RTO-TR-26
AC/323(AVT)TP/19

RTO-TR-26

NORTH ATLANTIC TREATY ORGANIZATION

RESEARCH AND TECHNOLOGY ORGANIZATION

BP 25, 7 RUE ANCELLE, F-92201 NEUILLY-SUR-SEINE CEDEX, FRANCE

RTO TECHNICAL REPORT 26

Verification and Validation Data for Computational Unsteady Aerodynamics

(Données de vérification et de validation pour l'aérodynamique instationnaire numérique)

Report of the Applied Vehicle Technology Panel (AVT) Task Group AVT-010.

Published October 2000

Distribution and Availability on Back Cover

RTO-TR-26
AC/323(AVT)TP/19

NORTH ATLANTIC TREATY ORGANIZATION

RESEARCH AND TECHNOLOGY ORGANIZATION

BP 25, 7 RUE ANCELLE, F-92201 NEUILLY-SUR-SEINE CEDEX, FRANCE

RTO TECHNICAL REPORT 26

Verification and Validation Data for Computational Unsteady Aerodynamics

(Données de vérification et de validation pour l'aérodynamique instationnaire numérique)

Report of the Applied Vehicle Technology Panel (AVT) Task Group AVT-010.

The Research and Technology Organization (RTO) of NATO

RTO is the single focus in NATO for Defence Research and Technology activities. Its mission is to conduct and promote cooperative research and information exchange. The objective is to support the development and effective use of national defence research and technology and to meet the military needs of the Alliance, to maintain a technological lead, and to provide advice to NATO and national decision makers. The RTO performs its mission with the support of an extensive network of national experts. It also ensures effective coordination with other NATO bodies involved in R&T activities.

RTO reports both to the Military Committee of NATO and to the Conference of National Armament Directors. It comprises a Research and Technology Board (RTB) as the highest level of national representation and the Research and Technology Agency (RTA), a dedicated staff with its headquarters in Neuilly, near Paris, France. In order to facilitate contacts with the military users and other NATO activities, a small part of the RTA staff is located in NATO Headquarters in Brussels. The Brussels staff also coordinates RTO's cooperation with nations in Middle and Eastern Europe, to which RTO attaches particular importance especially as working together in the field of research is one of the more promising areas of initial cooperation.

The total spectrum of R&T activities is covered by 7 Panels, dealing with:

- SAS Studies, Analysis and Simulation
- SCI Systems Concepts and Integration
- SET Sensors and Electronics Technology
- IST Information Systems Technology
- AVT Applied Vehicle Technology
- HFM Human Factors and Medicine
- MSG Modelling and Simulation

These Panels are made up of national representatives as well as generally recognised 'world class' scientists. The Panels also provide a communication link to military users and other NATO bodies. RTO's scientific and technological work is carried out by Technical Teams, created for specific activities and with a specific duration. Such Technical Teams can organise workshops, symposia, field trials, lecture series and training courses. An important function of these Technical Teams is to ensure the continuity of the expert networks.

RTO builds upon earlier cooperation in defence research and technology as set-up under the Advisory Group for Aerospace Research and Development (AGARD) and the Defence Research Group (DRG). AGARD and the DRG share common roots in that they were both established at the initiative of Dr Theodore von Kármán, a leading aerospace scientist, who early on recognised the importance of scientific support for the Allied Armed Forces. RTO is capitalising on these common roots in order to provide the Alliance and the NATO nations with a strong scientific and technological basis that will guarantee a solid base for the future.

The content of this publication has been reproduced
directly from material supplied by RTO or the authors.

Published October 2000

ISBN 92-837-1048-7

Printed by St. Joseph Ottawa/Hull
(A St. Joseph Corporation Company)
45 Sacré-Cœur Blvd., Hull (Québec), Canada J8X 1C6

Verification and Validation Data for Computational Unsteady Aerodynamics

(RTO TR-26)

Executive Summary

In the quest to improve the performance of civil and military aircraft, helicopters and missiles (lower structural weight, higher maneuverability, larger flight and firing/release envelopes, higher angles of attack, etc.) the designer increasingly faces the need to predict or understand complex unsteady aerodynamic phenomena. The continuous progress in hardware and software give the opportunity to simulate numerically many of these fluid dynamics problems. Consequently Computational Unsteady Aerodynamics (CUA) is finding its way as a useful and reliable tool, which can be routinely applied from the very early stages of the design and development process.

Before a specific code may be used with confidence it is essential to validate its capability to describe the physics of the flow correctly, for which purpose a comparison with accurate experimental data is needed. Unsteady wind tunnel testing is difficult and expensive; two factors which limit the number of organizations with the capability and/or resources to perform it. Thus, unsteady experimental data is scarce, often restricted and scattered in diverse documents. The present publication was conceived with the aim of collecting into a single easily accessible document as much of the good quality data as possible. Given the large amounts of information produced in unsteady experiments, and to facilitate its handling and use, the data is provided in machine-readable form in a CD-ROM that accompanies the report.

The type of experiment included in this publication falls under the general category of validation experiments, that is, those made on geometrically simple “generic shapes” designed to provide sufficiently detailed measured data for the verification of the physical representation provided by the CFD code. Wherever possible experiments have been selected which include different levels of physical difficulty and/or different flow phenomena so that the CFD researcher can use a staircase approach to the problem of validating the code. The test cases provided pertain to different categories: Flutter, Buffet, Stability & Control, Dynamic Stall, Cavity Flows, and Store Separation, which basically cover most of the areas of current interest in the field.

In addition to the experimental data, the publication includes computational results. Before a code can be validated, the developer must first verify that it solves accurately the mathematical model that it uses of the real world. Given the lack of analytical solutions to the 3-D versions of the various sets of equations of interest to CUA, verification is best achieved by means of comparison with another computational solution of the same set of equations. The numerical data may also be useful in cases where the CFD developer finds intriguing differences with experimental data, which cannot be attributed in a straightforward way to deficiencies in the numerical model, or in the test. Comparison with another computational result may clarify whether code improvements are required.

Données de vérification et de validation pour l'aérodynamique instationnaire numérique

(RTO TR-26)

Synthèse

Dans sa démarche d'amélioration des performances des aéronefs militaires et civils, ainsi que des hélicoptères et des missiles (masse structurale réduite, plus grande maniabilité, domaines de vol et de tir/de largage plus étendus, incidences plus fortes etc...) le concepteur est de plus en plus confronté à la nécessité de comprendre et de prévoir des phénomènes aérodynamiques instationnaires complexes. Les avancées permanentes réalisées dans le domaine de l'informatique nous offrent la possibilité de simuler de façon numérique bon nombre de ces problèmes de dynamique des fluides. Il en résulte que l'aérodynamique instationnaire numérique (CUA) est en passe de trouver un rôle d'outil pratique et fiable, qui peut être mis en œuvre dès les premières étapes du processus de conception et développement.

Avant de pouvoir utiliser un code quelconque avec confiance il est essentiel de valider sa capacité à décrire correctement la physique d'un écoulement, ce qui nécessite de faire la comparaison avec des données expérimentales fiables. Les essais d'aérodynamique instationnaire en soufflerie sont difficiles et coûteux à réaliser; ces deux facteurs ont pour effet de limiter le nombre d'organisations disposant d'installations et/ou de moyens permettant de le faire. Il s'ensuit que les données expérimentales instationnaires sont rares, souvent restreintes et dispersées dans de multiples documents. La présente publication a été conçue dans le but de recueillir dans un seul document le plus grand volume possible de données de bonne qualité disponibles à l'heure actuelle. Etant donné les masses d'informations produites par les essais instationnaires, et pour faciliter leur traitement et mise en œuvre, les données sont fournies sous une forme exploitable par une machine sur le CD-ROM qui accompagne ce rapport.

Le type d'expérimentation décrite dans cette publication appartient à la catégorie générale d'expérimentations de validation, c'est à dire à celles réalisées sur des « formes génériques » géométriquement simples, choisies pour fournir des données mesurées suffisamment détaillées pour permettre la vérification de la représentation physique donnée par le code CFD. Chaque fois qu'il s'est avéré possible, nous avons choisi des expérimentations comprenant des niveaux de difficulté physique différents et/ou des phénomènes d'écoulement différents pour permettre au chercheur en CFD d'adopter une approche par paliers du problème de la validation du code. Les cas d'essai présentés se rapportent à différentes catégories, à savoir : Le flottement, le tremblement, la stabilité et le contrôle, le décrochage dynamique, les écoulements en cavité, et le largage des emports, lesquelles catégories couvrent plus ou moins la totalité des domaines d'intérêt courants dans ce secteur.

En plus des données expérimentales, la publication inclut des résultats de calculs CFD. Avant de pouvoir procéder à la validation d'un code, le développeur doit vérifier sa capacité à résoudre correctement le modèle du monde réel qu'il exploite. Etant donné le manque de solutions analytiques des versions en trois dimensions des différents systèmes d'équations qui intéressent le CUA, le meilleur moyen de procéder à la vérification est de faire la comparaison avec une autre solution, obtenue par le calcul, du même système d'équations. Les données numériques peuvent également servir lorsque le développeur CFD découvre des différences significatives par rapport aux données expérimentales, qui ne peuvent pas être imputées directement à des insuffisances au niveau soit du modèle numérique, soit des essais. La comparaison avec un autre résultat obtenu par le calcul peut permettre d'établir si des améliorations sont nécessaires au niveau du code.

Click inside the blue boxes to view the corresponding section

Contents

		Page
Executive Summary		**iii**
Synthèse		**iv**
Publications of the RTO Applied Vehicle Technology Panel		**vii**
Members of the Applied Vehicle Technology Task Group AVT-010		**viii**
1.	**Presentation of the Database** by L.P. Ruiz-Calavera	**1**
2.	**Analytical Solutions for the Unsteady Compressible Flow Equations Serving as Test Cases for the Verification of Numerical Schemes** by S. Tsangaris and Th. Pappou	**9**
3E.	**Data from AGARD Report 702**	**29**
	3E1. NACA 64A006 Oscillating Flap by R.J. Zwaan	**33**
	3E3. NACA 0012 Oscillatory and Transient Pitching by R.H. Landon	**45**
	3E4. NLR 7301 Supercritical Airfoil Oscillatory Pitching and Oscillating Flap by R.J. Zwaan	**61**
	3E8. ZKP Wing, Oscillating Aileron by K. Dau, S. Vogel and H. Zimmermann	**79**
4.	**F-5 CFD Results** by M.J. de C. Henshaw and S. Guillemot	**97**
5E.	**F-5 Wing & F-5 Wing + Tip Store** by E.G.M. Geurts	**135**
6E.	**Test Cases for a Rectangular Supercritical Wing Undergoing Pitching Oscillations** by R.M. Bennett	**153**
7E.	**Test Cases for Flutter of the Benchmark Models Rectangular Wings on the Pitch and Plunge Apparatus** by R.M. Bennett	**173**
8E.	**Test Cases for the Benchmark Active Controls Model: Spoiler and Control Surface Oscillations and Flutter** by R.M. Bennett, R.C. Scott and C.D. Wieseman	**201**
8C.	**Benchmark Active Controls Technology (BACT) Wing CFD Results** by D.M. Schuster and R.E. Bartels	**225**
9E.	**Test Cases for a Clipped Delta Wing with Pitching and Trailing-Edge Control Surface Oscillations** by R.M. Bennett	**239**
10.	**Supersonic 2D Wing with Control Surfaces** by P. Naudin	**257**

11E.	**RAE Tests on AGARD Tailplane** by I.W. Kaynes	**271**
12.	**NAL SST Arrow Wing with Oscillating Flap** by M. Tamayama, K. Saitoh, H. Matsushita and J. Nakamichi	**295**
13E.	**Transonic Buffet of a Supercritical Airfoil** by X.Z. Huang	**319**
14E.	**Buffet Data from M2391 Diamond Wing** by I.W. Kaynes	**341**
15E.	**Wing and Fin Buffet on the Standard Dynamics Model** by S. Zan et al - reported by X.Z. Huang	**361**
16E.	**Selected Data Set from Static and Rolling Experiments on a 65° Delta Wing at High Incidence** by X.Z. Huang, T.C. Lui and E.S. Hanff	**383**
16C.	**Large-Amplitude, High-Rate Roll Oscillations of a 65° Delta Wing at High Incidence** by N.M. Chaderjian and L.B. Schiff	**407**
17E.	**Oscillating 65° Delta Wing, Experimental** by T. Loeser	**415**
17C.	**Oscillating 65° Delta Wing, Numerical** by W. Fritz	**431**
18E.	**Low Speed Straked Delta Wing** by E.G.M. Geurts	**437**
19E.	**Transonic Simple Straked Delta Wing** by E.G.M. Geurts	**453**
20.	**M219 Cavity Case** by M.J. deC. Henshaw	**473**
21E.	**DLR Cavity Pressure Oscillations, Experimental** by J. Delfs	**481**
22E.	**Dynamic Stall Data for 2-D and 3-D Test Cases** by R.A. McD Galbraith, F.N. Coton, R.B. Green and M. Vezza	**489**
23.	**Generic Wing, Pylon, and Moving Finned Store** by J.H. Fox	**535**

Publications of the RTO Applied Vehicle Technology Panel

MEETING PROCEEDINGS (MP)

Design for Low Cost Operation and Support
MP-37, September 2000

Gas Turbine Operation and Technology for Land, Sea and Air Propulsion and Power Systems (Unclassified)
MP-34, September 2000

Aerodynamic Design and Optimization of Flight Vehicles in a Concurrent Multi-Disciplinary Environment
MP-35, June 2000

Structural Aspects of Flexible Aircraft Control
MP-36, May 2000

New Metallic Materials for the Structure of Aging Aircraft
MP-25, April 2000

Small Rocket Motors and Gas Generators for Land, Sea and Air Launched Weapons Systems
MP-23, April 2000

Application of Damage Tolerance Principles for Improved Airworthiness of Rotorcraft
MP-24, January 2000

Gas Turbine Engine Combustion, Emissions and Alternative Fuels
MP-14, June 1999

Fatigue in the Presence of Corrosion
MP-18, March 1999

Qualification of Life Extension Schemes for Engine Components
MP-17, March 1999

Fluid Dynamics Problems of Vehicles Operation Near or in the Air-Sea Interface
MP-15, February 1999

Design Principles and Methods for Aircraft Gas Turbine Engines
MP-8, February 1999

Airframe Inspection Reliability under Field/Depot Conditions
MP-10, November 1998

Intelligent Processing of High Performance Materials
MP-9, November 1998

Exploitation of Structural Loads/Health Data for Reduced Cycle Costs
MP-7, November 1998

Missile Aerodynamics
MP-5, November 1998

EDUCATIONAL NOTES (EN)

Measurement Techniques for High Enthalpy and Plasma Flows
EN-8, April 2000

Development and Operation of UAVs for Military and Civil Applications
EN-9, April 2000

Planar Optical Measurements Methods for Gas Turbine Engine Life
EN-6, September 1999

High Order Methods for Computational Physics, Published jointly with Springer-Verlag, Germany
EN-5, March 1999

Fluid Dynamics Research on Supersonic Aircraft
EN-4, November 1998

Integrated Multidisciplinary Design of High Pressure Multistage Compressor Systems
EN-1, September 1998

TECHNICAL REPORTS (TR)

Verification and Validation Data for Computational Unsteady Aerodynamics
TR-26, October 2000

Recommended Practices for Monitoring Gas Turbine Engine Life Consumption
TR-28, April 2000

A Feasibility Study of Collaborative Multi-facility Windtunnel Testing for CFD Validation
TR-27, December 1999

Members of the Applied Vehicle Technology Task Group AVT-010 on Test Cases for Computational Unsteady Aerodynamics

Chairman: Luis P. Ruiz-Calavera
INTA
Aerodynamics Division
Carretera de Ajalvir Km 4.5
28850 Torrejon de Ardoz (Madrid)
Spain

CANADA
X.Z. Huang
National Research Council
Institute for Aerospace Research
M-10, Montreal Rd.
Ottawa, Ontario K1A 0R6

FRANCE
S. Guillemot
Dassault Aviation
Aerodynamics Division
78 Quai Marcel Dassault
Cedex 300
92214 Saint Cloud

P. Naudin
Structures Department
ONERA
29, avenue de la division Leclerc
BP 72, 92322 Châtillon Cedex

GERMANY
T. Löser
NWD Low Speed Wind Tunnel
DLR/DNW Braunschweig
Lilienthalplatz 7
D-38022 Braunschweig

GREECE
S. Tsangaris
Dept. of Mechanical Engineering
National Technical University of Athens
P.O. Box 64070
15710 Zografu-Athens

ITALY
A. Pagano
Aerodynamics and Propulsion Department
CIRA, Via Maiorise
81043 Capua (CE)

NETHERLANDS
E.G.M. Geurts
NLR
Aerodynamic Engineering and Aeroelasticity Department
Anthony Fokkerweg 2
1059 CM AMSTERDAM

TURKEY
M. Kavsaoglu
Middle East Technical University
Department of Aeronautical Engineering
Inonu Bulvari
06531 Ankara

UNITED KINGDOM
R.W. Galbraith
Department of Aerospace Engineering
University of Glasgow
Glasgow, G12 8QQ, Scotland

M.J. de C. Henshaw
British Aerospace (Operations) Ltd.
Military Aircraft and Aerostructures
Dept. of Aerodynamic Technology
Skillings Lane, Brough
East Riding of Yorkshire
HU15 1EQ, England

I.W. Kaynes
Room 1008, A9 Building
Aero-Structures Dept
DERA
Farnborough
Hants GU14 0LX

UNITED STATES
R. Bennett
Aeroelasticity Branch
Structures Division
Mail Stop 340
NASA Langley Research Center
Hampton, VA 23681-0001

J.H. Fox
Sverdrup Technology, Inc.
AEDC Group
740 Fourth Street
Arnold AFB, TN 37389-6001

L.J. Huttsell
AFRL/VASV
2130 Eighth St, Ste 1
Wright-Patterson AFB, OH 45433-7542

1. PRESENTATION OF THE DATABASE

Luis P. Ruiz-Calavera
INTA
Aerodynamics Division
Carretera de Ajalvir s/n
28850 Torrejon de Ardoz, Madrid, SPAIN

INTRODUCTION

With the continuous progress in hardware and numerical schemes, Computational Unsteady Aerodynamics (CUA), that is, the application of Computational Fluid Dynamics (CFD) to unsteady flowfields, is slowly finding its way as a useful and reliable tool (turbulence and transition modeling permitting) in the aircraft, helicopter, and missile design and development process. Before a specific code may be used with confidence it is essential to validate its capability to describe the physics of the flow correctly, or at least to the level of approximation required, for which purpose a comparison with accurate experimental data is needed. Unsteady wind tunnel testing is difficult and expensive; two factors which limit the number of organizations with the capability and/or resources to perform it. Thus, unsteady experimental data is scarce, often restricted and scattered in diverse documents. Additionally, access to the reports does not necessarily assure access to the data itself. The present publication was conceived with the aim of collecting into a single easily accessible document as much of the good quality data as possible.

The idea is not new. In 1982 AGARD's Structures and Material Panel (SMP) produced the AGARD Report No. 702 'Compendium of Unsteady Aerodynamic Measurements', which has found and continues to find extensive use within the CUA community. Report 702 is primarily focused on aeroelasticity, with particular attention paid to transonic conventional flutter. In 1995 AGARD's Fluid Dynamics Panel (FDP) decided to update and expand the former database with new geometries and physical phenomena and launched Working Group WG-22 on 'Validation Data for Computational Unsteady Aerodynamic Codes'. Shortly afterwards AGARD was reorganized as the RTO (Research and Technology Organization) and the WG was renamed as AVT (Applied Vehicle Technology) WG-003. The group, chaired by the author of this introductory chapter, first met in spring 1997 and closed its effort 5 meetings later in spring 1999 with the present publication. Special care was taken that both theoreticians and experimentalists were represented in the Working Group. Table 1 gives the complete list of WG members including address, telephone, fax and e-mail. Other contributors who were not formal members of the group are identified as authors of individual chapters.

REQUIREMENTS FOR EXPERIMENTS

The type of experiment included in this publication falls under the general category of validation experiments, that is, those made on geometrically simple "generic shapes" designed to provide sufficiently detailed measured data for the verification of the physical representation provided by the CFD code. This requires that the data be taken and presented in a form and level of detail consistent with CFD requirements and that the accuracy of the experimental data be thoroughly documented and understood. The ideal test case should provide:

a) Accurately measured model shape and surface finish.
b) The actual position and motion of all points of the model, including both static and dynamic elastic deformations.
c) Well defined state of the boundary layer on the model.
d) Inflow and outflow conditions.
e) Wall conditions and wall boundary layer.
f) Specification of support interference
g) Specification of the accuracy of measured data.

After a thorough screening of the candidate test cases available for general distribution, it was found that ideal test cases are rare indeed, so the acceptance criteria had to be dramatically modified to the minimum requirements of knowing the geometry, and the motion (rigid and elastic) as accurately as possible. Nevertheless the WG believe the test cases included in this report to be generally of very high quality.

It has been the aim to select cases with very detailed information (e.g. a lot of pressure points), but cases with less detailed information, but a wide range of flow conditions, have also been acceptable. Wherever possible experiments have been selected which include different levels of physical difficulty so that the CFD researcher can use a staircase approach to the problem of validating the code.

Generally, agreement on the steady pressure distribution is a prerequisite for agreement on the unsteady pressures, when comparing calculations with experimental data. In particular, when shock waves are present the experimental and theoretical distributions of unsteady pressure will not agree unless there is already agreement with the mean position and strength of the shock. For this reason a fair amount of steady data has also been included.

COMPUTATIONAL RESULTS

In addition to the experimental data, this publication includes computational results. Before a code can be validated, the developer must first verify that it solves accurately the mathematical model that it uses of the real world. Given the lack of analytical solutions to the 3-D versions of the various sets of equations of interest to CUA, verification is best achieved by means of comparison with another computational solution of the same set of equations.

To this aim a benchmark exercise was performed on the F-5 wing. Computational results covering the whole spectrum from Unsteady Transonic Small Perturbations to Navier-Stokes codes were generated and are provided in the database, thus facilitating the verification of the new code against the same level of physical modeling.

For the same reason, attempts have been made to complement each experimental data set with an example of a numerical calculation of at least one of its test points. These results may also be useful in cases where the CFD developer finds intriguing differences with experimental data, which cannot be attributed in a straightforward way to deficiencies in the numerical model, or in the test. Comparison with another computational result may clarify whether code improvement is required. Unfortunately it has not been possible to obtain numerical results for most of the test cases, but the door is left open for interested groups to submit their calculations to complete the picture. These 'late arrivals' could be compiled as an addendum to this document.

No claim is made that any of the CFD solutions included are free of discretization or solution errors. They should be treated as examples of what people with experience in the field have produced using mature codes, but not as absolute truth.

ORGANIZATION OF THE DATA BASE

The compendium consists of this general introduction, a chapter on analytical solutions, a review of AGARD-R-702, the F-5 benchmark exercise mentioned above, and 19 self-contained datasets, which are summarized in Table 2. For each test case the following information is provided:

- A brief overview of the purpose and salient features of the experiment
- Nomenclature information (no attempt has been made to assure uniformity of notation across the data sets).
- A standard form (taken directly from Report 702 as this was considered difficult to improve, with appropriate adaptations for some of the cases) with the key information about the test conditions and equipment that a user may require.
- Information on the layout of the data files when it was not self-explanatory
- Figures and pictures to illustrate the case

When available, the associated computational results are presented in a chapter immediately following the experimental counterpart.

The data itself is only provided in machine-readable form in the CD-ROM that accompanies this publication. Each case is included in a different folder, where the various relevant data files are stored. Most of the data files are plain ASCII, with some being written in TECPLOT format. In some cases it was necessary to provide geometry information by means of CATIA files. Figures are included in a number of well-known formats (eps, pdf, etc). A copy of the different chapters is also provided in Word 97 format.

OVERVIEW OF THE CASES

Immediately following this general review the reader will find a chapter on analytical solutions of the 1-D unsteady Euler equations as well as other simplified equations (Linear Advection, Burger's, etc.). Comparison with analytical solutions is a necessary (albeit often neglected) first step in the process of code verification. The classical problems described in the chapter:

- Shock Tube (Riemann) problem
- Propagation and reflection of a moving shock at the closed end of a tube
- Expansion and compression flows behind moving pistons

provide excellent opportunities to check respectively: the time-accuracy of shock convection (particularly for implicit methods); the numerical implementation of unsteady boundary conditions; and moving grids.

Next in line the reader will find a chapter devoted to the AGARD-R-702. The original Compendium has been revisited with the perspective of time, and those cases, which have found more use, are included here again. Nothing has been added to them, but the data is provided in electronic format, which will make the user's life easier. The reader will probably miss the well-known LANN wing. Different problems encountered in the preparation of the electronic data have prevented the group to incorporate this case, which would otherwise have been included as it has found extensive use in spite of (or perhaps because of) the difficulties introduced by its elastic deformation.

The already mentioned F-5 wing benchmark exercise follows next. Computational results covering the whole spectrum from Unsteady Transonic Small Perturbations (UTSP) to time-accurate Navier-Stokes codes, with different levels of grid refinement and/or geometrical simplifications (tip, trailing edge, etc) are included. While the steady solutions compared quite well, with differences being easily attributable to grid or viscous effects, the unsteady solutions show surprisingly large discrepancies. A detailed analysis can be found in Chapter 4.

The test cases themselves follow in the remaining chapters; they have been loosely classified under 6 categories:

- Flutter
- Buffet
- Stability & Control
- Dynamic Stall
- Cavity Flows
- Store Separation

Not surprisingly, the database is well populated with an assortment of flutter-type cases. The category seems to be well balanced, covering from very simple to more complicate geometries and from linear to highly non-linear flows. Some of the cases have been available for a long time (although it is the group's opinion that good data never ages) but they were considered to be still useful and relevant.

The database starts with the well-known F-5 wing tested in the High Speed Wind Tunnel of NLR. The original purpose of the experiment was to determine the unsteady airloads characteristics on a representative fighter type wing oscillating in pitch. It constitutes a very comprehensive data set, which progressively builds up in geometric complexity from the clean wing to a wing with a tip launcher and an A-A missile with canards and fins. From a computational point of view, the clean wing case can be considered as rather benign, as it involves only small static angles of attack, small amplitudes of oscillation and limited viscous effects. This fact together with its simple geometry and wide range of Mach numbers tested (from subcritical to low supersonic) make it an ideal 'first case' in the validation process of a new code. This was the main reason why it was selected for the benchmark exercise mentioned before. On the other hand, the wing plus launcher plus missile cases provide excellent opportunities to check the ability of the code to tackle rather complex geometries.

Test case 6E is the Rectangular Supercritical Wing model. The RSW was tested in the NASA Langley Transonic Dynamic Tunnel (TDT) with the specific aim of obtaining data for CFD comparison. It has a simple low aspect ratio unswept rectangular planform with no twist, a constant 12% thick supercritical airfoil and a tip of revolution. The model undergoes pitching oscillations. Data is provided corresponding to a wide range of flow conditions from low subsonic to strong transonic well beyond the design Mach number, as would be required for flutter verification beyond cruise conditions. A broad range of reduced frequencies is also covered. Special care has been taken to select data points, which illustrate the trends with Mach number, reduced frequency, amplitude of oscillation and static angle of attack. Some cases for high angle of attack (at low speed) and others for the effect of transition have been also included. Despite its simple geometry, the case has proved to be a difficult one to calculate. Typically for low-aspect ratio rectangular wings, transonic shock waves tend to sweep forward from root to tip such that there are strong three-dimensional effects. Additionally it has been found to be very sensitive to viscous and transition effects, specially on the undersurface.

Test cases 7E and 8E were part of NASA's Benchmark Model Program (BMP) which tested in Langley's TDT a number of models with the same rectangular planform but with different airfoils with diverse transonic characteristics. The first model had a NACA 0012 airfoil which develops strong shocks ahead of mid-chord; the second model had a NACA 64A010 airfoil with a milder evolution of the shock which initially forms at mid-chord; and the third model had a supercritical SC(2)-0414 airfoil with strong aft loading and the associated low upper surface curvature which generates weaker hard to capture shocks. In addition the Benchmark Active Control Technology (BACT) model had also a NACA 0012 airfoil but with a trailing edge control surface, and a pair of independently actuated upper and lower surface spoilers for use in flutter suppression and dynamic response excitations. All the models were mounted on the PAPA (Pitch and Plunge Apparatus) 2 Degrees of Freedom dynamic system, which allows rigid models to undergo flutter. Cases corresponding to classical pitch-plunge flutter, transonic stall flutter involving shock waves and separating and re-attaching flows during the cycle of motion, and a shock-induced plunge instability are included. The actual wing motion together with the corresponding pressures are provided, thus allowing a staircase approach to validation, from forced oscillations (using the measured pitch-plunge motion as input) to 'simple' aeroelastic simulations (using the known elastic characteristics of PAPA). Finally the transfer functions of control surface inputs measured with the BACT can be used to validate aeroservoelastic codes. These two cases together provide an extremely comprehensive dataset, which is sure to keep CFD developers busy for a long time.

The Clipped Delta Wing model of test case 9E was also tested in the NASA Langley TDT. The planform was derived by simplifying that of a Supersonic Civil Transport aircraft, resulting in a trapezoid wing with an unswept trailing edge and without twist and camber. The model undergoes pitching and trailing edge control surface oscillations. A rather thick (for a supersonic transport) 6% symmetrical circular arc section was used, which very much enhances transonic effects. Additionally the highly swept sharp leading edge separates the flow at relatively low angles of attack forming a leading edge vortex, which sometimes co-exists with a shock wave, making this a challenging case for any numerical method.

Case 10E was tested in ONERA S2 wind tunnel to obtain a database of the unsteady behavior of control surfaces in high supersonic conditions. It consists of a 5.5 aspect ratio rectangular wing with a 7% symmetric bi-convex airfoil and an oscillating trailing edge flap. Detailed pressure information was measured at the mid semi-span section, which at the supersonic Mach numbers tested is effectively in 2D conditions. Test points are provided that illustrate the effect on the unsteady airloads of: Mach number, steady angle of attack, mean flap deflection, flap oscillation amplitude and oscillation frequency.

The RAE Tailplane constituting case 11E was tested in RAE's 3 ft tunnel to provide data for the validation of codes for the prediction of unsteady pressures on low aspect ratio configurations suitable for wings or controls of military aircraft. The model has again a thick (for supersonic applications) NACA 64A010 airfoil, which was oscillated in pitch at a wide range of frequencies and Mach numbers. It constitutes an excellent challenge for any 3D supersonic code, with the added bonus that the model was build in carbon fiber, which provided both high stiffness and low inertia, thus minimizing aeroelastic distortions.

The opposite (in terms of aeroelastic deformations) is true for test case 12E. This model of a Supersonic Transport with a double-swept-back arrow wing, a fuselage and an oscillating trailing edge flap was tested at NAL's 2mx2m transonic wind tunnel with the specific purpose to accumulate validation data for CUA and ACT (Active Control Technology) codes. A NACA0003 airfoil was used, resulting in a very thin wing with non-negligible static and dynamic elastic deformations. These deformations were very carefully monitored tracing optical targets installed on the wing surface. Furthermore, in some cases the trailing edge was made to oscillate at frequencies close to the eigenfrequencies of the model. Although the flow characteristics are not very demanding (no strong shock waves appear) the elastic motion further complicates its accurate prediction. It thus constitutes an excellent test of the ability of the code to handle elastic problems. Results are included for different transonic Mach numbers, mean flap positions and frequencies of oscillation.

The buffet category starts with test case 13E corresponding to the shock-induced buffet of the BGK No 1 supercritical airfoil tested at IAR's 2D High Reynolds Wind Tunnel. This dataset provides very rich pressure information on a number of points outside, at, and well inside, the buffet onset boundary. Additionally skin friction data is available allowing the user to monitor the merging of the shock induced separation bubble with the trailing edge separation.

Test case 14E extends the buffet information to wing configurations with Model 2391 tested in DERA Bedford 13ftx9ft low speed wind tunnel. This is a low mass, high stiffness model designed to obtain data of the aerodynamic excitation arising from unsteady separated flow without the interferences due to model vibration and/or support natural frequencies. It is a 40° sweep diamond wing with a streamwise clipped tip. Two interchangeable fuselages were tested, respectively rectangular and chined, with the former providing a perpendicular wing-fuselage interface, and the later allowing the study of buffet due to mixed vortical flow. Very rich pressure information for angles of attack up to 30° is included, thus providing an excellent test case to validate the buffet part of any buffeting prediction code.

Finally, test case 15E1 closes the buffet category with the Standard Dynamic Model (SDM) tested in IAR's Low Speed Wind Tunnel to investigate the aerodynamic excitation during wing and/or fin buffet of a generic fighter aircraft configuration. It was also build extremely stiff so as to avoid any buffeting. Wing and fin buffet cases corresponding to bursting of strakes and/or forebody vortices (both symmetric and asymmetric) are presented. The rather complicated geometry together with the very difficult physics pose a real challenge for any CFD code.

The Stability & Control category is mainly devoted to high-angle of attack oscillations. Test cases 16E and 17E present similar 65° delta wings and explore their aerodynamic behavior during high performance maneuvers involving large amplitude, high-rate, pitching/rolling/yawing motions at high incidence. The first case, presented by IAR, was tested in two different wind tunnels using two different support systems with very similar results; so it can be assumed to be fairly free of support and wall interferences. It mainly presents global coefficients with limited pressure information. The second case, tested at DLR, has more extensive pressure data. It presents a range from simple attached flow, through fully developed vortex flow and vortex bursting upstream and downstream of the trailing edge, up to deadwater type flow on the upper surface; thus allowing a code validation with progressively more complex physics.

Test cases 18E and 19E can again be treated together. They correspond to straked delta wings tested at respectively subsonic and transonic speed in NLR's LST and HST wind tunnels, with the aim to improve understanding of unsteady loading on fighter like wings during pitch oscillations and maneuvers. They present a wide range of flow topologies, from attached to vortex breakdown over the whole model. Additionally the transonic test includes cases with shock induced trailing edge separation, leading edge separation and vortex breakdown at transonic speeds, and Limit Cycle Oscillations (LCO). The data points selected cover all the different flow types, including the influence of Mach number, static incidence and sideslip, amplitude and frequency of oscillation, thus proposing test points ranging from relatively easy to extremely difficult to calculate.

The cavity category is represented by 2 datasets (test cases 20E and 21E) produced respectively by BAe/DERA and DLR. In both cases very rich pressure information inside rectangular cavities at different Mach numbers is provided. Acoustics as well as loads and store separation specialist will benefit greatly from these test cases.

A whole set of dynamic stall test cases is included in chapter 22E. Both 2D and 3D configurations undergoing "ramp-up", "ramp-down" (to isolate the stalling mechanism from the re-attachment process) and harmonic pitching oscillations are considered. Detailed pressure and loads information for different pitch rates and mean angles of attack are included, thus providing the CFD developer with a variety of test data to assess the output of their codes, with many of the cases constituting a severe tests of the ability of the code to capture massively separated flows.

Finally a store separation case (test case 23E) is included The test was performed at AEDC by means of a CTS (Captive Trajectory Support) so that strictly speaking data is only quasi-steady. Nevertheless the case has been included because the modeled phenomena is unsteady by nature, and this type of data is comparatively difficult to find in the open literature. Additionally the store's boundary layer transition is very far aft and has a strong influence on global coefficients, which increases the challenge for NS solvers.

It is recognize that the database lacks an isolated missile type configuration. This is unfortunate, as missile aerodynamics is an area where unsteady effects are playing an increasingly important role with the permanent increases in maneuverability. It is hoped that such a case be offered in the near future.

ACKNOWLEDGMENTS

Funding for this work was provided in the first place by AGARD/RTO, the different AGARD/RTO national organizations and the individual member organization. Their contributions are gratefully acknowledged.

The author would like to thank all Working Group members and all contributors for their collaboration, excellent work and dedication.

The publication was reviewed by Dr. R.J. Zwaan from Delft University of Technology, and by Dr. T. E. Noll and Dr. J. W. Edwards from NASA Langley Research Center. Their experience and knowledge in the field contributed very much to the improvement of the output.

TABLE 1. WORKING GROUP MEMBERS

NAME	ADDRESS	TELEPHONE FAX E-MAIL
L.P. Ruiz-Calavera	INTA Aerodynamics Division Carretera de Ajalvir Km 4.5 28850 Torrejon de Ardoz, Spain	+34-1-520-1571 +34-1-520-1978 ruizcl@inta.es
S. Tsangaris	Dept. of Mechanical Engineering National Technical University of Athens P.O. Box 64070 15710 Zografu-Athens, Greece	+30-1-7721043 +30-1-7721057 sgt@fluid.mech.ntua.gr
P. Naudin	Structures Department ONERA 29, avenue de la division Leclerc BP 72 92322 Chatillon Cedex, France	+33-1-46734621 +33-1-46734143 naudin@onera.fr
S. Guillemot	Dassault Aviation Aerodynamics Division 78 Quai Marcel Dassault Cedex 300 92214 Saint Cloud, France	+33-1-47115562 +33-1-47114535 Stephane.Guillemot@dassault-aviation.fr
I. W. Kaynes	Room 1008, A9 Building Aero-Structures Dept DERA Farnborough Hants GU14 0LX, UK	+44-1252-395082 +44-1252-395875 iwkaynes@dra.hmg.gb
R. W. Galbraith	Department of Aerospace Engineering University of Glasgow Glasgow, G12 8QQ, Scotland, UK	+44-141-3305295 +44-141-3305560 r.a.m.galbraith@aero.gla.ac.uk
M. J. deC. Henshaw	British Aerospace (Operations) Ltd., Military Aircraft and Aerostructures, Dept. of Aerodynamic Technology, Skillings Lane, Brough. East Riding of Yorkshire. HU15 1EQ, England, UK	+44-1482-663169 +44-1482-663001 Michael.Henshaw@bae.co.uk
X. Huang	National Research Council Institute for Aerospace Research M-10, Montreal Rd. Ottawa, Ont., Canada, K1A 0R6	+1-613-990-6796 +1-613-952-7677 xingzhong.huang@nrc.ca
M. Kavsaoglu	Middle East Technical University Department of Aeronautical Engineering Inonu Bulvari 06531 Ankara, Turkey	+90-312-210-4290 +90-312-210-1272 kavsa@rorqual.cc.metu.edu.tr
E. G. M. Geurts	NLR Aerodynamic Engineering and Aeroelasticity Department Anthony Fokkerweg 2 1059 CM AMSTERDAM, The Netherlands	+31-20-511-3455 +31-20-511-3210 geurts@nlr.nl

R. Bennett	Aeroelasticity Branch Structures Division Mail Stop 340 NASA Langley Research Center, Hampton, VA USA 23681-0001	+1-757-864-2274 +1-757-864-8678 r.m.bennett@larc.nasa.gov
J. H. Fox	Sverdrup Technology, Inc. AEDC Group 740 Fourth Street Arnold AFB, TN 37389-6001, USA	+1-615-454-6692 +1-615-454-6658 fox@hap.arnold.af.mil
L. J. Huttsell	AFRL/VASV 2130 Eighth St Ste 1 Wright-Patterson AFB OH 45433-7542, USA	+1-937-255-8456 +1-937-255-3740 lawrence.huttsell@va.wpafb.af.mil
Th. Löser	NWB Low Speed Wind Tunnel DLR/DNW Braunschweig Lilienthalplatz 7, Braunschweig, Germany	+49-531-295-2454 +49-531-295-2829 Thomas.Loeser@dlr.de
A. Pagano	Aerodynamics and Propulsion Department CIRA Via Maiorise 81043 Capua (CE), Italy	+39-823-62-3331 +39-823-62-3335 a.pagano@cira.it

Table 2. Test cases

ID	Test case	Configuration	Motion	Speed Regime	CFD?
5E	NLR F-5 Wing & Wing+Store	Wing+Missile	Pitch	Subsonic to Supersonic	YES
6E	NASA RSW	Wing	Pitch	Subsonic to Transonic	
7E	NASA BMP Rectangular Wing	Wing	Pitch Plunge	Subsonic to Transonic	
8E	NASA BMP BACT	Wing + Flap + Spoiler	Flap spoiler	Subsonic to Transonic	YES
9E	NASA Clipped Delta Wing	Wing + Flap	Pitch Flap	Subsonic to Supersonic	
10E	ONERA 2D Supersonic TE Control	Airfoil + Flap	Flap	Supersonic	
11E	RAE Tailplane	Wing	Pitch	Supersonic	
12E	NAL SST	Wing + Flap + Fuselage	Flap	Transonic	
13E	IAR BGK Airfoil	Airfoil	Buffet	Transonic	
14E	DERA Model 2391	Wing + Fuselage	Buffet	Subsonic	
15E	IAR SDM Fin Buffet	Wing + Fuselage + Fin	Buffet	Subsonic	
16E	IAR 65° Delta Wing	Wing + Centerbody	Roll	Subsonic	YES
17E	DLR 65° Delta Wing	Wing + Centerbody	Pitch Yaw Roll	Subsonic	YES
18E	NLR Low Speed Straked Delta Wing	Wing	Pitch	Subsonic	
19E	NLR Transonic Simple Straked Delta Wing	Wing	Pitch	Subsonic to Transonic	
20E	BAe/DERA Cavity	Cavity	-	Subsonic to Supersonic	
21E	DLR COM TWG1	Cavity	-	Transonic Supersonic	
22E	Glasgow U. Dynamic Stall	Airfoil Wing	Pitch	Subsonic	
23E	AEDC Wing/Pylon/Moving Store	Wing + Pylon + Store	Drop	Transonic Supersonic	

2. ANALYTICAL SOLUTIONS FOR THE UNSTEADY COMPRESSIBLE FLOW EQUATIONS SERVING AS TEST CASES FOR THE VERIFICATION OF NUMERICAL SCHEMES

S.Tsangaris
Th.Pappou
Laboratory of Aerodynamics, National Technical University of Athens
P.O.BOX 64070, 15 710 Zografos-Athens, Greece

INTRODUCTION

The verification of numerical schemes for solving the equations of inviscid and viscous compressible unsteady flow equations is limited to a small number of analytical solutions of the equations governing the one-dimensional unsteady flow including moving discontinuities. Among them the most important were given first by B. Riemann (1859-1860) and later by W.J.M. Rankine (1870), P.H. Hugoniot (1887), Lord Rayleigh (1910) and G.I. Taylor (1910). The scope of the present chapter is to overview the analytical solutions, serving as test case for the accuracy of the numerical schemes. It is worth noting that the analytical solutions are of importance for Euler and Navier-Stokes equations for laminar flow and does not give any indication for the behaviour of the numerical schemes in the prediction of turbulent flows. For each analytical solution a corresponding FORTRAN program is attached.

LINEAR ADVECTION EQUATION

The linear advection equation is used as a simple model for contact discontinuities in fluid dynamics, and is the simplest model equation for the representation of wave propagation. The linear advection equation is:

$$u_t + c_0 u_x = 0 \tag{1}$$

where c_0 is a positive constant ($c_0 > 0$) called the velocity of the wave. The general solution of equation (1) is

$$u(x,t) = f(x - c_0 t) \tag{2}$$

$f(x)$ is an arbitrary function defined by the initial conditions of the problem

$$u(x,0) = f(x) \tag{3}$$

The solution (3) apparently describes a wave motion to the positive x-axis, since the initial profile $f(x)$ is translated unchanged in shape a distance $c_0 t$ to the right at time t [8].

Oscillatory solution of linear advection equation with a discontinuity in the derivative (case LADV-1)

The problem of oscillatory solution of linear advection equation is approached using the initial conditions [8]:

$$u(x,0) = f(x;\alpha,k) = \begin{cases} -\alpha \sin(k\pi x), x < 0 \\ x \ , \ x \geq 0 \end{cases} \quad \text{with } \alpha = 0.1 \text{ and } k = 6 \tag{4}$$

At x=-1 the boundary condition

$$u(-1,t) = 0 \tag{4a}$$

is imposed. The solution in accordance with the above consideration, is presented in Figure 1 at time instances t=0 and t=0.5

This test case gives information about the capability of a computational method to capture an oscillating solution with a discontinuity in the derivative.

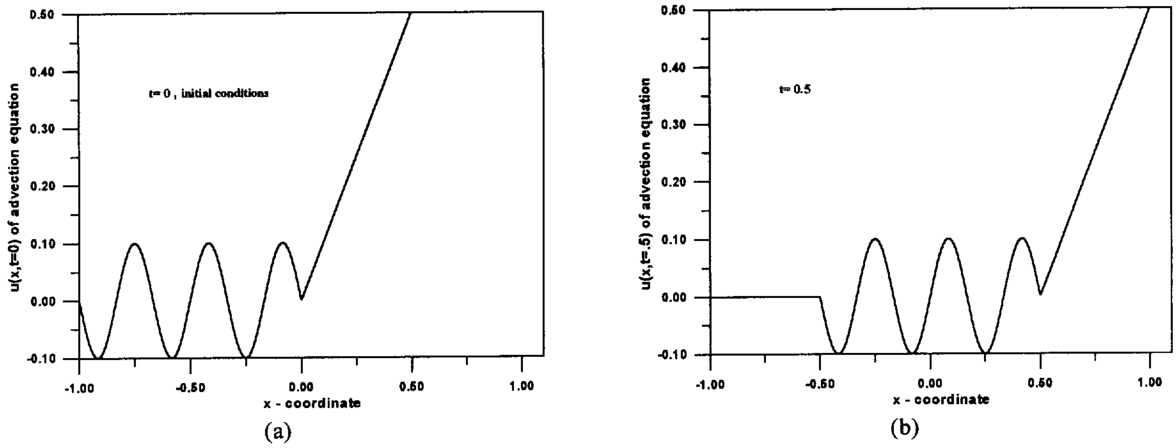

Figure 1: Oscillatory solution of linear advection equation with a discontinuity in the derivative

Simulation of discontinuities (case LADV-2)

To simulate discontinuities we again solve the linear advection equation, this time using piecewice continuous initial data:

$$u(x,0) = f(x;u_L,u_R) = \begin{cases} u_L, x < 0 \\ u_R, x \geq 0 \end{cases} \quad \text{with } u_L = 1 \text{ and } u_R = 0 \tag{5}$$

At x=-1 the boundary condition

$$u(-1,t) = 0 \tag{5a}$$

is imposed. The resultant solution is a square wave travelling with speed 1 to the right, as it is depicted in Figure 2 .

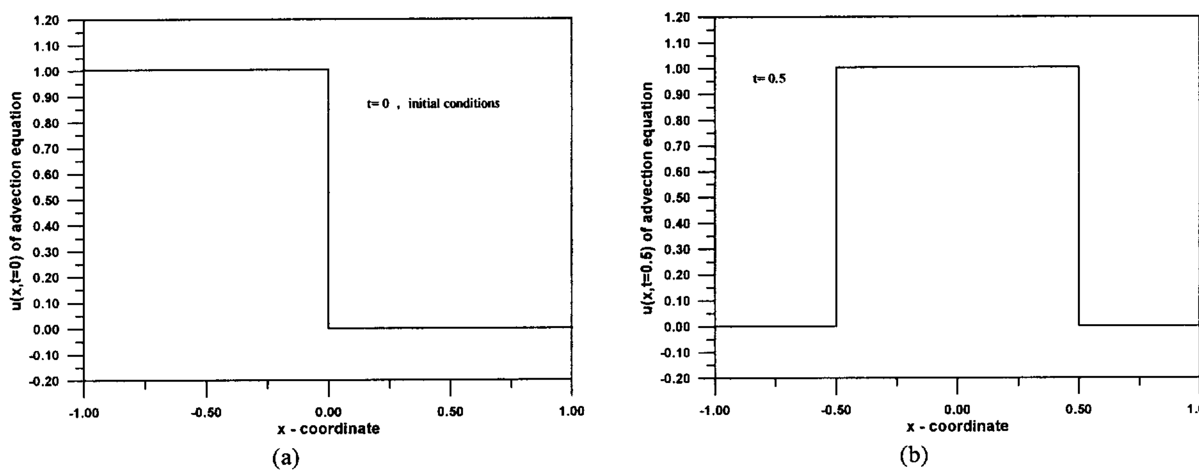

Figure 2: Contact discontinuity, advection equation.

BURGERS' EQUATION

Inviscid Burgers' equation.

The non linear first order equation:

$$u_t + uu_x = 0 \quad \text{or} \quad u_t + \left(\frac{u^2}{2}\right)_x = 0 \tag{6}$$

with Initial Conditions

$$u(x,0) = f(x) \quad \text{for} \quad -\infty < x < \infty \tag{6a}$$

is the x-momentum equation without pressure gradient or other external forces and it is so called inviscid Burgers' equation. The general solution of the above equation is given by:

$$du = 0 \quad \text{along the characteristic} \quad \frac{dx}{dt} = u \tag{7}$$

expressing that u remains constant on the characteristic.

For the above initial distribution of u(x,0)=f(x) the general solution is concluded in an implicit form, as follows [4]:

$$u(x,t) = f(x - ut) \tag{8}$$

The characteristics have a slope proportional to $1/f(x_0)$ in the (x,t) plane, where x_0 is a position at initial state, and if $f'(x_0)$ is positive , which is typical for an expansion profile, they will never intersect. On the other hand for a decreasing initial distribution of u, that means $f'(x_0) < 0$, the characteristics will intersect as for a typical compression profile. An initial profile with decreasing intensities will lead to a breakdown of a continuous solution and to the appearance of a shock discontinuity. The shock will appear at the time instance t_s , when the tangent to u(x) profiles becomes vertical:

$$t_s = \frac{-1}{\max|f'(x_0)|} \tag{9}$$

The shock wave velocity , u_s , satisfies the Rankine-Hugoniot relations and is equal to:

$$u_s = \frac{1}{2}(u_2 + u_1) \tag{10}$$

where u_1, u_2 are the values upstream and downstream of the shock.

At this point the following three types of initial conditions are proposed for the analyses of non oscillatory shock capturing methods.

Initial shock discontinuity (case IB-1)

For this case, the Riemann problem for Burgers' equation is solved. The test case is provided by an initial discontinuous distribution :

$$u(x,0) = f(x; u_L, u_R) = \begin{cases} u_L, x < 0 \\ u_R, x \geq 0 \end{cases} \quad \text{with} \quad u_L > u_R \tag{11}$$

At the left boundary the condition

$$u(x_L, t) = u_L \tag{11a}$$

is imposed. The solution of Burgers' equation gives a shock propagating at speed $(u_L + u_R)/2$ with unmodified intensity $[u] = u_L - u_R$, as shown in Figure 3. If $u_R = -u_L$, the shock is stationary and it is used as a non-linear test case for steady-state methods.

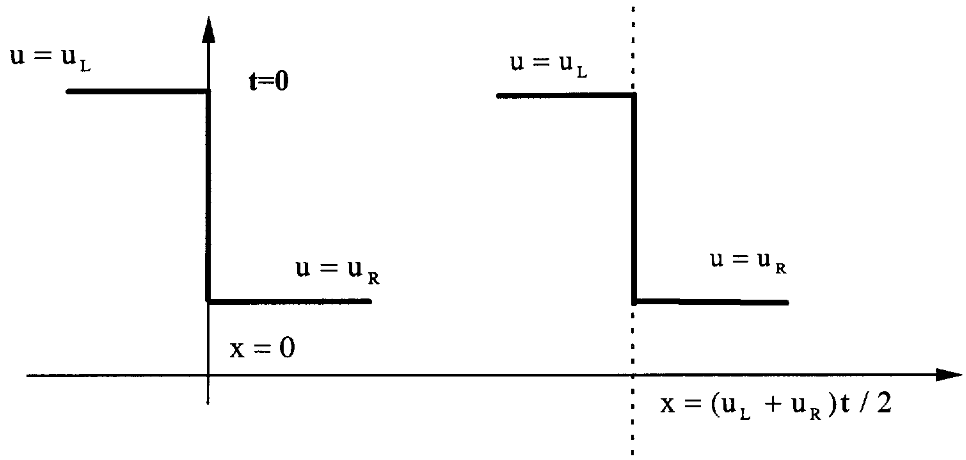

Figure 3 : Burgers' solution for a propagating discontinuity.

Initial linear discontinuity (case IB-2)

A different initial distribution with $f'(x_0) < 0$ leads to the same shock structure. The initial linear distribution is:

$$u(x,0) = f(x; u_L, u_R) = \begin{cases} u_L, & x < 0 \\ u_L\left(1 - \frac{x}{L}\right) + u_R \frac{x}{L}, & 0 \le x \le L \quad \text{with } u_L > u_R \\ u_R, & x > L \end{cases} \tag{12}$$

and at the left boundary the condition

$$u(x_L, t) = u_L \tag{12a}$$

is imposed. A shock is formed at time instance

$$t_s = \frac{L}{u_L - u_R} \tag{13}$$

and at position $x_s = t_s u_L = L + t_s u_R$. The solution of Figure 4 for $t > t_s$ is :

$$u(x,t) = \begin{cases} u_L \text{ for } x < \frac{u_L + u_R}{2} t \\ u_R \text{ for } x > \frac{u_L + u_R}{2} t \end{cases} \tag{14}$$

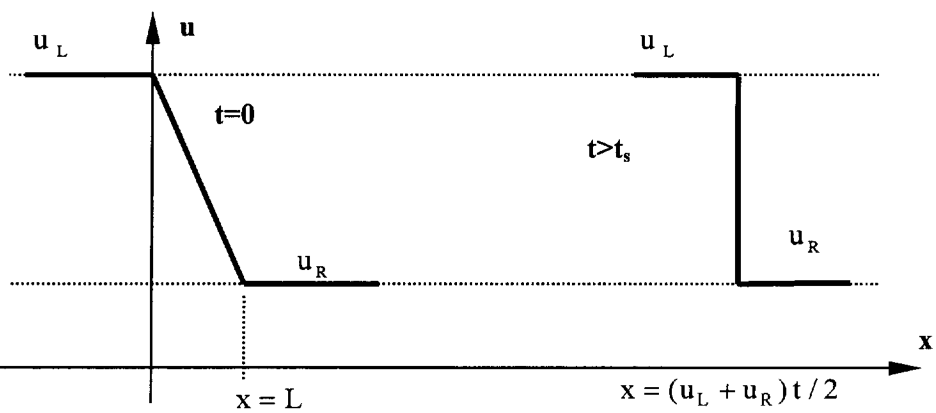

Figure 4 : Shock formation for an initial linear distribution

Burgers' equation for a rarefaction wave (case IB-3)

Burgers' equation with the following initial conditions gives a propagating rarefaction wave.

$$u(x,t=0)=f(x;u_L,u_R)=\begin{cases} u_L & x<0 \\ u_R & x>0 \end{cases} \text{ with } u_L<u_R \tag{15}$$

Between points $u_L t < x < u_R t$ the solution is not determined by the intersection of characteristics. So, a continuous solution is possible in the following form (Figure 5):

$$u(x,t)=\begin{cases} u_L & x/t<u_L \\ x/t & u_L<x/t<u_R \\ u_R & x/t>u_R \end{cases} \tag{16}$$

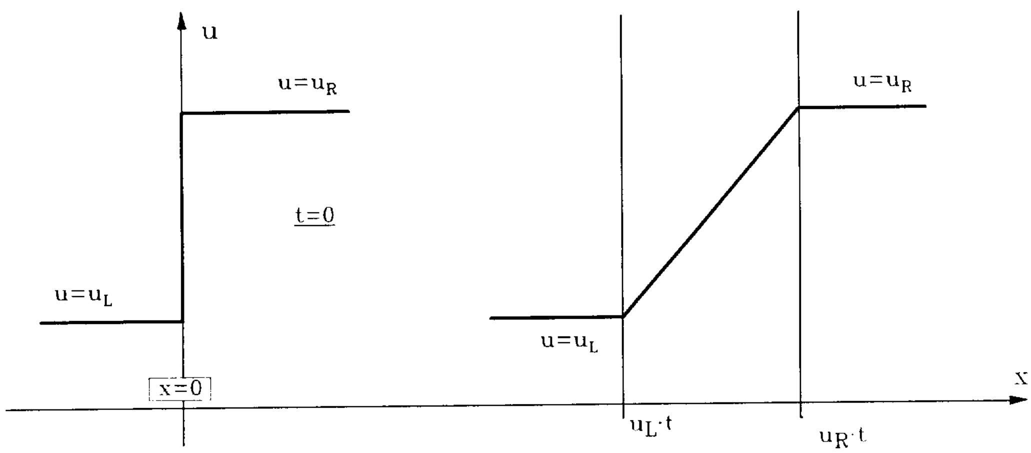

Figure 5 : Initial state and time evolution of a propagating rarefaction wave as a solution of Burgers' equation.

Viscous Burgers' equation (case VB-1)

The complete nonlinear Burgers' equation adding a viscous term is :

$$u_t+uu_x=\nu u_{xx} \text{ or } u_t+\left(\frac{u^2}{2}\right)_x=\nu u_{xx} \tag{17}$$

with Initial Conditions

$$u(x,0)=f(x) \text{ for } -\infty<x<\infty \tag{17a}$$

The "Viscous" Burgers' equation serves as a model equation for the boundary-layer equation, the "parabolized" Navier-Stokes equations and the complete Navier-Stokes equations.
The problem with the following initial values:

$$u(x,0)=f(x;u_L,u_R)=\begin{cases} u_L, x<0 \\ u_R, x\geq 0 \end{cases} \text{ with } u_L>u_R \tag{18}$$

and boundary conditions

$$u(x=-\infty,t)=u_L, u(x=\infty,t)=u_R \tag{18a}$$

has a solution of the form:

$$u = u_R + \frac{u_L - u_R}{1 + h\exp\frac{u_L - u_R}{2\nu}(x - Ut)} \;, \quad U = \frac{u_L + u_R}{2}$$

where:

$$h = \frac{\int_{-(x-u_R t)/\sqrt{4\nu t}}^{\infty} e^{-\zeta^2} d\zeta}{\int_{(x-u_L t)/\sqrt{4\nu t}}^{\infty} e^{-\zeta^2} d\zeta} \tag{19}$$

The diffusing shock still propagates with the "inviscid" velocity equal to U. Due to viscosity effects the inviscid discontinuities are transformed into continuous shaped "steps", as it is shown for the test case of Figure 6.

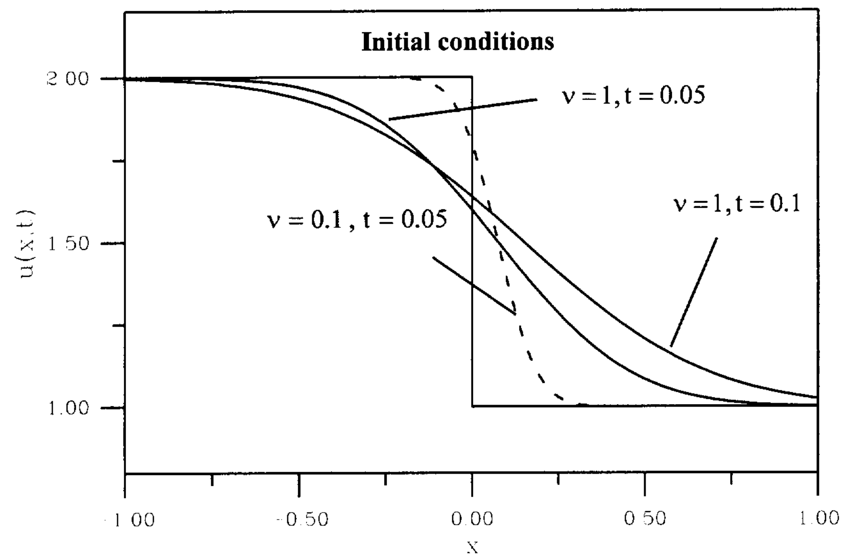

Figure 6 : Shock wave solution of viscous unsteady Burgers' equation ($u_L = 2$, $u_R = 1$).

UNSTEADY EULER EQUATIONS

Reflection of a moving shock on a closed boundary (case RMS-1)

The general discontinuity equations for the moving shock are shown in the literature reference [1] to be:

$$\frac{\hat{\rho}}{\rho} = \frac{u}{\hat{u}} \tag{20}$$

$$\frac{\hat{u}}{u} = 1 - \frac{2}{\gamma + 1}\left(1 - \frac{c^2}{u^2}\right) \tag{21}$$

$$\frac{\hat{p}}{p} = 1 + \frac{2\gamma}{\gamma + 1}\left(\frac{u^2}{c^2} - 1\right) \tag{22}$$

where u, $\hat{u}$ denotes the relative velocities in front and behind the moving shock

$$u = \upsilon - w, \qquad \hat{u} = \hat{\upsilon} - w \tag{23}$$

while $\upsilon, \hat{\upsilon}$ are the absolute velocities and w the velocity of the shock front. The velocity of sound c in front of the moving shock wave is given by:

$$c = \sqrt{\gamma \frac{p}{\rho}} \tag{24}$$

The test problem proposed here is the reflection of a shock wave moving with constant velocity towards the closed boundary of a tube (figure 7). The fluid behind the shock wave moving to the left, has a velocity with the absolute value υ_0 ($\upsilon = -\upsilon_0$, $\upsilon_0 > 0$), pressure and density p_0, ρ_0 ($p = p_0, \rho = \rho_0$) respectively, so that the velocity of sound be $c_0 = \sqrt{\gamma \frac{p_0}{\rho_0}}$. The given data are p_0, ρ_0, υ_0, which are the initial conditions of the problem at starting point. The reflection condition, which has to be satisfied is $\hat{\upsilon} = 0$.

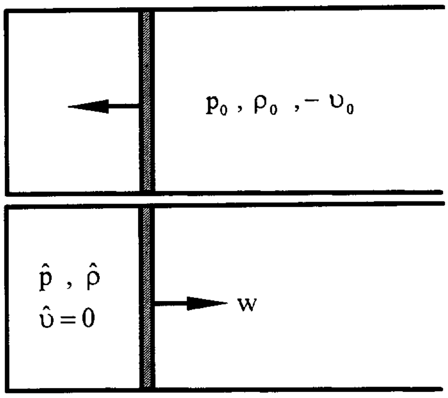

Figure 7 : Reflection of a moving on the left with constant velocity shock wave on the left closed boundary of a tube.

The velocity of the shock front after the reflection, the pressure and the density behind the reflected shock wave, are given by the following relationships [2]:

$$w = \frac{\gamma - 3}{4}\upsilon_0 + \sqrt{\left(\frac{\gamma + 1}{4}\upsilon_0\right)^2 + \gamma \frac{p_0}{\rho_0}} \tag{25}$$

$$\hat{p} = p_0 \left[1 + \frac{2\gamma}{\gamma + 1}\left(\frac{(\upsilon_0 + w)^2}{\gamma p_0}\rho_0 - 1\right)\right] \tag{26}$$

$$\hat{\rho} = \frac{\upsilon_0 + w}{w}\rho_0 \tag{27}$$

Analytical solutions for the unsteady inviscid, non-conducting fluid conservation equations

By neglecting viscous, heat-conduction effects and field forces, the unsteady compressible conservation equations of mass, momentum and energy, in one dimensional conservative form, which will be referred to as Euler equations, have the following form:

Continuity equation:

$$\frac{\partial \rho}{\partial t} + \frac{\partial (\rho u)}{\partial x} = 0 \tag{28}$$

Momentum equation:

$$\frac{\partial (\rho u)}{\partial t} + \frac{\partial (\rho u^2 + p)}{\partial x} = 0 \tag{29}$$

Energy equation:

$$\frac{\partial\left[\rho\left(e+\frac{1}{2}u^2\right)\right]}{\partial t}+\frac{\partial\left[\rho u\left(e+\frac{1}{2}u^2+\frac{p}{\rho}\right)\right]}{\partial x}=0 \tag{30}$$

The above system is closed by the constitutive equation, in the form of ***Gibbs relation***, namely:

$$Tds = de + pd\left(\frac{1}{\rho}\right) \tag{31}$$

Which leads to the entropy relation:

$$\frac{\partial(\rho s)}{\partial t}+\frac{\partial(\rho u s)}{\partial x}=0 \tag{32}$$

In the space - time plane the transformation of independent (x,t) to the new variables (ξ,η) (Figure 8) is introduced:

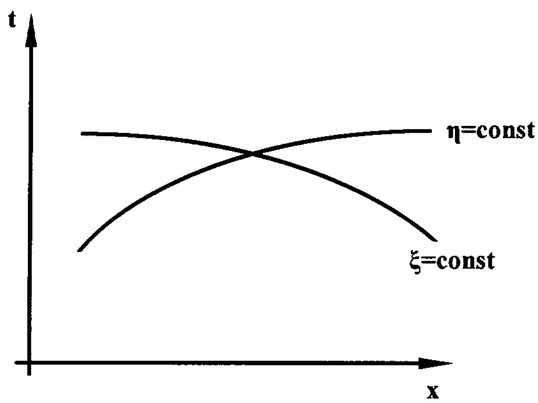

Figure 8: Sketch of the two families of characteristics in the (x,t) plane.

$$\xi=\xi(x,t), \eta=\eta(x,t) \tag{33}$$

so that:

$$\xi=\text{const}: \frac{dx}{dt}=u-c,\ \ \eta=\text{const}: \frac{dx}{dt}=u+c \tag{34}$$

where c is the isentropic velocity of sound:

$$c^2=\left(\frac{\partial p}{\partial \rho}\right)_s \tag{35}$$

Then it can be shown that the system of governing equations in terms of (ξ,η) takes the form:

$$\begin{aligned}\eta=\text{const}&: \frac{dx}{dt}=u+c,\ \ u+\omega=\text{const}\\ \xi=\text{const}&: \frac{dx}{dt}=u-c,\ \ u-\omega=\text{const}\end{aligned} \tag{36}$$

where:

$$\omega=\int\frac{c(\rho)}{\rho}d\rho \tag{37}$$

The $\xi = \text{const.}, \eta = \text{const.}$ are the two families of characteristics which are wave fronts of the kinematic discontinuities. The kinematic discontinuities in the considered one-dimensional case correspond to lines across which the first derivative of the flow quantities are discontinuous , while the flow quantities are continuous.

The last equation for ideal gas of constant coefficients of specific heat of ratio γ reduces to the form:

$$\omega = \frac{2}{\gamma - 1} c , \qquad c^2 = \gamma \frac{p}{\rho} \tag{38}$$

The reduced system of equations can be solved analytically in certain problems such as **moving piston** case (two sub-cases: expansion and compression) and the so called **Riemann** or **shock tube problem** which includes a shock wave, a contact discontinuity and an expansion wave [1], [3].

(a) Expansion flow behind a moving piston (case MP-1)

A piston is considered to move towards the negative x-direction, figure 9. This results to an expansion of the gas behind the piston.

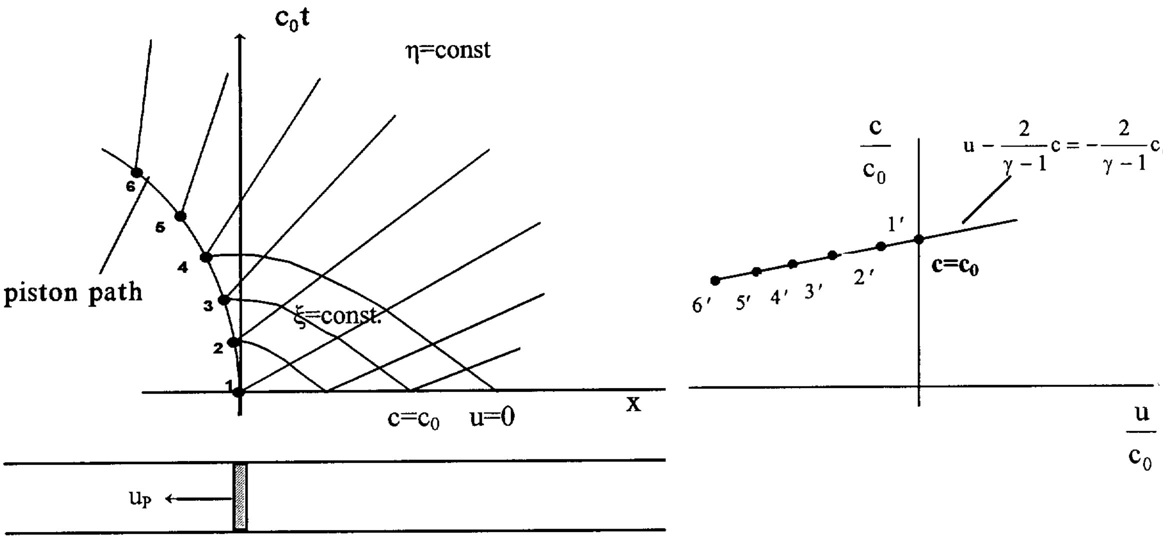

Figure 9: Expansion flow on the right of a left moving piston

The flow is studied in the plane x-t where the path of the piston $u=-u_0$ is shown. As an initial value of the problem a gas with zero velocity and a constant temperature (constant velocity of sound) will be considered.

$$u(x,0) = 0, \; c(x,0) = c_0 \quad x \geq 0 \tag{39}$$

As a boundary condition the equality of the gas velocity to the velocity of the piston is taken into account:

$$u(x_p, t) = u_p(t) = \dot{x}_p \tag{40}$$

Starting from the initial values $c = c_0, u = 0$ (for $t = 0$) we could easily observe that in the open region between the positive x-axis and the positively inclined characteristic ($\eta = \text{const.}$) originating from point 1 both families of characteristics are straight lines since they originate from the positive part of the x-axis where the constant initial conditions are valid.
The movement of the piston affects the flow field left of the characteristic originating from point 1. Since all the $\xi = \text{const}$ characteristics originate from the positive x-axis where the initial conditions are valid, across all the negatively inclined characteristics the following relation is valid:

$$\xi = \text{const}, \; u - \frac{2}{\gamma - 1} c = -\frac{2}{\gamma - 1} c_0 \tag{41}$$

All the $\xi = \text{const}$ characteristics end on the piston path, so that

$$\xi = \text{const} \quad u_p - \frac{2}{\gamma - 1} c_p = -\frac{2}{\gamma - 1} c_0 \tag{42}$$

while for the $\eta = \text{const}$ characteristics the following relation is valid:

$$\eta = \text{const} \quad u + \frac{2}{\gamma - 1} c = u_p + \frac{2}{\gamma - 1} c_p \tag{43}$$

By substracting the previous two equations for the region between the piston path and the positively inclined characteristic originating from point 1, the following relation along the positively inclined characteristics is valid :

$$\eta = \text{const} \quad u + \frac{2}{\gamma - 1} c = 2u_p + \frac{2}{\gamma - 1} c_0 \tag{44}$$

From the relations (42) and (43) we conclude that:

$$\eta = \text{const}, \quad u = u_p, c = c_p \tag{45}$$

Thus the values of u and c on each $\eta = \text{const}$ keep constant and this family of characteristics are straight lines with the following inclination :

$$\eta = \text{const}, \quad \frac{dx}{dt} = u_p + c_p = c_0 + \frac{\gamma + 1}{2} u_p \tag{46}$$

Note: From equation results a limit maximum piston velocity.

$$(u_p)_{max} = -\frac{2}{\gamma - 1} c_0 \quad c_p = 0 \tag{47}$$

With a piston velocity increasing further, a cavitation zone is developed behind the moving piston (where pressure vanishes). The cavitation area is located in the region between the piston path and the positively inclined characteristic with inclination w :

$$w = \frac{dx}{dt} = c_0 + \frac{\gamma + 1}{2} (u_p)_{max} = -\frac{2}{\gamma - 1} c_0 \tag{48}$$

This limit velocity $w \approx -5c_0$ is quite higher than the maximum isentropic steady flow velocity in vacuum ($u_{max} = \sqrt{5} c_0$). This shows the basic differences between the steady and unsteady flows. Of course, we should note that these regions are on the limit of continuums mechanics validity.

The whole phenomenon can be considered as simple wave. This is the case of the wave when one family of the characteristics are straight lines.

Special case I:
In the special case of a piston moving with constant velocity, so that the piston path is a straight line. The expansion region is limited to an angle around the axis origin, so that all the gas particles hold the constant velocity of the piston. The wave is called central simple expansion wave.

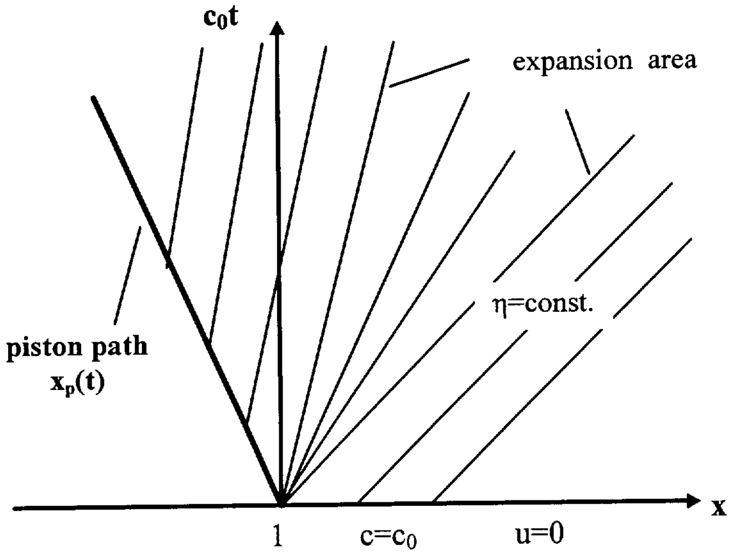

Figure 10 : Central expansion wave behind a piston moving with constant velocity

Special case II:

For the special case of the constant accelerating piston, for which the velocity argument is linearly increasing with time (U and t_o are constants):

$$u_p = -U\frac{t}{t_0} \tag{49}$$

leads to a fully analytical expression of the flow velocity and the isentropic velocity of sound in the expansion area, which are given by the relations:

$$u(x,t) = -\frac{1}{\gamma}\left(c_0 + \frac{\gamma+1}{2}U\frac{t}{t_0}\right) + \left(\frac{1}{\gamma^2}\left(c_0 + \frac{\gamma+1}{2}U\frac{t}{t_0}\right)^2 + \frac{2}{\gamma}\frac{U}{t_0}(x - c_0 t)\right)^{\frac{1}{2}} \tag{50}$$

$$c(x,t) = c_0 + \frac{\gamma-1}{2}u \tag{51}$$

The distribution of velocity as a function of the space variable x is shown in figure 11 for various time levels.

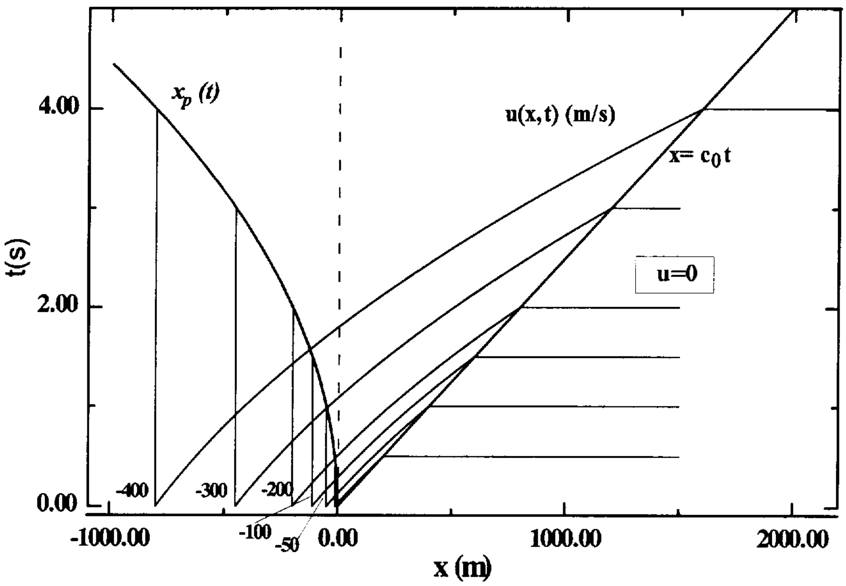

Figure 11: Velocity distribution as function of x for various times for the case of gas expansion due to the movement of a piston with a constant acceleration ($U = 100\,m/s, t_0 = 1s, c_0 = 400\,m/s, \gamma = 1.4$).

(b) Compression flow in front of a piston moving in a non-moving gas (MP-2)

The theory of isentropic flow for the compression flow in front of a piston obeys the same analysis as the expansion one (eqs (38)-(47)). One should remark in this case that the $\eta = \text{const}$ characteristics converge and form an envelope (Figure 12). The envelope can be in general shown that appears at earliest time at the point (x_c, t_c), that is defined as:

$$x_c = \frac{2c_0^2}{(\gamma+1)\ddot{u}_p(0)}, \quad t_c = \frac{2c_0}{(\gamma+1)\ddot{u}_p(0)} \tag{52}$$

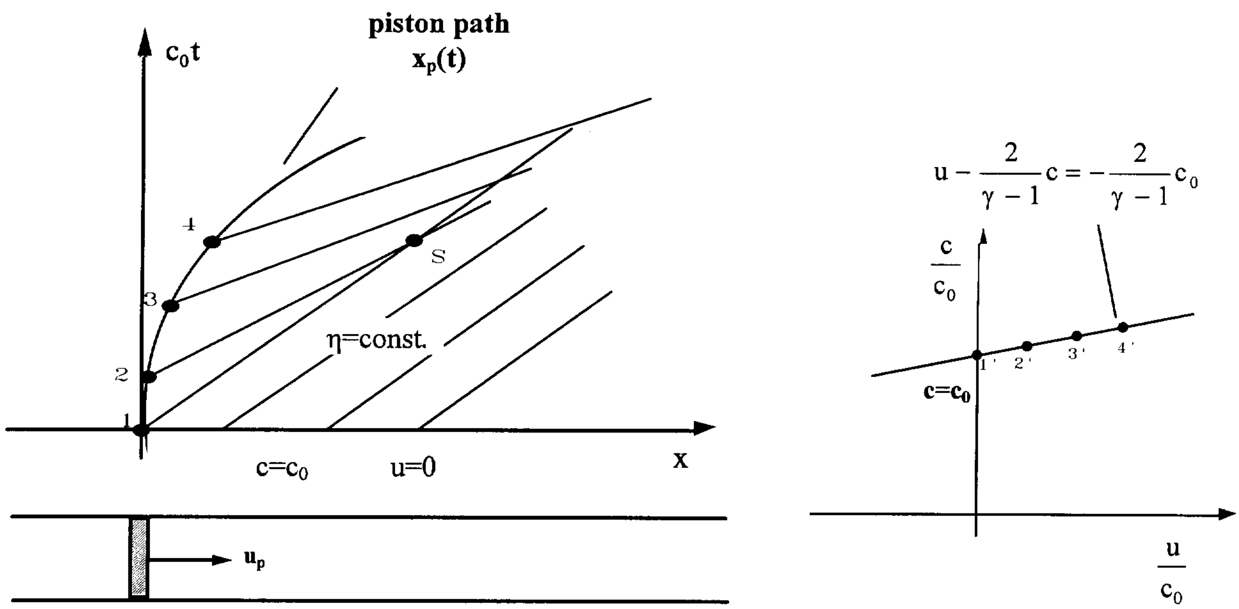

Figure 12 : Compression flow in front of a piston moving in a non-moving gas

After this point and for ($t > t_c$) a moving shock wave appears, which propagates in the gas at rest in the same direction with the piston and the flow is anisentropic. An analytic description of the flow field succeeds for the following two cases:

Special case III

In the case that the piston moves with constant velocity in a gas at rest:

$$u_p = U, \qquad U = \text{const} \tag{53}$$

so that the piston path is a straight line, figure 13, the $\eta = \text{const}$ characteristics are parallel to each other and a shock forms, which propagates with constant velocity u_s higher than that of the piston:

$$u_s = \frac{dx_s}{dt} = \frac{\gamma+1}{4}U + \sqrt{\left(\frac{\gamma+1}{4}U\right)^2 + c_0^2} \tag{54}$$

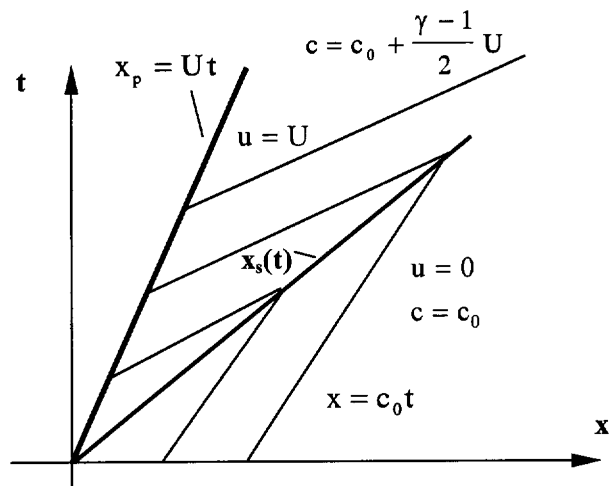

Figure 13 : Compression flow of a gas in front of a moving piston with a constant velocity

Special case IV

For the case of the compression flow of a gas in front of a moving piston with a velocity linearly increasing with time (constant accelerating piston):

$$u_p = U\frac{t}{t_0} \tag{55}$$

(U, t_0 constants), we lead as in the case II to a fully analytic expression for the flow field velocity in the isentropic region, that is before the appearance of the shock wave. The expression of the velocity in the isentropic compression region, can be shown to be similar to the expression of the expansion flow:

$$u(x,t) = -\frac{1}{\gamma}\left(c_0 - \frac{\gamma+1}{2}U\frac{t}{t_0}\right) + \sqrt{\frac{1}{\gamma^2}\left(c_0 - \frac{\gamma+1}{2}U\frac{t}{t_0}\right)^2 - \frac{2}{\gamma}\frac{U}{t_0}(x - c_0 t)} \tag{56}$$

$$c(x,t) = c_0 + \frac{\gamma-1}{2}u \tag{57}$$

and the point (x_c, t_c) is calculated as:

$$x_c = \frac{2c_0^2 t_0}{(\gamma+1)U}, \qquad t_c = \frac{2c_0 t_0}{(\gamma+1)U} \tag{58}$$

The distribution of velocity as function of the space variable x for various times t is shown in figure 14.

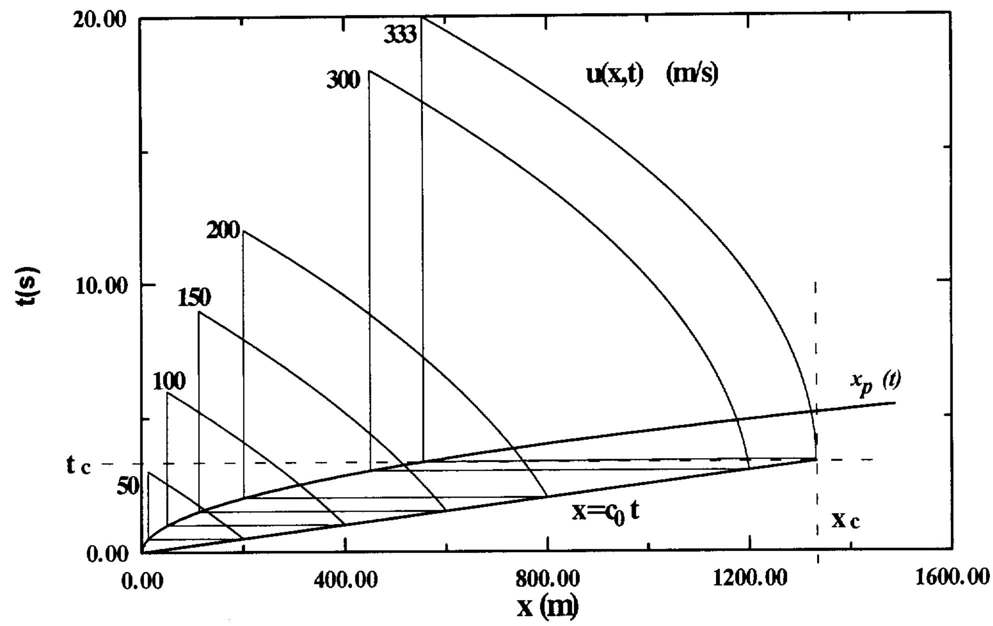

Figure 14 : Distribution of the velocity as a function of x for various t in the isentropic compression area of a gas in front of a constant accelerating piston ($U = 100\,m/s, t_0 = 1\,s, c_0 = 400\,m/s, \gamma = 1.4$).

(c) Moving shock in a shock tube or Riemann-problem (case ST-1)

The shock tube problem, often called Riemann problem, is the flow owing to the abrupt removal of the valve which separates a high pressure gas from a low pressure gas in the shock tube [1], [6]. The resulting wave effect of the propagation of the discontinuity and the relating nomenclature are shown in figure 15. The diaphragm located in position $x = 0$ at time $t = 0$ separates the space of high pressure $p_H \equiv p_4$ from the space of lowpressure $p_L \equiv p_1$. Thus, the basic parameter of the flow effect is the pressure ratio:

$$\frac{p_H}{p_L} = \frac{p_4}{p_1} \tag{59}$$

The two parts of the tube may have also different temperatures (T_4, T_1) and different gases (R_4, R_1).

At initial time the pressure distribution is a step distribution, figure 15a. This causes the separation of the problem in two problems, the propagation of a shock wave in the low pressure gas p_L and the propagation of an expansion wave in the high pressure gas p_H . The state behind the moving shock wave is indicated by the index 2 and the state behind the expansion wave with the index 3. The interface between the states 2 and 3 is a contact discontinuity. This is the contact point of the two gases, initially separated by the diaphragm, and have different temperatures and densities. On the other hand they should have the same velocities and pressures. The basic problem is how the flow quantities can be calculated with a given initial pressure ratio.

Introducing the following expressions:

$$P = \frac{p_2}{p_L}, \qquad \alpha = \frac{\gamma+1}{\gamma-1} \tag{60}$$

we have firstly the relations connecting the quantities on both sides of the moving shock wave:

Moving shock wave relations:

$$\frac{\rho_2}{\rho_L} = \frac{1+\alpha P}{\alpha + P} \text{ (Hugoniot relation)} \tag{61}$$

$$\frac{\upsilon_2 - \upsilon_L}{c_L} = \left(\frac{2}{\gamma(\gamma-1)}\right)^{\frac{1}{2}} \frac{P-1}{(1+\alpha P)^{\frac{1}{2}}} \tag{62}$$

$$\frac{c_2}{c_L} = \left(P \frac{\alpha + P}{1 + \alpha P} \right)^{\frac{1}{2}} \tag{63}$$

$$\frac{w - c_L}{c_L} = \left(\frac{\gamma - 1}{2\gamma} \right)^{\frac{1}{2}} (1 + \alpha P)^{\frac{1}{2}} \tag{64}$$

The pressure and velocity on both sides of the contact discontinuity are equal.

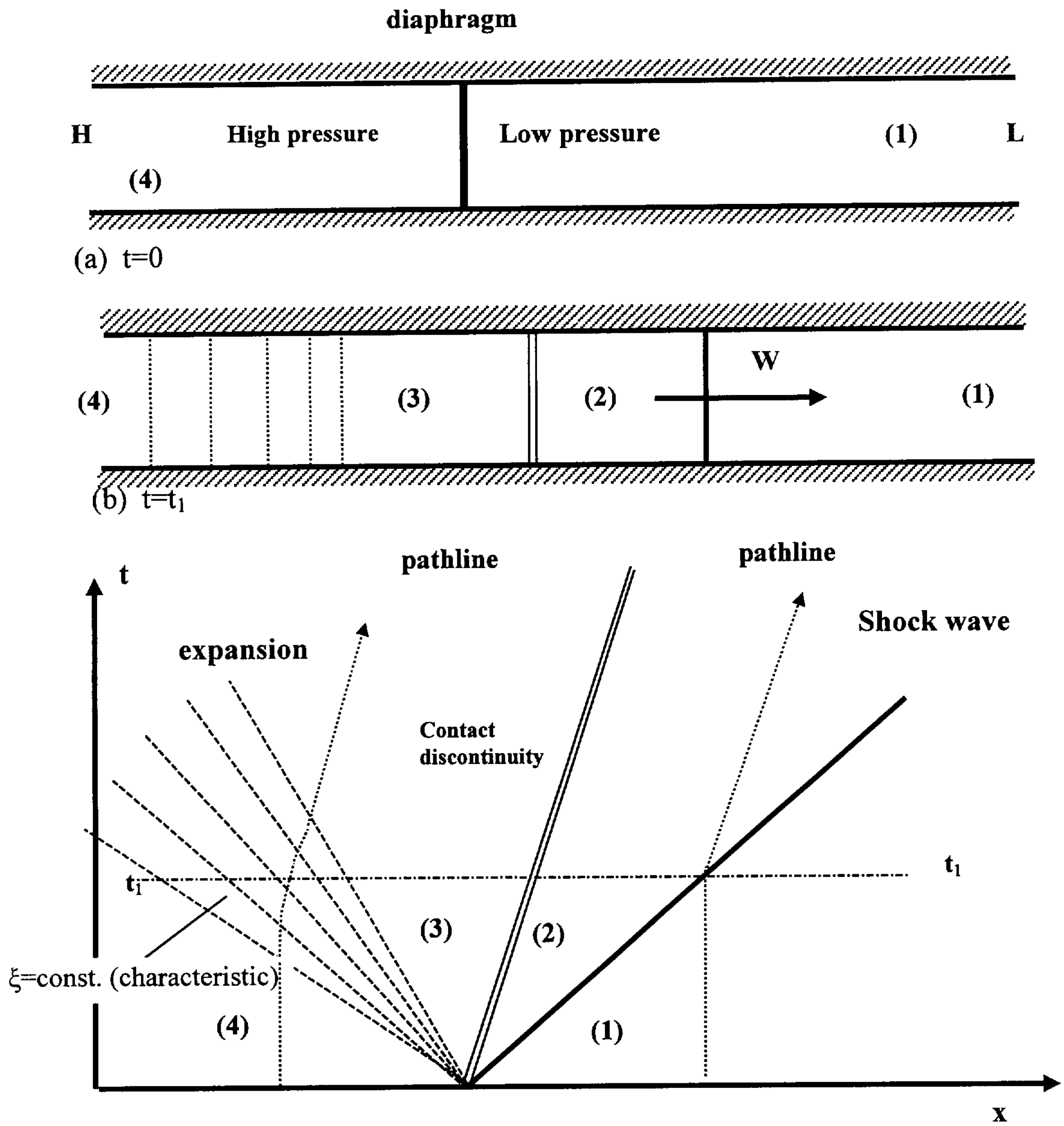

Figure 15 : Flow effects in a shock tube

Equations of the contact discontinuity:

$$\begin{aligned} p_3 &= p_2 \\ \upsilon_3 &= \upsilon_2 = v \end{aligned} \tag{65}$$

v is the velocity of the contact discontinuity.

Pressure and velocity in the regions 3 and $H \equiv 4$ are related with Riemann conditions on positive inclined characteristics $(\eta = \text{const})$.

Riemann equations across positive inclined characteristics:

$$\upsilon_3 - \upsilon_H = c_H \frac{2}{\gamma - 1}\left[1 - \left(\frac{p_3}{p_H}\right)^{\frac{\gamma-1}{2\gamma}}\right] \tag{66}$$

After eliminating unknowns from equations (61) , (64), (65) the following equation, which has as unknown the pressure relation P, is obtained:

$$\left(\frac{2}{\gamma(\gamma-1)}\right)^{\frac{1}{2}} \frac{P-1}{(1+\alpha P)^{\frac{1}{2}}} = \frac{c_H}{c_L}\frac{2}{\gamma-1}\left[1 - \left(\frac{p_L}{p_H}P\right)^{\frac{\gamma-1}{2\gamma}}\right] + \frac{\upsilon_H - \upsilon_L}{c_L} \tag{67}$$

The solution of the implicit algebraic equation (66) is accomplished by numerical integration.

Example:

For the following values of the variables:

$p_H = 10^5, \rho_H = 1, \quad \upsilon_H = 0, \quad p_L = 10^4, \quad \rho_L = 0.125, \quad \upsilon_L = 0, \gamma = 1.4$

the solution of equation (66) gives the following values of the unknown parameters:

$P = 3.0313, \quad p_2 = 30313, \quad \upsilon_2 = v = 203, \quad w = 544$

In figure 16 the variation of flow quantities are shown for the time instant $t = 6{,}110^{-3}$.

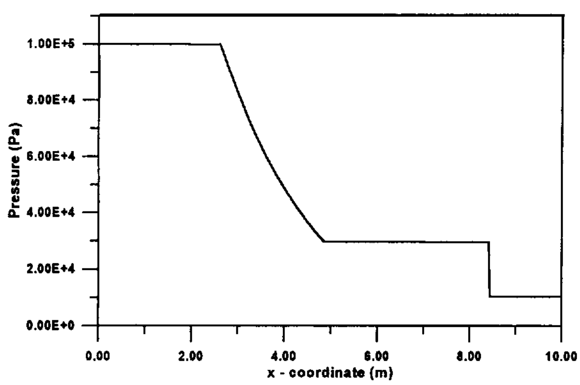

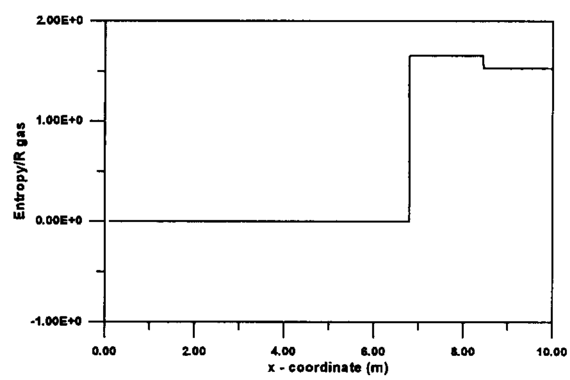

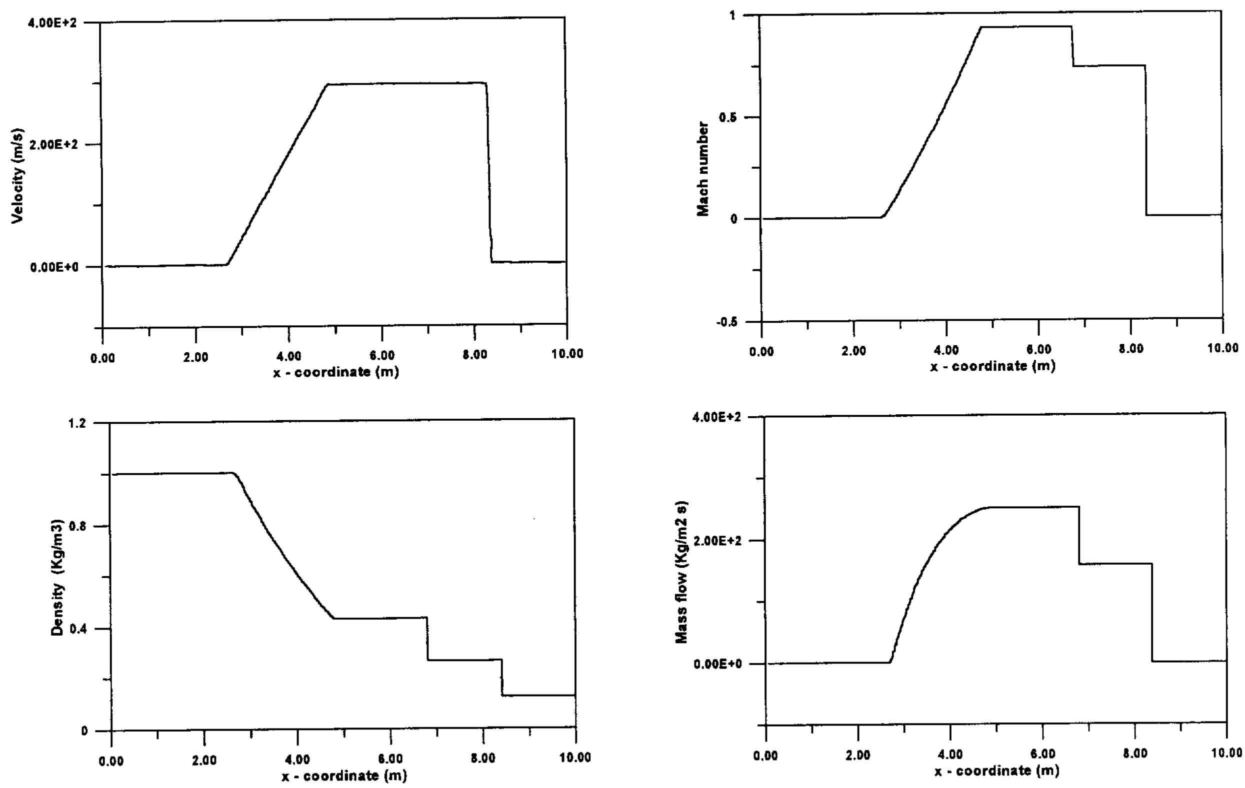

Figure 16 : Distribution of flow quantities at t=6,1 ms for $p_H = 10^5, \rho_H = 1, \quad \upsilon_H = 0, \quad p_L = 10^4, \rho_L = 0.125, \quad \upsilon_L = 0, \gamma = 1.4$

ANALYTICAL SOLUTIONS FOR THE UNSTEADY COMPRESSIBLE LAMINAR FLOW FOR HEAT CONDUCTING FLUID

The existing analytical solutions for the unsteady, compressible laminar flow for a heat conducting fluid concern only the Lighthill's approximation of finite amplitude sound waves, for the case of one-dimension. For the derivation of this theory we refer to the review of M.J.Lighthill [5]. This theory leads to the following equation for the velocity u derived from the equations of continuity, momentum and energy after simplifications coming from the assumption of sound waves of finite amplitude for a perfect gas of constant γ :

$$\frac{\partial u}{\partial t} + \left(c_0 + \frac{\gamma + 1}{2} u \right) \frac{\partial u}{\partial x} = \frac{\delta}{2} \frac{\partial^2 u}{\partial x^2} \tag{68}$$

δ is the Lighthill's diffusion coefficient for the sound waves of finite amplitudes propagating to the positive - x direction:

$$\delta = \frac{\overline{\mu}_0}{\rho_0} + \frac{(\gamma - 1)\lambda_0}{\rho_0 c_p} \tag{69}$$

$\overline{\mu}_0 = 2\mu + \mu'$, where μ μ' are the dynamic and volumetric viscosities of the gas , λ_0 is the coefficient of heat conductivity, c_p is the heat coefficient for constant pressure and ρ_0 is the undisturbed density.

$$u_0 = 0, \quad c = c_0 \tag{70}$$

Through the transformation:

$$X = x - c_0 t, \quad \overline{u} = c_0 + \frac{\gamma + 1}{4} u \tag{71}$$

the differential equation can be transformed to the following non-linear **Burgers'** equation (1940), which is the simplest non linear equation describing convective effects combined with diffusive one :

$$\frac{\partial \bar{u}}{\partial t} + \bar{u}\frac{\partial \bar{u}}{\partial X} = \frac{\delta}{2}\frac{\partial^2 \bar{u}}{\partial X^2} \tag{72}$$

The general solution of the Burgers' equation is defined by the introduction of a new dependent variable, the function ϕ defined by the following relations, satisfying the Burgers' equation:

$$\frac{\partial \phi}{\partial X} = -\bar{u}, \quad \frac{\partial \phi}{\partial t} = \frac{1}{2}\bar{u}^2 - \frac{\delta}{2}\frac{\partial \bar{u}}{\partial X} \tag{73}$$

The differential equation for ϕ leads by elimination of $\bar{u}$ from the previous equations:

$$\frac{\partial \phi}{\partial t} = \frac{1}{2}\left(\frac{\partial \phi}{\partial X}\right)^2 + \frac{\delta}{2}\frac{\partial^2 \phi}{\partial X^2} \tag{74}$$

By introducing again a new function ψ :

$$\phi = \delta \ln \psi \tag{75}$$

the equation which satisfies ψ is the standard linear equation for heat transfer by conduction:

$$\frac{\partial \psi}{\partial t} = \frac{1}{2}\delta\frac{\partial^2 \psi}{\partial X^2} \tag{76}$$

So, all the known solutions of the linear heat conduction equation are at the same time solution of the Burgers' equation, of course in the transformed variables.

The relations connecting ψ and $\bar{u}$ are:

$$\bar{u} = -\frac{\delta}{\psi}\frac{\partial \psi}{\partial X}, \qquad \psi = \exp\left(\frac{1}{\delta}\int_X^{\infty}\bar{u}\,dX\right) \tag{77}$$

As a first example we refer to the initial value problem owing to Laplace. When the initial value of the wave form is given by $\bar{u}(X,0)$, then the solution is defined by the integral:

$$\psi(X,t) = \frac{1}{\sqrt{2\pi\delta t}}\int_{-\infty}^{\infty}\psi(Y,0)\exp\left[-\frac{(X-Y)^2}{2\delta t}\right]dY \tag{78}$$

$$\bar{u}(X,t) = \frac{\int_{-\infty}^{\infty}\frac{X-Y}{t}\exp\frac{1}{\delta}\left\{\int_Y^{\infty}\bar{u}(Y,0)dY - \frac{(X-Y)^2}{2t}\right\}dY}{\int_{-\infty}^{\infty}\exp\frac{1}{\delta}\left\{\int_Y^{\infty}\bar{u}(Y,0)dY - \frac{(X-Y)^2}{2t}\right\}dY} \tag{79}$$

INDICATIONS FOR USE OF THE EXAMINED TEST CASES

The above test cases are frequently used for testing various properties of the examined numerical schemes. Specifically:

- The test case of linear advection equation (LADV-1) that results in oscillatory solution and contains discontinuity in the derivative, can be used to test the diffusion and dispersion properties of schemes and to define the accuracy of the scheme on smooth functions of the wave number k.
- The linear advection equation of propagating discontinuity with the velocity α (LADV-2) is important with regard to properties of the schemes at handling propagating discontinuities. If the discontinuity is an expansion shock, the numerical scheme can propagate and dump the expansion through an introduced entropy condition or any other form of dissipative mechanism.

- The behaviour of invisvid Burgers' equation against non linearities is representative of the examination of Euler equations behaviour due to the non linear term of Burgers' equation. Inviscid Burgers' equation (IB-1) with initial shock discontinuity gives information about the capability of the numerical scheme on shock capturing with the correct shock propagating speed (time accurate scheme). The shock capturing without the presentation of non physical oscillations in the vicinity of the discontinuity ensures the monotonicity of the numerical scheme or its property for total variations diminishing. . Inviscid Burgers' equation (IB-2) with initial linear discontinuity gives information about the diffusion and dispersion properties of the numerical scheme. IB-2, also ensures, as IB-1 for the shock capturing capability of the scheme and its characteristics about monotonicity. Inviscid Burgers' equation (IB-3) for a rarefaction wave is used to test the additional entropy condition that is imposed on the numerical schemes in order to capture expansion shocks for inviscid flow equation. Viscous Burgers' equation (VB-3) serves as a model equation for the boundary-layer equation or the "parabolized" Navier-Stokes equations and examines the capturing of diffusing shock.
- The problem of shock tube presents an exact solution to the full system of one-dimensional Euler equations containing simultaneously a shock wave, a contact discontinuity and an expansion fan. Consequently, it can be used for the testing of all the above properties of numerical schemes.

SOFTWARE

The analytical solutions for the above cases are also presented in the corresponding FORTRAN 90 programs that have been attached to the present paper. These programs are:

FORTRAN program	Input Data file	Test case
advection.for	*advect.int*	Linear advection equation
inv_Burgers.for	*inv_burg.int*	Inviscid Burgers' equation
vis_Burgers.for	*vis_burg.int*	Viscous Burgers' equation
expansion.for	*expansion.int*	Expansion flow behind a moving piston
compresion.for	*compression.int*	Compression flow in front of a moving piston in a non-moving gas
shock_tube.for	*shock.int*	Moving shock in a shock tube or Riemann problem

REFERENCES

1. H. Shapiro "The Dynamics and Thermodynamics of Compressible Fluid Flow" The Ronald Press Company, New York, vol II (1953).
2. Glaister P. "An Approximate linearised Riemann Solver for the Euler Equations of Real Gases" JCP, 74, 382-408 (1988).
3. R. Courant, K.O.Friedrichs "Supersonic flow and Shock Waves", Springer Verlag, New York (1976).
4. G.B. Whitham "Linear and Nonlinear waves", John Wiley & Sons (1974).
5. M.J.Lighthill "Viscosity effects in waves of finite amplitudes" In Surveys in Mechanics (ed. G.K. Batchelor & R.M. Davies) pp. 250-351, Cambridge Univ. Press (1956).
6. Hirsch C., 'Numerical computation of internal and external flows', Volume I, II, John Wiley & Sons (1988, 1990).
7. E.R. Benton and G.W.Platzman "A Table of solutions of the one-dimensional Burgers' equation", Quarterly of Applied Mathematics, pp.195-212 (1972).
8. B. Gustafsson and P.Olsson "Fourth-Order Difference Methods for Hyperbolic IBVPs", J. Comput. Phys., **117**, 300-317 (1995).

3E. DATA FROM AGARD REPORT 702

INTRODUCTION

In the late seventies a need was perceived for standard comparison cases and experimental data to aid the comparison and validation of the theoretical methods then emerging for unsteady aerodynamics. A Working Group of the AGARD Structures and Materials panel chose a set of 2-D and 3-D configurations and for each configuration defined a set of test cases, including a prioity subset, to be used for comparisons. These test cases were fully identified in ref.1 and 2. The chosen configurations were known as the AGARD Aeroelastic Configurations and the chosen cases were denoted as Computational Test (CT) cases. Some of the CT cases were entirely theoretical while others were also the subject of unsteady measurements.

The next step undertaken to aid the methods development was to produce an experimental data compendium (AGARD Report 702, ref.3) which was conceived with the idea of bringing together the experimental data most important for the comparisons. The report was followed by an Addendum, ref.4, which introduced two additional 3-D experiments. These reports established an admirable common base for providing experimntal data and their value has been demonstrated by the repeated use of the test cases for the entire period since publication. The report has served as a model for the present new compendium of experimental data.

It was decided that some of the data cases in the original Report 702 should be reproduced in this document in order to provide more complete coverage in this report with the additional bonus of making available the original data in electronic form to facilitate its continued use to validate calculations.

The data sets contained in ref.3 and 4 were:

Set 1	NLR	NACA 64A006 Oscillating Flap
Set 2	NASA Ames	NACA 64A010 Oscillatory Pitching
Set 3	ARA	NACA 0012 Oscillatory and Transient Pitching
Set 4	NLR	NLR 7301 Supercritical Airfoil Oscillatory Pitching and Oscillatory Flap
Set 5	NLR	NLR 7301 Supercritical airfoil Oscillatory Pitching
Set 6	RAE	RAE Wing A, Oscillating Flap
Set 7	RAE/NLR/ONERA	NORA model, Oscillation about a Swept Axis
Set 8	MBB/ONERA	ZKP wing, Oscillating Aileron
Set 9	NLR	LANN wing, Pitching Oscillation

The characterisitics of the nine experiments are summarised in the following two tables giving a guide to the characteristics of the motion in each experiment and the types of data measured.

Set	1	2	3	4	5	6	7	8	9
wing or section	NACA 64A006 symmetric 6%	NACA 64A010 symmetric 10%	NACA 0012 symmetric 12%	NLR 7301 supercritical 16.5%	NLR 7301 supercritical 16.5%	Wing Aspect ratio 6 LE sweep 36°	NORA aspect ratio 2 LE sweep 50°	ZKP, aspect ratio 9, LE sweep 30°	LANN, aspect ratio 8, LE sweep 28°
form of motion	flap 25%c	pitch about 25%c	pitch about 25%c	pitch about 40%c and flap 25%c	pitch about 40%c	mid-span flap, 30%c	"pitch" about swept axis	outboard flap, 22.6%c	pitch
Maximum amplitude	1°	2°	9.5° oscill ramp to 30°	1.5° pitch, 2° flap	2°	2°	1°	2°	1°
Mach range	0.5 - 1	0.5 - 0.85	0.3 - 0.87	0.5 - 0.8	0.4 - 0.85	0.4 - 0.95	0.6 - 1.1	0.5 - 0.83	0.6 - 0.95
mean chord (m)	0.18	0.5	0.1	0.18	0.5	0.16	0.44	0.95	0.268
Frequency range Hz	0 - 120	0 - 60	0 - 60	0 - 80 pitch 0 - 200 flap	0 - 60	0 - 90	0 - 60	6 - 21	0 - 72
Maximum reduced frequency	0.4	0.3	0.25	0.26 pitch 0.65 flap	0.3	0.26	0.31	0.3	0.15

Set	1	2	3	4	5	6	7	8	9
Steady pressures for mean conditions	Y	Y	N	Y	Y	Y	Y	Y	Y
Steady pressures for small changes from the mean conditions	Y	N	N	Y	N	N	N	Y	Y
Quasi-steady pressures	N	N	Y	N	N	Y	Y	Y	N
Unsteady pressures	Y	Y	Y	Y	Y	Y	Y	Y	Y
Steady section forces for the mean conditions by integration of pressures	Y	Y	N	Y	Y	N	Y	Y	Y
Steady section forces for small changes from the mean conditions by integration	Y	N	N	Y	N	N	N	N	Y
Quasi-steady section forces by integration	N	N	Y	Y	N	N	Y	Y	N
Unsteady section forces by integration	Y	Y	Y	Y	N	N	Y	Y	Y
Measurement of actual motion at points of the model	Y	Y	N	Y	Y	N	Y	Y	Y
Observation or measurement of boundary layer properties	N	Y	N	N	Y	Y	N	N	N
Visualisation of surface flow	N	Y	N	N	Y	Y	N	N	N
Visualisation of shock wave movements	Y	N	N	Y	N	N	N	N	N

The selection of sets for reproduction in this chapter was based on considerations of the form of data and the feasibility of transferring the data to electronic media, and also on the type of experiment, particularly the uniqueness of the data beside the new data presented in this report. The sets selected are:

Set 1	NLR	NACA 64A006 Oscillating Flap
Set 3	ARA	NACA 0012 Oscillatory and Transient Pitching
Set 4	NLR	NLR 7301 Supercritical Airfoil Oscillatory Pitching and Oscillatory Flap
Set 8	MBB/ONERA	ZKP wing, Oscillating Aileron

PRESENTATION OF DATA

The data for Sets 1, 4 and 8 are supplied on ASCII files in a common format. For each Set the main test data is on a single file with the format defined below. A FORTRAN program (RUNAD.FOR) is provided which demonstrates the extraction of the data and. The program includes a sample main segment which displays the data of a specific run or creates a file containing formatted tables of all the data in the Set, via a call to subroutine SELUNAD. This subroutine may be employed in a user's code to extract the data for a single table or to serve as a model for other data extraction codes.

SELUNAD subroutine

A description of the subroutine call and arguments follows:

```
C
      SUBROUTINE SELUNAD(NCH,FILNAM,KRUN,MAXP,MAXSEC,MAXCPV,VMACH,FREQ
     1,AERFM,AERFA,FLAPM,FLAPA,NSEC,LSEC,RTEXT,ICPST,ICPUS,IMACH,ICLM
     2,CL,CM,CP,VMST,XT,YT,NMT)
C
C-- This routine reads and selects data from a UNAD standardised unsteady aero
C   data file and returns the available data
C-- Arguments are as defined below:
C   Input values
C         NCH      FORTRAN channel number to be used for reading the input file
C         FILNAM   The name of the required input file
C         KRUN     Specifies the required run number
C         MAXP     The declared dimension in the calling routine for number of
C                  transducer locations in one section for one subclass of data
C                  unsteady
C         MAXSEC   The declared dimension in the calling routine for the number
C                  of sections in this data
```

```
C         MAXCPV   The declared dimension in the calling routine for the number
C                  of CP values,  a minimum of 3 is required for oscillatory
C                  data, number of time values for time history
C   Returned values
C         VMACH    Mach number for this run
C         FREQ     Oscillatory frequency for this run (Hz)
C         AERFM    Mean wing/aerofoil incidence for this run (deg)
C         AERFA    Wing/aerofoil incidence oscillation amplitude for run (deg)
C         FLAPM    Mean flap angle for this run (deg)
C         FLAPA    Flap angle oscillation amplitude for this run (deg)
C         NSEC     The number of sections in this data
C         LSEC(is) Integer array giving identifier number of each section
C         RTEXT    Character string giving optional description of this run
C The following four quantities are integers which return with the value of
C zero if the corresponding data is not given:
C         ICPST    Set positive if steady CP values given for this run
C         ICPUS    Set positive if oscillatory unsteady CP values given
C         IMACH    Set positive if local Mach number values are given
C         ICLM     Set positive if local CL,CM values given for sections
C
C The following array quantities are defined using specific variables :
C   i    for transducer location (1 to NMT)
C   j    as surface indicator (=1 upper surface, =2 lower surface)
C   is   section number (1 to NSEC)
C   it   quantity type (=1 steady, =2 unsteady)
C   k    variable quantity =1 for steady values, =2 for oscillatory real,
C                          =3 oscillatory imag
C
C         CL(i,k)          Lift coefficients for each section
C         CM(i,k)          Pitching moment coefficient for each section
C         CP(i,k,j,is)     Pressure coefficients
C         VMST(i,j,is)     Local Mach numbers
C         XT(i,it,j,is)    Chordwise locations of transducers, non-dimensionalised
C                          by dividing by local chord
C         YT(i,it,j,is)    Spanwise locations of transducers, non-dimensionalised
C                          by dividing by semi-span
C         NMT(it,j,is)     Numbers of locations of transducers in specific sections
C
      REAL CL(3,MAXSEC),CM(3,MAXSEC), CP(MAXP,MAXCPV,2,MAXSEC)
     1,VMST(MAXP,2,MAXSEC), XT(MAXP,2,2,MAXSEC), YT(MAXP,2,2,MAXSEC)
      INTEGER NMT(2,2,MAXSEC), LSEC(MAXSEC)
      CHARACTER *80 FILNAM, TITLE, RTEXT
C
```

UNAD data format

The UNAD data files are ASCII with free formatting within the structure of heading information followed by data with type determined by a control number. Each test is refered to by a run number, which in the pplication to the AGARD R702 data sets is generally the number of the corresponding tablein that report.

The first line of the file contains a text record of up to 80 characters describing the data on the file.

The second line of the file contains the lowest and highest run numbers for tests included on the file.

The remaining data on the file is in segments introduced by a control number (denoted here by NCON) on a single line at the start of the segment.

NCON=0 Marks the end of data on the file

NCON=1 This segment defines the data quantities included on this file. These integers are set zero if data is not included or positive if data is included for this run:

- ICPST if steady CP values given
- ICPUS if oscillatory unsteady CP values given as real & imag parts
- IMACH if local Mach number values are given
- ICLM if local CL, CM values given for each section

NCON=2 This segment defines transducer locations. Data is grourped into sections and each section may include locations for steady and unsteady transducers on upper and lower surfaces:
NSEC number of sections or groups of data on first record
For each of the NSEC sections the following data, starting on a new record:
First record contains an integer section identifier. Note that this does not appear if NSEC=1

The next record contains the number of transducers (NMT) of a particular type followed (if NMT>0) on the subsequent records by pairs of values giving the X and Y coordinates of the transducers. The chordwise location X is non-dimensionalised by local chord and the spanwise location Y by the semi-span. These data (number followed by X,Y array) are repeated in order for upper surface steady, upper surface unsteady, lower surface steady, lower surface unsteady.

NCON=3 This segment defines run data. First parametric values are given:

IRUN	integer run number
VMACH	Mach number for this run
FREQ	Frequency of oscillation (Hz)
AERFM	Mean wing/aerofoil flap angle for this run (deg)
AERFA	Wing/aerofoil oscillation amplitude for this run (deg)
FLAPM	Mean flap angle for this run (deg)
FLAPA	Flap oscillation amplitude for this run (deg)
ITEXT	Integer, if positive indicates that a run description text is given on the next record
RTEXT	Run descriptive text (if any, as specified by ITEXT). A single record up to 80 characters.

The data for this run is then given in the same order as for the transducer locations. For each steady set of data points are all CPST followed by all MACH if both are given for the current surface, thus data quantities if all appear are:

steady upper surface CP
steady upper surface local Mach number
unsteady upper surface CP real part
unsteady upper surface CP imaginary part
steady lower surface CP
steady lower surface local Mach number
unsteady lower surface CP real part
unsteady lower surface CP imaginary part
CL steady, CM steady
CL oscillatory real, imag, CM oscillatory real, imag

List of references

1 S R Bland. AGARD two-dimensional aeroelastic configurations. AGARD AR 156, August 1979.

2 S R Bland. AGARD three-dimensional aeroelastic configurations. AGARD AR 167, March 1982.

3 Compendium of unsteady aerodynamic measurements. AGARD Report No.702. August 1982.

4 Compendium of unsteady aerodynamic measurements. AGARD Report No.702 Addendum 1. May 1985.

3E1. NACA 64A006 OSCILLATING FLAP

R.J. Zwaan, NLR

INTRODUCTION

The wind tunnel model which had a NACA 64A006 airfoil section, was fitted with a trailing-edge flap of 25 per cent of the chord. The maximum thickness of this symmetrical airfoil is 6 per cent and is located at about 28 per cent of the chord. During the test the main surface was clamped at the wind tunnel side walls, whereas the flap could be driven in a harmonic motion about an axis at 75 per cent of the chord. The flap had no aerodynamic balance.

In the set of two-dimensional aeroelastic configurations this airfoil represents the category of small thickness and conventional airfoils (roof-top type). The characteristics are illustrated in figure 1, presenting the development of the steady and unsteady pressure distributions with Mach number for a given frequency. Passing the critical Mach number, $M^* \approx 0.85$, the measured unsteady pressure distributions start to deviate from the calculated distributions under the influence of shocks at both sides. The calculated results are based on lifting surface theory.

Lift and moment coefficients are given in figure 2 for a frequency of 120 Hz. An at least qualitative agreement exists between experiment and theory up to $M \approx 0.85$. Results are also given for $k = 0$, see figure 3. The differences between experiment and theory are appreciably larger now, which can be ascribed partly to tunnel wall interference.

LIST OF SYMBOLS AND DEFINITIONS

α_m	ALPHA	mean wing incidence, deg
δ_0	C	flap amplitude, deg; see note below
c		airfoil chord
C_p	CP	steady mean pressure coefficient
	DCP	oscillatory pressure coefficient ($k \neq 0$), tabulated as REal, IMaginary, MODulus and ARGument, equivalent to $- C_p / \delta_0$, in which $C_p / \delta_0 = (C'_p / \delta_0) + i\,(C''_p / \delta_0)$. RE, IM, MOD, in rad^{-1}, ARG in deg. If k=0, then $DCP = - [C_p(+\delta_0) - C_p(-\delta_0)] / 2\delta_0$
δ_m	DELTA	mean flap angle, deg
f	F	frequency, Hz
k	K	reduced frequency, $k = \pi fc/V$
k_c	KC	oscillatory wing lift coefficient, $C_L/\pi\delta_0$, rad^{-1}
M_L	M	mean local Mach number
m_c	MC	oscillatory wing pitching moment coefficient (about 0.25c)', $-2C_m/\pi\delta_0$, rad^{-1}
n_c	NC	oscillatory flap hinge moment coefficient, $-2C_h/\pi\delta_0$, rad^{-1}
p_t	PO	total pressure, Pa
q	Q	dynamic pressure, Pa
	RC	oscillatory flap lift coefficient, $C_{Lf}/\pi\delta$, rad^{-1}
R_e	RE	Reynolds number based on wing chord
x		chordwise coordinate of the airfoil (% chord)
z		vertical coordinate of the airfoil (% chord)
+ suffix		upper side
- suffix		lower side

Note: The oscillatory motion is defined as $\delta = \delta_0 \sin(\omega t)$. The equation for an oscillatory pressure reads: $p(t)=p_m + p' \sin(\omega t) + p'' \cos(\omega t)$ + etc. Similar expressions hold for the aerodynamic coefficients.

PRESENTATION OF DATA

The data which were presented in tables 5 to 18 of Report 702 for this test are supplied here as a single ASCII data file SET1.UND in RUNAD format as defined in the introduction to chapter 3. The table numbers are used as the "run numbers" for data selection by the program RUNAD. Tables 5 and 6 are reproduced here as samples with key parameters from the remaining tables. Note that for the zero-frequency tests the values of CL, CM and CP given as "steady" apply for the airfoil with undeflected flap and the values given as "real parts of oscillatory" CL and CM and the DCP values apply to the deflected flap configuration.

FORMULARY

1 General Description of model

1.1	Designation	NACA 64A006
1.2	Type	Roof top. 6 % thick symmetrical airfoil
1.3	Derivation	See Table 1 for geometry
1.4	Additional remarks	-
1.5	References	1

2 Model Geometry

2.1	Planform	Two-dimensional airfoil
2.2	Aspect ratio	NA
2.3	Leading edge sweep	0
2.4	Trailing edge sweep	0
2.5	Taper ratio	0
2.6	Twist	0
2.7	Wing centreline chord	0.18m
2.8	Semi-span of model	0.42m
2.9	Area of planform	0.0756 m^2
2.10	Location of reference sections and definition of profiles	See table 2
2.11	Lofting procedure between reference sections	NA
2.12	Form of wing-body junction	NA
2.13	Form of wing tip	NA
2.14	Control surface details	Flap hinge axis at 0.75c, gap width 0.1mm
2.15	Additional remarks	-
2.16	References	-

3 Wind Tunnel

3.1	Designation	NLR Pilot Tunnel
3.2	Type of tunnel	Continuous closed circuit
3.3	Test section dimensions	Rectangular, see fig. 4. height 0.55 m, width 0.42 m
3.4	Type of roof and floor	10 % slotted top and bottom walls, separate top and bottom plenums
3.5	Type of side walls	Solid side walls
3.6	Ventilation geometry	See fig. 4
3.7	Thickness of side wall boundary layer	Thickness 10 % of test section semi-width, no special treatment
3.8	Thickness of boundary layers at roof and floor	Not measured; probably comparable'with side wall boundary layers

3.9	Method of measuring Mach number	Derived from static pressure measured upstream of model and from total pressure measured in settling chamber
3.10	Flow angularity	-
3.11	Uniformity of Mach number over test section	See fig. 5.
3.12	Sources and levels of noise or turbulence in empty tunnel	See fig. 6 for turbulence/noise levels
3.13	Tunnel resonances	No evidence
3.14	Additional remarks	For two-dimesnionality of the flow see ref. 3
3.15	References on tunnel	2

4 Model motion

4.1	General description	Flap oscillation
4.2	Natural frequencies and normal modes of model and support system	No interference with natural vibration modes

5 Test Conditions

5.1	Model chord/tunnel width	0.435
5.2	Model chord/tunnel height	0.323
5.3	Blockage	-
5.4	Position of model in tunnel	-
5.5	Range of Mach numbers	M = 0.5 to 1.0
5.6	Range of tunnel total pressure	Atmospheric
5.7	Range of tunnel total temperature	313 ± 1 K
5.8	Range of model steady or mean incidence	α_m :-4 ° to 0 °; δ_m: -3 ° to 3 °
5.9	Definition of model incidence	Zero incidence defined by matching upper and lower static pressure distribution (applicable because of airfoil symmetry)
5.10	Position of transition, if free	NA
5.11	Position and type of trip, if transition fixed	2.5 mm strip of carborundum garins at 0.1c
5.12	Flow instabilities during tests	No evidence
5.13	Changes to mean shape of model due to steady aerodynamic load	-
5.14	Additional remarks	-
5.15	References describing tests	4

6 Measurements and Observations

6.1	Steady pressures for the mean conditions	Y
6.2	Steady pressures for small changes from the mean conditions	Y
6.3	Quasi-steady pressures	N
6.4	Unsteady pressures	Y
6.5	Steady section forces for the mean conditions by integration of pressures	Y
6.6	Steady section forces for small changes from the mean conditions by integration	Y
6.7	Quasi-steady section forces by integration	N
6.8	Unsteady section forces by integration	Y
6.9	Measurement of actual motion at points of model	Y
6.10	Observation or measurement of boundary	N

layer properties	
6.11 Visualisation of surface flow	N
6.12 Visualisation of shock wave movements	Y
6.13 Aditional remarks	N

7 Instrumentation

7.1 Steady pressure	
7.1.1 Position of orifices spanwise and chordwise	See 7.2.1
7.1.2 Type of measuring system	See 7.2.3
7.2 Unsteady pressure	
7.2.1 Position of orifices spanwise and chordwise	See figures 7 and 8
7.2.2 Diameter of orifices	0.8mm
7.2.3 Type of measuring system	38 pressure tubes + 6 in situ pressure transducers
7.2.4 Type of transducers	±2.5 psi and ±5 Psi Statham differential pressure transducers, and ±5 psi Kulite miniature pressure transducers
7.2.5 Principle and accuracy of calibration	Calibration uses transfer functions of pressure tubes. see Ref. 4; for accuracy see 9.10
7.3 Model motion	
7.3.1 Method of measuring motion reference coordinate	See fig. 7
7.3.2 Method of determining spatial mode of motion	
7.3.3 Accuracy of measured motion	See 9.10
7.4 Processing of unsteady measurements	
7.4.1 Method of acquiring and processing measurements	See fig. 9
7.4.2 Type of analysis	Signal analysis of TFA over 20 cycles for f = 30 Hz and 60 cycles for f = 120 Hz
7.4.3 Unsteady pressure quantities obtained and accuracies achieved	Fundamental harmonies; for accuracy see 9.10
7.4.4 Method of integration to obtain forces	Trapezoidal rule
7.5 Additional remarks	-
7.6 References on techniques	4 and 5

8 Data presentation

8.1 Test cases for which data could be made available	Table 3
8.2 Test cases for which data are included in this document	Table 4
8.3 Steady pressures	Mean pressures in tables 5 to 18
8.4 Quasi-steady or steady perturbation pressures	Steady pressure derivatives in Tables 5, 8, 11, 14 and 17
8.5 Unsteady pressures	Tables 6, 7, 9, 10, 12, 13, 15, 16 and 18
8.6 Steady forces or moments	-
8.7 Quasi-steady or unsteady perturbation forces	See 8.4
8.8 Unsteady forces and moments	See 8.5
8.9 Other forms in which data could be made available	-
8.10 Reference giving other representations of data	6

9 Comments on data

9.1 Accuracy	
9.1.1 Mach number	±0.002
9.1.2 Steady incidence	±0.02°
9.1.3 Reduced frequency	±0.0005
9.1.4 Steady pressure coefficients	Not known
9.1.5 Steady pressure derivatives	Not known
9.1.6 Unsteady pressure coefficients	Not known
9.2 Sensitivity to small changes of parameter	No evidence
9.3 Non-linearities	Part of analysis of experimental results, see ref. 4
9.4 Influence of tunnel total pressure	-
9.5 Effects on data of uncertainty, or variation, in mode of model motion	
9.6 Wall interference corrections	No corrections included
9.7 Other relevant tests on same model	None
9.8 Relevant tests on other models of nominally the same shapes	Unknown
9.9 Any remarks relevant to comparison between experiment and theory	Comparisons of experiment and theory including various calculation methods are given in ref. 4
9.10 Additional remarks	No systematic investigations of separate accuracies have been performed; accuracy of lift and moment coefficients is estimated to be 5 to 10 per cent in maginutde and 3 to 6 degrees in phase angle
9.11 References on discussion of data	4 and 7

10 Personal contact for further information

Evert G M Geurts
Department of Aerodynamics Engineering and Aeroelasticity
Phone: +31 20 5113455
Fax: +31 20 5113210
Email: geurts@nlr.nl

National Aerospace Laboratory NLR
Anthony Fokkerweg 2 P.O. Box 90502
NL 1059 CM Amsterdam NL 1006 BM Amsterdam
The Netherlands The Netherlands
Phone: +31 20 5113113
Fax: +31 20 5113210
Website: http://www.nlr.nl

11 List of references

1 I.H. Abbott, A.E. von Doenhoff. Theory of wing sections. Dover Publications, Inc., New York, 1959

2 J. Zwaaneveld. Principal data of the NLL Pilot Tunnel NLL Report MP 185, 1959

3 H.A. Dambrink. Investigation of the 2-dimensionality of the flow around a profile in the NLR 0.55x0.42 m2 transonic wind tunnel. NLR Memorandum AC-72-018, 1972

4 H. Tijdeman. Investigations of the transonic flow around oscillating airfoils. NLR TR 77090 U, 1977

5 P.H. Fuykschot L.J.M. Joosten. DYDRA - Data logger for dynamic measurements. NLR MP 69012 U, 1969

6 H. Tijdeman, P. Schippers. Results of pressure measurements on an airfoil with oscillating flap in two-dimensional high subsonic and transonic flow (zero incidence and zero mean flap position). NLR TR 73078 U, 1973

7 R. Houwink. Some remarks on boundary layer effects on unsteady airloads. AGARD-CP-296, 1981

8 S. R. Bland. AGARD Two-dimensional aeroelastic configurations. AGARD-AR-156, 1979

Table 1 **Contour data of the NACA 64A006 airfoil**

x (%c)	z (%c)	x (%c)	z (%c)	x (%c)	z (%c)
0	0	20	2.557	65	2.188
0.5	0.485	25	2.757	70	1.907
0.75	0.585	30	2.896	75	1.602
1.25	0.739	35	2.977	80	1.285
2.5	1.016	40	2.999	85	0.967
5.0	1.399	45	2.945	90	0.649
7.5	1.684	50	2.825	95	0.331
10	1.919	55	2.653	100	0.013
15	2.283	60	2.438		

L.E. radius: 0.246 %c

Table 2 **Actual Contour data of the NACA 64A006 airfoil model**

Actual contour data of the NACA 64A006 airfoil (measures per cent of chord)

x	z_{upper}	z_{lower}	x	z_{upper}	z_{lower}
1.25	0.724	-0.742	50.00	2.822	-2.819
2.50	1.025	-1.025	55.00	2.655	-2.642
5.00	1.405	-1.405	60.00	2.430	-2.425
7.50	1.686	-1.686	65.00	2.194	-2.169
10.00	1.919	-1.922	70.00	1.908	-1.894
15.00	2.283	-2.283	75.00	-	-
20.00	2.558	-2.555	80.00	1.310	-1.310
25.00	2.758	-2.758	85.00	0.989	-0.989
30.00	2.894	-2.889	90.00	0.668	-0.668
35.00	2.975	-2.969	95.00	0.346	-0.346
40.00	2.991	-2.989	100.00	0.027	-0.027
45.00	2.942	-2.936			

Table 3 Test program for the NACA 64A006 airfoil with flap

Amplitude of oscillation: $\delta_0 = 1\,^{o}$

Test Condition	Freq Hz	Mach number 0.50	0.75	0.775	0.80	0.825	0.85	0.875	0.90	0.92	0.94	0.96	0.98	1.00
$\alpha_m = 0^o$, $\delta_m = 0^o$	0	x	x		x	x	x	x	x	x	x	x	x	x
	10	x				x	x	x	x			x		
	20	x						x						
	30	x			x	x	x	x	x			x		
	90	x				x	x	x	x			x		
	120	x	x	x	x	x	x	x	x	x	x	x	x	x
$\alpha_m = 0^o$, $\delta_m = 3^o$	0	x	x		x	x	x	x	x	x	x	x	x	x
	30	x				x	x	x		x				
	120	x	x	x	x	x	x	x		x	x	x		
$\alpha_m = -2^o$, $\delta_m = 0^o$	0	x	x		x	x	x	x	x	x	x	x		
	30	x				x	x	x	x					
	120	x	x	x	x	x	x	x	x	x	x			
$\alpha_m = -2^o$, $\delta_m = -3^o$	0	x	x	x	x	x	x	x	x	x	x	x		
	30	x				x	x	x						
	120	x	x	x	x	x	x	x						
$\alpha_m = -4^o$, $\delta_m = 0^o$	0	x	x	x	x	x	x	x	x	x				
	10	x						x						
	30	x					x	x						
	120	x	x	x	x	x	x	x	x	x				

Table 4 Test cases for the NACA 64A006 airfoil with flap included in Data Set 1

	CT case				Data set 1						
Flow	No	M	δ_0	k	Run No	M	δ_0	δ_m	k	Re*10^{-6}	Table
Subsonic	z1	0.800	1.5	0	-	0.800	1.5	0	0	2.34	5
	1	0.800	1.0	0.064	40904	0.794	1.09	0.15	0.064	2.32	6
	2	0.800	1.0	0.253	40807	0.804	1.11	0.00	0.253	2.35	7
	z2	0.825	1.5	0	-	0.825	1.5	0	0	2.36	8
	3	0.825	1.0	0.062	40905	0.824	1.09	0.15	0.062	2.36	9
	4	0.825	2.0	0.062	No measurement						
	5	0.825	1.0	0.248	40305	0.822	0.95	0.20	0.248	2.28	10
Transonic	z3	0.850	1.5	0	-	0.850	1.5	0	0	2.39	11
	6	0.850	1.0	0.060	40906	0.853	1.10	0.16	0.060	2.40	12
	7	0.850	1.0	0.240	40806	0.854	1.05	0.02	0.240	2.41	13
	z4	0.875	1.5	0	-	0.875	1.5	0	0	2.43	14
	8*	0.875	1.0	0.059	40907	0.877	1.13	0.15	0.059	2.43	15
	9*	0.875	2.0	0.059	No measurement						
	10*	0.875	1.0	0.234	40807	0.879	1.08	0.01	0.234	2.44	16
	z5	0.960	1.5	0	-	0.960	1.5	0	0	2.51	17
	11	0.960	1.0	0.054	40911	0.960	1.03	0.00	0.54	2.53	18
	12	0.960	1.0	0.214	No measurement		0.18				

Comments on Table 4: Cases z1 to z5 are extra to the computational cases identified in reference 8. They correspond to zero-frequency (k=0) experimental data that are closely related to the CT cases for which $k \neq 0$. The asterisks denote priority cases. In all cases $\alpha_m = 0$. Transition is fixed at 0.15c.

Table 5

M=0.800	F =0	ALPHA=0.00	KC=1.32
		DELTA=0.00	MC=.612
		C = 1.5	NC=.0372

	UPPERSIDE				LOWERSIDE			
X/C	CP+	M+	DCP+		CP-	M-	DCP-	
			RE	IM			RE	IM
.010	-.005	.802	3.552	0.0	.029	.787	-3.609	0.0
.050	-.154	.870	2.292	0.0	-.143	.865	-2.253	0.0
.100	-.192	.887	1.833	0.0	-.179	.881	-1.833	0.0
.200	-.236	.907	1.680	0.0	-.238	.908	-1.719	0.0
.300	-.268	.922	1.719	0.0	-.273	.924	-1.852	0.0
.400	-.290	.932	1.890	0.0	-.293	.933	-2.005	0.0
.450	-.276	.926	1.967	0.0	-.267	.921	-1.986	0.0
.500	-.249	.913	1.890	0.0	-.250	.914	-2.024	0.0
.550	-.216	.898	1.948	0.0	-.213	.897	-1.986	0.0
.600	-.179	.881	2.005	0.0	-.176	.880	-2.158	0.0
.650	-.150	.868	2.215	0.0	-.144	.865	-2.349	0.0
.700	-.119	.854	2.597	0.0	-.103	.847	-2.616	0.0
.725	-.104	.847	2.941	0.0	-.084	.838	-2.826	0.0
.750	-.096	.843	4.431	0.0	.007	.797	-7.086	0.0
.775	-.071	.832	3.858	0.0	-.053	.824	-3.724	0.0
.800	-.046	.821	2.807	0.0	-.034	.815	-2.769	0.0
.850	-.010	.805	1.661	0.0	-.004	.802	-1.699	0.0
.900	.023	.790	.974	0.0	.030	.786	-.974	0.0
.950	.067	.770	.458	0.0	.072	.768	-.477	0.0

Table 6

RUNNO 40904

M=0.794	F=30.00	ALPHA=0
P0=10429		DELTA=.15
RE=1.04E+04	K=.064	C=1.09
Q=3037.30		

	RE	IM		RE	IM		
KC=	1.016	-0.26	RC=	.2766	.0112	X5=1.334E-03	1
MC=	.640	.010	NC=	.0385	.0028	X6=1.346E-03	0

			UPPERSIDE						LOWERSIDE			
X/C	CP+	M+	DCP+		DCP+		CP-	M-	DCP-		DCP-	
			RE	IM	MOD	ARG			RE	IM	MOD	ARG
.010	-0.035	.811	.671	-1.474	1.619	-65	.077	.759	-0.736	1.554	1.719	115
.050	-0.175	.873	.342	-0.753	.827	-66	-0.120	.847	-0.678	1.050	1.250	123
.100	-0.226	.897	.657	-0.853	1.077	-52	-0.166	.867	-0.737	0.895	1.159	129
.200	-0.252	.909	.991	-0.787	1.266	-38	-0.222	.893	-1.115	0.826	1.387	143
.300	-0.279	.921	1.245	-0.683	1.420	-29	-0.256	.908	-1.276	0.708	1.459	151
.400	-0.304	.932	1.628	-0.554	1.719	-19	-0.279	.919	-1.578	0.605	1.690	159
.450	-0.287	.925	1.744	-0.403	1.790	-13	-0.260	.910	-1.665	0.490	1.736	164
.500	-0.263	.914	1.826	-0.301	1.850	-9	-0.235	.898	-1.825	0.379	1.864	168
.550	-0.222	.895	1.915	-0.198	1.925	-6	-0.199	.882	-1.927	0.288	1.948	172
.600	-0.190	.881	2.034	-0.113	2.038	-3	-0.165	.867	-2.105	0.185	2.113	175
.650	-0.159	.866	2.155	-0.136	2.159	-4	-0.127	.850	-2.302	0.118	2.305	177
.700	-0.125	.851	2.258	-0.253	2.272	-6	-0.089	.833	-2.649	0.043	2.650	179
.725	-0.108	.844	2.658	-0.213	2.667	-5	-0.071	.825	-2.885	0.023	2.885	180
.750	-0.068	.825	4.948	.409	4.965	5	.013	.787	-5.276	1.571	5.505	163
.775	-0.085	.833	4.097	.224	4.103	3	-0.030	.806	-3.821	-0.047	3.822	181
.800	-0.058	.821	3.038	.335	3.057	6	-0.018	.801	-2.943	-0.141	2.946	183
.850	-0.018	.803	1.751	.212	1.764	7	0.006	.790	-1.738	-0.042	1.739	181
.900	.021	.786	.959	.100	.964	6	0.038	.776	-1.066	-0.090	1.069	185
.950	.069	.764	.374	.013	.374	2	.080	.757	-0.501	-0.043	.503	185

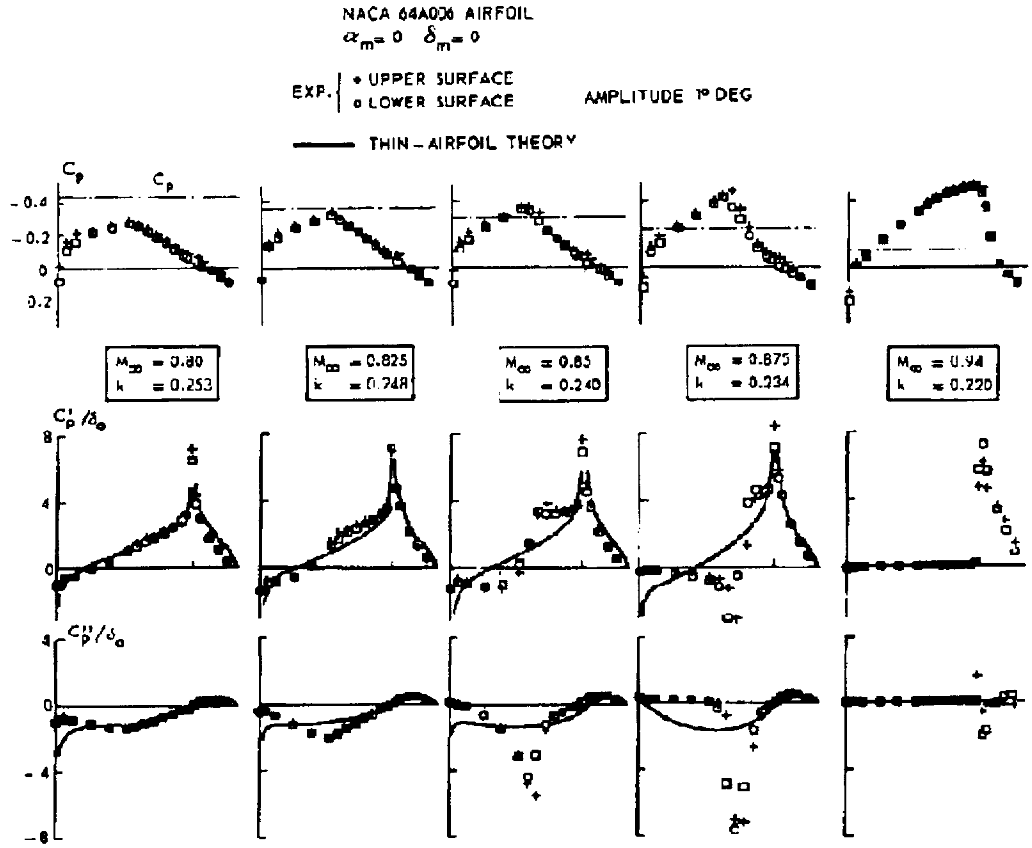

Fig. 1 Development of mean steady and unsteady pressure distributions with Mach number (f = 120 Hz)

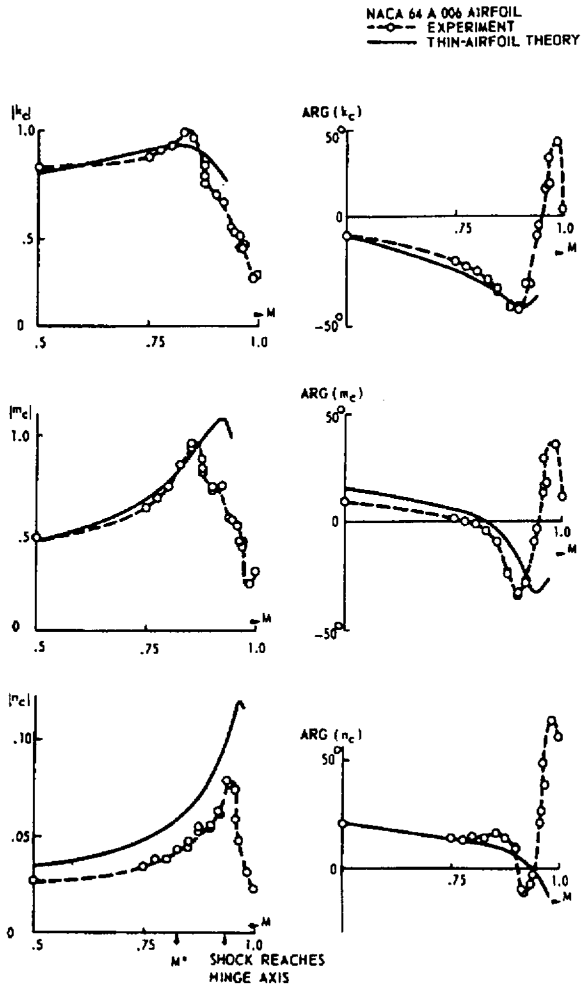

Fig. 2 Unsteady aerodynamic coefficients as a function of Mach number (f = 120 Hz)

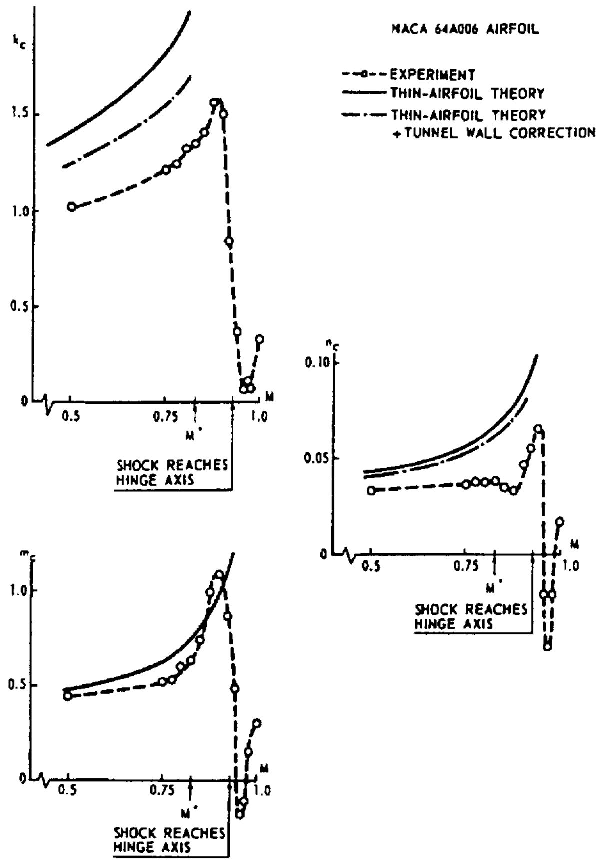

Fig. 3 Steady aerodynamic derivatives as a function of Mach number

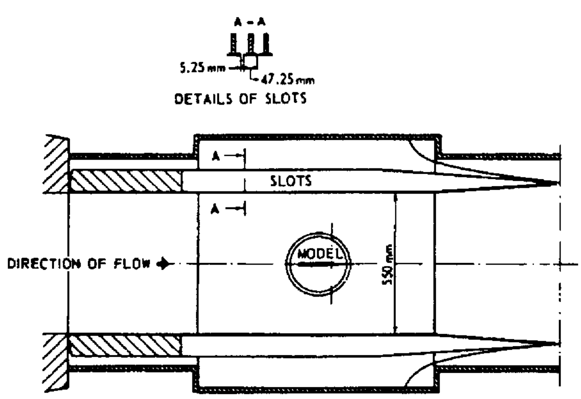

Fig. 4 Transonic test section of the NLR Pilot Tunnel

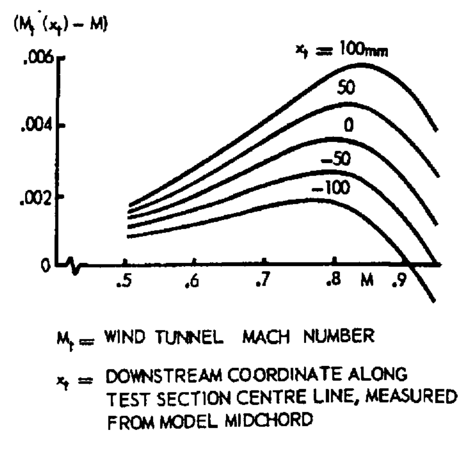

Fig. 5 Mach number distribution in NLR Pilot Tunnel test section

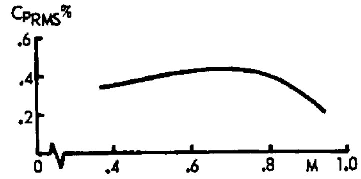

Fig. 6   Noise level in NLR Pilot Tunnel test section

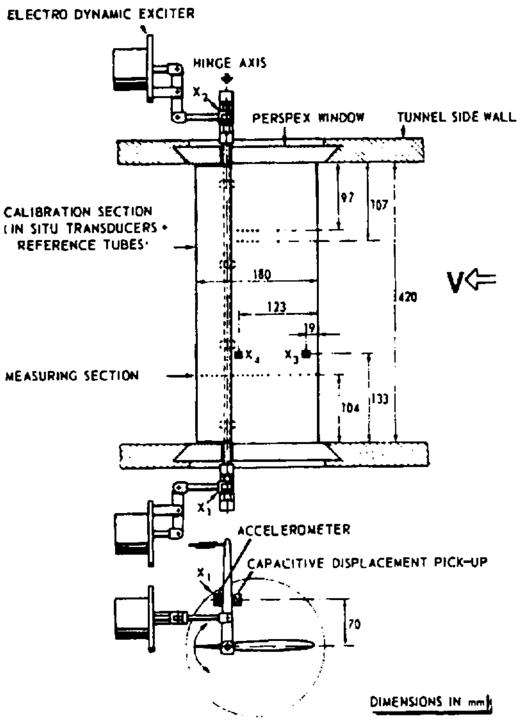

Fig. 7   Test set-up and instrumentation of the NACA 64A006 airfoil with flap

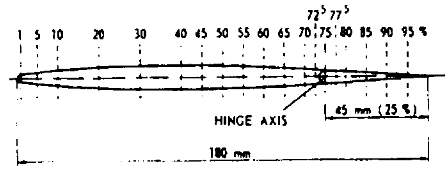

MEASURING SECTION (BOTH UPPER AND LOWER SURFACE)			
No. 1	x/c = .01	No. 11	x/c = .65
2	.05	12	.70
3	.10	13	.725
4	.20	14	.75
5	.30	15	.775
6	.40	16	.80
7	.45	17	.85
8	.50	18	.90
9	.55	19	.95
10	.60		

CALIBRATION SECTION (UPPER SURFACE ONLY)	
No. 1	x/c = .30
2	.50
3	.55
4	.60
5	.65
6	.70

Fig. 8   Location of pressure orifices on the NACA 64A006 airfoil with flap

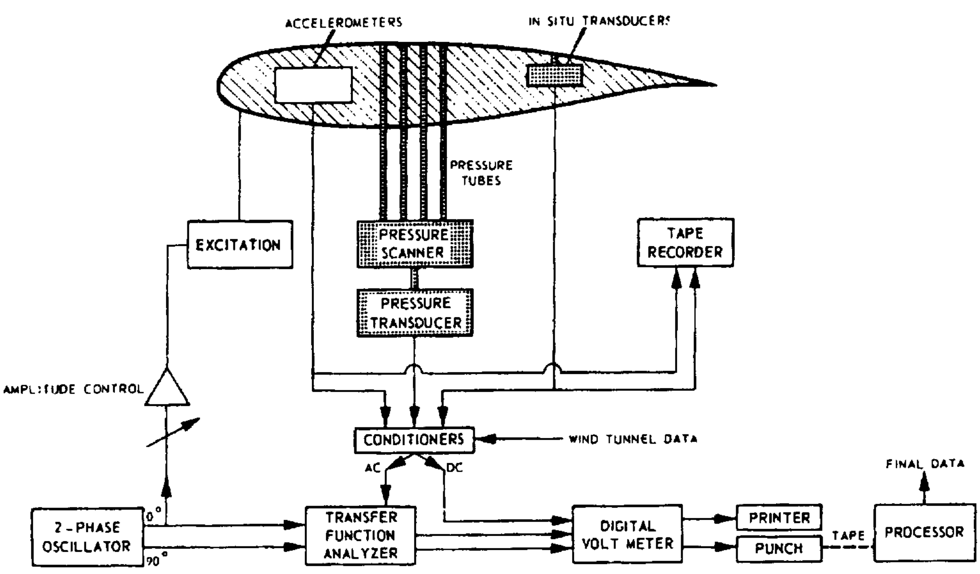

Fig. 9   Block diagram of measuring equipment

3E3. NACA 0012 OSCILLATORY AND TRANSIENT PITCHING

R. H. Landon, ARA

INTRODUCTION

These results are extracted from tabulations of wing pressures resulting from the 3rd series of pitching tests about 0.25c axis made in the ARA 2-dimensional tunnel, using the pitching and heaving rig, Ref 1.

The main purpose of these tests was to examine the conditions of dynamic stall and recovery at scaled time rates similar to those of a typical helicopter application. Dynamic similarity was maintained also in Reynolds number; the approximately quarter scale blade section was therefore run, for all the cases reported here, at a tunnel stagnation pressure of 4 bar to match low altitude flight of the helicopter. Consequently, no artificial boundary layer transition trips were applied to the test wing.

The output of dynamic pressure transducers was sampled at fixed intervals, the instantaneous pressures and reference conditions having a matched and filtered response within 3 dB up to 460 Hz.

The results represent one specific cycle, and are not averaged over a number of cycles. The data bank at ARA contains at least 4 cycles of each dynamic condition. Ramp motions have only a single transient.

Up to 6 increments of mean incidence and amplitude, singly or in combination, could be run: the present programme called for 3 increments (called programme steps or PSTEP) of mean incidence α_m.

The time-dependent results are presented without harmonic or spectral analysis. Note that the harmonic content of the pitching motion is relatively high, due to the intrusion of other modes of the drive system:

AGARD Case	f (Hz)	Harmonic content and phase angle relative to the fundamental			
		First	Second	Third	Fourth
1, 2, 3	50.32	2.44%, -10°	2.45%, -30°	0.5%, -51°	0.38%, 0°
5	62.5	0.22%, -13°	2.60%, -44°	0.37%, -61°	0.07%, -76°

The instantaneous Mach number varies in sympathy with the drag of the wing: the flow momentum loss changes the effective area of the choked throat that controls the flow down-stream of the model, thus making speed dependent on drag. Mach number is thus given for each data point in the results.

The heave mode (no results presented here) allowed the wing to be placed up to 63.5 mm (2.5 in) above and below the tunnel centre line. Some pitching tests are reported in Ref 2 to show possible effects on dynamic readings of wall proximity: there has been no analysis of unsteady tunnel interference, but corrections appropriate to steady interference have been applied to some of the measured quantities.

Notes on the data

The ordinates of the NACA 0012 airfoil are given in Table 1. The chordwise and spanwise locations of the 30 pressure holes and their channel numbers are given in Table 2, and the arrangement of the data is explained in Table 3.

Ten data sets are presented in tables 4 to 13 which provide experimental comparison with AGARD CT Cases. For the priority CT Case 1 the tabulated data are presented as 32 sets of pressure coefficients at equal time intervals during a cycle of oscillation, extracted from 64 sets in the original data. For the other CT Cases of oscillatory pitch the number is reduced to 8 sets. The ramp motion and quasi-steady data have 16 points, chosen to give approximately equal incidence increments, again taken from more closely spaced original data. Tables 4 to 7 include a pitch damping factor which is irrelevant for the present purpose and its value is also shown in each of the oscillatory plots. Note also that the ramp incidence rate is an approximate or nominal value: the incidence rate $d\alpha/dt$ is not constant, and when calculated from different ranges of incidences, will give different values. Approximate representations of the motions in Ref 6 are recommended for comparative calculations at given α. No measurements were made for strictly steady conditions, but instantaneous pressures were measured for very slow oscillations of incidence. The results of three of these quasi-steady tests are given in Tables 11 to 13.

Oscillatory pitch about 0.25c:

Related	Run No.	Experimental conditions							
AGARD CT case	and P step	M	α_m (deg)	α_0 (deg)	f (Hz)	k	Re x 10^{-6}	Sets	Data table
1	87-1	0.600	2.89	2.41	50.32	0.0808	4.8	32	4
2	89-1	0.600	3.16	4.59	50.32	0.0811	4.8	8	5
3	87-3	0.600	4.86	2.44	50.32	0.0810	4.8	8	6
5	128-1	0.755	0.016	2.51	62.5	0.0814	5.5	8	7

Ramp motion about 0.25c:

Related	Run No.	Experimental conditions					
AGARD CT case		M	α range (deg)	Re x 10^{-6}	Approx dα/dt (deg/s)	Sets	Data table
6	218	0.30	-0.03 to 15.54	2.7	1280	16	8
7	227	0.57	-0.01 to 14.80	4.6	425	16	9
8	230	0.56	-0.01 to 14.97	4.5	1380	16	10

Quasi-steady:

Run No.	M	α range in table (deg)	Re x 10^{-6}	Sets	Data table
6	0.30	-0.12 to 15.55	2.6	16	11
11	0.58	-0.13 to 11.56	4.6	16	12
151	0.75	-3.27 to 3.35	5.5	16	13

Figs 2 to 4 show typical results extracted from Ref 2 for oscillatory pitching at M = 0.6 and 0.75, showing the effect of reduced frequency parameter on normal force, pitching moment and a damping factor DF. The related AGARD CT cases 1, 2, 3 and 5 are included in these figures. Figs 2 and 3 are for respective amplitudes $\alpha_0 = 2.5^o$ and 5.0^o.

Fig 5 shows curves of C_N against α from the quasi-steady data and for the two ramp rates at M = 0.57 to illustrate the lag in the growth of C_N and the delayed stall under dynamic conditions.

LIST OF SYMBOLS AND DEFINITIONS

b	airfoil span and tunnel width
c	chord
C_N	normal force coefficient
C_m	pitching moment coefficient (about 0.25c)
f	frequency (Hz)
h	tunnel height
k	reduced frequency, $\omega c/2V$
M	Mach number
q	dynamic pressure
R, R_e	Reynolds number
t	time (seconds)
V	velocity

x,y,z	airfoil coordinates
α	incidence
α_m	mean incidence
α_o	pitch amplitude
δ^*	displacement thickness of boundary layer
ω	frequency (rad/sec)

For each chosen case, experimental dat are presented as sets of instantaneous values of the quantities Cp C_N C_m α and M for particular times t (in seconds) in tables 4 to 13.

Uncorrected coefficients C'_N and C'_m are evaluated by a curve fitting procedure from the integrals

$$C'_N = \int_0^1 (C_{pL} - C_{pU})\, d(x/c)$$

$$C'_m = \int_0^1 (C_{pL} - C_{pU})\,(0.25 - (x/c))\, d(x/c)$$

where $C_p = (p - p_\infty) / q$ is uncorrected and the suffices L and U denote lower and upper surfaces respectively.

Oscillatory motion is defined by

$$\alpha = \alpha_m + \alpha_0 \sin(\omega t + \varepsilon)$$

where ε is a phase angle dependent on the time datum.

The quantities α α_m α_0 C_N and C_m (but not C_p) have each been corrected for tunnel constraint effects. The corrections, as derived for steady conditions in refs 3, 4 and 5, are applied to each instantaneous condition as if it were steady.

PRESENTATION OF DATA

The data were presented in tables 4 to 13 of the original AGARD R702 report. In this document the first part of table 4 is supplied as a sample and the remaining tables are supplied in an ASCII data file SET3.DAT. A FORTRAN program (SET3.FOR) is provided which demonstrates the extraction of the data. The program includes a sample main segment which reproduces the data of a table via a call to subroutine SET3SEL, with output either online or to a formatted file. This subroutine may be employed in a user's code to extract the data for a single table or to serve as a model for other data extraction codes.

SET3SEL subroutine

A description of the subroutine call and arguments follows:

```
      SUBROUTINE SET3SEL(NCH,ITAB,MAXP,MAXT,RMACH
     1,VMACH,TIM,ALPHA,CN,CM,Q,CPST,NUMP,STN,NTIM)
C
C-- This routine reads and selects tables from the data file SET3.DAT
C   which contains the data of tables 4 to 13 of R702 data set 3 (ARA).
C-- Arguments are as defined below (all except NCH,ITAB, MAXP,MAXT must be
c   variables):
C   Input values
C         NCH     channel number to be used for reading the input file
C         ITAB    Specifies the required table number.
C         MAXP    The declared dimension in the calling routine of the
C                 array STN and leading dimension of CPST (must be >=30)
C         MAXT    The declared dimension in the calling routine of the
C                 time variation arrays VMACH...
C   Returned values:
C         RMACH   The nominal Mach number for this run
C   Time variable arrays of instantaneous values:
C         VMACH   Mach number
C         TIM     Time (sec)
C         ALPHA   Incidence (deg)
C         CN      Normal force coefficient
```

```
C        CM      Pitching moment coefficient (about 0.25c)
C        Q       dynamic pressure
C   Time and location array:
C        CPST    Instantaneous pressure coefficient [CPST(i,j,k) is the
C                value of CP at transducer i,and time value j and
C                surface k (1=upper, 2=lower)]
C
C        NUMP    The number of chordwise locations, 2-element integer array
C                with NUMP(1) the number of upper surface points
C                and NUMP(2) the number of lower surface points
C        STN     2-dimensional array of locations of transducers (X/C)
C                STN(i,j) is the i-th transducer on the upper (j=1) or
C                lower (j=2) surface
C        NTIM    The number of times at which data is given
C
      REAL CPST(MAXP,MAXT,2),VMACH(MAXT),TIM(MAXT),ALPHA(MAXT)
      REAL CN(MAXT),CM(MAXT),Q(MAXT),STN(MAXP,2)
      INTEGER NUMP(2)
```

FORMULARY

1 General Description of model

1.1	Designation	NACA 0012
1.2	Type	Symmetrical 12% thick
1.3	Derivation	
1.4	Additional remarks	Ordinates given in table 1
1.5	References	6, 7

2 Model Geometry

2.1	Planform	Two-dimensional airfoil
2.2	Aspect ratio	NA
2.3	Leading edge sweep	NA
2.4	Trailing edge sweep	NA
2.5	Taper ratio	NA
2.6	Twist	None
2.7	Wing centreline chord	0.1016 m
2.8	Span of model	0.2032 m
2.9	Area of planform	0.0206 m^2
2.10	Location of reference sections and definition of profiles	NA
2.11	Lofting procedure between reference sections	NA
2.12	Form of wing-body junction	NA
2.13	Form of wing tip	NA
2.14	Control surface details	NA
2.15	Additional remarks	Accuracy of profile see fig.1. Trailing edge thickness 0.383mm, approximately 0.127mm too thick
2.16	References	None

3 Wind Tunnel

3.1	Designation	ARA 2-dimensional tunnel
3.2	Type of tunnel	Intermittent blow down
3.3	Test section dimensions	h = 0.4572, b = 0.2032, length = 1.251 m
3.4	Type of roof and floor	Slotted, 3.2% open area ratio
3.5	Type of side walls	Solid
3.6	Ventilation geometry	Roof and floor each have 6 slots and 2 half slots at corners. Plenum chambers 133 mm deep connected by large ducts. Top and bottom walls diverge.
3.7	Thickness of side wall boundary layer	$2\,\delta^* / b = 0.015$
3.8	Thickness of boundary layers at roof and floor	Not known
3.9	Method of measuring Mach number	Static hole in side wall 5 chords ahead of model
3.10	Flow angularity	NA
3.11	Uniformity of Mach number over test section	Centre line distribution within $\pm$0.038 mm in region of model
3.12	Sources and levels of noise or turbulence in empty tunnel	No serious disturbances
3.13	Tunnel resonances	No evidence
3.14	Additional remarks	None
3.15	References on tunnel	Ref.8

4 Model motion

4.1	General description	Pitching about 0.25c, oscillation or ramp.
4.2	Natural frequencies and normal modes of model and support system	Lowest frequency is bending at 600 Hz

5 Test Conditions

5.1	Model chord/tunnel width	0.222
5.2	Model chord/tunnel height	0.5
5.3	Blockage	-
5.4	Position of model in tunnel	-
5.5	Range of Mach numbers	0.3 to 0.87
5.6	Range of tunnel total pressure	1.5 to 4 bar
5.7	Range of tunnel total temperature	Temperature 280^{o}K approx, uncontrolled
5.8	Range of model steady or mean incidence	$\pm 11^{o}$
5.9	Definition of model incidence	On chordline: datum matched on chordwise pressure distributions
5.10	Position of transition, if free	Not knwon
5.11	Position and type of trip, if transition fixed	No trips in presented data because model Re transition fixed consistent with full-scale helicopter blade
5.12	Flow instabilities during tests	No simple answer, refer to ARA
5.13	Changes to mean shape of model due to steady aerodynamic load	No significant distortion
5.14	Additional remarks	None
5.15	References describing tests	1, 2

6 Measurements and Observations

6.1	Steady pressures for the mean conditions	N
6.2	Steady pressures for small changes from the mean conditions	N
6.3	Quasi-steady pressures	Y
6.4	Unsteady pressures	Y
6.5	Steady section forces for the mean conditions by integration of pressures	N
6.6	Steady section forces for small changes from the mean conditions by integration	N
6.7	Quasi-steady section forces by integration	Y
6.8	Unsteady section forces by integration	Y
6.9	Measurement of actual motion at points of model	N
6.10	Observation or measurement of boundary layer properties	N
6.11	Visualisation of surface flow	N
6.12	Visualisation of shock wave movements	N
6.13	Aditional remarks	None

7 Instrumentation

7.1	Steady pressure	Pressures for quasi-steady conditions measured with same system used for unsteady pressures
	7.1.1 Position of orifices spanwise and chordwise	See 7.2
	7.1.2 Type of measuring system	See 7.2
7.2	Unsteady pressure	
	7.2.1 Position of orifices spanwise and chordwise	See table 2
	7.2.2 Diameter of orifices	0.25mm
	7.2.3 Type of measuring system	30 transducers in model (see ref. 1)
	7.2.4 Type of transducers	Kulite XCQL absolute
	7.2.5 Principle and accuracy of calibration	Calibrated under steady conditions against calibration Texas Quartz Pressure Test Set. Accuracy: $\pm$2.7 mb
7.3	Model motion	
	7.3.1 Method of measuring motion reference coordinate	Shaft encoder
	7.3.2 Method of determining spatial mode of motion	NA
	7.3.3 Accuracy of measured motion	Resolution $\pm$0.1 deg
7.4	Processing of unsteady measurements	
	7.4.1 Method of acquiring and processing measurements	Signals sampled at known time intervals, same points in cycle
	7.4.2 Type of analysis	Instantaneous pressures reduced to non-dimensional coefficients
	7.4.3 Unsteady pressure quantities obtained and accuracies achieved	Approximately $\pm$0.01 in C_p
	7.4.4 Method of integration to obtain forces	Standard curve fitting procedure
7.5	Additional remarks	Tabulated C_N and C_m are corrected for wall constraint
7.6	References on techniques	1, 9, 10

8 Data presentation

8.1	Test cases for which data could be made available	None. The test cases covered in the original test were listed in tables in AGARD R702. However, since the publication of the original report, this data has become unavailable from ARA.
8.2	Test cases for which data are included in this document	See Introduction
8.3	Steady pressures	No
8.4	Quasi-steady or steady perturbation pressures	Tables 11, 12, 13
8.5	Unsteady pressures	Tables 4 to 10
8.6	Steady forces or moments	No
8.7	Quasi-steady or unsteady perturbation forces	Tables 11, 12, 13
8.8	Unsteady forces and moments	Tables 4 to 10
8.9	Other forms in which data could be made available	None
8.10	Reference giving other representations of data	1

9 Comments on data

9.1	Accuracy	
	9.1.1 Mach number	± 0.0015
	9.1.2 Steady incidence	Instantaneous incidence to $\pm 0.1^{o}$
	9.1.3 Reduced frequency	Within about 1%
	9.1.4 Steady pressure coefficients	NA
	9.1.5 Steady pressure derivatives	NA
	9.1.6 Unsteady pressure coefficients	Instantaneous Cp to ± 0.01 (see ref 10)
9.2	Sensitivity to small changes of parameter	Not recorded
9.3	Non-linearities	Not recorded
9.4	Influence of tunnel total pressure	Not recorded
9.5	Effects on data of uncertainty, or variation, in mode of model motion	Not recorded
9.6	Wall interference corrections	Values of α, α_m, α_0, , C_N and C_m have been corrected on the basis of steady calibrations (see para 12). No corrections appear to be necessary for M
9.7	Other relevant tests on same model	None
9.8	Relevant tests on other models of nominally the same shapes	Ref.11 gives steady measurements on another model of NACA 0012 in same tunnel
9.9	Any remarks relevant to comparison between experiment and theory	None
9.10	Additional remarks	None
9.11	References on discussion of data	2

10 Personal contact for further information

Aircraft Research Association Ltd, Manton Lane, Bedford MK41 7PF, England

11 List of references

1 R H Landon. A description of the ARA 2-dimensional pitch and heave rig and some results from the NACA 0012 wing. ARA Memo 199, September 1977

2 Mrs M.E. Wood. Results of oscillatory pitch and ramp tests on the NACA 0012 blade section. ARA Memo 220, December 1979

3 A Harris. Calibration of ARA's 2-dimensional facility using 2.8% open area liners. April 1971, unpublished Memorandum

4 A Harris, A B Haines. Evidence on wall interference effects in the ARA 2-dimensional tunnel. ARA Memo 147, 1972

5 A B Haines. An evaluation of wall interference effects in ARA's 2-dimensional tunnel. Item 5, Tech Comm, June 1973

6 Ed. S R Bland. AGARD two-dimensional aeroelastic configurations. AGARD-AR-156, 1979

7 I H Abbott, A E Von Doenhoff. Theory of wing sections: including a summary of airfoil data. McGraw-Hill, New York 1949

8 B L F Hammond. Some notes on model testing in the ARA 2-dimensional facility. ARA Memo 170, 1975

9 R H Landon, Mrs M E Wood. Some sources of error with Kulite pressure transducers in the ARA pitch/heave rig. ARA Memo 204, 1978

10 R H Landon, Mrs M E Wood. The pitch/heave rig data selection and reduction program, and Corrigendum. ARA Memo 182, 1976

11 Mrs J Sawyer. Results of tests on aerofoil M.102/9 (NACA 0012(in the ARA 2-dimensional tunnel. ARA Model Test Note M.102/9, 1978

Table 1 NACA 0012 Section Ordinates

x/c	z/c				
0	0	0.2000	±0.05738	0.6500	±0.04132
0.0050	±0.01221	0.2500	±0.05941	0.7000	±0.03664
0.0125	±0.01894	0.3000	±0.06002	0.7500	±0.03160
0.0250	±0.02615	0.3500	±0.05949	0.8000	±0.02623
0.0500	±0.03555	0.4000	±0.05803	0.8500	±0.02053
0.0750	±0.04200	0.4500	±0.05581	0.9000	±0.01448
0.1000	±0.04683	0.5000	±0.05294	0.9500	±0.00807
0.1500	±0.05345	0.5500	±0.04952	1.0000	±0.00126
		0.6000	±0.04563		

Table 2 NACA 0012 Wing Pressure Locations And Channel Number Identities

Upper surface			Lower surface		
Channel No.	x/c	y/b	Channel No.	x/c	y/b
1	1.0 TE	0.52	21	0 LE	0.44
2	0.9	0.51	22	0.01	0.46
3	0.8	0.48	23	0.02	0.48
4	0.7	0.49	24	0.04	0.48
5	0.6	0.5	25	0.10	0.48
6	0.5	0.5	26	0.22	0.5
7	0.4	0.5	27	0.34	0.5
8	0.3	0.5	28	0.46	0.5
9	0.2	0.51	29	0.57	0.5
10	0.15	0.48	30	0.68	0.5
11	0.125	0.48	31	0.79	0.54
12	0.1	0.49	32	0.90	0.55
13	0.075	0.5			
14	0.05	0.51			
15	0.03	0.52			
16	0.02	0.53			
17	0.01	0.55			
18	0.005	0.56			

Table 3 Layout of Results in Tables 4 to 13.
Note the layout differs from that in AGARD R702.

t(sec)	M	α (deg)	C_N	C_m	q (lb/ft^2)				
C_{p+1}	C_{p+2}	C_{p+3}	C_{p+4}	C_{p+5}	C_{p+6}	C_{p+7}	C_{p+8}	C_{p+9}	C_{p+10}
C_{p+11}	C_{p+12}	C_{p+13}	C_{p+14}	C_{p+15}	C_{p+16}	C_{p+17}	C_{p+18}	C_{p-1}	C_{p-2}
C_{p-3}	C_{p-4}	C_{p-5}	C_{p-6}	C_{p-7}	C_{p-8}	C_{p-9}	C_{p-10}	C_{p-11}	C_{p-12}

where, in the arrangement above, C_{p+n} is the instantaneous value of C_p for channel n on the upper surface and C_{p-n} is the instantaneous value of C_p for channel n on the lower surface. Chordwise locations can be identified from the following key:

Upper									
1.00	0.90	0.80	0.70	0.60	0.50	0.40	0.30	0.10	0.15
Upper								Lower	
0.125	0.10	0.075	0.05	0.03	0.02	0.01	0.005	0	0.01
Lower									
0.02	0.04	0.10	0.22	0.34	0.46	0.57	0.68	0.79	0.90

Table 4 AGARD Case 1 - oscillatory pitch. Sample showing first part of data

M=0.600 NT=31 Re=8*10^6 $\omega c/2V$=0.0808 α_m=2.89 α_0=2.41 Damping=0.06708

0.00000	0.6020	2.97	0.3719	0.0014	1706.3				
0.1647	-0.0007	-0.1408	-0.2437	-0.3383	-0.4547	-0.5912	-0.7231	-0.8666	-0.9290
-1.0117	-1.0640	-1.1383	-1.1316	-1.1096	-0.9442	-0.7231	-0.5408	0.9766	0.6306
0.3993	0.1580	-0.1897	-0.2488	-0.2454	-0.1948	-0.1560	-0.1070	-0.0530	0.0263
0.00062	0.6020	3.42	0.4267	0.0022	1706.3				
0.1562	-0.0024	-0.1493	-0.2539	-0.3501	-0.4716	-0.5965	-0.7535	-0.9172	-0.9965
-1.0894	-1.1484	-1.2615	-1.2683	-1.2582	-1.0928	-0.8683	-0.6860	0.9191	0.7031
0.4752	0.2254	-0.1358	-0.2151	-0.2134	-0.1746	-0.1391	-0.0986	-0.0497	0.0263
0.00124	0.6020	3.84	0.4777	0.0043	1708.7				
0.1645	0.0044	-0.1439	-0.2518	-0.3512	-0.4760	-0.6057	-0.7760	-0.9597	-1.0507
-1.1519	-1.2277	-1.3979	-1.4097	-1.4148	-1.2328	-1.0103	-0.8316	0.8674	0.7747
0.5455	0.2977	-0.0731	-0.1759	-0.1810	-0.1473	-0.1203	-0.0815	-0.0343	0.0348
0.00187	0.6000	4.23	0.5285	0.0070	1696.6				
0.1657	0.0078	-0.1416	-0.2519	-0.3571	-0.4879	-0.6304	-0.8070	-1.0107	-1.1024
-1.2161	-1.3044	-1.5827	-1.5929	-1.5963	-1.3689	-1.1516	-0.9699	0.8158	0.8277
0.6036	0.3558	-0.0312	-0.1348	-0.1568	-0.1314	-0.1059	-0.0720	-0.0261	0.0367
0.00249	0.6020	4.56	0.5731	0.0083	1708.7				
0.1594	0.0044	-0.1473	-0.2586	-0.3681	-0.4996	-0.6445	-0.8299	-1.0406	-1.1434
-1.2446	-1.4333	-1.7570	-1.7772	-1.7182	-1.4772	-1.2581	-1.0878	0.7460	0.8572
0.6449	0.4005	0.0094	-0.0968	-0.1389	-0.1187	-0.0984	-0.0647	-0.0260	0.0398
0.00311	0.6050	4.83	0.6049	0.0124	1723.1				
0.1632	0.0094	-0.1394	-0.2530	-0.3616	-0.4954	-0.6441	-0.8296	-1.0419	-1.1271
-1.2191	-1.6887	-1.9077	-1.9043	-1.8024	-1.5817	-1.3528	-1.1940	0.6830	0.8936
0.6880	0.4540	0.0529	-0.0641	-0.1143	-0.0976	-0.0825	-0.0553	-0.0173	0.0378
0.00373	0.5960	4.98	0.6485	0.0149	1677.4				
0.1537	-0.0008	-0.1571	-0.2721	-0.3871	-0.5211	-0.6807	-0.8730	-1.0791	-1.1237
-1.4293	-1.9393	-2.0835	-2.0577	-1.9461	-1.7401	-1.4929	-1.3194	0.6413	0.9229
0.7186	0.4782	0.0627	-0.0661	-0.1193	-0.1038	-0.0953	-0.0643	-0.0283	0.0301
0.00435	0.5970	5.11	0.6717	0.0189	1684.6				
0.1479	0.0043	-0.1495	-0.2675	-0.3803	-0.5205	-0.6778	-0.8710	-1.0556	-1.1018
-1.8471	-2.0318	-2.1514	-2.1138	-1.9976	-1.8078	-1.5616	-1.3719	0.6010	0.9395
0.7343	0.5001	0.0830	-0.0521	-0.1085	-0.0948	-0.0880	-0.0640	-0.0264	0.0300
0.00497	0.6030	5.09	0.6725	0.0208	1711.1				
0.1559	0.0111	-0.1387	-0.2548	-0.3659	-0.5005	-0.6520	-0.8389	-0.9887	-1.0863
-2.0255	-2.0675	-2.1551	-2.1130	-2.0002	-1.8218	-1.5761	-1.3707	0.5750	0.9402
0.7433	0.5127	0.1003	-0.0326	-0.0949	-0.0781	-0.0781	-0.0545	-0.0158	0.0364
0.00559	0.6010	5.00	0.6756	0.0236	1701.5				
0.1533	0.0094	-0.1429	-0.2580	-0.3697	-0.5119	-0.6643	-0.8504	-0.9926	-1.1213
-2.0945	-2.1233	-2.1994	-2.1571	-2.0471	-1.8643	-1.6223	-1.3971	0.5646	0.9369
0.7440	0.5087	0.0940	-0.0414	-0.1057	-0.1006	-0.0888	-0.0685	-0.0261	0.0297
0.00621	0.5970	4.82	0.6694	0.0254	1679.7				
0.1553	0.0061	-0.1430	-0.2545	-0.3642	-0.5065	-0.6591	-0.8443	-0.9918	-1.0792
-2.1234	-2.1594	-2.2365	-2.1902	-2.0839	-1.8936	-1.6484	-1.4015	0.5737	0.9389
0.7400	0.5034	0.0833	-0.0522	-0.1207	-0.1122	-0.0967	-0.0710	-0.0333	0.0301
0.00683	0.6000	4.54	0.6422	0.0262	1699.1				
0.1552	0.0077	-0.1381	-0.2482	-0.3567	-0.4940	-0.6432	-0.8313	-0.9906	-0.9923
-1.9992	-2.1144	-2.1924	-2.1551	-2.0534	-1.8619	-1.6110	-1.3296	0.6027	0.9128
0.7145	0.4755	0.0653	-0.0686	-0.1313	-0.1177	-0.1025	-0.0770	-0.0364	0.0247
0.00745	0.6010	4.17	0.6039	0.0238	1706.4				
0.1494	0.0009	-0.1426	-0.2523	-0.3603	-0.4936	-0.6354	-0.8244	-1.0101	-1.0320
-1.4118	-2.0548	-2.1358	-2.1172	-2.0295	-1.8134	-1.5637	-1.2784	0.6237	0.8785
0.6743	0.4363	0.0313	-0.0936	-0.1510	-0.1392	-0.1189	-0.0903	-0.0447	0.0194
0.00807	0.5980	3.80	0.5738	0.0238	1687.0				
0.1597	0.0112	-0.1373	-0.2449	-0.3524	-0.4873	-0.6256	-0.8168	-1.0216	-1.1070
-1.0848	-1.9657	-2.0698	-2.0784	-2.0067	-1.7472	-1.4945	-1.2077	0.6889	0.8665
0.6582	0.4124	0.0095	-0.1151	-0.1698	-0.1527	-0.1271	-0.0947	-0.0486	0.0231

- - - - - - - - continued - - - - - - - - -

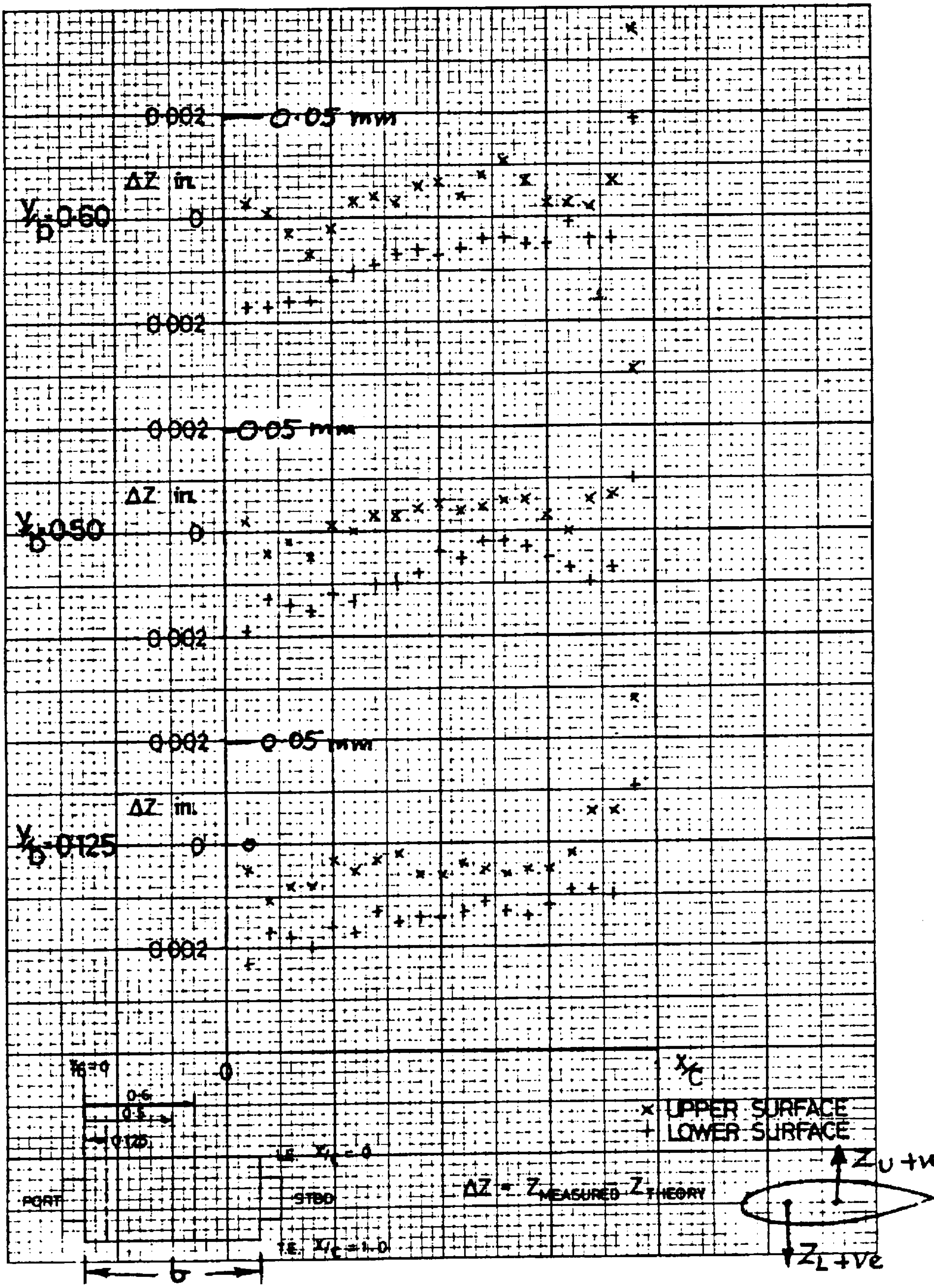

Fig.1 Profile inspection of NACA 0012 wing Z_m - Z_t

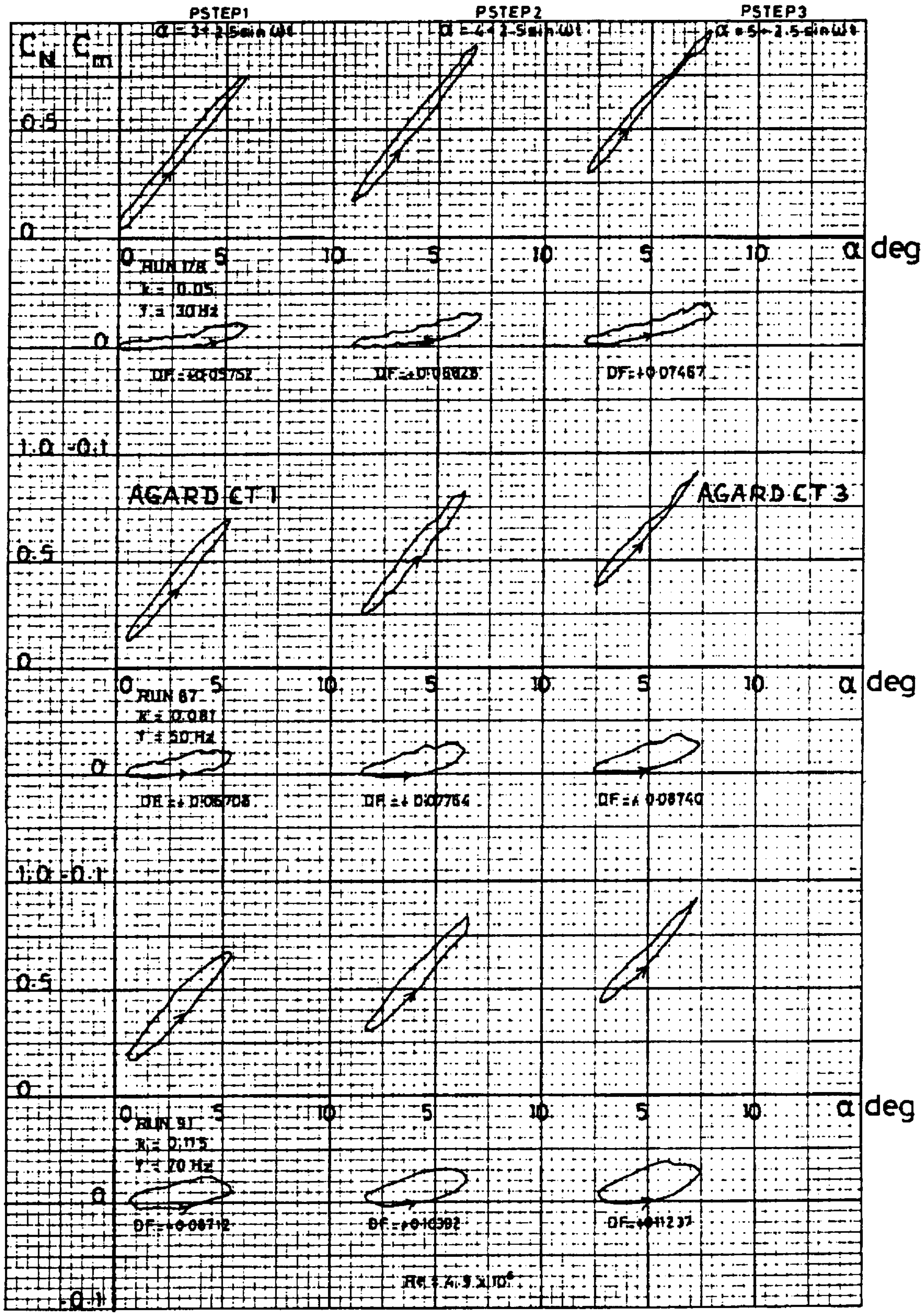

Fig. 2 C_N, C_m v incidence over range of $\alpha_m = 3°, 4°, 5°$; α_o=2.5°.
Effect of frequency k=0.05, 0.08, 0.12; M=0.6

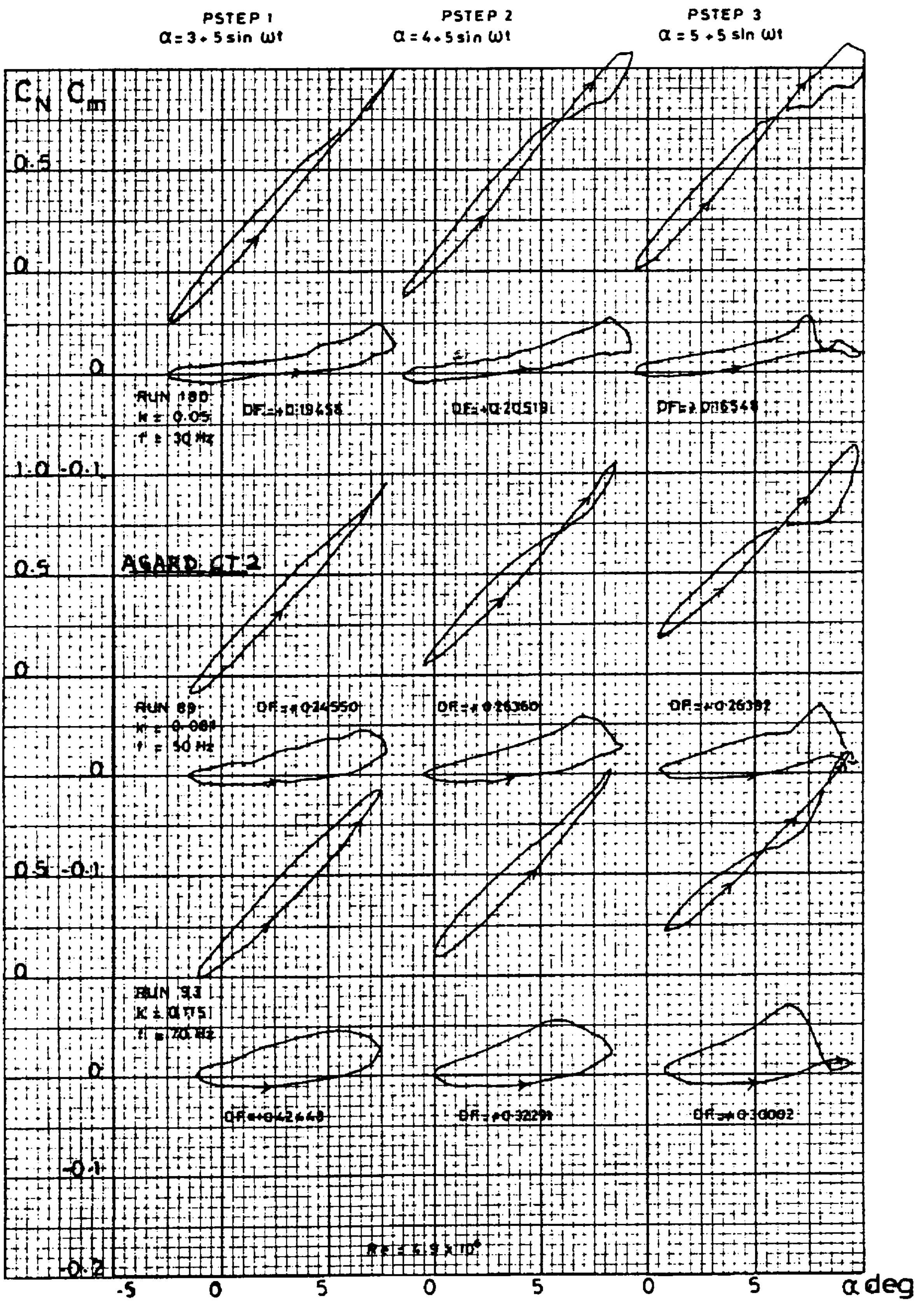

Fig. 3 C_N, C_m v incidence over range of $\alpha_m = 3°, 4°, 5°$; $\alpha_o=5°$.
Effect of frequency k=0.05, 0.08, 0.12; M=0.6

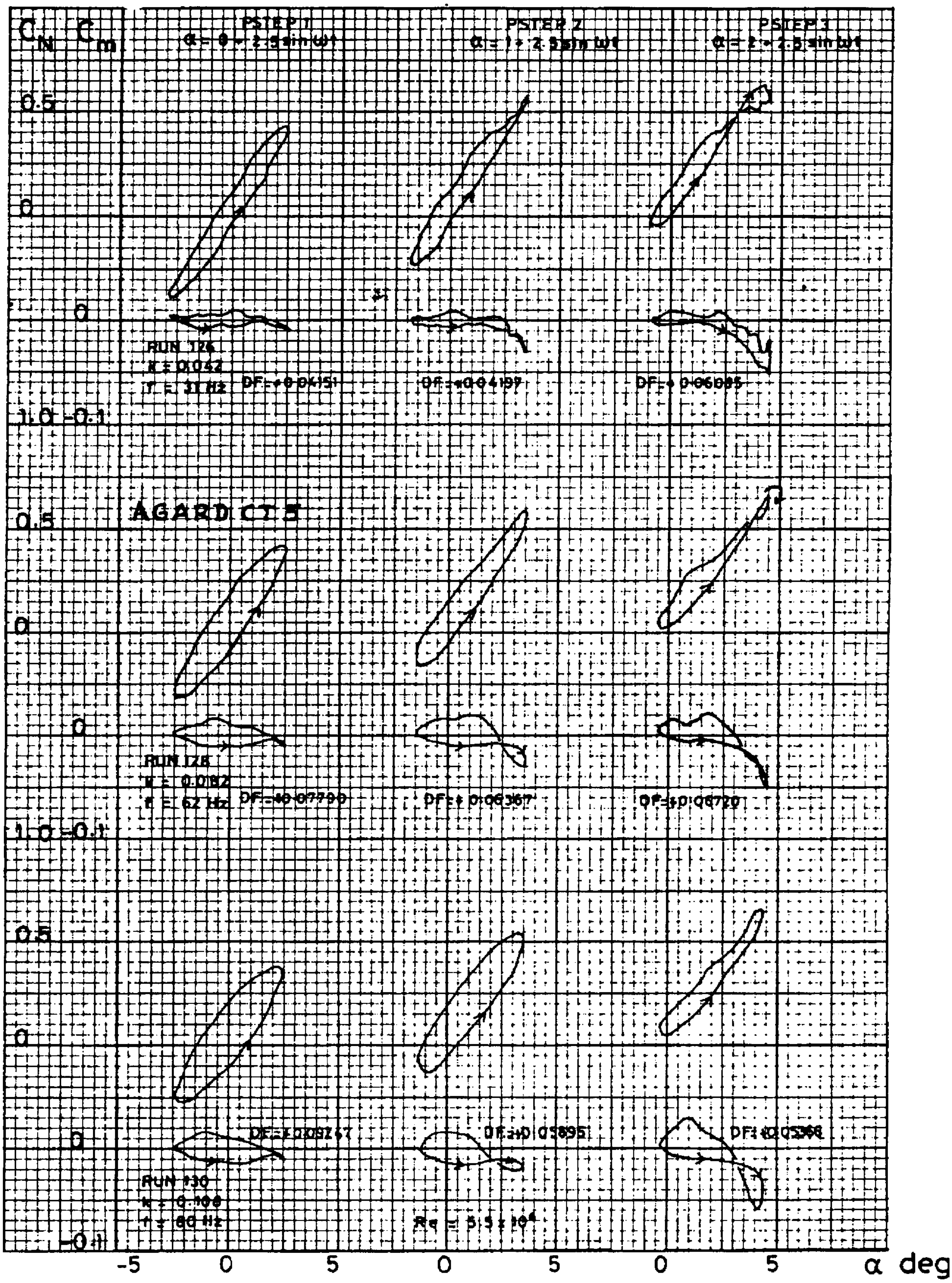

Fig. 4 C_N, C_m v incidence over range of α_m = 0°, 1°, 2°; α_o=2.5°.
Effect of frequency k=0.05, 0.08, 0.12; M=0.6

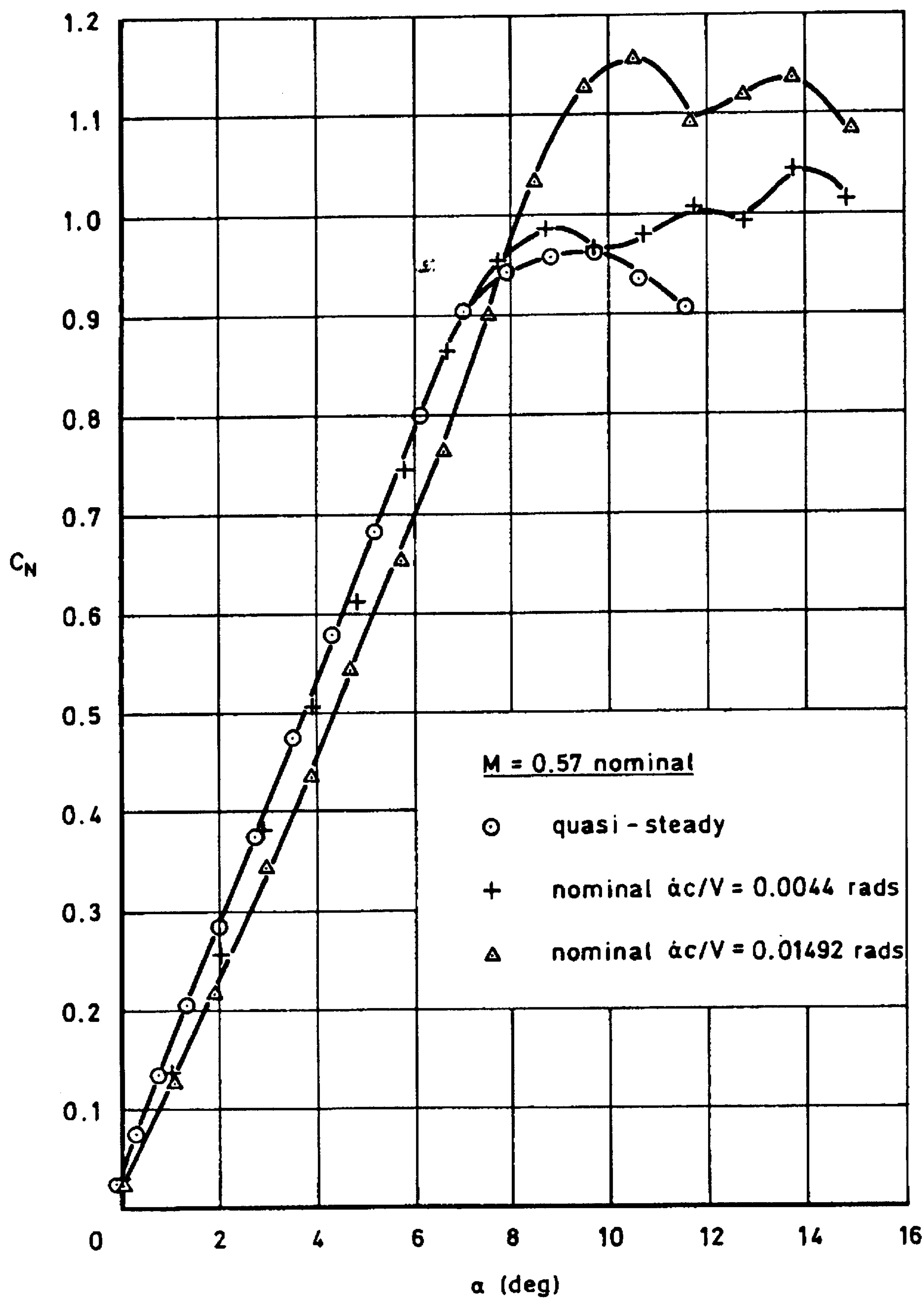

Fig.5 Lift v incidence for different rates of change

3E4. NLR 7301 SUPERCRITICAL AIRFOIL OSCILLATORY PITCHING AND OSCILLATING FLAP

R.J. Zwaan, NLR

INTRODUCTION

The supercritical airfoil NLR 7301 has a maximum thickness of 16.5 per cent of the chord. In the Set of two-dimensional aeroelastic configurations this airfoil represents the category of thick and blunt-nosed airfoils.

The airfoil was investigated in two windÄtunnel tests with different models. In the first test the model could be driven harmonically in a pitching motion about an axis at 40 per cent of the chord. Information about this configuration is designated with the letter "A". In the second test harmonic rotation of a trailing-edge flap was considered. The flap axis was located at 75 per cent of the chord; the flap had no aerodynamic balance. Information about this configuration is designated with the letter "B".

In transonic flow the contribution of the shock to the aerodynamic loading can of course be very different. As an illustration, pressure distributions on the upper surface are compared for a flow with a strong shock and a shock-free flow. Also results of thin-airfoil theory have been added. In the strong shock cases (A: Fig. 1, B: Fig. 5) the pressure peak due to the moving shock dominates in the pressure distribution, with a strength which diminishes with frequency. Although the flow conditions are the same for both configurations, the mean pressure distributions differ slightly. The cause of these differences could not be traced. In the shock-free cases (A: Fig. 2, B: Fig. 6) the pressure distribution shows a wide bulge. The pressure distributions of configuration A show very clearly that with increasing frequency the bulge decreases while at the same time a weak shock develops. Also here the mean pressure distributions should be the same. For unexplained reasons, however, shock-free flow could only be realized at slightly different Mach numbers.

Lift and moment coefficients are presented in figures 3 and 4 for configuration A and in figures 7 and 8 for configuration B. The influence of fixing boundary layer transition is remarkable. Configuration A shows only minor differences. Forced transition at 0.3c is obviously not so effective in this case. The differences are larger for configuration B, which includes also fixed transition at 0.07c. Characteristic changes occur in particular in the lift coefficient at low frequencies. Transition fixing has obviously the effect of reducing both the lift magnitude and the phase lag.

An aspect that emerges especially in the present case of a supercritical airfoil is the difference in the specification of theoretical and experimental shockÄfree flow. In the General Review it was pointed out that this difference is mainly due to viscous effects and tunnel interference. It was further proposed to choose the CT specification such that theory would produce a flow similar to that observed in the experiment. This is illustrated in figure 9 where the theoretical design pressure distribution calculated with a hodograph theory is compared with a shockÄfree pressure distribution measured at free transition.

LIST OF SYMBOLS AND DEFINITIONS

ALPHA	mean wing incidence, α_m, deg
AMPL	flap amplitude, δ_0 deg; see note below
C2	pitch amplitude, α_0, deg; see note below
CL	mean wing lift coefficient, C_L
CLIM	k_α'' in Tables 5 to 14; k_c'' in Tables 15 to 23
CLRE	k_α' in Tables 5 to 14; k_c' in Tables 15 to 23
CM	mean wing moment coefficient (about 0.25 c), C_m
CMIM	m_α'' in Tables 5 to 14; m_c'' in Tables 15 to 23
CMRE	m_α' in Tables 5 to 14; m_c' in Tables 15 to 23
CP	mean pressure coefficient C_p
CPIM	imaginary component of oscillatory pressure coefficient, rad^{-1}. In Tables 5 to 14 it represents C_p''/α_0, in Tables 15 to 23 it represents C_p''/δ_0
CPRE	real component of oscillatory pressure coefficient, rad^{-1}. In Tables 5 to 14 it represents C_p'/α_0, in Tables 15 to 23 it represents C_p'/δ_0 . If k=0, then CPRE = $[C_p(+\alpha_o) - C_p(-\alpha_0)] / 2\alpha_0$ and CPRE = $[C_p(+\delta_o) - C_p(-\delta_0)] / 2\delta_0$ respectively.
DELTA	mean flap angle, δ_m deg
FREQ.	frequency, f, Hz
HARM	order of harmonic

k_α	oscillatory wing lift coefficient, $C_L/\pi\alpha_0$ rad^{-1}
k_c	oscillatory wing lift coefficient, $C_L/\pi\delta_0$ rad^{-1}
M	mean local Mach number, M_L
MACH	free-stream Mach number, M
m_α	oscillatory wing moment coefficient, $-2\ C_m/\pi\alpha_0$, rad^{-1}
m_c	oscillatory wing moment coefficient, $-2\ C_m/\pi\delta_0$, rad^{-1}
MEETRUNNR	run number
NCRE, NCIM	real and imaginary components of oscillatory flap moment coefficient, $-2\ C_h/\ \pi\delta_0$, rad^{-1}
P0	total pressure, p_t , Pa
Q	dynamic pressure, q, Pa
RCRE, RCIM	real and imaginary components of oscillatory flap lift coefficient, $C_{Lf}/\pi\delta_0$
RE	Reynolds number based on wing chord, Re
RFREQ	reduced frequency, $k = \pi fc/V$
+	(suffix) upper side
-	(suffix) lower side
*	(superscript) critical value

Note: The oscillatory motions are defined as $\alpha = \alpha_0 \sin \omega t$ and $\delta = \delta_0 \sin \omega t$. The equation for a corresponding oscillatory pressure (including higher harmonics, if available) reads: $p(t) = p_m + p' \sin \omega t + p'' \cos \omega t + p_1' \sin 2\omega t + p_1'' \cos 2\omega t$ Similar expressions hold for the aerodynamic coefficients.

PRESENTATION OF DATA

The data which were presented in tables 1, 2, and 5 to 23 of the original AGARD R702 report for this test are supplied here in electronic form as ASCII files.

The file SET4TAB1.DAT contains the NLR7301 data given in table 1. The format is that the first record contains the number NU of upper surface points followed by NU records containing the Z value and X value for the points.After this the file contains the number NL of lower surface points followed by NL records containing the Z value and X value for the points.

The file SET4TAB2.DAT contains the model contour data given in table 2. The format is that the first record contains the number N of followed by N records containing Z, X upper surface, X lower surface for these N points.

The data which were presented in tables 5 to 23 are supplied here as a single ASCII data file SET4.UND in RUNAD format as defined in the introduction to chapter 3. The table numbers are used as the "run numbers" for data selection by the program RUNAD and the conditions corresponding to each table is given in table 4. Tables 6 and 16 are reproduced here as samples. Note that for the zero-frequency tests the values of CL, CM and CP given as "steady" apply for the airfoil with undeflected flap and the values given as "real parts of oscillatory" CL and CM and the DCP values apply to the deflected flap configuration.

FORMULARY

1 General Description of model

1.1	Designation	NLR 7301 (also NLR HT 7310810)
1.2	Type	Thick, aft-loaded, shock-free supercritical airfoil
1.3	Derivation	Airfoil designed by means of Boerstoel hodograph method
1.4	Additional remarks	Thickness/chord = 16.5%
1.5	References	-

2 Model Geometry

2.1	Planform	Two-dimensional airfoil
2.2	Aspect ratio	(2.33)

2.3	Leading edge sweep	0
2.4	Trailing edge sweep	0
2.5	Taper ratio	0
2.6	Twist	0
2.7	Wing centreline chord	0.18m
2.8	Span of model	0.42m
2.9	Area of planform	$0.0756m^2$
2.10	Location of reference sections and definition of profiles	See table 2
2.11	Lofting procedure between reference sections	NA
2.12	Form of wing-body junction	NA
2.13	Form of wing tip	NA
2.14	Control surface details	Flap with hinge at 75% chord, gap width 0.35mm
2.15	Additional remarks	Nose radius 0.05c Design condition - Potential flow hodograph theory M=0.721, C_L=0.595 Design pressure distribution (free transition, NLR Pilot Tunnel): M=0.747, C_L=0.455, see fig.9 "Shock-free" pressure distributions for configuration A shown in fig.2 and for configuration B in fig.6.
2.16	References	-

3 Wind Tunnel

3.1	Designation	NLR Pilot Tunnel
3.2	Type of tunnel	Continuous, closed circuit
3.3	Test section dimensions	Rectangular, see fig.10. Height 0.55m, width 0.42m.
3.4	Type of roof and floor	10% slotted top and bottom walls, separate top and bottom plenums
3.5	Type of side walls	Solid side walls
3.6	Ventilation geometry	See fig.10
3.7	Thickness of side wall boundary layer	Thickness 10% of test section semi-width, no special treatment
3.8	Thickness of boundary layers at roof and floor	Not measured. Probably comparable with side wall boundary layers
3.9	Method of measuring Mach number	Derived from static pressure measured upstream of model and from total pressure measured in settling chamber
3.10	Flow angularity	NA
3.11	Uniformity of Mach number over test section	See fig.11 (empty test section)
3.12	Sources and levels of noise or turbulence in empty tunnel	Turbulence/noise level, see fig.12
3.13	Tunnel resonances	No evidence
3.14	Additional remarks	For two-dimensionality of the flow see ref 3
3.15	References on tunnel	Ref 2

4 Model motion

4.1	General description	Hydraulic excitation at one side of the model. A pitching oscillation of airfoil B oscillation of trailing-edge flap
4.2	Natural frequencies and normal modes of model and support system	No interference with natural vibration modes

5 Test Conditions

5.1	Model chord/tunnel width	0.435
5.2	Model chord/tunnel height	0.323
5.3	Blockage	
5.4	Position of model in tunnel	
5.5	Range of Mach number	A: 0.5 to 0.8 B: 0.5 to 0.82
5.6	Range of tunnel total pressure	Atmospheric
5.7	Range of tunnel total temperature	$313 \pm 1°$ K
5.8	Range of model steady or mean incidence	A: $\alpha_m = 0°$ to $3°$ B: $\alpha_m = 0°$ to $3°$, $\delta_m = 0°$
5.9	Definition of model incidence	Incidence datum line α=0 relates to the x-axis as used in tables 1 and 2. Datum line is parallel to test section centre line for $\alpha_m = 0$
5.10	Position of transition, if free	Part of the tests performed with natural transition, position of transition not measured
5.11	Position and type of trip, if transition fixed	A: strip of carborundum grains at 0.3 c B: strip of carborundum grains at 0.07 c or 0.3 c
5.12	Flow instabilities during tests	No evidence
5.13	Changes to mean shape of model due to steady aerodynamic load	Negligible
5.14	Additional remarks	-
5.15	References describing tests	A: ref.4

6 Measurements and Observations

6.1	Steady pressures for the mean conditions	Y
6.2	Steady pressures for small changes from the mean conditions	Y
6.3	Quasi-steady pressures	N
6.4	Unsteady pressures	Y
6.5	Steady section forces for the mean conditions by integration of pressures	Y
6.6	Steady section forces for small changes from the mean conditions by integration	Y
6.7	Quasi-steady section forces by integration	N
6.8	Unsteady section forces by integration	Y
6.9	Measurement of actual motion at points of model	Y
6.10	Observation or measurement of boundary layer properties	N
6.11	Visualisation of surface flow	N
6.12	Visualisation of shock wave movements	Y
6.13	Additional remarks	N

7 Instrumentation

7.1 Steady pressure

7.1.1	Position of orifices spanwise and chordwise	See 7.2.1
7.1.2	Type of measuring system	See 7.2.3

7.2 Unsteady pressure

7.2.1	Position of orifices spanwise and	A: see fig.13 and 14

	chordwise	B: see fig.15 and 16
	7.2.2 Diameter of orifices	0.8mm
	7.2.3 Type of measuring system	A: 40 pressure tubes + 13 in situ pressure transducers B: 46 pressure tubes + 12 in situ pressure transducers
	7.2.4 Type of transducers	$\pm$7.5 psi Statham differential pressure transducers, and $\pm$5 psi Kulite miniature pressure transducers
	7.2.5 Principle and accuracy of calibration	Calibration uses transfer functions of pressure tubes, see ref.4, for accuracy see 9.10
7.3	Model motion	
	7.3.1 Method of measuring motion reference coordinate	A: with accelerometers, see fig.13 B: with accelerometers, see fig.15
	7.3.2 Method of determining spatial mode of motion	NA
	7.3.3 Accuracy of measured motion	See fig.10
7.4	Processing of unsteady measurements	
	7.4.1 Method of acquiring and processing measurements	See fig.17
	7.4.2 Type of analysis	A: signal analysis of TFA over 20 cycles for f=30, 80 Hz and 60 cycles for f=200 Hz B: signal length during TFA analysis was 1 sec
	7.4.3 Unsteady pressure quantities obtained and accuracies achieved	A: Fundamental harmonics B: Fundamental harmonics and occasionally second and third harmonics For accuracy see 9.10
	7.4.4 Method of integration to obtain forces	Trapezoidal rule
7.5	Additional remarks	-
7.6	References on techniques	A: ref 4 and 5 B: ref 6

8 Data presentation

8.1	Test cases for which data could be made available	A: see table 3 B: not available
8.2	Test cases for which data are included in this document	See table 4. Amplitude: A: $\alpha_0 = 0.1°$ to $1.5°$; B: $\delta_0 = 0.1°$ to $2°$ Frequency: A: f =0 to 80 Hz (k=0 to 0.26); B: f=0 to 200 Hz (k=0 to 0.65)
8.3	Steady pressures	Mean pressures for: A: tables 5 to 14 B: tables 15 to 23
8.4	Quasi-steady or steady perturbation pressures	Steady pressure derivatives for: A: tables 5, 8, 12 B: tables 15, 17, 19
8.5	Unsteady pressures	A: tables 6, 7, 9, 10, 11, 13, 14 B: tables 16, 18, 20 to 23
8.6	Steady forces or moments	See 8.3
8.7	Quasi-steady or unsteady perturbation forces	See 8.4
8.8	Unsteady forces and moments	See 8.5
8.9	Other forms in which data could be made available	NA
8.10	Reference giving other representations of data	NA

9 Comments on data

9.1	Accuracy	
	9.1.1 Mach number	$\pm$0.002. No corrections made for Mach number non-uniformity
	9.1.2 Steady incidence	$\pm0.02^\circ$
	9.1.3 Reduced frequency	$\pm$0.0005
	9.1.4 Steady pressure coefficients	Not known
	9.1.5 Steady pressure derivatives	Not applicable
	9.1.6 Unsteady pressure coefficients	Not known
9.2	Sensitivity to small changes of parameter	No evidence
9.3	Non-linearities	Part of analysis of experimental results, see ref.4
9.4	Influence of tunnel total pressure	NA
9.5	Effects on data of uncertainty, or variation, in mode of model motion	NA
9.6	Wall interference corrections	No corrections included, but under steady conditions it is normal to make the following steady corrections to measurements made in this tunnel: $\Delta\alpha_m = -1.4\, C_L + 0.56\, (C_m + 0.25\, C_L)/\, (1\text{-}M^2)^{-1/2}$ (deg) ($\pm$15%) $\Delta C_L = -0.015\, C_L\, /\, (1\text{-}M^2)$, ($\pm$30%) $\Delta C_m = -0.25\, \Delta C_L$ ($\pm$30%)
9.7	Other relevant tests on same model	None
9.8	Relevant tests on other models of nominally the same shapes	See data set 5 of R702.
9.9	Any remarks relevant to comparison between experiment and theory	-
9.10	Additional remarks	No systematic investigations of separate accuracies have been performed. Accuracy of lift and moment coefficients is estimated to be 5 to 10 per cent in magnitude and 3 to 6 degrees in phase angle.
9.11	References on discussion of data	A: ref.4

10 Personal contact for further information

Evert G M Geurts
Department of Aerodynamics Engineering and Aeroelasticity
Phone: +31 20 5113455
Fax: +31 20 5113210
Email: geurts@nlr.nl

National Aerospace Laboratory NLR

Anthony Fokkerweg 2	P.O. Box 90502
NL 1059 CM Amsterdam	NL 1006 BM Amsterdam
The Netherlands	The Netherlands

Phone: +31 20 5113113
Fax: +31 20 5113210
Website: http://www.nlr.nl

11 List of references

1 T Barche c.s. Experimental data base for computer program assessment. AGARD-AR-138, 1979

2 J Zwaaneveld Principal data of the NLL Pilot Tunnel. NLL Report MP 185, 1959

3 H A Dambrink Investigation of the 2-dimensionality of the flow around a profile in the NLR 0.55x0.42m transonic wind tunnel. NLR Memorandum AC-72-018, 1972

4 H Tijdeman Investigations of the transonic flow around oscillating airfoils. NLR TR 77090 U, 1977

5 P H Fuykschot, L J M Joosten DYDRA - Data logger for dynamic measurements. NLR MP 69012 U, 1969

6 P H Fuykschot PHAROS, processor for harmonic analysis of the response of oscillating surfaces. NLR MP 77012 U, 1977

7 S R Bland AGARD Two-dimensional aeroelastic configurations. AGARD-AR-156, 1979

Table 1 Contour data of the NLR 7301 airfoil

The contour data is contained in the file SET4TAB1.DAT

Table 2

Actual contour data of the NLR 7301 airfoil (conf. B) (measured in mm) is contained in the file SET4TAB2.DAT

Note regarding Tables 1 and 2:

In Ref. 7 the contour coordinates have been transformed to unit chord. The model was designed to shape given by Table 1, but the trailing edge was cut off at x/c=1.0. The actual measured shape of the model is given in the table above.

Table 3

Test program for the NLR 7301 airfoil (conf.A)

Basic program: amplitude of oscillation: $\alpha_0 = 0.5°$
frequencies: 0, 10, and 80 Hz
transition strip at x/c=0.3

Incidence α_m degrees	Mach number										
	0.5	0.6	0.65	0.675	0.70	0.725	0.74	0.75	0.76	0.775	0.80
0	x				x			x			
0.85	x	x	x	x	x	x	x	x	x	x	x
1.50	x				x			x			
3.00	x	x	x	x	x	x		x			

Influence of amplitude and frequency, transition strip at x/c=0.3

Incidence α_m degrees	Amplitude α_0 degrees	Frequency Hz	Mach number		
			0.5	0.7	0.75
0.85	0.1, 0.25, 0.75, 1.0, 1.5	10, 80	x	x	x
3.00	0.1, 0.25, 0.75, 1.0	10, 80		x	
0.85	0.5, 1.0	10, 30, 60, 80	x	x	x
3.00	0.5, 1.0	10, 30, 60, 80		x	

Additional tests with natural transition

Incidence α_m degrees	Amplitude α_0 degrees	Frequency Hz	Mach number		
			0.5	0.7	0.75
0.85	0.5, 1.0	10	x	x	x
0.85	0.5, 0.75	80	x	x	x
3.00	0.5, 1.0	10		x	
3.00	0.5, 0.75	80		x	
0.85	0.5	30, 60	x	x	x

Table 4 Test cases for the NLR 7301 airfoil (confs A and B) included in this Data Set

Motion	Flow	CT case					Data Set									
		N_0	M	α_m	α_0,δ_0	k	Run no.	M	α_m	δ_m	α_0, δ_0	k	$Re*10^{-6}$	transition	Harm.	Table
Pitching about 0.4c (conf.A)	Subsonic	z1	0.500	0.40	0.5	0	12201	0.499	0.85		0.50	0	1.70	0.3c	1	5
		1	0.500	0.40	0.5	0.098	1601	0.499	0.85		0.55	0.098	1.70	0.3c	1	6
		2	0.500	0.40	0.5	0.262	1301	0.498	0.85		0.44	0.262	1.70	0.3c	1	7
	Transonic with shock	z2	0.700	2.00	0.5	0	14405	0.696	3.00		0.50	0	2.11	0.3c	1	8
		3	0.700	2.00	0.5	0.072	3805	0.696	3.00		0.42	0.072	2.11	0.3c	1	9
		4	0.700	2.00	1.0	0.072	3905	0.696	3.00		0.98	0.072	2.11	0.3c	1	10
		5	0.700	2.00	0.5	0.192	52705	0.695	3.00		0.55	0.192	2.12	0.3c	1	11
	Supercritical design	z3	0.721	-0.19	0.5	0	16908	0.744			0.50	0	2.22	free	1	12
		6	0.721	-0.19	0.5	0.068	9608	0.744	0.85		0.46	0.068	2.23	free	1	13
		7	0.721	-0.19	1.0	0.068	xxx									
		8*	0.721	-0.19	0.5	0.181	6708	0.744	0.85		0.61	0.181	2.22	free	1	14
		9	0.721	-0.19	0.5	0.453	xxx									
Flap rotation (conf B)	Subsonic	z4	0.500	0.40	1.0	0	250	0.503	0	0.02	0.95	0	1.69	0.07c	1	15
		10	0.500	0.40	1.0	0.098	253	0.502	0	0.02	0.97	0.098	1.69	0.07c	1	16
	Transonic with shock	z5	0.700	2.00	1.0	0	129	0.702	3.00	-0.08	0.95	0	2.14	0.3c	1	17
		11	0.700	2.00	1.0	0.071	120	0.701	3.00	0.03	0.97	0.071	2.14	0.3c	1	18
	Supercritical design	z6	0.721	-0.19	1.0	0	160	0.754	0.85	0.01	0.96	0	2.23	free	1	19
		12	0.721	-0.19	1.0	0.067	148-150	0.755	0.85	0.01	0.95	0.067	2.23	free	1,2,3	20-22
		13*	0.721	-0.19	1.0	0.181	xxx									
		14	0.721	-0.19	1.0	0.445	162	0.756	0.85	-0.01	0.90	0.445	2.23	free	1	23

Remarks on Table 4

Cases z1 to z6 are extra to the computational cases identified in Ref. 7. They correspond to zero-frequency (k=0) experimental data that are closely related to the CT cases for which k≠0. The asterisks denote Priority Cases. xxx denotes cases for which no measurements are included.

Note that the table numbers in the right hand column are used as the reference number in the SET4.UND data file.

Sample table for configuration A - Table 6

RUN 1601

M	.499	C2	.55	STAT.		QUASI-INSTAT.		
ALPHA	.85	FREQ	30.			RE	IM	
P0	10398.	K	0.000	CL .311		1.481	-.170	
RE	1.70E6			CM .069		-.028	.151	
Q	1529.							
		UPPERSIDE				LOWERSIDE		
X/C	CP+	M-	CPRE+	CPIM+	CP-	M-	CPRE-	CPIM-
.01	-.070	.518	-10.560	2.296	.296	.417	6.804	-3.146
.05	-1.163	.776	-11.456	2.389	-.351	.586	7.090	-2.048
.10	-.846	.703	-8.108	1.833	-.373	.592	4.808	-1.920
.15	-.707	.672	-3.138	.552	-.383	.594	4.104	-1.096
.20	-.654	.659	-4.080	.853	-.400	.598	3.403	-.864
.25	-.633	.655	-3.339	.514	-.415	.602	2.854	-.738
.30	-.642	.657	-2.972	.213	-.413	.601	2.725	-.614
.35	-.599	.647	-2.920	.004	-.426	.604	2.671	.011
.40	-.594	.645	-2.415	.024	-.440	.608	2.356	.164
.45	-.582	.643	-2.089	-.054	-.440	.608	1.963	.091
.50	-.571	.640	-1.804	-.181	-.393	.597	1.688	.237
.55	-.562	.638	-1.398	-.139	-.297	.573	1.492	.238
.60	-.542	.633	-1.045	-.155	-.201	.550	1.089	.164
.65	-.494	.622	-.705	-.200	-.084	.520	.852	.296
.70	-.410	.602	-.412	-.227	.030	.491	.259	-.067
.75	-.307	.577	-.191	-.277	.130	.464	.547	.422
.80	-.195	.549	.054	-.279	.212	.441	.571	.457
.85	-.085	.522	.091	-.256	.269	.425	.562	.533
.90	.011	.497	-.090	-.152	.300	.416	.440	.431
.95	.086	.477	-.466	-.092	.302	.415	.250	.284

Sample table for configarion B - Table 16

FUNDAMENTAL FREQUENCY TEST DATA NLR 7301 WITH OSCILLATING FLAP

	UPPERSIDE				LOWERSIDE			
X/C	CP+	M-	CPRE+	CPIM+	CP-	M-	CPRE-	CPIM-
.010	.126	.469	-2.159	1.234	.069	.484	2.243	-1.519
.030	-.935	.728	-3.015	1.557	-.464	.618	2.675	-1.422
.050	-.867	.713	-.883	1.411	-.531	.634	.973	-1.323
.100	-.629	.658	-1.950	.987	-.472	.620	1.900	-.860
.150	-.570	.643	-1.384	.755	-.471	.620	1.389	-.839
.200	-.545	.638	-1.238	.629	-.474	.621	1.321	-.673
.250	-.534	.635	-1.237	.629	-.483	.623	1.201	-.568
.300	-.522	.632	-1.363	.483	-.488	.624	.976	-.584
.350	-.512	.630	-1.362	.484	-.488	.624	1.306	-.447
.400	-.509	.629	-1.290	.421	-.497	.626	1.419	-.439
.450	-.503	.628	-1.425	.411	-.483	.623	1.418	-.439
.500	-.501	.627	-1.551	.266	-.431	.610	1.521	-.320
.550	-.487	.624	-1.550	.266	-.328	.585	1.622	-.201
.600	-.470	.620	-1.820	.247	-.222	.559	1.776	-.024
.650	-.421	.608	-1.954	.239	-.107	.530	1.929	.152
.700	-.340	.588	-2.347	.078	.009	.500	1.970	.319
.725	-.283	.574	-2.416	.144	.057	.487	1.975	.205
.760	-.269	.571	-3.494	.072	.117	.471	2.123	.492
.775	-.233	.562	-2.728	-.215	.140	.465	1.788	.471
.800	-.172	.547	-1.711	-.213	.174	.455	1.565	.456
.850	-.067	.520	-.901	-.159	.228	.440	1.119	.429
.900	.022	.497	-.568	-.069	.261	.430	.955	.362
.950	.097	.476	-.425	-.194	.270	.428	.517	.225

TEST DATA		MODEL DATA			OVERALL DATA				
							STEADY	UNSTEADY	
								RE	IM
MEETRUNNR.	253	ALPHA	.00	DEG.					
MACH	.502	DELTA	.02	DEG.	NORMAL FORCE	CL	.172	.927	-.197
Q [PA]	15024	AMPL.	.97	DEG.	MOMENT(1/4C)	CM	.058	.418	.065
RE	1.69E6	FREQ.	30.0	HZ	FLAP FORCE	RC	.0625	.1705	.0376
HARM	1	RFREQ	.098		HINGE MOMENT	NC	.0059	.0255	.0077
IDENTNR.	10								

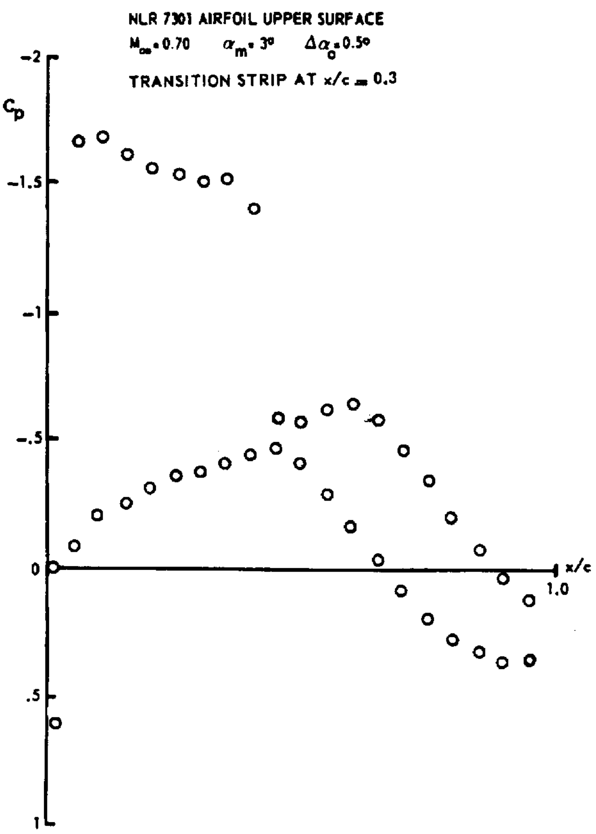

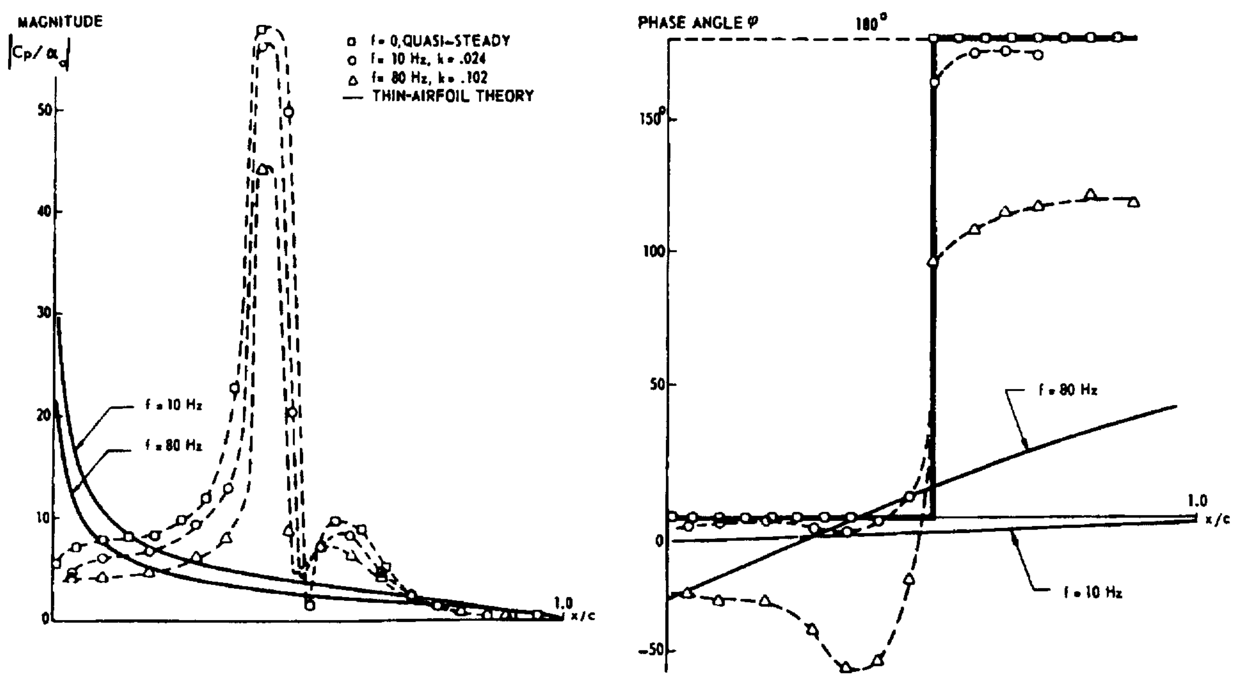

Fig. 1 Effect of shock wave on the unsteady pressure distributions; pitching oscillation

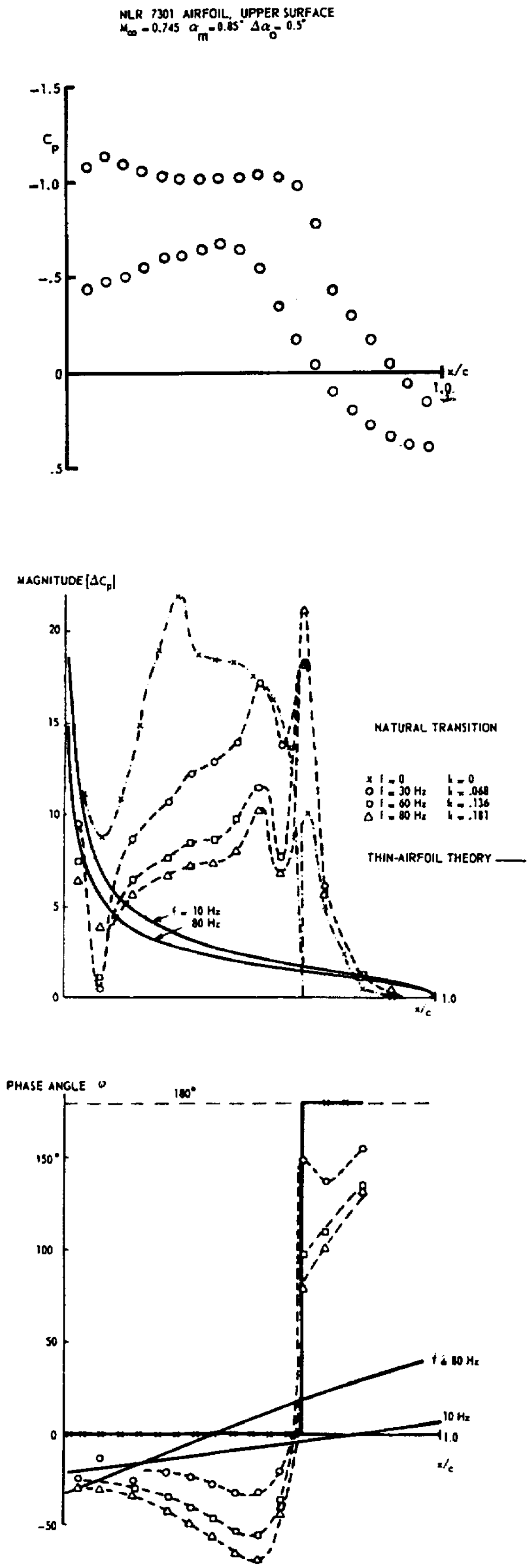

Fig. 2 Unsteady pressure distributions for the "shock-free" design point; pitching oscillation

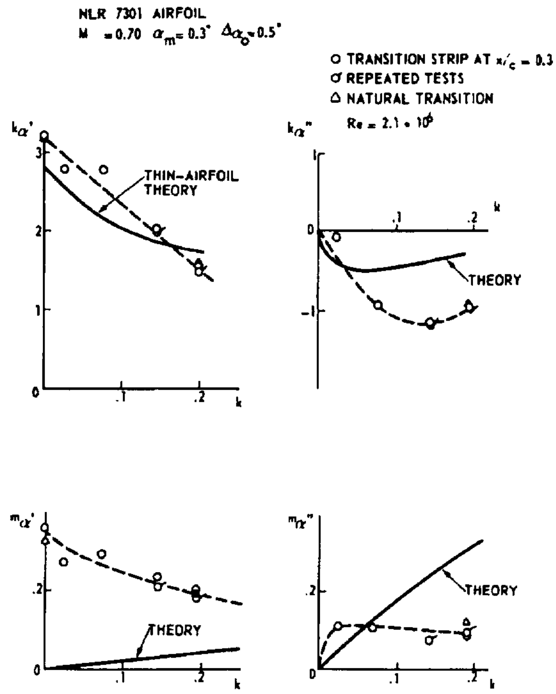

Fig. 3 Unsteady normal-force and moment coefficients as a function of frequency in transonic flow with a well-developed shock wave; pitching oscillation

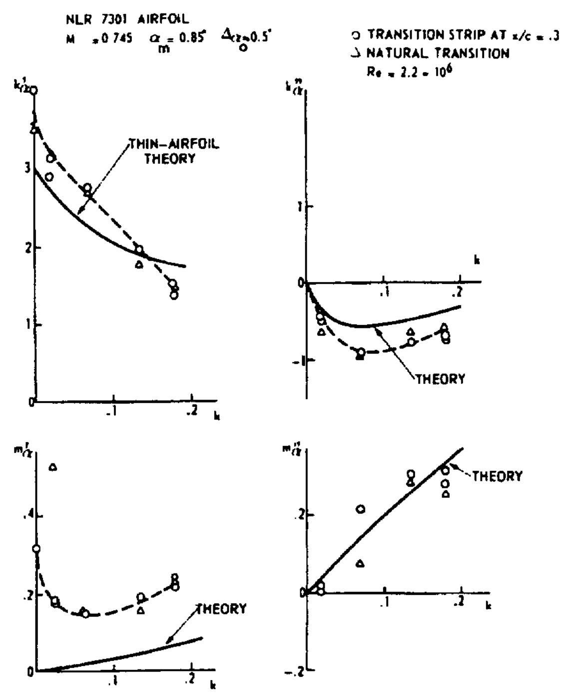

Fig. 4 Unsteady normal-force and moment coefficients as a function of frequency for the "shock-free" design point; pitching oscillation

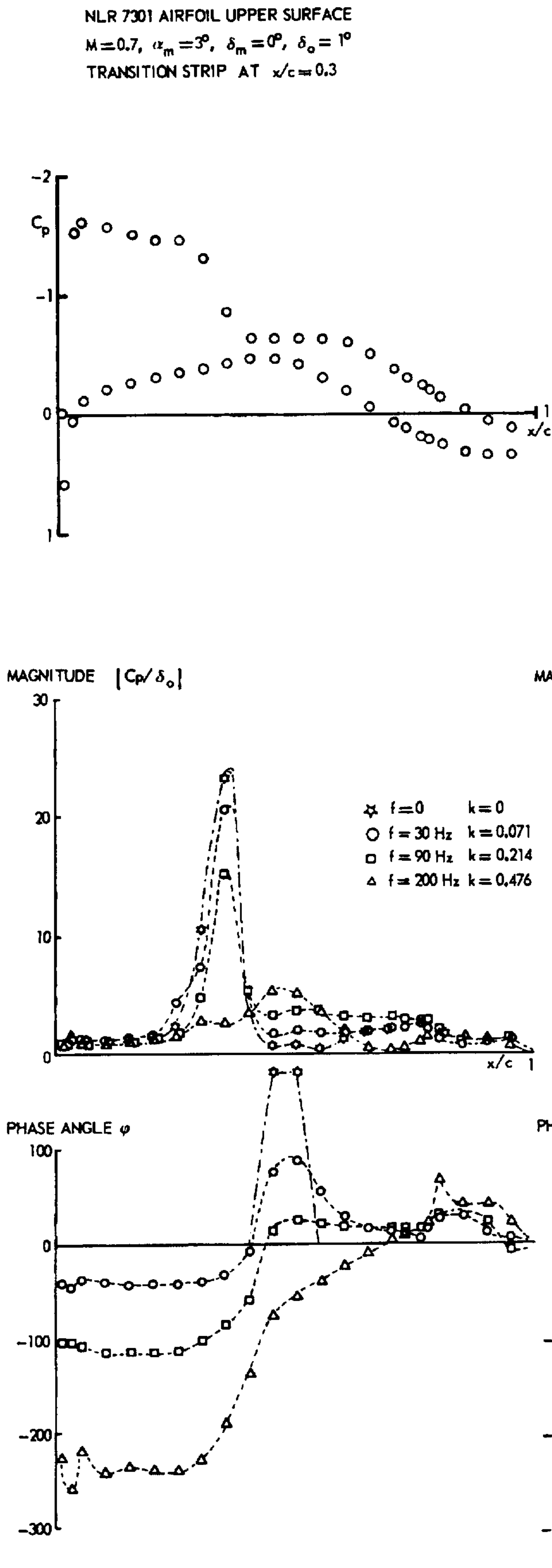

Fig. 5 Effect of shock wave on the unsteady pressure distributions; flap oscillation

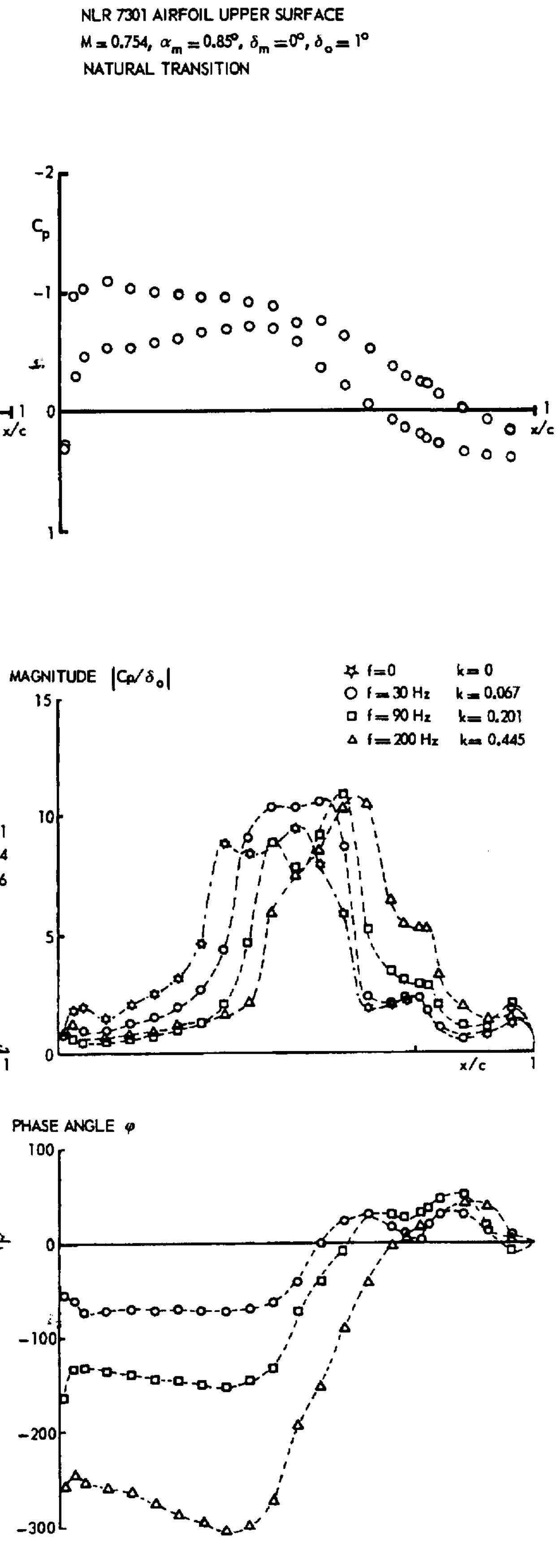

Fig. 6 Unsteady pressure distributions for the "shock-free" design point; flap oscillation

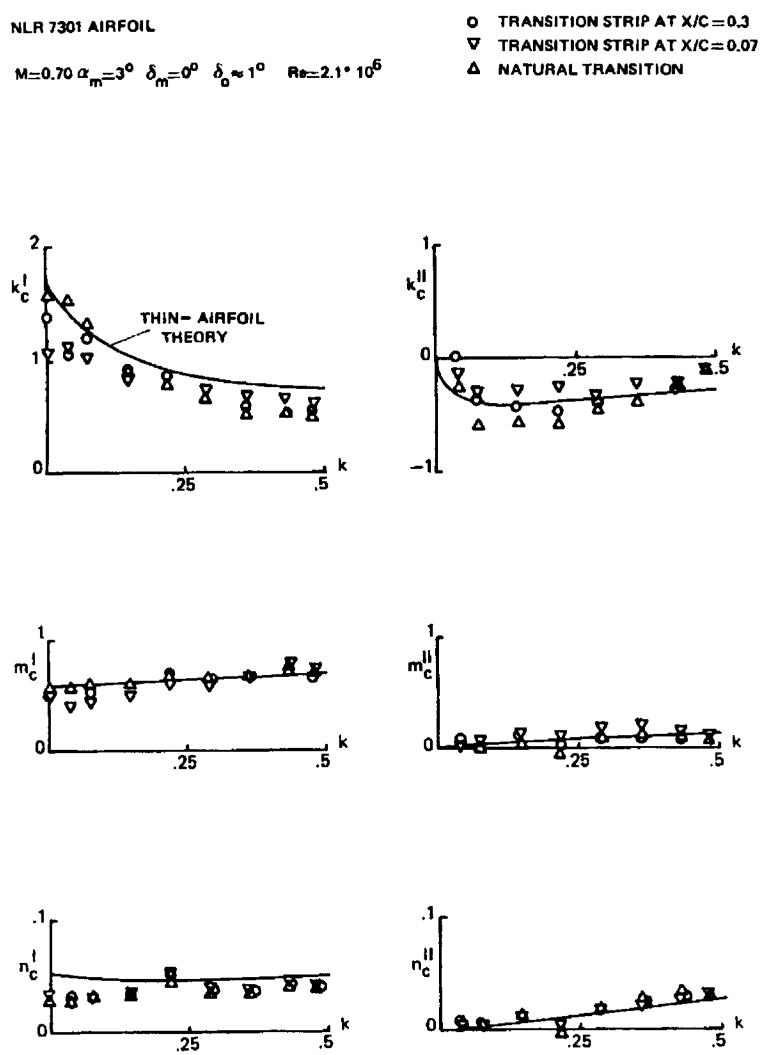

Fig. 7 Unsteady aerodynamic coefficients as functions of frequency in transonic flow with a well-developed shock wave; flap oscillation

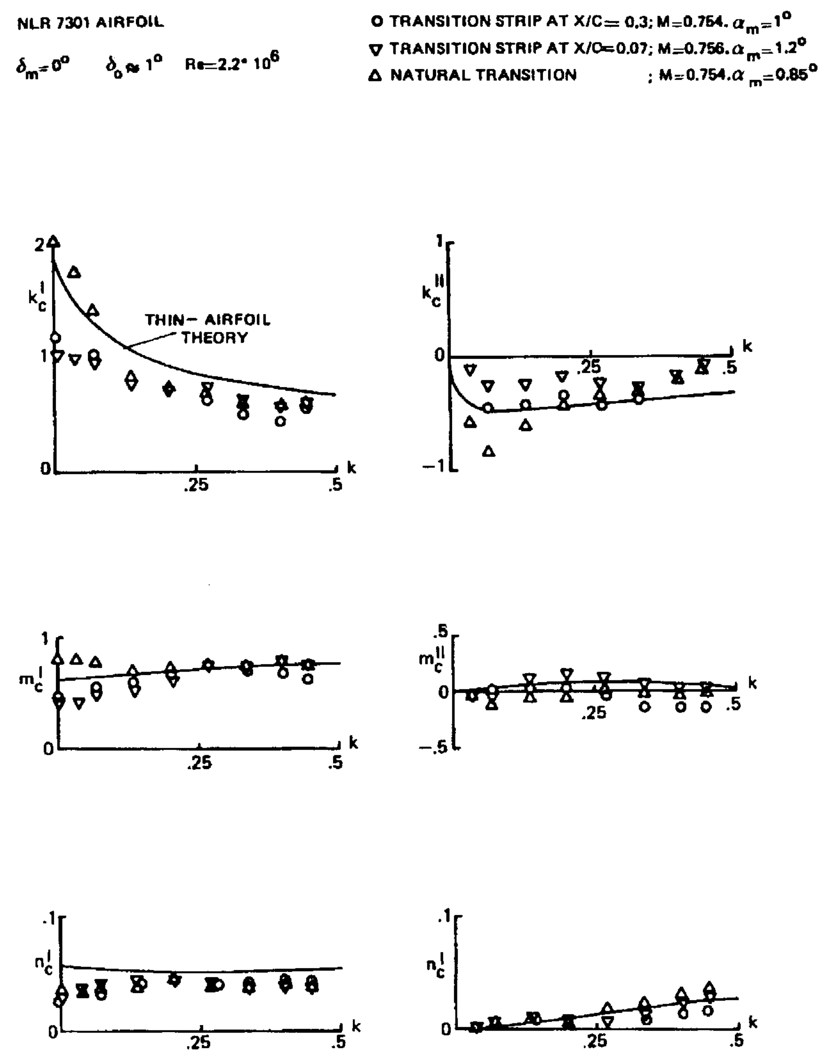

Fig. 8 Unsteady aerodynamic coefficients as functions of frequency for best "shock-free" steady flow; flap oscillation

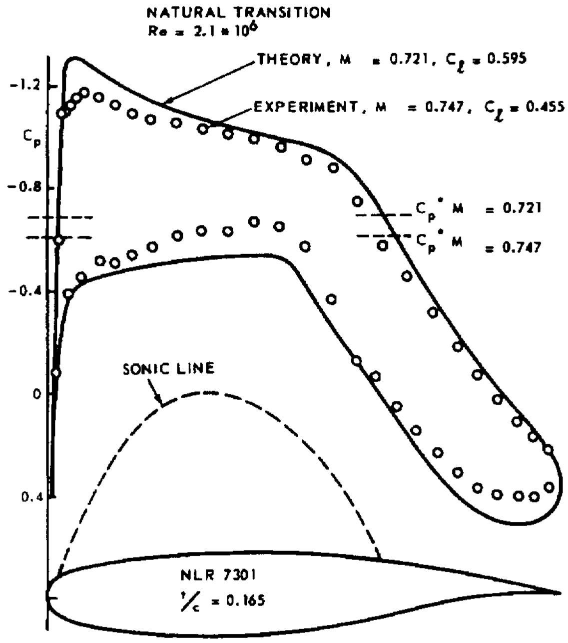

Fig. 9 Theoretical and experimental "shock-free" pressure distributions of the NLR 7301 airfoil (free transition)

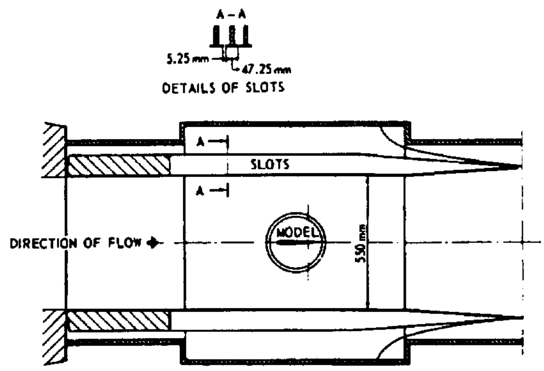

Fig. 10 Transonic test section of the NLR Pilot Tunnel

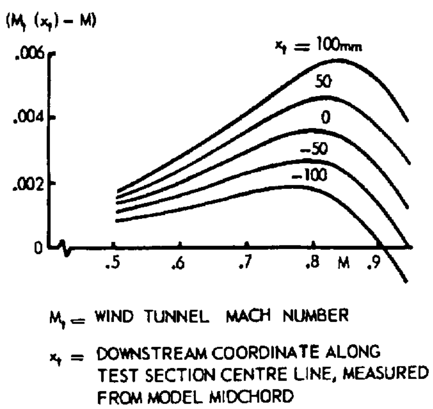

Fig. 11 Mach number distribution in NLR Pilot Tunnel test section

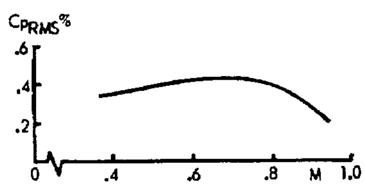

Fig. 12 Noise level in NLR Pilot Tunnel test section

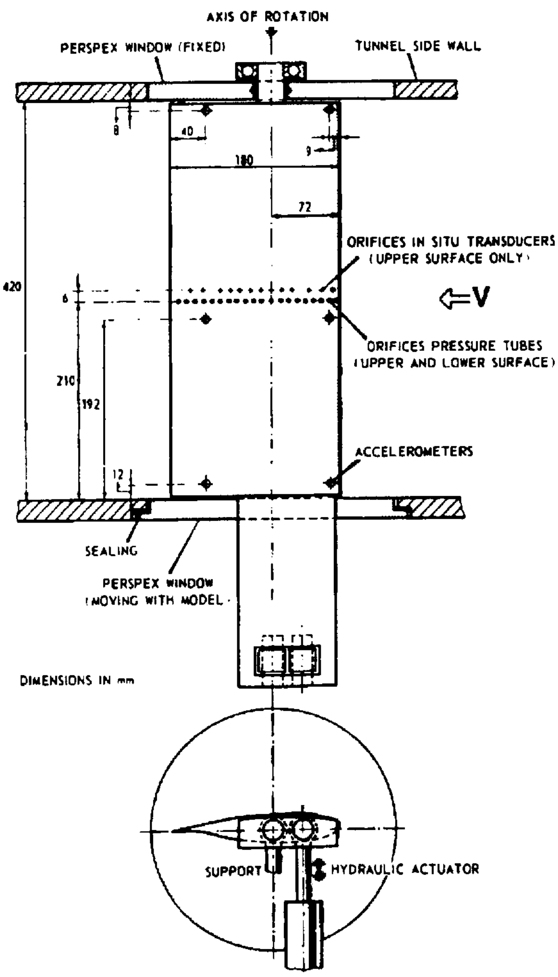

Fig. 13 Test set-up and instrumentation of the NLR 7301 airfoil (Conf. A)

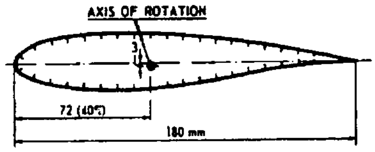

PRESSURE ORIFICES TUBING SYSTEM (BOTH UPPER AND LOWER SURFACE)				IN SITU TRANSDUCERS (UPPER SURFACE ONLY)			
No. 1	x/c = .01	No. 11	x/c = .50	No. 1	x/c = .04	No. 11	x/c = .70
2	.05	12	.55	2	.10	12	.80
3	.10	13	.60	3	.19	13	.88
4	.15	14	.65	4	.28		
5	.20	15	.70	5	.34		
6	.25	16	.75	6	.40		
7	.30	17	.80	7	.46		
8	.35	18	.85	8	.52		
9	.40	19	.90	9	.58		
10	.45	20	.95	10	.64		

Fig. 14 Location of pressure orifices of the NLR 7301 airfoil (Conf. A)

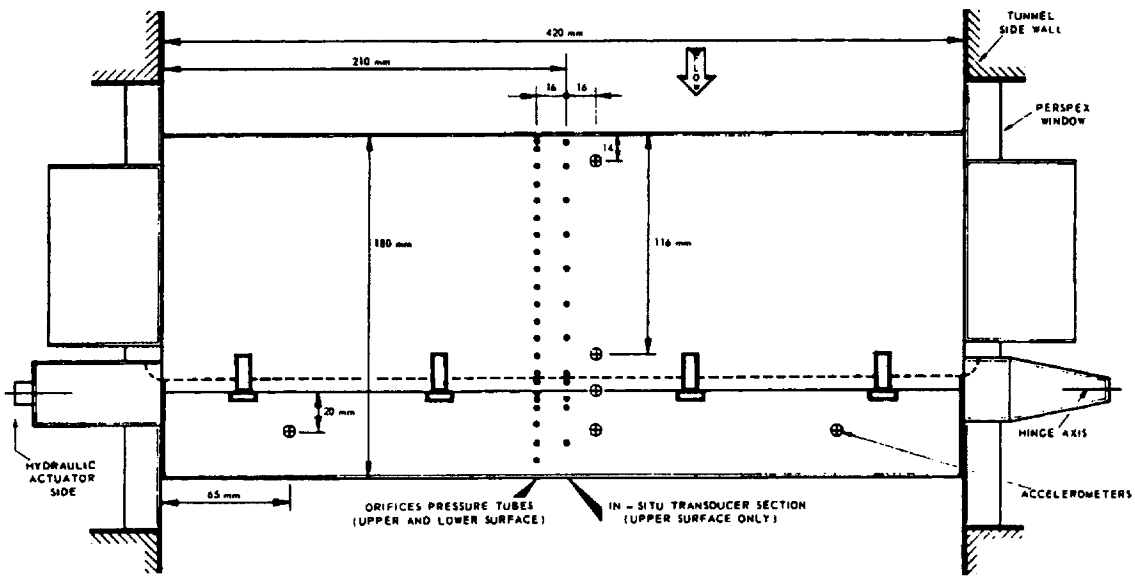

Fig. 15 Test set-up and instrumentation of the NLR 7301 airfoil with control surface (Conf. B)

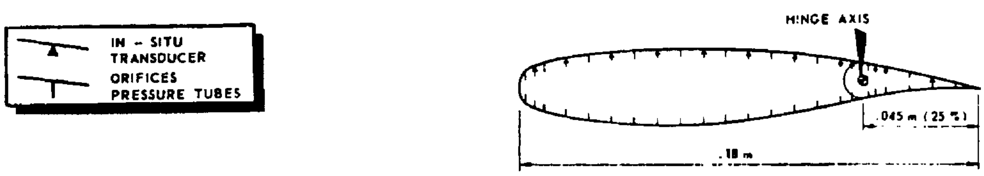

PRESSURE ORIFICES TUBING SYSTEM (both upper and lower surface)				IN SITU TRANSDUCERS (upper surface only)	
no. 1	x/c = .01	no. 13	x/c = .55	no. 1	x/c = .03
2	.03	14	.60	2	.10
3	.05	15	.65	3	.20
4	.10	16	.70	4	.30
5	.15	17	.725	5	.40
6	.20	18	.76	6	.50
7	.25	19	.775	7	.60
8	.30	20	.8	8	.70
9	.35	21	.85	9	.725
10	.40	22	.90	10	.775
11	.45	23	.95	11	.80
12	.50			12	.90

Fig. 16 Location of pressure orifices of the NLR 7301 airfoil with control surface (Conf. B)

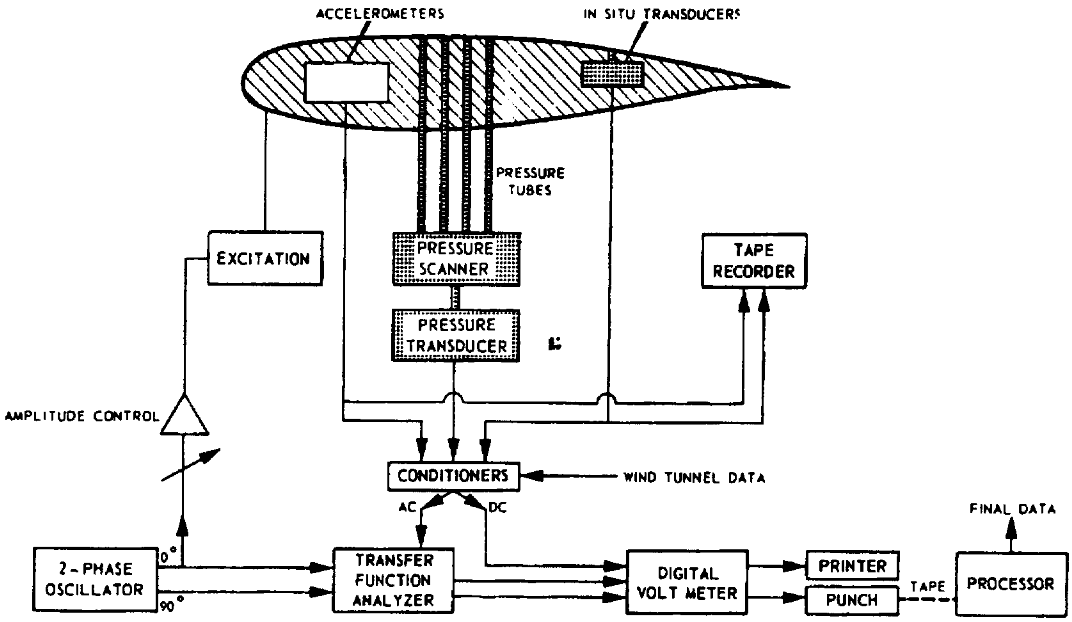

Fig. 17 Block diagram of measuring equipment (Conf. A). Similar equipment essentially for Conf. B

3E8. ZKP WING, OSCILLATING AILERON

by
Dipi. Ing. K.Dau
Dipi. Ing. S.Vogel
Dipi. Ing. H.Zimmermann
MBB Transport und Verkehrsflugzeuge
TE234
Postfach 10 78 45
2800 Bremen 1
Germany

INTRODUCTION

This Data Set contains pressure distributions measured on the ZKP wing for an oscillating aileron in the ONERA transonic 51 wind tunnel at Modane, France, in late 1982. The tests were part of a cooperative project between MBB, ONERA, and the Aerospatiale Corporation. The purpose of the tests was to obtain steady and unsteady pressures due to fast-moving control surfaces in transonic flow, likely to be encountered in the operation of active control systems for transport aircraft.

The following is a number of comments on the diagrams and tables.

GEOMETRY OF EXPERIMENTAL MODEL

The model geometry is shown in Fig. 3 to 5. Figure 3 shows the model including the major dimensions of the half-fuselage in a coordinate system parallel to the tunnel floor and walls. Figure 4 shows the dimensions of the wing and the aileron when rotated by the dihedral angle of 4.787 deg into the plane z = 0 of the coordinate system in which the profile coordinates are given by Ref. 1. Figure 5 shows the details of the aileron geometry in cross-section, including nose and gap geometry.

COMPARISON WITH AGARD COMPUTATIONAL PROGRAMME OF REF. 1

Model geometry

Unlike the computational model (Ref. 1, Fig. 7) the experimental model has a half-fuselage as shown in Fig. 3. This changes the definition of the root chord which is now smaller than the computational root chord because of the taper of the wing (see Fig. 4). The difference in the definition of the root chord affects the specifications of reduced frequency and Reynolds number as shown in Para. 12, NOTATION. Otherwise the two planforms and their coordinate origins are identical. Furthermore, the gap between aileron and wing spar (Fig. 5) of the experimental model was not sealed, as stated in Ref. 1. The gap is 0.3-0.5 mm wide.

Instrumentation

The number and location of the sections at which pressures were measured where changed from the values given in Ref. 1 to those given in Fig. 6.

Design Condition

The design condition of the experimental model is M = 0.78 and α_m = 1.5° as listed in Ref. 1, Sect. 3.4. The experimental lift coefficient may be somewhat different from the listed theoretical value of 0.5 at the design condition, depending on how the fuselage contribution is interpreted.

Experimental Cases

The experimental cases for which data are provided in the Data Set are not identical with the computational test cases originally suggested in Ref.1, Table 9; this may affect the choices for future calculations. The correspondence between the experimental and the original computational cases is shown in Table 2. It will be seen that, of the computational choices, only the three priority cases have closely related experimental cases. No experimental results are available for M = 0.73 to match the computational cases 2 and 3.

TEST SET-UP AND INSTRUMENTATION

The wind tunnel test set-up for measuring unsteady pressures on the wing is shown in Fig.1 and 2. To prevent the wing tip from executing large bending motions due to aileron forces, the wing tip was braced by four cables, all attached to a point of the wing tip, and lying in a plane roughly parallel to the aircraft plane of symmetry. The other ends of the cables were led outside the test section, and preloaded with a two-ton weight each.

Prior to every unsteady run the brakes on all cables were released permitting the wing to assume mean position under aerodynamic load without additional cable constraint, while the new mean test parameters (Mach no., wing and flap incidences) were established. The cables were then clamped, and remained clamped during aileron oscillation.

The aileron was actuated by a hydraulic servo motor producing a harmonic aileron rotation about ts swept hinge axis. The instantaneous aileron displacement was measured relative to the wing by potentiometers in the streamwise direction at the two aileron stations.

The wing was equipped with 509 pressure taps for steady pressures, and 387 Kulite transducers for unsteady pressures. The tap coordinates are listed in Tables 3 to 7 with their corresponding pressures.

The pressure taps were arrayed in streamwise wing sections as shown in Fig.6. For reasons of space the sections containing steady-pressure taps were not congruent with those for unsteady pressures, but are considered to be close enough to reflect flow conditions for the neighboring unsteady pressures with sufficient accuracy for most purposes.

Steady pressures were measured via tubing and scanivalve by tunnel system transducers, unsteady pressures were measured by Kulite transducers installed directly below each pressure tap. Furthermore 17 accelerometers were installed on the wing, one of them on the aileron, see Fig.7.

DATA PROCESSING

Only the fundamental component was recorded for each response signal. Response signal phase was defined to be relative to aileron motion. All listed pressures correspond to an aileron amplitude of $\delta_0=1°$, the aileron deflection angles δ_m, and δ_0 being defined in the streamwise direction.

Both steady and unsteady pressures are presented in uncorrected form. Those pressure values which were obviously spurious (transducer failure, etc.) were eliminated. Besides these data additional data, listed in Table 1, could be made available.

DISCUSSION

The unsteady pressures generally exhibit the distribution typical for ailerons on transport aircraft wings, i.e. they are virtually zero outside the neighborhood of the aileron sections. Therefore only the aileron section pressures are shown as plots against x/c on Fig.8 to 14.

Concerning the sectional lift and moment coefficients, which are listed in the same tables as the pressure distribution from which they were derived, it should be pointed out that they are uncorrected in the sense that no attempt has been made to introduce supplementary points where a pressure peak was obviously not properly defined by the array of pressure taps, see for instance Fig.11, top left plot. Furthermore the integration interval extended only from the first to the last tap on a given section. The section coefficients should therefore be viewed only as a rough guide to the spanwise distribution.

Because of the uncorrected values, the spanwise distribution of load coefficients is likely to show some fluctuation. The wiggle near the wing tip, however, seems to be genuine; and is believed to have been caused by a geometric irregularity behind the aileron gap.

During the course of the test program certain steady test cases were repeated a number of times for nominally the same test parameters. Since repeatability is a good indicator of data quality, the pressures on the mid-aileron section have been plotted on top of each other for a number of nominally identical cases, see Fig.15.

The right-hand plot corresponds to five runs, one of which (case 94) was made entirely without wing-tip cable braces, entailing a tunnel shut-down before the remaining cases were run. In spite of the shut-down, repeatability may be said to be very good. The left-hand plot shows pressures for a larger number of repetitions for the same case, with two intervening shut-downs. Agreement here is still good, but two runs show a marked deviation from the mean near the hinge position, which is known to be sensitive to changes in flow parameters. The two runs in question were separated by two shut-downs from the other runs of the series.

No comparable repetitions were made for unsteady pressures, but they are felt to be of the same quality as the steady ones.

LIST OF SYMBOLS AND DEFINITIONS

ALPHA	α_m	mean wing incidence, as defined in 5.9
C	c	local chord
CL	c_l	sectional lift coefficient
CM	c_m	sectional moment coefficient about quarter-chord point
CPL	C_p	lower surface
CPU	C_p	upper surface
CPL/RAD		lower surface) unsteady pressure coefficients
CPU/RAD		uppersurface) per unit amplitude
DELM	δ_m	mean streamwise aileron angle
	δ_0	streamwise aileron angle amplitude of oscillation
FREQ	f	frequency
K		reduced frequency based on half-chord at wing-body junction, AGARD k = 1.197k
PTOT	p	total pressure
QINF	q	dynamic pressure

RE		Reynolds number, based on chord at wing-body junction, AGARD Re = 1.197 Re
S	s	semi-span
T0	T_o	total temperature of flow
X/C		non-dimensional chordwise position aft of local leading edge
Y/S	η	spanwise position relative to plane of symmetry

PRESENTATION OF DATA

The data which were presented in tables 3 to 7 of Report 702 for this test are supplied here as a single ASCII data file SET8.UND in RUNAD format as defined in the introduction to chapter 3. The table numbers are used as the "run numbers" for data selection by the program RUNAD. Also supplied as an ASCII file SET8.TAB containing the data formatted into tables.

FORMULARY

General Description of model

1.1	Designation	ZKP Wing
1.2	Type	Half-model of wing fuselage combination, transport aircraft with oscillating aileron, no tail surfaces
1.3	Derivation	Research wing, representative of a medium-range transport aircraft with a supercritical wing
1.4	Additional remarks	None
1.5	References	None

Model Geometry

2.1	Planform	high aspect ratio, tapered
2.2	Aspect ratio	9
2.3	Leading edge sweep	30.08°
2.4	Trailing edge sweep	20.89° for outer wing
2.5	Taper ratio	0.26
2.6	Twist	washout type, see ref. 1, table 4
2.7	Root chord	1.5055m
2.8	Semi-span of model	4.0161m
2.9	Area of planform	$3.5989m^2$
2.10	Location of reference sections and definition of profiles	15%, 40%, and 85% semi-span (see ref.1 section 2.4)
2.11	Lofting procedure between reference sections	Linear on constnat-chord lines between reference sections (ss ref.1, section 2.4)
2.12	Form of wing-body junction	Gap between half-fuselage and floor sealed with brushes
2.13	Form of wing tip	rounded
2.14	Control surface details	unsealed aileron-wing gap about 0.3 to 0.5 mm wide (see fig.5)
2.15	Additional remarks	None
2.16	References	None

Wind Tunnel

3.1	Designation	ONERA S1 transonic tunnel, Modane, France
3.2	Type of tunnel	Closed circuit, ambient pressure
3.3	Test section dimensions	6.855m high and wide, 14.0m long (see fig.1 and 2)
3.4	Type of roof and floor	Solid, excpet for 2 slots (see also fig.1 and 2)
3.5	Type of side walls	Solid

3.6	Ventilation geometry	One slot each at intersection of floor with wind tunnel shell, 0.13m wide, running from 5m to 9m from test section entrance
3.7	Thickness of side wall boundary layer	about 0.1m
3.8	Thickness of boundary layers at roof and floor	about 0.1m
3.9	Method of measuring Mach number	by measurement of static pressure, 4.5m upstream of test section, and by previous calibration
3.10	Flow angularity	Not measured
3.11	Uniformity of velocity over test section	Not measured
3.12	Sources and levels of noise or turbulence in empty tunnel	Considered very small
3.13	Tunnel resonances	At f = N/5, N/6, N/5 + N/6, N=246 M
3.14	Additional remarks	None
3.15	References on tunnel	None

Model motion

4.1	General description	Aileron oscillation with braced wing tip. Amplitude 1 ° and 2°, frequency 6, 12, 21 Hz.
4.2	Natural frequencies and normal modes of model and support system	15.6, 27.3, 44.4 Hz with cable braces

Test Conditions

5.1	Model planform area/tunnel area	0.08
5.2	Model span/tunnel width	0.5858
5.3	Blockage	NA
5.4	Position of model in tunnel	x-mac 6.19m downstream of test section inlet (see fig.1)
5.5	Range of Mach number	0.5, 0.78, 0.83
5.6	Range of tunnel total pressure	0.9 bar
5.7	Range of tunnel total temperature	298 to 322° K
5.8	Range of model steady or mean incidence	-1 to +3°
5.9	Definition of model incidence	The model incidence α_m is defined to be zero when the fuselage reference line (FRL) is parallel to the tunnel walls. The FRL lies in the plane z=0 of the profile coordinate system as listed in ref.1.
5.10	Position of transition, if free	No
5.11	Position and type of trip, if transition fixed	x/c=0.07, upper and lower wing surface, 5mm wide band of 80K carborundum. Same type of trip on fuselage, 105mm from nose.
5.12	Flow instabilities during tests	None detected
5.13	Changes to mean shape of model due to steady aerodynamic load	Not measured
5.14	Additional remarks	None
5.15	References describing tests	None

Measurements and Observations

6.1	Steady pressures for the mean conditions	Y
6.2	Steady pressures for small changes from the mean conditions	Y
6.3	Quasi-steady pressures	6 Hz
6.4	Unsteady pressures	Y
6.5	Steady section forces for the mean conditions by integration of pressures	Y
6.6	Steady section forces for small changes from	N

	the mean conditions by integration	
6.7	Quasi-steady section forces by integration	6 Hz
6.8	Unsteady section forces by integration	Y
6.9	Measurement of actual motion at points of model	Y
6.10	Observation or measurement of boundary layer properties	N
6.11	Visualisation of surface flow	N
6.12	Visualisation of shock wave movements	N
6.13	Aditional remarks	None

Instrumentation

7.1	Steady pressure	
	7.1.1 Position of orifices spanwise and chordwise	See fig.6 and tables 3 to 7.
	7.1.2 Type of measuring system	Taps connected via tubing and Scanivalve to tunnel system transducers
7.2	Unsteady pressure	
	7.2.1 Position of orifices spanwise and chordwise	See fig.6 and tables 3 to 7.
	7.2.2 Diameter of orifices	0.3mm
	7.2.3 Type of measuring system	Transducer installed directly below each tap.
	7.2.4 Type of transducers	Kulite
	7.2.5 Principle and accuracy of calibration	Calibrated by 30 Hz sinusoidal signal before tests. Checked at various intervals during testing. Variation less than 1%.
7.3	Model motion	
	7.3.1 Method of measuring motion reference coordinate	Aileron angle measured relative to wing structure by rotary potentiometers on aileron. Aileron harmonic rotation about swept axis at the 77.4% chord line, measured at inboard and centre aileron section.
	7.3.2 Method of determining spatial mode of motion	By accelerometers on wing and aileron, and potentiometers on aileron.
	7.3.3 Accuracy of measured motion	2%
7.4	Processing of unsteady measurements	
	7.4.1 Method of acquiring and processing measurements	Signal digitized (12 bit ADC) and Fourier transformed. Transfer function for motion-pressure by HP 5451 Analyzer.
	7.4.2 Type of analysis	Only one harmonic kept.
	7.4.3 Unsteady pressure quantities obtained and accuracies achieved	Presented data are amplitudes of fundamental of all response signals. Response phases are defined relative to zero aileron deflection.
	7.4.4 Method of integration to obtain forces	Cubic spline, uncorrected for possible missed peaks. Integration interval between first and last pressure taps on section.
7.5	Additional remarks	None
7.6	References on techniques	None

Data presentation

8.1	Test cases for which data could be made available	Table 1.
8.2	Test cases for which data are included in this document	Table 2.
8.3	Steady pressures	Tables 3 to 7.
8.4	Quasi-steady or steady perturbation	6 Hz, unsteady pressures

	pressures	
8.5	Unsteady pressures	Tables 3 to 7.
8.6	Steady forces or moments	Tables 3 to 7.
8.7	Quasi-steady or unsteady perturbation forces	6 Hz, unsteady loads
8.8	Unsteady forces and moments	Tables 3 to 7.
8.9	Other forms in which data could be made available	Magnetic tape
8.10	Reference giving other representations of data	2

Comments on data

9.1	Accuracy	
	9.1.1 Mach number	About 0.002
	9.1.2 Steady incidence	About 0.1°
	9.1.3 Reduced frequency	About 2%
	9.1.4 Steady pressure coefficients	See discussion and fig.15
	9.1.5 Steady pressure derivatives	Not calculated
	9.1.6 Unsteady pressure coefficients	See discussion
9.2	Sensitivity to small changes of parameter	Not calculated
9.3	Non-linearities	None detected
9.4	Influence of tunnel total pressure	Total pressure was kept constant
9.5	Effects on data of uncertainty, or variation, in mode of model motion	Not checked
9.6	Wall interference corrections	All pressures are uncorrected
9.7	Other relevant tests on same model	None
9.8	Relevant tests on other models of nominally the same shapes	None
9.9	Any remarks relevant to comparison between experiment and theory	None
9.10	Additional remarks	None
9.11	References on discussion of data	2

Personal contact for further information

Dipl. Phys. H Zimmermann, MBB-Bremen, Abt. TE234 Hunefeldstr. 1-5, 2800 Bremen, Germany

List of references

1 S R Bland. AGARD three-dimensional aeroelastic configurations. AGARD Advisory Report 167, March 1982.

2 M Couston, J J Angelini, J P Meurzec. Compariason des champs de pression instationnaires calcules et mesures sur le modele ZKP. AGARD R-688, April 1980 (Also available as RAE Library translation 2061, November 1980).

Table 1 List of run numbers available

Run parameters						Run indices			
M	p_t (bar)	T_o (°K)	α_m (°)	δ_m (°)	δ_o (°)	Steady	6 Hz	12 Hz	21 Hz
0.50	0.9	297.7	3	-5	1	21	18	-	21
0.50	0.9	297.7	3	0	1	26	23	25 *	26
0.50	0.9	297.7	3	10	1	33	31	-	33
0.78	0.9	311.3	-1	-5	1	58	56	-	58
0.78	0.9	315.9	-1	0	1	75	61	64	75
0.78	0.9	317.4	-1	0	2	144	63	144	-
0.78	0.9	320.8	-1	5	1	80	78	-	80
0.78	0.9	322.6	0	-5	1	90	88	-	90 *
0.78	0.9	322.7	0	0	1	97	94	96	97 *
0.78	0.9	319.2	0	0	2	143	95	143	-
0.78	0.9	322.0	0	5	1	102	-	-	102
0.78	0.9	318.0	2	-5	1	109	107	-	109
0.78	0.9	319.2	2	0	1	116	112	115	116 *
0.78	0.9	316.5	2	0	2	145	114	145	-
0.78	0.9	319.4	2	5	1	119	119	-	121
0.83	0.9	321.6	0	-2	1	141	131	137	140 *
0.83	0.9	321.6	0	0	1	143	133	138	141
0.83	0.9	322.2	0	2	1	145	135	139	142

Note: the starred case numbers correspond to data in tables 3 to 7.

Table 2 Experimental cases for which data are included, related to computational cases of ref 1

Note that amplitude δ_o=1° for all these cases. * indicates priority case

Experimental Case						Computational Case				
Run Index	M	α_m (°)	δ_m (°)	f (Hz)		Case No.	M	α_m (°)	δ_m (°)	f (Hz)
25	0.50	3	0	12		1	0.30	0	-4.60	10
97	0.78	0	0	21		4 *	0.78	0	0	20
90	0.78	0	-5	21		5 *	0.78	0	-5.52	20
116	0.78	2	0	21		6 *	0.78	2	0	20
140	0.83	0	-2	21		7	0.83	0	-5.52	20

Run details for data supplied on electronic media.

Note that table number is used as the reference number in selection program RUNAD.

Table 3	Run index =25	M=0.50	α_m=3°	δ_m =0°	f= 12 Hz
	K=0.336	PTOT=0.900 bar	QINF = 0.133 bar	RE= 0.134E8	T0=297.85 ° K
Table 4	Run index =97	M=0.78	α_m=0°	δ_m =0°	f= 21 Hz
	K=0.375	PTOT=0.900 bar	QINF = 0.255 bar	RE= 0.163E8	T0=322.65 ° K
Table 5	Run index =90	M=0.78	α_m=0°	δ_m =-5°	f= 21 Hz
	K=0.375	PTOT=0.900 bar	QINF = 0.254 bar	RE= 0.163E8	T0=322.55 ° K
Table 6	Run index =116	M=0.78	α_m=2°	δ_m =0°	f= 21 Hz
	K=0.377	PTOT=0.900 bar	QINF = 0.254 bar	RE= 0.165E8	T0=319.15 ° K
Table 7	Run index =140	M=0.83	α_m=0°	δ_m =-2°	f= 21 Hz
	K=0.355	PTOT=0.900 bar	QINF = 0.275 bar	RE= 0.169E8	T0=322.55 ° K

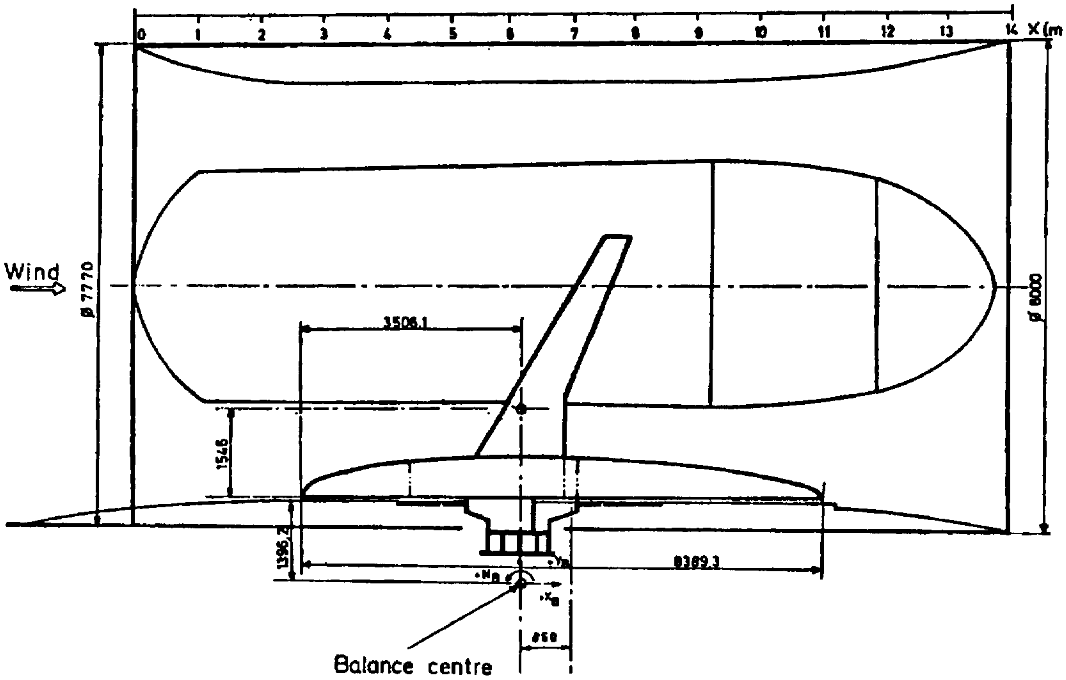

FIG. 1 Model set-up in test section, side view

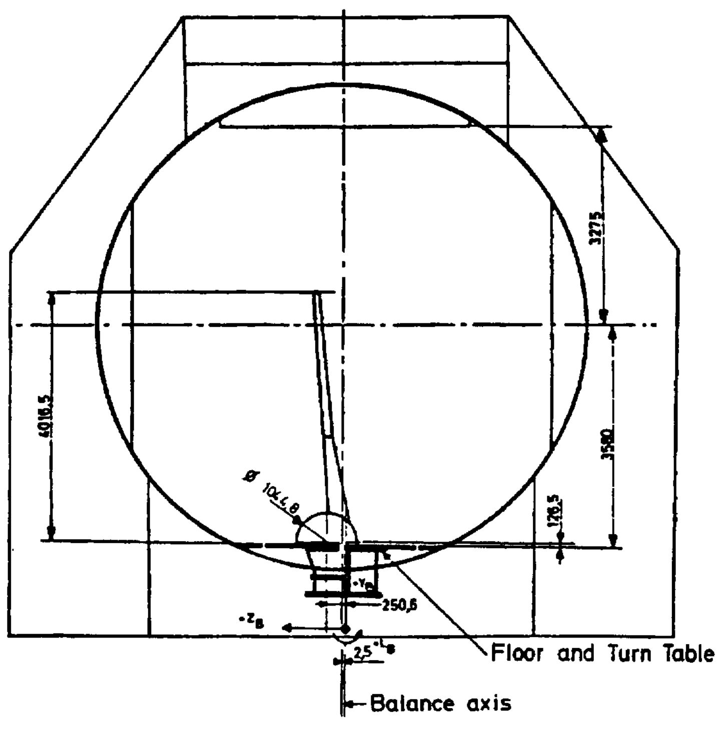

FIG. 2 Model set-up in test section, head-on view

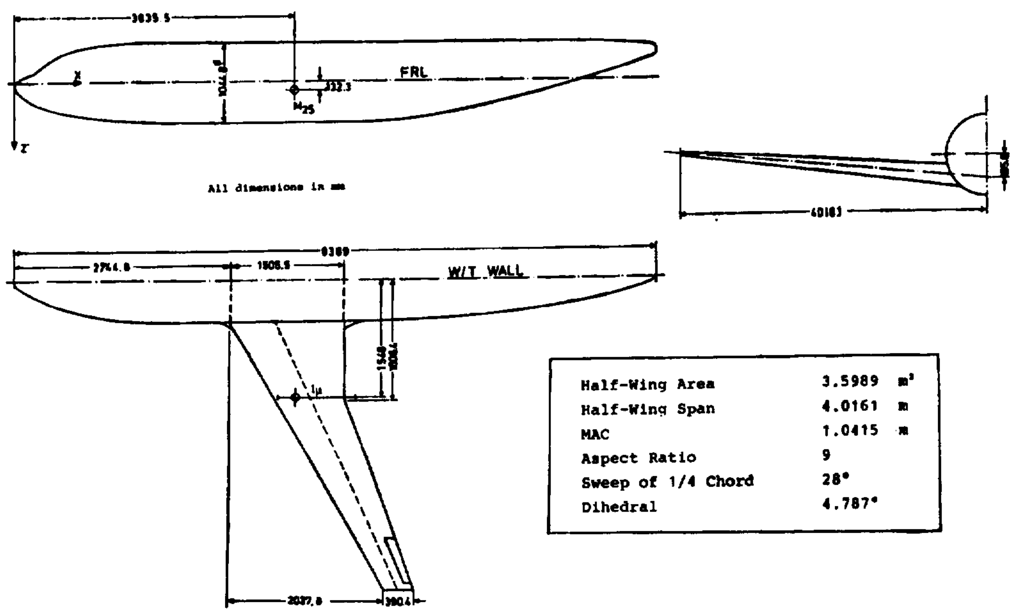

Half-Wing Area	3.5989 m²
Half-Wing Span	4.0161 m
MAC	1.0415 m
Aspect Ratio	9
Sweep of 1/4 Chord	28°
Dihedral	4.787°

FIG. 3 Geometry of experimental ZKP model

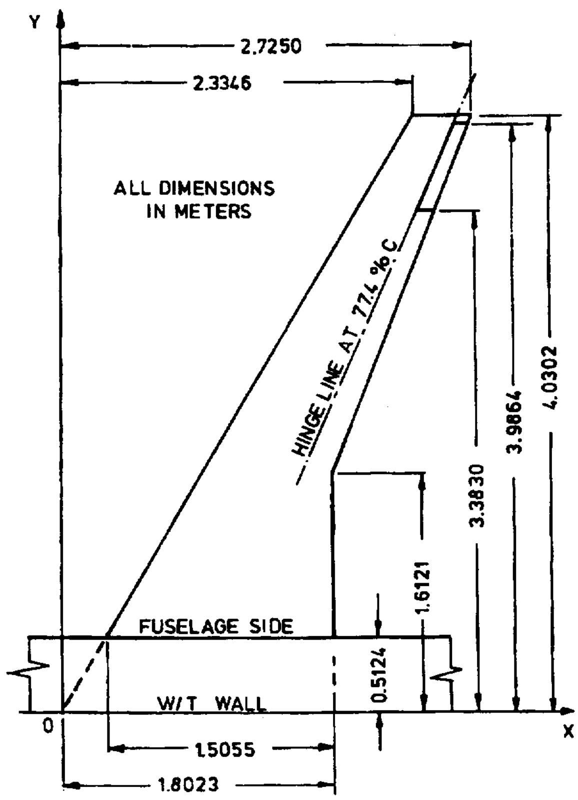

FIG. 4 Geometry of experimental ZKP wing, rotated into profile-coordinate plane by dihedral angle φ = 4.787 deg

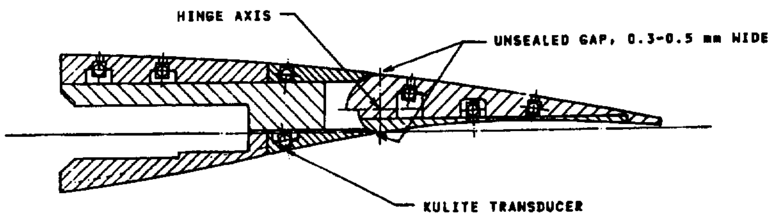

FIG. 5 Aileron geometry in cross-section at wing section 14

Steady press. taps		
Section	η	Number
DV1	0.250	45
DV2	0.357	45
DV3	0.450	3
DV4	0.483	56
DV5	0.528	2
DV6	0.573	53
DV7	0.588	3
DV8	0.618	52
DV9	0.669	56
DV10	0.703	2
DV11	0.755	54
DV12	0.800	2
DV13	0.850	65
DV14	0.889	45
DV15	0.940	46

Unsteady press. taps		
Section	η	Number
K1	0.264	31
K2	0.363	31
K3	0.450	18
K4	0.479	32
K5	0.528	19
K6	0.589	34
K7	0.584	5
K8	0.618	31
K9	0.665	37
K10	0.700	20
K11	0.751	35
K12	0.800	18
K13	0.854	28
K14	0.886	23
K15	0.944	23

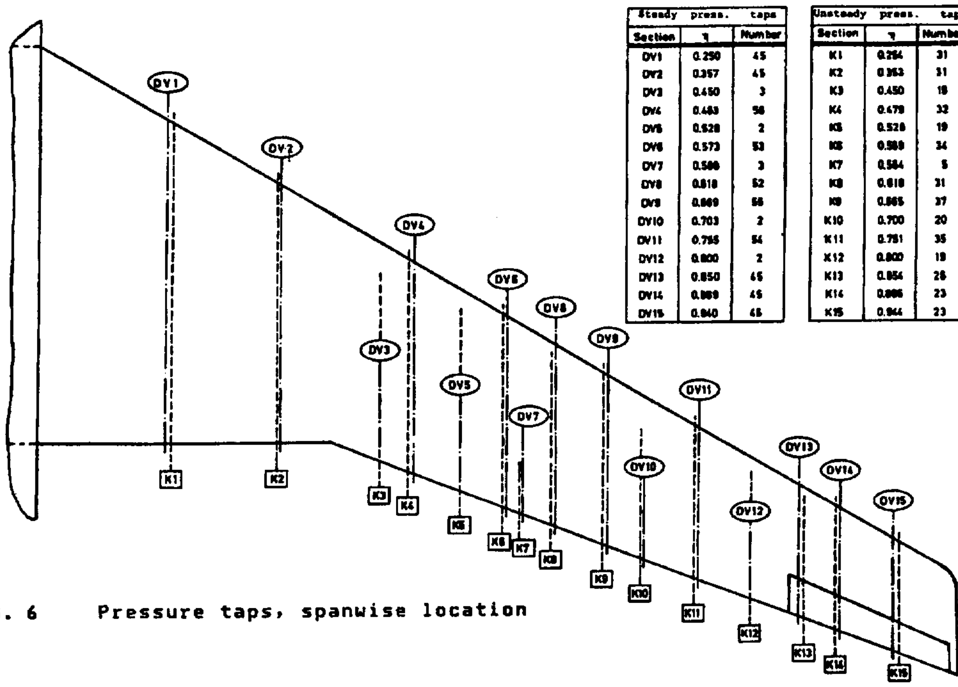

FIG. 6 Pressure taps, spanwise location

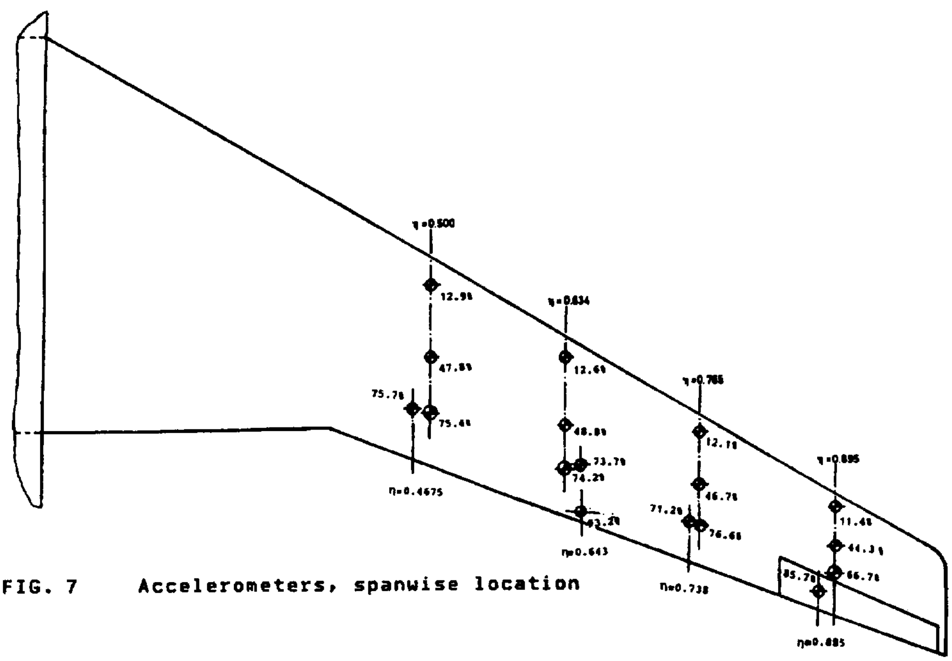

FIG. 7 Accelerometers, spanwise location

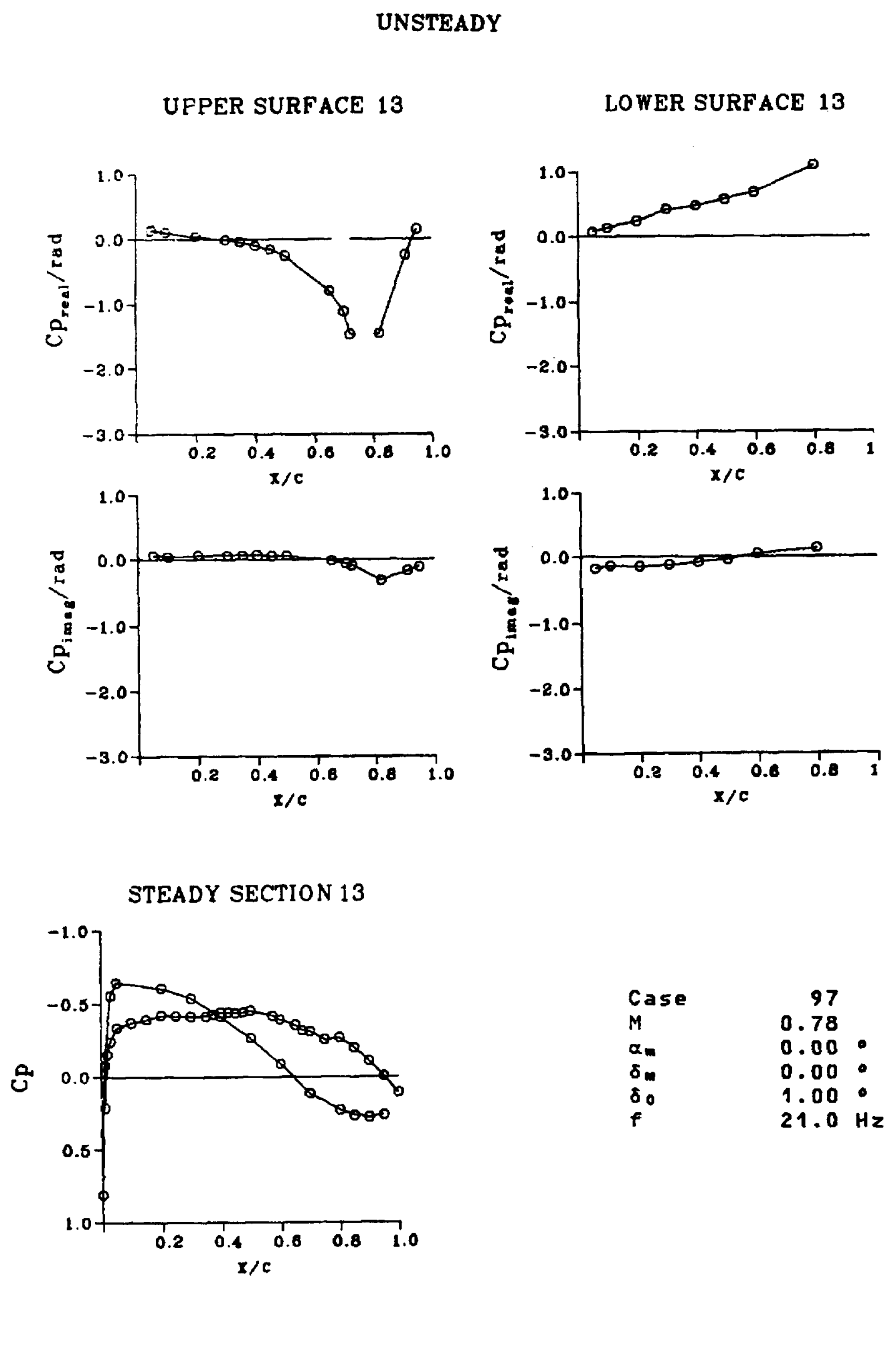

FIG. 8 Sample pressure distribution for aileron section

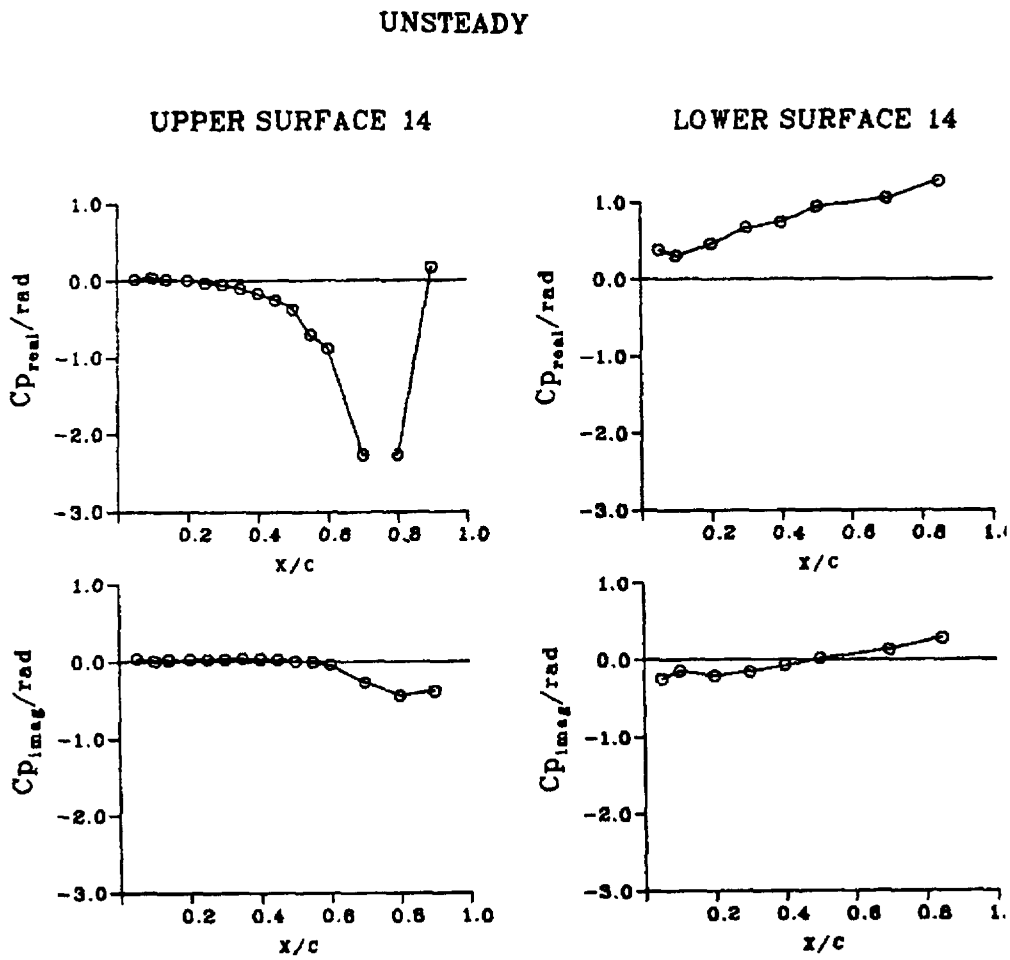

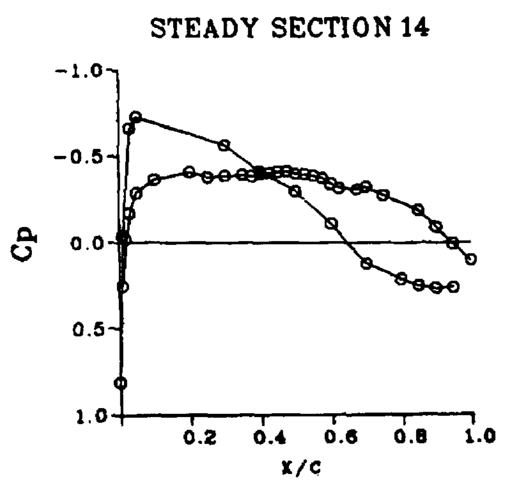

Case	97
M	0.78
α_m	0.00 °
δ_m	0.00 °
δ_0	1.00 °
f	21.0 Hz

FIG. 9 Sample pressure distribution for aileron section

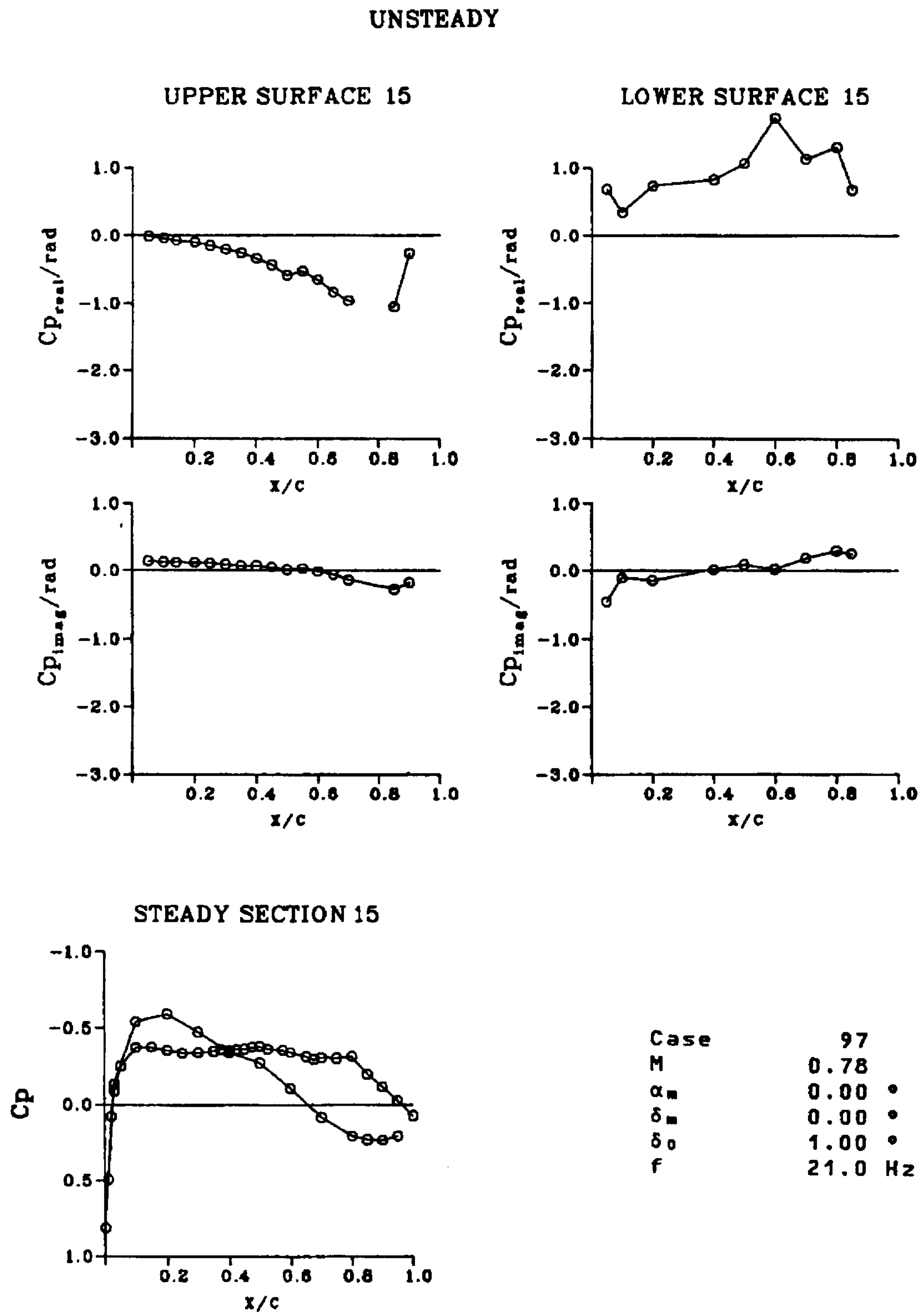

FIG. 10 Sample pressure distribution for aileron section

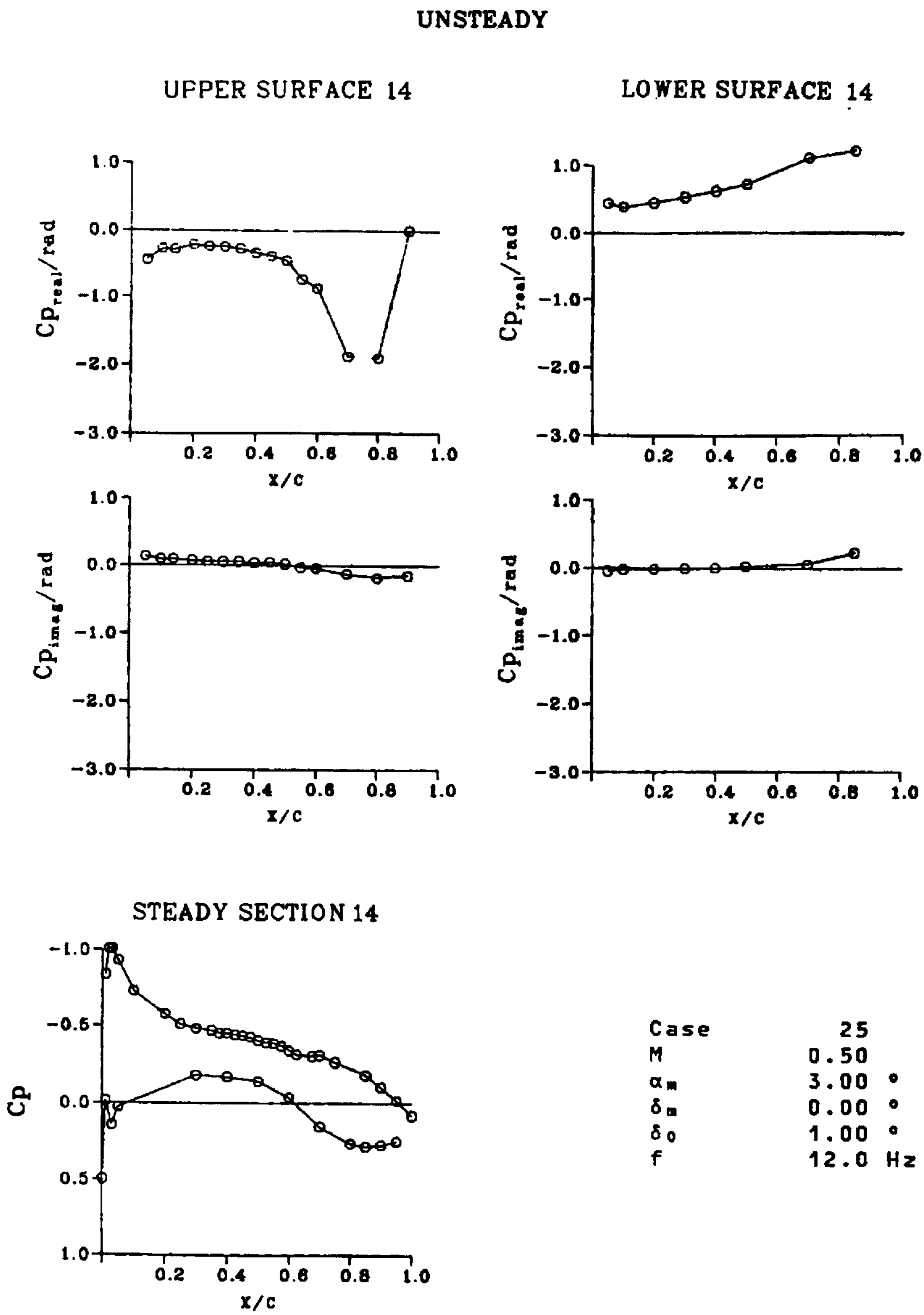

FIG. 11 Sample pressure distribution for aileron section

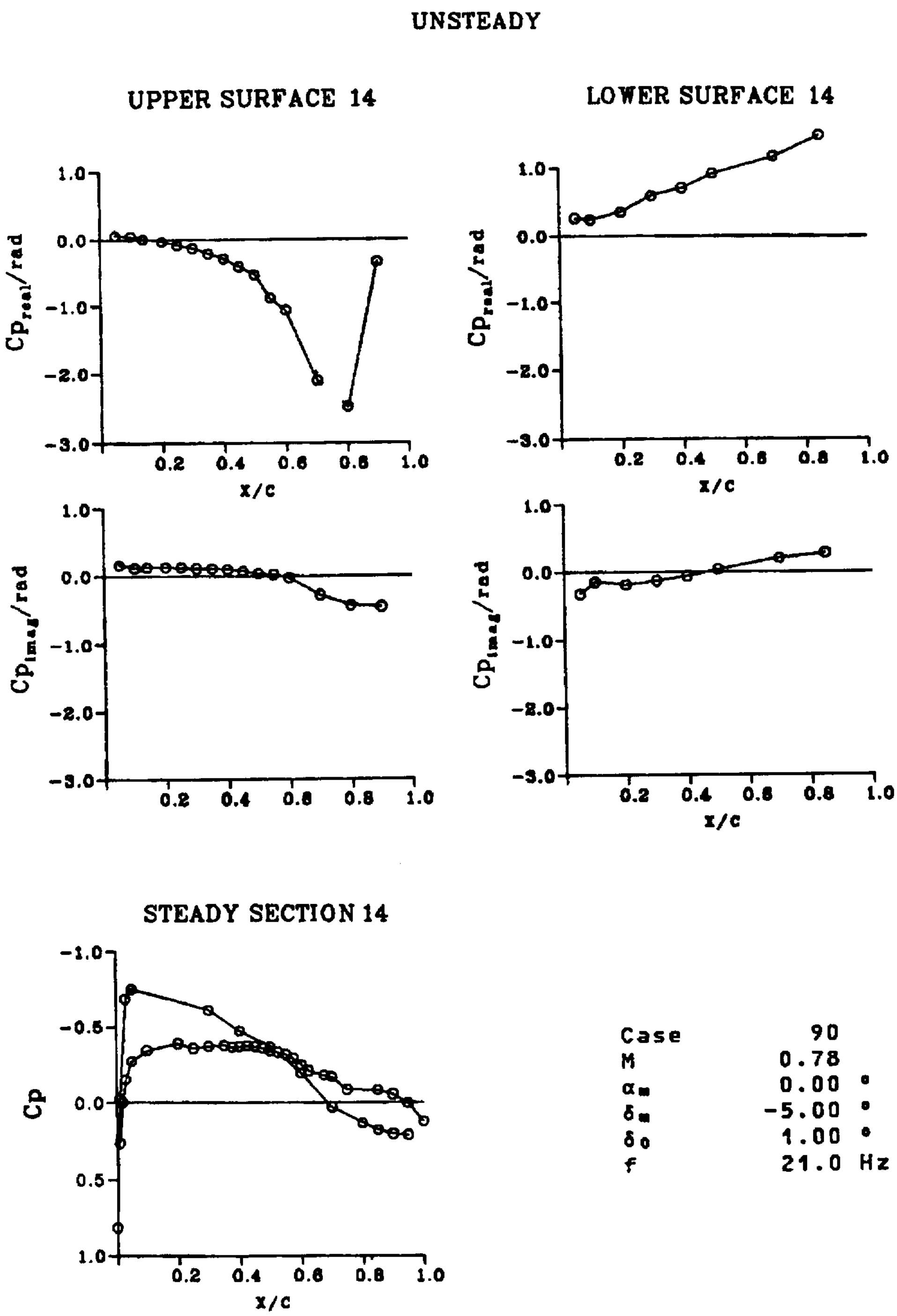

FIG. 12 Sample pressure distribution for aileron section

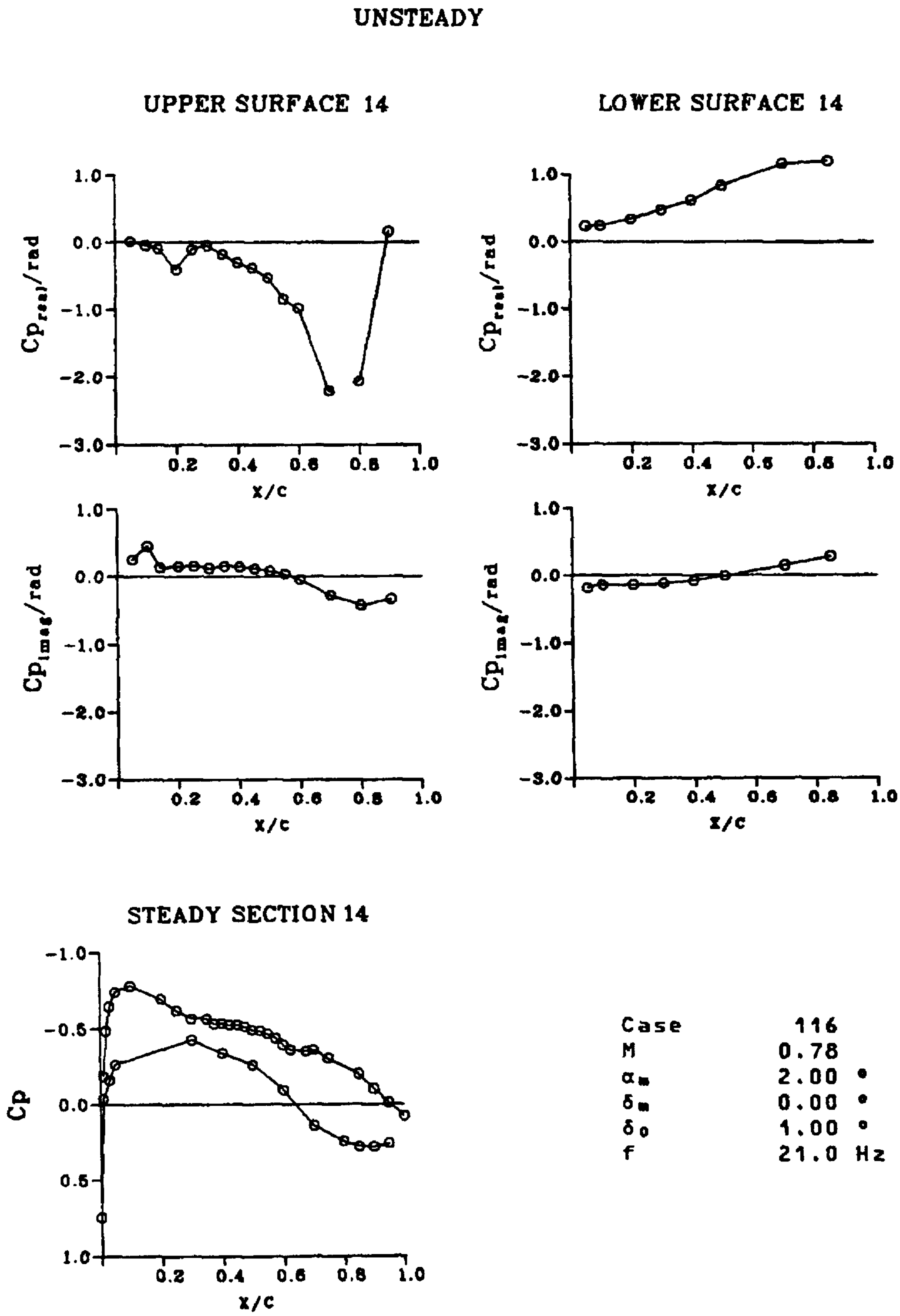

FIG. 13 Sample pressure distribution for aileron section

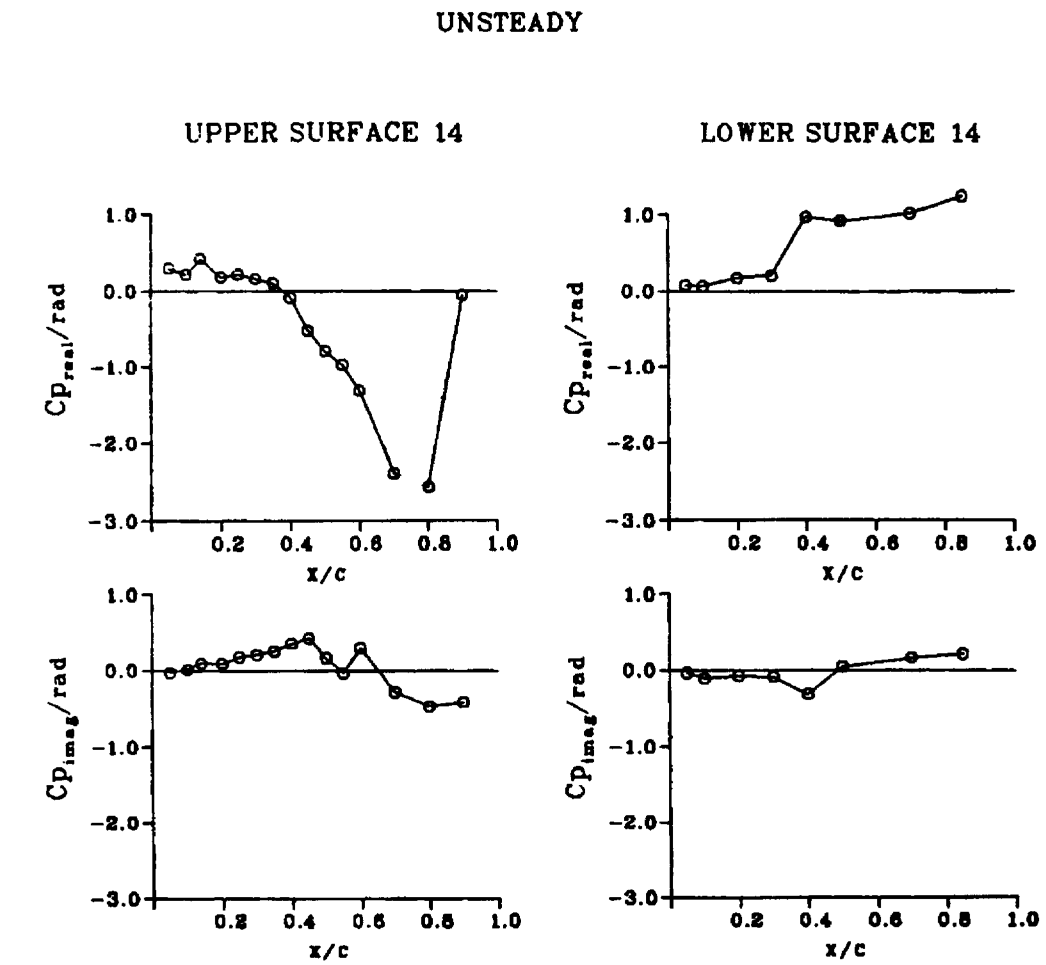

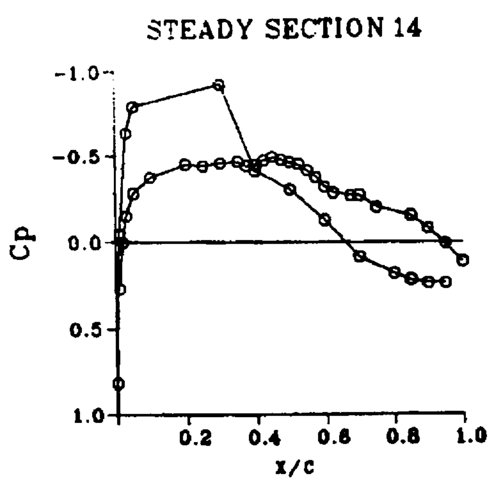

Case	140	
M	0.83	
α_m	0.00	°
δ_m	-2.00	°
δ_0	1.00	°
f	21.0	Hz

FIG. 14 Sample pressure distribution for aileron section

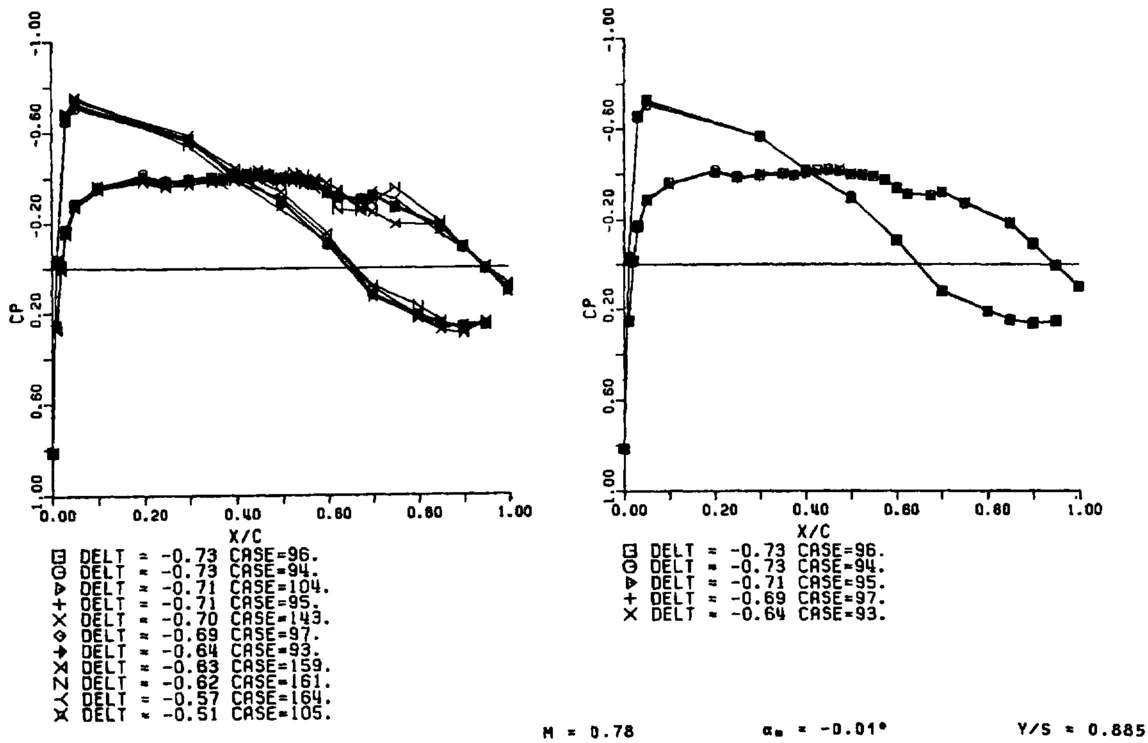

FIG. 15 Repeatability check for various cases

4. F-5 CFD RESULTS

Michael J de C Henshaw
British Aerospace (Operations) Ltd.
Military Aircraft and Aerostructures,
Brough, East Riding of Yorkshire,
HU15 1EQ
UK
michael.henshaw@bae.co.uk

Stephane Guillemot
Dassault Aviation
78, Quai Marcel Dassault,
F-92214, Saint Cloud,
CEDEX
France
stephane.guillemot@dassault-aviation.fr

NOMENCLATURE

α	Angle of attack (deg.)
κ	Reduced frequency ($=\pi F C_r / V_\infty$)
θ	Maximum pitch angle (deg.)
η	Normalised spanwise co-ordinate (=y/s)
$\overline{C}$	Mean geometric chord (=0.4183m)
C_l	Lift coefficient
Cp	Pressure coefficient (see definitions in chapter 5)
CpImag	Imaginary part of pressure coefficient for unsteady pressures (see definitions in chapter 5)
CpReal	Real part of pressure coefficient for unsteady pressures (see definitions in chapter 5)
C_r	Root chord (=0.6396 m)
F	Frequency of modal oscillation (Hz)
M	Mach number
Re	Reynold's number based on the mean geometric chord.
s	Span of wing
V_∞	Free-stream velocity (m/s)
y	Spanwise co-ordinate
Y+	Normalised wall distance of first cell height

INTRODUCTION

The F-5 test series (see chapter 5) provides a succession of geometries of increasing complexity [Ref. 1, Ref. 2], which will be useful for validating CFD codes during their development. In this chapter a range of CFD results are provided for the clean wing configuration at selected flow conditions, and a more limited set for one complex configuration. Results from essentially state of the art UTSP (Unsteady Transonic Small Perturbation), Full Potential, Euler, and NS (Navier-Stokes) codes are presented, this will allow the reader to gauge anticipated modelling accuracy for code development purposes. Table 1 summarises the methods used by contributors reported herein, the methods themselves are described in a standard pro-forma and the results collated as a series of plots. The flow conditions calculated are summarised in Table 2 and Table 4. Two or more methods are presented for each level of modelling approximation in order to assist the reader in gauging the likely level of variation in solution at a particular level of approximation.

Level of approximation	Contributor organisation	Method name/ identification label	Method type
UTSP	BAe.	UTSPV21	Cartesian/finite difference
UTSP	NASA	CAP-ASP	Cartesian/finite difference
Full Potential	CIRA	HELIFP	Structured/finite volume
Full Potential	Dassault Aviation	TCITRON	Structured/finite difference
Euler	INTA	EUL3DU	Structured/explicit/multiblock
Euler	Glasgow University	PMB3D	Structured multiblock/implicit
Euler	Dassault Aviation	EUGENIE	Unstructured finite volume / implicit
Euler	BAe.	UEMB	Structured/explicit/multiblock
Euler	NASA	ENS3DAE	Structured/finite difference
Navier-Stokes	NASA	ENS3DAE	Structured/finite difference

Table 1 CFD Methods

CFD METHODS

DESCRIPTIONS OF CODES

A table of information is provided for each CFD code, which will allow the reader to make comparisons with codes under development. The first section of the code formulary gives a general description of the method type, but in the case of the NS code, only the turbulence and transition modelling actually used for data presented herein are described (additional models may also be available). The manner in which convergence is determined is described in item 1.10, and techniques used to accelerate the overall convergence of the method are also specified (item 1.6). Where available, performance data is also provided (items 4.2-4.4), and coupled with information of platform (item 4.1) the reader will be able to gauge, in a general manner, the comparative performance of newly developing computing techniques with the contemporary techniques reported herein.

Section 2 of the code formulary gives details about the specific grid used in the studies reported here; where the grid is completely structured the grid dimensions are given as chordwise X spanwise X normal. The grid size is specified as number of cells, number of vertices, or both. Any modifications to the geometry (e.g. treatment of wing tip) are noted in item 2.6.

The presentation of the results is detailed below; only a limited number of CFD solutions have been plotted in this written report, but many more are plotted in the electronic report. In section 3 of the code formulary the run numbers (as indexed in chapter 5) of those cases presented in either the written or electronic report are listed.

Interpolation details are provided where interpolation from CFD grid locations to specific points has taken place (item 3.3). Where no interpolation has been used, the data is extracted directly from the computational grid points (vertices or cell centres as appropriate to that particular method).

UTSP CODES

1 CODE	**UTSPV21**
1.1 Type	UTSP (Unsteady Transonic Small Perturbation)
1.2 Name	UTSP v2.1
1.3 Description	Inviscid, linearised or non-linear TSP equations for single lifting surface with up to 2 control surfaces.
1.4 Available grid types	Geometry transformed to rectangular wing with 60 X 20 X 40 grid dimensions for optimised performance.
1.5 Artificial viscosity	None
1.6 Convergence acceleration techniques	None
1.7 Turbulence model	N/A
1.8 Transition model	N/A
1.9 Time-step	The Mach number and the planform geometry determine the allowable Δt for stability, with the leading edge sweep having a particularly strong influence. For the F-5 case a value of Δt=0.002 has been used.
1.10 Convergence	Not specified
1.11 References	Ref. 10
2 GRID	
2.1 Size of grid	120 X 20 X 40
2.2 Y+	N/A
2.3 Number of Surface grid points	78 X 17 (i.e. 39 on each surface)
2.4 Grid type	C-grid (transformed)
2.5 Distance of outer boundaries from the wing	Not specified
2.6 Modifications to geometry	None

3 RESULTS

3.1 Written Report	152 (sections 1,3,5,7), 370 (1 & 7)
3.2 Electronic data	138 (sections 1-8), 152 (1-8), 191 (1-8), 370 (1 & 7)
3.3 Interpolation details	Linear interpolation to spanwise station

4 ADDITIONAL INFORMATION

4.1 Platform	Cray YMP
4.2 CPU	
4.2.1 Total	Not given
4.2.2 per iteration	Not given
4.2.3 per cycle	Not given
4.3 Convergence	Not given
4.4 Memory	Not given
4.5 Contact for further information	M J de C Henshaw, British Aerospace (Operations) Ltd, Military Aircraft and Aerostructures, Brough, East Riding of Yorkshire, HU15 1EQ, UK. michael.henshaw@bae.co.uk

1 CODE — CAP-ASP

1.1 Type	UTSP
1.2 Name	CAP-ASP
1.3 Description	Advanced TSP with revised streamwise flux and revised mass-flux boundary conditions. Boundary conditions applied on mean plane. AF algorithm for finite difference solution.
1.4 Available grid types	Single Cartesian grid mapped to plan-form
1.5 Artificial viscosity	None
1.6 Convergence acceleration techniques	N/A
1.7 Turbulence model	N/A
1.8 Transition model	N/A
1.9 Time-step	On the order of .01 or .02 (only steady cases provided)
1.10 Convergence	Residual reduced to E-4 to E-5 (3-4 orders of magnitude)
1.11 References	None - derivative of CAP-TSD. Ref. 6

2 GRID

2.1 Size of grid	180 X 45 X 90 = 729 000 grid points
2.2 Y+	N/A
2.3 Number of Surface grid points	90 X 30 = 2700 each on upper and lower surface
2.4 Grid type	Single Cartesian grid mapped to plan-form
2.5 Distance of outer boundaries from the wing	10 root chords upstream, downstream, above, and below the wing. 2 semi-spans
2.6 Modifications to geometry	None; airfoil constant throughout including tip

3 RESULTS

3.1 Written Report	137 (sections 1,3,5,7), 152 (1,3,5,7), 168 (1,3,5,7)
3.2 Electronic data	137, 138, 152, 158, 168, 190, 191 (steady runs only, sections 1 -

	8)
3.3 Interpolation details	Linear spanwise interpolation on unit square to measurement chords

4 ADDITIONAL INFORMATION

4.1 Platform	Cray C-90
4.2 CPU	
4.2.1 Total	2000-4000 time steps required on the order of 1500-3000 sec
4.2.2 per iteration	.75 sec
4.2.3 per cycle	N/A
4.3 Convergence	Varied by case, see 1.10
4.4 Memory	31 mega words
4.5 Contact for further information	R. Bennett, Aeroelasticity Branch, Structures Div., NASA, Mail stop 340, NASA Langley Research Center, Hampton, VA. 23681-2199 , USA r.m.bennett@larc.nasa.gov

FULL POTENTIAL CODES

1 CODE

HELIFP

1.1 Type	Unsteady Full Potential equation in conservative form.
1.2 Name	HELIFP Developed by CIRA, DERA, NLR, PMI, GKN-Westland, AGUSTA during the BRITE/EURAM project HELISHAPE(1993-96)
1.3 Description	Finite volume discretisation with velocity potential at the vertex and flux quantities at the cell centre.
1.4 Available grid types	Structured C-H topology.
1.5 Artificial viscosity	Streamwise density flux biasing.
1.6 Convergence acceleration techniques	Approximate factorisation with Newton iterations.
1.7 Turbulence model	N/A
1.8 Transition model	N/A
1.9 Time-step	CFL number 100-->500
1.10 Convergence	Two convergence criteria are used in HELIFP: the correction of the velocity potential between two pseudo-time steps, and the behaviour of the number of supersonic points in the field. For transonic cases the second method is more reliable.
1.11 References	Ref. 3, Ref. 4

2 GRID

2.1 Size of grid	161 X 32 X 24
2.2 Y+	N/A
2.3 Number of Surface grid points	116 X 22
2.4 Grid type	C-H
2.5 Distance of outer boundaries from the wing	Distance of C-outer boundary = 7 root chords Location of the last H-outer boundary = 1.5 semi-span
2.6 Modifications to geometry	Linear closing of T.E. sharp closing of wing tip.

3 RESULTS

3.1 Written Report	152 (sections 1,3,5,7 + convergence plots), 370 (1 & 7), 373 (1 & 7), 383 (1 & 7)
3.2 Electronic data	151, 152, 168, 190, 160, 172, 370, 373, 383 (sections 1 – 8)
3.3 Interpolation details	Pressure coefficients linearly interpolated onto experimental stations.

4 ADDITIONAL INFORMATION

4.1 Platform	SGI Power Challenge
4.2 CPU	
4.2.1 Total	(RUN 370): 8540 sec
4.2.2 per iteration	(RUN 370): 2.527 sec
4.2.3 per cycle	(RUN 370): 3638 sec.
4.3 Convergence	N. iterations (RUN 370): 3380 (500 convergence +2 cycles of 720 steps with 2 Newton it. = 500 + 2880)
4.4 Memory	85 Mb
4.5 Contact for further information	A Pagano, Aerodynamics and Propulsion department, CIRA, Via Maiorise, 81043, Capua, CE, Italy. a.pagano@cira.it

1 CODE

TCITRON

1.1 Type	Full Potential
1.2 Name	TCITRON
1.3 Description	Finite difference discretisation based on a non-conservative formulation with implicit time and semi-implicit space schemes. 3D, but only for wing geometries (with a wake surface). Steady Boundary Layer coupling capability. Resolution of the dynamic aeroelasticity equation in a reduced modal basis. Unsteady motion is applied through a transpiration boundary condition.
1.4 Available grid types	Structured C-H topology type.
1.5 Artificial viscosity	Due to non-conservative formulation
1.6 Convergence acceleration techniques	Full multigrid scheme (3 levels)
1.7 Turbulence model	N/A
1.8 Transition model	N/A
1.9 Time-step	From 12 to 360 Δt / cycles
1.10 Convergence	6 orders of perturbation potential correction
1.11 References	

2 GRID

2.1 Size of grid	185 X 21 X 22
2.2 Y+	N/A
2.3 Number of Surface grid points	113 X 14
2.4 Grid type	C-H
2.5 Distance of outer boundaries from the wing	Distance of C-outer boundary = from 5 to 8 root chords Location of the last H-outer boundary = 1.5 semi-span

2.6 Modifications to geometry	Tip fairing is modelled, but with closure 4mm from the experimental tip.

3 RESULTS

3.1 Written Report	137, 152, 168 (sections 1,3,5,7), 370 (1 & 7)
3.2 Electronic data	137, 138, 151, 152, 158, 168, 160, 370, 383 (sections 1 – 8)
3.3 Interpolation details	Spanwise grid distribution adjusted to coincide with experimental stations. No interpolation needed

4 ADDITIONAL INFORMATION

4.1 Platform	SGI O_2 (R 10000)
4.2 CPU	
4.2.1 Total	(RUN 370): 1570 sec (2 cycles)
4.2.2 per iteration	(RUN 370): 1.18 sec
4.2.3 per cycle	(RUN 370): 765 sec.
4.3 Convergence	300 steady iterations + 2 cycles of 72 x 10 unsteady iterations
4.4 Memory	12 Mb
4.5 Contact for further information	S. Guillemot, Dassault Aviation - 78, Quai Marcel Dassault, F-92214, Saint Cloud, CEDEX, France. Stephane.guillemot@dassault-aviation.fr

EULER CODES

Five Euler methods have been used, although not all are represented in the written report. There are four structured grid codes, of which three are multiblock, and one unstructured grid code. Two of the codes (ENS3DAE and PMB3D) are in fact Navier-Stokes codes, but for the purposes of this set of results they have been run in Euler mode. This sample of methods covers explicit, semi-implicit and fully implicit formulations.

1 CODE

	EUL3DU
1.1 Type	Euler
1.2 Name	EUL3DU
1.3 Description	Finite-Volume, Cell centred, 2nd order central flux approximation, 2nd order 5 stage Runge-Kutta time integration. Unsteady motion is introduced through moving grid: grid is fixed at the outer boundary, but follows wing movement at inner boundary. Smooth transition in between outer and inner boundaries that ensures geometry conservation law is satisfied.
1.4 Available grid types	Structured O-H, monoblock.
1.5 Artificial viscosity	Jameson's type blending of 2nd and 4th order terms
1.6 Convergence acceleration techniques	Implicit residual smoothing, dual time-stepping, local time stepping (steady only), enthalpy damping (steady only).
1.7 Turbulence model	N/A
1.8 Transition model	N/A
1.9 Time-step	Maximum local Δt^* (dimensionless time with root chord and free-stream velocity) corresponding to a CFL of 6 for steady cases. $\Delta t^*=0.001$ for unsteady cases (dual time stepping not used), selected for accuracy, not for stability reasons.

1.10 Convergence	5000 Iterations with a reduction in maximum residual of at least 6 orders of magnitude for steady cases (Figure 4a). 3 periods for unsteady cases, the last period is Fourier analysed (Figure 4c)
1.11 References	Ref. 5

2 GRID

2.1 Size of grid	160 x 31 x 32 cells
2.2 Y+	N/A
2.3 Number of Surface grid points	160 x 21
2.4 Grid type	O-H
2.5 Distance of outer boundaries from the wing	9 root-chords / 2 semi-span
2.6 Modifications to geometry	Linear closing of T.E. Sharp closing of wing tip

3 RESULTS

3.1 Written Report	137, 168 (sections 1,3,5,7), 152 (1,3,5,7,8 + convergence plots), 172 (convergence plots), 370, 373, 383 (1 & 7)
3.2 Electronic data	137, 138, 151, 152, 158, 168, 190, 191, 383, 370, 160, 373, 172, 193 (sections 1-8)
3.3 Interpolation details	Spanwise grid distribution adjusted to coincide with experimental stations. No interpolation needed

4 ADDITIONAL INFORMATION

4.1 Platform	Cray YMP-EL
4.2 CPU	
4.2.1 Total	10900 secs. (Case 152, 5000 iterations)
4.2.2 per iteration	13.7×10^{-6} secs. /cell/iteration
4.2.3 per cycle	58890 secs. (Case 172, 27000 iterations)
4.3 Convergence	See 1.10 above.
4.4 Memory	8 MWords
4.5 Contact for further information	L P Ruiz-Calavera, INTA, Aerodynamics Division, Carretera de Ajalvir Km 4.5, 28850 Torrejon de Ardoz, SPAIN. ruizcl@inta.es

1 CODE

PMB3D

1.1 Type	Euler
1.2 Name	PMB3D
1.3 Description	A fully Implicit structured, cell-centred Parallel multiblock solver. The convective terms are discretised using Osher's upwind flux difference splitting scheme with MUSCL variable extrapolation. The unsteady equations solved using the classical dual time method introduced by Jameson Unsteady motion introduced by rigid rotation of the grid with the boundary velocities, using a first order difference.
1.4 Available grid types	Structured multiblock

1.5 Artificial viscosity	Through Van-Albada Limiting of MUSCL
1.6 Convergence acceleration techniques	The Implicit Jacobian matrix is approximated to reduce storage and is solved using a Krylov subspace method preconditioned with BILU(0). Only the pre-conditioned is decoupled across blocks
1.7 Turbulence model	N/A
1.8 Transition model	N/A
1.9 Time-step	Explicit start-up 0.4 Implicit 250. With at least 3 Cycles for unsteady runs.
1.10 Convergence	Steady cases are 8 orders in the L2 norm of the starting residual. Unsteady results are 6 orders. See Figure 4.
1.11 References	Ref. 12, also http://www.aero.gla.ac.uk/Research/CFD

2 GRID

2.1 Size of grid	180224 nodes, 225888 cells
2.2 Y+	N/A
2.3 Number of Surface grid points	84 X 34 = 2,856 cells
2.4 Grid type	Multiblock
2.5 Distance of outer boundaries from the wing	10 (root) chords streamwise and normal to wing, 3 spans from wing tip in spanwise direction.
2.6 Modifications to geometry	Tip fairing modelled, but with closure 4mm from experimental tip.

3 RESULTS

3.1 Written Report	152 (sections 1,3,5,7, + convergence plots), 172 (convergence plots), 370 (1 & 7)
3.2 Electronic data	138, 152, 191, 383, 370, 160, 373, 193 (sections 1 – 8)
3.3 Interpolation details	Linear interpolation in spanwise direction to measurement stations.

4 ADDITIONAL INFORMATION

4.1 Platform	Ppro 200's
4.2 CPU	5-7 work units per implicit iteration.
4.2.1 Total	Not given
4.2.2 per iteration	Not given
4.2.3 per cycle	Not given
4.3 Convergence	Explicit start up, followed by implicit to converge to at least 6 orders of magnitude on residuals. At least 3 cycles used for unsteady. See Figure 4.
4.4 Memory	2.1 Kbytes per cell
4.5 Contact for further information	B E Richards, Aerospace Engineering, James Watt Building, Glasgow University, Glasgow, Scotland, G12 8QQ, UK. bryan@aero.gla.ac.uk

1 CODE

EUGENIE

1.1 Type	Euler
1.2 Name	EUGENIE
1.3 Description	Galerkin finite volume approx. using a modified Lax-Wendroff scheme with implicit low storage time integration for steady,

	implicit 2nd order time integration (Gear method) for unsteady calculations. For steady flow calculations viscous effects are included using a boundary layer method: Laminar and Turbulent Boundary Layer with integral method. Boundary Layer coupling with "transpiration" velocities. Unsteady motion applied using a transpiration boundary condition.
1.4 Available grid types	Unstructured
1.5 Artificial viscosity	2nd order Lax-Wendroff
1.6 Convergence acceleration techniques	Jacobi method and dual time stepping strategy
1.7 Turbulence model	N/A
1.8 Transition model	Granville criteria for smooth transition and modified with Schlichting correction for roughness. Used for viscous coupled calculations.
1.9 Time-step	Corresponding to a maximum CFL of 10 / Δt.
1.10 Convergence	L_2 residual on all the variables (5 orders)
1.11 References	Paper to appear in M^2AN

2 GRID

2.1 Size of grid	51 539 nodes, 294 851 cells
2.2 Y+	N/A
2.3 Number of Surface grid points	2 865
2.4 Grid type	Unstructured
2.5 Distance of outer boundaries from the wing	Between 10 to 15 root chord.
2.6 Modifications to geometry	Tip fairing is modelled, but with closure 4mm from the experimental tip.

3 RESULTS

3.1 Written Report	Euler: 370, 373, 383 (sections 1 & 7), Euler+boundary layer: 137, 152, 168 (1,3,5,7)
3.2 Electronic data	137, 138, 151, 152, 158, 168, 190, 191 383, 370, 160, 373, 172, 193. (1 - 8)
3.3 Interpolation details	Pressure coefficients interpolated onto experimental stations.

4 ADDITIONAL INFORMATION

4.1 Platform	IBM SP2
4.2 CPU	All CPU times given for 1 processor
4.2.1 Total	(RUN 370): 27,440 sec ≈ 7h30 (2 cycles)
4.2.2 per iteration	(RUN 370): 12.25 sec.
4.2.3 per cycle	(RUN 370): 8,200 sec ≈ 2h30
4.3 Convergence	4 orders on L_2 residual for unsteady steps.
4.4 Memory	65 Mb
4.5 Contact for further information	S. Guillemot, Dassault Aviation - 78, Quai Marcel Dassault, F-92214, Saint Cloud, CEDEX, France. Stephane.guillemot@dassault-aviation.fr

1 CODE

	UEMB
1.1 Type	Euler, Multiblock
1.2 Name	UEMB
1.3 Description	Explicit, Euler multiblock code which uses structured grid within the blocks, but unstructured arrangements of blocks. Based on a steady code that uses Jameson type Runge-Kutta scheme. Cell centred. Unsteady motion is introduced using a transpiration velocity boundary condition applied at the cell centres of moving surfaces. A 2D strip theory boundary layer method is coupled to the Euler code to introduce viscous effects for some steady flow cases.
1.4 Available grid types	Structured grid within blocks, C, H and O type grids are all available.
1.5 Artificial viscosity	2[nd] and 4[th] order blended artificial viscosity.
1.6 Convergence acceleration techniques	None employed, although time-step constraint is relaxed for unsteady calculations.
1.7 Turbulence model	N/A
1.8 Transition model	N/A
1.9 Time-step	Local.
1.10 Convergence	Based on residuals, and C_l.
1.11 References	Ref. 13 for basis of steady code.

2 GRID

2.1 Size of grid	225,888 grid cells in 88 blocks.
2.2 Y+	N/A
2.3 Number of Surface grid points	84 X 34 = 2,856 cells
2.4 Grid type	C grid around wing
2.5 Distance of outer boundaries from the wing	10 (root) chords streamwise and normal to wing, 3 spans from wing tip in spanwise direction.
2.6 Modifications to geometry	Tip fairing is modelled, but with closure 4mm from the experimental tip.

3 RESULTS

3.1 Written Report	Euler: 152 (sections 1,3,5,7), 370 (1 & 7) Euler+boundary layer (8)
3.2 Electronic data	138, 152, 158, 191 (sections 1 – 8), 383, 193 (1,3,5,7), 370 (1 & 7)
3.3 Interpolation details	Linear interpolation in spanwise direction to measurement stations.

4 ADDITIONAL INFORMATION

4.1 Platform	Cray YMP.
4.2 CPU	
4.2.1 Total	Not given
4.2.2 per iteration	Not given
4.2.3 per cycle	Not given
4.3 Convergence	Not given

4.4 Memory	Not given
4.5 Contact for further information	M J de C Henshaw, British Aerospace (Operations) Ltd, Military Aircraft and Aerostructures, Brough, East Riding of Yorkshire, HU15 1EQ, UK. michael.henshaw@bae.co.uk

1 CODE

ENS3DAE

1.1 Type	3-D Compressible Full (not thin layer) Reynolds Averaged Navier-Stokes
1.2 Name	ENS3DAE run as Euler
1.3 Description	Beam Warming implicit central finite difference scheme. Second order accurate in space and time. Local time stepping for steady state cases.
1.4 Available grid types	Multi-block structured
1.5 Artificial viscosity	Pressure switched second/fourth order non-linear explicit with spectral radius scaling. Second order implicit
1.6 Convergence acceleration techniques	Local time stepping for steady state. Grid sequencing
1.7 Turbulence model	N/A
1.8 Transition model	N/A
1.9 Time-step	Local time stepping, CFL=4.0
1.10 Convergence	3000 iterations at M=0.90
1.11 References	Ref. 7, Ref. 8, Ref. 9

2 GRID

2.1 Size of grid	201 x 49 x 33 = 325,017 points
2.2 Y+	N/A
2.3 Number of Surface grid points	153 x 25 = 3825 points
2.4 Grid type	Single-zone C-H structured grid
2.5 Distance of outer boundaries from the wing	6 root chords forward and aft of wing. 4 root chords above and below. 4 semi-spans
2.6 Modifications to geometry	None; airfoil constant throughout span

3 RESULTS

3.1 Written Report	-
3.2 Electronic data	137, 151, 158, 168, 190 (steady only, sections 1 – 8)
3.3 Interpolation details	Linear interpolation to experimental stations

4 ADDITIONAL INFORMATION

4.1 Platform	Cray C-90 at NASA Ames, multitasked on 8 shared processors
4.2 CPU	
4.2.1 Total	Approx. 5 hrs (3000 iterations)
4.2.2 per iteration	Approx. 6 sec., 1.85 x 10-5 sec/iteration/grid point
4.2.3 per cycle	(Steady only)
4.3 Convergence	2.5 orders of magnitude on L2 norm of residual
4.4 Memory	32 million words (multitasked on 8 processors)

4.5 Contact for further information	d.m.schuster@larc.nasa.gov

NAVIER-STOKES CODES

1 CODE

	ENS3DAE
1.1 Type	3-D Compressible Full (not thin layer) Reynolds Averaged Navier-Stokes
1.2 Name	ENS3DAE
1.3 Description	Beam Warming implicit central finite difference scheme. Second order accurate in space and time. Local time stepping for steady state cases.
1.4 Available grid types	Multi-block structured
1.5 Artificial viscosity	Pressure switched second/fourth order non-linear explicit with spectral radius scaling. Second order implicit
1.6 Convergence acceleration techniques	Local time stepping for steady state. Grid sequencing
1.7 Turbulence model	Baldwin-Lomax algebraic with FMAX search limiter to force FMAX to occur in viscous layer near surface. 3-D eddy viscosity smoothing to provide spatial history effects (helpful in separated flows)
1.8 Transition model	Fully turbulent
1.9 Time-step	Local time stepping, CFL=4.0
1.10 Convergence	2000 iterations most cases, more at M=0.90
1.11 References	Ref. 7, Ref. 8, Ref. 9

2 GRID

2.1 Size of grid	201 x 49 x 41 = 403,809 points
2.2 Y+	Minimum, 3.8; maximum, 15.2; average, 7.4
2.3 Number of Surface grid points	153 x 25 = 3825 points
2.4 Grid type	Single-zone C-H structured grid
2.5 Distance of outer boundaries from the wing	6 root chords forward and aft of wing. 4 root chords above and below. 4 semi-spans
2.6 Modifications to geometry	None; airfoil constant throughout span

3 RESULTS

3.1 Written Report	137, 168 (sections 1,3,5,7)
3.2 Electronic data	137, 151, 158, 168, 190 (steady only, sections 1 – 8)
3.3 Interpolation details	Linear interpolation to experimental stations

4 ADDITIONAL INFORMATION

4.1 Platform	Cray C-90 at NASA Ames, multitasked on 8 shared processors
4.2 CPU	
4.2.1 Total	15,720 sec = 4.367 hrs (2000 iterations) CPU, 54 min Wall.
4.2.2 per iteration	7.860 sec., 1.95×10^{-5} sec/iteration/grid point
4.2.3 per cycle	(Steady only)
4.3 Convergence	2.5 orders of magnitude on L_2 norm of residual
4.4 Memory	40 million words (multitasked on 8 processors)
4.5 Contact for further information	d.m.schuster@larc.nasa.gov

CFD SOLUTIONS

CLEAN WING TEST CASES

There are 14 cases (8 steady and 6 unsteady) as detailed in Table 2, in all cases the (equilibrium) angle of attack is close to zero, and the Mach number range includes sub-critical, transonic and supersonic flow conditions. Viscous effects are comparatively insignificant for these conditions.

Solutions are presented (on the CDROM) for upper and lower surfaces at 8 spanwise stations, as specified in Table 3 (see also figure 1 of chapter 5), and sample results are plotted at a few selected conditions and spanwise locations in this chapter. A selection of convergence plots is also provided.

The reader should note that the first data point on the upper surface for sections 3 and 5 are faulty pressure points (see Ref. 2) and should not be considered in evaluations. This can be observed in figures 5 to 10, particularly Figure 10.

Run No.	Mach No.	α (deg.)	freq. (Hz)	κ	θ (deg.)	Re X10^6
Steady cases						
137	0.597	-0.005	-	-	-	4.79
138	0.597	+0.493	-	-	-	4.77
151	0.897	-0.004	-	-	-	5.79
152	0.896	+0.497	-	-	-	5.79
158	0.946	-0.004	-	-	-	5.89
168	1.093	-0.002	-	-	-	6.01
190	1.328	-0.005	-	-	-	4.07
191	1.327	+0.500	-	-	-	4.08
Unsteady cases						
383	0.597	0.004	40	0.399	0.115	4.57
370	0.896	0.001	40	0.275	0.111	5.73
160	0.947	-0.006	20	0.132	0.523	5.91
373	1.092	0.003	10	0.058	0.113	5.92
172	1.093	0.003	20	0.116	0.267	6.02
193	1.336	-0.001	40	0.198	0.222	4.10

Table 2 Flow conditions used for comparisons

Section No.	η (=y/s)	y (m)
1	0.181	0.1127
2	0.352	0.2192
3	0.512	0.3188
4	0.641	0.3991
5	0.721	0.4489
6	0.817	0.5087
7	0.875	0.5448
8	0.977	0.6082

Table 3 Spanwise measurement stations on F-5 Wing.

WING TIP

In the absence of the launcher and missile a wing tip fairing was attached to the model; this is defined in the geometry specification (see chapter 5). Three stations define the fairing, and the last of these is 4 mm short of the actual wing tip, which allows the possibility of some variation in the modelling of the geometry. CFD results generated within this benchmark exercise have indicated that minor compromises to the geometry in this region are insignificant compared to changes in grid density and/or model physics. Indeed a linear extrapolation of the wing section to the full span with a simple closure at the tip is a reasonable compromise of the actual geometry.

Overall the codes UEMB and EUL3DU were found to give almost identical results, the main differences being due only to the grid density (particularly around the leading edge). The tip geometry was defined differently in these two sets of results; for UEMB the fairing definition (three stations) is used, but the last (undefined) 4-mm are truncated and the tip closed with a flat surface. In the EUL3DU geometry, on the other hand, the tip is modelled by extending the constant wing section to the tip, which is located at 0.6476 m. Thus the wing has the span of the tested wing, but the change in shape of the fairing is not modelled at all. The tip is closed by collapsing the grid to a plane in a section located about 13 mm from the tip, which actually gives additional span to the wing.

The Cp distribution at station 8 (97.7%) is shown in Figure 2, for run 152 ($M=0.896$, $\alpha=0.497°$).

On the lower surface the EUL3DU results show sharper and earlier peak suction than the UEMB results, but this is explained by the difference in mesh density. In fact the EUL3DU grid has 160 chordwise points compared to 84 for the UEMB grid. Overall the EUL3DU lower surface results agree more closely with the experimental points. On the upper surface this position is somewhat reversed, with the UEMB results closer to the experimental points. Once again the grid density is seen to make a difference, manifested by the sharpness of the shock wave.

For information, an UEMB result obtained using viscous coupling is also plotted. This shows closer agreement in terms of shock position and peak pressures on the upper surface, the difference is less pronounced on the lower surface. Although the results with the two geometry definitions show variation, these variations appear to be associated with different grid density rather than differences in the geometry definition per se. Overall, it is concluded that the Cp variations, due to these differences in tip geometry modelling, are not significant.

CONVERGENCE

There is some variation in the metrics used by the different methods to monitor convergence, the metric(s) used by each method are noted in the formulary above. For information the convergence for a sample of codes is plotted for two of the run conditions run 152 (steady) and run 172 (unsteady) in Figure 3 (Full potential) and Figure 4 (Euler). These are typical plots and will inform the reader of the general level of convergence that has been achieved for the results presented herein.

STEADY SOLUTIONS

Steady solutions are presented as sectional Cp plots at spanwise stations 1, 3, 5, 7 for a selection of the flow conditions, and data for all stations and all the steady conditions specified in Table 2 are available on the accompanying CDROM. The reader is invited to plot these data for the purposes of more extensive comparison. Code to code comparisons are made for the transonic case, run 152, in Figure 5 (UTSP and Full Potential) and Figure 6 (Euler and Navier-Stokes). For clarity a reduced set of results which compare the four different levels of approximation are shown in Figure 7 (run 137, subsonic), Figure 8 (run 152, transonic) and Figure 10 (run 168, supersonic).

The various methods are in *overall* agreement, but differ somewhat in detail. The inboard pressures tend to be overpredicted by all the methods, but this is almost certainly due to the sidewall boundary layer affecting the experimental results. The tip pressure detail is sensitive to spanwise grid clustering, and it is suggested that this is as significant as the changes in tip geometry mentioned above.

At Mach numbers near 0.9, and above, a leading edge shock appears, and this is somewhat sensitive to the grid spacing around the leading edge for the inviscid methods. For Navier-Stokes methods particular attention to cell clustering in this region may be required, and it is not clear whether the flow near the leading edge should be laminar or turbulent.

The two UTSP methods show fairly close agreement (Figure 5), although UTSPV21 fails to capture the leading edge peak pressure (lower surface) and the sharpness of the shock (upper surface); this is due to the differences in grid fineness. CAP-ASP uses more than twice as many chordwise grid points, and this indicates that of the order of 90 (on each surface) are required. It may be noted that the shock is further aft for CAP-ASP, particularly at the tip, however, this agrees well with the EUL3DU (Euler) predicted position (Figure 8) and other fine grid Euler results (Ref. 11). Both Full Potential methods capture the leading edge peak better than the UTSP results.

There is a significant difference in the shock position between the two Full Potential methods. HELIFP and TCITRON use similar grid densities (although HELIFP uses more spanwise stations) and the difference is attributed to the different formulations: HELIFP is a conservative formulation and TCITRON is non-conservative.

The difference in shock position for the Euler methods UEMB and EUL3DU (Figure 6) is once again entirely attributable to the different grid densities, however, the difference between PMB3D and UEMB is less easily explained, as these methods were run on the same grid. The implicit formulation (PMB3D) in fact shows closest agreement with EUGENIE, an unstructured grid code that in this case is used with boundary layer coupling to model the effects of viscosity. Figure 9 shows a comparison between UEMB and EUGENIE (i.e. structured and unstructured grids respectively) both run in Euler and Euler with viscous coupling mode. There appears to be no significant difference between the grid technologies, and the inclusion of viscous coupling achieves the correct shock position in both cases.

For the subsonic case (Figure 7) there is virtually no difference between the various levels of approximation, although the trailing edge treatment for the codes results in some differences in pressure. The two methods that include viscosity (RANS code ENS3DAE and EUGENIE with boundary layer coupling) show a similar trend in Cp at the trailing edge. For the supersonic case there is again variation in the trailing edge treatment, although overall the various levels of approximation appear to agree well. Euler with boundary layer coupling (EUGENIE) matches most closely to experiment, and the Full Potential method shows the least agreement with other methods or experiment.

UNSTEADY SOLUTIONS

Unsteady solutions are presented as sectional plots of the real and imaginary parts of the pressure coefficient (CpReal and CpImag) at spanwise stations 1 and 7 for a selection of flow conditions. Data for all the stations and all the unsteady flow conditions specified in Table 2 are available on the accompanying CDROM. The reader is invited to plot these data for the purposes of more extensive comparison.

Code to code comparisons are presented for run 370 (transonic) in Figure 11 (UTSP and Full Potential) and Figure 12 (Euler). A reduced set of results which compare the three different levels of approximation are shown in Figure 13 (run 383, subsonic), Figure 14 (run 370, transonic), and Figure 15 (run 373, supersonic).

The reader should note that the first experimental point on section 1, upper surface, for run 370 appears to be in error; although no error has been identified in the experimental dataset for this point. The point is not included in the plots reported here (e.g. Figure 11), although it remains in the experimental data included on the CDROM.

Only one set of UTSP data is available (UTSPV21, run 370, Figure 11) and this underestimates the peaks in the real and imaginary pressures. As before this is due to the coarseness of the mesh used in this code. The Full Potential codes show reasonable agreement with each other, although the position of the peak in CpImag agrees less well on the outboard stations. HELIFP (with conservative formulation) appears to match experiment most closely for this case. The Euler methods also show reasonable agreement with each other (Figure 12) although the EUL3DU method tends to predict larger outboard peaks for both real and imaginary parts. Overall, EUGENIE matches most closely to the experimental values.

The predictions for subsonic and supersonic flow show fairly close agreement between all the methods (Figure 13 and Figure 15), although the outboard peak Cp (real and imaginary) is rather reduced for the Full Potential code at supersonic conditions.

No differences in the results are attributed to differences in the way that unsteady motion is introduced (e.g. transpiration boundary conditions or mesh movement), however, the oscillation amplitude is comparatively small for this test case.

COMPLEX CONFIGURATION TEST CASES

The F-5 test series includes a range of geometries, increasing in complexity from the clean wing to the wing with stores and attendant components, as defined in chapter 5, tables 3 and 4. Computational solutions are presented for the geometry described by table 3d, of chapter 5, i.e. F-5 wing with tip launcher + missile body + aft fins + canard fins, at the flow conditions specified in Table 4.

RUN	MACH	κ	α	Re	F	θ
Steady Cases						
320	.897	0	-.000	5.65	-	-
Unsteady Cases						
348	.595	.401	.004	4.62	40.000	.111
352	.897	.069	-.002	5.73	10.000	.115
355	.896	.275	.004	5.73	40.000	.117
302	1.327	.199	.016	4.20	40.000	.221

Table 4 Wing With Tip Launcher + Missile Body + Aft Fins + Canard Fins

The Euler methods UEMB (structured) and EUGENIE (unstructured) have provided results for the complex configurations, the grids were as follows: -

UEMB: Multiblock: 290 blocks, 238,263 cells (11,712 surface cells).

EUGENIE: 120,307 grid nodes (6,770 surface nodes)

Although there is an increase in the number of grid points, compared to the number for the clean wing, in both cases the increase is comparatively modest compared to the increase in complexity of the geometry. This is especially true of the structured code (UEMB), where some compromise in surface density has been necessary to minimise the number of cells used. The grids are illustrated in plots provided on the CDROM (in directory 'Grids')

STEADY SOLUTIONS

Results are presented for steady flow case, run 320, in the form of Cp maps only. The plots may be viewed from the CDROM in directory Chapter4/ComplexWing/Steady/Run320, and are in postscript form. Detailed Cp plots of the missile, calculated using EUGENIE, are given in EU_EUGENIE_SURF and EU_EUGENIE_SURFZ (an enlargement of the aft fins area). The results for EUGENIE and UEMB are compared in EU_EUGENIE_UEMB_XCUT (field plot) and EU_EUGENIE_UEMB_WING (wing surface). For these figures the reader should note that EUGENIE is equivalent to the DAv label, and UEMB to the BAe label. The agreement between the two methods appears to be good for this steady flow condition.

UNSTEADY SOLUTIONS

Sectional plots are provided at sections 1, 3, 7, and 8 (Table 3) for the real and imaginary components of the pressure coefficient for the cases defined in Table 4. Plots for the three cases with pitch frequency of 40 Hz are included below. The agreement of the codes, and with experiment, is close for the subsonic and supersonic flow conditions for the real component of Cp (Figure 16 and Figure 20), but less good for the imaginary Cps. EUGENIE appears to underestimate Cp compared to experiment, whereas UEMB achieves fairly good agreement except at the outermost section (Figure 17and Figure 21). For the transonic flow case (run 355) the codes show a basic agreement in trend, but differ in detail (Figure 18 and Figure 19), however, the agreement with experiment is less well determined, especially at the outboard stations. The peaks in CpReal and CpImag, identified by the codes (which exhibit the same trends) are not present at the measurement locations of the experimental results.

DATA LAYOUT

The data relevant to this chapter is held in directories chapter4 and chapter5 (experimental). The structure for the CFD data (chapter 4) is shown in Figure 1.

The location of results for particular runs is self-evident from the structure of the chapter directory tree. Each RUN*** directory contains all the CFD results for that particular run number (see Table 2 and Table 4) with a designation according to the following key: -

MM_CCCC_SS

Where MM is the method identifier, CCCC is the code identifier, and SS the section number.

$$\left\{\begin{matrix}\text{UT}\\\text{FP}\\\text{EU}\\\text{NS}\end{matrix}\right\} - \left\{\begin{matrix}\text{UTSPV21}\\\text{CAPASP}\\\text{HELIFP}\\\text{TCITRON}\\\text{EUL3DU}\\\text{PMB3D}\\\text{EUGENIE}\\\text{EUGENIE + BL}\\\text{UEMB}\\\text{ENS3DAE}\end{matrix}\right\} - \left\{\begin{matrix}\text{S1}\\\text{S2}\\\text{S3}\\\text{S4}\\\text{S5}\\\text{S6}\\\text{S7}\\\text{S8}\end{matrix}\right\}$$

For example, section 5 of data for run 151 using the code EUL3DU has the code EU_ EUL3DU_S5 and held in directory RUN151.

Some RUN*** directories also contain a directory entitled 'Plotting', and this contains files for producing the plots printed below, with one or two additional cases for further information. To produce plots execute Xmgr.xxx_sh, this uses the corresponding set.xxx and graph.uCp files. Ensure that the directory is correctly set in Xmgr.xxx_sh by modifying the 'DIR=' line appropriately. Different sections may be plotted using the scripts, by editting the filenames in Xmgr.xxx_sh.

Postscript files illustrating some of the grids used in this exercise are provided in the directory 'Grids'

Two movie files are provided for the clean wing unsteady case, run160, these are both generated from results from the EUGENIE code. The first 'skin.mov' shows the upper surface shaded according to Cp value through two pitch cycles, the second ('profil.mov') shows the Cp plot at a section at 0.535 m span as it pitches through two cycles.

A full list of contents is given in the README file.

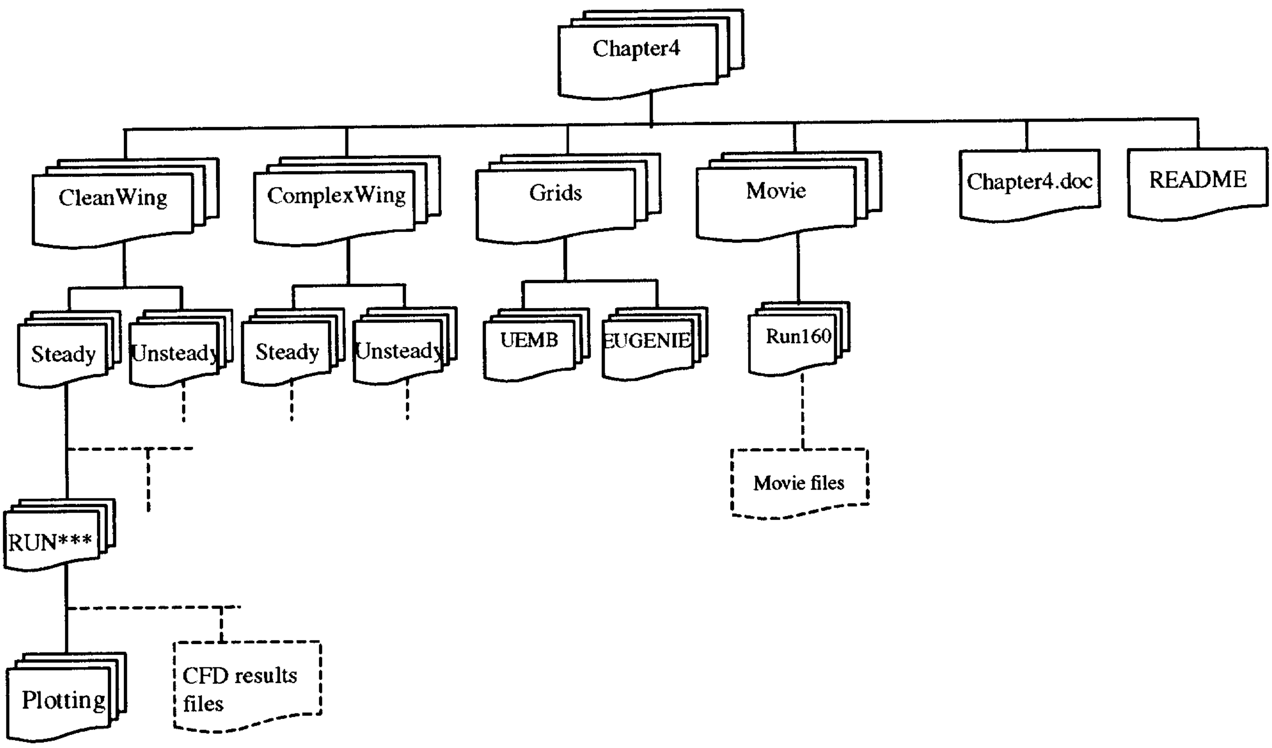

Figure 1 **Directory structure for Chapter 4 on CDROM.**

a)

b)

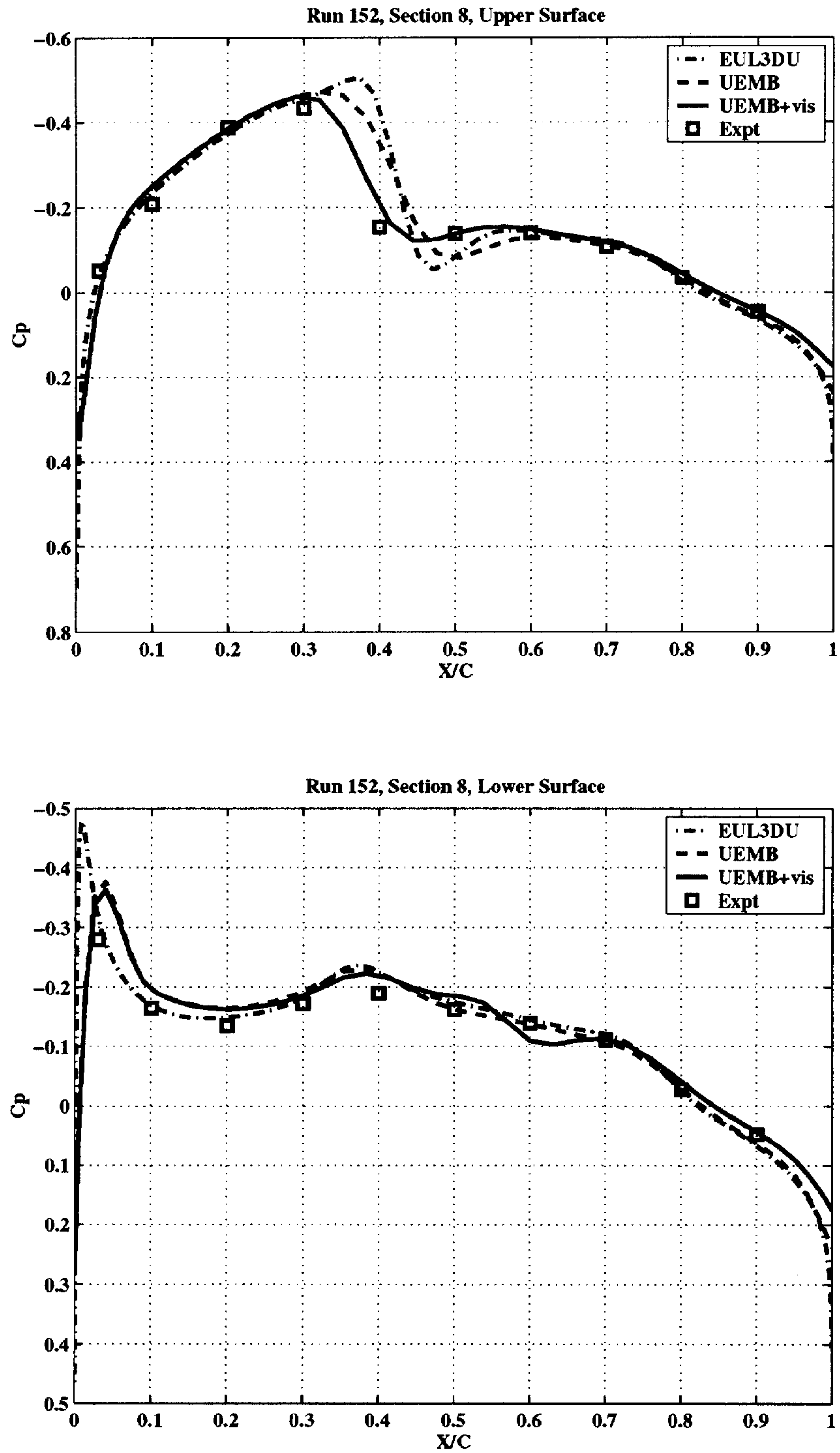

Figure 2 Comparison of EUL3DU and UEMB at section 8 for run 152. Cp is plotted for a) upper surface, and b) lower surface. This figure shows that different tip modelling has less effect than other factors (such as inclusion of viscosity, designated UEMB+vis)

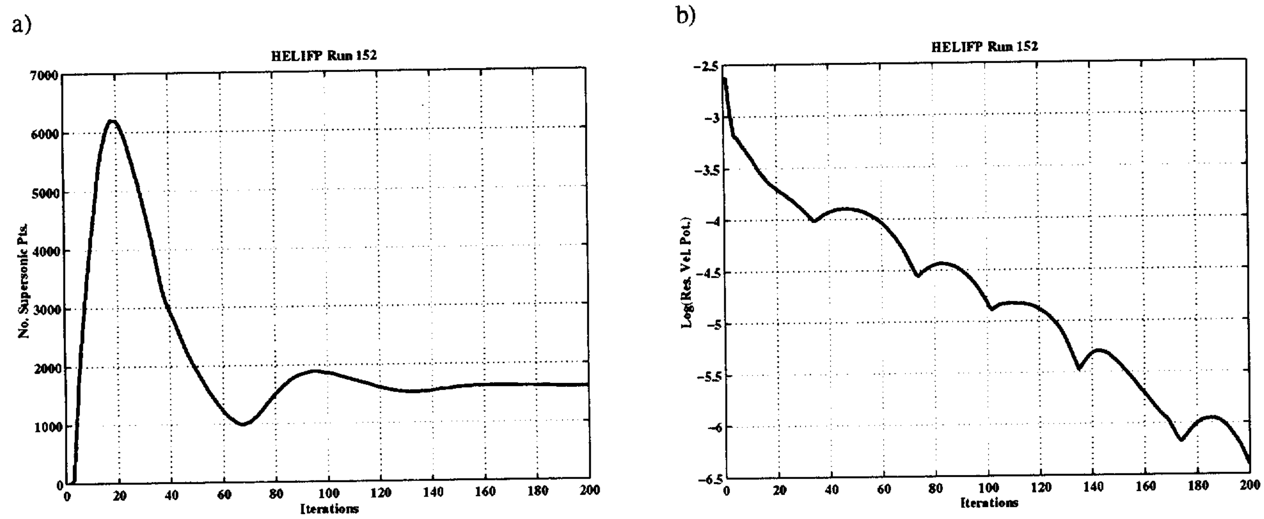

Figure 3 Convergence plots for Full Potential methods. Convergence for the code HELIFP is illustrated for run 152. a) Number of supersonic points plotted against iteration number, b) residual of velocity potential plotted against iteration number.

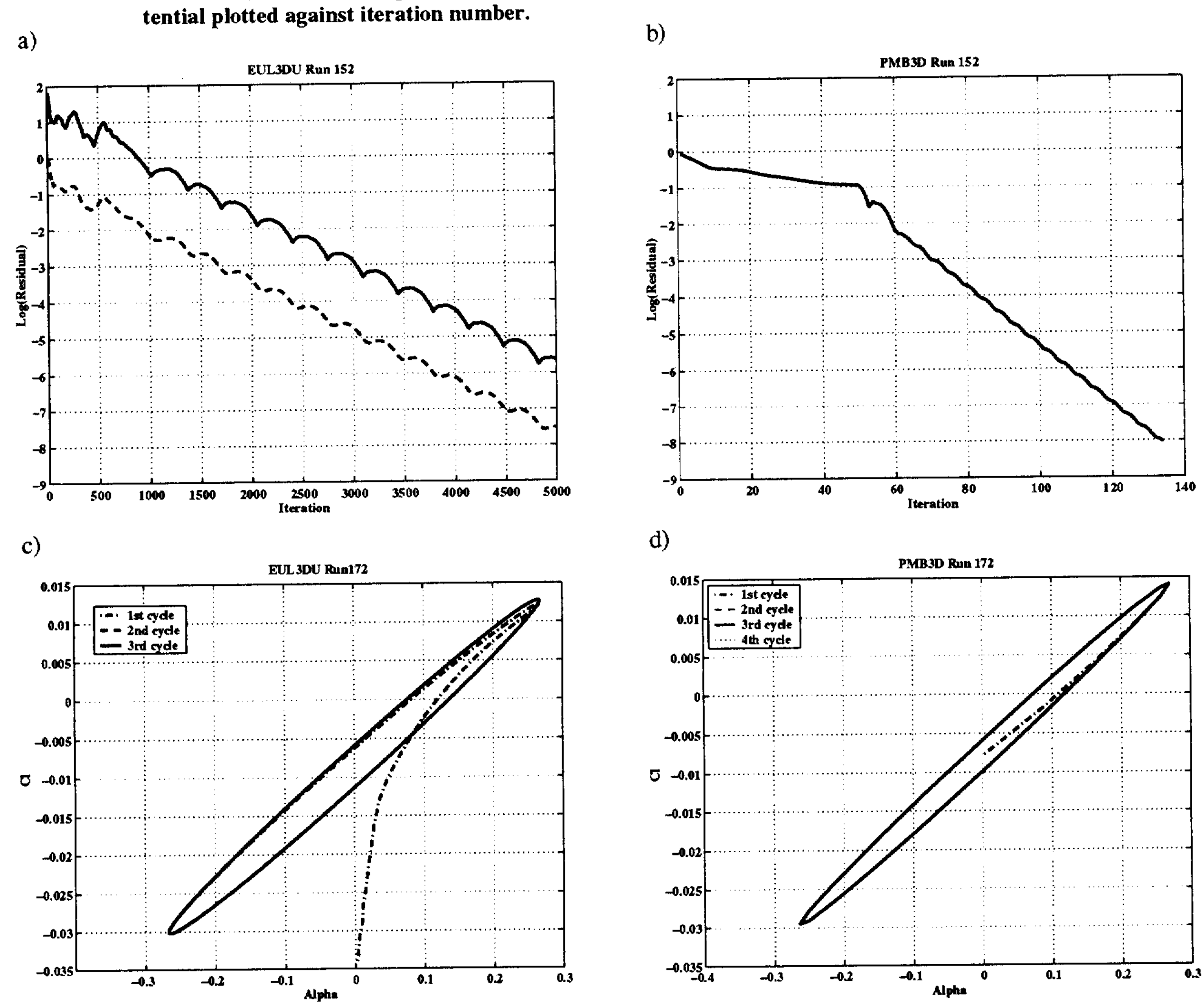

Figure 4 Convergence plots for Euler methods. Explicit (EUL3DU) and implicit (PMB3DU) algorithms are illustrated. a) EUL3DU for run 152 (steady), residual vs. iteration; b) PMB3D for run 152 (steady), residual vs. iteration; c) EUL3DU for run 172 (unsteady), Cl vs. α for 3 pitch oscillations; d) PMB3D for run 172 (unsteady), Cl vs. α for 3.25 pitch oscillations.

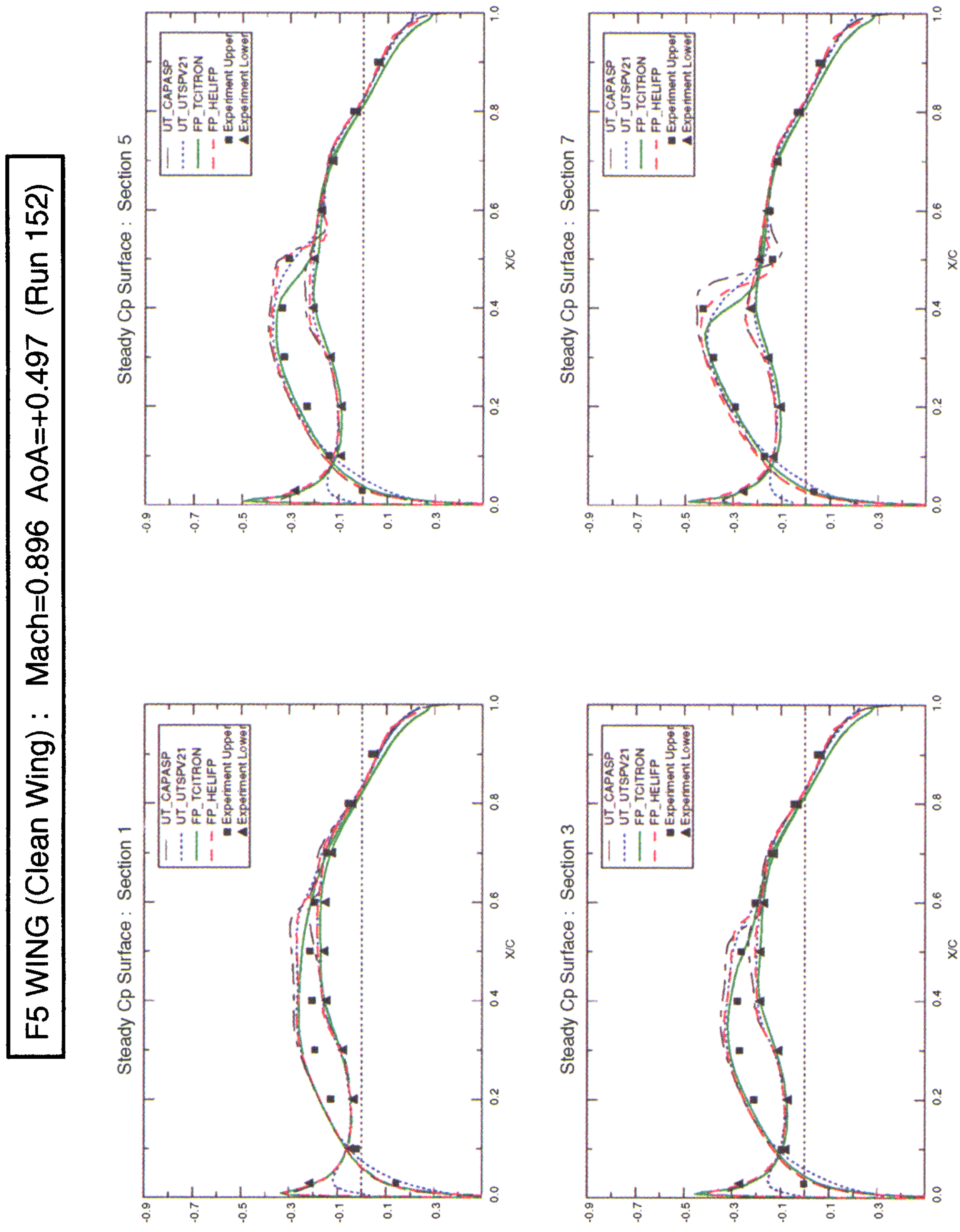

Figure 5 **Code comparisons, steady flow. Run 152 (M=0.896, α=0.497°), Cp vs. X/C for UTSP and Full Potential codes (UTSPV21, CAP-ASP, TCITRON and HELIFP) at sections 1, 3, 5, and 7.**

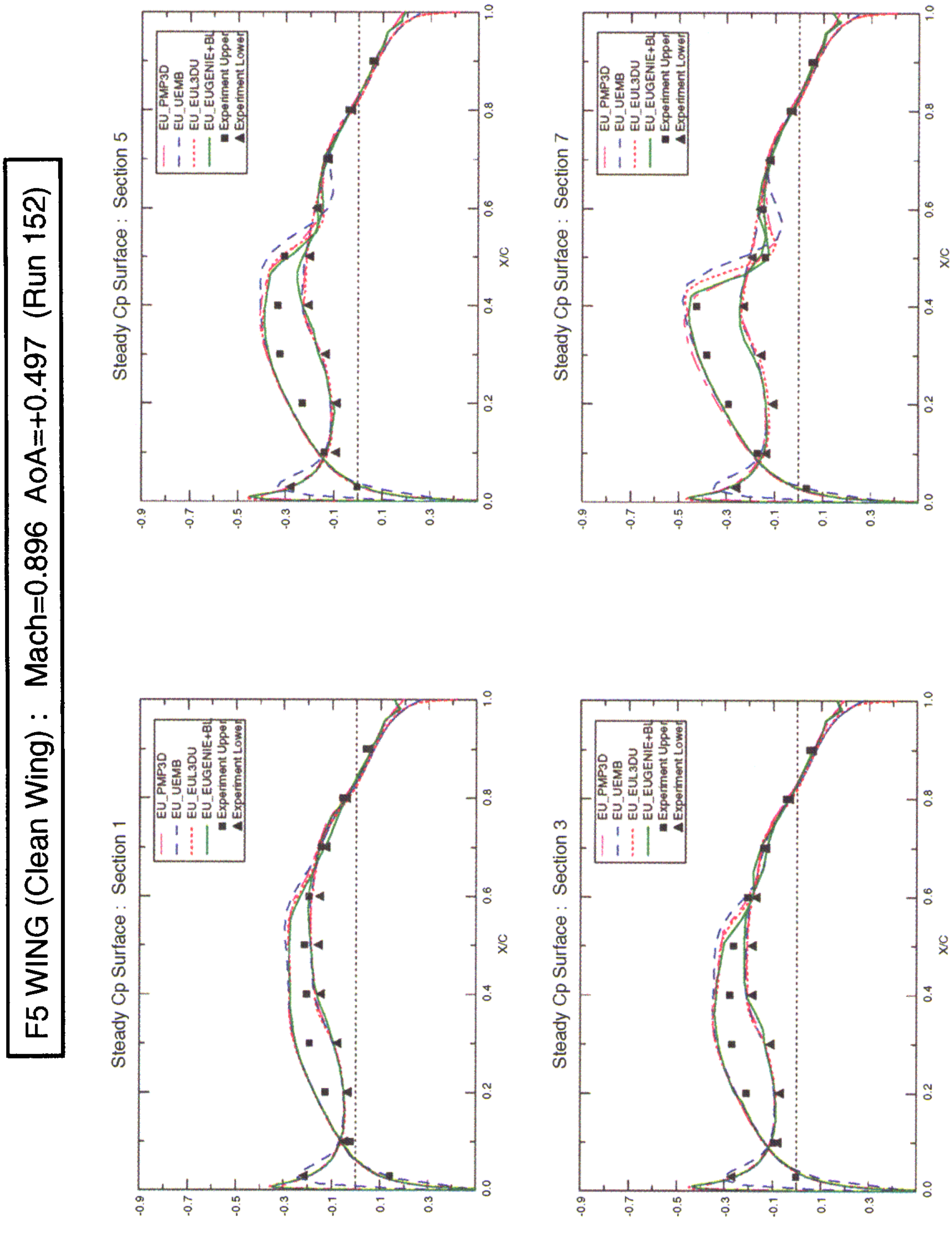

Figure 6 **Code comparisons, steady flow. Run 152 (M=0.896, α=0.497°), Cp vs. X/C for Euler codes (PMB3D, UEMB, EUL3DU and EUGENIE) at sections 1, 3, 5, and 7. Note that for viscous effects are included in EUGENIE through boundary layer coupling.**

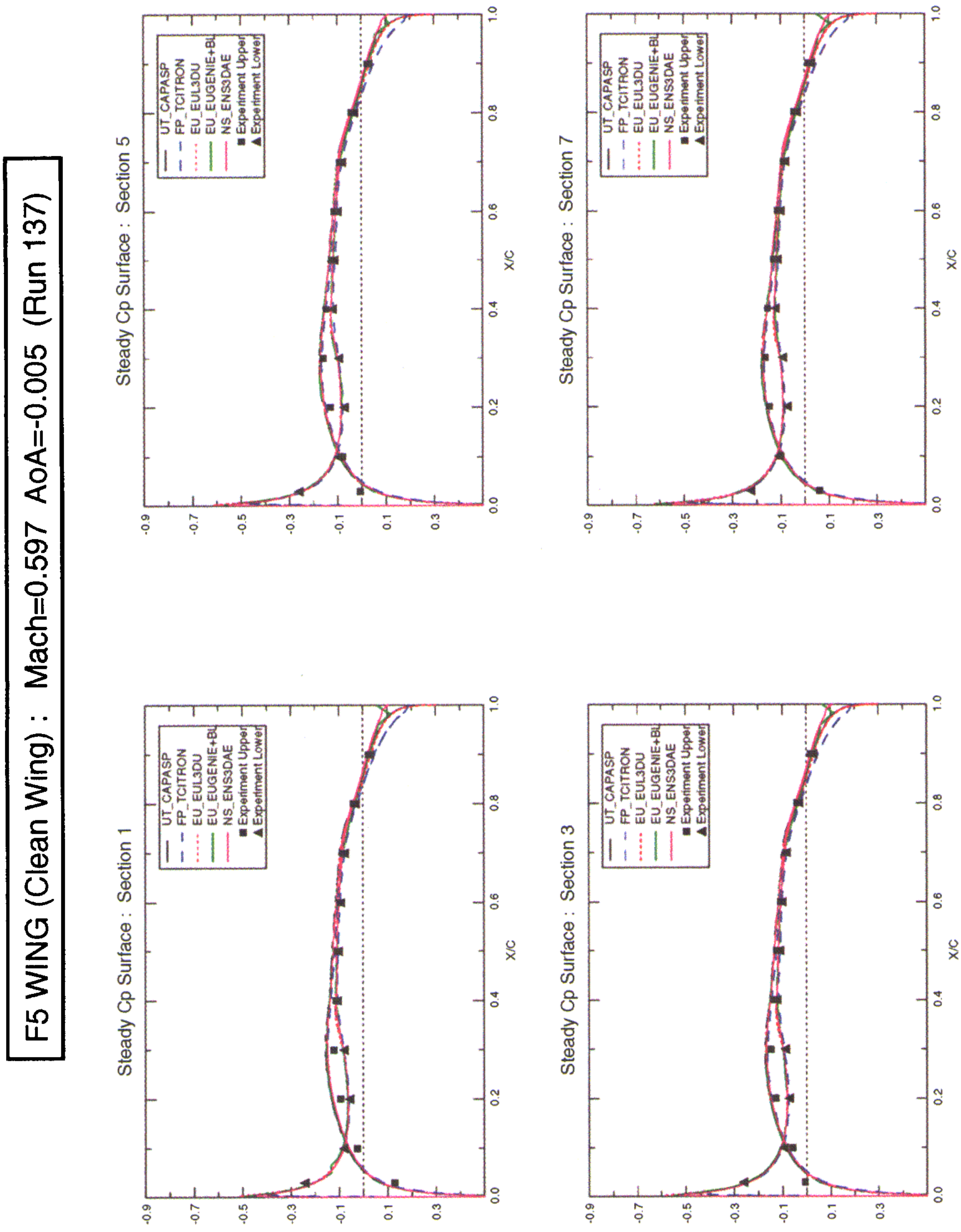

Figure 7 **Method comparisons, steady flow. Run 137 (M=0.597, α=-0.005°), Cp vs. X/C for a selection of UTSP, Full Potential, Euler and Navier-Stokes methods at sections 1, 3, 5, and 7. Note that viscous effects are also introduced into EUGENIE through boundary layer coupling.**

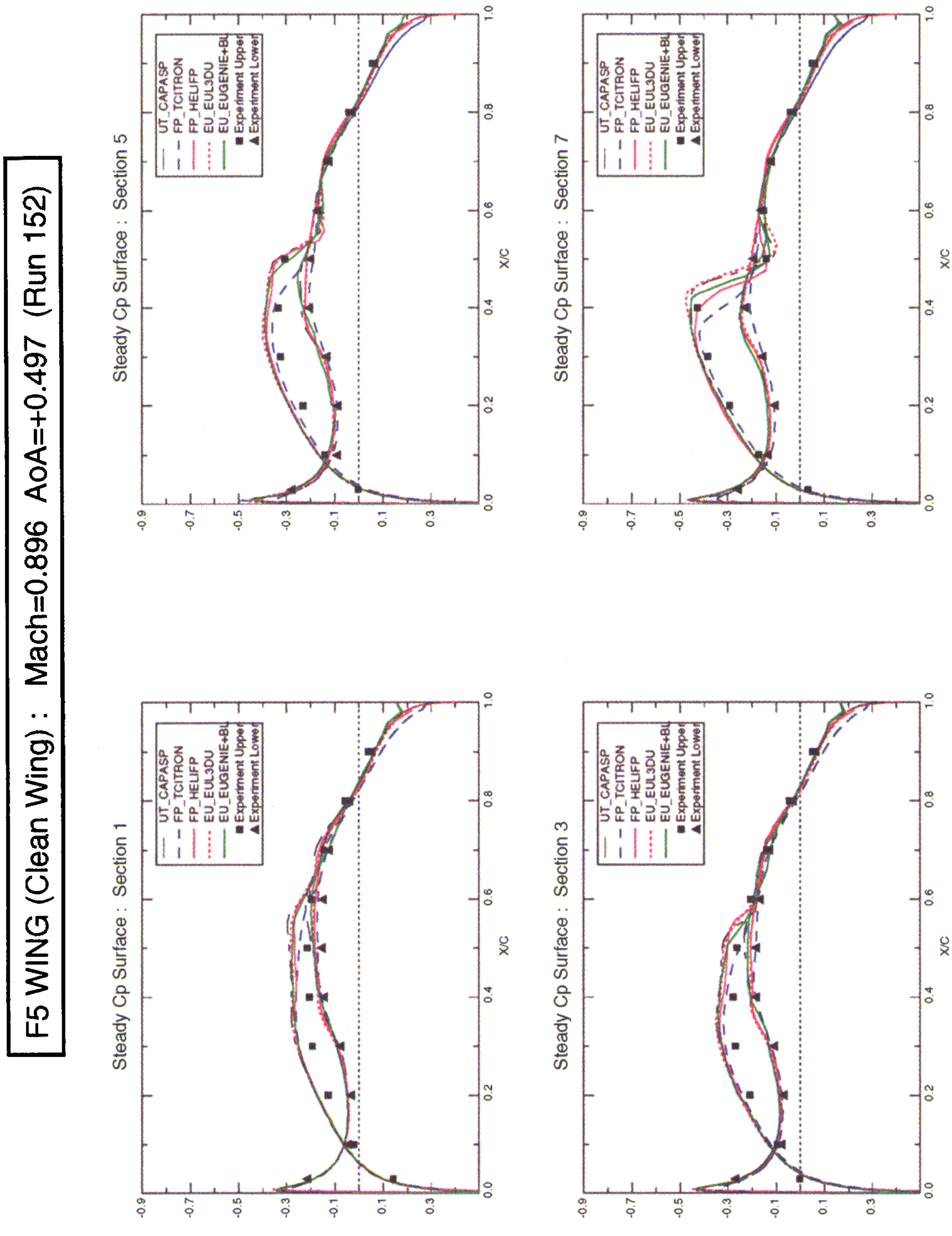

Figure 8 **Method comparisons, steady flow. Run 152 (M=0.896, α=+0.497°), Cp vs. X/C for UTSP, Full Potential and Euler methods at sections 1,3, 5, and 7. Note that EUGENIE includes viscous effects through boundary layer coupling.**

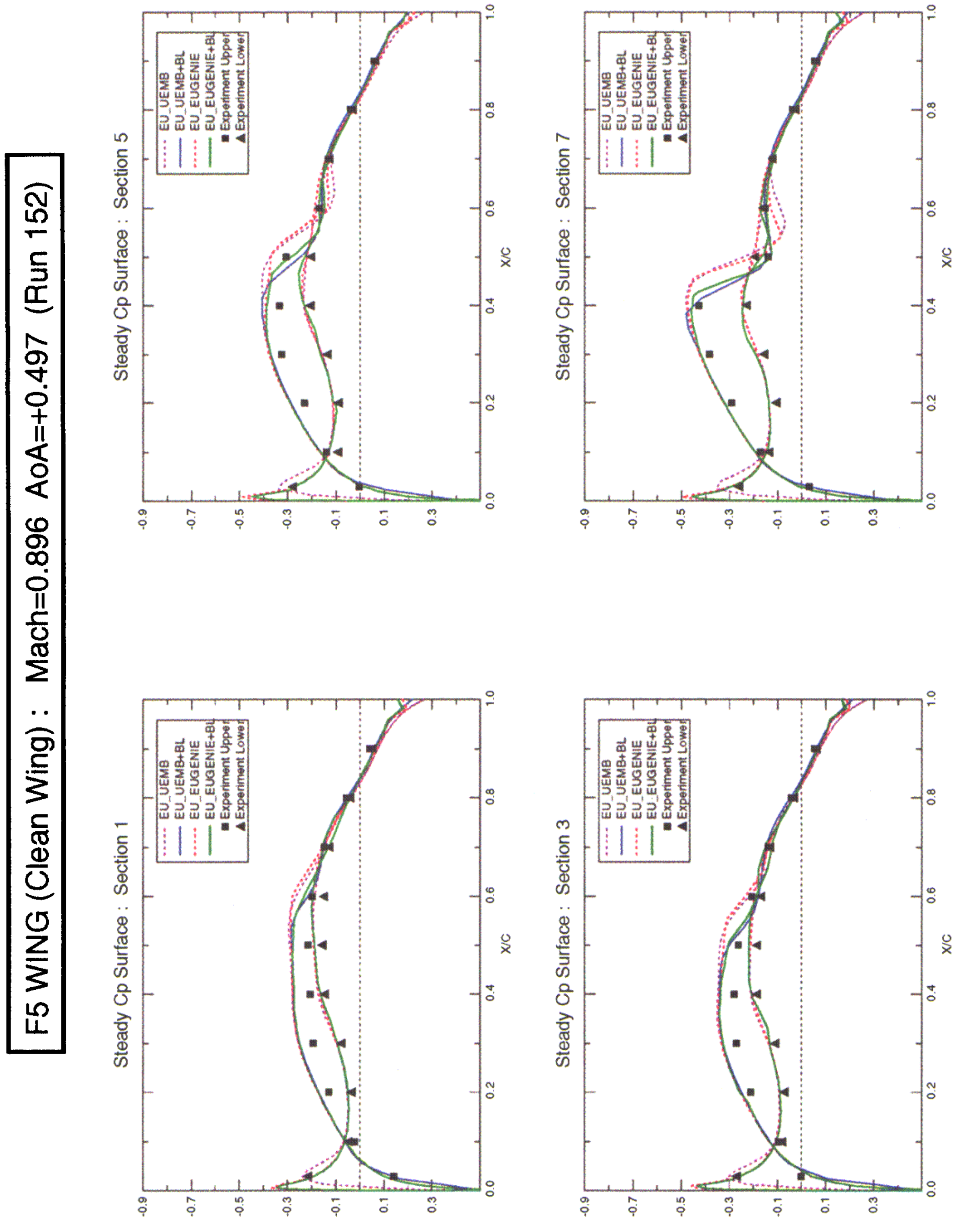

Figure 9 **Code Comparison, steady flow. Run 152 (M=0.896, α=+0.497°), Cp vs. X/C at sections 1, 3, 5 and 7. Euler methods with and without viscous coupling. UEMB (Structured) and EUGENIE (Unstructured).**

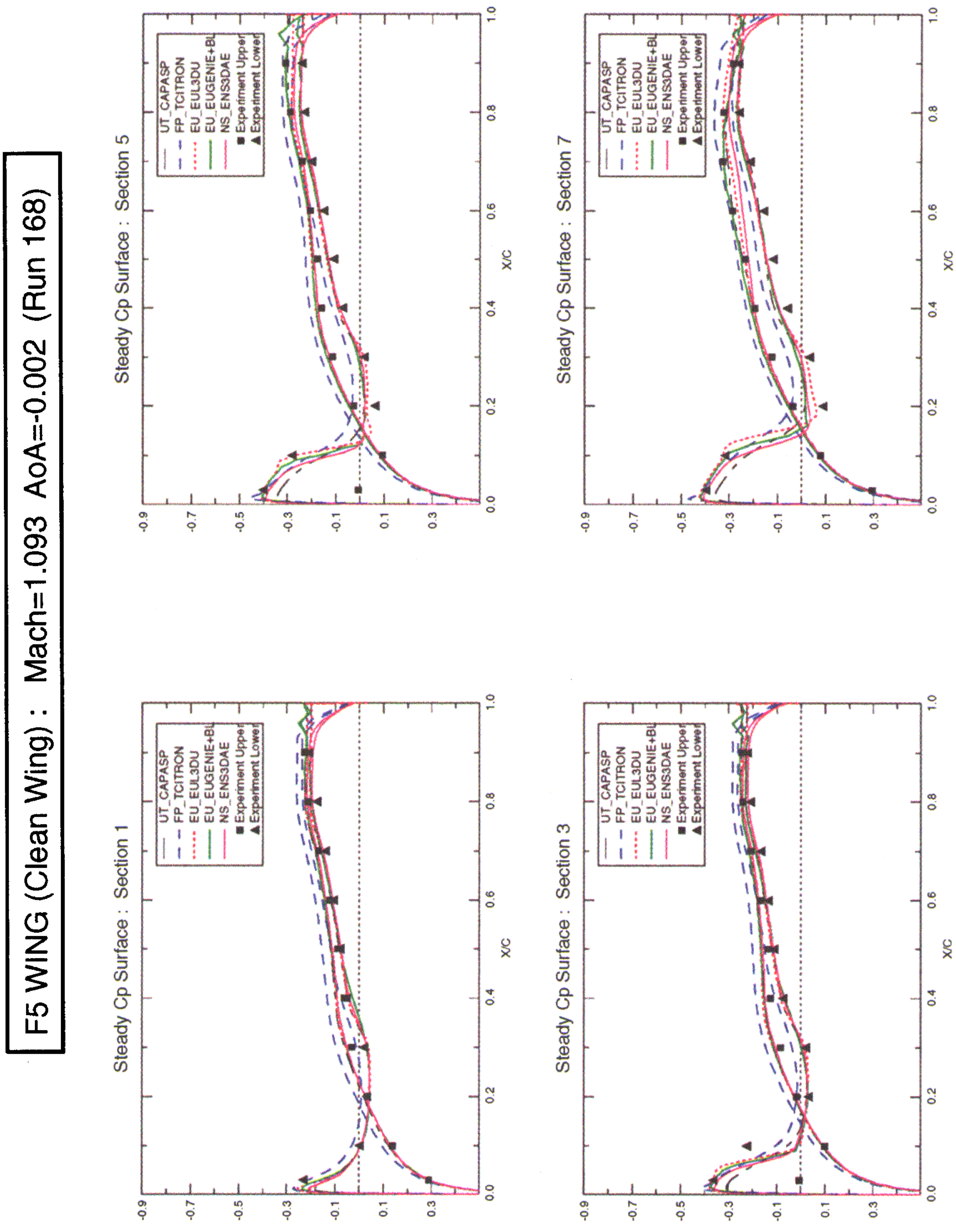

Figure 10 **Method comparisons, steady flow. Run 168 (M=1.093, α=-0.002°), Cp vs. X/C for UTSP, Full Potential, Euler and Navier-Stokes codes at sections 1, 3, 5, and 7. Note that EUGENIE includes viscous effects through boundary layer coupling.**

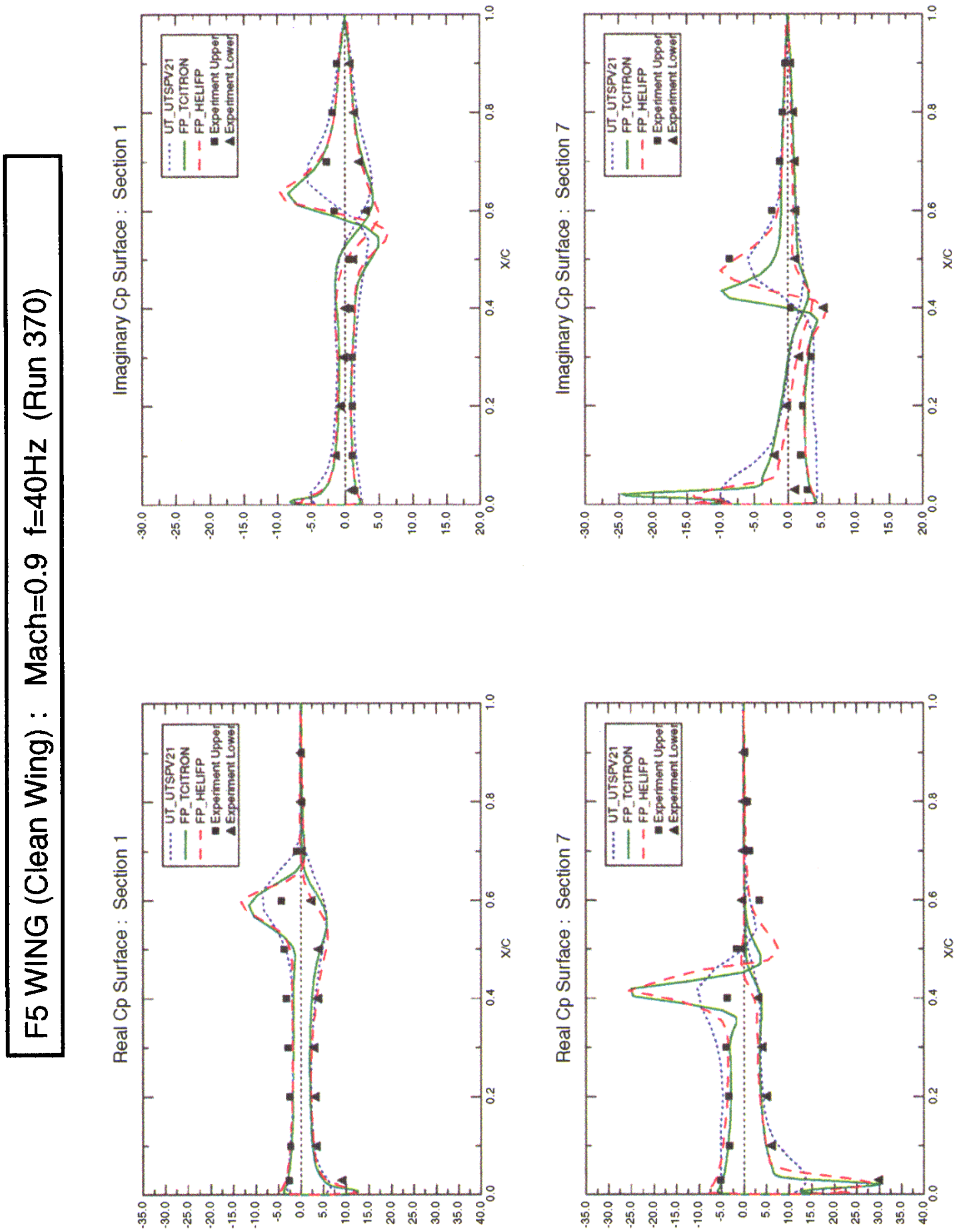

Figure 11 **Code comparisons, unsteady flow. Run 370 (M=0.896, α=0.001°, F=40 Hz, θ=0.111°), CpReal and CpImag vs. X/C for UTSP and Full Potential codes (UTSPV21, TCITRON AND HELIFP) at sections 1 and 7.**

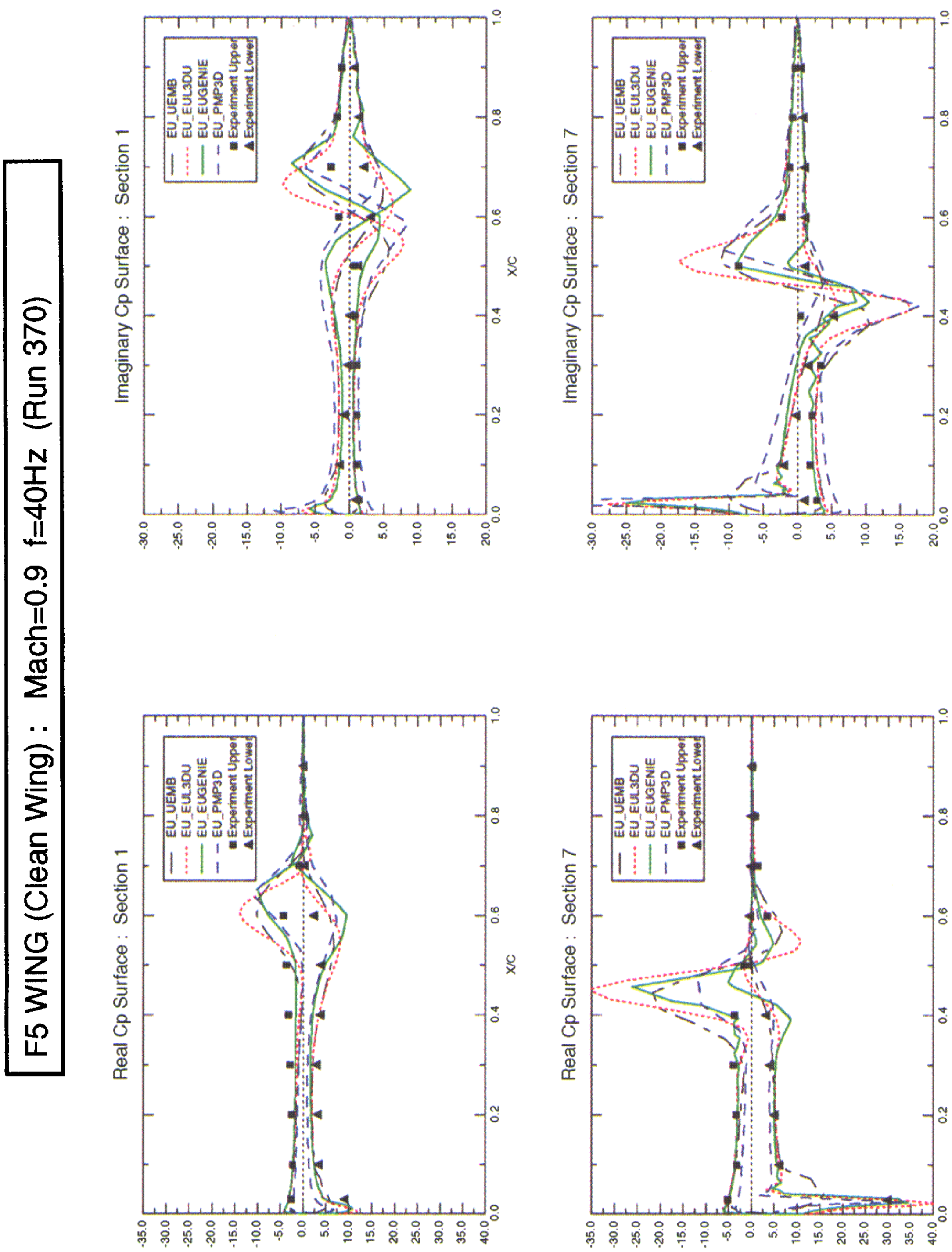

Figure 12 **Code comparisons, unsteady flow. Run 370 (M=0.896, α=0.001°, F=40 Hz, θ=0.111°), CpReal and CpImag vs. X/C for Euler codes (UEMB, EUL3DU, EUGENIE, and PMB3D) at sections 1 and 7.**

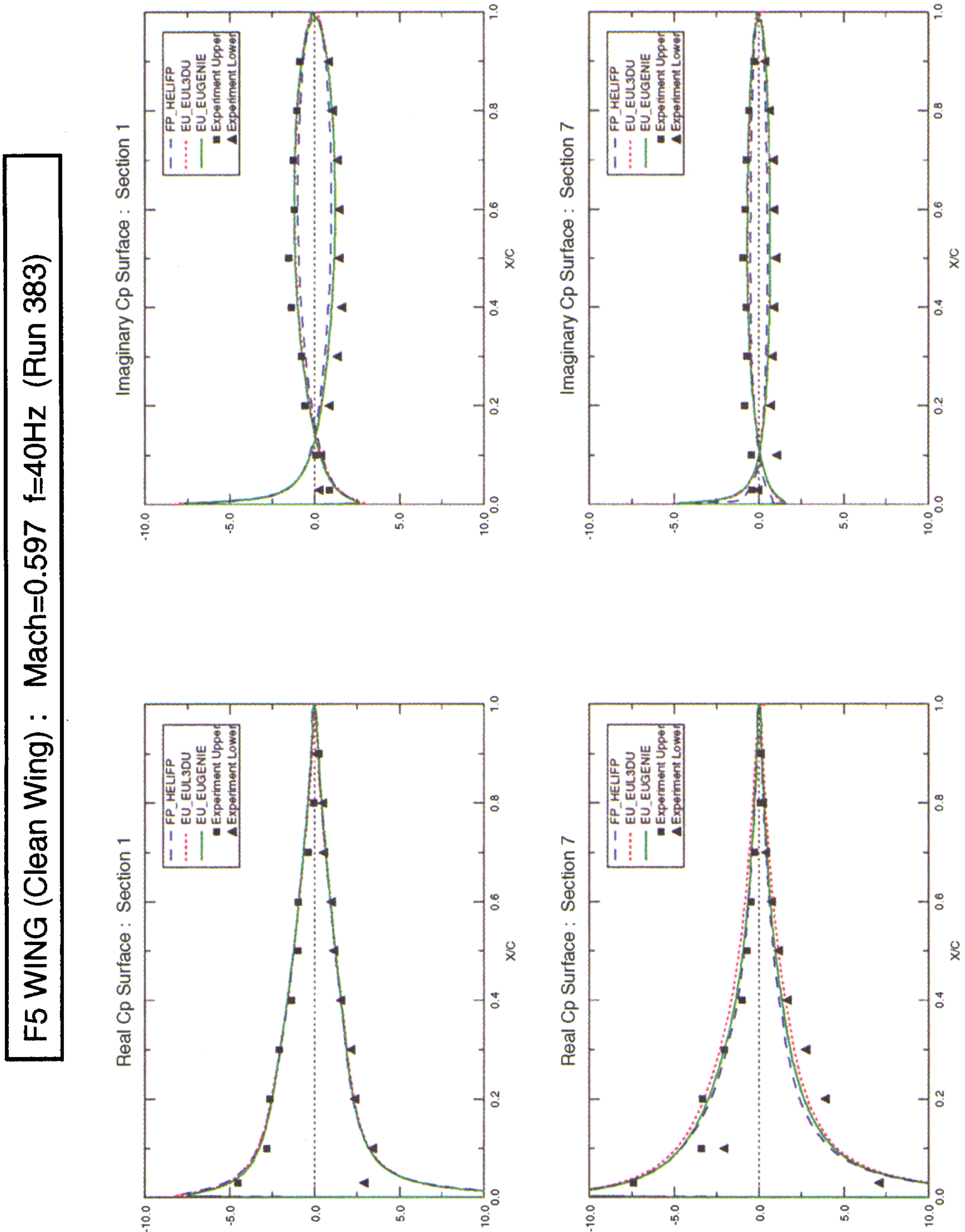

Figure 13 **Method comparisons, unsteady flow. Run 383 (M=0.597, α=0.004°, F=40 Hz, θ=0.399°), CpReal and CpImag vs. X/C for Full Potential and Euler methods at sections 1 and 7.**

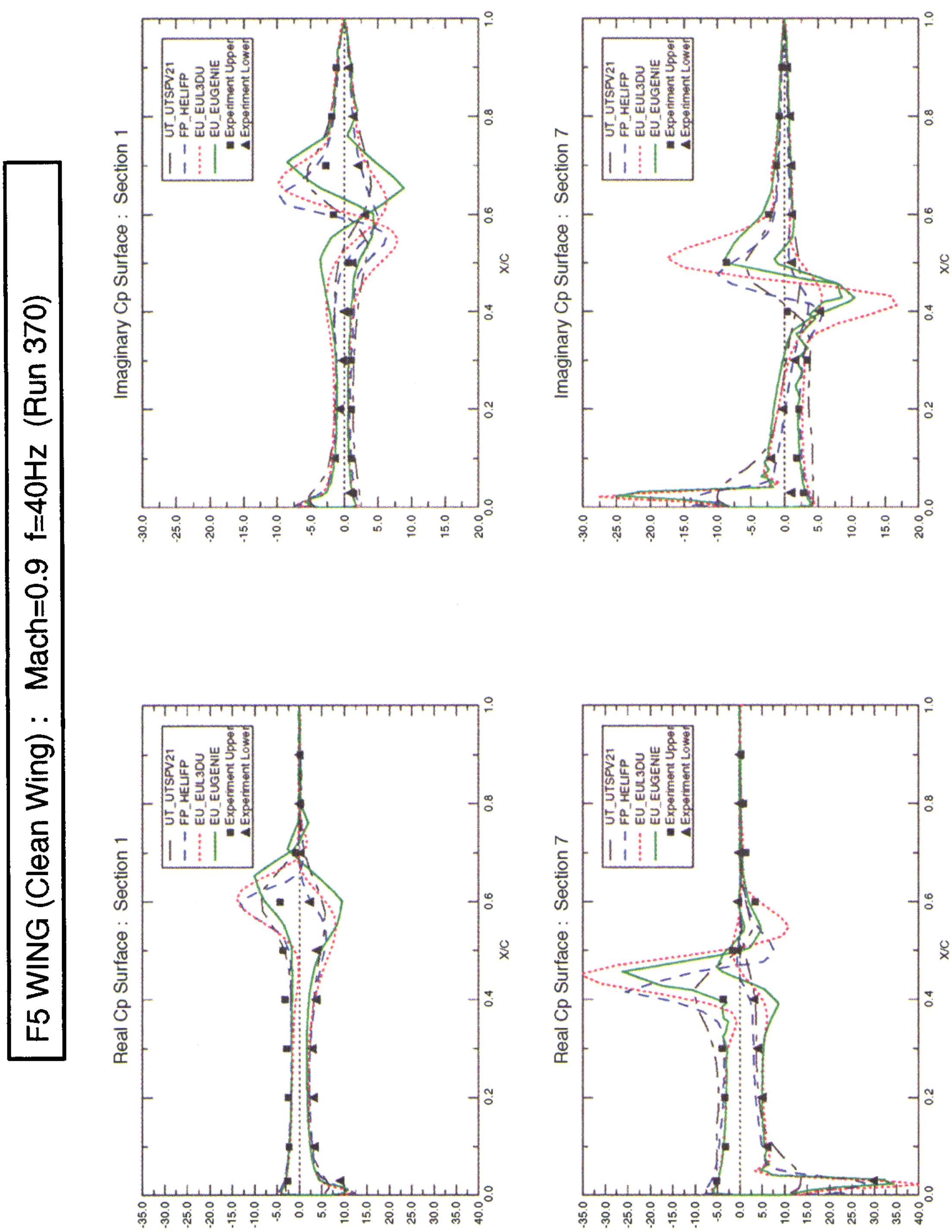

Figure 14 **Method comparisons, unsteady flow. Run 370 (M=0.896, α=0.001°, F=40 Hz, θ=0.275°), CpReal and CpImag vs. X/C for UTSP, Full Potential and Euler codes at sections 1 and 7.**

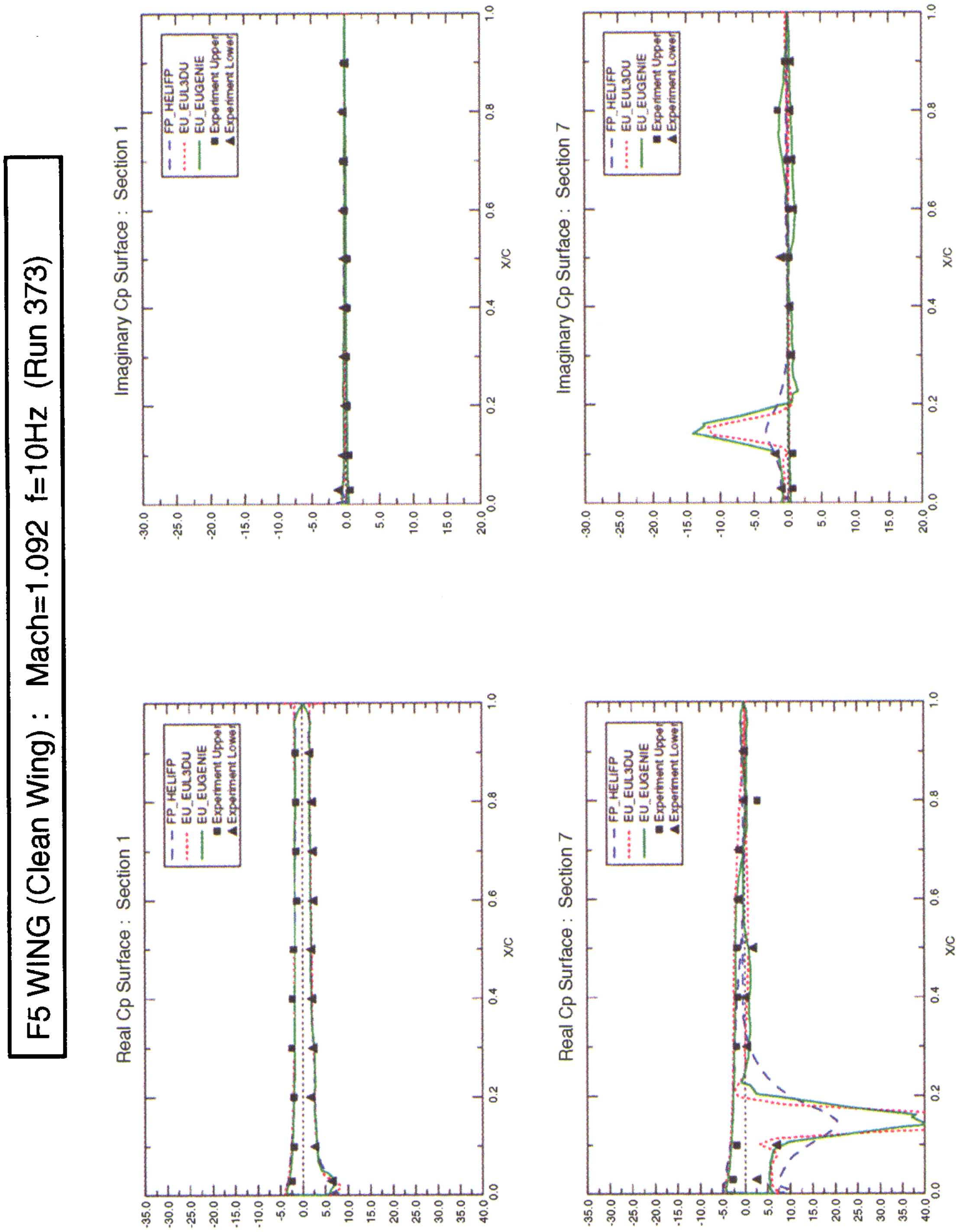

Figure 15 Method comparisons, unsteady flow. Run 373 (M=1.092, α=0.003°, F=10 Hz, θ=0.058°), CpReal and CpImag vs. X/C for Full Potential and Euler codes at sections 1 and 7.

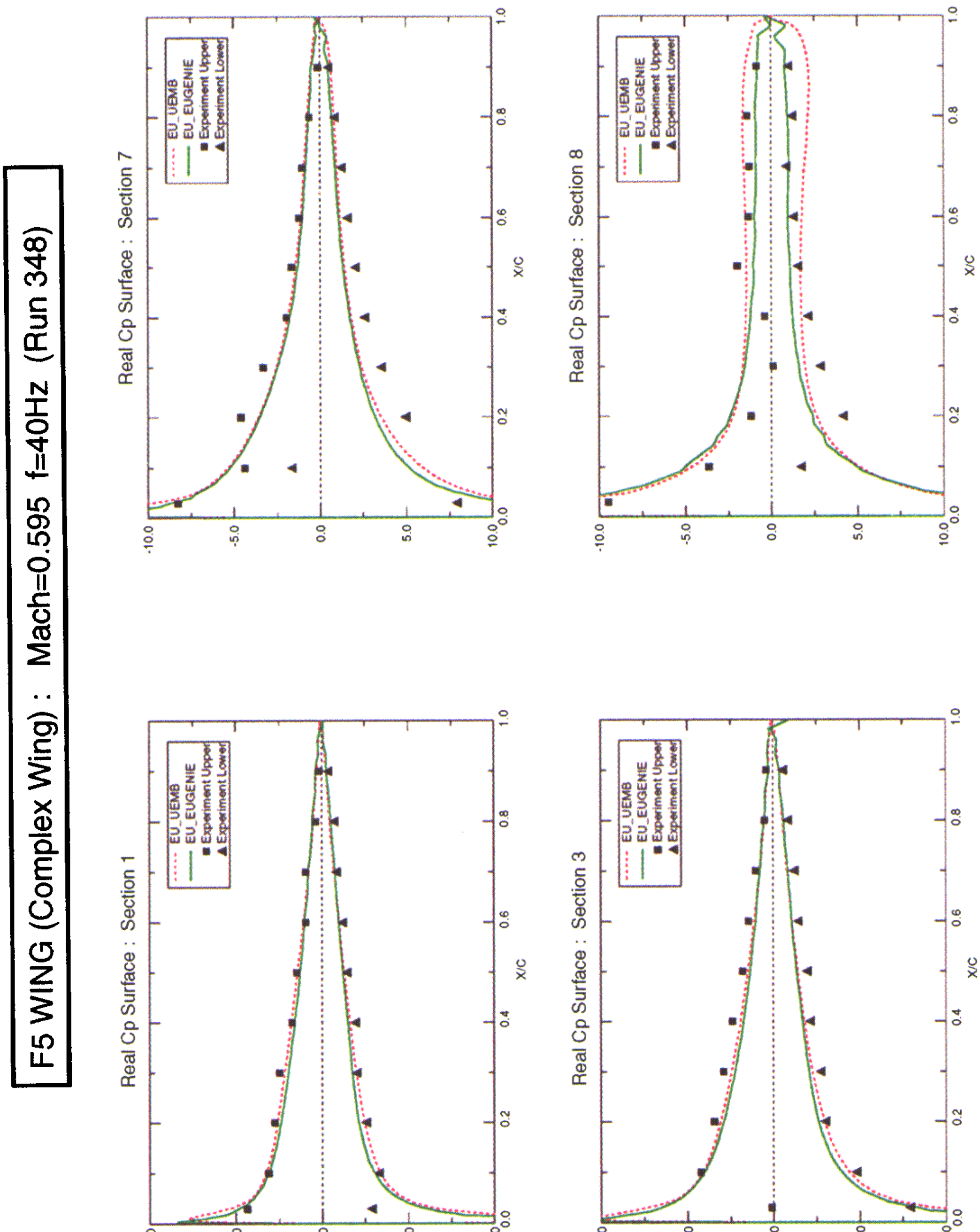

Figure 16 **Code Comparison, unsteady flow. Run 348 (complex geometry, M=0.595, F=40 Hz, α=0.004°, θ=0.111°), CpReal vs. X/C for Euler methods (EUGENIE and UEMB) at sections 1,3,7 and 8.**

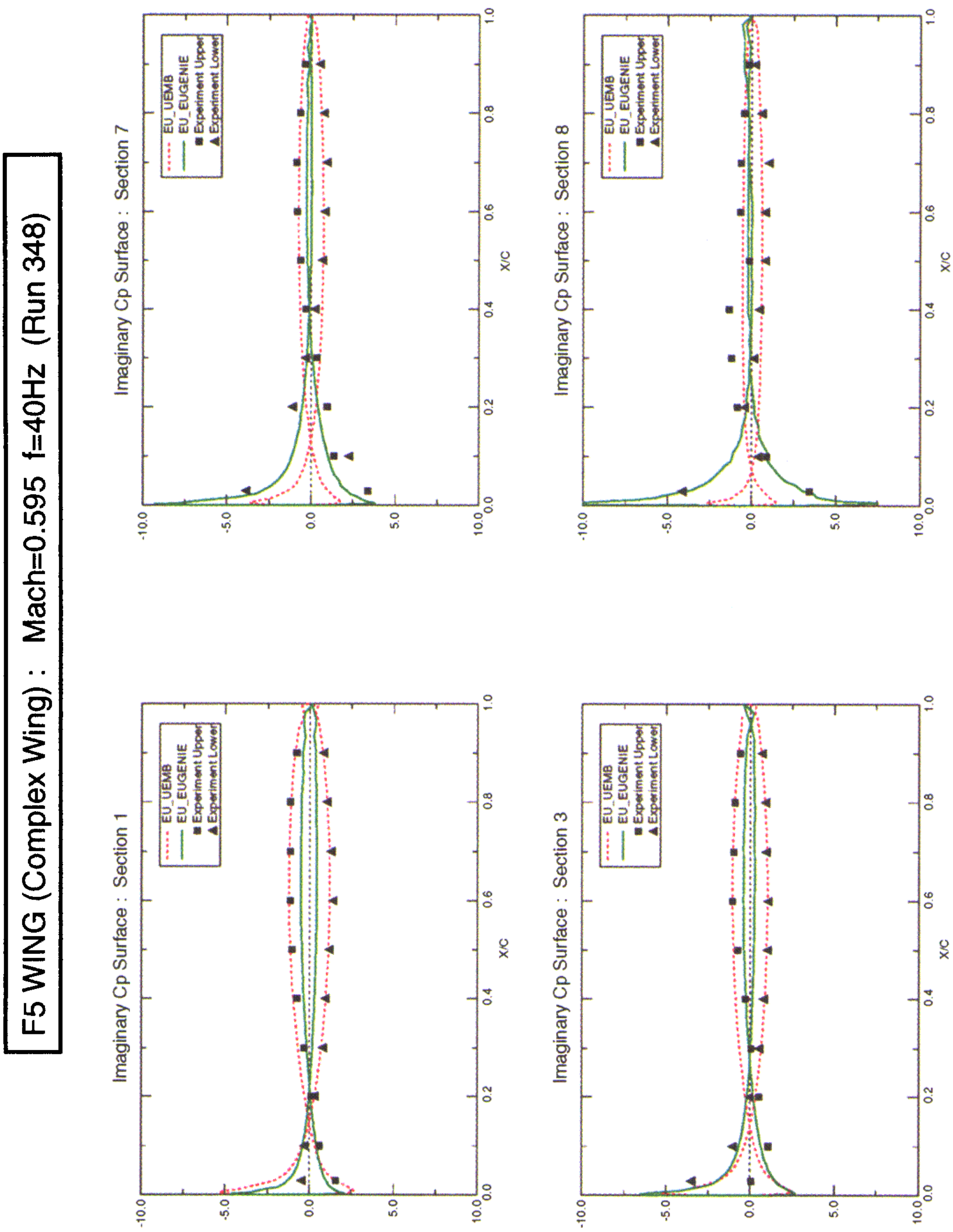

Figure 17 **Method Comparison, unsteady flow. Run 348 (complex geometry, M=0.595, F=40 Hz, α=0.004°, θ=0.111°), CpImag vs. X/C for Euler methods (EUGENIE and UEMB) at sections 1, 3, 7 and 8.**

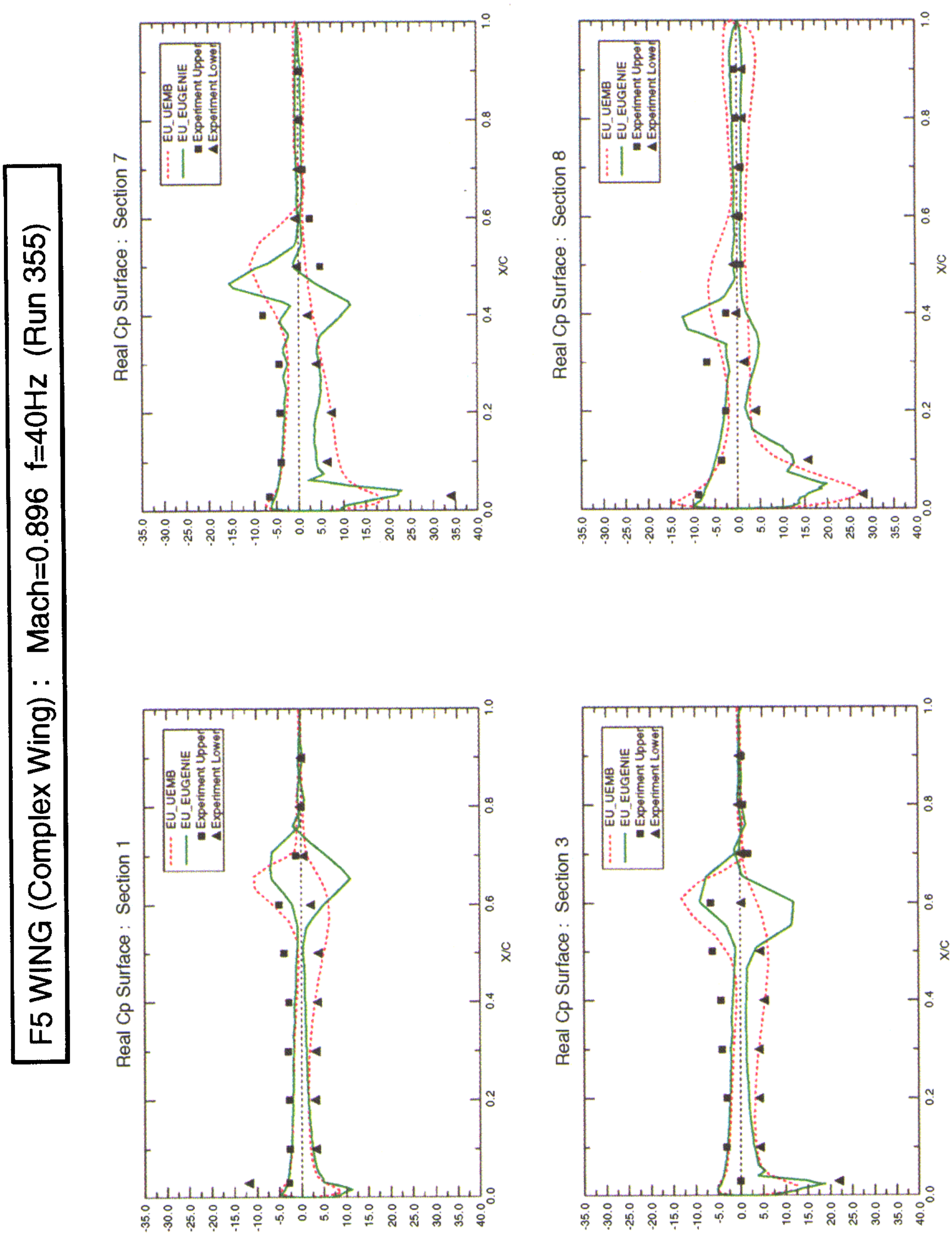

Figure 18 Code Comparison, unsteady flow. Run 355 (complex geometry, M=0.869, F=40 Hz, α=0.004°,θ=0.117°) CpReal vs. X/C for Euler methods (EUGENIE and UEMB) at sections 1, 3, 7 and 8.

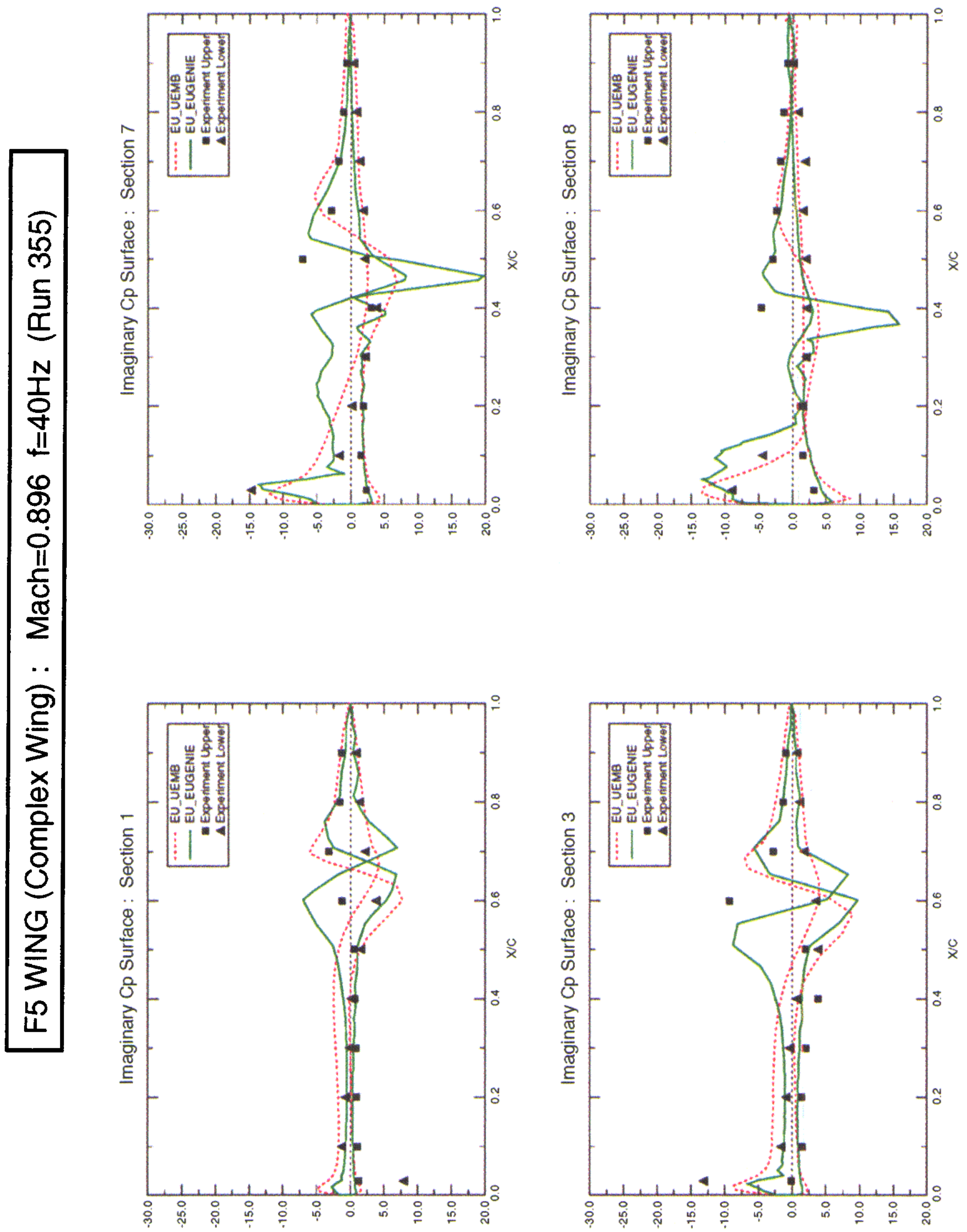

Figure 19 **Code Comparison, unsteady flow. Run 355 (complex geometry, M=0.869, F=40 Hz, α=0.004°,θ=0.117°) CpImag vs. X/C for Euler methods (EUGENIE and UEMB) at sections 1, 3, 7 and 8.**

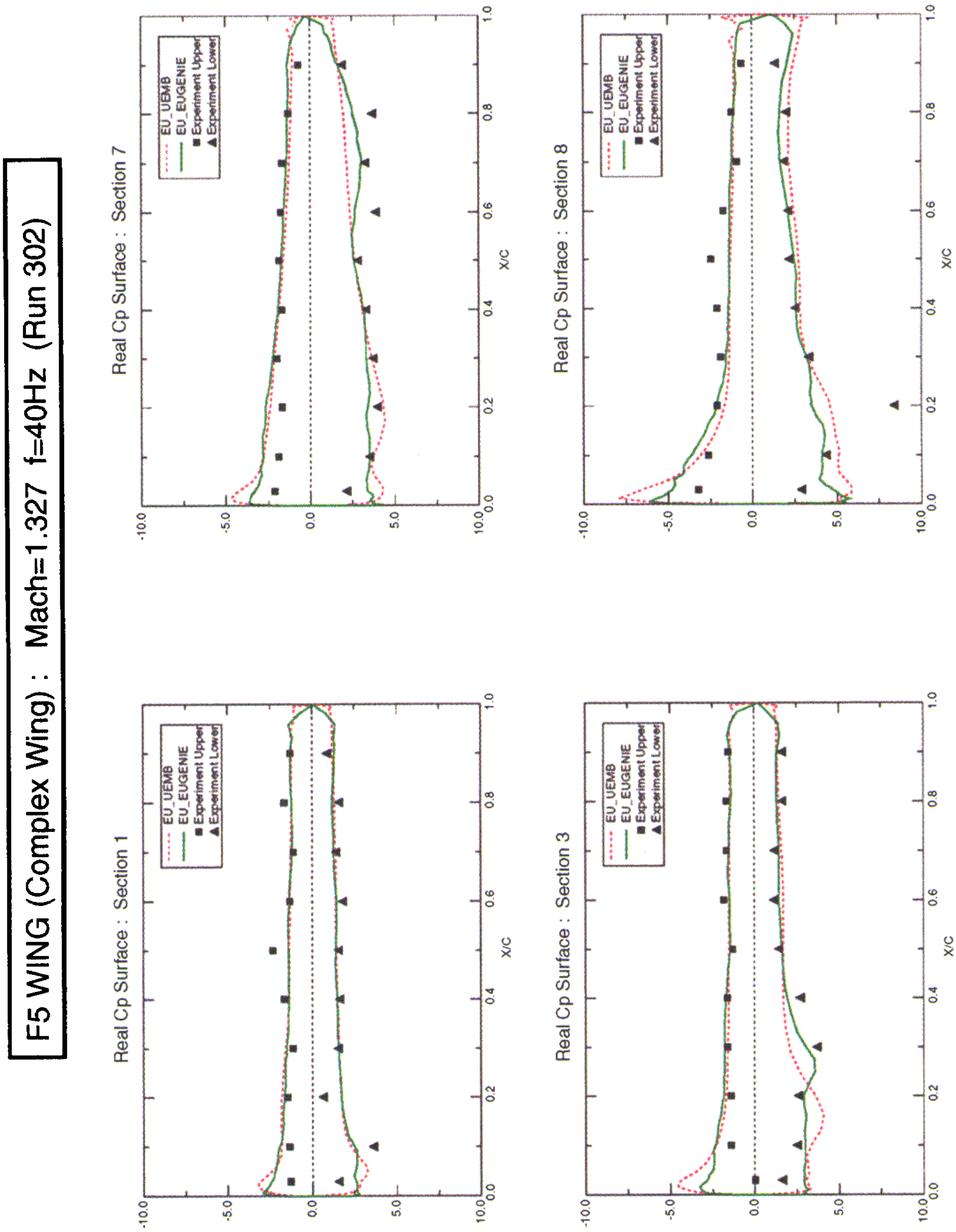

Figure 20 Code Comparison, unsteady flow. Run 302 (complex geometry, M=1.327, F=40 Hz, α=0.16°, θ=0.221°) CpReal vs. X/C for Euler (EUGENIE and UEMB) at sections 1, 3, 7 and 8.

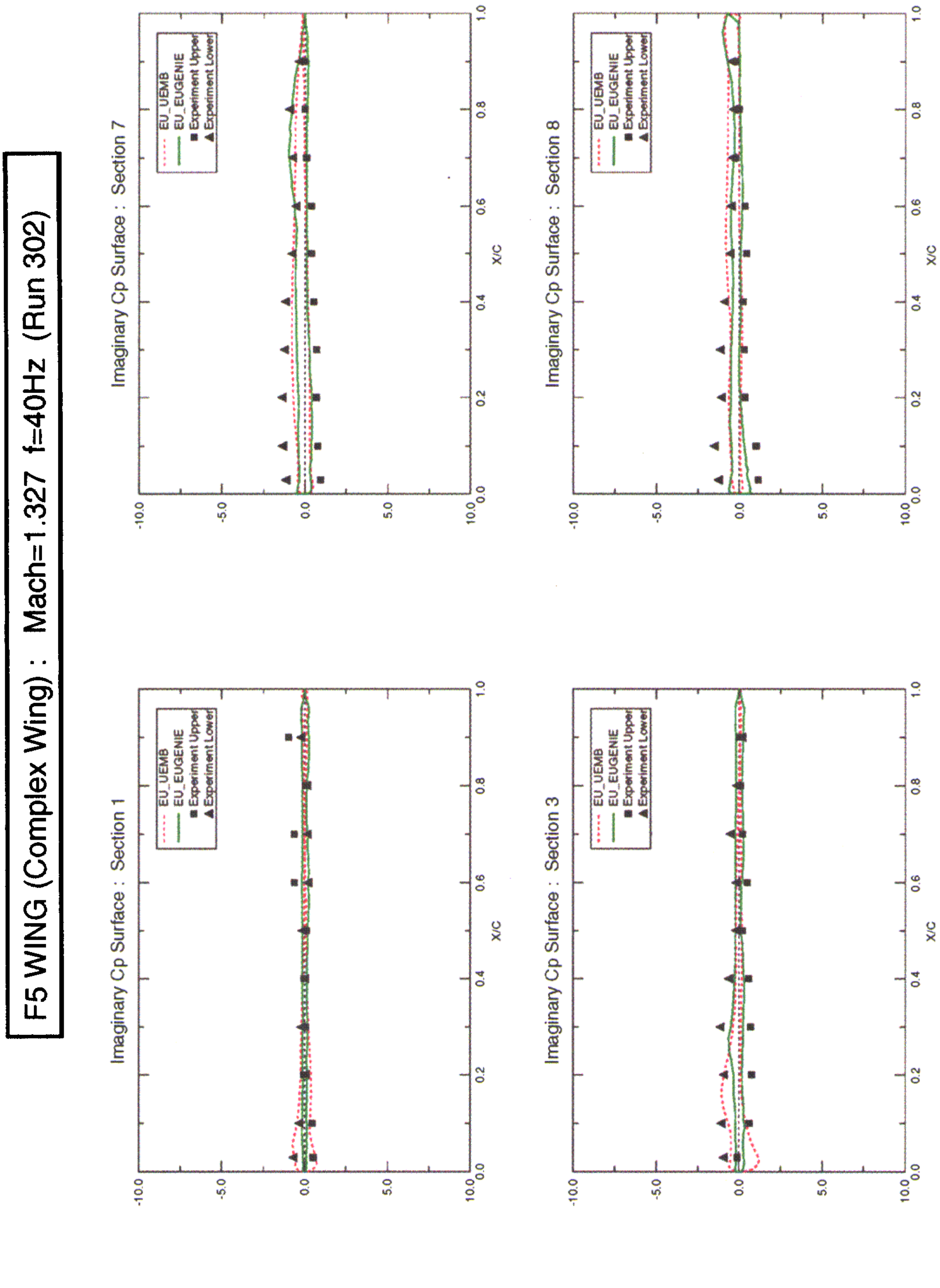

Figure 21 Code Comparison, unsteady flow. Run 302 (complex geometry, M=1.327, F=40 Hz, α=0.16°, θ=0.221°) CpImag vs. X/C for Euler (EUGENIE and UEMB) at sections 1, 3, 7 and 8.

REFERENCES

Ref. 1 Van Nunen J. W. G., Tijdeman H., et. al. (1978), 'Results of transonic wind tunnel measurements on an oscillating wing with external store (data report)', NLR TR 78030 U.

Ref. 2 Tijdeman H., Van Nunen J. W. G., et. al., (1978), 'Transonic wind tunnel tests of an oscillating wing with external store', Parts I-IV, NLR TR 78106 U.

Ref. 3 Pagano A., Renzoni P., Miller J. V., Hounjet M. H. L., Costes M., Le Balleur J. C., Gasparini L., Vigevano L., Kokkalis A., 'Formulation and Solution Algorithm of the Full Potential Code', HELISHAPE Report HELI/R/2/ONERA/02/A, June 1994.

Ref. 4 Costes M. & Le Balleur J. C., Gasparini L. & Vigevano L., Hounjet M. H. L., Kokkalis A. Miller J. V. & Spruce M., Pagano A. & Renzoni P., Rocchetto A., Toulmay F., 'Development of a Common European Unsteady Full Potential Code for Helicopter Rotors in Hover and Forward Flight', presented at American Helicopter Society 53rd Annual Forum, Virginia Beach, Virginia, April 29-May 1, 1997.

Ref. 5 Ruiz-Calavera L. P., 'Parametric Studies of a Time-Accurate Finite-Volume Euler code in the NWT parallel Computer'; AGARD-CP-578; Paper 38, 1995

Ref. 6 Batina, J. T.; Seidel, D. A.; Bland, S. R.; and Bennett, R. M., 'Unsteady Transonic Flow Calculations for Realistic Aircraft Configurations.' J. of Aircraft, vol. 26, no. 1, pp. 21-28, Jan. 1989.

Ref. 7 Schuster, D. M.; Vadyak, J.; and Atta, E.: *Static Aeroelastic Analysis of Fighter Aircraft Using a Three-Dimensional Navier-Stokes Algorithm.* Journal of Aircraft, vol. 27, no. 9, Sep. 1990, pp. 820-825.

Ref. 8 Schuster, D.M., Vadyak, J., and Atta, E., *Flight Loads Prediction Methods for Fighter Aircraft.* WRDC-TR-89-3104, Wright Research and Development Center, Wright-Patterson Air Force Base, OH, November, 1989

Ref. 9 Schuster, D. M.; Beran, P. S.; and Huttsell, L. J.: *Application of the ENSDAE/Navier-Stokes Aeroelastic Method.* Paper No. 3 in Numerical Unsteady Aerodynamics and Aeroelastic Simulation, AGARD Report 822, Mar. 1998.

Ref. 10 Knott M. J., 'Transonic Aeroelastic Calculations in Both the Time and Frequency Domains', in AGARD-CP-507 (73rd SMP), Oct. 1991.

Ref. 11 Anderson W. K. and Batina J. T., 'Accurate solutions, parameter studies, and comparisons for the Euler and potential flow equations', paper no. 15 presented at the AGARD 62nd Meeting of the Fluid Dynamics Panel Symposium on Validation of Computational Fluid Dynamics, Lisbon, Portugal, May 2-5, 1988.

Ref. 12 Dubac L., Cantariti F., Woodgate M., Gribben B., Badcock K. J. and Richards B. E., 'Solution of the unsteady Euler equations using an implicit dual time method', AIAA Journal, Vol. 36, 1417, 1998.

Ref. 13 Jameson A., Schmidt W., and Turkel E., 'Numerical solutions of the Euler equations by finite volumne methods using Runge-Kutta time-stepping schemes', AIAA paper 81-1259, 1981.

ACKNOWLEDGEMENTS

Contributions to this exercise were received from working group members and others outside the working group; the following contributors are acknowledged: R. M. Bennett and D M Schuster (NASA), L. P. Ruiz-Calavera (INTA), A. Pagano (CIRA), M. Woodgate, K. Badcock and F Cantarti (University of Glasgow), D.D. McKiernan (BAe.), E Geurts (NLR).

5E. F-5 WING & F-5 WING + TIP STORE

Evert G.M. Geurts
National Aerospace Laboratory NLR, The Netherlands

INTRODUCTION

This data set relates to a transonic wind tunnel investigation carried out in 1977 on an oscillating, slightly modified model of the outer part of a Northrop F-5 wing with and without an external store. The store represented an AIM-9J missile including its launcher. These tests were reported in references 1, 2 and 3. The model proceeded from an F-5 wing model for subsonic tests by a slight reduction of the model span, needed to accommodate the tip store considered in the document. In streamwise direction the wing possesses a modified NACA 65-A-004.8 airfoil, characterised by a droopnose, extending from the leading edge towards the point of maximum thickness at 40 per cent of the chord.

The aim of the experiments was to determine the unsteady aerodynamic loads on a representative fighter type wing in the transonic and low supersonic speed regimes. Detailed steady and unsteady pressure distributions were measured over the wing, while on the store strain gauge balances obtained aerodynamic loads (Ref. 4). To study the effect of the external store on the unsteady wing loading (interference effects) as well as the unsteady loads on the store itself and its components, the model was tested in various stages of completeness. Starting with the clean wing, successively more parts of the store (launcher, missile body, aft wings, canard fins) were added. Data presented here refer accordingly to the F-5 clean wing configuration, growing in steps to the configuration of the F-5 wing with complete tip store. The model geometry described in the Formulary concerns only the clean wing; geometry data concerning the tip store are not described in this document. However, they are presented in the figures and they are contained in the database on the CD-ROM, accompanying this chapter. Simultaneously with these measurements also wind tunnel wall pressures were recorded to support wall interference effect studies. In the same test also various stages of an underwing missile were measured (pylon, launcher, missile body with aft wings, complete missile). However, no underwing missile data are included in this document.

Subsonic tests on the unmodified wing model in different tip store and underwing configurations were extensively reported in references 5 and 6. Tests on the same wing but with an inboard control surface were reported in reference 7.

The tests on the F-5 wing and F-5 wing with tip store were carried out in the High Speed Tunnel of the National Aerospace Laboratory NLR, in Amsterdam, The Netherlands. The tests covered the Mach number range between Ma = 0.6 and Ma = 1.35, and frequencies up to 40 Hz. An overview of the selected data is given in table 1. For steady measurements steady values are presented; for unsteady measurements mean values are represented as well as real and imaginary part of the unsteady values.

LIST OF SYMBOLS AND DEFINITIONS

Definition of axes systems

Figure 1 shows the body-fixed co-ordinate system used for non-dimensionalisation.

Figure 2 shows the body-fixed axis system (CATIA origin)

x-axis: chordwise co-ordinate in wing reference plane: apex: x = 0

y-axis: spanwise co-ordinate in wing reference plane; y-axis = rotation axis or pitching axis at $x/C_r = 50.00$ %

z-axis: co-ordinate in plane of symmetry normal to wing reference plane

Definitions of pressure, force and moment coefficients for the wing

Steady and mean

Pressure coefficient $C_p = (P_{loc} - P) / Q$

Sectional normal force $C_z = Z / (Q * C) = - \int_0^1 (C_{p+} - C_{p-}) \, d(x/C)$

Sectional pitching moment about quarter-chord point (positive nose down) $C_m = M / (Q * C^2) = - \int_0^1 (C_{p+} - C_{p-}) (x/C - 0.25) \, d(x/C)$

Unsteady

Pressure coefficient $C_{pi} = \mathrm{Re}\, C_{pi} + i\, \mathrm{Im}\, C_{pi} = P_i / (Q * \theta)$

Sectional normal force	$C_{zi} = \text{Re}\, C_{zi} + i\, \text{Im}\, C_{zi} = Z_i / (\pi Q C \theta) = (1/\pi) \int_0^1 (C_{pi-} - C_{pi+})\, d(x/C)$
Sectional pitching moment about quarter-chord point (positive nose down)	$C_{mi} = \text{Re}\, C_{mi} + i\, \text{Im}\, C_{mi} = M_i / (\tfrac{1}{2}\pi Q C^2 \theta) = (2/\pi) \int_0^1 (C_{pi-} - C_{pi+})(x/C - 0.25)\, d(x/C)$

Quasi-Steady at zero incidence ($\omega = 0;\ \alpha_0 = 0$)

Pressure coefficient	$C_{pq} = \Delta C_p / \Delta\alpha = \{C_p(\alpha_0 + \Delta\alpha_1) - C_p(\alpha_0 - \Delta\alpha_2)\} / \{\Delta\alpha_1 + \Delta\alpha_2\}$
Sectional normal force	$C_{zq} = Z_q / (\pi Q C \theta) = \{C_z(\alpha_0 + \Delta\alpha_1) - C_z(\alpha_0 - \Delta\alpha_2)\} / \pi \{\Delta\alpha_1 + \Delta\alpha_2\}$
Sectional pitching moment (positive nose down)	$C_{mq} = M_q / (\tfrac{1}{2}\pi Q C^2 \theta) = 2\{C_m(\alpha_0 + \Delta\alpha_1) - C_m(\alpha_0 - \Delta\alpha_2)\} / \pi \{\Delta\alpha_1 + \Delta\alpha_2\}$

Definitions of force and moment coefficients of pylon and store

Steady and mean

Normal force	$C_z = Z / (Q * \bar{c} * S)$
Side force	$C_y = Y / (Q * \bar{c} * S)$
Pitching moment about balance centre (positive nose up)	$C_m = M / (Q * \bar{c}^2 * S)$
Yawing moment about balance centre (positive nose inward)	$C_n = N / (Q * \bar{c}^2 * S)$

Unsteady

Normal force	$C_{zi} = \text{Re}\, C_{zi} + i\, \text{Im}\, C_{zi} = Z_i / (\pi Q \bar{c} S \theta)$
Side force	$C_{yi} = \text{Re}\, C_{yi} + i\, \text{Im}\, C_{yi} = Y_i / (\pi Q \bar{c} S \theta)$
Pitching moment about balance centre (positive nose up)	$C_{mi} = \text{Re}\, C_{mi} + i\, \text{Im}\, C_{mi} = M_i / (\tfrac{1}{2}\pi Q \bar{c}^2 S \theta)$
Yawing moment about balance centre (positive nose inward)	$C_{ni} = \text{Re}\, C_{ni} + i\, \text{Im}\, C_{ni} = N_i / (\tfrac{1}{2}\pi Q \bar{c}^2 S \theta)$

Quasi-Steady at zero incidence ($\omega = 0;\ \alpha_0 = 0$)

Normal force	$C_{zq} = Z_i / (\pi Q \bar{c} S \theta) = \{C_z(\alpha_0 + \Delta\alpha_1) - C_z(\alpha_0 - \Delta\alpha_2)\} / \pi \{\Delta\alpha_1 + \Delta\alpha_2\}$
Side force	$C_{yq} = Y_i / (\pi Q \bar{c} S \theta) = \{C_y(\alpha_0 + \Delta\alpha_1) - C_y(\alpha_0 - \Delta\alpha_2)\} / \pi \{\Delta\alpha_1 + \Delta\alpha_2\}$
Pitching moment about balance centre (positive nose up)	$C_{mq} = M_i / (\tfrac{1}{2}\pi Q \bar{c}^2 \theta) = 2\{C_m(\alpha_0 + \Delta\alpha_1) - C_m(\alpha_0 - \Delta\alpha_2)\} / \pi \{\Delta\alpha_1 + \Delta\alpha_2\}$
Yawing moment about balance centre (positive nose inward)	$C_{nq} = N_i / (\tfrac{1}{2}\pi Q \bar{c}^2 \theta) = 2\{C_n(\alpha_0 + \Delta\alpha_1) - C_n(\alpha_0 - \Delta\alpha_2)\} / \pi \{\Delta\alpha_1 + \Delta\alpha_2\}$

Symbols

ALPHA, alpha, α	(°)	incidence, positive nose up
C	(m)	local chord
C	(-)	coefficient (followed by symbol or subscript)
C_r	(m)	root chord: $C_r = 0.6396$ m
$\bar{c}$	(m)	mean geometric chord: $\bar{c} = 0.4183$ m
F	(Hz)	frequency, frequency of model oscillation

K	(-)	reduced frequency, $K = \pi * F * C_r / V$
Ma, MA	(-)	freestream Mach number
M	(Nm)	pitching moment
N	(N)	wing normal force
P	(Pa)	freestream static pressure
P_0, P0	(Pa)	stagnation pressure
P_{loc}, PLOC	(Pa)	local static pressure
P_i	(Pa)	unsteady pressure at model surface
PPL	(Pa)	settling chamber pressure
Q	(Pa)	dynamic pressure
Re, RE	(-)	Reynolds number (x 10^{-6}) based on $\bar{c}$
S	(m)	semi-span: S = 0.6226 m
t	(s)	time
T0	(° C)	stagnation temperature
THETA, theta, θ	(°, rad)	amplitude of oscillation in section of accelerometers 1 and 2; positive nose up
V	(m/s)	freestream velocity
x	(m)	chordwise ordinate (see Definitions)
y	(m)	spanwise ordinate (see Definitions)
Y	(N)	side force
z	(m)	co-ordinate in plane of symmetry normal to WRP (see Definitions)
Z	(N)	normal force
α, ALPHA, alpha	(°)	incidence; positive nose up
θ, THETA, theta	(°, rad)	amplitude of oscillation in the section of accelerometers 1 and 2; positive nose up
ω	(rad/s)	angular velocity; $\omega = 2\pi * F$

Subscripts

I, i	referring to unsteady quantities
Q, q	referring to quasi-steady quantities

Suffices

+	denotes upper surface
-	denotes lower surface

Abbreviations

LVDT	Linear Variable Displacement Transducer
RE, Re	real part of complex number
IM, Im	imaginary part of complex number
WRP	Wing Reference Plane (Definition: Figure 1)

FORMULARY

1 General Description of model

1.1	Designation	F5 wing + store
1.2	Type	Semi-span model with modified NACA 65-A-004.8 airfoil
1.3	Derivation	Fighter-type wing
1.4	Additional remarks	AIM-9J launcher/missile
1.5	References	-

2 Model Geometry

2.1	Planform	Trapezoidal (swept tapered)
2.2	Aspect ratio	2.977
2.3	Leading edge sweep	31.917° (31°55')
2.4	Trailing edge sweep	5.033° (5°2')
2.5	Taper ratio	0.308
2.6	Twist	-
2.7	Root chord	0.6396
2.8	Semi-span of model	0.6226 (fairing excluded)
2.9	Area of planform	0.2604
2.10	Leading edge flap	-
2.11	Trailing edge flap	-
2.12	Reference locations and profile definitions	NACA 65-A-004.8 up to 40%, further backwards symmetrical (co-ordinates included in database in file "f5w.crd")
2.13	Form of wing body- or wing-root junction	No body
2.14	Form of wing tip	Fairing for clean wing, co-ordinates at 4 sections, See Table 2; see Figure 1
2.15	Additional remarks	Geometry data of all configurations are included as CATIA files in the database on CD-ROM
2.16	References	-

3 Wind Tunnel

3.1	Designation	NLR High Speed Tunnel (HST)
3.2	Type of tunnel	Continuous, variable pressure
3.3	Test section dimensions	Height: 1.6 m, width: 2.0 m, enclosed in large plenum chamber
3.4	Type of roof and floor	Slotted, 6 slots per wall
3.5	Type of side walls	Solid
3.6	Ventilation geometry	Roof and floor: open ratio 12%
3.7	Displacement thickness of side wall boundary layer	~ 7 mm
3.8	Thickness of boundary layers at roof and floor	Not measured
3.9	Method of measuring Mach number	Derived from settling chamber stagnation and plenum chamber static pressures
3.10	Flow angularity	< 0.1° in centre of test section, less than 0.25° elsewhere
3.11	Uniformity of Mach number over test section	< 0.4% in ΔM/M at supersonic Mach numbers
3.12	Sources and levels of noise or turbulence in empty tunnel	< 1% in rms p/q for M=0.8

3.13	Tunnel resonance	No evidence of resonance
3.14	Additional remarks	Information on flow angularity and Mach number uniformity available only along test section centreline
3.15	References on tunnel	Ref. 8.

4 Model motion

4.1	General description	Sinusoidal pitching about axis normal to wind tunnel side wall. Axis location at 50% root chord
4.2	Reference co-ordinate and definition of motion	Oscillation amplitude measured with LVDT on actuator
4.3	Range of amplitude	Between 0.1° and 0.5°.
4.4	Range of frequency	10, 20, 30 and 40 Hz
4.5	Method of applying motion	Electro-hydraulic shaker system (HYDRA), see Ref.10
4.6	Timewise purity of motion	Adequate purity of sinusoid
4.7	Natural frequencies and normal modes of model	Not traceable, but far enough from driving frequencies
4.8	Method of applying motion	Actual modes measured with accelerometers: Wing 8, store 4 (position and output of accelerometers included in database files)
4.9	Additional remarks	-

5 Test Conditions

5.1	Model planform area/tunnel area	0.0814
5.2	Model span/tunnel width	0.3113
5.3	Blockage	Negligible
5.4	Position of model in tunnel	Standard sidewall position
5.5	Range of Mach number	0.6 to 1.35
5.6	Range of tunnel total pressure	70 kPa and 100 kPa
5.7	Range of tunnel total temperature	Total temperature included in data point information
5.8	Range of model steady or mean incidence	-0.5°, 0.0°, +0.5°
5.9	Definition of model incidence	Relative to line of symmetry of rear part
5.10	Position of transition, if free	Not measured
5.11	Position and type of trip, if transition fixed	No transition trips
5.12	Flow instabilities during tests	None encountered
5.13	Changes to mean shape of model due to steady aerodynamic load	Not measured
5.14	Additional remarks	-
5.15	References describing tests	References 1 and 2

6 Measurements and Observations

6.1	Steady pressures for the mean conditions	Wing	Yes
		Slotted top wall	Yes
6.2	Steady pressures for small changes from the mean conditions	Wing	Yes
6.3	Quasi-steady pressures	Wing	Yes
6.4	Unsteady pressures	Wing	Yes
		Slotted top wall	Yes
6.5	Steady forces for the mean conditions	Store: measured directly	Yes
		Wing: Integrated pressures	Yes
6.6	Steady forces for small changes from the	Store: measured directly	Yes

	mean conditions		
		Wing: Integrated pressures	Yes
6.7	Quasi-steady forces	Store: measured directly	Yes
		Wing: Integrated pressures	Yes
6.8	Unsteady forces	Store: measured directly	Yes
		Wing: Integrated pressures	Yes
6.9	Measurement of actual motion at points of model		Yes
6.10	Observation or measurement of boundary layer properties		No
6.11	Visualisation of (surface) flow		No
6.12	Visualisation of shock wave movements		No
6.13	Additional remarks	-	

7 Instrumentation

7.1 Steady pressure

7.1.1 Position of orifices spanwise and chordwise	8 spanwise sections, 10 upper and 10 lower, see Figure 1 and CD-ROM file "sensors.txt"
7.1.2 Type of measuring system	PHAROS (Ref.9): combination of 160 orifices and connecting tubes and 8 miniature pressure transducers

7.2 Unsteady pressure

7.2.1 Position of orifices spanwise and chordwise	See Figure 1 and CD-ROM file "sensors.txt"
7.2.2 Diameter of orifices	0.8 mm
7.2.3 Type of measuring system	PHAROS (Ref.9)
7.2.4 Type of transducers	Scanning valves: Statham. In situ transducers: Kulite and Endevco
7.2.5 Principle and accuracy of calibration	Data acquisition system was calibrated daily, pressure transducers before and after wind tunnel test. Accuracy less/equal 1%

7.3 Model motion

7.3.1 Method of measuring motion reference co-ordinate	LVDT: Sangamo
7.3.2 Method of determining spatial mode of motion	8 accelerometers on wing, 4 accelerometers on store
7.3.3 Accuracy of measured motion	Accelerometers: about 1%, LVDT: better than 0.015 mm

7.4 Processing of unsteady measurements

7.4.1 Method of acquiring and processing measurements	Direct Fourier Transform of time signals to harmonic components
7.4.2 Type of analysis	Averaging and determination of first (and higher) harmonics took place over signal lengths of 1 s (steady), or about 1 s with round-off to integral number of cycles (unsteady)
7.4.3 Unsteady pressure quantities obtained and accuracies achieved	Fundamental harmonics and occasionally second and third harmonics for accuracy see 9.1.6
7.4.4 Method of integration to obtain forces	Trapezoidal rule

7.5	Additional remarks	Position of accelerometers, see Figure 1 and CD-ROM
7.6	References on techniques	-

8 Data presentation

8.1	Test cases for which data could be made available	See Tables 3, 4 and 5
8.2	Test cases for which data are included in this document	See Table 1

8.3	Steady pressures	See Tables 3, 4 and 5
8.4	Quasi-steady or steady perturbation pressures	See Tables 3, 4 and 5
8.5	Unsteady pressures	See Tables 3, 4 and 5
8.6	Steady forces or moments	See Tables 3, 4 and 5; integrated pressures on wing, measured directly on store
8.7	Quasi-steady or unsteady perturbation forces	See Tables 3, 4 and 5; integrated pressures on wing, measured directly on store
8.8	Unsteady forces and moments	See Tables 3, 4 and 5; integrated pressures on wing, measured directly on store
8.9	Other forms in which data could be made available	-
8.10	Ref. giving other representations of data	Ref.1

9 Comments on data

9.1	Accuracy	
	9.1.1 Mach number	+/- 0.001
	9.1.2 Steady incidence	+/- 0.01° at LVDT position
	9.1.3 Reduced frequency	+/- 0.0005
	9.1.4 Steady pressure coefficients	+/- 0.5 percent
	9.1.5 Steady pressure derivatives	-
	9.1.6 Unsteady pressure coefficients	Uncertainty in the real and imaginary parts of the coefficients is probably +/- (0.02 + 0.05 Q), where Q = |R| or |I|
9.2	Sensitivity to small changes of parameter	-
9.3	Non-linearity's	-
9.4	Influence of tunnel total pressure	-
9.5	Effects on data of uncertainty, or variation, in mode of model motion	-
9.6	Wall interference corrections	Unsteady wall pressures measured, no correction applied
9.7	Other relevant tests on same model	References 5 and 6: Same wing, F5 + tip-tank and store (Data possibly not available) Reference 7: Same wing, F5 + inboard flap
9.8	Relevant tests on other models of nominally the same shapes	See above
9.9	Any remarks relevant to comparison between experiment and theory	This publication, Chapter 4
9.10	Additional remarks	An example of a database file is included in table 6. Structure of file set-up is included in README file in database.
9.11	References on discussion of data	-

10 Personal contact for further information

Evert G.M. Geurts
Department of Aerodynamic Engineering and Aeroelasticity
Phone: +31 20 5113455
Fax: +31 20 5113210
Email: geurts@nlr.nl

National Aerospace Laboratory NLR
Anthony Fokkerweg 2 P.O. Box 90502
NL 1059 CM Amsterdam NL 1006 BM Amsterdam
The Netherlands The Netherlands
Phone: +31 20 5113113
Fax: +31 20 5113210
Website: http://www.nlr.nl

11 List of references

1 van Nunen, J.W.G., Tijdeman, H., et.al., "Results of transonic wind tunnel measurements on an oscillating wing with external store (data report)", NLR TR 78030 U, 1978

2 Tijdeman, H., van Nunen, J.W.G. et.al., "Transonic Wind Tunnel Tests of an Oscillating Wing with External Store",

Part I: General description

Part II: The clean wing

Part III: The wing with tip store

Part IV: The wing with under wing-store

NLR TR 78106 U, 1978 (also AFFDL TR 78-194, 1978)

3 Roos, R., "Unsteady airloads on a harmonically pitching wing with external stores", Proceedings of the AIAA/ASME 21st Structures, Structural Dynamics and Materials Conference, Seattle, Washington, May 12-14, AIAA paper 80-733, 1980, (also NLR MP 80004 U, 1980

4 Persoon, A.J., "Measuring unsteady loads on wing-mounted stores", NLR TR 79013 U, 1979

5 Renirie, L., van Nunen, J.W.G. et.al., "Unsteady pressure measurements on a wing with stores in subsonic flow",

Part I: Description of tests,

Part II: Tabulated results,

NLR TR 75155C, 1975

6 Van Nunen, J.W.G., Roos, R., Meijer, J.J., "Investigation of the unsteady airloads on wing-store configurations in subsonic flow", AGARD CP227: Unsteady Aerodynamics, (also NLR MP 77025 U, 1977)

7 Persoon, A.J., Roos, R., Schippers, P., "Transonic and low supersonic wind tunnel tests on a wing with inboard control surface",

Part I: General description,

Part II: Tabulated results,

NLR TR 80070 L, 1980

8 NN., "Users guide to the High Speed Tunnel (HST): edition 1977

9 Fuykschot, P.H., "PHAROS, Processor for harmonic analysis of the response of oscillating surfaces", NLR MP 77012 U, 1977

10 Poestkoke, R., "Hydraulic test rig for oscillating wind-tunnel models", NLR MP 76020 U, 1976

Selected Steady Cases				Selected Unsteady Cases						
RUN	Ma	ALPHA	Re	RUN	Ma	K	ALPHA	Re	F	THETA
WING										
137	.597	-.005	4.77	383	.597	.399	.004	4.57	40.000	.115
138	.597	.493	4.77	370	.896	.275	.001	5.73	40.000	.111
151	.897	-.004	5.79	160	.947	.132	-.006	5.91	20.000	.523
152	.896	.497	5.79	373	1.092	.058	.003	5.92	10.000	.113
158	.946	-.004	5.89	172	1.093	.116	.003	6.02	20.000	.267
168	1.093	-.002	6.01	193	1.336	.198	-.001	4.10	40.000	.222
190	1.328	-.005	4.07							
191	1.327	.500	4.08							
WING WITH TIP LAUNCHER										
198	.597	-.004	4.73	204	.598	.402	-.007	4.80	40.000	.114
208	.897	-.009	5.94	211	.898	.276	.010	5.84	40.000	.224
218	1.329	-.256	4.27	222	1.323	.200	.000	4.24	40.000	.115
WING WITH TIP LAUNCHER + MISSILE BODY										
256	.597	.001	4.62	259	.593	.402	-.006	4.60	40.000	.221
251	.894	-.010	5.68	254	.894	.276	-.005	5.69	40.000	.223
234	1.327	-.004	4.21	237	1.327	.199	.003	4.25	40.000	.111
WING WITH TIP LAUNCHER + MISSILE BODY + AFT FINS										
286	.596	-.004	4.68	289	.597	.401	-.004	4.68	40.000	.220
281	.894	-.004	5.94	284	.894	.279	-.004	5.95	40.000	.222
265	1.315	-.003	4.27	268	1.321	.200	-.004	4.33	40.000	.220
WING WITH TIP LAUNCHER + MISSILE BODY + AFT FINS + CANARD FINS										
341	.596	.005	4.59	348	.595	.401	.004	4.62	40.000	.111
320	.897	-.000	5.65	352	.897	.069	-.002	5.73	10.000	.115
297	1.330	-.003	4.41	355	.896	.275	.004	5.73	40.000	.117
				302	1.327	.199	.016	4.20	40.000	.221

Table 1: Selected test cases

Remark:
For the different configurations tested, the steady normal force and pitching moment acting on the store were measured with a strain gage balance; the unsteady normal force and pitching moment were measured with the same balance. For test cases above 30 Hz doubts have been expressed concerning the store loads. For that reason all 40 Hz cases were omitted from the database files.

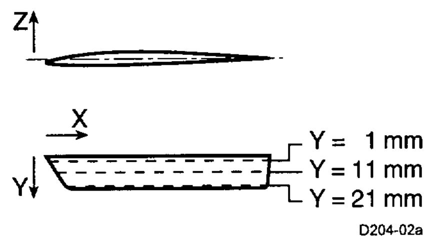

x mm	y mm
0.46	1.00
3.56	6.00
6.66	11.00
9.80	16.00
14.58	21.00
16.00	22.00
17.78	23.00
20.24	24.00
30.00	24.98
100.00	25.00
160.00	25.02
170.00	24.90
180.00	24.38
190.00	23.54
192.00	23.08
194.00	21.52
196.10	1.00

	y = 1.00 mm		y = 11.00 mm		y = 21.00 mm	
x mm	z_{upper} mm	z_{lower} mm	Z_{upper} mm	Z_{lower} mm	Z_{upper} mm	Z_{lower} mm
1	-1.58	-2.68				
5	-0.38	-3.18				
7			-1.66	-2.58		
10	0.56	-3.38	-0.58	-3.06		
15			0.42	-3.28	-1.54	-2.66
20	1.94	-3.68	1.18	-3.44	0.20	-3.20
25			1.80	-3.70	1.02	-3.38
30	2.86	-3.90			1.66	-3.50
40	3.56	-4.12	3.12	-3.90	2.64	-3.72
50	4.06	-4.32	3.70	-4.10	3.32	-3.92
60	4.38	-4.48	4.08	-4.28	3.78	-4.08
70	4.56	-4.60	4.34	-4.40	4.08	-4.22
80	4.62	-4.64	4.44	-4.48	4.24	-4.30
90	4.56	-4.64	4.43	-4.52	4.26	-4.36
100	4.46	-4.54	4.34	-4.44	4.18	-4.32
110	4.28	-4.36	4.18	-4.28	4.04	-4.18
120	4.00	-4.10	3.94	-4.02	3.80	-3.96
130	3.70	-3.76	3.62	-3.70	3.52	-3.66
140	3.30	-3.32	3.24	-3.28	3.14	-3.26
150	2.80	-2.80	2.76	-2.76	2.68	-2.74
160	2.24	-2.26	2.18	-2.20	2.12	-2.18
170	1.64	-1.68	1.59	-1.64	1.52	-1.60
180	1.02	-1.12	0.98	-1.08	0.90	-1.03
190	0.40	-0.54	0.40	-0.52	0.28	-0.46
194					0.00	-0.22
195	0.13	-0.19	0.04	-0.22		

Table 2: Co-ordinates of tip fairing of F-5 clean wing configuration

STEADY TESTS			
RUN	Ma	ALPHA	Re
136	0.598	-.504	4.76
137	0.597	-.005	4.77
138	0.597	0.493	4.77
145	0.799	-.508	5.63
146	0.796	-.004	5.63
147	0.797	0.493	5.54
150	0.899	-.504	5.78
151	0.897	-.004	5.79
152	0.896	0.497	5.79
157	0.949	-.511	5.89
158	0.946	-.004	5.89
159	0.946	0.496	5.90
162	1.046	-.506	6.04
163	1.044	-.004	6.04
164	1.044	0.494	6.06
167	1.096	-.512	6.00
168	1.093	-.002	6.01
169	1.093	0.498	6.02
184	1.184	-.506	4.28
185	1.185	-.005	4.25
186	1.186	0.495	4.26
189	1.333	-.504	4.12
190	1.328	-.005	4.07
191	1.327	0.500	4.08

UNSTEADY TESTS						
RUN	Ma	K	ALPHA	Re	F	THETA
380	0.596	0.100	0.003	4.57	10.000	0.108
382	0.598	0.199	0.004	4.57	20.000	0.106
381	0.597	0.299	0.005	4.57	30.000	0.110
383	0.597	0.399	0.004	4.57	40.000	0.115
367	0.800	0.153	0.004	5.48	20.000	0.108
368	0.796	0.307	0.001	5.47	40.000	0.113
378	0.899	0.068	0.001	5.65	10.000	0.108
369	0.899	0.137	0.002	5.73	20.000	0.109
379	0.896	0.206	0.002	5.66	30.000	0.108
370	0.896	0.275	0.001	5.73	40.000	0.111
160	0.947	0.132	-.006	5.91	20.000	0.523
161	0.948	0.264	-.013	5.92	40.000	0.222
375	0.996	0.125	0.005	5.79	20.000	0.107
376	0.994	0.250	0.000	5.80	40.000	0.112
165	1.045	0.122	-.003	6.07	20.000	0.522
166	1.044	0.243	0.004	6.08	40.000	0.219
373	1.092	0.058	0.003	5.92	10.000	0.113
172	1.093	0.116	0.003	6.02	20.000	0.267
374	1.092	0.173	0.004	5.92	30.000	0.110
372	1.093	0.231	-.000	5.92	40.000	0.112
187	1.188	0.109	-.010	4.28	20.000	0.524
188	1.186	0.218	-.008	4.29	40.000	0.222
192	1.328	0.100	-.008	4.09	20.000	0.523
193	1.336	0.198	-.001	4.10	40.000	0.222

Table 3: Test programme F-5 WING

STEADY TESTS			
RUN	Ma	ALPHA	Re
197	0.599	-.505	4.78
198	0.597	-.004	4.73
199	0.596	0.497	4.73
206	0.899	-.510	5.90
208	0.897	-.009	5.94
209	0.896	0.496	5.95
212	1.095	-.514	6.10
213	1.092	-.005	5.98
214	1.092	0.496	6.00
223	1.089	-.502	4.19
224	1.086	-.002	4.26
225	1.091	0.494	4.29
217	1.327	-.504	4.37
218	1.329	-.256	4.27
220	1.330	0.499	4.28

UNSTEADY TESTS						
RUN	Ma	K	ALPHA	Re	F	THETA
202	0.596	0.202	-.004	4.76	20.000	0.111
204	0.598	0.402	-.007	4.80	40.000	0.114
210	0.897	0.138	0.006	5.83	20.000	0.530
211	0.898	0.276	0.010	5.84	40.000	0.224
215	1.092	0.116	-.007	6.01	20.000	0.531
216	1.095	0.232	-.005	6.02	40.000	0.226
226	1.088	0.117	-.006	4.99	20.000	0.526
227	1.091	0.234	-.000	4.32	40.000	0.117
221	1.329	0.100	-.001	4.22	20.000	0.529
222	1.323	0.200	0.000	4.24	40.000	0.115

Table 4a: Test programme F-5 WING WITH TIP LAUNCHER

STEADY TESTS			
RUN	Ma	ALPHA	Re
255	0.592	-.512	4.56
256	0.597	0.001	4.62
257	0.594	0.495	4.60
249	0.897	-.512	5.61
251	0.894	-.010	5.68
252	0.893	0.498	5.68
244	1.092	-.512	5.91
245	1.089	-.001	5.91
246	1.089	0.497	5.92
233	1.324	-.508	4.50
234	1.327	-.004	4.21
235	1.327	0.499	4.23

UNSTEADY TESTS						
RUN	Ma	K	ALPHA	Re	F	THETA
258	0.595	0.201	-.001	4.60	20.000	0.524
259	0.593	0.402	-.006	4.60	40.000	0.221
253	0.895	0.138	-.008	5.69	20.000	0.532
254	0.894	0.276	-.005	5.69	40.000	0.223
247	1.090	0.116	-.003	5.92	20.000	0.530
248	1.089	0.232	0.001	5.93	40.000	0.230
242	1.086	0.116	-.008	4.19	20.000	0.525
243	1.085	0.233	-.003	4.20	40.000	0.223
236	1.322	0.100	-.004	4.24	20.000	0.532
237	1.327	0.199	0.003	4.25	40.000	0.111

Table 4b: Test programme F-5 WING WITH TIP LAUNCHER + MISSILE BODY

STEADY TESTS			
RUN	Ma	ALPHA	Re
285	0.592	-.509	4.67
286	0.596	-.004	4.68
287	0.596	0.497	4.68
280	0.896	-.508	5.62
281	0.894	-.004	5.94
282	0.894	0.494	5.94
274	1.089	-.508	6.03
275	1.089	-.002	5.91
276	1.089	0.492	5.93
269	1.086	-.511	4.13
270	1.082	-.006	4.22
271	1.084	0.498	4.23
264	1.319	-.505	4.29
265	1.315	-.003	4.27
266	1.315	0.496	4.29

UNSTEADY TESTS						
RUN	Ma	K	ALPHA	Re	F	THETA
288	0.598	0.201	-.009	4.70	20.000	0.525
289	0.597	0.401	-.004	4.68	40.000	0.220
283	0.896	0.139	-.007	5.95	20.000	0.534
284	0.894	0.279	-.004	5.95	40.000	0.222
277	1.089	0.116	-.009	5.93	20.000	0.522
278	1.090	0.232	-.006	5.92	40.000	0.226
272	1.084	0.117	-.008	4.23	20.000	0.524
273	1.087	0.234	-.003	4.26	40.000	0.113
267	1.319	0.100	-.006	4.32	20.000	0.527
268	1.321	0.200	-.004	4.33	40.000	0.220

Table 4c: Test programme F-5 WING WITH TIP LAUNCHER + MISSILE BODY + AFT FINS

STEADY TESTS			
RUN	Ma	ALPHA	Re
340	0.598	-.502	4.58
341	0.596	0.005	4.59
342	0.595	0.505	4.60
333	0.696	-.500	5.10
334	0.696	0.005	5.11
335	0.696	0.506	5.11
326	0.797	-.500	5.44
327	0.797	-.001	5.43
328	0.796	0.499	5.45
319	0.896	-.494	5.65
320	0.897	-.000	5.65
321	0.897	0.505	5.68
312	1.096	-.499	5.97
313	1.093	0.003	5.95
314	1.091	0.504	5.95
303	1.092	-.522	4.14
306	1.090	0.018	4.25
307	1.094	0.499	4.28
295	1.332	-.495	4.43
297	1.330	-.003	4.41
298	1.329	0.495	4.43

UNSTEADY TESTS						
RUN	Ma	K	ALPHA	Re	F	THETA
351	0.595	0.100	0.005	4.63	10.000	0.109
350	0.596	0.200	0.004	4.63	20.000	0.114
344	0.596	0.200	0.001	4.61	20.000	0.527
349	0.596	0.300	0.013	4.63	30.000	0.109
348	0.595	0.401	0.004	4.62	40.000	0.111
336	0.697	0.086	0.001	5.13	10.000	0.535
337	0.697	0.173	-.001	5.13	20.000	0.528
338	0.696	0.260	0.002	5.14	30.000	0.375
339	0.697	0.346	0.005	5.14	40.000	0.225
357	0.798	0.076	0.003	5.40	10.000	0.110
358	0.797	0.153	0.001	5.40	20.000	0.108
359	0.797	0.229	0.006	5.40	30.000	0.110
360	0.797	0.305	0.004	5.41	40.000	0.115
352	0.897	0.069	-.002	5.73	10.000	0.115
353	0.896	0.138	-.000	5.72	20.000	0.110
354	0.895	0.207	0.003	5.72	30.000	0.110
355	0.896	0.275	0.004	5.73	40.000	0.117
315	1.094	0.058	-.004	5.96	10.000	0.547
316	1.092	0.116	-.003	5.97	20.000	0.527
317	1.094	0.174	-.005	5.99	30.000	0.376
318	1.093	0.231	0.003	5.99	40.000	0.228
308	1.092	0.058	-.013	4.29	10.000	0.536
309	1.091	0.117	-.013	4.30	20.000	0.519
310	1.091	0.175	0.003	4.30	30.000	0.375
311	1.091	0.234	0.007	4.32	40.000	0.224
299	1.329	0.051	0.006	4.45	10.000	0.532
300	1.330	0.101	0.011	4.37	20.000	0.526
301	1.328	0.149	0.012	4.18	30.000	0.374
302	1.327	0.199	0.016	4.20	40.000	0.221

Table 4d: Test programme F-5 WING WITH TIP LAUNCHER + MISSILE BODY + AFT FINS + CANARD FINS

STEADY TESTS			
RUN	Ma	ALPHA	Re
125	0.598	-.507	4.47
126	0.595	-.001	4.58
127	0.596	0.496	4.58
120	0.897	-.499	5.54
121	0.898	0.000	5.59
122	0.897	0.499	5.59
116	1.094	-.504	5.96
117	1.094	-.003	5.96
118	1.094	0.496	5.97
106	1.092	-.505	4.13
107	1.089	-.002	4.24
108	1.089	0.502	4.25
101	1.333	-.503	4.53
102	1.331	-.001	4.19

UNSTEADY TESTS						
RUN	Ma	K	ALPHA	Re	F	THETA
128	0.599	0.199	-.003	4.60	20.000	0.526
129	0.597	0.399	0.002	4.58	40.000	0.223
123	0.898	0.137	-.003	5.60	20.000	0.529
124	0.898	0.273	-.001	5.60	40.000	0.221
114	1.095	0.115	-.004	5.94	20.000	0.532
115	1.094	0.231	-.003	5.95	40.000	0.220
109	1.090	0.117	-.009	4.26	20.000	0.524
110	1.093	0.233	-.001	4.28	40.000	0.223
104	1.331	0.099	-.002	4.20	20.000	0.528
105	1.331	0.199	-.001	4.21	40.000	0.223

Table 5a: Test programme F-5 WING WITH PYLON

STEADY TESTS			
RUN	Ma	ALPHA	Re
54	0.600	-.498	3.42
55	0.597	-.001	3.33
56	0.597	0.500	3.33
61	0.897	-.497	4.19
62	0.896	-.001	4.22
63	0.897	0.513	4.04
68	1.090	-.499	4.35
69	1.089	-.004	4.36
70	1.088	0.495	4.38
75	1.331	-.493	4.18
76	1.325	-.002	4.20
77	1.329	0.495	4.22

UNSTEADY TESTS						
RUN	Ma	K	ALPHA	Re	F	THETA
57	0.597	0.101	0.001	3.34	10.000	0.523
58	0.599	0.201	0.001	3.36	20.000	0.518
59	0.597	0.303	0.002	3.35	30.000	0.370
60	0.597	0.403	0.003	3.36	40.000	0.229
64	0.897	0.070	0.038	3.83	10.000	0.533
65	0.898	0.140	0.003	4.18	20.000	0.519
66	0.895	0.210	0.008	4.18	30.000	0.375
67	0.898	0.279	0.009	4.20	40.000	0.226
71	1.090	0.059	0.005	4.41	10.000	0.534
72	1.089	0.118	0.001	4.42	20.000	0.526
73	1.090	0.176	0.004	4.35	30.000	0.371
74	1.089	0.234	0.001	4.36	40.000	0.223
78	1.331	0.050	-.002	4.20	10.000	0.529
79	1.328	0.099	-.003	4.22	20.000	0.524
80	1.331	0.149	-.001	4.23	30.000	0.372
81	1.329	0.199	-.001	4.25	40.000	0.228

Table 5b: Test programme F-5 WING WITH PYLON + LAUNCHER

STEADY TESTS			
RUN	Ma	ALPHA	Re
40	0.598	-.500	4.75
41	0.596	-.002	4.75
42	0.598	0.498	4.74
45	0.899	-.501	5.80
46	0.898	-.018	5.81
47	0.898	0.498	2.54

UNSTEADY TESTS						
RUN	Ma	K	ALPHA	Re	F	THETA
43	0.597	0.201	0.001	4.71	20.000	0.527
44	0.599	0.400	-.001	4.67	40.000	0.230
48	0.898	0.138	0.001	5.79	20.000	0.524
49	0.897	0.081	0.006	0.36	40.000	0.225

Table 5c: Test programme F-5 WING WITH PYLON + LAUNCHER + MISSILE

STEADY TESTS			
RUN	Ma	ALPHA	Re
89	1.093	-.500	4.26
90	1.088	0.001	4.28
91	1.089	0.500	4.29
94	1.333	-.506	4.25
95	1.332	0.001	4.16
96	1.333	0.502	4.17

UNSTEADY TESTS						
RUN	Ma	K	ALPHA	Re	F	THETA
88	0.899	0.141	0.003	6.21	20.000	0.521
87	0.902	0.281	0.003	6.20	40.000	0.226
92	1.089	0.118	0.003	4.30	20.000	0.521
93	1.090	0.235	0.001	4.31	40.000	0.222
97	1.335	0.099	-.002	4.20	20.000	0.522
98	1.330	0.199	-.002	4.23	40.000	0.223

Table 5d: Test programme F-5 WING WITH PYLON + LAUNCHER + MISSILE WITHOUT CANARD FINS

NATIONAL AEROSPACE LABORATORY NLR
NLR TR78030 U

TABLE 1.1

RUN 383 10111977 NF-5 WING

TEST CONDITIONS		DISPLACEMENTS NR	MOD	ARG
MA	= .597	1	.897	-178.6
PO	= 99458.	2	1.000	0.0
PPL	=78039.	3	.334	-172.6
Q	=19503.	4	1.041	-2.0
TO	= 31.00	5	.254	-16.3
RE	= 4.57	6	1.097	-3.9
K	= .399	7	.259	-23.8
F	= 40.000	8	1.205	-5.3
ALPHA=	.004	9	0.000	0.0
THETA=	.115	10	0.000	0.0
		11	0.000	0.0
		12	0.000	0.0

FORCE AND MOMENT COEFFICIENTS STAT	INSTAT RE	IM

WING

SEC NR	CZ	CZI RE	CZI IM	CM	CMI RE	CMI IM
1	-.017	.88	.58	.008	.021	.357
2	-.009	1.02	.54	.007	-.052	.357
3	-.009	1.19	.50	.008	-.036	.320
4	.000	1.16	.44	.008	-.093	.307
5	-.001	1.16	.48	.008	-.025	.257
6	.002	1.00	.46	.007	-.037	.217
7	.005	.92	.42	.007	-.053	.183
8	.011	.40	.33	.005	-.065	.130

WINGSECTION 1

X/C	UPPERSIDE MLOC	CP	CPI RE	CPI IM	LOWERSIDE MLOC	CP	CPI RE	CPI IM
.03	.555	.130	-4.519	.882	.674	-.245	2.910	.232
.10	.605	-.025	-2.821	.066	.624	-.084	3.380	.344
.20	.627	-.096	-2.624	-.571	.616	-.059	2.347	.835
.30	.636	-.122	-2.106	-.787	.622	-.078	2.134	1.324
.40	.634	-.116	-1.393	-1.394	.631	-.107	1.524	1.601
.50	.632	-.109	-1.032	-1.518	.630	-.103	1.122	1.431
.60	.629	-.100	-.988	-1.189	.626	-.091	.972	1.447
.70	.623	-.083	-.398	-1.268	.622	-.078	.510	1.329
.80	.609	-.036	-.061	-1.060	.607	-.031	.462	1.020
.90	.590	.022	.236	-.856	.588	.028	.073	.811

WINGSECTION 2

X/C	UPPERSIDE MLOC	CP	CPI RE	CPI IM	LOWERSIDE MLOC	CP	CPI RE	CPI IM
.03	.566	.097	-4.544	.447	.679	-.263	8.541	-1.319
.10	.616	-.059	-3.263	.095	.627	-.093	4.076	.615
.20	.638	-.130	-2.429	-.373	.619	-.069	2.778	1.033
.30	.645	-.151	-1.945	-.770	.624	-.086	2.203	1.215
.40	.640	-.135	-1.502	-.933	.633	-.113	1.259	1.679
.50	.633	-.112	-1.228	-1.276	.631	-.108	1.125	1.405
.60	.630	-.104	-.684	-1.297	.628	-.096	.884	1.474
.70	.624	-.085	-.403	-1.252	.622	-.080	.381	1.585
.80	.609	-.037	-.246	-1.022	.607	-.031	.357	.844
.90	.589	.024	.228	-.688	.587	.030	.013	.918

1

Table 6: Example of a database file (included in the database)

Remark: For files of the clean wing with any tip configuration, force and moment coefficients (which are blank in the above example) refer to values measured by the wing tip balance for that particular configuration.
For the different configurations tested, the steady normal force and pitching moment acting on the store were measured; the unsteady normal force and pitching moment were measured with the same balance. For test cases above 30 Hz doubts have been expressed concerning the store loads. For that reason all 40 Hz cases were omitted from the database files.

NATIONAL AEROSPACE LABORATORY NLR
NLR TR78030 U

TABLE 1.2

RUN 383 10111977 NF-5 WING

WINGSECTION 3

X/C	UPPERSIDE MLOC	CP	CPI RE	CPI IM	LOWERSIDE MLOC	CP	CPI RE	CPI IM
.03	.599	-.006	.002	-.047	.681	-.269	8.569	-1.276
.10	.616	-.061	-4.234	-.189	.627	-.096	5.190	.342
.20	.637	-.127	-3.121	-.705	.621	-.074	2.969	.679
.30	.644	-.149	-2.444	-.776	.625	-.087	2.370	1.205
.40	.640	-.136	-1.755	-1.098	.635	-.121	1.601	1.346
.50	.636	-.123	-1.140	-1.389	.632	-.109	1.432	1.331
.60	.632	-.109	-.876	-1.336	.628	-.099	.911	1.235
.70	.624	-.086	-.493	-1.111	.623	-.081	.660	.987
.80	.608	-.036	-.177	-.916	.606	-.029	.429	.958
.90	.590	.022	.002	-.702	.588	.029	.124	.673

WINGSECTION 4

X/C	UPPERSIDE MLOC	CP	CPI RE	CPI IM	LOWERSIDE MLOC	CP	CPI RE	CPI IM
.03	.573	.076	-5.379	.450	.681	-.268	8.299	-1.950
.10	.623	-.082	-3.592	-.064	.627	-.094	7.206	.280
.20	.644	-.150	-2.932	-.371	.622	-.079	3.354	.829
.30	.650	-.167	-2.259	-.773	.625	-.089	2.543	1.019
.40	.645	-.153	-1.972	-.951	.634	-.117	1.801	1.256
.50	.639	-.132	1.391	-1.295	.632	-.111	1.239	1.290
.60	.630	-.106	-1.122	-.987	.628	-.098	1.008	1.239
.70	.625	-.087	-.597	-.987	.623	-.082	.494	1.077
.80	.610	-.040	-.180	-.854	.608	-.033	.272	.920
.90	.590	.023	.090	-.573	.588	.030	.091	.703

WINGSECTION 5

X/C	UPPERSIDE MLOC	CP	CPI RE	CPI IM	LOWERSIDE MLOC	CP	CPI RE	CPI IM
.03	.599	-.006	-.002	.045	.679	-.263	4.996	.311
.10	.623	-.082	-4.410	-.203	.629	-.100	5.360	.410
.20	.639	-.133	-3.141	-.683	.621	-.075	3.504	.804
.30	.649	-.164	-2.409	-.718	.626	-.093	2.614	1.015
.40	.644	-.150	-1.566	-.859	.635	-.121	1.903	1.304
.50	.637	-.127	-.974	-1.134	.632	-.112	1.338	1.240
.60	.633	-.113	-.849	-1.059	.629	-.100	.970	1.060
.70	.626	-.090	-.506	-.971	.623	-.080	.593	1.064
.80	.610	-.042	-.175	-.755	.607	-.031	.351	.882
.90	.589	.024	.112	-.486	.588	.030	.154	.496

WINGSECTION 6

X/C	UPPERSIDE MLOC	CP	CPI RE	CPI IM	LOWERSIDE MLOC	CP	CPI RE	CPI IM
.03	.586	.036	-6.548	-.064	.679	-.264	7.256	-.447
.10	.625	-.087	-1.961	-.392	.627	-.094	1.204	1.286
.20	.644	-.148	-3.539	-.646	.621	-.077	3.754	.786
.30	.649	-.166	-2.320	-1.192	.626	-.093	2.528	.887
.40	.645	-.153	-1.631	-.863	.635	-.120	1.477	1.063
.50	.637	-.127	-.915	-1.068	.633	-.112	1.132	1.010
.60	.632	-.111	-.640	-.860	.628	-.099	.878	1.024
.70	.626	-.090	-.389	-.841	.623	-.082	.418	.870
.80	.610	-.040	-.117	-.691	.607	-.031	.151	.630
.90	.589	.025	.109	-.426	.588	.029	.038	.461

WINGSECTION 7

X/C	UPPERSIDE MLOC	CP	CPI RE	CPI IM	LOWERSIDE MLOC	CP	CPI RE	CPI IM
.03	.578	.059	-7.403	-.409	.669	-.228	7.063	-.077
.10	.629	-.101	-3.428	-.453	.630	-.105	-2.076	1.054
.20	.645	-.151	-3.326	-.839	.621	-.075	3.891	.699
.30	.649	-.166	-2.069	-.730	.626	-.090	2.752	.786
.40	.646	-.155	-1.020	-.764	.636	-.122	1.656	.880
.50	.637	-.127	-.721	-.927	.633	-.112	1.133	.989
.60	.633	-.112	-.491	-.817	.628	-.099	.718	.871
.70	.625	-.087	-.260	-.751	.622	-.079	.392	.848
.80	.609	-.039	.052	-.587	.607	-.030	.174	.596
.90	.591	.020	.126	-.306	.588	.028	.050	.356

WINGSECTION 8

X/C	UPPERSIDE MLOC	CP	CPI RE	CPI IM	LOWERSIDE MLOC	CP	CPI RE	CPI IM
.03	.597	.000	-5.596	-.436	.665	-.217	6.286	.311
.10	.634	-.116	-3.036	-.297	.628	-.098	-3.654	.369
.20	.649	-.165	.384	-.501	.620	-.072	3.838	.741
.30	.647	-.159	2.200	-.827	.623	-.082	1.877	.647
.40	.640	-.135	2.005	-1.067	.629	-.100	1.095	.751
.50	.631	-.106	-.230	-.476	.627	-.096	.863	.738
.60	.627	-.094	-1.248	-.433	.624	-.086	.543	.627
.70	.622	-.078	-.317	-.522	.620	-.073	.088	.509
.80	.608	-.035	-.004	-.363	.605	-.026	.000	.452
.90	.589	.024	.075	-.174	.588	.028	-.085	.394

1

NATIONAL AEROSPACE LABORATORY NLR
NLR TR78030 U

TABLE 1.3

RUN 383 10111977 NF-5 WING

X/C	CP-KULILES RE	CP-KULILES IM
.10	-3.729	.365
.20	-2.546	-.509
.30	-2.146	-.713
.40	-1.533	-.973
.50	-.921	-1.098
.60	-.738	-1.188
.70	-.585	-.991
.80	-.397	-.851

1

Table 6 (continued): Example of a database file (included in the database)

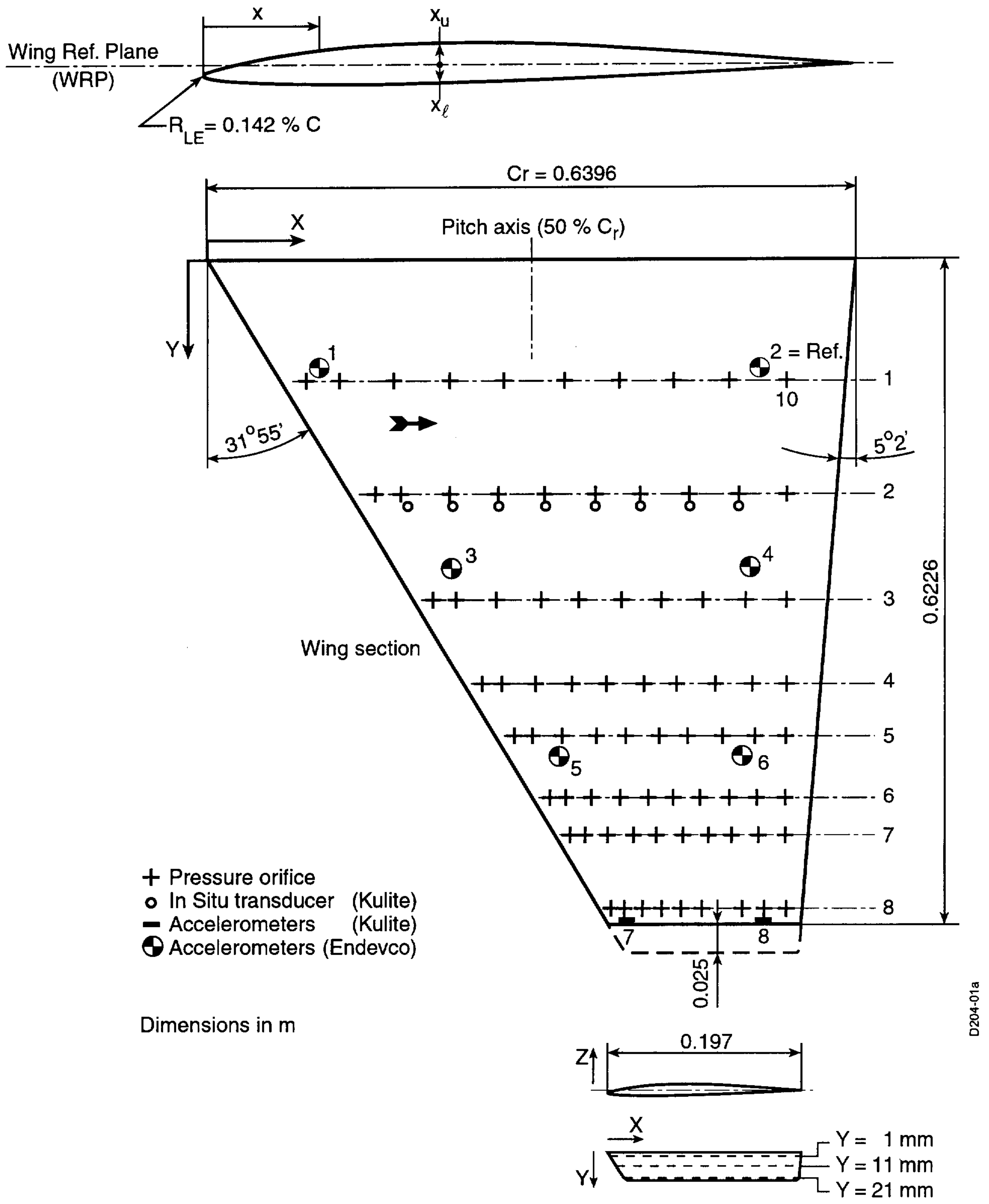

Figure 1: NLR F-5 clean wing, location of pressure orifices and transducers

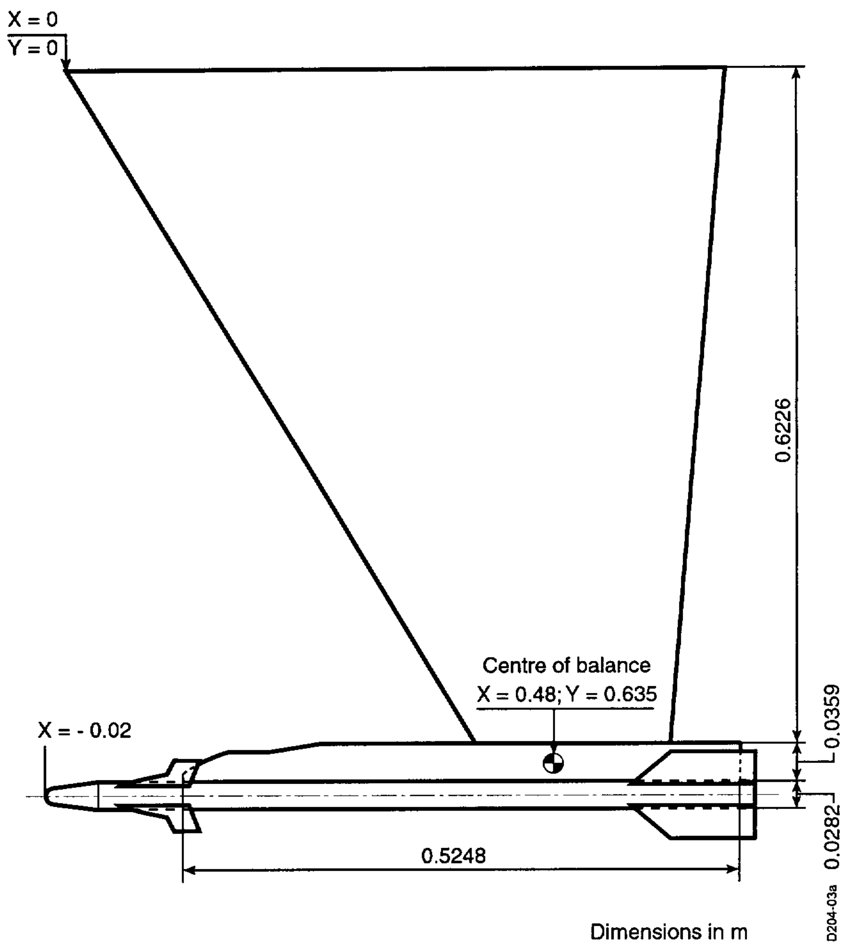

Figure 2a: Position of the store and strain gage balances

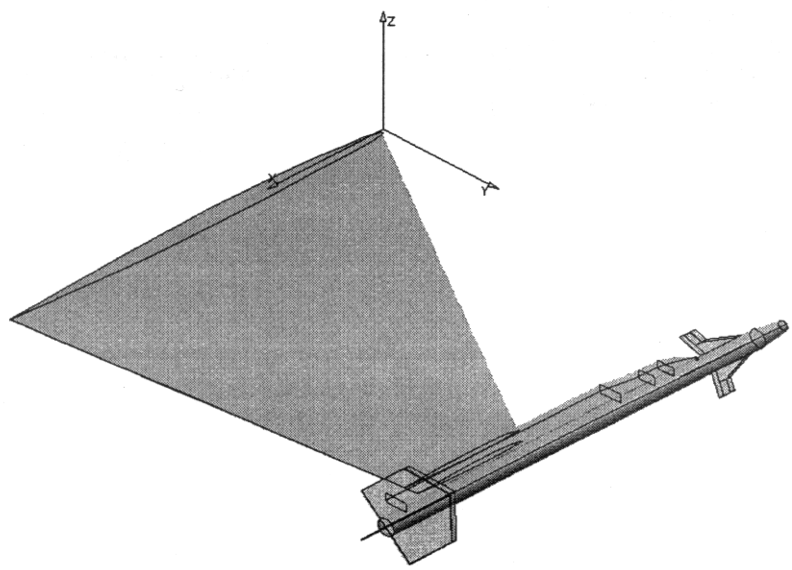

Figure 2b: CATIA example of F5 wing with tip store

6E. TEST CASES FOR A RECTANGULAR SUPERCRITICAL WING UNDERGOING PITCHING OSCILLATIONS

Submitted by

Robert M. Bennett
Senior Aerospace Engineer
Aeroelasticity Branch, Structures and Materials
Mail Stop 340
NASA Langley Research Center
Hampton, VA 23681-2199 USA
r.m.bennett@larc.nasa.gov

INTRODUCTION

Steady and unsteady measured pressures for a Rectangular Supercritical Wing (RSW) undergoing pitching oscillations have been presented in Ref 1 to 3. From the several hundred compiled data points, 27 static and 36 pitching oscillation cases have been proposed for computational Test Cases to illustrate the trends with Mach number, reduced frequency, and angle of attack.

The wing was designed to be a simple configuration for Computational Fluid Dynamics (CFD) comparisons. The wing had an unswept rectangular planform plus a tip of revolution, a panel aspect ratio of 2.0, a twelve per cent thick supercritical airfoil section, and no twist. The model was tested over a wide range of Mach numbers, from 0.27 to 0.90, corresponding to low subsonic flows up to strong transonic flows. The higher Mach numbers are well beyond the design Mach number such as might be required for flutter verification beyond cruise conditions. The pitching oscillations covered a broad range of reduced frequencies.

Some early calculations for this wing are given for lifting pressure in Ref 3 and 4 as calculated from a linear lifting surface program and from a transonic small perturbation program. The unsteady results were given primarily for a mild transonic condition at M = 0.70. For these cases the agreement with the data was only fair, possibly resulting from the omission of viscous effects. Supercritical airfoil sections are known to be sensitive to viscous effects (for example, one case cited in Ref 4). Calculations using a higher level code with the full potential equations have been presented in Ref 5 for one of the same cases, and with the Euler equations in Ref 6. The agreement around the leading edge was improved, but overall the agreement was not completely satisfactory. Typically for low-aspect-ratio rectangular wings, transonic shock waves on the wing tend to sweep forward from root to tip such that there are strong three-dimensional effects. It might also be noted that for most of the test, the model was tested with free transition, but a few points were taken with an added transition strip for comparison. Some unpublished results of a rigid wing of the same airfoil and planform that was tested on the pitch and plunge apparatus mount system (PAPA, Ref 7-8) showed effects of the lower surface transition strip on flutter at the lower subsonic Mach numbers. Significant effects of a transition strip were also obtained on a wing with a thicker supercritical section on the PAPA mount system (Ref 9). Both of these flutter tests on the PAPA resulted in very low reduced frequencies that may be a factor in this influence of the transition strip. However, these results indicate that correlation studies for RSW may require some attention to the estimation of transition location to accurately treat viscous effects.

In this report several Test Cases are selected to illustrate trends for a variety of different conditions with emphasis on transonic flow effects. An overview of the model and tests is given and the standard formulary for these data is listed. Sample data points are presented in both tabular and graphical form. A complete tabulation and plotting of all the Test Cases is given in Ref 10. Only the static pressures and the real and imaginary parts of the first harmonic of the unsteady pressures are available. All the data for the test are available in electronic file form and are printed in the tables of Ref 1. The Test Cases are also available as separate electronic files.

LIST OF SYMBOLS AND DEFINITIONS

c	local chord
c_r	wing root chord, ft (m)
C_p	pressure coefficient, $(p - p_\infty)/q_\infty$ steady; $(p - p_{mean})/q_\infty$ unsteady
f	frequency, Hz
H_o	freestream total pressure, psf (kPa)
k	reduced frequency, $\omega c_r/(2V_\infty)$
M	Mach number
p	pressure, psf (kPa)
p_{mean}	mean local pressure, psf (kPa)
p_∞	freestream static pressure, psf (kPa)
q_∞	dynamic pressure, psf (kPa)

R	local radius of tip section
Rn	Reynolds number based on chord
s	semispan
T_o	total or stagnation temperature, °R (°C)
V_∞	freestream velocity, ft/sec (m/sec)
x	streamwise distance from leading edge
x/c	steamwise fraction of local chord
y	spanwise coordinate normal to freestream
z_u, z_l	airfoil vertical upper and lower ordinate normal to freestream, positive up
α_o	mean angle of attack, degrees
θ	amplitude of pitch oscillations, degrees or radians
η	fraction of span, y/s
γ	ratio of specific heats for test gas
ω	frequency, radians/second

MODEL AND TESTS

The rectangular supercritical wing model was tested in the NASA Langley Transonic Dynamics Tunnel (TDT). The tunnel has a slotted test section 16-feet (4.064 m) square with cropped corners. At the time of these tests, it could be operated with air or a heavy gas, R-12, as a test medium at pressures from very low to near atmospheric values. Currently the TDT can be operated with air or R-134a as a test medium. An early description of this facility is given in Ref 11 and the early data system in Ref 12. More recent descriptions of the facility are given in Ref 13-14, and of the recent data system in Ref 15 and 16. Based on cone transition results (Ref 17-18), the turbulence level for this tunnel is in the "average large transonic tunnel" category. Some low speed turbulence measurements in air have also been presented in Ref 19.

A photograph of the model and splitter plate as installed in the TDT is shown in Fig 1 and the dimensions of the model and splitter plate setup are detailed in the sketch of Fig 2. The unswept rectangular planform was 48 inches (1219 mm) in span plus a tip of revolution of maximum radius of 1.434 inches (36.4 mm) such that the maximum spanwise extent was 49.43 inches (1255 mm). The chord was 24 inches (609.6 mm). The model was mounted on a splitter plate offset from the wall. It was oscillated in pitch about 46 percent root chord with a shaft that was directly driven by a rotary hydraulic actuator located behind the tunnel wall. It could be set at various mean angles, and the amplitude and frequency of oscillation could be varied.

The wing was constructed in three sections. The center section was made of aluminum with the upper and lower halves pinned and bonded together. The leading and trailing edge portions were made of balsa and Kevlar sandwich material to minimize the inertia loading. The leading and trailing edge sections were joined at 0.23 and 0.69 of the chord, respectively. Some stiffness measurements are given in Ref 3.

Unsteady pressures were measured on four chords. There were 14 measurement locations along each chord on both upper and lower surfaces and one location in the nose for a total of 29 points per chord as shown in Fig 3 and listed in Table 1. The transducers in the center portion of the wing were in-situ measurements. The transducers in the leading and trailing edges were mounted near the joints of the leading or trailing edge sections to the center beam. Equal length tubes were used between the orifices and these transducers. Other transducers were located by the first row of in-situ transducers and had tubes of the same length located in the center beam. These transducers were used to correct for dynamic effects of the tubes of the transducers in the leading and trailing edges. Each transducer was referenced to the tunnel static pressure and was used to measure both static and unsteady pressures. Eight accelerometers were located on the center section for dynamic measurements. Fig 4 (from Ref 1) shows C_L versus Mach number as integrated from the pressure data, and gives an overall indication of the performance of the wing.

The airfoil for the RSW is illustrated in Fig 5. This airfoil was derived by ratioing the thickness of an 11 percent airfoil (Ref 20) to 12 percent while keeping the same mean camber line. The trailing edge thickness was increased to 0.7 percent chord by rotating the lower cusp area as described in Ref 21. The design Mach number and lift coefficient for the 2-dimensional airfoil is quoted as M = 0.80, and C_L = 0.6 (Ref 3). The design ordinates and the measured ordinates for five spanwise stations are given in Table 2. The design wing tip-shape is also presented in Table 2. The quoted accuracy of the measured ordinates is .00040 in. (.0010 mm). The measured airfoil ordinates are compared with the theoretical ordinates in Fig 6. The measured ordinates agree very well with the theoretical ones but with some small deviation in the lower surface aft, or cove, region.

By CFD standards, the theoretical and measured ordinates were given on a medium to coarse grid. In order to develop a common set of ordinates for CFD applications, the measured ordinates have been interpolated at each span station. The measured ordinates were fit with a spline using arc-length as the independent parameter and running from upper surface trailing edge around the nose to the lower surface trailing edge. Three passes of a local 5-point least-squares cubic smoothing patch were made, and the resulting curve interpolated for the ordinates. These smoothed ordinates at the five span stations were interpolated for 206 values of x/c for each span station and included as a file for the data set. They are also listed in a table in Ref 10. One airfoil section after smoothing and the corresponding streamwise slopes are presented in Fig 7. For this wing, the measured spanwise sections are nearly identical, except at the lower surface trailing edge where the slope varies by about 8 per cent. It should also be noted that the slope varies quite rapidly near the inflection point in the cove region of the airfoil lower surface (Fig 7).

As can been seen in Fig 1, the model was tested with the sidewall slots of the test section open. Some recent unpublished results for a model having about six times the root chord of this model and mounted directly to the wind tunnel wall, have shown an influence of closing the slots on static lift curve slope of the order of ten percent (similar to those measured in Ref 22). Significantly less influence would be anticipated for this much smaller model mounted on a splitter plate.

TEST CASES

The static Test Cases for the rectangular supercritical wing are given in Table 3, and the dynamic Test Cases are presented in Table 4. The point number is used to identify the test conditions and are in the order taken during the test. The cases are chosen to indicate trends with Mach number at two degrees angle of attack, and also at zero and four degrees angle of attack with a coarse increment. Some cases for high angles of attack at M=0.40, some cases for the effect of transition at M=0.825, and some cases for air as the test medium are listed. The dynamic cases are chosen to evaluate unsteady effects at these static conditions. The cases illustrate variations with Mach number for nearly constant reduced frequency, and variations with reduced frequency at constant Mach numbers. Some cases are chosen also to indicate the effects of angle of attack, transition strip, and amplitude. The plot of C_L versus Mach number as integrated from the pressure data (Fig 4) was used as a guide in selecting the Test Cases.

Sample data for the static Test Cases are tabulated and shown in composite plots in Fig 8. Sample data for the dynamic cases are also tabulated and shown in the plots of Fig 9 in terms of in-phase and out-of-phase parts (real and imaginary) of the pressure normalized by the amplitude of the pitching oscillation. The phase is referenced to the pitching motion. More digits than are significant are retained in the tables to accurately reproduce the phase angles of the original tabulations. No further screening of bad transducer output points have been performed in this report.

The files included on the CD-ROM are ascii files and a readme file is included. The file for the static data is named rswstat and a Fortran subprogram to read it, rswstrd.f, is furnished. The dynamic data is on file rswdynmc and the subprogram to read it is rswdyrd.f. The data files consist of contiguous data points in the format shown in the figures. Both theoretical and measured ordinates are given in file rsword and the interpolated and smoothed ordinates are given in file rswordint.

Note that most of the tests for RSW were conducted with the heavy gas, R-12, as the test medium. The ratio of specific heats, γ, is tabulated for each point in the figures. It varies from about 1.129 to 1.132 and a value of 1.132 is suggested for use in computational comparisons. The corresponding value of Prandtl number is calculated to range from 0.77 to 0.78 for the conditions of this test assuming 0.99 for the fraction of heavy gas in the heavy gas-air mixture.

FORMULARY

1 General Description of Model

1.1	Designation	Rectangular Supercritical Wing (RSW)
1.2	Type	Semispan wing
1.3	Derivation	None
1.4	Additional remarks	Shown mounted in tunnel in Fig 1 and setup sketched in Fig 2
1.5	References	Ref 1-3 are the original sources

2 Model Geometry

2.1	Planform	Rectangular plus tip of revolution
2.2	Aspect ratio	2.0 for panel (without tip)
2.3	Leading edge sweep	Unswept
2.4	Trailing edge sweep	Unswept
2.5	Taper ratio	1.0
2.6	Twist	None
2.7	Wing centreline chord	24.0 inches (609.6 mm)
2.8	Semi-span of model	48.0 inches (1219 mm)plus tip
2.9	Area of planform	1152 sq. in (1.786 sq m)
2.10	Location of reference sections and definition of profiles	See Table 2, Fig 5-7, and files rsword and rswordint
2.11	Lofting procedure between reference sections	Constant percent thickness airfoil
2.12	Form of wing-body junction	No fairing

2.13	Form of wing tip	Tip of rotation. Each spanwise section formed by half circle with radius half the local thickness and rotated about the mean line
2.14	Control surface details	No control surfaces
2.15	Additional remarks	See Fig 1-3 for overview
2.16	References	Ref 1-3

3 Wind Tunnel

3.1	Designation	NASA LaRC Transonic Dynamics Tunnel (TDT)
3.2	Type of tunnel	Continuous flow, single return
3.3	Test section dimensions	16 ft x 16 ft (4.064 x 4.064 m)
3.4	Type of roof and floor	Three slots each
3.5	Type of side walls	Two sidewall slots
3.6	Ventilation geometry	Constant width slots in test region
3.7	Thickness of side wall boundary layer	Some documentation in Ref 11. Model tested with splitter plate
3.8	Thickness of boundary layers at roof and floor	Not documented
3.9	Method of measuring velocity	Calculated from static pressures measured in plenum and total pressure measured upstream of entrance nozzle of test section
3.10	Flow angularity	Not documented, considered small
3.11	Uniformity of velocity over test section	Not documented, considered nearly uniform
3.12	Sources and levels of noise or turbulence in empty tunnel	Generally unknown. Some low speed measurements are presented in Ref 19. Cone transition measurements are presented in Ref 17 and 18
3.13	Tunnel resonances	Unknown
3.14	Additional remarks	Tests generally performed in heavy gas, R-12. Ratio of specific heats, γ, is 1.129-1.132. For computations, 1.132 is recommended. For the conditions of this test, the Prandtl number is calculated to be 0.77-0.78
3.15	References on tunnel	Ref 11, 13, and 14

4 Model Motion

4.1	General description	Pitching about 46% of root chord for wing, 11.04 inches (280.4 mm) aft of leading edge
4.2	Reference coordinate and definition of motion	Pitch about axis normal to freestream
4.3	Range of amplitude	Pitch amplitude of 0.50, 1.00, and 1.50 degrees
4.4	Range of frequency	5, 10, 15, and 20 Hz with a few lower frequencies
4.5	Method of applying motion	Pitch oscillations shaft-driven with a rotary hydraulic actuator
4.6	Timewise purity of motion	Not documented
4.7	Natural frequencies and normal modes of model and support system	First natural frequency was 34.8 Hz; maximum test frequency was 20 Hz
4.8	Actual mode of applied motion including any elastic deformation	Some accelerometer measurements given in Ref 2. Elastic deformations not expected to be significant, but stiffness measurements available in Ref 3
4.9	Additional remarks	None

5 Test Conditions

5.1	Model planform area/tunnel area	.03
5.2	Model span/tunnel height	.25
5.3	Blockage	Model less than 0.4%
5.4	Position of model in tunnel	Mounted from splitter plate on wall and in the center of the tunnel

5.5	Range of Mach number	0.40 to 0.90
5.6	Range of tunnel total pressure	175 to 2025 psf (8.38 to 812 kPa)
5.7	Range of tunnel total temperature	Not documented but generally in the range of 520 to 580 degrees Rankine (16 to 49° C)
5.8	Range of model steady or mean incidence	Generally -1 to 7 degrees, a few points from -4 to 14 degrees
5.9	Definition of model incidence	From chord line or wing reference plane of airfoil, see Fig 5-7
5.10	Position of transition, if free	Unknown except for a few points with transition strip. Although the joint was quite smooth, an initial estimate of transition might be considered to be at the joint between the leading edge section and the main spar (23 per cent chord)
5.11	Position and type of trip, if transition fixed	Generally free transition. A few points measured with transition strip of number 60 grit located at 6 percent chord on upper and lower surfaces (number is approximate grains per inch (per 25.4 mm)).
5.12	Flow instabilities during tests	None defined
5.13	Changes to mean shape of model due to steady aerodynamic load	Not measured
5.14	Additional remarks	Generally, a heavy gas, R-12, was used as a test medium for the Test Cases. The ratio of specific heats, γ, is tabulated for each point and varies from about 1.129 to 1.132. A value of 1.132 is suggested for use in computational comparisons. The corresponding value of Prandtl number is 0.77-0.78. A few points were also measured in air
5.15	References describing tests	Ref 1- 3

6 Measurements and Observations

6.1	Steady pressures for the mean conditions	yes
6.2	Steady pressures for small changes from the mean conditions	yes
6.3	Quasi-steady pressures	no
6.4	Unsteady pressures	yes
6.5	Steady section forces for the mean conditions by integration of pressures	no
6.6	Steady section forces for small changes from the mean conditions by integration	no
6.7	Quasi-steady section forces by integration	no
6.8	Unsteady section forces by integration	no
6.9	Measurement of actual motion at points of model	no
6.10	Observation or measurement of boundary layer properties	no
6.11	Visualisation of surface flow	no
6.12	Visualisation of shock wave movements	no
6.13	Aditional remarks	no

7 Instrumentation

7.1	Steady pressure	
7.1.1	Position of orifices spanwise and chordwise	29 chordwise locations at 4 spanwise stations. See Fig 3
7.1.2	Type of measuring system	Kulite
7.2	Unsteady pressure	
7.2.1	Position of orifices spanwise and chordwise	Same transducers measured steady and unsteady pressures

	7.2.2 Diameter of orifices	Not documented
	7.2.3 Type of measuring system	In situ pressure gages and short tubes to unsteady gages with tube calibrations
	7.2.4 Type of transducers	Kulites
	7.2.5 Principle and accuracy of calibration	Statically calibrated through reference tubes
7.3	Model motion	
	7.3.1 Method of measuring motion reference coordinate	Potentiometer
	7.3.2 Method of determining spatial mode of motion	Some verification with accelerometers
	7.3.3 Accuracy of measured motion	Undocumented
7.4	Processing of unsteady measurements	
	7.4.1 Method of acquiring and processing measurements	Analog signals digitized at about 300 samples/sec for 75-100 cycles depending on frequency
	7.4.2 Type of analysis	Fourier analysis
	7.4.3 Unsteady pressure quantities obtained and accuracies achieved	Amplitude and phase of each pressure signal. Accuracy not specified
	7.4.4 Method of integration to obtain forces	None
7.5	Additional remarks	None
7.6	References on techniques	Data system overview for test given in Ref 12

8 Data Presentation

8.1	Test Cases for which data could be made available	See Ref 2
8.2	Test Cases for which data are included in this document	See Tables 3 and 4
8.3	Steady pressures	Generally available for each Test Case
8.4	Quasi-steady or steady perturbation pressures	Steady pressures measured for several angles of attack
8.5	Unsteady pressures	Primary data. First harmonic only. No time histories or mean values saved. C_p magnitude and phase of Ref 2 converted to real and imaginary parts and normalised by amplitude of oscillation (in radians) for this report.
8.6	Steady forces or moments	None
8.7	Quasi-steady or unsteady perturbation forces	None
8.8	Unsteady forces and moments	None
8.9	Other forms in which data could be made available	None
8.10	References giving other representations of data	Ref 1-6

9 Comments on Data

9.1	Accuracy	
	9.1.1 Mach number	Not documented
	9.1.2 Steady incidence	Not documented
	9.1.3 Reduced frequency	Should be accurate
	9.1.4 Steady pressure coefficients	Not documented
	9.1.5 Steady pressure derivatives	None
	9.1.6 Unsteady pressure coefficients	Not documented, but each gage individually calibrated dynamically and monitored statically

9.2	Sensitivity to small changes of parameter	None indicated. Amplitudes of oscillation was varied in test
9.3	Non-linearities	Many flow conditions involve shock waves
9.4	Influence of tunnel total pressure	Some variation during test. Most of the test at constant dynamic pressure
9.5	Effects on data of uncertainty, or variation, in mode of model motion	Unknown, not expected to be appreciable.
9.6	Wall interference corrections	None applied
9.7	Other relevant tests on same model	None
9.8	Relevant tests on other models of nominally the same shapes	None
9.9	Any remarks relevant to comparison between experiment and theory	Generally free transition. R_n from 1×10^6 to 8×10^6 but generally about 4×10^6. Test Reynolds number included for each Test Case
9.10	Additional remarks	Upper and lower surfaces instrumented symmetrically. Reduced frequency based on root semichord, 12.0 inches (304.8 mm)
9.11	References on discussion of data	Ref 1-6

10 Personal Contact for Further Information

Head, Aeroelasticity Branch
Mail Stop 340
NASA Langley Research Center
Hampton, VA 23681-2199 USA

Phone: +1-(757)-864-2820
FAX: +1-(757)-864-8678

LIST OF REFERENCES

1. Ricketts, Rodney H.; Sandford, Maynard C.; Seidel, David A.; and Watson, Judith J: *Transonic Pressure Distributions on a Rectangular Supercritical Wing Oscillated in Pitch.* Journal of Aircraft, vol. 21, no. 8, August 1984, pp 576-582. (Also AIAA Paper 83-0923, May 1983 which is available as NASA TM 84616, Mar. 1983).

2. Ricketts, Rodney H.; Sandford, Maynard C.; Watson, Judith J.; and Seidel, David A.: *Subsonic and Transonic Unsteady- and Steady-Pressure Measurements on a Rectangular Supercritical Wing Oscillated in Pitch.* NASA TM 85765, August 1984.

3. Ricketts, Rodney H.; Sandford, Maynard C.; Watson, Judith J.; and Seidel, David A.: *Geometric and Structural Properties of a Rectangular Supercritical Wing Oscillated in Pitch for Measurements of Unsteady Transonic Pressure Distributions.* NASA TM 85673, Nov. 1983.

4. Seidel, David A.; Bennett, Robert M.; and Ricketts, Rodney H.: *Some Recent Applications of XTRAN3S.* AIAA Paper 83-1811, July 1983. (Also available as NASA TM 85641, May 1983).

5. Hounjet, M. H. L.: *NLR Inviscid Transonic Unsteady Loads Prediction Methods in Aeroelasticity.* Paper No. 12 in "Transonic Unsteady Aerodynamics and Aeroelasticity," AGARD CP-507, March 1992.

6. Brenneis, A.; and Eberle, A.: *Application of an Implicit Relaxation Method Solving the Euler Equations for Time-Accurate Unsteady Problems.* Journal of Fluids Engineering, Transactions of the ASME, Vol 112, Dec. 1990, pp. 510-520.

7. Farmer, Moses G.: *A Two-Degree-of Freedom Flutter Mount System with Low Damping for Testing Rigid Wings at Different Angles of ttack.* NASA TM 83302, 1982.

8. Farmer, Moses G.: *Model Mount System for Testing Flutter.* U. S. Patent No. 4,475,385, Oct. 9, 1984.

9. Dansberry, B.E.; Durham, M.H.; Bennett, R.M.; Rivera, J.A., Jr.; Silva, W.A.; Wieseman, C.D.; and Turnock, D.L.: *Experimental Unsteady Pressures at Flutter on the Supercritical Wing Benchmark Model.* AIAA Paper No. 93-1592, April 1993.

10. Bennett, Robert M.; Walker, Charlotte, E.: *Computational Test Cases for a Rectangular Supercritical Wing Undergoing Pitching Oscillations.* NASA/TM-1999-209130, Apr. 1999.

11. Aeroelasticity Branch Staff: *The Langley Transonic Dynamics Tunnel.* LWP-799, Sep. 1969.

12. Cole, Patricia H.: *Wind Tunnel Real-Time Data Acquisition System.* NASA TM-80081, 1979.

13. Cole, Stanley C., and Rivera, Jose, A., Jr.: *The New Heavy Gas Testing Capability in the NASA Langley Transonic Dynamics Tunnel.* Paper No. 4, presented at the Royal Aeronautical Society Wind Tunnels and Wind Tunnel Test Techniques Forum, Churchill College, Cambridge, UK, Apr. 1997.

14. Corliss, James M.; and Cole, Stanley R.: *Heavy Gas Conversion of the NASA Langley Transonic Dynamics Tunnel.* AIAA Paper 98-2710, June 1998.

15. Wieseman, Carol D.; and Hoadley, Sherwood, T.: *Versatile Software Package for Near Real-Time Analysis of Experimental Data.* AIAA Paper 98-2722, June 1998.

16. Bryant, C.; and Hoadley, S. T.: Open Architecture Dynamic Data System at Langley's Transonic Dynamics Tunnel. AAIA Paper 98-0343, Jan. 1998.

17. Dougherty, N. Sam, Jr.: *Influence of Wind Tunnel Noise on the Location of Boundary-Layer Transition on a Slender Cone at Mach Numbers from 0.2 to 5.5.* Volume I. - Experimental Methods and Summary of Results. Volume II. - Tabulated and Plotted Data. AEDC --TR-78-44, March 1980.

18. Dougherty, N. S., Jr.; and Fisher, D. F.: *Boundary-Layer Transition on a 10-Degree Cone: Wind Tunnel/Flight Correlation.* AIAA Paper 80-0154, January 1980.

19. Sleeper, Robert K.; Keller, Donald F.; Perry, Boyd, III; and Sandford, Maynard C.: *Characteristics of Vertical and Lateral Tunnel Turbulence Measured in Air in the Langley Transonic Dynamics Tunnel.* NASA TM 107734, March 1993.

20. Whitcomb, Richard T.: *Review of NASA Supercritical Airfoils.* ICAS Paper No.74-10, presented at the Ninth Congress of the International Council of The Aeronautical Sciences, Aug. 1974, Haifa, Israel.

21. Harris, Charles D.: *Wind-Tunnel Investigation of Effects of Trailing-Edge Geometry on a NASA Supercritical Airfoil Section.* NASA TM X-2336, Sept. 1971.

22. Lambourne, N.; Destuynder, R.; Kienappel, K.; and Roos, R.: *Comparative Measurements in Four European Wind Tunnels of the Unsteady Pressures on an Oscillating Model (The NORA Experiments).* AGARD Report No. 673, Feb. 1980.

ACKNOWLEDGMENT

Appreciation is extended to David A. Seidel of the Boeing Company, Seattle WA, USA for making the data files available from the NASA Langley archives. The considerable assistance of Charlotte E. Walker in generating the tables and figures for this report is also gratefully acknowledged.

Table 1. Pressure Orifice Locations and Type

x/c	Type
0.000	Tube to Transducer
.003	Tube to Transducer
.050	Tube to Transducer
.100	Tube to Transducer
.200	Tube to Transducer
.260	In Situ
.320	In Situ
.380	In Situ
.440	In Situ
.500	In Situ
.560	In Situ
.620	In Situ
.700	Tube to Transducer
.800	Tube to Transducer
.900	Tube to Transducer

Table 2. Design and Measured Ordinates

		Design Values		Measured Values					
				y = 1.000 in		y = 14.932 in		y = 28.324 in	
x, in	x/c	z_u, in	z_l, in	z_u, in	z_l, in	z_u, in	z_l, in	z_u, in	z_l, in
0.0000	0.0000	0.0000	0.0000	0.0000	0.0000	0.0000	0.0000	0.0000	0.0000
0.1800	0.0075	0.4610	-0.4610	0.4571	-0.4726	0.4535	-0.4701	0.4514	-0.4624
0.3000	0.0125	0.5630	-0.5650	0.5602	-0.5750	0.5557	-0.5717	0.5572	-0.5669
0.6000	0.0250	0.7230	-0.7350	0.7193	-0.7435	0.7156	-0.7376	0.7197	-0.7380
0.9000	0.0375	0.8280	-0.8470	0.8226	-0.8569	0.8234	-0.8498	0.8242	-0.8492
1.2000	0.0500	0.9100	-0.9360	0.9050	-0.9436	0.9050	-0.9383	0.9062	-0.9365
1.8000	0.0750	1.0330	-1.0670	1.0289	-1.0720	1.0290	-1.0693	1.0295	-1.0683
2.4000	0.1000	1.1220	-1.1610	1.1191	-1.1638	1.1176	-1.1620	1.1176	-1.1603
3.0000	0.1250	1.1930	-1.2340	1.1901	-1.2372	1.1895	-1.2345	1.1910	-1.2346
3.6000	0.1500	1.2480	-1.2890	1.2466	-1.2928	1.2459	-1.2902	1.2465	-1.2898
4.2000	0.1750	1.2930	-1.3330	1.2936	-1.3378	1.2916	-1.3345	1.2925	-1.3330
4.8000	0.2000	1.3290	-1.3650	1.3335	-1.3691	1.3287	-1.3670	1.3300	-1.3665
6.0000	0.2500	1.3840	-1.4130	1.3876	-1.4147	1.3846	-1.4122	1.3839	-1.4116
7.2000	0.3000	1.4150	-1.4340	1.4177	-1.4343	1.4147	-1.4320	1.4148	-1.4308
8.4000	0.3500	1.4320	-1.4370	1.4343	-1.4374	1.4331	-1.4343	1.4329	-1.4326
9.6000	0.4000	1.4390	-1.4170	1.4421	-1.4153	1.4396	-1.4127	1.4397	-1.4130
10.8000	0.4500	1.4320	-1.3750	1.4354	-1.3739	1.4341	-1.3717	1.4354	-1.3721
12.0000	0.5000	1.4170	-1.3060	1.4194	-1.3069	1.4177	-1.3036	1.4190	-1.3036
13.2000	0.5500	1.3870	-1.2000	1.3893	-1.2011	1.3892	-1.1971	1.3891	-1.1978
13.8000	0.5750	1.3690	-1.1260	1.3713	-1.1266	1.3702	-1.1224	1.3697	-1.1228
14.4000	0.6000	1.3450	-1.0330	1.3492	-1.0332	1.3487	-1.0284	1.3467	-1.0291
15.0000	0.6250	1.3200	-0.9140	1.3235	-0.9129	1.3225	-0.9084	1.3216	-0.9096
15.6000	0.6500	1.2880	-0.7620	1.2920	-0.7606	1.2912	-0.7569	1.2905	-0.7564
16.2000	0.6750	1.2500	-0.5940	1.2554	-0.5942	1.2543	-0.5896	1.2531	-0.5888
16.8000	0.7000	1.2110	-0.4390	1.2091	-0.4419	1.2169	-0.4370	1.2158	-0.4352
17.4000	0.7250	1.1640	-0.3010	1.1623	-0.3074	1.1737	-0.2994	1.1744	-0.2998
18.0000	0.7500	1.1130	-0.1750	1.1133	-0.1801	1.1232	-0.1697	1.1243	-0.1731
18.6000	0.7750	1.0580	-0.0650	1.0593	-0.0670	1.0675	-0.0608	1.0702	-0.0598
19.2000	0.8000	0.9930	0.0290	0.9948	0.0284	1.0032	0.0354	1.0066	0.0369
19.8000	0.8250	0.9190	0.1080	0.9224	0.1088	0.9285	0.1237	0.9327	0.1169
20.4000	0.8500	0.8330	0.1650	0.8387	0.1685	0.8446	0.1772	0.8472	0.1755
21.0000	0.8750	0.7380	0.2030	0.7440	0.2064	0.7494	0.2154	0.7518	0.2150
21.6000	0.9000	0.6250	0.2110	0.6317	0.2147	0.6371	0.2211	0.6412	0.2231
22.2000	0.9250	0.4980	0.1870	0.5046	0.1920	0.5076	0.2004	0.5140	0.1988
22.8000	0.9500	0.3500	0.1190	0.3574	0.1255	0.3580	0.1314	0.3632	0.1333
23.4000	0.9750	0.1790	-0.0010	0.1864	0.0053	0.1829	0.0104	0.1895	0.0128
24.0000	1.0000	-0.0190	-0.1870	-0.0077	-0.1765	-0.0217	-0.1796	-0.0184	-0.1734

Table 2. Concluded.

		Measured Values				Design Values
		y = 38.932 in		y = 45.948 in		Wing Tip Radius
x, in	x/c	z_u, in	z_l, in	z_u, in	z_l, in	R, in.
0.0000	0.0000	0.0000	0.0000	0.0000	0.0000	0.000
0.1800	0.0075	0.4580	-0.4583	0.4648	-0.4585	0.461
0.3000	0.0125	0.5625	-0.5640	0.5681	-0.5613	0.564
0.6000	0.0250	0.7248	-0.7321	0.7250	-0.7271	0.729
0.9000	0.0375	0.8299	-0.8446	0.8316	-0.8402	0.837
1.2000	0.0500	0.9103	-0.9320	0.9109	-0.9273	0.923
1.8000	0.0750	1.0330	-1.0639	1.0301	-1.0552	1.050
2.4000	0.1000	1.1199	-1.1560	1.1161	-1.1480	1.141
3.0000	0.1250	1.1900	-1.2284	1.1842	-1.2206	1.214
3.6000	0.1500	1.2454	-1.2836	1.2417	-1.2780	1.268
4.2000	0.1750	1.2929	-1.3283	1.2887	-1.3270	1.313
4.8000	0.2000	1.3324	-1.3631	1.3308	-1.3633	1.347
6.0000	0.2500	1.3833	-1.4117	1.3877	-1.4143	1.398
7.2000	0.3000	1.4138	-1.4310	1.4174	-1.4363	1.424
8.4000	0.3500	1.4310	-1.4283	1.4336	-1.4394	1.434
9.6000	0.4000	1.4369	-1.4073	1.4397	-1.4176	1.428
10.8000	0.4500	1.4329	-1.3670	1.4362	-1.3743	1.403
12.0000	0.5000	1.4168	-1.3004	1.4208	-1.3049	1.361
13.2000	0.5500	1.3876	-1.1963	1.3909	-1.1989	1.293
13.8000	0.5750	1.3689	-1.1224	1.3708	-1.1250	1.248
14.4000	0.6000	1.3461	-1.0287	1.3476	-1.0315	1.189
15.0000	0.6250	1.3204	-0.9091	1.3215	-0.9128	1.117
15.6000	0.6500	1.2891	-0.7564	1.2893	-0.7598	1.025
16.2000	0.6750	1.2520	-0.5891	1.2509	-0.5927	0.922
16.8000	0.7000	1.2128	-0.4338	1.2144	-0.4376	0.825
17.4000	0.7250	1.1698	-0.2965	1.1687	-0.3019	0.732
18.0000	0.7500	1.1225	-0.1706	1.1209	-0.1761	0.644
18.6000	0.7750	1.0688	-0.0577	1.0665	-0.0598	0.561
19.2000	0.8000	1.0052	0.0397	1.0004	0.0357	0.482
19.8000	0.8250	0.9320	0.1198	0.9280	0.1171	0.405
20.4000	0.8500	0.8493	0.1811	0.8447	0.1753	0.334
21.0000	0.8750	0.7546	0.2194	0.7506	0.2131	0.267
21.6000	0.9000	0.6446	0.2282	0.6387	0.2184	0.207
22.2000	0.9250	0.5153	0.2058	0.5083	0.1999	0.155
22.8000	0.9500	0.3661	0.1395	0.3586	0.1306	0.115
23.4000	0.9750	0.1892	0.0174	0.1809	0.0091	0.090
24.0000	1.0000	-0.0061	-0.1671	-0.0139	-0.1757	0.084

Table 3. Static Test Cases for the Rectangular Supercritical Wing

Test Case No.	Point	M	α_o, deg.	Comments
6E1	212	.404	2.22	Versus M @ $\alpha_o = 2^\circ$
6E2	394	.604	2.00	
6E3	364	.701	2.00	
6E4	331	.753	2.05	
6E5	152	.802	2.00	
6E6	462	.828	2.00	
6E7	276	.850	2.01	
6E8	423	.876	2.00	
6E9	251	.907	2.00	
6E10	489	.803	1.99	Repeat of 152
6E11	214	.403	.21	Versus M @ $\alpha_o = 0^\circ$
6E12	154	.801	.03	
6E13	464	.821	-.01	
6E14	253	.901	.00	
6E15	210	.403	4.20	Versus M @ $\alpha_o = 4^\circ$
6E16	150	.803	3.99	
6E17	460	.828	4.00	
6E18	249	.903	4.00	
6E19	604	.400	7.01	Versus α_o @ M=.4
6E20	607	.400	9.97	
6E21	609	.401	12.00	
6E22	628	.826	.00	With transition strip
6E23	626	.825	2.00	
6E24	624	.826	4.00	
6E25	52	.802	-.05	Air
6E26	53	.802	2.01	
6E27	54	.801	4.01	

Table 4. Dynamic Test Cases for the Rectangular Supercritical Wing

Test Case No.	Point	M	q psf	α_o deg.	θ deg.	f Hz	k	Comments
6E28	514	.402	54.8	1.97	1.003	10.00	.309	
6E29	344	.750	100.8	2.05	1.052	14.99	.249	
6E30	316	.802	107.6	2.08	1.035	15.03	.233	Versus
6E31	475	.826	108.1	1.97	1.023	15.01	.228	M @ $\alpha_o = 2°$
6E32	289	.854	113.7	1.99	1.006	14.96	.219	
6E33	435	.875	115.2	1.96	.987	14.99	.215	
6E34	264	.894	116.8	2.01	1.032	14.99	.210	
6E35	513	.403	54.7	1.97	1.008	5.02	.155	vs k, $\alpha_o = 2°$
6E36	515	.402	54.7	1.98	1.020	15.06	.466	M = .40
6E37	516	.402	54.8	1.98	1.060	19.97	.617	
6E38	494	.803	106.1	2.19	1.069	1.98	.031	
6E39	493	.802	105.8	1.89	1.025	3.00	.047	Versus
6E40	495	.803	106.1	1.84	1.080	3.95	.062	k @ $\alpha_o = 2°$
6E41	314	.803	107.7	2.10	1.080	4.95	.077	M = .80
6E42	315	.804	107.9	2.08	1.057	9.96	.154	
6E43	317	.802	107.5	2.07	1.039	20.01	.311	
6E44	473	.825	107.8	1.98	1.070	4.97	.076	Versus
6E45	474	.825	107.8	1.97	1.038	9.96	.152	k @ $\alpha_o = 2°$
6E46	476	.825	108.0	1.97	1.035	20.07	.305	M = .825
6E47	262	.896	117.1	2.00	1.022	4.96	.069	Versus
6E48	263	.896	117.1	2.00	.989	9.95	.139	k @ $\alpha_o = 2°$
6E49	265	.902	118.3	2.01	1.055	19.99	.278	M = .90
6E50	481	.823	107.6	-.03	1.023	15.01	.229	Versus
6E51	469	.822	107.2	3.99	1.018	15.04	.230	α_o,@ M = .825
6E52	269	.901	118.2	-.03	1.065	14.98	.208	Versus
6E53	258	.900	117.9	4.03	1.024	14.95	.208	α_o @ M = .90
6E54	632	.825	108.7	1.98	1.014	10.03	.152	With Transition
6E55	633	.826	108.9	1.98	.984	15.03	.228	Strip, M = .825
6E56	634	.826	108.9	1.98	1.005	20.09	.305	
6E57	180	.802	108.0	3.30	.500	15.12	.234	Versus
6E58	184	.801	107.8	3.30	.983	15.03	.233	θ @ $\alpha_o = 3.3°$
6E59	189	.802	108.2	3.29	1.513	14.99	.232	M = .80
6E60	613	.402	54.4	11.99	1.004	5.00	.155	Versus
6E61	614	.401	54.2	12.00	.998	10.02	.312	k, @ $\alpha_o = 12°$
6E62	615	.401	54.2	12.01	1.012	14.99	.466	M = .40
6E63	616	.401	54.3	12.02	1.087	19.99	.621	

Figure 1. Rectangular supercritical wing installed in wind tunnel.

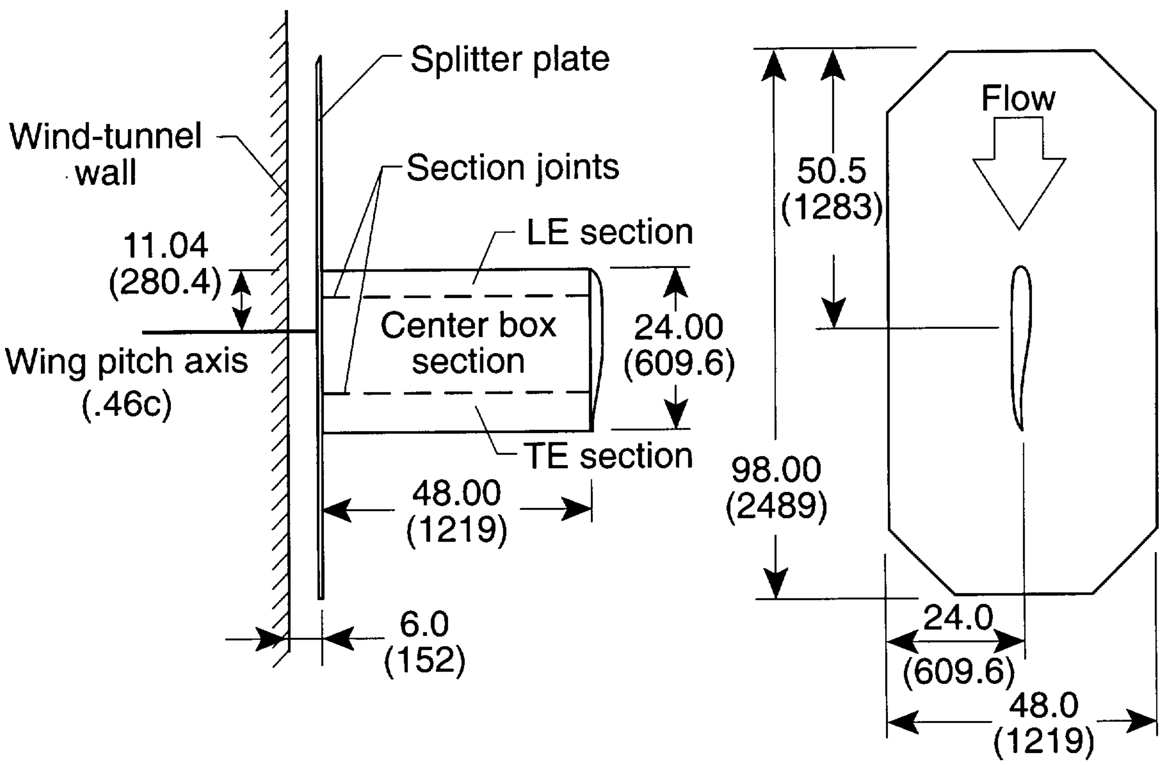

Figure 2. Diagram of wing and splitter plate in wind tunnel. Dimensions in inches (mm).

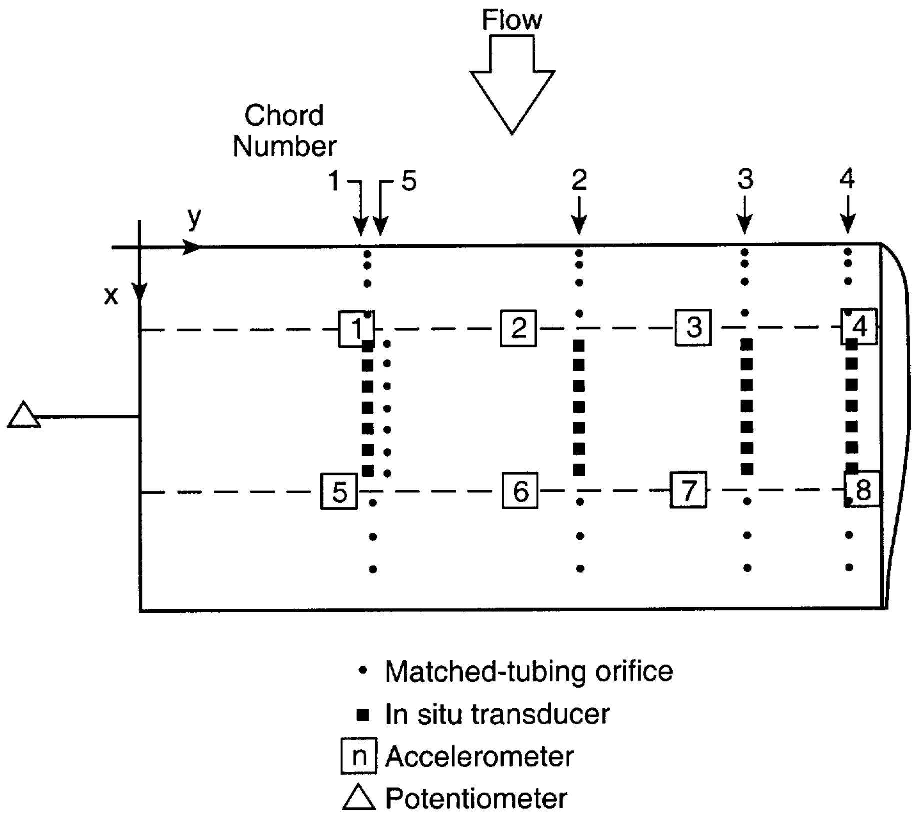

Figure 3. Instrumentation layout for the RSW model.

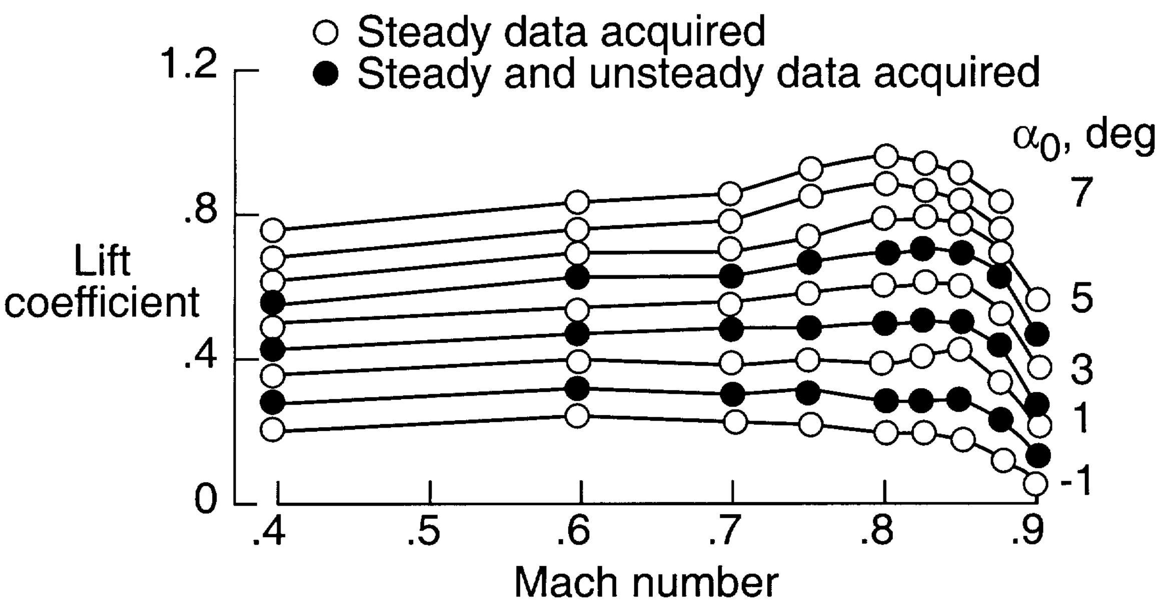

Figure 4. Lift coefficient vs. Mach number.

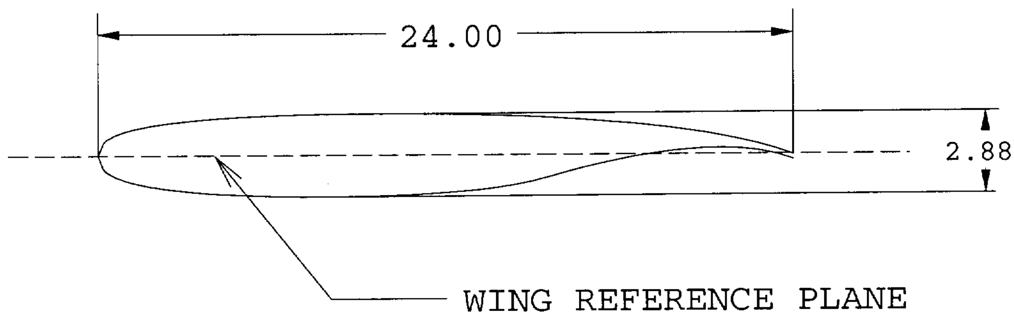

Figure 5. Airfoil for rectangular supercritical wing.

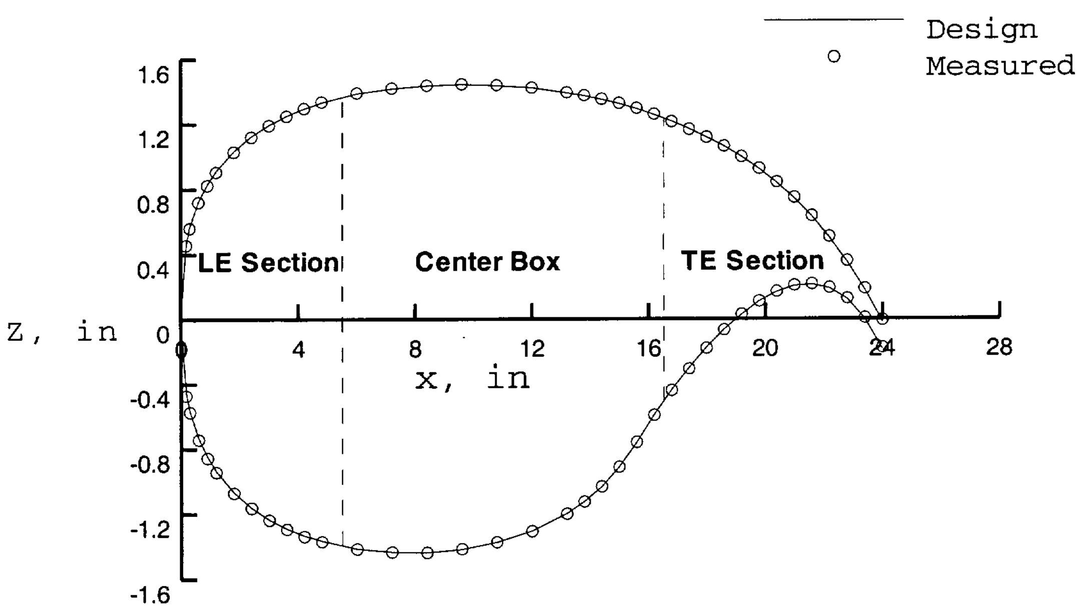

(a) Span station 1.000 in.

Figure 6. Comparison of the design and measured coordinates.

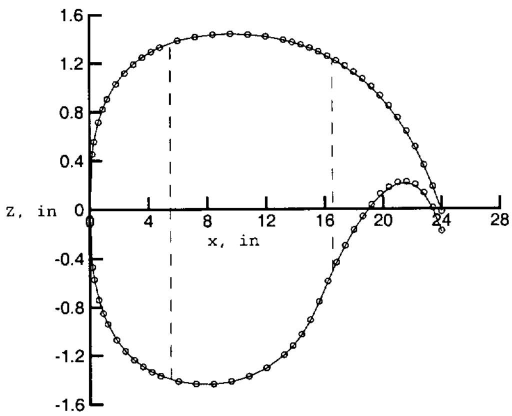

(b) Span station 14.932 in.

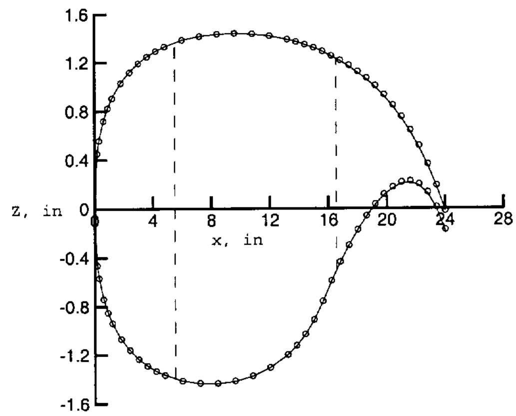

(c) Span station 28.324 in.

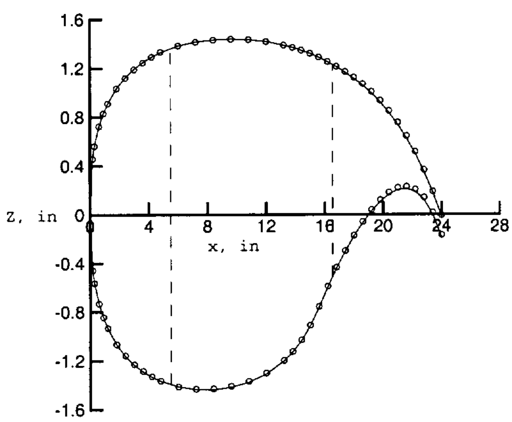

(d) Span station 38.932 in.

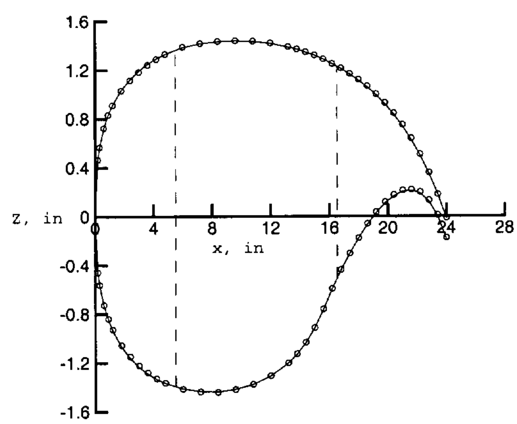

(e) Span station 45.948 in.

Figure 6. Concluded.

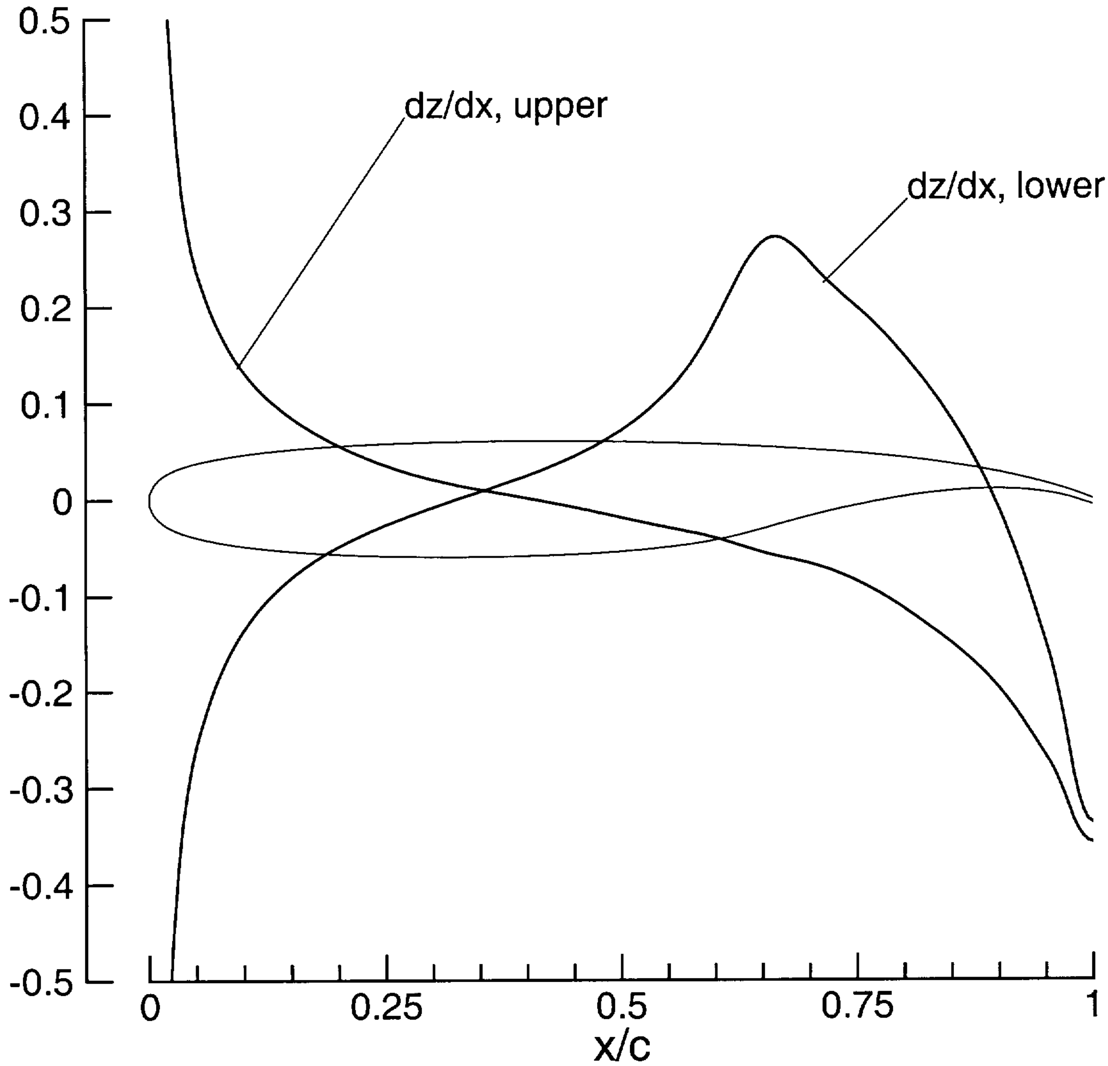

Figure 7. Plot of interpolated ordinates and slopes of smoothed measured airfoil, y = 28.324 in.

Point Number = 152 Mach Number = 0.802 Alphao = 2.00, deg.

q	H	V	Rn	gamma	Cp*
106.1	415.9	403.5	.401E+07	1.133	-0.479

	y/s =0.309		y/s =0.588		y/s =0.809		y/s =0.951	
x/c	Cpu	Cpl	Cpu	Cpl	Cpu	Cpl	Cpu	Cpl
.000	1.187		1.164		1.166		1.159	
.025	-0.666	-0.092	-0.826	-0.151	-0.845	-0.117	-0.739	-0.156
.050	-0.906	-0.310	-0.857	-0.201	-0.944	-0.307	-0.995	-0.398
.100	-0.930	-0.399	-0.904	-0.381	-0.961	-0.460	-0.824	-0.416
.200	-0.907	-0.350	-0.897	-0.414	-0.874	-0.362	-0.429	-0.370
.260	-0.936	-0.378	-0.945	-0.399	-0.362	-0.324	-0.340	-0.345
.320	-0.849	-0.296	-0.841	-0.314	-0.336	-0.283	-0.265	-0.274
.380	-0.471	-0.289	-0.230	-0.359	-0.323	-0.292	-0.263	-0.247
.440	-0.183	-0.329	-0.318	-0.269	-0.310	0.000	-0.275	-0.313
.500	-0.404	-0.344	-0.391	-0.366	-0.342	-0.366	-0.249	-0.303
.560	-0.444	-0.291	-0.374	-0.398	-0.358	-0.331	-0.230	-0.335
.620	-0.511	-0.013	-0.451	-0.093	-0.373	-0.113	-0.226	-0.193
.700	-0.550	0.260	-0.522	0.258	-0.402	0.204	-0.258	0.130
.800	-0.608	0.392	-0.553	0.440	-0.478	0.335	-0.313	0.314
.900	-0.319	0.499	-0.353	0.602	-0.338	0.478	-0.396	0.393

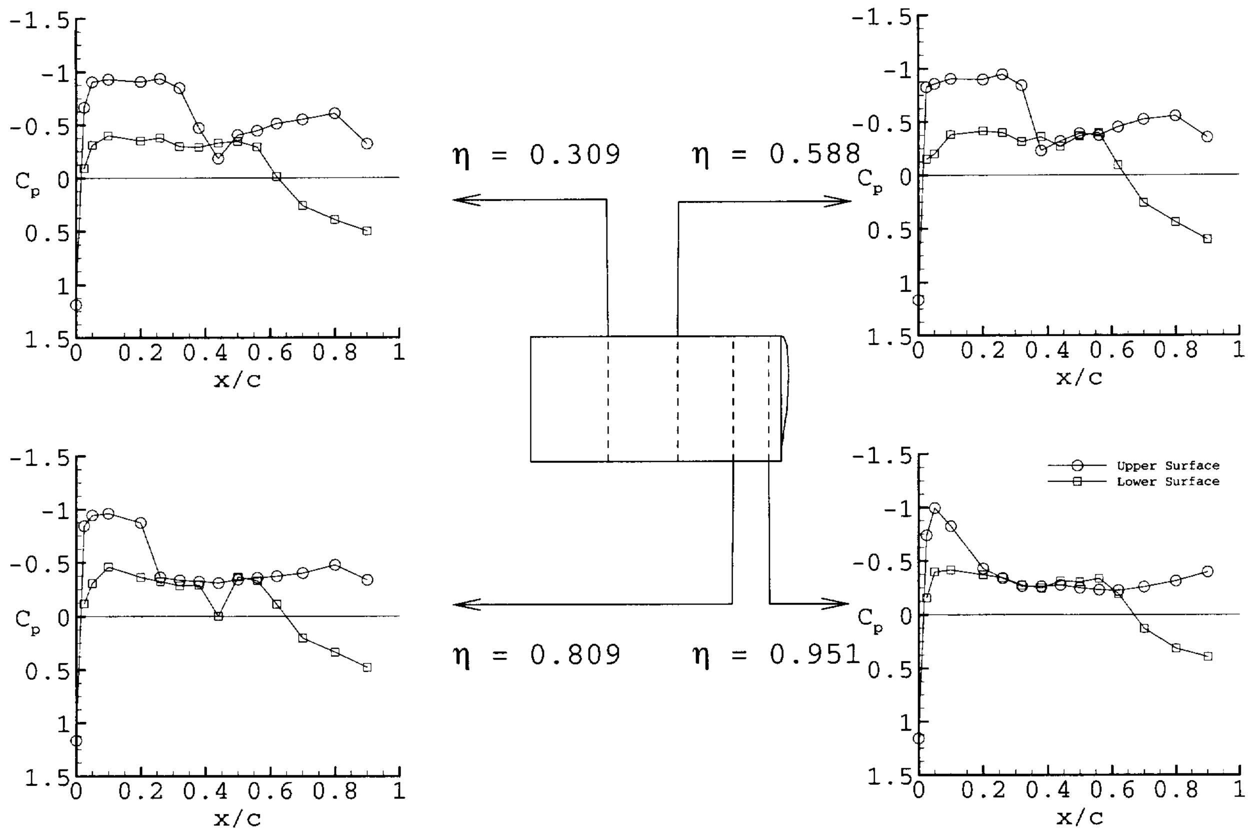

Figure 8. Sample static data, Test Case 6E3 (point 152).

Point Number = 315 Mach Number = 0.804 Alphao = 2.08, deg.

q,psf	H,psf	V,fps	Rn	gamma	freq,Hz	k	theta,deg
107.9	422.2	405.5	.401E+07	1.131	9.96	0.154	1.057

	y/s = 0.309				y/s = 0.588			
x/c	ReCpu/t	ImCpu/t	ReCpl/t	ImCpl/t	ReCpu/t	ImCpu/t	ReCpl/t	ImCpl/t
.000	-0.492	0.426			-0.569	0.415		
.025	-6.080	3.343	6.761	-2.800	-4.855	2.758	6.959	-3.026
.050	-6.356	3.626	6.721	-2.895	-7.377	4.022	6.142	-2.594
.100	-5.686	3.270	6.260	-2.131	-5.373	2.942	5.600	-2.049
.200	-5.786	3.830	4.620	-0.948	-5.532	3.524	4.146	-0.828
.260	-7.307	5.251	3.740	-0.059	-11.959	7.560	3.402	0.292
.320	-14.397	10.888	3.183	0.312	-18.215	9.849	2.634	0.342
.380	-16.559	10.428	2.602	0.534	-10.416	5.917	2.142	0.594
.440	-9.467	0.596	2.046	0.533	2.422	-6.618	1.822	0.699
.500	1.327	-8.571	1.499	0.630	1.672	-5.610	1.001	0.831
.560	2.087	-7.183	0.430	1.170	1.173	-4.231	0.249	1.055
.620	1.942	-3.998	-1.187	1.616	1.015	-3.033	-0.489	1.147
.700	2.124	-2.604	1.623	0.105	0.793	-1.294	0.972	0.340
.800	1.269	1.183	2.228	-0.851	0.773	0.595	1.582	-0.711
.900	-0.369	1.750	1.710	-1.048	-0.332	1.647	1.330	-0.838

	y/s = 0.809				y/s = 0.951			
x/c	ReCpu/t	ImCpu/t	ReCpl/t	ImCpl/t	ReCpu/t	ImCpu/t	ReCpl/t	ImCpl/t
.000	-0.550	0.348			-0.465	0.279		
.025	-4.582	2.467	5.469	-2.514	-6.241	3.031	5.484	-2.050
.050	-7.607	4.165	5.454	-2.269	-5.423	2.847	5.467	-1.936
.100	-4.777	2.562	3.519	-1.822	-7.007	3.679	3.604	-0.773
.200	-10.130	7.360	1.776	-0.372	-2.313	0.581	1.789	0.009
.260	-9.064	4.539	1.191	0.152	-2.847	0.678	1.096	0.470
.320	-1.827	-1.448	0.958	0.345	-1.662	-0.245	-0.027	0.975
.380	-1.387	-1.737	0.698	0.638	-1.358	-0.546	0.625	0.430
.440	-0.870	-1.807	-0.554	0.000	-0.988	-0.761	0.356	0.478
.500	-0.319	-2.035	0.463	0.647	-0.569	-0.792	0.063	0.647
.560	0.012	-1.735	-0.063	0.971	-0.210	-0.785	-0.219	0.612
.620	0.195	-1.505	-0.750	1.078	0.012	-0.705	-0.828	0.613
.700	0.253	-0.942	0.292	0.380	-0.033	-0.487	0.061	0.319
.800	0.050	0.649	0.538	-0.168	-0.990	0.286	0.542	0.012
.900	-0.179	0.904	0.249	-0.536	-3.406	1.545	0.257	0.085

(a) Tabulated data for Test Case 6E42

Figure 9. Sample data for pitch oscillation, Test Case 6E42 (point 315).

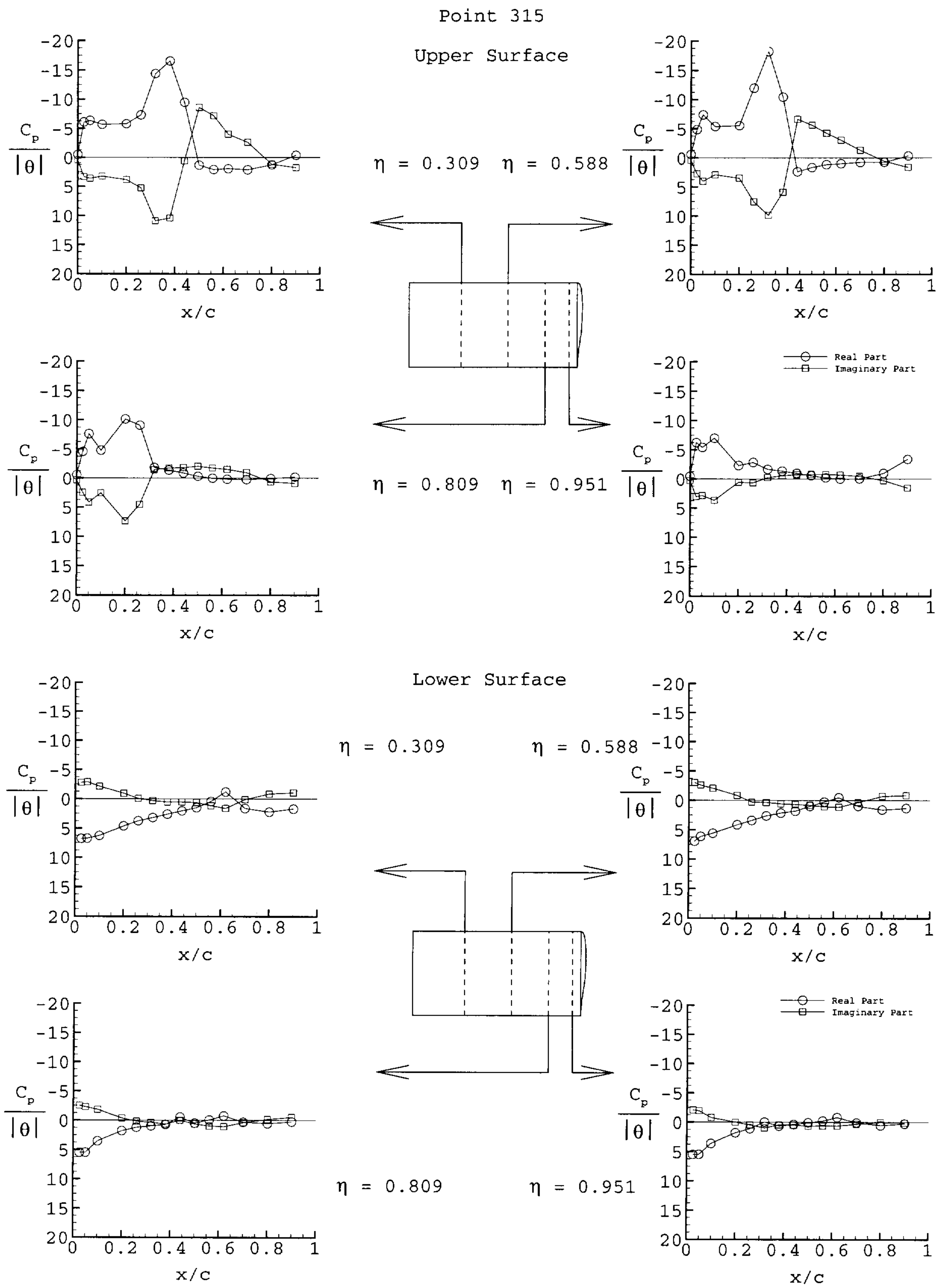

(b) Plot of data for Test Case 6E42
Figure 9. Concluded.

7E. TEST CASES FOR FLUTTER OF THE BENCHMARK MODELS RECTANGULAR WINGS ON THE PITCH AND PLUNGE APPARATUS

Submitted by

Robert M. Bennett
Senior Aerospace Engineer
Aeroelasticity Branch, Structures and Materials
Mail Stop 340
NASA Langley Research Center
Hampton, VA 23681-2199 USA
r.m.bennett@larc.nasa.gov

INTRODUCTION

As a portion of the Benchmark Models Program at NASA Langley (Ref 1), three models with the same rectangular planform, but with different airfoils were flutter tested on the Pitch and Plunge Apparatus (PAPA, Ref 2-3). These models were designed and tested to provide flutter data for evaluating Computational Aeroelasticity (CA) programs with emphasis on transonic flows. The geometry of the wings was kept simple to reduce the complexity of the geometry processing for computation and in the interpretation of the results. One model was built with the NACA 0012 airfoil called the B0012, one with the NACA 64A010 airfoil called the B64A010, and one with an NASA SC(2)-0414 airfoil called BSCW. These airfoils, shown in Fig 1, were not selected to provide a systematic empirical trend study of thickness or airfoil type, but to provide flutter data for wings with different transonic airfoil characteristics. The NACA 0012 airfoil has a forward loading and for transonic flows, a shock forms initially ahead of midchord. The NACA 64A010 airfoil has a more mild evolution of the shock which forms initially near midchord. The NASA SC(2)-0414 has a strong aft loading and the associated low aft upper surface curvature. There was considerable experience in two dimensions with the NACA 0012 and 64A010 airfoils based on comparisons with the early two-dimensional unsteady aerodynamic data of Ref 4. The supercritical airfoil (Ref 5) was chosen as a relatively modern airfoil for comparison.

The B0012 model was tested first. Three different types of flutter instability boundaries were encountered, a classical flutter boundary, a transonic stall flutter boundary at angle of attack, and a plunge instability near M = 0.9 and for zero angle of attack. This test was made in air and was Transonic Dynamics Tunnel (TDT) Test 468 (Ref 1, 6-8). The BSCW model (for Benchmark SuperCritical Wing) was tested next as TDT Test 470 (Ref 9-11). It was tested using both with air and a heavy gas, R-12, as a test medium. The effect of a transition strip on flutter was evaluated in air. The B64A010 model was subsequently tested as TDT Test 493 (Ref 1).

Some further analysis of the experimental data for the B0012 wing is presented in Ref 12. Transonic calculations using the parameters for the B0012 wing in a two-dimensional typical section flutter analysis are given in Ref 13.

These data are supplemented with data from the Benchmark Active Controls Technology model (BACT) given in Ref 14-15 and in the next chapter of this document. The BACT model was of the same planform and airfoil as the B0012 model, but with spoilers and a trailing edge control. It was tested in the heavy gas R-12, and was instrumented mostly at the 60 per cent span. The flutter data obtained on PAPA and the static aerodynamic test cases from BACT serve as additional data for the B0012 model. All three types of flutter are included in the BACT Test Cases.

In this report several test cases are selected to illustrate trends for a variety of different conditions with emphasis on transonic flutter. Cases are selected for classical and stall flutter for the BSCW model, for classical and plunge for the B64A010 model, and for classical flutter for the B0012 model. Test Cases are also presented for BSCW for static angles of attack. Only the mean pressures and the real and imaginary parts of the first harmonic of the pressures are included in the data for the test cases, but digitized time histories have been archived. The data for the test cases are available as separate electronic files. An overview of the model and tests is given, the standard formulary for these data is listed, and some sample results are presented.

LIST OF SYMBOLS AND DEFINITIONS

a	speed of sound, ft/sec
A_z	amplitude of the plunge free vibration envelope, inches
A_θ	amplitude of the pitch free vibration envelope, degrees
b	semichord, c/2
c	wing chord, ft (m)
C_p	pressure coefficient, $(p - p_\infty) / q_\infty$ steady; $(p - p_{mean}) / q_\infty$ unsteady
f	frequency, Hz
h	plunge displacement, inches

k	reduced frequency, $\omega c/(2V_\infty)$
M	Mach number
p	pressure, psf
p_∞	freestream static pressure, psf
q_∞	dynamic pressure, psf (kPa)
s	semispan, 32 inches
R_n	Reynolds number based on chord
T_o	total or stagnation temperature, ^oR
V_∞	freestream velocity, ft/sec (m/sec)
V	velocity, ft/sec (m/sec)
V_I	flutter speed index, $V_f / \left(b\omega_\theta\sqrt{\mu}\right)$
x/c	streamwise fraction of local chord
y	spanwise coordinate normal to freestream
α_m	mean angle of attack, degrees
ϕ	phase angle referenced to pitch displacement, degrees
θ	pitch angle, degrees
η	fraction of span, y/s
μ	mass ratio, wing mass/($\left(\pi b^2 \rho \text{span}\right)$
ρ	density
γ	ratio of specific heats for test gas
ω	frequency, radians/second
ζ_z	fraction of critical damping for plunge
ζ_θ	fraction of critical damping for pitch
$\lvert \; \rvert$	absolute value

subscripts

0	steady value
f	flutter
m	mean value
h	plunge mode
z	vertical displacement
θ	pitch mode

MODEL AND TESTS

The BMP rectangular wing models were tested in the NASA Langley Transonic Dynamics Tunnel (TDT). The tunnel has a slotted test section 16-feet (4.064 m) square with cropped corners. At the time of these tests, it could be operated with air or a heavy gas, R-12, as a test medium at pressures from very low to near atmospheric values. Currently the TDT can be operated with air or R-134a as a test medium. An early description of this facility is given in Ref 16 and more recent descriptions of the facility are given in Ref 17 and 18. The early data system is described in Ref 19 and the recent data system given in Ref 20 and 21, but the data system used in the BMP tests was a version between these systems. Based on cone transition results (Ref 22-23), the turbulence level for this tunnel is in the average large transonic tunnel category. Some low speed measurements in air have also been presented in Ref 24.

The three wing models were very similar but differed somewhat in detail. These models were of rectangular planform with a span of 32 inches (813 mm) plus a tip of revolution, and a chord of 16 inches (406 mm). The wings were machined from aluminum, were very smooth, and were tested either with free transition or with a transition strip at 7.5 per cent chord on both upper and lower surfaces. They were fabricated in three parts as shown in Fig 2, with two main sections and a tip section to facilitate access to the pressure instrumentation.

The assembled BSCW model is shown installed in the wind tunnel in Fig 3 and an overall view of the BSCW model and splitter plate installed in the TDT test section is shown in Fig 4. The model was mounted on a large splitter plate set out approximately 40 inches (1.02 m) from tunnel sidewall. An end plate that moved with the model was attached to the root of the model, and moved within a recessed or undercut section of the splitter plate. A large fairing behind the splitter plate isolated the equipment between the splitter plate and the tunnel sidewall from the airstream. Some recent tests (Ref 25) of the splitter plate arrangement without a wing have shown some nonuniformity of the flow along the splitter plate resulting from the flow around the leading edge of the splitter plate for Mach numbers above M = 0.80. The data for the models may be affected somewhat above M = 0.80.

These models were flutter tested using the Pitch and Plunge Apparatus (PAPA, Ref 2-3) as shown in the photograph of Fig 5 and illustrated in the sketch of Fig 6. The PAPA system permits rigid body pitch and plunge motion of the wing and flutter of the system by using four circular rods for flexibility. This system has sufficient strength to permit flutter testing at moderate angles of attack including some stall flutter cases. The rods are arranged such that the elastic axis is at the midchord and the model is balanced to place the center of gravity on the midchord. The system thus gives essentially uncoupled pitch and plunge modes about the midchord of the model. The summary of the modal parameters is given in Table 1. The generalized masses given here are the effective mass and pitch inertia calculated from the frequency and stiffness values. Higher modes of this system have been determined for the BSCW model (Ref 10) and are considered typical for all three models. Some amplitude effects on frequency and damping were analyzed (Ref 10) and can be summarized by the following equations.

$$f_z = 3.339978 - 0.638404\, A_z + 0.09185239\, A_z^2 \qquad \zeta_z = 0.0006913 + 0.0021713\, A_z$$

$$f_\theta = 5.1987 \quad - 0.008994\, A_\theta + 0.0056696\, A_\theta^2 \qquad \zeta_\theta = 0.0004379 + 0.0003561\, A_\theta$$

where A_z is the amplitude of the plunge free vibration envelope in inches, and A_θ is the amplitude of pitch free vibration envelope in degrees. The effects of amplitude are quite small for the frequencies (third or fourth significant figure) but are significant on damping. Detailed wind-off free decay records have been archived.

In addition to the testing on the PAPA, the B0012 and BSCW models were tested with the PAPA mount system rigidized for static pressure measurements. The model could be pitched statically with the turntable, but there was no balance in this system for force measurements. Only static data for BSCW are included as test cases. Static data, including force measurements, for a similar 0012 model is available in the next chapter of this document for the BACT model.

Both the model and the plate that constrains the model end of the PAPA system are large in mass. The resulting mass ratio at flutter is thus very large and consequently the reduced frequency at flutter is very low. The reduced frequency may be more comparable to those for rigid body modes for an aircraft than typical of flutter. The flutter crossings are relatively mild and unpublished calculations for the B0012 model have indicated some sensitivity to torsional aerodynamic damping.

The models were instrumented for unsteady pressures at two chords and for dynamic motions. The list of transducers is given in Table 2. The primary dynamic motion measurements were made with the PAPA strain gages and accelerometers, although four wing accelerometers were included. There were 40 unsteady pressure transducers located along the chord at 60 per cent span and 40 located at 95 per cent span. The distribution for BSCW is illustrated in figure 7. The chordwise distribution of unsteady pressure transducers was slightly different for each model and is summarized in Table 3. In addition to the pressure measurements on the wing, there were transducers located in the splitter plate as illustrated in figure 8 and listed in Table 4. However the data measured on the splitter plate are not included in the data sets for the Test Cases of these wings.

It might be noted that some flow visualization work on these low aspect ratio planforms indicated that wing surface separation tended to occur in an inboard aft cell. The row of pressure transducers at 60 per cent chord was in the outer portion of this cell, whereas the row at 95 per cent span was dominated by the tip flow.

Data from all channels were acquired simultaneously at a rate of 1000 or 500 samples/second (depending on the test) for 20 seconds for the dynamic data and for 10 seconds for the static data.. Each recorded data set was stored in digital form on disk, and assigned an index called a Point No. which is given in the Tables. Although it was intended to use 200 Hz or 400 Hz low pass filters in the data stream prior to digitizing the data to avoid aliasing, the filters were later thought to be set at 1000 Hz as a result of a data system problem. The data are thus considered aliased with a foldover frequency of 500 Hz. For the flutter data, which was in the 4 to 10 Hz range, in order for the 1st harmonic to be contaminated, there would have to be significant signals at 990-996 Hz for the 1000 samples/sec case and at 490-510 and 990-996 Hz for the 500 samples/sec cases. It is not considered likely that there are significant disturbances in these frequency ranges.

Detailed geometry measurements were performed for each of these wings along several sections. The measured ordinates are not included in this report, but they are available as electronic files. Design ordinates are given in Table 5 only for the BSCW and B64A010 models since the NACA 0012 airfoil is analytically defined. The thickness of the aft end of the NACA 64A010 airfoil was increased to permit smooth installation of the aft-facing transducers in the trailing edge. The trailing edge thickness was increased and a line was drawn to be tangent to the original airfoil. Therefore the modified B64A010 airfoil has a somewhat larger linear aft section than the standard 64A010 which is linear in thickness from 0.80 to the trailing edge. Table 5b lists the design ordinates with interpolation of the airfoil to 104 points along the chord.

TEST CASES

The flutter Test Cases for the three models on the PAPA system are listed in Tables 6-8. In the Test Case Number, the leading portion is 7E for the Chapter number, followed by the Model designation, SW = BSCW model, 64 for the B64A010 model, and 12 for the B0012 model. Flutter is denoted by F with a following letter for the type of flutter, C = classical, S = stall, and P = plunge.

The BSCW model was tested both in air and in the heavy gas, R-12. The classical flutter boundaries for both the air and R-12 tests are given in Fig 9 in terms of dynamic pressure versus Mach number and flutter frequency versus Mach number. The flutter dynamic pressure increases with Mach number. This is an unusual trend that is apparently a result of the specific aeroelastic configuration of this model on the PAPA system. The boundary flattens near M = 0.78-0.80 and then rises which is interpreted as the transonic "dip" for this system. The boundaries obtained in air and in R-12 show generally good agreement.

A few points of stall flutter near $\alpha = 5^o$ and M = 0.80 were obtained with the BSCW model and are included in Table 6. The corresponding flutter boundary is given in Fig 10. The boundary is not fully defined with angle of attack, but the stall flutter boundary appears to be nearly vertical near $\alpha = 5^o$. These points are thought to involve shock waves and separating and reattaching flows during the cycle of motion. No plunge instability points were defined for the BSCW model, possibly because the condition of zero lift could not be obtained without hitting the stops within the mechanical setup. For the NASA supercritical airfoils of this type, the two-dimensional design lift coefficient occurs at $\alpha = 0^o$. For the SC(2)-0414 airfoil, the design lift coefficient is 0.4.

An earlier unpublished test of a supercritical wing on the PAPA system had indicated an effect of transition strip on flutter. It was found that a forward transition strip on the lower surface had a significant influence at the lower subsonic Mach numbers. Some variations of the transition strips were thus explored in this test with air as the test medium. A few Test Cases are included for the free transition test for BSCW in Table 6.

The Test Cases for static angles of attack for BSCW are presented in Table 9. The angles of attack given generally encompass the range of the flutter data in the Test Cases. A listing of a sample of the static data file illustrating the format is given in Fig 11. For each pressure transducer, the time-averaged mean, the minimum and maximum values, and the standard deviation (generally called channel statistics) of the pressure coefficient is listed. The static pressures for Test Cases 7ESWA24 and 7ESWA30 are presented in Fig 12. Test Case 7ESWA24 shows little lift at the instrumented chords except over the aft section, whereas for Test Case 7ESWA30 there is significant lift and a strong shock on the inboard section.

A listing of a sample of the flutter data file illustrating the format is given in Fig 13. The mean, minimum, maximum, and standard deviation are listed with the real and imaginary parts of the first harmonic of the unsteady pressures. The unsteady pressures are referenced to pitch displacement. The minimum, maximum, and standard deviation include the unsteady components and thus their interpretation is not straightforward. The mean pressures and the in-phase (or real) and the out-of-phase (or imaginary) components of the unsteady pressures for a classical flutter case, Test Case 7ESWFC6, are given in Fig 14. Similar data for a stall flutter Test Case, 7ESWA30 are presented in Fig 15. For the classical flutter case (Fig 14), the imaginary components of the pressure are small, but for the stall flutter Test Case the imaginary components of the pressure can be as large as the real components (Fig 15).

The unsteady pressures presented and included in the files have not been normalized by amplitude of motion. Case to case comparisons of pressures may need to be normalized by pitch or plunge amplitude values listed with the Test Case.

The flutter data for the B0012 model is given in Table 8. Only flutter Test Cases in air were obtained for this model and only classical flutter points are included as Test Cases. Corresponding flutter points for a model in R-12 with the NACA 0012 airfoil including stall and plunge flutter cases are given in the next Chapter for the Benchmark Active Controls Technology (BACT) model. The flutter boundaries for the B0012 and BSCW models are quite similar indicating that the supercritical design permits about two percent more thickness for corresponding transonic effects on flutter.

The flutter data for the B64A010 model is given in Table 9. It might be noted that the available flutter data for this model listed the plunge displacement to one significant figure (Table 9). For this thinner airfoil, the rise in the flutter boundary occurs at somewhat higher Mach number. No stall flutter points were defined for this model as sufficient angle of attack could not be obtained without hitting the stops within the mechanical setup. Two flutter points are included and labeled plunge flutter near M=0.95. They are of significantly lower frequency, but also include a significant pitch amplitude (Table 9).

Only the mean pressures and the real and imaginary parts of the first harmonic of the pressures are included in the data for the Test Cases, but digitized time histories have been archived. The data for the Test Cases are available as separate electronic files. For the flutter cases, calculations for flutter can be made and compared with measured boundaries. However in calculations, the analytical model can be forced to duplicate the measured combined pitch and plunge motion and the pressures compared directly. It might be noted that the transition strip (at 7.5 per cent chord) has an influence on the first transducer downstream of the strip that varies with angle of attack or other test conditions.

The files on the CD-ROM are ascii files and readme files are included. For BSCW, the file for the static data is named bscwstat and a Fortran program to read it, bscwstrd.f, is furnished. The BSCW flutter data is in file bscwflut, and the Fortran program to read it, bscwftrd.f, is included. The data files consist of contiguous data points in the sequence given in the tables. The design ordinates are on file bscwordt, and the measured ordinates are given on file bscworde. In the measured ordinates for BSCW, some points may need to be omitted as they were on the edge of the orifices. For the B0012 model, the flutter data is in file b12flut, and the Fortran program to read it, b12ftrd.f, is included. The design ordinates are on file b12ordt, and the measured ordinates are given on file b12orde. For the B64A010 model, the flutter data is in file b64flut, and the Fortran program to read it, b64ftrd.f, is included. The design ordinates are in file b64ordt, and the measured ordinates are given in file b64orde.

Note that the tests for these BMP models were conducted both in air and in the heavy gas, R-12. For CFD calculations, care must be exercised to select the correct gas properties are used for each Test Case. For R-12, the ratio of specific heats, γ, is calculated to be 1.132 to 1.135 for the conditions of the tests assuming 0.99 for the fraction of heavy gas in the heavy gas-air mixture. A value of 1.132 is suggested for use in computational comparisons. The corresponding value of Prandtl number is calculated to range from 0.77 to 0.78 for the conditions of these tests. For some cases, the calculated values of γ and Prandl number are included in the data files.

FORMULARY

1 General Description of Model

1.1	Designation	Three models, Benchmark Supercritical Wing Model, BSCW, Benchmark 0012 Model, B0012, and Benchmark 64A010 Model, B64A010
1.2	Type	Semispan wing
1.3	Derivation	Same planform as Benchmark Active Controls Model with 0012 airfoil, BACT (see Introduction)
1.4	Additional remarks	Overall view given in Fig 2 and shown mounted in tunnel in Figs 3 and 4
1.5	References	Refs 1, 6-11 describe tests and data

2 Model Geometry

2.1	Planform	Rectangular
2.2	Aspect ratio	2.0 for the panel (neglecting tip of rotation)
2.3	Leading edge sweep	Unswept
2.4	Trailing edge sweep	Unswept
2.5	Taper ratio	1.0
2.6	Twist	None
2.7	Wing centreline chord	16 inches (406.4 mm)
2.8	Semi-span of model	32 inches (812.8 mm) plus tip of rotation
2.9	Area of planform	512 sq. in. (0.3303 sq. m) neglecting tip
2.10	Location of reference sections and definition of profiles	Measured ordinates are given in files on the CDROM
2.11	Lofting procedure between reference sections	Constant design airfoil section
2.12	Form of wing-body junction	No fairing and plate overlapped at splitter plate
2.13	Form of wing tip	Tip of rotation
2.14	Control surface details	No control surfaces
2.15	Additional remarks	See Fig 1 for overview
2.16	References	Refs 1, 6-11

3 Wind Tunnel

3.1	Designation	NASA LaRC Transonic Dynamics Tunnel (TDT)
3.2	Type of tunnel	Continuous flow, single return
3.3	Test section dimensions	16 ft x 16 ft (4.064 x 4.064 m)
3.4	Type of roof and floor	Three slots each
3.5	Type of side walls	Two sidewall slots
3.6	Ventilation geometry	Constant width slots in test region
3.7	Thickness of side wall boundary layer	Model tested on large splitter plate set out approximately 40 inches (1.02 m) from tunnel side wall (see Fig 3). Some documentation of tunnel wall boundary layer in Ref 16
3.8	Thickness of boundary layers at roof and floor	Not documented
3.9	Method of measuring velocity	Calculated from static pressures measured in plenum and total pressure measured upstream of entrance nozzle of test section
3.10	Flow angularity	Not documented, considered small
3.11	Uniformity of velocity over test section	Not documented, considered nearly uniform, some nonuniformity over splitter plate above M = 0.80

3.12	Sources and levels of noise or turbulence in empty tunnel	Generally unknown. Some low speed measurements are presented in Ref 24. Cone transition measurements are presented in Ref 22 and 23
3.13	Tunnel resonances	Unknown
3.14	Additional remarks	Some tests performed in air and some in heavy gas, R-12. For R-12, ratio of specific heats, γ, is 1.132-1.135. For R-12 computations, 1.132 is recommended. For the conditions of this test, the R-12 Prandtl number is calculated to be 0.77-0.78
3.15	References on tunnel	Ref 16-18

4 Model Motion

4.1	General description	Flutter with combined pitch and plunge motions
4.2	Reference coordinate and definition of motion	Pitch and plunge motions referenced to midchord
4.3	Range of amplitude	Varies for each case, tabulated
4.4	Range of frequency	Generally 0 to 5 Hz
4.5	Method of applying motion	Self-excited flutter, measured values of pitch and plunge are listed with each data point
4.6	Timewise purity of motion	Not documented
4.7	Natural frequencies and normal modes of model and support system	See Table 1 for plunge and pitch on PAPA. For higher modes see Ref 10. Not documented for rigid strut
4.8	Actual mode of applied motion including any elastic deformation	Combined pitch and plunge measured. Very stiff model with flutter below 5 Hz with next vertical mode at 37 Hz
4.9	Additional remarks	None

5 Test Conditions

5.1	Model planform area/tunnel area	.015
5.2	Model span/tunnel height	.17
5.3	Blockage	Model less than 0.2% but splitter plate and equipment fairing is near 4%
5.4	Position of model in tunnel	Mounted from large splitter plate out from wall and on the tunnel centerline, Fig 3
5.5	Range of Mach number	0.30 to 0.90
5.6	Range of tunnel total pressure	Approximately 500 to 1000 psf (24 to 48 kPa)
5.7	Range of tunnel total temperature	512 to 576 degrees Rankine (23 to 47^{o} C)
5.8	Range of model steady or mean incidence	-3^{o} to 5^{o} pitch
5.9	Definition of model incidence	From chord line of symmetric airfoils or reference chord line of BSCW
5.10	Position of transition, if free	Transition strip used
5.11	Position and type of trip, if transition fixed	Grit strip at 7.5% chord on upper and lower surfaces when used
5.12	Flow instabilities during tests	None defined
5.13	Changes to mean shape of model due to steady aerodynamic load	Not measured but considered very stiff
5.14	Additional remarks	Tests performed both in air and in heavy gas, R-12. For R-12 ratio of specific heats, γ, is 1.132-1.135. For R-12 computations, 1.132 is recommended. For the conditions of this test, the R-12 Prandtl number is calculated to be 0.77-0.78. Some data files include values of γ and Prandl number
5.15	References describing tests	Refs 1, 6-11

6 Measurements and Observations

6.1	Steady pressures for the mean conditions	BSCW only
6.2	Steady pressures for small changes from the mean conditions	no
6.3	Quasi-steady pressures	no
6.4	Unsteady pressures	yes
6.5	Steady section forces for the mean conditions by integration of pressures	no
6.6	Steady section forces for small changes from the mean conditions by integration	no
6.7	Quasi-steady section forces by integration	no
6.8	Unsteady section forces by integration	no
6.9	Measurement of actual motion at points of model	yes
6.10	Observation or measurement of boundary layer properties	no
6.11	Visualisation of surface flow	no
6.12	Visualisation of shock wave movements	no
6.13	Additional remarks	no

7 Instrumentation

7.1	Steady pressure	
	7.1.1 Position of orifices spanwise and chordwise	40 locations at 60% span and 40 at 95% span. See Fig 7 and Table 3
	7.1.2 Type of measuring system	Used same transducers as unsteady pressure measurements
7.2	Unsteady pressure	
	7.2.1 Position of orifices spanwise and chordwise	Same transducers as steady measurements. See Fig 7 and Table 3
	7.2.2 Diameter of orifices	.020 inches (.51 mm)
	7.2.3 Type of measuring system	In situ pressure gages
	7.2.4 Type of transducers	Kulites
	7.2.5 Principle and accuracy of calibration	Statically calibrated and monitored through reference tubes
7.3	Model motion	
	7.3.1 Method of measuring motion reference coordinate	Strain gages on PAPA system
	7.3.2 Method of determining spatial mode of motion	Wind-off verification with accelerometers
	7.3.3 Accuracy of measured motion	Undocumented
7.4	Processing of unsteady measurements	
	7.4.1 Method of acquiring and processing measurements	Analog signals digitized at 500 or 1000 samples/sec for 10-20 seconds depending on data type
	7.4.2 Type of analysis	Fourier analysis
	7.4.3 Unsteady pressure quantities obtained and accuracies achieved	Amplitude and phase of each pressure signal. Accuracy not specified
	7.4.4 Method of integration to obtain forces	None
7.5	Additional remarks	None
7.6	References on techniques	Data system for test similar to one described in Refs 19-20

8 Data Presentation

8.1	Test Cases for which data could be made available	See Ref 6-11
8.2	Test Cases for which data are included in this document	See Tables 6-9
8.3	Steady pressures	BSCW only
8.4	Quasi-steady or steady perturbation pressures	BSCW only given in CDROM
8.5	Unsteady pressures	C_p real and imaginary parts for first harmonic only included in CDROM. Time histories have been archived. Pressures have not been normalized by motion amplitude
8.6	Steady forces or moments	None
8.7	Quasi-steady or unsteady perturbation forces	None
8.8	Unsteady forces and moments	None
8.9	Other forms in which data could be made available	Time histories archived
8.10	Reference giving other representations of data	Ref 12

9 Comments on Data

9.1	Accuracy	
	9.1.1 Mach number	Not documented
	9.1.2 Steady incidence	Unknown
	9.1.3 Reduced frequency	Should be accurate
	9.1.4 Steady pressure coefficients	Not documented
	9.1.5 Steady pressure derivatives	None
	9.1.6 Unsteady pressure coefficients	Each gage individually calibrated and monitored statically through reference tubes
9.2	Sensitivity to small changes of parameter	None indicated. Amplitudes of oscillation varied in tests
9.3	Non-linearities	Many flow conditions involve shock waves and separation
9.4	Influence of tunnel total pressure	Not evaluated. Most of the tests at nearly constant dynamic pressure
9.5	Effects on data of uncertainty, or variation, in mode of model motion	Unknown, not expected to be appreciable
9.6	Wall interference corrections	None applied
9.7	Other relevant tests on same model	None
9.8	Relevant tests on other models of nominally the same shapes	Aerodynamic and flutter tests on similar 0012 model with spoilers and trailing edge control surface (BACT), Ref 15 and next Chapter
9.9	Any remarks relevant to comparison between experiment and theory	Some included under Model and Tests
9.10	Additional remarks	None
9.11	References on discussion of data	Ref 1 and 6-13

10 Personal Contact for Further Information

Head, Aeroelasticity Branch
Mail Stop 340
NASA Langley Research Center
Hampton, VA 23681-2199 USA

Phone: +1-(757)-864-2820
FAX: +1-(757)-864-8678

LIST OF REFERENCES

1 Bennett, Robert M.; Eckstrom, Clinton V.; Rivera, Jose, A.; Dansberry, Bryan E.; Farmer, Moses G.; and Durham, Michael H.: *The Benchmark Aeroelastic Models Program - Description and Highlights of Initial Results.* Paper No. 25 in Transonic Unsteady Aerodynamics and Aeroelasticity, AGARD CP 507, Mar. 1992. Also available as NASA TM-104180, 1991.

2 Farmer, Moses G.: *A Two-Degree-of-Freedom Flutter Mount System with Low Damping for Testing Rigid Wings at Different Angles of Attack.* NASA TM 83302, 1982.

3 Farmer, Moses G.: Mount System for Testing Flutter. U.S Patent No. 4,475,385, Oct. 9, 1984.

4 "*Compendium of Unsteady Aerodynamic Measurements,*" AGARD Report No. 702, Aug. 1982.

5 Harris, Charles D.: *NASA Supercritical Airfoils--A Matrix of Family-Related Airfoils,* NASA TP 2969, March 1990.

6 Rivera, Jose A., Jr.; Dansberry, Bryan E.; Durham, Michael, H.; Bennett, Robert M.; and Silva, Walter A.: *Pressure Measurements on a Rectangular Wing with A NACA 0012 Airfoil During Conventional Flutter.* NASA TM 104211, July 1992.

7 Rivera, Jose A.; Dansberry, Bryan E.; Bennett, Robert M.; Durham, Michael, H.; and Silva, Walter A.: *NACA 0012 Benchmark Model Experimental Flutter Results With Unsteady Pressure Distributions.* AIAA Paper 92-2396, Apr. 1992. Also available as NASA TM 107581, Mar. 1992.

8 Rivera, Jose A.; Dansberry, Bryan E.; Farmer, Moses G.; Eckstrom, Clinton, V.; Seidel, David A.; and Bennett, Robert M.: *Experimental Flutter Boundaries with Unsteady Pressure Distributions for the NACA 0012 Benchmark Model.* AIAA 91-1010, 1991. Also available as NASA TM 104072, 1991.

9 Dansberry, Bryan E.; Durham, Michael, H.; Bennett, Robert M.; Rivera, Jose A.; Silva, Walter A.; and Wieseman, Carol D.: *Experimental Unsteady Pressures at Flutter on the Supercritical Wing Benchmark Model.* AIAA 93-1592, Apr. 1993.

10 Dansberry, Bryan E.; Durham, Michael, H.; Bennett, Robert M.; Turnock, David L.; Silva, Walter A.; and Rivera, Jose A., Jr.: *Physical Properties of the Benchmark Models Program Supercritical Wing.* NASA TM 4457, Sep. 1993.

11 Dansberry, Bryan E.: *Dynamic Characteristics of a Benchmark Models Program Supercritical Wing.* AIAA 92-2368, Apr. 1992.

12 Finaish, F.: Frigerio, J.; and Bennett, R. M.: *Unsteady Pressure Distributions Around an Aeroelastic Wing in Transonic Flows.* AIAA Paper 95-0311, Jan. 1995.

13 Bendiksen, Oddvar O.; Hwang, Guang-Yaw; and Piersol, John: *Nonlinear Aeroelastic and Aeroservoelastic Calculations for Transonic Wings.* AIAA Paper 98-1898, April 1998.

14 Durham, Michael H.; Keller, Donald F.; Bennett, Robert M.; and Wieseman, Carol D.: *A Status Report on a Model for Benchmark Active Controls Testing.* AIAA Paper 91-1011, Apr. 1991. Also available as NASA TM 107582, 1991.

15 Scott, Robert C.; Hoadley, Sherwood T.; Wieseman, Carol D.; and Durham, Michael H.: *The Benchmark Active Controls Technology Model Aerodynamic Data.* AIAA Paper 97-0829, Jan. 1997.

16 Aeroelasticity Branch Staff: *The Langley Transonic Dynamics Tunnel.* LWP-799, Sep. 1969.

17 Cole, Stanley, R.; and Rivera, Jose, A, Jr.: *The New Heavy Gas Testing Capability in the NASA Langley Transonic Dynamics Tunnel.* Paper No. 4, presented at the Royal Aeronautical Society Wind Tunnels and Wind Tunnel Test Techniques Forum, Churchill College, Cambridge, UK, Apr. 1997.

18 Corliss, James M.; and Cole, Stanley R.: *Heavy Gas Conversion of the NASA Langley Transonic Dynamics Tunnel.* AIAA Paper 98-2710, June 1998.

19 Cole, Patricia H.: *Wind Tunnel Real-Time Data Acquisition System.* NASA TM 80081, 1979.

20 Bryant, C.; and Hoadley, S. T.: *Open Architecture Dynamic Data System at Langley's Transonic Dynamics Tunnel.* AAIA Paper 98-0343, Jan. 1998.

21 Wieseman, Carol D.; and Hoadley, Sherwood, T.: *Versatile Software Package for Near Real-Time Analysis of Experimental Data.* AIAA Paper 98-2722, June 1999.

22 Dougherty, N. Sam, Jr.: *Influence of Wind Tunnel Noise on the Location of Boundary-Layer Transition on a Slender Cone at Mach Numbers from 0.2 to 5.5. Volume I. - Experimental Methods and Summary of Results. Volume II. - Tabulated and Plotted Data.* AEDC--TR-78-44, March 1980.

23 Dougherty, N. Sam, Jr.; and Fisher, D. F.: *Boundary-Layer Transition on a 10-Deg. Cone: Wind Tunnel/Flight Correlation.* AIAA Paper 80-0154, Jan. 1980.

24 Sleeper, Robert K.; Keller, Donald F.; Perry, Boyd, III; and Sandford, Maynard C.: *Characteristics of Vertical and Lateral Tunnel Turbulence Measured in Air in the Langley Transonic Dynamics Tunnel.* NASA TM 107734, March 1993.

25 Schuster, David M: *Aerodynamic Measurements on a Large Splitter Plate for the NASA Langley Transonic Dynamics Tunnel.* Proposed NASA TM 1999.

Table 1. Measured Nominal Structural Dynamic Parameters

	Plunge Mode	Pitch Mode
Frequency	3.33 Hz.	5.20 Hz.
Stiffness	2637 lb/ft	2964 ft-lb/rad
Damping Ratio, ζ	0.001	0.001
Effective Mass or Inertia	6.01 slugs	2.78 slug-ft^2

Table 2. Instrumentation

Instrument	Quantity
Model Pressure Transducers	80
Splitter Plate Pressure Transducers	20
Boundary Layer Rake Pressure Transducers	10
Model Accelerometers	4
PAPA Strain Gage Bridges	2
PAPA Accelerometers	2
Turntable AOA Accelerometer	1
Model AOA Accelerometer	1

Table 3. Nominal Location of Wing Pressure Orifices

BSCW x/c		B64A010 x/c		B0012 x/c	
Upper	Lower	Upper	Lower	Upper	Lower
0.000		0.000		0.000	
0.010	0.010	0.010	0.010	0.010	0.010
0.025	0.025	0.025	0.025	0.020	0.020
0.050	0.050	0.050	0.050	0.030	0.030
0.100	0.100	0.100	0.100	0.040	
0.150		0.150		0.050	0.050
0.200	0.200	0.200	0.200	0.100	0.100
0.250		0.250		0.200	0.200
0.300	0.300	0.300	0.300	0.250	
0.350		0.350		0.300	0.300
0.400	0.400	0.400	0.400	0.350	
0.450		0.450		0.400	0.400
0.500	0.500	0.500	0.500	0.450	
0.550	0.550	0.550	0.550	0.500	0.500
0.600	0.600	0.600	0.600	0.550	
0.650	0.650	0.650	0.650	0.600	0.600
0.700	0.700	0.700	0.700	0.650	
0.750	0.750	0.750	0.750	0.700	0.700
0.800	0.800	0.800	0.800	0.750	
0.850	0.850	0.850	0.850	0.800	0.800
0.900	0.900	0.900	0.900	0.850	
0.950	0.950	0.950	0.950	0.900	0.900
1.000		1.000		0.950	0.950
				1.000	

Table 4. Locations of Pressure Orifices on the Splitter-Plate

x, in.	y, in.	z, in.
Horizontal Row		
64	0	0
48	0	0
24	0	0
20	0	0
16	0	0
0	0	0
-4	0	0
-8	0	0
-32	0	0
-48	0	0
Vertical Row 1		
0	0	16
0	0	8
0	0	4
0	0	-4
0	0	-16
Vertical Row 2		
16	0	16
16	0	8
16	0	4
16	0	-4
16	0	-16
Boundary Layer Rake		
32	0.25	16
32	0.50	16
32	0.75	16
32	1.00	16
32	1.50	16
32	2.00	16
32	2.50	16
32	3.00	16
32	4.00	16
32	5.00	16

Table 5. Design Ordinates for SC(2)-0414 and B64A010 Airfoils
(a) SC(2)-0414 Airfoil Design Coordinates

x/c	z/c upper	z/c lower	x/c	z/c upper	z/c lower
0.00000	0.00000	0.00000	0.50000	0.06840	-0.06420
0.00200	0.01080	-0.01080	0.51000	0.06800	-0.06330
0.00500	0.01660	-0.01660	0.52000	0.06760	-0.06230
0.01000	0.02250	-0.02250	0.53000	0.06720	-0.06120
0.02000	0.02990	-0.02990	0.54000	0.06670	-0.06000
0.03000	0.03500	-0.03500	0.55000	0.06620	-0.05870
0.04000	0.03890	-0.03890	0.56000	0.06560	-0.05730
0.05000	0.04210	-0.04210	0.57000	0.06500	-0.05580
0.06000	0.04480	-0.04480	0.58000	0.06430	-0.05430
0.07000	0.04710	-0.04720	0.59000	0.06360	-0.05270
0.08000	0.04910	-0.04930	0.60000	0.06280	-0.05100
0.09000	0.05100	-0.05120	0.61000	0.06200	-0.04920
0.10000	0.05270	-0.05290	0.62000	0.06110	-0.04740
0.11000	0.05420	-0.05450	0.63000	0.06020	-0.04550
0.12000	0.05560	-0.05600	0.64000	0.05930	-0.04350
0.13000	0.05690	-0.05730	0.65000	0.05830	-0.04150
0.14000	0.05810	-0.05850	0.66000	0.05730	-0.03940
0.15000	0.05920	-0.05970	0.67000	0.05620	-0.03730
0.16000	0.06020	-0.06080	0.68000	0.05510	-0.03520
0.17000	0.06120	-0.06180	0.69000	0.05400	-0.03300
0.18000	0.06210	-0.06270	0.70000	0.05280	-0.03080
0.19000	0.06290	-0.06360	0.71000	0.05160	-0.02860
0.20000	0.06370	-0.06440	0.72000	0.05030	-0.02640
0.21000	0.06440	-0.06510	0.73000	0.04900	-0.02420
0.22000	0.06510	-0.06580	0.74000	0.04770	-0.02200
0.23000	0.06570	-0.06640	0.75000	0.04640	-0.01980
0.24000	0.06630	-0.06700	0.76000	0.04500	-0.01770
0.25000	0.06680	-0.06750	0.77000	0.04360	-0.01560
0.26000	0.06730	-0.06800	0.78000	0.04220	-0.01360
0.27000	0.06770	-0.06840	0.79000	0.04070	-0.01160
0.28000	0.06810	-0.06880	0.80000	0.03920	-0.00970
0.29000	0.06850	-0.06910	0.81000	0.03770	-0.00780
0.30000	0.06880	-0.06940	0.82000	0.03620	-0.00600
0.31000	0.06910	-0.06960	0.83000	0.03460	-0.00430
0.32000	0.06930	-0.06980	0.84000	0.03300	-0.00270
0.33000	0.06950	-0.06990	0.85000	0.03140	-0.00120
0.34000	0.06970	-0.07000	0.86000	0.02980	0.00010
0.35000	0.06990	-0.07000	0.87000	0.02810	0.00130
0.36000	0.07000	-0.07000	0.88000	0.02640	0.00230
0.37000	0.07010	-0.06990	0.89000	0.02470	0.00320
0.38000	0.07020	-0.06980	0.90000	0.02290	0.00390
0.39000	0.07020	-0.06970	0.91000	0.02110	0.00440
0.40000	0.07020	-0.06950	0.92000	0.01930	0.00460
0.41000	0.07020	-0.06930	0.93000	0.01750	0.00460
0.42000	0.07010	-0.06900	0.94000	0.01560	0.00430
0.43000	0.07000	-0.06860	0.95000	0.01370	0.00380
0.44000	0.06990	-0.06820	0.96000	0.01170	0.00310
0.45000	0.06970	-0.06770	0.97000	0.00970	0.00210
0.46000	0.06950	-0.06720	0.98000	0.00760	0.00080
0.47000	0.06930	-0.06660	0.99000	0.00550	-0.00080
0.48000	0.06900	-0.06590	1.00000	0.00330	-0.00270
0.49000	0.06870	-0.06510			

Table 5. Concluded
(b) B64A010 Airfoil Design Coordinates

x/c	z/c	x/c	z/c
.000000	.000000	.490000	.047344
.001000	.003622	.500000	.046851
.002000	.005124	.510000	.046323
.005000	.008035	.520000	.045761
.010000	.011193	.530000	.045166
.020000	.015365	.540000	.044541
.030000	.018465	.550000	.043886
.040000	.021129	.560000	.043203
.050000	.023452	.570000	.042494
.060000	.025502	.580000	.041758
.070000	.027340	.590000	.040997
.080000	.029021	.600000	.040212
.090000	.030583	.610000	.039404
.100000	.032043	.620000	.038574
.110000	.033417	.630000	.037722
.120000	.034713	.640000	.036850
.130000	.035935	.650000	.035959
.140000	.037087	.660000	.035050
.150000	.038173	.670000	.034124
.160000	.039198	.680000	.033183
.170000	.040165	.690000	.032229
.180000	.041076	.700000	.031263
.190000	.041934	.710000	.030287
.200000	.042741	.720000	.029302
.210000	.043500	.730000	.028310
.220000	.044212	.740000	.027313
.230000	.044880	.750000	.026312
.240000	.045504	.760000	.025308
.250000	.046085	.770000	.024304
.260000	.046627	.780000	.023298
.270000	.047127	.790000	.022292
.280000	.047588	.800000	.021286
.290000	.048010	.810000	.020281
.300000	.048391	.820000	.019277
.310000	.048734	.830000	.018274
.320000	.049036	.840000	.017271
.330000	.049298	.850000	.016269
.340000	.049517	.860000	.015267
.350000	.049694	.870000	.014266
.360000	.049826	.880000	.013264
.370000	.049914	.890000	.012263
.380000	.049956	.900000	.011262
.390000	.049951	.910000	.010261
.400000	.049898	.920000	.009260
.410000	.049798	.930000	.008259
.420000	.049649	.940000	.007258
.430000	.049453	.950000	.006257
.440000	.049211	.960000	.005255
.450000	.048923	.970000	.004254
.460000	.048591	.980000	.003253
.470000	.048216	.990000	.002251
.480000	.047800	1.000000	.001250

Table 6. Experimental Flutter Results for BSCW in R-12 with Fixed Transition Using #35 Grit

Test Case No.	Point No.	α_m deg	M	q lb/ft^2	a ft/sec	V ft/sec	ρ slugs/ft3	R_n x10-6	μ	V_I	f_f Hz	f_f / f_θ	k	$\lvert h \rvert$ in.	ϕ_h deg	$\lvert \theta \rvert$ deg
Classical Flutter in R-12 with Fixed Transition, #35 Grit																
7ESWFC1	492	-0.3	.435	157.4	506.5	220.4	.006482	7.03	253	.630	4.53	.863	.0861	.28	-172.5	1.20
7ESWFC2	488	-0.2	.579	162.4	508.0	294.2	.003752	5.44	437	.640	4.45	.848	.0633	.29	-174.0	1.03
7ESWFC3	485	-0.2	.689	169.3	507.9	350.0	.002764	4.77	593	.654	4.35	.829	.0521	.49	-174.7	1.42
7ESWFC4	480	-0.1	.742	168.8	506.6	375.7	.002392	4.45	685	.653	4.30	.819	.0480	.38	-175.2	1.01
7ESWFC5	465	0.0	.797	172.6	510.9	407.4	.002080	4.15	788	.660	4.14	.789	.0425	.70	-173.9	1.40
7ESWFC6	472	0.0	.803	170.7	510.0	409.3	.002038	4.09	805	.656	4.15	.790	.0424	.37	-174.8	0.73
7ESWFC7	457	1.3	.799	166.9	509.7	407.3	.002012	4.03	815	.649	4.14	.789	.0425	.35	-174.5	0.69
7ESWFC8	470	0.0	.817	178.8	511.5	417.7	.002050	4.19	800	.672	4.05	.771	.0407	.62	-173.4	1.01
7ESWFC9	466	0.0	.823	177.5	510.0	419.7	.002016	4.16	813	.669	4.13	.787	.0412	.24	-174.5	0.42
Classical Flutter in Air with Fixed Transition, #35 Grit																
7ESWFC10	341	0.0	.335	155.5	1139.	381.9	.002132	2.81	769	.626	4.55	.867	.0499	.25	-175.8	1.09
7ESWFC11	333	-0.2	.503	160.1	1132.	569.5	.000987	1.96	1660	.636	4.47	.851	.0329	.37	-176.7	1.37
7ESWFC12	329	-0.4	.619	168.2	1125.	696.9	.000693	1.71	2366	.652	4.39	.836	.0264	.57	-177.0	1.74
7ESWFC13	321	-0.1	.679	171.1	1123.	763.0	.000588	1.59	2789	.657	4.36	.830	.0239	.37	-177.0	1.08
7ESWFC14	319	-0.1	.738	177.6	1118.	825.0	.000522	1.53	3142	.669	4.27	.813	.0217	.51	-176.8	1.26
7ESWFC15	315	-0.1	.762	173.8	1116.	850.8	.000480	1.45	3413	.662	4.23	.806	.0208	.31	-177.5	0.73
Classical Flutter in Air with Free Transition																
7ESWFC16	72	-0.1	.319	140.3	1142.	364.4	.002113	2.65	776	.595	4.60	.876	.0529	.21	-175.4	1.05
7ESWFC17	57	0.0	.509	152.2	1130.	574.7	.000922	1.85	1779	.620	4.47	.851	.0326	.21	-176.3	0.86
7ESWFC18	141	-0.2	.730	172.4	1120.	817.6	.000516	1.49	3569	.622	4.23	.806	.0217	.59	-176.6	1.47
7ESWFC19	133	0.0	.769	168.9	1115.	857.6	.000459	1.41	3178	.692	4.14	.789	.0202	.44	-176.3	0.94
7ESWFC20	74	1.0	.326	145.1	1140.	372.0	.002097	2.69	782	.605	4.55	.867	.0513	.26	-175.1	1.23
7ESWFC21	60	1.0	.513	156.4	1130.	580.0	.000930	1.89	1763	.628	4.43	.844	.0320	.28	-175.8	1.12
7ESWFC22	139	1.2	.725	170.2	1121.	812.4	.000516	1.48	3180	.655	4.19	.798	.0216	.71	-175.7	1.94
7ESWFC23	137	1.2	.766	169.3	1118.	856.8	.000461	1.40	3556	.653	4.09	.779	.0200	.82	-175.4	1.92
Stall Flutter in R-12 with Fixed Transition, #35 Grit																
7ESWFS1	427	5.4	.801	124.7	507.2	406.1	.001512	3.04	1084	.561	4.87	.928	.0503	.08	-162.9	0.69
7ESWFS2	403	5.3	.799	105.5	505.6	404.0	.001293	2.60	1268	.516	4.89	.931	.0507	.05	-168.0	0.43
7ESWFS3	395	5.5	.798	93.6	503.6	402.0	.001158	2.33	1416	.486	4.97	.947	.0518	.08	-167.5	0.90

Table 7. Experimental Classical Flutter Results for B0012 in Air with Fixed Transition Using #35 Grit

Test Case No.	Point No.	α_m deg	M	q lb/ft^2	a ft/sec	V ft/sec	ρ slugs/ft3	R_n x10-6	μ	V_I	f_f Hz	f_f / f_θ	k	$\|h\|$ in.	ϕ_h deg	$\|\theta\|$ deg
7E12FC1	94	.07	0.30	131.7	1127.2	338.2	0.002303	2.736	696	0.538	4.56	0.877	0.0565	0.27	-175.5	1.63
7E12FC2	84	.07	0.39	137.2	1132.3	441.6	0.001407	2.168	1139	0.549	4.51	0.867	0.0428	0.35	-176.2	1.93
7E12FC3	79	.06	0.45	137.7	1129.5	508.3	0.001066	1.897	1503	0.550	4.47	0.860	0.0368	0.23	-176.7	1.22
7E12FC4	74	.06	0.51	141.9	1121.6	572.0	0.000867	1.755	1848	0.558	4.43	0.852	0.0324	0.32	-177.0	1.49
7E12FC5	67	.05	0.61	144.6	1108.8	676.4	0.000632	1.540	2535	0.564	4.34	0.835	0.0269	0.25	-177.3	1.01
7E12FC6	62	.05	0.67	146.5	1096.0	734.3	0.000543	1.463	2951	0.567	4.28	0.823	0.0244	0.34	-177.1	1.22
7E12FC7	48	.04	0.71	146.9	1106.6	785.7	0.000476	1.316	3366	0.568	4.25	0.817	0.0227	0.26	-177.2	0.89
7E12FC8	42	.07	0.77	144.2	1097.1	844.8	0.000404	1.251	3966	0.563	4.13	0.794	0.0205	0.36	-177.1	0.99
7E12FC9	129	.06	0.80	147.2	1109.1	887.3	0.000374	1.196	4284	0.567	4.09	0.787	0.0193	0.25	-177.4	0.60
7E12FC10	134	.07	0.82	159.9	1111.6	911.5	0.000385	1.259	4162	0.593	4.07	0.783	0.0187	0.21	-176.5	0.42

Table 8. Experimental Flutter Results for B64A010 in R-12 with Fixed Transition Using #35 Grit

Test Case No.	Point No.	α_m deg	M	q lb/ft^2	a ft/sec	V ft/sec	ρ slugs/ft3	R_n x10-6	μ	V_I	f_f Hz	f_f / f_θ	k	|h| in.	ϕ_h deg	|θ| deg
							Classical	Flutter								
7E64FC1	256	0.48	0.543	148.7	500.9	272.0	0.004020	5.57	405	0.619	4.462	0.856	0.069	0.3	-174.3	1.26
7E64FC2	253	0.48	0.588	149.4	500.9	294.5	0.003446	5.18	472	0.621	4.440	0.852	0.063	0.3	-173.9	1.23
7E64FC3	250	0.48	0.630	150.8	500.6	315.4	0.003033	4.89	537	0.624	4.407	0.846	0.059	0.2	-174.0	0.80
7E64FC4	246	0.48	0.674	152.8	500.6	337.4	0.002685	4.64	606	0.628	4.370	0.839	0.054	0.3	-174.3	0.98
7E64FC5	242	0.48	0.691	152.3	499.7	345.3	0.002554	4.54	637	0.627	4.365	0.838	0.053	0.2	-174.5	0.90
7E64FC6	326	0.43	0.728	158.0	503.4	366.5	0.002352	4.37	692	0.638	4.300	0.825	0.049	0.5	-174.4	1.49
7E64FC7	236	0.48	0.731	158.8	502.1	367.0	0.002359	4.42	690	0.640	4.286	0.823	0.049	0.4	-174.3	1.32
7E64FC8	230	0.48	0.742	156.1	501.6	372.2	0.002255	4.29	722	0.635	4.290	0.823	0.048	0.3	-174.7	0.93
7E64FC9	226	0.48	0.750	153.7	500.5	375.4	0.002182	4.20	746	0.630	4.296	0.825	0.048	0.2	-174.3	0.64
7E64FC10	222	0.47	0.781	159.2	500.8	391.1	0.002082	4.18	782	0.641	4.218	0.810	0.045	0.4	-174.3	1.07
7E64FC11	322	0.43	0.781	159.8	503.3	393.1	0.002069	4.13	787	0.642	4.228	0.812	0.045	0.6	-174.5	1.58
7E64FC12	218	0.40	0.799	159.8	501.3	400.5	0.001993	4.09	817	0.642	4.192	0.805	0.044	0.3	-174.3	0.77
7E64FC13	317	0.42	0.801	159.2	503.7	403.5	0.001956	4.01	832	0.641	4.200	0.806	0.044	0.3	-174.8	0.82
7E64FC14	215	0.46	0.816	159.6	500.5	408.4	0.001914	4.02	851	0.642	4.162	0.799	0.043	0.3	-174.3	0.72
7E64FC15	373	0.45	0.856	174.5	504.3	431.7	0.001873	4.10	869	0.671	4.070	0.781	0.040	0.3	-173.7	0.59
7E64FC16	311	0.42	0.861	176.8	502.8	432.9	0.001887	4.16	863	0.675	4.090	0.785	0.040	0.2	-172.2	0.42
							Plunge	Flutter								
7E64FP1	299	0.00	0.937	178.7	502.5	470.8	0.001613	3.88	1009	0.679	3.592	0.689	0.032	0.4	-174.3	0.91
7E64FP2	290	-0.10	0.947	172.5	502.7	476.1	0.001523	3.70	1069	0.667	3.600	0.691	0.032	0.4	-174.5	0.82

Table 9. Conditions for Static Test Cases for BSCW in R-12 with Fixed Transition, #35 Grit

Test Case No.	Point No.	M	α deg.	q psf	Wind-Off Zero Point No.
7ESWA1	608	0.582	-2.83	169.4	597
7ESWA2	609	0.583	-1.84	169.6	597
7ESWA3	610	0.583	-0.86	169.6	597
7ESWA4	611	0.581	0.10	168.8	597
7ESWA5	612	0.583	0.62	169.8	597
7ESWA6	613	0.583	1.15	169.7	597
7ESWA7	614	0.582	2.11	169.3	597
7ESWA8	615	0.583	3.14	169.7	597
7ESWA9	616	0.581	4.14	169.1	597
7ESWA10	617	0.582	4.83	169.3	597
7ESWA11	582	0.741	-2.88	170.2	581
7ESWA12	583	0.741	-1.90	170.3	581
7ESWA13	584	0.740	-0.91	170.1	581
7ESWA14	585	0.739	0.20	169.9	581
7ESWA15	586	0.739	0.65	170.0	581
7ESWA16	587	0.741	1.15	170.7	581
7ESWA17	588	0.740	2.24	170.3	581
7ESWA18	589	0.740	3.15	170.6	581
7ESWA19	590	0.741	4.16	170.9	581
7ESWA20	591	0.738	4.89	170.1	581
7ESWA21	550	0.803	-2.88	169.7	539
7ESWA22	551	0.803	-1.85	169.6	539
7ESWA23	552	0.801	-0.90	169.3	539
7ESWA24	553	0.802	0.10	169.7	539
7ESWA25	554	0.801	0.62	169.5	539
7ESWA26	555	0.802	1.10	169.8	539
7ESWA27	556	0.802	2.12	169.9	539
7ESWA28	557	0.803	3.12	170.1	539
7ESWA29	558	0.802	4.12	170.1	539
7ESWA30	559	0.802	4.83	170.2	539
7ESWA31	540	0.819	-2.90	169.7	539
7ESWA32	541	0.819	-1.87	169.8	539
7ESWA33	542	0.818	-0.89	169.7	539
7ESWA34	543	0.828	0.11	172.9	539
7ESWA35	544	0.820	0.63	170.5	539
7ESWA36	545	0.823	1.11	171.4	539
7ESWA37	546	0.823	2.11	171.6	539
7ESWA38	547	0.821	3.12	171.1	539
7ESWA39	548	0.820	4.10	170.9	539
7ESWA40	549	0.821	4.83	171.4	539
7ESWA41	513	0.882	-0.92	170.7	508
7ESWA42	510	0.877	0.00	170.8	508
7ESWA43	516	0.879	1.11	170.7	508
7ESWA44	518	0.875	3.09	170.1	508
7ESWA45	524	0.900	-0.97	178.7	508
7ESWA46	523	0.904	0.05	179.4	508
7ESWA47	522	0.900	1.07	178.3	508
7ESWA48	521	0.899	3.14	177.7	508

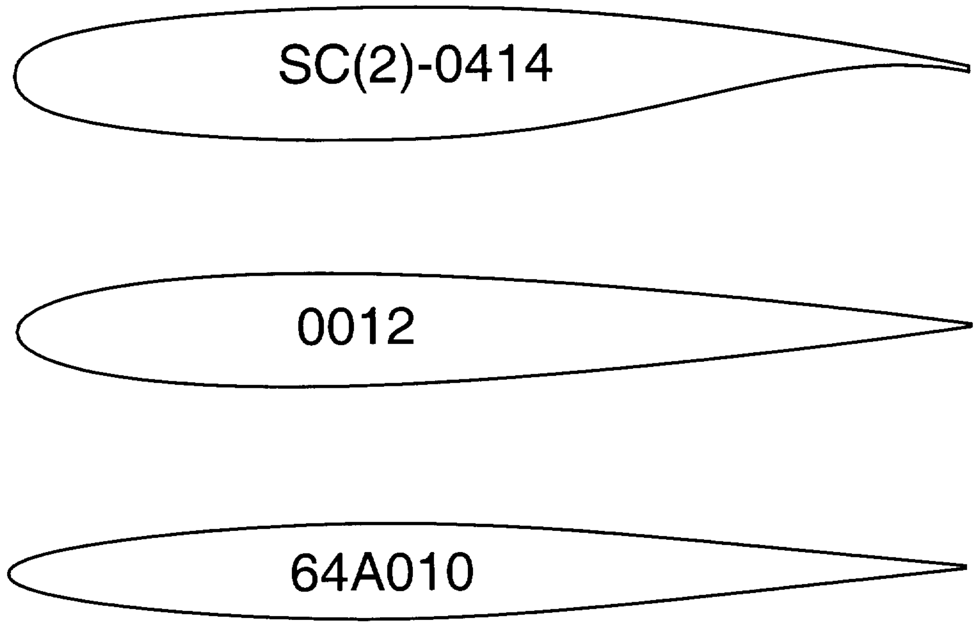

Figure 1. Airfoils used for the three Benchmark Models rectangular wings.

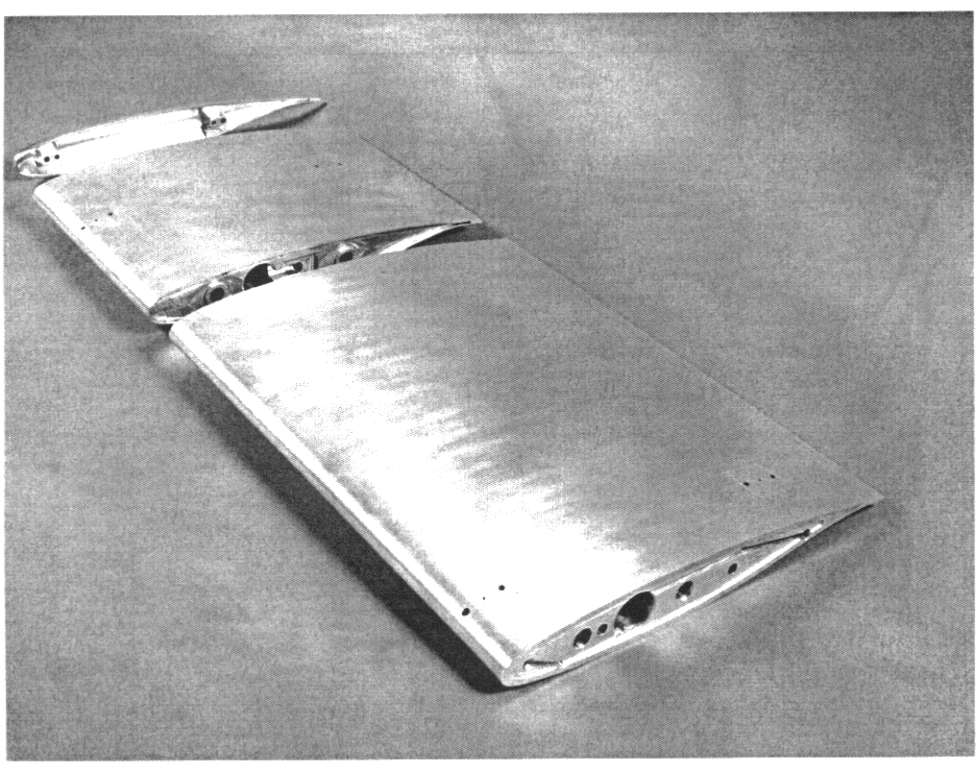

Figure 2. Photograph of Benchmark Supercritical Wing Model before assembly.

Figure 3. Photograph of Benchmark Supercritical Wing Model mounted in the wind tunnel.

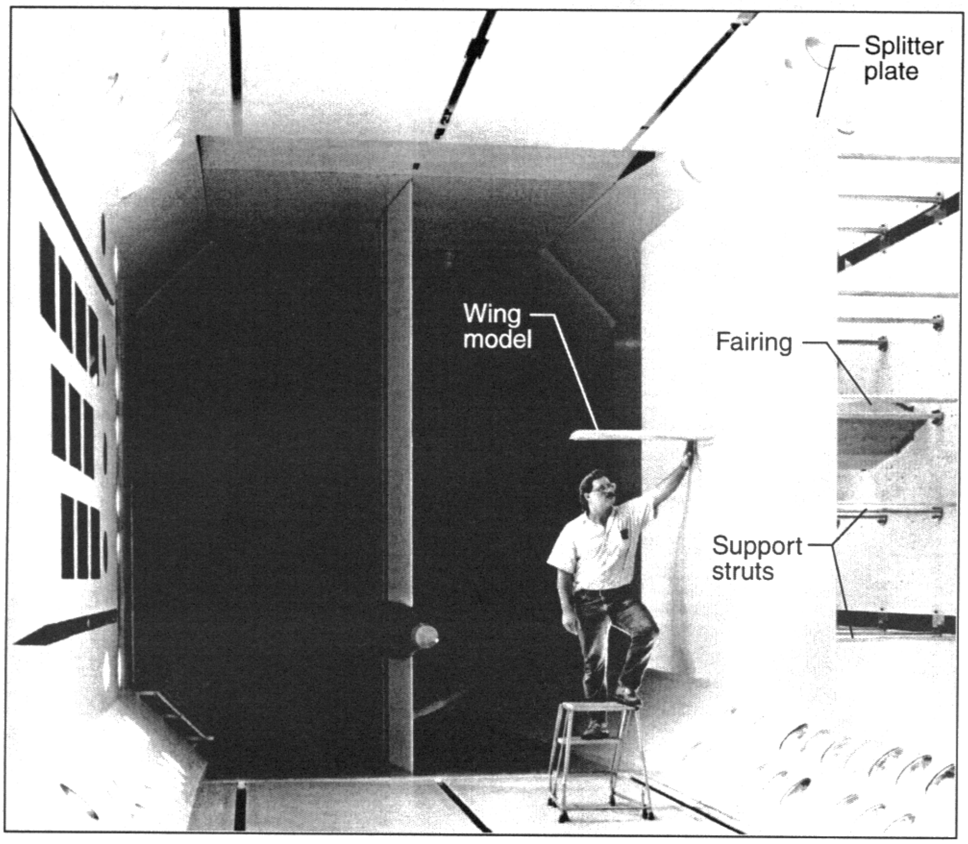

Figure 4. Photograph showing general arrangement of BSCW model and splitter plate.

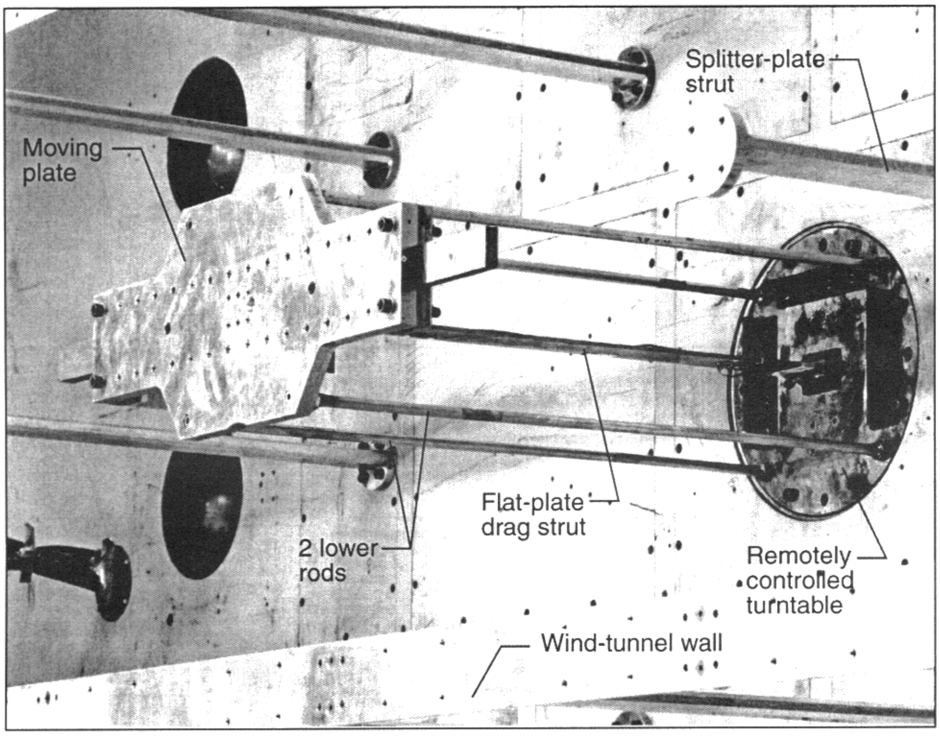

Figure 5. Photograph of Pitch and Plunge Apparatus mounted in the wind tunnel.

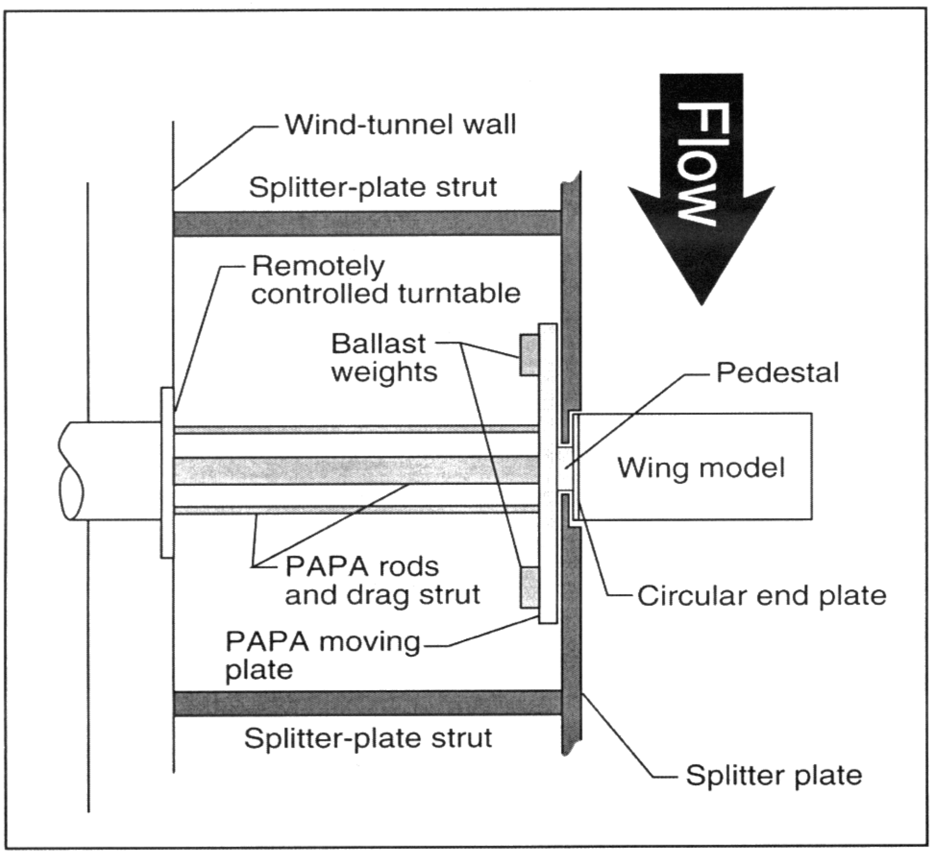

Figure 6. Sketch of model mounted on the Pitch and Plunge Apparatus.

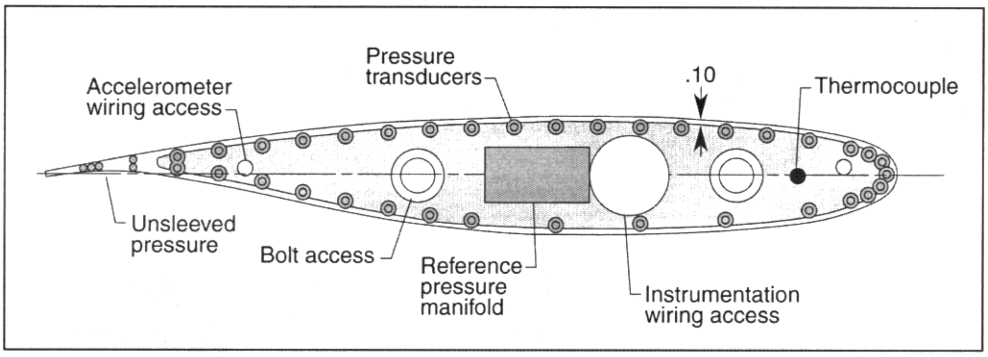

Figure 7. Pressure transducer locations on the Benchmark Supercritical Wing model.

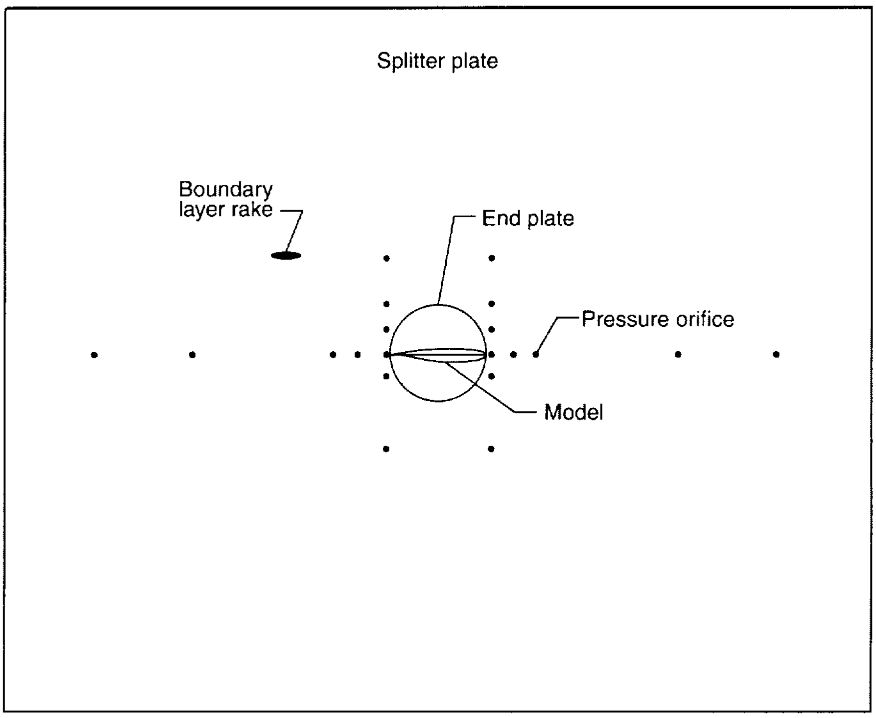

Figure 8. Sketch of pressure transducer locations on the splitter plate.

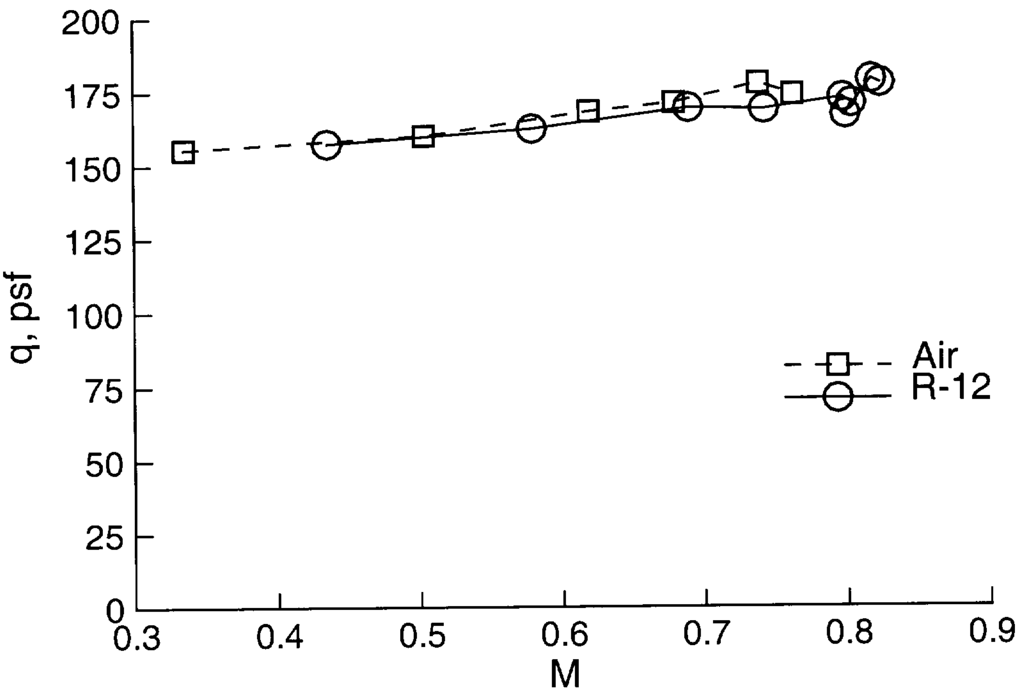

(a) Flutter dynamic pressure

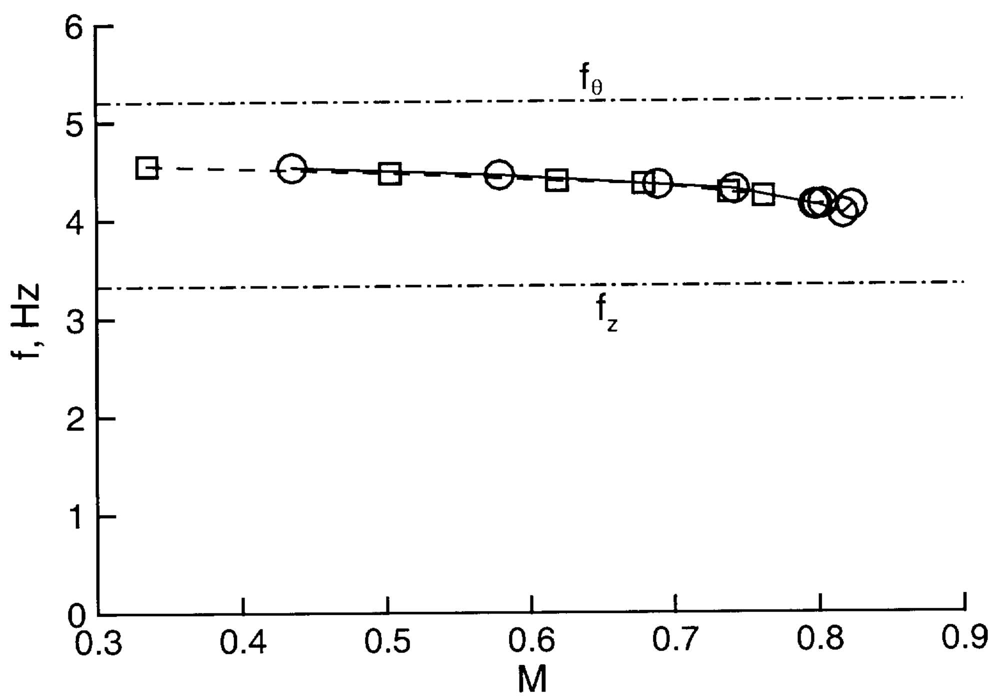

(b) Flutter frequency

Figure 9. Flutter boundaries for the BSCW in air and in R-12 (#35 grit), Test Cases 7ESWFC1-15.

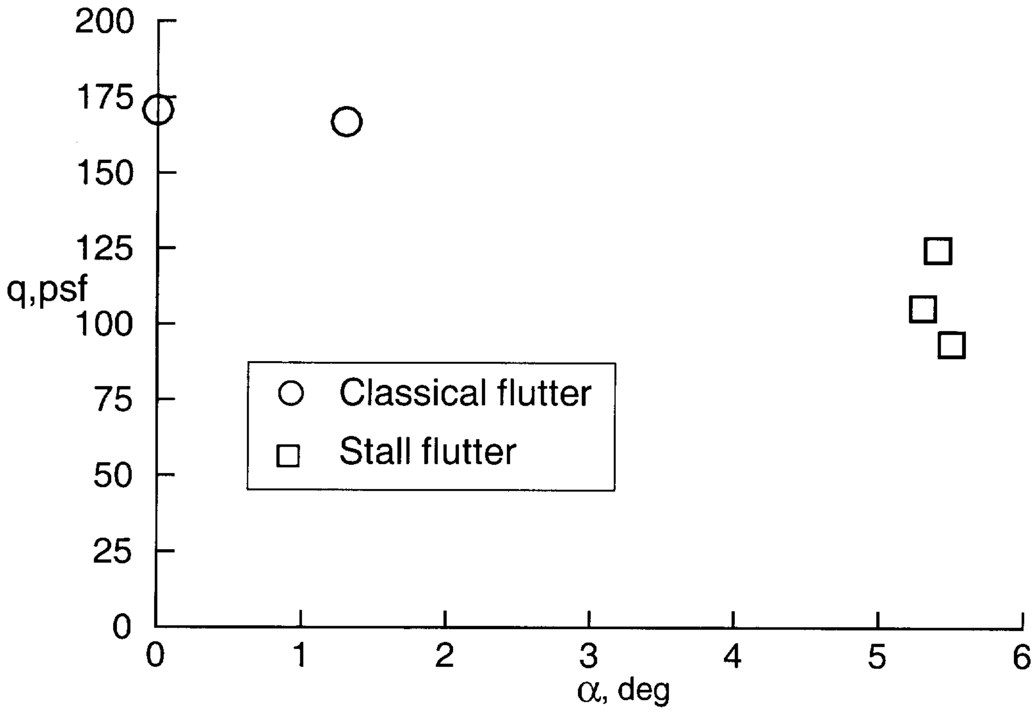

(a) Flutter dynamic pressure

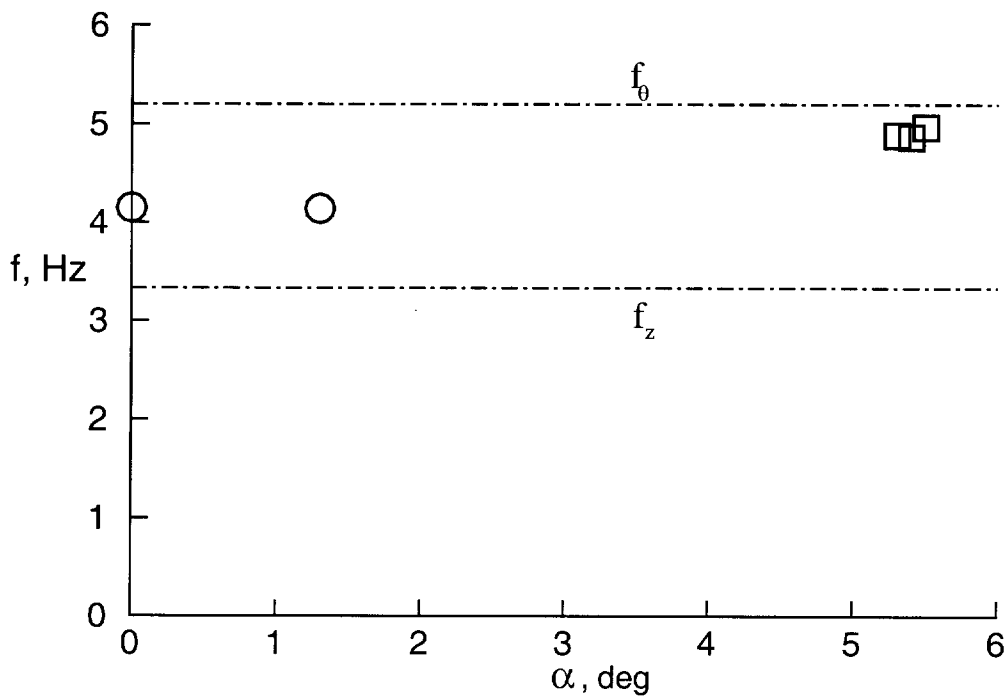

(b) Flutter frequency

Figure 10. Flutter at angle of attack for BSCW in R-12, (#35 grit), Test Cases 7ESWFS1-3, and 7ESWFC6-7, M =0.80.

Test Case	Point No	Wind-Off Zero Pt	TDT Test 470
7ESWA1	608	597	BmpBSCW/Static

Mach No	alphao,deg	q, psf	V,fps	Rn*10**-6	Prandl No	gamma
0.582	-2.83	169.4	297.0	5.72	0.748	1.136

Upper surface at ETA = 0.60

x/c	Cp Mean	Cp Min	Cp Max	CpStdDev	Chl No
0.000	0.000	0.000	0.000	0.000	1
0.010	0.546	0.499	0.585	0.013	2
0.025	0.107	0.059	0.144	0.012	3
0.050	-0.141	-0.184	-0.107	0.011	4
0.100	-0.181	-0.217	-0.150	0.009	5
0.150	-0.220	-0.252	-0.191	0.009	6
0.200	-0.249	-0.284	-0.218	0.009	7
0.250	-0.271	-0.306	-0.240	0.008	8
0.300	-0.285	-0.320	-0.252	0.009	9
0.350	-0.273	-0.304	-0.240	0.009	10
0.400	-0.289	-0.325	-0.254	0.009	11
0.450	-0.317	-0.354	-0.286	0.009	12
0.500	-0.325	-0.358	-0.293	0.009	13
0.550	-0.334	-0.366	-0.304	0.009	14
0.600	-0.302	-0.338	-0.269	0.009	15
0.650	-0.276	-0.308	-0.245	0.008	16
0.700	-0.236	-0.269	-0.204	0.009	17
0.750	-0.193	-0.227	-0.161	0.008	18
0.800	-0.166	-0.196	-0.140	0.007	19
0.850	-0.094	-0.120	-0.068	0.007	20
0.900	-0.047	-0.080	-0.021	0.007	21
0.950	0.025	-0.001	0.051	0.006	22
1.000	0.078	0.052	0.105	0.007	23

Lower surface at ETA = 0.60

x/c	Cp Mean	Cp Min	Cp Max	CpStdDev	Chl No
0.010	-0.497	-0.568	-0.442	0.019	24
0.025	-0.929	-0.995	-0.877	0.018	25
0.050	-0.915	-0.962	-0.872	0.015	26
0.100	-0.731	-0.771	-0.693	0.013	27
0.200	-0.583	-0.612	-0.555	0.009	28
0.300	-0.538	-0.571	-0.502	0.010	29
0.400	-0.496	-0.533	-0.454	0.011	30
0.500	-0.426	-0.466	-0.389	0.010	31
0.550	-0.358	-0.392	-0.325	0.009	32
0.600	-0.213	-0.247	-0.181	0.009	33
0.650	-0.087	-0.121	-0.059	0.007	34
0.700	0.048	0.019	0.074	0.008	35
0.750	0.154	0.127	0.181	0.007	36
0.800	0.232	0.210	0.257	0.006	37
0.850	0.274	0.249	0.299	0.008	38
0.900	0.314	0.289	0.337	0.007	39
0.950	0.330	0.301	0.362	0.008	40

Upper surface at ETA = 0.95

x/c	Cp Mean	Cp Min	Cp Max	CpStdDev	Chl No
0.000	1.052	1.028	1.080	0.011	69
		.			
		.			
1.000	0.000	0.000	0.000	0.000	91

Lower surface at ETA = 0.95

x/c	Cp Mean	Cp Min	Cp Max	CpStdDev	Chl No
0.010	-0.311	-0.362	-0.249	0.017	92
		.			
		.			
0.950	0.322	0.294	0.347	0.008	108

Figure 11. Example of static data file for BSCW.

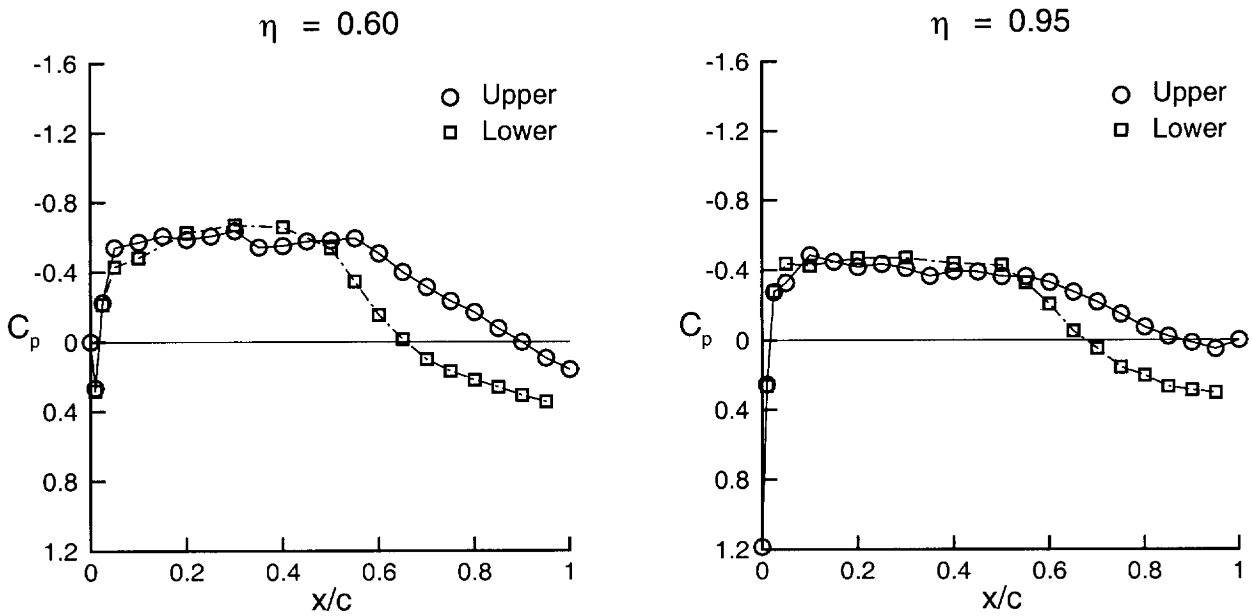

(a) Test Case 7ESWA24, α = 0.10.

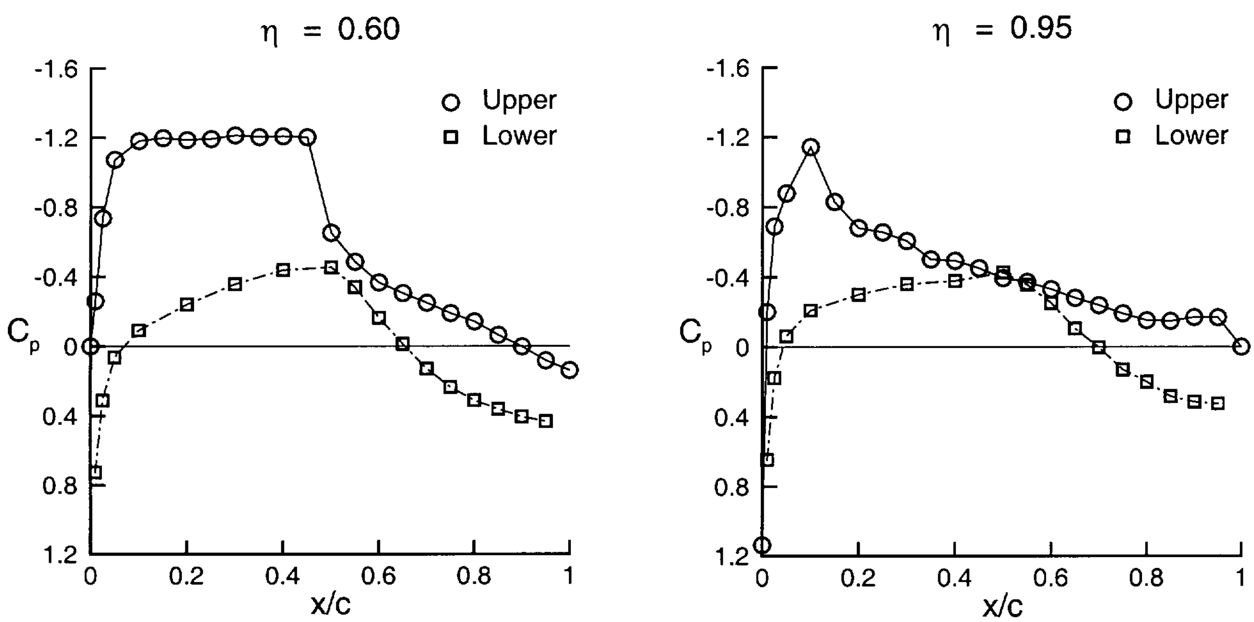

(b) Test Case 7ESWA30, α = 4.83.

Figure 12. Mean pressure coefficients for BSCW, Static Test Cases 7ESWA24and 7ESWA30, M = 0.802.

Test Case	Point No	Wind-Off Zero Pt	TDT Test 470
7ESWFC6	472	442	BmpBSCW/PAPA

Mach No	alphao,deg	q, psf	V,fps	rho,sl/ft3	Rn*10**-6	Prandl No	gamma
0.803	0.00	170.7	409.3	0.002038	4.09	0.755	1.134

FSI	ff/ft	kf	mass ratio	flt-frq,Hz	Real(h)	Imag(h)	theta,deg
0.656	0.790	0.0424	805.	4.150	-0.368	-0.034	0.73

Upper surface at ETA = 0.60

x/c	Cp Mean	Cp Min	Cp Max	CpStdDev	Real(Cp)	Imag(Cp)	Chl No
0.000	0.000	0.000	0.000	0.000	0.0000	0.0000	1
0.010	0.269	0.052	0.491	0.125	-0.1746	0.0061	2
0.025	-0.186	-0.410	0.063	0.136	-0.1889	0.0063	3
0.050	-0.412	-0.596	-0.194	0.109	-0.1516	0.0025	4
0.100	-0.665	-0.959	-0.305	0.240	-0.3233	0.0119	5
0.150	-0.613	-0.962	-0.319	0.194	-0.2477	0.0056	6
0.200	-0.557	-0.914	-0.319	0.135	-0.1511	-0.0044	7
0.250	-0.548	-0.854	-0.321	0.078	-0.0790	-0.0144	8
0.300	-0.540	-0.738	-0.328	0.078	-0.0772	-0.0152	9
0.350	-0.516	-0.749	-0.307	0.062	-0.0539	-0.0113	10
0.400	-0.532	-0.719	-0.312	0.061	-0.0468	-0.0105	11
0.450	-0.521	-0.725	-0.326	0.064	-0.0419	-0.0103	12
0.500	-0.529	-0.734	-0.315	0.065	-0.0320	-0.0097	13
0.550	-0.521	-0.748	-0.343	0.064	-0.0243	-0.0080	14
0.600	-0.464	-0.740	-0.293	0.053	-0.0124	-0.0064	15
0.650	-0.383	-0.571	-0.257	0.037	-0.0063	-0.0046	16
0.700	-0.303	-0.436	-0.198	0.031	-0.0035	-0.0035	17
0.750	-0.228	-0.344	-0.128	0.025	-0.0020	-0.0027	18
0.800	-0.142	-0.236	-0.063	0.019	-0.0011	-0.0019	19
0.850	-0.076	-0.149	-0.017	0.017	-0.0006	-0.0010	20
0.900	0.017	-0.044	0.074	0.015	-0.0011	-0.0004	21
0.950	0.111	0.065	0.167	0.013	-0.0039	-0.0004	22
1.000	0.154	0.111	0.209	0.012	-0.0086	-0.0008	23

Lower surface at ETA = 0.60

x/c	Cp Mean	Cp Min	Cp Max	CpStdDev	Real(Cp)	Imag(Cp)	Chl No
0.010	0.270	0.061	0.486	0.121	0.1683	-0.0017	24
0.025	-0.214	-0.434	0.026	0.133	0.1851	-0.0063	25
0.050	-0.311	-0.494	-0.132	0.098	0.1357	-0.0015	26
0.100	-0.671	-0.982	-0.280	0.251	0.3394	-0.0051	27
0.200	-0.638	-0.962	-0.425	0.140	0.1718	-0.0145	28
0.300	-0.624	-0.896	-0.421	0.072	0.0676	0.0163	29
0.400	-0.613	-0.857	-0.352	0.082	0.0452	0.0129	30
0.500	-0.508	-0.875	-0.299	0.075	-0.0059	0.0048	31
0.550	-0.314	-0.461	-0.195	0.035	-0.0046	0.0043	32
0.600	-0.178	-0.265	-0.084	0.023	-0.0108	0.0038	33
0.650	-0.008	-0.061	0.065	0.015	-0.0037	0.0046	34
0.700	0.098	0.040	0.160	0.015	0.0103	0.0058	35
0.750	0.164	0.092	0.226	0.021	0.0221	0.0067	36
0.800	0.206	0.140	0.274	0.025	0.0290	0.0068	37
0.850	0.251	0.173	0.322	0.028	0.0337	0.0072	38
0.900	0.284	0.203	0.351	0.029	0.0359	0.0058	39
0.950	0.329	0.245	0.400	0.029	0.0354	0.0055	40

Upper surface at ETA = 0.95

x/c	Cp Mean	Cp Min	Cp Max	CpStdDev	Real(Cp)	Imag(Cp)	Chl No
0.000	1.165	1.137	1.194	0.007	0.0026	0.0006	69
0.010	0.252	0.062	0.458	0.105	-0.1468	0.0005	70
0.900	0.004	-0.062	0.066	0.018	-0.0145	-0.0007	89
			⋮				
0.950	0.042	-0.040	0.108	0.024	-0.0256	-0.0009	90
1.000	0.000	0.000	0.000	0.000	0.0000	0.0000	91

Lower surface at ETA = 0.95

x/c	Cp Mean	Cp Min	Cp Max	CpStdDev	Real(Cp)	Imag(Cp)	Chl No
0.010	0.230	0.043	0.416	0.103	0.1436	-0.0016	92
0.025	-0.295	-0.498	-0.089	0.117	0.1628	-0.0035	93
			⋮				
0.900	0.286	0.241	0.333	0.012	0.0037	0.0019	107
0.950	0.311	0.259	0.378	0.015	-0.0070	0.0015	108

Figure 13. Example of flutter data file for BSCW.

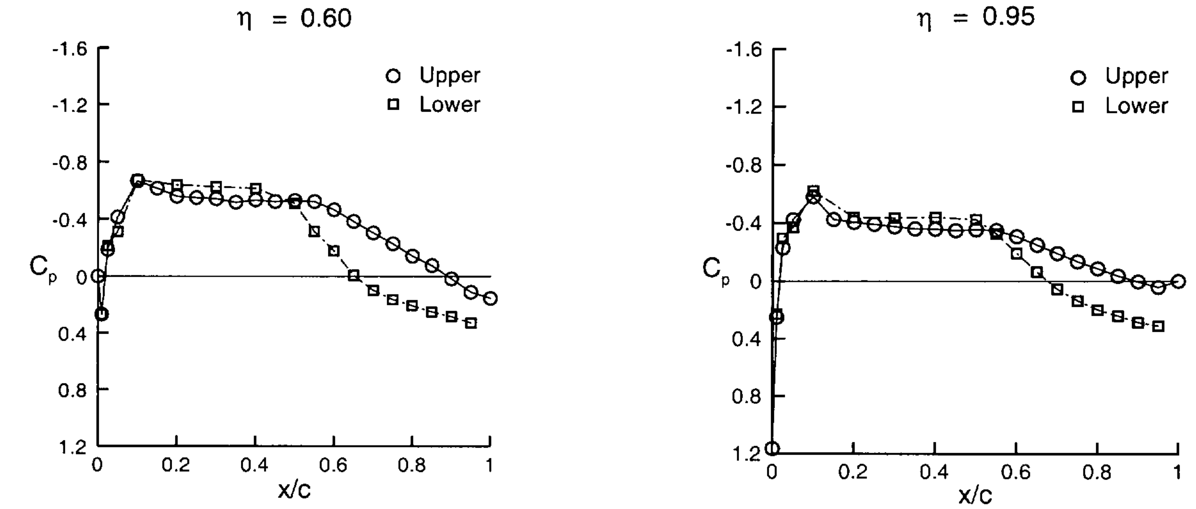

(a) Mean pressure coefficient during flutter

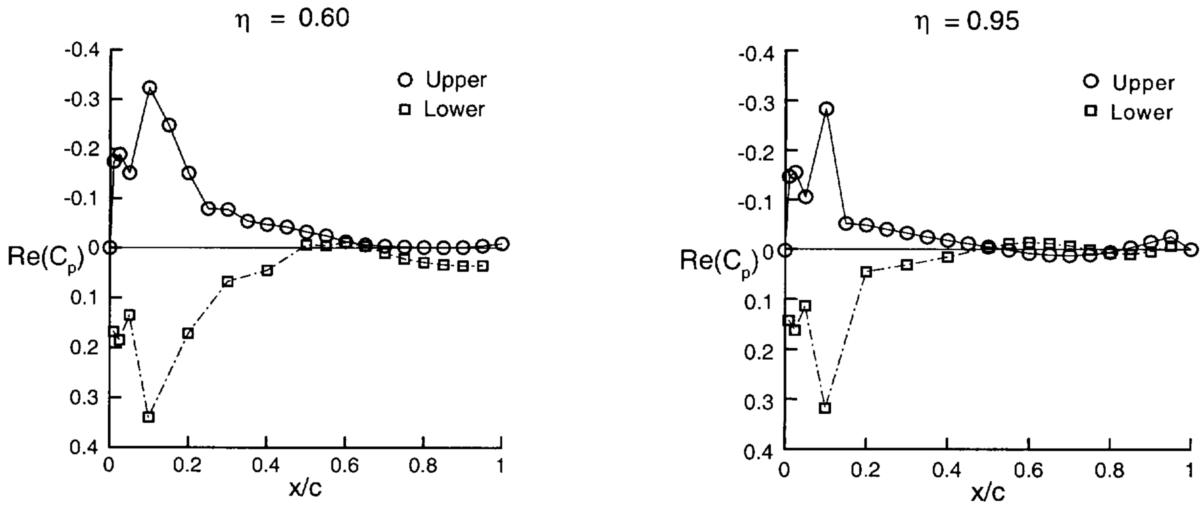

(b) Real part of pressure coefficient during flutter

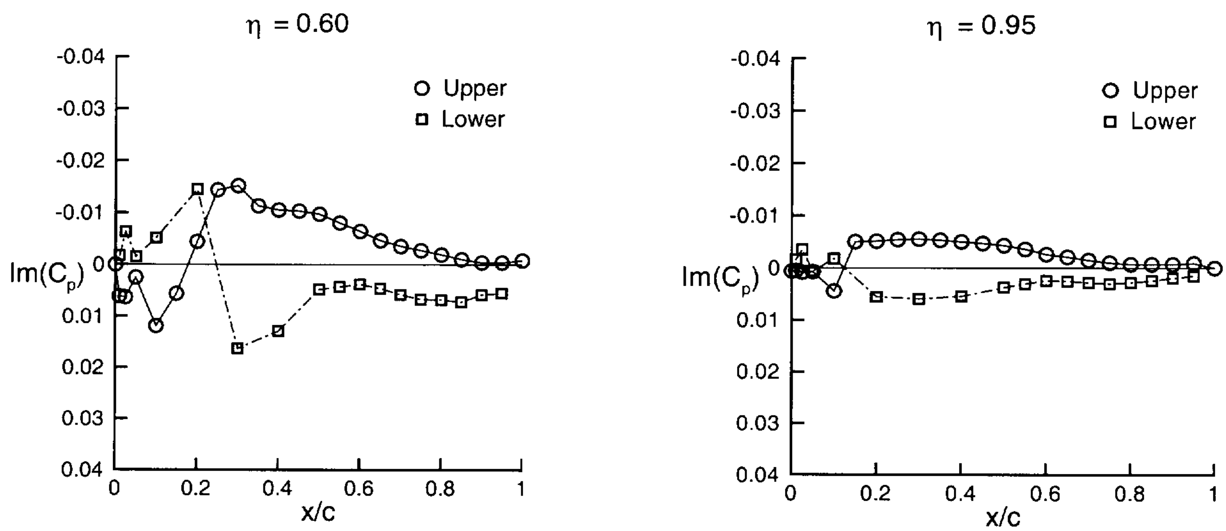

(c) Imaginary part of pressure coefficient during flutter

Figure 14. Measured pressures for BSCW during flutter, Test Case 7ESWFC6, M= 0.803, $\alpha = 0$.

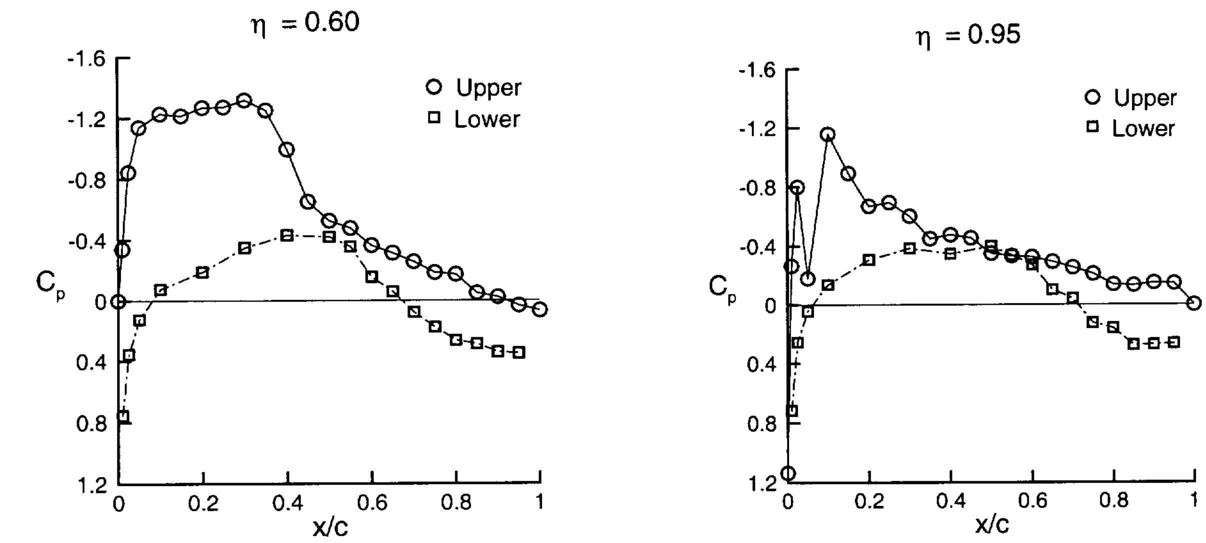

(a) Mean pressure coefficient during flutter

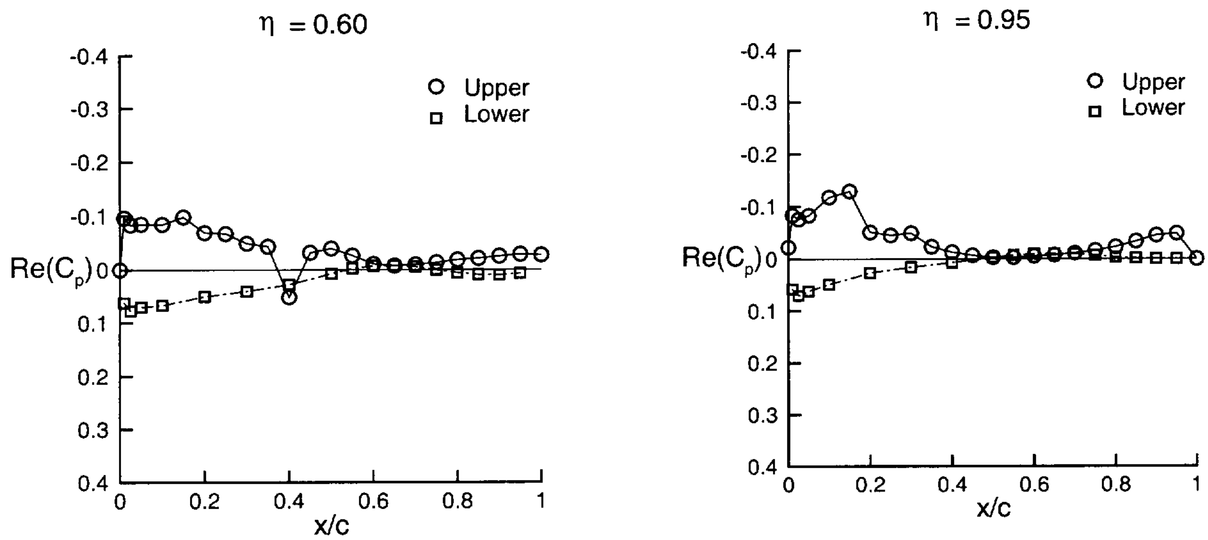

(b) Real part of pressure coefficient during flutter

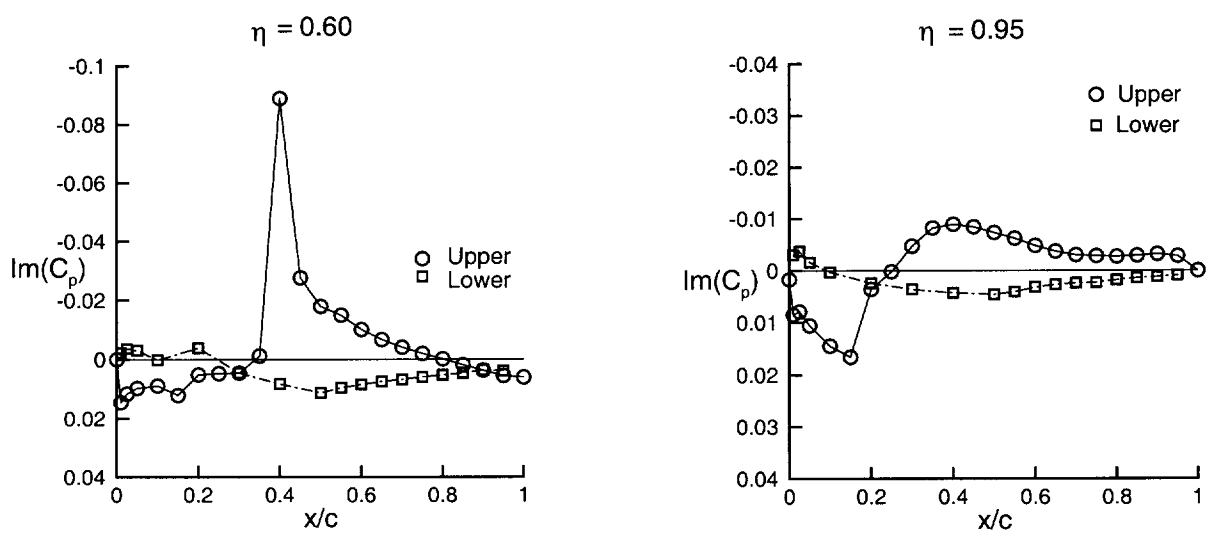

(c) Imaginary part of pressure coefficient during flutter

Figure 15. Measured pressures for BSCW during flutter, Test Case 7ESWFS3, M= 0.798, $\alpha = 5.5$ degrees.

8E. TEST CASES FOR THE BENCHMARK ACTIVE CONTROLS MODEL: SPOILER AND CONTROL SURFACE OSCILLATIONS AND FLUTTER

Submitted by

Robert M. Bennett
Senior Aerospace Engineer
r.m.bennett@larc.nasa.gov

Robert C. Scott
Aerospace Engineer
r.c.scott @larc.nasa.gov

Carol D. Wieseman
Aerospace Engineer
c.d.wieseman @larc.nasa.gov

Aeroelasticity Branch, Structures and Materials
Mail Stop 340
NASA Langley Research Center
Hampton, VA 23681-2199 USA

INTRODUCTION

As a portion of the Benchmark Models Program at NASA Langley (Ref 1-2), a simple generic model was developed for active controls research and was called BACT for Benchmark Active Controls Technology model. This model was based on the previously-tested Benchmark Models rectangular wing with the NACA 0012 airfoil section that was mounted on the Pitch and Plunge Apparatus (PAPA) for flutter testing (Ref 1, 3-5). The BACT model had an upper surface spoiler, a lower surface spoiler, and a trailing edge control surface for use in flutter suppression and dynamic response excitation. Previous experience with flutter suppression (Ref 6-7) indicated a need for measured control surface aerodynamics for accurate control law design. Three different types of flutter instability boundaries had also been determined for the NACA 0012/PAPA model, a classical flutter boundary, a transonic stall flutter boundary at angle of attack, and a plunge instability near M = 0.9 (Ref 1, 3-5). Therefore an extensive set of steady and control surface oscillation data was generated spanning the range of the three types of instabilities (Ref 8). This information was subsequently used to design control laws to suppress each flutter instability.

There have been three tests of the BACT model. The objective of the first test, TDT Test 485, was to generate a data set of steady and unsteady control surface effectiveness data, and to determine the open loop dynamic characteristics of the control systems including the actuators. Unsteady pressures, loads, and transfer functions were measured. The other two tests, TDT Test 502 and TDT Test 518, were primarily oriented towards active controls research, but some data supplementary to the first test were obtained. Dynamic response of the flexible system to control surface excitation and open loop flutter characteristics were determined during Test 502. Loads were not measured during the last two tests. During these tests, a database of over 3000 data sets was obtained. A reasonably extensive subset of the data sets from the first two tests have been chosen for Test Cases for computational comparisons concentrating on static conditions and cases with harmonically oscillating control surfaces. Several flutter Test Cases from both tests have also been included.

Some aerodynamic comparisons with the BACT data have been made using computational fluid dynamics codes at the Navier-Stokes level in Ref 9-11 (and in the accompanying chapter 8C). Some mechanical and active control studies have been presented in Ref 12-17.

In this report several Test Cases are selected to illustrate trends for a variety of different conditions with emphasis on transonic flow effects. Cases for static angles of attack, static trailing-edge and upper-surface spoiler deflections are included for a range of conditions near those for the oscillation cases. Cases for trailing-edge control and upper-surface spoiler oscillations for a range of Mach numbers, angle of attack, and static control deflections are included. Cases for all three types of flutter instability are selected. In addition some cases are included for dynamic response measurements during forced oscillations of the controls on the flexible mount. An overview of the model and tests is given, and the standard formulary for these data is listed. Some sample data and sample results of calculations are presented. Only the static pressures and the first harmonic real and imaginary parts of the pressures are included in the data for the Test Cases, but digitized time histories have been archived. The data for the Test Cases are also available as separate electronic files.

LIST OF SYMBOLS AND DEFINITIONS

c	wing chord, ft (m)
C_p	pressure coefficient, $(p - p_\infty)/q_\infty$ steady; $(p - p_{mean})/q_\infty$ unsteady
f	frequency, Hz
k	reduced frequency, $\omega c/(2V_\infty)$
M	Mach number
MILEA	model inboard leading edge accelerometer
MITEA	model inboard trailing edge accelerometer
MOLEA	model outboard leading edge accelerometer
MOTEA	model outboard trailing edge accelerometer
p	pressure, psf (kPa)
p_∞	freestream static pressure, psf (kPa)

q_∞	dynamic pressure, psf (kPa)
R_N	Reynolds number based on average chord
T_o	total or stagnation temperature, °R (°C)
V_∞	freestream velocity, ft/sec (m/sec)
x/c	streamwise fraction of local chord
y	spanwise coordinate normal to freestream
α_o	mean angle of attack, degrees
δ_{te}	trailing edge control surface deflection, degrees or radians, Fig 1
δ_{us}	upper spoiler deflection, degrees or radians, Fig 1
η	fraction of span, y/s
γ	ratio of specific heats for test gas
ω	frequency, radians/second
	subscript 0 = steady value

MODEL AND TESTS

The BACT model was tested in the NASA Langley Transonic Dynamics Tunnel (TDT). The tunnel has a slotted test section 16-feet (4.064 m) square with cropped corners. At the time of these tests, it could be operated with air or a heavy gas, R-12, as a test medium at pressures from very low to near atmospheric values. Currently the TDT can be operated with air or R-134a as a test medium. An early description of this facility is given in Ref 18 and more recent descriptions of the facility are given in Ref 19 and 20. The early data system is described in Ref 21 and the recent data system given in Ref 22 and 23, but the data system used in the BACT tests was a version between these systems. Based on cone transition results (Ref 24-25), the turbulence level for this tunnel is in the average large transonic tunnel category. Some low speed turbulence measurements in air have also been presented in Ref 26.

An overall view of the BACT model is shown in Fig 1. It is a rectangular planform wing with a span of 32 inches (813 mm) plus a tip of revolution and a chord of 16 inches (406 mm). It has a trailing edge control surface of 25 per cent chord, hinged at 75 per cent chord, extending between 45 percent and 75 percent span. Upper and lower surface spoilers of 15 per cent chord length were located directly ahead of the trailing edge control surface, were of the same span, and were hinged at 60 per cent chord (Fig 1). The outward surface of the spoilers was flat, and a relatively thin trailing edges extended to near the round leading edge radius of the trailing edge control surface. When both spoilers were deployed, the cavity underneath was open permitting flow between upper and lower surfaces. The cavity contained plumbing for the actuators, wiring, and the shape is undocumented. The wing was machined from aluminum and was very smooth (the screws for the hatch covers shown in Fig 1 were filled in for the tests) and was tested with a transition strip at 5 per cent chord. The control surfaces were of composite construction and were driven with miniature hydraulic actuators located within the wing.

The BACT model is shown installed in the TDT in Fig 2. It was mounted on a large splitter plate set out approximately 40 inches (1.02 m) from tunnel sidewall. The model had an end plate fixed to its root that moved with the model within a recessed or undercut section of the splitter plate. A large fairing behind the splitter plate isolated the equipment between the splitter plate and the tunnel sidewall from the airstream. Some recent tests (Ref 27) of the splitter plate arrangement without a wing have shown some nonuniformity of the flow resulting from the flow around the splitter plate leading edge for Mach numbers above M = 0.80 and the data may be somewhat affected.

The BACT model was tested with two different mounting systems shown in Fig 3. For the first test, TDT Test 485, a circular strut extended from the turntable to the balance that was attached to the wing for force measurements (Fig 3a). The model could be pitched statically with the turntable, and the controls were powered for static and dynamic measurements. Most of the Test Cases for control surface oscillation were determined from this setup.

The model was also tested using the Pitch and Plunge Apparatus (PAPA, Ref 28-29) as illustrated in Fig 3b. The PAPA system permits rigid body pitch and plunge motion of the wing and flutter of the system by using four circular rods for flexibility. This system has sufficient strength to permit flutter testing at moderate angles of attack including some stall flutter cases. The rods are arranged such that the elastic axis is at the midchord and the model is balanced to place the total center of gravity on the midchord. The system thus gives primarily pitch and plunge uncoupled modes about the midchord of the model. The summary of the modal parameters is given in Table 1. The generalized masses given here are the effective mass and pitch inertia calculated from the frequency and stiffness values. Higher modes of this system have been explored with a different model and given in Ref 30. Some amplitude effects on frequency and damping were presented in Ref 30 also, but may not apply to BACT as a result of the addition of hydraulic lines spanning the PAPA system. Detailed wind-off free decay records have been archived. A remotely operable restraining or snubber system was installed and was used to suppress flutter when it grew near the amplitude limits and many flutter points were obtained. Some additional mass parameters relating to the control surfaces are available in Ref 12-14.

Both the model and the plate that constrains the model end of the PAPA system are large in mass. The resulting mass ratio at flutter is thus very large and consequently the reduced frequency at flutter is very low. The flutter crossings are relatively mild and unpublished calculations have indicated some sensitivity to torsional aerodynamic damping.

The model was instrumented for unsteady pressures at two chords and for dynamic motions. The list of transducers is given in Table 2 and shown in Fig 4. There were 58 unsteady pressure transducers located along the chord at 60 per cent span that is at the midspan of the control surfaces. There were 5 transducers on each spoiler and 7 on each of the upper and lower surfaces of the trailing edge control surface. This relatively dense spacing of the transducers was selected to define the pressures near the control surface hinge lines. In addition there were 17 unsteady pressure transducers located at 40 percent span over the aft portion of the chord that were placed to examine the carry-over loading near the side edge of the control surfaces. Space limitations prevented further pressure instrumentation at other chords. It might be noted that some flow visualization work on these low aspect ratio planforms indicated that wing surface separation tended to occur in an inboard aft cell. The row of pressure transducers at 60 per cent chord was in the outer portion of this cell.

Dynamic data from all channels were acquired simultaneously at a rate of 500 samples/second and stored in digital form on disk. For the static data, at least 10 seconds of data was acquired for averaging and for the oscillating control cases, 8-10 seconds of data was acquired and analyzed. For the flutter cases, data was selected for nearly constant amplitude, and ran from 3 to 30 seconds. The number of samples used is included in the data files for the dynamic cases. Each recorded data set was assigned an index called a Point No. which is given in the Tables. Although it was intended to use 200 Hz low pass filters in the data stream prior to digitizing the data to avoid aliasing, the filters were later thought to be set at 1000 Hz as a result of a data system problem. The data are thus considered aliased with a foldover frequency of 250 Hz. For the flutter data, which was in the 4 to 10 Hz range, in order for the 1st harmonic to be contaminated, there would have to be significant signals at 490-510 Hz or at 990-996 Hz. It is not considered likely that there are significant disturbances in these frequency ranges.

Detailed geometry measurements were performed for this wing along several sections as illustrated in Fig 5. The measured ordinates are not included in this report, but they are available as an electronic file on the CD.

TEST CASES

An extensive set of Test Cases is selected with emphasis on transonic flow effects. The Test Case Number begins with 8E for the chapter identifier. There are several configurations and variables such that a few cases per configuration results in a fairly large number, but one would normally not be concerned with all configurations. The aerodynamic Test Cases selected generally include four Mach numbers, M = 0.65, which is subsonic at low angles of attack, M = 0.77, which is transonic and near the bottom of the flutter "bucket", M = 0.82, which is strongly transonic, and M = 0.90 which is significantly beyond normal applications for this airfoil. Control surface deflection cases are generally selected for angles of attack of zero and four degrees. It might be noted that the transition strip (at five per cent chord) has an influence on the first transducer downstream of the strip. The effect varies with angle of attack and other test conditions.

The Test Cases for static angles of attack, static trailing-edge control surface deflections, and static upper-surface spoiler deflections are presented in Tables 3-5, respectively. The Test Case Number, the TDT Test Number, and Test Point Number are included. In the Test Case Number, S =static conditions, T = trailing edge control surface, and U = upper surface spoiler. The test conditions are listed are the actual values from the data files. A listing of a sample of one of the static data files illustrating the format is given in Fig 6. For each pressure transducer, the time-averaged mean, the minimum value, the maximum value, and the standard deviation of the pressure coefficient is listed (these are generally called the channel statistics). An example of an application of the BACT data is given in Fig 7. Static pressures are shown for $\alpha = 4^o$ and $\delta_{te} = -10^o$ at both M = 0.65 and M = 0.75, and are compared with linear theory aerodynamics (Ref 31-32 for example). Significant transonic effects are shown at the higher Mach number over the forward portion of the chord. One feature of the BACT data set is an irregular pressure distribution at the spoiler hinge line that can be seen in Fig 7b. This feature is possibly related to the geometric details of the hinge line area or to a small flow through the hinge line.

The Test Cases for harmonic oscillation of the trailing edge control surface are given in Table 6, and for upper spoiler oscillations in Table 7. In the Test Case Number, O = harmonic oscillation, and again T = trailing edge control surface, and U = upper surface spoiler. There was no provision for oscillating the main wing and no Test Cases are included for an open lower surface spoiler. There are also no Test Cases included for both spoilers open. A listing of a sample of a data file for an oscillating trailing edge control case illustrating the format is given in Fig 8. The mean, minimum, maximum, and standard deviation are listed with the real and imaginary parts of the first harmonic of the unsteady pressures. The unsteady pressures are referenced to pitch displacement. The minimum, maximum, and standard deviation include the unsteady components and thus their interpretation is not straightforward. Measured pressure data for Test Case 8EOT31, a trailing edge control surface oscillation case, are shown in Fig 9. Large unsteady pressure components are evident both near the hinge line at x/c of 0.75, and at the shock located near x/c of 0.30.

The flutter conditions are shown in Fig 10 in terms of dynamic pressure versus Mach number and for zero control surface deflections. The classical flutter boundary is shown as a conventional boundary with Mach number with a minimum near M = 0.77, and a subsequent rise. Both the classical flutter boundary and the plunge instability are at small angles of attack, but the stall flutter points are at angles of attack of the order of 5^o. Thus α is an independent variable for stall flutter that is not shown in Fig 10. The plunge instability occurs near zero lift, and it was found that opening the upper spoiler a small amount would suppress it. Earlier investigations could go around it by going to a higher angle of attack. Cases for all three types of flutter are selected and are listed in Table 8. In the Test Case Number, F = flutter, C =classical, S = stall, and P = plunge. The majority of the flutter points are included as Test Cases, except for nearly coincident points. For the flutter cases, calculations for flutter can be made and compared with measured boundaries. However, the model can also be forced to duplicate the measured combined pitch and plunge motions and the pressures compared directly. Only first harmonics are included in the data set, but time histories have been archived. In addition some cases are included for dynamic response measurements on the PAPA mount during forced oscillations of the control surfaces and are presented in Tables 9 and 10. In the Test Case Number, R = response, T = trailing edge control surface, and U = upper surface spoiler. Again calculations can be made including the structural response, or using the measured motion. The data file format for the flutter and response measurements is identical in format to the files for the oscillating controls (Fig 8) except that the line for mean aerodynamic coefficients from the balance is replaced by the measured values of pitch and plunge displacement.

The unsteady pressures presented and included in the files have not been normalized by amplitude of motion. Case to case comparisons of pressures may need to be normalized by the pitch, plunge, or control surface amplitude value listed with the Test Case. For instances of pressures transducers malfunction, the pressures are set to zero.

The files included on the CD-ROM are ascii files and a readme file is included. There are separate files for each type of static and dynamic data organized in the manner of Tables 3-10. The file for static angle of attack is bactsa, for static trailing edge control is bactste, and for upper spoiler deflection is bactsus. A Fortran subprogram to read the static files, bactrdst.f, is included. The static data include the averaged pressures along with the mean, maximum and standard deviation for each channel of data. The data for oscillating control surfaces are on files bactdteo, and bactduso and the subprogram to read these files is bactrdos.f. The flutter and dynamic response data are on files bactdflt, bactdfter, and bactdfusr and the subprogram to read the files is bactftrd.f. The data files consist of contiguous data points. The measured ordinates are included on file bactorde.

Note that all of the data included for BACT were conducted with the heavy gas, R-12, as the test medium. The ratio of specific heats, γ, is calculated to be 1.132 to 1.135 for the conditions of the test assuming 0.99 for the fraction of heavy gas in the heavy gas-air mixture. A value of 1.132 is suggested for use in computational comparisons. The corresponding value of Prandtl number is calculated to range from 0.77 to 0.78 for the test conditions. For some cases, the calculated values of γ and Prandl number are included in the data files.

FORMULARY

1 General Description of Model

1.1	Designation	Benchmark Active Controls Technology Model (BACT)
1.2	Type	Semispan wing
1.3	Derivation	Same airfoil and planform as Benchmark NACA 0012/PAPA model (see Introduction)
1.4	Additional remarks	Overall view given in Fig 1 and shown mounted in tunnel in Fig 2
1.5	References	Ref 8 describes tests and data

2 Model Geometry

2.1	Planform	Rectangular
2.2	Aspect ratio	2.0 for the panel (neglecting tip of rotation)
2.3	Leading edge sweep	Unswept
2.4	Trailing edge sweep	Unswept
2.5	Taper ratio	1.0
2.6	Twist	None
2.7	Wing centreline chord	16 inches (406.4 mm)
2.8	Semi-span of model	32 inches (812.8 mm) plus tip of rotation
2.9	Area of planform	512 sq. in. (0.3303 sq. m) neglecting tip
2.10	Location of reference sections and definition of profiles	NACA 0012 airfoil throughout except for flat spoiler surfaces. Measured ordinates available as an electronic file
2.11	Lofting procedure between reference sections	Constant design airfoil section
2.12	Form of wing-body junction	No fairing and plate overlapped at splitter plate
2.13	Form of wing tip	Tip of rotation
2.14	Control surface details	Trailing edge control surface of 25% chord between 45% span and 75% span. Circular leading edge with hinge line not sealed, but a gap of less than .016 in (0.40 mm) between the spoiler trailing edge and the trailing edge control leading edge. Side edges open with a gap of the order of .031 in (0.80 mm). Upper and lower surface spoilers of 15% chord, hinged at 60% chord, and also running between 45% span and 75% span
2.15	Additional remarks	See Fig 1 for overview
2.16	References	Ref 8

3 Wind Tunnel

3.1	Designation	NASA LaRC Transonic Dynamics Tunnel (TDT)

3.2	Type of tunnel	Continuous flow, single return
3.3	Test section dimensions	16 ft x 16 ft (4.064 x 4.064 m)
3.4	Type of roof and floor	Three slots each
3.5	Type of side walls	Two sidewall slots
3.6	Ventilation geometry	Constant width slots in test region
3.7	Thickness of side wall boundary layer	Model tested on large splitter plate set out approximately 40 inches (1.02 m) from tunnel side wall (see Fig 2). Some documentation of tunnel wall boundary layer in Ref 18. Some results for the boundary layer on the splitter plate are presented in Ref 27
3.8	Thickness of boundary layers at roof and floor	Not documented
3.9	Method of measuring velocity	Calculated from static pressures measured in plenum and total pressure measured upstream of entrance nozzle of test section
3.10	Flow angularity	Not documented, considered small
3.11	Uniformity of velocity over test section	Not documented, considered nearly uniform, some nonuniformity over splitter plate above M = 0.80
3.12	Sources and levels of noise or turbulence in empty tunnel	Generally unknown. Some low speed measurements are presented in Ref 26. Cone transition measurements are presented in Ref 24 and 25.
3.13	Tunnel resonances	Unknown
3.14	Additional remarks	Tests performed in heavy gas, R-12. Ratio of specific heats, γ, is 1.132-1.135. For computations, 1.132 is recommended. For the conditions of this test, the Prandtl number is calculated to be 0.77-0.78
3.15	References on tunnel	Ref 18-20

4 Model Motion

4.1	General description	Oscillations about hinge line of control surfaces, and dynamic response and flutter on PAPA
4.2	Reference coordinate and definition of motion	Unswept hinge lines, see Fig 1 for conventions
4.3	Range of amplitude	Trailing edge control surface oscillation of 1, 2, and 4 degrees, spoiler up to 10 degrees
4.4	Range of frequency	Generally 0 to 10 Hz
4.5	Method of applying motion	Control surface oscillations driven by miniature hydraulic actuators at control surfaces. Flutter self excited or by control surface
4.6	Timewise purity of motion	Not documented
4.7	Natural frequencies and normal modes of model and support system	See Table 1 for plunge and pitch on PAPA. For higher modes see Ref 30. Not documented for rigid strut and balance
4.8	Actual mode of applied motion including any elastic deformation	Combined pitch and plunge measured for flutter and control surface rotations measured. Very stiff model with flutter below 5 Hz and control surface oscillations below 10 Hz and next vertical mode at 37 Hz
4.9	Additional remarks	None

5 Test Conditions

5.1	Model planform area/tunnel area	.015
5.2	Model span/tunnel height	.17
5.3	Blockage	Model less than 0.2% but splitter plate and equipment fairing is near 4%
5.4	Position of model in tunnel	Mounted from large splitter plate out from wall and on the tunnel centerline, Fig 2

5.5 Range of Mach number	0.63 to 0.94
5.6 Range of tunnel total pressure	Approximately 500 to 1000 psf (24 to 48 kPa)
5.7 Range of tunnel total temperature	512 to 576 degrees Rankine (23 to 47° C)
5.8 Range of model steady or mean incidence	-4° to 10° pitch, 0 to 40° spoiler deflection, and -10° to 12° trailing edge control surface deflection
5.9 Definition of model incidence	From chord line of symmetric airfoil
5.10 Position of transition, if free	Transition strip used
5.11 Position and type of trip, if transition fixed	Grit strip at 5% chord on upper and lower surfaces.
5.12 Flow instabilities during tests	None defined
5.13 Changes to mean shape of model due to steady aerodynamic load	Not measured but considered very stiff
5.14 Additional remarks	Tests performed in heavy gas, R-12. Ratio of specific heats, γ, is 1.132-1.135. For computations, 1.132 is recommended. For the conditions of this test, the Prandtl number is calculated to be 0.77-0.78
5.15 References describing tests	Ref 8

6 Measurements and Observations

6.1 Steady pressures for the mean conditions	yes
6.2 Steady pressures for small changes from the mean conditions	yes
6.3 Quasi-steady pressures	no
6.4 Unsteady pressures	yes
6.5 Steady section forces for the mean conditions by integration of pressures	no
6.6 Steady section forces for small changes from the mean conditions by integration	no
6.7 Quasi-steady section forces by integration	no
6.8 Unsteady section forces by integration	no
6.9 Measurement of actual motion at points of model	yes
6.10 Observation or measurement of boundary layer properties	no
6.11 Visualisation of surface flow	no
6.12 Visualisation of shock wave movements	no
6.13 Additional remarks	no

7 Instrumentation

7.1 Steady pressure	
7.1.1 Position of orifices spanwise and chordwise	58 locations at 60% span and 17 at 40% span. See Figs 1 and 4
7.1.2 Type of measuring system	Used same transducers as unsteady pressure measurements
7.2 Unsteady pressure	
7.2.1 Position of orifices spanwise and chordwise	Same transducers as steady measurements. . See Figs 1 and 4
7.2.2 Diameter of orifices	.020 inches (.51 mm)
7.2.3 Type of measuring system	In situ pressure gages
7.2.4 Type of transducers	Kulites
7.2.5 Principle and accuracy of calibration	Statically calibrated and monitored through reference tubes
7.3 Model motion	
7.3.1 Method of measuring motion reference coordinate	Undocumented
7.3.2 Method of determining spatial mode of motion	Wind-off verification with accelerometers

	7.3.3 Accuracy of measured motion	Undocumented
7.4	Processing of unsteady measurements	
	7.4.1 Method of acquiring and processing measurements	Analog signals digitized at 500 samples/sec for 8-30 seconds depending on data type
	7.4.2 Type of analysis	Fourier analysis
	7.4.3 Unsteady pressure quantities obtained and accuracies achieved	Amplitude and phase of each pressure signal. Accuracy not specified
	7.4.4 Method of integration to obtain forces	None
7.5	Additional remarks	None
7.6	References on techniques	Data system for test similar to one described in Ref 22

8 Data Presentation

8.1	Test Cases for which data could be made available	See Ref 8
8.2	Test Cases for which data are included in this document	See Tables 3-10
8.3	Steady pressures	Available for each Test Case
8.4	Quasi-steady or steady perturbation pressures	Steady pressures measured for several angles of attack
8.5	Unsteady pressures	Primary data is C_p mean, magnitude and phase for first harmonic only. Time histories have been archived
8.6	Steady forces or moments	5 component force balance used for static force measurements
8.7	Quasi-steady or unsteady perturbation forces	None
8.8	Unsteady forces and moments	None
8.9	Other forms in which data could be made available	None
8.10	Reference giving other representations of data	Ref 8-17

9 Comments on Data

9.1	Accuracy	
	9.1.1 Mach number	Not documented
	9.1.2 Steady incidence	Unknown
	9.1.3 Reduced frequency	Should be accurate
	9.1.4 Steady pressure coefficients	Not documented
	9.1.5 Steady pressure derivatives	None
	9.1.6 Unsteady pressure coefficients	Each gage individually calibrated and monitored statically through reference tube
9.2	Sensitivity to small changes of parameter	None indicated. Amplitudes of oscillation varied in test
9.3	Non-linearities	Many flow conditions involve shock waves and some with separation
9.4	Influence of tunnel total pressure	Not evaluated. Most of the test at constant dynamic pressure
9.5	Effects on data of uncertainty, or variation, in mode of model motion	Unknown, not expected to be appreciable
9.6	Wall interference corrections	None applied
9.7	Other relevant tests on same model	None
9.8	Relevant tests on other models of nominally the same shapes	Flutter tests on similar planform on PAPA presented in Ref 3-5
9.9	Any remarks relevant to comparison between experiment and theory	Some included under Model and Tests. Reynolds number included for each Test Case
9.10	Additional remarks	Reduced frequency based on root semichord of 8 inches (203.2 mm)
9.11	References on discussion of data	Ref 1-2 and 8-12

10 Personal Contact for Further Information

Head, Aeroelasticity Branch
Mail Stop 340
NASA Langley Research Center
Hampton, VA 23681-2199 USA

Phone: +1-(757)-864-2820
FAX: +1-(757)-864-8678

11 List of references

1. Bennett, Robert M.; Eckstrom, Clinton V.; Rivera, Jose, A.; Dansberry, Bryan E.; Farmer, Moses G.; and Durham, Michael H.: *The Benchmark Aeroelastic Models Program - Description and Highlights of Initial Results.* Paper No. 25 in Transonic Unsteady Aerodynamics and Aeroelasticity, AGARD CP 507, Mar. 1992. Also available as NASA TM-104180, 1991.

2. Durham, Michael H.; Keller, Donald F.; Bennett, Robert M.; and Wieseman, Carol D.: *A Status Report on a Model for Benchmark Active Controls Testing.* AIAA Paper 91-1011, Apr. 1991. Also available as NASA TM 107582, 1991.

3. Rivera, Jose A., Jr.; Dansberry, Bryan E.; Durham, Michael, H.; Bennett, Robert M.; and Silva, Walter A.: *Pressure Measurements on a Rectangular Wing with A NACA 0012 Airfoil During Conventional Flutter.* NASA TM 104211, July 1992.

4. Rivera, Jose A.; Dansberry, Bryan E.; Bennett, Robert M.; Durham, Michael, H.; and Silva, Walter A.: *NACA 0012 Benchmark Model Experimental Flutter Results with Unsteady Pressure Distributions.* AIAA Paper 92-2396, Apr. 1992. Also available as NASA TM 107581, Mar. 1992.

5. Rivera, Jose A.; Dansberry, Bryan E.; Farmer, Moses G.; Eckstrom, Clinton, V.; Seidel, David A.; and Bennett, Robert M.: *Experimental Flutter Boundaries with Unsteady Pressure Distributions for the NACA 0012 Benchmark Model.* AIAA 91-1010, 1991. Also available as NASA TM 104072, 1991.

6. Perry, Boyd, III; Cole, Stanley R.; and Miller, Gerald D.: *Summary of an Active Flexible Wing Program.* Journal of Aircraft, vol. 32, no. 1, Jan.-Feb. 1995, pp 10-15.

7. Sandford, Maynard C.; Abel, Irving; and Gray, David L.: *Development and Demonstration of a Flutter-Suppression System Using Active Controls.* NASA TR R-450, 1974.

8. Scott, Robert C.; Hoadley, Sherwood T.; Wieseman, Carol D.; and Durham, Michael H.: *The Benchmark Active Controls Technology Model Aerodynamic Data.* AIAA Paper 97-0829, Jan. 1997.

9. Bartels, R. E.; and Schuster, David M.: *A Comparison of Two Navier-Stokes Aeroelastic Methods Using BACT Benchmark Experimental Data.* AIAA Paper 99-3157, June 1999.

10. Schuster, David M.; Beran, Philip S.; and Huttsell, Lawrence J.: *Application of the ENS3DAE/Navier-Stokes Aeroelastic Method.* Paper No. 3 in Numerical Unsteady Aerodynamics and Aeroelastic Simulation, AGARD Report 822, Mar. 1998.

11. Roughen, K. M.; Baker, M. L.; and Fogarty T.: *CFD and Doublet-Lattice Calculation of Unsteady Control Surface Aerodynamics and Correlation with Wind Tunnel Test.* AAIA Paper 99-1469, Jan. 1999.

12. Waszak, Martin R.: *Modeling the Benchmark Active Control Technology Wind-Tunnel Model for Active Control Design Applications.* NASA/TP-1998-206270, June 1998.

13. Waszak, Martin R.: *Modeling the Benchmark Active Controls Technology Wind-Tunnel Model for Application to Flutter Suppression.* AIAA 96-3437, July 1996.

14. Waszak, Marty R. and Fung, James: *Parameter Identification and Analysis of Actuators for the BACT Wind-Tunnel Model.* AIAA Paper 96-3362, July 1996.

15. Lichtenwalner, P.; Little, G.; and Scott, R.: *Adaptive Neural Control of Aeroelastic Response.* SPIE 1996 Symposium on Smart Structures and Materials, San Diego, CA, Feb. 1996.

16. Lichtenwalner, P.; Little, G.; Pado, L.; and Scott, R.: *Adaptive Neural Control for Active Flutter Suppression.* SPIE 1997 Symposium on Smart Structures and Materials, San Diego, CA, Mar. 1997.

17. D'Cruz, Jonathan: A Determination of the External Forces Required to Move the Benchmark Active Controls Testing Model *in Pure Plunge and Pure Pitch.* NASA TM 107743, July 1993.

18. Aeroelasticity Branch Staff: The Langley Transonic Dynamics Tunnel. LWP-799, Sep. 1969.

19. Cole, Stanley, R.; and Rivera, Jose, A, Jr.: *The New Heavy Gas Testing Capability in the NASA Langley Transonic Dynamics Tunnel.* Paper No. 4, presented at the Royal Aeronautical Society Wind Tunnels and Wind Tunnel Test Techniques Forum, Churchill College, Cambridge, UK, Apr. 1997.

20. Corliss, James M.; and Cole, Stanley R.: *Heavy Gas Conversion of the NASA Langley Transonic Dynamics Tunnel.* AIAA Paper 98-2710, June 1998.

21. Cole, Patricia H.: *Wind Tunnel Real-Time Data Acquisition System.* NASA TM 80081, 1979.

22. Bryant, C.; and Hoadley, S. T.: *Open Architecture Dynamic Data System at Langley's Transonic Dynamics Tunnel.* AAIA Paper 98-0343, Jan. 1998.

23. Wieseman, Carol D.; and Hoadley, Sherwood, T.: *Versatile Software Package for Near Real-Time Analysis of Experimental Data.* AIAA Paper 98-2722, June 1999.

24. Dougherty, N. Sam, Jr.: *Influence of Wind Tunnel Noise on the Location of Boundary-Layer Transition on a Slender Cone at Mach Numbers from 0.2 to 5.5. Volume I. - Experimental Methods and Summary of Results. Volume II. - Tabulated and Plotted Data.* AEDC--TR-78-44, March 1980.

25. Dougherty, N. Sam, Jr.; and Fisher, D. F.: *Boundary-Layer Transition on a 10-Deg. Cone: Wind Tunnel/Flight Correlation.* AIAA Paper 80-0154, Jan. 1980.

26. Sleeper, Robert K.; Keller, Donald F.; Perry, Boyd, III; and Sandford, Maynard C.: *Characteristics of Vertical and Lateral Tunnel Turbulence Measured in Air in the Langley Transonic Dynamics Tunnel.* NASA TM 107734, March 1993.

27. Schuster, David M: *Aerodynamic Measurements on a Large Splitter Plate for the NASA Langley Transonic Dynamics Tunnel.* Proposed NASA TM, 1999.

28. Farmer, Moses G.: *A Two-Degree-of-Freedom Flutter Mount System with Low Damping for Testing Rigid Wings at Different Angles of Attack. NASA* TM 83302, 1982.

29. Farmer, Moses G.: *Mount System for Testing Flutter.* U.S Patent No. 4,475,385, Oct. 9, 1984.

30. Dansberry, Bryan E.; Durham, Michael, H.; Bennett, Robert M.; Turnock, David L.; Silva, Walter A.; and Rivera, Jose A., Jr.: *Physical Properties of the Benchmark Models Program Supercritical Wing.* NASA TM 4457, Sep. 1993.

31. Rowe, W. S.; Redman, M. C.; Ehlers, F. E.; and Sebastian, J. D.: *Prediction of Unsteady Aerodynamic Loadings Caused by Leading Edge and Trailing Edge Control Surface Motions in Subsonic Compressible Flow—Analysis and Results.* NASA CR-2543, May 1975.

32. Giesing, J. P.; Kalman, T. P.; and Rodden, W. P.: *Subsonic Unsteady Aerodynamics for General Configurations, Part I – Vol. I – Direct Application of the Nonplanar Doublet Lattice Method.* AFFDL-TR-71-5, Nov. 1971.

Table 1. Measured Nominal Structural Dynamic Parameters

	Plunge Mode	Pitch Mode
Frequency	3.34 Hz.	5.21 Hz.
Stiffness	2,686 lb/ft	3,000 ft-lb/rad
Damping Ratio, ζ	0.0014	0.0010
Effective Mass or Inertia	6.08 slug	2.80 slug-ft^2

Table 2. Instrumentation

Instrument	Quantity
Model Pressure Transducers	75
Splitter Plate Pressure Transducers (Test 485 only)	20
Boundary Layer Rake Pressure Transducers (Test 485 only)	10
Model Accelerometers	4
Control Surface Accelerometers	6
Control Surface Potentiometers	3
Control Surface Command Signals	3
Hydraulic Pressure Transducers	6
Balance Components (Rigid support only)	5
PAPA Strain Gage Bridges (Flexible support only)	2
PAPA Accelerometers (Flexible support only)	2
Turntable AOA Accelerometer	1
Model AOA Accelerometer	1

Table 3. Static Test Cases for Angle Of Attack

Test Case No.	Test	Run	Point No.	M	q psf	α deg.	δ_{te_0} deg.	δ_{us_0} deg.	δ_{ls_0} deg.	Wind-Off Zero Point No.
8ESA1	485	27	1911	0.650	145.0	-0.03	0.3	0.2	0.2	1910
8ESA2	485	27	1912	0.648	144.2	0.51	0.3	0.2	0.2	1910
8ESA3	485	27	1913	0.650	144.8	1.01	0.3	0.2	0.2	1910
8ESA4	485	27	1914	0.650	145.1	2.05	0.3	0.2	0.2	1910
8ESA5	485	27	1915	0.649	144.6	3.99	0.3	0.2	0.2	1910
8ESA6	485	27	1916	0.651	145.3	6.01	0.3	0.2	0.2	1910
8ESA7	485	27	1917	0.650	145.1	-2.01	0.3	0.2	0.2	1910
8ESA8	485	27	1918	0.649	144.8	-4.01	0.3	0.2	0.2	1910
8ESA9	485	5	136	0.768	140.4	-0.01	0.0	0.2	0.0	132
8ESA10	485	5	137	0.771	141.6	0.51	0.0	0.2	0.0	132
8ESA11	485	5	138	0.772	142.1	1.01	0.0	0.2	0.0	132
8ESA12	485	5	139	0.769	141.6	2.00	0.0	0.2	0.0	132
8ESA13	485	5	140	0.769	141.7	3.01	0.0	0.2	0.0	132
8ESA14	485	5	141	0.768	141.5	3.99	0.0	0.2	0.0	132
8ESA15	485	5	142	0.769	141.7	5.00	0.0	0.2	0.0	132
8ESA16	485	5	143	0.770	142.3	6.01	0.0	0.2	0.0	132
8ESA17	485	5	144	0.768	141.7	7.02	0.0	0.2	0.0	132
8ESA18	485	5	145	0.769	142.2	8.02	0.0	0.2	0.0	132
8ESA19	485	5	146	0.769	142.2	9.00	0.0	0.1	0.0	132
8ESA20	485	5	147	0.770	142.6	6.02	0.0	0.2	0.0	132
8ESA21	485	5	148	0.769	142.6	4.02	0.0	0.2	0.0	132
8ESA22	485	5	150	0.769	142.8	-0.03	0.0	0.1	0.0	132
8ESA23	485	5	151	0.769	142.8	-2.02	0.0	0.1	0.0	132
8ESA24	485	5	152	0.769	142.9	-4.02	0.0	0.1	0.0	132
8ESA25	485	21	1405	0.821	169.2	-0.01	0.3	0.2	0.2	1404
8ESA26	485	21	1406	0.817	168.5	0.50	0.3	0.2	0.2	1404
8ESA27	485	21	1407	0.817	168.5	1.03	0.3	0.2	0.2	1404
8ESA28	485	21	1408	0.819	169.0	2.05	0.3	0.2	0.2	1404
8ESA29	485	21	1409	0.819	169.1	3.12	0.3	0.2	0.2	1404
8ESA30	485	21	1410	0.821	169.9	3.99	0.3	0.2	0.2	1404
8ESA31	485	21	1411	0.819	169.5	5.01	0.3	0.2	0.2	1404
8ESA32	485	21	1412	0.819	169.4	6.00	0.3	0.2	0.2	1404
8ESA33	485	21	1413	0.819	169.4	7.04	0.3	0.2	0.2	1404
8ESA34	485	21	1414	0.820	169.7	8.04	0.3	0.1	0.2	1404
8ESA35	485	21	1415	0.819	169.6	9.04	0.3	0.1	0.2	1404
8ESA36	485	21	1416	0.819	169.8	10.04	0.3	0.1	0.2	1404
8ESA37	485	21	1418	0.816	169.2	6.01	0.3	0.2	0.2	1404
8ESA38	485	21	1420	0.818	169.7	1.99	0.3	0.2	0.2	1404
8ESA39	485	21	1421	0.818	169.8	-0.06	0.3	0.2	0.2	1404
8ESA40	485	21	1423	0.818	169.8	-4.01	0.3	0.2	0.2	1404
8ESA41	485	25	1715	0.902	134.5	0.00	0.2	0.3	0.1	1714
8ESA42	485	25	1716	0.903	134.7	0.26	0.2	0.4	0.1	1714
8ESA43	485	25	1717	0.899	134.0	0.50	0.2	0.4	0.2	1714
8ESA44	485	25	1718	0.900	134.2	0.75	0.2	0.3	0.4	1714
8ESA45	485	25	1719	0.902	134.7	1.02	0.2	0.3	0.4	1714
8ESA46	485	25	1720	0.897	133.9	1.52	0.2	0.4	0.5	1714
8ESA47	485	25	1721	0.899	134.4	2.00	0.2	0.3	0.4	1714
8ESA48	485	25	1722	0.896	133.9	3.01	0.2	0.3	0.4	1714

Table 4. Static Test Cases for Trailing Edge Control Surface Deflection

Test Case No.	Test	Run	Point No.	M	q psf	α deg.	δ_{te_0} deg.	δ_{us_0} deg	δ_{ls_0} deg	Wind-Off Zero Point No.
8EST1	485	27	1929	0.649	145.0	0.01	-9.7	0.2	0.2	1910
8EST2	485	27	1930	0.648	144.8	0.01	-4.8	0.2	0.4	1910
8EST3	485	27	1931	0.648	144.7	0.01	-1.7	0.2	0.2	1910
8EST4	485	27	1932	0.648	144.7	0.01	0.3	0.2	0.3	1910
8EST5	485	27	1933	0.650	145.4	0.01	2.3	0.2	0.3	1910
8EST6	485	27	1934	0.650	145.2	0.01	5.3	0.2	0.2	1910
8EST7	485	27	1935	0.651	145.6	0.01	10.3	0.2	0.2	1910
8EST8	485	27	1937	0.649	145.1	1.99	-9.8	0.2	0.1	1910
8EST9	485	27	1938	0.650	145.4	1.99	-4.8	0.2	0.2	1910
8EST10	485	27	1939	0.650	145.3	1.99	-1.7	0.2	0.1	1910
8EST11	485	27	1940	0.650	145.4	1.99	0.3	0.2	0.1	1910
8EST12	485	27	1941	0.650	145.6	1.99	2.3	0.2	0.2	1910
8EST13	485	27	1942	0.649	145.3	1.99	5.3	0.2	0.2	1910
8EST14	485	27	1943	0.649	145.3	1.99	10.3	0.2	0.2	1910
8EST15	485	5	156	0.767	142.9	0.03	-10.0	0.1	-0.1	132
8EST16	485	5	157	0.768	143.1	0.03	-5.0	0.1	-0.1	132
8EST17	485	5	158	0.771	143.9	0.03	-2.0	0.1	-0.1	132
8EST18	485	5	159	0.768	143.1	0.03	0.0	0.1	-0.1	132
8EST19	485	5	160	0.772	144.4	0.03	0.5	0.1	-0.1	132
8EST20	485	5	161	0.769	143.5	0.03	1.0	0.1	-0.1	132
8EST21	485	5	162	0.768	143.4	0.03	2.0	0.1	-0.1	132
8EST22	485	5	163	0.770	143.9	0.03	3.0	0.1	0.0	132
8EST23	485	5	164	0.769	143.7	0.03	5.0	0.1	0.0	132
8EST24	485	5	165	0.770	144.1	0.03	10.0	0.1	-0.1	132
8EST25	485	5	166	0.770	144.1	0.03	12.0	0.1	-0.1	132
8EST26	485	5	193	0.770	145.2	3.99	-9.9	0.1	-0.1	132
8EST27	485	5	195	0.769	145.1	3.99	-5.0	0.1	-0.1	132
8EST28	485	5	196	0.770	145.5	3.99	-1.9	0.1	-0.1	132
8EST29	485	5	197	0.769	145.3	3.99	0.0	0.1	-0.1	132
8EST30	485	5	200	0.768	145.1	3.99	1.0	0.1	-0.1	132
8EST31	485	5	201	0.769	145.3	3.99	2.0	0.1	-0.1	132
8EST32	485	5	202	0.770	145.6	3.99	3.0	0.1	-0.1	132
8EST33	485	5	203	0.769	145.4	3.99	5.0	0.1	-0.1	132
8EST34	485	5	204	0.769	145.4	3.99	10.0	0.1	-0.1	132
8EST35	485	5	205	0.770	145.6	3.99	12.0	0.1	-0.1	132

Table 4. Concluded

Test Case No.	Test	Run	Point No.	M	q psf	α deg.	δ_{te_o} deg.	δ_{us_0} deg.	δ_{ls_0} deg	Wind-Off Zero Point No.
8EST36	485	21	1425	0.818	170.0	0.03	-9.7	-0.2	0.2	1404
8EST37	485	21	1426	0.820	170.6	0.03	-4.7	-0.1	0.2	1404
8EST38	485	21	1427	0.818	170.0	0.03	-1.7	-0.1	0.2	1404
8EST39	485	21	1428	0.817	170.0	0.03	0.3	-0.1	0.2	1404
8EST40	485	21	1429	0.820	170.7	0.03	1.3	-0.1	0.2	1404
8EST41	485	21	1430	0.819	170.5	0.03	2.3	-0.1	0.2	1404
8EST42	485	21	1431	0.818	170.3	0.03	3.3	-0.1	0.2	1404
8EST43	485	21	1432	0.817	170.0	0.03	5.3	-0.1	0.2	1404
8EST44	485	21	1433	0.818	170.3	0.03	10.3	-0.1	0.2	1404
8EST45	485	21	1434	0.821	171.1	0.03	12.3	-0.1	0.2	1404
8EST46	485	21	1447	0.817	170.3	4.01	-9.7	-0.1	0.2	1404
8EST47	485	21	1448	0.819	170.9	4.01	-4.7	-0.1	0.2	1404
8EST48	485	21	1449	0.818	170.8	4.01	-1.7	-0.1	0.2	1404
8EST49	485	21	1450	0.817	170.5	4.01	0.3	-0.1	0.2	1404
8EST50	485	21	1451	0.817	170.7	4.01	1.3	-0.1	0.2	1404
8EST51	485	21	1452	0.818	170.9	4.01	2.3	-0.1	0.2	1404
8EST52	485	21	1453	0.818	170.9	4.01	3.4	-0.1	0.2	1404
8EST53	485	21	1454	0.817	170.5	4.01	5.4	-0.1	0.2	1404
8EST54	485	21	1455	0.816	170.3	4.01	10.3	-0.1	0.2	1404
8EST55	485	21	1456	0.818	170.8	4.00	12.3	-0.1	0.2	1404
8EST56	485	25	1735	0.896	134.9	-0.05	-4.8	0.3	0.3	1714
8EST57	485	25	1737	0.899	135.6	-0.05	-1.7	0.2	0.3	1714
8EST58	485	25	1738	0.896	135.2	-0.05	-0.7	0.2	0.3	1714
8EST59	485	25	1739	0.896	135.2	-0.05	-0.3	0.2	0.3	1714
8EST60	485	25	1740	0.897	135.3	-0.05	0.3	0.2	0.3	1714
8EST61	485	25	1741	0.897	135.4	-0.05	0.7	0.2	0.3	1714
8EST62	485	25	1742	0.898	135.5	-0.05	1.3	0.2	0.3	1714
8EST63	485	25	1745	0.897	135.7	-0.05	1.8	0.2	0.2	1714
8EST64	485	25	1746	0.899	136.0	-0.05	2.2	0.2	0.1	1714
8EST65	485	25	1747	0.901	136.4	-0.05	5.2	0.3	0.1	1714

Table 5. Static Test Cases for Upper Spoiler Deflection

Test Case No.	Test	Run	Point No.	M	q psf	α deg.	δ_{te_0} deg.	δ_{us_0} deg.	δ_{ls_0} deg.	Wind-Off Zero Point No.
8ESU1	485	27	1953	0.648	145.0	0.00	0.2	0.2	0.2	1910
8ESU2	485	27	1954	0.649	145.3	0.00	0.2	-4.8	0.2	1910
8ESU3	485	27	1955	0.649	145.5	0.00	0.2	-9.8	0.2	1910
8ESU4	485	27	1956	0.648	144.9	0.00	0.2	-20.0	0.2	1910
8ESU5	485	27	1957	0.649	145.4	0.00	0.2	-40.1	0.2	1910
8ESU6	485	27	1959	0.649	145.6	3.98	0.2	0.3	0.2	1910
8ESU7	485	27	1960	0.647	145.0	3.98	0.2	-4.8	0.2	1910
8ESU8	485	27	1961	0.649	145.4	3.98	0.2	-9.8	0.2	1910
8ESU9	485	27	1962	0.649	145.6	3.98	0.2	-19.9	0.2	1910
8ESU10	485	27	1963	0.649	145.5	3.98	0.2	-40.2	0.2	1910
8ESU11	485	8	361	0.771	146.4	-0.01	0.0	-0.2	0.0	360
8ESU12	485	8	362	0.775	146.7	-0.01	0.0	-0.5	0.0	360
8ESU13	485	8	363	0.772	146.0	-0.01	0.0	-0.5	0.0	360
8ESU14	485	8	364	0.772	145.9	-0.01	0.1	-1.0	0.0	360
8ESU15	485	8	365	0.770	145.6	-0.01	0.1	-2.0	0.0	360
8ESU16	485	8	366	0.770	145.6	-0.01	0.1	-5.0	0.0	360
8ESU17	485	8	367	0.772	146.3	-0.01	0.0	-9.9	0.0	360
8ESU18	485	8	368	0.769	145.5	-0.01	0.0	-15.0	0.0	360
8ESU19	485	8	369	0.770	146.0	-0.01	0.0	-20.0	0.0	360
8ESU20	485	8	370	0.770	146.0	-0.01	0.0	-25.0	0.0	360
8ESU21	485	8	371	0.772	146.9	-0.02	0.0	-35.1	0.0	360
8ESU22	485	21	1458	0.817	171.0	-0.02	0.3	-0.1	0.1	1404
8ESU23	485	21	1459	0.816	170.6	-0.03	0.3	-0.9	0.2	1404
8ESU24	485	21	1460	0.819	171.3	-0.03	0.3	-2.0	0.2	1404
8ESU25	485	21	1461	0.818	171.4	-0.03	0.3	-4.9	0.2	1404
8ESU26	485	21	1462	0.820	171.8	-0.03	0.3	-10.0	0.2	1404
8ESU27	485	21	1463	0.818	171.2	-0.03	0.3	-14.9	0.2	1404
8ESU28	485	21	1464	0.817	171.0	-0.03	0.3	-19.8	0.2	1404
8ESU29	485	25	1775	0.899	137.2	-0.03	0.2	0.3	0.3	1714
8ESU30	485	25	1776	0.897	137.1	-0.03	0.3	-0.9	0.3	1714
8ESU31	485	25	1777	0.895	136.9	-0.03	0.2	-2.0	0.3	1714
8ESU32	485	25	1778	0.897	137.1	-0.03	0.3	-3.0	0.2	1714

Table 6. Test Cases for Trailing Edge Control Surface Oscillation, $\delta_{us_0} = 0$

Test Case No.	Test	Run	Point No.	M	q psf	α deg.	δ_{te_0} deg.	δ_{te} deg.	k	Frequency Hz	Wind-Off Zero Point No.
8EOT1	485	27	1966	0.648	145.3	0.04	0.25	4.05	0.0257	2.00	1910
8EOT2	485	27	1967	0.648	145.2	0.09	0.27	4.04	0.0645	5.01	1910
8EOT3	485	27	1968	0.647	145.1	0.05	0.27	3.83	0.1291	10.02	1910
8EOT4	485	27	1972	0.648	145.5	4.03	0.25	4.05	0.0257	2.00	1910
8EOT5	485	27	1973	0.647	145.1	4.02	0.27	4.04	0.0646	5.01	1910
8EOT6	485	27	1974	0.648	145.5	4.00	0.27	3.83	0.1289	10.02	1910
8EOT7	485	14	901	0.768	151.2	-0.03	0.05	1.07	0.1076	9.93	879
8EOT8	485	14	904	0.767	151.4	0.04	0.05	2.04	0.0108	1.00	879
8EOT9	485	14	905	0.768	151.6	-0.06	0.05	2.05	0.0217	2.00	879
8EOT10	485	14	906	0.769	152.0	0.07	0.05	2.05	0.0325	3.00	879
8EOT11	485	14	907	0.769	151.9	0.01	0.05	2.06	0.0431	3.99	879
8EOT12	485	14	908	0.766	151.2	0.04	0.05	2.07	0.0544	5.01	879
8EOT13	485	14	909	0.768	152.0	-0.06	0.06	2.08	0.0650	6.00	879
8EOT14	485	14	910	0.769	152.2	0.04	0.08	2.08	0.0868	8.03	879
8EOT15	485	14	911	0.768	151.8	-0.02	0.08	2.07	0.1076	9.93	879
8EOT16	485	14	916	0.770	152.6	0.13	0.08	3.00	0.1073	9.93	879
8EOT17	485	14	919	0.769	152.5	0.07	0.07	4.06	0.0216	2.00	879
8EOT18	485	14	920	0.769	152.6	0.10	0.08	4.06	0.0542	5.01	879
8EOT19	485	14	921	0.769	152.6	0.12	0.08	3.89	0.1074	9.93	879
8EOT20	485	14	933	0.769	153.3	-0.04	5.09	2.03	0.1073	9.93	879
8EOT21	485	14	936	0.768	153.1	-0.03	5.08	4.05	0.0216	2.00	879
8EOT22	485	14	937	0.768	153.1	-0.03	5.10	4.03	0.0542	5.01	879
8EOT23	485	14	938	0.768	153.0	-0.02	5.08	3.84	0.1075	9.93	879
8EOT24	485	16	1049	0.765	145.0	2.01	0.08	4.05	0.0218	2.00	963
8EOT25	485	16	1050	0.767	145.4	2.04	0.10	4.05	0.0544	5.01	963
8EOT26	485	16	1051	0.768	145.8	2.08	0.10	3.88	0.1086	10.02	963
8EOT27	485	17	1083	0.767	147.4	4.10	0.09	1.07	0.1088	10.02	1060
8EOT28	485	17	1088	0.768	148.0	4.04	0.09	2.05	0.1086	10.02	1060
8EOT29	485	17	1092	0.769	148.3	4.05	0.08	4.04	0.0217	2.00	1060
8EOT30	485	17	1093	0.768	148.3	4.15	0.10	4.04	0.0543	5.01	1060
8EOT31	485	17	1094	0.771	149.0	4.01	0.10	3.87	0.1083	10.02	1060
8EOT32	485	17	1121	0.767	148.7	4.99	0.08	4.04	0.0217	2.00	1060
8EOT33	485	17	1124	0.767	149.1	4.93	0.09	4.04	0.0543	5.01	1060
8EOT34	485	17	1126	0.767	149.2	5.08	0.10	3.87	0.1087	10.02	1060
8EOT35	485	18	1165	0.769	151.8	5.93	0.08	4.04	0.0217	2.00	1154
8EOT36	485	18	1166	0.770	152.2	5.87	0.10	4.04	0.0542	5.01	1154
8EOT37	485	18	1167	0.767	151.4	5.98	0.10	3.87	0.1088	10.02	1154
8EOT38	485	22	1557	0.818	175.2	0.02	0.04	4.04	0.0204	2.00	1519
8EOT39	485	22	1558	0.819	175.2	0.03	0.05	4.04	0.0510	5.01	1519
8EOT40	485	22	1560	0.819	175.4	0.06	0.06	3.88	0.1019	10.02	1519
8EOT41	485	22	1568	0.817	175.2	3.97	0.04	4.04	0.0204	2.00	1519
8EOT42	485	22	1569	0.817	175.1	3.97	0.06	4.04	0.0511	5.01	1519
8EOT43	485	22	1570	0.817	175.1	4.03	0.07	3.86	0.1022	10.02	1519
8EOT44	485	25	1789	0.900	138.5	-0.19	0.25	2.04	0.0186	2.00	1714
8EOT45	485	25	1790	0.899	138.3	-0.23	0.25	2.06	0.0466	5.01	1714
8EOT46	485	25	1791	0.898	138.2	-0.21	0.26	2.06	0.0934	10.02	1714
8EOT47	485	25	1798	0.898	138.4	0.34	0.26	2.05	0.0933	10.02	1714

Table 7. Test Cases for Upper Spoiler Oscillations, $\delta_{te_0} = 0$

Test Case No.	Test	Run	Point No.	M	q psf	α deg.	δ_{us_0} deg.	δ_{us} deg.	k	Frequency Hz	Wind-Off Zero Point No.
8EOU1	485	27	1978	0.648	145.5	-0.02	-9.86	2.12	0.0257	2.00	1910
8EOU2	485	27	1979	0.648	145.4	-0.02	-9.84	2.17	0.0645	5.01	1910
8EOU3	485	27	1980	0.647	145.3	-0.02	-9.82	2.29	0.1291	10.02	1910
8EOU4	485	27	1988	0.648	145.7	3.99	-10.60	2.17	0.0257	2.00	1910
8EOU5	485	27	1989	0.648	145.7	3.99	-10.58	2.21	0.0645	5.01	1910
8EOU6	485	27	1990	0.648	145.9	3.99	-10.54	2.37	0.1289	10.02	1910
8EOU7	485	18	1188	0.769	152.7	-0.01	-5.06	2.36	0.1085	10.02	1154
8EOU8	485	18	1197	0.770	153.1	-0.01	-5.01	4.47	0.1084	10.02	1154
8EOU9	485	18	1201	0.769	153.0	-0.01	-10.06	2.10	0.0216	2.00	1154
8EOU10	485	18	1202	0.769	153.0	-0.01	-10.04	2.16	0.0543	5.01	1154
8EOU11	485	18	1203	0.768	152.6	-0.01	-10.02	2.26	0.1087	10.02	1154
8EOU12	485	18	1207	0.769	153.2	-0.01	-10.09	10.44	0.1085	10.02	1154
8EOU13	485	18	1211	0.768	152.9	-0.01	-20.01	2.09	0.0217	2.00	1154
8EOU14	485	18	1212	0.768	153.0	-0.01	-20.00	2.05	0.0543	5.01	1154
8EOU15	485	18	1213	0.768	152.9	-0.01	-19.97	2.10	0.1086	10.02	1154
8EOU16	485	18	1217	0.769	153.4	-0.01	-19.65	10.18	0.1085	10.02	1154
8EOU17	485	20	1369	0.768	150.7	5.01	-19.52	10.25	0.1086	10.02	1298
8EOU18	485	22	1574	0.818	175.6	0.00	-9.94	2.15	0.0204	2.00	1519
8EOU19	485	22	1575	0.819	176.1	0.00	-9.93	2.18	0.0509	5.01	1519
8EOU20	485	22	1576	0.818	175.8	0.00	-9.90	2.27	0.1020	10.02	1519
8EOU21	485	22	1580	0.819	176.0	0.00	-10.09	10.36	0.1020	10.02	1519
8EOU22	485	22	1584	0.815	174.9	0.00	-19.89	2.11	0.0204	2.00	1519
8EOU23	485	22	1585	0.818	175.8	0.00	-19.89	2.08	0.0510	5.01	1519
8EOU24	485	22	1586	0.819	176.4	0.00	-19.84	2.14	0.1019	10.02	1519
8EOU25	485	22	1590	0.819	176.3	0.00	-19.43	10.15	0.1020	10.02	1519
8EOU26	485	23	1618	0.819	177.4	4.01	-19.51	10.26	0.1020	10.02	1608
8EOU27	485	25	1802	0.896	138.4	-0.01	-2.02	2.16	0.0187	2.00	1714

Table 8. BACT Flutter Test Cases

Test Case No.	Test	Run	Point No.	M	q psf	α deg.	Type	k	Flutter Freq., Hz	Wind-Off Zero Point No.
8EFC1	502	25	1438	0.631	158.2	1.64	Classical	0.0574	4.31	1379
8EFC2	502	25	1394	0.747	151.6	1.78	Classical	0.0470	4.14	1379
8EFC3	502	27	1524	0.770	145.2	1.72	Classical	0.0458	4.19	1484
8EFC4	502	26	1469	0.793	146.5	1.81	Classical	0.0439	4.13	1450
8EFC5	502	28	1685	0.801	151.7	2.09	Classical	0.0436	4.17	1569
8EFC6	502	26	1472	0.804	149.9	1.86	Classical	0.0430	4.10	1450
8EFC7	502	26	1477	0.842	161.1	1.83	Classical	0.0420	4.20	1450
8EFC8	502	25	1405	0.859	191.8	1.85	Classical	0.0408	4.10	1379
8EFP1	485	36	2324	0.928	163.7	-0.06	Plunge	0.0304	3.37	2300
8EFP2	485	41	2490	0.935	124.2	-0.06	Plunge	0.0299	3.31	2481
8EFP3	485	33	2240	0.937	133.8	0.03	Plunge	0.0294	3.27	2205
8EFP4	485	41	2488	0.939	124.7	-0.05	Plunge	0.0289	3.21	2481
8EFS1	485	43	2648	0.768	124.2	6.34	Stall	0.0520	4.77	2604
8EFS2	485	42	2571	0.799	126.9	5.43	Stall	0.0506	4.83	2543
8EFS3	485	36	2332	0.799	137.6	5.15	Stall	0.0497	4.74	2300

Table 9. Test Cases for Forced Response with Trailing Edge Control Surface on PAPA, $\delta_{us_o} = \delta_{te_o} = 0$

Test Case No.	Test	Run	Point No.	M	q psf	α deg.	δ_{te} deg.	k	Frequency Hz	Wind-Off Zero Point No.
8ERT1	485	38	2377	0.648	112.6	2.02	1.56	0.0445	3.45	2355
8ERT2	485	38	2380	0.649	113.0	2.02	4.08	0.0579	4.50	2355
8ERT3	485	43	2618	0.771	123.6	1.99	1.04	0.0374	3.44	2604
8ERT4	485	43	2619	0.770	123.4	1.98	2.07	0.0467	4.30	2604
8ERT5	485	42	2573	0.796	126.4	4.94	1.05	0.0492	4.69	2543
8ERT6	485	42	2551	0.798	125.0	2.09	2.06	0.0362	3.45	2543
8ERT7	485	42	2553	0.795	124.5	2.09	4.09	0.0456	4.32	2543
8ERT8	485	46	2723	0.875	129.5	2.02	1.04	0.0333	3.44	2718
8ERT9	485	46	2724	0.879	130.5	1.96	4.07	0.0450	4.69	2718

Table 10. Test Cases for Forced Response with Upper Surface Spoiler on PAPA, $\delta_{te_o} = 0$

Test Case No.	Test	Run	Point No.	M	q psf	α deg.	δ_{us_o} deg.	δ_{us} deg.	k	Frequency Hz	Wind-Off Zero Point No.
8ERU1	485	39	2434	0.649	116.3	1.89	-10.03	1.00	0.0452	3.50	2398
8ERU2	485	39	2435	0.649	115.7	1.90	-10.02	2.07	0.0582	4.50	2398
8ERU3	485	43	2630	0.768	123.5	1.92	-4.97	2.11	0.0375	3.44	2604
8ERU4	485	43	2631	0.770	124.0	1.93	-4.97	0.99	0.0469	4.32	2604
8ERU5	485	42	2587	0.799	127.7	5.24	-5.09	1.00	0.0504	4.81	2543
8ERU6	485	42	2562	0.795	125.6	2.04	-5.07	2.07	0.0382	3.63	2543
8ERU7	485	42	2563	0.800	126.7	2.02	-5.07	2.05	0.0452	4.32	2543
8ERU8	485	46	2729	0.873	130.2	1.99	-5.07	4.15	0.0332	3.44	2718
8ERU9	485	46	2730	0.874	130.3	2.00	-5.07	4.16	0.0452	4.69	2718

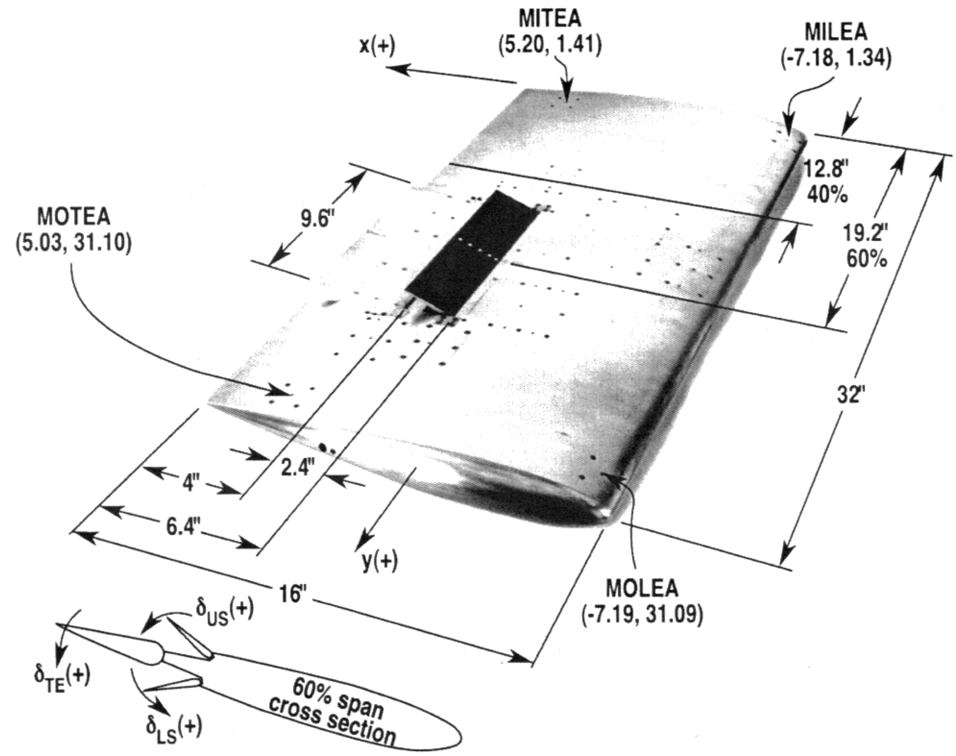

Figure 1. BACT model, dimensions in inches and origin at root midchord.

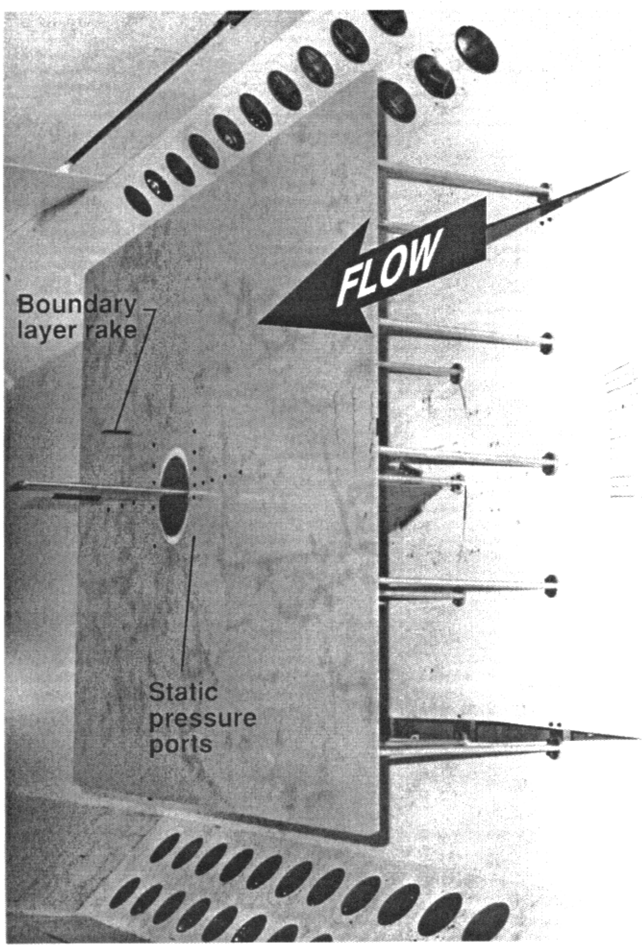

Figure 2. BACT model installed in Transonic Dynamics Tunnel

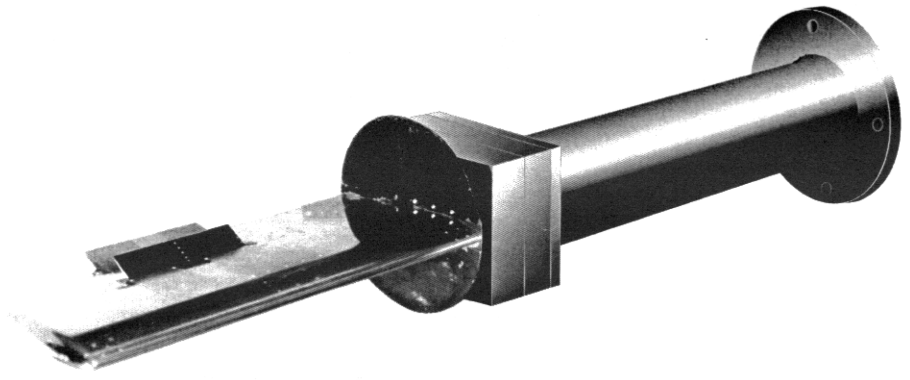

a) Model on the rigid mount (balance and strut).

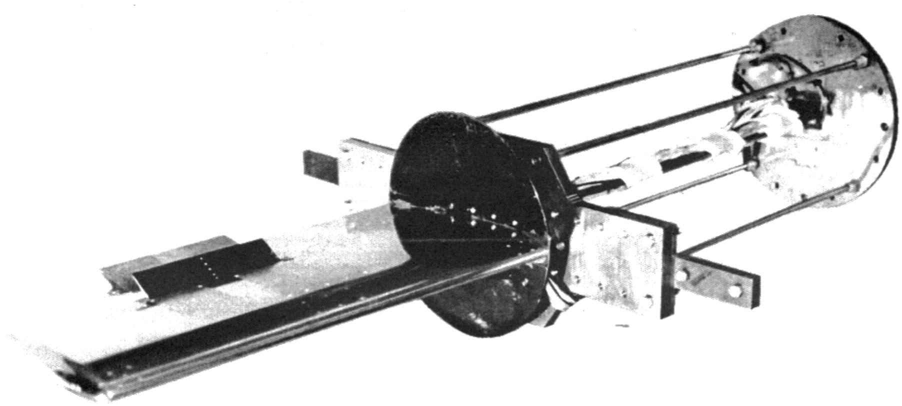

b) Model on the flexible mount (PAPA).

Figure 3. BACT model on rigid and flexible mount systems.

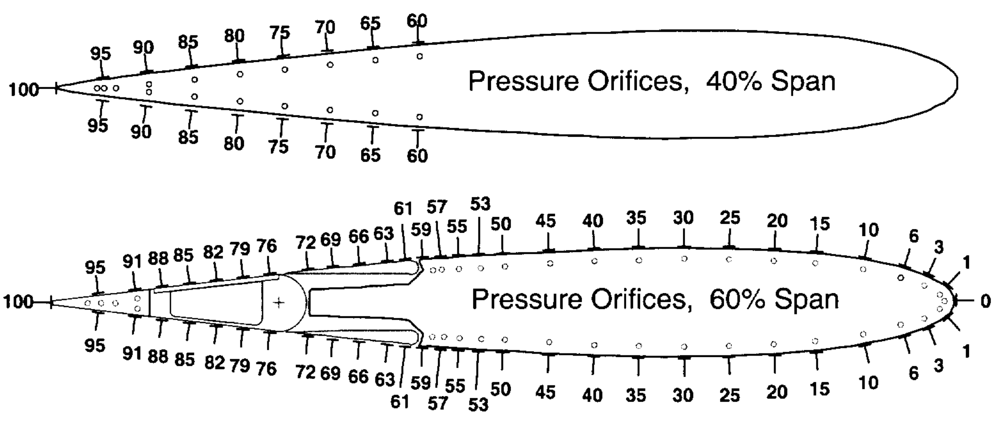

Figure 4. Pressure orifice locations, percent chord.

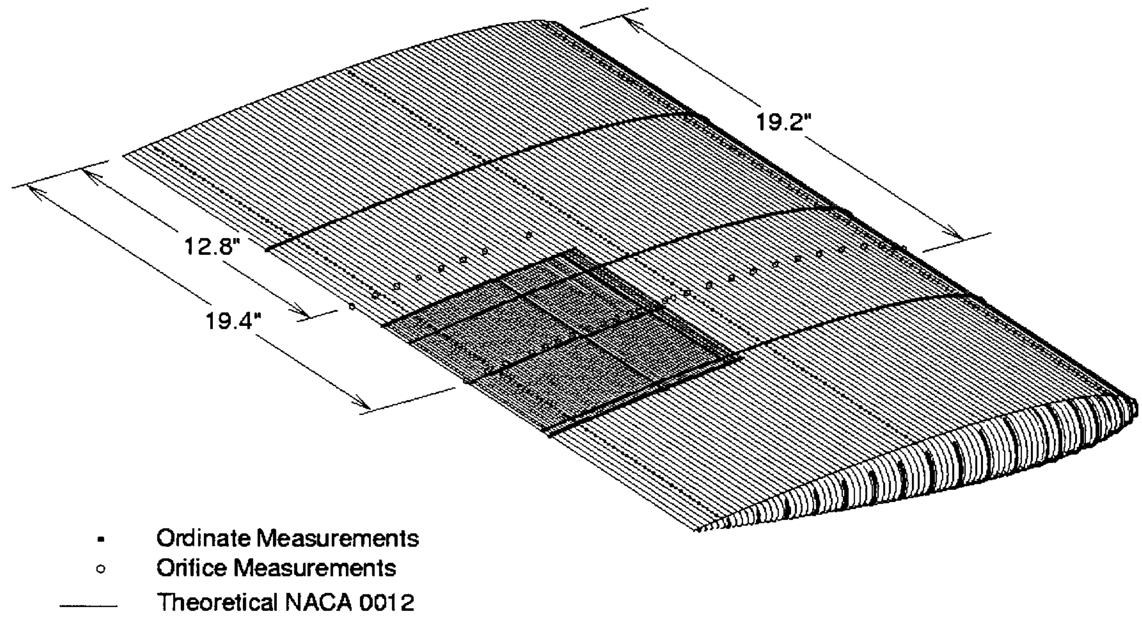

a) Ordinate measurements for entire model.

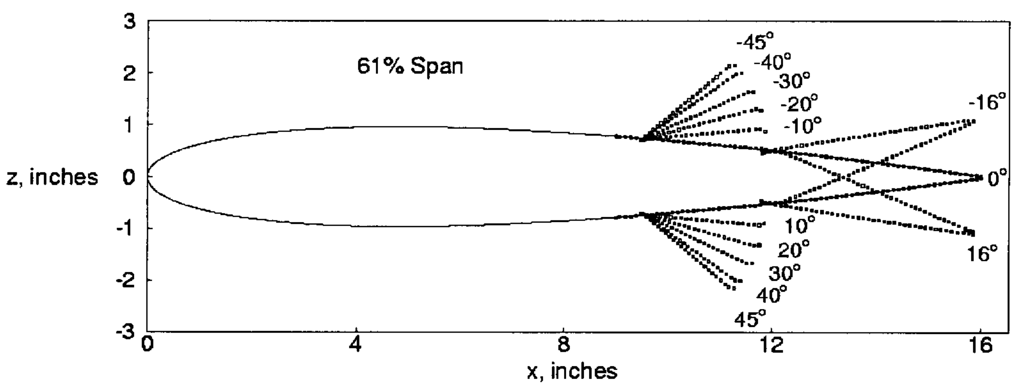

b) Ordinate measurements at 60% span.

Figure 5. Ordinate measurements for the BACT model.

```
 Test Case   Point No   Wind-Off Zero Pt      TDT Test 485
   8EST33       203                132       BmpBACT/Static

   Mach No      q, psf    Rn*10**-6   gamma
     0.769      145.4       3.83      1.132

    alphao   delta te   delta us   delta ls    (degees)
      3.99      5.00       0.10      -0.10

  C-Normal F  C-Pitch M  C-Axial F  C-Roll M  C-Yaw M
     0.3675     0.1022     0.0108    0.2751    0.0216

                Upper surface at ETA = 0.60
   x/c     Cp Mean    Cp Min     Cp Max   CpStdDev   Chl No
  0.000     1.106      1.078      1.135     0.018       82
  0.010    -0.336     -0.386     -0.283     0.017       83
  0.030    -0.686     -0.728     -0.641     0.017       84
  0.060    -0.636     -0.687     -0.583     0.017       85
  0.100    -1.119     -1.139     -1.098     0.017       86
  0.150    -1.218     -1.246     -1.188     0.018       87
  0.200    -1.315     -1.353     -1.270     0.021       88
  0.250    -1.340     -1.377     -1.297     0.022       89
  0.300    -1.065     -1.336     -0.583     0.170       90
  0.350    -0.545     -0.746     -0.422     0.043       91
  0.400    -0.399     -0.495     -0.322     0.024       92
  0.450    -0.336     -0.453     -0.219     0.033       93
  0.500    -0.296     -0.393     -0.200     0.027       94
  0.530    -0.270     -0.367     -0.159     0.027       95
  0.550    -0.298     -0.382     -0.189     0.027       96
  0.570    -0.278     -0.359     -0.186     0.025       97
  0.590    -0.230     -0.297     -0.168     0.017       98
  0.610    -0.279     -0.399     -0.153     0.032      129
  0.630    -0.252     -0.349     -0.157     0.028      130
  0.660    -0.226     -0.314     -0.104     0.027      131
  0.690    -0.227     -0.307     -0.127     0.026      132
  0.720    -0.235     -0.312     -0.137     0.024      133
  0.760    -0.296     -0.397     -0.172     0.030      134
  0.790    -0.157     -0.234     -0.058     0.024      135
  0.820    -0.073     -0.142      0.010     0.021      136
  0.850    -0.015     -0.077      0.063     0.019      137
  0.880     0.045     -0.012      0.104     0.017      138
  0.910     0.110      0.059      0.158     0.014      139
  0.950     0.162      0.112      0.213     0.014      140
  1.000     0.213      0.169      0.259     0.013      141

                Lower surface at ETA = 0.60
   x/c     Cp Mean    Cp Min     Cp Max   CpStdDev   Chl No
  0.010     0.720      0.674      0.771     0.017      114
  0.030     0.284      0.228      0.342     0.016      113
  0.060     0.065      0.015      0.118     0.014      112
                                 .
                                 .
  0.910     0.110      0.066      0.150     0.012      143
  0.950     0.155      0.132      0.177     0.007      142

                Upper surface at ETA = 0.40
   x/c     Cp Mean    Cp Min     Cp Max   CpStdDev   Chl No
  0.600    -0.198     -0.304     -0.099     0.027       65
  0.650    -0.160     -0.244     -0.072     0.026       66
                                 .
                                 .
  0.950     0.124      0.081      0.185     0.015       72
  1.000     0.212      0.181      0.254     0.010       73

                Lower surface at ETA = 0.40
   x/c     Cp Mean    Cp Min     Cp Max   CpStdDev   Chl No
  0.600    -0.126     -0.202     -0.025     0.023       81
  0.650    -0.083     -0.142     -0.007     0.019       80
                                 .
                                 .
  0.900     0.085      0.035      0.146     0.014       75
  0.950     0.127      0.081      0.181     0.014       74
```

Figure 6. Example of static control surface deflection data file for BACT.

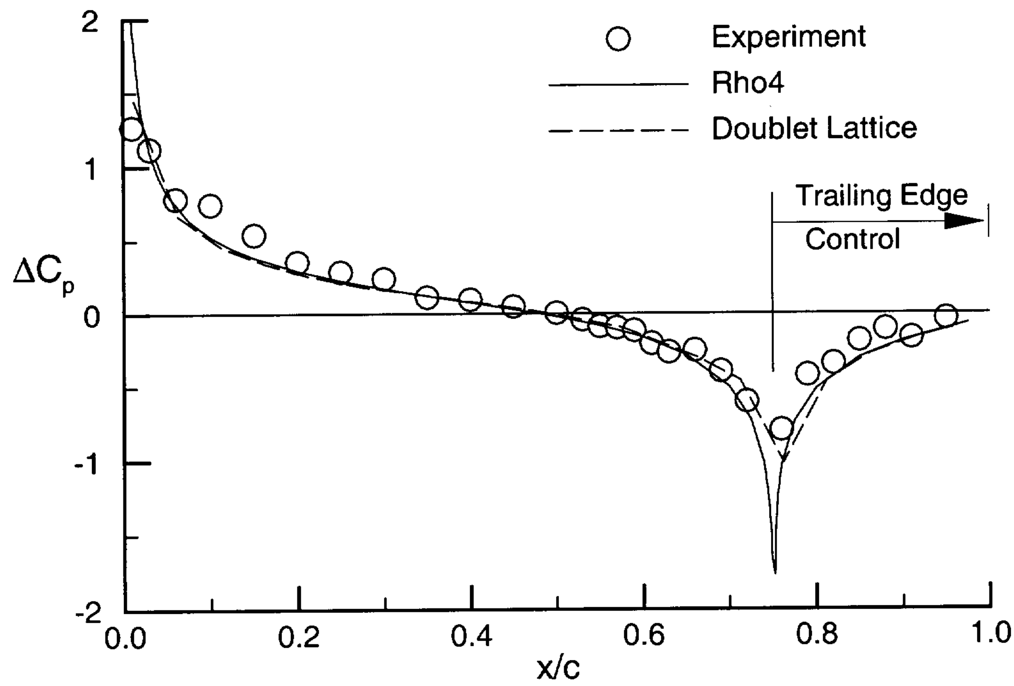

a) M=0.65, Test 485, Point 1945.

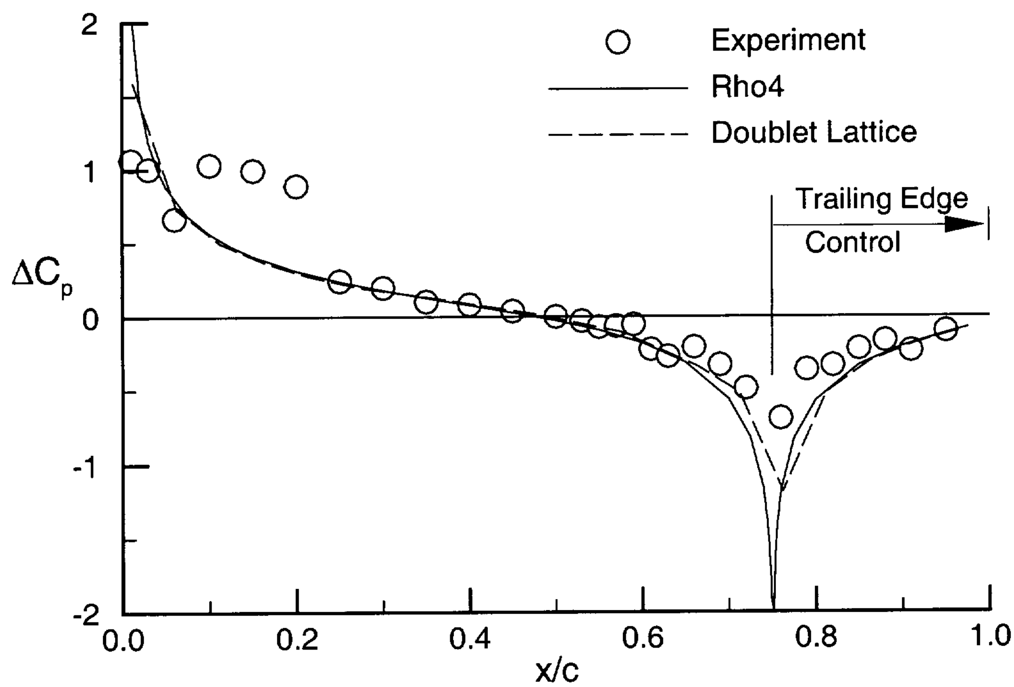

b) M=0.75, Test 485, Point 1686.

Figure 7. Comparison of BACT static results with linear aerodynamics, α=4° and δ_{TE}=-10°.

Test Case	Point No	Wind-Off Zero Pt	TDT Test 485
8EOT31	1094	1060	BmpBACT/TE Oscillations

Mach No	q, psf	Rn*10**-6	gamma	Vel, fps	freq, Hz	k
0.771	149.00	3.86	1.132	387.7	10.020	0.1083

alphao	delta teo	delta uso	delta lso	te osc ampl (degees)
4.01	0.10	-0.12	0.14	3.87

C-Normal-F	C-Pitch-M	C-Axial-F	C-Roll-M	C-Yaw-M (means)	nsamples
0.3013	0.0987	0.0079	0.2227	0.0161	4989

Upper surface at ETA = 0.60

x/c	Cp Mean	Cp Min	Cp Max	CpStdDev	Real(Cp)	Imag(Cp)	Chl No
0.000	1.093	1.065	1.131	0.008	-0.0021	0.0029	82
0.010	-0.328	-0.397	-0.267	0.019	-0.0068	0.0118	83
0.030	-0.705	-0.762	-0.645	0.016	-0.0053	0.0112	84
0.060	-0.638	-0.718	-0.578	0.018	-0.0068	0.0119	85
0.100	-1.096	-1.111	-1.076	0.005	-0.0007	0.0017	86
0.150	-1.228	-1.248	-1.203	0.006	-0.0017	0.0035	87
0.200	-1.252	-1.295	-1.205	0.012	-0.0041	0.0079	88
0.250	-1.288	-1.335	-1.224	0.014	-0.0049	0.0085	89
0.300	-0.926	-1.344	-0.514	0.203	-0.1579	0.0967	90
0.350	-0.493	-0.733	-0.358	0.051	-0.0383	0.0175	91
0.400	-0.401	-0.524	-0.318	0.029	-0.0211	0.0027	92
0.450	-0.334	-0.473	-0.213	0.037	-0.0205	-0.0032	93
0.500	-0.289	-0.418	-0.184	0.031	-0.0236	-0.0034	94
0.530	-0.270	-0.384	-0.153	0.032	-0.0261	-0.0036	95
0.550	-0.233	-0.342	-0.125	0.032	-0.0285	-0.0035	96
0.570	-0.223	-0.328	-0.122	0.032	-0.0306	-0.0034	97
0.590	-0.215	-0.301	-0.139	0.026	-0.0283	-0.0025	98
0.610	-0.227	-0.401	-0.072	0.056	-0.0657	-0.0055	129
0.630	-0.190	-0.355	-0.041	0.055	-0.0670	-0.0055	130
0.660	-0.167	-0.327	0.004	0.058	-0.0726	-0.0069	131
0.690	-0.150	-0.311	0.029	0.065	-0.0857	-0.0083	132
0.720	-0.100	-0.268	0.088	0.078	-0.1061	-0.0107	133
0.760	-0.087	-0.356	0.157	0.128	-0.1762	-0.0195	134
0.790	-0.057	-0.224	0.114	0.074	-0.0982	-0.0168	135
0.820	0.008	-0.106	0.134	0.049	-0.0612	-0.0146	136
0.850	0.052	-0.043	0.146	0.033	-0.0365	-0.0129	137
0.880	0.055	-0.019	0.135	0.023	-0.0193	-0.0107	138
0.910	0.155	0.100	0.218	0.016	-0.0098	-0.0087	139
0.950	0.197	0.148	0.251	0.015	-0.0005	-0.0059	140
1.000	0.266	0.209	0.316	0.015	-0.0052	-0.0017	141

Lower surface at ETA = 0.60

x/c	Cp Mean	Cp Min	Cp Max	CpStdDev	Real(Cp)	Imag(Cp)	Chl No
0.010	0.716	0.665	0.780	0.014	0.0057	-0.0071	114
0.030	0.272	0.211	0.340	0.017	0.0073	-0.0080	113
0.060	0.010	-0.046	0.069	0.016	0.0078	-0.0078	112
			.				
			.				
0.910	0.064	0.016	0.118	0.015	0.0080	0.0087	143
0.950	0.191	0.166	0.216	0.008	-0.0014	0.0059	142

Upper surface at ETA = 0.40

x/c	Cp Mean	Cp Min	Cp Max	CpStdDev	Real(Cp)	Imag(Cp)	Chl No
0.600	-0.201	-0.312	-0.082	0.033	-0.0270	-0.0050	65
0.650	-0.162	-0.269	-0.054	0.033	-0.0307	-0.0052	66
			.				
			.				
0.950	0.166	0.123	0.217	0.014	-0.0041	-0.0011	72
1.000	0.307	0.278	0.338	0.009	-0.0002	-0.0007	73

Lower surface at ETA = 0.40

x/c	Cp Mean	Cp Min	Cp Max	CpStdDev	Real(Cp)	Imag(Cp)	Chl No
0.600	-0.144	-0.249	-0.032	0.033	0.0310	-0.0018	81
0.650	-0.111	-0.206	-0.012	0.033	0.0356	-0.0007	80
0.700	-0.077	-0.168	0.038	0.035	0.0398	0.0011	79
			.				
			.				
0.900	0.094	0.030	0.154	0.019	0.0154	0.0019	75
0.950	0.160	0.105	0.216	0.016	0.0078	0.0008	74

Figure 8. Example of oscillating control surface data file for BACT.

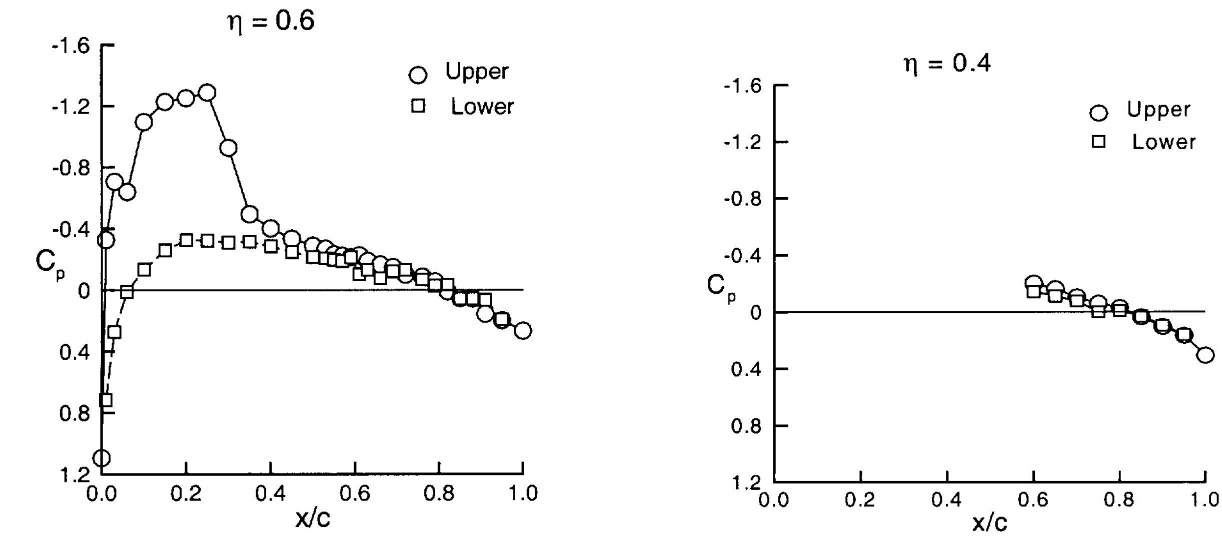

(a) Mean pressure coefficient during control surface oscillation

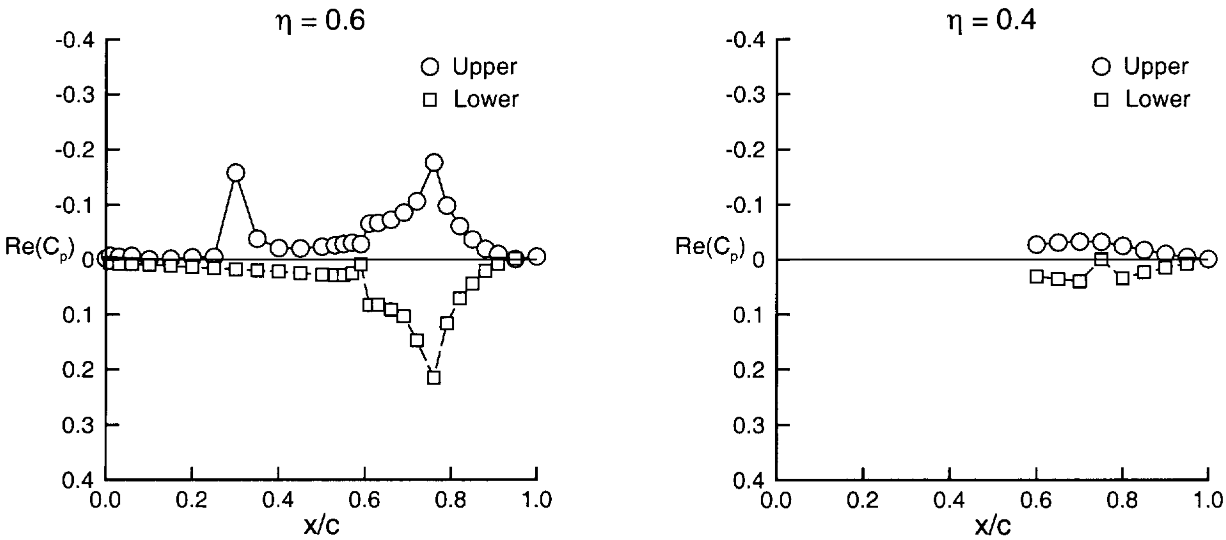

(b) Real part of pressure coefficient during control surface oscillation

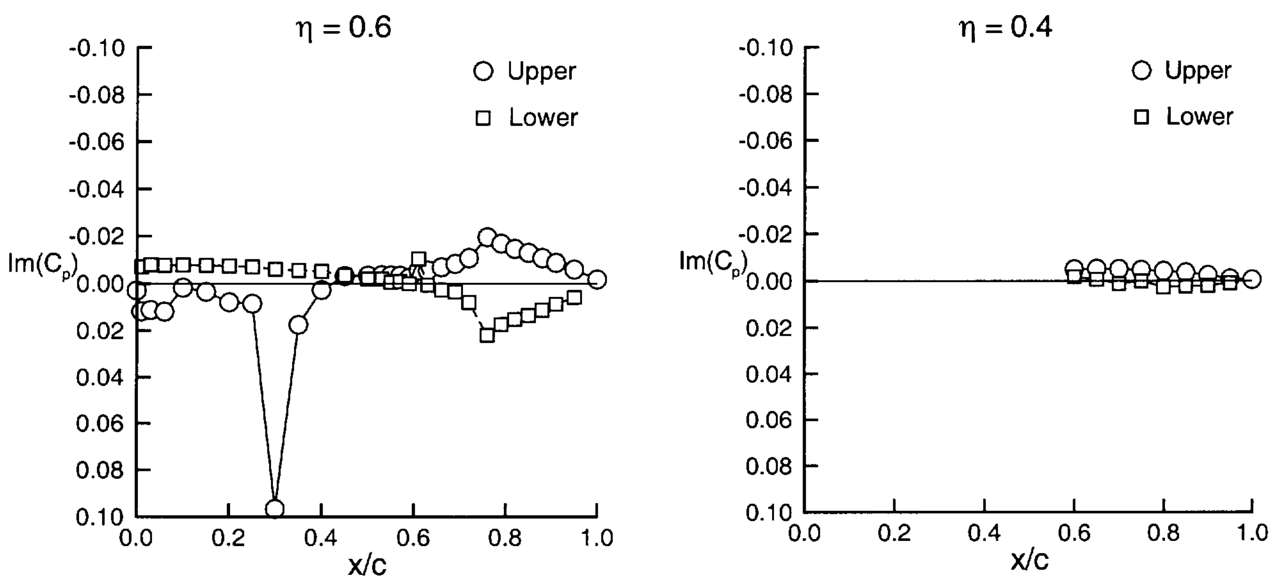

(c) Imaginary part of pressure coefficient during control surface oscillation

Figure 9. Unsteady pressures measured during trailing edge control oscillations, Test Case 8EOT31, M=0.77, $\alpha = 4^{\circ}$.

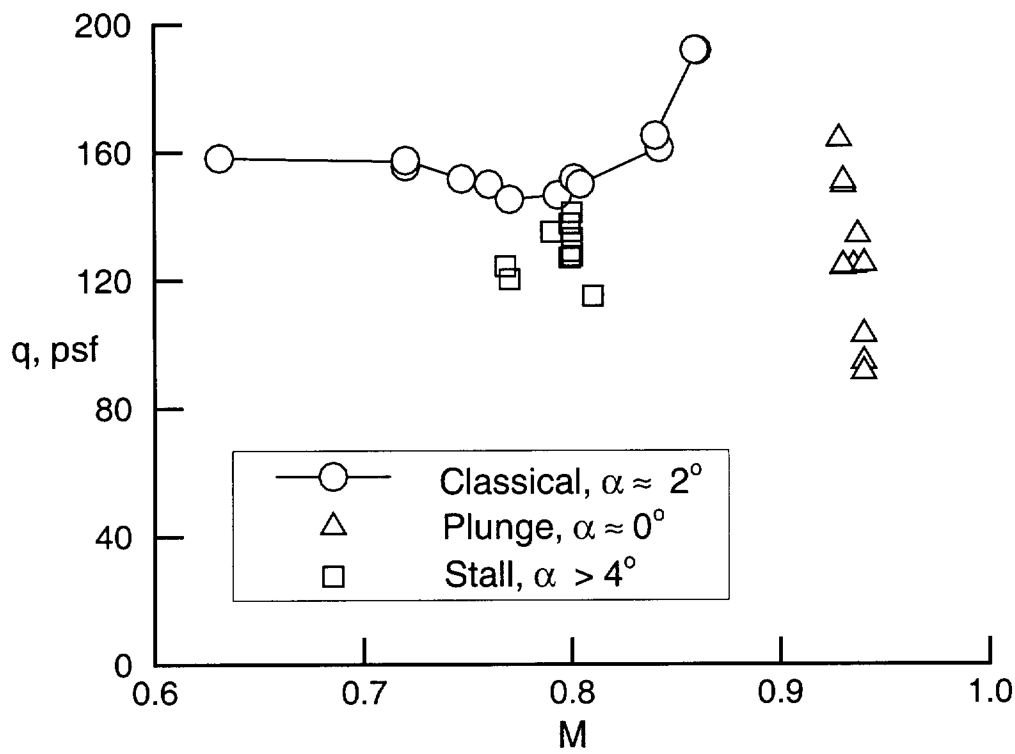

(a) Flutter dynamic pressure.

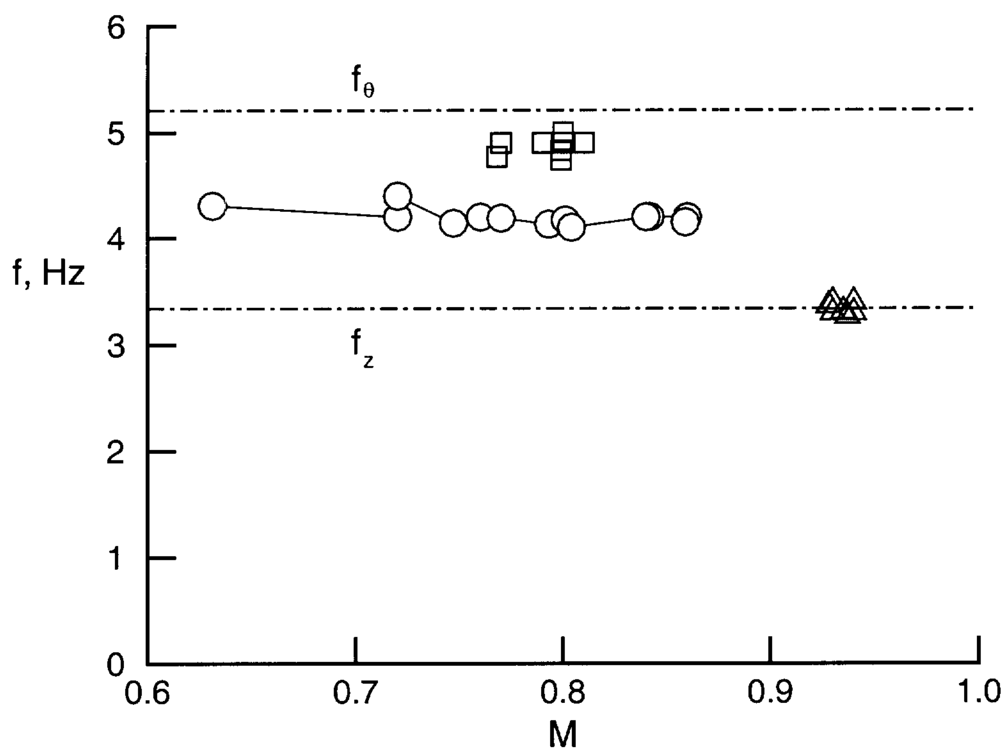

(a) Flutter frequencies.

Figure 10. BACT flutter instabilities.

8C. BENCHMARK ACTIVE CONTROLS TECHNOLOGY (BACT) WING CFD RESULTS

David M. Schuster
Aerospace Engineer
D.M.Schuster@LaRC.nasa.gov

Robert E. Bartels
Aerospace Engineer
R.E.Bartels@LaRC.nasa.gov

Aeroelasticity Branch, Structures and Materials
Mail Stop 340
NASA Langley Research Center,
Aeroelasticity Branch,
Hampton, Virginia 23681-2199 USA

NOMENCLATURE

α	Angle of attack (deg.)	f	Frequency of aileron oscillation (Hz)
δ_{TE}	Aileron mean deflection angle (deg.)	C	Wing chord (16 in.)
δ_{SP}	Spoiler deflection angle (deg.)	M	Mach number
η	Spanwise coordinate (=y/ytip)	Re	Reynolds number, based on wing chord
θ_{TE}	Aileron oscillation amplitude (deg.)		

INTRODUCTION

The Benchmark Active Controls Technology (BACT) wing test (see chapter 8E) provides data for the validation of aerodynamic, aeroelastic, and active aeroelastic control simulation codes. These data provide a rich database for development and validation of computational aeroelastic and aeroservoelastic methods. In this vein, high-level viscous CFD analyses of the BACT wing have been performed for a subset of the test conditions available in the dataset. The computations presented in this section investigate the aerodynamic characteristics of the rigid clean wing configuration as well as simulations of the wing with a static and oscillating aileron and spoiler deflection. Two computational aeroelasticity codes extensively used at NASA Langley Research Center are implemented in this simulation. They are the ENS3DAE and CFL3DAE computational aeroelasticity programs. Both of these methods solve the three-dimensional compressible Navier-Stokes equations for both rigid and flexible vehicles, but they use significantly different approaches to the solution of the aerodynamic equations of motion. Detailed descriptions of both methods are presented in the following section.

CFD METHODS

Two three-dimensional compressible Euler/Navier-Stokes aeroelastic methods are used to compute the steady and unsteady flow about the BACT geometry. The first method, known as ENS3DAE was developed in the late 1980's by Lockheed-Georgia under contract to the United States Air Force Wright Laboratory. This program has been used to solve numerous aerodynamic and aeroelastic problems about a wide range of geometries including wings, wing/fuselage, propulsion, and integrated airframe/propulsion configurations. The second method, known as CFL3DAE has been developed more recently at the NASA Langley Research Center. While several aeroelastic versions of CFL3D have had limited application, the aerodynamic base version of the code has also been used to analyze a very wide range of problems and has become a staple for computational aerodynamics research throughout the industry.

DESCRIPTIONS OF CODES

The ENS3DAE computational aeroelasticity method is described in Table 1. ENS3DAE solves the full three-dimensional compressible Reynolds averaged Navier-Stokes equations using an implicit approximate factorization algorithm. Central finite differences are used to spatially discretize the problem. A three-dimensional implementation of the Beam-Warming implicit scheme is employed for the temporal integration. Blended second and fourth order dissipation is added to the explicit right-hand-side of the equations, and implicit second order dissipation is added to improve the diagonal dominance of the matrix system. The method accepts either single or multiple block curvilinear grid topologies and can be run in a steady state or time-accurate mode by specifying local or global time stepping, respectively. Turbulence characteristics are predicted using the Baldwin-Lomax algebraic turbulence model or the Johnson-King model. For the present calculations, the Baldwin-Lomax model is used with transition assumed to be at the leading edge of the wing. A multigrid option for steady flows has recently been added to the method and the code has been explicitly written to take advantage of vectorization. Directives for parallel operation on shared memory processors are also included in the programming and the method is regularly run on 8 or more processors. Since dynamic aeroelastic and oscillating control surface simulations require grid models that deform in time, a Geometric Conservation Law (GCL) has also been incorporated in this code and in the code CFL3DAE.

The CFL3DAE computational aeroelasticity method is described in Table 2. CFL3DAE solves the thin-layer three-dimensional compressible Reynolds averaged Navier-Stokes equations. The integral form of the equations is spatially discretized with volume integrals evaluated at cell centers and fluxes evaluated at cell faces. Typically, upwind differencing of the fluxes is used. Here, third order upwind-biased Roe's flux difference splitting and a minmod flux limiter and second order accurate backward time differencing are used. An implicit approximate factorization algorithm is used to solve the equations. Pseudo time sub-iteration (τ-TS) is used to accelerate convergence at each time step. CFL3D version 5.0, on which the current aeroelastic version of the code is based, includes many turbulence models. The turbulence model used in the present computations is the Spalart-Allmaras model, used here because of its performance in the presence of separated flow and because of past excellent performance in computations with large time step. The flow is assumed to be fully turbulent beginning at the wing leading edge. There have been several aeroelastic versions of the code developed. The present version incorporates a new deforming mesh scheme based on the spring analogy and incorporates the GCL in the Navier-Stokes equations. Special attention has been paid to treatment of the grid at wall boundaries and in the wake. In particular, the orthogonality of the grid points within the boundary layer is maintained even at large surface deflection. Although not used in the computations discussed in this paper, the code also has an aeroelastic capability. Static and dynamic aeroelastic computations are possible. For the simulation of unsteady responses, a closely coupled time marching solution of the aeroelastic equations of motion is obtained using a predictor-corrector linear finite dimensional state space formulation of the uncoupled modal equations.

Another primary difference between ENS3DAE and CFL3DAE is the approach used to deform the grids for problems involving elastic and control surface deflections. ENS3DAE uses a simple, one-dimensional algebraic grid shearing method to deform the grid. This algorithm has proven to be very efficient and robust for many problems of interest. However, deformation of the grid using this approach does not properly account for rigid body rotation. Thus for control surface motions, as analyzed in this research, some stretching of the control surface is realized as it cycles through its range of motion.. The present CFL3DAE code models prescribed wing or control surface motion as true solid body motion, eliminating this potential source of error. The movement of the wake cut has also been addressed. CFL3DAE extends the wake cut from the trailing edge by bisecting the trailing edge upper and lower surfaces. An exponential decay down stream returns the wake cut to a horizontal asymptote well before one chord length has passed. In contrast, ENS3DAE maintains the original trajectory of the wake downstream of the trailing edge, allowing the wake cut to simply float up and down with the motion of the trailing edge.

The specific grids used in this study are also detailed in Tables 1 and 2. Both ENS3DAE and CFL3DAE used grids having identical dimensions and nearly identical grid spacing for the static aileron cases. The two codes used identically dimensioned grids for the dynamic case, however, with somewhat different clustering at the hinge line. The solution with CFL3DAE was made with more clustering of grids in the stream wise direction at the hinge line, which will account for some of the differences in the dynamic results to follow. Furthermore, differences in the grid motion algorithms employed by the codes during the dynamic motion of the aileron caused the grids to differ as the dynamic solution progressed. The grid dimensions given in the tables are organized as chordwise X spanwise X normal. The grid size is specified as the number of vertices in the grid. The grid type specified in item 2.4 refers specifically to the grid used for these solutions. Both ENS3DAE and CFL3DAE are capable of analyzing a wide range of structured grid topologies.

The computational modeling of the aileron is an important issue in these analyses. The aileron is modeled as a continuous surface with the wing. There are no gaps modeled at the hinge line or at the spanwise edges of the control surface. Therefore, the flow near these edges is not modeled accurately, especially for large control surface deflections. The impact of this approximation is difficult to assess using the BACT data since there are not detailed pressure measurements in close proximity to the spanwise edges of the aileron. The available experimental data does not appear to indicate a problem with this approximation for the cases analyzed. The spoiler is modeled in the computations as a ramp of finite span and backward facing step. There are three surface grids that are spaced out over the backward step surface. The spoiler deflection is modeled with the correct rigid body rotation of the control surface about the spoiler hinge line. This approach to modeling the spoiler clearly does not model the effect of the cavity beneath the spoiler, nor the gap between the spoiler and flap leading edge.

TEST CASES

Data for six test cases are presented in this section. There are five steady cases and one unsteady case as detailed in Table 3. ENS3DAE data is available for the first four steady cases and the unsteady case, while CFL3DAE data is available for cases 8EST23, 8EST24, 8ESU18 and 8EOT12. All computations were performed with the Mach number fixed at 0.77, and the Reynolds number is approximately 3.96 million. The experimental data for these cases were acquired in a test medium composed of R-12 gas, so the numerical value used for the ratio of specific heats was set to 1.132.

Solutions are presented for the upper and lower wing surface at two spanwise stations located at 40 and 60 percent span. The 40 percent span station is just inboard of the inboard edge of the aileron, while the 60 percent span station is located along the spanwise center of the aileron. The static data is presented as pressure coefficient versus X/C. The dynamic pressure data is decomposed into real and imaginary parts with the real part being the component of pressure that is in phase with the aileron motion, and the imaginary part the component of pressure which lags the aileron motion by 90 degrees phase. The real and imaginary parts of the dynamic pressure are scaled by the amplitude of the aileron motion in radians.

STEADY SOLUTIONS

Figures 1 through 4 show numerical computations for statically deflected aileron cases 8ESA9, 8ESA13, 8EST23, and 8EST24. Figures 1 and 2 compare numerical data from the ENS3DAE code with TDT experimental data for the clean wing with no aileron deflection. Data is presented at 40 and 60 percent span, and it should be noted that grid stations were located precisely at these stations, so no interpolation of the numerical data was required for this comparison. The zero degree angle-of-attack case presented in Figure 1 shows overall good agreement with the experimental data with ENS3DAE slightly under predicting the pressure coefficient on the forward part of the wing. Figure 2 shows the comparison at three degrees angle-of-attack. In this case, a shock has formed on the upper surface of the wing, and ENS3DAE over predicts the pressure on the forward portion of the wing and also predicts a shock location aft of the experimental data. The pressures on the aft portion of the wing and on the lower surface agree favorably with the experimental data. Figures 3 and 4 compare analyses using both ENS3DAE and CFL3DAE with experimental data for two cases with a statically deflected aileron. Figure 3 presents data for the aileron deflected five degrees with the wing at zero degrees angle-of-attack. Both ENS3DAE and CFL3DAE reasonably predict the pressure distribution for this case with ENS3DAE under predicting the pressures in the mid chord region slightly more than CFL3DAE. Figure 4 presents the same comparison for a case with the aileron deflected at ten degrees. Again, both ENS3DAE and CFL3DAE predict the pressure distribution at the 40 percent span station and on the lower surface of the 60 percent station very well. However, the experimental data indicates separation on the upper surface of the aileron at 60 percent span that is not predicted by either code. Both codes under predict the pressure near the aileron hinge line with ENS3DAE computing a pressure which is closer to the experimental data, but still in significant disagreement.

Figure 5 presents numerical computations for the statically deflected spoiler case 8ESU18. The grid used in this case is finer than that used in the deflected aileron computations. This is to resolve the additional surface slope discontinuities of the spoiler geometry compared to those of the trailing edge control surface cases. Grid points in the direction normal to the surface were added to somewhat better capture the reversed flow region and shear layer behind the spoiler trailing edge. In order to better capture the three dimensional character of the reversed flow behind the spoiler, the Navier-Stokes equation set for this computation included the thin layer viscous terms in all three coordinate directions. Note also that surface grid lines are again located at the 40 and 60 percent span locations, corresponding to the data stations at those locations. These are just inboard and mid span of the spoiler surface, which has spanwise edges at 45 and 75 percent span. The computed results show good agreement with the experiment, especially in the region of and aft of the spoiler. One minor exception to the overall agreement is at the 60 percent span station where a slight disagreement with the data is observed just ahead of the spoiler trailing edge and just ahead of the shock.

UNSTEADY SOLUTIONS

Both ENS3DAE and CFL3DAE have been used to analyze a dynamically oscillating aileron case. The flow conditions for this analysis are M = 0.77, zero degrees angle-of-attack, zero degrees mean aileron deflection, two degree aileron deflection amplitude and an aileron oscillation frequency of 5 Hz. These simulations were accomplished by performing a time-accurate solution of the Navier-Stokes equations using a user-specified time step. The simulation was run long enough to obtain 3 cycles of aileron motion, using a static analysis at the mean flow conditions as a starting point for the unsteady solution. Comparison of the second and third cycles of oscillation showed virtually no difference in the computed values of pressure over the period of the cycle. Thus all transients due to the impulsive start from the static solution were assumed to have passed by the end of the second cycle of oscillation. The third cycle of motion was then used to extract the mean pressure distribution as well as the components of pressure that are in-phase and out-of-phase with the aileron motion. The mean pressure distribution computed during this analysis is shown in Figure 6 which shows good agreement between ENS3DAE, CFL3DAE, and the experimental data. The real and imaginary pressure coefficients, normalized by the amplitude of the aileron motion, are presented in Figure 7 and 8. Figure 7 compares ENS3DAE, CFL3DAE, and experimental data obtained at the 40 percent span station. The upper plot displays the real component of the pressure while the lower plot shows the imaginary part of the pressure. The real component of pressure for all three sets of data compare very well over the entire length of the airfoil at this span station. Some variation is seen in the imaginary component of the pressure, but it should be noted that the scale on this plot has been significantly expanded over that of the real pressure component. Therefore, this component of the pressure is actually very small as compared to the real component of the pressure, and differences between the three sets of data are much smaller than they appear in this figure. Figure 8 compares the unsteady pressures at 60 percent span. Again both ENS3DAE and CFL3DAE compare very favorably with the experimental real component of the pressure with CFL3DAE capturing the peak in pressure near the aileron hinge line slightly better than ENS3DAE. As with the 40 percent span section, the imaginary pressure component at this station shows more variation between the three methods. As before, the scale is greatly expanded, and the actual differences between the data are quite small.

REFERENCES

1. Schuster, D. M.; Vadyak, J.; and Atta, E.: *Static Aeroelastic Analysis of Fighter Aircraft Using a Three-Dimensional Navier-Stokes Algorithm.* Journal of Aircraft, vol. 27, no. 9, Sep. 1990, pp. 820-825.

2. Schuster, D.M., Vadyak, J., and Atta, E.. *Flight Loads Prediction Methods for Fighter Aircraft.* WRDC-TR-89-3104, Wright Research and Development Center, Wright-Patterson Air Force Base, OH, November, 1989

3. Schuster, David M.; Beran, Philip S.; and Huttsell, Lawrence J.: *Application of the ENSDAE Euler/Navier-Stokes Aeroelastic Method.* Paper No. 3 in Numerical Unsteady Aerodynamics and Aeroelastic Simulation, AGARD Report 822, Mar. 1998.

4. Bartels, R. E. and Schuster, D. M., *Comparison of Two Navier-Stokes Aeroelastic Methods Using BACT Benchmark Experimental Data,* AIAA Paper 99-3157-CP, 17th AIAA Applied Aerodynamics Conference, Norfolk, VA, June, 1999.

5. Bartels, R. E., *An Elasticity Based Mesh Scheme Applied to the Computation of Unsteady Three-Dimensional Spoiler and Aeroelastic Problems,* AIAA Paper 99-3301-CP, 14th AIAA Computational Fluid Dynamics Conference, Norfolk, VA, June, 1999.

6. Rumsey, C., Biedron, R., and Thomas, J., *CFL3D: Its History and Some Recent Applications,* NASA TM-112861, May, 1997.

7. Krist, S. L., Biedron, R. T., and Rumsey, C. L., *CFL3D User's Manual (Version 5.0),* NASA TM-208444, June, 1998.

1 CODE	
1.1 Type	3-D Compressible Full (not thin layer) Reynolds Averaged Navier-Stokes.
1.2 Name	ENS3DAE
1.3 Description	Beam Warming implicit central finite difference scheme. Second order accurate in space and time. Local time stepping for steady state cases.
1.4 Available grid types	Multi-block structured.
1.5 Artificial viscosity	Pressure switched second/fourth order nonlinear explicit with spectral radius scaling. Second order implicit.
1.6 Convergence acceleration techniques	Local time stepping for steady-state. Grid sequencing.
1.7 Turbulence model	Baldwin-Lomax algebraic with FMAX search limiter to force FMAX to occur in viscous layer near surface. 3-D eddy viscosity smoothing to provide spatial history effects (helpful in separated flows).
1.8 Transition model	Fully turbulent.
1.9 Time-step	Local time stepping for static cases. Global time stepping for dynamic cases.
1.10 Convergence	Steady state forces for static cases, at least three cycles of motion for dynamic cases.
1.11 References	References 1, 2, 3
2 GRID	
2.1 Size of grid	153 x 53 x 41 = 332,469 points.
2.2 Y+	Less than 6.0 for entire wing surface.
2.3 Number of Surface grid points	113 x 41 = 4633 points.
2.4 Grid type	Single-zone C-H structured grid.
2.5 Distance of outer boundaries from the wing	6 root chords forward and aft of wing. 6 root chords above and below. Spanwise boundary 4 semi spans from centerline.
2.6 Modifications to geometry	None, theoretical NACA0012 airfoil section constant throughout span.
3 RESULTS	
3.1 Written Report	References 3, 4
3.2 Electronic data	Pressures.
3.3 Interpolation details	None
4 ADDITIONAL INFORMATION	
4.1 Platform	Cray C-90 at NASA Ames, multitasked on 8 shared processors.
4.2 CPU	
4.2.1 Total	Varies with case.
4.2.2 per iteration	19.5×10^{-6} sec/iteration/grid point.
4.2.3 per cycle	10,500 sec./cycle.
4.3 Convergence	Steady state loads for static cases, 3 cycles of motion for dynamic cases.
4.4 Memory	33 million words (multitasked on 8 processors).
4.5 Contact for further information	d.m.schuster@larc.nasa.gov

Table 1. ENS3DAE computational aeroelasticity code specifications.

1 CODE	
1.1 Type	3-D Compressible Thin Layer Reynolds Averaged Navier-Stokes.
1.2 Name	CFL3DAE
1.3 Description	Upwind finite volume implicit scheme. Second order accurate in time and upwind biased third order in space. Local time stepping and multigrid for steady state cases. Subiteration with CFL based local time stepping and multigrid for time accurate cases.
1.4 Available grid types	Multi-block structured.
1.5 Artificial viscosity	Flux difference (Roe) and flux vector (Van Leer) splitting. Min-mod flux limiter.
1.6 Convergence acceleration techniques	Local time stepping for steady-state. Multigrid.
1.7 Turbulence model	Spalart –Allmaras turbulence model.
1.8 Transition model	Fully turbulent.
1.9 Time-step	Local time stepping for static cases, Global time stepping with local time step subiteration for dynamic cases.
1.10 Convergence	Steady state forces for static cases, at least three cycles of motion for dynamic cases.
1.11 References	References 5, 6, 7
2 GRID	
2.1 Size of grid	153 x 53 x 41 = 332,469 points (aileron case). 201 x 73 x 73 = 1,071,129 points (spoiler case)
2.2 Y+	Less than 6.0 for entire wing surface.
2.3 Number of Surface grid points	113 x 41 = 4633 points (aileron case). 169 x 49 = 8281 points (spoiler case).
2.4 Grid type	Single-zone C-H structured grid.
2.5 Distance of outer boundaries from the wing	6 root chords forward and aft of wing. 6 root chords above and below. Spanwise boundary 4 semi spans from centerline.
2.6 Modifications to geometry	None, theoretical NACA0012 airfoil section constant throughout span.
3 RESULTS	
3.1 Written Report	Reference 4,5
3.2 Electronic data	Pressures.
3.3 Interpolation details	None.
4 ADDITIONAL INFORMATION	
4.1 Platform	Cray C-90 at NASA Ames, SGI Origin 2000.
4.2 CPU	
4.2.1 Total	Varies.
4.2.2 per iteration	13 X 10^{-6} sec/iteration/grid point (Cray C-90).
4.2.3 per cycle	2100 sec./cycle.
4.3 Convergence	Steady state loads for static cases, 3 cycles of motion for dynamic cases.
4.4 Memory	
4.5 Contact for further information	r.e.bartels@larc.nasa.gov

Table 2. CFL3DAE computational aeroelasticity code specifications.

Test Case	Mach No.	α (deg.)	freq. (Hz)	δ (deg.)	δ_{sp} (deg.)	Re $X10^6$
8ESA9	0.77	0.0	0.0	0.0	0.0	3.96
8ESA13	0.77	3.0	0.0	0.0	0.0	3.96
8EST23	0.77	0.0	0.0	5.0	0.0	3.96
8EST24	0.77	0.0	0.0	10.0	0.0	3.96
8ESU18	0.77	0.0	0.0	0.0	15.0	3.96
8EOT12	0.77	0.0	5.0	2.0	0.0	3.96

Table 3 Flow conditions used for comparisons.

BACT Viscous Analysis

M = 0.77, α = 0.0°, δ_{TE} = 0.0°, θ_{TE} = 0.0°, δ_{SP} = 0.0°, f = 0 Hz.

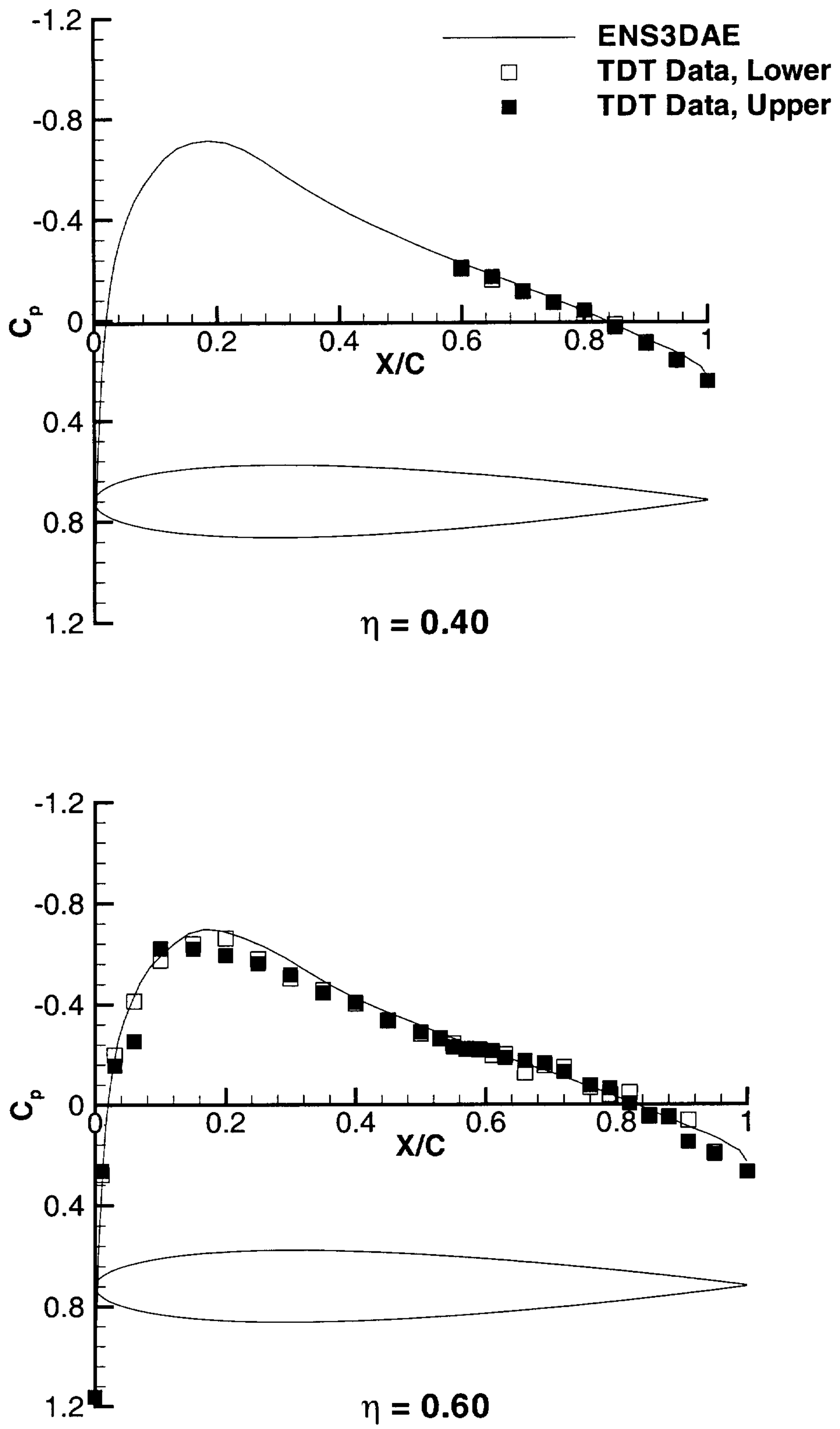

Figure 1. Comparison of theoretical and experimental results for the BACT wing at M = 0.77, α = 0.0°, δ_{TE} = 0.0°, θ_{TE} = 0.0°, δ_{SP} = 0.0°, f = 0.0 Hz, Re = 3.96 million.

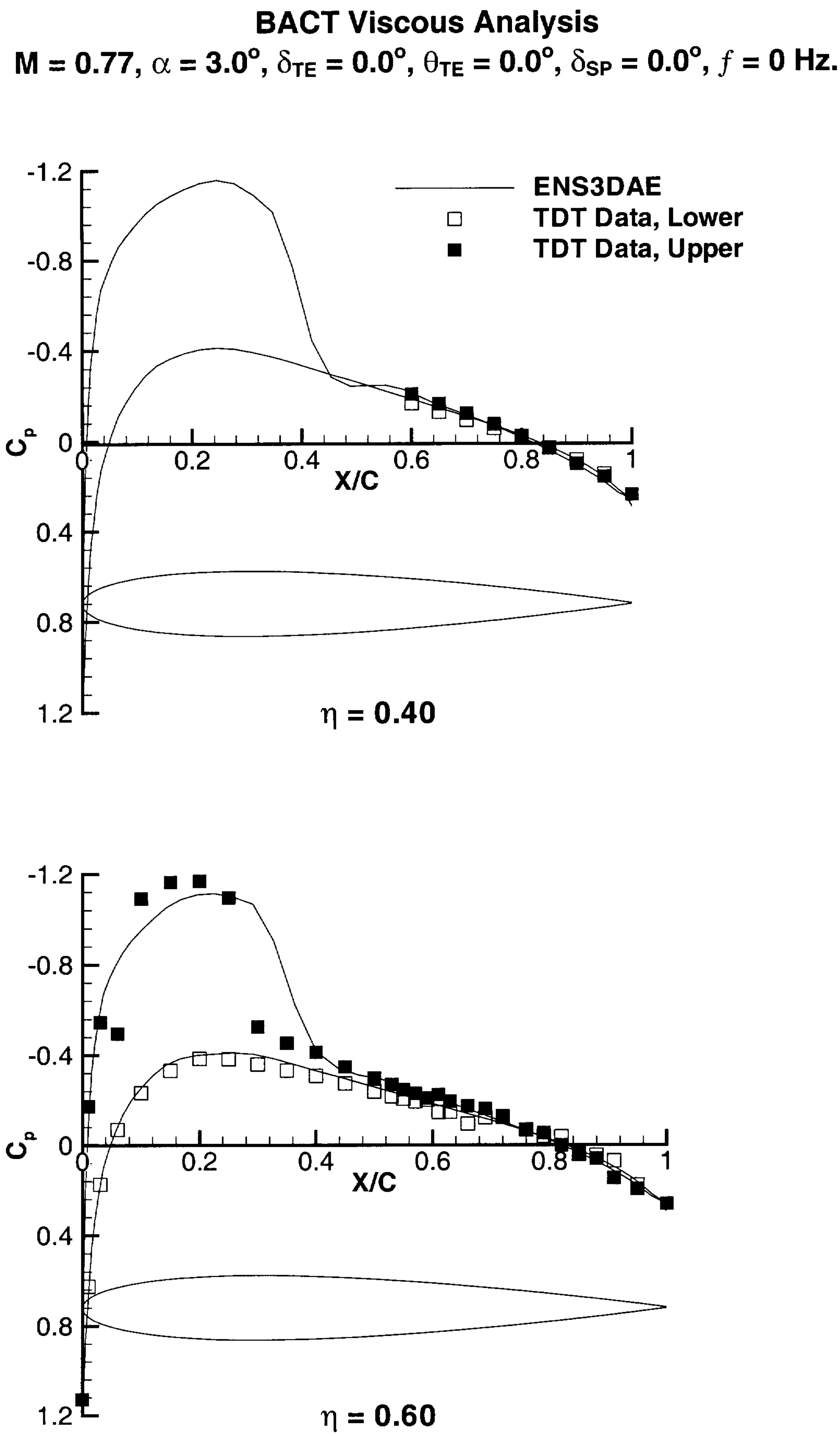

Figure 2. Comparison of theoretical and experimental results for the BACT wing at M = 0.77, $\alpha = 3.0^{\circ}$, $\delta_{TE} = 0.0^{\circ}$, $\theta_{TE} = 0.0^{\circ}$, $\delta_{SP} = 0.0^{\circ}$, $f = 0.0$ Hz, Re = 3.96 million.

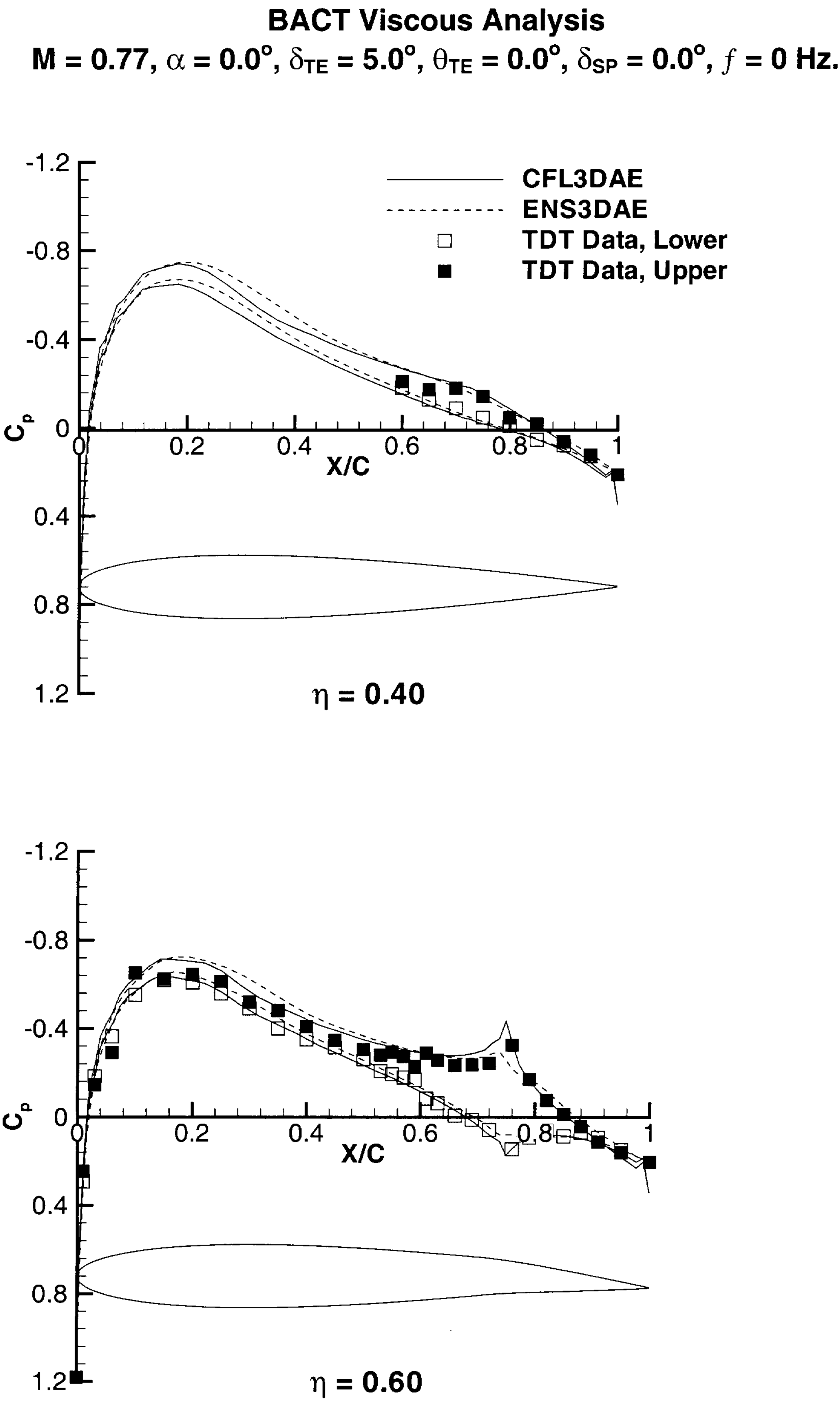

Figure 3. Comparison of theoretical and experimental results for the BACT wing at M = 0.77, $\alpha = 0.0^{\circ}$, $\delta_{TE} = 5.0^{\circ}$, $\theta_{TE} = 0.0^{\circ}$, $\delta_{SP} = 0.0^{\circ}$, $f = 0.0$ Hz, Re = 3.96 million.

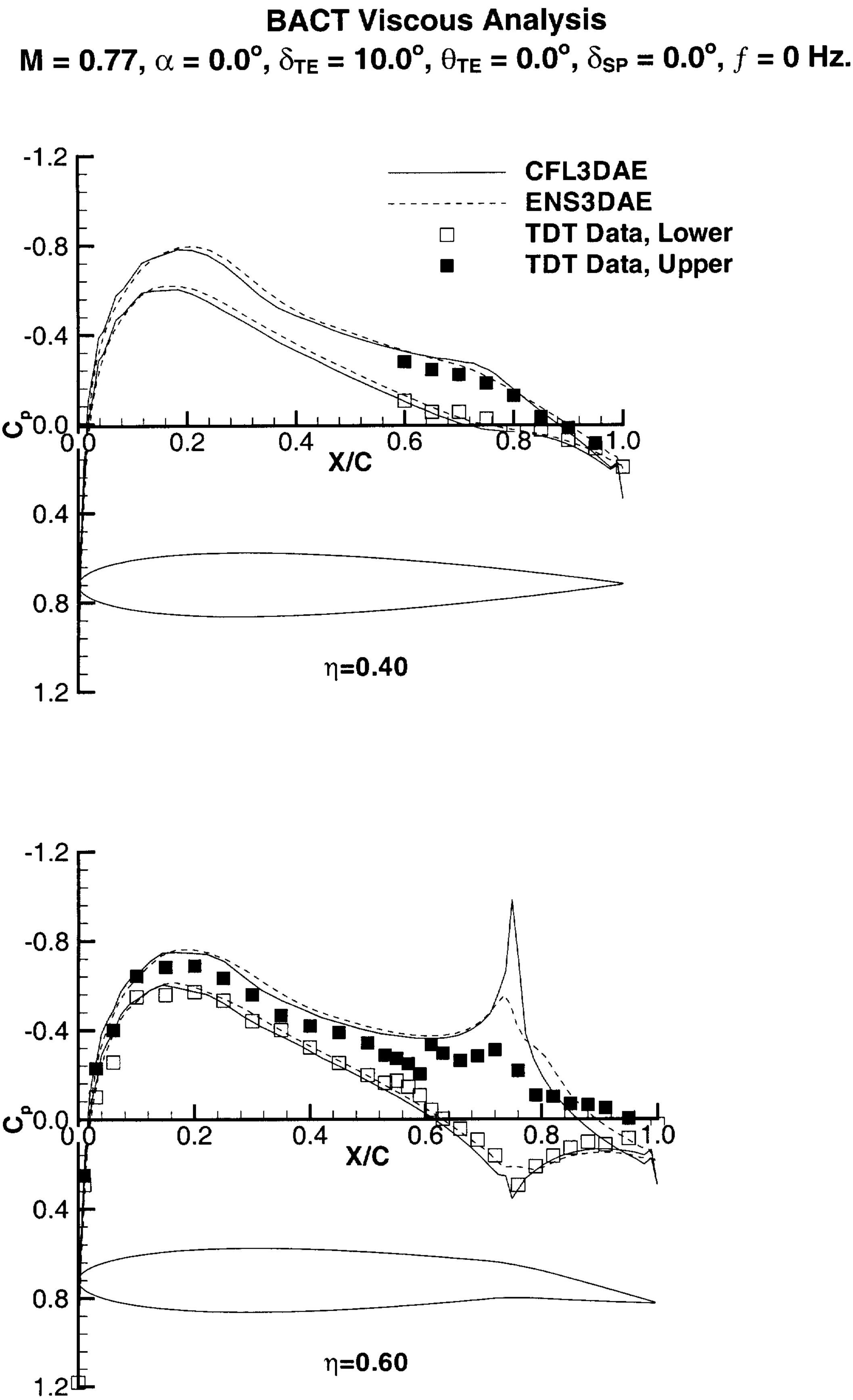

Figure 4. Comparison of theoretical and experimental results for the BACT wing at M = 0.77, $\alpha = 0.0^{\circ}$, $\delta_{TE} = 10.0^{\circ}$, $\theta_{TE} = 0.0^{\circ}$, $\delta_{SP} = 0.0^{\circ}$, $f = 0.0$ Hz, Re = 3.96 million.

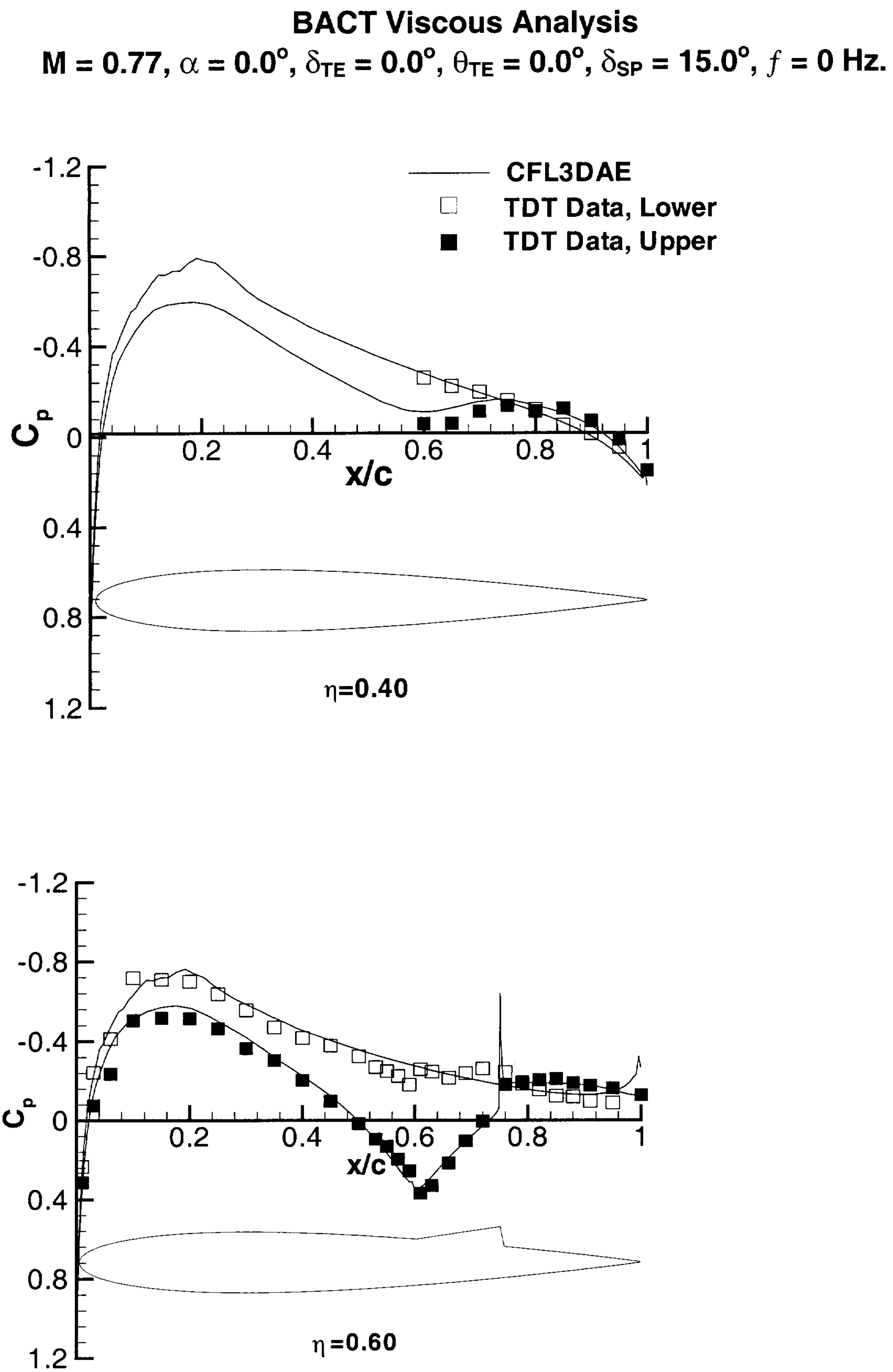

Figure 5. Comparison of theoretical and experimental results for the BACT wing at M = 0.77, $\alpha = 0.0^{\circ}$, $\delta_{TE} = 0.0^{\circ}$, $\theta_{TE} = 0.0^{\circ}$, $\delta_{SP} = 15.0^{\circ}$, $f = 0.0$ Hz, Re = 3.96 million.

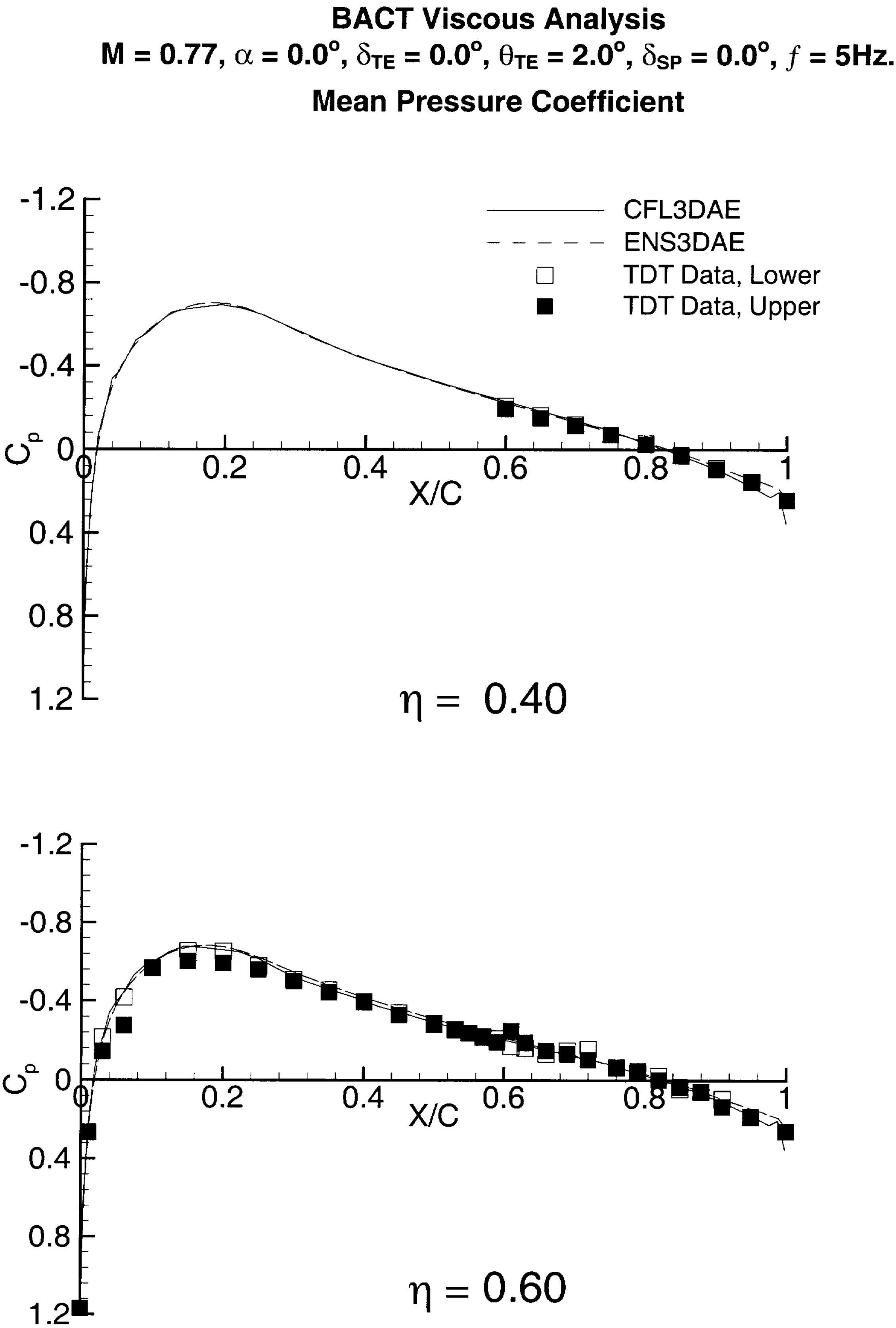

Figure 6. Comparison of theoretical and experimental mean pressures for the BACT wing at $M = 0.77$, $\alpha = 0.0^{\circ}$, $\delta_{TE} = 0.0^{\circ}$, $\theta_{TE} = 2.0^{\circ}$, $\delta_{SP} = 0.0^{\circ}$, $f = 5.0$ Hz, Re = 3.96 million.

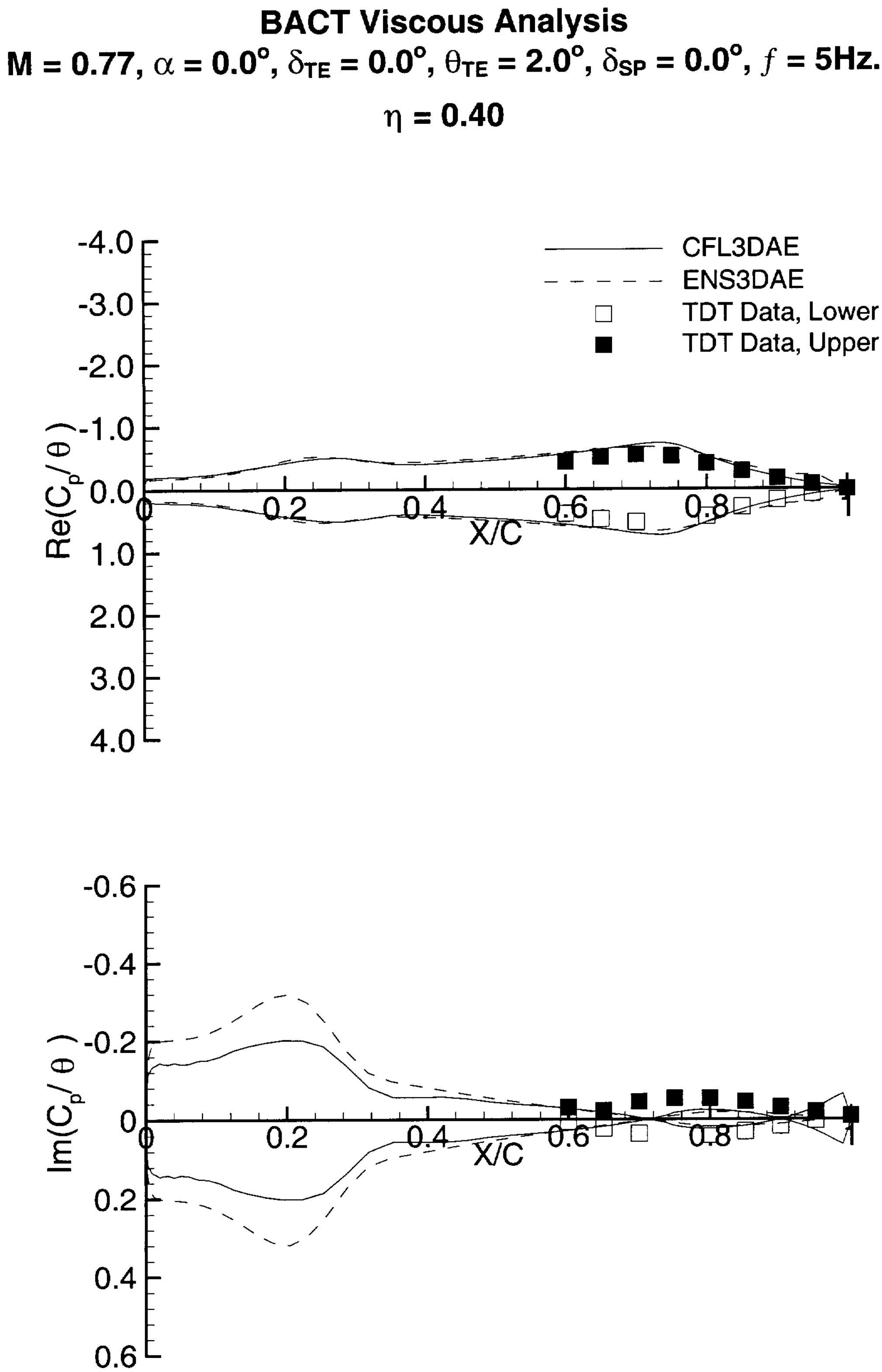

Figure 7. Comparison of theoretical and experimental unsteady pressures for the BACT wing at 40 percent span, M = 0.77, $\alpha = 0.0^{\circ}$, $\delta_{TE} = 0.0^{\circ}$, $\theta_{TE} = 2.0^{\circ}$, $\delta_{SP} = 0.0^{\circ}$, $f = 5.0$ Hz, Re = 3.96 million.

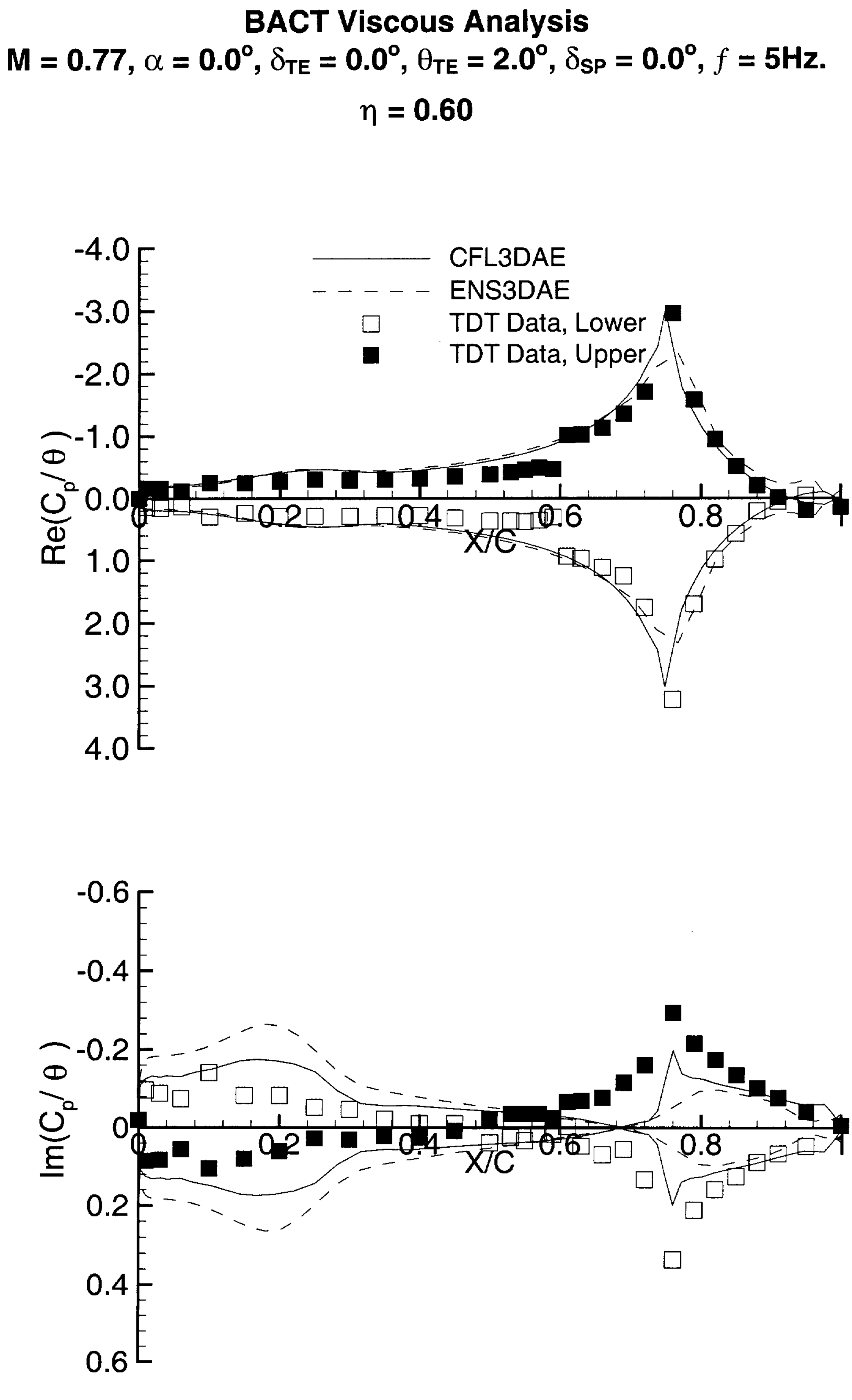

Figure 8. Comparison of theoretical and experimental unsteady pressures for the BACT wing at 60 percent span, M = 0.77, $\alpha = 0.0^{\circ}$, $\delta_{TE} = 0.0^{\circ}$, $\theta_{TE} = 2.0^{\circ}$, $\delta_{SP} = 0.0^{\circ}$, $f = 5.0$ Hz, Re = 3.96 million.

9E. TEST CASES FOR A CLIPPED DELTA WING WITH PITCHING AND TRAILING-EDGE CONTROL SURFACE OSCILLATIONS

Submitted by

Robert M. Bennett
Senior Aerospace Engineer
Aeroelasticity Branch, Materials and Structures
Mail Stop 340
NASA Langley Research Center
Hampton, VA 23681-2199 USA
r.m.bennett@larc.nasa.gov

INTRODUCTION

Steady and unsteady measured pressures for a Clipped Delta Wing (CDW) undergoing pitching oscillations and trailing-edge control surface oscillations have been presented in Ref 1 and 2. From the several hundred compiled data points, 22 static cases, 12 pitching-oscillation cases, and 12 control-surface-oscillation cases have been proposed for Computational Test Cases to illustrate the trends with Mach number, reduced frequency, and angle of attack.

The planform for this wing was derived by simplifying the planform of a proposed design for a supersonic transport which is described (Ref 3) as the Boeing 2707-300. The strake was deleted, the resulting planform was approximated by a trapezoid with an unswept trailing edge, and the twist and camber were removed. In order to facilitate pressure instrumentation, the thickness was increased to 6 percent from the typical 2.5 to 3 percent for the supersonic transport. The airfoil is thus a symmetrical circular arc section with $t/c = 0.06$. A wing of similar planform but with a thinner airfoil of $t/c = 0.03$ was used in the flutter investigations of Ref 4 and 5, and the buffet and stall flutter investigation of Ref 6. Flutter results are also reported both for the 3 per cent thick simplified wing and for a more complex SST model in Ref 7.

One of the consequences of the increased thickness of the clipped delta wing is that transonic effects are enhanced for Mach numbers near one. They are significantly stronger than would be the case for the thinner wing. Also, with the combination of high leading edge sweep of 50.5° and the sharp leading edge, a leading edge vortex forms on the wing at relatively low angles of attack, on the order of three degrees. The Appendix of Ref 1 discusses some of the vortex flow effects. In addition, a shock develops over the aft portion of the wing at transonic speeds such that at some angles of attack, there is both a leading edge vortex and a shock wave on the wing. Such cases are a computational challenge. Some previous applications of this data set have been for the evaluation of an aerodynamic panel method (Ref 8) and for evaluation of a Navier-Stokes capability (Ref 9-11). Linear theory and panel method results are also presented in Ref 1, which demonstrated the need for inclusion of transonic effects. Flutter calculations for the related wing with $t/c=0.03$ are given in Ref 4 and 12.

In this report several Test Cases are selected to illustrate trends for a variety of different conditions with emphasis on transonic flow effects. An overview of the model and tests are given, and the standard formulary for these data is listed. For each type of data, a sample table and a sample plot of the measured pressures are presented. A complete tabulation and plotting of the Test Cases is given in Ref 13. Only the static pressures and the1st harmonic real and imaginary parts of the pressures are available. All of the data for the test are included in a microfiche document in the original report (Ref 1) and are available in electronic file form. The Test Cases are also available as separate electronic files.

LIST OF SYMBOLS AND DEFINITIONS

c	local chord, ft (m)
c_r	wing root chord, ft (m)
C_p	pressure coefficient, $(p - p_\infty)/q_\infty$ steady; $(p - p_{mean})/q_\infty$ unsteady
f	frequency, Hz
H_o	freestream total pressure, psf (kPa)
k	reduced frequency, $\omega c_r/(2V_\infty)$
M	Mach number
p	pressure, psf (kPa)
p_{mean}	mean local pressure, psf (kPa)
p_∞	freestream static pressure, psf (kPa)
q_∞	dynamic pressure, psf (kPa)
R_N	Reynolds number based on average chord
s	semispan, ft (m)

t/c	airfoil thickness to chord ratio
T_o	total or stagnation temperature, ^oR (^oC)
V_∞	freestream velocity, ft/sec (m/sec)
x/c	streamwise fraction of local chord
y	spanwise coordinate normal to freestream
α_o	mean angle of attack, degrees
θ	amplitude of pitch oscillations, degrees or radians
δ	amplitude of control surface oscillations, degrees or radians
δ_o	mean control surface deflection, degrees or radians
η	fraction of span, y/s
γ	ratio of specific heats for test gas
ω	frequency, radians/second

MODEL AND TESTS

The clipped delta wing model was tested in the NASA Langley Transonic Dynamics Tunnel (TDT). The tunnel has a slotted test section 16-feet (4.064 m) square with cropped corners. At the time of these tests, it could be operated with air or a heavy gas, R-12, as a test medium at pressures from very low to near atmospheric values. Currently the TDT can be operated with air or R-134a as a test medium. An early description of this facility is given in Ref 14 and the early data system is described in Ref 15. More recent descriptions of the facility are given in Ref 16 and 17, and of the recent data system given in Ref 18 and 19. Based on cone transition results (Ref 20-21), the turbulence level for this tunnel is in the average large transonic tunnel category. Some low speed turbulence measurements in air have also been presented in Ref 22.

The model is shown installed in the TDT in Fig 1, the basic structure is illustrated in Fig 2, and the overall planform and instrumentation layout is given in Fig 3. It was mounted on a splitter plate offset from the wall. The model had an end plate fixed to its root that moved with the model. To prevent leakage between the end plate and the splitter plate, the region where the splitter plate overlapped the end plate was sealed. The leading edge control surface shown in Figs 1 and 2 was fixed and the side edges smoothly faired into the wing. The hinge line at 15 per cent chord was sealed but not smoothed. The trailing-edge control surface (Figs 1-3) had a hinge line at 80 per cent chord that was sealed but not smoothed. The side edges were not sealed. The model was oscillated in pitch as a mass-spring system with a large spring mechanism located behind the tunnel wall that was driven hydraulically. It could be set at various mean angles, and the amplitude and frequency of oscillation varied. The trailing edge control surface was oscillated with a miniature hydraulic actuator located within the wing at the control surface and attached directly to the shaft along the control hinge line.

The wing was constructed with stainless steel ribs and spars and Kevlar-epoxy skins. Although no stiffness measurements were made, it was considered very stiff. Based on accelerometer measurements, the wind-off node lines showed only modest variation with frequencies in the range of interest (Fig 4). The control surface was constructed with ribs, spars, and skin of graphite-epoxy for low weight and high stiffness.

The instrumentation was mostly on the upper surface (shown in Fig 3) with a few transducers on the lower surface to establish symmetry and zero angle of attack. There are 5 chordwise locations for the transducers, with chord C consisting of a few transducers near the edges of the control surfaces. Static and dynamic measurements were made separately, with a static orifice adjacent to each dynamic transducer. The locations of the static orifices are given in Table 1, and locations of the orifices for the dynamic transducers are given in Table 2. The static pressure tubing was also connected to the reference side of the corresponding dynamic orifices through 35 feet (10.7 m) of .020 inch (.51 mm) diameter tubing to damp out unsteady effects on the reference pressure.

Although ordinates were measured for this wing, it was concluded that the basic definition of a t/c=0.06 circular arc was adequate to describe the airfoil geometry of the wing and the measured ordinates were not published. It was noted (Ref 1) that the control surface had two degrees of twist, which was averaged by setting the inboard portion low and the outboard portion high.

As can been seen in Fig 1, the model was tested with the sidewall slots of the test section open. Some recent unpublished results for a model of about twice the root chord of this model and mounted directly to the wind tunnel wall have shown an order of ten percent influence of closing the slots on static lift curve slope (similar to those measured in Ref 23). Significantly less influence would be anticipated for this smaller model which was mounted on a splitter plate.

TEST CASES

The static Test Cases chosen for the Clipped Delta Wing (CDW) are given in Table 3, and the dynamic Test Cases are presented in Tables 4 and 5. The code, or point index, for the cases are designated with a two-digit value of the test Mach number, followed by an S for static or D for dynamic, and followed by a sequence number for each Mach number (Ref 1). The pitch cases are chosen to indicate trends with Mach number at zero angle of attack, trends with Mach number for small values of angle of attack, and trends with angle of attack at one low and one transonic Mach number (including some cases with leading-edge vortex flows). The trailing edge control cases also illustrate trends with Mach number and static deflection amplitude of the trailing-edge control surface. The dynamic cases are chosen to evaluate unsteady effects at these static conditions. One feature of this data set is a relatively high Reynolds number for the test, of the order of 10×10^6 based on the average chord.

A sample data point for the static Test Cases is tabulated and shown in the composite plot of Fig 5. The data for the dynamic cases are also tabulated and shown in the plots of Figs 6 and 7 in terms of in-phase and out-of-phase parts (real and imaginary) of the pressure normalized by the amplitude of the dynamic motion, either pitch or control-surface oscillation (in radians). The phase reference is the input dynamic motion. More figures than are significant are retained in the Tables to accurately reproduce the phase angles of the original tabulations. For each of these cases, the data points are connected by straight lines for visual continuity only and the lines are not intended to be considered a fairing of the data. No further screening of bad points have been performed in this report. In the original data set, the output of bad transducers was set to zero.

The files included on the CD-ROM are ascii files and a readme file is included. The file for the static data is named cdwstat and a Fortran subprogram to read it, cdwstrd.f, is furnished. The dynamic data is on file cdwdynmc and the subprogram to read it is cdwdyrd.f. The data files consist of contiguous data points in the format shown in the figures.

Note that all of the tests for the CDW were conducted with the heavy gas, R-12, as the test medium. The ratio of specific heats, γ, is calculated to be 1.132 to 1.135 for the conditions of the test assuming 0.99 for the fraction of heavy gas in the heavy gas-air mixture. A value of 1.132 is suggested for use in computational comparisons. The corresponding value of Prandtl number is calculated to range from 0.77 to 0.78 for the conditions of this test.

FORMULARY

1 General Description of Model

1.1	Designation	Clipped Delta Wing (CDW)
1.2	Type	Semispan wing
1.3	Derivation	Simplified version of early SST with thicker airfoil (see Introduction)
1.4	Additional remarks	Shown mounted in tunnel in Fig 1
1.5	References	Ref 1 and 2 are the original source

2 Model Geometry

2.1	Planform	Trapezoidal
2.2	Aspect ratio	1.242 for panel
2.3	Leading edge sweep	50.4 deg.
2.4	Trailing edge sweep	Unswept
2.5	Taper ratio	0.1423
2.6	Twist	None
2.7	Wing centreline chord	63.55 inches (1614 mm)
2.8	Semi-span of model	45.08 inches (1145 mm)
2.9	Area of planform	1635.88 sq. in. (1.0554 sq. m)
2.10	Location of reference sections and definition of profiles	Six per cent circular arc airfoil section
2.11	Lofting procedure between reference sections	Constant per cent thickness airfoil
2.12	Form of wing-body junction	No fairing, sealed at splitter plate
2.13	Form of wing tip	Sharply cut off
2.14	Control surface details	Trailing edge control, 80% chord between 56.6% span and 82.9% span. Hinge line sealed, but side edges open. About two degrees twist in control surface, with inboard trailing edge low and outboard high
2.15	Additional remarks	See Fig 3 for overview
2.16	References	Ref 1 and 2

3 Wind Tunnel

3.1	Designation	NASA LaRC Transonic Dynamics Tunnel (TDT)
3.2	Type of tunnel	Continuous flow, single return
3.3	Test section dimensions	16 ft x 16 ft (4.064 x 4.064 m)
3.4	Type of roof and floor	Three slots each
3.5	Type of side walls	Two sidewall slots
3.6	Ventilation geometry	Constant width slots in test region
3.7	Thickness of side wall boundary layer	Some documentation in Ref 14. Model tested with splitter plate
3.8	Thickness of boundary layers at roof and floor	Not documented
3.9	Method of measuring velocity	Calculated from static pressures measured in plenum and total pressure measured upstream of entrance nozzle of test section
3.10	Flow angularity	Not documented, considered small
3.11	Uniformity of velocity over test section	Not documented, considered nearly uniform
3.12	Sources and levels of noise or turbulence in empty tunnel	Generally unknown. Some low speed measurements are presented in Ref 22. Cone transition measurements are presented in Ref 20 and 21.
3.13	Tunnel resonances	Unknown
3.14	Additional remarks	Tests performed in heavy gas, R-12. Ratio of specific heats, γ, is 1.132-1.135. For computations, 1.132 is recommended. For the conditions of this test, the Prandtl number is calculated to be 0.77-0.78
3.15	References on tunnel	Ref 14, 16, and 17

4 Model Motion

4.1	General description	Pitching about 65.22% of root chord for wing. Oscillation about control hinge line
4.2	Reference coordinate and definition of motion	Pitch about axis normal to freestream. Control oscillation about 80% chord line of wing
4.3	Range of amplitude	Pitch amplitude of 0.25 and 0.50 degrees. Control oscillation of 2, 4, and 6 degrees
4.4	Range of frequency	4, 8, and 16 Hz for wing pitch, and 8, 16, and 22 Hz for control surface oscillations
4.5	Method of applying motion	Pitch oscillations generated as spring-mass system driven by hydraulic actuator. Control surface oscillations driven by miniature hydraulic actuator at control surface
4.6	Timewise purity of motion	Not documented
4.7	Natural frequencies and normal modes of model and support system	First natural frequency was 28 Hz
4.8	Actual mode of applied motion including any elastic deformation	Not documented except for node lines for wind-off conditions. (Fig 4). Elastic deformations not expected to be significant
4.9	Additional remarks	None

5 Test Conditions

5.1	Model planform area/tunnel area	.05
5.2	Model span/tunnel height	.23
5.3	Blockage	Model less than 0.3%
5.4	Position of model in tunnel	Mounted from splitter plate on wall and in the center of the tunnel
5.5	Range of Mach number	0.40 to 1.12
5.6	Range of tunnel total pressure	530 to 1005 psf (25.4 to 48.1 kPa)
5.7	Range of tunnel total temperature	512 to 576 degrees Rankine (23 to 47° C)

5.8	Range of model steady or mean incidence	0 to 5.5 degrees
5.9	Definition of model incidence	From chord line of symmetric airfoil
5.10	Position of transition, if free	Transition strip used
5.11	Position and type of trip, if transition fixed	Grit strip 0.1 inch wide (2.5 mm) at 8 % chord on upper and lower surfaces. Number 70 grit from root to midspan and number 90 from midspan to tip (number is approximately grains per inch (per 25.4 mm))
5.12	Flow instabilities during tests	None defined
5.13	Changes to mean shape of model due to steady aerodynamic load	Not measured but considered very stiff
5.14	Additional remarks	Tests performed in heavy gas, R-12. Ratio of specific heats, γ, is 1.132-1.135. For computations, 1.132 is recommended. For the conditions of this test, the Prandtl number is calculated to be 0.77-0.78
5.15	References describing tests	Ref 1 and 2

6 Measurements and Observations

6.1	Steady pressures for the mean conditions	yes
6.2	Steady pressures for small changes from the mean conditions	yes
6.3	Quasi-steady pressures	no
6.4	Unsteady pressures	yes
6.5	Steady section forces for the mean conditions by integration of pressures	no
6.6	Steady section forces for small changes from the mean conditions by integration	no
6.7	Quasi-steady section forces by integration	no
6.8	Unsteady section forces by integration	no
6.9	Measurement of actual motion at points of model	no
6.10	Observation or measurement of boundary layer properties	no
6.11	Visualisation of surface flow	no
6.12	Visualisation of shock wave movements	no
6.13	Additional remarks	no

7 Instrumentation

7.1	Steady pressure	
	7.1.1 Position of orifices spanwise and chordwise	7 to 16 chordwise locations at 5 spanwise stations. See Fig 3 and Table 1
	7.1.2 Type of measuring system	Scani-valve
7.2	Unsteady pressure	
	7.2.1 Position of orifices spanwise and chordwise	7 to 16 chordwise locations at 5 spanwise stations. See Fig 3 and Table 2. Slightly different locations than steady.
	7.2.2 Diameter of orifices	.056 inches (1.4 mm)
	7.2.3 Type of measuring system	In situ pressure gages
	7.2.4 Type of transducers	Kulite
	7.2.5 Principle and accuracy of calibration	Calibrated dynamically using method of Ref 24. Also statically calibrated through reference tubes

7.3 Model motion	
7.3.1 Method of measuring motion reference coordinate	Undocumented
7.3.2 Method of determining spatial mode of motion	Wind-off verification with accelerometers
7.3.3 Accuracy of measured motion	Undocumented
7.4 Processing of unsteady measurements	
7.4.1 Method of acquiring and processing measurements	Analog signals digitized at about 940 samples/sec for 10-30 seconds depending on frequency
7.4.2 Type of analysis	Fourier analysis
7.4.3 Unsteady pressure quantities obtained and accuracies achieved	Amplitude and phase of each pressure signal. Accuracy not specified
7.4.4 Method of integration to obtain forces	None
7.5 Additional remarks	None
7.6 References on techniques	Data system overview for test given in Ref 15

8 Data Presentation

8.1 Test Cases for which data could be made available	See Ref 1 and 2
8.2 Test Cases for which data are included in this document	See Tables 3 and 4
8.3 Steady pressures	Available for each Test Case
8.4 Quasi-steady or steady perturbation pressures	Steady pressures measured for several angles of attack
8.5 Unsteady pressures	Primary data. First harmonic only. No time histories saved. C_p magnitude and phase of Ref 1 converted to real and imaginary parts and normalized by amplitude of oscillation (in radians)
8.6 Steady forces or moments	Some static hinge moments for control surface plotted in Ref 1. No other force measurements
8.7 Quasi-steady or unsteady perturbation forces	None
8.8 Unsteady forces and moments	None
8.9 Other forms in which data could be made available	None
8.10 References giving other representations of data	Ref 1-2 and 8-11

9 Comments on Data

9.1 Accuracy	
9.1.1 Mach number	Not documented
9.1.2 Steady incidence	Zero set by pressure difference. Accuracy of other values unknown
9.1.3 Reduced frequency	Should be accurate
9.1.4 Steady pressure coefficients	Not documented
9.1.5 Steady pressure derivatives	None
9.1.6 Unsteady pressure coefficients	Not documented, but each gage individually calibrated dynamically and monitored statically
9.2 Sensitivity to small changes of parameter	None indicated. Amplitudes of oscillation varied in test
9.3 Non-linearities	Plotted (Ref 2) hinge moments show some nonlinearity. Many flow conditions involve shock waves; some with leading edge vortex flows
9.4 Influence of tunnel total pressure	Not evaluated. Most of the test at constant dynamic pressure

9.5	Effects on data of uncertainty, or variation, in mode of model motion	Unknown, not expected to be appreciable. Wind-off measurements shown in Fig 4
9.6	Wall interference corrections	None applied
9.7	Other relevant tests on same model	None
9.8	Relevant tests on other models of nominally the same shapes	Flutter tests on similar planform but with thinner airfoil presented in Ref 4-7
9.9	Any remarks relevant to comparison between experiment and theory	Leading edge vortex forms near 3 degrees angle of attack. Some cases have both vortex flow and shock waves. Test Reynolds number included for each Test Case. Reduced frequency based on root semichord, 31.775 inches (807.1 mm) for all Test Cases
9.10	Additional remarks	Wing mostly instrumented on one side. Upper and lower surface data assembled from varying angle of attack
9.11	References on discussion of data	Ref 1-2 and 8-11

10 Personal Contact for Further Information

Head, Aeroelasticity Branch
Mail Stop 340
NASA Langley Research Center
Hampton, VA 23681-2199 USA

Phone: +1-(757)-864-2820
FAX: +1-(757)-864-8678

LIST OF REFERENCES

1 Hess, Robert W.; Cazier, F. W., Jr.; and Wynne, Eleanor C.: *Steady and Unsteady Transonic Pressure Measurements on a Clipped Delta Wing for Pitching and Control-Surface Oscillations.* NASA TP-2594, Oct. 1986.

2 Hess, R. W.; Cazier, F. W.,Jr.; and Wynne, E. C.: *Static and Unsteady Pressure Measurements on a 50 degree Clipped Delta Wing at M = 0.9.* AIAA Paper 82-0686, 1982. Also available as NASA TM-83297, 1982.

3 Bhatia, Kumar G.; and Wertheimer, Jiri: *Aeroelastic Challenges for a High Speed Civil Transport.* AIAA Paper 93-1478, May 1993.

4 Sandford, Maynard C.; Abel, Irving; and Gray, David L.: *Development and Demonstration of a Flutter-Suppression System Using Active Controls.* NASA TR R-450, 1974.

5 Sandford, Maynard C.; Ruhlin, Charles L.; and Abel, Irving: *Transonic Flutter Study of a 50.5-Deg. Cropped-Delta Wing with Two Rearward-Mounted Nacelles.* NASA TN D-7544, 1974.

6 Goetz, Robert C.: *Exploratory Study of Buffet and Stall Flutter of Space Vehicle Wing Concepts.* NASA LWP-872, May 1970.

7 Ruhlin, Charles L.; Destuynder, Roger M.; and Gregory, Richard A.: *Some Wind Tunnel Wall Effects on Transonic Flutter.* Journal of Aircraft, vol. 12, no. 3, Mar. 1975, pp 162-167.

8 Yates, E. Carson, Jr.; Cunningham, Herbert J.; Desmarais, Robert N.; Silva, Walter A.; and Drobenko, Bohdan: *Subsonic Aerodynamic and Flutter Characteristics of Several Wings Calculated by the SOUSSA P1.1 Panel Method.* AIAA Paper 82-0727, May 1982.

9 Guruswamy, Guru P.; and Obayashi, Shigeru: *Transonic Aeroelastic Computations on Wings Using Navier-Stokes Equations.* Paper No. 22 in "Transonic Unsteady Aerodynamics and Aeroelasticity", AGARD-CP-507, Mar. 1992.

10 Obayashi, Shigeru; and Guruswamy, Guru P.: *Unsteady Shock-Vortex Interaction on a Flexible Delta Wing.* Journal of Aircraft, vol. 29, no. 5, Sept.-Oct. 1992, pp 790-798.

11 Obayashi, Shigeru; and Guruswamy, Guru P.: *Navier-Stokes Computations for Oscillating Control Surfaces.* Journal of Aircraft, vol. 31, no. 3, May-June 1994, pp. 631-636.

12 Bennett, Robert M.; Batina, John T.; and Cunningham, H. J.: *Wing-Flutter Calculations with the CAP-TSD Unsteady Transonic Small-Disturbance Program.* Journal of Aircraft, vol. 26, no. 9, Sep. 1989, pp. 876-882.

13 Bennett, Robert M.; Walker, Charlotte, E.: *Computational Test Cases For a Clipped Delta Wing with Pitching and Trailing-Edge Control Surface Oscillations.* NASA/TM-1999-209104, Mar.1999.

14 Aeroelasticity Branch Staff: *The Langley Transonic Dynamics Tunnel.* LWP-799, Sep. 1969.

15 Cole, Patricia H.: *Wind Tunnel Real-Time Data Acquisition System.* NASA TM 80081, 1979.

16 Cole, Stanley, R.; and Rivera, Jose, A, Jr.: *The New Heavy Gas Testing Capability in the NASA Langley Transonic Dynamics Tunnel.* Paper No. 4, presented at the Royal Aeronautical Society Wind Tunnels and Wind Tunnel Test Techniques Forum, Churchill College, Cambridge, UK, Apr. 1997.

17 Corliss, James M.; and Cole, Stanley R.: *Heavy Gas Conversion of the NASA Langley Transonic Dynamics Tunnel.* AIAA Paper 98-2710, June 1998.

18 Wieseman, Carol D.; and Hoadley, Sherwood, T.: *Versatile Software Package for Near Real-Time Analysis of Experimental Data.* AIAA Paper 98-2722, June 1998.

19 Bryant, C.; and Hoadley , S. T.: *Open Architecture Dynamic Data System at Langley's Transonic Dynamics Tunnel.* AAIA Paper 98-0343, Jan. 1998.

20 Dougherty, N. Sam, Jr.: *Influence of Wind Tunnel Noise on the Location of Boundary-Layer Transition on a Slender Cone at Mach Numbers from 0.2 to 5.5. Volume I. - Experimental Methods and Summary of Results. Volume II. - Tabulated and Plotted Data.* AEDC--TR-78-44, March 1980.

21 Dougherty, N. Sam, Jr.; and Fisher, D. F.: *Boundary-Layer Transition on a 10-Deg. Cone: Wind Tunnel/Flight Correlation.* AIAA Paper 80-0154, January 1980.

22 Sleeper, Robert K.; Keller, Donald F.; Perry, Boyd, III; and Sandford, Maynard C.: *Characteristics of Vertical and Lateral Tunnel Turbulence Measured in Air in the Langley Transonic Dynamics Tunnel.* NASA TM 107734, March 1993.

23 Lambourne, N.; Destuynder, R.; Kienappel, K.; and Roos, R.: *Comparative Measurements in Four European Wind Tunnels of the Unsteady Pressures on an Oscillating Model (The NORA Experiments).* AGARD Report No. 673, Feb. 1980.

24 Bolt, Pamela C.; Hess, Robert W.; and Davis William T.: *Portable Dynamic Pressure Generator for Static and Dynamic Calibration of In-Situ Pressure Transducers.* NASA TM 85687, 1983.

ACKNOWLEDGMENT

The considerable assistance of Charlotte E. Walker in generating the tables and figures for this report is gratefully acknowledged.

Table 1. Orifice Locations for Steady Measurements

Chord A	Chord B	Chord C	Chord D	Chord E
y/s				
0.332	0.541	0.587	0.694	0.851
x/c				
0.0778	0.0687	0.0818	0.0675	0.2070
0.1264	0.1282	0.1318	0.1151	0.2559
0.2020	0.2529	0.2099	0.1980	0.3016
0.2523	0.3041	0.7875	0.2559	0.3537
0.3023	0.3531	0.8522	0.3041	0.4583
0.3519	0.4530	0.9017	0.3545	0.5562
0.4510	0.5036	0.9514	0.4537	0.6074
0.5523	0.5534		0.5025	0.6577
0.6025	0.6040		0.5527	0.7071
0.6515	0.6528		0.6038	0.7975
0.6991	0.7030		0.6538	
0.7813	0.7694		0.7025	
0.8505	0.8967		0.7754	
0.9001	0.9512		0.8553	
0.9596			0.9037	
			0.9526	

Table 2. Orifice Locations for Unsteady Measurements

Chord A	Chord B	Chord C	Chord D	Chord E
y/s				
0.337	0.546	0.590	0.698	0.856
x/c				
0.0731	0.0681	0.0767	0.0754	0.1955
0.1120	0.1237	0.1271	0.1237	0.2458
0.1974	0.2485	0.1993	0.1980	0.2915
0.2478	0.3004	0.7802	0.2502	0.3454
0.2987	0.3481	0.8514	0.3001	0.4519
0.3486	0.4487	0.9016	0.3476	0.5497
0.4477	0.4997	0.9511	0.4495	0.6025
0.5506	0.5500		0.4974	0.6545
0.6009	0.6014		0.5484	0.7049
0.6459	0.6494		0.6007	0.7808
0.6979	0.6995		0.6514	
0.7805	0.7747		0.7000	
0.8500	0.8964		0.7795	
0.8996			0.8547	
0.9495			0.9033	
			0.9522	

Table 3. Static Test Cases

Test Case No.	Point (Code[1])	M	α_o deg.	δ_o deg.	Comments
9E1	.40-S-1	.399	.05	0.	Versus M @ $\alpha_o = 0^\circ$
9E2	.88-S-1	.883	.05	0.	
9E3	.90-S-1	.899	.05	0.	
9E4	.92-S-1	.921	.05	0.	
9E5	.94-S-1	.944	.05	0.	
9E6	. 96-S-1	.965	.00	0.	
9E7	1.12-S-1	1.120	.00	0.	
9E8	.40-S-6	.400	1.03	0.	Versus M @ $\alpha_o = 1^\circ$
9E9	.90-S-5	.909	.99	0.	
9E10	.94-S-6	.943	.97	0.	
9E11	1.12-S-6	1.120	.99	0.	
9E12	.40-S-11	.404	3.04	0.	Versus α_o @M
9E13	.40-S-15	.403	5.04	0.	
9E14	.90-S-19	.900	2.99	0.	
9E15	.90-S-38	.901	4.24	0.	
9E16	.40-S-3	.406	.05	4.	Versus δ_o @ $\alpha_o = 0$
9E17	.90-S-2	.898	.05	2.	
9E18	.90-S-3	.896	.05	4.	
9E19	.94-S-3	.944	.05	4.	
9E20	1.12-S-3	1.120	.00	4.	
9E21	.90-S-21	.901	2.99	4.	Versus δ_o @ α_o
9E22	.90-S-24	.896	2.99	-4.	

[1] Ref 1

Table 4. Test Cases for Pitching Oscillations, $\delta_0 = 0$

Test Case No.	Point (Code[1])	M	α_o deg.	θ deg.	f Hz	k	Comments
9E23	.40-D-5	.403	.05	.47	4.00	.194	Versus M
9E24	.88-D-5	.885	.05	.48	7.98	.173	
9E25	.90-D-5	.904	.00	.46	7.99	.167	
9E26	.92-D-5	.921	.05	.47	7.97	.166	
9E27	.94-D-5	.945	.05	.47	7.98	.162	
9E28	.96-D-4	.961	.04	.50	7.99	.158	
9E29	1.12-D-5	1.120	.00	.47	8.00	.136	
9E30	.90-D-2	.905	.00	.24	7.99	.168	Lower θ
9E31	.90-D-4	.904	.00	.50	4.01	.084	Lower k
9E32	.90-D-6	.909	.00	.46	16.01	.335	Higher k
9E33	.40-D-24	.403	5.02	..50	4.00	.189	Higher α_o
9E34	.90-D-29	.902	3.97	.46	7.99	.169	

[1] Ref 1

Table 5. Test Cases for Control Surface Oscillations, $\delta_0 = 0$

Test Case No.	Point (Code[1])	M	α_o deg.	δ deg.	f Hz	k	Comments
9E35	.40-D-32	.405	.05	3.90	7.99	.376	Versus M
9E36	.88-D-34	.878	.05	3.88	16.00	.350	
9E37	.90-D-35	.901	.05	4.00	16.00	.338	
9E38	.92-D-33	.923	.05	3.93	15.98	.337	
9E39	.94-D-34	.942	.05	3.96	15.98	.326	
9E40	.96-D-10	.960	.05	4.54	16.00	.315	
9E41	1.12-D-11	1.120	.00	4.37	16.01	.273	
9E42	.90-D-32	.898	.05	3.48	7.99	.170	Lower k
9E43	.92-D-36	.924	.05	3.89	22.00	.459	Higher k
9E44	.90-D-34	.898	.05	1.97	16.00	.339	Lower δ
9E45	.90-D-36	.899	.04	5.82	16.01	.340	Higher δ
9E46	.90-D-59	.901	2.99	4.39	16.01	.337	Higher α_o

[1] Ref 1

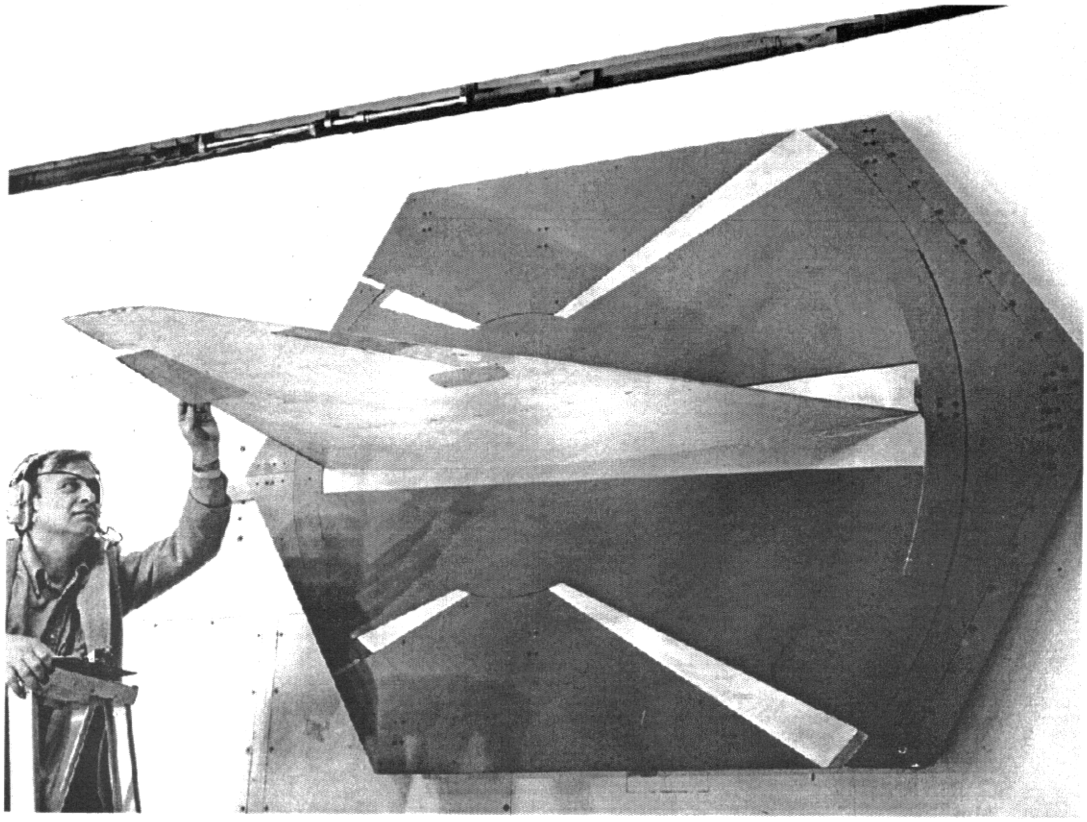

Figure 1. Clipped delta wing installed in wind tunnel.

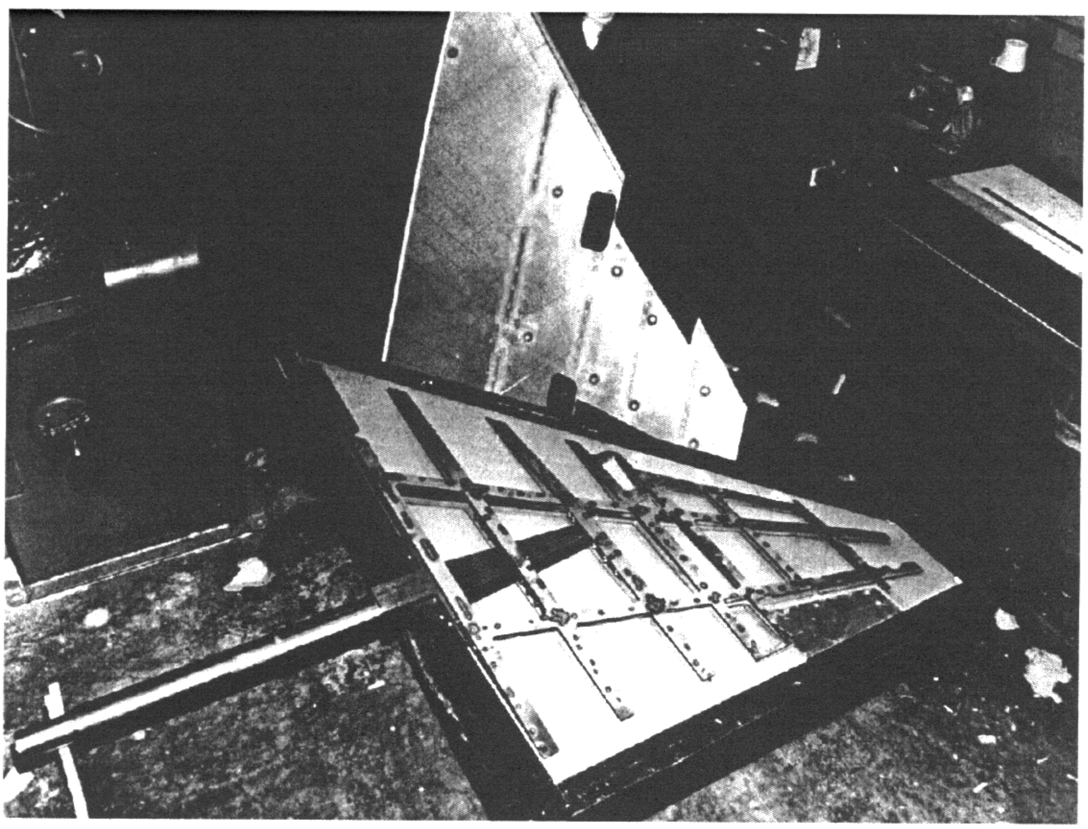

Figure 2. Construction of clipped delta wing.

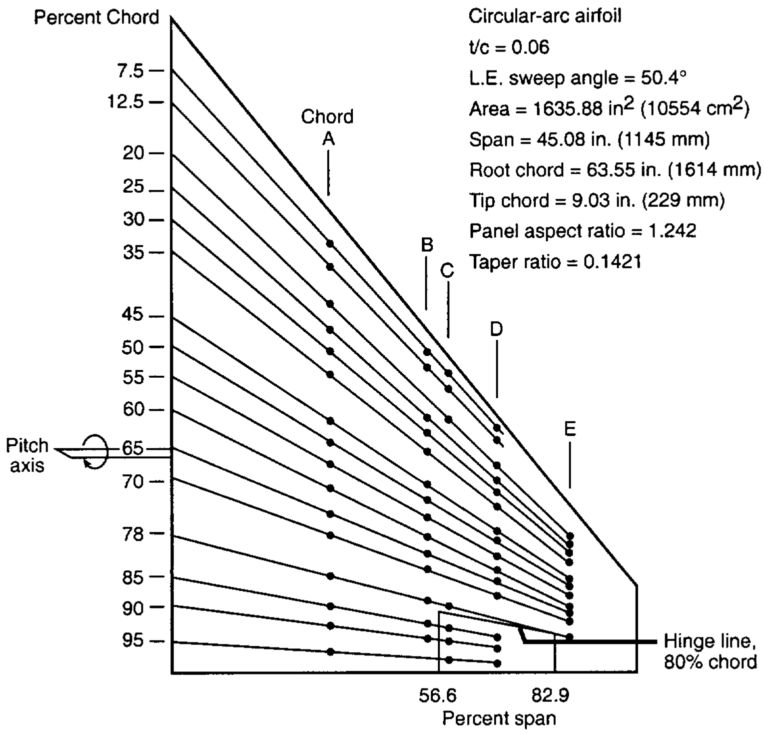

Figure 3. Planform geometry and instrumentation layout.

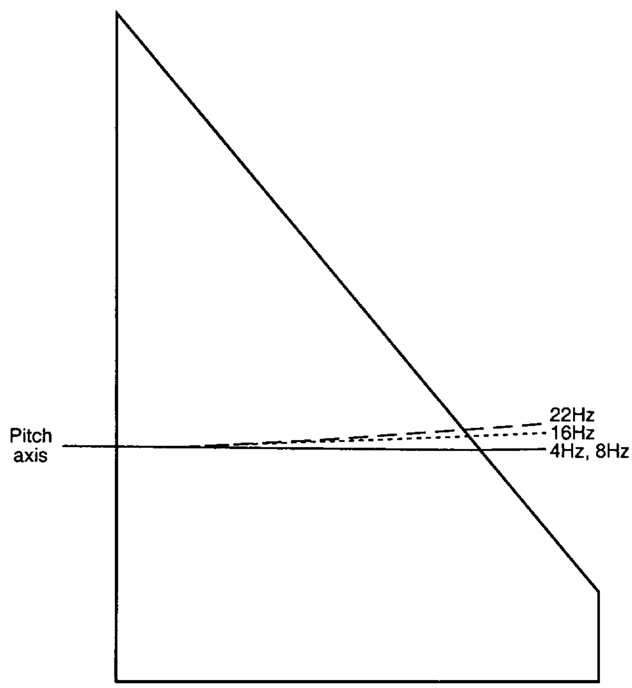

Figure 4. Node lines for test frequencies in still air.

.90-S-1

MACH	q	To	H	ALPHAo	THETA	DELTA	RN
	psf	deg R	psf	deg	deg	deg	
0.899	191.2	565.3	651.8	0.05	0.00	0.00	9.77 *10**6

y/s = 0.332

x/c	Cpu	Cpl
.0778	0.0217	
.1264	-.0318	
.2020	-.0802	
.2523	-.1134	
.3023	-.1580	
.3519	-.1620	
.4510	-.2456	
.5523	-.2424	
.6025	-.3011	
.6515	-.3778	
.6991	-.3374	
.7813	-.2514	
.8505	-.1069	
.9001	-.0362	
.9596	0.0812	

y/s = 0.541

x/c	Cpu	Cpl
.0687	0.0049	
.1282	-.0788	
.2529	-.1548	
.3041	-.2251	
.3531	-.2484	
.4530	-.2859	
.5036	-.3258	
.5534	-.3261	
.6040	-.3542	
.6528	-.3646	
.7030	-.3350	
.7694	-.1980	
.8967	0.0138	

y/s = 0.587

x/c	Cpu	Cpl
.0818	0.0229	
.1318	-.0596	
.2099	-.1477	
.7875	-.1491	
.8522	-.0710	
.9017	0.0186	
.9514	0.0988	

y/s = 0.694

x/c	Cpu	Cpl
.0675	-.0528	
.1151	-.0572	
.1980	-.1748	
.2559	-.2408	
.3041	-.2481	
.3545	-.2905	
.4537	-.3831	
.5025	-.3628	
.5527	-.3760	
.6038	-.3990	
.6538	-.3987	
.7025	-.3588	
.7754	-.1191	
.8553	-.0617	
.9037	0.0126	
.9526	0.0999	

y/s = 0.851

x/c	Cpu	Cpl
.2070	-.2689	
.2559	-.3260	
.3016	-.2912	
.3537	-.3057	
.4583	-.4098	
.5562	-.4368	
.6074	-.3943	
.6577	-.3388	
.7071	-.2408	
.7975	-.0879	

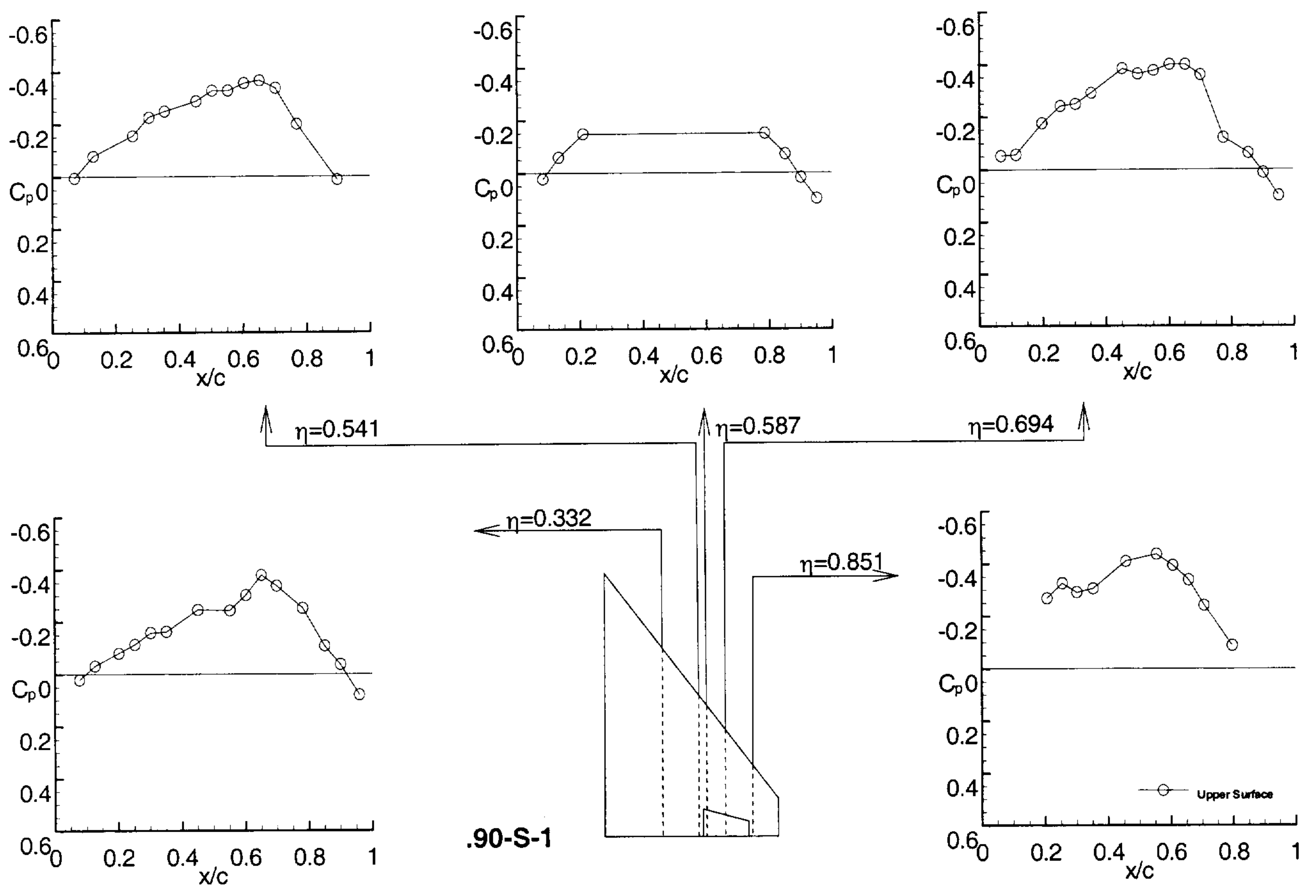

Figure 5. Static case, Test Case number 9E3 (point .90-S-1).

.90-D-5

MACH	q	To	H	ALPHAo	THETA	DELTA	RN
	psf	deg R	psf	deg	deg	deg	
0.904	200.3	566.2	679.5	0.00	0.46	0.00	10.13*10**6

f = 7.99 Hz k = 0.167

y/s = 0.337

	Upper		Lower	
x/c	Real	Imag	Real	Imag
.0731	-2.4667	0.7920		
.1120	-2.1392	0.5334		
.1974	-2.1072	0.3867		
.2478	-2.1140	0.2596		
.2987	-1.0684	0.0766		
.3486	-2.2901	0.0880		
.4477	-1.8757	-0.1377		
.5506	-2.0993	-0.1542		
.6009	-2.1938	-0.4623		
.6459	-2.5171	-0.6136		
.6979	-4.0662	-0.8791		
.7805	0.2918	-3.4253		
.8500	0.8783	-0.8655		
.8996	0.7067	-0.4199		
.9495	0.4162	-0.1668		

y/s = 0.546

	Upper		Lower	
x/c	Real	Imag	Real	Imag
.0681	-3.8789	1.2007		
.1217	-3.2047	0.8407		
.2485	-2.4548	0.4240		
.3004	-2.0958	0.3020		
.3481	-1.3275	0.2174		
.4487	-2.9393	0.0359		
.4997	-2.1027	-0.0992		
.5500	-2.4586	0.1935		
.6014	-2.6647	0.0651		
.6494	-4.7044	-0.1889		
.6995	-4.5903	-2.0919		
.7747	1.0737	-2.1090		
.8964	0.3784	-0.5410		

y/s = 0.590

	Upper		Lower	
x/c	Real	Imag	Real	Imag
.0767	-3.6778	1.2163		
.1271	-3.2311	0.9326		
.1993	-2.9437	0.7558		
.7802	1.6063	-1.4734		
.8514	0.3705	-0.2741		
.9016	0.6694	-0.3851		
.9511	0.6307	-0.0754		

y/s = 0.698

	Upper		Lower	
x/c	Real	Imag	Real	Imag
.0754	-2.2762	0.2674		
.1237	-4.1315	1.0378		
.1980	-3.8566	0.7217		
.2502	0.6121	-3.4714		
.3001	-1.4630	0.1409		
.3476	-3.2697	0.3494		
.4495	-3.1492	0.3032		
.4974	-2.9312	0.3495		
.5484	-2.5658	0.0134		
.6007	-3.1078	-0.1955		
.6514	-4.3593	-1.4164		
.7000	-2.1524	-2.9626		
.7795	0.6742	-0.4254		
.8547	0.5982	-0.1213		
.9033	0.5532	-0.1917		
.9522	0.6080	-0.0529		

y/s = 0.856

	Upper		Lower	
x/c	Real	Imag	Real	Imag
.1955	-3.1322	0.5975		
.2458	-4.2549	0.8271		
.2915	-4.8539	1.0672		
.3454	-1.7394	3.0372		
.4519	-3.6992	0.0323		
.5497	-4.8832	-0.6950		
.6025	-4.2134	-2.8634		
.6545	1.1374	-4.1181		
.7049	3.4864	-0.9446		
.7808	1.0075	0.0537		

(a) Tabulated data for 9E25

Figure 6. Pitching oscillation, Test Case number 9E25 (point 90-D-5).

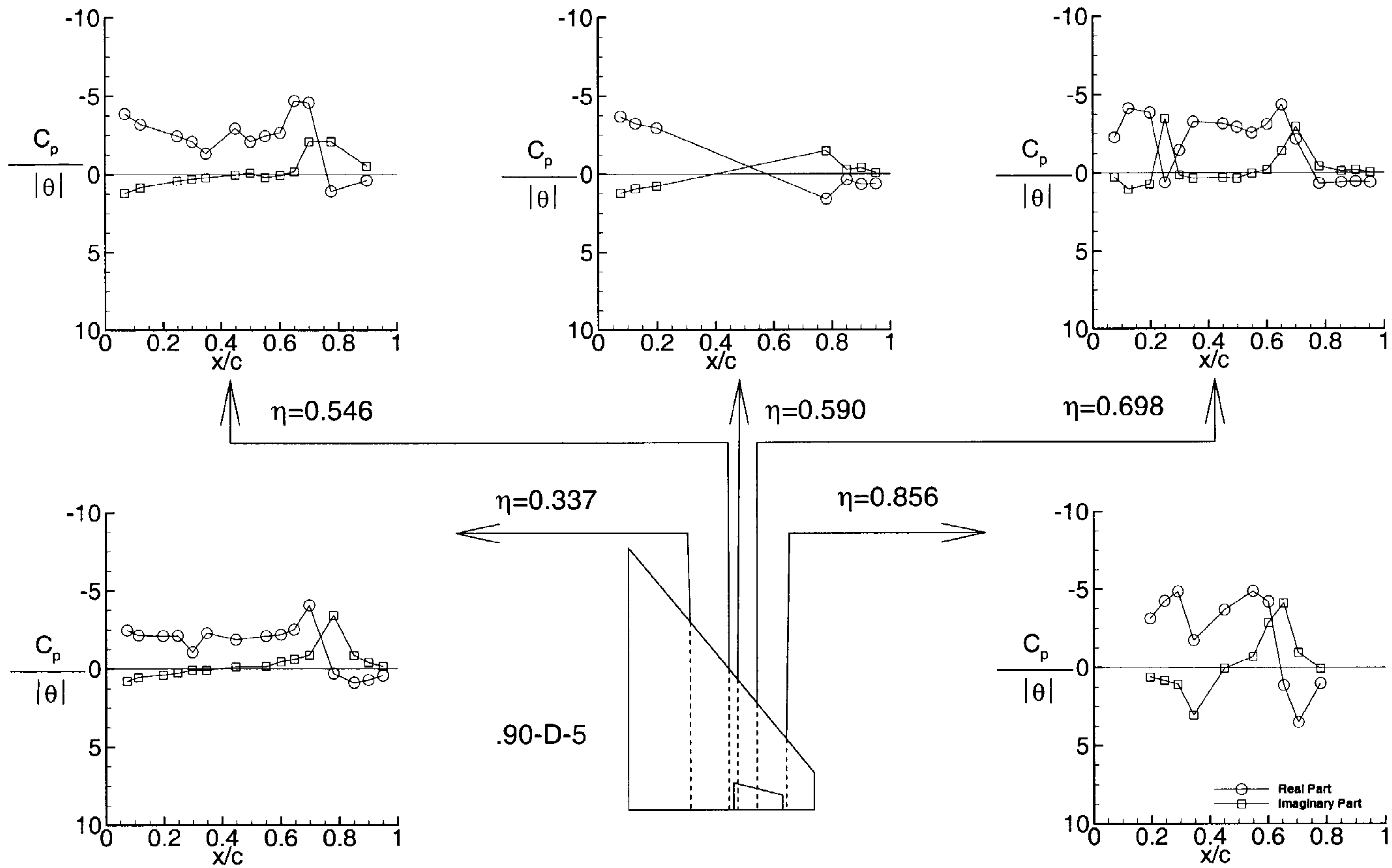

(b) Plot of data for 9E25

Figure 6. Concluded.

.90-D-35

MACH	q psf	To deg R	H psf	ALPHAo deg	THETA deg	DELTA deg	RN
0.901	192.0	565.2	654.1	0.05	0.00	4.00	9.84*10**6

f = 16.00 Hz   k = 0.338

y/s = 0.337

x/c	Upper Real	Upper Imag	Lower Real	Lower Imag
.0731	-0.3013	0.0483		
.1120	-0.2954	0.0389		
.1974	-0.2567	0.0238		
.2478	-0.2545	0.0151		
.2987	-0.0003	0.0014		
.3486	-0.2807	0.0059		
.4477	-0.2034	0.0025		
.5506	-0.1782	-0.0175		
.6009	-0.2402	0.0139		
.6459	-0.3362	0.0563		
.6979	-0.2748	-0.0416		
.7805	0.0218	-0.1008		
.8500	0.0343	-0.0304		
.8996	0.0133	-0.0053		
.9495	-0.0012	0.0085		

y/s = 0.546

x/c	Upper Real	Upper Imag	Lower Real	Lower Imag
.0681	-0.1346	0.0014		
.1217	-0.3132	0.0346		
.2485	-0.2704	0.0128		
.3004	-0.2546	0.0142		
.3481	-0.0008	0.0012		
.4487	-0.4544	0.0703		
.4997	-0.2319	0.0081		
.5500	-0.2116	-0.0122		
.6014	-0.2879	-0.0030		
.6494	-0.3553	-0.1293		
.6995	-0.2401	-0.1589		
.7747	0.0796	-0.0610		
.8964	0.0180	-0.0142		

y/s = 0.590

x/c	Upper Real	Upper Imag	Lower Real	Lower Imag
.0767	-0.7556	0.1278		
.1271	-0.5800	0.0825		
.1993	-0.4027	0.0466		
.7802	0.0688	-0.0562		
.8514	-0.0005	0.0028		
.9016	0.0258	-0.0002		
.9511	0.0037	0.0123		

y/s = 0.698

x/c	Upper Real	Upper Imag	Lower Real	Lower Imag
.0754	-0.2543	0.0182		
.1237	-0.1991	0.0010		
.1980	-0.2930	0.0195		
.2502	-0.3981	0.0489		
.3001	-0.0006	0.0013		
.3476	-0.4392	0.0547		
.4495	-0.3093	0.0070		
.4974	-0.3492	0.0140		
.5484	-0.3953	0.0048		
.6007	-0.4157	-0.0673		
.6514	-0.3653	-0.2793		
.7000	0.2386	-0.3260		
.7795	0.0521	-0.0096		
.8547	0.0902	0.0036		
.9033	0.0968	-0.0106		
.9522	-0.0052	0.0068		

y/s = 0.856

x/c	Upper Real	Upper Imag	Lower Real	Lower Imag
.1955	-0.2882	0.0252		
.2458	-0.4349	0.0220		
.2915	-0.3566	0.0056		
.3454	-0.4440	0.0008		
.4519	-0.4439	0.0108		
.5497	-0.3540	-0.2255		
.6025	0.2054	-0.2757		
.6545	0.4322	-0.1017		
.7049	0.1496	0.0151		
.7808	0.0026	0.0199		

(c) Tabulated data for 9E37

Figure 7. Control surface oscillation, Test Case number 9E37 (point 90-D-35).

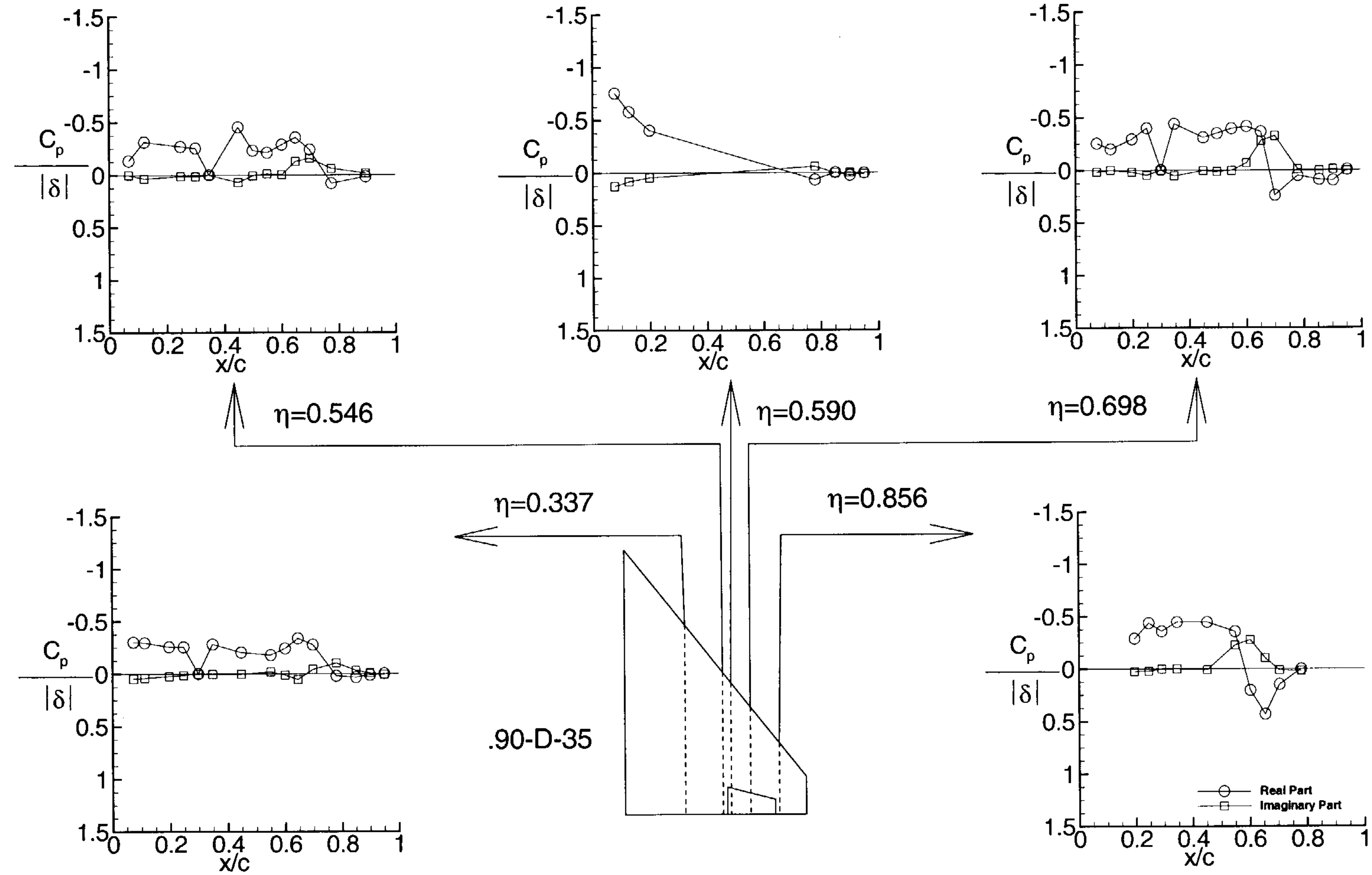

(d) Plot of data for 9E37

Figure 7. Concluded.

10. SUPERSONIC 2D WING WITH CONTROL SURFACES

P. Naudin
ONERA
29, Av. de la Div. Leclerc 92320 Chatillon
France

INTRODUCTION

For some years ONERA, in collaboration with AEROSPATIALE, has undertaken research into improvement of CFD codes, in the framework of studies on a new supersonic plane. The main goal has been to take unsteady effects, induced by movements of control surfaces such as spoilers or trailing edge flaps, into account with improved accuracy. For this purpose a wind tunnel test was carried out to provide an extensive database of unsteady behavior of control surfaces in supersonic conditions. ONERA has designed a generic 2D rigid model with two control surfaces: a spoiler and a trailing edge flap. These two control surfaces were moved in rotation by electro-hydraulic actuators, allowing an adjustment in static position as well as a harmonic excitation. A model with steady and unsteady pressure transducers, and accelerometers, was installed in the ONERA S2 wind tunnel at Modane in March 1994 (figures 1 and 2).

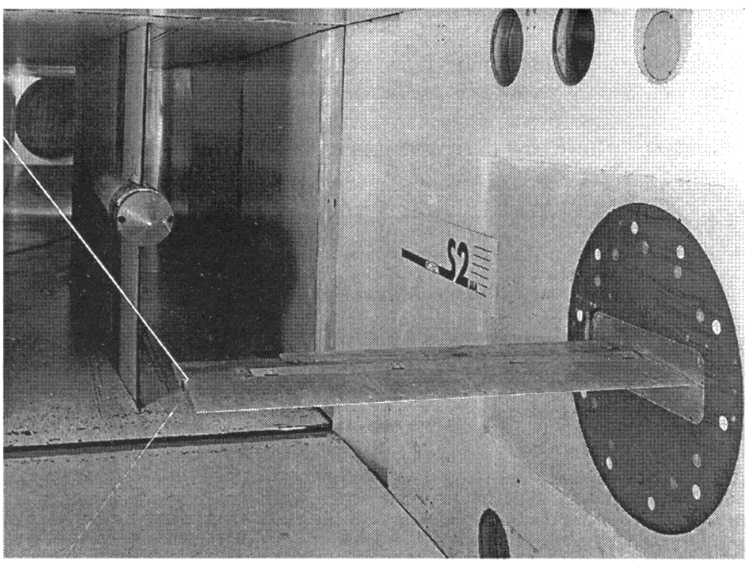

Figure 1: Model in the wind-tunnel section

LIST OF SYMBOLS AND DEFINITIONS

A	amplitude of harmonic excitation, (deg.)
α	angle of attack, alpha
β	deflection of the trailing edge flap, beta
c	wing chord
Cp	unsteady pressure coefficient $Cp = \frac{P_i . e^{i(\omega_0 t + \Phi_0)}}{Q_0 . A}$
Cpm	mean pressure coefficient
Cpq	quasi-steady pressure coefficient $Cpq = \frac{Cpm(\beta + \Delta\beta) - Cpm(\beta - \Delta\beta)}{2.\Delta\beta}$
F	excitation frequency
M	Mach number
P_i	modulus of the unsteady pressure at excitation frequency ω_0
Pi0	stagnation pressure

Q0	dynamic pressure
R	Reynolds number referred to model chord (0.4 m)
Ti0	stagnation temperature
x/c	non-dimensional chord location

TESTING EQUIPMENT

MODEL

The model, a rectangular wing of 1.1 m span and 0.4 m chord was manufactured in aluminum alloy. Figure 3 shows general dimensions of the model. The airfoil had a biconvex symmetrical shape of 7 % relative thickness with a sharp leading edge as indicated in figure 4. Co-ordinates are shown in table 1 and in a separate file "airfoil.txt". The spoiler and trailing edge flap have chords, respectively, of 10% and 20% of the root chord. Spans of these control surfaces were limited in order to minimize their inertia and to preserve a good quality of the supersonic flow on the measured sections for the lower Mach number (M= 1.65).

In order to improve the dynamic behavior of the model, guys lines were connected to the middle of the wing tip (visible on the left side of the figure 1). A tension of 1500 N increased the first bending frequency by about 50 %.

Other details of the test apparatus are presented in the formulary.

INSTRUMENTATION

Instrumentation of the model consists of two pressure sections with 53 steady and unsteady pressure taps each. Details of span locations and chord distribution of these pressure taps are presented on figures 5 - 6 and table 2. Kulite transducers (type XCQL093D) were used for unsteady pressure measurements. In order to obtain more accurate pressure measurements, pressure taps do not have the same layout on the lower and the upper surfaces. Pressure taps on upper surface are mainly put around the spoiler while they are concentrated near the flap hinge on the lower surface.

There was no steady deflection measurement of the model. Steady torsion was indirectly observed through Cpm distribution on the outside measurement section. This effect was almost non-existent on the mid-span section.

Dynamic deflection of the model was measured with 16 accelerometers, 6 on the spoiler, 4 on the flap and 6 on the fixed part. Locations of these accelerometers are shown on Figure 6 and Table 3.

Control surface motion was measured by two rotating potentiometers located on hydraulic actuator's shaft.

AVAILABLE DATA

Only measurements with trailing edge flap motion are provided in this data base, none relevant to the spoiler configuration are included. In order to limit the amount of data, a reduced number of representative data points has been chosen; these points and the corresponding test conditions are listed on table 4. The pressure data file "pressure.txt" includes steady, quasi-steady and unsteady pressure distributions on the mid-span section (upper and lower surface at Y= 509 mm). A self-explanatory listing of one data set is presented, with corresponding graphs, in the appendix. Accelerometer measurements are also included for all the selected points in a separate data file "accelero.txt".

CONTENTS OF NUMERICAL DATA FILES

The folder includes three ASCII data files. The file named 'airfoil.txt' contains the co-ordinates of the theoretical airfoil shape as presented in table1 (Size = 2 KB).

The file named 'pressure.txt' contains all steady, quasi-steady and unsteady pressure measurements for the data points listed in table 4 (Size = 59 KB). An example of the format used is presented in the appendix; it is self-explanatory, and all symbols are listed above. Quasi-steady values were calculated from 2 steady measurements with 2 different flap deflections (+0.5 and -0.5 deg. from the indicated deflection). Quasi-steady distributions are comparable with unsteady Cp distribution modulus at low frequency.

Accelerometer measurements, and locations, are included in the file 'accelero.txt' (Size = 22 KB). The values presented correspond to the transfer function between acceleration and angle measured at the flap root. Two frequencies are presented, so there are two complex values, measured by accelerometer in (m/s^2)/deg.

FORMULARY

1 General Description of model

1.1	Designation	ONERA 2D Supersonic wing
1.2	Type	Generic model
1.3	Derivation	Model manufactured at ONERA
1.4	Additional remarks	None
1.5	References	1

2 Model Geometry

2.1	Planform	Rectangular
2.2	Aspect ratio	2.75
2.3	Leading edge sweep	0°
2.4	Trailing edge sweep	0°
2.5	Taper ratio	N/A
2.6	Twist	0°
2.7	Wing chord	400 mm
2.8	Semi-span of model	1100 mm
2.9	Area of planform	0.44 m^2
2.10	Definition of profiles	7 % supersonic airfoil, bi-convex symmetric sharp leading edge (see figure 4, table 1 and file "airfoil.txt" for co-ordinates)
2.11	Wing-body	None
2.12	Form of wing tip	Straight
2.14	Control surface details	2 rectangular control surfaces (flap and spoiler) (see figure 3 for positions and dimensions, and figure 4 for maximum steady amplitude)
2.15	Additional remarks	Two guys were fixed between the middle of the wing tip and the right side wall for improving dynamic behavior of the model. Tension in guys was about 1500 N. Attachment point on the model was on the rotating axis (see figure 1).

3 Wind Tunnel

3.1	Designation	ONERA S2 at Modane
3.2	Type of tunnel	Continuous, variable pressure
3.3	Test section dimensions	Height = 1.935 m, width = 1.75 m
3.4	Type of roof and floor	Solid
3.5	Type of side walls	Solid
3.6	Ventilation geometry	N/A
3.7	Thickness of side wall boundary layer	150 mm at model location (empty tunnel, for any Mach number)
3.8	Thickness of boundary layers at roof and floor	150 mm at model location (empty tunnel, for any Mach number)
3.9	Method of measuring velocity	Not Available
3.10	Flow angularity	Not Available
3.11	Uniformity of velocity over test section	Not Available
3.12	Sources and levels of noise or turbulence in empty tunnel	Not Available
3.13	Tunnel resonance's	Fan blade resonance's
3.14	Additional remarks	None

3.15	References on tunnel	None

4 Model motion

4.1	General description	Steady incidence about an axis normal to wind tunnel side-wall located on the middle of root chord.
4.2	Natural frequencies and normal modes of model and support system	First bending mode at 37 Hz, torsion at 76.9 Hz, second bending mode at 96.3 Hz (with the tensioned guy lines). The values of excitation frequencies have been chosen between modal frequencies in order to avoid dynamic deformation of the wing. Only rotation of the trailing edge has to be taken into account in CFD simulations. Acceleration measurements are provided to check that dynamic motion of the wing is negligible.

5 Test Conditions

5.1	Model planform area/tunnel area	13 %
5.2	Model span/tunnel width	62.86 %
5.3	Blockage	1.2 % max.
5.4	Position of model in tunnel	Model fixed on a wall turret on the left side wall
5.5	Range of Mach number	1.65, 2.0, 2.5
5.6	Range of tunnel total pressure	0.9 bar
5.7	Range of tunnel total temperature	300 K
5.8	Range of model steady or mean incidence	-2, 0, +2 deg.
5.9	Definition of model incidence	model incidence defined relative to horizontal wind tunnel axis
5.10	Position of transition, if free	Not available
5.11	Position and type of strip, if transition fixed	Free transition (no transition strip).
5.12	Flow instabilities during tests	Not available
5.13	Changes to mean shape of model due to steady aerodynamic load	Not measured
5.14	Additional remarks	None
5.15	References describing tests	1

6 Measurements and Observations

6.1	Steady pressures for the mean conditions	Yes
6.2	Steady pressures for small changes from the mean conditions	Yes
6.3	Quasi-steady pressures	Yes
6.4	Unsteady pressures	Yes
6.5	Steady section forces for the mean conditions by integration of pressures	No
6.6	Steady section forces for small changes from the mean conditions by integration	No
6.7	Quasi-steady section forces by integration	No
6.8	Unsteady section forces by integration	No
6.9	Measurement of dynamic motion at points of model	Yes
6.10	Observation or measurement of boundary layer properties	No
6.11	Visualisation of surface flow	No
6.12	Visualisation of shock wave movements	No
6.13	Additional remarks	None

7 Instrumentation

7.1 Steady pressure	2 sections with 53 taps each (total number 106)
7.1.1 Position of orifices spanwise and chordwise	Sections were located at Y= 504 and 704 mm. For each section there was 29 taps on the upper surface and 24 taps on the lower surface (see figure 5 and table 2 for locations).
7.1.2 Type of measuring system	PSI system
7.2 Unsteady pressure	2 sections with 53 pressure transducers each (total number 106)
7.2.1 Position of orifices spanwise and chordwise	Sections were located at Y= 509 and 709 mm. Chordwise layout is the same than steady pressure taps (see figure 4 and table 2 for locations.
7.2.2 Diameter of orifices	0.8 mm
7.2.3 Type of measuring system	ONERA's conditioners and amplifiers
7.2.4 Type of transducers	Kulite XCQL 093 5D
7.2.5 Principle and accuracy of calibration	Calibrated in situ with an harmonic pressure generator.
7.3 Model and control surfaces motion	
7.3.1 Method of measuring motion reference co-ordinate	Rotating potentiometer
7.3.2 Method of determining spatial mode of motion	16 accelerometers: 6 on the spoiler, 4 on the flap and 6 on the fixed part. Locations of these accelerometers are shown in Fig. 6 and Table 3
7.3.3 Accuracy of measured motion	0.01° (angle measurement with potentiometer)
7.4 Processing of unsteady measurements	
7.4.1 Method of acquiring and processing measurements	Sampling frequency was 32 times the frequency of the sinusoidal excitation
7.4.2 Type of analysis	Real time FFT
7.4.3 Unsteady pressure quantities obtained and accuracies achieved	Cp referenced to control surface motion
7.4.4 Method of integration to obtain forces	N/A
7.5 Additional remarks	Accelerometers measurements in file "accelero.txt"
7.6 References on techniques	None

8 Data presentation

8.1 Test cases for which data could be made available	---
8.2 Test cases for which data are included in this document	See Table 4
8.3 Steady pressures	See file "pressure.txt"
8.4 Quasi-steady or steady perturbation pressures	See file "pressure.txt"
8.5 Unsteady pressures	See file "pressure.txt" (2 frequencies)
8.6 Steady forces or moments	No
8.7 Quasi-steady or unsteady perturbation forces	No
8.8 Unsteady forces and moments	No
8.9 Other forms in which data could be made available	None
8.10 Reference giving other representations of data	None

9 Comments on data

9.1 Accuracy

	9.1.1 Mach number	±0.001 M
	9.1.2 Steady incidence	±0.01deg
	9.1.3 Reduced frequency	Not Available
	9.1.4 Steady pressure coefficients	Better than ±0.002 Cpm
	9.1.5 Steady pressure derivatives	Not Available
	9.1.6 Unsteady pressure coefficients	Not Available
9.2	Sensitivity to small changes of parameter	Not Available
9.3	Non-linearities	Not Available
9.4	Influence of tunnel total pressure	N/A (Constant pressure 0.9 bar)
9.5	Effects on data of uncertainty, or variation, in mode of model motion	Not Available
9.6	Wall interference corrections	Not Available
9.7	Other relevant tests on same model	None
9.8	Relevant tests on other models of nominally the same shapes	None
9.9	Any remarks relevant to comparison between experiment and theory	None
9.10	Additional remarks	None
9.11	References on discussion of data	N/A

10 Personal contact for further information

P. NAUDIN; ONERA, 29 Av. de la Div. Leclerc 92320 Chatillon, France

Tel: 33 01 46 73 46 21

Fax: 33 01 46 73 41 43

Email: naudin@onera.fr

11 List of references

1 P. Naudin, Résultats d'essais d'une maquette bi-dimensionnelle munie d'un spoiler et d'une gouverne en supersonique. Avril 1996 ONERA Report n° 24/5115RN031R

x/c	z/c	x/c	z/c	x/c	z/c
0	0	.38	3.232093E-02	.66	3.311437E-02
.02	5.966748E-03	.4	.0328363	.68	3.231008E-02
.04	9.564082E-03	.42	3.330968E-02	.7	3.138345E-02
.06	1.263181E-02	.44	3.374017E-02	.72	3.021743E-02
.08	1.534582E-02	.36	3.175883E-02	.74	2.896985E-02
.1	1.771105E-02	.38	3.232093E-02	.76	2.747098E-02
.12	1.972565E-02	.4	.0328363	.78	.0258573
.14	2.148475E-02	.42	3.330968E-02	.8	2.406145E-02
.16	2.299185E-02	.44	3.374017E-02	.82	2.209795E-02
.18	.0243222	.46	3.412692E-02	.84	2.001825E-02
.2	2.549977E-02	.48	.0344435	.86	1.775008E-02
.22	2.654872E-02	.5	3.469358E-02	.88	1.542041E-02
.24	2.748777E-02	.52	.0348817	.9	1.292678E-02
.26	2.833828E-02	.54	3.498145E-02	.92	1.041014E-02
.28	2.911947E-02	.56	3.496132E-02	.94	7.797632E-03
.3	.0298445	.58	3.485948E-02	.96	5.181032E-03
.32	3.052228E-02	.6	3.463373E-02	.98	2.590508E-03
.34	3.115928E-02	.62	.0342517	1	0
.36	3.175883E-02	.64	3.378113E-02		

Table 1: Theoretical airfoil co-ordinates

Upper Surface		Lower Surface	
X from L.E.(mm)	X/C (%)	X from L.E.(mm)	X/C (%)
20	5	20	5
40	10	40	10
60	15	60	15
80	20	80	20
100	25	100	25
120	30	120	30
140	35	140	35
152	38	164	41
160	40	188	47
168	42	212	53
175	43.75	236	59
182	45.5	260	65
188	47	272	68
194	48.5	284	71
204	51	294	73.5
212	53	304	76
220	55	312	78
228	57	326	81.5
236	59	335	83.75
244	61	344	86
252	63	353	88.25
260	65	362	90.5
268	67	371	92.75
276	69	380	95
284	71		
304	76		
326	81.5		
344	86		
362	90.5		

Table 2: Locations of unsteady pressure taps for sections at Y= 509 or 709 mm

	Nbr Accelero.	X from L.E.(mm)	X/C (%)	Y from root (mm)
Wing	1	80	20	242
	4	300	75	242
	7	80	20	542
	10	300	75	542
	13	80	20	948
	16	300	75	948
Flap	2	208	52	242
	3	234	58.5	242
	8	208	52	542
	9	234	58.2	542
	14	208	52	948
	15	234	58.2	948
Spoiler	5	336	84	242
	6	380	95	242
	11	336	84	542
	12	380	95	542

Table 3: Locations of accelerometers

Mach	Steady Angle of attack	Flap Deflection	Run Number	Steady Measur.	Quasi.-steady	1st Unsteady freq. (Hz)	2nd Unsteady freq. (Hz)
1.65	$\alpha1 = -2°$	$\beta1 = 0°$	301	x	x	60 (A=0.5)	125 (A=0.3)
	$\alpha2 = 0°$	$\beta1 = 0°$	305	x	x	60 (A=0.5)	130 (A=0.15)
		$\beta2 = 2°$	310	x	x	60 (A=0.5)	130 (A=0.2)
		$\beta3 = 4°$	313	x	x	70 (A=0.5)	130 (A=0.2)
	$\alpha3 = 2°$	$\beta1 = 0°$	317	x	x	70 (A=0.5)	130 (A=0.2)
2.0	$\alpha2 = 0°$	$\beta1 = 0°$	342	x	x	60 (A=0.5)	130 (A=0.2)
		$\beta2 = 2°$	348	x	x	60 (A=0.5)	130 (A=0.2)
		$\beta3 = 4°$	353	x	x	60 (A=0.5)	130 (A=0.2)
	$\alpha3 = 2°$	$\beta1 = 0°$	327	x	x	60 (A=0.5)	130 (A=0.2)
		$\beta2 = 2°$	332	x	x	60 (A=0.5)	130 (A=0.2)
2.5	$\alpha2 = 0°$	$\beta1 = 0°$	391	x	x	60 (A=0.5)	120 (A=0.2)
		$\beta2 = 2°$	397	x	x	60 (A=0.5)	120 (A=0.2)
		$\beta3 = 4°$	402	x	x	60 (A=0.5)	120 (A=0.2)
	$\alpha3 = 2°$	$\beta1 = 0°$	407	x	x	60 (A=0.5)	120 (A=0.2)
		$\beta2 = 2°$	412	x	x	60 (A=0.5)	120 (A=0.2)

Table 4: List of selected data points

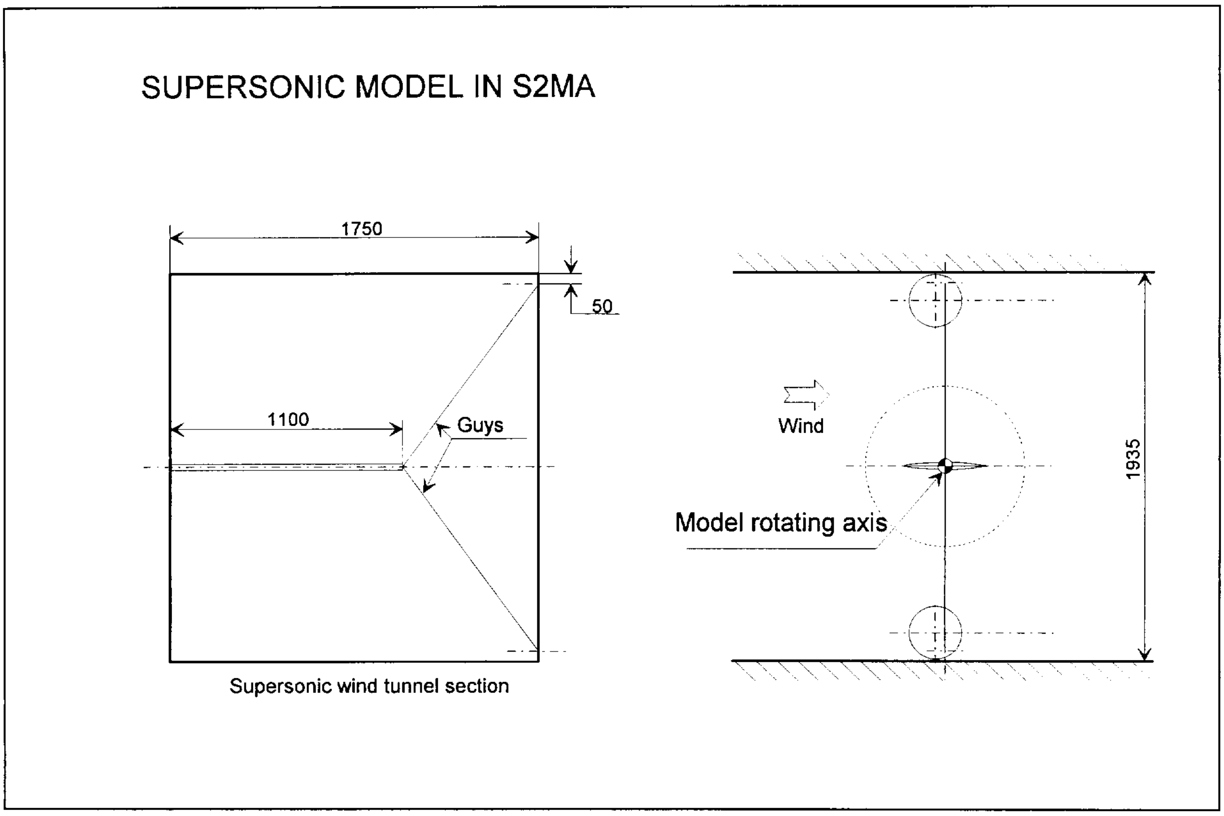

Figure 2: Dimensions of the wind-tunnel test section

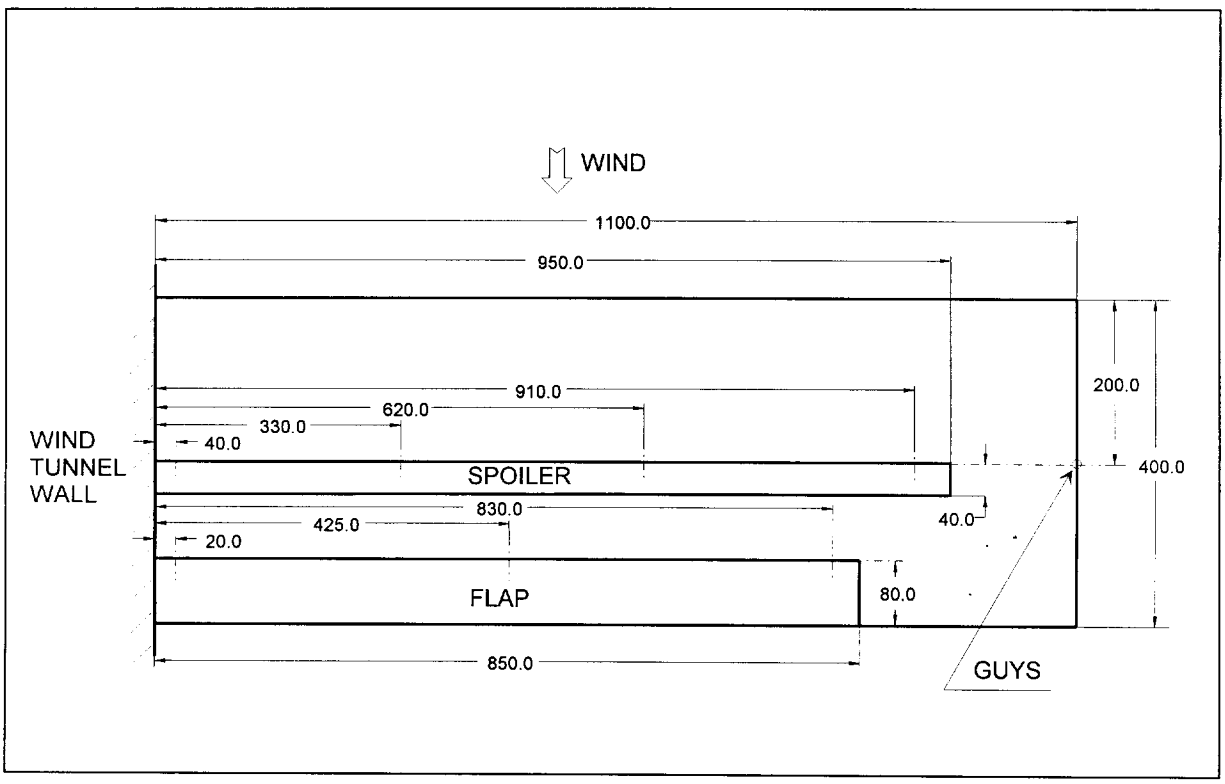

Figure 3: Dimensions of the model

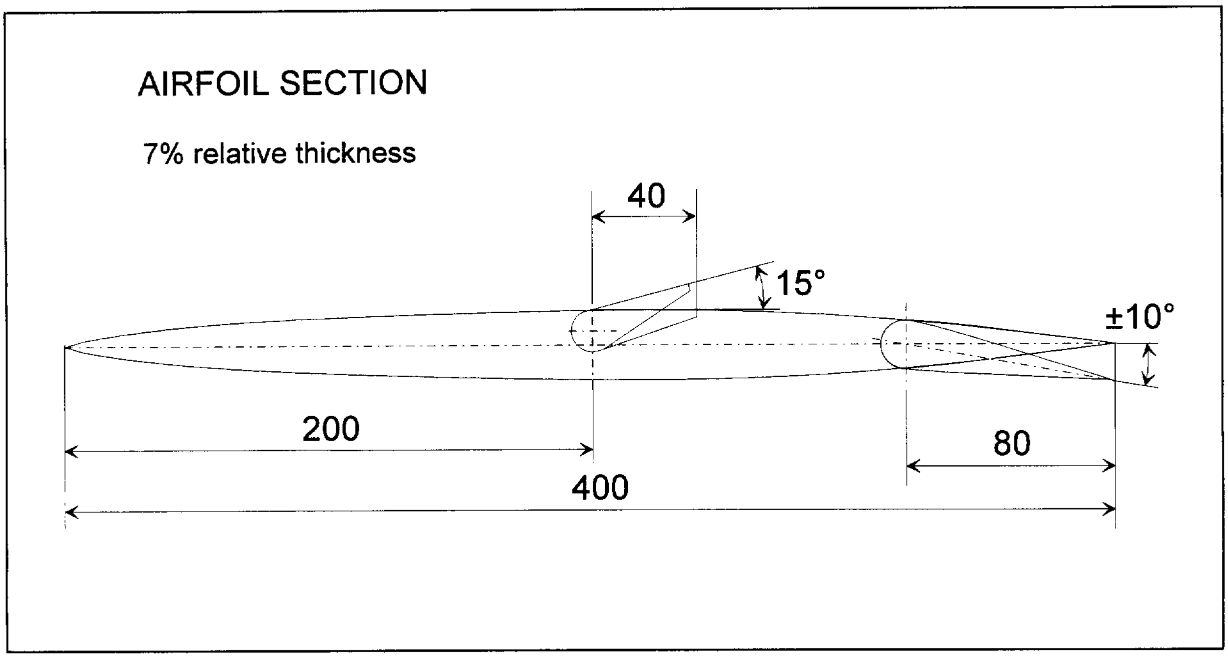

Figure 4: Airfoil and control surfaces

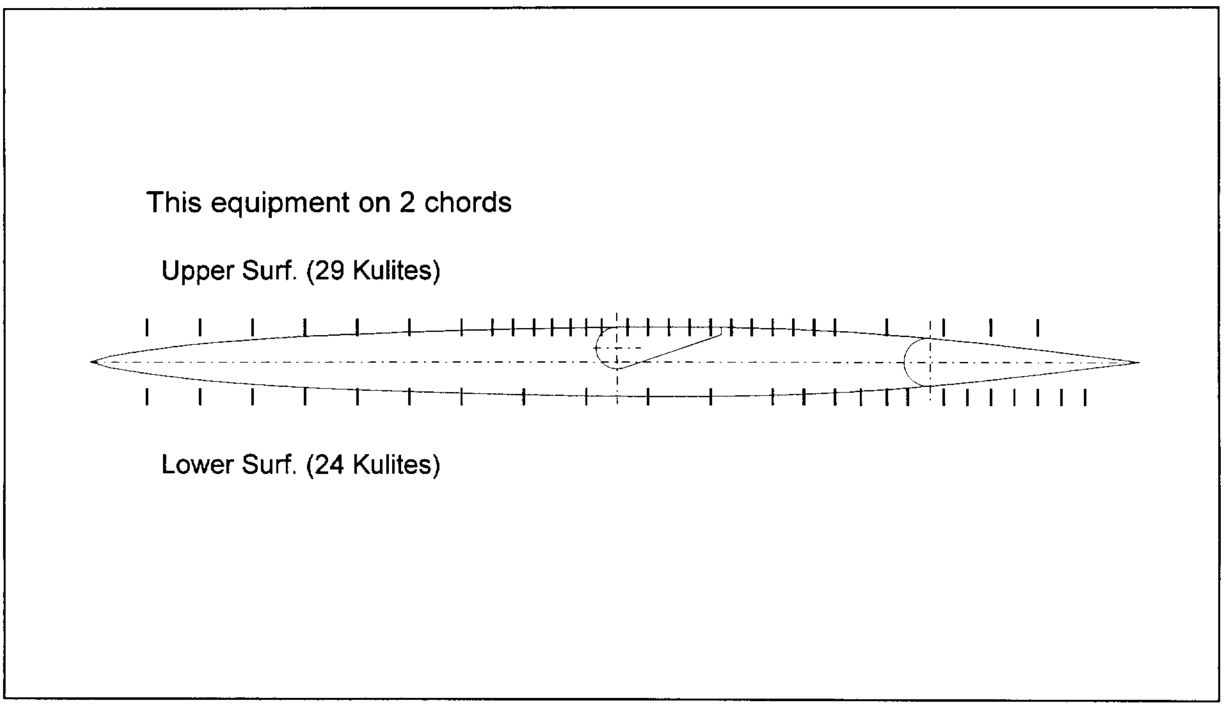

Figure 5: Transducers location

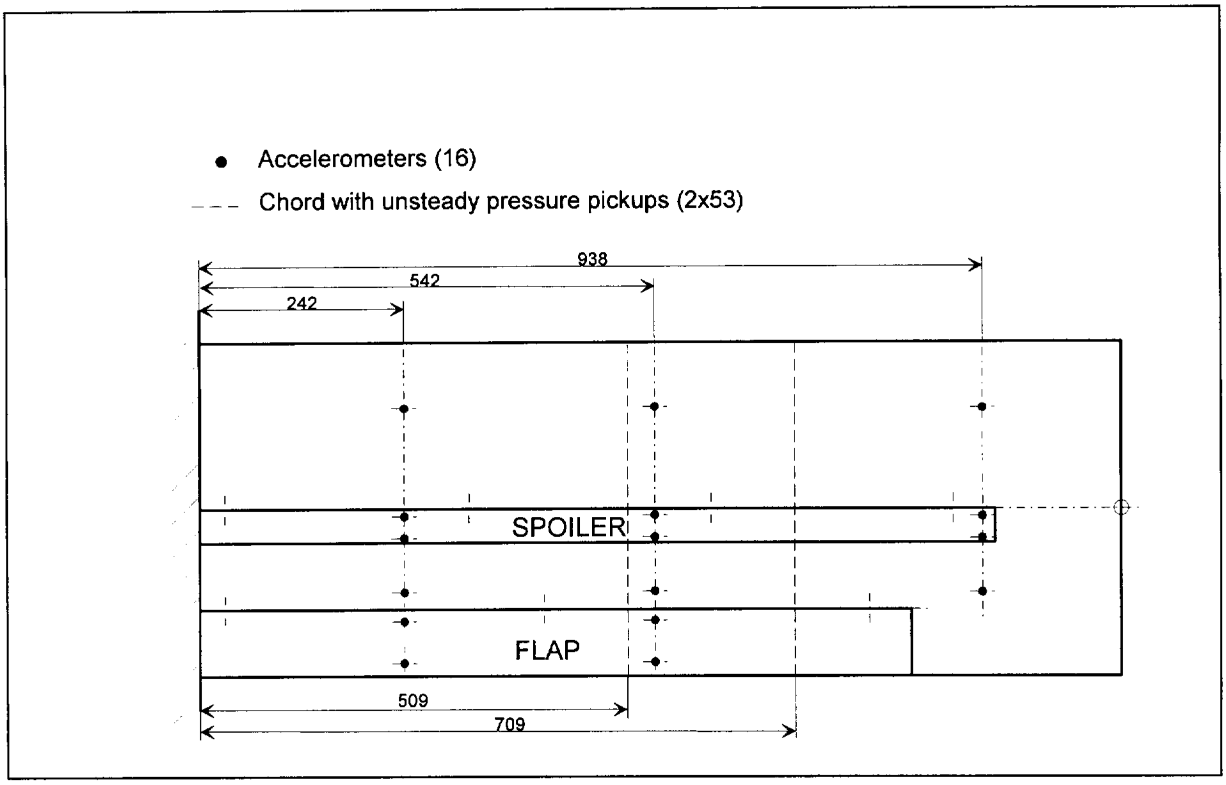

Figure 6: Placement of unsteady transducers

APPENDIX

Hereafter, an example of the formatted data file 'pressure.txt'. This part of file shows data relative to Run N° 305 (M= 1.65, alpha= 0, beta= 0). Steady and unsteady pressure coefficients distribution for this run are presented in Figures 7, 8 and 9.

```
Run= 305
M= 1.649    Pi0(Pa)= 89943    Ti0(K)= 299.83    Q0(Pa)= 37447.1
R= 5.04 million    alpha(deg.)= 0.008    beta(deg.)= -0.020
```

Upper Surface

			F:60 Hz	A:0.5	F:130 Hz	A:0.15
x/c	Cpm	Cpq	Re(Cp)	Im(Cp)	Re(Cp)	Im(Cp)
0.0500	-0.3018	0.0535	0.0189	0.0037	0.0786	-0.0108
0.1000	-0.1983	0.1083	0.0166	-0.0146	0.0316	0.0011
0.1500	-0.1393	0.0403	0.0145	-0.0032	0.1115	0.0033
0.2000	-0.1023	0.0764	0.0193	-0.0050	0.0460	-0.0048
0.2500	-0.0792	0.0116	0.0157	0.0006	0.0561	-0.0275
0.3000	-0.0641	0.0496	0.0085	0.0004	0.0640	-0.0153
0.3500	-0.0563	0.0729	0.0123	-0.0019	0.0479	-0.0151
0.3800	-0.0547	0.0328	0.0123	-0.0077	0.0569	0.0004
0.4000	-0.0553	0.1448	0.0180	-0.0088	0.0469	-0.0122
0.4200	-0.0505	0.0647	0.0215	-0.0040	0.0309	0.0001
0.4375	-0.0508	-0.0172	0.0198	-0.0011	0.0462	0.0007
0.4550	-0.0473	0.0073	0.0161	-0.0029	0.0641	0.0119
0.4700	-0.0429	0.0400	0.0142	-0.0015	0.0483	0.0044
0.4850	-0.0288	0.0071	0.0130	-0.0023	0.0405	0.0270
0.5100	-0.0146	0.0295	0.0123	0.0048	0.1255	-0.0270
0.5300	-0.0102	0.0047	0.0138	0.0002	0.0996	-0.0165
0.5500	-0.0254	0.0136	0.0092	-0.0044	0.1223	0.0030
0.5700	-0.0233	0.0302	0.0032	-0.0108	-0.0063	-0.1106
0.5900	-0.0081	-0.0601	0.0109	-0.0046	0.1268	0.0099
0.6100	0.0149	0.0350	0.0087	-0.0148	-0.0320	-0.0291
0.6300	0.0219	0.0347	0.0110	-0.0137	-0.0352	-0.0225
0.6500	0.0390	0.0330	0.0132	-0.0134	-0.0506	-0.0261
0.6700	0.0433	0.0881	0.0108	-0.0103	-0.0159	-0.0291
0.6900	0.0548	0.0156	0.0102	-0.0109	-0.0001	-0.0338
0.7100	0.0721	-0.0550	0.0078	-0.0131	-0.0153	-0.0366
0.7600	0.1009	-0.0197	0.0019	-0.0148	-0.0011	-0.0345
0.8150	0.1388	-0.8926	-1.0267	-0.0237	-3.3390	0.1980
0.8600	0.1449	-0.9555	-1.0544	0.0238	-3.3092	0.4860
0.9050	0.1428	-0.9722	-1.0674	0.0176	-3.2185	0.3293

Lower Surface

			F:60 Hz	A:0.5	F:130 Hz	A:0.15
x/c	Cpm	Cpq	Re(Cp)	Im(Cp)	Re(Cp)	Im(Cp)
0.0500	-0.3093	-0.0078	-0.0178	0.0005	-0.0861	-0.0276
0.1000	-0.2001	-0.0211	-0.0184	0.0015	-0.0837	0.0177

0.1500	-0.1347	-0.0097	-0.0220	0.0136	-0.0817	-0.0134
0.2000	-0.1009	0.0290	-0.0095	0.0060	-0.0849	-0.0212
0.2500	-0.0767	0.0345	-0.0075	0.0005	-0.0697	-0.0244
0.3000	-0.0620	0.0496	-0.0016	0.0029	-0.0639	-0.0019
0.3500	-0.0549	-0.0220	-0.0111	0.0045	-0.0463	0.0054
0.4100	-0.0445	-0.0240	-0.0133	0.0061	-0.0711	-0.0081
0.4700	-0.0376	-0.0174	-0.0073	-0.0004	-0.0643	-0.0270
0.5300	-0.0211	-0.0566	-0.0100	0.0048	-0.0748	-0.0228
0.5900	0.0003	-0.0413	-0.0123	0.0056	-0.0496	0.0007
0.6500	0.0289	0.0338	-0.0204	-0.0114	-0.0699	-0.0728
0.6800	0.0425	-0.0004	-0.0124	-0.0112	-0.0504	-0.0833
0.7100	0.0642	0.0162	-0.0110	-0.0115	-0.0637	-0.0670
0.7350	0.0771	-0.0033	-0.0113	-0.0100	-0.0556	-0.0646
0.7600	0.0872	0.0134	-0.0121	-0.0108	-0.0446	-0.0745
0.7800	0.0990	0.0034	-0.0134	-0.0127	-0.0501	-0.0814
0.8150	0.1336	0.8978	1.0383	-0.0236	3.3105	-0.3136
0.8375	0.1391	1.0306	1.0813	-0.0497	3.3478	-0.4582
0.8600	0.1428	0.9907	1.0888	-0.0709	3.2548	-0.5421
0.8825	0.1459	1.0320	1.1130	-0.0456	3.2976	-0.3863
0.9050	0.1507	0.9905	1.1055	-0.0051	3.3169	-0.1975
0.9275	0.1523	0.9821	1.0826	-0.0453	3.1006	-0.3928
0.9500	0.1570	1.0509	1.1165	0.0210	3.2651	-0.0127

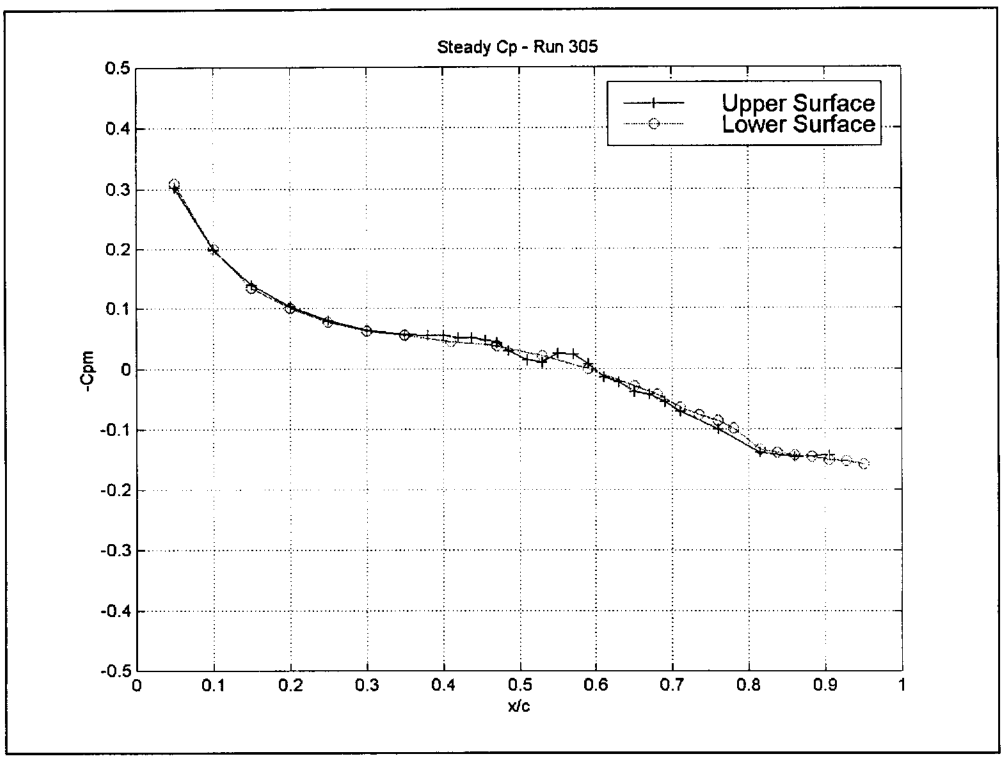

Figure 7

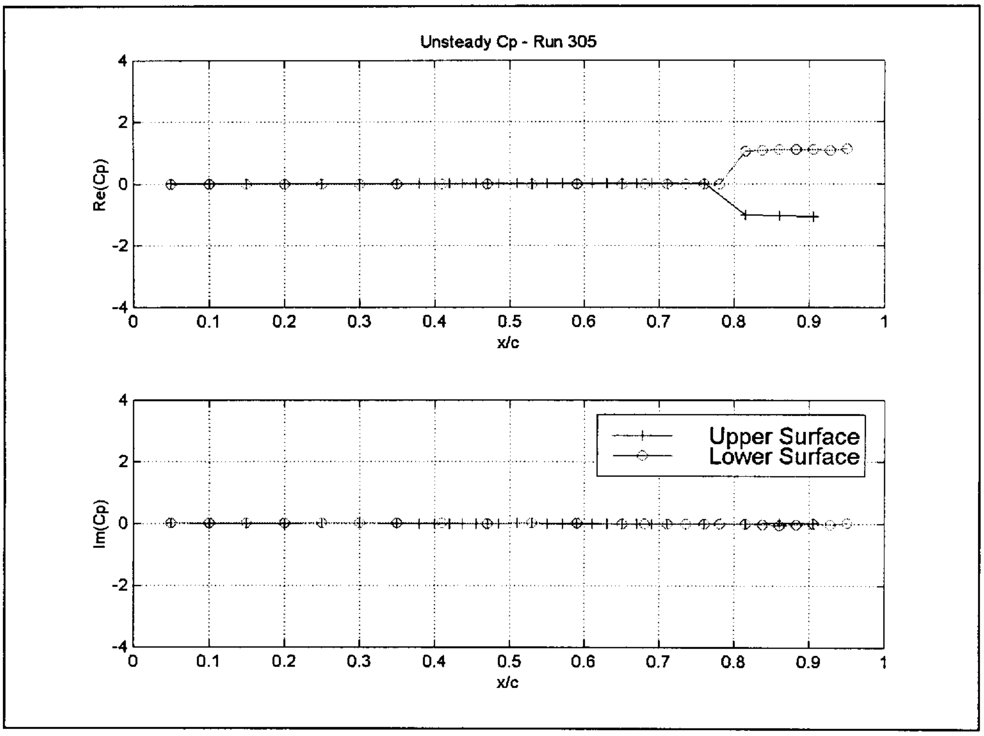

Figure 8: Cp F=60 Hz

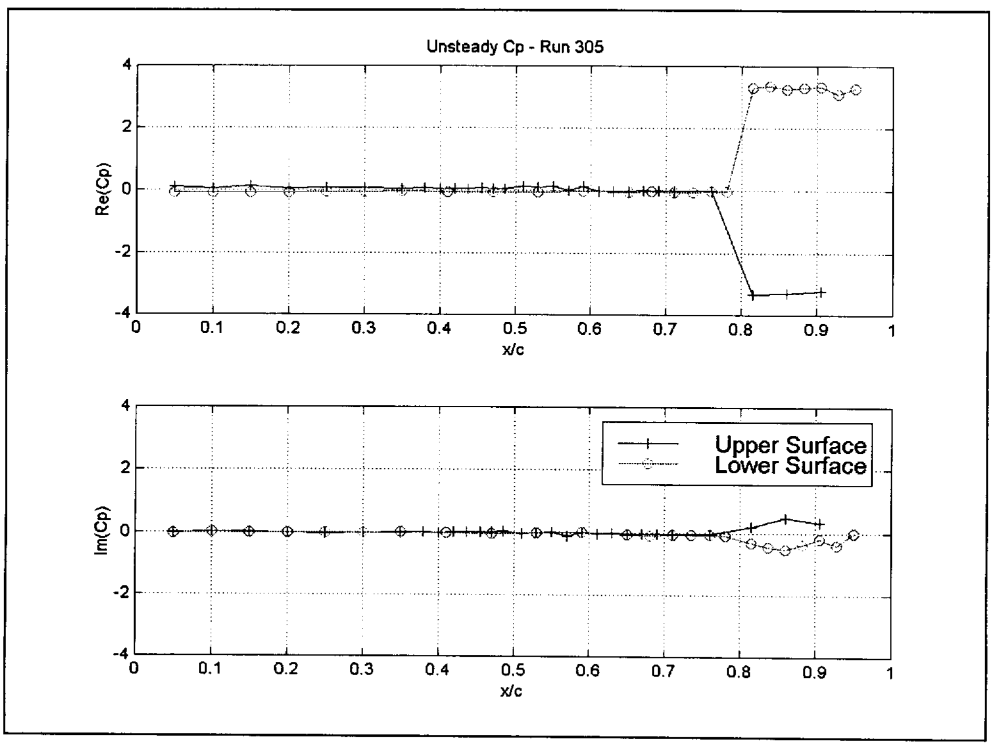

Figure 9: Cp F=130 Hz

11E. RAE TESTS ON AGARD TAILPLANE

Reported by
I W Kaynes
1008, A9
DERA
Farnborough
GU14 0LX
UK

INTRODUCTION

This data set relates to tests at RAE which were carried out and reported by D G Mabey, B L Welsh and B E Cripps, ref.1. The tests were undertaken to provide data for the validation of codes for the prediction of both steady and unsteady pressures on low aspect ratio configurations, suitable for the wings or controls of military aircraft. Comprehensive measurements have not been available to verify such codes, although some measurements were obtained during the NORA programme. This was a collaborative test on a low aspect ratio model oscillating about a swept axis, with the main aim of investigating dynamic interference in transonic wind tunnels. NORA was named after the participating organisations: NLR, ONERA, RAE, and AVA (branch of DFVLR). For the verification of transonic theories, a serious limitation of the NORA tests was that the steady and unsteady pressures were measured at different sections, with only a few measurements at each section. To overcome the lack of comprehensive measurements on a low aspect ratio configuration it was decided to make extensive measurements of steady and unsteady pressures on a model of the AGARD SMP (Structures and Materials Panel) tailplane, which has a planform similar to that of the wings and controls used on many military aircraft.

Previous tests have shown that for experiments in time-dependent aerodynamics it is essential to minimise aeroelastic distortion when the model is driven. To avoid measured pressures with a significant contribution due to the distortion in the present tests, the model had to move almost as a rigid body when it was oscillated at high frequencies. Hence the model was constructed in carbon fibre, which provided both high stiffness and low inertia. The high stiffness was aided by the 10% thickness of the section used, which is significantly thicker than the sections usually employed on combat aircraft. These two parameters ensured that the first bending frequency was high for a model of this size, 180 Hz when bolted to a large mass reducing to 120 Hz when the model was mounted on the drive system. This determined the maximum drive frequency to about 70 Hz, up to which frequency the model distortions were small.

This paper considers the measurements made in the RAE 3ft Wind Tunnel at Bedford in December 1982. The same model has been tested over a wider range of conditions in the DFVLR 1m Tunnel at Göttingen in October 1983 under a collaborative programme.

LIST OF SYMBOLS AND DEFINITIONS

c	local chord
C_p	pressure coefficient, $(p - p_\infty)/q$
C_{pm}	mean pressure coefficient, $(p - p_m)/q$
CPMAG	magnitude of oscillatory pressure coefficient C_p
CPPHASE	phase angle of oscillatory pressure coefficient C_p (deg)
CPST	steady pressure coefficients, mean value during oscillation C_{pm}
F	frequency (Hz)
M	free stream Mach number
M_e	local Mach number external to boundary layer
p	pressure
$\bar{p}$	root mean square pressure fluctuation
p_m	mean pressure during oscillation
p_∞	static pressure
q	dynamic pressure
Re	Reynolds number, based on wing semi-span

VMST	local Mach number
α	geometric angle of incidence (deg)
α_m	model angle of incidence corrected for flow angle (deg)
δ	pitch amplitude (deg)
ε	root mean square wing root strain
η	non-dimensional spanwise coordinate (based on model semi-span)
Λ_L, Λ_T	Sweep angle, leading edge and trailing edge, deg
ξ	non-dimensional chordwise coordinate (x/c)

PRESENTATION OF DATA

Sample flow visualisations are presented as data files VIS9A3.JPG, VIS9A5.JPG, VIS11A3.JPG, and VIS131A0.JPG (see 6.11)

The sectional geometry is given as an ASCII file RAEGEOM.DAT for 6 sections. The data are in the format of heading denoting the section station followed by 51 values of chordwise position and height.

The data for all runs are included on a single ASCII data file RAETPSEL.DAT. A FORTRAN program (RAETPR.FOR) is provided which demonstrates the extraction of the data. The program includes a sample main segment which lists the data of a run via a call to subroutine RAESEL. This subroutine may be employed in a user's code to extract the data for a single run or to serve as a model for other data extraction codes.

RAESEL subroutine

A description of the subroutine arguments follows:

```
      CALL RAESEL(NCH,IRUN,IPASS,VMACH,FREQ,DISPL,ALPHA,RE,V
     1 ,CPST,VMST,CPMAG,CPPHASE,NUMP,STN,IFAULT)
C
C-- Arguments are as defined below (all except NCH must be variables):
C   Input values
C         NCH     channel number to be used for reading the input file
C         IRUN    Specifies the required run number.
C   Returned values
C         IPASS   The data recording pass for this run
C         VMACH   The Mach number for this run
C         FREQ    The oscillatory frequency for this run (Hz)
C         DISPL   The oscillation amplitude for this run (deg)
C         ALPHA   The steady incidence for this run (deg)
C         RE      The Reynolds number for this run
C         V       The airspeed for this run (m/s)
C   The following 4 quantities are arrays of values at each chordwise location
C   on the 1 or 2 chords for which data is given in this pass
C         CPST    Static pressure coefficients
C         VMST    Local Mach numbers
C         CPMAG   Oscillatory pressure coefficients magnitude
C         CPPHASE Oscillatory pressure coefficients phase angle (deg)
C
C         NUMP    The number of data points in the above arrays
C         STN     The chordwise locations of transducers (same on each chord)
C                 array of size 20
C         IFAULT  Indicator of any faulty transducers in this data set
C                 (see table 2).  Integer array size 40, array elements are
C                 set non-zero for faulty transducer positions
```

Sample data

Sample output from RAEPTR for the data of run 459 is given below.

```
RUN 459 M=    1.31  FREQ=   70.31  AMPLITUDE=   .575  MEAN  ALPHA= -2.16
     stn      CP mag    CP phase      CP real    CP imag      CP steady
    .015      2.6315      -32.6       2.2161    -1.4191         .1384
    .025      2.7004      -31.2       2.3086    -1.4009         .0405
    .050      2.2566      -29.1       1.9708    -1.0991         .0157
    .100      1.4835      -28.2       1.3080     -.7000         .0879
    .150      1.3652      -23.8       1.2494     -.5503         .0652
    .200      1.2337      -20.0       1.1595     -.4214        -.0273
    .250      1.2614      -16.7       1.2082     -.3623        -.0812
    .300      1.1907      -14.2       1.1541     -.2930        -.1075
    .350  F    .0982      -46.6        .0675     -.0713         .0042
    .400      1.0141       -9.3       1.0007     -.1642        -.1608
    .450       .9494      -10.9        .9323     -.1795        -.2019
    .500       .9290       -6.9        .9223     -.1113        -.1699
    .550       .9190       -7.1        .9119     -.1141        -.1427
    .600       .9412      -12.6        .9186     -.2051        -.1333
    .650       .7965        8.8        .7872      .1214        -.1557
    .700       .7911        7.8        .7838      .1069        -.2055
    .750       .8691        5.3        .8653      .0809        -.2070
    .800       .8397        9.7        .8276      .1422        -.1573
    .850  F    .8146       13.3        .7929      .1869        -.0426
    .900       .8695       19.7        .8188      .2926        -.1339
```

FORMULARY

General Description of model

1.1	Designation	AGARD SMP Tailplane
1.2	Type	Low aspect ratio tailplane
1.3	Derivation	Planform used as standard configuration for prediction method evaluation
1.4	Additional remarks	
1.5	References	1

Model Geometry

2.1	Planform	Tapered low aspect ratio tailplane, see fig.1
2.2	Aspect ratio	2.42
2.3	Leading edge sweep	50.2°
2.4	Trailing edge sweep	14°
2.5	Taper ratio	0.27
2.6	Twist	0
2.7	Wing centreline chord	0.575m
2.8	Semi-span of model	0.442m
2.9	Area of planform	$0.161 m^2$
2.10	Location of reference sections and definition of profiles	NACA 64A010. See coordinates for 6 sections given in the data file RAEGEOM.DAT
2.11	Lofting procedure between reference sections	Constant section
2.12	Form of wing-body junction	None
2.13	Form of wing tip	Straight, no rounding
2.14	Control surface details	None

2.15	Additional remarks	For details of model structure see fig.2.
2.16	References	1

Wind Tunnel

3.1	Designation	RAE 3ft Tunnel
3.2	Type of tunnel	Transonic/supersonic
3.3	Test section dimensions	0.91m high, 0.64m wide
3.4	Type of roof and floor	Transonic: slotted; supersonic: closed
3.5	Type of side walls	Solid
3.6	Ventilation geometry	6% open area ratio
3.7	Thickness of side wall boundary layer	Not known
3.8	Thickness of boundary layers at roof and floor	Not known
3.9	Method of measuring Mach number	Sidewall static with a correction derived from calibration.
3.10	Flow angularity	Flow direction was considered to be the main factor in the observed angle of incidence for zero bending moment which varied from about +0.4° for M in range 0.65 to 0.9 to -0.4° for M=1.1 and 0° for M=1.2. Tests at zero mean aerodynamic incidence are included in the data, for comparison with the bulk of measurements which were made at zero mean geometric incidence. The geometric incidence for zero steady bending moment is given in table 1.
3.11	Uniformity of velocity over test section	Not known
3.12	Sources and levels of noise or turbulence in empty tunnel	See ref.2
3.13	Tunnel resonances	Significant preessure fluctuations at 3 Hz in subsonic tests
3.14	Additional remarks	For model installed in wind tunnel see fig.3.
3.15	References on tunnel	2, 3

Model motion

4.1	General description	Oscillated in pitch about an axis at 68.2% root chord.
4.2	Natural frequencies and normal modes of model and support system	Lowest frequency mode (fundamental bending) of model alone on fixed base 180 Hz, reduced to 120 Hz when model mounted on the drive system. This is significantly above the maximum oscillation frequency of 70 Hz.

Test Conditions

5.1	Model planform area/tunnel area	
5.2	Model span/tunnel height	0.486
5.3	Blockage	
5.4	Position of model in tunnel	Centrally mounted on side wall.
5.5	Range of velocities	
5.6	Range of tunnel total pressure	Tests presented here were all at 0.47 bar
5.7	Range of tunnel total temperature	Close to 293° K
5.8	Range of model steady or mean incidence	-5 to +5°
5.9	Definition of model incidence	Measured at root chord
5.10	Position of transition, if free	NA
5.11	Position and type of trip, if transition fixed	Band of ballotini 2mm wide at 0.075c. Ballotini diameter was 0.076mm for the subsonic and transonic tests (M<1.2) and 0.180mm for the supersonic tests.
5.12	Flow instabilities during tests	None recorded

5.13	Changes to mean shape of model due to steady aerodynamic load	Negligible
5.14	Additional remarks	-
5.15	References describing tests	1

Measurements and Observations

6.1	Steady pressures for the mean conditions	Y
6.2	Steady pressures for small changes from the mean conditions	N
6.3	Quasi-steady pressures	Y
6.4	Unsteady pressures	Y
6.5	Steady section forces for the mean conditions by integration of pressures	N
6.6	Steady section forces for small changes from the mean conditions by integration	N
6.7	Quasi-steady section forces by integration	N
6.8	Unsteady section forces by integration	N
6.9	Measurement of actual motion at points of model	N
6.10	Observation or measurement of boundary layer properties	N
6.11	Visualisation of surface flow	Y Visualisations made on prototype of the model (identical except for having only 2 pressure transducers). Sample visualisations are presented as data files VIS9A3, VIS9A5, VIS11A3, and VIS131A0. A sample is shown in fig. 4b (VIS9A5); note that these visualisations do not correspond to the conditions of specific test runs in the data.
6.12	Visualisation of shock wave movements	N
6.13	Aditional remarks	None

Instrumentation

7.1	Steady pressure	Measured with same transducers as unsteady pressure
	7.1.1 Position of orifices spanwise and chordwise	See 7.2.1
	7.1.2 Type of measuring system	See 7.2.3
7.2	Unsteady pressure	
	7.2.1 Position of orifices spanwise and chordwise	Instrumented sections on one surface at non-dimensional span η = 0.14, 0.42, 0.65, 0.84, 0.96. Each section has 20 chordwise measurement positions, at locations ξ = 0.015 0.025 0.05 0.1 0.15 0.2 0.25 0.3 0.35 0.4 0.45 0.5 0.55 0.6 0.65 0.7 0.75 0.8 0.85 0.9 Note that faults observed in specific transducers are recorded in table 2.
	7.2.2 Diameter of orifices	
	7.2.3 Type of measuring system	
	7.2.4 Type of transducers	Kulite pressure transducers type XCQL 093/25A mounted on lower surface of the model
	7.2.5 Principle and accuracy of calibration	Laboratory calibration as defined in ref.4
7.3	Model motion	
	7.3.1 Method of measuring motion reference coordinate	Steady incidence measured by a potentiometer on hydraulic actuator. Dynamic pitch amplitude derived from double integration of the signal from an accelerometer close to the model leading edge, see ref.1 appendix A.
	7.3.2 Method of determining spatial mode	Model distortion during the pitching excitation was assessed as

	of motion	very small by analysis
	7.3.3 Accuracy of measured motion	
7.4	Processing of unsteady measurements	
	7.4.1 Method of acquiring and processing measurements	Recorded on Presto system with capacity for 64 channel unsteady data. Note that to record data from all 5 sections runs were repeated three times (as shown in table 3, pass numbers 1, 2 ,3)
	7.4.2 Type of analysis	Harmonic analysis to give magnitude and phase angle of the unsteady pressure from each transducer.
	7.4.3 Unsteady pressure quantities obtained and accuracies achieved	Magnitude and phase of unsteady pressures. Repeatability very good for same conditions, ±0.06 for both real and imaginary parts of CP
	7.4.4 Method of integration to obtain forces	NA
7.5	Additional remarks	No
7.6	References on techniques	4, 5

Data presentation

8.1	Test cases for which data could be made available	See table 3
8.2	Test cases for which data are included in this document	See table 4. The test points which are not included here are those cases assessed as having large wind tunnel interference, those with large model motion, the sweep excitations, and the 3 Hz runs in the transonic section. Note that some of the runs which are included here are for conditions above the buffet threshold indicated in fig.4 (marked B in table 4).
8.3	Steady pressures	CPST
8.4	Quasi-steady or steady perturbation pressures	No
8.5	Unsteady pressures	Given in data as magnitude CPMAG and phase angle CPPHASE A sample contour plot of local Mach number and pressure for sample zero incidence case is given in figure 7.
8.6	Steady forces or moments	No
8.7	Quasi-steady or unsteady perturbation forces	No
8.8	Unsteady forces and moments	Unsteady root strain rms values shown in figures 4, 5, 6
8.9	Other forms in which data could be made available	Original data available from the author for all runs listed in table 3 in the same format used here for the runs of table 4
8.10	Reference giving other representations of data	1

Comments on data

9.1	Accuracy	
	9.1.1 Mach number	
	9.1.2 Steady incidence	Of the order of ±0.03°
	9.1.3 Reduced frequency	
	9.1.4 Steady pressure coefficients	Pressure measurement repeatability about ±0.002 at subsonic and transonic speeds, and about ±0.006 at supersonic speeds
	9.1.5 Steady pressure derivatives	NA
	9.1.6 Unsteady pressure coefficients	Repeatability of real or imaginary components estimated as ±0.06
9.2	Sensitivity to small changes of parameter	
9.3	Non-linearities	Minor effects found. Runs investigated the effects of oscillation amplitudes 0.4, 0.8, 1.2°.
9.4	Influence of tunnel total pressure	For a limited number of tests at M=0.86 α=0° the total pressure was increased by 50% (test 6). Both steady and unsteady measurements were virtually unaffected compared to the

		corresponding data for the regular total pressure.
9.5	Effects on data of uncertainty, or variation, in mode of model motion	For a pitch amplitude of 0.52°at M=0.86 the model distortion estimated to give an incidence of 0.03° at the wing tip for the worst-case frequency of 70 Hz.
9.6	Wall interference corrections	-
9.7	Other relevant tests on same model	The model was also tested in the 1m Tunnel at Göttingen
9.8	Relevant tests on other models of nominally the same shapes	-
9.9	Any remarks relevant to comparison between experiment and theory	-
9.10	Additional remarks	-
9.11	References on discussion of data	1

Personal contact for further information

Dr J Gibb
Unsteady Aerodynamics Team
DERA Bedford
Clapham
Bedford
England
MK41 6AE

jgibb@dera.gov.uk

List of references

1 D G Mabey, B L Welsh and B E Cripps. Measurements of steady and oscillatory pressures on a low aspect ratio model at subsonic and supersonic speeds. RAE TR 98095, 1984

2 D G Mabey. Flow unsteadiness in the new perforated working section of the 3ftx3ft tunnel. 1968

3 E P Sutton et al. Performance of the 3x2.9ft slotted transonic working section of the RAE Bedford 3ft wind tunnel. ARC R&M 3228.

4 B.L. Welsh, D.M. McOwat. Presto: a system for the measurement and analysis of time-dependent signals. RAE Technical Report 79135 (1979)

5 B.L. Welsh. A method to improve the temperature stability of semi-conductor strain gauge pressure transducers. RAE Technical Report 77155 (1977)

Table 1 Geometric incidence for zero steady bending moment

M	α	M	α
0.65	-0.31	1.10	+0.21
0.80	-0.31	1.20	0
0.86	-0.41	1.32	-0.1
0.90	-0.41	1.52	+0.2
0.95	-0.40	1.62	+0.1
1.05	+0.41	1.72	+0.1

Table 2 Pressure transducer faults

Transducer or cable faults were noted for the following conditions:

Run numbers	Section	η	ξ
1 to 353 (slotted transonic section)	1	0.14	0.35, 0.85
	2	0.42	0.40, 0.90
	3	0.65	0.20, 0.85
	4	0.84	0.45, 0.60(intermittent), 0.85
	5	0.96	-
354 to 499 (closed supersonic section)	1	0.14	0.35, 0.85
	2	0.42	0.40
	3	0.65	0.20, 0.85
	4	0.84	0.45, 0.60
	5	0.96	0.60, 0.80

Table 3 Tests for which data is available

Tests 1 to 6 — Slotted transonic section, Tests 7 to 10 — Closed supersonic section
Nominal Reynolds number $3*10^6$ for all tests except Test 6 at $4.5*10^6$

TEST 1 ZERO GEOMETRIC INCIDENCE

				Data points for sections		
α	M	δ	f	1 pass 3	2&3 pass 1	4&5 pass 2
0	0.65	0	0	238	136	2/7
0	0.65	0.4	3	239	137	—
0	0.65	0.4	12	240	138	3/9
0	0.65	0.4	33	241	139	4/10
0	0.65	0.4	70	242	140	5/11
0	0.65	0.4	S	243	141	6/12
0	0.80	0	0	244	142	13
0	0.80	0.4	3	245	143	14
0	0.80	0.4	12	246	144	15
0	0.80	0.4	33	247	145	16
0	0.80	0.4	70	248	146	17
0	0.80	0.4	S	249	147	18
0	0.86	0	0	250	148	19/55
0	0.86	0.4	3	251	149	20/56
0	0.86	0.4	12	252	150	21/57
0	0.86	0.4	33	253	151	22/58
0	0.86	0.4	70	254	152	23/59
0	0.86	0.4	S	255	153	24
0	0.90	0	0	256	154	25
0	0.90	0.4	3	257	155	26
0	0.90	0.4	12	258	156	27
0	0.90	0.4	33	259	157	28
0	0.90	0.4	70	260	158	29
0	0.90	0.4	S	261	159	30
0	0.95	0	0	262	160	31
0	0.95	0.4	3	263	161	32
0	0.95	0.4	12	264	162	33
0	0.95	0.4	33	265	163	34
0	0.95	0.4	70	266	164	35
0	0.95	0.4	S	267	165	36
0	1.05**	0	0	268	166	37
0	1.05**	0.4	3	269	167	38
0	1.05**	0.4	12	270	168	39
0	1.05**	0.4	33	271	169	40
0	1.05**	0.4	70	272	170	41
0	1.05**	0.4	S	273	171	42
0	1.10**	0	0	274	172	43
0	1.10**	0.4	3	275	173	44
0	1.10**	0.4	12	276	174	45
0	1.10**	0.4	33	277	175	46
0	1.10**	0.4	70	278	176	47
0	1.10**	0.4	S	279	177	48
0	1.20	0	0	280	178	49
0	1.20	0.4	3	281	179	50
0	1.20	0.4	12	282	180	51
0	1.20	0.4	33	283	181	52
0	1.20	0.4	70	284	182	53
0	1.20	0.4	S	285	183	54

TEST 1A ZERO AERODYNAMIC INCIDENCE

-0.37	0.86	0	0	332	190	—
-0.37	0.86	0.4	3	333	191	—
-0.37	0.86	0.4	12	334	192	—
-0.37	0.86	0.4	33	335	193	—
-0.37	0.86	0.4	70	336	194	—

Table 3 continued   Tests for which data is available

Tests 1 to 6 — Slotted transonic section, Tests 7 to 10 — Closed supersonic section
Nominal Reynolds number $3*10^6$ for all tests except Test 6 at $4.5*10^6$

TEST 1B ZERO AERODYNAMIC INCIDENCE

α	M	δ	f	Data points for sections 1 pass 3	2&3 pass 1	4&5 pass 2
-0.37	0.86	0.4	S	340	—	—
-0.37	0.86	0.8	S	341*	—	—

TEST 2 +2° GEOMETRIC INCIDENCE

α	M	δ	f	1 pass 3	2&3 pass 1	4&5 pass 2
+2	0.86	0	0	286	196	62
+2	0.86	0.4	3	287	197	63/74
+2	0.86	0.4	12	288	198	64
+2	0.86	0.4	33	289	199	65
+2	0.86	0.4	70	290	200	66
+2	0.86	0.4	S	291	201	67
-2	0.86**	0	0	292	202	68
-2	0.86**	0.4	3	293	203	69/77
-2	0.86**	0.4	12	294	204	70
-2	0.86**	0.4	33	295	205	71/72
-2	0.86**	0.4	70	296	206	90
-2	0.86**	0.4	S	297	207	73

TEST 3 TEST OF LINEARITY

α	M	δ	f	1 pass 3	2&3 pass 1	4&5 pass 2
+2	0.86	0.4	3	298	208	74/63
+2	0.86	0.8	3	299	209	75
+2	0.86	1.2	3	300	210	76
+2	0.86	0.4	12	301	211	86
+2	0.86	0.8	12	302	212	87
-2	0.86**	0.4	3	303	216	77
-2	0.86**	0.8	3	304	217	78
-2	0.86**	1.2	3	305	218	79
-2	0.86**	0.4	12	306	219	88
-2	0.86**	0.8	12	307	220	89

TEST 4 ±4° GEOMETRIC INCIDENCE

α	M	δ	f	1 pass 3	2&3 pass 1	4&5 pass 2
+4	0.86	0	0	308	—	80
+4	0.86	0.4	3	309	221	81
+4	0.86	0.4	S	310	222	82
-4	0.86**	0	0	311	—	83
-4	0.86**	0.4	3	312	223	84
-4	0.86**	0.4	S	313	224	85

Table 3 continued Tests for which data is available

Tests 1 to 6 — Slotted transonic section, Tests 7 to 10 — Closed supersonic section
Nominal Reynolds number $3*10^6$ for all tests except Test 6 at $4.5*10^6$

TEST 5 ±5° GEOMETRIC INCIDENCE

α	M	δ	f	Data points for sections 1 pass 3	2&3 pass 1	4&5 pass 2
+5	0.65	0	0	—	—	92
+5	0.65	0.4	3	—	—	93
+5	0.65	0.4	12	—	—	94
+5	0.65	0.4	33	—	—	95
+5	0.65	0.4	70	—	—	96
+5	0.65	0.4	S	—	—	97
+5	0.80	0	0	—	—	105
+5	0.80	0.4	3	—	—	106
+5	0.80	0.4	12	—	—	107
+5	0.80	0.4	33	—	—	108
+5	0.80	0.4	70	—	—	109
+5	0.80	0.4	S	—	—	110
+5	0.86	0	0	314	225	117
+5	0.86	0.4	3	315	226	118
+5	0.86	0.4	12	316	227	119
+5	0.86	0.4	33	317	228	120
+5	0.86	0.4	70	318	229	121
+5	0.86	0.4	S	319	230	122
-5	0.65	0	0	—	—	98
-5	0.65	0.4	3	—	—	99
-5	0.65	0.4	12	—	—	100
-5	0.65	0.4	33	—	—	101
-5	0.65	0.4	70	—	—	102
-5	0.65	0.4	S	—	—	103/104
-5	0.80	0	0	—	—	111
-5	0.80	0.4	3	—	—	112
-5	0.80	0.4	12	—	—	113
-5	0.80	0.4	33	—	—	114
-5	0.80	0.4	70	—	—	115
-5	0.80	0.4	S	—	—	116
-5	0.86**	0	0	326	231	123
-5	0.86**	0.4	3	327	232	124
-5	0.86**	0.4	12	328	233	125
-5	0.86**	0.4	33	329	234	126
-5	0.86**	0.4	70	330	235	127
-5	0.86**	0.4	S	331	236	—

TEST 6 ZERO GEOMETRIC INCIDENCE — HIGH REYNOLDS NUMBER

0	0.86	0	0	348	—	129
0	0.86	0.4	3	349	—	130
0	0.86	0.4	12	350	—	131
0	0.86	0.4	33	351	—	132
0	0.86	0.4	70	352	—	133
0	0.86	0.4	S	353	—	134/13

Table 3 continued   Tests for which data is available

Tests 1 to 6 — Slotted transonic section, Tests 7 to 10 — Closed supersonic section
Nominal Reynolds number $3*10^6$ for all tests except Test 6 at $4.5*10^6$

TEST 7   M = 1.32

				Data points for sections		
α	M	δ	f	1 pass 3	2&3 pass 1	4&5 pass 2
-0.13	1.32	0.4	3	456	410	354
-0.13	1.32	0.4	12	462	411	355
-0.13	1.32	0.4	33	466	412	356
-0.13	1.32	0.4	70	460	413	357
1.87	1.32	0.4	3	457	414/416	358
1.87	1.32	0.4	12	463	415	359
1.87	1.32	0.4	33	467	—	360
1.87	1.32	0.4	70	461	419	361
-2.13	1.32	0.4	3	458	420	362
-2.13	1.32	0.4	12	464	421	363
-2.13	1.32	0.4	33	465	417	364
-2.13	1.32	0.4	70	459	418	365
4.87	1.32	0.4	3	468	422	366
4.87	1.32	0.4	12	472	425	367
4.87	1.32	0.4	33	475	426	—
4.87	1.32	0.4	70	471	429	369
-5.13	1.32	0.4	3	469	423	370
-5.13	1.32	0.4	12	473	424	371
-5.13	1.32	0.4	33	474	427	—
-5.13	1.32	0.4	70	470	428	373
TEST 8 M = 1.52						
0	1.52	0.4	3	476	432	374
0	1.52	0.4	12	482	438	375
0	1.52	0.4	33	486	441	376
0	1.52	0.4	70	480	435	377
+5	1.52	0.4	3	477	433	378
+5	1.52	0.4	12	483	439	379
+5	1.52	0.4	33	487	442	380
+5	1.52	0.4	70	481	436	381
-5	1.52	0.4	3	478	434	382
-5	1.52	0.4	12	484	440	383
-5	1.52	0.4	33	485	443	384
-5	1.52	0.4	70	479	437	385
TEST 9 M = 1.62						
0	1.62	0.4	3	—	—	386
0	1.62	0.4	12	—	—	387
0	1.62	0.4	33	—	—	388
0	1.62	0.4	70	—	—	389
+5	1.62	0.4	3	—	—	390
+5	1.62	0.4	12	—	—	391
+5	1.62	0.4	33	—	—	392
+5	1.62	0.4	70	—	—	393
-5	1.62	0.4	3	—	—	394
-5	1.62	0.4	12	—	—	395
-5	1.62	0.4	33	—	—	396
-5	1.62	0.4	70	—	—	397

Table 3 continued   Tests for which data is available

Tests 1 to 6 — Slotted transonic section, Tests 7 to 10 — Closed supersonic section

TEST 10 M = 1.72

				Data points for sections		
α	M	δ	f	1	2&3	4&5
				pass 3	pass 1	pass 2
0	1.72	0.4	3	488	444	398
0	1.72	0.4	12	494	450	399
0	1.72	0.4	33	498	454	400
0	1.72	0.4	70	492	448	401
+5	1.72	0.4	3	489	445	402
+5	1.72	0.4	12	495	451	403
+5	1.72	0.4	33	499	455	404
+5	1.72	0.4	70	493	449	405
-5	1.72	0.4	3	490	446	406
-5	1.72	0.4	12	496	452	407
-5	1.72	0.4	33	497	453	408
-5	1.72	0.4	70	491	447	409

* Very large model amplitude
** Tunnel interference serious
S Denotes frequency sweep, from 5 to 75 Hz in 10 sec. Logarithmic sweep up to run 85, Linear sweep from run 116

Table 4 Tests for which data is presented in this report

Tests 1 to 6 — Slotted transonic section, Tests 7 to 10 — Closed supersonic section
Nominal Reynolds number 3*10^6 for all tests except Test 6 at 4.5*10^6

TEST 1 ZERO GEOMETRIC INCIDENCE

α	M	δ	f	Data points for sections 1 pass 3	2&3 pass 1	4&5 pass 2
0	0.65	0	0	238	136	2/7
0	0.65	0.4	12	240	138	3/9
0	0.65	0.4	33	241	139	4/10
0	0.65	0.4	70	242	140	5/11
0	0.80	0	0	244	142	13
0	0.80	0.4	12	246	144	15
0	0.80	0.4	33	247	145	16
0	0.80	0.4	70	248	146	17
0	0.86	0	0	250	148	19/55
0	0.86	0.4	12	252	150	21/57
0	0.86	0.4	33	253	151	22/58
0	0.86	0.4	70	254	152	23/59
0	0.90	0	0	256	154	25
0	0.90	0.4	12	258	156	27
0	0.90	0.4	33	259	157	28
0	0.90	0.4	70	260	158	29
0	0.95	0	0	262	160	31
0	0.95	0.4	12	264	162	33
0	0.95	0.4	33	265	163	34
0	0.95	0.4	70	266	164	35
0	1.20	0	0	280	178	49
0	1.20	0.4	12	282	180	51
0	1.20	0.4	33	283	181	52
0	1.20	0.4	70	284	182	53

TEST 1A ZERO AERODYNAMIC INCIDENCE

-0.37	0.86	0	0	332	190	—
-0.37	0.86	0.4	12	334	192	—
-0.37	0.86	0.4	33	335	193	—
-0.37	0.86	0.4	70	336	194	—

TEST 1B ZERO AERODYNAMIC INCIDENCE

-0.37	0.86	0.4	33	337	—	—
-0.37	0.86	0.8	33	338	—	—
-0.37	0.86	1.2	33	339	—	—

TEST 2 +2^O GEOMETRIC INCIDENCE

+2	0.86	0	0	286	196	62
+2	0.86	0.4	12	288	198	64
+2	0.86	0.4	33	289	199	65
+2	0.86	0.4	70	290	200	66

TEST 4 4^O GEOMETRIC INCIDENCE

+4	B 0.86	0	0	308	—	80
+4	B 0.86	0.4	3	309	221	81

Table 4 continued Tests for which data is presented in this report

Tests 1 to 6 — Slotted transonic section, Tests 7 to 10 — Closed supersonic section
Nominal Reynolds number $3*10^6$ for all tests except Test 6 at $4.5*10^6$

TEST 5 ±5° GEOMETRIC INCIDENCE

α	M	δ	f	Data points for sections 1 pass 3	2&3 pass 1	4&5 pass 2
+5	0.65	0	0	—	—	92
+5	0.65	0.4	12	—	—	94
+5	0.65	0.4	33	—	—	95
+5	0.65	0.4	70	—	—	96
+5	0.80	0	0	—	—	105
+5	0.80	0.4	12	—	—	107
+5	0.80	0.4	33	—	—	108
+5	0.80	0.4	70	—	—	109
+5	B 0.86	0	0	314	225	117
+5	B 0.86	0.4	12	316	227	119
+5	B 0.86	0.4	33	317	228	120
+5	B 0.86	0.4	70	318	229	121
-5	0.65	0	0	—	—	98
-5	0.65	0.4	12	—	—	100
-5	0.65	0.4	33	—	—	101
-5	0.65	0.4	70	—	—	102
-5	0.80	0	0	—	—	111
-5	0.80	0.4	12	—	—	113
-5	0.80	0.4	33	—	—	114
-5	0.80	0.4	70	—	—	115

TEST 6 ZERO GEOMETRIC INCIDENCE — HIGH REYNOLDS NUMBER

0	0.86	0	0	348	—	129
0	0.86	0.4	12	350	—	131
0	0.86	0.4	33	351	—	132
0	0.86	0.4	70	352	—	133

TEST 7 M = 1.32

-0.13	1.32	0.4	3	456	410	354
-0.13	1.32	0.4	12	462	411	355
-0.13	1.32	0.4	33	466	412	356
-0.13	1.32	0.4	70	460	413	357
1.87	1.32	0.4	3	457	414/416	358
1.87	1.32	0.4	12	463	415	359
1.87	1.32	0.4	33	467	—	360
1.87	1.32	0.4	70	461	419	361
-2.13	1.32	0.4	3	458	420	362
-2.13	1.32	0.4	12	464	421	363
-2.13	1.32	0.4	33	465	417	364
-2.13	1.32	0.4	70	459	418	365
4.87	1.32	0.4	3	468	422	366
4.87	1.32	0.4	12	472	425	367
4.87	1.32	0.4	33	475	426	—
4.87	1.32	0.4	70	471	429	369
-5.13	1.32	0.4	3	469	423	370
-5.13	1.32	0.4	12	473	424	371
-5.13	1.32	0.4	33	474	427	—
-5.13	1.32	0.4	70	470	428	373

Table 4 continued Tests for which data is presented in this report

Tests 1 to 6 — Slotted transonic section, Tests 7 to 10 — Closed supersonic section
Nominal Reynolds number $3*10^6$ for all tests except Test 6 at $4.5*10^6$

TEST 8 M = 1.52

α	M	δ	f	Data points for sections 1 pass 3	2&3 pass 1	4&5 pass 2
0	1.52	0.4	3	476	432	374
0	1.52	0.4	12	482	438	375
0	1.52	0.4	33	486	441	376
0	1.52	0.4	70	480	435	377
+5	1.52	0.4	3	477	433	378
+5	1.52	0.4	12	483	439	379
+5	1.52	0.4	33	487	442	380
+5	1.52	0.4	70	481	436	381
-5	1.52	0.4	3	478	434	382
-5	1.52	0.4	12	484	440	383
-5	1.52	0.4	33	485	443	384
-5	1.52	0.4	70	479	437	385

TEST 9 M = 1.62

α	M	δ	f	1 pass 3	2&3 pass 1	4&5 pass 2
0	1.62	0.4	3	—	—	386
0	1.62	0.4	12	—	—	387
0	1.62	0.4	33	—	—	388
0	1.62	0.4	70	—	—	389
+5	1.62	0.4	3	—	—	390
+5	1.62	0.4	12	—	—	391
+5	1.62	0.4	33	—	—	392
+5	1.62	0.4	70	—	—	393
-5	1.62	0.4	3	—	—	394
-5	1.62	0.4	12	—	—	395
-5	1.62	0.4	33	—	—	396
-5	1.62	0.4	70	—	—	397

TEST 10 M = 1.72

α	M	δ	f	1 pass 3	2&3 pass 1	4&5 pass 2
0	1.72	0.4	3	488	444	398
0	1.72	0.4	12	494	450	399
0	1.72	0.4	33	498	454	400
0	1.72	0.4	70	492	448	401
+5	1.72	0.4	3	489	445	402
+5	1.72	0.4	12	495	451	403
+5	1.72	0.4	33	499	455	404
+5	1.72	0.4	70	493	449	405
-5	1.72	0.4	3	490	446	406
-5	1.72	0.4	12	496	452	407
-5	1.72	0.4	33	497	453	408
-5	1.72	0.4	70	491	447	409

B : runs at conditions above the onset of Buffet as given in fig.4

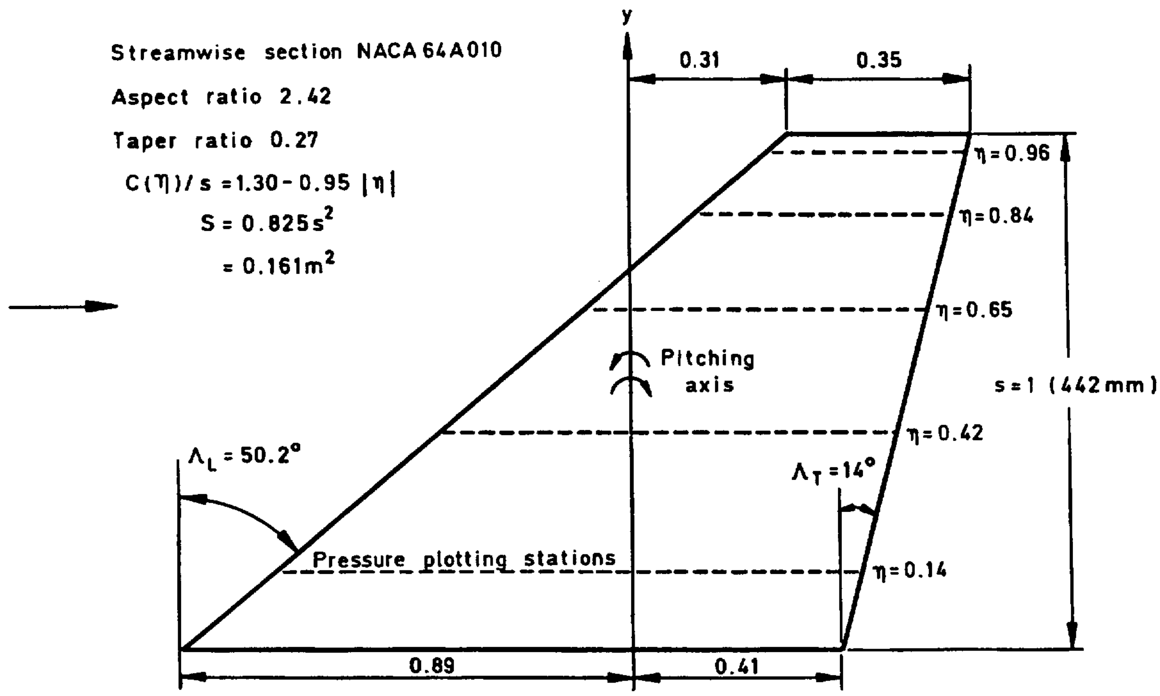

Fig.1 Planform of model (AGARD SMP tailplane)

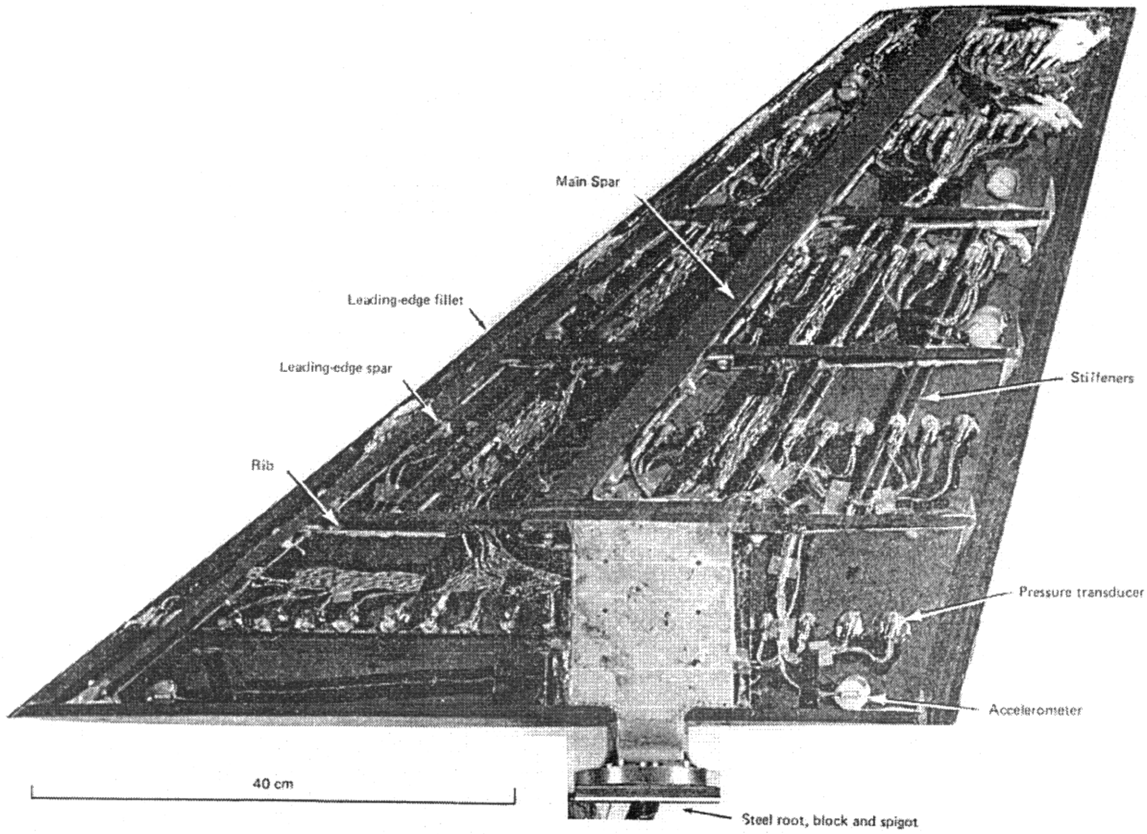

Fig.2 Interior of model

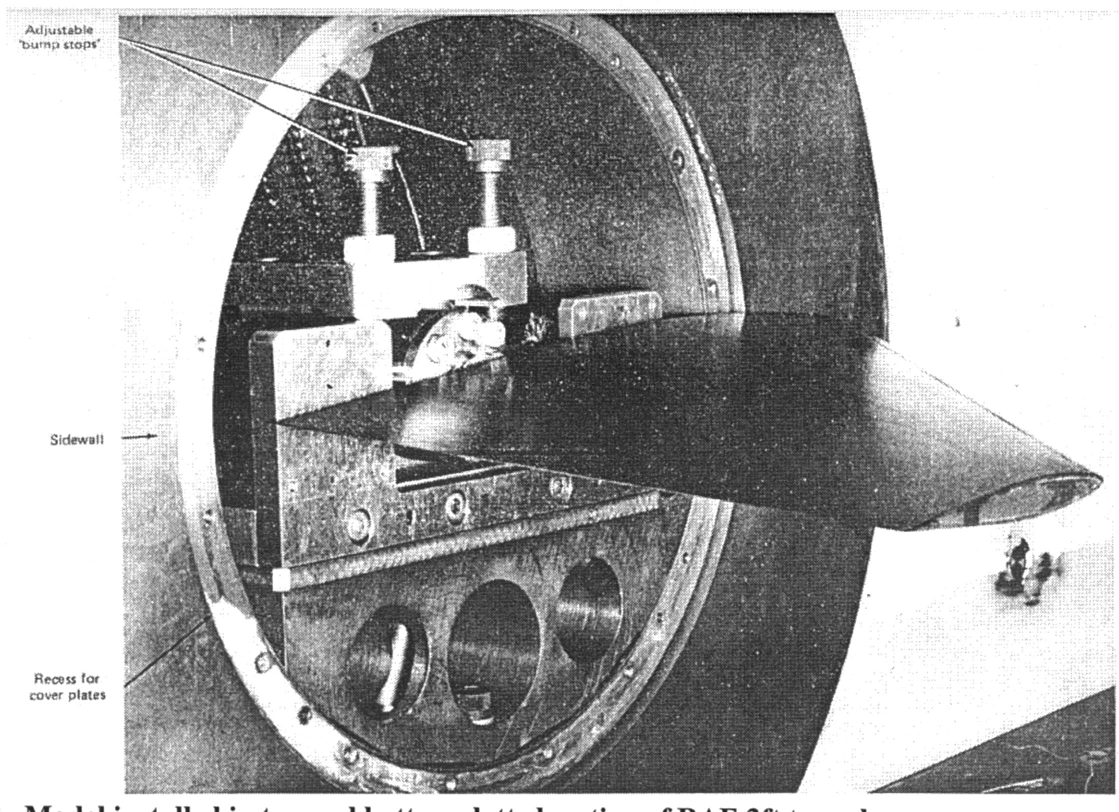

Fig.3 Model installed in top and bottom slotted section of RAE 3ft tunnel

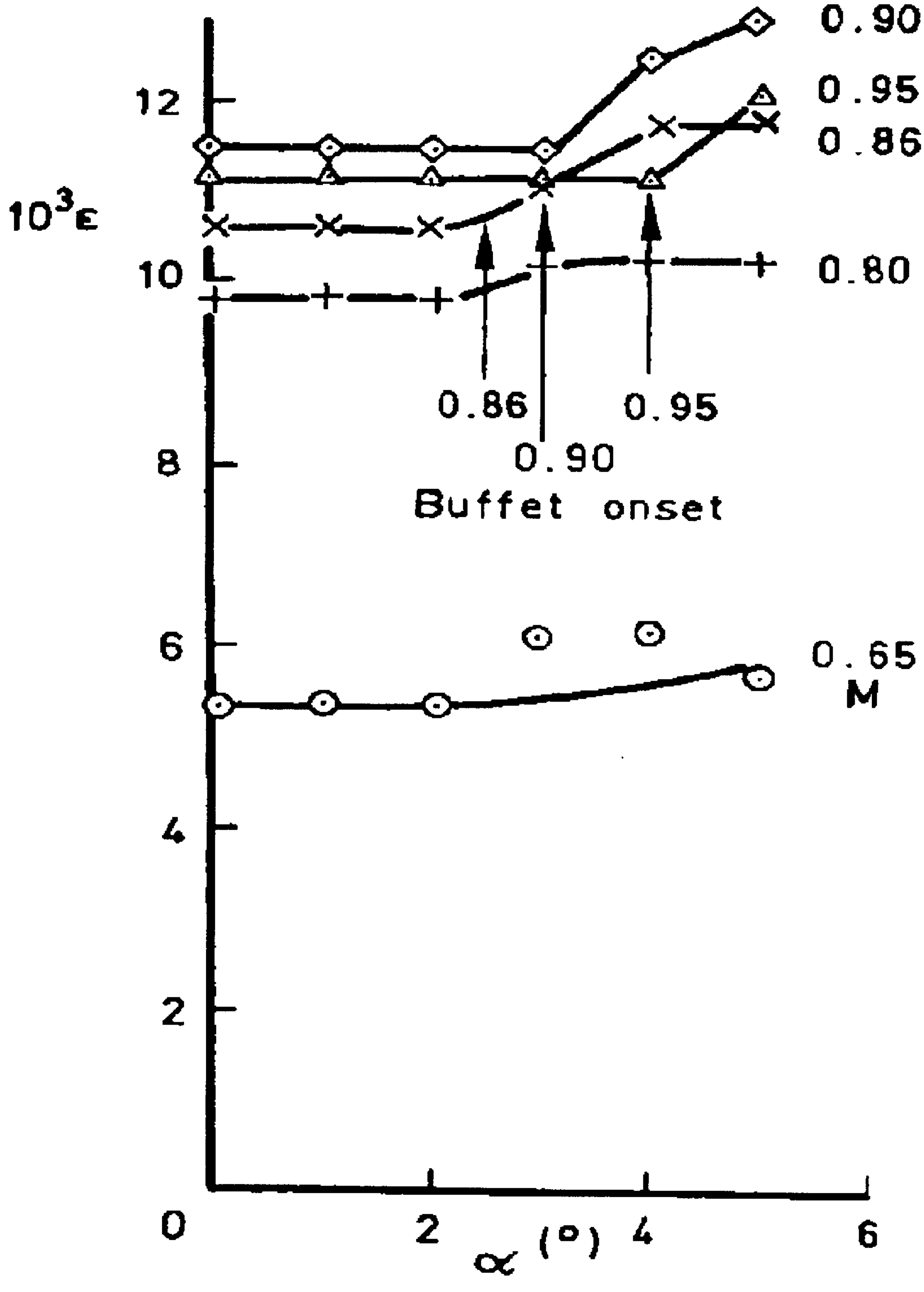

(a) rms unsteady root strain

Fig.4 Slotted section - subsonic and transonic speeds. Unsteady root strain and flow visualisation v incidence and Mach number

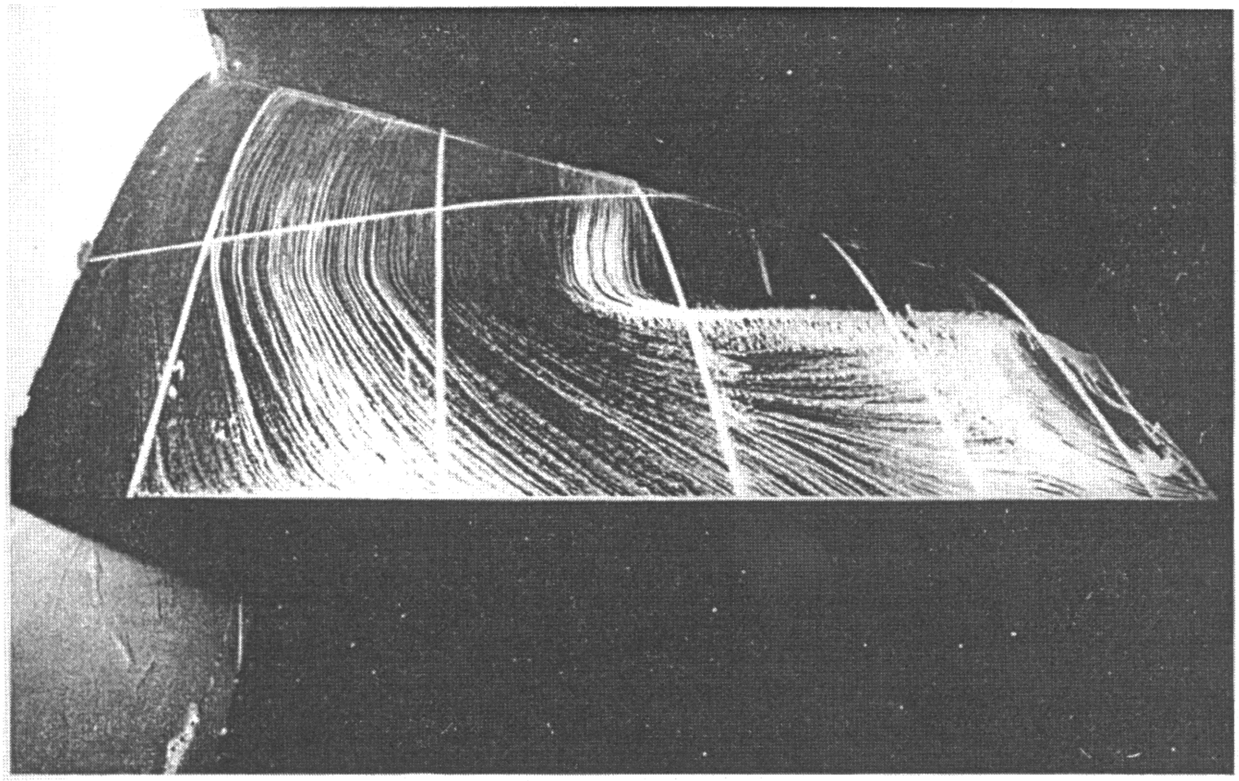

Flow visualisation, M = 0.90, α = 5°

Fig. 4b

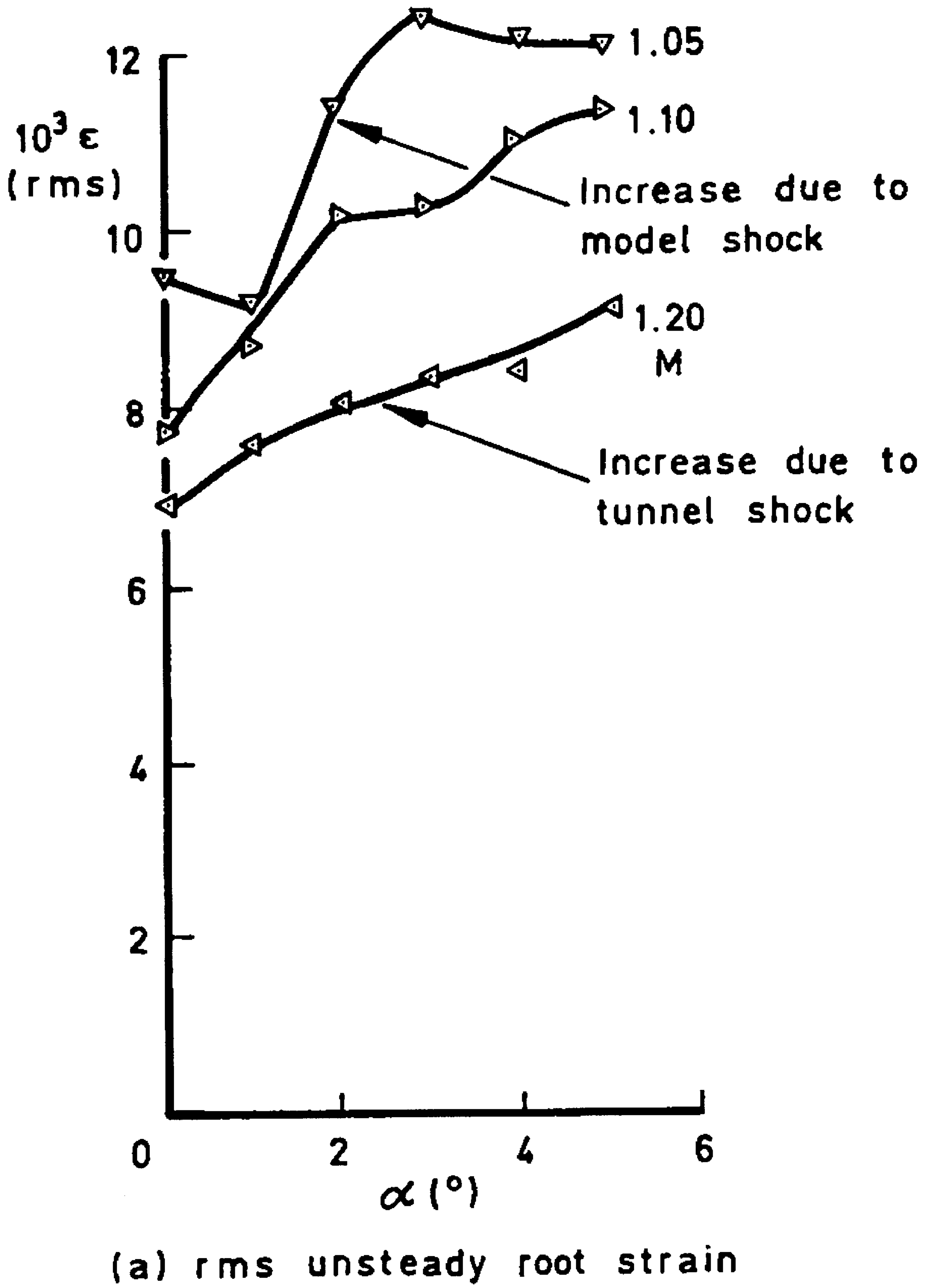

Fig. 5 Slotted section - supersonic speeds. Unsteady root strain and flow visualisation v incidence and Mach number

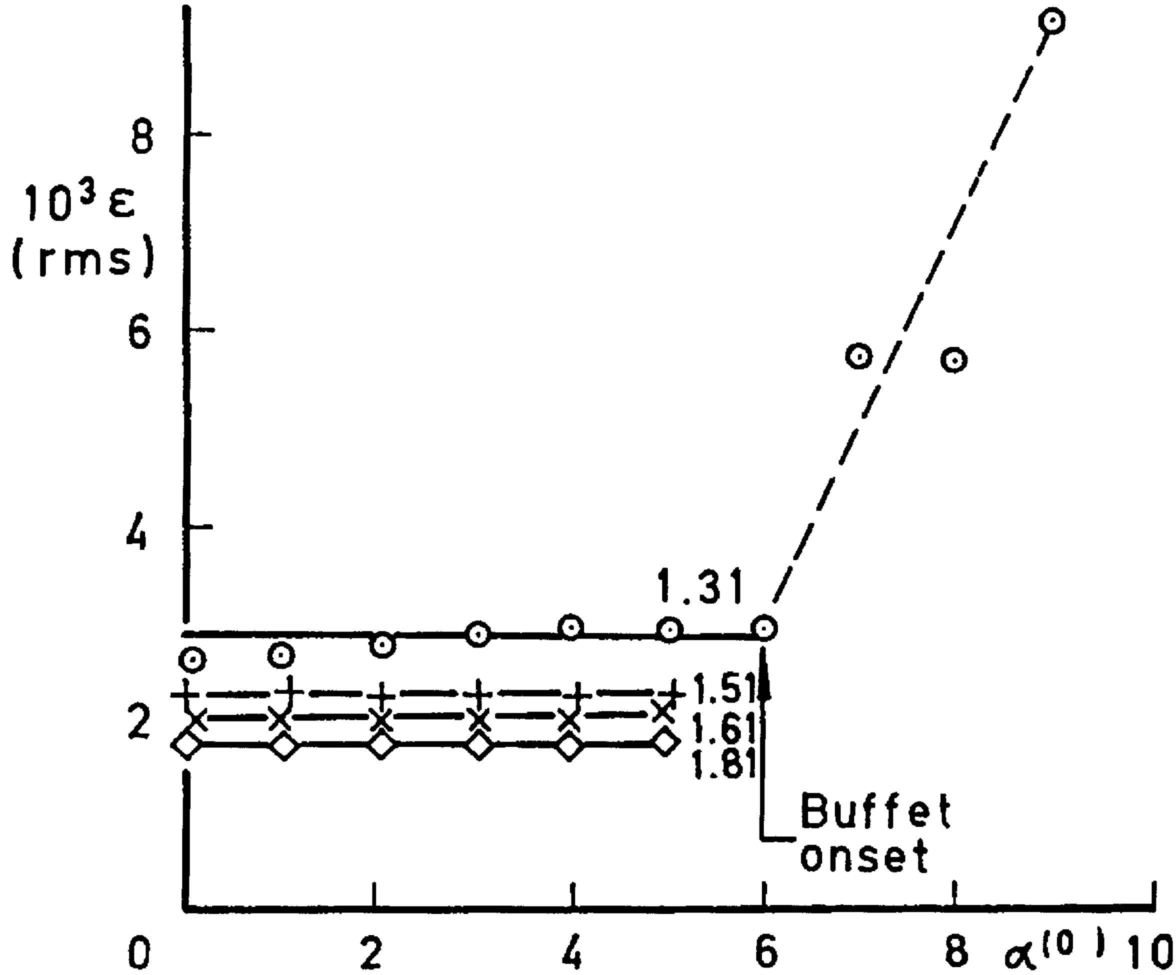

(a) rms unsteady root strain

Fig. 6 Closed section - supersonic speeds. Unsteady root strain and flow visualisation

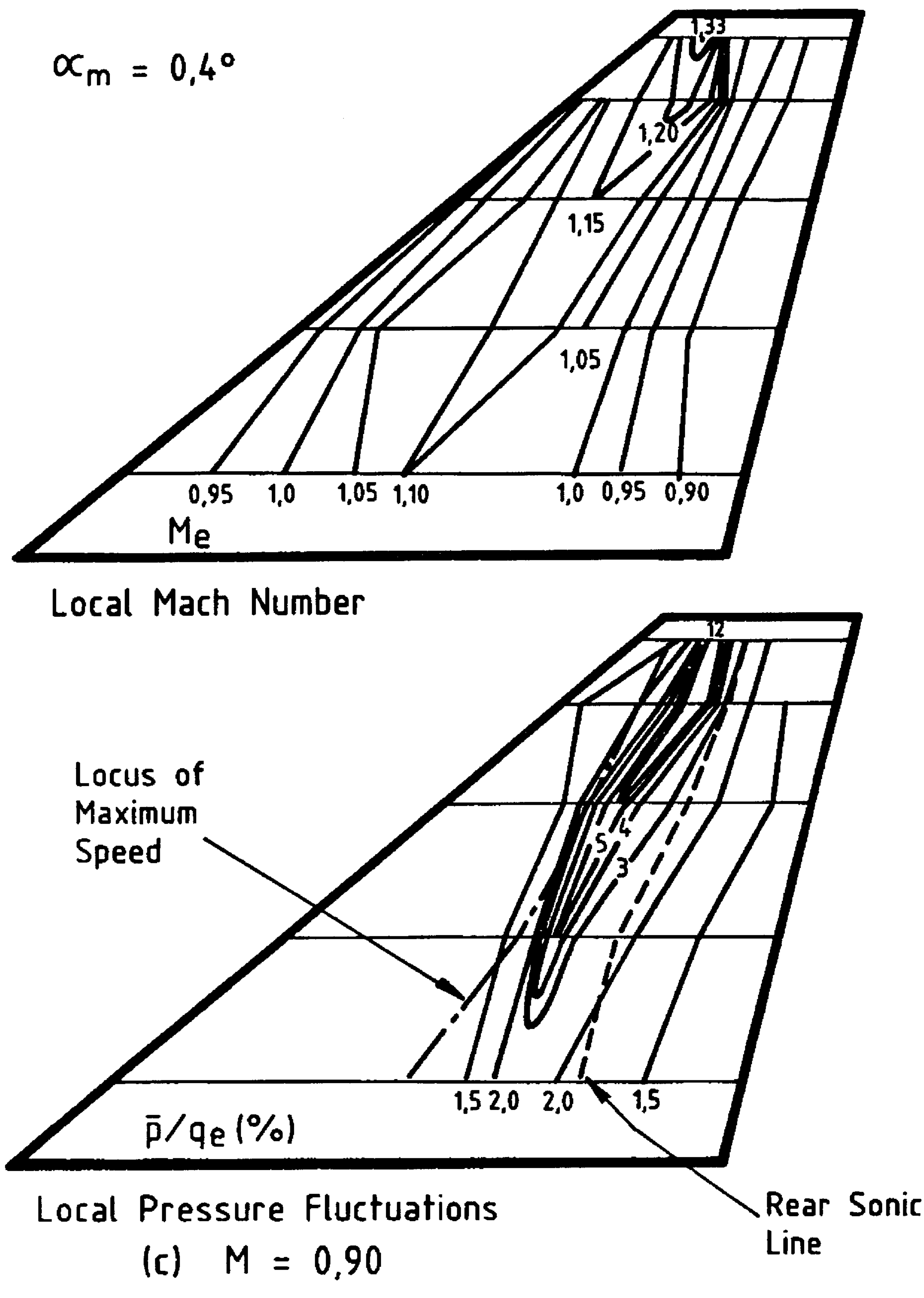

Fig. 7 Contour plots of local Mach numbers and rms pressure fluctuations at transonic speeds at $\alpha=0°$

12. NAL SST ARROW WING WITH OSCILLATING FLAP

M. Tamayama, K. Saitoh, H. Matsushita and J. Nakamichi

NAL, Tokyo

INTRODUCTION

A wind tunnel model of a SST(Supersonic Transport) arrow wing was tested in transonic regime. The purpose of this experiment is to accumulate verification data for the establishment of aeroelasticity related CFD codes and ACT (Active Control Technology) in the Japanese SST program.

The model is a semi-span arrow wing with a fuselage. The leading edge is double-swept-backed as shown in Fig. 1 and 2. The inboard sections of the model was constructed mainly with 7 mm thickness aluminum plate. A NACA0003 airfoil was, then, shaped by urethane resin. The dimensionless coordinates are shown in Table 1. At outboard sections, the NACA0003 airfoil was directly manufactured by cutting down an aluminum alloy. The detailed information on the model fuselage is shown in Table 2. Table 6 shows the model's natural frequencies acquired by both FEM analysis and a vibration test. Figure 5 shows the contours of model natural modes acquired by FEM analysis.

There is a flap, which can oscillate in the rear part of the inboard wing. The flap was driven by an electric motor around a hinge shaft which is parallel with the trailing edge. The deflection angle of the flap was measured using an appropriate transducer with installed inside the model fuselage. Downward motion was measured as positive angle.

Main measurement items presented here are pressures and deformations of the model. Steady and unsteady components of pressures were measured independently in order to remove the effect of thermal drift of pressure transducers. The pressure orifices are located at positions shown in Table 3 and Fig. 3. Chord positions in Table 3 are those for unsteady pressure transducers. The positions of steady pressure orifices are slightly different, because the span positions deviates 0.4% from the unsteady pressure orifices. The steady pressure orifice No.15 was not available because of the blockage of the vinyl tube, and it is not included in the experimental data provided.

The dynamic deformation of the model was measured by tracing optical targets installed in the wing surface. The positions of the optical targets are shown in Table 4 and Fig. 4. Multiple targets distributed in spanwise direction were measured with a single CCD camera. Four CCD cameras were used. While there were problems with the light intensity and some of the camera measurement systems failed, dynamic deformations were obtained at the target positions shown in Table 7.1. Four accelerometers are installed in the model. The locations are shown in Table 5 and Fig. 4. The accelerometer signals are useful for the verification of the dynamic deformation measurement system.

Tables 8.1 to 8.6 included in the accompanying CD-ROM show the results of steady and unsteady components of pressure coefficient, unsteady aerodynamic forces, steady and dynamic optical target displacement, and unsteady accelerometer signals. The unsteady results are presented only by the fundamental and 2nd harmonic components based on the flap frequency. The FFT function of Matlab was utilized in the frequency analysis. After data were FFT-processed in several intervals beginning from different time, they were averaged. The data length was double the sample frequency for each FFT-processing. The unsteady results presented in Tables 8.1 to 8.6 are not normalized by the flap amplitude. The phase characteristics are presented with respect to the flap motion. The results are also shown in Figs. 6, 7.1 to 7.12, 8.1, 8.2 and 9.1 to 9.6 (the whole set of figures is included in the accompanying CD-ROM here only some examples are presented). In these figures, only the fundamental component normalized by flap amplitude is shown.

LIST OF SYMBOLS AND DEFINITIONS

c	Local chord length
Cl	Unsteady section lift coefficient (normalized with c)
Cm	Unsteady section moment coefficient about 25% local chord (normalized with c^2)
c_{mean}	Mean geometrical chord length (1.27 m)
Cp	Steady pressure coefficient
c_r	Root chord length

f	Frequency
k	Reduced frequency. $f\pi c_{mean}/U$
M	Free stream Mach number
P	Unsteady Pressure above plenum chamber
P'	Real component of fundamental of P
P"	Imaginary component of fundamental of P
P1'	Real component of 2nd harmonic of P
P1"	Imaginary component of 2nd harmonic of P
Po	Free stream total pressure
q	Free stream dynamic pressure
Re	Reynolds number based on free stream conditions and c_r
s	Semi-span width
To	Free stream total temperature
U	Free stream velocity
x	Chordwise coordinate
y	Spanwise coordinate
z	Model deformation
z'	Real component of fundamental of z
z"	Imaginary component of fundamental of z
z1'	Real component of 2nd harmonic of z
z1"	Imaginary component of 2nd harmonic of z
α (alpha)	Angle of incidence
δ (delta)	Mean angle of flap deflection
δo (delta_o)	Amplitude of flap deflection
η (eta)	Dimensionless spanwise coordinate, y/s
Λ (lambda)	Sweepback angle
ξ (xi)	Dimensionless chordwise coordinate, x/c
θ (theta)	Phase lag of pressure with respect to flap motion

FORMULARY

1 General Description of model

1.1	Designation	NAL SST Arrow Wing with Fuselage
1.2	Type	Double swept-back semi-span model
1.3	Derivation	Proposed by Society of Japan Aircraft Company (SJAC).
1.4	Additional remarks	---
1.5	References	Ref. 1, 2

2 Model Geometry

2.1	Planform	Double tapered
2.2	Aspect ratio	2.01
2.3	Leading edge sweep	72.81 deg. (inboard) / 51.57 deg. (outboard)
2.4	Trailing edge sweep	6.57 deg. (inboard) / 16.94 deg. (outboard)
2.5	Taper ratio	$1.0_{\eta=0\%}$: $0.274_{57\%}$: $0.0783_{100\%}$
2.6	Twist	0
2.7	Wing root chord	2103.3 mm
2.8	Semi-span of model	1000.0 mm (From fuselage symmetry axis to wing tip. 35mm thickness base plate inserted between fuselage symmetry plane and tunnel side wall. See Table 2.)
2.9	Area of planform	0.8890 m^2 (only wing) [fuselage : 0.2778 m^2, base : 0.135 m^2]
2.10	Location of reference sections and definition of profiles	NACA0003 at 8 %, 57 % and 100 % semi-span positions (see Table 1)
2.11	Lofting procedure between reference sections	Straight line generators
2.12	Form of wing-body junction	Wing root supported from 52.8 % to 81.4 % chord-stations at 3 points (see Fig. 2). Rest of root free to deform, so it presented vertical displacements when the wing oscillated. A 1 mm clearance was thus given between fuselage and wing root section without any fairing.
2.13	Form of wing tip	Fairing using complex curve at 100 % semi-span position (semi-span length is slightly wider than 1000 mm. See Fig. 2)
2.14	Control surface details	Semi-span position : η=20.0 - 50.0 %
		Hinge-line : 110.0 mm upstream from trailing edge
		Small chordwise and spanwise gaps (see Ref. 1)
2.15	Additional remarks	Wing surface consist of aluminum alloy and urethane resin. Accuracy of wing section shape considered within 0.25 and 1.0 mm respectively for aluminum and urethane surfaces.
		Fuselage swell to cover the flap actuator presented in Table 2.
2.16	References	Ref. 1, 2

3 Wind Tunnel

3.1	Designation	NAL 2m x 2m transonic wind tunnel
3.2	Type of tunnel	Continuous and pressurized / depressurized
3.3	Test section dimensions	Height : 2000 mm, Width : 2000 mm Length : 4130 mm
3.4	Type of roof and floor	Slotted
3.5	Type of side walls	Closed
3.6	Ventilation geometry	6 slots on each of roof and floor. 6 % open ratio
3.7	Thickness of side wall boundary layer	ca. 0.1 m
3.8	Thickness of boundary layers at roof and floor	ca. 0.1 m (thicker than 0.1 m at slot sections)
3.9	Method of measuring Mach number	Derived from total and static pressures measured in settling and plenum chambers, respectively. Ratio of specific heats assumed 1.4.
3.10	Flow angularity	Less than 0.1 deg. (upwash).
3.11	Uniformity of Mach number over test section	Standard deviation of Mach number is less than 0.0025 for flow of Mach number less than 1.0.
3.12	Sources and levels of noise or turbulence in empty tunnel	At flow condition of M=0.7, Po=98kPa and To=310K, sound pressure levels based on $2x10^{-5}$ Pa are less than 130dB for each noise of 1st and 2nd fans and tunnel resonance.
3.13	Tunnel resonances	About 1 kHz corresponding to 1st natural frequency of test section plate.
3.14	Additional remarks	---
3.15	References on tunnel	Ref. 3 and 4 written in Japanese

4 Model motion

4.1	General description	Sinusoidal pitching of flap about swept hinge line
4.2	Definition of motion	Flap deflection angle relative to hinge line measured with a cam attached to hinge axis and a depth meter installed in fuselage.
4.3	Range of amplitude	Maximum command signal is 2 deg. with mean deflection angles of 0, 5 and -5 deg.
4.4	Range of frequency	0, 5, 10, 15(applied only to the mean deflection angle of 0 deg.), 20, 25 and 30 Hz
4.5	Method of applying motion	Forced by an electric motor
4.6	Timewise purity of motion	Adequate purity of sinusoid
4.7	Natural frequencies and normal modes of model and support system	First bending frequency at 9.79 Hz and second bending frequency at 40.25 Hz with 3 point support. Analytic and tested results shown in Table 6. Analytic natural modes presented in Fig. 5.
4.8	Actual mode of applied motion including any elastic deformation	Model dynamic deformation measured by observing optical targets installed in model. See Tables 8.1 to 8.6. Model 1st resonant frequency is almost 13.5 Hz with airflow. Flap oscillations at and below 15 Hz produce significant elastic deformations that influence unsteady pressure distributions and should be included in the calculations. Model deformation takes

		place most prominently in the 1st bending mode (Fig. 5). Detailed definition of the first 8 modes is included in the CD-ROM as file "FEM.txt"
4.9	Additional remarks	---
4.10	References	Ref. 1, 2

5 Test Conditions

5.1	Model planform area/tunnel area	0.222 (wing only). 0.325 (wing with fuselage and base plate)
5.2	Model span/tunnel width	0.500 (wing and fuselage). 0.518 (model with base plate)
5.3	Blockage	1.27%
5.4	Position of model in tunnel	Side mounted at middle height
5.5	Range of Mach number	0.80, 0.85, 0.90 and 0.95
5.6	Range of tunnel total pressure	70 and 80 kPa
5.7	Range of tunnel total temperature	306 to 315 deg. K
5.8	Range of model steady or mean incidence	-4, -3, -2, -1, 0, 1 and 2 deg.
5.9	Definition of model incidence	Model set to zero incidence in horizontal plane.
5.10	Position of transition, if free	Not measured
5.11	Position and type of trip, if transition fixed	---
5.12	Flow instabilities during tests	No remarkable instabilities detected.
5.13	Changes to mean shape of model due to steady aerodynamic load	About 7.5 mm wing tip displacement at M=0.85 and Po=80 kPa. See Tables 8.1 to 8.6.
5.14	Additional remarks	---
5.15	References describing tests	---

6 Measurements and Observations

6.1	Steady pressures for the mean conditions	Available
6.2	Steady pressures for small changes from the mean conditions	Not Available
6.3	Quasi-steady pressures	Not Available
6.4	Unsteady pressures	Available
6.5	Steady section forces for the mean conditions by integration of pressures	Not Available
6.6	Steady section forces for small changes from the mean conditions by integration	Not Available
6.7	Quasi-steady section forces by integration	Not Available
6.8	Unsteady section forces by integration	Available
6.9	Measurement of actual motion at points of model	Available
6.10	Observation or measurement of boundary layer properties	Not Available
6.11	Visualisation of surface flow	Not Available
6.12	Visualisation of shock wave movements	Not Available
6.13	Additional remarks	Accelerometer signals also measured.

6.14 References	Ref. 2

7 Instrumentation

7.1 Steady pressure	
7.1.1 Position of orifices	See Table 3 and Fig. 3
7.1.2 Type of measuring system	Orifices connected to scannivalves through vinyl tubes.
7.2 Unsteady pressure	
7.2.1 Position of orifices	See Table 3 and Fig. 3
7.2.2 Diameter of orifices	1.0 mm
7.2.3 Type of measuring system	Individual in situ transducers
7.2.4 Type of transducers	Kulite XCS-062 range 15 PSI
7.2.5 Principle and accuracy of calibration	Steady calibration against DPI601 using reference tube of pressure transducer. Accuracy of the device is 0.05%.
7.3 Model motion	
7.3.1 Method of measuring motion reference coordinates	Distance measured by depth meter mounted in fuselage and cam attached to hinge root.
7.3.2 Method of determining spatial mode of motion	Not measured for flap, but for wing itself. Optical targets set in the model were traced with CCD cameras. The position of targets presented in Table 4 and Fig. 4.
7.3.3 Accuracy of measured motion	Time response of angular transducer is less than 1 msec, which is equal to 10.8 deg. phase lag at 30 Hz flap motion. Accuracy of magnitude is less than 1 % taking into account non-linearity of depth meter and cam, and temperature characteristics of depth meter and its amplifier.
7.4 Processing of unsteady measurements	
7.4.1 Method of acquiring and processing measurements	Pressure above the plenum chamber, accelerometer signal, flap control signal and its actual motion sampled simultaneously at 25.6 kHz and stored. Data processed off-line to 256 Hz. Dynamic model deformation measured by another system at 333 Hz and stored.
7.4.2 Type of analysis	Complex components of Cp using about 5 seconds data for each flap frequency. Averaging conducted. See INTRODUCTION.
7.4.3 Unsteady pressure quantities obtained and accuracies achieved	Fundamental and 2nd harmonic components for each flap frequency presented. Although no unsteady calibrations were conducted, accuracy shown in 9.1.6 is expected.
7.4.4 Method of integration to obtain forces	Simpson method. Discretely divided distributions using spline interpolation. Leading edge unsteady Cp assumed to zero. At outboard section, trailing edge unsteady Cp assumed to mean of values extrapolated on each of upper and lower surfaces.
7.5 Additional remarks	4 accelerometers installed in wing (see Table 5 and Fig. 4).
7.6 References on techniques	Ref. 1

8 Data presentation

8.1 Test cases for which data could be made available	Table 7.2 (Included in accompanying CD-ROM)

8.2	Test cases for which data are included in this document	Table 7.1
8.3	Steady pressures	Tables 8.1 to 8.6 (Included in accompanying CD-ROM)
8.4	Quasi-steady or steady perturbation pressures	---
8.5	Unsteady pressures	Tables 8.1 to 8.6 (Included in accompanying CD-ROM)
8.6	Steady forces or moments	---
8.7	Quasi-steady or unsteady perturbation forces	---
8.8	Unsteady forces and moments	Tables 8.1 to 8.6 (Included in accompanying CD-ROM)
8.9	Other forms in which data could be made available	Static and dynamic model deformations presented in Tables 8.1 to 8.6. Accelerometer signals also presented in Tables 8.1 to 8.6.
8.10	Reference giving other representations of data	---

9 Comments on data

9.1	Accuracy	
	9.1.1 Mach number	Less than 0.001
	9.1.2 Steady incidence	0.1 deg.
	9.1.3 Reduced frequency	Less than 0.12%
	9.1.4 Steady pressure coefficients	Less than $(7.9\times Cp^2 + 5.9)^{0.5} \times 0.001$
	9.1.5 Steady pressure derivatives	---
	9.1.6 Unsteady pressure coefficients	Accuracy of $\mid P/q \mid$ less than $(0.22\times\mid P/q \mid^2 + 1.2)^{0.5} \times 0.01$. Effects of repeatability and temperature sensitivity of pressure transducer and calibration error were considered.
9.2	Sensitivity to small changes of parameter	Not examined
9.3	Non-linearities	Expansion waves seemed to appear only on the flap at higher Mach number. Unsteady pressure distribution affected by non-linearity of dynamic model deformation at model 1st resonant frequency.
9.4	Influence of tunnel total pressure	Total pressure of 70 and 80 kPa examined.
9.5	Effects on data of uncertainty, or variation, in mode of model motion	Not estimated yet
9.6	Wall interference corrections	None
9.7	Other relevant tests on same model	Ref. 1
9.8	Relevant tests on other models of nominally the same shapes	---
9.9	Any remarks relevant to comparison between experiment and theory	---
9.10	Additional remarks	---
9.11	References on discussion of data	Ref. 2

10 Personal contact for further information

Masato Tamayama

Aeroelasticity Laboratory, Structures Division

National Aerospace Laboratory

7-44-1, Jindaiji-Higashi-Machi,
Chofu, Tokyo 182-8522, JAPAN
Phone : +81-422-40-3392
Fax : +81-422-40-3376
E-mail : masato@nal.go.jp

11 List of references

1 M. Tamayama, H. Miwa, J. Nakamichi; Unsteady Aerodynamics Measurements on an Elastic Wing Model of SST, AIAA 97-0836, 1997

2 M. Tamayama, K. Saitoh, H. Matsushita; Measurements of Unsteady Pressure Distributions and Dynamic Deformations on an SST Elastic Wing Model, CEAS International Forum on Aeroelasticity and Structural Dynamics, Rome, Italy, 1997, Vol.3, pp.231-238.

3 N. Kawai, Y. Oguni, M. Suzuki; Measurements of Free-Stream Turbulence and Disturbance in NAL 2m x 2m Transonic Windtunnel, NAL TM-342, 1978 (in Japanese).

4 K. Suzuki, et al; Refurbishment of the NAL 2m x 2m Transonic Wind Tunnel Test Section, NAL TM-674, 1995 (in Japanese).

Table 1 Airfoil Section Shape

Airfoil NACA0003

$z_t(\xi) / c = 5 \times 0.03 \times \{ a_0\xi^{1/2} + a_1\xi + a_2\xi^2 + a_3\xi^3 + a_4\xi^4 \}$

$a_0 = 0.2969$, $a_1 = -0.1260$, $a_2 = -0.3516$

$a_3 = 0.2843$, $a_4 = -0.1015$

$z_t(\xi)$:Local airfoil thickness

ξ	$z_t(\xi)$	ξ	$z_t(\xi)$
0.00	0.00000	0.52	0.01291
0.04	0.00807	0.56	0.01220
0.08	0.01077	0.60	0.01141
0.12	0.01247	0.64	0.01055
0.16	0.01360	0.68	0.00964
0.20	0.01434	0.72	0.00867
0.24	0.01478	0.76	0.00764
0.28	0.01498	0.80	0.00656
0.32	0.01498	0.84	0.00542
0.36	0.01482	0.88	0.00423
0.40	0.01451	0.92	0.00299
0.44	0.01408	0.96	0.00168
0.48	0.01354	1.00	0.00031

Table 2 Definition of Fuselage

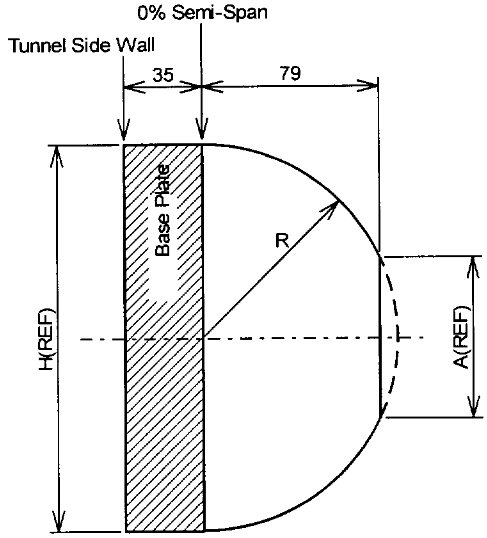

(unit : mm)

STA	R	H(REF)	A(REF)
-760	0.00	0.00	-----
-700	15.31	30.63	-----
-600	36.65	73.31	-----
-500	53.27	106.54	-----
-400	65.76	131.52	-----
-300	74.71	149.42	-----
-200	80.71	161.41	33.02
-100	84.34	168.69	59.10
0	86.21	172.43	69.04
100	86.90	173.80	72.41
190	87.00	174.00	72.88
200 : 1700	87.00	174.00	72.88
1824.4 : 2204.4	*(control surface actuator swell)		
2300 : 2400	87.00	174.00	72.88
2500	86.62	173.24	71.05
2600	84.04	168.08	57.32
2700	78.02	156.04	-----
2800	68.56	137.12	-----
2900	55.52	111.04	-----
3000	37.32	74.64	-----
3100	0.00	0.00	-----

The origin of STA is the wing leading edge at 8% semi-span position (wing-fuselage junction).

*(control surface actuator swell)

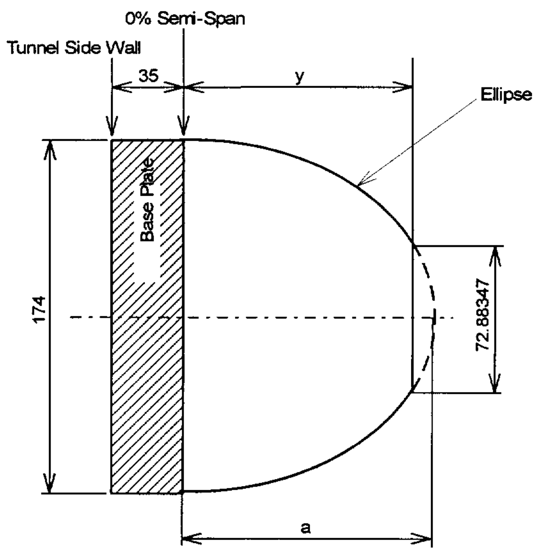

(unit : mm)

STA	y	a
1824.4	80.00	88.10
1864.4	85.50	94.16
1904.4	95.50	105.17
1944.4	109.50	120.59
1984.4	115.00	126.64
2024.4	114.00	125.54
2064.4	107.00	117.83
2104.4	94.00	103.52
2144.4	84.00	92.51
2184.4	80.00	88.10
2204.4	79.50	87.55

Table 3 Pressure Orifice Locations

η= 38.4% span (Steady) 38% span (Unsteady)				η= 73.5% span (Steady) 73.9% span (Unsteady)			
Upper Surface		Lower Surface		Upper Surface		Lower Surface	
ch	x/c [%]	ch	x/c [%]	ch	x/c [%]	ch	x/c [%]
1	2.5	22	70.0	30	10.0	39	79.0
2	5.0	23	60.0	31	20.0	40	66.0
3	7.5	24	50.0	32	30.0	41	54.2
4	10.0	25	40.0	33	35.0	42	48.0
5	15.0	26	30.0	34	41.8	43	41.8
6	20.0	27	20.0	35	48.0	44	30.0
7	30.0	28	10.0	36	54.2	45	20.0
8	40.0	29	5.0	37	66.0	46	10.0
9	50.0			38	80.0		
10	60.0						
11	70.0						
12	80.0						
13	82.5						
14	85.0						
15	86.5*						
16	88.0						
17	91.6						
18	93.1						
19	94.6						
20	96.1						
21	100.0*						

* : Only for Unsteady Measurement

Table 4 Optical Target Locations

No.	η %	ξ %	No.	η %	ξ %
* 1	96.0	13.0	11	41.0	43.2
* 2	96.0	38.6	12	41.0	63.2
3	96.0	64.2	* 13	41.0	74.0
4	76.0	28.2	* 14	41.0	83.4
* 5	76.0	48.5	15	18.0	38.2
* 6	76.0	66.3	16	18.0	59.9
7	60.0	3.4	* 17	18.0	73.0
8	60.0	41.4	* 18	18.0	80.2
* 9	60.0	59.1	* 19	18.0	87.1
10	41.0	5.0	* 20	60.0	74.5
			21	18.0	20.6

* Available

Table 5 Position of Accelerometers

66.8% Semi-Span		84.7% Semi-Span	
No.	% x/c	No.	% x/c
1	30.0	2	30.0
3	65.0	4	65.0

Table 6 Model Natural Frequencies

Mode	Natural Frequency[Hz]		Generalized Mass [kg]
	FEM	Vibration Test	
1	11.09	9.79	5.1982
2	41.65	---	2.3109
3	44.00	40.25	3.2874
4	56.26	47.91	1.9764
5	89.49	65.19	1.4333
6	119.23	90.57	0.7928
7	145.44	111.04	2.0683
8	163.58	122.39	1.2810

Table 7.1 SUMMARY OF PRESENTED DATA

Test ID No.	M	Po [kPa]	To [°K]	Re x 10^{-7}	k/f [/Hz]	f [Hz]	α [°]	δ [°]	Target data available
AC100803	0.8002	79.925	310.36	2.142	0.0150	5, 10, 15, 20, 25, 30	0	0	1, 2, 5, 6, 9, 13, 14, 18, 19, 20
AC100804	0.8004	79.963	310.52	2.141	0.0150	5, 10, 20, 25, 30	0	5	1, 2, 5, 6, 9, 20
AC100901	0.8507	80.000	310.34	2.207	0.0143	5, 10, 15, 20, 25, 30	0	0	1, 2, 5, 6, 9, 13, 14, 17, 18, 19, 20
AC100902	0.8489	79.936	310.78	2.199	0.0143	5, 10, 20, 25, 30	0	-5	1, 2, 5, 6, 9, 13, 14, 17, 18, 19, 20
AC100907	0.9001	80.083	311.87	2.247	0.0135	5, 10, 15, 20, 25, 30	0	0	1, 2, 5, 6, 9, 13, 14, 17, 18, 19, 20
AC100908	0.9005	79.956	312.34	2.239	0.0135	5, 10, 20, 25, 30	0	5	1, 2, 5, 6, 9, 13, 17, 18, 20

Table 8.1 Result / AC100803

```
| Test No. AC100803                                  |
| M = 0.8002,  Po = 79.925 kPa,  To = 310.36 deg. K  |
| Re = 2.142*10^7,  k/f = 0.0150 /Hz                 |
| Alpha =  0 deg.,  Delta =  0 deg.                  |
~~~~~~~~~~~~~~~~~~~~~~~~~~~~~~~~~~~~~~~~~~~~~~~~~~~~~~
```

[STEADY DATA]

< PRESSURE COEFFICIENT (Cp) >

Eta = 38.4%						Eta = 73.5%					
Upper surface			Lower surface			Upper surface			Lower surface		
Orifice No.	Xi	Cp	Orifice No.	Xi	Cp	Orifice No.	Xi	Cp	Orifice No.	Xi	Cp
1	0.025	-0.0229	22	0.700	-0.0458	30	0.100	-0.1239	39	0.790	-0.0149
2	0.050	-0.0400	23	0.600	-0.0551	31	0.200	-0.1254	40	0.660	-0.0479
3	0.075	-0.0420	24	0.500	-0.0605	32	0.300	-0.0941	41	0.542	-0.0532
4	0.100	-0.0440	25	0.400	-0.0545	33	0.350	-0.0848	42	0.480	-0.0622
5	0.150	-0.0496	26	0.300	-0.0600	34	0.418	-0.0785	43	0.418	-0.1022
6	0.200	-0.0571	27	0.200	-0.0529	35	0.480	-0.0695	44	0.300	-0.1081
7	0.300	-0.0613	28	0.100	-0.0403	36	0.542	-0.0702	45	0.200	-0.1247
8	0.400	-0.0667	29	0.050	-0.0563	37	0.660	-0.0492	46	0.100	-0.1151
9	0.500	-0.0573				38	0.800	-0.0448			
10	0.600	-0.0494									
11	0.700	-0.0426									
12	0.800	-0.0222									
13	0.825	-0.0327									
14	0.850	-0.0368									
16	0.880	-0.0235									
17	0.900	-0.0338									
18	0.920	-0.0211									
19	0.950	-0.0138									
20	0.970	+0.0447									

< DEFORMATION FROM NO-FLOW CONDITION >

Target NO.	
1	+8.9354e-003
2	+9.2979e-003
5	+6.6282e-003
6	+6.9474e-003
9	+4.5407e-003
13	+2.4733e-003
18	+9.0811e-004
19	+1.2350e-003
20	+4.9521e-003
	[unit : m]

[UNSTEADY DATA]

f = 5.0 Hz   Delta_o = 1.407 deg.

< PRESSURE >

No.	P'/q	P''/q	P1'/q	P1''/q	No.	P'/q	P''/q	P1'/q	P1''/q
1	+7.8672e-004	+4.3709e-005	+8.0516e-005	-5.8224e-005	24	-1.1412e-003	+4.8577e-005	-3.5234e-004	-5.9388e-005
2	+7.5615e-004	+3.6843e-005	+8.3223e-005	-5.1448e-005	25	-1.1946e-003	+9.3217e-005	-3.3515e-004	-4.4607e-005
3	+7.2296e-004	+1.7149e-005	+9.1091e-005	-2.5512e-005	26	-9.6874e-004	+5.0285e-005	-2.5858e-004	-3.5429e-005
4	+7.1944e-004	+5.0864e-005	+8.6095e-005	-5.9453e-005	27	-7.9342e-004	+5.6215e-005	-2.2098e-004	-3.3815e-005
5	+8.0283e-004	+3.0358e-005	+1.2223e-004	-8.6025e-005	28	-8.8828e-004	+6.7967e-005	-1.9143e-004	-2.8182e-005
6	+6.6100e-004	+7.0002e-005	+1.2902e-004	-8.9684e-005	29	-7.8033e-004	+4.7247e-005	-1.6621e-004	-3.8227e-005
7	+1.0015e-003	+1.0361e-004	+1.3800e-004	-8.1173e-005	30	+4.6798e-003	+2.3276e-004	+9.8975e-004	-9.0601e-005
8	+1.3027e-003	+6.1052e-005	+2.1992e-004	-1.1785e-004	31	+1.9328e-003	+1.4899e-004	+5.4238e-004	-6.5775e-005
9	+1.1805e-003	+8.9660e-005	+2.1234e-004	-1.0954e-004	32	+9.2340e-005	+1.4845e-004	+2.0084e-004	-7.4948e-005
10	+7.8312e-004	+3.6655e-005	+1.5814e-004	-1.1425e-004	33	-3.8883e-004	+1.4808e-004	+1.9665e-004	-1.0070e-004
11	-9.8334e-004	-1.0328e-004	-7.1924e-005	-2.0106e-004	34	-9.4809e-004	+1.0313e-004	+9.0647e-005	-1.1219e-004
12	-5.7040e-003	-6.1674e-004	-7.0427e-004	-4.4130e-004	35	-1.5268e-003	+1.0638e-004	-3.5361e-006	-9.9731e-005
13	-8.5204e-003	-6.2376e-004	-1.0955e-003	-4.4207e-004	36	-1.9714e-003	+9.2792e-005	-6.7405e-005	-1.1752e-004
14	-1.2701e-002	-1.0577e-003	-1.6996e-003	-5.5173e-004	37	-1.9822e-003	+7.4661e-005	-4.9516e-005	-1.4588e-004
15	-1.6012e-002	-1.3849e-003	-2.1815e-003	-6.0164e-004	38	-1.5498e-003	+8.7056e-005	-9.5056e-005	-1.3375e-004
16	-2.7111e-002	-2.5209e-003	-3.8842e-003	-8.6146e-004	39	+1.5977e-003	+2.0498e-004	-6.9301e-005	-1.3918e-004
17	-6.5368e-002	-4.4412e-003	-5.8103e-003	-1.5791e-003	40	+2.0575e-003	+2.2058e-004	-6.3125e-005	-1.3469e-004
18	-4.1524e-002	-3.3402e-003	-4.1162e-003	-1.1320e-003	41	+1.9475e-003	+1.8157e-004	-1.2719e-004	-1.4087e-004
19	-2.7545e-002	-2.5878e-003	-2.8568e-003	-9.0288e-004	42	+1.5229e-003	+1.6212e-004	-2.1213e-004	-1.4390e-004
20	-1.7642e-002	-1.9067e-003	-1.9389e-003	-7.1725e-004	43	+1.0206e-003	+1.0437e-004	-3.2457e-004	-1.5941e-004
21	+1.5456e-004	+2.1606e-004	+2.1787e-004	-6.7360e-005	44	-4.6880e-004	+7.7942e-005	-5.3641e-004	-1.5246e-004
22	+7.3478e-004	+2.3072e-004	-1.9087e-004	-1.9774e-006	45	-2.0729e-003	+3.9180e-005	-7.7220e-004	-1.8623e-004
23	-9.1626e-004	+9.5325e-005	-3.8716e-004	-6.6705e-005	46	-4.9538e-003	-4.0297e-005	-1.3125e-003	-2.3554e-004

< AERODYNAMIC FORCE >

	real(fundamental)	imag(fundamental)	real(2nd harmonic)	imag(2nd harmonic)
Cl inboard	+4.4811e-003	+5.4617e-004	+3.0432e-004	+2.4205e-004
Cl outboard	+1.9189e-004	-2.9888e-006	-5.3971e-004	-4.7549e-005
Cm inboard	-3.5334e-003	-3.4665e-004	-3.4419e-004	-1.3376e-004
Cm outboard	-9.4222e-004	-2.7897e-005	-4.0941e-005	+3.2761e-007

< DYNAMIC DEFORMATION >

Target NO.	real(fundamental)	imag(fundamental)	real(2nd harmonic)	imag(2nd harmonic)
1	+3.0206e-003	-5.5430e-005	+2.9867e-004	-5.6899e-004
2	+3.1819e-003	-5.8974e-005	+3.1358e-004	-5.9964e-004
5	+2.3323e-003	-2.5983e-004	+1.4506e-004	-4.6065e-004
6	+2.5142e-003	-4.4531e-005	+2.4202e-004	-4.5089e-004
9	+1.7175e-003	-1.9038e-004	+1.0799e-004	-3.2052e-004
13	+9.6971e-004	-1.0812e-004	+5.9302e-005	-1.7505e-004
14	+1.1849e-003	-1.3701e-004	+6.6696e-005	-2.1126e-004
18	+2.1879e-004	-2.4470e-005	+1.4574e-005	-3.7917e-005
19	+3.6009e-004	-5.5330e-005	+1.9597e-005	-5.7822e-005
20	+1.9133e-003	-2.1409e-004	+1.1434e-004	-3.5716e-004

[unit : m]

< ACCELERATION >

Acc. NO.	real(fundamental)	imag(fundamental)	real(2nd harmonic)	imag(2nd harmonic)
1	-1.6517e+000	-1.0160e-001	-1.3742e+000	-1.0738e-001
2	-2.6439e+000	-1.7970e-001	-2.2206e+000	-1.5267e-001
3	-1.8257e+000	-4.7501e-002	-1.6589e+000	-1.1162e-001
4	-2.8493e+000	-1.5522e-001	-2.4137e+000	-1.4551e-001

[unit : m/s^2]

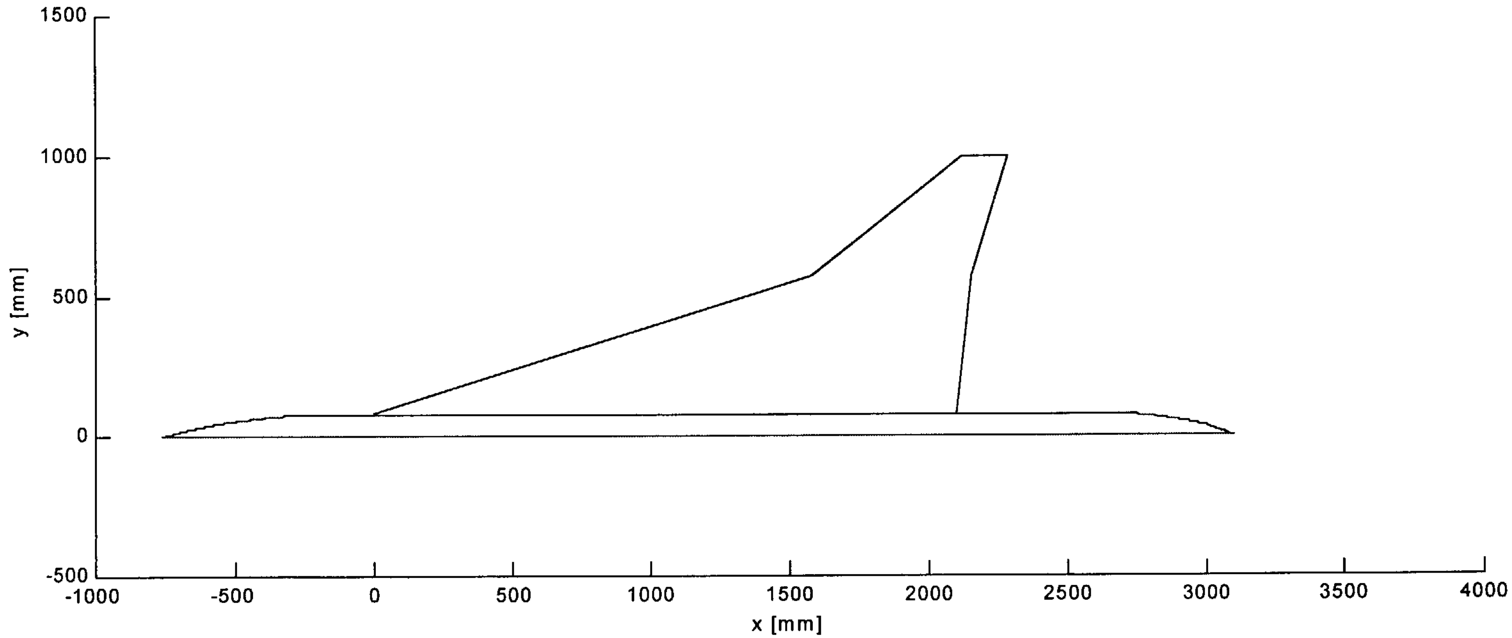

Figure 1 Semi-span Planform of SST Arrow Wing Model

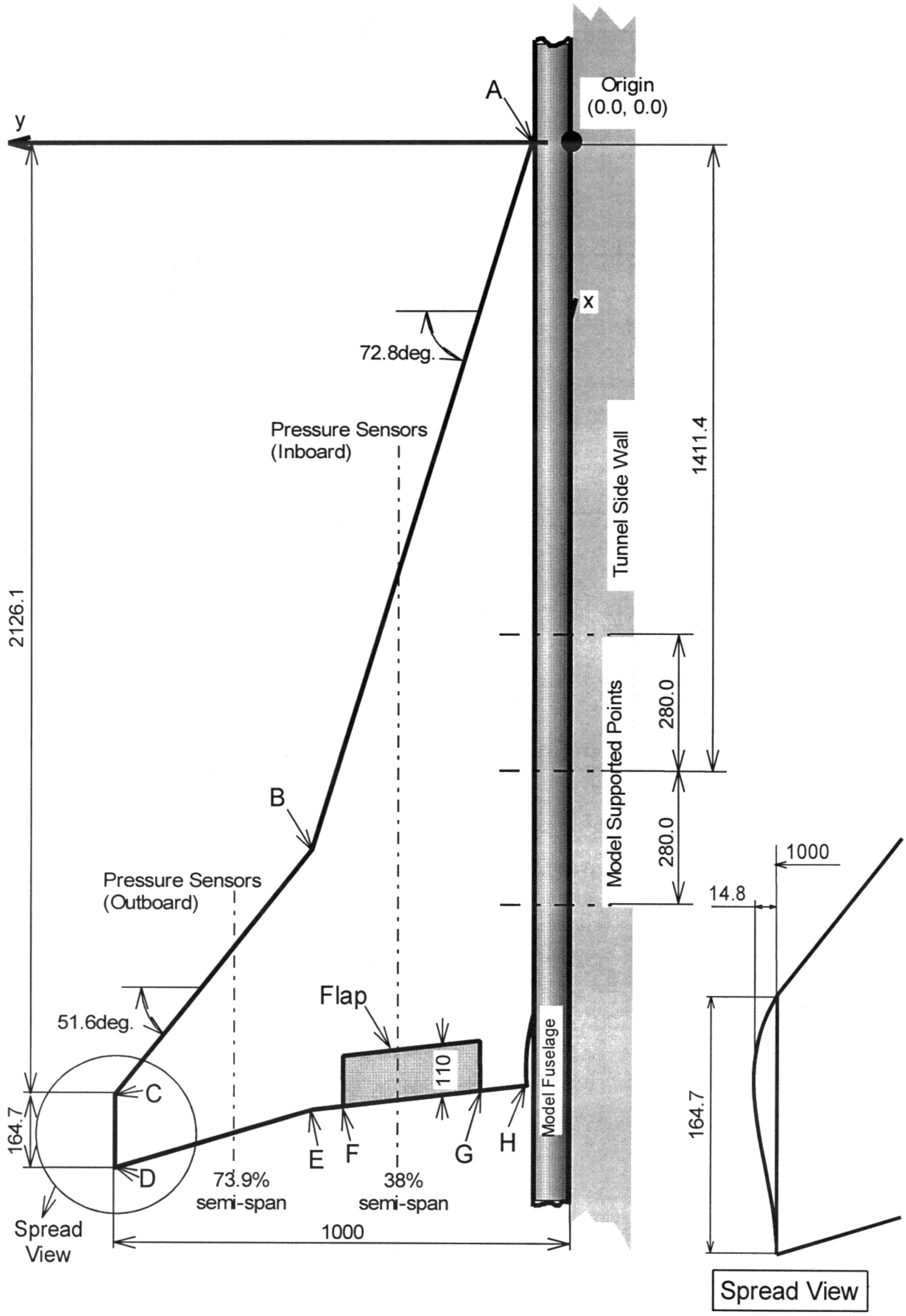

Figure 2 Model Planform (wing part)

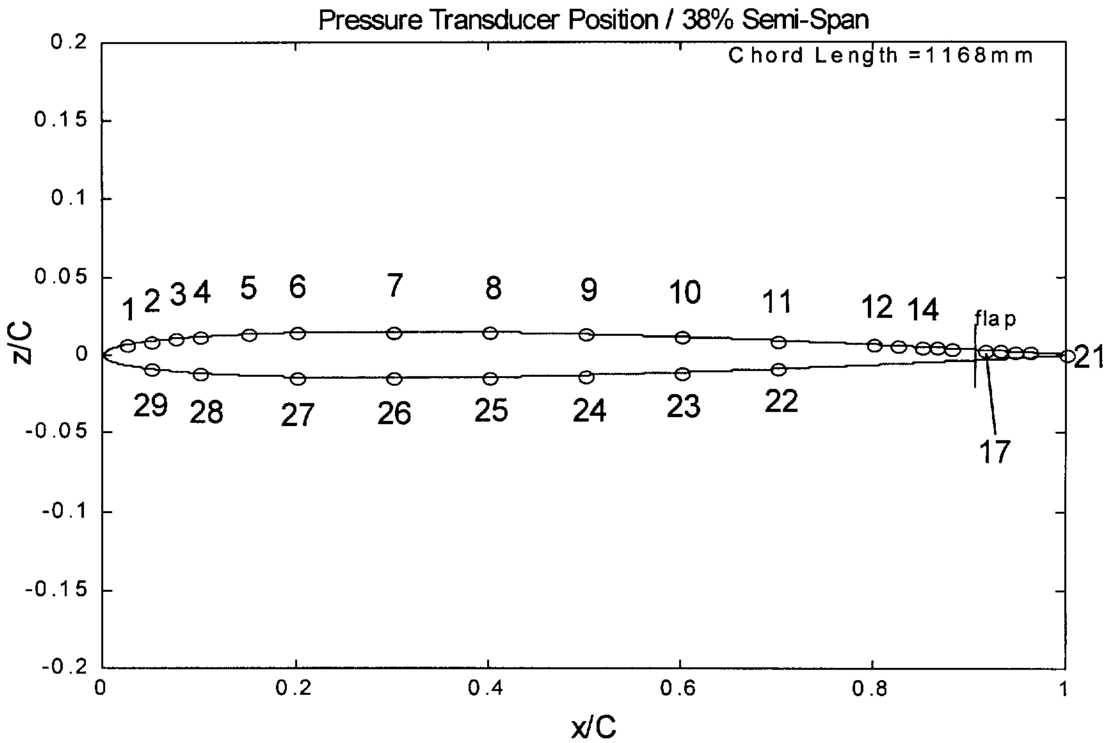

(a) 38 % semi-span

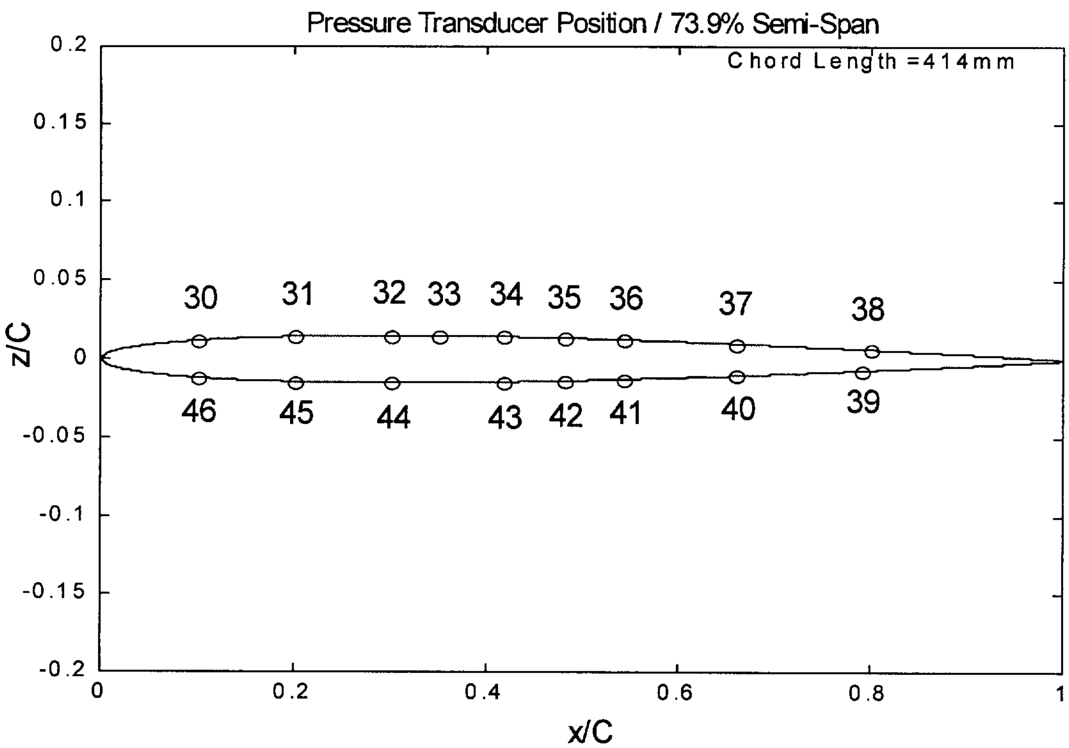

(b) 73.9 % semi-span

Figure 3 Pressure Orifice Positions

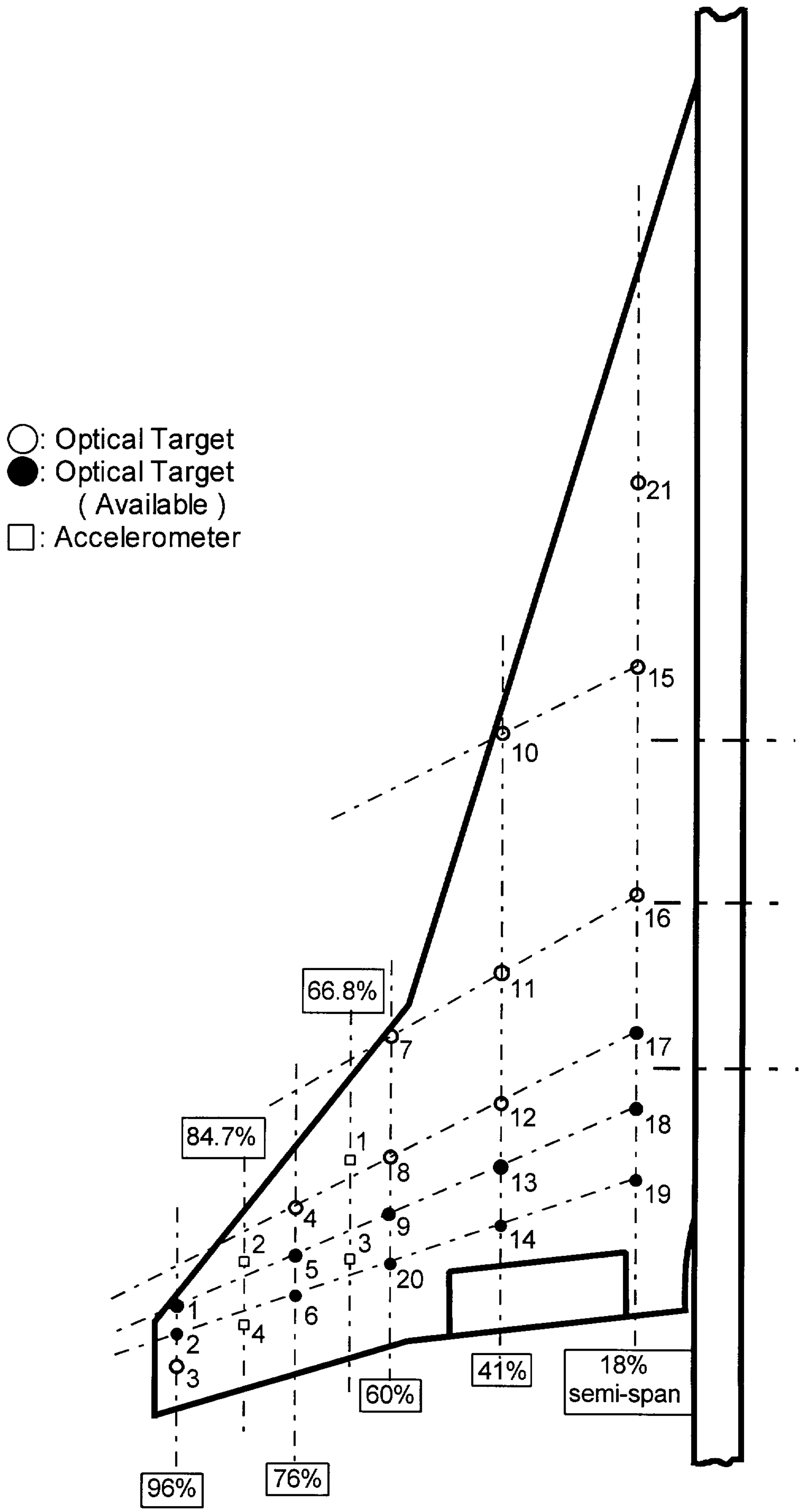

Figure 4 Positions of Optical Targets

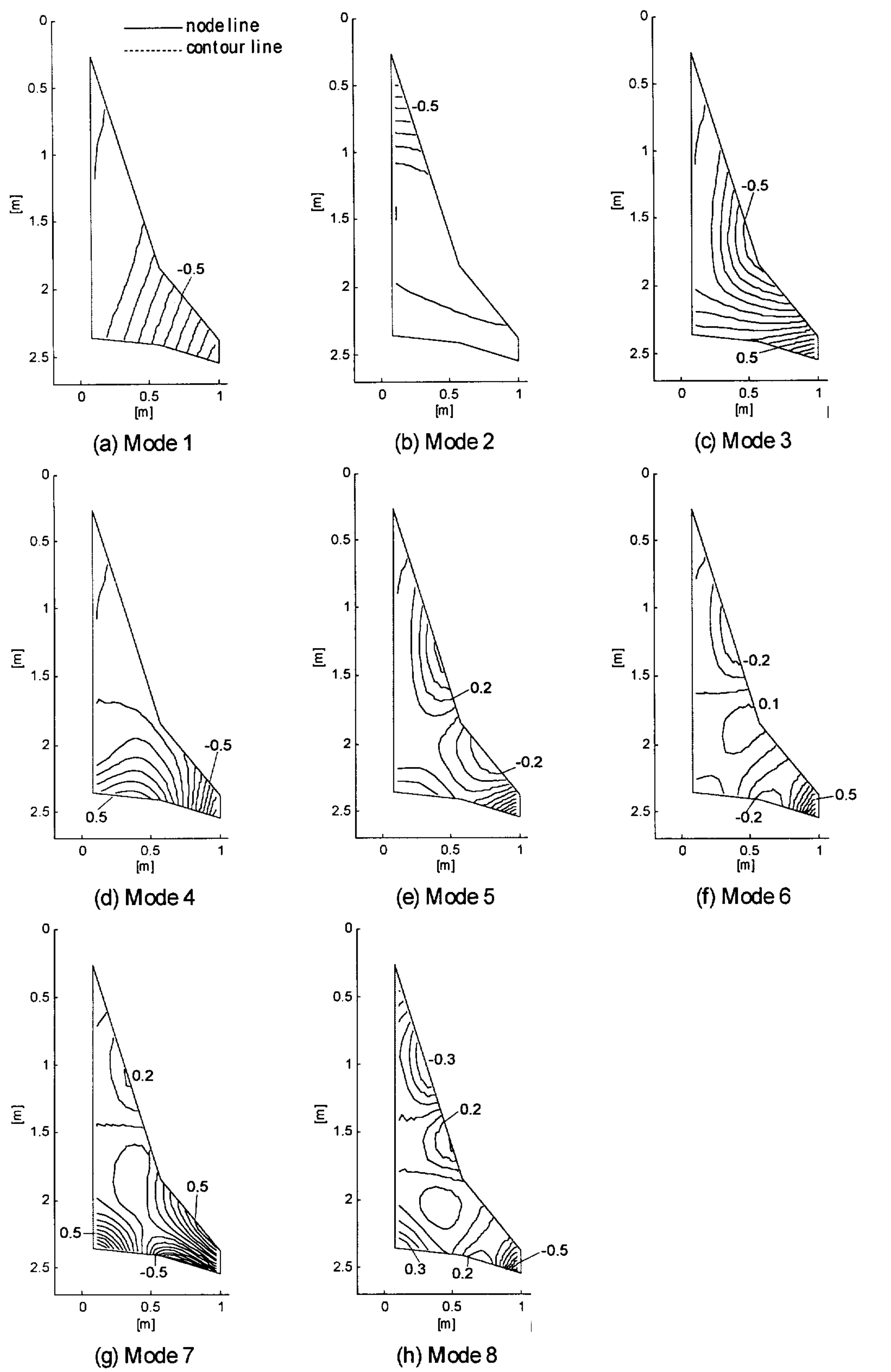

Figure 5 Model Natural Mode Contours Acquired by FEM
(Contours are normalized with the maximum displacement)

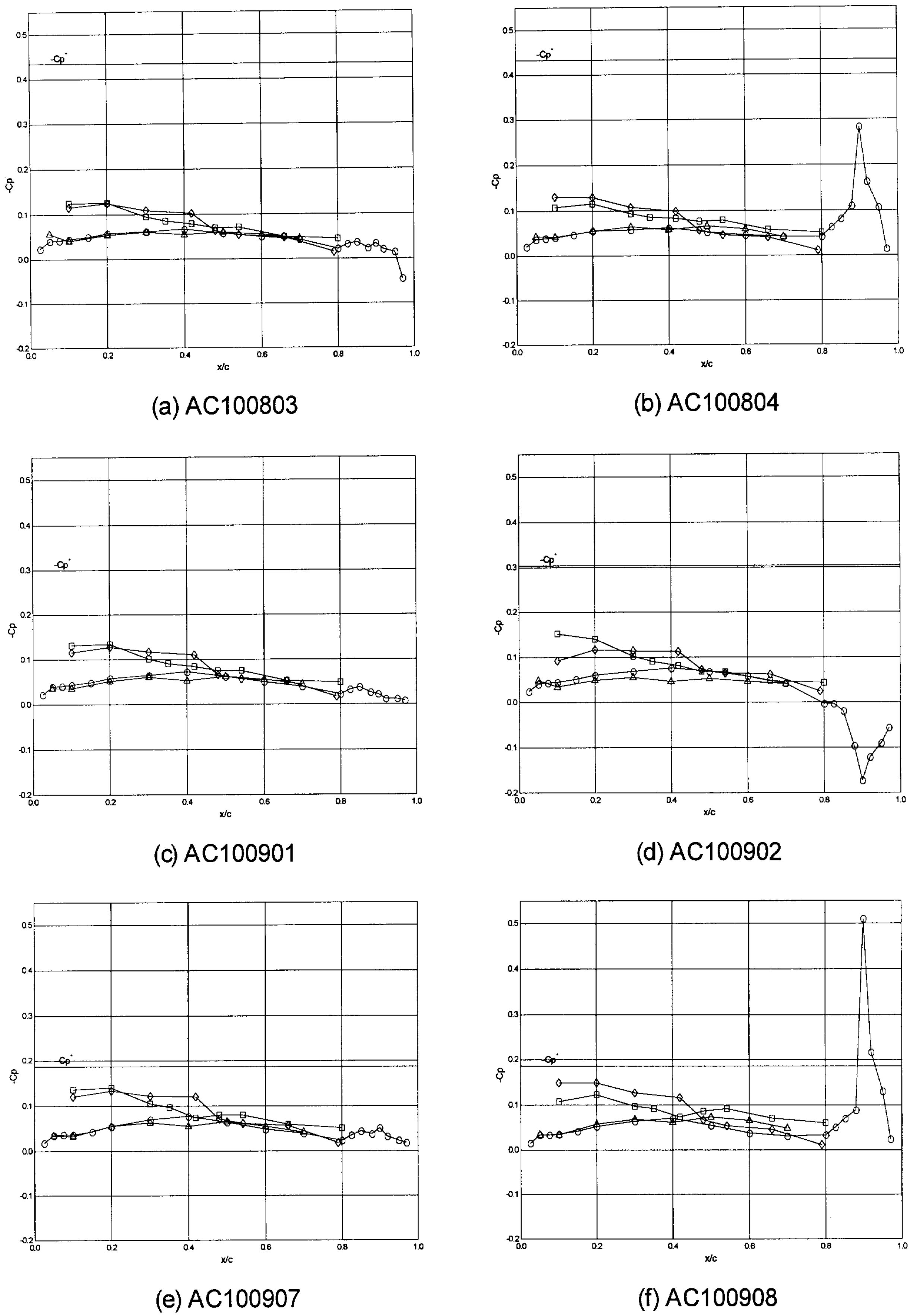

Figure 6 Steady Pressure Coefficient Distributions.
(O: Inboard Upper , Δ: Lower , □: Outboard Upper, ◊: Lower)

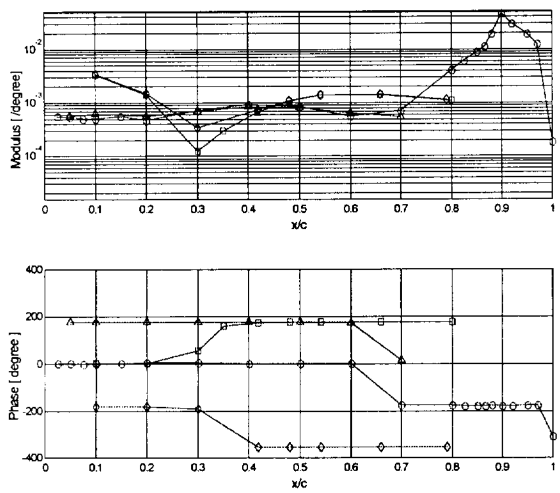

(a) f = 5 [Hz]

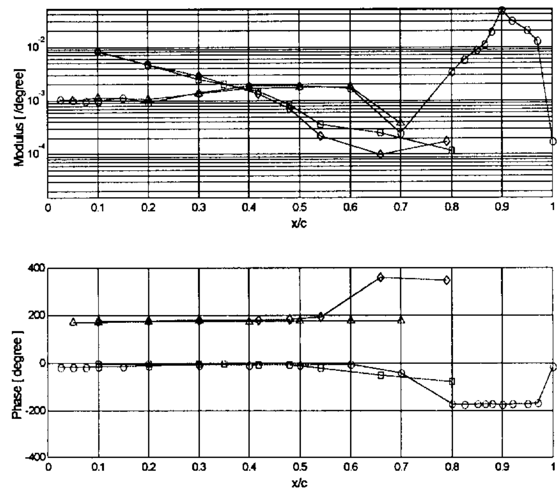

(b) f = 10 [Hz]

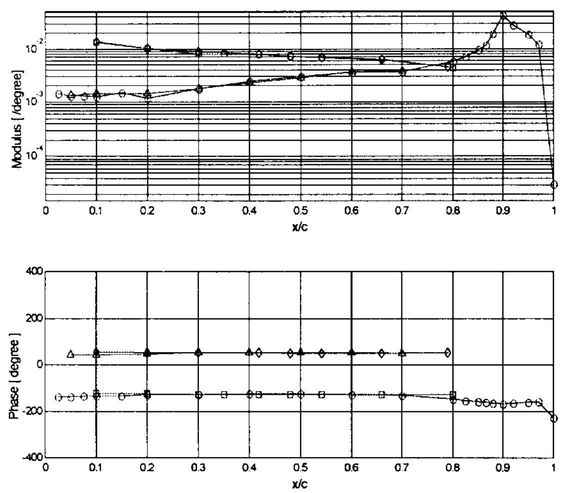

(c) f = 15 [Hz]

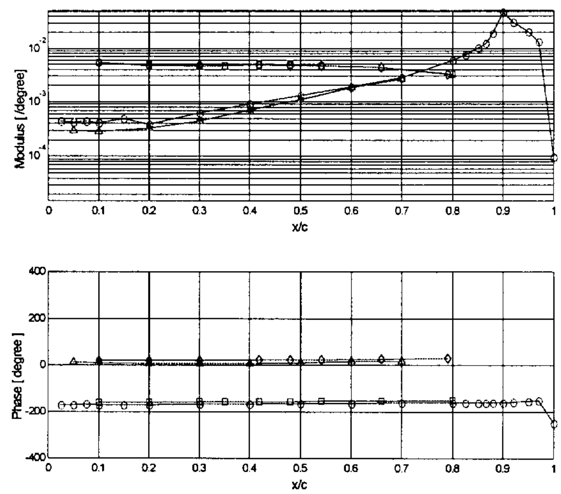

(d) f = 20 [Hz]

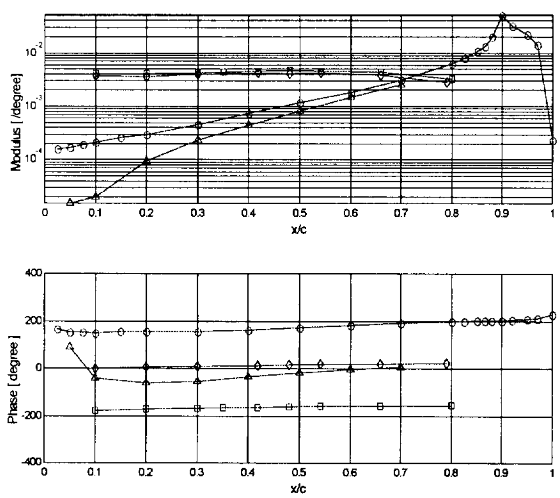

(e) f = 25 [Hz]

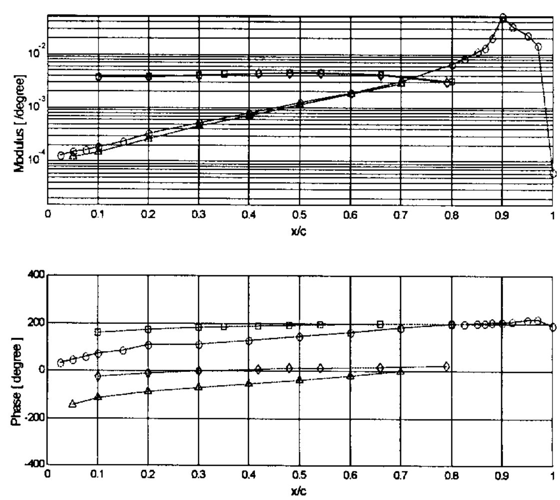

(f) f = 30 [Hz]

Figure 7.1 Unsteady Pressure Distributions. x/c vs Modulus & Phase.
Test Case AC100803 M = 0.8002, Po = 79.925 kPa,
Re = 2.142 * 10^7 , Alpha = 0 deg., Delta = 0 deg.
(O: Inboard Upper , Δ: Lower , □: Outboard Upper, ◊: Lower)

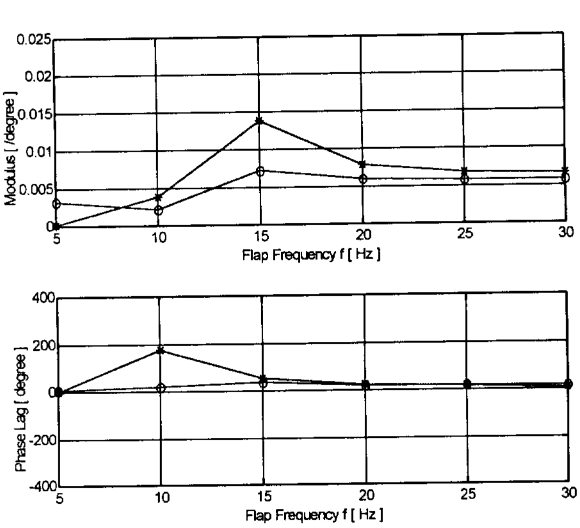

(a) AC100803, M=0.8002, Cl

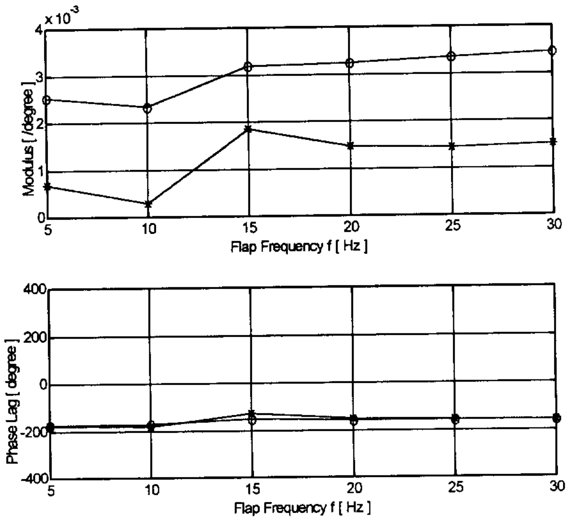

(b) AC100803, M=0.8002, Cm

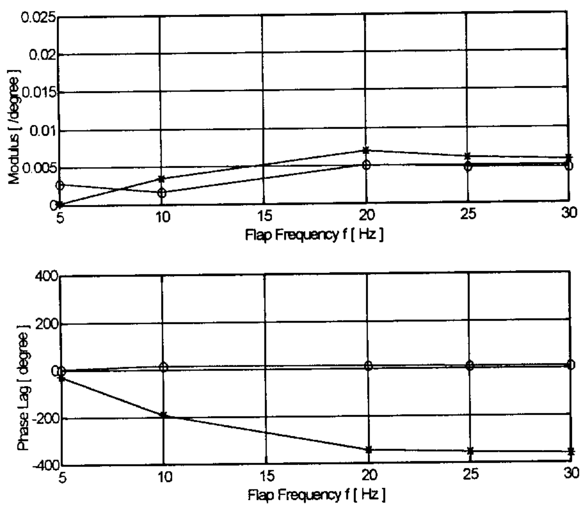

(c) AC100804, M=0.8004, Cl

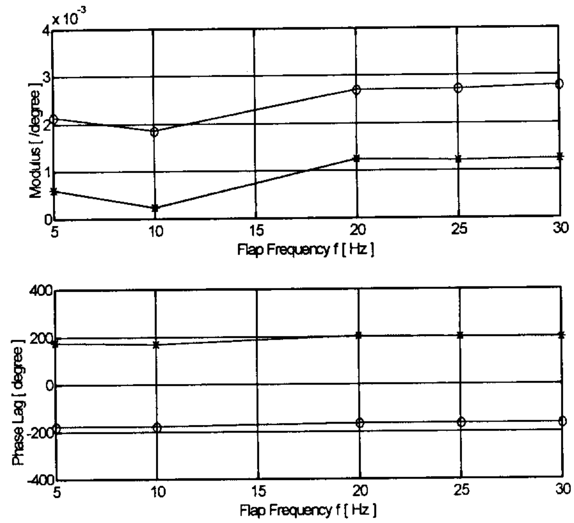

(d) AC100804, M=0.8004, Cm

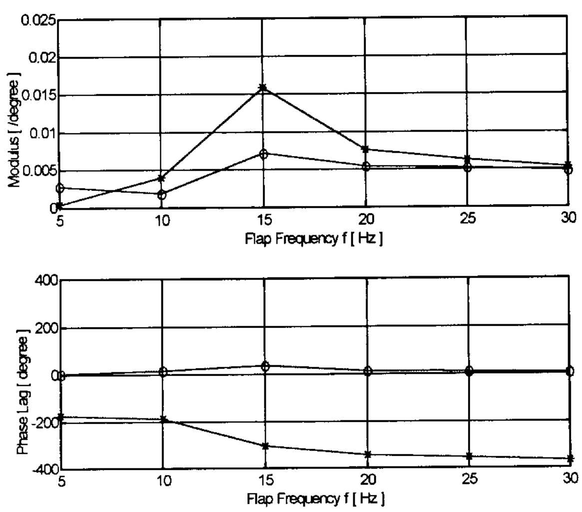

(e) AC100901, M=0.8507, Cl

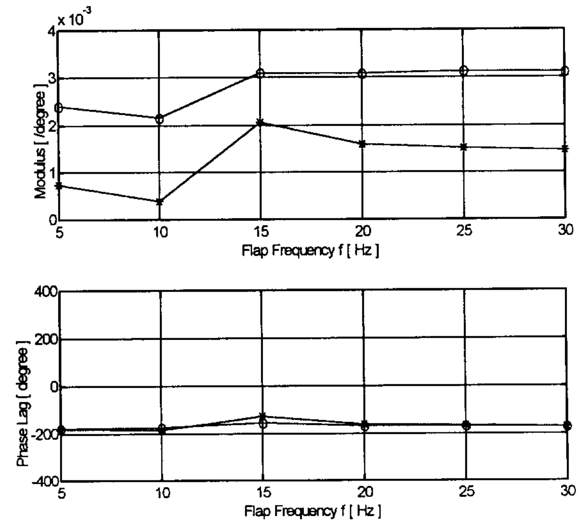

(f) AC100901, M=0.8507, Cm

Figure 8.1 Unsteady Aerodynamic Force Coefficients.
x/c vs Modulus & Phase.
(O: Inboard, ★: Outboard)

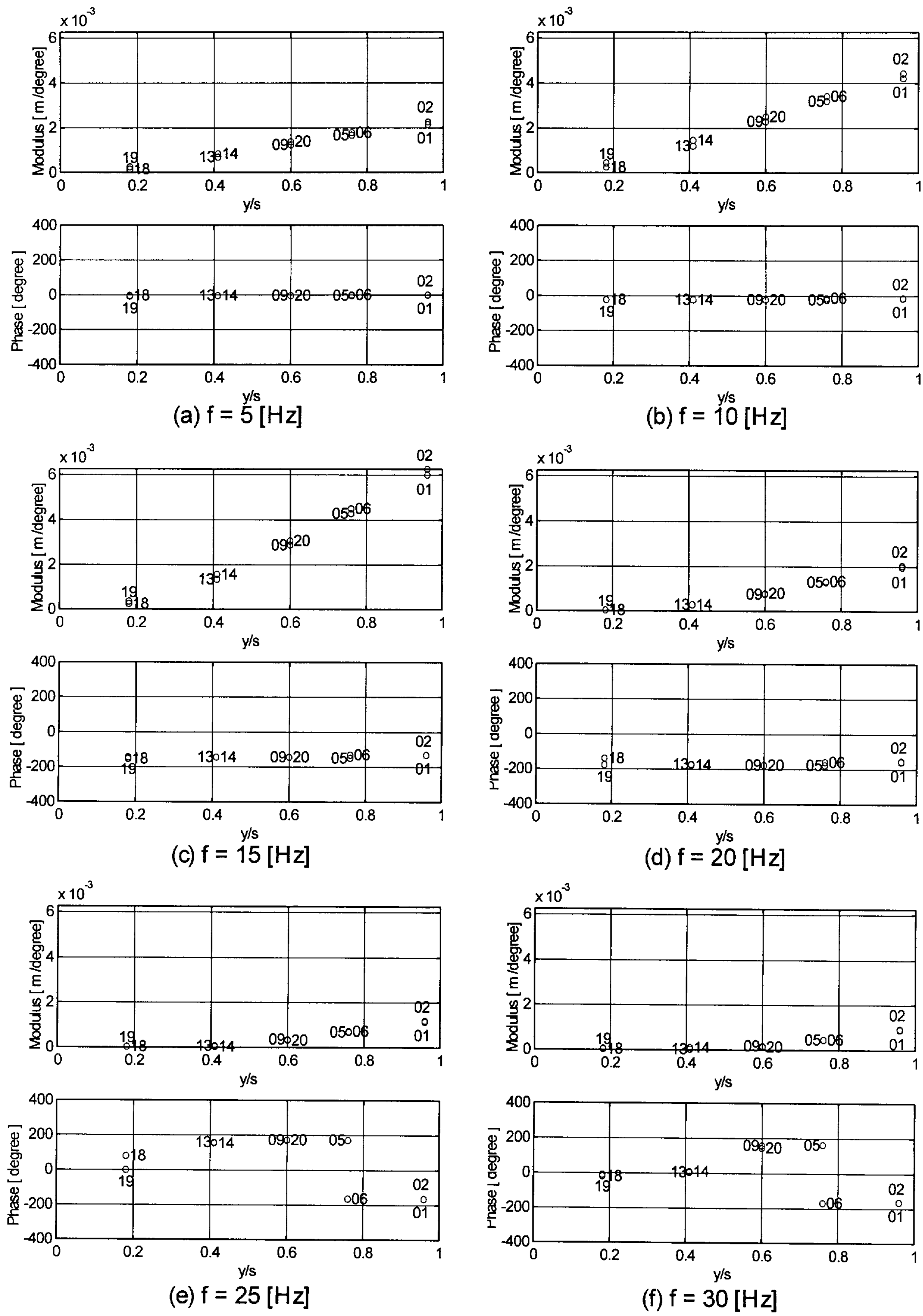

Figure 9.1 Unsteady Model Deformations. x/c vs Modulus & Phase.
Test Case AC100803 M = 0.8002, Po = 79.925 kPa,
Re = 2.142 * 10^7 , Alpha = 0 deg., Delta = 0 deg.

13E TRANSONIC BUFFET OF A SUPERCRITICAL AIRFOIL

Reported by
X.Z. Huang
of work by
B.H.K. Lee and F.C. Tang, et al

INTRODUCTION

This investigation was carried out in the Institute for Aerospace Research (IAR) 2D High Reynolds Test Facility (Ref. 1 to Ref. 3 and Fig. 1) to study the buffet characteristics of a supercritical airfoil, BGK No. 1 (Fig. 2). Steady, unsteady surface pressure and normal force were measured at various angles of attack and Mach numbers. The statistical properties of the normal force and pressure were carried out by spectral analyses. Buffet onset boundaries were evaluated from the divergence of the fluctuating normal force while buffet intensities were determined from the normal force measurements. The attached and separated flow regions on the airfoil as well as the merging of a shock induced separation bubble with the trailing edge separation region were determined by skin friction measurements.

The test program is presented in Table 1. There are two BGK No.1 models. One has normal static pressure orifices and 6 pressure ports to measure pressure fluctuations (BGK-1). Another has 15 fast response transducers (BGK-1(m)). The model's coordinates and the locations of pressure orifices and transducers are listed in Table 2 Table 3 respectively (in CD ROM). The experimental arrangement and results have been described in detail in Ref. 4 to Ref. 9. Tabulated data and illustrations are presented in Table 4 to Table 7 and Fig. 3 to Fig. 16 in CD ROM with part of the illustrations shown here.

Fig. 3 and Table 4 show the fluctuating normal force on BGK–1 model for various Mach numbers. Typical power spectra of the normal force are shown in Fig. 4. The frequencies of the shock motion vary from 70-80 Hz for the Mach number range of 0.688~0.796 and are partly listed in Table 5. The flow conditions where discrete shock oscillations were detected are summarized in Fig. 5. The test program for BGK-1(m) in Table 1 can be sorted in three cases as seen in Fig. 5: 1) points A, B, C, D, and E; 2) points a, b, c, d and e; and 3) points 1, 2, 3, 4, and 5 respectively. The shaded region was obtained by fixing a Mach number but varying the incidence in the experiment. A power spectra plot of the normal force was computed at each α and the presence of shock waves was determined from observing whether the 70-80 Hz peak was present or not. The buffet boundary, which was obtained from divergence of the fluctuating normal force, is included in this figure for reference. This buffet onset is identified from the divergence of the normal force fluctuations by noting the point on the curve with a slope $dC_N' /dC_L=0.1$. This value is arbitrarily chosen, but in those cases where buffet onset is primarily due to trailing edge separations, this criterion for deriving the buffet boundary is found to give consistent results and agrees with values computed from trailing edge pressure divergence.

The static surface pressure distributions are listed in Table 6 with some examples shown here from Fig. 6 to Fig. 8. The cross-hatched and open bar symbols in Fig. 7 and Fig. 8 denote regions of attached and separated flows determined from skin friction measurements.

Table 7 presents the unsteady pressure or the pressure intensities along airfoil chord of BGK-1 and BGK-1(m) models. The corresponding figures are shown in Fig. 10 and Fig. 11.

The statistical properties such as power and cross power spectral density, auto and cross correlation functions, as well as coherence functions of pressure and normal force have been measured at different Mach numbers and angles of attack. As examples Fig. 12 shows a set of the spectral analyses at the condition of M=0.753 and α=5.66° for BGK-1 model. The frequency response of the installed transducers was calibrated and established to be flat up to approximately 200 Hz. The normal force signal was obtained at the sampling frequency of 1.6 kHz. Power spectra of unsteady pressure on upper surface of BGK-1(m) at different locations are shown from Fig. 13a to Fig. 13c. Fig. 14 shows the cross correlation functions between different transducers at M=0.688 and α=3.99°, 6.43° and 9°.

The pressure-time histories on BGK-1(m) model at M=0.71 and various α are presented in Fig. 15. The unsteady pressure fluctuations behind the periodic shock wave have two contributions. One is from a random component associated with the turbulent motion in the separated flow region. Another is a deterministic part from the pressure field as a result of shock wave oscillation. Thus, approximately 175 ensemble averages of the pressure signals were performed. Each ensemble, which was synchronized to the zero crossings decided from balance normal force spectra, had 32 samples. A Fourier analysis was then performed to obtain the fundamental and harmonics of the oscillatory pressure field.

For supercritical airfoils such as the BGK No. 1, it is found that at the lower Mach number range, separation can occur behind the shock wave as a bubble and propagates downstream as the angle of incidence is increased. Trailing edge separation can occur at the same time and it moves upstream and the two separated regions will eventually merge. An investigation on the model was carried out at M=0.688 using a Preston tube to measure the skin friction on the surface at various angles of attack. The typical distributions of the skin friction coefficient are presented in Fig. 16. The results show that at α=4.67°, a small separation bubble begins to form behind the shock wave. The separation bubble grows as the incidence increased and at α=6.15°, trailing edge separation has already begun and has moved to nearly 90% of the chord as seen in Fig. 16.

LIST OF SYMBOLS AND DEFINITIONS

b	model span	
c	model chord	
C_L	lift coefficient	$=\frac{L}{qbc}$
C_{Ldes}	design lift coefficient	
C_N	normal force coefficient	$=\frac{N}{qbc}$
C_P	pressure coefficient	$=\frac{p-p_\infty}{q}$
$\overline{C}_p$	ensemble-averaged pressure coefficient	
C_p'	fluctuating pressure coefficient	$=\frac{P_{rms}}{q}$
C_N'	fluctuating normal force coefficient	$=\frac{N_{rms}}{qbc}$
f	frequency	
L	lift	
M	free stream Mach number	
M_{des}	design Mach number	
M_{dr}	drag rise Mach number	
N	Normal force	
$\overline{N}$	time-averaged normal force	
N_{rms}	rms value of normal force	$Nrms=\sqrt{\lim_{T\to\infty}\frac{1}{T}\int_0^T(N-\overline{N})^2(t)dt}$
P	local static pressure	
P_∞	free stream static pressure	
$\overline{P}$	time-averaged pressure	
P_{rms}	rms value of the fluctuating pressure	$P_{rms}=\sqrt{\lim_{T\to\infty}\frac{1}{T}\int_0^T(P-\overline{P})^2(t)dt}$
Q,q	free stream dynamic pressure	

Re	Reynolds number based on chord	
$R_x(\tau)$	auto correlation function of x(t)	$R_x(\tau) = \lim_{T\to\infty} \frac{1}{T}\int_0^T x(t)\cdot x(t+\tau)dt$
$R_{xy}(t)$	cross correlation function of x(t) and y(t)	$R_{xy}(\tau) = \lim_{T\to\infty} \frac{1}{T}\int_0^T x(t)\cdot y(t+\tau)dt$
$S_x(f)$	power spectral density of x(t)	$S_x(f) = 2\int_{-\infty}^{\infty} R_x(\tau)e^{-i2\pi f\tau}d\tau$
$S_{xy}(f)$	cross power spectral density of x(t) and y(t)	$S_{xy}(f) = 2\int_{-\infty}^{\infty} R_{xy}(\tau)e^{-i2\pi f\tau}d\tau$
t,T	time	
x	distance measured along chord from the leading edge	
x(t)	random signal	
y(t)	random signal	
α	mean wing incidence	
γ^2_{xy}	coherence function of x(t) and y(t)	$\gamma^2_{xy} = \frac{\left|S_{xy(f)}\right|^2}{S_x(f)\cdot S_y(f)}$
τ	time delay	

FORMULARY

1 General Description of model

1.1	Designation	Bauer-Garabedian-Korn (BGK No. 1) airfoil
1.2	Type	Aft-loaded, natural laminar flow-capable, shock-free supercritical airfoil
1.3	Design condition	Potential flow M_{des}=0.72, M_{dr}=0.75, C_{Ldes}=0.63
1.4	Additional remarks	
1.5	References	Ref. 10

2 Model Geometry

2.1	Chord length	10 in
2.2	Span	15 in
2.3	Model coordinate	See Table 2 in CD ROM
2.4	Nose radius	-
2.5	Maximum thickness	t/c = 11.8%
2.6	Trailing edge thickness	0.1% of the chord
2.7	Additional remarks	
2.8	References	Ref. 4, 10

3 Wind Tunnel

3.1	Designation	IAR 2D High Reynolds Test Facility
3.2	Type of tunnel	Blowdown, closed test section
3.3	Test section dimensions	Rectangular, height 60 in, width 15 in, (see Fig. 1a)

3.4	Length of parallel section	141 in.
3.5	Floor and ceiling porosity	20.5%
3.6	Side wall boundary layer	A gap between inlet and nozzle section permit bleeding into the plenum chamber of fairly thick side wall boundary layer (~2 in.), see Fig. 1b.
3.7	Side wall near model area	Additional porous with boundary layer suction to atmospheric, see Fig. 1c.
3.8	Ventilation geometry	See Fig. 1d.
3.9	Range of Mach numbers	0.1 to 1.1
3.10	Re	40×10^6/ft at M=1, 10 seconds total run time
3.11	Wake traverse probe	7 wafer (12 ports) Statham miniature transducer unit
3.12	Turbulence intensity level	0.1% for Re/ft $\leq 6 \times 10^6$ 0.16~0.24% for Re/ft 10×10^6~27×10^6
3.13	Turbulence intensity level	0.1% for Re/ft $\leq 6 \times 10^6$ 0.16~0.24% for Re/ft 10×10^6~27×10^6
3.14	Reference on tunnel	Ref. 1, 2 and 3

4 Measurements and Observations

4.1	Steady pressure for the mean conditions	measured directly
4.2	Unsteady pressure for the mean conditions	measured directly
4.3	Steady forces for the mean conditions	measured directly
4.4	Unsteady forces for the mean conditions	measured directly
4.5	Spectral analysis of the pressure	yes
4.6	Spectral analysis of the loads	yes
4.7	Local skin friction	yes
4.8	Buffet boundaries	yes
4.9	Synchronous Cp time histories	yes

5 Test Conditions

5.1	Tunnel height/model chord ratio	6
5.2	Tunnel width/model chord ratio	1.5
5.3	Range of Mach number	0.501 ~ 0.805
5.4	Incidence range	-0.36 ~ 11.74
5.5	Reynolds number range	15×10^6 ~ 20×10^6
5.6	Range of tunnel total pressure	300 psi
5.7	Maximum mass flow	10 lbm/sec
5.8	Definition of model incidence	between "x" of model axis (Fig. 2) and tunnel axis
5.9	Position of transition, if free	Not applicable
5.10	Flow instabilities during tests	No evidence
5.11	Model deformation under the loads	Negligible
5.12	References describing tests	Ref. 4 to Ref. 9

6 Instrumentation

6.1 Steady pressure measurements for BGK-

1 model	
6.1.1 Position of orifices	See Fig. 2a and Table 3 in CD ROM
6.1.2 Type of measuring system	70 pressure tubes + 15 in situ pressure transducers
6.2 Unsteady pressure measurements for BGK-1 model	
6.2.1 Location of transducers	See Fig. 2a (in the middle chord) and Table 3 in CD ROM
6.2.2 Type of transducers	6 Kulite TQ 360 25 psid transducers
6.2.3 Dynamic response	Flat up to approximately 200 Hz.
6.2.4 Signal record	Recorded on FM tape for subsequent analysis.
6.2.5 Data reduction	
6.3 Unsteady pressure measurement for model BGK-1(m) model	
6.3.1 Location of transducers	See Fig. 2b and Table 3 in CD ROM
6.3.2 Type of transducers	16 of 25 psid custom made CQ-062-25D differential Kulite transducers
6.3.3 Diameter of screen	0.042 in.
6.3.4 Type of screen	0.005 in thick with 0.062 in diameter holes in a mesh pattern
6.3.5 Signal measurements	Signals were filtered by a four pole low pass filter having a 300 Hz 3db point and a –24 db/octave slope beyond 600 Hz.
6.3.6 Sampling rate	1.6 kHz
6.4 Loads measurement	
6.4.1 Type of sensors	strain gages
6.4.2 Balance	3 component side balance with max capacity of N=20,000 lbf, *m*=22,500 in.lb and X=2,000 lbf
6.4.3 Pitch drive system	Range: 55° maximum angular rate: 12° /sec, fully loaded step program: 0.25°, 0.5°, 1°, 2°, 5° ramp program: 0° – 10°/sec
6.4.4 Sampling rate	1.6 kHz
6.5 Skin friction measurement	
6.5.1 Type of transducers	Given by the difference between the total and static pressures
6.5.2 Method of measurement	Preston tube to determine the pitot pressure
6.5.3 Spatial resolution	0.05c for x > 0.6c and 0.02c for x < 0.6c respectively

7 Data presentation

7.1 Test cases	See Table 1
7.2 Normal force fluctuation	Fig. 3, Fig. 4 and Table 4 in CD ROM
7.3 Shock oscillation frequencies	Table 5 in CD ROM
7.4 Region of shock oscillation	Fig. 5
7.5 Steady pressure	Fig. 6 to Fig. 9 and Table 6 in CD ROM
7.6 Unsteady pressure	Fig. 10, Fig. 11 and Table 7 in CD ROM
7.7 Spectral analysis	Fig. 12, Fig. 13 and Fig. 14
7.7.1 Power spectral density	Fig. 12a and Fig. 13

7.7.2	Auto correlation functions	Fig. 12b
7.7.3	Cross correlation functions	Fig. 12c and Fig. 14
7.7.4	Cross power spectral density	Fig. 12d
7.7.5	Coherence function	Fig. 12e
7.7.6	Cross power spectral density and coherence function between pressure and normal force	Fig. 12f
7.7.7	Pressure-time histories	Fig. 15
7.8	Skin friction	Fig. 16
7.9	Example illustrations of results	Fig. 6, Fig. 7, Fig. 8, Fig. 10 to Fig. 16

8 Comments on data

8.1	Mach number	Mach number be maintained constant by control system
8.2	Steady incidence	measured by a potentiometer
8.3	Balance linearity	maximum 0.3% and generally < 0.1%
8.4	Balance interaction	<1.26%
8.5	Balance natural frequencies	140, 215, 320, 360 Hz, buffet excitation frequencies=70-80 Hz
8.6	Unsteady pressure coefficients	a discrete frequency of ≈420 Hz was detected due to tunnel disturbances (See Fig. 4)
8.7	Wall interference corrections	distributed suction was applied through porous plates in the vicinity of the model to minimize any three-dimensional effects

9 Personal contact for further information

X.Z. Huang, Aerodynamics Laboratory, Institute for Aerospace Research, National Research Council of Canada
M-10, IAR/NRC, Montreal Rd. Ottawa, Ontario, Canada, K1A 0R6
e-mail: xingzhong.huang@nrc.ca

10 List of references

[1] Ohman, L.H., "The NAE High Reynolds Number 15" x 60" Two-Dimensional Test Facility", National Research Council, NAE LTR-HA-4, Part 1, April 1970.

[2] Khalid, M., Ellis, F. and Ohman, H., "Flow Quality Measurements in the NAE 2D High Reynolds Number Trisonic Test Facility," NAE HAS-384, 1988.

[3] Chan, Y.Y., Tang, F.C. and Wolfe, S.M., "Analysis of the Boundary Layer Development on the Sidewalls of the NAE 2-D Test Facility," NAE LTR-HA-34, 1978.

[4] Lee, B.H.K. and Ohman, L.H., "Unsteady Pressure and Force Measurements Associated with Transonic Buffeting of a Two-Dimensional Supercritical Airfoil", National Research Council of Canada, AN-14, June 1983.

[5] Lee, B.H.K. and Ohman, L.H., "Unsteady Pressures and Forces During Transonic Buffeting of a Supercritical Airfoil", Journal of Aircraft, Vol. 21, No. 6, June 1986, pp. 439-441.

[6] Lee, B.H.K., Tang, F.C., Ellis, F.A. and Bureau, J., "Measurements of Buffet Characteristics of Supercritical Airfoils", 69th Semi-Annual Meeting of the Supersonic Tunnel Association, Manhattan Beach, California, May 1988.

[7] Lee, B.H.K., "Investigation of Flow Separation on a Supercritical Airfoil", Journal of Aircraft, Vol. 26, November 1989, pp. 1032-1037.

[8] Lee, B.H.K., "Transonic Buffet on a Supercritical Aerofoil", Aeronautical Journal, Vol. 94, No. 935, May 1990, pp. 143-152.

[9] Lee, B.H.K., "Flow Separation on a Supercritical Airfoil", Canadian Aeronautics and Space Institute Journal, Vol. 36, No. 2, June 1990, pp. 81-89.

[10] Kacprzynski, J.J., “An Experimental Analysis and Buffet investigation of the Shockless Lifting Airfoil No.1,” NRC/NAE LR-569, Aug. 1973.

[11] Redeker, G. and Proksch, H.J., “The Prediction of Buffet Onset and Light Buffet by Means of Computational Methods,” AGARD CP-204, 1977.

Table 1 Test matrix

M_∞	$Re_c x10^{-6}$	$\alpha°$	C_L	Model	Cases in Fig. 5
0.501	21.0	11.74	1.124	BGK-1	
0.703	21.3	-0.31, 6.77,8.71	0.278, 1.077, 1.02	BGK-1	
0.753	21.1	5.66	0.945	BGK-1	
0.775	15.3	2.55, 3.57, 4.61	0.762,0.859, 0.868	BGK-1	
0.783	21.0	-0.34, 2.55, 3.55, 4.57, 5.60, 6.61	0.304, 0.756, 0.807, 0.820, 0.827, 0.84(	BGK-1	
0.805	20.9	-0.36,3.52	0.314,0.727	BGK-1	
0.597	20.0	5.95		BGK-1(m)	a
0.688	20.0	3.99, 4.95, 6.43, 6.94, 9.0	0.981, 1.052, 1.059, 1.052, 1.069	BGK-1(m)	A,B,C,D,E
0.688	20.0	3.99, 4.45, 4.67, 4.95, 5.16, 5.44 5.65, 5.92, 6.15, 6.43, 6.67		BGK-1(m) skin friction	b
0.71	20.0	-0.316, 1.396, 3.017, 4.905, 6.97	0.322, 0.610, 0.886, 1.034, 1.016	BGK-1(m)	1,2,3,4,5
0.722	20.0	5.98		BGK-1(m)	c
0.747	20.0	6.01	0.916	BGK-1(m)	d
0.772	20.0	6.04		BGK-1(m)	e

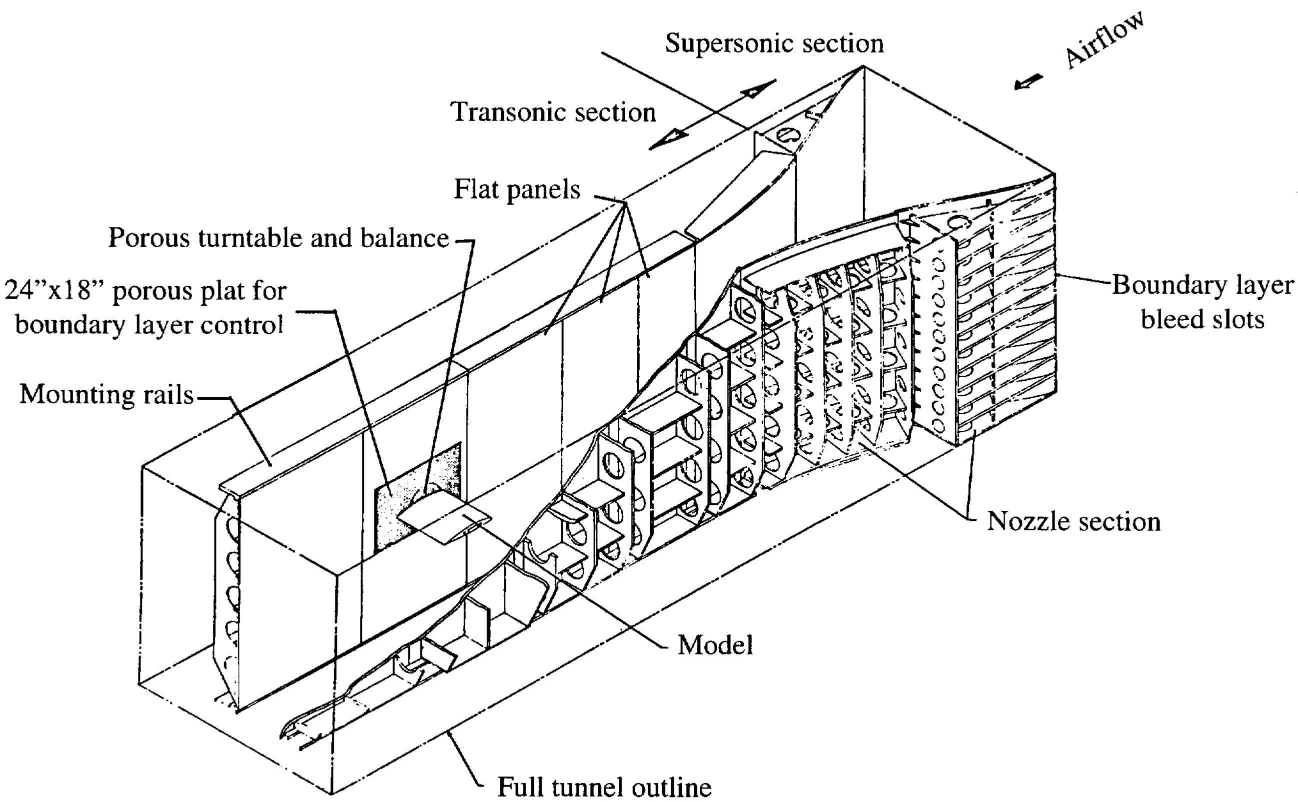

Fig. 1a IAR 15 in x 60 in 2-D insert

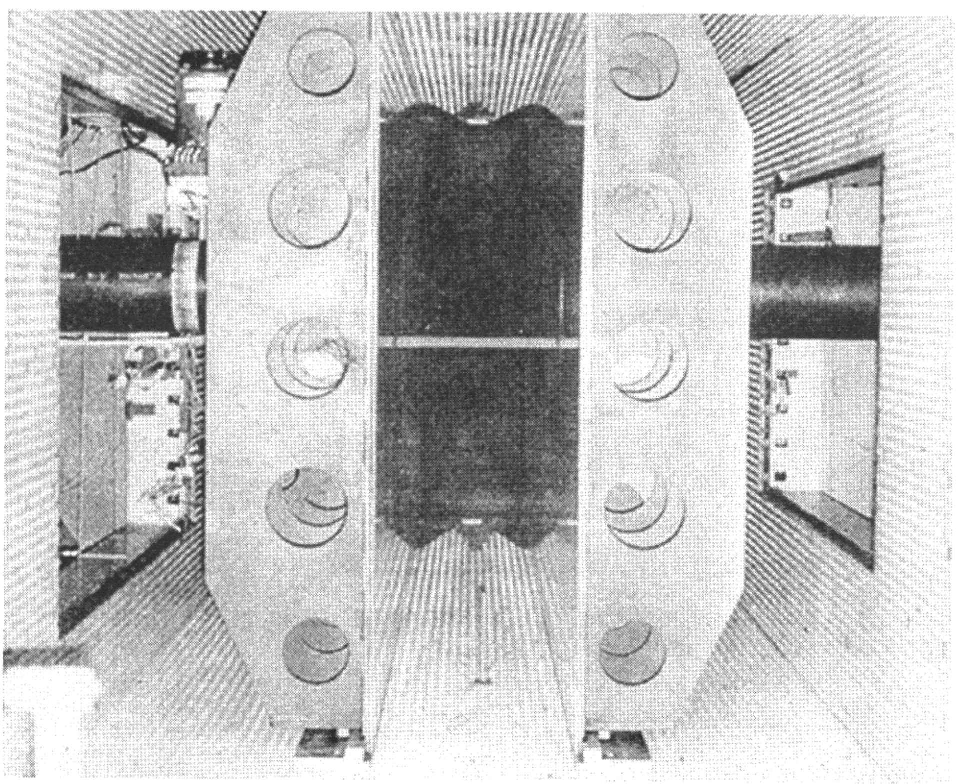

Fig. 1b Downstream view of 2-D insert

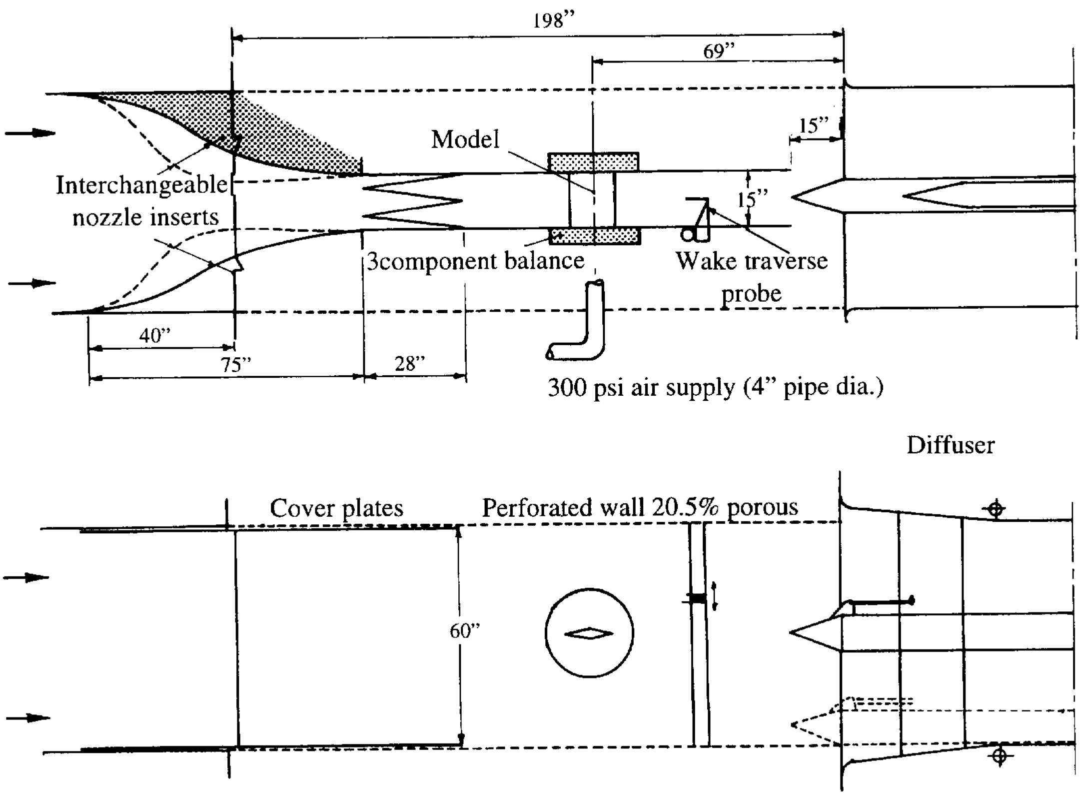

Fig. 1c 2D section arrangement for IAR 5ft x5ft wind tunnel

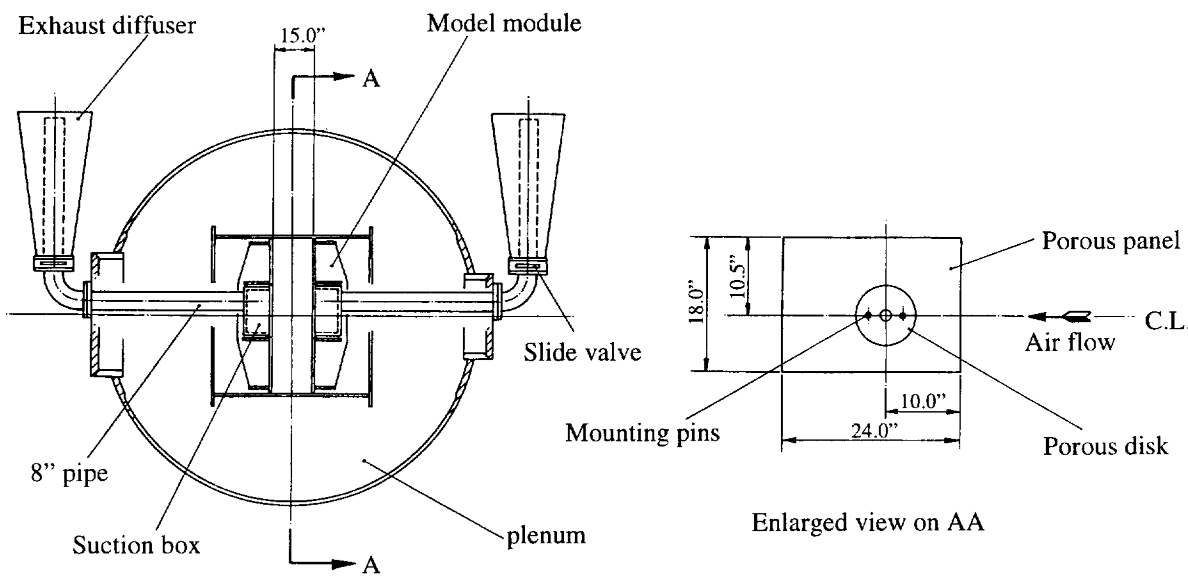

Fig. 1d Suction arrangement

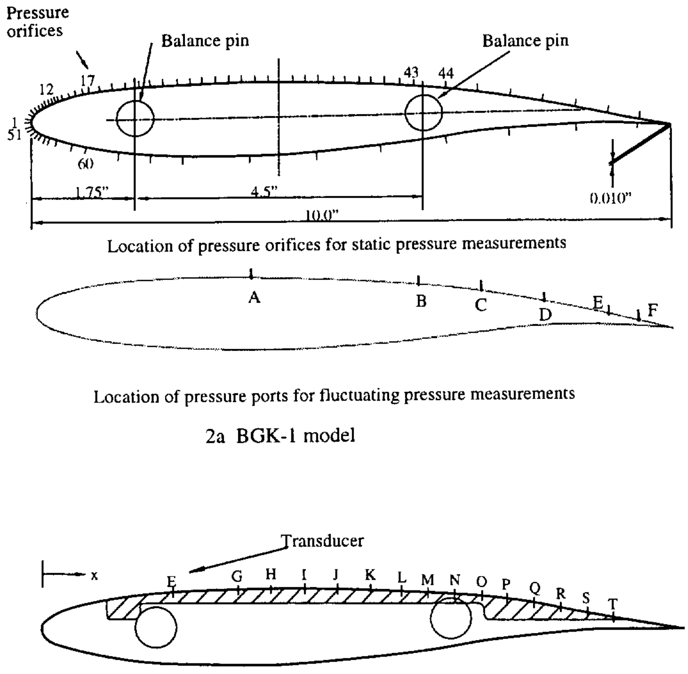

Fig. 2 BGK No. 1 supercritical airfoil

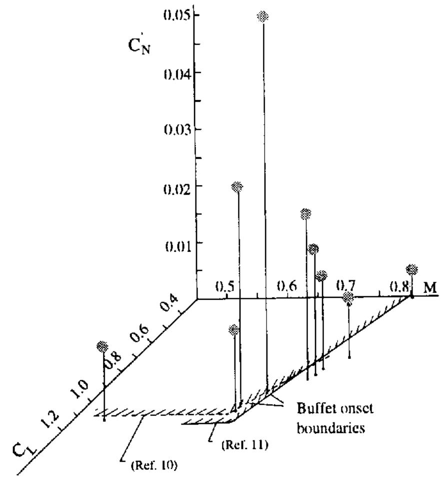

Fig. 3 Variation of the fluctuating normal force coefficient with Mach number and steady state lift coefficient

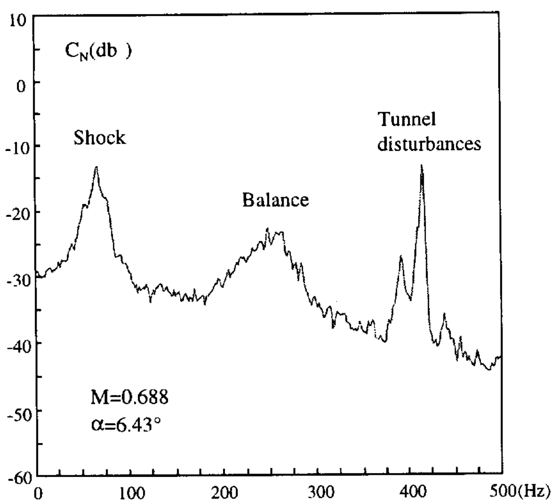

Fig. 4 Power spectra of normal force

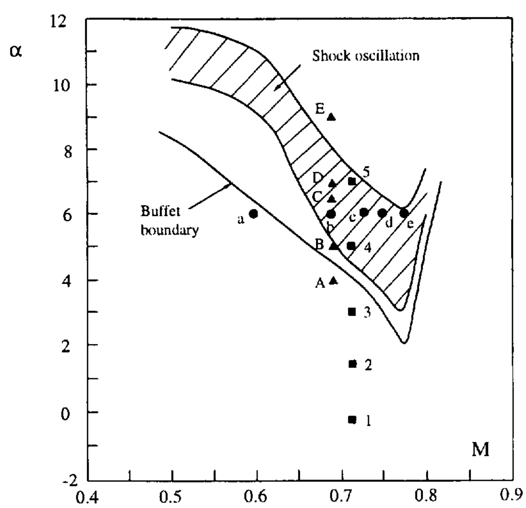

Fig. 5 Region of shock oscillation

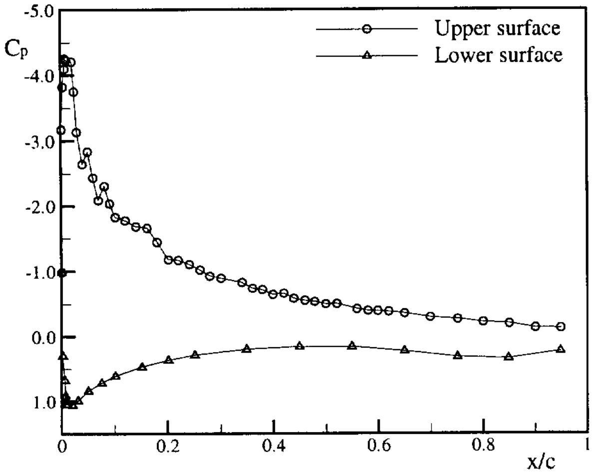

6a M=0.501, α=11.8°

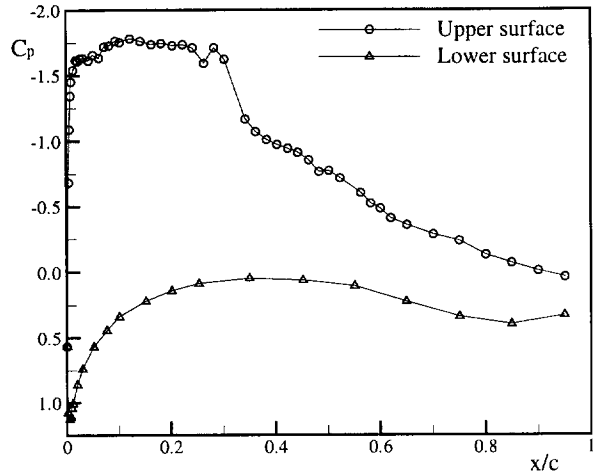

6b M=0.704, α=6.79°

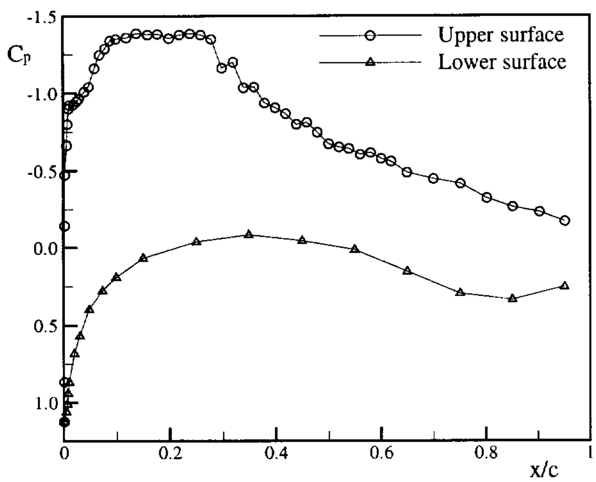

6c M=0.757, α=5.57°

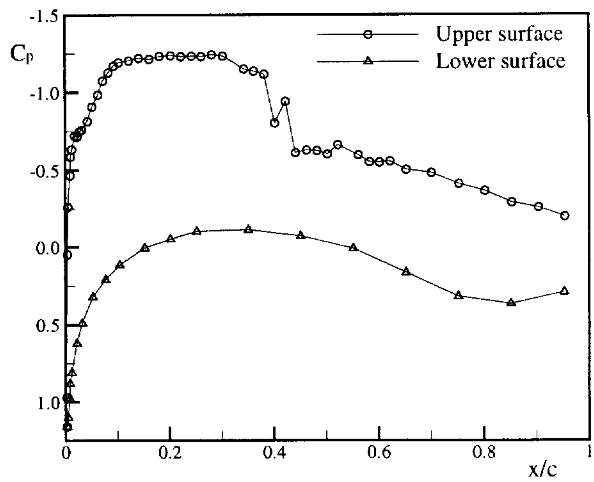

6d M=0.773, α=4.60°

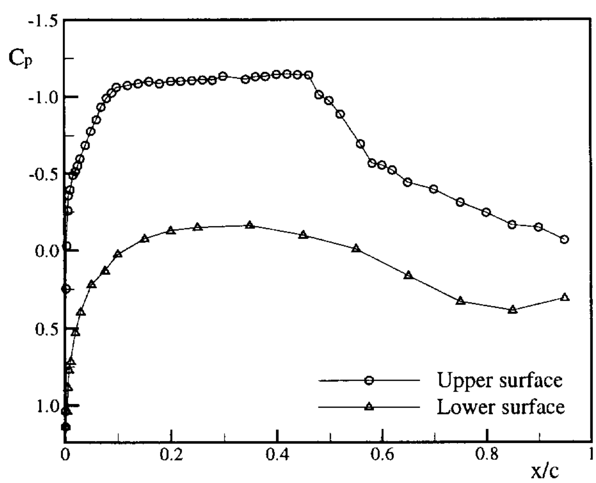

6e M=0.784, α=3.58°

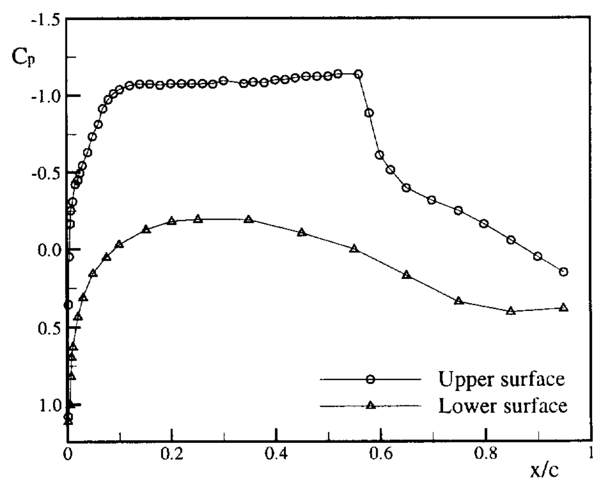

6f M=0.773, α=2.59°

Fig. 6 Steady pressure distributions

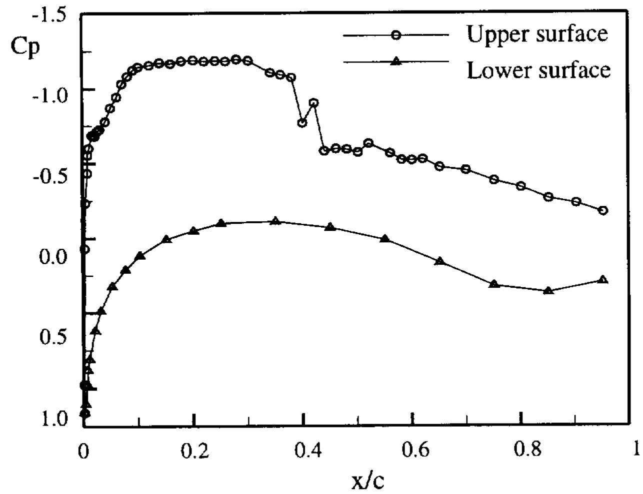

6g M=0.804, α=3.54°

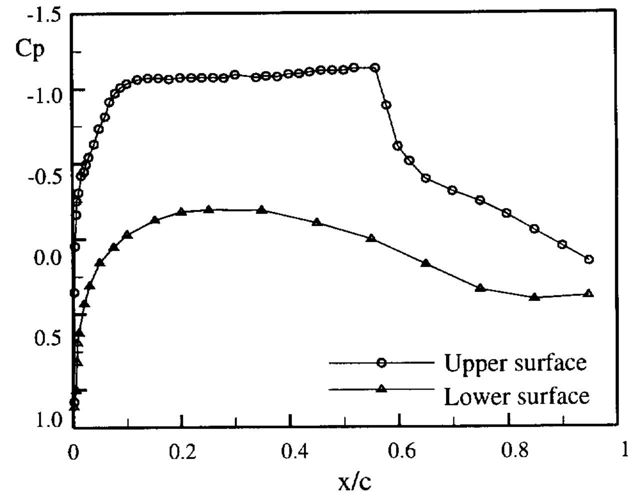

6h M=0.804, α=0.33°

Fig. 6(cont.) Steady pressure distributions

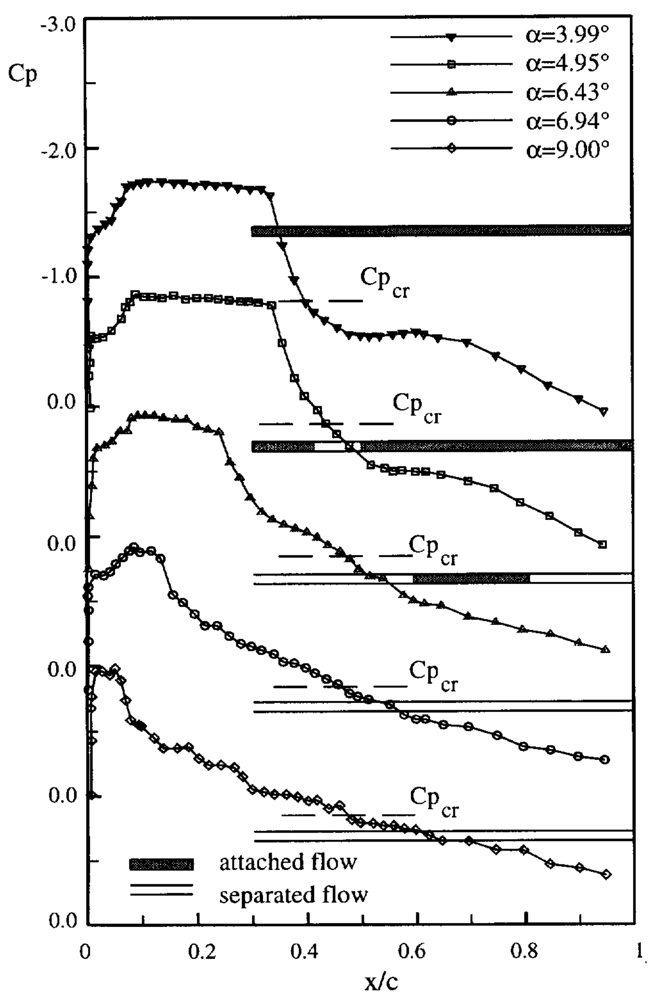

Fig. 7 Steady pressure distributions on upper surface at M=0.688

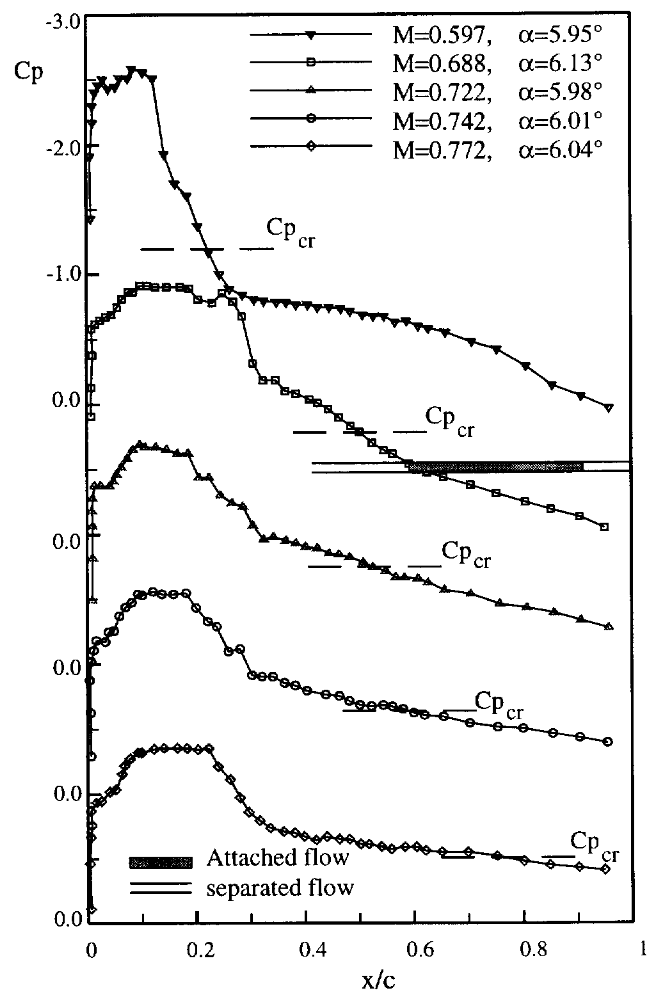

Fig. 8 Steady pressure distributions on upper surface at various Much numbers

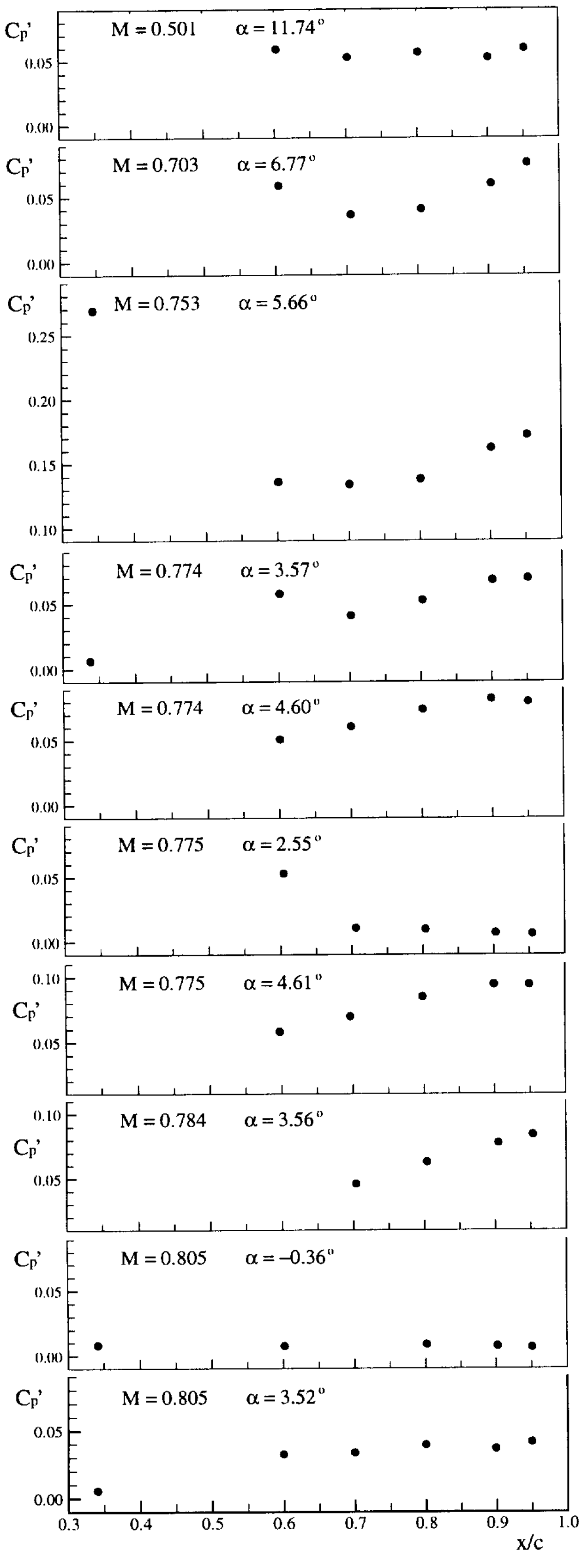

Fig.10 Variation of pressure intensities along airfoil chord

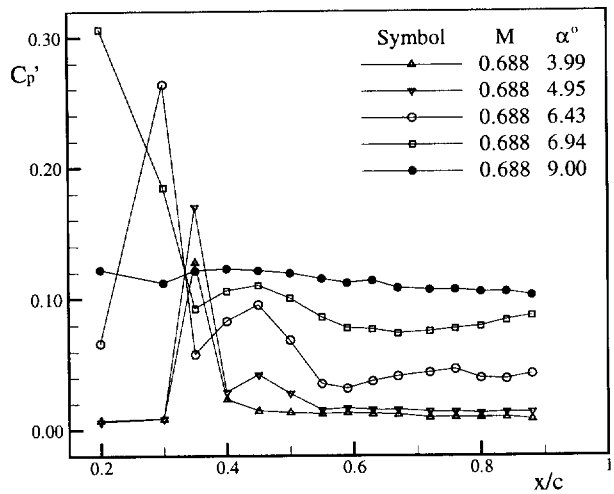

11a for points A,B,C,D and E in Fig.5

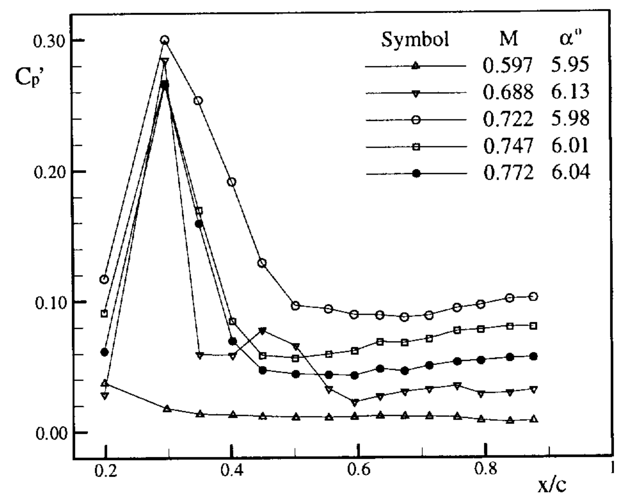

11b for points a,b,c,d and e in Fig.5

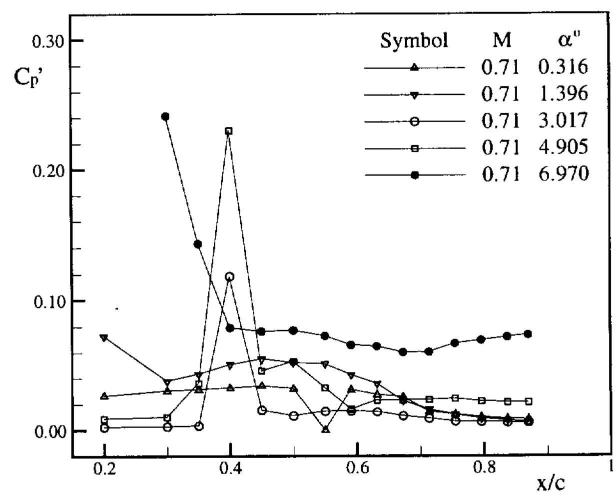

11c for points 1,2,3,4 and 5 in Fig.5

Fig.11 Unsteady pressure distributions

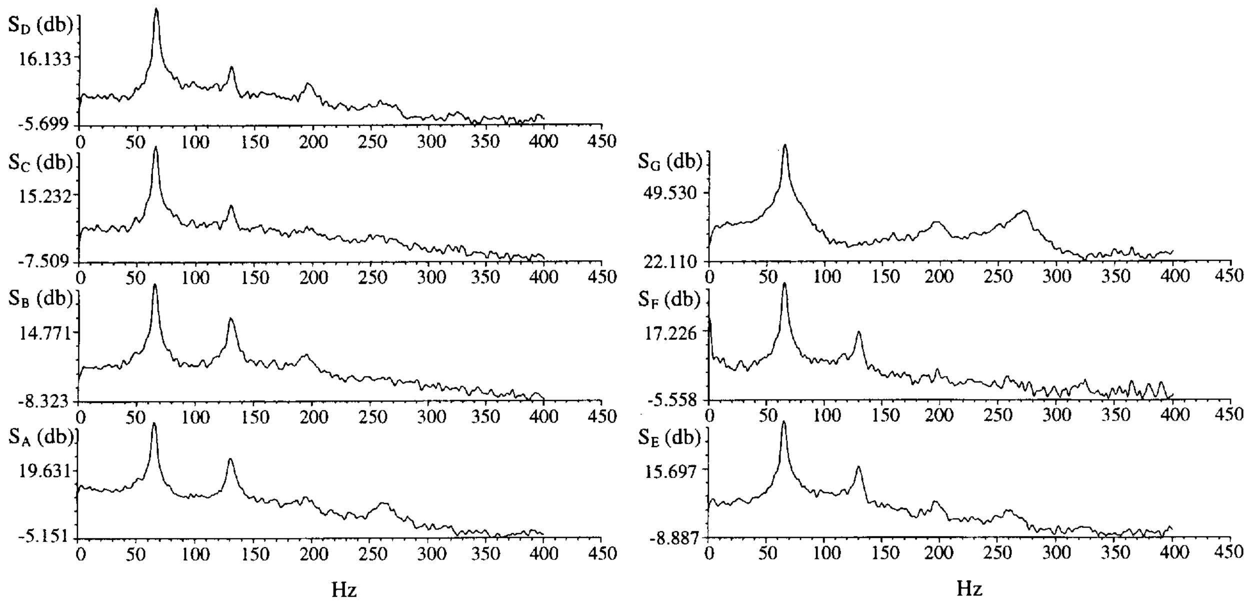

Fig. 12a Power spectral density for M_∞=0.753, C_L=0.945, q=24.5 psi

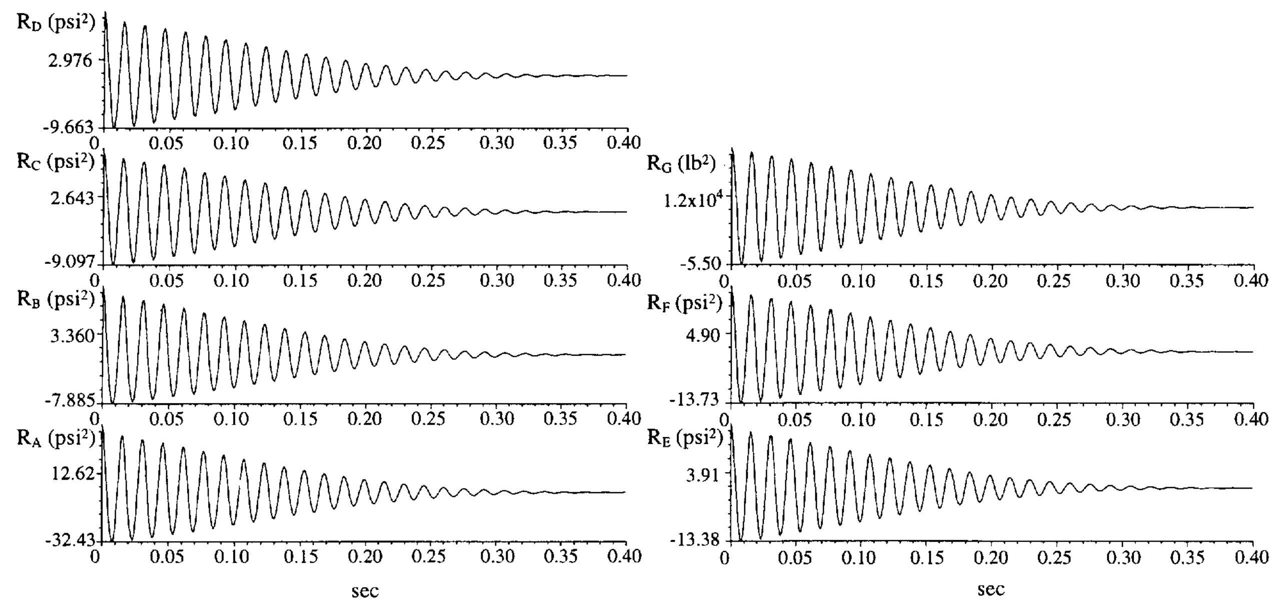

Fig. 12b Auto correlation functions for M_∞=0.753, C_L=0.945, q=24.5 psi

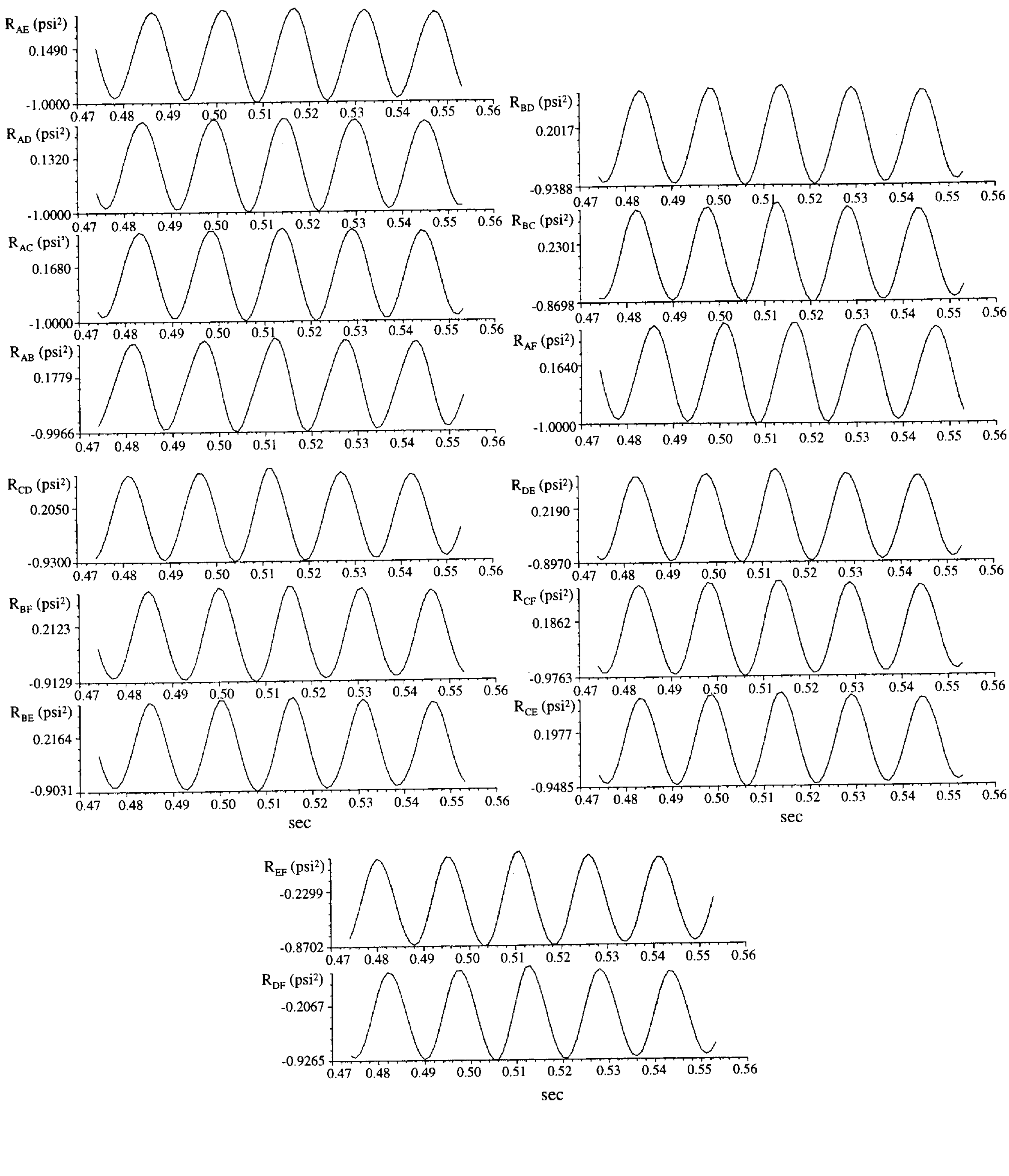

Fig. 12c Cross correlation functions for M_∞=0.753, C_L=0.945, q=24.5 psi

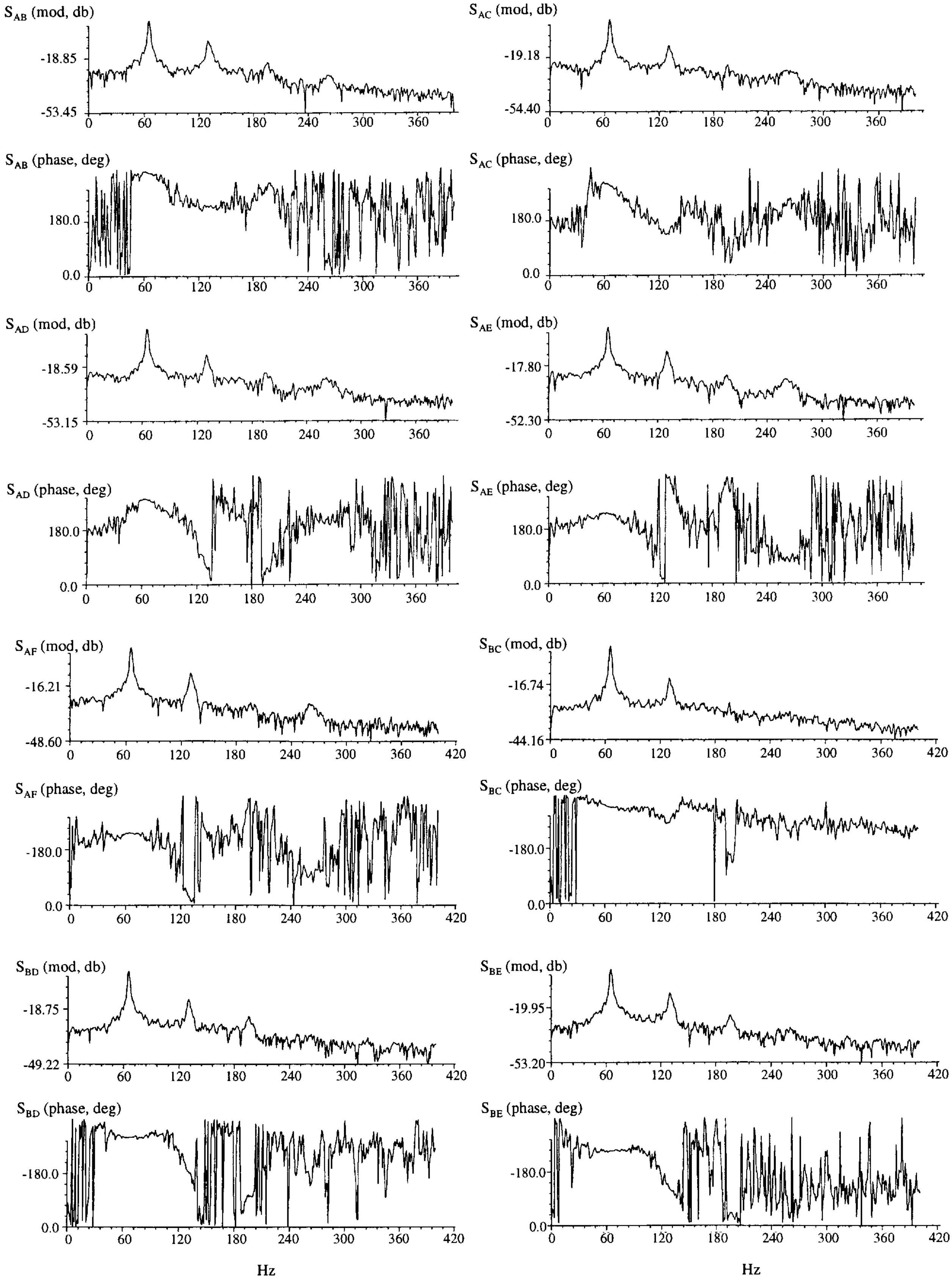

Fig. 12d Cross power spectral density for M_∞=0.753, C_L=0.945, q=24.5 psi

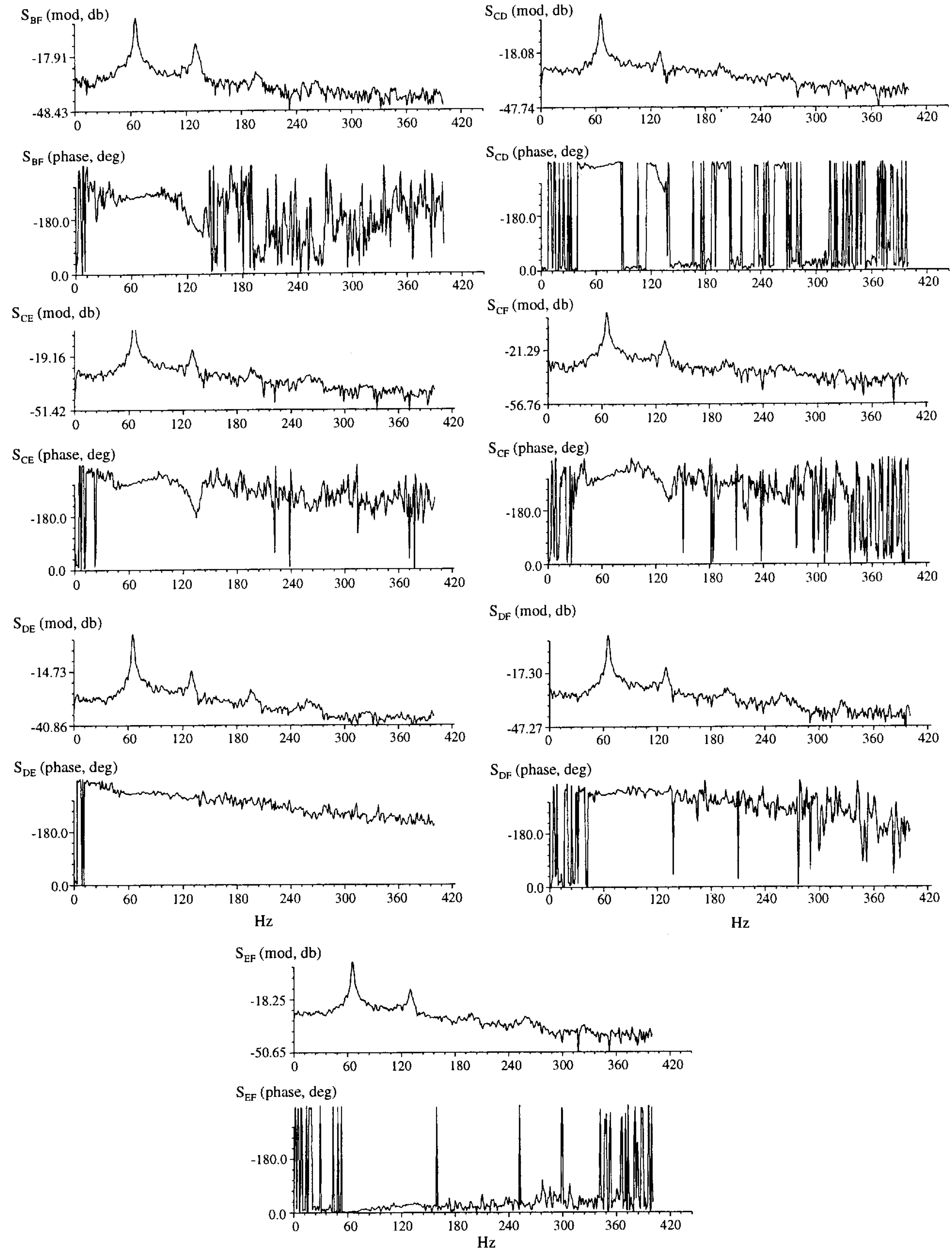

Fig. 12d (cont.) Cross power spectral density for M_∞=0.753, C_L=0.945, q=24.5 psi

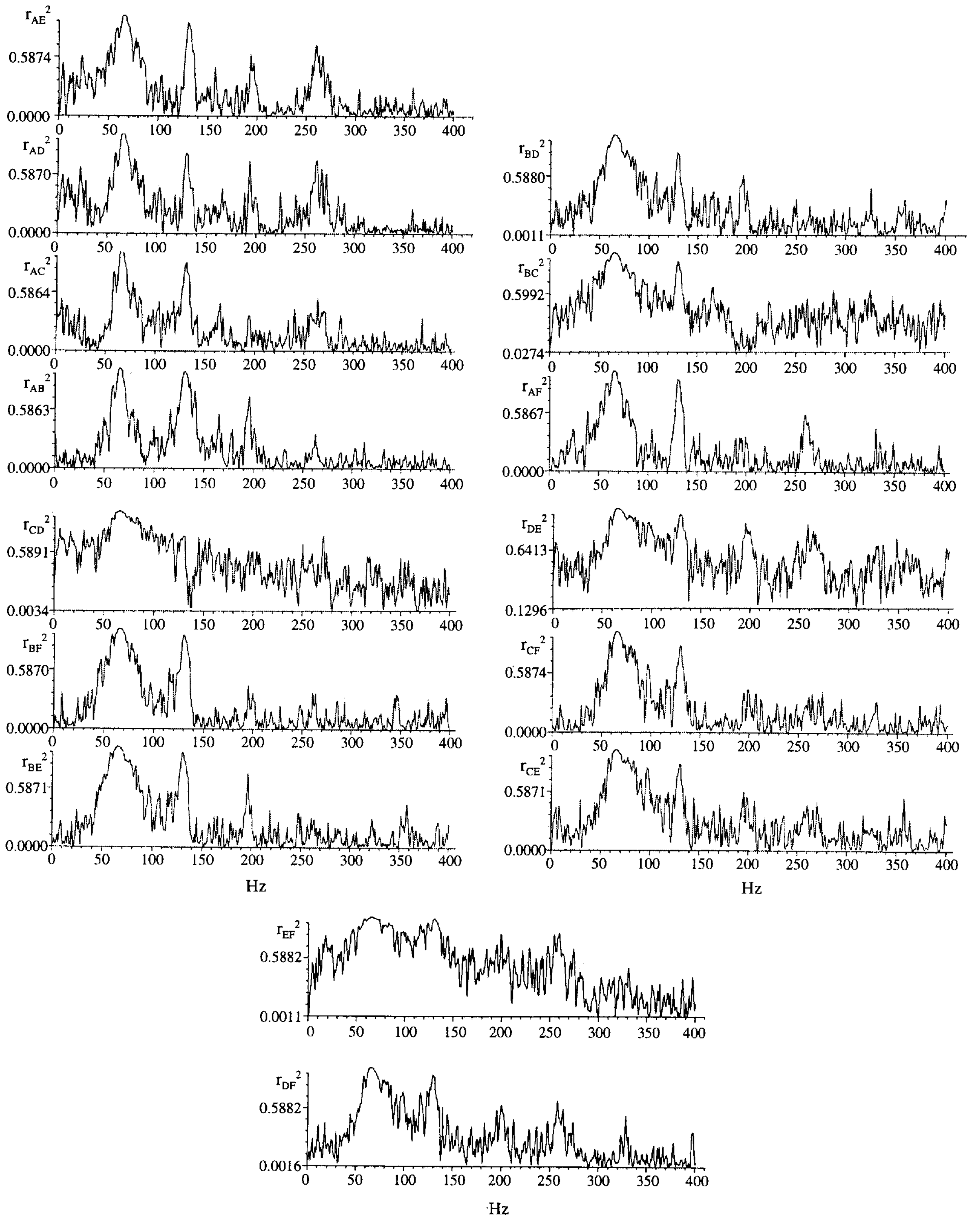

Fig. 12e Coherence functions for M_∞=0.753, C_L=0.945, q=24.5 psi

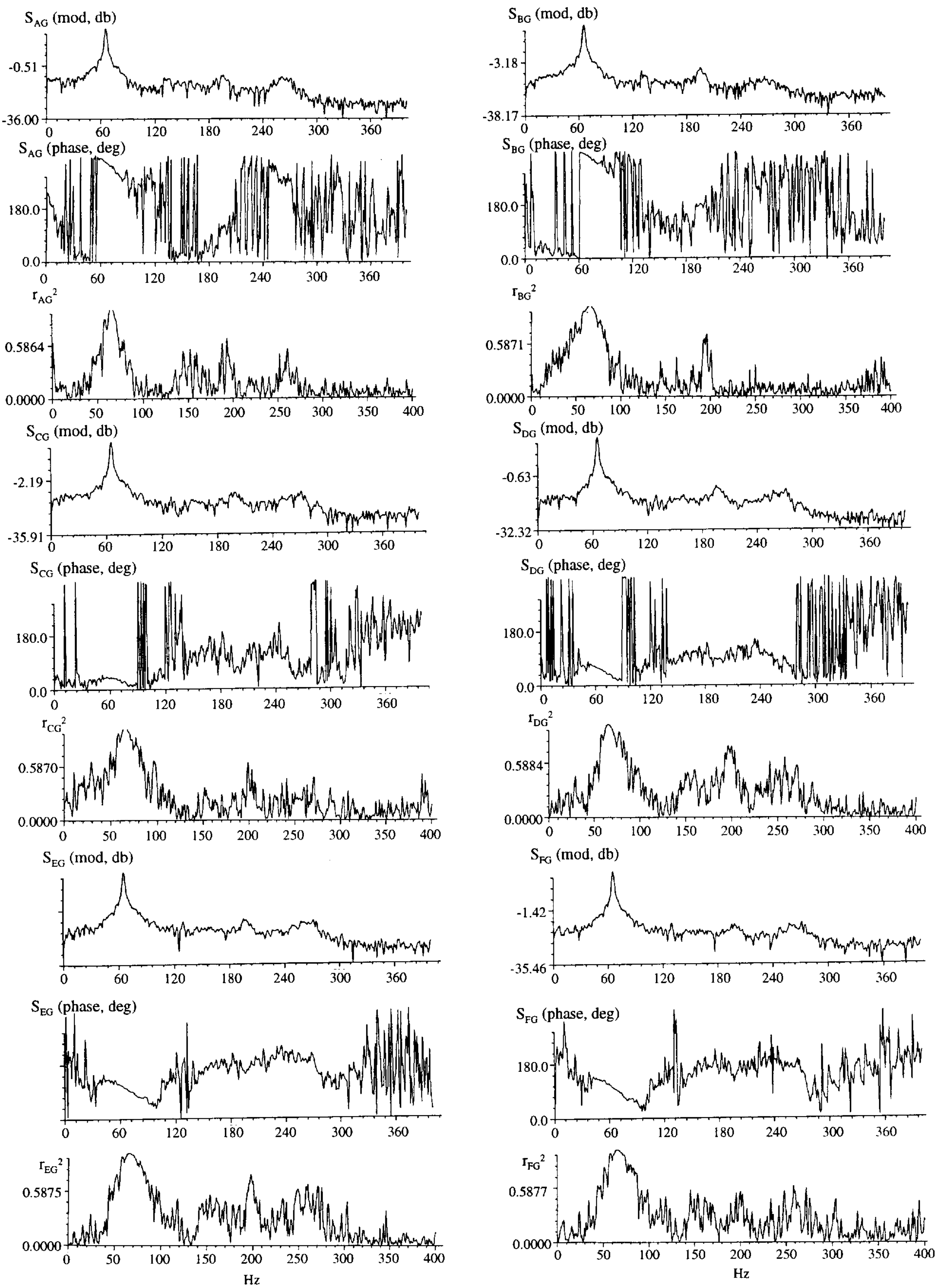

Fig. 12f Cross power spectral density and coherence function between pressure and normal force for M_∞=0.753, C_L=0.945, q=24.5 psi

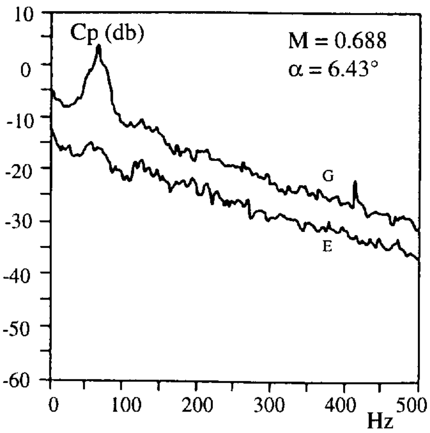

13a transducers located before and after shock

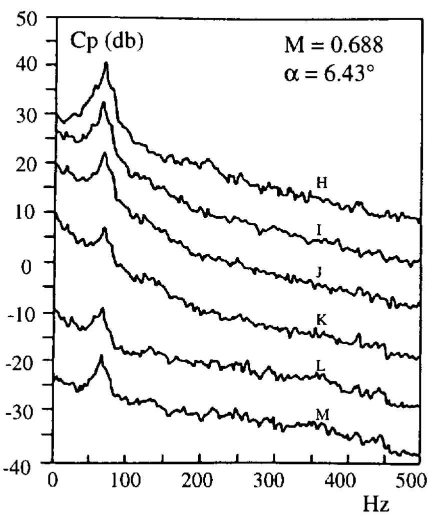

13b transducers located in the separation bubble

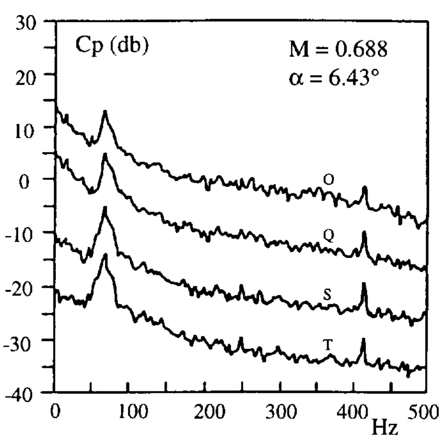

13c transducers located in the attachment and trailing-edge separation regions

Fig. 13 Power spectra of pressure on upper surface

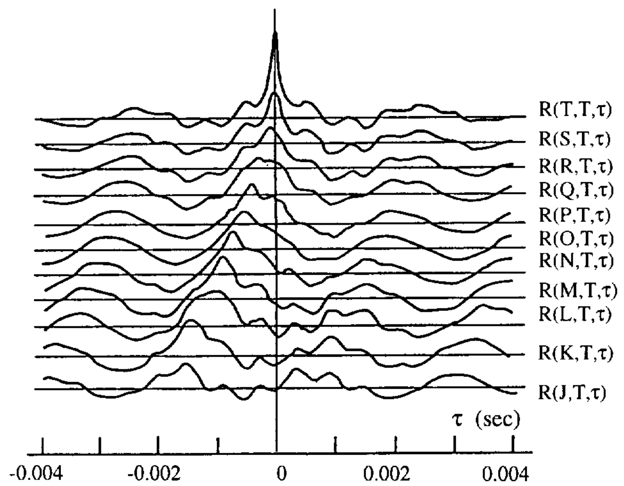

14a M = 0.688, α = 3.99°

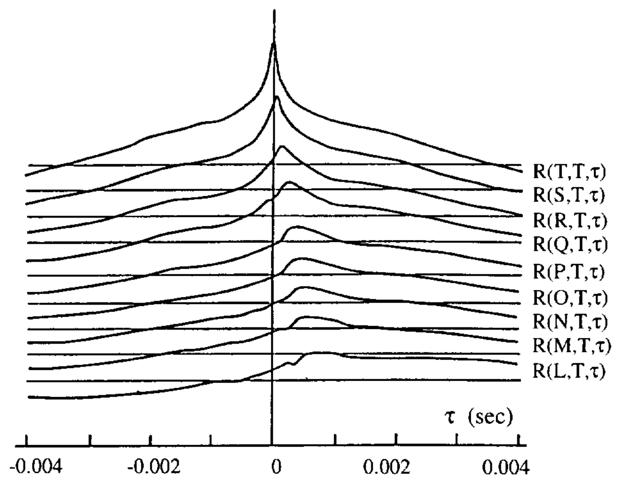

14b M = 0.688, α = 6.43°

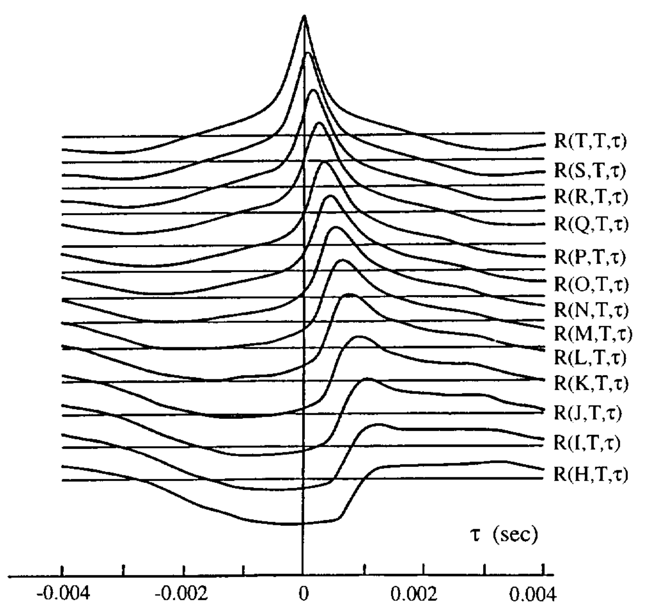

14c M = 0.688, α = 9°

Fig. 14 Cross-correlation functions of pressure

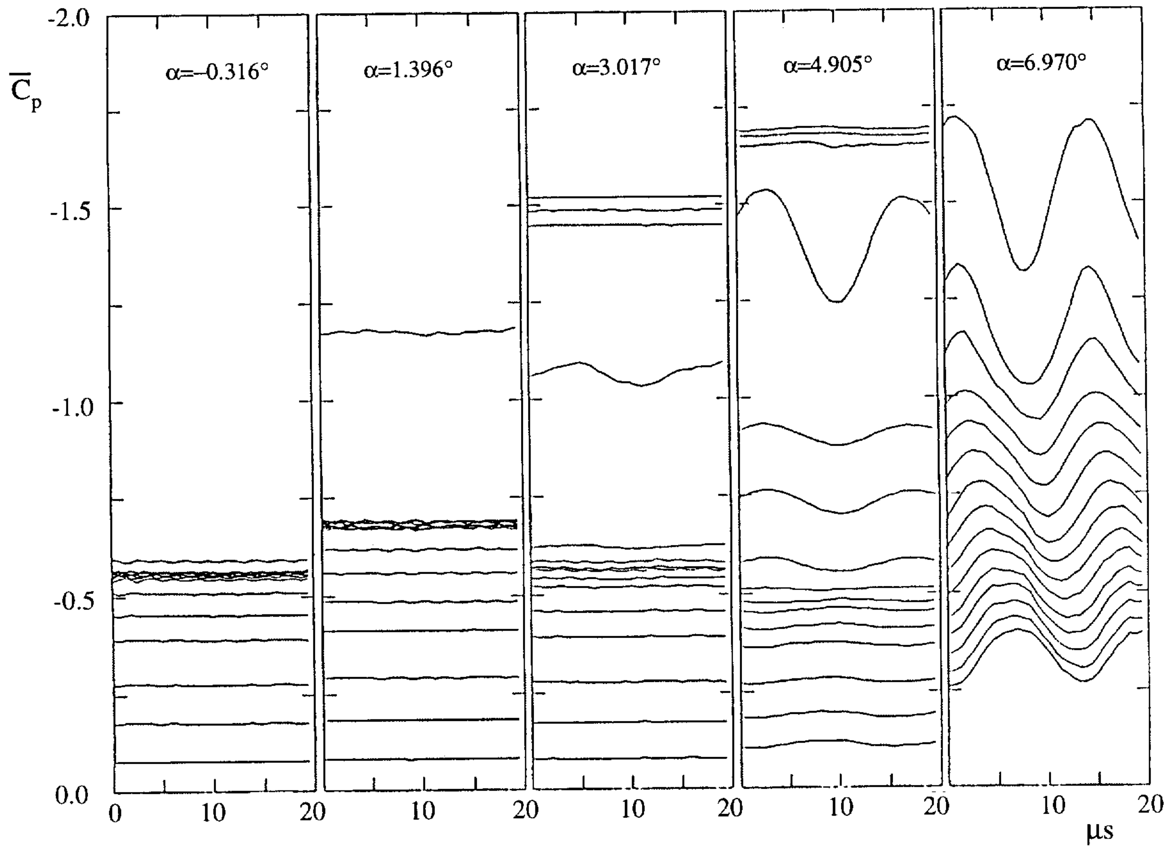

Fig. 15 Pressure-time histories at M=0.71 and various α

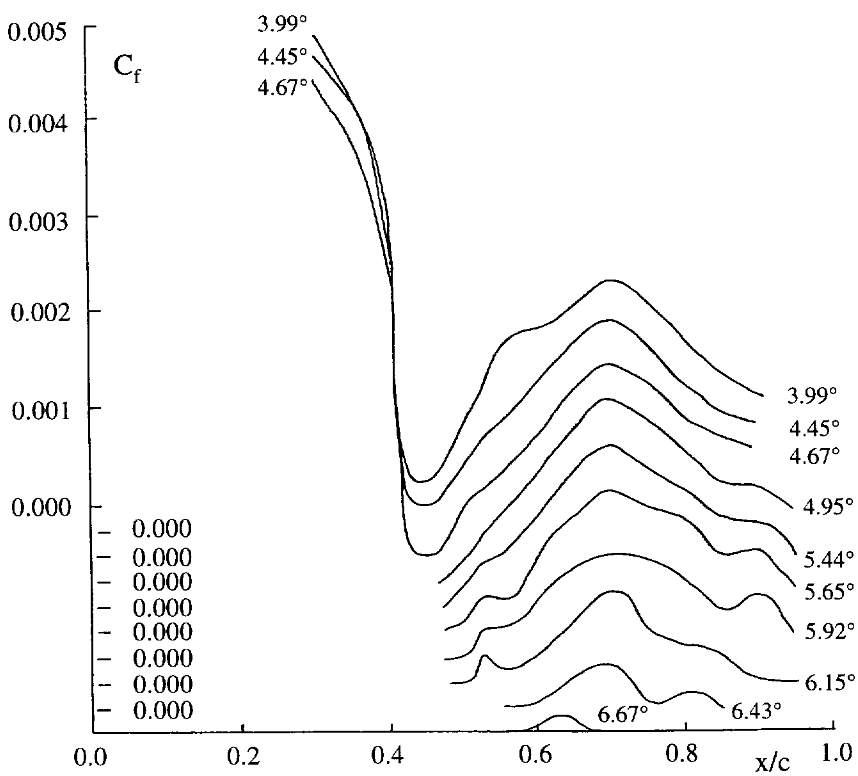

Fig. 16 Skin friction coefficient at M=0.688 and various α

14E. BUFFET DATA FROM M2391 DIAMOND WING

Reported by
I W Kaynes
1008, A9
DERA
Farnborough
GU14 0LX
UK

INTRODUCTION

Unsteady aerodynamic loads may be described in terms of the aerodynamic excitation arising from unsteady separated flows (buffet) or the associated uncoupled structural response (buffeting). Buffeting response measurements are usually made on nominally rigid or aero-elastically tuned models, with buffeting levels determined from the narrow band response of wing root strain gauges or wing tip mounted accelerometers. In such cases the model structural dynamics are tuned to provide sufficient buffeting response.

Detailed studies have suggested that the first stage in the successful prediction of full scale "buffeting" must be the prediction of "buffet", unless a dynamically scaled structure can be employed. Early in the design stage, the structural characteristics of a configuration are generally unknown. Dynamically scaled models are also expensive to design and manufacture and are therefore not considered a practical solution. The use of traditional construction "flexible" models to measure "buffet" can lead to serious difficulties in the interpretation of aerodynamic data with the measured buffet excitation comprising components due to the unsteady flow field and components due to model vibration. Furthermore, the combination of a conventional wind tunnel model on a typical steel wind tunnel support structure frequently results in combined model and support natural frequencies in the region of aerodynamic interest for buffet measurement.

A buffet test technique was therefore developed at DERA Bedford to enable "pure" unsteady aerodynamic data to be acquired free from model and support structure interference. The technique centres around the use of low mass, high stiffness models with structural frequencies above the frequency range of aerodynamic interest and a new low natural frequency model support system referred to as the Buffet Support Fixture (BSF).

The BSF is shown in Figure 1 and comprises a 2-tonne mounting block attached to two stiff lateral box beams. The box structure is in turn suspended from the tunnel floor on flexible elastomeric bearings. The combination of a large mass on low stiffness mountings provides a support structure with only low natural frequency modes of vibration. The support system natural frequencies are lower than the buffet excitation frequencies expected for half models in the 13ft x 9ft low speed tunnel and are typically less than 17Hz. The BSF natural frequency can be tuned by the addition of extra mass to the block or by modification of the elastomeric bearings. High natural frequency buffet models are provided by low mass, high stiffness models fabricated using a carbon fibre and foam core construction technique. The combined model and support system structural interference is restricted to limits outside of the domain of aerodynamic interest providing a wide frequency window within which "pure" aerodynamic data can be measured.

The first wing buffet planform to be manufactured at DERA Bedford was model M2391. This model is a 40 degree leading edge sweep, half model diamond wing with a stream-wise clipped tip as shown in figure 2. The model was constructed using a carbon fibre and foam-core construction technique. A rigid foam core (Rohacell 51) was bonded to a 50mm thick aluminium root block and numerically-controlled machined from solid to the desired profile. The assembly was slotted to support internal instrumentation and skinned with an 8 layer carbon fibre laminate, each layer 0.125mm thick. A cold cure technique was employed, with each successive layer rotated through an additional 45^{o} to provide the required directional strength. Although the 10% t/c ratio wing section shape is not representative it was generally agreed that the large scale buffet distribution and magnitude would be dominated by the low aspect ratio of the planform.

Model M2391 has interchangeable rectangular and chined fuselages, with the rectangular fuselage providing a perpendicular wing-fuselage interface. The chined fuselage allows the buffet due to mixed vortical flows to be studied. Figure 3 shows the model mounted in the DERA Bedford 13ft x 9ft low speed wind tunnel.

LIST OF SYMBOLS AND DEFINITIONS

α	model incidence, degrees
C_L	Lift coefficient -lift force (N)/qS
C_M	Pitching moment coefficient (about 25% mean aerodynamic chord)- Pitching moment (Nm)/qSc_{mac}
c_{mac}	Mean aerodynamic chord (m)

C_p	Pressure coefficient - $(P_{loc}-P_\infty)/q$
P_{loc}	Local static pressure (Nm^{-2})
P_∞	Freestream static pressure (Nm^{-2})
P_{RMS}	Root mean square pressure fluctuations(Nm^{-2})
q	Freestream dynamic pressure (Nm^{-2})

PRESENTATION OF DATA

The data are supplied in ASCII files describe din the following paragraphs:

The file COORDS.DAT contains the coordinates of the 205 transducers, as given in table 1 but to greater precision in the file. Each record of the file contains the name of the transducer (5-characters) followed by the non-dimensional coordinates x/c and y/b in format 2F9.6.

The files CPxxDEG.TXT contain the steady C_p data and unsteady data as P_{RMS}/q for each transducer position for a test at incidence xx as specified in the file name. The first line is a heading and subsequent lines each contain a transducer name (5-characters) followed by the steady pressure in format F9.5 and the unsteady pressure value in format F9.6.

The files SPxxDEG.TXT contain the spectral data for each pressure transducer versus frequency. The data has been processed using 256 spectral lines giving a frequency resolution of 1.465 Hz with a maximum frequency of 300 Hz. The first line of the file contains the transducer names (format 204A6) and each subsequent line contains a frequency value (Hz) followed by the 204 spectral values, with all values in format E12.5. A sample of the data is given in table 3, showing the first 5 transducers and first frequencies and first 8 frequencies for the test at 24^o incidence from file SP24DEG.TXT.

A FORTRAN code CH14.FOR is provided which demonstrates the reading of the data. The program includes a sample main segment which calls the data input subroutine CH14SEL and then lists the number of points read.. This subroutine may be employed in a user's code to extract the data to serve as a model for other data extraction codes.

CH14SEL subroutine

A description of the subroutine call and arguments follows:

```
      SUBROUTINE CH14SEL(NCH,INCID,TRAN,XYTRAN,FREQ,VAL,MAXF,MAXP,NF,NP)
C
C-- This routine reads and selects tables from the data file SET1.DAT
C   which contains the data of tables 5 to 18 of R702 data set 1.
C-- Arguments are as defined below (all except NCH must be variables):
C   Input values
C         NCH     channel number to be used for reading the input file
C         INCID   Specifies the required incidence (integer, degrees)
C         MAXF    The frequency-dimension of arrays in calling segment >=204
C         MAXP    The transducer-dimension of arrays in calling segment >=205
C   Returned values
C         NF      The number of frequency values
C         NP      The number of transducers
C         TRAN    The single element array of transducer names
C         XYTRAN  The two-dimension array of transducer locations
C                 XYTRAN(i,j) denotes the chordwise (i=1) and spanwise (i=2)
C                 position of the j-th transducer
C         FREQ    The single dimension array of frequency values
C         VAL     The values with VAL(i,j) denoting the value for the i-th
C                 frequency at the j-th transducer location
C
      REAL FREQ(MAXF), VAL(MAXF,MAXP), XYTRAN(2,MAXP)
      CHARACTER *5 TRAN(MAXP),BUF
```

FORMULARY

1 General Description of model

1.1	Designation	M2391
1.2	Type	Half model
1.3	Derivation	Diamond wing
1.4	Additional remarks	Interchangeable fuselages, rectangular and chined
1.5	References	1

2 Model Geometry

2.1	Planform	Diamond wing
2.2	Aspect ratio	2.27
2.3	Leading edge sweep	$+40^{o}$
2.4	Trailing edge sweep	-40^{o}
2.5	Taper ratio	0.024
2.6	Twist	None
2.7	Wing centreline chord	1.994 m
2.8	Semi-span of model	1.160 m
2.9	Area of planform	1.185 m^2 gross wing area
2.10	Location of reference sections and definition of profiles	Bi-convex section with constant 10% t/c ratio except at tip as noted below. Rounded leading and trailing edge radius with constant radius 3mm.
2.11	Lofting procedure between reference sections	Linear taper
2.12	Form of wing-body junction	a) Rectangular fuselage has perpendicular wing-fuselage interface b) Chined fuselage angled intersection with wing
2.13	Form of wing tip	Freestream aligned. Increased t/c at tip over last 50mm of span to permit flat upper and lower surfaces.
2.14	Control surface details	None
2.15	Additional remarks	Detailed drawings of model available from technical contact (Section 10).
2.16	References	1

3 Wind Tunnel

3.1	Designation	DERA Bedford 13ft x 9ft low speed wind tunnel
3.2	Type of tunnel	Continuous atmospheric with closed return circuit
3.3	Test section dimensions	Height 9ft (2.74m), width 13ft (3.96m), length= 36ft (10.97m)
3.4	Type of roof and floor	Closed – vented at trailing edge of working section
3.5	Type of side walls	Closed – vented at trailing edge of working section
3.6	Ventilation geometry	Vents at downstream of the working section - a ring of 118 slots 260mm long, 50mm wide, ducted to chamber with one way flaps to atmosphere.
3.7	Thickness of side wall boundary layer	Approx. 0.1m
3.8	Thickness of boundary layers at roof and floor	Approx. 0.1m
3.9	Method of measuring velocity	Working section and settling chamber static pressure tappings related to tunnel speed calibration.
3.10	Flow angularity	not available
3.11	Uniformity of velocity over test section	dynamic pressure constant to within 0.05% over a $2m^2$ reference plane normal to the flow axis in the working section.
3.12	Sources and levels of noise or turbulence in empty tunnel	Turbulence rms levels in 2 Hz to 1 KHz bandwidth: longitudinal 0.02% of u at 15 m/s rising to 0.04% at 61 m/s; vertical and lateral components 0.02% rising to 0.1% for the same speed range.
3.13	Tunnel resonances	Not available
3.14	Additional remarks	None
3.15	References on tunnel	2

4 Model motion

4.1	General description	High natural frequency model mounted on Buffet Support Fixture (BSF), a large mass/low stiffness support to give low frequency mounting.
4.2	Natural frequencies and normal modes of model and support system	Model wing first bending approx. 153 Hz, wing second bending and first torsion approx. 350 Hz. Highest frequency of BSF mounting system was rigid body roll at 17 Hz

5 Test Conditions

5.1	Model planform area/tunnel area	0.11
5.2	Model span/tunnel height	0.42
5.3	Blockage	Function of angle of attack
5.4	Position of model in tunnel	Mounted from floor
5.5	Range of velocities	50 m/s
5.6	Range of tunnel total pressure	102.9kPa
5.7	Range of tunnel total temperature	Approximately 2°C to 13°C according to atmospheric conditions
5.8	Range of model steady or mean incidence	0 to 30°
5.9	Definition of model incidence	Mean planform plane of symmetric model was used as datum for incidence
5.10	Position of transition, if free	Unknown.
5.11	Position and type of trip, if transition fixed	None
5.12	Flow instabilities during tests	Not measured
5.13	Changes to mean shape of model due to steady aerodynamic load	Not measured but considered negligible due to high model stiffness.
5.14	Additional remarks	None
5.15	References describing tests	1

6 Measurements and Observations

6.1	Steady pressures for the mean conditions	Yes
6.2	Steady pressures for small changes from the mean conditions	No
6.3	Quasi-steady pressures	No
6.4	Unsteady pressures	Yes
6.5	Steady section forces for the mean conditions by integration of pressures	No
6.6	Steady section forces for small changes from the mean conditions by integration	No
6.7	Quasi-steady section forces by integration	No
6.8	Unsteady section forces by integration	No
6.9	Measurement of actual motion at points of model	No
6.10	Observation or measurement of boundary layer properties	No
6.11	Visualisation of surface flow	Yes
6.12	Visualisation of shock wave movements	No
6.13	Aditional remarks	Steady forces measured on half model balance

7 Instrumentation

7.1 Steady pressure	
7.1.1 Position of orifices spanwise and chordwise	205 pressure tappings, located on 13 spanwise stations, see figure 2 and table 1. The data of table 1 is also presented as an electronic file.
7.1.2 Type of measuring system	Druck differential pressure transducers (±7 kPa) mounted in each Scanivalve.
7.2 Unsteady pressure	
7.2.1 Position of orifices spanwise and chordwise	a) 16 unsteady pressure transducers , see figure 2 b) Unsteady data also extracted from the 205 static pressure tappings – see ref 1 and 3
7.2.2 Diameter of orifices	1mm
7.2.3 Type of measuring system	a) Unsteady pressure transducers b) Unsteady data extracted from Scanivalve pressure fluctuations – see ref 1 and 3
7.2.4 Type of transducers	a) Entran EPE-55 (± 2 psi) pressure transducers b) see 7.1.2
7.2.5 Principle and accuracy of calibration	a) Steady state sensitivity from applied reference and calibration pressures. Accuracy as stated by transducer manufacturer. b) Frequency domain corrections applied to data to correct for frequency response of pressure tubes. See ref. 3
7.3 Model motion	None
7.3.1 Method of measuring motion reference coordinate	N/A
7.3.2 Method of determining spatial mode of motion	N/A
7.3.3 Accuracy of measured motion	N/A
7.4 Processing of unsteady measurements	
7.4.1 Method of acquiring and processing measurements	Pressure transducer, accelerometer and Scanivalve signals recorded using an AD16V 16 bit ADC within a Concurrent Maxion 9000 series workstation. Signal quantisation and aliasing errors were reduced by amplification and filtering of the signals using Kemo VBF-35 phase matched programmable filter-amplifiers.
7.4.2 Type of analysis	Power Spectral Density spectra (PSD) obtained from pressure fluctuations after correction for the frequency response function of the pressure tubes (e.g. figure 4 and ref.3). Broad band RMS values were integrated from the PSD spectra between the limits of support and model dynamics (between 20 Hz and 150 Hz).
7.4.3 Unsteady pressure quantities obtained and accuracies achieved	Broadband RMS pressures and PSD functions. RMS repeatability indicated by RMS standard deviation of 0.8%. Good agreement has been demonstrated between data from unsteady transducers and the data processed from the steady pressure tappings at nearby locations. This is shown in figure 5 for two sample locations
7.4.4 Method of integration to obtain forces	None
7.5 Additional remarks	Steady state forces and moments were measured on the wind tunnel model balance.
7.6 References on techniques	1

8 Data presentation

8.1 Test cases for which data could be made available	50 m/s for incidence from 0^o to 40^o
8.2 Test cases for which data are included in	50 m/s for incidence from 0^o to 28^o

	this document	
8.3	Steady pressures	Values for each case
8.4	Quasi-steady or steady perturbation pressures	No
8.5	Unsteady pressures	Spectra and RMS for each pressure tapping and unsteady pressure transducer at each incidence
8.6	Steady forces or moments	Figure 6
8.7	Quasi-steady or unsteady perturbation forces	No
8.8	Unsteady forces and moments	No
8.9	Other forms in which data could be made available	Surface oil visualisations, figures 7 and 8
8.10	Reference giving other representations of data	1

9 Comments on data

9.1	Accuracy	
	9.1.1 Mach number	± 0.1% of set speed
	9.1.2 Steady incidence	± 0.01 degrees
	9.1.3 Reduced frequency	N/A
	9.1.4 Steady pressure coefficients	N/A
	9.1.5 Steady pressure derivatives	N/A
	9.1.6 Unsteady pressure coefficients	± 1.0% - see 7.4.3
9.2	Sensitivity to small changes of parameter	N/A
9.3	Non-linearities	N/A
9.4	Influence of tunnel total pressure	Not examined
9.5	Effects on data of uncertainty, or variation, in mode of model motion	N/A
9.6	Wall interference corrections	Longitudinal change in freestream static pressure applied to measured pressures as an increment in local static pressure coefficient. Steady forces processed with model solid and separated wake blockage.
9.7	Other relevant tests on same model	None
9.8	Relevant tests on other models of nominally the same shapes	See ref 4
9.9	Any remarks relevant to comparison between experiment and theory	None
9.10	Additional remarks	None
9.11	References on discussion of data	1

10 Personal contact for further information

Dr J Gibb
DERA
Clapham
Bedford
Bedfordshire MK41 6AE
UK
Tel +44 1234 225849
Email: jgibb@dera.gov.uk

11 List of references

1 R Lynn, J Gibb, A Shires. 'Buffet tests on a 40 degree diamond wing – Model M2391', DERA/MSS4/TR98309/1.0, August 1998.

2 M H Hunter. 'A guide to the DERA 13ft x 9ft Low Speed Wind Tunnel facility', DERA/AS/HWA/TR97636/1.0, June 1998.

3 R J Lynn. 'Dynamic calibration of tube-transducer systems for unsteady pressure measurements', DERA/AS/HWA/TR980022/1.0, January 1998.

4 M Woods, N J Wood. 'Unsteady aerodynamic phenomenon on novel wing planforms', ICAS 96, Vol.2, 11.2, 1996.

Table 1. Pressure tapping nomenclature and absolute co-ordinates

tapping	(x/c)	(y/b)	tapping	(x/c)	(y/b)	tapping	(x/c)	(y/b)
S0101	0.010	0.087	S0303	0.054	0.230	S0417	0.474	0.301
S0102	0.036	0.087	S0304	0.074	0.230	S0418	0.531	0.301
S0103	0.053	0.087	S0305	0.092	0.230	S0419	0.588	0.301
S0104	0.074	0.087	S0306	0.120	0.230	S0420	0.647	0.301
S0105	0.097	0.087	S0307	0.146	0.230	S0421	0.707	0.301
S0106	0.121	0.087	S0308	0.179	0.230	S0422	0.768	0.301
S0107	0.149	0.087	S0309	0.221	0.230	S0423	0.832	0.301
S0108	0.184	0.087	S0310	0.248	0.230	S0424	0.896	0.301
S0109	0.251	0.087	S0311	0.297	0.230	S0501	0.010	0.373
S0110	0.347	0.087	S0312	0.341	0.230	S0502	0.037	0.373
S0111	0.429	0.087	S0313	0.381	0.230	S0503	0.060	0.373
S0112	0.531	0.087	S0314	0.426	0.230	S0504	0.080	0.373
S0113	0.647	0.087	S0315	0.476	0.230	S0505	0.099	0.373
S0114	0.768	0.087	S0316	0.531	0.230	S0506	0.123	0.373
S0115	0.896	0.087	S0317	0.588	0.230	S0507	0.152	0.373
S0201	0.010	0.159	S0318	0.647	0.230	S0508	0.184	0.373
S0202	0.033	0.159	S0319	0.768	0.230	S0509	0.223	0.373
S0203	0.053	0.159	S0320	0.896	0.230	S0510	0.254	0.373
S0204	0.069	0.159	S0401	0.010	0.301	S0511	0.306	0.373
S0205	0.090	0.159	S0402	0.036	0.301	S0512	0.338	0.373
S0206	0.123	0.159	S0403	0.055	0.301	S0513	0.369	0.373
S0207	0.151	0.159	S0404	0.082	0.301	S0514	0.425	0.372
S0208	0.180	0.159	S0405	0.100	0.301	S0515	0.479	0.373
S0209	0.218	0.159	S0406	0.116	0.301	S0516	0.531	0.373
S0210	0.288	0.159	S0407	0.132	0.301	S0517	0.588	0.373
S0211	0.335	0.159	S0408	0.154	0.301	S0518	0.647	0.373
S0212	0.378	0.159	S0409	0.184	0.301	S0519	0.707	0.373
S0213	0.432	0.159	S0410	0.213	0.301	S0520	0.768	0.373
S0214	0.531	0.159	S0411	0.249	0.301	S0521	0.832	0.373
S0215	0.647	0.159	S0412	0.278	0.301	S0522	0.896	0.373
S0216	0.768	0.159	S0413	0.304	0.301	S0601	0.010	0.444
S0217	0.896	0.159	S0414	0.339	0.301	S0602	0.036	0.444
S0302	0.036	0.230	S0416	0.432	0.301	S0604	0.085	0.444
S0301	0.010	0.230	S0415	0.389	0.301	S0603	0.059	0.444

Table 1 (continued) Pressure tapping nomenclature and absolute co-ordinates

tapping	(x/c)	(y/b)	tapping	(x/c)	(y/b)	tapping	(x/c)	(y/b)
S0605	0.102	0.444	S0718	0.769	0.515	S1007	0.437	0.729
S0606	0.125	0.444	S0719	0.832	0.515	S1008	0.532	0.729
S0607	0.148	0.444	S0720	0.897	0.515	S1009	0.647	0.729
S0608	0.190	0.444	S0801	0.010	0.587	S1010	0.769	0.729
S0609	0.223	0.444	S0802	0.040	0.587	S1011	0.897	0.729
S0610	0.259	0.444	S0803	0.060	0.587	S1101	0.035	0.800
S0611	0.302	0.444	S0804	0.094	0.587	S1102	0.086	0.800
S0612	0.338	0.444	S0805	0.134	0.587	S1103	0.125	0.800
S0613	0.386	0.444	S0806	0.183	0.587	S1104	0.208	0.800
S0614	0.438	0.444	S0807	0.260	0.586	S1105	0.243	0.800
S0615	0.482	0.444	S0808	0.350	0.587	S1106	0.342	0.800
S0616	0.531	0.444	S0809	0.439	0.587	S1107	0.418	0.800
S0617	0.588	0.444	S0810	0.531	0.587	S1108	0.532	0.800
S0618	0.647	0.444	S0811	0.647	0.587	S1109	0.648	0.800
S0619	0.707	0.444	S0812	0.707	0.587	S1110	0.769	0.800
S0620	0.769	0.444	S0813	0.769	0.587	S1111	0.897	0.800
S0621	0.832	0.444	S0814	0.832	0.587	S1201	0.075	0.872
S0622	0.896	0.444	S0815	0.896	0.587	S1202	0.126	0.872
S0701	0.012	0.515	S0901	0.017	0.658	S1203	0.186	0.872
S0702	0.036	0.515	S0902	0.064	0.658	S1204	0.270	0.872
S0703	0.053	0.515	S0903	0.124	0.658	S1205	0.327	0.872
S0704	0.076	0.515	S0904	0.194	0.658	S1206	0.434	0.872
S0705	0.102	0.515	S0905	0.245	0.658	S1207	0.533	0.872
S0706	0.119	0.515	S0906	0.341	0.658	S1208	0.649	0.872
Sf0707	0.185	0.515	S0907	0.427	0.658	S1209	0.769	0.872
S0708	0.252	0.515	S0908	0.532	0.658	S1210	0.897	0.872
S0709	0.293	0.515	S0909	0.647	0.658	S1301	0.182	0.943
S0710	0.333	0.515	S0910	0.769	0.658	S1302	0.280	0.943
S0711	0.385	0.515	S0911	0.897	0.658	S1303	0.377	0.943
S0712	0.429	0.515	S1001	0.037	0.729	S1304	0.533	0.943
S0713	0.479	0.515	S1002	0.075	0.729	S1305	0.649	0.943
S0714	0.531	0.515	S1003	0.124	0.729	S1306	0.771	0.943
S0715	0.588	0.515	S1004	0.184	0.729	S1307	0.896	0.943
S0716	0.647	0.515	S1005	0.278	0.729			
S0717	0.707	0.515	S1006	0.335	0.729			

Table 2. Sample of the pressure data contained on file CP04DEG.TXT (4° incidence case)

Tapping	Cp	Prms/q
S0101	-0.37640	0.023467
S0102	-0.28155	0.002484
S0103	-0.28481	0.002203
S0104	-0.28982	0.002091
S0105	-0.29281	0.002144
S0106	-0.30844	0.001996
S0107	-0.31755	0.002199
S0108	-0.34170	0.002024
S0109	-0.35270	0.002112
S0110	-0.35830	0.002114
S0111	-0.35752	0.002333
S0112	-0.34437	0.002141
S0113	-0.29906	0.002916
S0114	-0.23422	0.003456
S0115	-0.10474	0.003520
S0201	-0.87056	0.025597
S0202	-0.29125	0.015539
S0203	-0.28305	0.005993
S0204	-0.29880	0.003571
S0205	-0.31469	0.002751
S0206	-0.32718	0.002511
S0207	-0.33356	0.002437
S0208	-0.34307	0.002363
S0209	-0.35147	0.002418
S0210	-0.36885	0.002345
S0211	-0.36995	0.002143
S0212	-0.37711	0.002298
S0213	-0.37581	0.002357
S0214	-0.36195	0.002496
S0215	-0.32725	0.002135
S0216	-0.24705	0.002331
S0217	-0.11529	0.002394
S0301	-0.86001	0.035587
S0302	-0.31338	0.038050
S0303	-0.27934	0.010804
S0304	-0.30551	0.005938
S0305	-0.30668	0.004459
S0306	-0.32744	0.003329
S0307	-0.34131	0.002923
S0308	-0.35602	0.002720
S0309	-0.37132	0.002517
S0310	-0.38056	0.002213
S0311	-0.38981	0.002191
S0312	-0.38844	0.002713
S0313	-0.39196	0.002233
S0314	-0.39209	0.002373
S0315	-0.38707	0.002198
S0316	-0.37542	0.002247
S0317	-0.35342	0.002314
S0318	-0.33988	0.002098
S0319	-0.26144	0.002151
S0320	-0.12675	0.002499
S0401	-0.84810	0.024064
S0402	-0.52046	0.052762
S0403	-0.27022	0.020923
S0404	-0.30420	0.008472
S0405	-0.32133	0.005961
S0406	-0.34268	0.004220
S0407	-0.34020	0.003850
S0408	-0.35101	0.003413
S0409	-0.37041	0.002779
S0410	-0.33858	0.003149
S0411	-0.33584	0.002886
S0412	-0.40452	0.002208
S0413	-0.39287	0.002355
S0414	-0.40335	0.002127
S0415	-0.41344	0.002184
S0416	-0.40348	0.002403
S0417	-0.39411	0.002200
S0418	-0.39039	0.002308
S0419	-0.36670	0.002203
S0420	-0.35108	0.002062
S0421	-0.31729	0.002115
S0422	-0.26925	0.002267
S0423	-0.19946	0.002375
S0424	-0.13202	0.002312
S0501	-0.79374	0.022483
S0502	-0.65215	0.034271
S0503	-0.37757	0.027267
S0504	-0.33910	0.015499
S0505	-0.33597	0.010158
S0506	-0.30577	0.007574
S0507	-0.32575	0.005536
S0508	-0.34483	0.004293
S0509	-0.34079	0.003774
S0510	-0.37360	0.003189
S0511	-0.38493	0.003231
S0512	-0.38388	0.003716
S0513	-0.41891	0.002550
S0514	-0.41429	0.002530
S0515	-0.40901	0.002329
S0516	-0.39938	0.002348
S0517	-0.39163	0.002118
S0518	-0.35947	0.002062
S0519	-0.32881	0.002250
S0520	-0.26502	0.002143
S0521	-0.21222	0.002198
S0522	-0.13716	0.002596
S0601	-0.82069	0.022663
S0602	-0.82603	0.026817
S0603	-0.44775	0.043792
S0604	-0.31788	0.016914
S0605	-0.34014	0.010818
S0606	-0.35381	0.006754
S0607	-0.32627	0.005527
S0608	-0.35361	0.003715
S0609	-0.37021	0.003248
S0610	-0.38096	0.003305
S0611	-0.42262	0.002554
S0612	-0.44182	0.002436
S0613	-0.43876	0.002319
S0614	-0.42496	0.002434
S0615	-0.41383	0.002324
S0616	-0.40400	0.002642
S0617	-0.40244	0.002048
S0618	-0.37210	0.002047
S0619	-0.33949	0.002034
S0620	-0.27550	0.002081
S0621	-0.21808	0.002226
S0622	-0.14810	0.002331
S0701	-0.81464	0.021984
S0702	-0.83573	0.021538
S0703	-0.69668	0.042468
S0704	-0.42027	0.033537
S0705	-0.36605	0.014286
S0706	-0.37399	0.010536
S0707	-0.41031	0.005538
S0708	-0.44202	0.003965
S0709	-0.44358	0.003469
S0710	-0.44338	0.003180
S0711	-0.44286	0.002975
S0712	-0.44182	0.002819
S0713	-0.42678	0.002833
S0714	-0.42067	0.002856
S0715	-0.40387	0.002455
S0716	-0.36676	0.002642
S0717	-0.33643	0.002385
S0718	-0.28663	0.002120
S0719	-0.22732	0.002231
S0720	-0.15643	0.002586
S0801	-0.88729	0.020439
S0802	-0.77675	0.020439
S0803	-0.60834	0.029906
S0804	-0.43388	0.021484
S0805	-0.42281	0.010071
S0806	-0.43863	0.006713
S0807	-0.45491	0.005028
S0808	-0.46396	0.003342
S0809	-0.46194	0.002734
S0810	-0.44000	0.002853
S0811	-0.38024	0.002541
S0812	-0.33871	0.002427
S0813	-0.29366	0.002509
S0814	-0.23383	0.002483
S0815	-0.16535	0.003741
S0901	-0.94601	0.021361
S0902	-0.68757	0.044259
S0903	-0.41819	0.016281
S0904	-0.45621	0.008037
S0905	-0.47769	0.005517
S0906	-0.48433	0.003565
S0907	-0.46148	0.003261
S0908	-0.44827	0.002641
S0909	-0.39951	0.002472
S0910	-0.30713	0.002349
S0911	-0.17726	0.002768
S1001	-1.07328	0.028864
S1002	-0.65176	0.051230
S1003	-0.46337	0.017044
S1004	-0.48199	0.010793
S1005	-0.48720	0.006489
S1006	-0.49755	0.005017
S1007	-0.47867	0.003765
S1008	-0.45120	0.003446
S1009	-0.40224	0.002763
S1010	-0.31820	0.002555
S1011	-0.19386	0.002865
S1101	-1.05257	0.031377
S1102	-0.80579	0.048765
S1103	-0.55145	0.029608
S1104	-0.50360	0.011432
S1105	-0.51258	0.009152
S1106	-0.51545	0.005814
S1107	-0.50965	0.004757
S1108	-0.46955	0.003723
S1109	-0.42945	0.003250
S1110	-0.34248	0.002939
S1111	-0.21313	0.004897
S1201	-0.85734	0.022554
S1202	-0.77239	0.022466
S1203	-0.68711	0.025096
S1204	-0.56772	0.014972
S1205	-0.53888	0.011371
S1206	-0.51278	0.007208
S1207	-0.49455	0.005736
S1208	-0.44325	0.004686
S1209	-0.36852	0.004213
S1210	-0.25675	0.004392
S1301	-0.82037	0.030708
S1302	-0.61694	0.012421
S1303	-0.56961	0.007469
S1304	-0.49149	0.005062
S1305	-0.45784	0.004208
S1306	-0.44579	0.003354
S1307	-0.37757	0.003019

Table 3. Sample data from spectrum file SP24DEG.TXT

Test at incidence 24° sample values shown for the first 5 transducers and first 8 frequencies

Freq. (Hz)	S0101	S0102	S0103	S0104	S0105
1.46500E+00	4.07630E-05	4.27847E-05	5.71330E-05	3.45853E-05	3.15013E-05
2.93000E+00	4.53870E-05	4.73784E-05	6.22269E-05	5.23849E-05	3.04545E-05
4.39500E+00	4.39129E-05	3.14200E-05	4.84005E-05	4.90865E-05	2.49529E-05
5.85900E+00	4.29258E-05	2.27708E-05	3.53050E-05	2.95438E-05	2.44439E-05
7.32400E+00	2.92946E-05	2.14469E-05	2.46458E-05	2.15162E-05	1.49071E-05
8.78900E+00	1.93204E-05	2.00130E-05	1.81076E-05	1.34836E-05	9.41825E-06
1.02540E+01	1.62893E-05	1.18886E-05	1.53177E-05	1.08384E-05	8.76493E-06
1.17190E+01	1.74268E-05	1.52507E-05	1.57682E-05	9.42644E-06	7.28511E-06

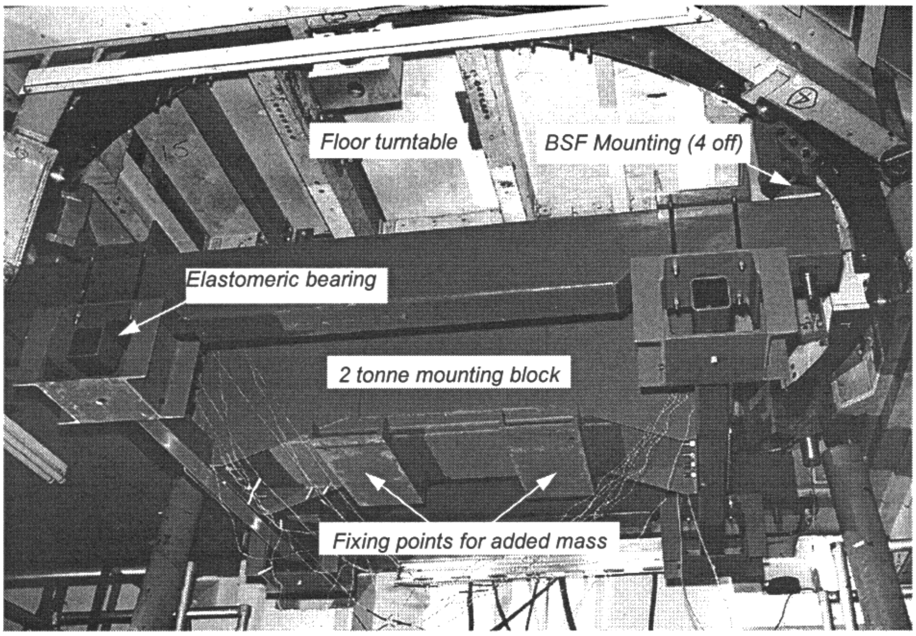

Figure 1

Buffet Support Fixture (BSF) mounted beneath the 13ft x 9ft Low Speed tunnel turntable

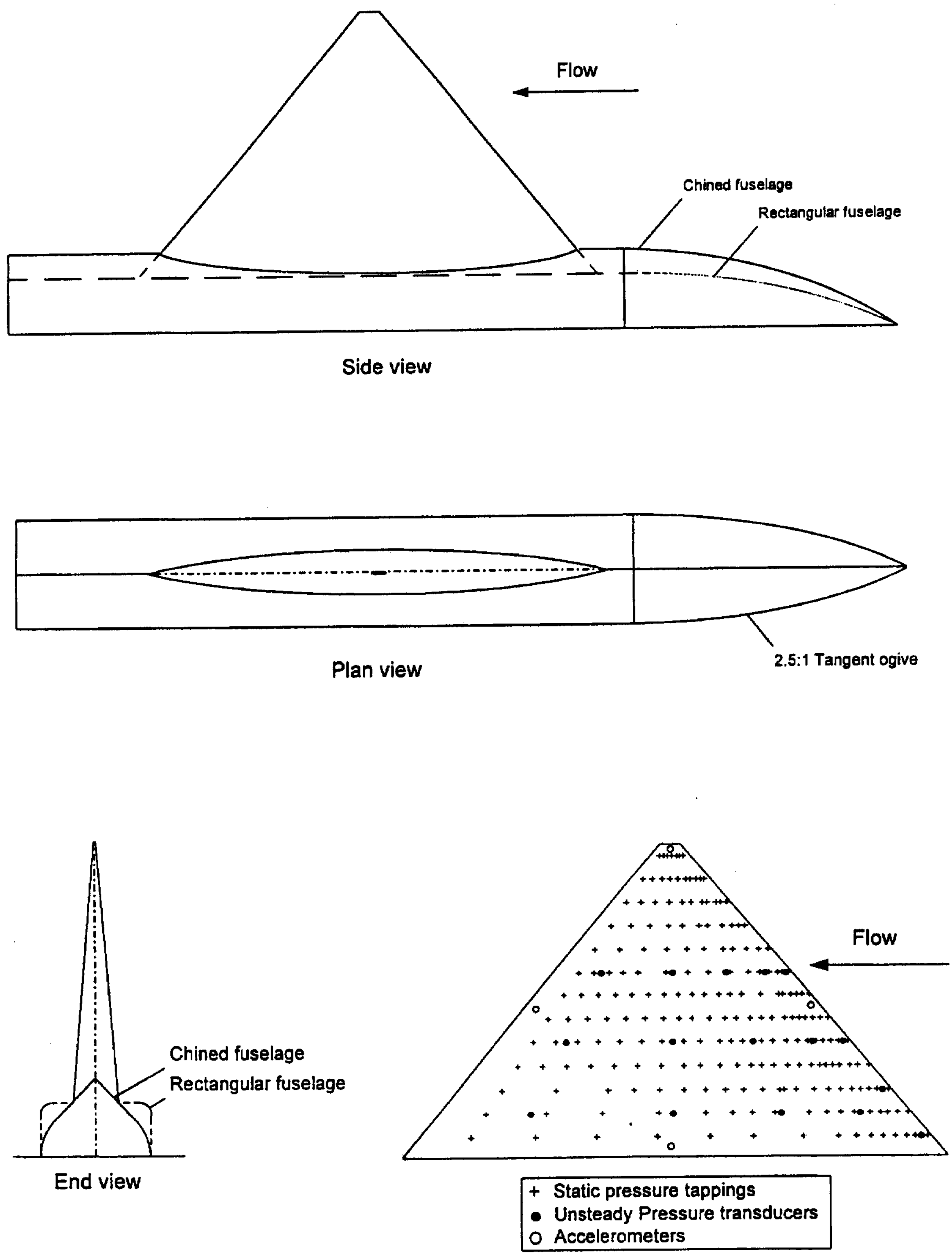

Figure 2

General arrangement of diamond wing half-model - M2391.

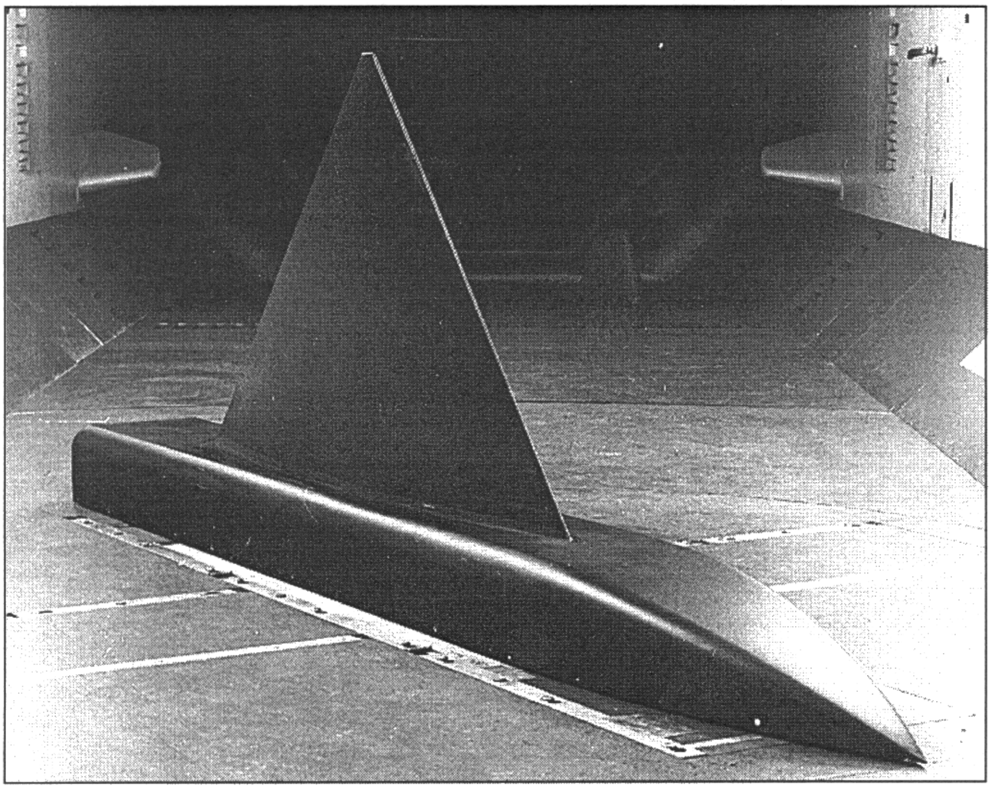

Figure 3

M2391 with chined fuselage installed in the DERA 13ft x 9ft low speed wind tunnel

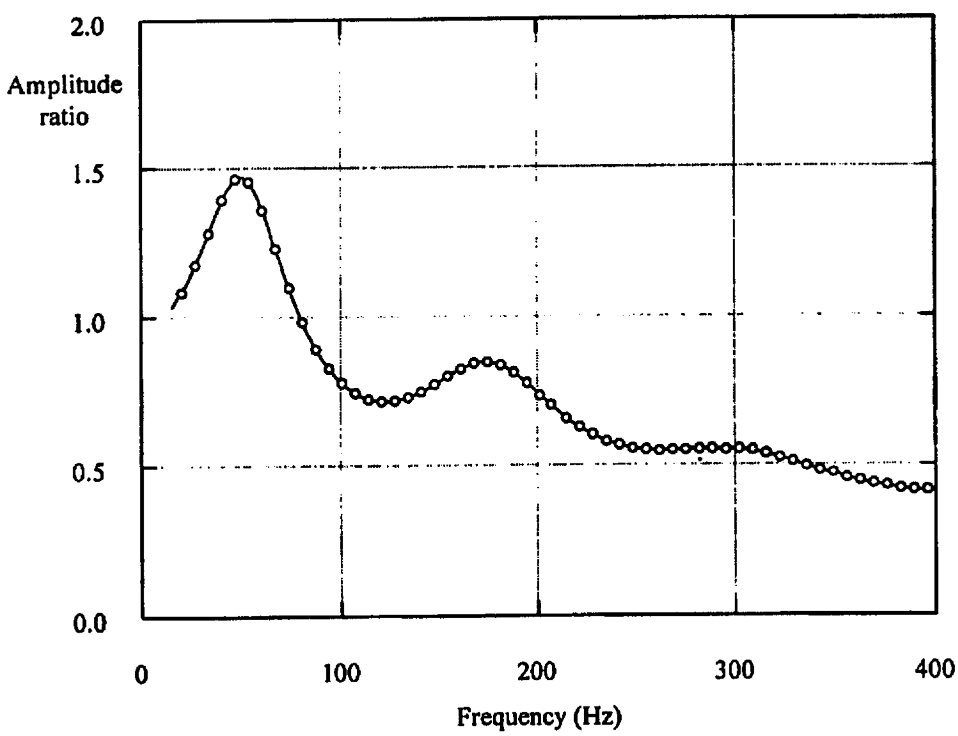

Figure 4

Typical frequency response function of M2391 tube transducer installation

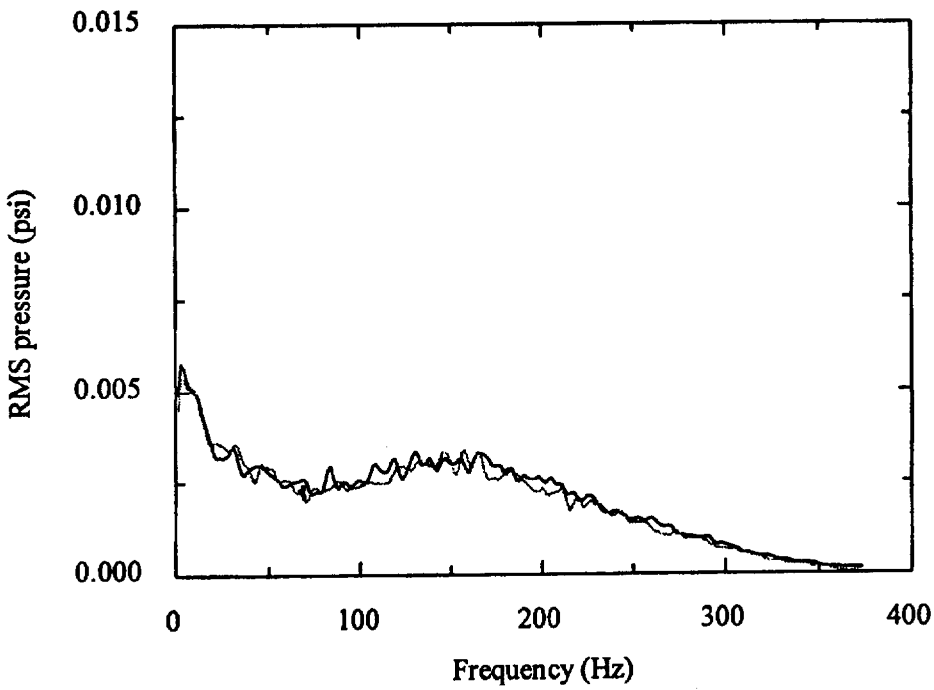

(a) Excitation at leading edge (α = 4°)

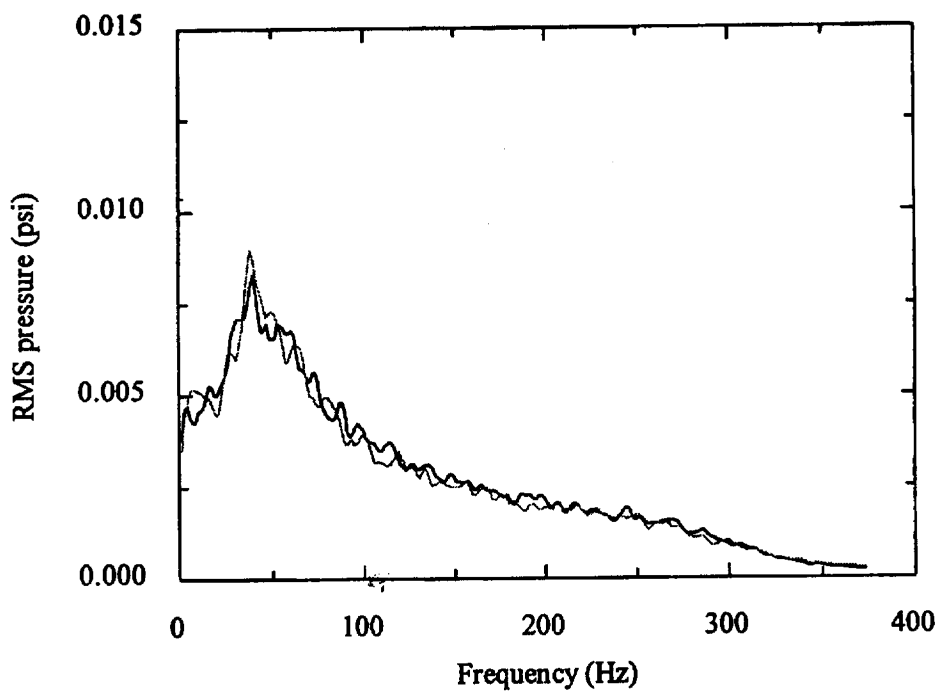

(b) Excitation near primary attachment (α = 6°)

Figure 5

Accuracy of spectral correction technique at two measurement stations

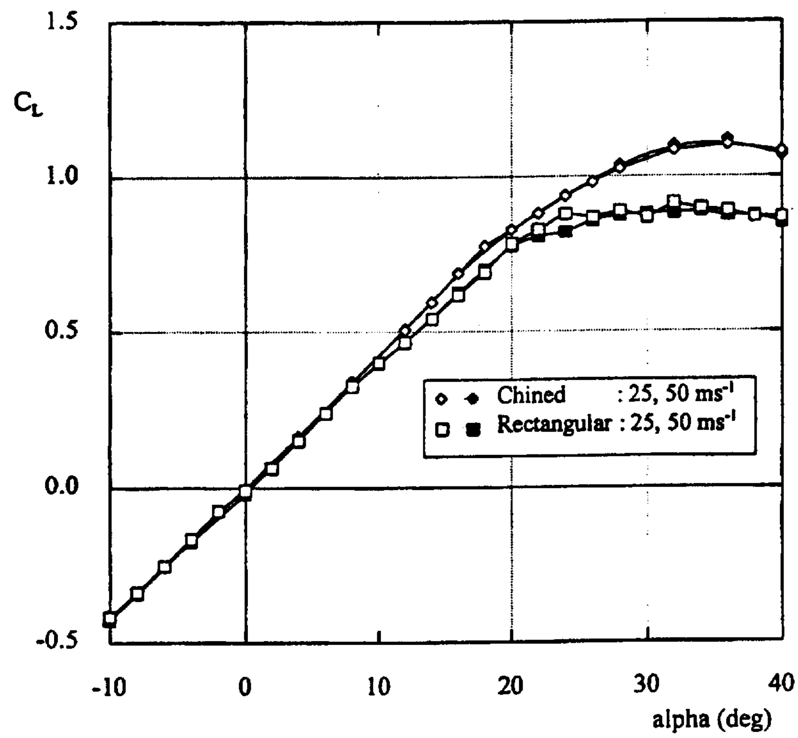

a) Variation of lift coefficient with incidence

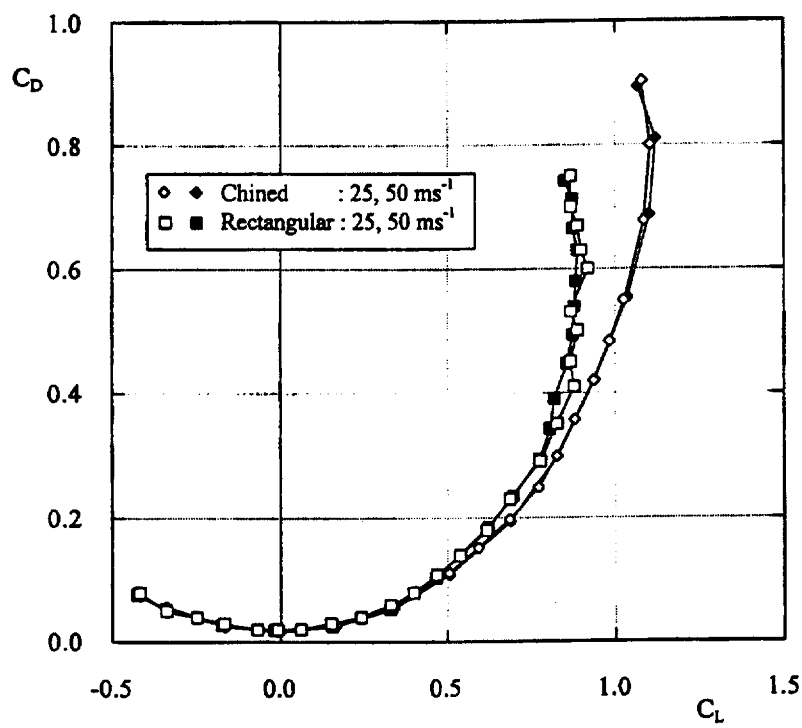

b) C_D vs C_L polar

***Figure* 6**

Model M2391 steady state force and moment results from half model balance

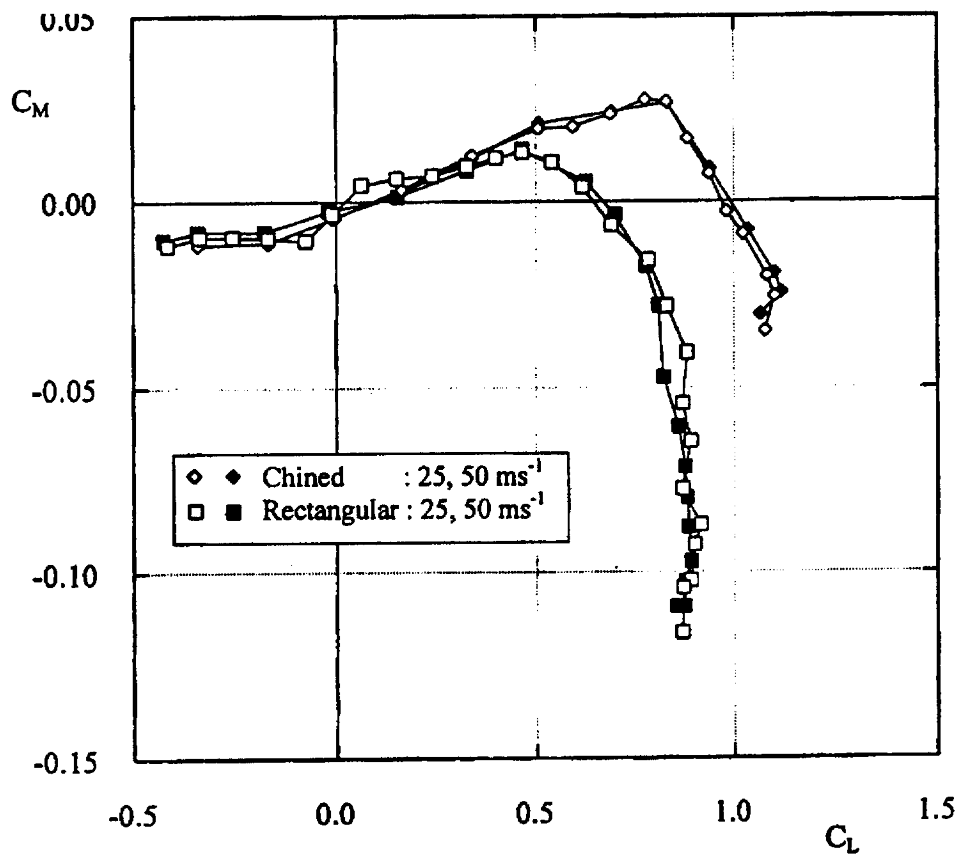

c) C_M vs C_L polar

***Figure** 6 (continued)*

Model M2391 steady state force and moment results from half model balance.

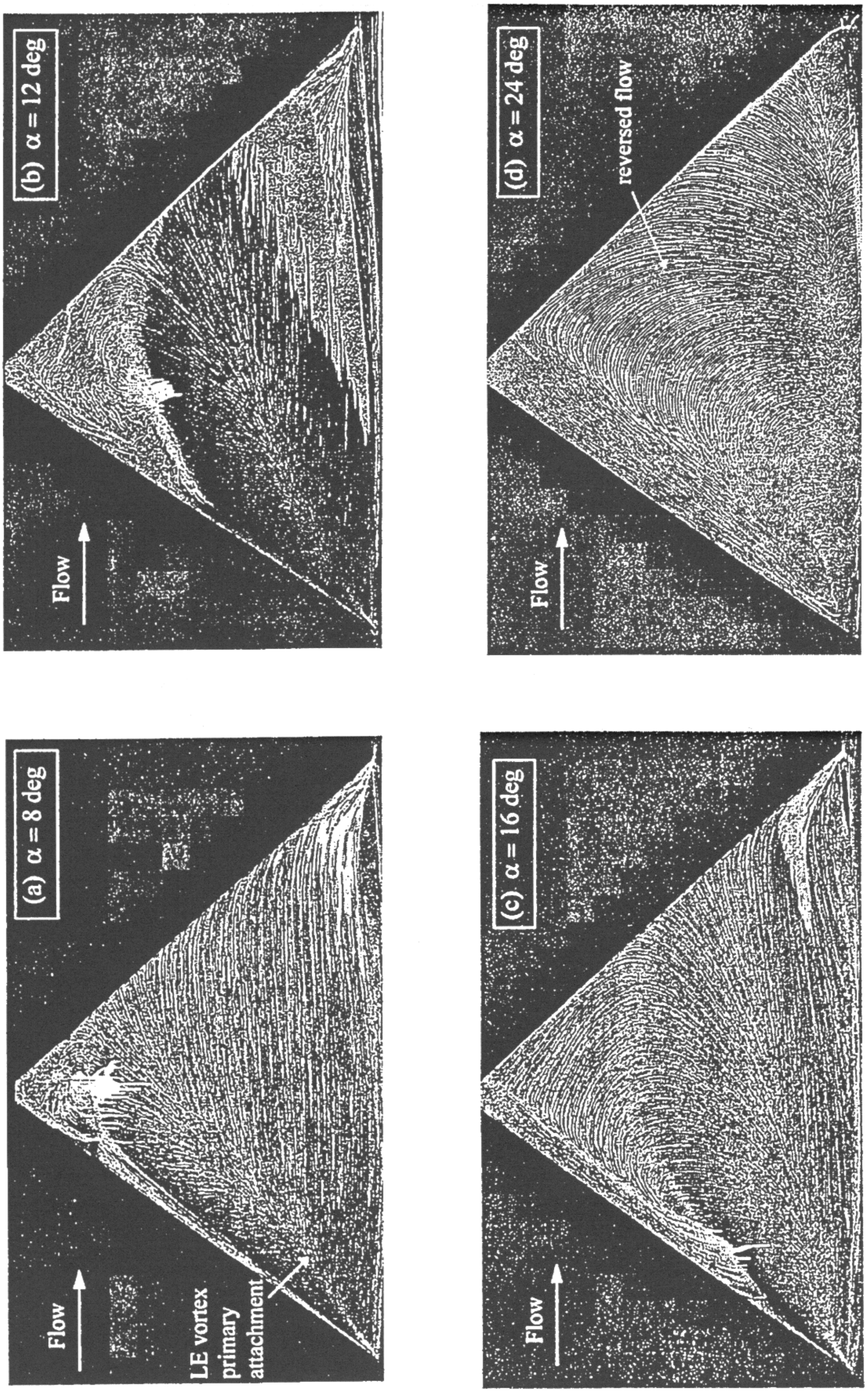

Figure 7

M2391 surface oil flow visualisation - rectangular fuselage configuration, $V = 50ms^{-1}$.

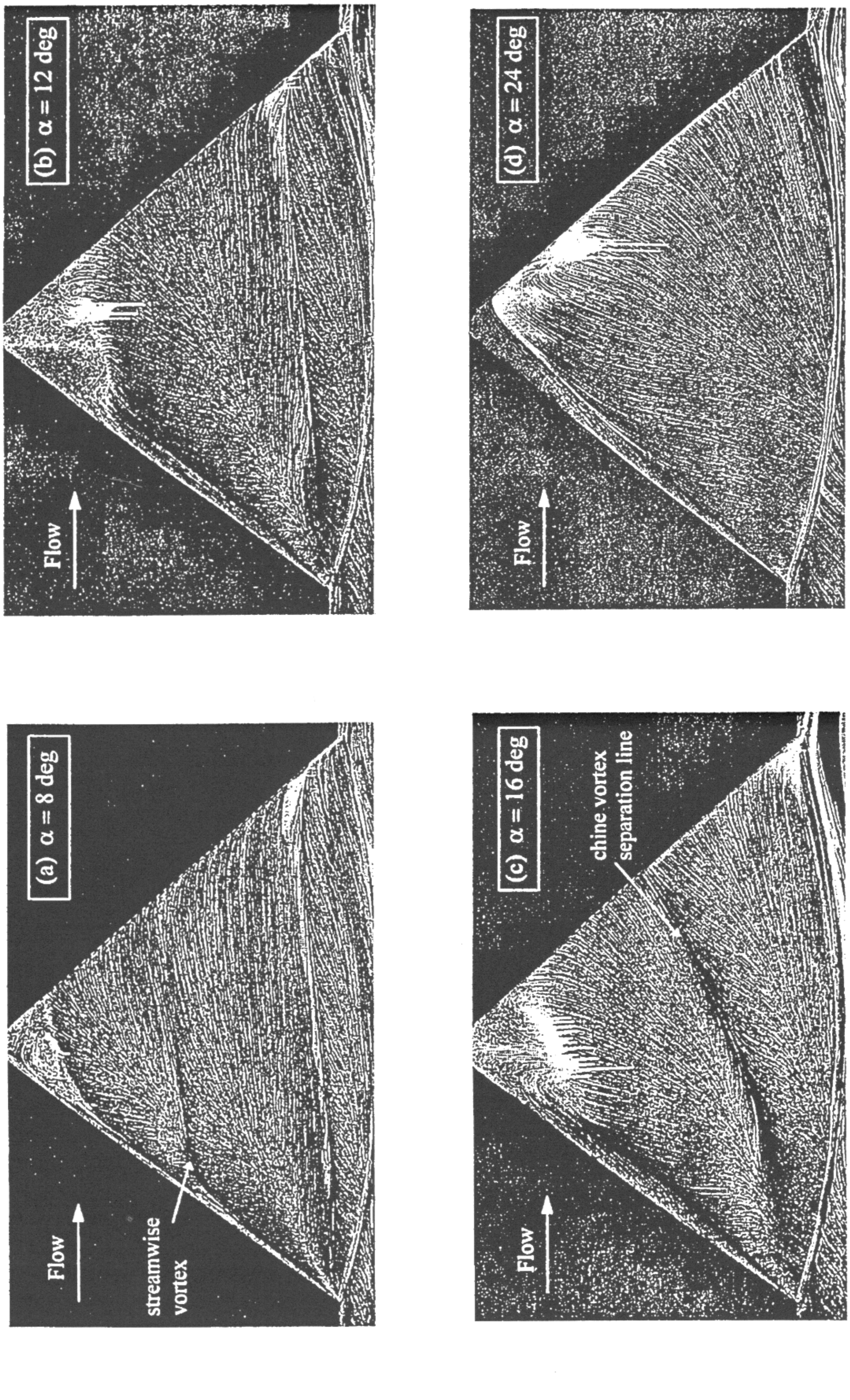

Figure 8

M2391 surface oil flow visualisation - chined fuselage configuration, $V=50\ ms^{-1}$.

15E. WING AND FIN BUFFET ON THE STANDARD DYNAMICS MODEL

Reported by X. Z. Huang
of work by S. Zan et al.
IAR/NRC, Canada

INTRODUCTION

For modern aircraft with higher sweep angles flying at higher incidence, unsteady and burst vortex flow in the vicinity of the wing and downstream lifting surface lead to strong unsteady airloads and buffeting[1]. Thus, investigations were conducted in the Institute for Aerospace Research (IAR) Low Speed Wind Tunnel (LSWT)[2] to study the buffet characteristics of the Standard Dynamics Model (SDM)[3], a generic fighter aircraft configuration.

Since the spectrum of the aerodynamic input load is reasonably flat over the frequency range of interest, the solution to the equation of the motion is easily solved in the frequency domain for a given aerodynamic loads and vice versa. Following Jones[4] and Mabey[5], it is suggested that $\sqrt{nG(n)}$ is the best parameter to use as a measure of buffet excitation due to flow separations and unsteadiness and to denote this as the buffet excitation parameter.

Buffeting is presented for three modes – the fin bending mode (VFB) and the wing symmetric and anti-symmetric bending modes (WSB and WAB)[6]. The strain gauges were mounted approximately on the node line of the torsional mode. It should be emphasized that since the model is rigid and the deformation of the structure and its damping are negligible, this measurement is linearly related to the buffet excitation. In addition, experimental results of static coefficients at angles of attack ranging from 0° to 90° are also included[7] for the understanding of the flow behavior during the experiments.

The geometry of SDM is shown in Fig. 1. There are two SDM models with ratio of 0.375 (SDM-L and SDM-S) used for buffet/dynamic stability and static experiments respectively.

The SDM model was sting-mounted in the wind tunnel[8], which in turn was protruded from a strut cantilevered in the wind tunnel floor as shown in Fig. 2 and Fig. 3. The pitch angle is obtained by turning the strut through the center of the turntable. Sideslip angle setting is effected by banking the model about the body axis.

The flow visualization results show that at $\beta = 0°$, separation becomes evident on the wing at $\alpha \approx 4°$ in the case of strakes removed and $\alpha \approx 15°$ in the case of strakes installed. At $\alpha \approx 20°$, the vortex burst reaches the wing trailing edge while it breaks down completely over the wing at $\alpha \approx 29°$. The onset of asymmetrical forebody vortices appears at $\alpha \approx 40°$.

The test matrix for the buffet characteristics is presented in Table 1. The experimental results of static coefficients and buffet characteristics at different conditions are listed in Table 2 and Table 3 in the CD-ROM and illustrated from Fig. 4 to Fig. 6 and Fig. 10 to Fig. 14 respectively. The reference center for the moment is at 35% of MAC. The results with a dummy strut which was installed on the tunnel ceiling to investigate the asymmetrical effect of the strut are shown in Fig. 10 (cont.). In addition, Fig. 7 to Fig. 9 shows the shapes of different modes for the purpose of locating the strain gauges.

In general, the level of fin buffeting exceeds that of wing buffeting by an order of magnitude. In connecting with static measurements and flow visualizations this severe fin buffeting arises from the fact that the fin is immersed in the wake of the burst of strake and/or forebody vortices. The peak of fin buffet excitation is near an angle of attack corresponding to the onset of asymmetrical forebody flow. The magnitude of the wing buffet excitation parameter did not exceed 0.003, which arose from the interaction of the strake and wing vortices or simply from separated flow unsteadiness over the wing.

LIST OF SYMBOLS AND DEFINITIONS

B	wingspan (m)
$\bar{c}$	wing mean aerodynamic chord (MAC, m)
C_ℓ	rolling moment coefficient ($=\ell$/qsB)
C_m	pitching moment ($=m/qs\bar{c}$)
C_n	yawing moment (=n/qsB)
C_Y	side force coefficient (=Y/qs)
C_Z	normal force coefficient (=Z/qs)

d	body diameter at base (m)
d_r	ratio of diameters ($=d_s/d$)
d_s	sting diameter (m)
f	frequency (Hz)
f_0	modal frequency (Hz)
ℓ, m, n	rolling, pitching and yawing moment around body axes system
m	mode generalized mass
n	reduced frequency parameter ($=f\bar{c}/U_\infty$)
$\sqrt{nF(n)}$	unsteady pressure fluctuations
$\sqrt{nG(n)}$	buffet excitation parameter due to flow separations and flow unsteadiness
q	free stream dynamic pressure (N/m^2)
F(n)	non-dimensional power spectral density of unsteady pressure fluctuations
G(n)	non-dimensional power spectral density of excitation
Re_D	Reynolds number based on ogive base diameter
SDM	Standard Dynamics Model
s	wing area (m^2)
Stks	strakes
U_∞	free-stream velocity (m/sec)
VFB	vertical fin bending mode (376 Hz)
WAB	wing anti-symmetric bending mode (319 Hz)
WSB	wing symmetric bending mode (276 Hz)
X,Y,Z	axial, side and normal force around body axes system
α	angle of attack (deg)
β	angle of sideslip (deg)
θ	amplitude (deg)
σ	aerodynamic pitch angle (deg)
ϕ	roll angle (deg)
ω	circular frequency (rad/sec)

FORMULARY

1 General Description of model

1.1	Designation	Standard Dynamics Model (SDM)
1.2	Type	Full model
1.3	Derivation	F-16
1.4	Additional remarks	Interchangeable strakes (LEX)
1.5	References	Ref. 3

2 Model Geometry

2.1	Wing	
2.1.1	Planform	Cropped delta wing

2.1.2	Aspect ratio	3.0
2.1.3	Dihedral angle	0°
2.1.4	Leading edge sweep	40°
2.1.5	Trailing edge sweep	0°
2.1.6	Taper ratio	0.227
2.1.7	Twist	0°
2.1.8	Wing centerline chord	0.3310 m (SDM-L)
2.1.9	Wing tip chord	0.0752 m (SDM-L)
2.1.10	Wing span	0.6096 m (SDM-L)
2.1.11	Mean aerodynamic chord	0.2299 m (SDM-L)
2.1.12	Area of planform	0.1238 m^2 (SDM-L)
2.1.13	Form of wing-body junction	With an interchangeable strakes (LEX)
2.1.14	Location of reference sections and definition of profiles	Double wedged with 4.5% at the root chord
2.1.15	Lofting procedure between reference sections	Linear taper
2.1.16	Lead-edge bevel	15° on both sides
2.1.17	Trailing edge bevel	15° on both sides
2.1.18	LEX angle	Double sweep back angles (73° and 83°)
2.1.19	Form of wing tip	Free stream aligned
2.2	Fuselage	
2.2.1	Length	0.9429 m (SDM-L)
2.2.2	Diameter at base	0.1347 m (SDM-L)
2.2.3	Fineness ratio	7
2.2.4	Nose	Tangent ogive
2.2.5	Fineness ratio of nose	3
2.2.6	Semi-apex angle of nose	18.92°
2.3	Horizontal stabilizer	
2.3.1	Planform	Cropped delta wing
2.3.2	Aspect ratio	1.88
2.3.3	Taper ratio	0.2126
2.3.4	Dihedral angle	-10°
2.3.5	Leading edge sweep	40°
2.3.6	Trailing edge sweep	0°
2.3.7	Lead-edge bevel	14°
2.3.8	Trailing edge bevel	15°
2.3.9	Twist	0°
2.3.10	Full span	0.3548 m (SDM-L)
2.3.11	Area of planform	0.06697 m^2 (SDM-L)
2.3.10	Centre line chord	0.1919 m (SDM-L)
2.3.12	Tip chord	0.0408 m (SDM-L)
2.3.13	Location of reference sections and definition of profiles	Double wedged with 6.3% at the root chord
2.3.14	Lofting procedure between reference sections	Linear taper

2.3.15	Form of stabilizer -body junction	Fillet
2.3.16	Form of tip	Free stream aligned
2.4	Vertical stabilizer	
2.4.1	Planform	Trapezoid
2.4.2	Taper ratio	0.53
2.4.3	Leading edge sweep	47.5°
2.4.4	Trailing edge sweep	61.8°
2.4.5	Twist	0°
2.4.6	Height	0.1472 m (SDM-L)
2.4.7	Area of planform	0.01840 m^2 (SDM-L)
2.4.8	Form of stabilizer -body junction	Fillet
2.4.9	Form of tip	Free stream aligned
2.5	Ventral fin	
2.1	Platform	Cropped trapezoid with LEX
2.2	Area of platform	0.003406 m^2 (SDM-L)
2.3	Height	0.0481 m (SDM-L)
2.4	Leading-edge sweep	30°
2.5	Trailing edge sweep	0°
2.6	Reference	Detail drawings (Ref. 3) can be provided on the request

3 Wind Tunnel

3.1	Designation	IAR 6ft x 9ft low speed wind tunnel
3.2	Type of tunnel	Continuous atmospheric with closed return circuit
3.3	Test section dimensions	Height: 6 ft, width: 9ft, length: 15 ft
3.4	Type of roof	Solid with large optical quality plexiglass
3.5	Type of floor	Solid with turn table
3.6	Type of side walls	Solid with large optical quality plexiglass windows
3.7	Maximum speed	390 ft/sec
3.8	Contraction ratio	9
3.9	Support	Sting attached to wind tunnel strut (see Fig. 2 and Fig. 3)
3.10	Turbulence in empty tunnel	≤ 0.12% at free stream speed of 100 ft/sec
3.11	Acoustic noise in working section ($\sqrt{nF(n)}$)	≤0.0028
3.12	Mean flow angularity	±0.1°
3.13	Wind tunnel acoustic resonance	The resonance of 416 and 475 Hz were eliminated before the buffet experiments
3.14	Velocity variation	±0.25% at free-stream speed of 27.4 m/s
3.15	Variation in total ad static pressure	±0.5% at free-stream speed of 27.4 m/s
3.16	References on tunnel	Ref. 2

4 Model motion (SDM-L)

4.1	General description	High natural frequency model mounted on the support with a large mass/low stiffness support
4.2	Model properties for three relevant modes	
4.2.1	Generalised mass (grams)	WSB=124, WAB=152, VFB=20.4
4.2.2	Characteristic area (m^2)	WSB=0.083, WAB=0.083, VFB=0.01459

4.2.3	First bending frequency (Hz)	WSB=276, WAB=319, VFB=377
4.3	Mode shapes	
4.3.1	Single wing	See Fig. 7
4.3.2	Vertical fin	See Fig. 8
4.3.3	Complete model modes	See Fig. 9

5 Test Conditions

5.1	Model planform area/tunnel area	0.0357 (SDM-L)
5.2	Model span/tunnel height	0.333 (SDM-L)
5.3	Blockage	Function of angle of attack
5.4	Position of model in tunnel	Standard side position
5.5	Range of velocities	25 m/s to 110 m/s for obtain different non-dimensional frequency.
5.6	Range of tunnel static pressure	Close to atmospheric pressure
5.7	Range of tunnel total temperature	Room temperature
5.8	Range of model steady or mean incidence	0° to 54°
5.9	Definition of model incidence	Angle between free-stream velocity vector and body axis in model's symmetric planform plane.
5.10	Position of transition, if free	N/A
5.11	Position and type of trip, if transition fixed	Two devices were used on the forebody: 1) A thin circumferential ring of adhesive tape fixed around the nose approximately 1.5 cm from the apex. 2) Two strips of #80 grit with 1.5 mm wide located on the windward side of the forebody at $\phi=\pm40°$ extended from apex to within 2 cm of the intake
5.12	Flow instabilities during tests	±0.3 m/s
5.13	Model deformations	Negligible
5.14	References describing tests	Ref. 6, 7, 8

6 Measurements and Observations

6.1	Steady pressures for the mean conditions	Yes
6.2	Quasi-steady pressures	-
6.3	Unsteady pressures	-
6.4	Steady aerodynamic loads	Yes
6.5	Dynamic derivatives	Available but not included
6.6	Power spectral density of excitation	Yes
6.7	Buffet excitation parameter	Yes
6.8	Oscillation frequency	Yes
6.9	Single wing mode shapes	Yes (fundamental bending, torsion and overtone bending modes)
6.10	Fin mode shapes	Yes (bending and torsion modes)
6.11	Complete model modes	Yes (WSB, WAB and VFB modes)
6.12	Visualisation of surface flow	Yes but not included
6.13	Comparisons between free and fixed transition	Yes
6.14	Comparisons between strakes on and off	Yes

7 Instrumentation

7.1	Steady loads (SDM-S)	
7.1.1	Type of transducers	Strain gauges.
7.1.2	Type of measuring system	Six components balance (TASK balance)
7.1.3	Range of measuring system	Forward normal force Z_1=445 N

		Aft normal force Z_2=445 N
		Forward side force Y_1=133 N
		Aft side force Y_2=133 N
		Rolling moment L=5.65 N-m
		Axial force X=133N
7.1.4	Method of calibration	Static calibration was performed on in situ in the wind tunnel
7.1.5	Principle and accuracy of calibration including interaction and temperature effect	≤1% of full-load output
7.2	Buffet excitation measurement	
7.2.1	Range of angle of attack	0° to 54°
7.2.2	Type of analysis	Measuring buffet excitation parameter, $\sqrt{nG(n)}$ obtained from the output of strain gauge bridges
7.2.3	Method of measurements	Strain gauges mounted approximately on the node line of the torsional mode (about 74% root chord of the wing and 37% root chord of the vertical tail).
7.2.4	Method of acquiring and processing measurement about wing buffet	Four gauges near the leading-edge were used to detect the symmetric bending mode and another four gauges aft were used to detect the anti-symmetric bending mode.
7.2.5	Method of acquiring and processing measurement about fin buffet	Four gauges near the leading-edge to detect the fin bending mode.
7.2.6	Sample rates	5500 Hz for the data channel of WSB mode and 7000 Hz for the channels of WAB and VFB modes
7.2.7	Windowing techniques	A Hanning window was used
7.2.8	Frequency range over which analysis is valid	WSB mode: 0.58<n<1.28; WAB mode: 0.66<n<1.47; VFB mode 0.96<n<1.73
7.2.9	A/D conversion details	12 bit A/D, 32k samples per condition, Anti-aliasing filters were used with a cut-off frequency of 2500 Hz for the WSB channel and 3500 Hz for the WAB and VFB channels
7.3	References on techniques	See Ref. 6, 7

8 Data presentation

8.1	Test cases for which data could be made available	See Table 1
8.2	Test cases for which data are included in this document	See Table 1
8.3	Steady forces or moments	See Fig. 4 to Fig. 6 and Table 2 in CD ROM
8.4	Quasi-steady or unsteady perturbation forces	N/A
8.5	Buffet excitation	See Fig. 10 to Fig. 14 and Table 3 in CD ROM
8.6	Other forms in which data could be made available	N/A

9 Comments on data

9.1	Accuracy	-
9.1.1	Mach number	±0.1% of set speed
9.1.2	Steady incidence	±0.01°
9.1.3	Reduced frequency	-
9.1.4	Steady aerodynamic loads coefficients	≤1% of full-load output
9.2	Influence of tunnel total pressure	Not examined
9.3	Effects on data of uncertainty, or	-

	variation, in mode of model motion	
9.4	Wall interference corrections	Following standard procedures the dynamic pressure was corrected for solid blockage and corrections were applied to the angle of attack to account for upwash caused by the tunnel walls
9.5	Wake blockage corrections	The correction to dynamic pressure due to wake blockage is ≤1% and was not corrected for
9.6	Other relevant tests on same model	Dummy strut tests was conducted and found the support interference effects were small
9.7	Relevant tests on other models of nominally the same shapes	-
9.8	Any remarks relevant to comparison between experiment and theory	-
9.9	References on discussion of data	Ref. 6, 7

10 Personal contact for further information

Xing Zhong Huang, Aerodynamics Laboratory, Institute for Aerospace Research, National Research Council of Canada
Building M-10, 1500 Montreal Rd. Ottawa, Ontario, Canada. K1A 0R6
e-mail xingzhong.huang@nrc.ca

11 List of references

1. Edwards, J.W., "Unsteady Airloads Due to Separated Flow on Airfoils and Wings," AGARD-CP-483.
2. Brown, T.R., "Description of the 6 ft x 9 ft Low Speed Wind Tunnel," NRC, NAE LTR-LA-285, Nov. 1986.
3 Huang, X.Z., "Standard Dynamics Model," T87-277-U, 1987.
4 Jones, J.G. "A Survey of the dynamic Analysis of Buffering and Related Phenomena," RAE TR 72197, 1973.
5 Mabey, D.G., "Some Aspect of Aircraft Dynamic Loads Due to Flow Separation," AGARD-R-750
6. Zan, S.J., "Measurements of Wing and Fin Buffeting on the Standard Dynamics Model," NRC No. 32158, IAR-AN-76, 1993.
7. Huang, X.Z. and Beyers, M.E., "Subsonic Aerodynamic Coefficients of the SDM at Angles of Attack up to 90°," NAE LTR-UA-93, 1990.
8. Hansen, K., "Installation of Models in the 6 ft x 9 ft Low Speed Wind Tunnel," NAE LTR-LA-286, Aug. 1986.

Table 1 Test matrix of wing and fin buffet experiments (SDM-L)

U_∞	α°	β°	Strakes	Transition	Dummy strut	Data (Run number) in CD-ROM
50,70,90	0≤39	0	On	No	No	104,105,106
110	0≤25	0	On	No	No	107
70	0≤39	±5,±10	On	No	No	108,109,110,111
50,70,90	0≤39	0	On	fixed	No	113,114,115
50,70	20,29	0	On	fixed	Yes	116,117
70	20	0, ±5	On	No	Yes	118
50	20,29	0	On	No	Yes	119
110	11≤14	0	On	fixed	No	122
50,70,90,	0≤39	0,±5,±10	Off	No	No	156,157,158,161,162,163,164
50,70,90	0≤39	0	Off	fixed	No	166,167,168
50,70	20,29	0	Off	fixed	Yes	169,170
50	20	0, ±5	Off	No	Yes	171
70	20,29	0	Off	No	Yes	172
70	24,30,36	-10≤10	Off	No	No	173,174,175
60,70	35≤53	0,5,10	On	No	No	200,201,202
70	42	-10≤10	On	No	No	203
70	35≤53	0	On	fixed	No	204
70	35≤53	0	Off	fixed	No	205
70	35≤53	0,5,10	Off	No	No	206,207,208
70	42	-10≤10	Off	No	No	209

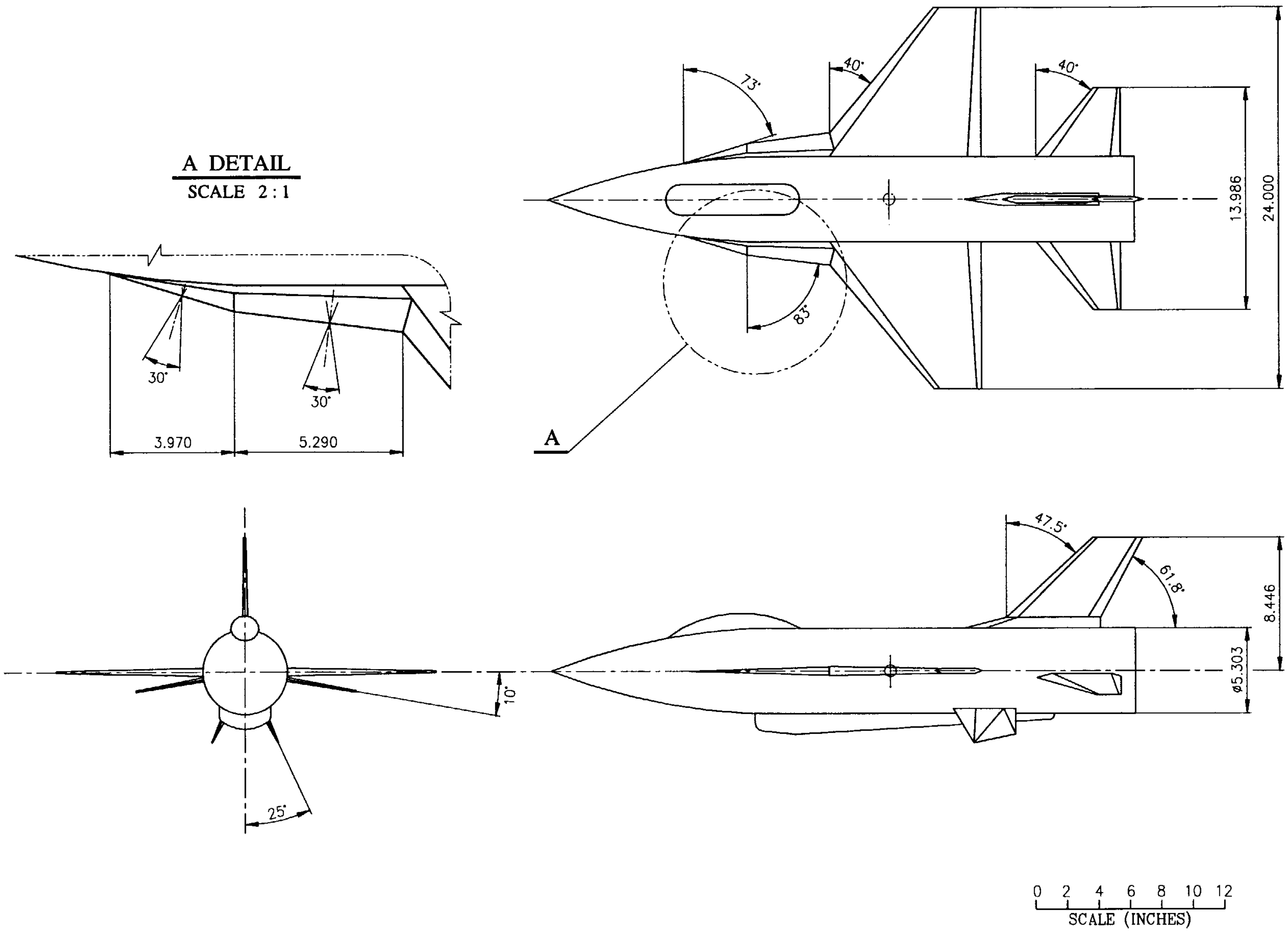

Fig. 1 Standard Dynamics Model

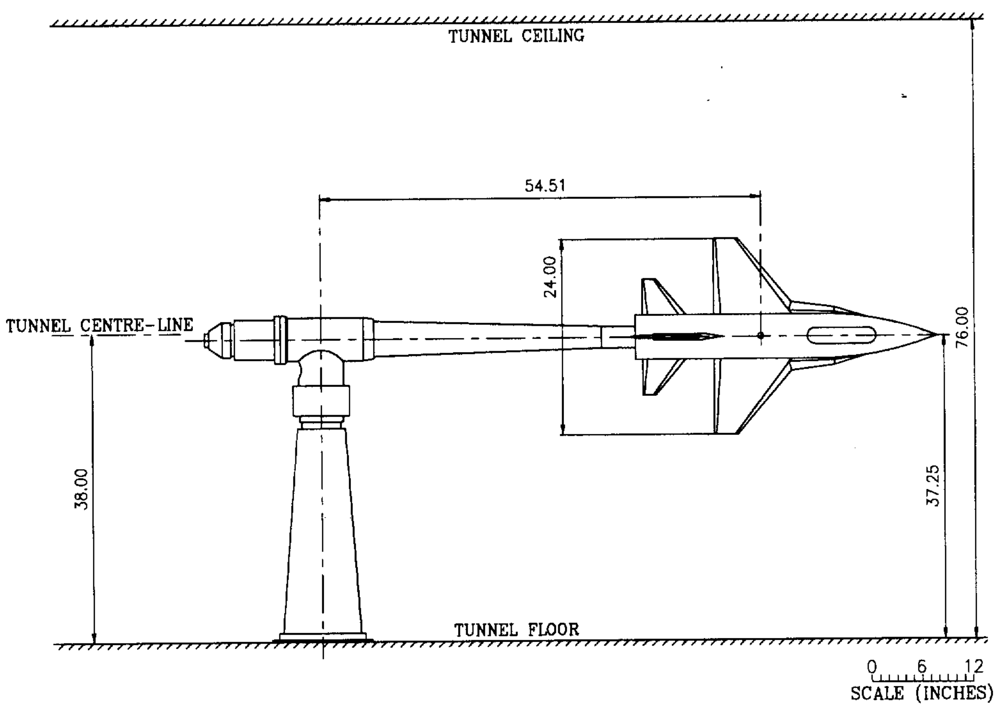

Fig 2 Side view of SDM-L model in the IAR 6 x 9 foot wind tunnel

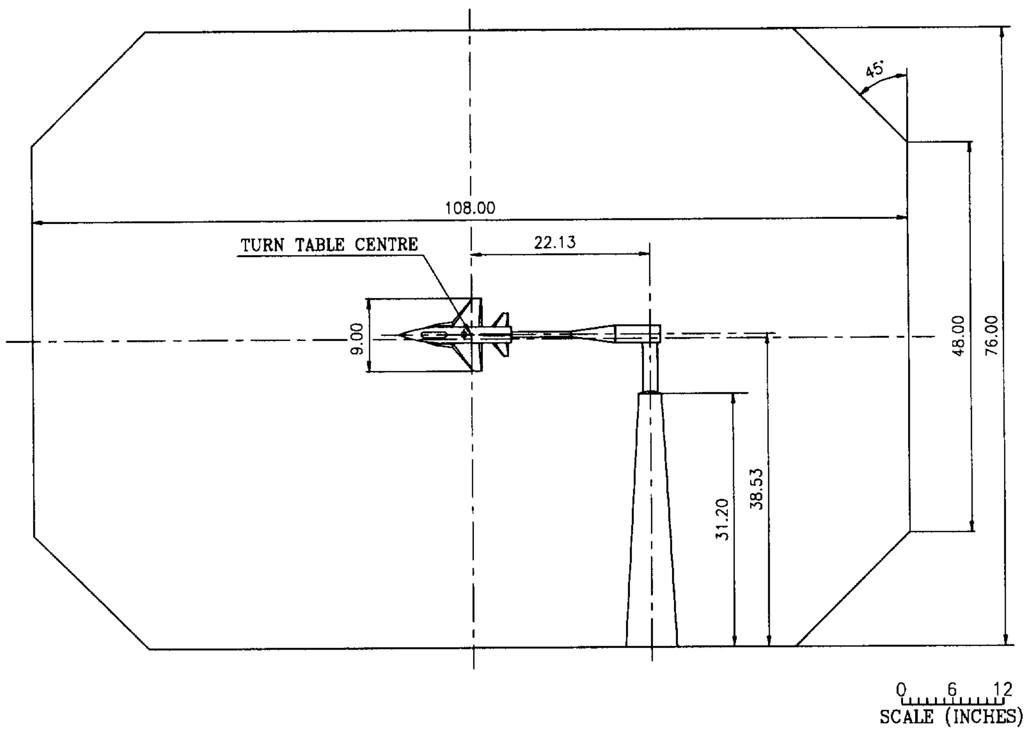

Fig. 3 Front view of SDM-S model in the IAR 6 x 9 foot wind tunnel

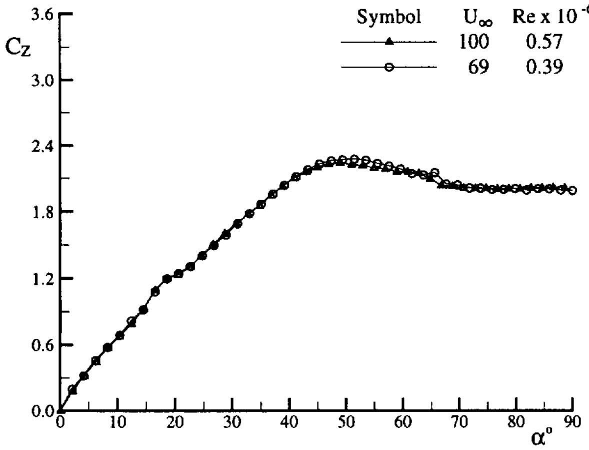

4a Normal force coefficient

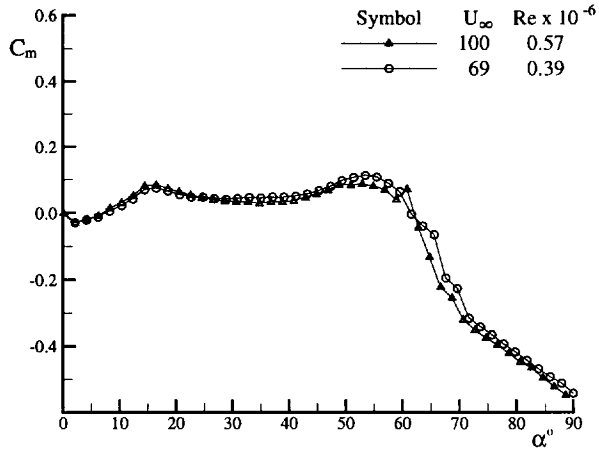

4b Pitching moment coefficient

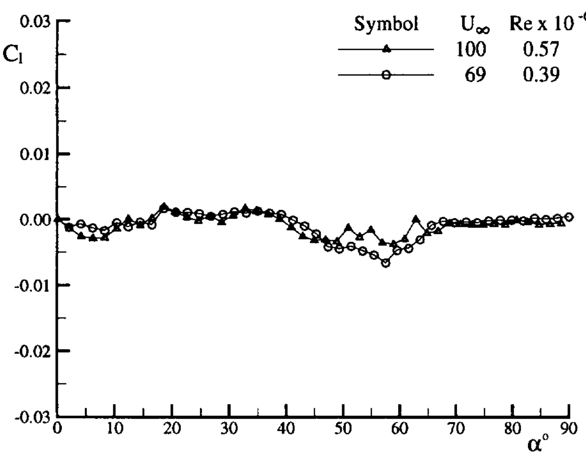

4c Rolling moment coefficient

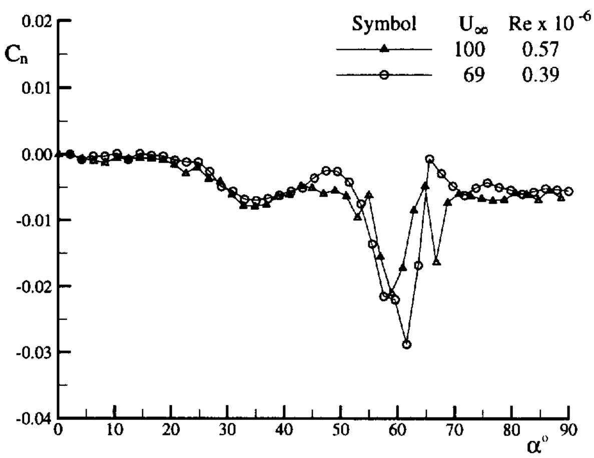

4d Yawing moment coefficient

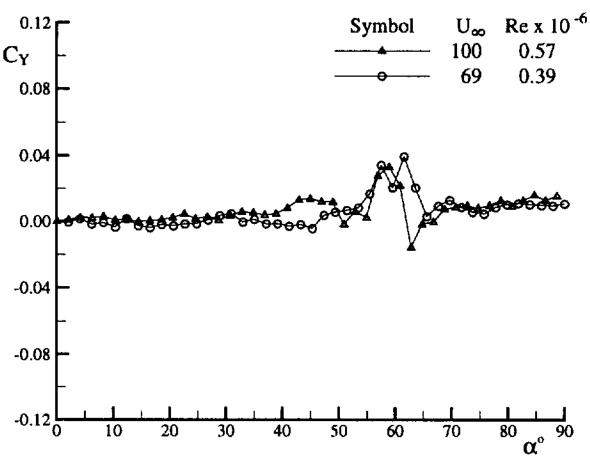

4e Side force coefficient

Fig. 4 Aerodynamic coefficients of SDM-S model at different velocities

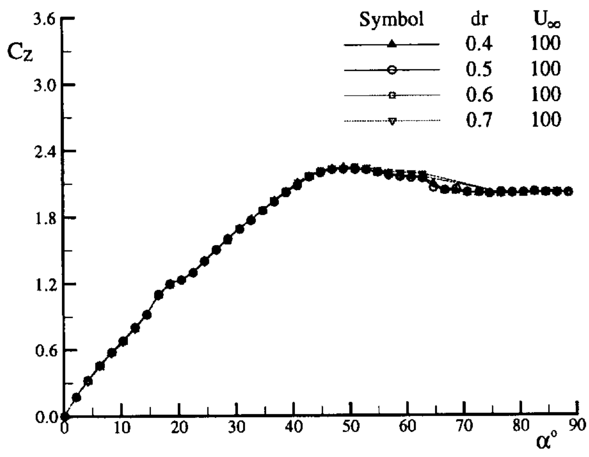

5a Normal force coefficient

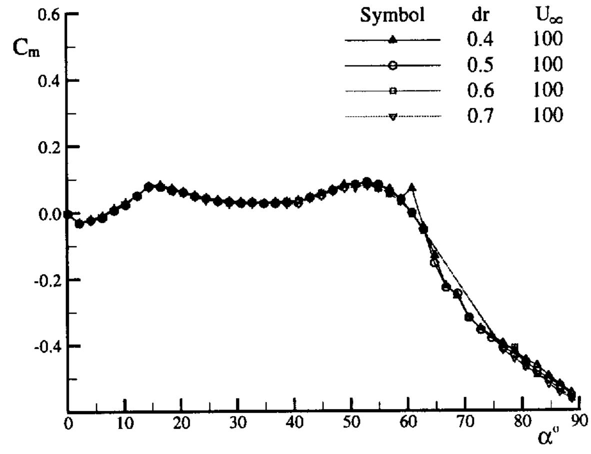

5b Pitching moment coefficient

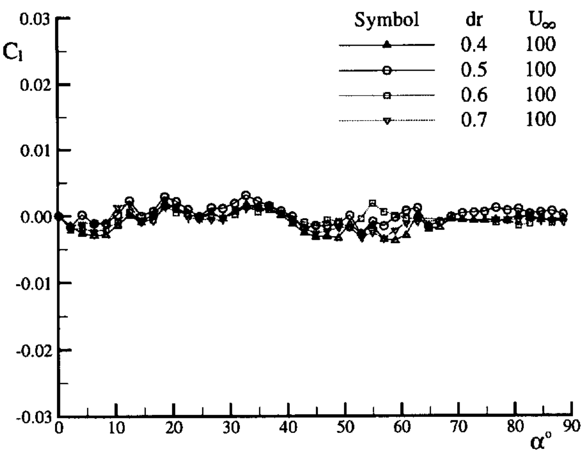

5c Rolling moment coefficient

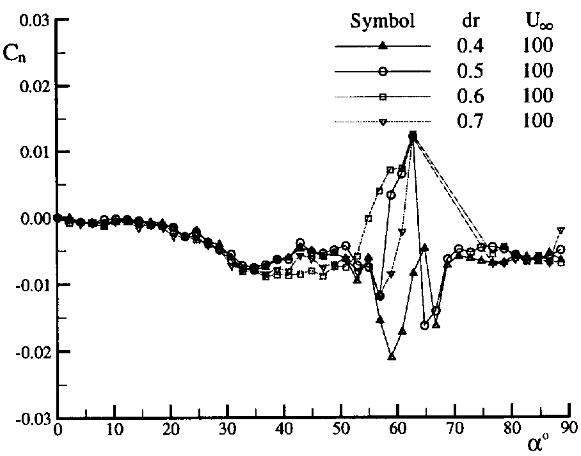

5d Yawing moment coefficient

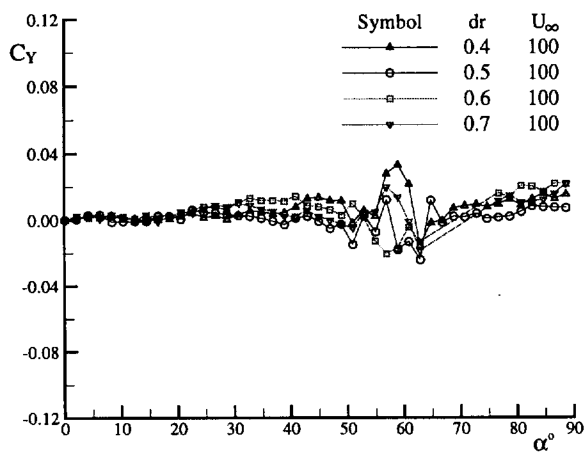

5e Side force coefficient

Fig. 5 Aerodynamic coefficients of SDM-S model at different sting diameters

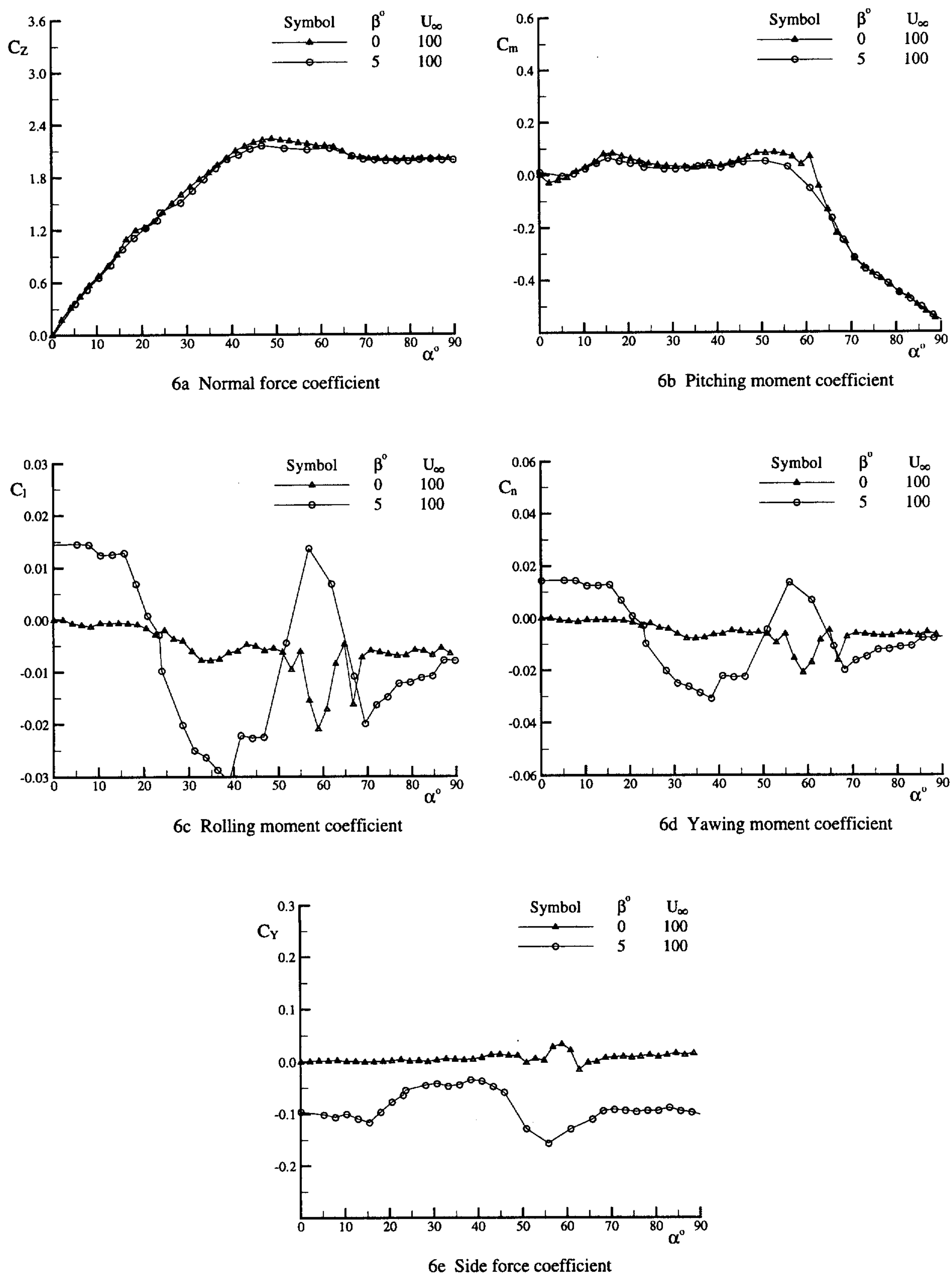

Fig. 6 Aerodynamic coefficients of SDM-S model at different sideslip angles

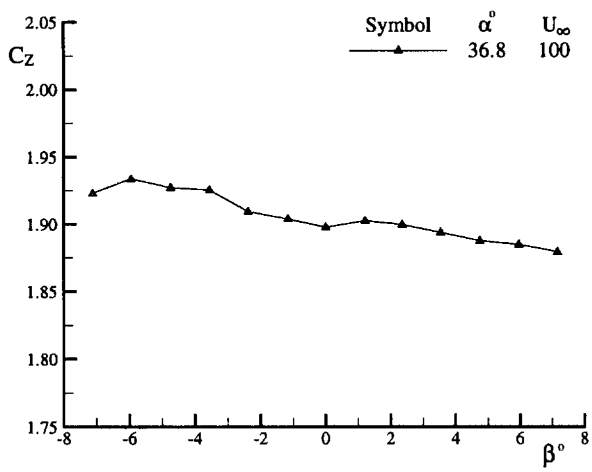

6f Normal force coefficient

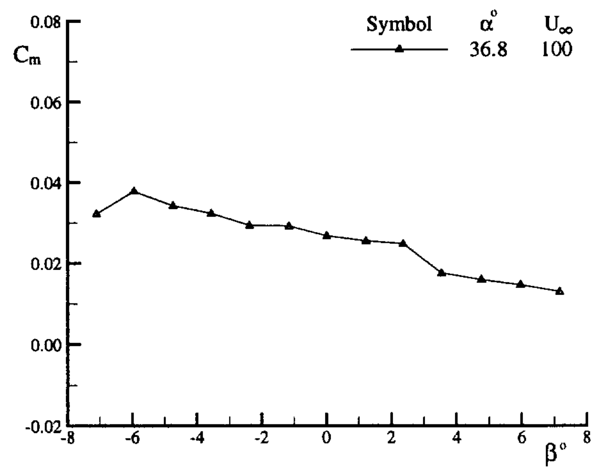

6g Pitching moment coefficient

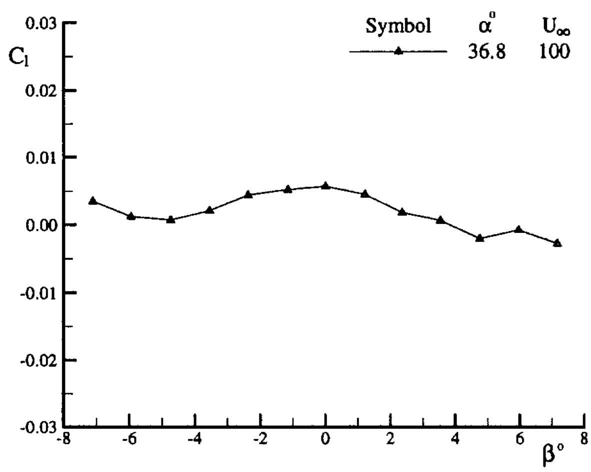

6h Rolling moment coefficient

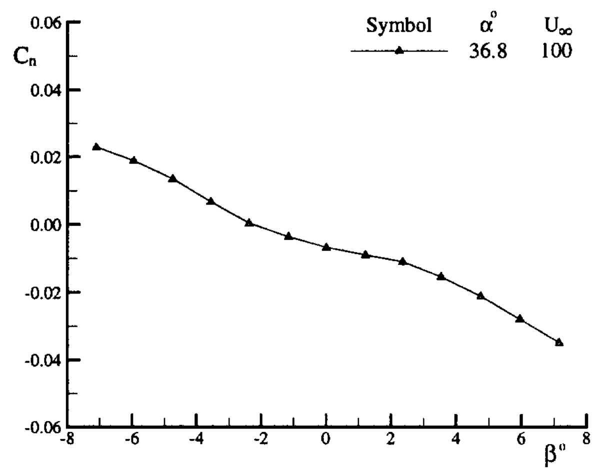

6i Yawing moment coefficient

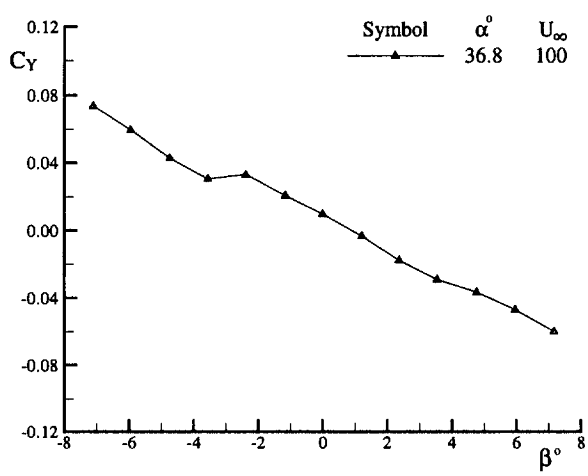

6j Side force coefficient

Fig. 6(cont.) Aerodynamic coefficients of SDM-S model at different sideslip angles

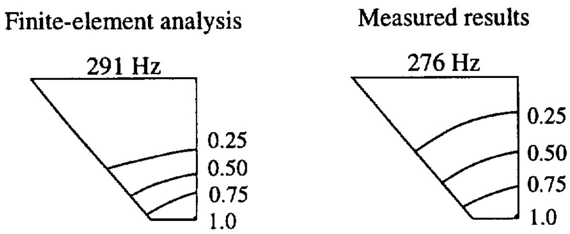

7a Fundamental bending

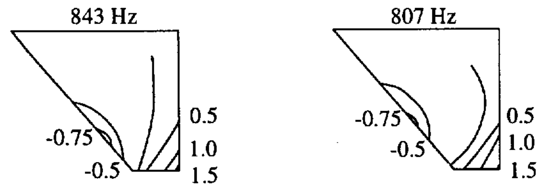

7b Torsion

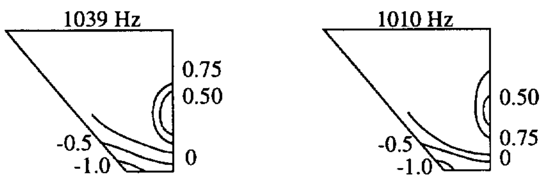

7c Overtone bending

Fig. 7 Single-wing mode shapes

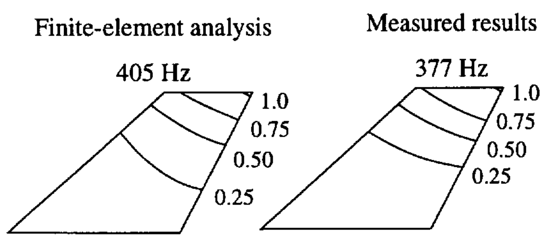

8a Bending

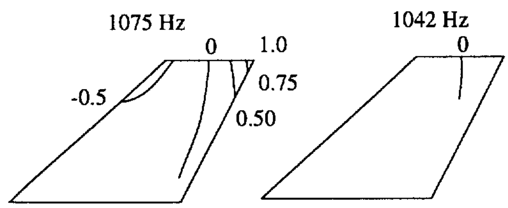

8b Torsion

Fig.8 Vertical fin mode shapes

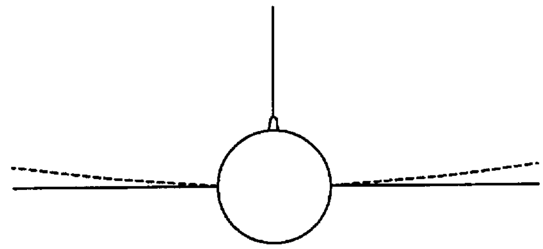

WSB mode 277 Hz

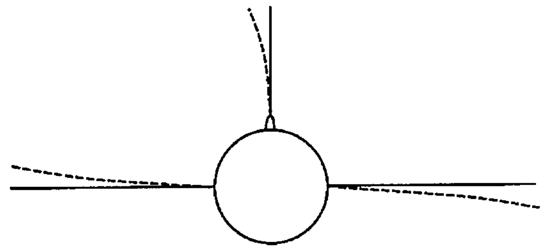

WAB mode 319 Hz

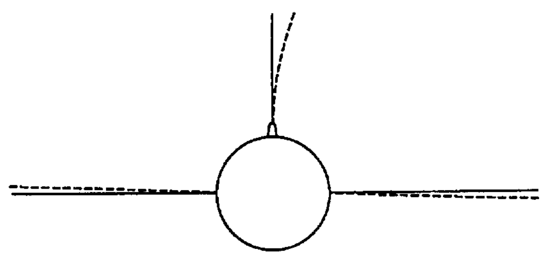

VFB mode 377 Hz

Fig. 9 Complete model modes

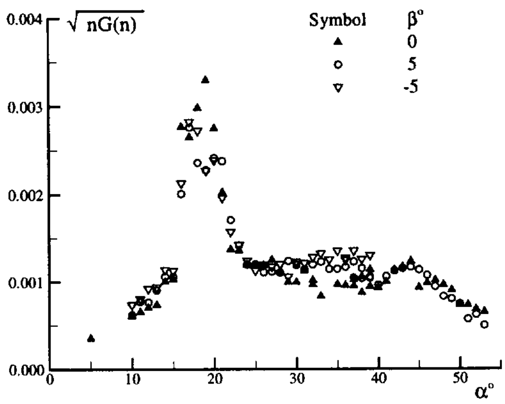

10a n=0.91, strakes on, transition fixed

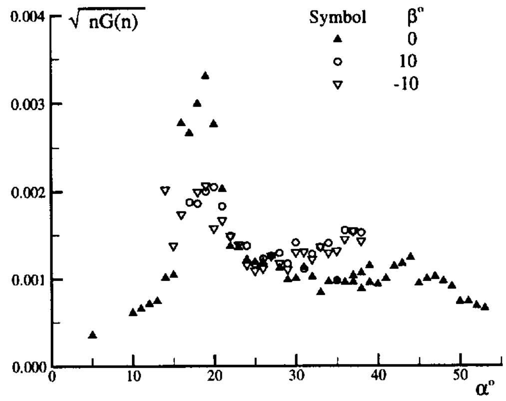

10b n=0.91, strakes on, transition fixed

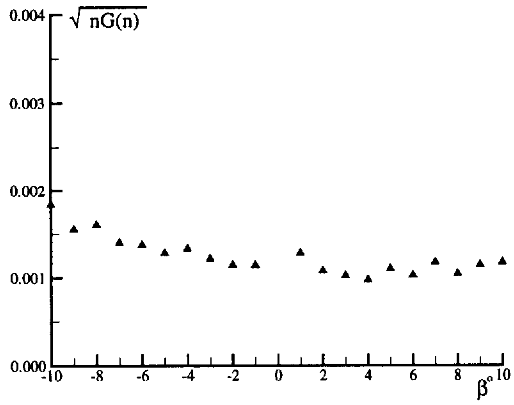

10c n=0.91, α=42°, strakes on, transition fixed

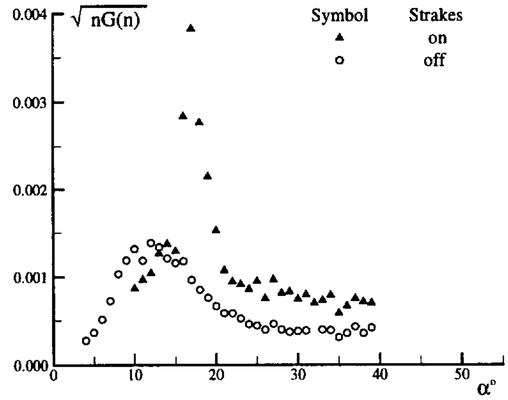

10d n=1.28, β=0°, transition fixed

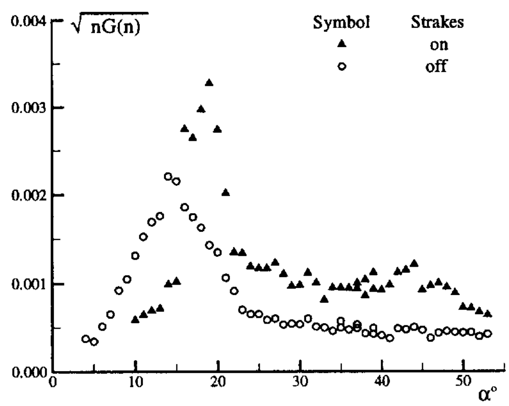

10e n=0.91, β=0°, transition fixed

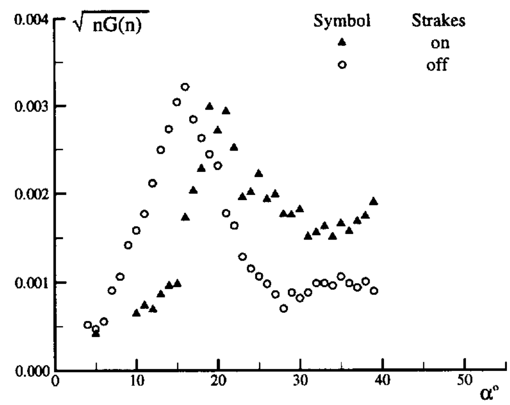

10f n=0.71, β=0°, transition fixed

Fig. 10 Wing buffet excitation parameter of SDM-L model at different conditions (WSB mode)

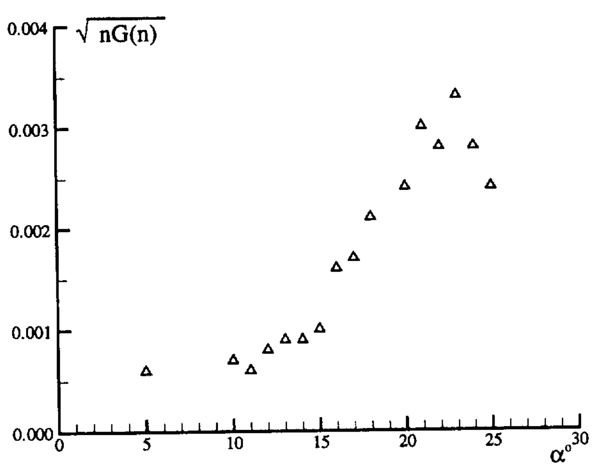

10g n=0.58, β=0°, strakes on, transition fixed

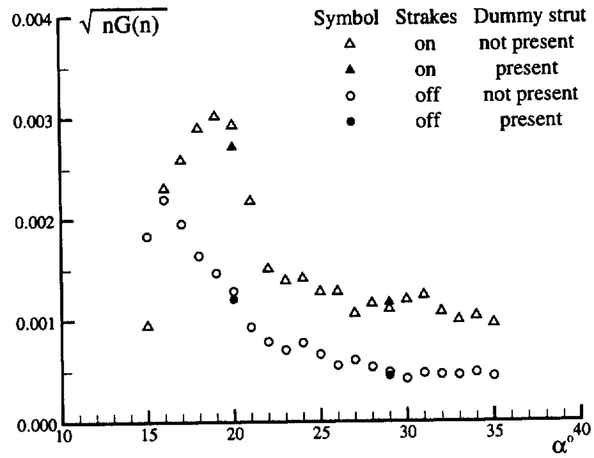

10h n=1.24, β=0°, free transition

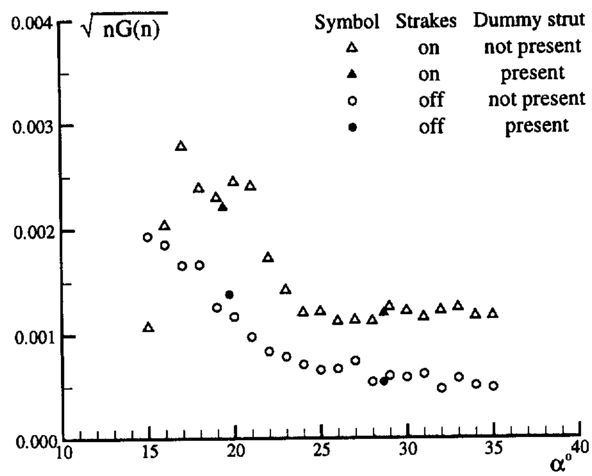

10i n=1.24, β=5°, free transition

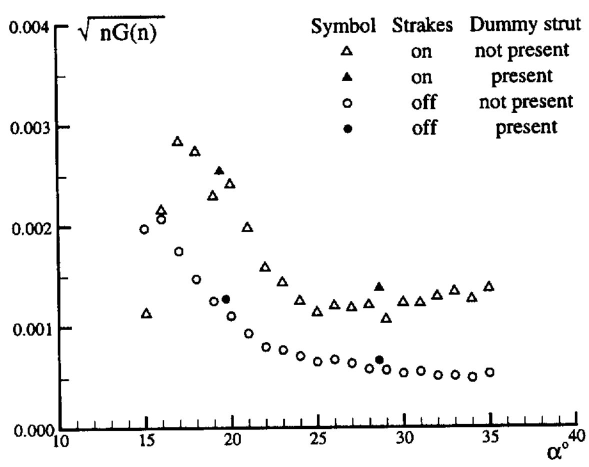

10j n=1.24, β=-5°, free transition

Fig. 10(cont.) Wing buffet excitation parameter of SDM-L model at different conditions (WSB mode)

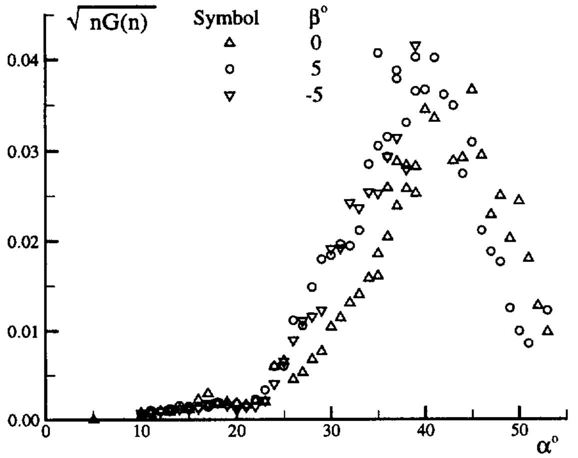

11a n=1.24, strakes on, free transition

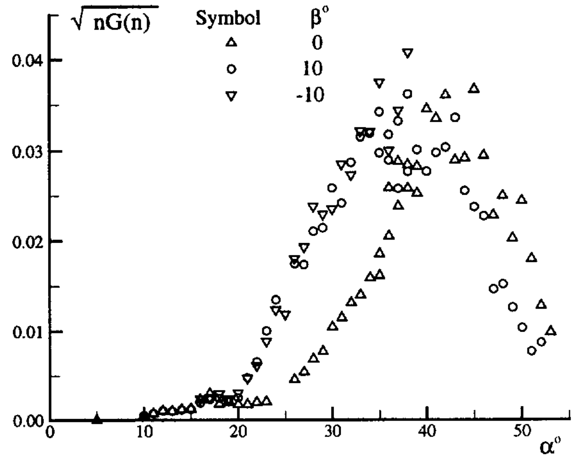

11b n=1.24, strakes on, free transition

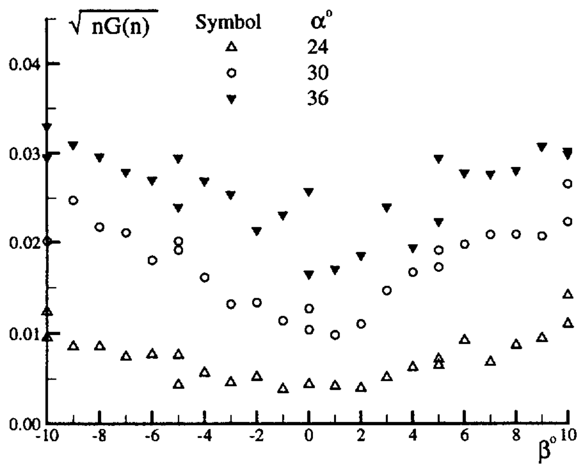

11c n=1.24, strakes on, free transition

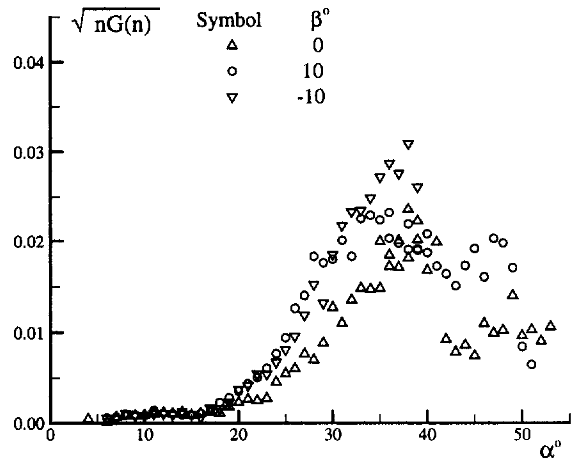

11d n=1.24, strakes off, free transition

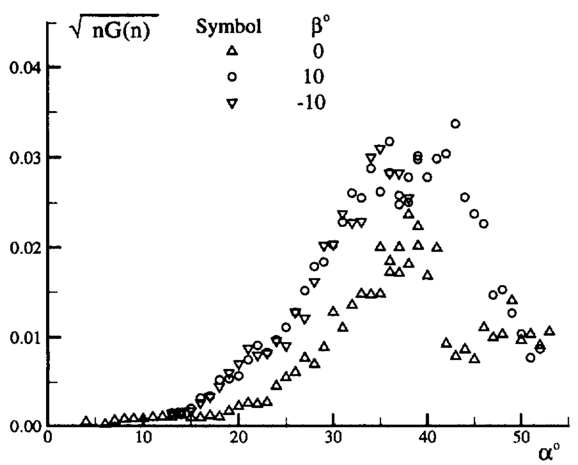

11e n=1.24, strakes off, free transition

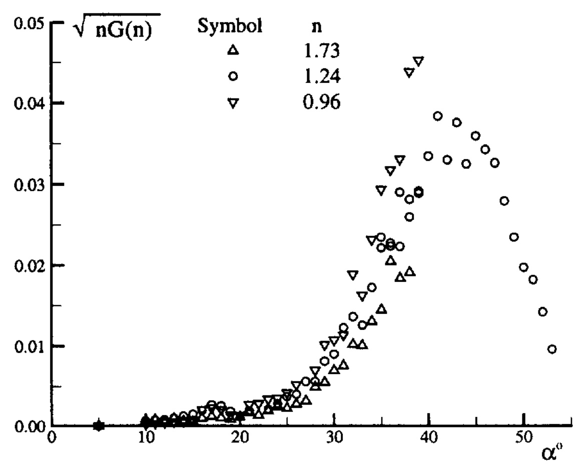

11f β=0°, strakes on, transition fixed

Fig. 11 Fin buffet excitation parameter of SDM-L model
at different conditions (FVB mode)

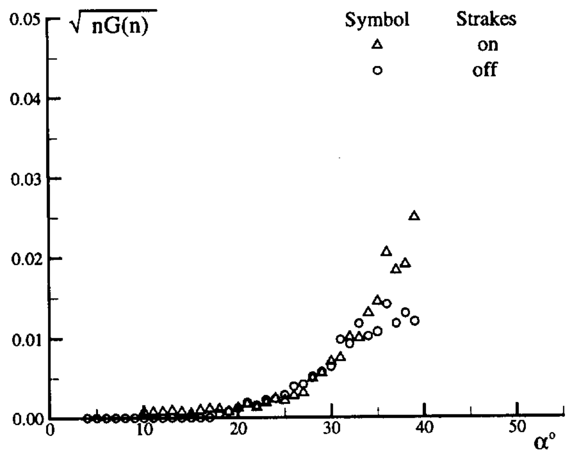

11g n=1.73, β=0°, transition fixed

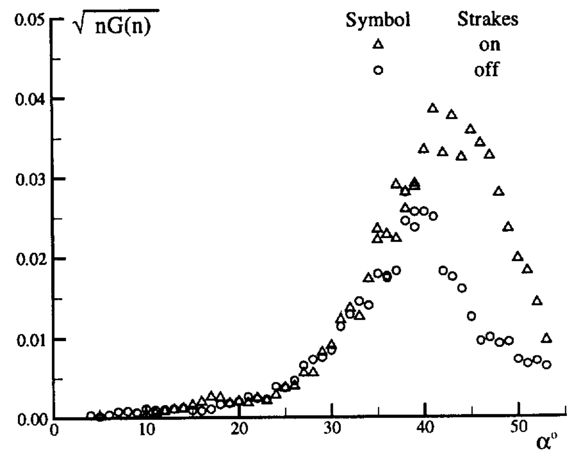

11h n=1.24, β=0°, transition fixed

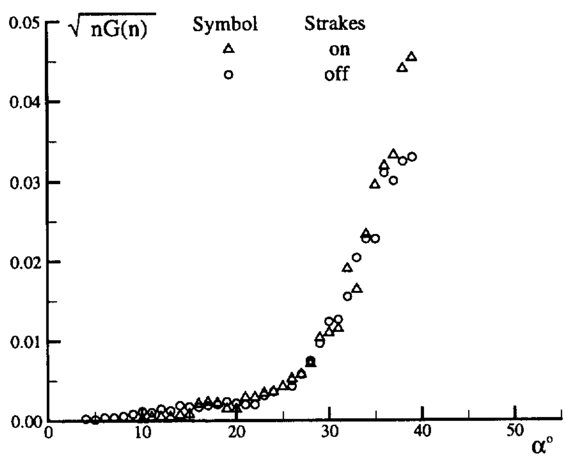

11i n=0.96, β=0°, transition fixed

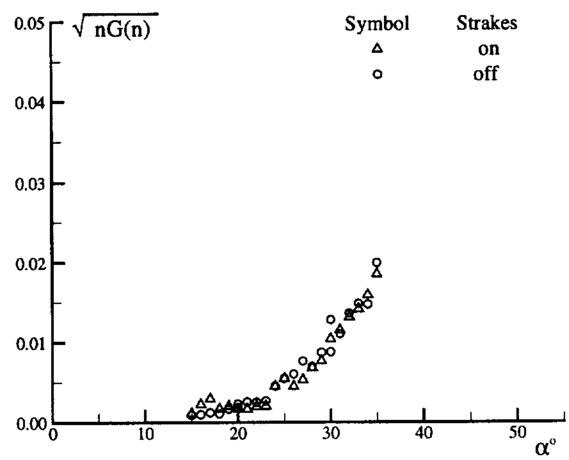

11j n=1.24, β=0°, free transition

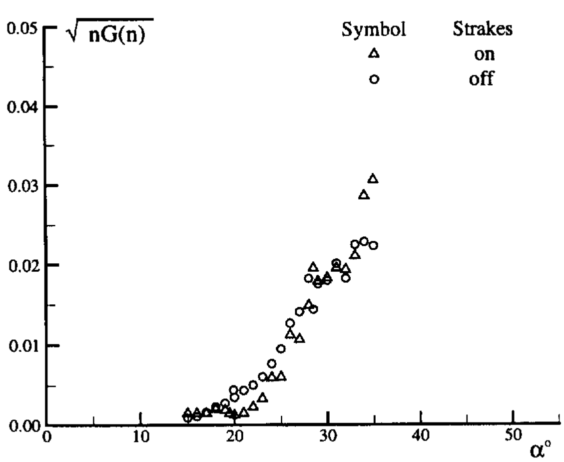

11k n=1.24, β=5°, free transition

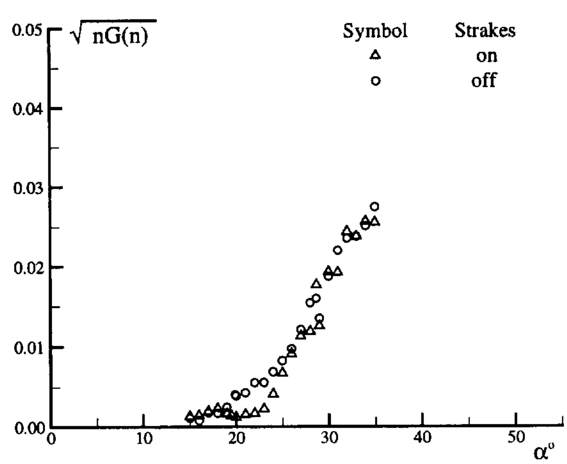

11l n=1.24, β=-5°, free transition

Fig.11(cont.) Fin buffet excitation parameter of SDM-L model at different conditions (FVB mode)

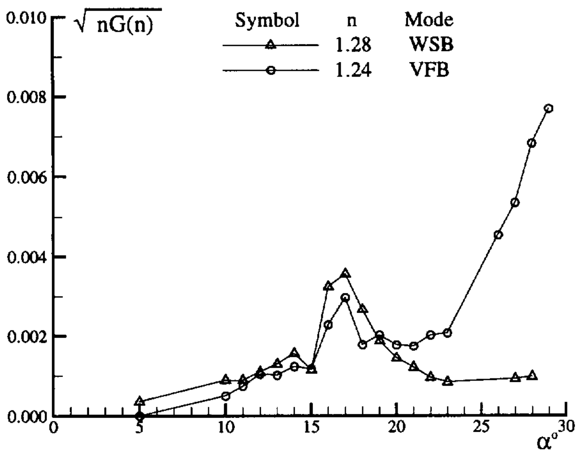

12a n=1.28, 1.24, strakes on

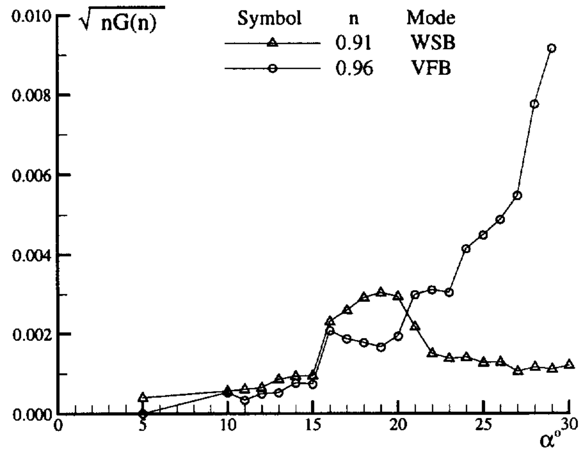

12b n=0.91, 0.96, strakes on

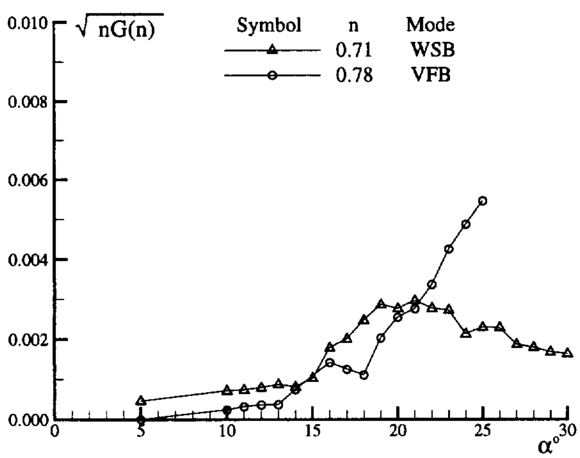

12c n=0.71, 0.78, strakes on

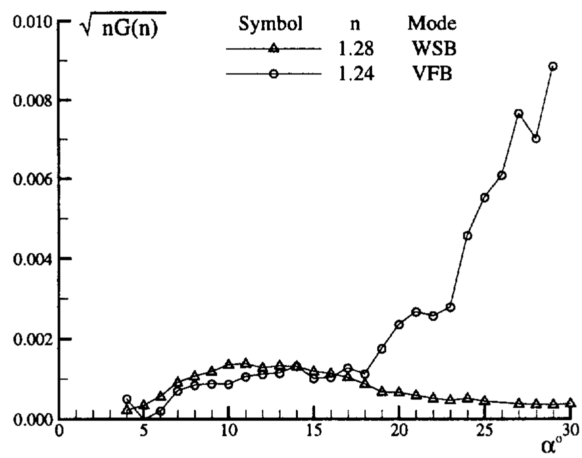

12d n=1.28, 1.24, strakes off

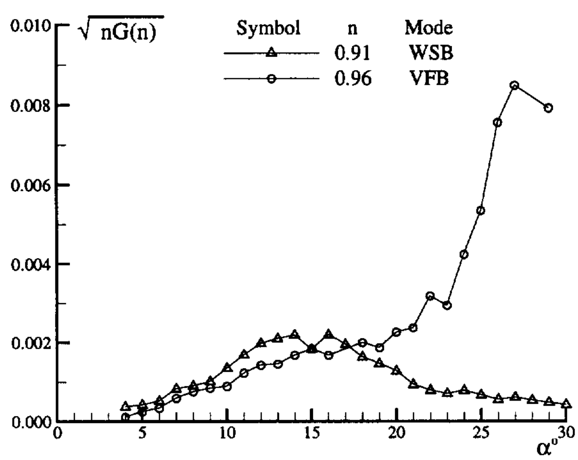

12e n=0.91, 0.96, strakes off

Fig. 12 Comparison of wing and fin buffet excitation ($\beta=0^{\circ}$, free transition)

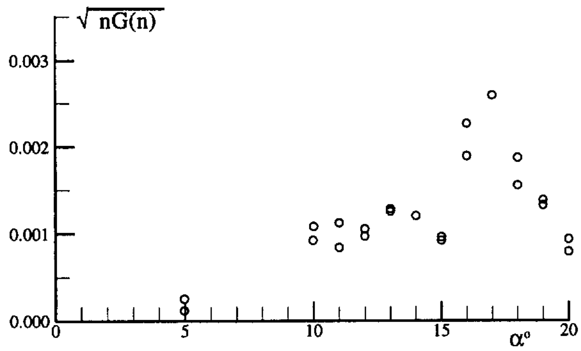

13a n=1.47, strakes on

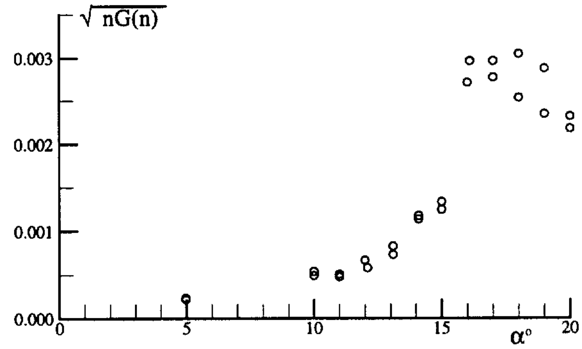

13b n=1.05, strakes on

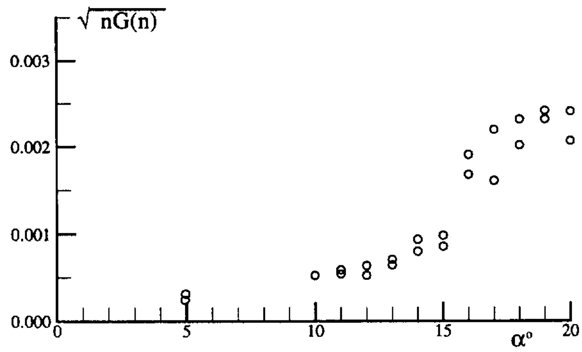

13c n=0.82, strakes on

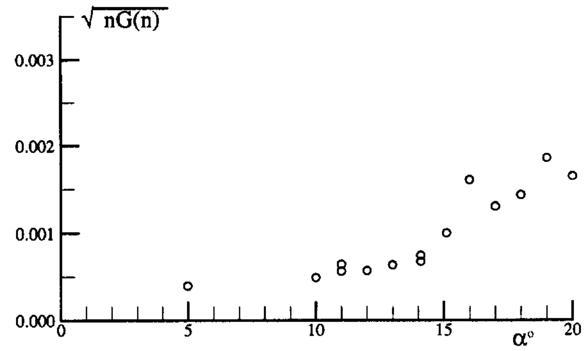

13d n=0.66, strakes on

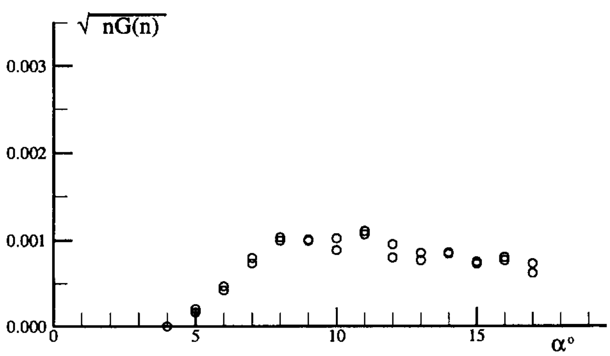

13e n=1.47, strakes off

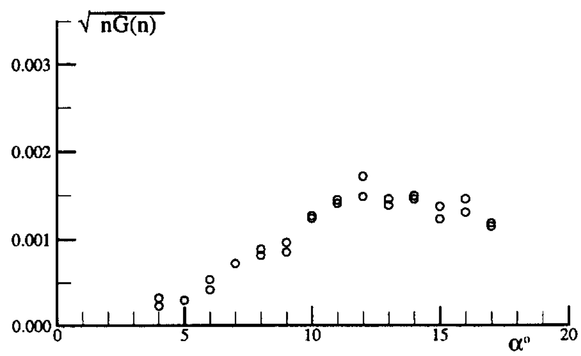

13f n=1.05, strakes off

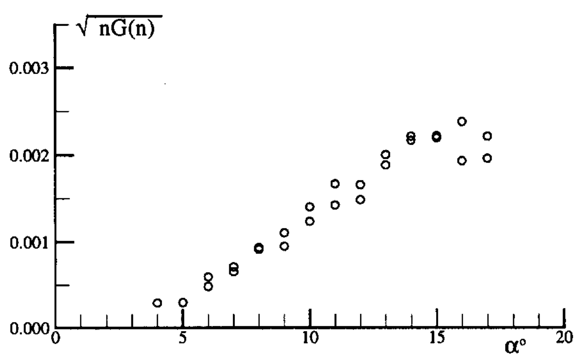

13g n=0.82, strakes off

Fig. 13 Wing buffet excitation parameter of SDM-L model at different coditions (WAB mode, $\beta = 0°$)

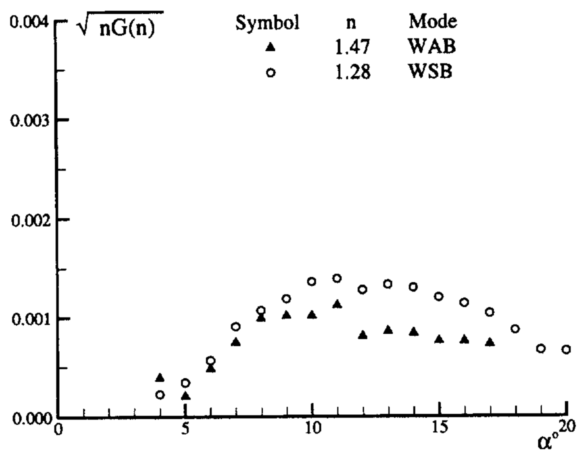

14a n=1.47 and 1.28

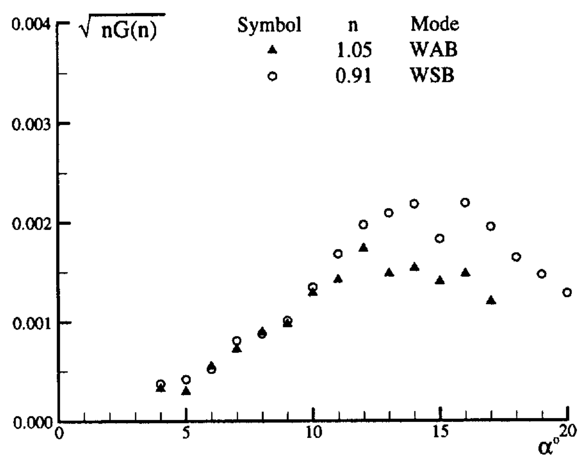

14b n=1.05 and 0.91

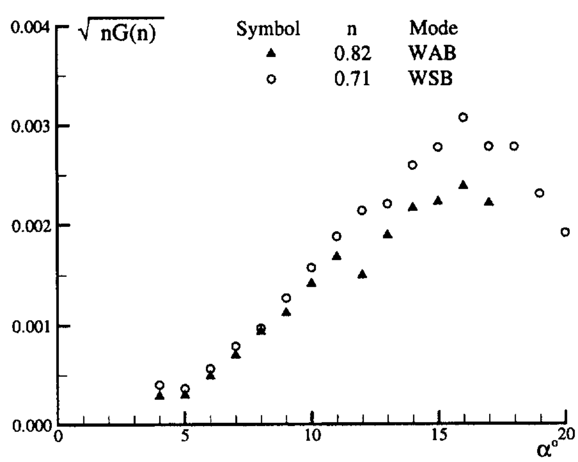

14c n=0.82 and 0.71

Fig. 14 Model independence on wing buffet excitation of SDM-L model (strakes off, $\beta=0°$, free transition)

16E. SELECTED DATA SET FROM STATIC AND ROLLING EXPERIMENTS ON A 65° DELTA WING AT HIGH INCIDENCE

X.Z. Huang, T.C. Lui and E.S. Hanff
IAR/NRC, Canada

INTRODUCTION

This data set is selected from an extensive set of experimental results obtained for configurations with a 65° delta wing under static as well as large-amplitude high-rate rolling or pitching conditions at high incidence. The experiments were performed under a joint research program on "Non-Linear Aerodynamics under Dynamic Maneuvers" by the National Research Council of Canada (NRC (IAR)), the U.S. Air Force (USAF (AFOSR, AFRL)) and the Canadian Dept. for National Defence (DND). NASA Ames informally participated in the program through its substantial CFD work on specific test conditions. The experimental results provide both detail pressure measurements and a wide range of flow conditions covering from simple attached flow, through fully developed vortex and vortex burst flow, up to fully-stalled flow at very high incidence. Since this data set includes different levels of physical difficulty, the computational researchers working in unsteady aerodynamics can use it as a staircase approach to the problem of validating their corresponding code. Four schematic and representative configurations[1] were selected in the experiments (Fig. 1 to Fig. 3):

1) 65° delta wing;
2) 80/65° double delta wing;
3) 65° delta wing with a single vertical tail and a circular ogive forebody,
4) 65° delta wing with a single vertical tail and an elliptical cross section forebody whose major axis could be installed either horizontally or vertically.

Experiments with the above models include the following test parameters:

1) motion variables (rolling or pitching),
2) modes (static or dynamic),
3) motion waveform (harmonic, ramp-and-hold, free-to-roll and "forced" free-to-roll),
4) observed variables (flow visualization, motion history, steady and unsteady loads and surface pressure),
5) wind tunnel interference assessment (by repeat tests in different wind tunnels),
6) support interference assessment (by repeat tests with different supports).

The words of "forced" free-to-roll refer to the experiments performed in the forced mode with the same motion as observed under free-to-roll condition so that the unsteady surface pressures prevailing during free-to-roll motions could be obtained.

Fig. 4 to Fig. 7 show the installation and support arrangements in the two wind tunnels. The models, rolling rig and pitching rig were designed by IAR. Experiments were conducted both at the IAR and AFRL wind tunnels (LSWT and SARL respectively) and Table 1 summarizes the test matrix. A complete list of tests with corresponding conditions can be found in Ref.1-4. The comparisons of repeat tests conducted in different wind tunnels and supports shown in Ref. 1 confirm that both wind-tunnel as well as support interference are negligible.

Due to large number of tests conducted, this data set contains only ten typical cases for the 65° delta wing, listed in Table 2. These cases were selected to cover typical sets of tests such as static tests and harmonic, ramp-and-hold, free-to-roll and "forced" free-to-roll dynamic tests. Seven spanwise-distributed surface pressure transducers on the up surface of the port wing were used to measure the instantaneous surface pressure during the motion. Three typical sting angles: σ=15°, 30° and 35° were selected as being representative of different leading-edge vortex behavior. In the absence of sideslip, at σ=15° the leading-edge vortex is intact over the full length of the model, leading to small non-linearities and time dependence; at σ=30° vortex breakdown occurs over the aft part of the wing leading to severe non-linearities and time dependence; and finally, at σ=35° vortex breakdown is present over the forward portion of the wing resulting in different characteristics.

LIST OF SYMBOLS AND DEFINITIONS

B	wing span, (in)
c	chord, (in)
c_0	mean aerodynamic chord, (in)

C_p	pressure coefficient $=(p-p_0)/qs$
C_{pi}	pressure coefficient measured from transducer at "i" station
C_ℓ	rolling moment coefficient $=\ell/qsB$
C_m	pitching moment coefficient $=m/qsc_0$
C_N	normal force coefficient =N/qs
C_p	pressure coefficient $=(p-p_0)/qs$
C_{pi}	pressure coefficient measured from transducer at "i" station
f	frequency, (Hz)
k	reduced frequency $=\pi fB/V_0$
ℓ	rolling moment, (lbs-in)
M	Mach number
m	pitching moment related to 35% MAC, (lbs-in)
N	normal force, (lbs)
n	yawing moment related to 35% MAC, (lbs-in)
p	pressure, (psi)
p_0	free stream static pressure, (psi)
p_{atm}	atmospheric pressure (psi)
q	dynamic pressure, (psi)
s	wing area, (in^2)
S	local semi-span, (in)
T_0	static temperature, (°C)
t	time, (sec)
V_0	free stream velocity, (ft/sec)
x,y,z	body axes coordinates
x_{Cp}	center of pressure in x axis, (in)
y_{Cp}	center of pressure in y axis, (in)
Y	side force, (lbs)
α	angle of attack, (°)
σ	sting angle (between body axis and tunnel axis), (°)
$\phi°$	roll angle, (°)
ϕ_0	mean roll angle or initial roll angle, (°)
ϕ_1	roll angle at end of ramp-and-hold motion, (°)
ϕ_t	roll angle in free-to-roll motion at wind-off condition, (°)
ϕ_w	roll angle in free-to-roll motion at wind-on condition, (°)
$\Delta\phi$	amplitude, (°)
$\dot{\phi}$	roll angular rate, (rad/sec)
$\dot{\Phi}$	non-dimensional rolling frequency $= \dot{\phi}B/2V_0$

FORMULARY

1 General Description of model

1.1	Designation	IAR/AFRL 65° delta wing
1.2	Type	Full model
1.3	References	Ref. 1 (Fig. 1 to Fig. 3)

2 Model Geometry

2.1	Planform	Delta wing
2.2	Aspect ratio	1.866
2.3	Leading edge sweep	65°
2.4	Trailing edge sweep	0°
2.5	Span	22.835 in
2.6	Root chord	24.485 in
2.7	Area of planform	279.486 in^2
2.8	Twist	0°
2.9	Leading-edge bevel (leeward)	10° (perpendicular to leading-edge)
2.10	Leading-edge bevel (windward)	10° (perpendicular to leading-edge)
2.11	Trailing edge bevel (leeward)	10° (perpendicular to trailing edge)
2.12	Trailing edge bevel (windward)	10° (perpendicular to trailing edge)
2.13	Area of planform	279.486 in^2
2.14	Leading-edge radius	0.020 in
2.15	Tolerance of leading-edge radius	±10%
2.16	Mean aerodynamic chord	16.323 in
2.17	Thickness of flat area	0.375 in
2.18	Reference center	13.875 aft of the apex
2.19	Center-body diameter	3.150 in
2.20	Radius of forebody	$r = \sqrt{24.103^2 - (12.243 - x)^2} - 22.528$ in

3 Wind Tunnel

3.1	Designation	LSWT (IAR)
3.1.1	Type of tunnel	Close-circuit atmospheric type
3.1.2	Test section dimensions	Height: 6 ft, width: 9ft, length: 15 ft
3.1.3	Type of roof and floor	Solid with large optical quality plexiglass windows
3.1.4	Maximum speed	390 ft/sec
3.1.5	Contraction ratio	9
3.1.6	Turbulence in empty tunnel	$\leq$ 0.12% at free stream speed of 100 ft/sec
3.1.7	Support	Sting attached to wind tunnel strut (Fig. 4)
3.1.8	Type of side walls	Solid with large optical quality plexiglass windows
3.1.9	Type of roof	Solid with large optical quality plexiglass windows
3.1.10	Tunnel resonance	No evidence of resonance in present test
3.1.11	Reference	Ref. 5
3.2	Designation	SARL wind tunnel (AFRL)
3.2.1	Type of tunnel	Open-circuit atmospheric type
3.2.2	Test section dimensions	Height: 10 ft, width: 7ft, length: 15 ft
3.2.3	Maximum speed	660 ft/sec
3.2.4	Contraction ratio	36
3.2.5	Turbulence in empty tunnel	$\leq$ 0.1%
3.2.6	Type of side walls	Solid with large optical quality plexiglass windows

3.2.7	Type of roof	Solid with large optical quality plexiglass windows
3.2.8	Support	Roll rig is shown in Fig. 4 and Fig. 5 while pitch rig is shown in Fig. 6 and Fig. 7
3.2.9	Tunnel resonance	No evidence of resonance in present test
3.2.10	Reference	Ref. 6

4 Model motion

4.1	General description	Rolling about body axis with following motions: Sinusoidal (§4.6) Ramp-and-hold (§4.7) Free-to-roll and "forced" free-to-roll (§4.8)
4.2	Method of applying motion	Inexorable hydraulic system (3,000 psi, 50 hp)
4.3	Model deformation	Negligible
4.4	Roll angle precision	0.175°
4.5	Sting angle precision	0.1°
4.6	Sinusoidal motion	
4.6.1	Maximum oscillation amplitude	40°
4.6.2	Maximum mean roll angle	± 50°
4.6.3	Maximum frequency	18 Hz
4.7	Ramp-and hold motion	
4.7.1	Waveform	Constant velocity with constant acceleration at both ends, or Only constant acceleration at both ends (double parabola)
4.7.2	Maximum of angular rate	4500 °/sec
4.7.3	Maximum of angular acceleration	500,000 °/sec^2
4.8	Free-to-roll and "forced" free-to-roll	
4.8.1	Maximum initial roll angle	90°
4.8.2	Tare friction	Approximately constant (independent of rate)

5 Test Conditions

5.1	Model planform area/tunnel area	0.0296 (SARL) and 0.0357 (LSWT)
5.2	Model span/tunnel height	0.300 (LSWT)
5.3	Model span/tunnel width	0.272 (SARL)
5.4	Model center chord/ tunnel height	0.204 (SARL)
5.5	Model center chord/ tunnel width	0.227 (LSWT)
5.6	Blockage at α=30°	0.0148 (SARL) and 0.0179 (LSWT)
5.7	Position of model in tunnel	Standard side position (LSWT) Standard upright position (SARL)
5.8	Rolling moment of inertia	0.15 lbs-in-sec^2
5.9	Range of tunnel total pressure	Atmospheric (SARL) Atmospheric static pressure (LSWT)
5.10	Definition of model sting angle	Angle between body axis and tunnel axis
5.11	Sting deformation under static loads	Negligible in (LSWT) and 1°at σ=30° in (SARL)

6 Measurements and Observations

6.1	Steady pressure for static conditions	Yes
6.2	Unsteady pressures for dynamic conditions	Yes
6.3	Steady forces for static conditions	Measured directly
6.4	Unsteady forces for dynamic conditions	Measured directly
6.5	Measurement of actual motion of model	Yes
6.6	Measurement of free-to-roll motion history	Yes
6.7	Observation or measurement of boundary layer properties	Yes
6.8	Visualisation of surface flow	Yes
6.9	Visualization of off-surface flow	Yes
6.10	Wind tunnel interference assessment	Yes
6.11	Support interference assessment	Yes

7 Instrumentation

7.1 Steady pressure

7.1.1	Position of orifices spanwise and chordwise	see Fig. 1
7.1.2	Type of measuring system Operation mode Sensitivity range Zero pressure output:	Kulite pressure transducers (LQ-47-25A) with "B" screen Absolute 3.21~4.46 mv/psi <±5% full scale
7.1.3	Installation of transducers	Using RTV adhesive flush ($^{0.000}_{-0.005}$) to upper surface. Fill trough with clear epoxy filler fair to upper surface.
7.1.4	Principle and accuracy of calibration	Kulite: static calibration at beginning of tunnel entry, offset measurement every 30 minutes.

7.2 Unsteady pressure

7.2.1	Position of orifices	See Fig. 1
7.2.2	Type of transducers	Same as §7.1.1
7.2.3	Method and accuracy of calibration	Kulite: static calibration at beginning of tunnel entry, offset measurement every 30 minutes

7.3 Steady loads

7.3.1	Type of transducers	Strain gauge
7.3.2	Type of measuring system	Five components balance with maximum range: Normal force N=2,000 lbs Side force Y=1,000 lbs Rolling moment ℓ=3,000 lb-in
7.3.3	Method and accuracy of calibration	Maximum and relative deviations: Normal force ΔN_{max} =±2 lbs, δN_{max}=0.1% Pitch moment Δm_{max}=±5 lbs-in (Δx_{max}= 0.005 in) Side force ΔY_{max} =±2 lbs, δY_{max}=0.1% Yawing moment Δn_{max}=±5 lbs-in (Δy_{max}= 0.005 in) Rolling moment $\Delta \ell_{max}$=±6 lbs-in $\delta C\ell_{max}$=0.2%

7.4 Unsteady loads

7.4.1	Type of transducers	Strain gauge
7.4.2	Measurement method	Ensemble average of coherent samples taken over several cycles
7.4.3	Method and accuracy of calibration	

7.5 Model motion

7.5.1	Method of measurement	Angular encoder on driveshaft aft end
7.5.2	Accuracy	±0.1°
7.5.3	Sting acceleration (horiz. and vert.)	Accelerometer EGA-125*-10D Non-linearity: ±1% Range: ±10 g Limit: ±50 g Them.Z ±1%FS/100°F TSS ±2.5% /100°F

7.6 Processing of unsteady measurements

7.6.1	Pressure signal acquisition	See Fig. 8a (up to 1991)
7.6.2	Loads signal acquisition	See Fig. 8b (up to 1991)
7.6.3	Processing data	Ensemble average over more than 30 (harmonic motion), or 9 cycles (ramp-and-hold motion)

8 Data presentation

8.1	Test cases for which data could be made available	Table 1
8.2	Test cases for which data are included in this document	Table 2
8.3	Data presentation	See CD-ROM (in Tecplot format)
8.4	Electronic data file index	Table 3
8.5	Examples of lay-out of data files	Table 4 at page 23
8.6	Some illustration of results	See page 17 to 22

9 Personal contact for further information

Xing Zhong Huang and Ernest S. Hanff, Aerodynamics Laboratory, Institute for Aerospace Research, National Research Council of Canada, Montreal Rd. Ottawa, Canada, K1A 0R6.
e-mail address: xingzhong.huang@nrc.ca and ernest.hanff@nrc.ca

10 List of references

[1]. Hanff, E.S. and Huang, X.Z., "Rolling and Pitching Experiments on Configurations with a 65° Delta Wing at High Incidence" NRC/IAR LTR-A-013, 1997.

[2]. Jenkins, J.E. and Hanff, E.S., "Highlights of the IAR/WL Delta Wing Program" AIAA Atmospheric Flight Mechanics Conference, Workshop III, August 1995

[3]. Hanff, E.S. and Jenkins, S.B., "Large-Amplitude High-Rate Roll Experiments on a Delta and Double Delta Wing," AIAA Paper 90-0224, 1990.

[4]. Hanff, E.S., Kapoor, K, Anstey, C.R. and Prini, A., "Large-Amplitude High-Rate Roll Oscillation System for the Measurement of Non-Linear Airloads," AIAA Paper 90-1426, 1990.

[5]. Brown, T.R., "Description of the 6-ft x 9-ft Low Speed Wind Tunnel," NRC, NAE LTR-LA-285, Nov. 1986.

[6]. Presdorf, T.A., "Subsonic Aerodynamic Research Laboratory," USAF WL-TR-92-3053, Aug., 1992.

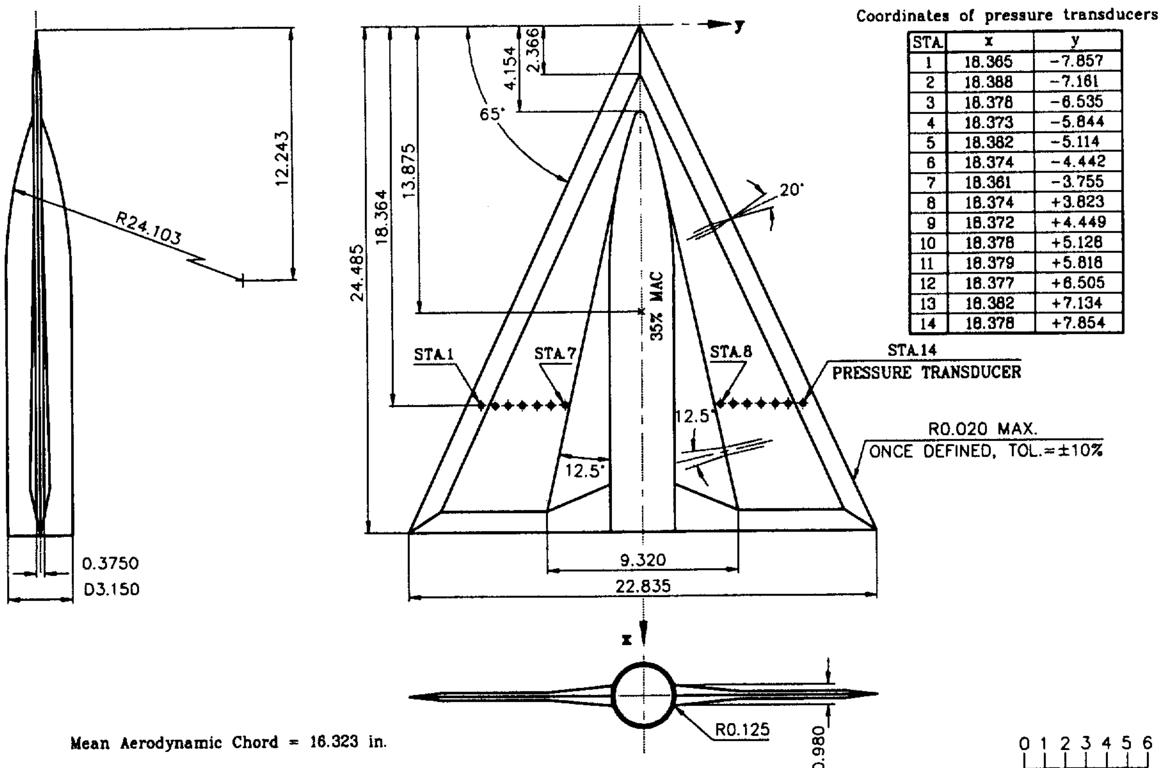

Coordinates of pressure transducers

STA.	x	y
1	18.365	-7.857
2	18.388	-7.161
3	18.378	-6.535
4	18.373	-5.844
5	18.382	-5.114
6	18.374	-4.442
7	18.361	-3.755
8	18.374	+3.823
9	18.372	+4.449
10	18.378	+5.128
11	18.379	+5.818
12	18.377	+6.505
13	18.382	+7.134
14	18.378	+7.854

Fig. 1 65° delta wing

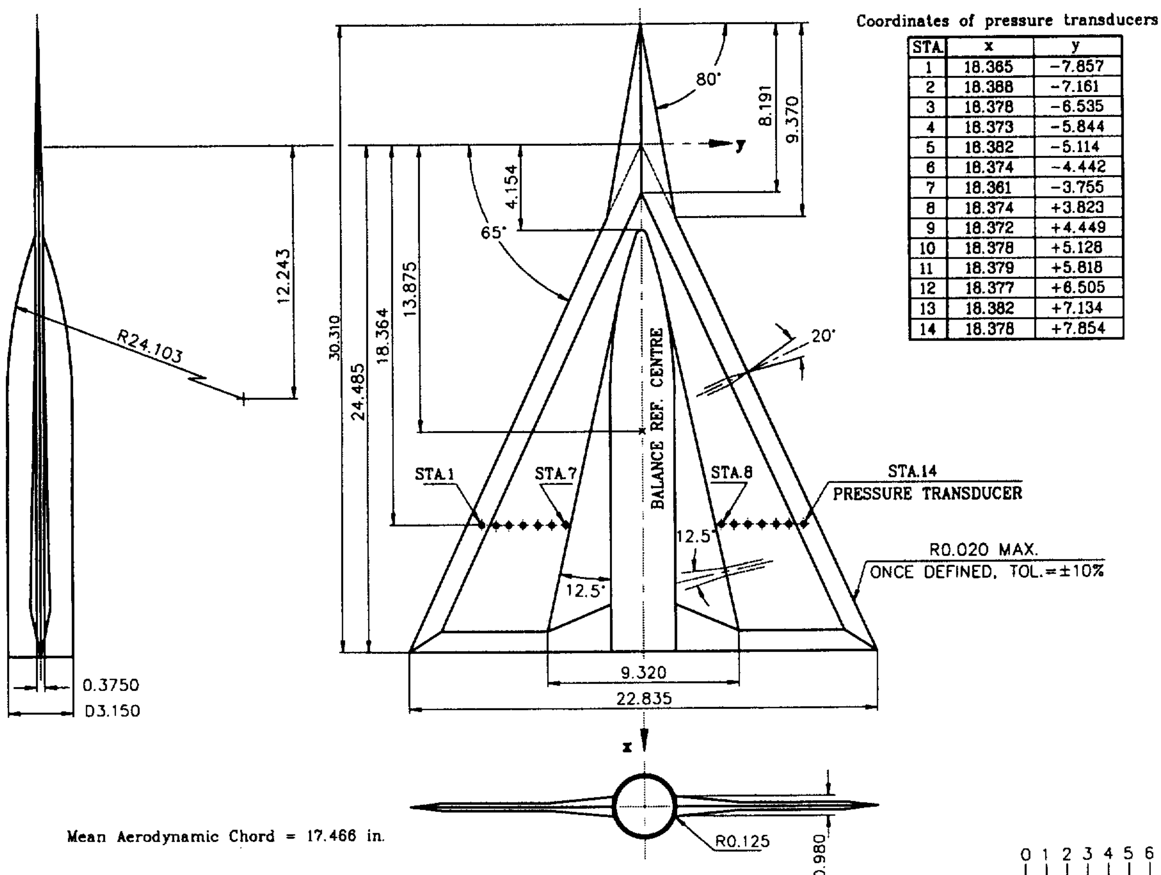

Coordinates of pressure transducers

STA.	x	y
1	18.365	-7.857
2	18.388	-7.161
3	18.378	-6.535
4	18.373	-5.844
5	18.382	-5.114
6	18.374	-4.442
7	18.361	-3.755
8	18.374	+3.823
9	18.372	+4.449
10	18.378	+5.128
11	18.379	+5.818
12	18.377	+6.505
13	18.382	+7.134
14	18.378	+7.854

Fig. 2 80°/65° double delta wing

Coordinates of pressure transducers

STA.	x	y
1	6.121	+7.850
2	6.121	+7.170
3	6.121	+6.490
4	6.121	+5.810
5	6.121	+5.130
6	6.121	+4.450
7	6.121	+3.770
8	1.347	+9.891
9	1.347	+7.321
10	1.347	+4.750
11	6.121	−5.810
12	12.242	+5.233
13	12.242	+3.873
14	12.242	+2.513

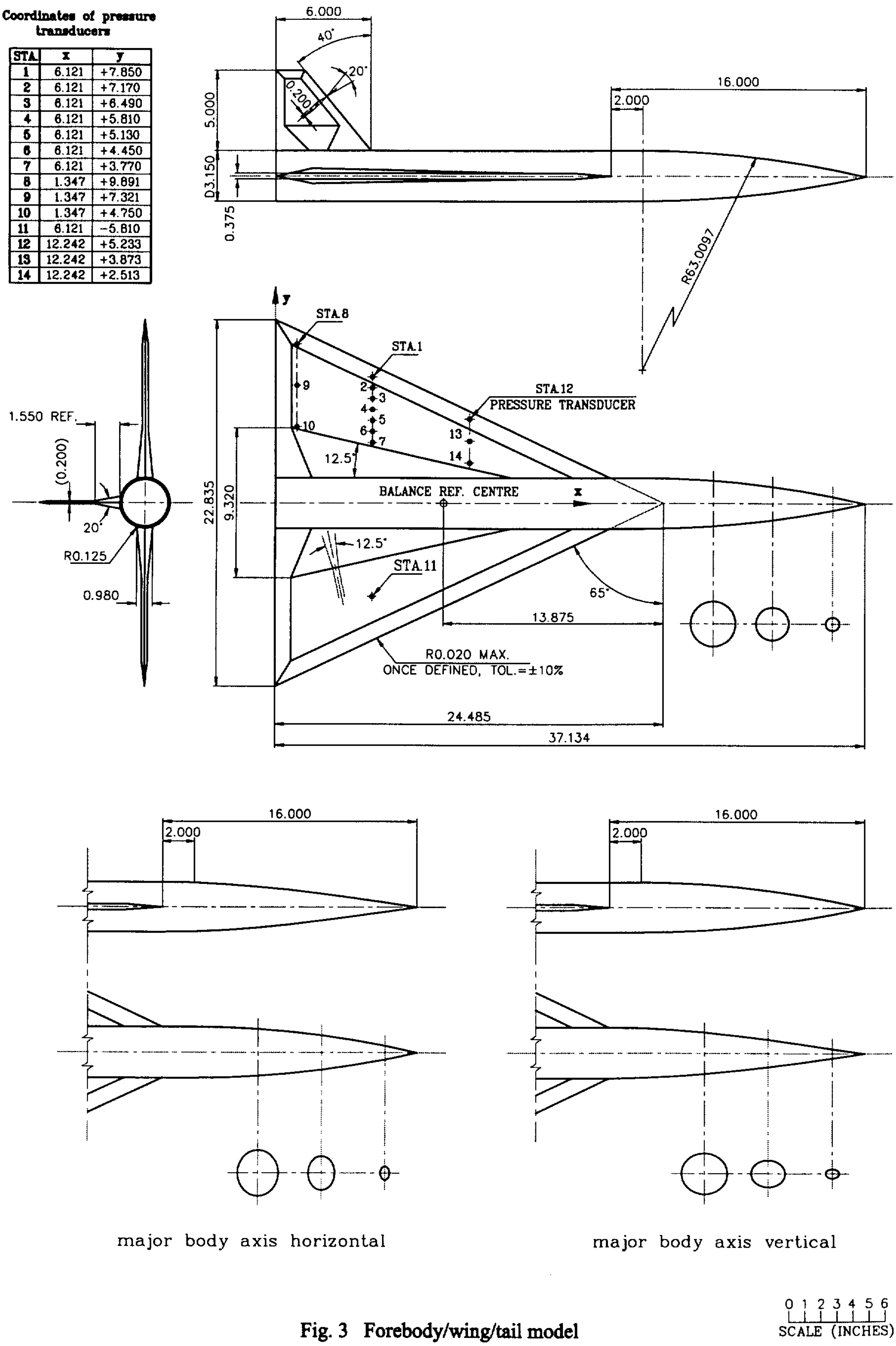

Fig. 3 Forebody/wing/tail model

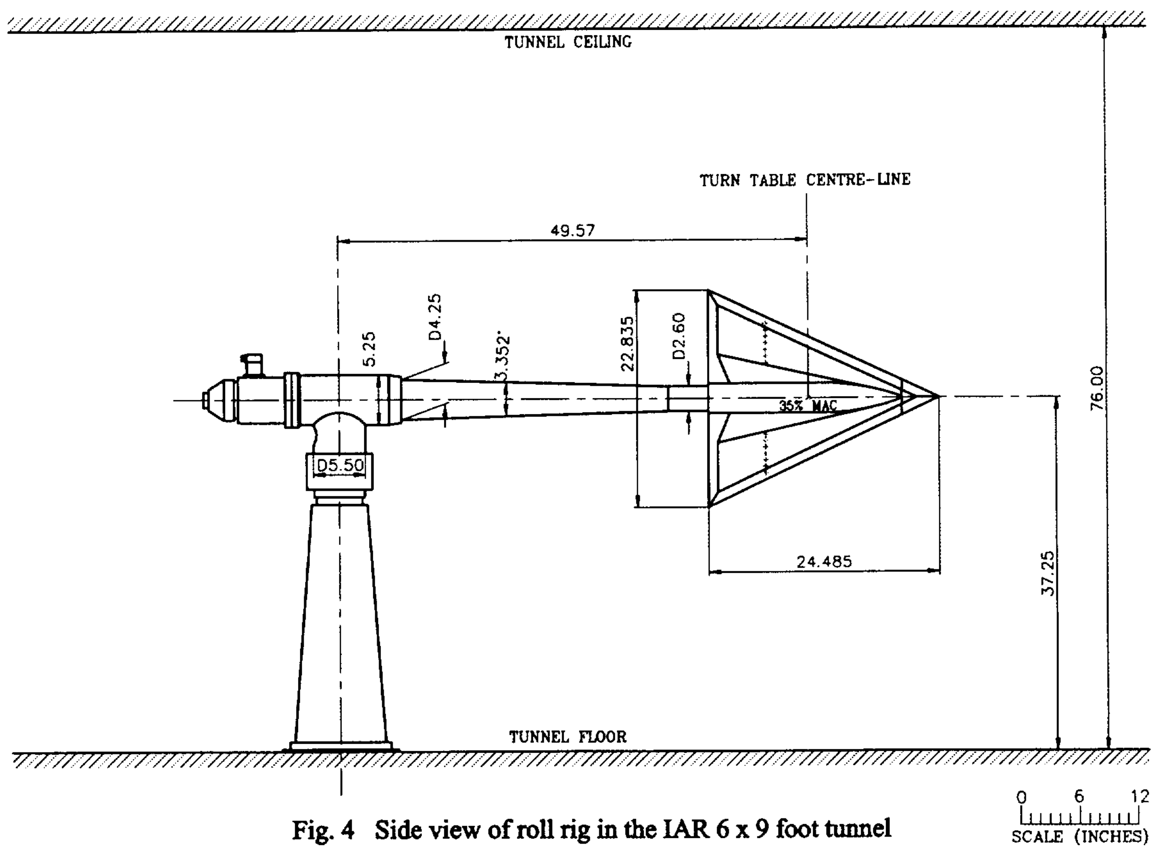

Fig. 4 Side view of roll rig in the IAR 6 x 9 foot tunnel

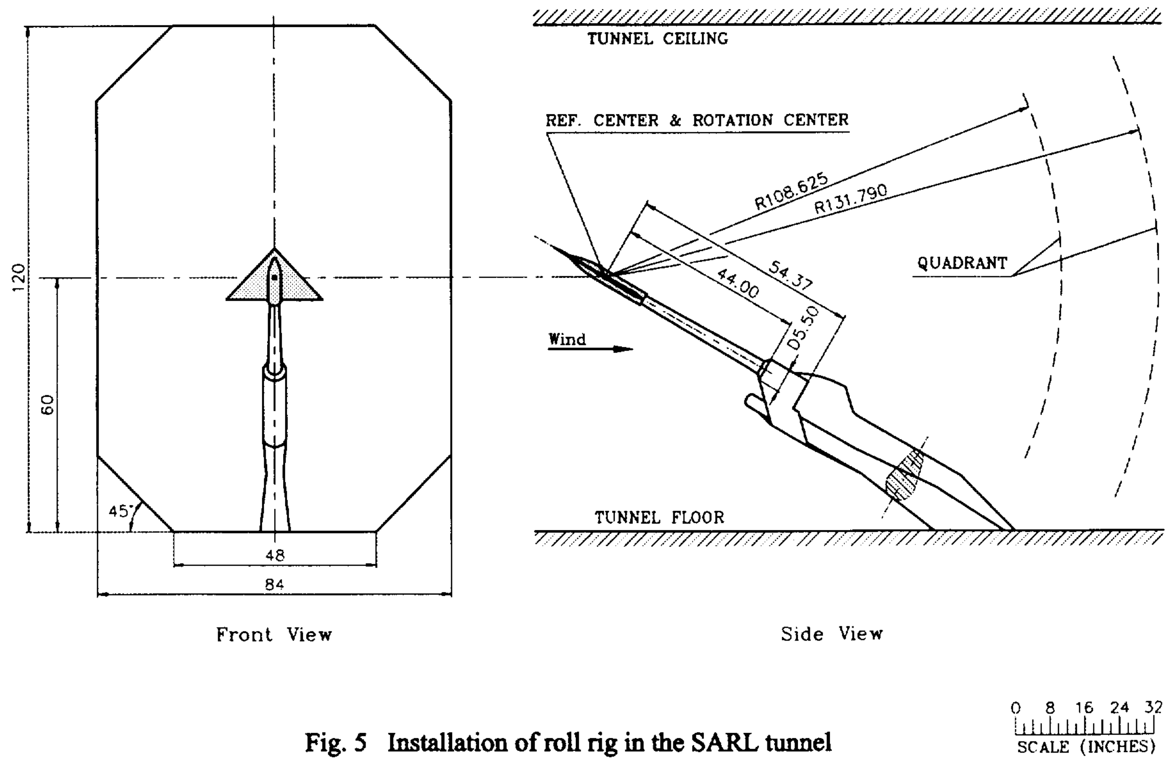

Fig. 5 Installation of roll rig in the SARL tunnel

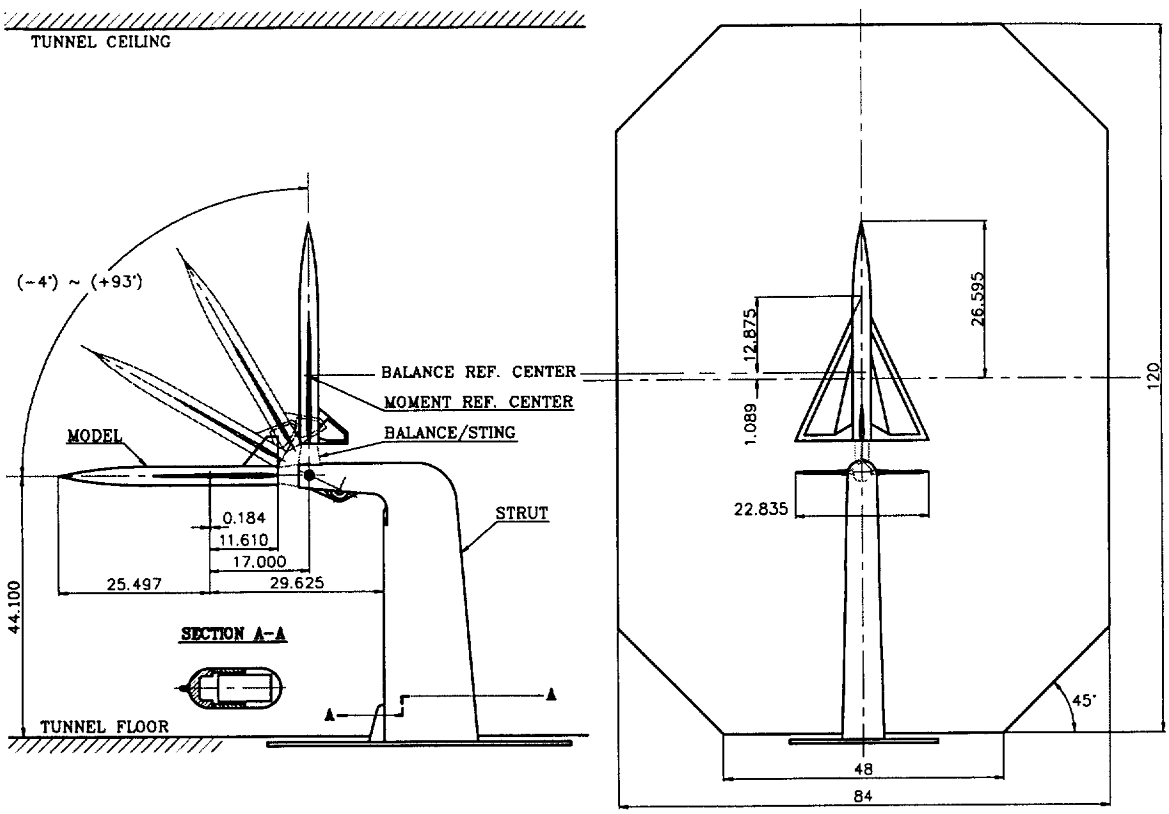

Fig. 6 Installation of pitch rig in SARL wind tunnel

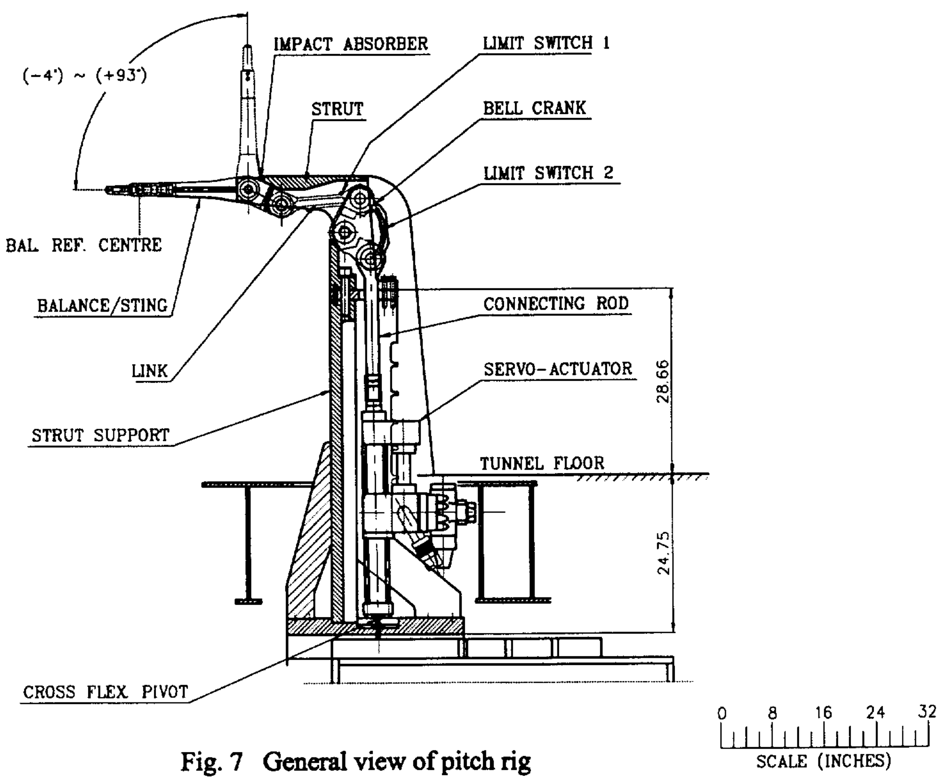

Fig. 7 General view of pitch rig

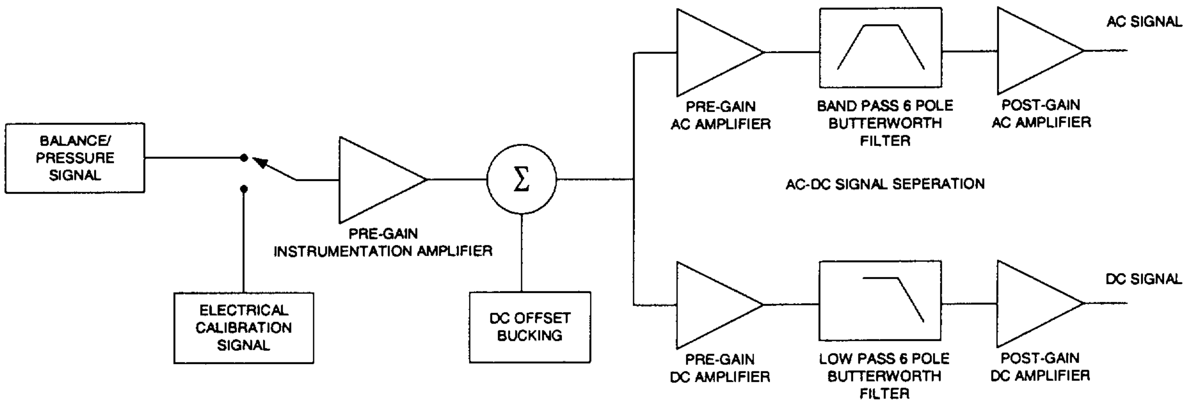

Fig. 8a Signal conditioning for data acquisition used up to 1991

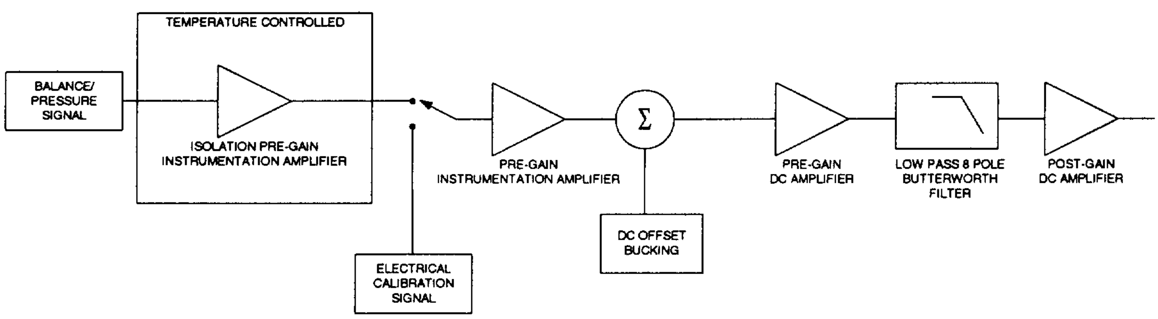

Fig. 8b Signal conditioning for data acquisition used after 1991

Table 1 Roll and pitch test conditions
(1989~1994)

Mode	Tests	Motion	Model	V_0(ft/s)	σ(°)	Δφ(°)	$φ_0$(°)	f(Hz), or roll rate and Δt in ramp motion	
Roll	Flow Vis.	Static	65,80/65	160,300,580,	15,17.5, 20,22.5, 25,30, 35,40,		-42,-35,-28,-21,-14,-7,-1,0,1,1.2,2.5,2.6, 3,4.6,4.8,5,5.2,5.4,6,6.5,7,7.5,8.4,9, 11,11.2,13,17,19,21,27,35,37,47,49, 51,55,57,58,59,60,61,62,67, 2~52,Δφ=2;		
		Dynamic	65,80/65	39.5,69,79,92, 121,138,158, 160,277,300, 345,395,580,	30,40	5,12,19,26,33,40	0,14,28,42	f(Hz)	1,1.1,2.2,4,4.4,7,7.7,
	Loads/pressure	Static	65,80/65 W+B(e)	300,330,580,	15,17.5,20, 25,30,33, 34,35,40, 44.5,-35		-90~90, Δφ=2.0; -23.8~23.8,Δφ=0.2; -10~27.5,Δφ=0.5; 49.5~54.5,Δφ=0.25; 61.5~64.5,Δφ=0.25; -85,-55,-49,-47,-45,-35,-25,-15,-11,-6.3, 0.9,1.1,1.9,2.1,2.9,3,3.1,3.7,3.9,4.1,4.9,5,5.1,5.9, 6.1,6.25,6.3,6.75,6.9,7.1,7.25,7.3,7.75,7.9,9,9.1, 9.9,10.9,11.1,11.9,13.9,14.1,14.5,27.8,27.9, 28.1,28.2,28.6,28.8,33,35,39,41.5,41.6,41.8, 41.9,42.1,42.9,43,45,47,48.5,55,55.5,56.1,56.3, 57,57.3,57.6,61,65,69.9,70.1,71.5,71.6,		
		Harmonic	65,80/65, W+B (c)	123,162, 280,300,330, 540,550, 580,	15,30,35,	2,3,4,5,6,8,10,12,15, 16,17,18,19,22,23,24, 26,27,30,31,32,33,34, 36,38,39,40,	-55,-35,-30,-28,-20,-10,-6,-2,0,1,2,2.5,3,4,5,6, 6.5,7,8,9.5,9.7,10,11,12,13,14, 15,18,18.5,20,21,21.5,25,27,28,30, 37.5,40,41,42,50,54,55,60,62,	f(Hz)	1.1,2.2,3.3,4,4.4,5.5,7,7.7,8.8,10,11,
		Ramp/vis.	65, W+B(e)	330	15,30,35	-30~-28,-26,-25,-24,-22,-20,-18,-16,-15, -30~-14,-12,-10,-5,0,5,10, -25~-20,-18,-16,-14,-12,-10,-8,-6,-4,25, -16~16, -12~12, -10~26,-24,-22,-20,-18,-17,-16,-15,-14,-12,12 -7~3, -4~4,6,7,9,10, -2~22, -1~0,2,3,5,7, 0~-7,9, 2~3,5,7,18, 3~-1,0,2, 5~8,10,17, 6~7,9,10,12,20, 7~-4,-1,0,2,3,4,5,6, 8~9,10,11,12,13,14,15,16,17,18,19,20, 9~10,12,20,26,29,35,60,80, 10~-30,-25.-20,-15,-10,-6,-5,-4,-2,0,4,5,6,7,9. 10~10,18,19,20,21,22,40, 12~9,24,26,29,35, 17~5,8,10, 19~21,22,40, 20~-20,6,7,9,10,12,18,19,32, 25~10,11,12,13,14,15,16,17,18,19,20,21,22,23, 30~-15,-10,-5,0,5,10,15,20,25, 35~9,10,12,26,29, 40~-40,9,10,18,19,21,22,40,53,56,61,63,64,70, 45~60, 56~68, 64~53,56,		roll rate (rad/ms)	0.5.1,4,7, 1.1,3.56,3.59,6.08,7.93,8.58,11.1,12.3, 13.6,16.1,16.7,17.3,18.5,21,23.5,25.4, 26,28.5,29.7,31,33.5,34.1,34.7,34.8,
								Δt(ms)	36,38.5,41,42.8,43.5,46,47.2,48.5,51, 51.6,52.2,53.5,55.9,58.4,60.3,60.7, 60.9,63.4,64.6,69,69.6,69.7,73.4,75.9, 77.7,78.4,82.1, 86.5,86.9,87.1,90.8, 95.2, 98,99.6,100,104,105,108,113,122, 123,126,130,134.5,139,140,157,174,176, 192,209,217,221.7,227,244,262,279, 296,309,314,331,348,349,366,,384, 401,419,436,454,489,523,541,558, 628,698,744,838,872,1082,1117,1239, 1396,1745,1780,2234,2478,2792,
	Free-to-roll			330,580	30,35		-2,-2.9,-3,-3.4,-3.5,-3.8,-6.8,-8.6,-9.8,-21, -23.1,-27,-27.7,-32.7,-35.6,-36.1, -37.8,-38.4, -43.8,-44.6,-45.7,-53.9,-54.1,-54.2, -55.6,-59.5,-59.8,-62.1,-62.7, -65.9,-68.6,-69.1,-69.3,-71.5,-80.8 0,4.9,5.2,5.6,6.9,9,18.9,18.6,20.9,22.5, 23.8,29.3,30.5,35.3,39.8,44.5,47.7,48.1, 50.6,50.8,53.7,55.2,56.2,58.1,59.1,59.2, 60.5,60.6,61.1,61.2,61.8,62.6,62.7,62.8, 63.6,64.2,64.5,64.8,64.9,65.3,65.7, 66.9,67.5,68.1,70.2,		

Table 1 Roll and pitch test conditions
(1989~1994)

Mode	Motion	Tests	Model	V_0(ft/s)	f(°)	Δα(°)	α_0(°)	Δt(ms)
Pitch	Flow vis.	static	65	330	0		0,1,2,5,10,12,14,15,17,20,22,24, 24.6,24.8,25,25.2,25.4,25.5,25.6, 25.8,26,26.2,27,28,29,30,31, 32.5,35,37,38,39,40,44,45,45.5,	
		Dynamic	65	330	0	10,20,30,40,50,60,70,80,90,	0,1,2,	47.4,50,72.3,75,97.2,100,105,122,147,150,172,194,199, 200,209,225,250,314,419,524,628,675,733,838,942, 1047,1257,1466,1885,
						-10,10,20,30,40,50,60,70,79,	10,	50,75,100,105,150,175,199,209,225,249,250,299,314, 349,399,419,524,628,675,733,838,
						-20,-18,-10,10,20,30,40,50,60,70,	20,	50,75,100,105,150,199,209,225,249,250,299, 314,349,419,524,628,675,733,
						-28,-20,-10,10,20,30,40,50,60,	30,	25,50,75,100,105,150,199,209,225,249,250,299, 314,349,419,524,628,675,
						-38,-30,-20,-10,10,20,30,40,50,	40,	25,50,75,100,105,120,150,199,209,225,249,250,299, 314,349,419,524,628,675,
						-48,-40,-30,-20,-10,10,20,30,38,	50,	50,75,100,105,150,199,209,225,244,249,250,314, 419,524,675,
						-59,-50,-40,-30,-20,-10,10,20,29,166+167	60,	50,75,100,105,125,150,209,225,250,314,419,524,628,675,
						-69,-60,-50,-40,-30,-20,-10,10,20,	70,	50,75,100,105,209,225,250,314,349,419,524,628,675,733,
						-80,-70,-60,-50,-40,-30,-20,-10,10,	80,	50,75,100,105,150,175,194,199,209,225,250,314,349,399, 419,524,628,675,733,838,
						-59,-49,	88,89,	75,225,244,294,344,524,628,675,
						-90-80-70-60-40-30-20-10	90,	105,209,225,250,314,419,628,675,733,838,942,
	Loads/pressure	Static	65	330,580,	0		0~90, Δα=1; 25.5,32.5; 34.5~48.5,Δα=1 24.6,24.8,25.2,25.4,25.6,25.8,26.2,38.8,39.2, 39.4,39.6,39.8,40.5,44.5,45.8,46.2,46.4,46.6	
		Harmonic	65	330	0	10,20,22,24,26,30,40,43,44,45,46,47,48, 50,60,70,80,90(88)	0,	49.9,75,99.7,104.7,149.6,199.5,209.4, 225,249.3,314.2,418.9, 523.6,628.3,675,733,837.8,942.5,
						39,49,59,	1,	47.4,72.3,97.2,122.2,147.1,172,194.5,225, 244.3,294.2,344.1,
						68,78,88,	2,	75,194.5,225,339.1,389,428.9,438.8,675,
						-10,10,12,14,16,20,30,40,50,60,70,80,	10,	49.9,75,99.7,104.7,149.6,174.5,199.5,209.4,225, 249.3,299.2,314.2,349.1,398.9,418.9,523.6, 628.3,675,733,837.8,
						-20,-10,10,20,23,24,25,26,27,30,40,50,60,70,	20,	49.9,75,99.7,104.7,149.6,199.5,209.4,225,249.3, 299.2,314.2,418.9,523.6,628.3,675,733,
						-30,-28,-20,-10,10,20,30,40,50,60,	30,	24.9,49.9,75,94.7,99.7,104.7,209.4,314.2, 418.9,523.6,
						-7.8,-9.8,-11.8,	35,	225,675,
						-40,-38,-30,-20,-10,10,20,30,40,50,	40,	24.9,49.9,74.8,75,99.7,104.7,119.7,149.6, 194.5,209.4,314.2,418.9,523.6,
						-17.8,-19.8,-21.8,	45,	225,675,
						-48,-40,-30,-20,-10,10,20,30,38,40,	50,	24.9,49.9,75,99.7,104.7,149.6,199.5,209.4,225, 244.3,314.2,418.9,523.6,
						-59,-50,-40,-30,-20,-10,10,20,29,30	60,	49.9,75,99.7,104.7,124.7,149.6,209.4, 225,249.3,299.2,314.2,418.9,523.6,628.3,675,
						-15.9,-17.9,-19.9,	65,	225,675,
						-70,-69,-60,-50,-40,-30,-20,-10,10,20,	70,	74.8,75,99.7,104.7,149.6,199.5,209.6,225, 249.3,314.2,349.1,418.9,523.6,628.3,733,675,
						-80,-70,-60,-50,-40,-30,-20,-10,10,	80,	75,99.7,104.7,149.6,174.5,194.5,199.5,209.6,225, 314.2,418.9,523.6,628.3,675,733,837.8,895.3,
						-37.9,-39.9,-41.9,	85,	225,675,
						-90,-80,-70,-60,-50,-40,-30,-20,-10,	90(88),	75,104.7,209.6,225,244.3,294.2,314.2,344.1, 393.9,418.9,523.6,628.3,675,733,837.8,942.5,
		Ramp	65	330	0	2, -2,	22,24,26,43,45,47, 23.2,25.2,27.2,45.1,47.1,49.1,	10.06 10.06

Table 2 Selected test cases

Case	Motion	σ°	Condition				Measurement	Run No.	Year	Tunnel
			φ°	Δφ	f	M				
1	static	15	-42~42			0.3	loads	L02211~02231	1991	SARL
2	static	15	0~42			0.3	pressure	L11001~11014	1991	SARL
3	harmonic	15	0.1	18.7	7.7	0.3	loads	L02158	1991	SARL
	harmonic	15	0.1	25.4	7.7	0.3	loads	L02157	1991	SARL
	harmonic	15	0.1	32.3	7.7	0.3	loads	L02156	1991	SARL
	harmonic	15	0.2	39.1	7.7	0.3	loads	L02155	1991	SARL
	harmonic	15	13.6	18.7	7.7	0.3	loads	L02178	1991	SARL
	harmonic	15	13.6	25.4	7.7	0.3	loads	L02177	1991	SARL
	harmonic	15	13.5	32.1	7.7	0.3	loads	L02176	1991	SARL
	harmonic	15	13.5	38.9	7.7	0.3	loads	L02175	1991	SARL
	harmonic	15	0.4	39.7	7.7	0.3	pressure	L11273	1991	SARL
	harmonic	15	0.4	32.8	7.7	0.3	pressure	L11274	1991	SARL
	harmonic	15	0.4	25.9	7.7	0.3	pressure	L11275	1991	SARL
	harmonic	15	0.4	19	7.7	0.3	pressure	L11276	1991	SARL
4	ramp	15	0~9			0.3	loads	DW3411	1994	SARL
	ramp	15	12~9			0.3	loads	DW3412	1994	SARL
	ramp	15	20~9			0.3	loads	DW3413	1994	SARL
	ramp	15	40~-40			0.3	loads	DW3414	1994	SARL
	ramp	15	0~9			0.3	loads	DW3415	1994	SARL
	ramp	15	12~9			0.3	loads	DW3416	1994	SARL
	ramp	15	20~9			0.3	loads	DW3417	1994	SARL
	ramp	15	40~-40			0.3	loads	DW3418	1994	SARL
	ramp	15	0~9			0.3	loads	DW3419	1994	SARL
	ramp	15	12~9			0.3	loads	DW3420	1994	SARL
	ramp	15	20~9			0.3	loads	DW3421	1994	SARL
	ramp	15	40~-40			0.3	loads	DW3422	1994	SARL
	ramp	15	0~9			0.3	loads	DW3423	1994	SARL
	ramp	15	12~9			0.3	loads	DW3424	1994	SARL
	ramp	15	20~9			0.3	loads	DW3425	1994	SARL
	ramp	15	40~-40			0.3	loads	DW3426	1994	SARL
5	static	30	-64~64			0.3	loads	SW01000~1141	1994	SARL
6	harmonic	30	0	28.2	10	0.3	loads	L00371	1989	IAR
	harmonic	30	-0.1	18.4	7	0.3	Loads	L00354	1989	IAR
	harmonic	30	0	18.4	7	0.3	pressure	L10290	1990	IAR
	harmonic	30	28	31.9	10	0.3	loads	L00384	1989	IAR
	harmonic	30	14	18.5	7	0.3	loads	L00359	1989	IAR
	harmonic	30	14	18.5	7	0.3	pressure	L10293	1990	IAR
7	ramp	30	-16~16			0.3	loads	DW3000	1994	SARL
	ramp	30	16~-16			0.3	loads	DW3001	1994	SARL
	ramp	30	-16~16			0.3	loads	DW3002	1994	SARL
	ramp	30	16~-16			0.3	loads	DW3003	1994	SARL
	ramp	30	-16~16			0.3	loads	DW3004	1994	SARL
	ramp	30	16~-16			0.3	loads	DW3005	1994	SARL
	ramp	30	-16~16			0.3	loads	DW3006	1994	SARL
	ramp	30	16~-16			0.3	loads	DW3007	1994	SARL
	ramp	30	-4~4			0.3	loads	DW3036	1994	SARL
	ramp	30	-4~6			0.3	loads	DW3037	1994	SARL
	ramp	30	-4~7			0.3	loads	DW3038	1994	SARL
	ramp	30	-4~4			0.3	loads	DW3039	1994	SARL
	ramp	30	-4~6			0.3	loads	DW3040	1994	SARL
	ramp	30	-4~7			0.3	loads	DW3041	1994	SARL
	ramp	30	-4~4			0.3	loads	DW3042	1994	SARL
	ramp	30	-4~6			0.3	loads	DW3043	1994	SARL
	ramp	30	-4~7			0.3	loads	DW3044	1994	SARL
	ramp	30	7~-4			0.3	loads	DW3050	1994	SARL
	ramp	30	7~-4			0.3	loads	DW3053	1994	SARL
	ramp	30	7~-4			0.3	loads	DW3055	1994	SARL
8	static	35	-60~68			0.3	loads	SW1142~1314	1994	SARL
9	harmonic	35	0	5.2	4	0.3	loads	L01360	1989	IAR
	harmonic	35	0	5.2	4	0.3	pressure	L10379	1990	IAR
	harmonic	35	33.6	28	7	0.3	loads	L1111	1989	IAR
	harmonic	35	33.8	27.9	7	0.3	pressure	L10447	1990	IAR
10	forced	30	64.5			0.3	pressure	TW0001	1991	SARL
	free-to-roll	30	53			0.3	pressure	TW0016	1991	SARL
		35	66.7			0.3	pressure	TW0032	1991	SARL
		35	53			0.3	pressure	TW0036	1991	SARL

Table 3 Electronic data file index

Page	Case	Motion	Data	Measurement	Run No.	File Name
1	1	static	Case 1 (Data and Test Conditions)	loads	L02211-L02231	data-cs3-1-2-3
	2	static	Case 2 (Data and Test Conditions)	pressure	L11000-L11014	
	3	harmonic	Case 3 (Test Conditions)	loads/pressure		
2-6			Case 3 (Data Run No. L02158)	loads	L02158	data-case3 / c3-2
7-11			Case 3 (Data Run No. L02157)	loads	L02157	
12-16			Case 3 (Data Run No. L02156)	loads	L02156	
17-21			Case 3 (Data Run No. L02155)	loads	L02155	
22-26			Case 3 (Data Run No. L02178)	loads	L02178	
27-31			Case 3 (Data Run No. L02177)	loads	L02177	
32-36			Case 3 (Data Run No. L02176)	loads	L02176	
37-41			Case 3 (Data Run No. L02175)	loads	L02175	
42-46			Case 3 (Data Run No. L11273)	pressure	L11273	data-case3 / c3-3
47-51			Case 3 (Data Run No. L11274)	pressure	L11274	
52-56			Case 3 (Data Run No. L11275)	pressure	L11275	
57-61			Case 3 (Data Run No. L11276)	pressure	L11276	
62	4	ramp	Case 4 (Test Conditions)	loads		data-case4 / c4-1
63-67			Case 4 (Data Run No. DW03411)	loads	DW03411	data-case4 / c4-2
68-72			Case 4 (Data Run No. DW03412)	loads	DW03412	
73-77			Case 4 (Data Run No. DW03413)	loads	DW03413	
78-82			Case 4 (Data Run No. DW03414)	loads	DW03414	
83-87			Case 4 (Data Run No. DW03415)	loads	DW03415	
88-92			Case 4 (Data Run No. DW03416)	loads	DW03416	
93-97			Case 4 (Data Run No. DW03417)	loads	DW03417	
98-102			Case 4 (Data Run No. DW03418)	loads	DW03418	
103-107			Case 4 (Data Run No. DW03419)	loads	DW03419	
108-112			Case 4 (Data Run No. DW03420)	loads	DW03420	
113-117			Case 4 (Data Run No. DW03421)	loads	DW03421	
118-122			Case 4 (Data Run No. DW03422)	loads	DW03422	
123-127			Case 4 (Data Run No. DW03423)	loads	DW03423	
128-132			Case 4 (Data Run No. DW03424)	loads	DW03424	
133-137			Case 4 (Data Run No. DW03425)	loads	DW03425	
138-142			Case 4 (Data Run No. DW03426)	loads	DW03426	
143-146	5	static	Case 5 (Data and Test Conditions)	loads	SW01000-01316	data-case5 / c5-1
147	6	harmonic	Case 6 (Test Conditions)	loads/pressure		data-case6 / c6-1
148-152			Case 6 (Data Run No. L00371)	loads	L00371	data-case6 / c6-2
153-157			Case 6 (Data Run No. L00354)	loads	L00354	
158-162			Case 6 (Data Run No. L10290)	pressure	L10290	data-case6 / c6-3
163-167			Case 6 (Data Run No. L00384)	loads	L00384	data-case6 / c6-4
168-172			Case 6 (Data Run No. L00359)	loads	L00359	
173-177			Case 6 (Data Run No. L10293)	pressure	L10293	data-case6 / c6-5
178	7	ramp	Case 7 (Test Conditions)	loads		data-case7 / c7-1
179-183			Case 7 (Data Run No. DW03000)	loads	DW03000	data-case7 / c7-2
184-188			Case 7 (Data Run No. DW03001)	loads	DW03001	
189-193			Case 7 (Data Run No. DW03002)	loads	DW03002	
194-198			Case 7 (Data Run No. DW03003)	loads	DW03003	
199-203			Case 7 (Data Run No. DW03004)	loads	DW03004	
204-208			Case 7 (Data Run No. DW03005)	loads	DW03005	
209-213			Case 7 (Data Run No. DW03006)	loads	DW03006	
214-218			Case 7 (Data Run No. DW03007)	loads	DW03007	
219-223			Case 7 (Data Run No. DW03036)	loads	DW03036	
224-228			Case 7 (Data Run No. DW03037)	loads	DW03037	

Table 3(cont.) Electronic data file index

Page	Case	Motion	Data	Measurement	Run No.	File Name
229-233	7	ramp	Case 7 (Data Run No. DW03038)	loads	DW03038	data-case7 / c7-2
234-238			Case 7 (Data Run No. DW03039)	loads	DW03039	
239-243			Case 7 (Data Run No. DW03040)	loads	DW03040	
244-248			Case 7 (Data Run No. DW03041)	loads	DW03041	
249-253			Case 7 (Data Run No. DW03042)	loads	DW03042	
254-258			Case 7 (Data Run No. DW03043)	loads	DW03043	
259-263			Case 7 (Data Run No. DW03044)	loads	DW03044	
264-268			Case 7 (Data Run No. DW03050)	loads	DW03050	
269-273			Case 7 (Data Run No. DW03053)	loads	DW03053	
274-278			Case 7 (Data Run No. DW03055)	loads	DW03055	
279-281	8	static	Case 8 (Data and Test Conditions)		SW01142-01262	data-case8 / c8-1
282	9	harmonic	Case 9 (Test Conditions)	loads/pressure		data-case9 / c9-1
283-287			Case 9 (Data Run No. L01360)	loads	L01360	data-case9 / c9-2
288-292			Case 9 (Data Run No. L10379)	pressure	L10379	data-case9 / c9-3
293-297			Case 9 (Data Run No. L01111)	loads	L01111	data-case9 / c9-4
298-302			Case 9 (Data Run No. L10447)	pressure	L10447	data-case9 / c9-5
303	10	forced free-to-roll	Case 10 (Test Conditions)	pressure		data-case10 / c10-1
304-309			Case 10 (Data Run No. TW00001 / TT00001)	pressure	TW00001 / TT00001	data-case10 / c10-2
310-315			Case 10 (Data Run No. TW00009 / TT00009)	pressure	TW00009 / TT00009	data-case10 / c10-2
316-321			Case 10 (Data Run No. TW00032 / TT00040)	pressure	TW00032 / TT00040	data-case10 / c10-2
322-327			Case 10 (Data Run No. TW00046 / TT00034)	pressure	TW00046 / TT00034	data-case10 / c10-2

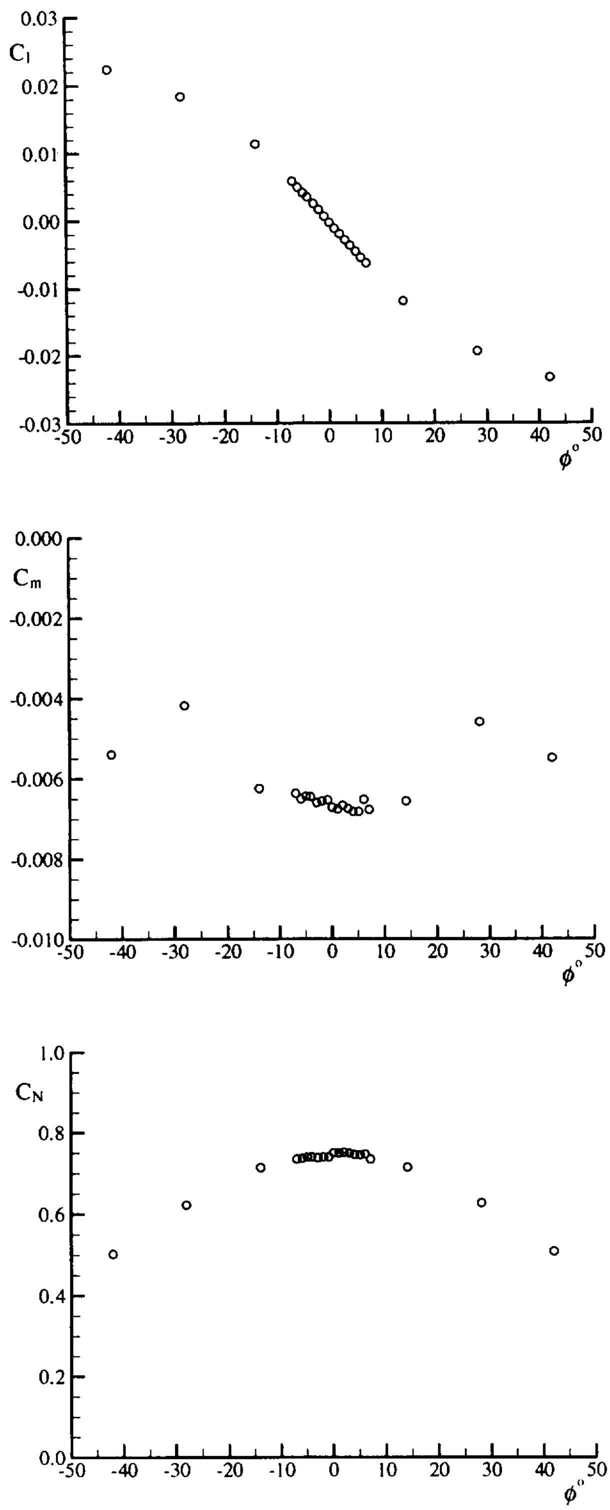

Fig.Case 1 Run No. L02211 - L02231

$\sigma = 15^\circ$ $P_o = 13.355$ psi
$\phi = -42^\circ \sim +42^\circ$
$M = 0.29$

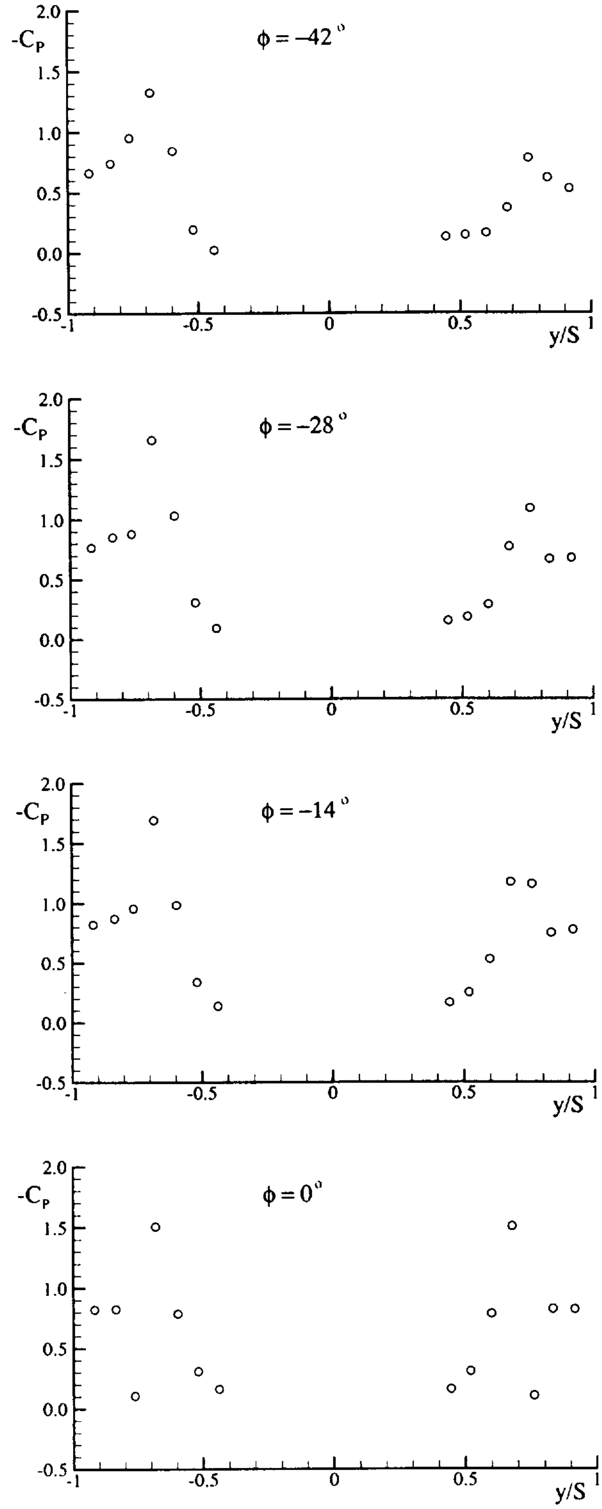

Fig.Case 2-1 Run No. 11000 - L11014

$\sigma = 15^\circ$ $P_o = 13.427$ psi
$T_o = 22.2^\circ$ $q = 0.806$ psi
$M = 0.29$ $P_{atm} = 14.254$ psi

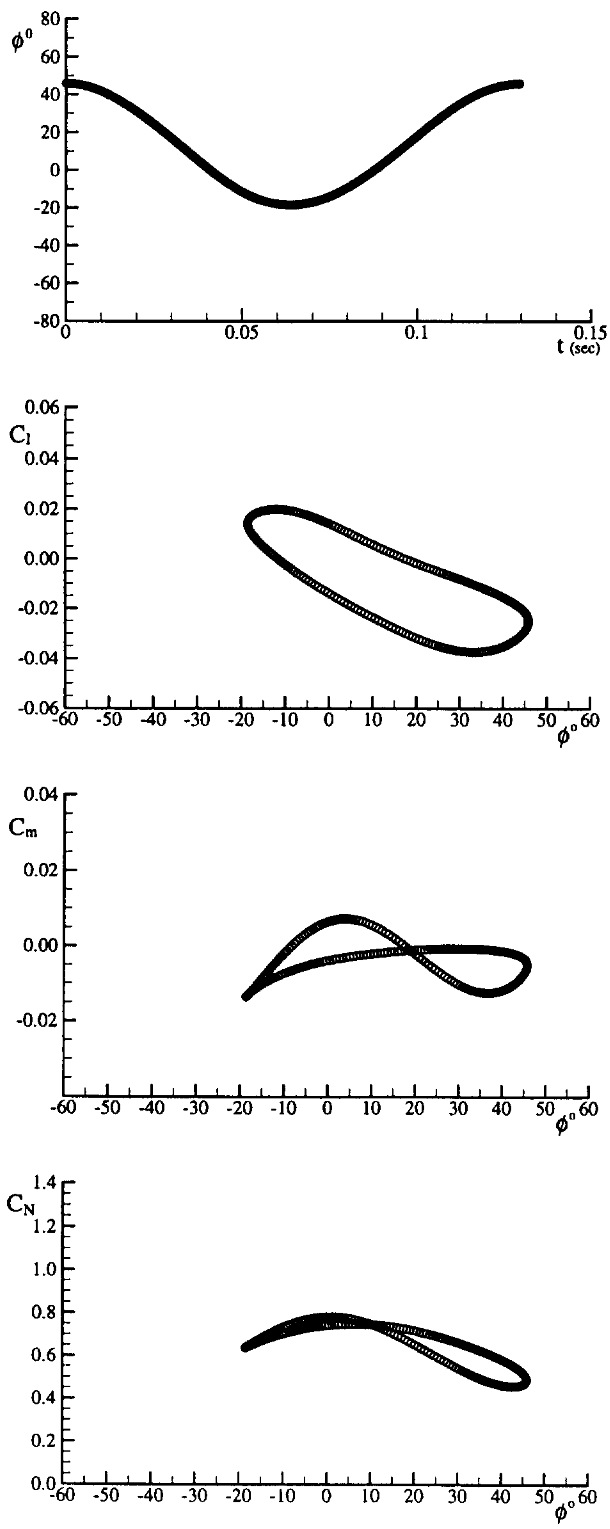

Fig.Case 3-7 Run No. L02176

$\sigma = 15^\circ$ $f = 7.7$
$\phi_o = 13.645^\circ$ $P_o = 13.427$ psi
$\Delta\phi = 32.176^\circ$ $M = 0.29$

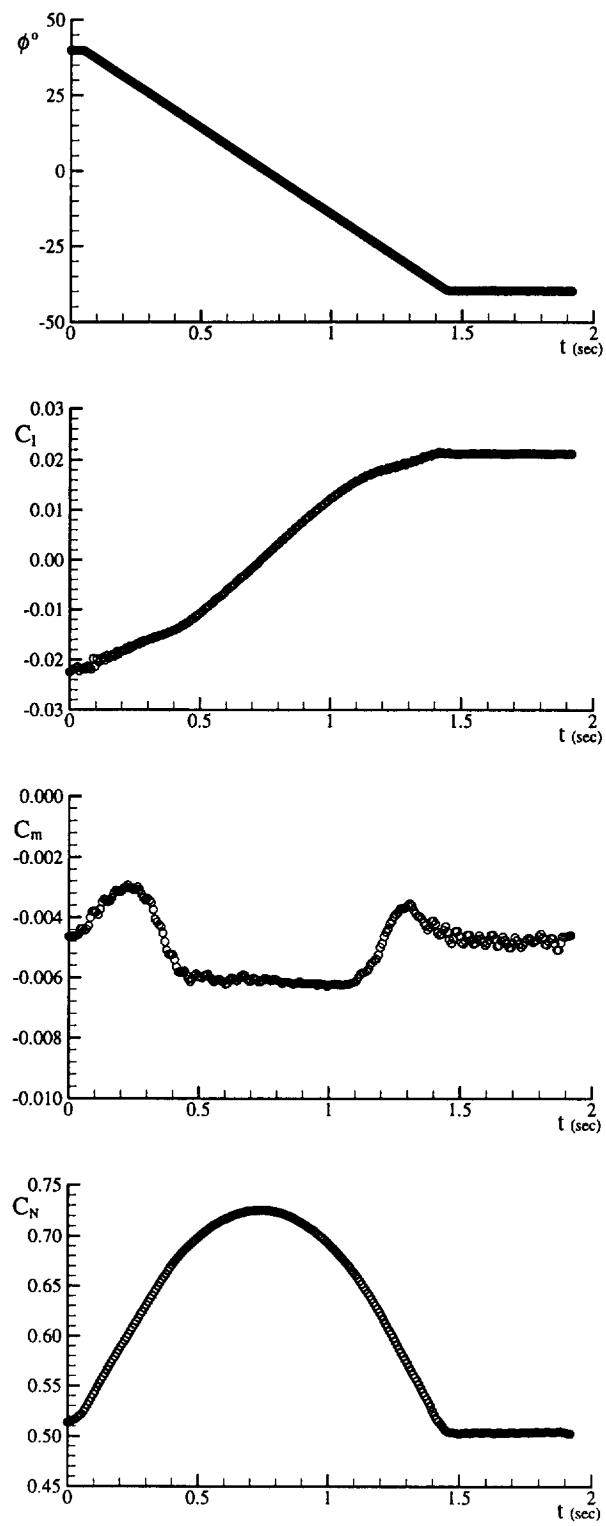

Fig.Case 4-8 Run No. DW03418

$\sigma = 15^\circ$ $\dot{\Phi} = 1$ rad/sec
$\phi_o = 40^\circ$ $P_o = 13.378$ psi
$\phi_l = -40^\circ$ $M = 0.29$

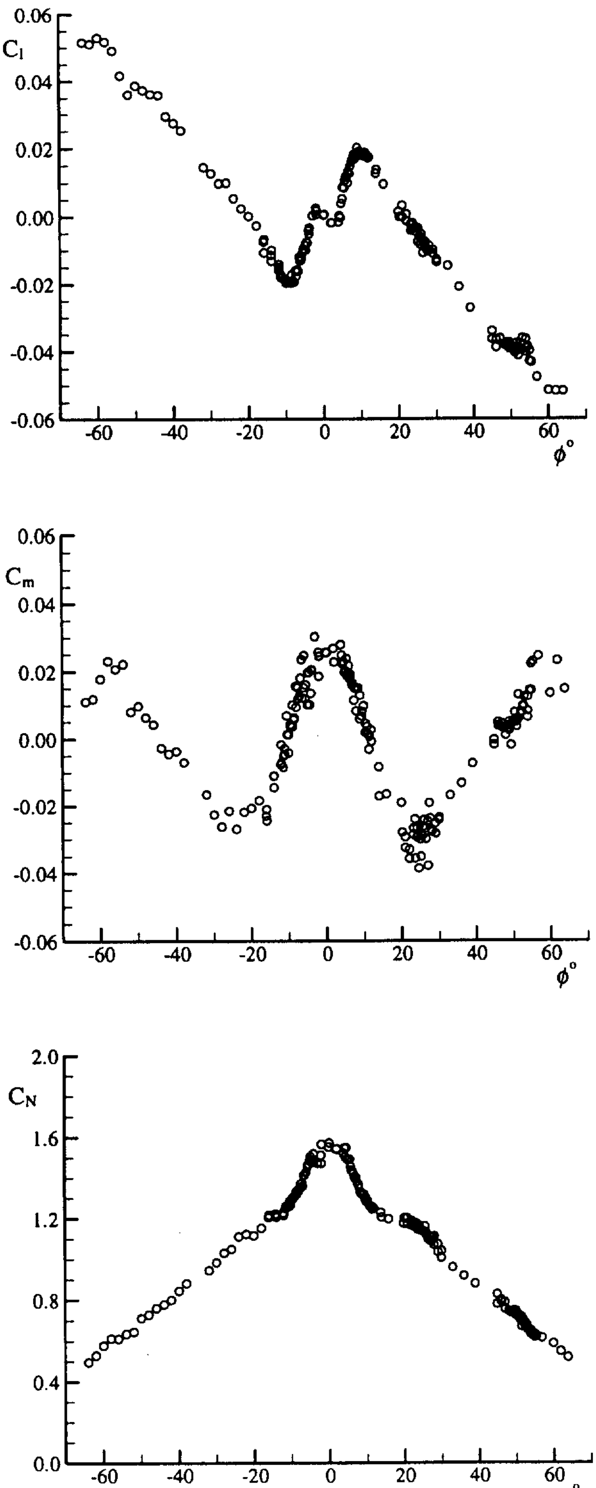

Fig.Case 5 Run No. SW01000 - 01141
SW01290 - 01420

$\sigma = 30^{\circ}$ $P_o = 13.355$ psi
$\phi = -64^{\circ} \sim +64^{\circ}$ $M = 0.29 \sim 0.31$

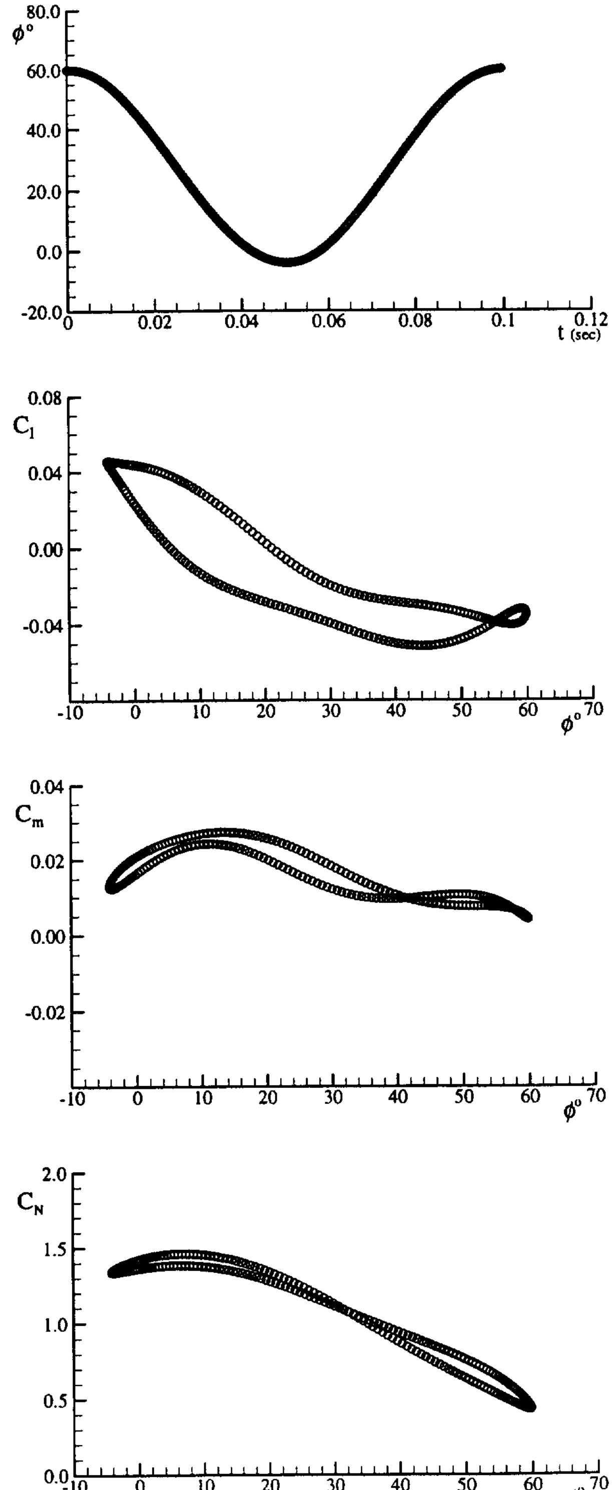

Fig.Case 6-4 Run No. L00384

$\sigma = 30^{\circ}$ $f = 10$
$\phi_o = 27.359^{\circ}$ $P_o = 14.602$ psi
$\Delta\phi = 31.502^{\circ}$ $M = 0.264$

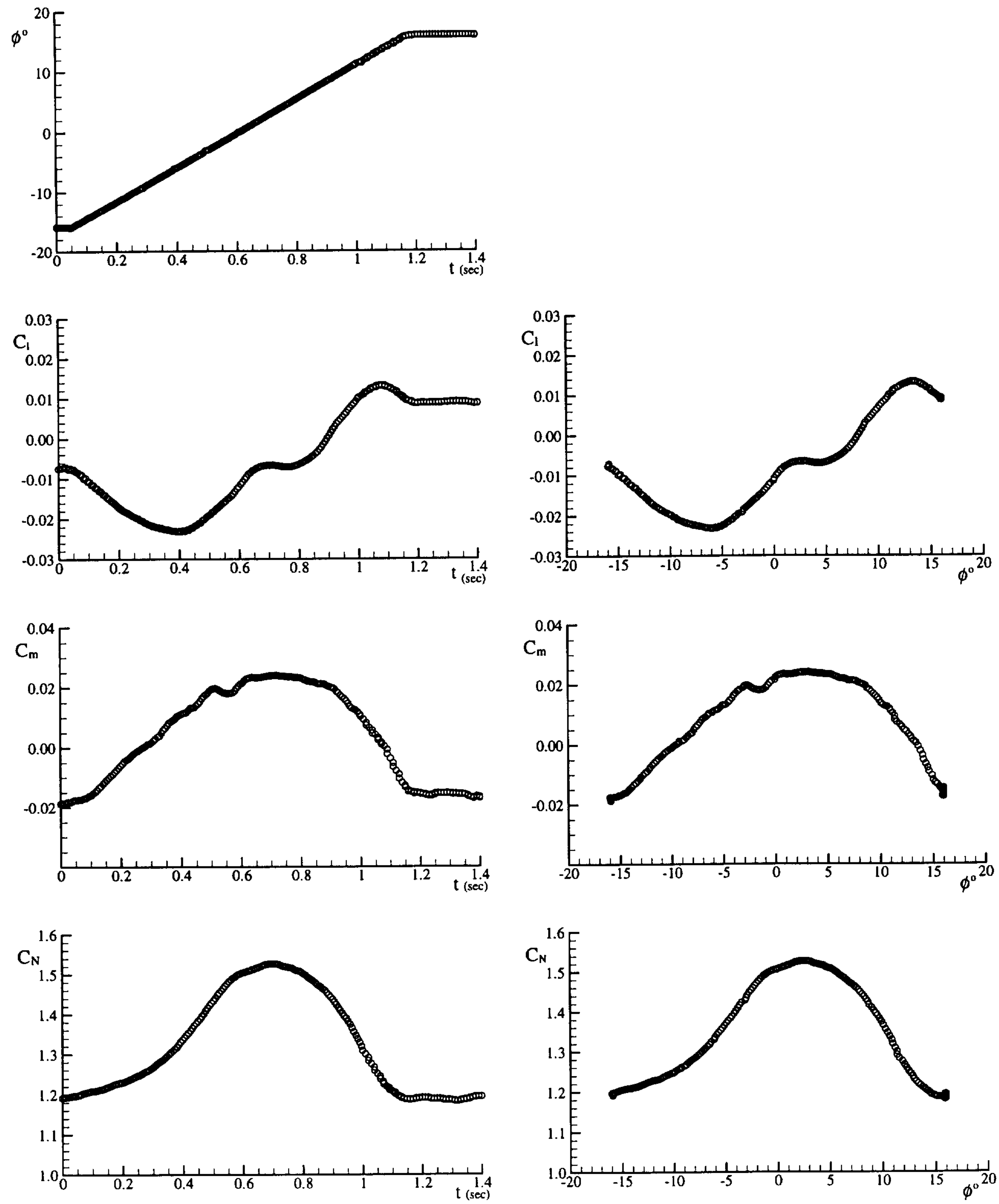

Fig.Case 7-1 Run No. DW03000

$\sigma = 30^\circ$	$\dot{\Phi} = 0.5$ rad/sec
$\phi_o = -16^\circ$	$P_o = 13.574$ psi
$\phi_1 = 16^\circ$	$M = 0.30$

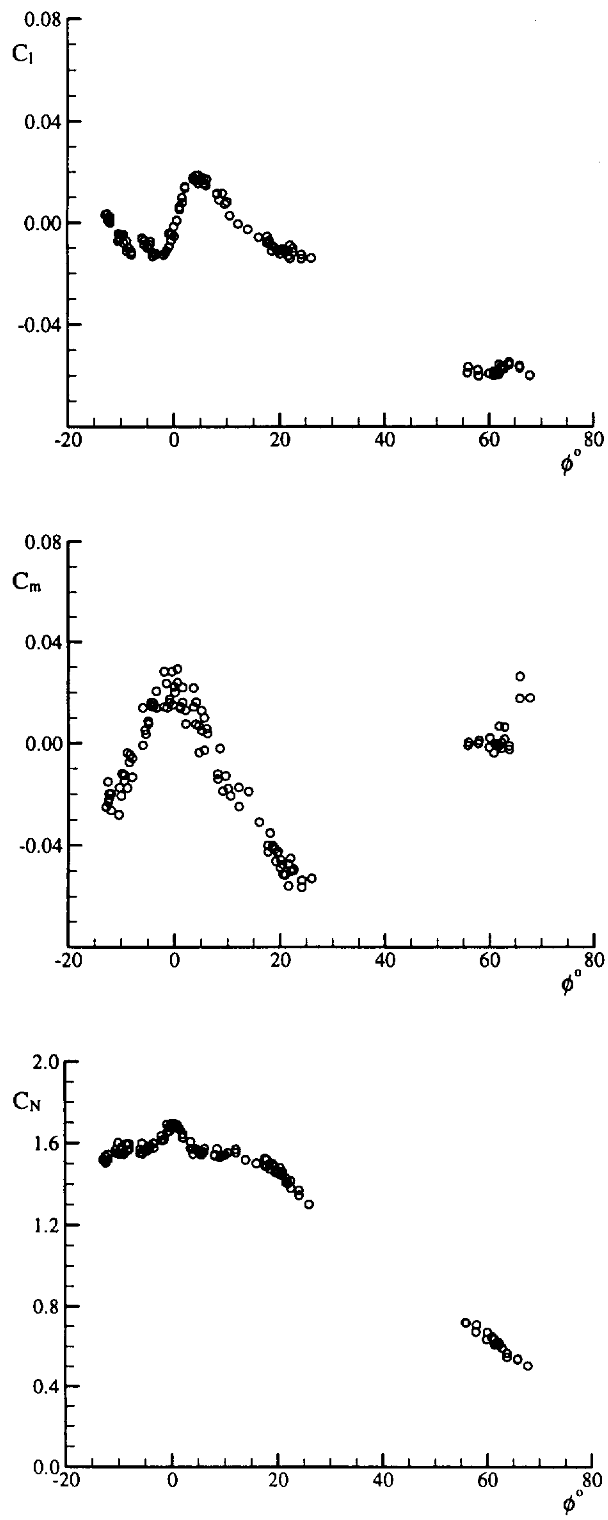

Fig.Case 8 Run No. SW01142 - 01262

$\sigma = 35°$ M = 0.30

$\phi = -12° \sim +68°$

$P_o = 13.342 \sim 13.432$ psi

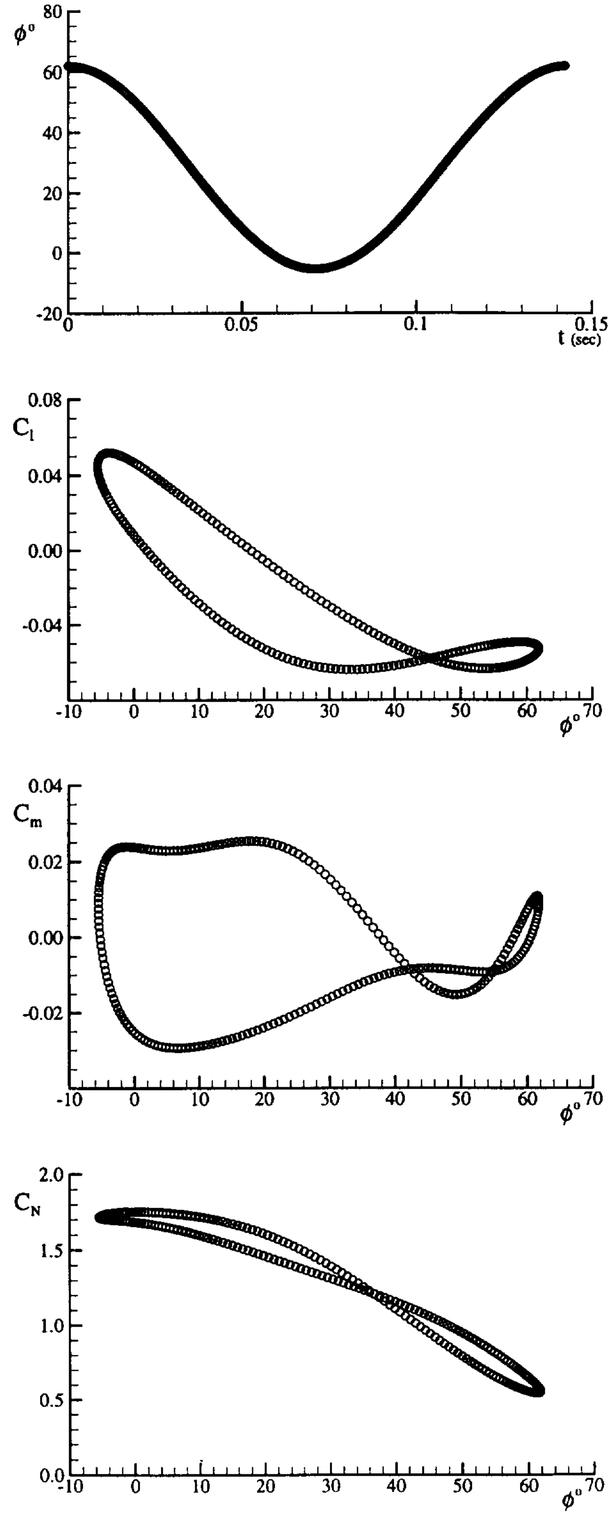

Fig.Case 9-3 Run No. L01111

$\sigma = 35°$ f = 7

$\phi_o = 28.176°$ $P_o = 14.672$ psi

$\Delta\phi = 33.646°$ M = 0.264

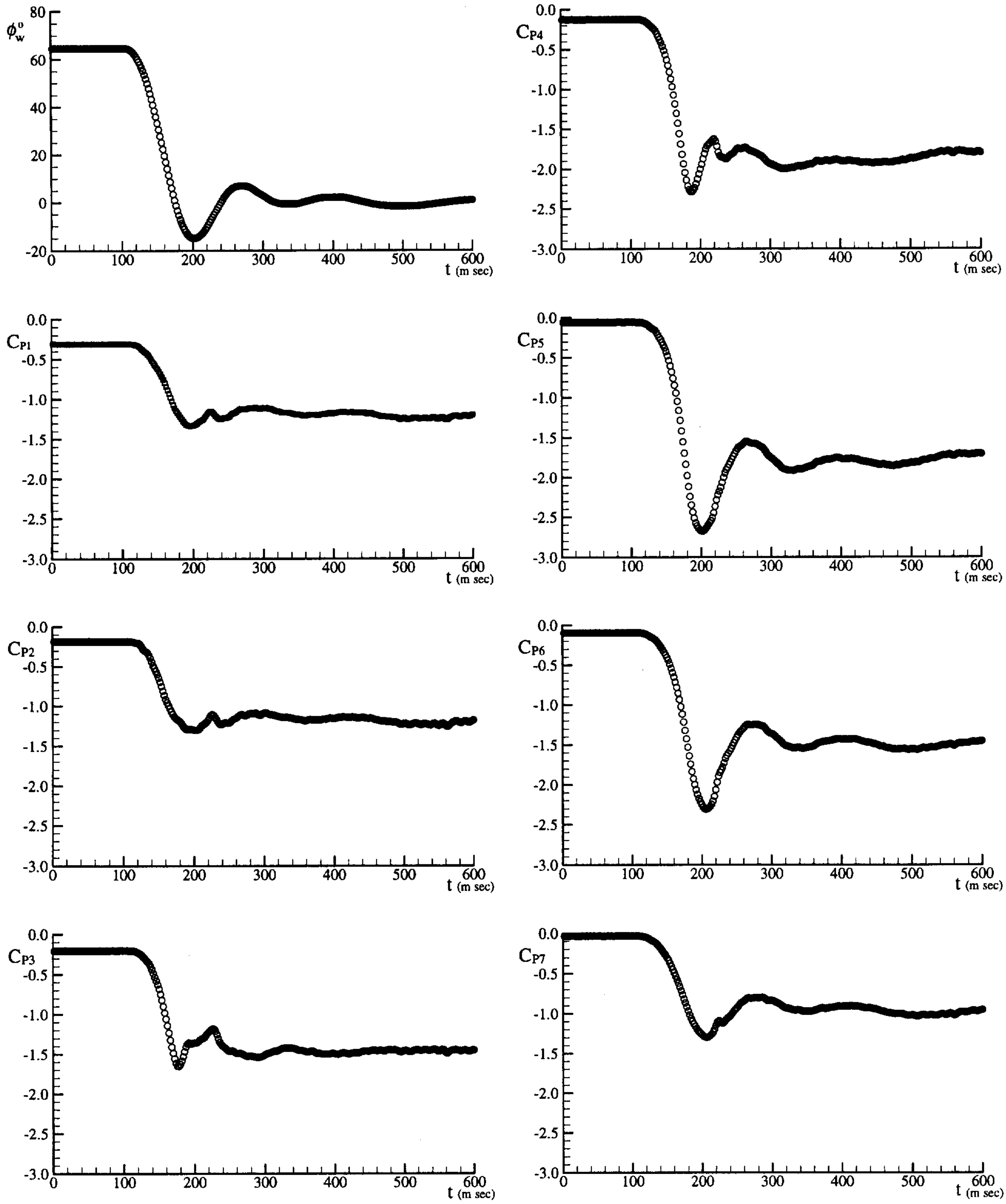

Fig.Case 10-1 Run No. TW00001 / TT00001

$\sigma = 30^\circ$ M = 0.27 (TW00001)

$\phi_o = 64.000^\circ$ M = 0.00 (TT00001)

$P_o = 13.572$ psi

Table 4 Examples of lay-out of data files

Case 1 (Data and Test Conditions)

Run No.	σ°	ϕ°	C_l	C_m	C_N	C_Y	C_n	T_0 (°C)	P_0 (psi)	M	V_0 (ft/sec)	q (psi)	atm (psi)
L02211	15	-41.995	0.0224	-0.0054	0.502	0.01275	-0.00007	20.5	13.355	0.29	329.0	0.799	14.181
L02212	15	-28.044	0.0184	-0.0042	0.623	0.01009	-0.00025	20.5	13.355	0.29	329.0	0.799	14.181
L02213	15	-13.912	0.0113	-0.0062	0.713	0.00491	0.00003	20.5	13.355	0.29	329.0	0.799	14.181

Case 2 (Data and Test Conditions)

Run No.	σ°	ϕ°	Cp_1	Cp_2	Cp_3	Cp_4	Cp_5	Cp_6	Cp_7	T_0 °C	P_0 (psi)	M	V_0 (ft/sec)	q (psi)	atm (psi)
L11000	15	-41.881	-0.6722	-0.7502	-0.9437	-1.3365	-0.8449	-0.1978	-0.0265	22.2	13.427	0.29	331.0	0.806	14.254
L11001	15	-27.975	-0.7451	-0.8353	-0.9074	-1.6457	-1.0368	-0.3017	-0.0835	22.2	13.427	0.29	331.0	0.806	14.254
L11002	15	-13.909	-0.8262	-0.8823	-0.9569	-1.6905	-0.9928	-0.3431	-0.1414	22.2	13.427	0.29	331.0	0.806	14.254

Case 3 (Data Run No. L02158)

σ°	ϕ_0°	$\Delta\phi^\circ$	f	P_0 (psi)	M	V_0 (ft/sec)	q (psi)
15	-0.046	18.752	7.7	13.398	0.29	329	0.856

No.	Time (sec)	$\phi(t)^\circ$	C_l	C_m	C_N	C_y	C_n
1	0.000000	18.704	-0.0163	-0.0064	0.654	-0.02070	0.00177
2	0.000507	18.690	-0.0165	-0.0064	0.654	-0.02088	0.00176
3	0.001015	18.666	-0.0167	-0.0064	0.654	-0.02104	0.00175

Case 3 (DataRun No. L11273)

σ°	ϕ_0°	$\Delta\phi^\circ$	f	T_0 (°C)	P_0 (psi)	M	V_0 (ft/sec)	q (psi)	atm (psi)
15	-0.397	39.759	7.7	24.9	13.456	0.29	333.05	0.813	14.297

No.	Time (sec)	$\phi(t)^\circ$	Cp_1	Cp_2	Cp_3	Cp_4	Cp_5	Cp_6	Cp_7
1	0.000000	39.326	-0.5731	-0.6263	-0.8655	-0.4511	-0.1785	-0.1421	-0.1335
2	0.000507	39.272	-0.5755	-0.6297	-0.8688	-0.4543	-0.1804	-0.1437	-0.1349
3	0.001015	39.193	-0.5780	-0.6331	-0.8725	-0.4579	-0.1825	-0.1454	-0.1363

Case 4 (Data Run No. DW03413)

σ°	ϕ_0°	ϕ_1°	$\dot{\phi}$ (rad/sec)	P_0 (psi)	M	V_0 (ft/sec)	q (psi)
15	20	9	0.5	13.378	0.30	336.4	0.856

No.	Time (sec)	$\phi(t)^\circ$	C_l	C_m	C_N	C_y	C_n
1	0.00000	19.978	-0.0150	-0.0057	0.671	-0.00668	0.00033
2	0.00357	19.978	-0.0150	-0.0057	0.671	-0.00574	0.00061
3	0.00714	19.978	-0.0150	-0.0057	0.671	-0.00798	0.00048

Case 5 (Data and Test Conditions)

Run No.	σ°	ϕ°	C_l	C_m	C_N	C_Y	C_n	T_0 (°C)	P_0 (psi)	M	V_0 (ft/sec)	q (psi)	atm (psi)
SW01000	30	-15.978	-0.0107	-0.0210	1.207	-0.03297	0.00314	19.3	13.401	0.30	330.5	0.825	14.181
SW01001	30	-13.981	-0.0132	-0.0144	1.215	-0.11537	-0.00040	19.0	13.407	0.30	330.1	0.824	14.426
SW01002	30	-11.998	-0.0159	-0.0017	1.227	-0.05010	0.00196	18.9	13.400	0.30	331.5	0.830	14.263

Case 10 (Data Run No. TW00001 / TT00001)

Run No.	σ°	ϕ_0°	T_0 (°C)	M	P_0 (psi)	V_0 (ft/sec)	q (psi)	atm (psi)
TW00001	30	64.000	21.27	0.27	13.572	300.0	1.421	14.268
TT00001	30	64.000	25.65	0.00	13.572	0.0	0.000	13.543

Time (ms)	ϕ_w°	ϕ_t°	Cp_1	Cp_2	Cp_3	Cp_4	Cp_5	Cp_6	Cp_7
2	64.512	64.152	-0.3090	-0.1860	-0.2060	-0.1270	-0.0610	-0.0990	-0.0350
4	64.512	64.116	-0.3080	-0.1860	-0.2070	-0.1240	-0.0590	-0.0990	-0.0370
6	64.512	64.116	-0.3090	-0.1870	-0.2060	-0.1260	-0.0610	-0.0990	-0.0360

16C. LARGE-AMPLITUDE, HIGH-RATE ROLL OSCILLATIONS OF A 65° DELTA WING AT HIGH INCIDENCE

Neal M. Chaderjian and Lewis B. Schiff
NASA Ames Research Center
Moffett Field, California, U.S.A.

INTRODUCTION

The IAR/WL 65° delta wing experimental results provide both detail pressure measurements and a wide range of flow conditions covering from simple attached flow, through fully developed vortex and vortex burst flow, up to fully-stalled flow at very high incidence. Thus, the Computational Unsteady Aerodynamics researchers can use it at different level of validating the corresponding code. In this section a range of CFD results are provided for the 65° delta wing at selected flow conditions. The time-dependent, three-dimensional, Reynolds-averaged, Navier-Stokes (RANS) equations are used to numerically simulate the unsteady vortical flow. Two sting angles and two large-amplitude, high-rate, forced-roll motions and a damped free-to-roll motion are presented. The free-to-roll motion is computed by coupling the time-dependent RANS equations to the flight dynamic equation of motion. The computed results are compared with experimental pressures, forces, moments and roll angle time history. In addition, surface and off-surface flow particle streaks are also presented.

LIST OF SYMBOLS AND DEFINITIONS

B	wing span, (in)
c	root chord, (in)
c_0	mean aerodynamic chord, (in)
C_p	pressure coefficient $=(p-p_0)/qs$
C_ℓ	rolling moment coefficient $=\ell/qsB$
C_N	normal force coefficient $=N/qs$
f	frequency, (Hz)
k	reduced frequency $=\pi fB/V_0$
ℓ	rolling moment, (lbs-in)
M_∞	Mach number
m	pitching moment, (lbs-in)
N	normal force, (lbs)
n	yawing moment, (lbs-in)
p	pressure, (psi)
p_0	static pressure, (psi)
q	dynamic pressure, (psi)
Re	Reynolds number, based on root chord
s	wing area, (in^2)
S	semi span, (in)
T_0	static temperature, (°C)
t	time (sec)
V_0	free stream velocity (ft/sec)
x,y,z	body axes coordinates
X_{Cp}	center of pressure in x axis, (in)
α	angle of attack, (°)
σ	sting angle (between body axis and tunnel axis), (°)
ϕ	roll angle, (°)
ϕ_0	mean roll angle or initial roll angle, (°)
$\Delta\phi$	amplitude, (°)

$\dot{\phi}$	roll angular rate, (rad/sec)
CCW	counter clockwise
CW	clockwise
CFD	Computational Fluid Dynamics
NSS	Navier-Stokes Simulation
RANS	Reynolds-averaged, Navier-Stokes Equations

FORMULARY

General Description of model

1.1	Designation	IAR Delta Wing
1.2	Derivation	IAR Dynamic Experimental Model
1.3	Type	Full model
1.4	References	Ref. 1 (Fig. 1)

Model Geometry

2.1	Planform	Delta wing-body, See Fig. 1
2.2	Aspect ratio	1.866
2.3	Mean aerodynamic chord	16.323 in
2.4	Root chord	24.485 in
2.5	Span	22.835 in
2.6	Reference center	13.875 aft of the apex
2.7	Leading edge sweep	65°
2.8	Trailing edge sweep	0°
2.9	Taper ratio	0
2.10	Twist	0°
2.11	Dihedral	0°
2.12	Area of planform	279.486 in^2
2.13	Leading-edge bevel (leeward)	9° (perpendicular to leading-edge)
2.14	Leading-edge bevel (windward)	9° (perpendicular to leading-edge)
2.15	Trailing edge bevel (leeward)	9° (perpendicular to trailing edge)
2.16	Trailing edge bevel (windward)	9° (perpendicular to trailing edge)
2.17	Leading-edge radius	0.020 in
2.18	Tolerance of leading-edge radius	±10%
2.19	Definition of profiles	0.375 inch thick flat-plate wing with double-bevelled (18° included angle) sharp leading and trailing edge
2.20	Center body	Ogive-cylinder
2.21	Form of wing-body junction	Bevelled, see Fig. 1
2.22	Form of wing tip	Sharp
2.23	Control surface details	None
2.24	Center-body diameter	3.150 in
2.25	Radius of forebody	$r = \sqrt{24.103^2 - (12.243 - x)^2} - 22.528$ in
2.26	References	Ref. 1 (Fig. 1)

CFD Grid Details

3.1 RANS grid size	67 axial x 209 circumferential x 49 normal points (baseline grid); 113 x 421 x 97 points (finest grid), See Fig. 2
3.2 Additional Remarks	Full-body grids used in all cases; zonal grids used in axial directio to fit machine memory; zonal boundaries are one-to-one matching

CFD Code used

4.1 RANS code	Novier-Stokes Simulation (NSS) code, Beam-Warming, block or diagonal, central differencing, blended 2nd- and 4th-order dissipation, reduced dissipation in boundary layer
4.2 Turbulence model	Baldwin-Lomax with Degani-Schiff modifications, no fixed transition
4.3 Computational time step	$3.62 \times 10^{-3} < \tau < 5.0 \times 10^{-3}$, 6.67×10^{-6} sec $< \Delta t < 9.0 \times 10^{-6}$ sec
4.4 Computation time	80 hours per oscillation cycle on a CRAY C-90 single processor - block version (15,000 steps per cycle of oscillation)
4.5 Additional remarks	Unsteady computation started with steady solution at ϕmax. Solution converged after 2-3 cycles
4.6 Reference on code	Ref. [5]

Model Motion

5.1 Mode of applied motion	Sinusoidal roll oscillations and free-to-roll motion about longitudinal axis of symmetry
5.2 Range of amplitude	28.2°, 31.9°, 40.0°
5.3 Reduced frequency	f = 7 Hz, 10 Hz; k = 0.14, 0.20
5.4 Additional Remarks	oscillations about ϕ_0 = 0.0°, 28.0°

Boundary Conditions

6.1 Mach Number	0.27
6.2 Reynolds Number	$Re_c = 3.67 \times 10^6$, based on root chord
6.3 Temperature	300° K
6.4 Range of model incidence	15° and 30°
6.5 Definition of model incidence	Model incidence defined relative to model axis of symmetry
6.6 Additional Remarks	Distance of far field boundary is 5 root chords normal to wing, 2 root chords upstream and downstream of wing

Data Presentation

7.1 Static Cases	Roll moment versus roll angle
	Normal force versus roll angle
	Center of pressure versus roll angle
	Leeward surface pressure distributions for various roll angles
	Surface flow patterns for various roll angles
	Vortex breakdown point versus roll angle
7.2 Forced Roll Oscillations	Instantaneous roll moment versus roll angle
	Instantaneous normal force versus roll angle
	Center of pressure versus roll angle
7.3 Free-to-Roll Oscillations	Roll angle history versus time
7.4 Sample illustrations	Fig. 3 to Fig. 10

7.5	Additional Remarks	All above quantities are compared against IAR experiments (Case No. 2, No. 3, No. 5, No. 6 and No. 10)

Personal contact for further information

Dr. Neal M. Chaderjian, T27B-2, NASA Ames Research Center, Moffett Field, California U. S. A
Phone: (650) 604-4472, E-mail: nchaderjian@mail.arc.nasa.gov

List of references

[1]. N. M. Chaderjian, "Navier-Stokes Prediction of Large-Amplitude Delta-Wing Roll Oscillations," *Journal of Aircraft*, Vol. 31, No. 6, pp. 1333-1340.

[2]. N. M. Chaderjian and L. B. Schiff, "Navier-Stokes Prediction of a Delta Wing in Roll with Vortex Breakdown," AIAA Paper 93-3495, 11th Applied Aerodynamics Conference, Monterey CA, August 1993.

[3]. N. M. Chaderjian and L. B. Schiff, "Numerical Simulation of Forced and Free-to-Roll Delta-Wing Motions," *Journal of Aircraft*, Vol. 33, No. 1, pp. 93-99.

[4]. N. M. Chaderjian and L. B. Schiff, "Navier-Stokes Analysis of a Delta Wing in Static and Dynamic Roll," AIAA Paper 95-1868, 13th Applied Aerodynamics Conference, San Diego, CA, June 1995.

[5]. N. M. Chaderjian, "Comparison of Two Navier-Stokes Codes for Simulating High-Incidence Vortical Flow", *Journal of Aircraft*, Vol. 30, No. 3, pp. 357-364.

[6]. E. S. Hanff and X. Z. Huang, "Roll-Induced Cross-Loads on a Delta Wing at High Incidence," AIAA Paper 91-3223, September 1991

[7]. E. S. Hanff and S.B. Jenkins, "Large-Amplitude High-Rate Roll Experiments on a Delta and Double Delta Wing," AIAA paper 90-0224, January 1990.

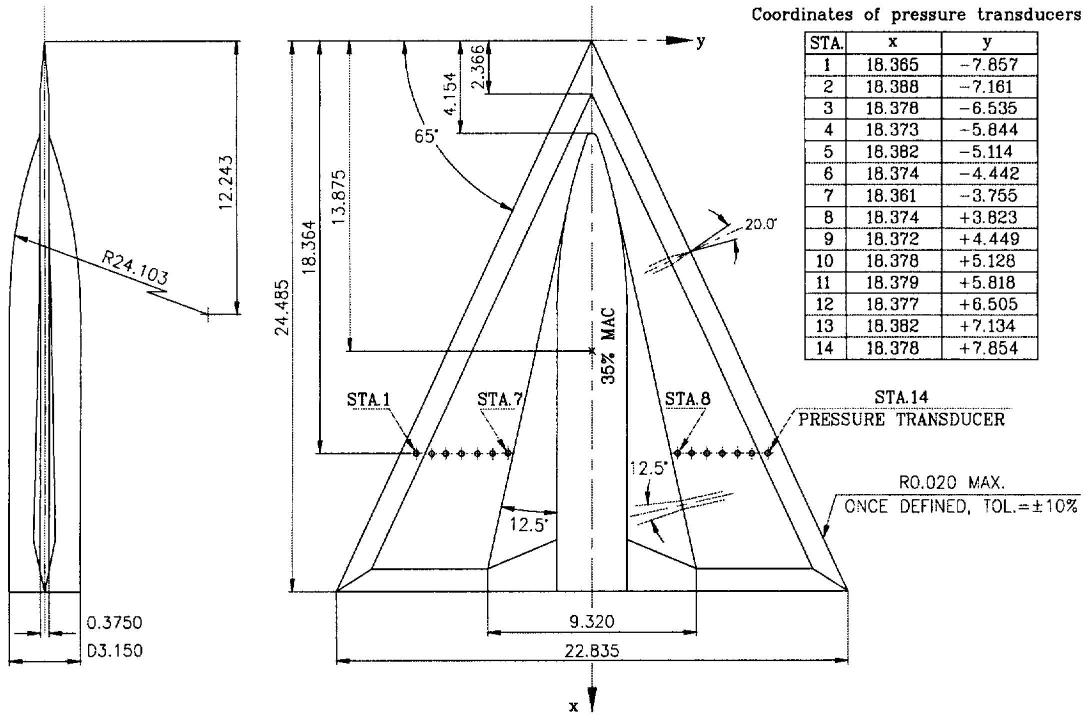

STA.	x	y
1	18.365	-7.857
2	18.388	-7.161
3	18.378	-6.535
4	18.373	-5.844
5	18.382	-5.114
6	18.374	-4.442
7	18.361	-3.755
8	18.374	+3.823
9	18.372	+4.449
10	18.378	+5.128
11	18.379	+5.818
12	18.377	+6.505
13	18.382	+7.134
14	18.378	+7.854

Fig. 1 65° delta wing model

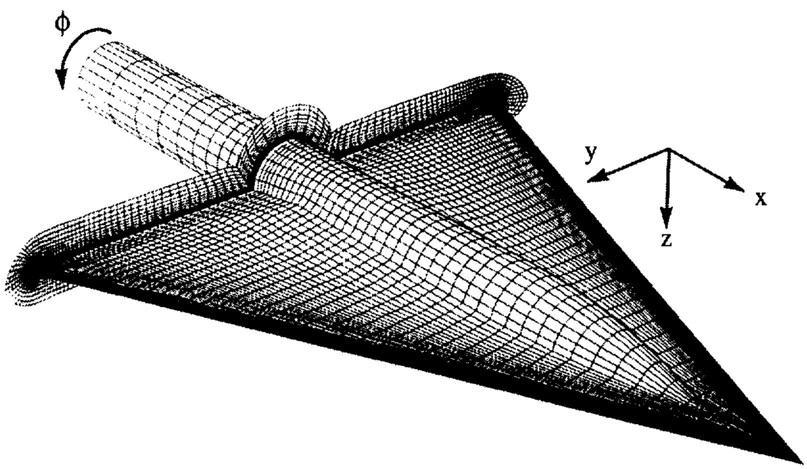

Fig. 2 Perspective view of the computational grid

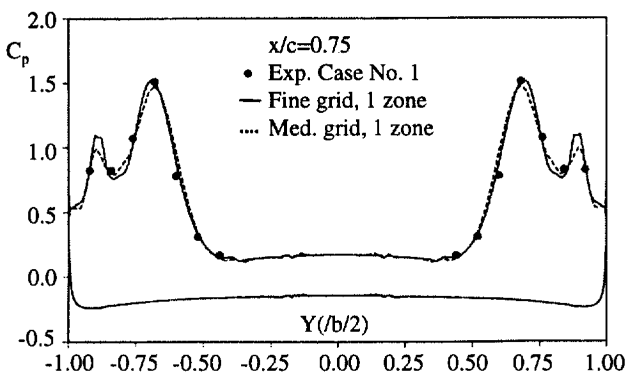

Fig. 3 Effects of grid refinement and zonal boundary condition treatment on the pressure coefficients
M_∞=0.27, α=15°, φ=0, Re=3.67 million

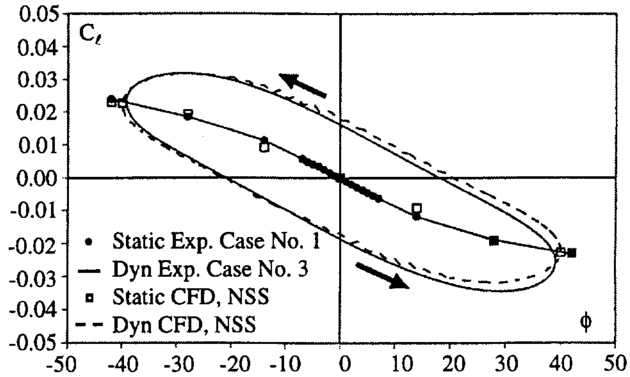

Fig. 4 Comparison of computational and experimental rolling moment coefficients for dynamic and static cases
M_∞=0.27, σ=15°, Δφ=40°,k=0.14, Re=3.67 million

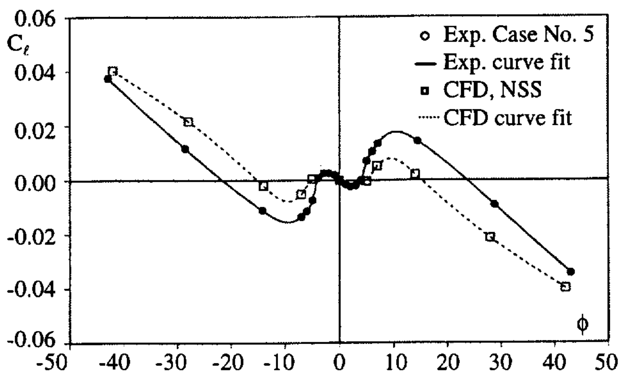

Fig. 5 Comparison of mean computed and experimental rolling moment coefficients for static roll angles
M_∞=0.27, σ=30°, Re=3.67 million

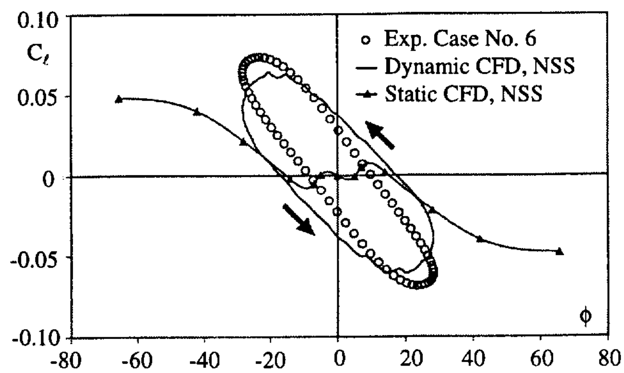

Fig. 6 Dynamic and static rolling-moment coefficients
M_∞=0.27, σ=30°, ϕ_0=0°, Δφ=28.2°,k=0.20, Re=3.67 million

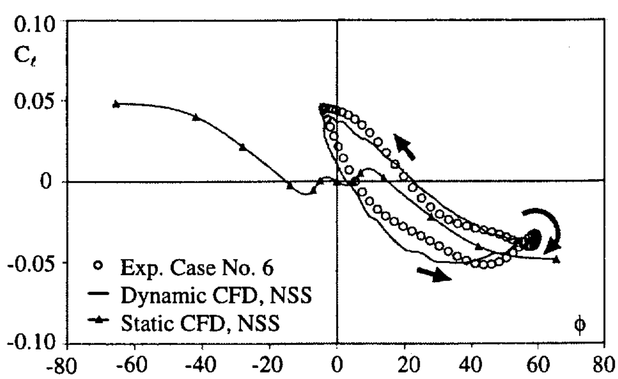

Fig. 7 Dynamic and static rolling-moment coefficients
M_∞=0.27, σ=30°, ϕ_0=28°, Δφ=31.9°, Re=3.67 million

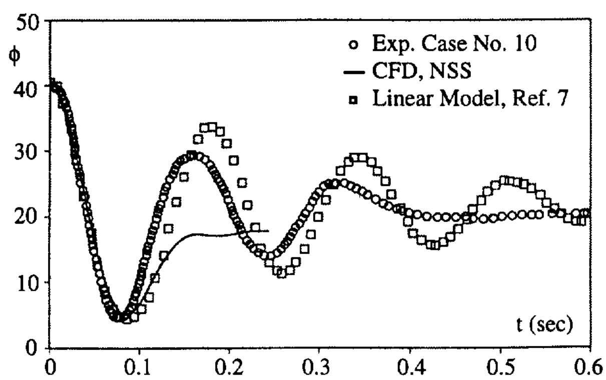

Fig. 8 Time history of roll angle for free-to-roll motion
M_∞=0.27, σ=30°, ϕ_0=40.5°, Re=3.67 million

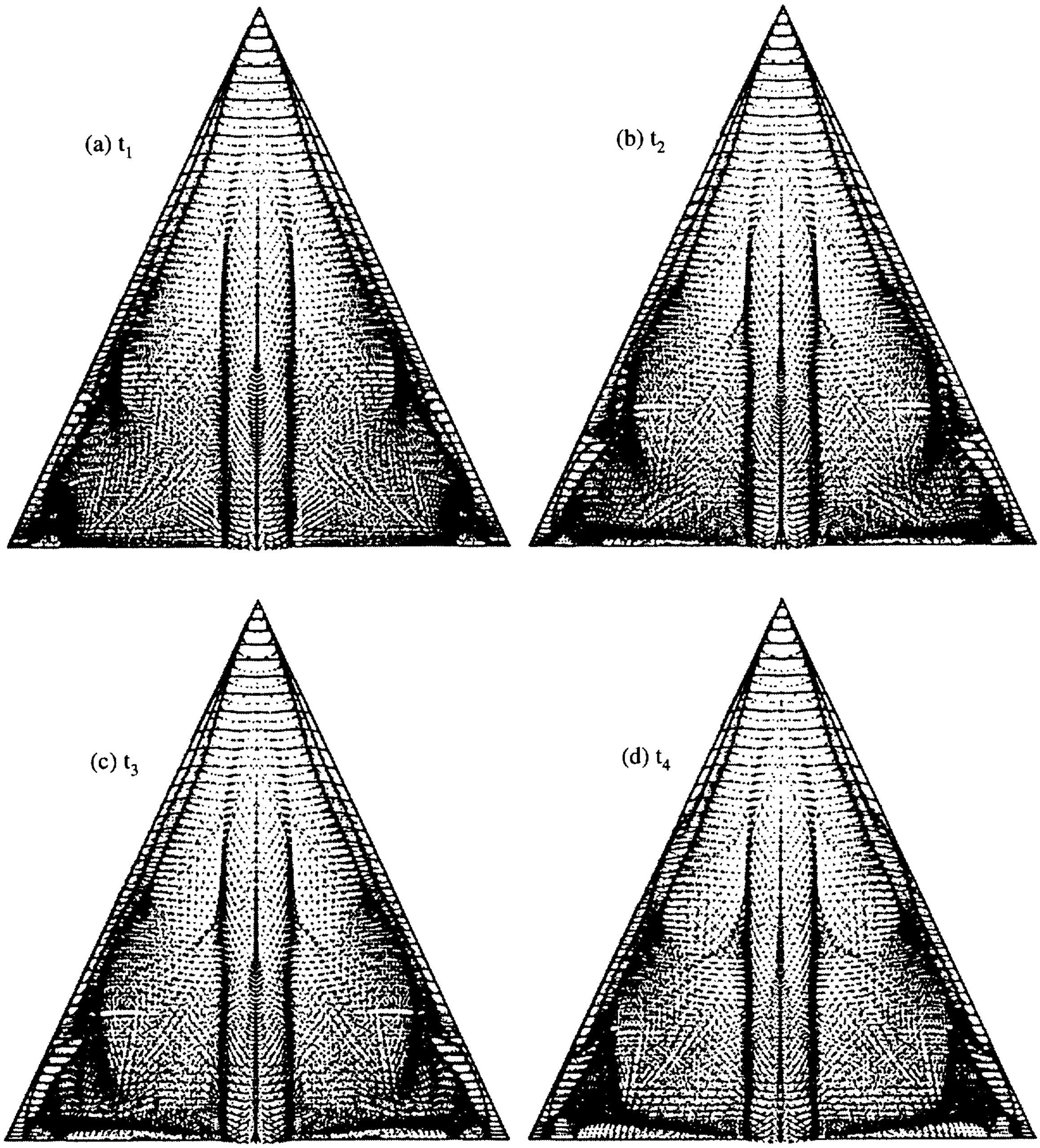

Fig. 9 Computed unsteady surface-flow particle-streaks at four sequential times
M_∞=0.27, α=30°, ϕ=0°, Re=3.67 million

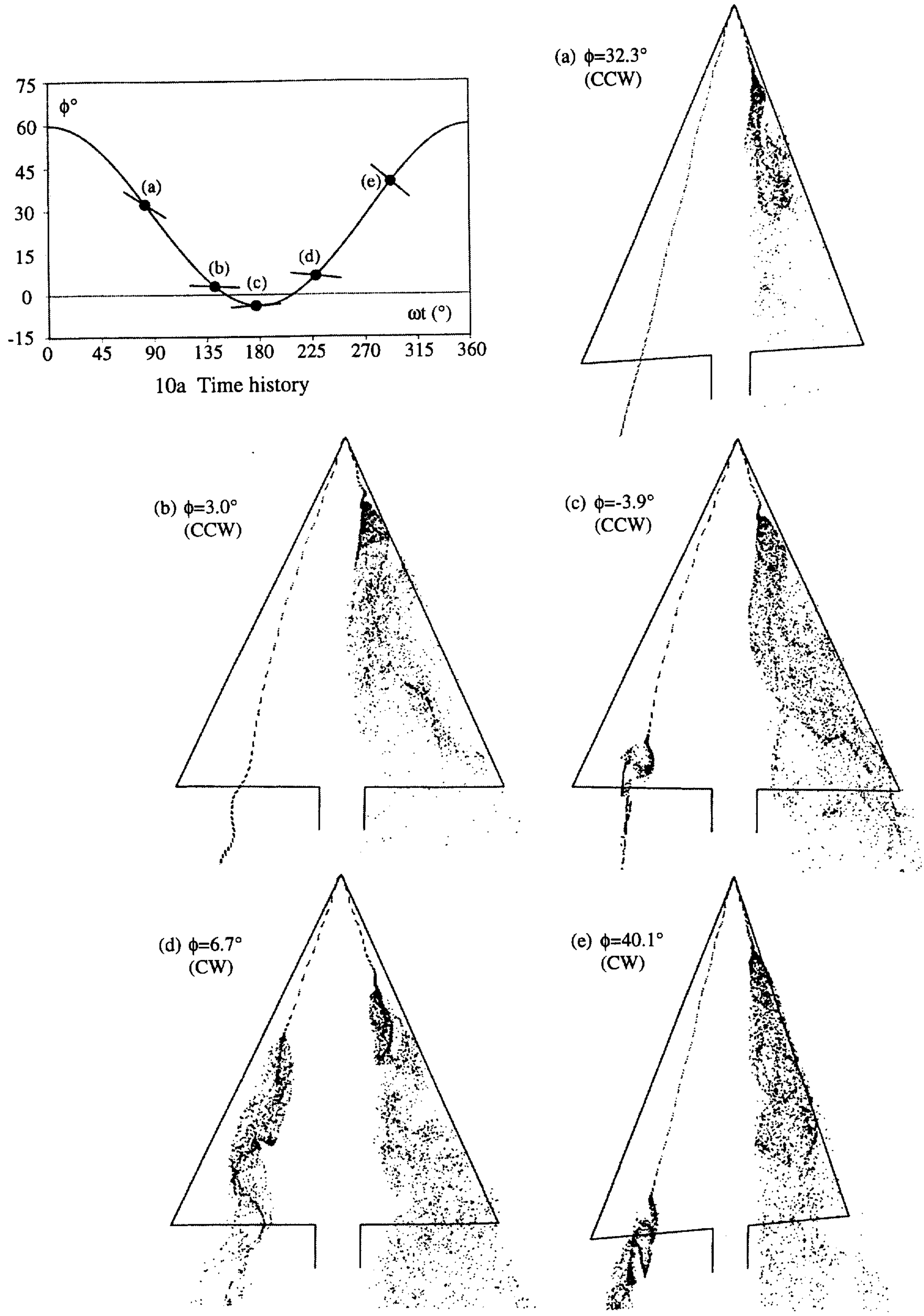

Fig. 10 Periodic formation and disappearance of vortex breakdown over left wing
M_∞=0.27, α=30°, ϕ_0=28°, Δϕ=31.9°, k=0.20, Re=3.67 million

17E. OSCILLATING 65° DELTA WING, EXPERIMENTAL

Thomas Loeser
German – Dutch Wind Tunnel
DNW - NWB
Braunschweig, Germany

INTRODUCTION

This data set contains force and pressure data resulting from static and dynamic measurements on a sharp-edged cropped delta wing with a leading edge sweep of 65° oscillating in different modes. Motivation for the experiment were the provision of experimental data for validation of unsteady computational codes and understanding of the flow past an oscillating delta wing.

The model geometry is identical to a geometry used in the Vortex Flow Experiment for Computer Code Validation (VFE), a multinational cooperation which provided experimental data of delta wing configurations in the mid eighties [3], [4]. The geometry of the wing is also used for steady and unsteady calculations within the Western European Armament Group (WEAG, formerly IEPG) TA - 15.

The experiments have been performed in 1994 (force measurements) and 1995 (pressure measurements). They were performed in the German-Dutch wind tunnel DNW-NWB at low speeds, the model undergoing pitching, yawing or rolling motions about wind-fixed axes. The choice of the mean angles of attack was closely related to the expected flow types:

$\alpha_0 = 0°$: In this case the vortex formation will alternate between the upper and the lower surface of the configuration during the pitching motion.

$\alpha_0 = 9°$: Vortices will be present over the upper surface of the configuration and no vortex breakdown will occur during the whole cycle of the pitching motion.

$\alpha_0 = 15°$ and

$\alpha_0 = 21°$: These conditions are related to mixed cases without vortex breakdown over the configuration at low angles of attack and with vortex breakdown at high angles of attack during the cycle of motion.

$\alpha_0 = 27°$: Vortices with vortex breakdown are expected to occur over the upper surface of the configuration and this type of flow will be present during the whole cycle of the pitching motion.

$\alpha_0 = 42°$: During the cycle of the pitching motion the flow is expected to switch between a vortex-type flow with vortex breakdown and a dead-water-type flow.

$\alpha_0 = 48°$: In this case a deadwater-type flow is expected during the whole cycle of motion.

The mean angles of attack at which no vortex breakdown occurs during the complete cycle of motion are simpler to treat numerically. Therefore the pitching oscillations about $\alpha_0 = 9°$ was the first case to be included in a WEAG TA-15 common exercise. The other case included in that common exercise is the pitching oscillation about $\alpha_0 = 21°$, the reduced frequency being 0.56 for all mean angles of attack. Results from unsteady Euler and Navier-Stokes calculations of pitching oscillation about $\alpha_0 = 9°$ with an amplitude of $\Delta\alpha = 3°$ by W. Fritz are included in the following chapter 17C.

LIST OF SYMBOLS AND DEFINITIONS

$b = 2s$	wing span
c	chord
c_i	root chord
C_L, C_D, C_m	lift, drag and pitching moment coefficients, reference length for C_m: c_i, see figs. 1 and 3 for reference point
C_Y, C_l, C_n	side force, rolling moment and yawing moment coefficients, reference length for C_l and C_n: s, see figs. 1 and 3 for reference point
C_p	static pressure coefficient, $C_p = (p - p_\infty)/q_\infty$
d	fuselage diameter, see fig. 3
DNW - NWB	Deutsch-Niederländischer Windkanal - Niedergeschwindigkeits-Windkanal Braunschweig
f_0	model oscillation frequency
FS	full scale
F_x, F_y, F_z	forces in x, y, z -direction in balance-fixed coordinate system
LE	leading edge
m0	unsteady mean value of force and pressure values, see fig. 7
m1, m2, m3	amplitudes of the first, second and third harmonic of force and pressure values, see fig. 7
M_x, M_y, M_z	moments about balance-fixed x, y, z-axis
q_∞	dynamic pressure
Re	Reynolds number, $Re = V_\infty \cdot c_i / \nu$
TE	trailing edge
V_∞	free stream velocity
t	time
x, y, z	rectangular wing-fixed coordinate system, origin at apex, see fig. 3
α	angle of attack
α_0	mean angle of attack
$\Delta\alpha$	amplitude of pitching oscillation
β	angle of sideslip

β_0	mean angle of sideslip
$\Delta\beta$	amplitude of yawing oscillation
η	dimensionless span-wise coordinate, $\eta = y/s(x)$
$\Delta\Phi$	amplitude of rolling oscillation
φ_i	phase angle of the *i*th harmonic with respect to the model motion
ω^*	reduced frequency, $\omega^* = 2\pi \cdot f_0 \cdot c_i / V_\infty$ (pitching motion), $\omega^* = 2\pi \cdot f_0 \cdot s / V_\infty$ (yawing and rolling motion)

FORMULARY

1 General description of model

1.1 Designation	VFE WB1 - SLE
1.2 Type	full model
1.3 Derivation	NLR 65°-wing, Ref. 1
1.4 Additional remarks	none
1.5 References	1

2 Model geometry

2.1 Planform	cropped delta wing
2.2 Aspect ratio	1.378
2.3 Leading edge sweep	65°
2.4 Trailing edge sweep	0°
2.5 Taper ratio	0.15
2.6 Twist	0°
2.7 Root chord	1200 mm
2.8 Span of model	951 mm
2.9 Area of planform	0.6564 m^2
2.10 Definition of profiles	symmetrical with sharp leading edge (radius approx. 0.25 mm); 5% rel. thickness; arc segment from leading edge (LE) to $x/c = 0.4$; airfoil NACA 64A005 from $x/c = 0.4$ to $x/c = 0.75$; straight line with 3° inclination from $x/c = 0.75$ to trailing edge (TE). A sketch of the airfoil including the coordinates of the NACA airfoil used is presented in fig. 8.
2.11 Lofting procedure between reference sections	N/A
2.12 Form of wing-body junction	sharp
2.13 Form of wing tip	square cut
2.14 Control surface details	N/A
2.15 Additional remarks	definition of fuselage: below the wing, the cross section being semicircular at its bottom half and having a constant width at its upper half below the wing. The section of the fuselage protruding above the wing has cylindrical shape again. The fuselage consists basically of three parts: a tapered nose section from $x/c_i = 0.0$ to $x/c_i = 0.358$ (see figs. 2, 3 and 4 for details), a cylindrical section with a width (diameter d) of 160 mm from $x/c_i = 0.358$ to $x/c_i = 1.0$ and a conical section aft of the TE with a length of 50 mm and a taper angle of 15°. The fuselage centreline is located 50 mm below the wing plane ($z/c_i = -0.042$). All dimensions given are nomimal dimensions.
2.16 References	1,2

3 Wind tunnel

3.1 Designation	Low Speed Wind Tunnel Braunschweig DNW - NWB
3.2 Type of tunnel	continuous, atmospheric pressure
3.3 Test section dimensions	height: 2.85 m, width: 3.25 m, Length: 6 m (open) 8 m (closed), open or closed. Open section used.

3.4 Type of roof and floor	open section used
3.5 Type of side walls	open section used
3.6 Ventilation geometry	open section used
3.7 Thickness of side wall boundary layer	open section used
3.8 Thickness of boundary layers at roof and floor	open section used
3.9 Method of measuring velocity	derived from contraction reference pressures
3.10 Flow angularity	0.08°
3.11 Uniformity of Mach number over test section	$\Delta V/V_\infty < 0.1$ % in jet core
3.12 Sources and levels of noise in empty tunnel	no specs
3.13 Tunnel resonances	no evidence of resonance in tests
3.14 Additional remarks	accuracy of wind speed < 0.06 %
3.15 References on tunnel	3

4 Model motion

4.1 General description	
4.1.1 Pitching motion	sinusoidal motion about axis parallel to model Y-axis. Axis location: $x/c_i = 0.5625$, axis located 50 mm ($z/c_i = -0.042$) below wing plane, see fig. 3.
4.1.2 Yawing motion	sinusoidal motion about axis parallel to wind tunnel Z-axis. Oscillation axis intersects with point $x/c_i = 0.5625$, $z/c_i = -0.042$ at all angles of attack, see fig 1.
4.1.3 Rolling motion	sinusoidal motion about axis parallel to wind axis. Oscillation axis intersects with point $x/c_i = 0.5625$, $z/c_i = -0.042$ at all angles of attack, see fig 1.
4.2 Natural frequencies and normal modes of model and support system	no interference with applied frequencies. Lowest natural frequencies above 15 Hz
4.3 Range of amplitude	pitch: 3° and 6°; yaw: 2.5° and 5.0°; roll: 4.5°
4.4.Range of frequency	1.5 Hz and 3.0 Hz, yielding reduced frequencies $0.28 \leq \omega^* \leq 1.12$ (pitching motion), $0.11 \leq \omega^* \leq 0.44$ (yawing and rolling motion)
4.5 Method of applying motion	forced by electric motor
4.6 Timewise purity of motion	fourier analysis of position signal indicates a 2nd harmonic of 0.8%, 1.7% and 3.1% amplitude of the first harmonic and a 3rd harmonic of 0.21%, 0.2% and 0.5% of the first harmonic (typical values for pitching, yawing and rolling motion).
4.7 Actual mode of applied motion including any elastic deformation	see 4.6
4.8 Additional remarks	measurements with oscillating model have been performed in symmetrical flow ($\beta_0 = 0°$)

5 Test conditions

5.1 Model planform area/tunnel area	0.072 (based upon nozzle exit area)
5.2 Model span/tunnel width	0.28
5.3 Blockage	0.56% (frontal blockage) 5 % (projected area at $\alpha = 45°$)
5.4 Position of model in tunnel	standard upright position, center of test section, belly sting axis 2400 mm behind nozzle exit plane
5.5 Range of freestream velocity	20 m/s, 40 m/s 50 m/s at static tests only)
5.6 Range of tunnel total pressure	atmospheric
5.7 Range of tunnel total temperature	293 K ± 5 K
5.8 Range of model incidence	
5.8.1 Range of steady model incidence	$-7.5° < \alpha < 59.2°$

5.8.2 Range of mean model incidence	$\alpha_0 = 0°, 9°, 15°, 21°, 27°, 42°$ (pitching) $\alpha_0 = 9°, 15°, 27°, 42°$ (yawing) $\alpha_0 = 0°, 9°, 27°$ (rolling)
5.9 Definition of model incidence	model incidence defined relative to the wing plane
5.10 Position of transition, if free	not measured
5.11 Position and type of trip, if transition fixed	no trip used
5.12 Flow instabilities during tests	none encountered
5.13 Changes to mean shape of model due to steady aerodynamic load	not measured, negligible
5.14 Additional remarks	none
5.15 References describing tests	2, 4

6 Measurements and observations

6.1 Steady pressures for the mean conditions	yes
6.2 Steady pressures for small changes from the mean conditions	no
6.3 Quasi-steady pressures	yes
6.4 Unsteady pressures	yes
6.5 Steady forces for the mean conditions	
6.5.1 Steady forces for the mean conditions by integration of pressures	no
6.5.2 Steady forces for the mean conditions by direct measurement	yes
6.6 Steady forces for small changes from the mean conditions by integration	no
6.7 Quasi-steady forces by integration	no
6.8 Unsteady forces	no
6.8.1 Unsteady forces by integration	no
6.8.2 Unsteady forces by direct measurement	yes
6.9 Measurement of actual motion at points on model	no
6.10 Observation or measurement of boundary-layer properties	no
6.11 Visualisation of surface flow	yes
6.12 Visualisation of shock wave movements	N/A
6.13 Additional remarks	steady forces and pressures have been measured with increasing angle of attack, control measurements with increasing and decreasing angle of attack have been performed to ensure the absence of hysteresis effects. Forces and pressures have been measured during different wind tunnel entries.

7 Instrumentation

7.1 Steady pressures	pressures for steady conditions measured with same system used for unsteady measurements with the only difference being that the static measurements have been performed with all 10 psi transducers connected simultanously whereas the dynamic measurements have been performed with 2 transducers connected simultanously.
7.1.1 Position of orifices span-wise and chord-wise	see tables 1 and 2.
7.1.2 Diameter of orifices	0.6 mm
7.1.3 Type of measuring system	see 7.2.3
7.2 Unsteady pressures	
7.2.1 Position of orifices span-wise and chord-wise	see tables 1 and 2.
7.2.2 Diameter of orifices	see 7.1.2

7.2.3 Type of measuring system

230 pressure orifices connected with short pressure tubes of equal length to 10 PSI pressure transducers, which are located in the wing of the model. 9 of these orifices are also connected to Kulite pressure transducers by means of tubes of approximately 10 cm length
PSI System 780 B, 16bit ADC.
Sampling frequencies: 74.35 Hz (PSI), 1000 Hz (Kulites)

7.2.4 Type of transducers

PSI modules used: ESP-16 SL, ESP-32 SL and ESP-48 SL, range: 0.35 psi and 1.0 psi.
Kulites used: XCW-062 and XCW 093, range 0.35 bar (= 5.0 psi)

7.2.5 Principle and accuracy of calibration

PSI: 3 calibration pressures (magnitudes adapted to the expected values of the experiment) applied to each module every 30 minutes. Manufacturers claimed accuracy: 0.1 % full scale (FS) worst case, 0.07 % typical, wind tunnel operators checked accuracy: 0.05 % FS
Kulite: static calibration at beginning of tunnel entry, offset measurement every 30 minutes.

7.3 Steady forces

steady and unsteady forces measured with six component strain gauge balance of type "Emmen 196-6"

7.4 Unsteady forces

see 7.3

7.5 Model motion

7.5.1 Method of measurement

spring-loaded foil strain gauges on steel flexures

7.5.2 Accuracy of measured motions

better than 1%

7.6 Processing of unsteady measurements

7.6.1 Method of acquiring and processing measurements

pressure measurements: see fig 6
force measurements: see fig 6

7.6.2 Type of analysis

fourier analysis, then analysis of variance

7.6.3 Unsteady pressure quantities obtained and accuracies achieved

amplitudes and phases up to the 3rd harmonic. Confidence intervals for amplitudes and phases of each harmonic specified in data files

7.6.4 Method of integration to obtain forces

N/A

7.7 Additional remarks

process of calculating the phase angles of the harmonics:

1. calculate position signal $\alpha(t)$ from raw data
2. calculate Pressure Coefficients -Cp(t) from raw data:
   $-Cp = (p_\infty - p)/q_\infty$
3. Set the number of data values to be used for Fourier analysis to cover an integer number of model oscillations
4. Perform Fourier analysis on position signal and calculate phase of its first harmonic according to
   $\varphi_{1,Pos} = -\mathrm{atan}(Im_{1,Pos}/Re_{1,Pos})$
5. Perform Fourier analysis on pressure signals -Cp(t). Calculate phase angles of the i-th harmonic according to $\varphi_{i,-Cp} = -\mathrm{atan}(Im_i/Re_i)$. Account for the phase of the position signal by subtracting it from the phases of the harmonics according to $\varphi_{i,-cp} = \varphi_{i,-cp} - i \cdot \varphi_{1,Pos}$. This is equivalent with letting the fourier analysis start at an instant where the position signal has a phase angle $\varphi_{1,Pos}$ of 0°. The phases are then (if necessary) modified to lie again within the range
   $-180^\circ <= \varphi_{i,-Cp} <= +180^\circ$
6. The pressure signal now can be represented by
   $$-Cp(t) = -Cp_0 + \sum_{i=1}^{3} -\hat{C}p_i \cdot \cos(i\omega t + \varphi_i),$$
   $-\hat{C}p_i$ being the amplitude of the i-th harmonic and $-Cp_0$ the constant offset of the signal as presented in the data files.
7. The procedure above applies also to the force measurements.

It is important to note the negative sign in the definition of the

	phase angles and the resulting "+" sign in the equation in step 6. Furthermore it should be noted that the phase angles of the harmonics are counted with respect to their maxima, as can be seen in fig. 5.
7.8 References on techniques	7, 8, 9, 10

8 Data presentation

8.1 Test cases for which data could be made available	
8.1.1 Steady pressures	-6° <= α <= 48° in approximately 1° intervals for $\beta = 0°$; -5° <= β <= +5° in approximately 1° intervals for α = 9°, 15°, 27° and 42°
8.1.2 Unsteady pressures	see tables 4, 6 and 8
8.1.3 Steady forces	-7.5° <= α <= 58.5° in 1.5° intervals at Re = $1.55 \cdot 10^6$, Re = $3.1 \cdot 10^6$ and Re = $3.9 \cdot 10^6$, for $\beta = 0°$; β = -5°, -3°,-3°,0°,+1°,+3° and +5° for 0° <= α <= 54° in approx. 3° or 6° intervals for Re = $3.1 \cdot 10^6$.
8.1.4 Unsteady forces	see tables 3, 5 and 7
8.2 Test cases for which data are included in this document	
8.2.1 Steady pressures	α = 0°, 9°, 15°, 21°, 27° and 42° for $\beta = 0°$, Re = $1.55 \cdot 10^6$ and/or Re = $3.1 \cdot 10^6$; β = -5°, 0°, +5° for α = 9°, 15°, 27° and 42° for Re = $3.1 \cdot 10^6$.
8.2.2 Unsteady pressures	see tables 4, 6 and 8
8.2.3 Steady forces	-7.5° <= α <= 58.5° in 1.5° intervals at Re = $1.55 \cdot 10^6$, Re = $3.1 \cdot 10^6$ and Re = $3.9 \cdot 10^6$, $\beta = 0°$; β = -5°, 0° and +5° for 0° <= α <= 54° in approx. 3° or 6° intervals for Re = $3.1 \cdot 10^6$
8.2.4 Unsteady forces	see tables 3, 5 and 7
8.3 Other forms in which data could be made available	none
8.4 References giving other presentation of data	2
8.5 Additional remarks	force coefficients given for steady measurements at $\beta = 0°$ and for pitching motion: C_L, C_D and C_m; force coefficients given for steady measurements at $\beta \neq 0°$ and for yawing and rolling motion: C_L, C_D C_Y, C_l , C_m, and C_n

9 Comments on data

9.1 Accuracy	
9.1.1 Mach number	see 3.14
9.1.2 Steady incidence	±0.01°
9.1.3 Reduced frequency	±0.1 %
9.1.4 Steady pressure coefficients	see 7.2.5
9.1.5 Unsteady pressure coefficients	confidence interval is result of Analysis of Variance
9.1.4 Steady force coefficients	accuracy according to balance manufacturer: 0.1 – 0.3 % of balance design point values (F_x = 350 N, F_y = 250 N, F_z = 1200 N, M_x = 100 Nm, M_y = 120 Nm, M_z = 130 Nm)
9.1.5 Unsteady force coefficients	confidence interval is result of Analysis of Variance
9.2 Sensitivity to small changes of parameter	no evidence
9.4 Influence of tunnel total pressure	no evidence
9.5 Effects on data of uncertainty, or variation, in mode of model motion	N/A
9.6 Wall interference corrections	no corrections applied
9.7 Other relevant tests on same model	none
9.8 Relevant tests on other models of nominally the same shapes	static tests have been performed within the Vortex Flow Experiment, see references 1, 5, 6
9.9 Any remarks relevant to comparison between	the presence of the fuselage below the wing is believed to be of

experiment and theory	importance for the upper surface flow at small angles of attack and at angles of attack at which vortex breakdown occurs.
9.10 Additional remarks	none
9.11 References on discussion of data	4

Personal contact for further information

Thomas Loeser
DNW - NWB
Lilienthalplatz 7
38108 Braunschweig, Germany
phone: +49 - 531 – 295 - 2454
thomas.loeser@dlr.de

List of references

1 R.H.C.M. Hirdes: US/European Vortex Flow Experiment - Test Report of Wind-Tunnel Measurements on the 65° Wing in the NLR High Speed Wind Tunnel HST; NLR TR 85046 L

2 T. Loeser: Dynamic Force and Pressure Measurements on an Oscillating Delta Wing at Low Speeds; DLR IB 129-96/9

3 G. Kausche, H. Otto, D. Christ, R. Siebert: The Low-Speed Wind Tunnel at DFVLR in Braunschweig (Status 1988); DFVLR-Mitteilung 88-25, 1988

4 D. Hummel, T. Loeser: Low Speed Wind Tunnel Experiments on a Delta Wing Oscillating in Pitch; ICAS-98-3.9.3, Sept. 1998

5 G. Drougge: The international vortex flow experiment for computer code validation; ICAS-Proc. 1988, Vol. 1, pp. XXXV – XLI

6 A. Elsenaar, L. Hjelmberg, K. Bütefisch, W.J. Bannink: The International Vortex Flow Experiment; AGARD-CP-437 (1988), Vol. 1 , pp. 9-1 to 9-23

7 N.L. Johnson, F.C. Leone: Statistics and Experimental Design in Engineering and the Physical Sciences, Vol. II second edition; John Wiley & Sons, New York, 1964

8 R. Mason, R. Gunst, J. Hess: Statistical Design and Analysis of Experiments; John Wiley & Sons, New York, 1989

9 D. Vanmol: Experimental Design and Statistical Analysis applied to Hypersonic Ground Testing; Progress Meeting "Manned Space Transportation Programme", Köln, January 26 & 27 1995

10 H. Coleman, W.G. Steele Jr.: Experimentation and Uncertainty Analysis for Engineers; John Wiley & Sons, New York, 1989

FORMAT OF DATA SET

The static and dynamic pressure and force data are stored in ASCII files. They are located in a directory tree, which is described in a README-file placed in the root directory of this data set. For example, data of dynamic pressure measurements of the pitching motion at 9° mean angle of attack can be found in the subdirectory `pressure/dynamic/pitch/alpha_09`. The naming conventions for the files are also described in the README-file. Additional information with respect to the contents of the files is available at the top of the file, comment lines have a # in the first column. The first lines of a data file containing dynamic pressure data is listed below.

```
###############################################################################
#
# Analysis of Variance on constant offset and first 3 Harmonics
# of Magnitudes and Phases of Pressure Coefficients -Cp
# Dimension of Phase Angle : Degrees
# Model                    : VOMO-model WEAG WB1, SLE, Ci = 1200 mm
# Program                  : ./2fd.pl -n -a 27 -f1 theta -f2 omega -d 0 -q 980 -no_wild_plot -print -eps -30o
# Date of Analysis         : Wed Feb 14 00:51:50 MET 1996
#
# alpha                    : 27 degrees
# mode                     : pitch
# Reynolds Number          : 3.10*10^6
# 1. Factor                : theta with levels 3.0 6.0
# 2. Factor                : omega with levels 0.28 0.56
# Prob. for Confid. Inteval: 0.95
# Risk for Significance    : 1 %
# location of pressure taps: x/Ci = 0.3, upper side
#
# Each dim'less spanwise coordinate eta is followed by 7 lines, which
# contain the following data
# m0: Constant Offset of Signal
# m1: Magnitude of 1. Harmonic
# p1: Phase     of 1. Harmonic
# m2: Magnitude of 2. Harmonic
# p2: Phase     of 2. Harmonic
# m3: Magnitude of 3. Harmonic
# p3: Phase     of 3. Harmonic
#
# meaning of the columns:
# 1.column: value for theta 3.0 and omega 0.28
# 2.column: value for theta 3.0 and omega 0.56
# 3.column: value for theta 6.0 and omega 0.28
# 4.column: value for theta 6.0 and omega 0.56
# 5.column: Confidence Interval for above mentioned probability
# 6.column: S, if influence of theta is significant, N if not
```

```
# 7.column: S, if influence of omega is significant, N if not
# 8.column: S, if influence of interaction of theta with omega is significant, N if not
#
#
# eta = +0.000
#
    0.624    0.623    0.626    0.621    +-    0.007  N  N  N
    0.075    0.079    0.162    0.163    +-    0.003  S  N  N
     11.8     14.1      9.3     13.0    +-      2.5  N  S  N
    0.003    0.003    0.003    0.003    +-    0.002  N  N  N
    108.5    101.3     58.7    111.6    +-     51.1  N  S  N
    0.001    0.002    0.005    0.004    +-    0.002  S  N  N
     -9.5    -69.0    -76.0    -93.7    +-     79.9  N  N  N
#
# eta = +0.100
#
    0.627    0.627    0.631    0.627    +-    0.008  N  N  N
    0.077    0.081    0.164    0.166    +-    0.004  S  S  N
     12.5     14.0      9.8     13.4    +-      2.8  N  S  N
    0.003    0.003    0.003    0.003    +-    0.002  N  N  N
    110.0    113.0     44.4     90.5    +-     52.9  S  S  N
    0.001    0.001    0.005    0.003    +-    0.002  S  N  N
    -22.4    -63.0    -70.5    -96.9    +-     87.7  N  N  N
#
```

TABLES

$x/c_i = 0.3$		$x/c_i = 0.6$		$x/c_i = 0.8$	
η	Range / kPa	η	Range / kPa	η	Range / kPa
		-0.980	6.9	-0.980	6.9
-0.960	6.9	-0.960	6.9	-0.960	6.9
-0.940	6.9	-0.940	6.9	-0.940	6.9
-0.920	6.9	-0.920	6.9	-0.920	6.9
-0.900	6.9	-0.900	6.9	-0.900	6.9
-0.875	6.9	**-0.875**	6.9	-0.875	6.9
-0.850	6.9	-0.850	6.9	**-0.850**	6.9
-0.825	6.9	-0.825	6.9	-0.825	6.9
-0.800	6.9	-0.800	6.9	-0.800	6.9
-0.775	6.9	-0.775	6.9	-0.775	6.9
-0.750	6.9	-0.750	6.9	-0.750	6.9
-0.725	6.9	-0.725	6.9	-0.725	6.9
-0.700	6.9	**-0.700**	6.9	**-0.700**	6.9
-0.675	6.9			-0.675	6.9
-0.650	6.9	-0.650	6.9	-0.650	6.9
-0.600	6.9	-0.600	6.9	-0.600	6.9
-0.550	6.9	-0.550	6.9	-0.550	6.9
-0.500	6.9	-0.500	6.9	-0.500	6.9
-0.400	6.9	-0.400	6.9	-0.400	6.9
-0.300	6.9	-0.300	6.9	-0.300	6.9
-0.200	6.9	-0.200	6.9	-0.200	6.9
-0.100	6.9	-0.100	6.9		
0.000	6.9				
+0.100	6.9	+0.100	6.9		
+0.200	6.9	+0.200	6.9	+0.200	6.9
+0.300	6.9	+0.300	6.9	+0.300	6.9
+0.400	6.9	+0.400	6.9	+0.400	6.9
+0.500	6.9	+0.500	6.9	+0.500	6.9
+0.550	6.9	+0.550	6.9	+0.550	6.9
+0.600	6.9	+0.600	6.9	+0.600	6.9
+0.650	6.9	+0.650	6.9	+0.650	6.9
+0.675	6.9			+0.675	6.9
+0.700	6.9	**+0.700**	6.9	**+0.700**	6.9
+0.725	6.9	+0.725	6.9	+0.725	6.9
+0.750	6.9	+0.750	6.9	+0.750	6.9
+0.775	6.9	+0.775	6.9	+0.775	6.9
+0.800	6.9	+0.800	6.9	+0.800	6.9
+0.825	6.9	+0.825	6.9	+0.825	6.9
+0.850	6.9	+0.850	6.9	+0.850	6.9
+0.875	6.9	+0.875	6.9	+0.875	6.9
+0.900	6.9	+0.900	6.9	+0.900	6.9

+0.920	6.9	+0.920	6.9	+0.920	6.9
+0.940	6.9	+0.940	6.9	+0.940	6.9
+0.960	6.9	+0.960	6.9	+0.960	6.9
		+0.980	6.9	+0.980	6.9

Table 1: Location of the pressure taps, upper side, Kulite locations printed bold

$x/c_i = 0.3$		$x/c_i = 0.6$		$x/c_i = 0.8$	
η	Range / kPa	η	Range / kPa	η	Range / kPa
		-0.980	6.9	-0.980	6.9
-0.960	6.9	-0.960	6.9	-0.960	6.9
-0.940	6.9	-0.940	6.9	-0.940	2.4
-0.920	6.9	-0.920	2.4		
-0.900	6.9	-0.900	2.4	-0.900	2.4
		-0.875	2.4	-0.875	2.4
-0.850	2.4	-0.850	2.4	-0.850	2.4
-0.825	2.4	-0.825	2.4	-0.825	2.4
-0.800	2.4	-0.800	2.4	-0.800	2.4
-0.775	2.4	-0.775	2.4		
-0.750	2.4	-0.750	2.4	-0.750	2.4
-0.725	2.4	-0.725	2.4		
-0.700	2.4	-0.700	2.4	-0.700	2.4
-0.675	2.4				
-0.650	2.4	-0.650	2.4	-0.650	2.4
-0.600	2.4	-0.600	2.4	-0.600	2.4
-0.550	2.4	-0.550	2.4	-0.550	2.4
-0.500	2.4	-0.500	2.4	-0.500	2.4
		-0.400	2.4	-0.400	2.4
		-0.300	2.4	-0.300	2.4
				-0.200	2.4
				+0.200	2.4
		+0.300	2.4	+0.300	2.4
		+0.400	2.4	+0.400	2.4
+0.500	2.4	+0.500	2.4	+0.500	2.4
+0.550	2.4	+0.550	2.4	+0.550	2.4
+0.600	2.4	+0.600	2.4	+0.600	2.4
+0.650	2.4	+0.650	2.4	+0.650	2.4
+0.675	2.4				
+0.700	2.4	+0.700	2.4	+0.700	2.4
+0.725	2.4	+0.725	2.4		
+0.750	2.4	+0.750	2.4	+0.750	2.4
+0.775	2.4	+0.775	2.4		
+0.800	2.4	+0.800	2.4	+0.800	2.4
+0.825	2.4	+0.825	2.4	+0.825	2.4
+0.850	2.4	+0.850	2.4	+0.850	2.4
+0.875	6.9	+0.875	2.4	+0.875	2.4
+0.900	6.9	+0.900	2.4	+0.900	2.4
+0.920	6.9	+0.920	2.4		
+0.940	6.9	+0.940	6.9	+0.940	2.4
+0.960	6.9	+0.960	6.9	+0.960	6.9
		+0.980	6.9	+0.980	6.9

Table 2: Location of the pressure taps, lower side

α_0/degrees	Re/10^6	$\Delta\alpha$/degrees
0	**1.6, 3.1**	**6**
9	**1.6, 3.1**	**3,6**
15	**3.1**	**3, 6**
21	**1.6, 3.1**	**6**
27	**1.6, 3.1**	**3, 6**
42	**3.1**	**6**
48	**3.1**	**6**

Table 3: Force Measurements, Pitching Motion

α_0/degrees	Re/10^6	$\Delta\alpha$/degrees
0	**1.6,** 3.1	**6**
9	**1.6, 3.1**	**3, 6**
15	**1.6, 3.1**	**3, 6**
21	**1.6, 3.1**	**3, 6**
27	**1.6, 3.1**	**3, 6**
42	1.6, **3.1**	**6**

Table 4: Pressure Measurements, Pitching Motion

α/degrees	Re/10^6	$\Delta\beta$/degrees
9	1.6, **3.1**	**2.5, 5**
15	**3.1**	**2.5, 5**
27	1.6, **3.1**	**2.5, 5**
42	**3.1**	**5**
48	**3.1**	**5**

Table 5: Force Measurements, Yawing Motion

α/degrees	Re/10^6	$\Delta\beta$/degrees
9	**1.6, 3.1**	**2.5, 5**
15	**1.6, 3.1**	**5**
27	**1.6, 3.1**	**2.5, 5**
42	**1.6, 3.1**	**5**

Table 6: Pressure Measurements, Yawing Motion

α/degrees	Re/10^6	$\Delta\Phi$/degrees
0	1.6, **3.1**	**4.5**
9	1.6, **3.1**	**4.5**
27	1.6, **3.1**	**4.5**

Table 7: Force Measurements, Rolling Motion

α/degrees	Re/10^6	$\Delta\Phi$/degrees
0	1.6, 3.1	4.5
9	**1.6, 3.1**	**4.5**
27	1.6, 3.1	4.5

Table 8: Pressure Measurements, Rolling Motion

All measurements listed in the tables 3 to 8 have been carried out at model oscillation frequencies of f_0 = 1.5 Hz and f_0 = 3.0 Hz. Measurements, which are included in this document, are printed in bold letters.

FIGURES

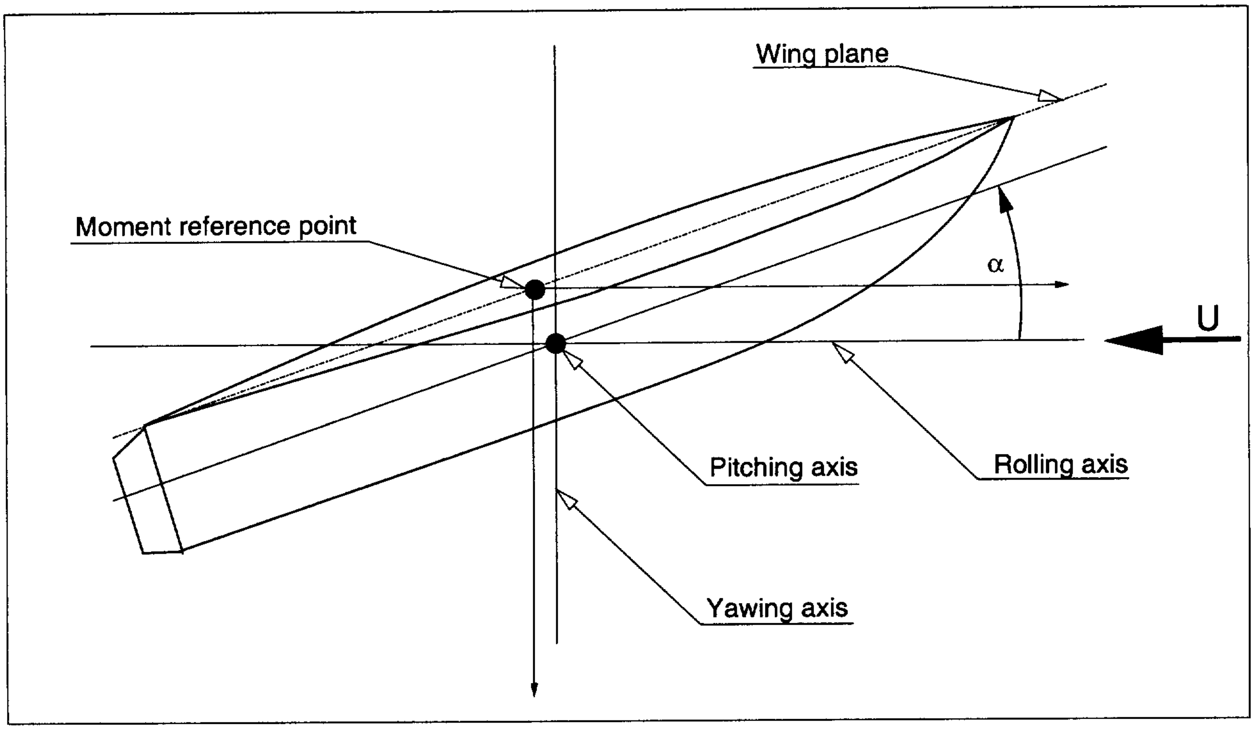

Figure 1: Location of the oscillation axes and the moment reference point

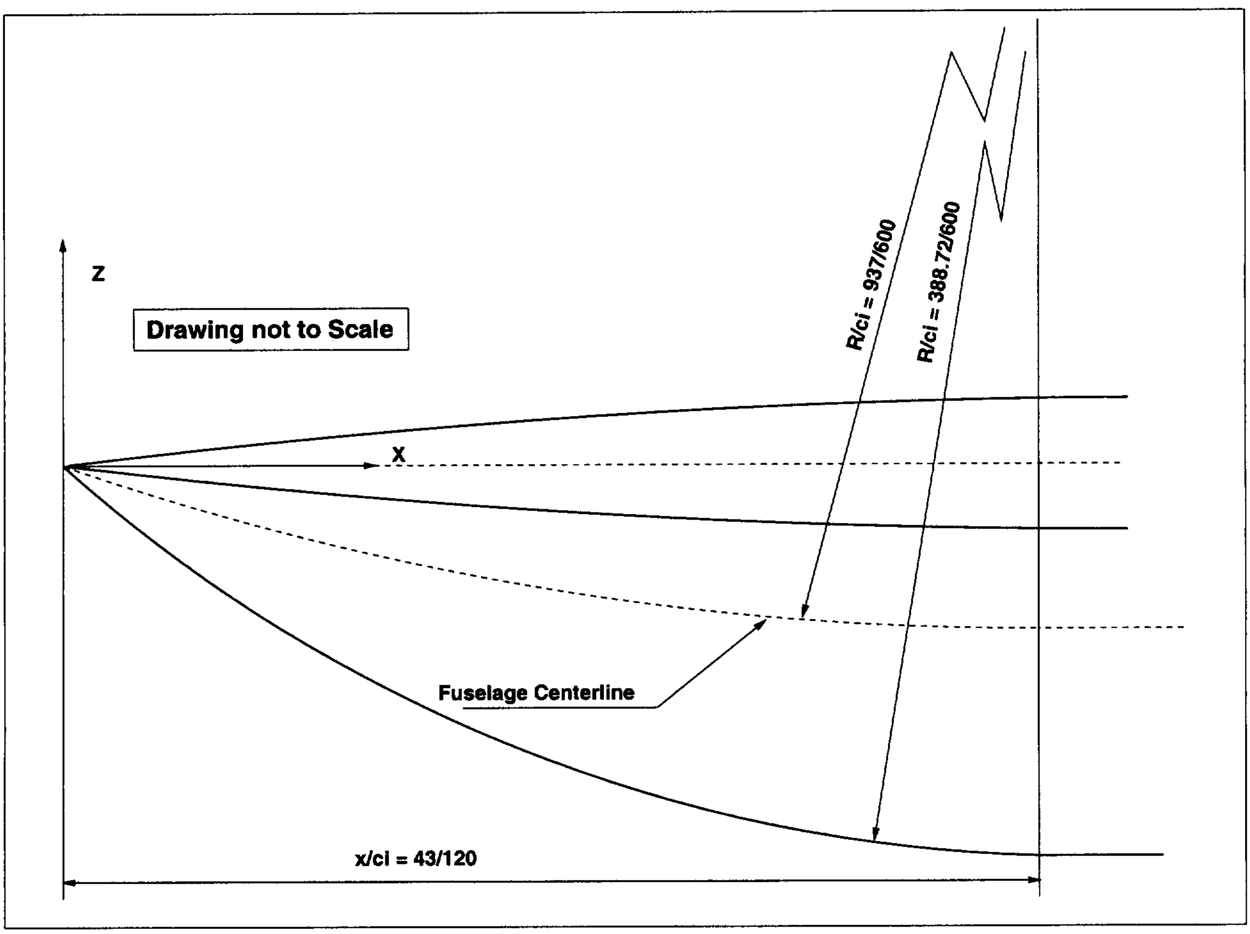

Figure 2: Geometry of the fuselage nose

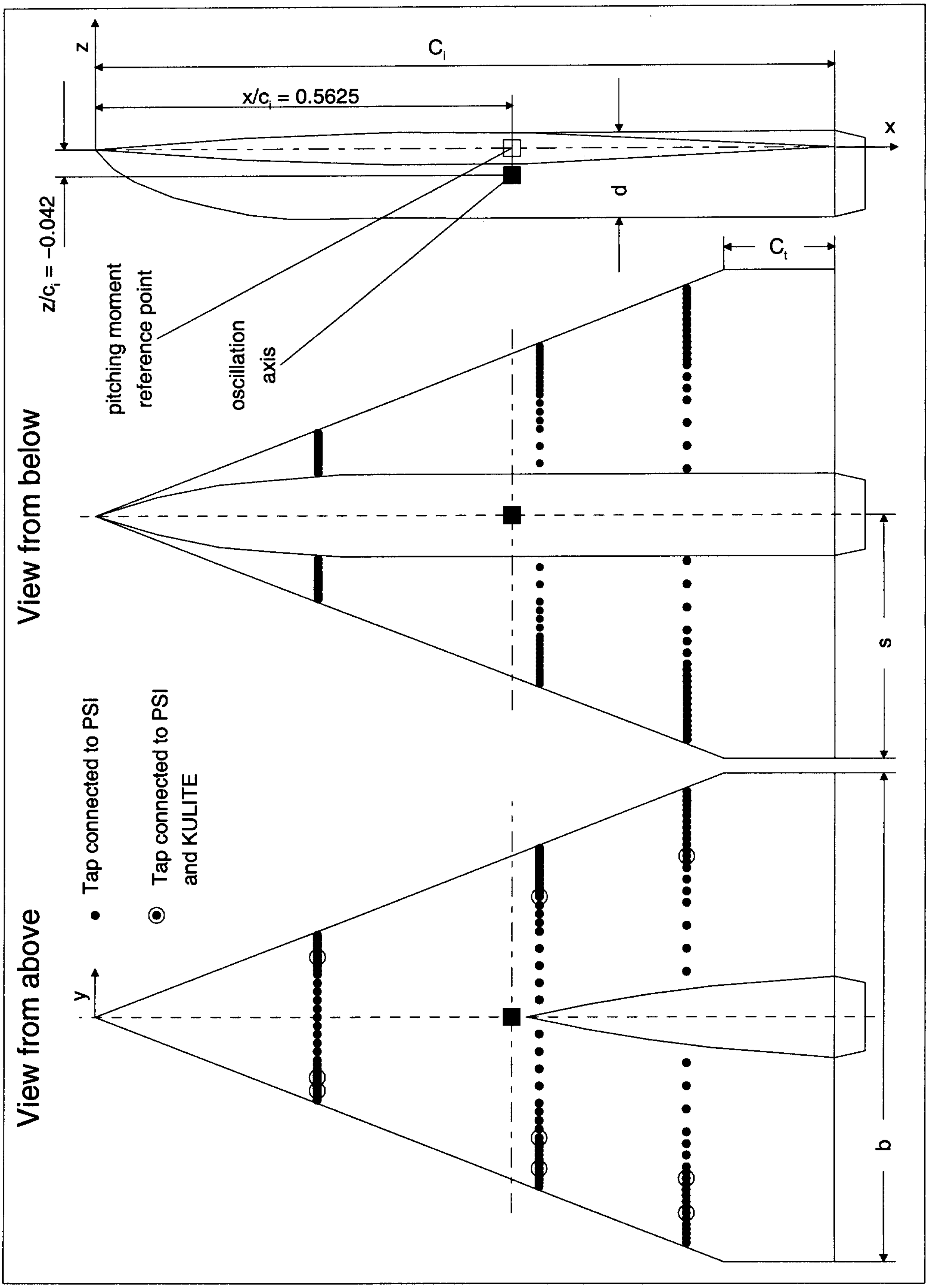

Figure 3: Sketch of the wind tunnel model

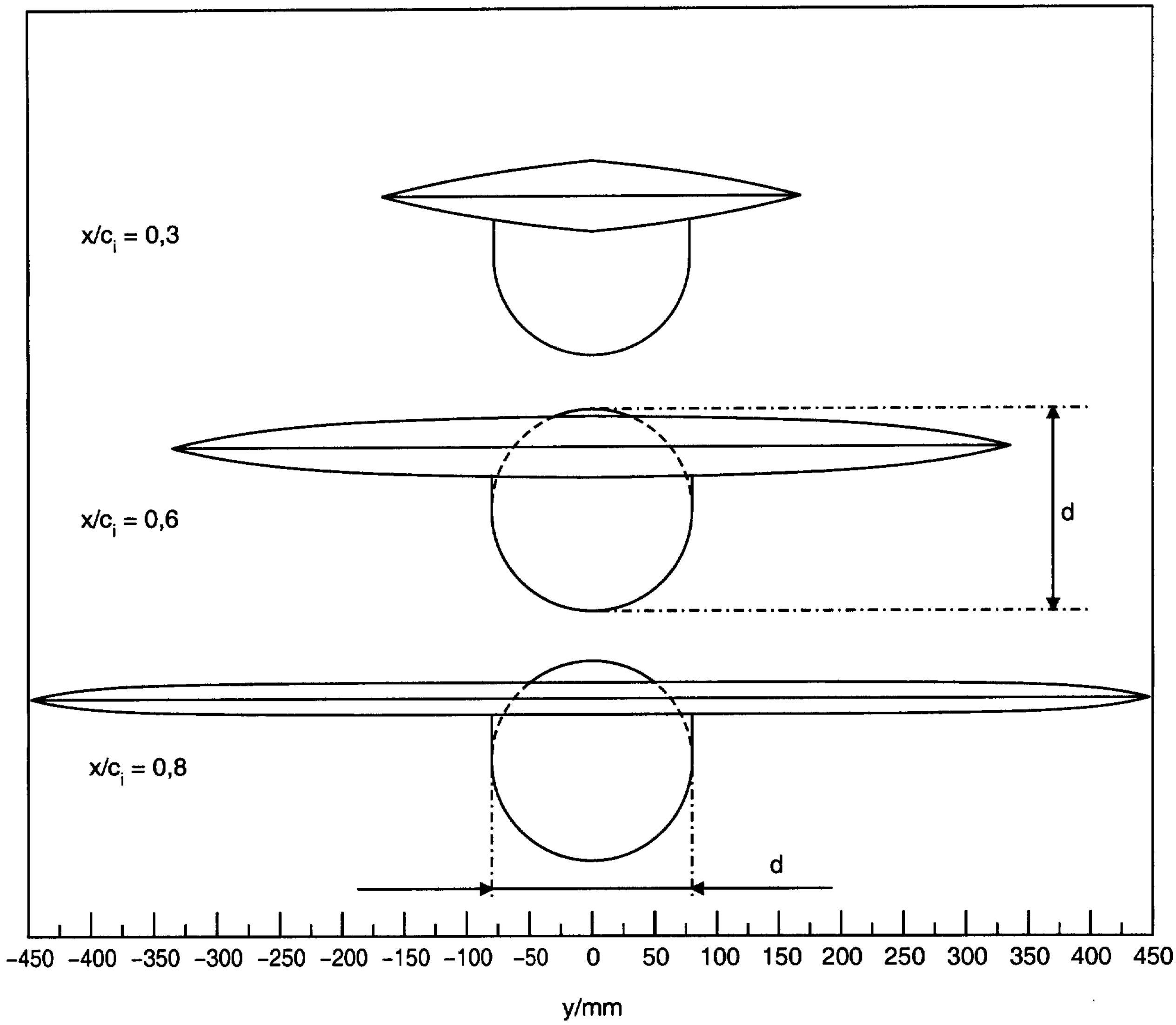

Figure 4: Cross sections of the wind tunnel model at the positions of the pressure taps

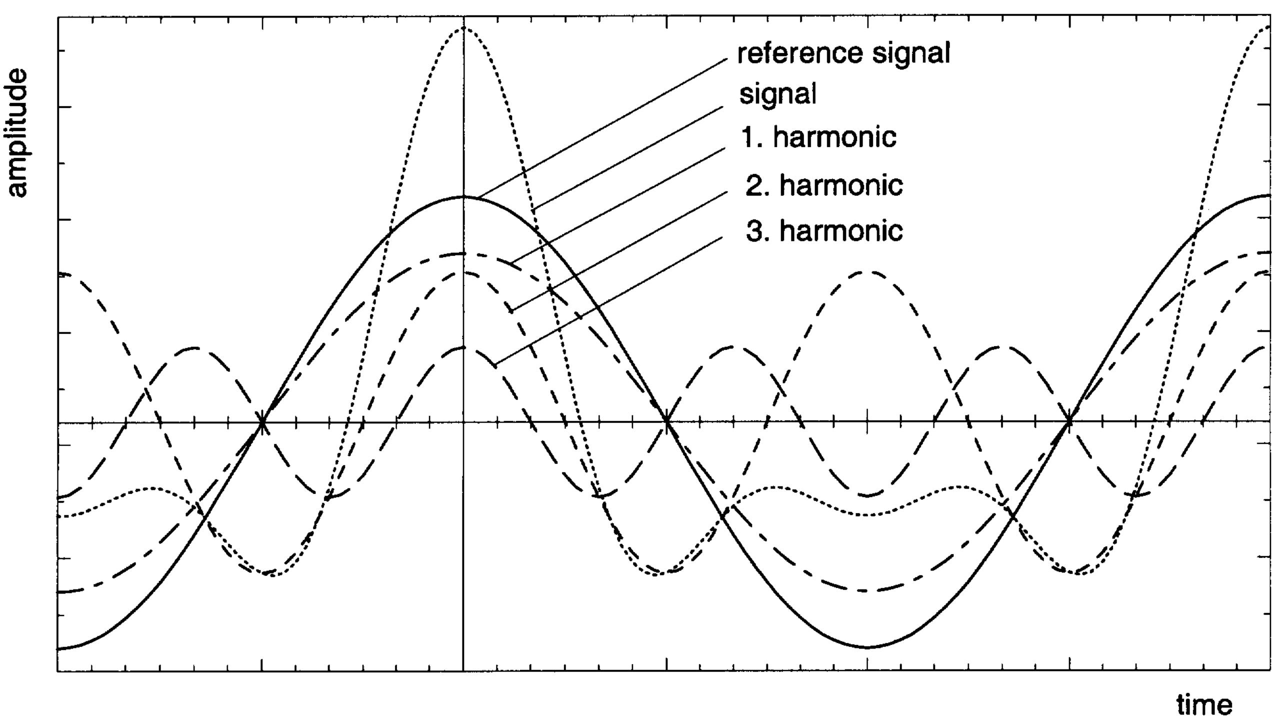

Figure 5: Schematic view of arbitrary signal with harmonics having phase angles $\varphi_i = 0$

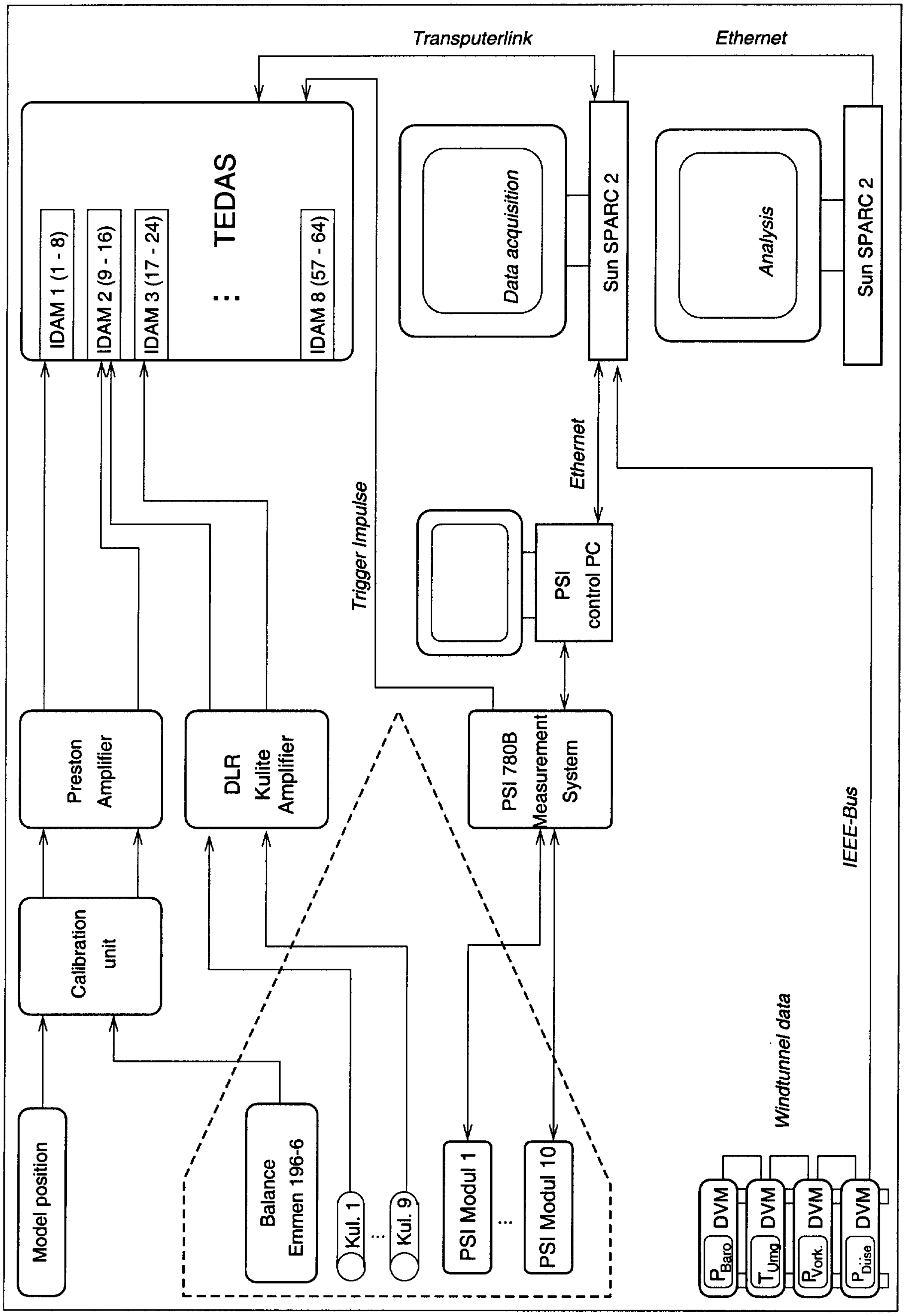

Figure 6: Schematic view of data acquisition

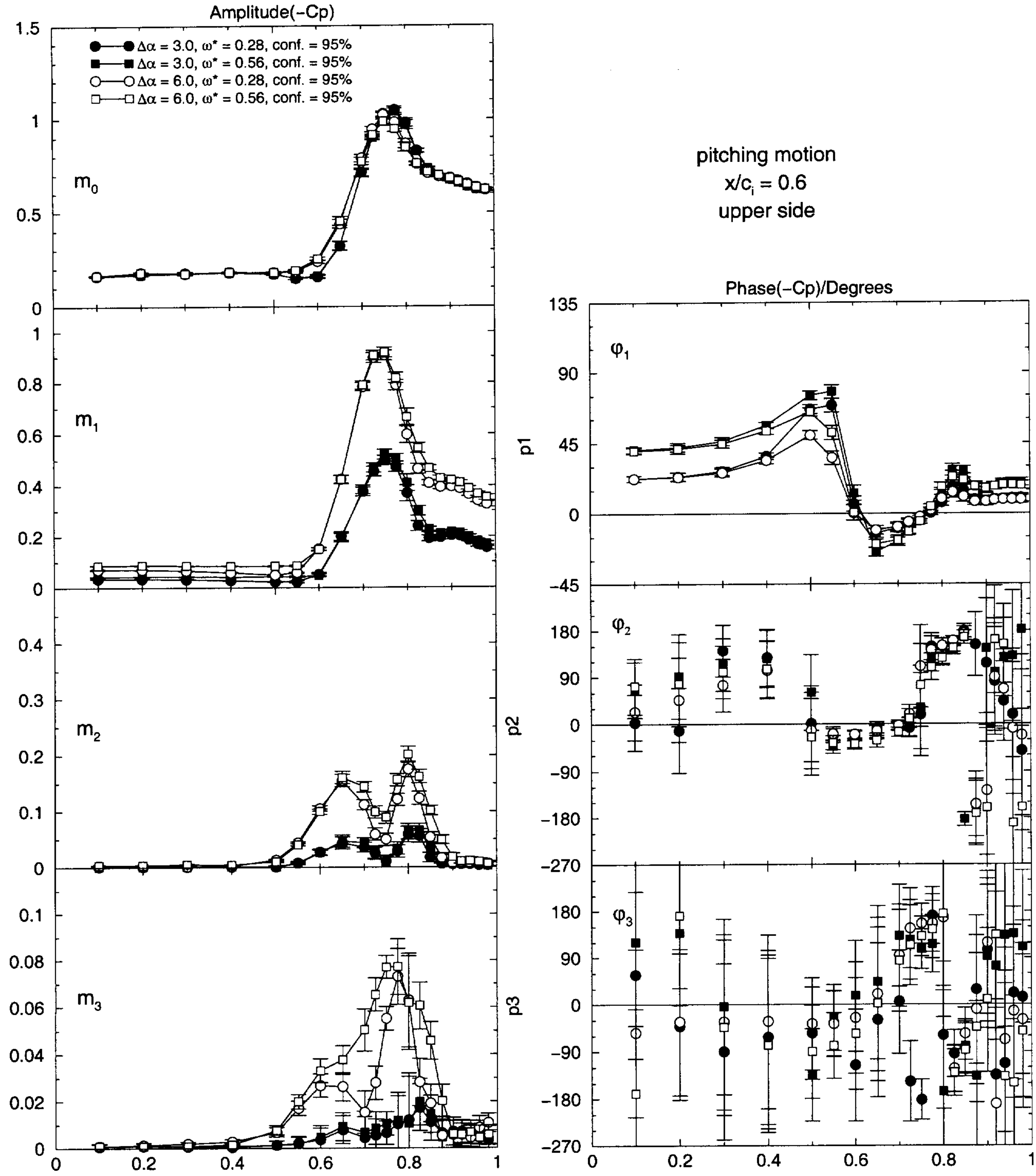

Figure 7: Typical result of an analysis of variance for the unsteady pressure distribution Cp(η) in the section $x/c_i = 0.6$. Pitching motion with $\alpha_0 = 9°$ and factors Δα and ω* at Re = $3.1*10^6$, error bars indicate confidence intervals of 95%. Top to bottom: unsteady mean value, amplitude m1 and phase φ_1 of the first harmonic, amplitude m2 and phase φ_2 of the second harmonic, amplitude m3 and phase φ_3 of the third harmonic.

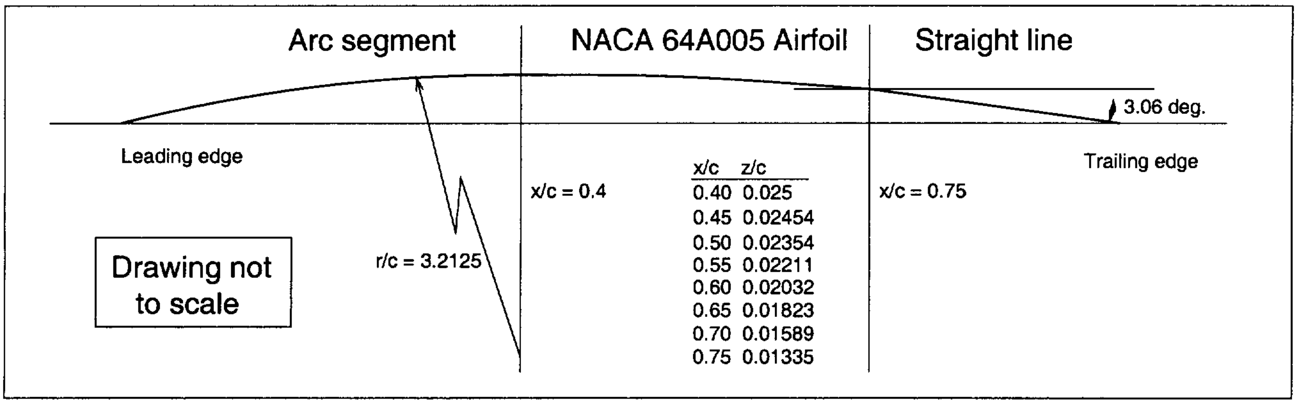

Figure 8: Definition of the airfoil

17C. OSCILLATING 65° DELTA WING, NUMERICAL

Willy Fritz
DaimlerChrysler Aerospace
Military Aircraft
81663 Munich (Ottobrunn)
Germany

INTRODUCTION

This data set consists of steady and unsteady numerical solutions of a sharp-edged cropped delta wing with a leading edge sweep of 65° undergoing a pitching oscillation. The geometry of the wing corresponds with the geometry of the wind tunnel model described in the previous data set (chapter 17E), the difference being the absence of the fuselage in the numerical model. The presence of the fuselage on the upper surface flow is believed to have an effect at small angles of attack only on the forward region of the wing and to have an effect on the location of vortex breakdown at large angles of attack.
The pitching oscillation has an amplitude of 3°, the mean angle of attack is 9°. The position of the oscillation axis and the reduced frequency have been set to match one of the reduced frequencies of the aforementioned experiment, while the Mach number has been increased from the experiment's Mach number 0.12 to 0.4 to reduce computational time.
The data set includes field solutions from Euler as well as from Reynolds averaged Navier-Stokes (RANS) calculations for four equidistant instants within one oscillation cycle and for the corresponding static solution ($\alpha = 9°$). Comparison of the Euler and RANS solutions shows the well known differences in strength and spanwise location of the primary vortex-induced suction peak due to the absence of a secondary vortex in the Euler solution. The agreement with the experimental results is very good.

LIST OF SYMBOLS AND DEFINITIONS

C_p	static pressure coefficient, $C_p = (p-p_\infty)/q_\infty$
LE	leading edge
M_∞	freestream Mach number
RANS	Reynolds averaged Navier-Stokes
Re_∞	Reynolds number
TE	trailing edge
T_∞	freestream temperature
U_∞	freestream velocity
$b = 2s$	wing span
c_i	root chord
f_0	model oscillation frequency
q_∞	dynamic pressure
α	angle of attack, degrees
α_0	mean angle of attack, degrees
$\Delta\alpha$	oscillation amplitude
β	angle of sideslip
ω^*	reduced frequency, $\omega^* = 2\pi f_0 c_i/U_\infty$

FORMULARY

1 General description of model

1.1 Designation	VFE WB1 - SLE
1.2 Type	cropped delta wing
1.3 Derivation	NLR 65°-wing,
1.4 Additional remarks	none
1.5 References	1

2 Model geometry

2.1 Planform	cropped delta wing, see Fig. 1
2.2 Aspect ratio	1.378
2.3 Leading edge sweep	65°
2.4 Trailing edge sweep	0°
2.5 Taper ratio	0.15
2.6 Twist	0°
2.7 Root chord	1.0

2.8 Semi span of model	0.3964
2.9 Area of planform	0.4558
2.10 Definition of profiles	symmetrical with sharp leading edge; 5% rel. thickness; arc segment from LE to x/c = 0.4; airfoil NACA 64A005 from x/c = 0.4 to x/c = 0.75; straight line with 3° inclination from x/c = 0.75 to TE, see Fig. 4
2.11 Lofting procedure between reference sections	N/A
2.12 Form of wing-body junction	N/A, no fuselage
2.13 Form of wing tip	rounded, see Fig. 2
2.14 Control surface details	N/A
2.15 Grid type	structured grid
2.16 Grid size	Euler grid: 96 * 32 * 80 cells RANS grid: 192 * 80 * 128 cells
2.17 Additional remarks	Euler grid identical with WEAG-TA 15 CE III "Fine Grid"
2.18 References on model geometry	1

3 CFD code used

3.1 Euler code	DASA code, using modified Jameson type scheme (dual timestepping)
3.2 RANS code	FLOWer Version 112.1 using modified Jameson type scheme (dual timestepping)
3.3 Turbulence model	Baldwin-Lomax with Degani-Schiff modification, no fixed transition
3.4 Computational time	Euler: 6-8 hours per oscillation cycle RANS: 60 hours per oscillation cycle on a SGI Power Challenge, 1 processor used
3.5 Additional remarks	unsteady calculation started with steady solution ($\alpha = 9°$), unsteady solution converged after 2 - 3 model oscillation cycles
3.6 References on CFD code	2

4 Model motion

4.1 Mode of applied motion	sinusoidal pitching motion about axis parallel to model Y-axis. Axis location: $x/c_i = 0.5625$, axis located below wing plane, $z/c_i = 0.042$
4.2 Range of amplitude	$\Delta\alpha = 3°, 6°$
4.3 Range of frequency	$\omega^* = 2\pi f_0 c_i / U_\infty = 0.56$
4.4 Additional remarks	none

5 Boundary conditions

5.1 Mach number	0.4
5.2 Total pressure	atmospheric
5.3 Temperature	T = 300 K
5.4 Range of model incidence	$\alpha_0 = 9°$
5.5 Definition of model incidence	model incidence defined relative to the wing plane
5.6 Position of transition, if free	N/A
5.7 Additional remarks	distance of far field $\pm 3 \cdot c_i$ in x direction, $6 \cdot s$ in y direction, $\pm 3 \cdot c_i$ in z direction

6 Data presentation

6.1 Test cases for which data could be made available	$\alpha = 9°$, $\Delta\alpha = 3°$ and $\Delta\alpha = 6°$, $Re = 3.1 \cdot 10^6$, $\omega^* = 0.56$, Ma = 0.4, Euler and RANS solutions
6.2 Test cases for which data are included in this document	$\alpha = 9°$, $\Delta\alpha = 3°$, $Re = 3.1 * 10^6$, $\omega^* = 0.56$, Ma = 0.4, Euler and RANS solutions
6.3 Variables included	x, y, z, u/U_∞, v/U_∞, w/U_∞, C_p, total pressure loss, enthalpy

6.4 Data available as	field solution for $\alpha = 9°$ static case, $\alpha = 9°$ dynamic case (upstroke), $\alpha = 12°$ dynamic case, $\alpha = 9°$ dynamic case (downstroke), $\alpha = 6°$ dynamic case, see Fig. 3.
6.5 Steady forces and moments	no
6.6 Unsteady forces and moments	no
6.7 Other forms in which data could be made available	no
6.8 References on data presentation	3, 4
6.9 Additional remarks	data of RANS solution available for every other grid point in each direction. Data for Euler and RANS solutions formatted as TECPLOT® input file

7 Comments on data

7.1 Accuracy	2nd order in time, 2nd order spatial (Euler and RANS)
7.2 Other relevant calculations on same model	none, but unsteady Euler calculations on the presented grid for the cases $\alpha = 9° \pm 6°$ and $\alpha = 21° \pm 6°$ are part of the CE IV of WEAG TA-15
7.3 Relevant calculations on other models of nominally the same airfoil	no, but comparison of RANS results with experimental data of same dynamic parameters from chapter 17E1 is shown in Fig. 5.

Personal contact for further information

Willy Fritz
DaimlerChrysler Aerospace
Dept. MT63 Build. 70.N
P.O. Box 80 11 60
81663 Munich, Germany
Phone: +49-(0)89-607-24529
Email: Willy.Fritz@m.dasa.de

List of references

1 M. T. Arthur: WEAG TA 15 Common Exercise III on Grid Adaptation in Vortical Flow Simulations; Part 1: Euler Solutions. DRA/AS/ASD/TR96073/1, April 1997

2 N. Kroll, R. Radespiel, C.-C. Rossow: Accurate and Efficient Flow Solvers for 3D Applications on Structured Meshes. Lecture Series 1994-05 of the von Karman Institute for Fluid Dynamics, March 1994

3 W. Fritz: Numerische Simulation der instationären Strömung um hochangestellte, oszillierende Deltaflügel. 10. DGLR Fach-Symposium "Strömungen mit Ablösung", Braunschweig, Nov.11th - Nov. 13th 1996

4 W. Fritz: Unsteady Navier-Stokes calculations for a delta wing oscillating in pitch. ICAS-98, Melbourne, Sept. 1998

FORMAT OF DATA SET

As mentioned in section 6.9, the data set is submitted as a series of TECPLOT® input files The files are ASCII files, their size has been reduced with the UNIX command `compress` . The contents of the files can be deduced from their names, all files containing Euler solutions start with the letters eu_, whereas all files containing Navier-Stokes solutions start with the letters ns_. The numbers following those letters indicate the angle of attack. Finally, the letters _up indicate upstroke movement (α increasing) of the model, the letters _dn indicate downstroke movement and the letters _st indicate a steady solution.
As an example, the first lines of an arbitrary data file are printed below. Three columns have been omitted.

```
TITLE = "TA15 Delta Wing 3D-Volume Data"
VARIABLES = "X", "Y", "Z", "U", "V", "W", "CP" ,"TPL", "ENTP"
ZONE F=POINT, I=          97 J=          33K=          81
   0.00000E+00   0.00000E+00   0.00000E+00   0.70126E+00   -0.52673E-01 ... -0.59724E-01
   0.13577E-02   0.17011E-03   0.12071E-14   0.82930E+00   -0.11842E+00 ... -0.10498E+00
   0.28747E-02   0.35948E-03   0.24797E-14   0.93920E+00   -0.98587E-01 ... -0.13640E+00
   0.45697E-02   0.57019E-03   0.38084E-14   0.99580E+00   -0.61080E-01 ... -0.15771E+00
   0.64634E-02   0.80454E-03   0.51794E-14   0.10214E+01   -0.29753E-01 ... -0.17151E+00
   0.85793E-02   0.10650E-02   0.65733E-14   0.10340E+01   -0.80058E-02 ... -0.17954E+00
   0.10943E-01   0.13544E-02   0.79636E-14   0.10422E+01    0.62073E-02 ... -0.18298E+00
   0.13585E-01   0.16756E-02   0.93157E-14   0.10491E+01    0.15155E-01 ... -0.18273E+00
   0.16536E-01   0.20318E-02   0.10585E-13   0.10556E+01    0.20517E-01 ... -0.17949E+00
```

Since the data are written as ASCII files, they can be read by any other program using the Fortran 77 code fragment below. In the data files each row of data corresponds to a data point and each column corresponds to a variable. The order of the variables is specified in one of the first rows, starting with the tecplot-specific keyword VARIABLES. The dimensions in i-, j- and k-direction are specified in the line starting with the keyword ZONE.

```
      do 1, kmax
          do 1, jmax
```

```
            do 1, imax
                do 1, var = 1, numvar
                    read *, array(var, i, j, k)
                end do
            end do
        end do
    end do
```

FIGURES

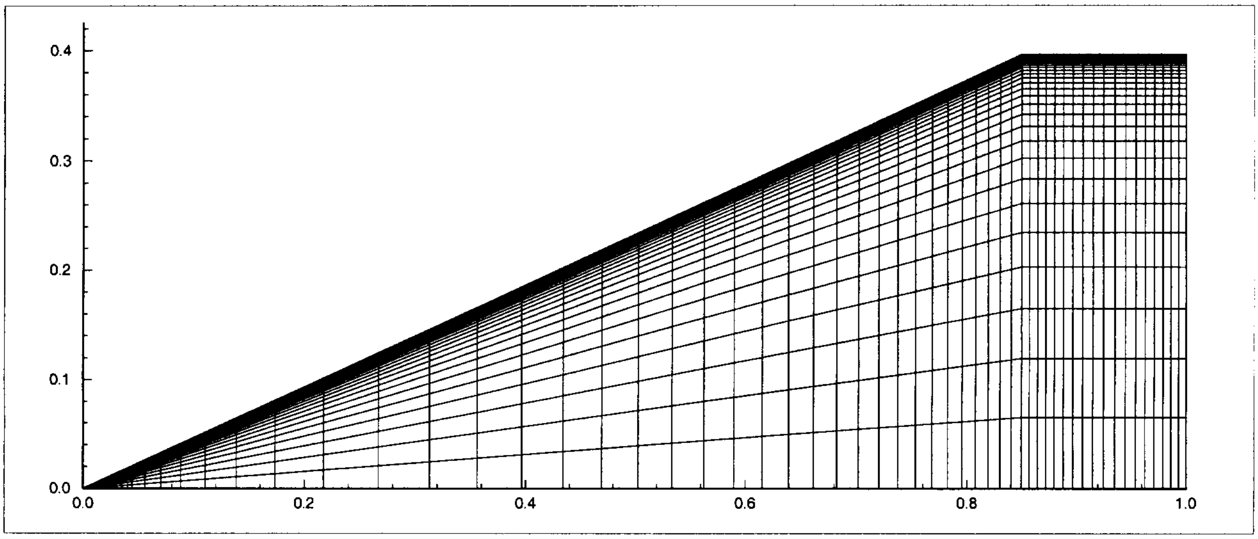

Figure 1: Geometry of the delta wing, RANS grid, every other gridline shown

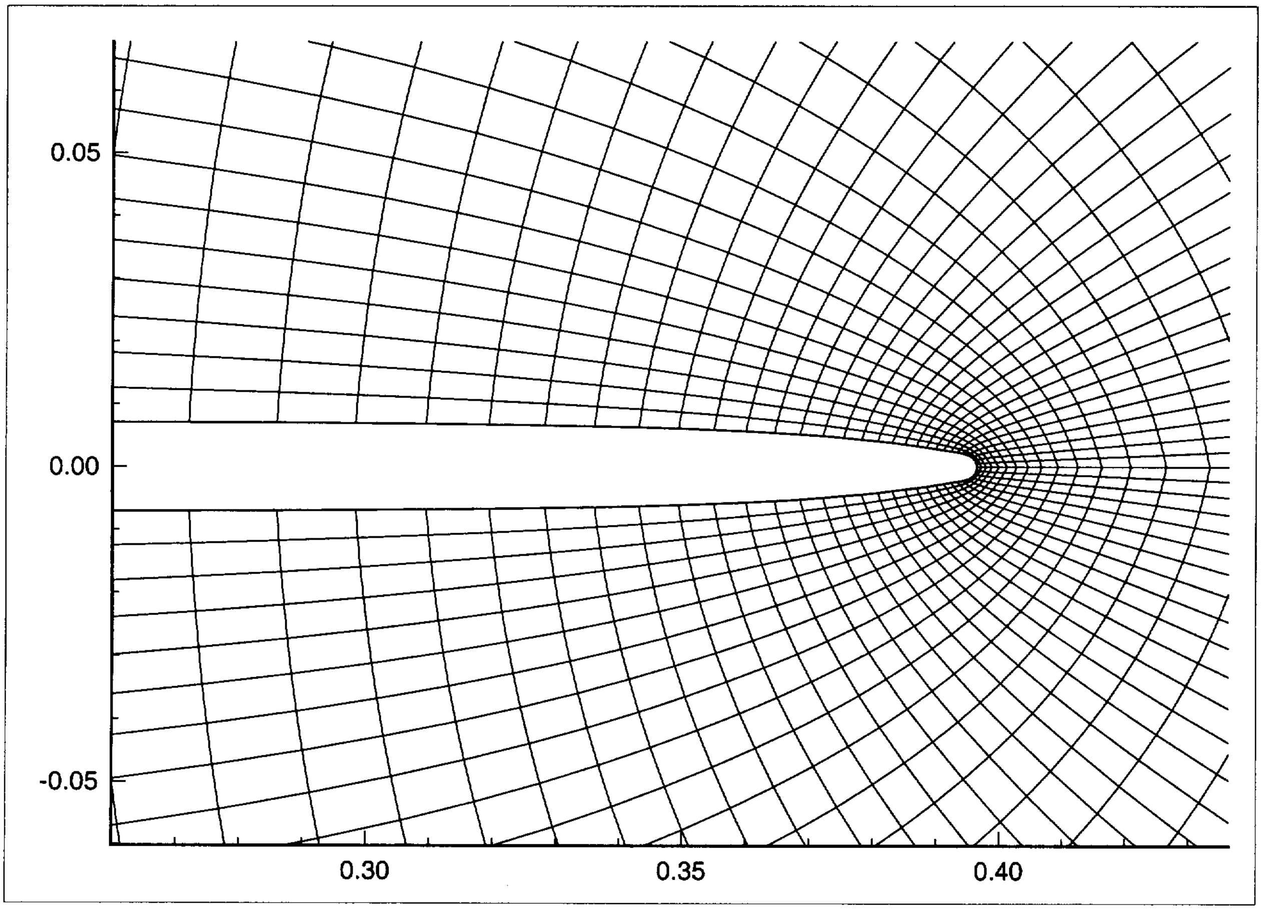

Figure 2: Geometry of wingtip at $x/c_i = 0.9$, Euler grid

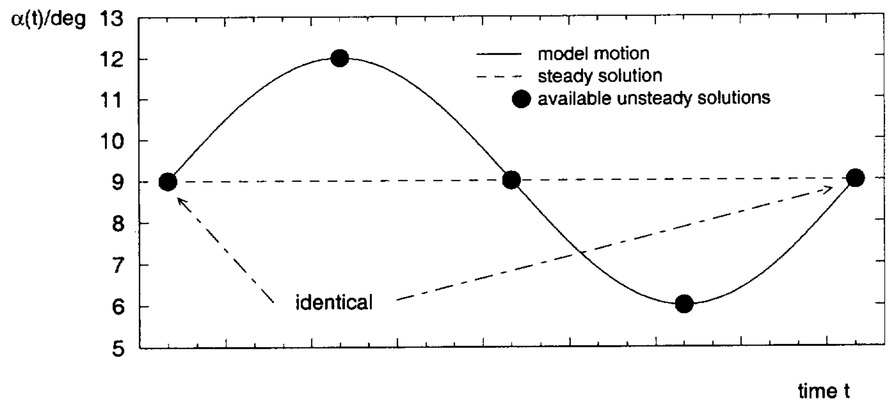

Figure 3: Available steady and unsteady solutions

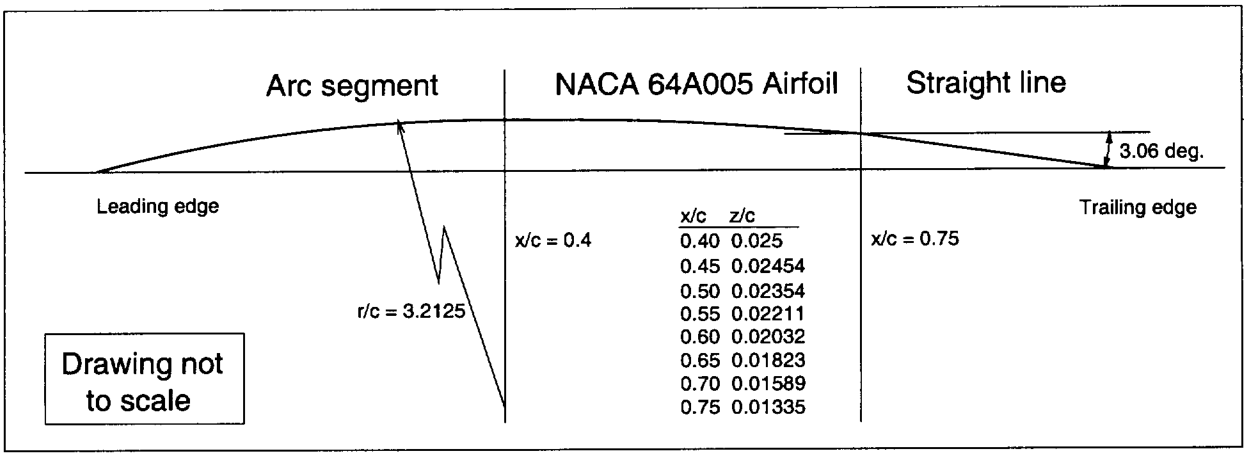

Figure 4: Definition of airfoil

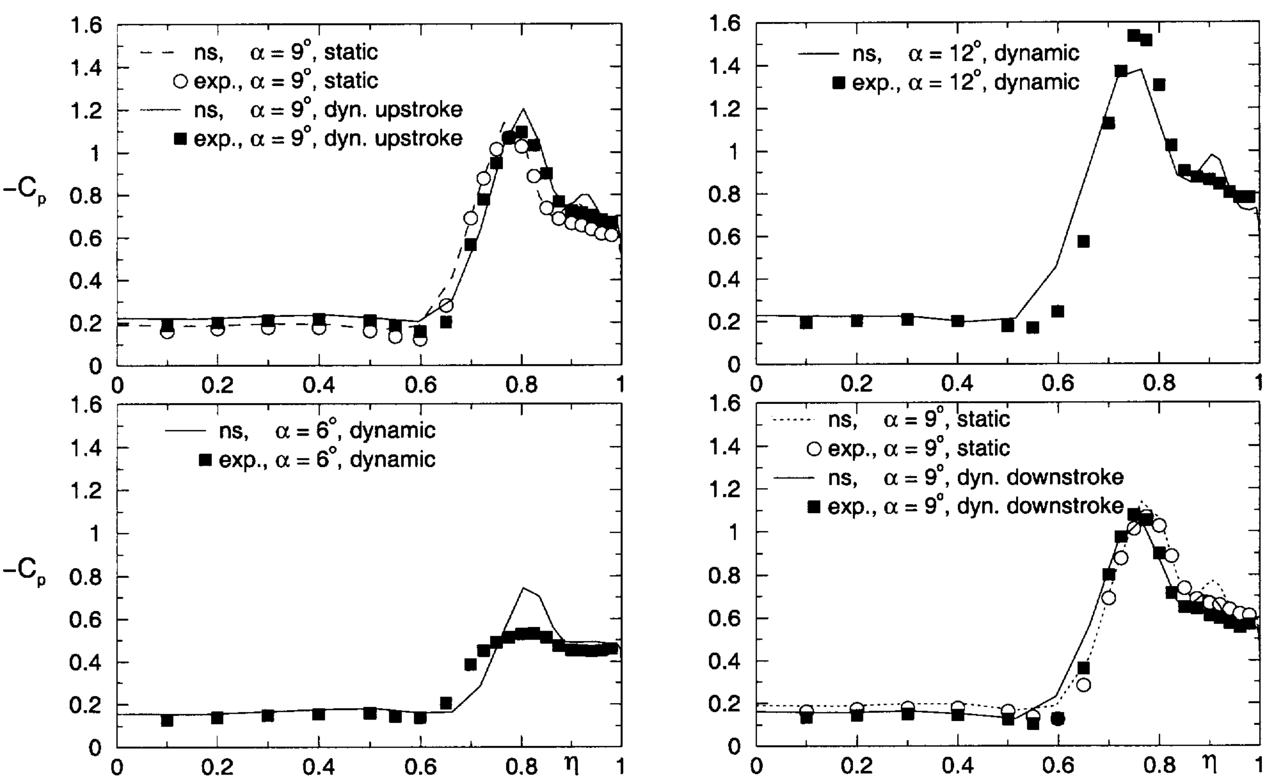

Figure 5: Comparison of results from RANS calculation with experimental data ($\alpha = 9°$, $\Delta\alpha = 3°$, $\omega^* = 0.56$)

18E. LOW SPEED STRAKED DELTA WING

Evert G.M. Geurts
National Aerospace Laboratory NLR, Amsterdam, The Netherlands

INTRODUCTION

Straked wings have become common features of advanced fighter-type aircraft. The strakes are designed to generate vortices from their highly swept leading edges, which stabilise the flow over the wing and provide additional lift up to high angles of attack. In this way the strakes contribute much to a high manoeuvrability. The vortex lift capability of straked wings has been extensively explored and experimental data concerning aerodynamic loading are available for various planforms and Mach numbers. The knowledge of unsteady loading on straked wings is less developed, both in the cases where the loading is due to wing oscillations - as required for aircraft stability and flutter analysis - and in cases where fluctuations in the flow are induced by vortex burst (or vortex breakdown) - as required for stall and buffet predictions.

Some physical aspects of the unsteady vortex flow are described briefly below.

Vortices are shed from the leading edges of the strake and the wing. The sharp leading edges generate vortex sheets, even at low incidence, which roll up spirally into the strake vortices and flow downstream over the wing. The vortices induce strong lateral velocities at the strake and wing upper surface, giving rise to suction peaks at the position of the vortex cores. When the lateral velocities are large enough, secondary flow separations occur, leading to secondary vortices spiralling opposite to the primary vortices. At moderate incidences vortex sheets start to develop from the wing leading edges, starting at the kinks. At higher incidences vortex burst or vortex breakdown occurs, initially for the wing vortices, followed by the strake vortices. An important consequence of vortex burst is that the corresponding suction peaks become weaker and that the vortices lose their ability to produce additional lift. A normal behaviour of vortex burst is that it will move upstream when the incidence increases. At still higher incidences large-scale boundary layer or stall separation occurs, starting often at the trailing edge.

The explanation of the above vortex flow becomes increasingly complicated in case of interactions of strake and wing vortices, their influence on vortex burst and flow separation and, at high enough speeds their interactions with shock waves.

When the straked delta wing is oscillating, the strength and the position of the wing and strake vortices will oscillate. As the vortices are being fed through the vortex sheets emanating from the leading edges, it is to be expected that the oscillations of vortex strength and position will lag the wing oscillation.

Some phenomena can be distinguished in the results of the steady measurements, shown in figure 1, at some characteristic incidence ranges:

- up to 9° attached ("linear") flow
- 9° to 19° fully developed vortex flow
- 19° to 38° vortex burst extending from trailing edge
- beyond 38° vortex burst penetrating the strake, almost fully stalled flow

For the data selection special interest was placed on incidences which mark transition of flow characteristics, or were typical for the flow characteristics in some incidence range. These incidences were 9°, 19°, 22°, 36° and 42°.

- alpha = 9° attached flow
- alpha = 19° onset to vortex burst
- alpha = 22° burst vortex flow
- alpha = 36° maximum CN, change of 180° in phase angle of unsteady pitching
- alpha = 42° fully separated flow

The above values are the correct geometric incidences as are included in the database files; in the data point overview adjusted values are indicated. For the above characteristic values of incidence a large number of test conditions was explored. Though there is a full-span model, and conditions for plus and minus 5 degrees side-slip are expected to give the same results, both cases are included, because pressure transducers were situated only in the right half-wing. Both conditions are necessary to understand side-slip effects. This all leads to a selection of test cases as indicated in table 1.

LIST OF SYMBOLS AND DEFINITIONS

Definitions

Figure 2a is included as an example of the CATIA based geometry file, included in the database, with the CATIA body-fixed axis system. The CATIA file provides half of the model geometry. The wind tunnel model was a full model, but because of its symmetry only half of the model had to be designed in CATIA.

x-axis: chord-wise co-ordinate in wing reference plane; at apex x = 0

y-axis: span-wise co-ordinate in wing reference plane; y'-axis = rotation axis or pitching axis at x/cr = 73.27 %

z-axis: co-ordinate in plane of symmetry normal to wing reference plane

Figure 2b shows the definitions and sign conventions used for non-dimensionalisation.

Non-dimensionalisation

Mean	**Unsteady**
steady component	First harmonic component (sometimes also second) the unsteady component is indicated by the suffix i, each unsteady component has been decomposed into a real (in-phase) and an imaginary (out-of-phase) part; e.g.(C#)i = Re (C#) + i * Im (C#)

Pressures

(Cp)m	= (p – ps) / q	(Cp)i	= $(p)_i$ / (Q * dα)

Balance loads

(Cl)m	= l / (Q * S * bw)	(Cl)i	= l_i / (Q * S * bw * dα)
(Cm)m	= m / (Q * S * cr)	(Cm)i	= m_i/ (Q * S * cr * dα)
(CN)m	= N / (Q * S)	(CN)i	= N_i / (Q * S * dα)
(Cn)m	= n / (Q * S * bw)	(Cn)i	= n_i / (Q * S * bw * dα)
(CT)m	= T / (Q * S)	(CN)i	= T_i / (Q * S * dα)
(CY)m	= Y / (Q * S)	(CY)i	= Y_i / (Q * S * dα)

Note: Each harmonic component has been non-dimensionalized by the first harmonic of dα (in radians).

Symbols and abbreviations

ALPHA, alpha, α	(°)	wing incidence
b	(m)	local wing span
bw	(m)	wing span; reference span bw = 0.8000 m
BETA, beta, β	(°)	sideslip angle
c	(m)	local chord
CD	(-)	wing drag force coefficient
CL	(-)	wing lift force coefficient
Cl	(-)	wing rolling moment coefficient
Cm	(-)	wing pitching moment coefficient; reference axis = rotation axis x/cr = 73.27 %
CN	(-)	wing normal force coefficient
Cn	(-)	wing yawing moment coefficient
Cp	(-)	pressure coefficient
cr	(m)	root chord; reference chord cr = 0.7855 m
CT	(-)	wing tangential force coefficient
CY	(-)	wing side force coefficient
D	(N)	wing drag force
DALPHA, dalpha, dα	(°, rad)	harmonic oscillations: amplitude of unsteady wing incidence (1-cosine) inputs: magnitude of wing incidence variation
(d)i	(mm/rad)	unsteady displacement of accelerometer relative to angular displacement of wing
DPN		Data point number
FREQ, freq, f	(Hz)	frequency, frequency of model oscillation
HARM, harm, h		harmonic component; harm = 0: mean, harm = 1: first harmonic
i		$\sqrt{-1}$
L	(N)	wing lift force

l	(Nm)	wing rolling moment
LVDT		Linear Variable Displacement Transducer
m	(Nm)	wing pitching moment; rotation axis x/cr = 73.27 %
MACH	(-)	freestream Mach number
N	(N)	wing normal force
n	(Nm)	wing yawing moment
NO		number of pressure transducers
p	(Pa)	pressure at model surface
ps	(Pa)	freestream static pressure
pt	(Pa)	total pressure
PHI, φ	(°)	phase angle
Q	(Pa)	dynamic pressure
REDFR	(-)	reduced frequency, REDFR = π * f * cr / V
RUN		run number, data point
S	(m^2)	wing area; wing reference area S = 0.2640 m^2
T	(°C)	stagnation temperature in settling chamber
T	(N)	wing tangential force
T	(s)	harmonic oscillation: period of oscillation (1-cosine) inputs: duration of a (1-cos) input
t	(s)	time
V	(m/s)	freestream velocity
WRP		Wing Reference Plane
x	(m)	chordwise ordinate (see Definitions)
Y	(N)	wing side force
y	(m)	spanwise ordinate (see Definitions)
z	(m)	ordinate (see Definitions)

Subscripts

a, _a	adjusted
g	geometric
m	mean
i	unsteady
ref	reference value

FORMULARY

1 General Description of model

1.1	Designation	Low Speed Straked Delta Wing
1.2	Type	Full-span model, supported by struts
1.3	Derivation	Research fighter-type wing
1.4	Additional remarks	-
1.5	References	Ref. 1, Ref. 2, Ref. 6

2 Model Geometry

2.1	Planform	Trapezoidal main wing with simple strake
2.2	Aspect ratio	2.422

2.3	Leading edge sweep	Wing: 40°, strake: 76°
2.4	Trailing edge sweep	No
2.5	Taper ratio	-
2.6	Twist	No
2.7	Root chord	0.7855 m
2.8	Span of model	0.800 m
2.9	Area of planform	0.264 m^2
2.10	Leading-edge flap	Not present
2.11	Trailing-edge flap	Not present
2.12	Location of reference sections and definition of profiles	Measured upper and lower co-ordinates at 4 chordwise sections (3 on port and starboard side and one at line of symmetry) and at 5 spanwise sections
2.13	Form of wing-body or wing-root junction	No fuselage and empennage, middle of main wing thickened to accommodate balance
2.14	Form of wing tip	Fairing: geometry included in CATIA file in database
2.15	Additional remarks	Outboard wing: NACA 64A005 airfoil, Strake: diamond shaped with sharp LE Geometry data included as CATIA file in database
2.16	References	Ref. 2, Ref. 6 Part I, Appendix A

3 Wind Tunnel

3.1	Designation	NLR Low Speed Wind Tunnel LST
3.2	Type of tunnel	Atmospheric, closed-circuit, interchangeable test sections
3.3	Test section dimensions	Width 3 m, height 2.25 m, length 8.75 m (5.75 m forward part for aeronautical testing, aft part for non-aerodynamical (industrial) testing
3.4	Type of roof and floor	Solid
3.5	Type of side walls	Solid
3.6	Ventilation geometry	-
3.7	Displacement thickness of side wall boundary layer	Aeronautical testing (forward part): 10 to 11 mm, nonaeronautical testing (aft part): 15 to 20 mm
3.8	Displacement thickness of boundary layers at roof and floor	About the same as in 3.7
3.9	Method of measuring Mach number in the contraction and a calibration correction	Combination of 4 total pressures in settling chamber, 4 static pressures
3.10	Flow angularity	Well within 0.1%
3.11	Variation in flow velocity across the test section	Less than 0.2%
3.12	Variation in static pressure along length of test section	Less than 0.5% of established dynamic pressure
3.13	Sources and levels of noise or turbulence in empty tunnel	0.02% - 0.03%
3.14	Tunnel resonance	-
3.15	Additional remarks	-
3.16	References on tunnel	-

4 Model motion

4.1	General description	Harmonic sinusoidal pitching motion, (1-cos) pitch manoeuvres
4.2	Reference co-ordinate and definition of motion	LVDT between model and support gave correct geometric incidence, which included deformation of balance
4.3	Range of amplitude	1° to 18°
4.4	Range of frequency	1 to 16 Hz

4.5	Method of applying motion	Electro-hydraulic shaker system (Ref. 8)
4.6	Timewise purity of motion	Adequate purity
4.7	Natural frequencies and normal modes of model and support system	Natural frequencies: 31.97 Hz (yaw), 38.66 Hz (roll), 45.36 Hz (roll + pitch), 53.03 Hz (pitch), also higher frequencies; see Ref. 3
4.8	Actual mode of applied motion including any elastic deformation	Measured with 9 accelerometers; elastic deformation negligible Position and output included in database files.
4.9	Additional remarks	-

5 Test Conditions

5.1	Model planform area/tunnel area	0.0391
5.2	Model span/tunnel height	0.2667
5.3	Blockage	Solid blockage negligible, corrected for wake blockage according standard procedure
5.4	Position of model in tunnel	Supported by struts, Wing reference plane in centre of tunnel
5.5	Range of velocities	80, 55 and 30 m/s (Mach numbers: 0.225, 0.155, 0.085)
5.6	Range of tunnel total pressure	Atmospheric
5.7	Range of tunnel total temperature	Actual total temperature value included in database files
5.8	Range of model steady or mean incidence and sideslip angles	Adjusted incidences: -10° to 55° Sideslip angles: -5°, 0°, +5°
5.9	Definition of model incidence	Relative to WRP
5.10	Position of transition, if free	-
5.11	Position and type of trip, if transition fixed	-
5.12	Flow instabilities during tests	-
5.13	Changes to mean shape of model due to steady aerodynamic load	Not measured
5.14	Additional remarks	Correct geometric incidences and amplitudes in data files
5.15	References describing tests	Refs. 5, 6 and 9

6 Measurements and Observations

6.1	Steady pressures for the mean conditions		Yes
6.2	Steady pressures for small changes from the mean conditions		No
6.3	Quasi-steady pressures		No
6.4	Unsteady pressures	Measured directly	
		- harmonic components	Yes
		- time histories	Yes
6.5	Steady loads for the mean conditions	Measured directly	Yes
6.6	Steady loads for small changes from the mean conditions		No
6.7	Quasi-steady loads		No
6.8	Unsteady loads	Measured directly	
		- harmonic components	Yes
		- time histories	Yes
		- Power Spectral Densities	Yes
		- manoeuvres	Yes
6.9	Measurement of actual motion at points on model		Yes
6.10	Observation or measurement of boundary		No

	layer properties	
6.11	Visualisation of flow	Yes
6.12	Visualisation of shock wave movements	No
6.13	Additional remarks	-

7 Instrumentation

7.1	Steady pressure	
	7.1.1 Position of orifices spanwise and chordwise	See Figure 3: positions included in database files of pressures
	7.1.2 Type of measuring system	42 in situ miniature pressure transducers
7.2	Unsteady pressure	
	7.2.1 Position of orifices spanwise and chordwise	See Figure 3: positions included in database files of pressures
	7.2.2 Diameter of orifices	0.8 mm
	7.2.3 Type of measuring system	Processor for measuring harmonic components; see Ref.7
	7.2.4 Type of transducers	Endevco 8507-5, Kulite CQL-080-5D, Kulite XCS-093-5D
	7.2.5 Principle of calibration	Data acquisition system was calibrated daily, pressure transducers before the wind tunnel test
	7.2.6 Accuracy of calibration	~1%
7.3	Model motion	
	7.3.1 Method of measuring motion	LVDT: type Sangamo AFG 5.0 S
	7.3.2 Method of determining spatial mode of motion	9 accelerometers: 5 Endevco 2220 C, 4 Kulite GY-155
	7.3.3 Accuracy of measured motion	LVDT: better than 0.015 mm
7.4	Processing of unsteady measurements	
	7.4.1 Method of acquiring and processing measurements	Processor for measuring harmonic components
	7.4.2 Type of analysis	Fundamental harmonics: pressures, balance loads time histories: pressures, balance loads PSD plots: balance loads vortex core positions: visualisation
	7.4.3 Unsteady pressure quantities obtained and accuracy's achieved	Fundamental harmonics and time histories, for accuracy see 9.1.6
7.5	Additional remarks	-
7.6	References on techniques	-

8 Data presentation

8.1	Test cases for which data could be made available	see Tables 2 to 5
8.2	Test cases for which data are included in this document	Summarised and motivated in Introduction
8.3	Steady pressures	Mean values; see Low Speed Straked Delta Wing Database
8.4	Quasi-steady or steady perturbation pressures	
8.5	Unsteady pressures	Mean values and first harmonics; see Low Speed Straked Delta Wing Database
8.6	Steady loads	Mean values; see Low Speed Straked Delta Wing Database
8.7	Quasi-steady or unsteady perturbation forces	
8.8	Unsteady loads	Mean values and first harmonic; see Low Speed Straked Delta Wing Database
8.9	Other forms in which data could be made	-

	available	
8.10	Reference giving other representations of data	References 9 to 15

9 Comments on data

9.1	Accuracy	
	9.1.1 Mach number	+/- 0.001
	9.1.2 Steady incidence	+/- 0.01 at LVDT position
	9.1.3 Reduced frequency	+/- 0.0005
	9.1.4 Steady pressure coefficients	+/- 0.5 percent
	9.1.5 Steady pressure derivatives	-
	9.1.6 Unsteady pressure coefficients	+/- 0.5 percent
9.2	Spanwise variations	Dynamic pressure distribution around model in relation to dynamic pressure, measured by tunnel reference system, measured for zero-lift condition
9.3	Non-linearity's	-
9.4	Influence of tunnel total pressure	-
9.5	Effects on data of uncertainty, or variation, in mode of model motion	-
9.6	Wall interference corrections	Not measured
9.7	Other relevant tests on same model	Ref. 5
9.8	Relevant tests on other models of nominally the same shapes	Ref. 4
9.9	Any remarks relevant to comparison between experiment and theory	-
9.10	Additional remarks	An example of a database file and its explanation is included in table 6. Structure of file set-up is included in README file in database
9.11	References on discussion of data	References 9 to 15

10 Personal contact for further information

Evert G.M. Geurts
Department of Aerodynamic Engineering and Aeroelasticity
Phone: +31 20 5113455
Fax: +31 20 5113210
Email: geurts@nlr.nl

National Aerospace Laboratory NLR

Anthony Fokkerweg 2	P.O. Box 90502
NL 1059 CM Amsterdam	NL 1006 BM Amsterdam
The Netherlands	The Netherlands

Phone: +31 20 5113113
Fax: +31 20 5113210
Website: http://www.nlr.nl

11 List of references

1 Horsten, J.J., Kannemans, H., "Joint General Dynamics/NLR (Netherlands) wind-tunnel test program for an oscillating straked wing in low speed vortex flow", NLR Memorandum AE-82-015 U, 1982.

2 Horsten, J.J., "Design of the GD/NLR straked wing model and support system", NLR Memorandum AE-85-005 U, 1985.

3 den Boer, R.G., Persoon, A.J., "Vibration test of the GD/NLR straked wing model and support system", NLR Memorandum AE-85-014 U, 1985.

4 Persoon, A.J., Retel, A.P., "Some experiments with flow visualization of vortices over a vibrating straked wing", NLR Memorandum AE-86-001 L, 1986.

5 de Vries, O., "Force measurements in a low-speed wind tunnel on a model of a straked wing, suspended in wires", NLR TR 86047 C, 1986.

6 Cunningham, Jr., A.M., den Boer, R.G., et.al., "Unsteady low speed wind tunnel test of a straked delta wing, oscillating in pitch",

Part I General description and discussion of results

Part II Plots of steady and zeroth and first order harmonic unsteady pressure distributions

Part III Plots of zeroth and first order harmonic unsteady pressure distributions (concluded) and plots of steady and zeroth and first order harmonic overall loads

Part IV Plots of time histories of pressures and overall loads

Part V Plots of the overall loads spectra and the response of overall loads to single step (1-cos) inputs

Part VI Presentation of the visualization program

NLR TR 87146 L Parts I through VI, (also "published" in April 1988 as AFWAL-TR-8-3098, Parts I-VI).

7 Fuykschot, P.H., "PHAROS, Processor for harmonic analysis of the response of oscillating surfaces", NLR MP 77012 U, 1977.

8 Poestkoke, R., "Hydraulic test rig for oscillating wind-tunnel models", NLR MP 76020 U, 1976.

9 den Boer, R.G., Cunningham Jr., A.M., "A wind tunnel investigation at low speed of the flow about a straked delta wing, oscillating in pitch", Proceedings of the AIAA Atmospheric Flight Mechanics Conference, Monterey, August 1987, (also NLR MP 87046 U, 1987).

10 Cunningham Jr., A.M., den Boer, R.G., "Harmonic analysis of force and pressure data results for an oscillating straked wing at high angles", Proceedings of the AIAA Atmospheric Flight Mechanics Conference, Monterey, California, 17-19 August 1987, AIAA Paper No. 87-2494.

11 Cunningham Jr., A.M., "A critique of the Experimental Aerodynamic Database for an Oscillating Straked Wing at High Angles", Proceedings Fourth Symposium on Numerical and Physical Aspects of Aerodynamic Flows, California State University, Long Beach, California, 16-19 January 1989.

12 den Boer, R.G., Cunningham Jr., A.M., "Low-Speed Unsteady Aerodynamics of a Pitching Straked Wing at High Incidence - Part I: Test Program", Journal of Aircraft, Volume 27, Number 1, January 1990, Pages 23-30, (also NLR TP 89150 L, 1989).

13 Cunningham Jr., A.M., den Boer, R.G., "Low-Speed Unsteady Aerodynamics of a Pitching Straked Wing at High Incidence - Part II: Harmonic Analysis", Journal of Aircraft, Volume 27, Number 1, January 1990, Pages 31-41.

14 Cunningham Jr., A.M., den Boer, R.G., "Steady and Unsteady Aerodynamics of a Pitching Straked Wing Model at High Angles of Attack", AGARD FDP Conference Proceedings 494 Paper 29: Vortex Flow Aerodynamics, Scheveningen, The Netherlands, 1-4 October 1990.

15 Cunningham Jr., A.M., den Boer, R.G., "Analysis of Unsteady Force, Pressure and Flow-Visualization Data for a Pitching Straked Wing Model at High Angles of Attack", AGARD FDP Conference Proceedings 497 Paper 8: Maneuvering Aerodynamics, Toulouse, France, 1-2 May 1991

Incidence [°] (adjusted)	8	22	22	22	22	22	38
Amplitude [°]	4	4	8	8	8	8	8
Frequency [Hz]	5	6	6	8	8	8	6
Side-slip [°]	0	0	0	0	+5	-5	0
Velocity [m/s]	80	80	80	80	80	80	80
Steady Pressures (Cp_s)	13	20	20	20			54
Unsteady Pressures (Cp0,Cp1)	1036	524	526	532, 976	919	929	593
Time histories of pressures	1036			976			
Time histories of balance loads				532	919	929	
Manoeuvres				3017			

Table 1: Selected test cases for Low Speed Straked Delta Wing (Values in shaded area indicate data point numbers)

α_a	$\beta = 0.0°$, V ~ 80 m/s
-10° (2°) 54°, 55°	without wire suspension blocks
4° (4°) 40°	with wire suspension blocks

Table 2: Steady test program

Oscillating amplitudes at alpha/frequency combinations								
$\beta = 0.0°$, V ~ 80m/s								
f	2	3	4	5	8	10	12	16
α_a								
-4		2,4		2,4	2,4		2	2
0		2,4,8		2,4,8	2,4,8		2	2
4		2,4,8,12		2,4,8,12	2,4,8		2	2
8		2,4,8,12,16		2,4,8,12,16	2,4,8		2	2
12	4,8	2,4,8,12		2,4,8,12	2,4,8		2	2
16	2,4,6,8,10,12	2,4,6,8,10,12	2,4,6,8,10,12	2,4,6,8,10,12	2,4,6,8		2	2
18	2,4,6,8,10,12,14	2,4,6,8,10,12,14	2,4,6,8,10,12,14	2,4,6,8,10,12,14	2,4,6,8		2	2
20	2,4,6,8,10,12,14,16	2,4,6,8,10,12,14,16	2,4,6,8,10,12,14,16	2,4,6,8,10,12,14,16	2,4,6,8		2	2
22	2,4,6,8,10,12,14,16,18	2,4,6,8,10,12,14,16,18	2,4,6,8,10,12,14,16,18	2,4,6,8,10,12,14,16,18 (6Hz) 2,4,6,8,10,12	2,4,6,8	2,4	2	2
24		2,4,6,8,10,12,14,16		2,4,6,8,10,12,14,16	2,4,6,8		2	2
26		2,4,6,8,10,12,14		2,4,6,8,10,12,14	2,4,6,8		2	2
28		2,4,6,8,10,12		2,4,6,8,10,12	2,4,6,8		2	2
30		2,4,6,8,10		2,4,6,8,10	2,4,6,8		2	2
32		2,4,6,8,10,12		2,4,6,8,10,12	2,4,6,8		2	2
34		2,4,6,8,10,12,14		2,4,6,8,10,12,14	2,4,6,8		2	2
36		2,4,6,8,10,12,14,16		2,4,6,8,10,12,14,16	2,4,6,8		2	2
38	2,4,6,8,10,12,14,16	2,4,6,8,10,12,14,16	2,4,6,8,10,12,14,16	2,4,6,8,10,12,14,16 (6Hz) 2,4,6,8,10	2,4,6,8	2,4	2	2
40		2,4,6,8,10,12,14		2,4,6,8,10,12,14	2,4,6,8		2	2
42		2,4,6,8,10,12		2,4,6,8,10,12	2,4,6,8		2	2
44		2,4,6,8,10		2,4,6,8,10	2,4,6,8		2	2
46		2,4,6,8 (also.1,1,3)		2,4,6,8	2,4,6,8		2	2
48		2,4,8		2,4,8	2,4,8		2	2
50		2,4		2,4	2,4		2	2
52		2		2	2		2	2
54		1		1	1		1	1

Table 3a: Unsteady test program (FUNDAMENTAL HARMONICS, BASIC PROGRAM)

Oscillating amplitudes at alpha/frequency combinations									
$\beta = +5°$, V ~ 80 m/s					$\beta = -5°$, V ~ 80 m/s				
frequency	3	5	8	16	frequency	3	5	8	16
α_a					α_a				
8	4,8,16	4,8,16	2,4,8	2	8	4,8,16	4,8,16	2,4,8	2
18	4,8,14	4,8,14	2,4,8	2	18	4,8,14	4,8,14	2,4,8	2
22	4,8,16	4,8,16	2,4,8	2	22	4,8,16	4,8,16	2,4,8	2
38	4,8,16	4,8,16	2,4,8	2	38	4,8,16	4,8,16	2,4,8	2
46	4,8	4,8	2,4,8	2	46	4,8	4,8	2,4,8	2

Table 3b: Unsteady test program (FUNDAMENTAL HARMONICS, SIDESLIP INFLUENCE)

Oscillating amplitudes at alpha/frequency combinations										
$\beta = 0.0°$, V ~ 55 m/s					$\beta = 0.0°$, V ~ 30 m/s					
frequency	2.06	3.44	5.50	11.0	frequency	1.13	1.88	3.0	6.0	12.0
α_a					α_a					
8	4,8,16	4,8,16	4,8	2	8	4,8,16	4,8,16	4,8,16	2,4,8	2
16	4,8,12	4,8,12	4,8	2						
18	4,8,14	4,8,14	4,8	2	18	4,8,14	4,8,14	4,8,14	2,4,8	2
20	4,8,16	4,8,16	2,4,8	2						
22	4,8,16	4,8,16	4,8	2	22	4,8,16	4,8,16	4,8,16	2,4,8	2
24	4,8,16	4,8,16	4,8	2						
36	4,8,16	4,8,16	4,8	2						
38	4,8,16	4,8,16	4,8	2	38	4,8,16	4,8,16	4,8,16	2,4,8	2
42	4,8,16	4,8,12	4,8	2						
44	4,8,10	4,8,10	4,8	2						
46	4,8	4,8	4,8	4	46	4,8	4,8	4,8,16	2,4,8	4

Table 3c: Unsteady test program (FUNDAMENTAL HARMONICS, VELOCITY INFLUENCE)

Oscillating amplitudes at alpha/frequency combinations						
$\beta = +0°$, V ~ 80 m/s						
frequency	2	3	4	5	8	16
α_a						
8		4,8,16		4,8,16	4,8	2
18	8,14	8,14	4,8	4,8,14	4,8	2
20	4,8,14		4,8,14		4,8	2
22	4,8,14	4,8,14	4,8,14	4,8,14	4,8	2
38		4,8,14		4,8,14	4,8	2
46		4,8		4,8	4,8	2

Table 4a: Unsteady test program (TIME HISTORIES of PRESSURES)

Oscillating amplitudes at alpha/frequency combinations									
	$\beta = +0°$, V ~ 80 m/s			$\beta = +5°$, V ~ 80 m/s			$\beta = -5°$, V ~ 80 m/s		
frequency	3	5	8	3	5	8	3	5	8
α_a									
0	8	8	8						
4	8,12	8,12	8						
8	8,12,16	8,12,16	8	8,16	8,16	8	8,16	8,16	8
12	8,12	8,12	8						
16	8,12	8,12							
18	8,12	8,12	8	8	8	8	8	8	8
20	8,12,16	8,12,16	8						
22	8,12,16,18	8,12,16,18	8	8,16	8,16	8	8,16	8,16	8
24	8,12,16	8,12,16	8						
26	8,12	8,12	8						
28	8,12	8,12	8						
30	8	8	8						
32	8,12	8,12	8						
34	12	8,12	8						
36	8,12	8,12	8						
38	8,12,16	8,12,16	8	8,16	8,16	8	8,16	8,16	8
40	8,12	8,12	8						
42	8,12	8,12	8						
44	8	8	8						
46	8	8	8	8	8	8	8	8	8

Table 4b: Unsteady test program (TIME HISTORIES of OVERALL LOADS, PSD'S)

Oscillating amplitudes at alpha/T combinations						
$\beta = +0°$, V ~ 80 m/s						
T	0.500	0.330	0.250	0.200	0.125	0.083
α_a						
8	8,16,24,32	8,16,24,32	8,16,24,32	8,16,24,32	8,16	8
16	24	24	24	24		
22	8,16,24,32	8,16,24,32	8,16,24,32	8,16,24,32	8,16	8
24	16	16	16	16	16	
30	24	24	24	24		
32	8	8	8	8	8	8
38	16	16	16	16	16	
46	8	8	8	8	8	8

Table 5: Unsteady test program: (1 - COSINE) INPUTS

```
File organization of "sel_st" and "sel_uns" (STeadu and UNSteady)
=================================================================
Selection of zeroth and first order harmonic (un)steady pressures
```

Description	FORMAT
DPN,HARM,ALPHA,Re(DALPHA),Im(DALPHA),FREQ,MACH	2i5,5f10.5
VELOCITY,REDFR,Q,ps,T,BETA,S	2f10.5,f10.2,4f10.5
NO,xref,x/xref,yref,y/yref,(Cp)m,Re(Cp),Im(Cp)	44*(i2,7f10.5,/)
(CN)m,Re(CN),Im(CN),(Cn)m,Re(Cn),Im(Cn)	6f10.5
(CY)m,Re(CY),Im(CY),(Cm)m,Re(Cm),Im(Cm)	6f10.5
(CT)m,Re(CT),Im(CT),(Cl)m,Re(Cl),Im(Cl)	6f10.5
NO,xref,x/xref,yref,y/yref,Re(d),Im(d)	9*(i2,6f10.5,/)

```
NB. Improper values represented as: 9999.99
```

Table 6a: Example of explanation of file organisation of pressure data files

```
1036    1   9.97900     .05941    -.02431    5.00000     .22346
  77.60194     .15900    3613.07102086.920 303.00000   0.00000     .26400
  1 785.50000      .40420   79.16000     .068109999990.009999990.009999990.00
  2 785.50000      .40420   79.16000     .204309999990.009999990.009999990.00
  3 785.50000      .40420   79.16000     .340609999990.009999990.009999990.00
  4 785.50000      .40420   79.16000     .476809999990.009999990.009999990.00
  5 785.50000      .40420   79.16000     .54480    -.45169   -5.93639     .79971
  6 785.50000      .40420   79.16000     .612909999990.00   -7.10090     .92673
  7 785.50000      .40420   79.16000     .68100    -.77757   -5.86580     .45257
  8 785.50000      .40420   79.16000     .749209999990.009999990.009999990.00
  9 785.50000      .40420   79.16000     .81730    -.62521   -2.84359    -.26235
 10 785.50000      .40420   79.16000     .88540    -.69598   -2.79452    -.21200
 11 785.50000      .65880 225.00000     .13110    -.24250    -.64196    -.29332
 12 785.50000      .65880 225.00000     .26000    -.28479   -1.37241    -.14200
 13 785.50000      .65880 225.00000     .32440    -.29590   -3.22860     .26914
 14 785.50000      .65880 225.00000     .38890    -.57053   -4.92005     .50296
 15 785.50000      .65880 225.00000     .42930    -.87438   -5.33319     .37613
 16 785.50000      .65880 225.00000     .46930    -.85384   -3.98634    -.47575
 17 785.50000      .65880 225.00000     .50980    -.52407   -3.34236    -.14527
 18 785.50000      .65880 225.00000     .55020    -.44519   -2.48929     .05060
 19 785.50000      .65880 225.00000     .59020    -.42339   -2.77352    -.11098
 20 785.50000      .65880 225.00000     .63070    -.35628   -1.92341    -.17372
 21 785.50000      .65880 225.00000     .67070    -.31453   -1.31876    -.18386
 22 785.50000      .65880 225.00000     .71110    -.28706   -1.64119    -.15489
 23 785.50000      .65880 225.00000     .75560    -.67130   -5.41212    -.85584
 24 785.50000      .65880 225.00000     .80000   -2.21298  -18.60173     .19867
 25 785.50000      .65880 225.00000     .84440   -1.79432   -5.78206    -.32753
 26 785.50000      .65880 225.00000     .88890   -1.48771   -3.35132    -.54125
 27 785.50000      .65880 225.00000     .933309999990.00   -2.65331    -.55818
 28 785.50000      .65880 225.00000     .97780   -1.27615   -2.93168    -.64424
 29 785.50000      .96820 400.00000     .20000    -.018249999990.009999990.00
 30 785.50000      .96820 400.00000     .30000    -.10672    -.47488     .08081
 31 785.50000      .96820 400.00000     .40000    -.02891    -.90136     .01624
 32 785.50000      .96820 400.00000     .50000    -.00183    -.37925    -.12307
 33 785.50000      .96820 400.00000     .60000    -.07435   -1.18126    -.05478
 34 785.50000      .96820 400.00000     .70000    -.24055   -3.67764     .32366
 35 785.50000      .96820 400.00000     .80000    -.37085   -2.92309    -.07185
 36 785.50000      .96820 400.00000     .90000    -.33002   -1.53550    -.41388
 37 321.38000      .05720 400.00000     .40000   -2.870869999990.009999990.00
 22 321.38000      .16610 400.00000     .40000    -.28706   -1.64119    -.15489
 38 321.38000      .29210 400.00000     .40000    -.27462   -1.47719     .04282
 39 321.38000      .41820 400.00000     .40000    -.38444   -2.34909     .06812
 40 321.38000      .54420 400.00000     .40000    -.25250   -1.12146    -.06194
 41 321.38000      .67020 400.00000     .40000    -.19045    -.68371    -.15309
 42 321.38000      .79620 400.00000     .400009999990.00    -.54453    -.11307
 31 321.38000      .92220 400.00000     .40000    -.02891    -.90136     .01624
     .50894    3.00332     .31524     .00007    -.00037     .00039
     .00163     .01840     .00893     .03635     .21730    -.02732
    -.00451     .00380    -.01719     .00126     .00285    -.00096
  1 785.50000      .82750 400.00000      .86250 -70.42357    1.72442
  2 785.50000      .92940 400.00000      .86250-128.70087     .16808
  3 785.50000      .82750 400.00000     -.86250-140.47656 -43.30425
  4 785.50000      .92940 400.00000     -.86250-1265.5269-1767.7434
  5 785.50000      .92940 400.00000     -.37500    0.00000    0.00000
  6 785.50000      .93700 400.00000     0.00000     .66343     .49160
  7 785.50000      .46720 400.00000     0.00000 221.16983   72.80017
  8 785.50000      .21260 400.00000     0.00000 470.46179  148.68518
  9 785.50000      .62380 400.00000     -.37500 118.99069   61.73772
```

Table 6a: Example of an unsteady pressure measurement database file

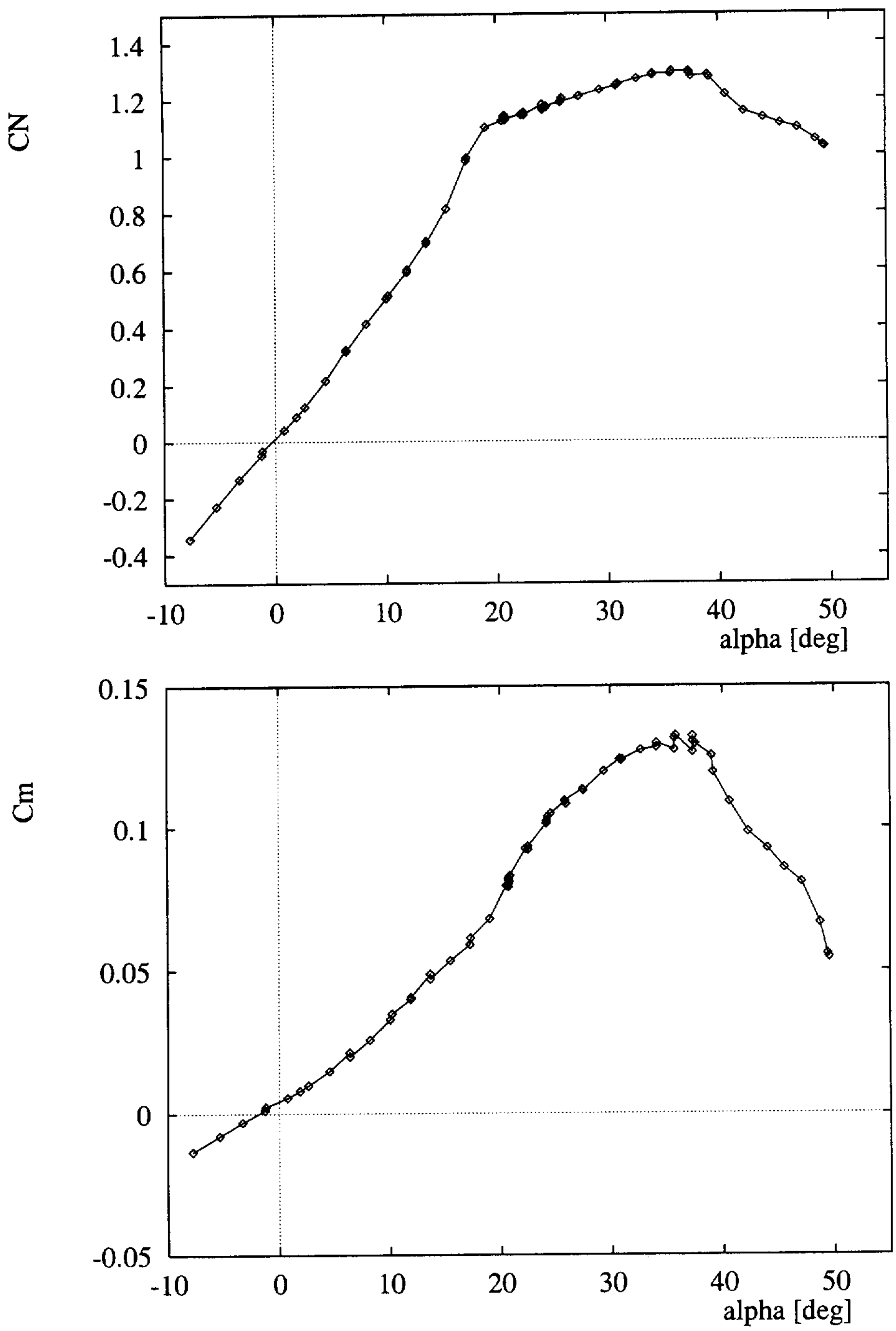

Figure 1: Low Speed Straked Delta Wing: Steady Normal Force and Pitching Moment vs. alpha.

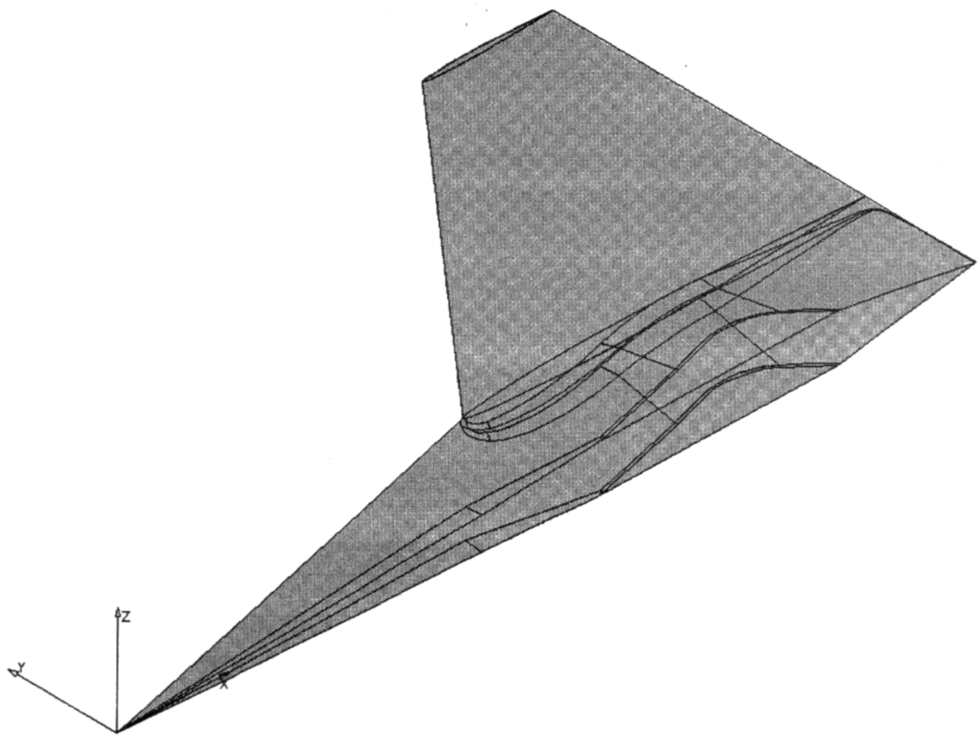

Figure 2a: CATIA example of NLR Low Speed Straked Delta Wing.

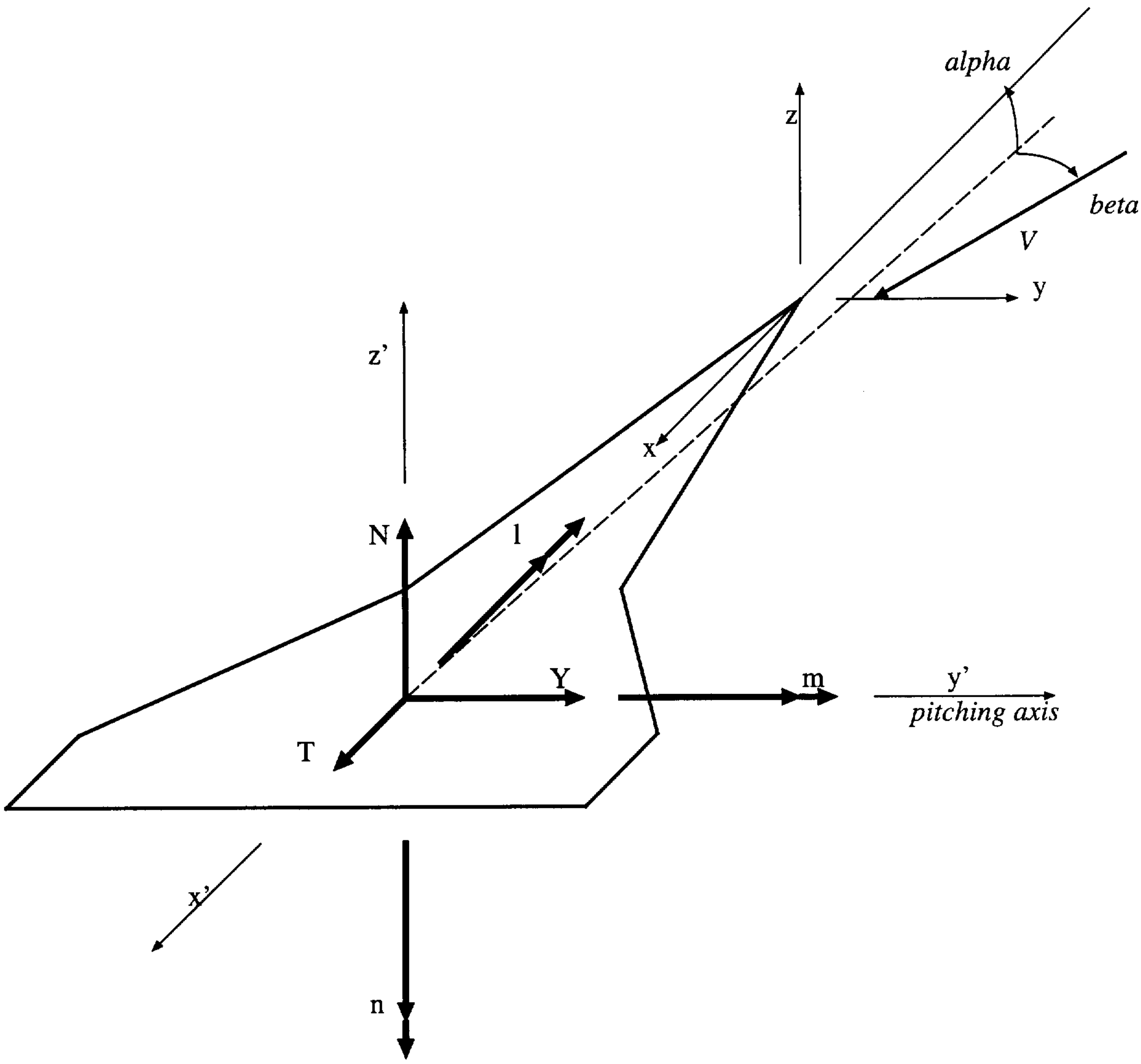

Figure 2b: Definitions and sign conventions

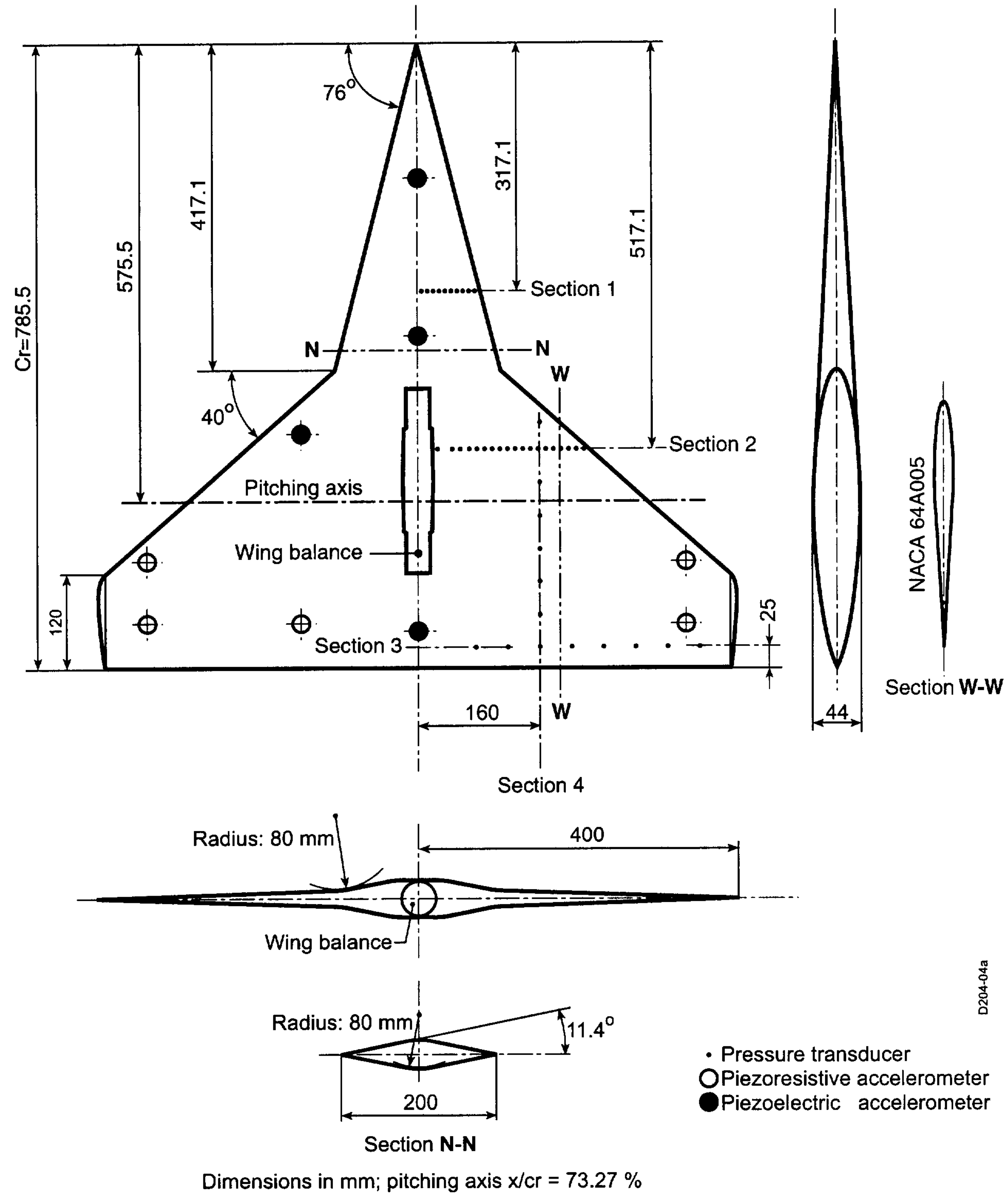

Figure 3: NLR Low Speed Straked Delta Wing, planform and model instrumentation

19E. TRANSONIC SIMPLE STRAKED DELTA WING

Evert G.M. Geurts
National Aerospace Laboratory NLR, The Netherlands

INTRODUCTION

The unsteady transonic flow during manoeuvres of fighters is not very well understood. For instance, large time delays and severe dynamic overshoots in normal force may occur, which cannot be predicted accurately by numerical methods. As a consequence, to be conservative structures must be over-designed or flight envelopes must be unnecessarily restricted. Therefore, a better understanding of the unsteady transonic flows, which occur during manoeuvres, is of interest for the development and operation of fighters.

This data set relates to an unsteady transonic wind tunnel test, on a highly instrumented semi-span simple straked delta wing model. Harmonic pitch as well as manoeuvre simulations were performed.
The objectives of the test were:

- To develop a better understanding of the physics of the unsteady vortex flow about a simple straked delta wing,
- The generation of a steady and unsteady airloads database for the use in the validation of CFD codes.

A first selection of test data for the validation of unsteady CFD codes related to this test is given in the following table and is motivated below. For harmonic oscillation the selected data points were chosen to highlight:

- Vortex flow breakdown
- Onset to Shock-Induced Trailing Edge Separation (SITES) and leading edge separation at transonic speeds.

Harmonic oscillation				
Mach	incidence	amplitude	frequency	data point
0.225	22.0	8.0	5.7	151
0.600	22.0	8.0	5.7	375
0.600	10.0	4.0	5.7	358
0.900	6.0	4.0	5.7	566
0.900	22.0	8.0	5.7	580
0.900	10.0	4.0	7.6	593
0.900	10.0	8.0	7.6	602
0.900	22.0	8.0	7.6	605

The y=0 plane was located on a distance of 7 mm from the tunnel sidewall which corresponded to the local displacement thickness of the tunnel sidewall boundary layer. To impose the start of the vortex on the apex to avoid interference of vortex with sidewall boundary layer, a little flat plate, the filler plate was attached to the model apex. As starting point for transonic calculation data point 566 was chosen, where conditions are stable. As primary point of interest the effect of Mach number is covered by the selection of data points 151, 375 and 580. At M = 0.225, data point 151 shows the effect of the model oscillating between 14° and 30° incidence at 5.7 Hz. With vortex bursting starting at about 22°, this oscillation provides a maximum pitch rate at the burst point. Similar data are given for M = 0.6 in data point 375 where vortex breakdown apparently begins between 23° and 24° and for M=0.9 in data point 580. Data point 605 was chosen at M = 0.9 and at the higher frequency of 7.6 Hz to provide an approximately constant reduced frequency when compared with data point 375 at M = 0.6. In the case of data point 605, vortex bursting begins at about 18° incidence.

The onset to SITES and leading edge separation at M = 0.9 occurs at an incidence between 10° and 12°. Data point 593 was chosen to show these effects. In order to highlight these transonic transitions, data point 358 was chosen to show how aerodynamics responded to oscillations of 4° amplitude at 10° mean angle and M = 0.6, where no such transitions occur. Frequency for the M = 0.6 case was 5.7 Hz and for the M = 0.9 case 7.6 Hz in order to maintain an approximately constant reduced frequency. Data point 580 was added to show frequency effects when compered with data point 605; data point 602 shows amplitude effects when compared with data point 593. Data are presented as the first seven harmonics of the pressures, balance data and accelerations.

Manoeuvres				
Mach	incidence	amplitude	frequency	data point
0.225	22.0	16.0	3.8	306
0.600	22.0	16.0	3.8	480
0.900	22.0	16.0	3.8	656

To cover the manoeuvring part of the test the large amplitude motions of 16° amplitude centred on a mean angle of 22°, were chosen to provide a dynamic variation of flow fields covering attached, vortex, burst vortex and developing separated flows for incidences from 7° to 37°. The three Mach numbers are represented by data points 306 (M=0.225), 480 (M=0.60) and 656 (M=0.90). In all cases the frequency was held constant at 3.8 Hz in order to simulate the same manoeuvre at different speeds.

Since these data points are for transient and not for oscillatory motions, they are represented in a time history format and thus do not have the harmonic part that is used in the selected data points for harmonic oscillations.

LIST OF SYMBOLS AND DEFINITIONS

Definitions

Figure 1 shows an example of a presentation from the geometry file (CATIA) included in the database and the origin of the body fixed axis system.

x-axis In the Wing Reference Plane following the root chord line of the basic wing panel[1] at a distance of 62.3 mm (see figure 2). The root chord line of the basic wing panel and the line connecting the 0 % chord points (Leading Edge) define the Wing Reference Plane (WRP).

y-axis In the Wing Reference Plane, perpendicular to the x axis, going through 48.24 % of the root chord line of the basic wing panel (= 73.27 % of the root chord line of the strake). The y-axis coincides with the rotation axis or pitching axis of the experiment.

z-axis Perpendicular to x-axis and y-axis. The z = 0 plane is the Wing Reference Plane. Both the root chord line of the strake, the rotation axis and the line connecting the 0 % chord points are in this plane.

The Trailing Edge is one straight line. Due to the twist, this line is crossing the Wing Reference Plane at the root chord of the basic wing panel. Although the apex of the strake is in the Wing Reference Plane, the chord line of the y = 0 section is not precisely in the Wing Reference Plane; it has a 0.0803° more positive angle of attack than the root chord line of the basic wing panel.

Non-dimensionalisation

Mean (NOT steady)

suffix 0 indicates the zero-th harmonic component

Unsteady

all unsteady signals have been decomposed into harmonic components

the harmonic component is indicated by suffix h,

- each harmonic component has been decomposed into
- a real (in-phase) and an imaginary (out-of-phase) part, e.g. Cp h = Re (Cp h) + i * Im (Cp h)

Pressures

Mean		Unsteady	
Cp 0	= (p 0 - ps) / q	Cp h	= (p h) / q * dalpha

Balance loads

Mean		Unsteady	
CN 0	= Normal Force / (q * Sref)	CN h	= Normal Force / (q * Sref * dalpha)
Cm 0	= Pitching Moment / (q * Sref * cref)	Cm h	= Pitching Moment / (q * Sref * cref * dalpha)
Cl 0	= Rolling Moment / (q * Sref * bref)	Cl h	= Rolling Moment / (q * Sref * bref * dalpha)

Chordwise sectional loads

$$CN\_u\ 0 = -\int_0^1 (Cp^+\ 0)\ d(x/c) \qquad CN\_u\ h = -\int_0^1 (Cp^+\ h)\ d(x/c)$$

$$CN\_l\ 0 = +\int_0^1 (Cp^-\ 0)\ d(x/c) \qquad CN\_l\ h = +\int_0^1 (Cp^-\ h)\ d(x/c)$$

$$CN\_t\ 0 = +\int_0^1 (Cp^-\ 0 - Cp^+\ 0)\ d(x/c) \qquad CN\_t\ h = +\int_0^1 (Cp^-\ h - Cp^+\ h)\ d(x/c)$$

[1] Since a common outboard wing was part of two different wind tunnel models, this common part was defined as the basic wing panel. For this test integration with a simple strake was realised.

$$Cm\_u\ 0 = -\int_0^1 (Cp^+\ 0)\ (x/c-0.25)\ d(x/c)$$

$$Cm\_l\ 0 = +\int_0^1 (Cp^-\ 0)\ (x/c-0.25)\ d(x/c)$$

$$Cm\_t\ 0 = +\int_0^1 (Cp^-\ 0 - Cp^+\ 0)(x/c-0.25)\ d(x/c)$$

$$Cm\_u\ h = -\int_0^1 (Cp^+\ h)\ (x/c-0.25)\ d(x/c)$$

$$Cm\_l\ h = +\int_0^1 (Cp^-\ h)\ (x/c-0.25)\ d(x/c)$$

$$Cm\_t\ h = +\int_0^1 (Cp^-\ h - Cp^+\ h)(x/c-0.25)\ d(x/c)$$

Spanwise sectional loads

$$CN\_u\ 0 = -\int_0^1 (Cp^+\ 0)\ d(y/b)$$

$$Cl\_u\ 0 = -\int_0^1 (Cp^+\ 0)\ (y/b)\ d(y/b)$$

$$CN\_u\ h = -\int_0^1 (Cp^+\ h)\ d(y/b)$$

$$Cl\_u\ h = -\int_0^1 (Cp^+\ h)\ (y/b)\ d(y/b)$$

Notes:

- All harmonic (h>0) components have been non-dimensionalised by the first harmonic of dalpha (in radians).
- For layout reasons, the 0 indicating the zero-th harmonic component (mean value) is sometimes omitted.
- Pitching moment: - Wing: about the rotation axis
  - Sections: about 25 % local chord
- Coefficients of spanwise sections: integration from y=0 to tip; rolling moment about y=0.
- The section number of the section coefficients is either indicated at the left hand side of the presented values (e.g. see table 3) or an additional suffix is used according to the following convention:

C1_2_3 h:	1_	2_	3_	h
	N: normal force	u: upper	section number	harmonic number
	M: pitching moment	l: lower		
	l: rolling moment	t: total		

- Chordwise sectional load integration: Between leading edge and first pressure transducer the static pressure and the unsteady pressure were assumed to be constant and equal to the values of the first pressure transducer. At the trailing edge the static pressure coefficient was assumed to be zero. Between the trailing edge and the last pressure transducer the unsteady pressure was assumed to be constant and equal to the values of the last pressure transducer.
- Spanwise sectional load integration: Between the symmetry plane and the first pressure transducer the steady pressure and the unsteady pressure were assumed to be constant and equal to the values of the first pressure transducer. At the tip the static pressure was assumed to be zero. Between the tip and the last pressure transducer the unsteady pressure was assumed to be constant and equal to the values of the last pressure transducer.
- The result of the pressure integration was NOT multiplied by $1/\pi$ or $2/\pi$.

Symbols and definitions

acc	(m/s^2)	acceleration (acc_11 is acceleration measured by accelerometer 11: see table 3)
alpha, α	(°)	incidence relative to x-axis as determined from LVDT signal
		(Note that incidence relative to root chord is alpha + 0.0803°)
		harmonic oscillations: zero-th harmonic component of the signal
		manoeuvres: half the sum of maximum and minimum of (1-cos) input
b	(m)	(local) span: measured from strake root chord (y = 0)

bref	(m)	reference span used in non-dimensionalising rolling moment: (distance between y=0 and tip section, excluding wing tip fairing): bref = 0.417900 (m)
c	(m, mm)	(local) chord
Cl	(-)	rolling moment coefficient
Cm	(-)	pitching moment coefficient
CN	(-)	normal force coefficient
Cp	(-)	pressure coefficient
cr, cref	(m, mm)	length of reference chord: root chord (at y = 0): cref = 0.820700 (m)
dalpha, dα	(°, rad)	model amplitude as determined from LVDT signal harmonic oscillations: first harmonic component manoeuvres: half of top-top value of (1-cos) input
DPN, dpn		data point number
freq, f	(Hz)	frequency, frequency of model oscillation
harm, h		harmonic component: harm = 1 refers to the excitation frequency of the model
i		$\sqrt{-1}$
Im		Imaginary part, e.g. CN h= Re (CN h) + i * Im (CN h)
k	(-)	reduced frequency, k = π * f * cref / V
LVDT		Linear Variable Differential Transducer, refers to displacement transducer mounted between a fixture on the turntable and a crank on the main axis
M, Mach	(-)	freestream Mach number
P, p	(Pa)	pressure
p.a.		pitching axis, rotation axis (see figure 2)
p_d	(°)	pitch deflection of main balance (> 0 nose up)
PHARAO		Processor for Harmonic And RAndom Oscillations
ps	(Pa)	freestream static pressure
q, Q	(Pa)	freestream dynamic pressure
r_d	(°)	roll deflection of main balance (>0 port-side down)
Re	(-)	Reynolds number, Re = V * cref / ν
Re		Real part, e.g. CN h= Re (CN h) + i * Im (CN h)
SiS		Simple Strake
SITES		Shock-Induced Trailing Edge Separation
Sref	(m^2)	wing reference area: wing area, including strake, Sref = 0.144406 (m^2)
T	(s)	duration of a full (1-cos) input, T= 1/3.8
T	(K)	Temperature
V	(m/s)	Freestream velocity
WRP		Wing Reference Plane (see Definitions)
x	(mm)	ordinate (see Definitions)
x/c	(-, %)	relative chordwise position
y	(mm)	spanwise ordinate (see Definitions)
y/b	(-, %)	relative spanwise position
z	(mm)	ordinate (see Definitions)

Greek

α	(°)	incidence relative to x-axis as determined from LVDT signal (Note that incidence relative to root chord is alpha + 0.0803°) harmonic oscillations: zero-th harmonic component of the signal manoeuvres: half the sum of maximum and minimum of (1-cos) input

dα, dalpha	(°, rad)	model amplitude as determined from LVDT signal
		harmonic oscillations: first harmonic component
		manoeuvres: half of top-top value of (1-cos) input
ν	(m^2/s)	(freestream) kinematic viscosity

Superscripts and postscripts

+	upper
-	lower
h	harmonic; when no harmonic is indicated the mean value is presented
i	instationary
tot	total
_in	inertia part
_l	lower
_m	mean (zero-th harmonic)
_u	upper
_t	total
0	(zero-th harmonic) mean: when no harmonic is indicated the mean value is presented

FORMULARY

1 General Description of model

1.1	Designation	Transonic Simple Straked Delta Wing
1.2	Type	Half model
1.3	Derivation	Outboard wing: Modified NACA 64A204, linearly lofted between root and tip Strake: diamond shaped with sharp leading edge
1.4	Additional remarks	Filler plate attached to model apex (remark in introduction)
1.5	References	Refs. 1, 2, 3, 7

2 Model Geometry

2.1	Planform	Trapezoidal outboard wing with simple strake (see figure 2)
2.2	Aspect ratio	2.4187
2.3	Leading edge sweep	Wing: 40°, Strake: 76°
2.4	Trailing edge sweep	No
2.5	Taper ratio	-
2.6	Twist	-3.0°, the y = -62.3 section has 0.0° incidence with respect to WRP, the y = -417.9 section (tip) has –3.0° incidence; the panel is linearly lofted between root and tip. Twist is applied by rotation about the leading edge
2.7	Root chord	0.8207 m
2.8	Semi-span of model	0.4179 m
2.9	Area of planform	0.144406 m^2
2.10	Leading-edge flap	Present, but not deflected
2.11	Trailing-edge flap	Present, but not deflected
2.12	Reference locations and profile definitions	See CATIA geometry file
2.13	Form of wing-body or wing-root junction	Area between outboard wing and strake smoothed
2.14	Form of wing tip	Tip fairing present (geometry included in CATIA file in database)
2.15	Additional remarks	Planform identical to (half of) full-span model of Low Speed

	Straked Delta Wing (case 18.E)
	Geometry included as CATIA file in database
2.16 References	Refs. 2, 3, 7

3 Wind Tunnel

3.1 Designation	NLR High Speed Tunnel (HST)
3.2 Type of tunnel	Continuous, variable pressure
3.3 Test section dimensions	Height: 1.6 m, width: 2.0 m, enclosed in large plenum chamber
3.4 Type of roof and floor	Slotted, 6 slots per wall
3.5 Type of side walls	Solid
3.6 Ventilation geometry	Roof and floor: open ratio 12%
3.7 Displacement thickness of side wall boundary layer	~ 7 mm.
3.8 Thickness of boundary layers at roof and floor	-
3.9 Method of measuring Mach number	Derived from settling chamber stagnation pressure and plenum chamber static pressure
3.10 Flow angularity	< 0.1° in centre of test section, < 0.25° elsewhere
3.11 Uniformity of Mach number over test section	< 0.4% in $\Delta M/M$ at supersonic Mach numbers
3.12 Sources and levels of noise or turbulence in empty tunnel	< 1% in rms p/q for M=0.8
3.13 Tunnel resonance	No evidence of resonance in present test
3.14 Additional remarks	Information on flow angularity and Mach number uniformity available only along test section centre line
3.15 References on tunnel	Ref. 8

4 Model motion

4.1 General description	Sinusoidal pitching and manoeuvre simulations (half/full [1-cosine], half/full cosine inputs). Pitching axis location at 73.27 % root chord
4.2 Reference co-ordinate and definition of motion	Oscillation amplitude measured with LVDT on actuator
4.3 Range of amplitude	0.5°, 2°, 4°, 8° and 16°
4.4 Range of frequency	3.8, 5.7, 7.6, 11.4 and 15.2 Hz
4.5 Method of applying motion	Electro-hydraulic shaker system (HYDRA), Ref. 9
4.6 Timewise purity of motion	Adequate purity of sinusoid
4.7 Natural frequencies and normal modes of model and support system	Lowest: 91.2 Hz (balance torsion combined with model pitching) Further: 136.6 Hz and 166.5 Hz and higher
4.8 Actual mode of applied motion including any elastic deformation	Measured with 15 accelerometers (12 wing, 3 strake) Position and output included in database files. The angular deflections, calculated from the total balance loads and stiffness matrices are presented in the database files.
4.9 Additional remarks	Rotation axis location at same position as in Low Speed Straked Delta Wing Test

5 Test Conditions

5.1 Model planform area/tunnel area	0.0451
5.2 Model span/tunnel height	0.2090
5.3 Blockage	Estimated 3 % of dynamic pressure: no blockage or upwash corrections applied due to scarce information at extreme conditions

5.4	Position of model in tunnel	Standard sidewall mounting
5.5	Range of Mach number	0.225, 0.6 and 0.9
5.6	Range of tunnel total pressure (Reynolds number)	$Re \approx 3.8 \times 10^6$ for M=0.225, $Re \approx 8.0 \times 10^6$ for M=0.225, 0.6 and 0.9 $Re \approx 14.0 \times 10^6$ for M=0.9
5.7	Range of tunnel total temperature	Actual total temperature value included in database files
5.8	Range of model steady or mean incidence	4° to 48° (adjusted values)
5.9	Definition of model incidence	Relative to WRP (see Definitions)
5.10	Position of transition, if free	-
5.11	Position and type of trip, if transition fixed	Strips of 2mm width on upper and lower side of outboard wing (y < -108.65 mm), starting 14.5 mm downstream of leading edge, measured perpendicular to the leading edge. Grit size: 88 μm (Carborundum 150)
5.12	Flow instabilities during tests	None encountered
5.13	Changes to mean shape of model due to steady aerodynamic load	Not measured
5.14	Additional remarks	In test programme and introduction nominal adjusted values are indicated; correct geometric values are in the database files
5.15	References describing tests	Ref. 7

6 Measurements and Observations

6.1	Steady pressures for the mean conditions		Yes
6.2	Steady pressures for small changes from the mean conditions		No
6.3	Quasi-steady pressures (6 Hz)		Yes
6.4	Unsteady pressures	• Harmonic components	Yes
		• Time histories	Yes
6.5	Steady loads for the mean conditions	• Measured directly (total)	Yes
		• Integrated sectional pressures (see Definitions)	Yes
6.6	Steady loads for small changes from the mean conditions		No
6.7	Quasi-steady loads (6 Hz)	• Measured directly (total)	Yes
		• Integrated sectional pressures (see Definitions)	Yes
6.8	Unsteady loads	• Measured directly (total)	Yes
		• Integrated sectional pressures (see Definitions)	Yes
6.9	Measurement of actual motion at points on model		Yes
6.10	Observation or measurement of boundary layer properties		No
6.11	Visualisation of flow (demonstration)		Yes
6.12	Visualisation of shock wave movements		No
6.13	Additional remarks	Demonstration during this test resulted in a flow visualization test in August 1996 (Refs. 16, 19, 20, 21, 22)	

7 Instrumentation

7.1	Steady pressure	
7.1.1	Position of orifices spanwise and chordwise	See figure 2 and table 3
7.1.2	Type of measuring system	95 in situ pressure transducers, DC part of time signal measured in

		conditioning units
7.2	Unsteady pressure	
	7.2.1 Position of orifices spanwise and chordwise	See figure 2 and table 3
	7.2.2 Diameter of orifices	0.8 mm
	7.2.3 Type of measuring system	AC part of time signals measured by PHARAO (Ref. 14)
	7.2.4 Type of transducers	Endevco: 8514-10, 8507B-15, 8507-5M, Kulite: XCS 093-5D
	7.2.5 Principle and accuracy of calibration	Calibration of data acquisition system before test
7.3	Model motion	
	7.3.1 Method of measuring motion	LVDT: Sangamo AFG 5.0 S
	7.3.2 Method of determining spatial mode of motion	15 accelerometers (12 in wing, 3 in strake) Endevco: 2222B/2222C, Kulite: GY-155-100/250
	7.3.3 Accuracy	better than 0.015 mm
7.4	Processing of unsteady measurements	
	7.4.1 Method of acquiring and processing measurements	Application of Phase Locked Time Domain Averaging on time traces and processed to first seven harmonics
	7.4.2 Type of analysis	Harmonic components (0 to 7) and time histories
	7.4.3 Unsteady pressure quantities obtained and accuracy's achieved	Harmonic components and time histories, for accuracy see 9.1.6; application of sensor characteristics, correction for zero measurements applied
	7.4.4 Method of integration to obtain forces	Trapezoidal rule with specials at leading and trailing edge
7.5	Additional remarks	Positions of instrumentation included in output files (see table 3)
7.6	References on techniques	Refs. 4, 5, 14

8 Data presentation

8.1	Test cases for which data could be made available	See tables 1 and 2
8.2	Test cases for which data are included in this document	Summarized and motivated in Introduction
8.3	Steady pressures	Mean values; example in table 3 (see Database)
8.4	Quasi-steady or steady perturbation pressures	Example in table 3 and table 4 (see Database)
8.5	Unsteady pressures	Harmonic measurements: first seven harmonics Manoeuvres: time data Examples in table 3 and table 4 (see Database)
8.6	Steady forces or moments	Example in table 3 (see Database)
8.7	Quasi-steady or unsteady perturbation forces	
8.8	Unsteady forces and moments	Harmonic measurements: first seven harmonics Manoeuvres: time data examples in table 3 and table 4 (see Database)
8.9	Other forms in which data could be made available	Harmonic measurements: time traces
8.10	Reference giving other representations of data	Refs. 10, 11, 12, 13, 16

9 Comments on data

9.1	Accuracy	
	9.1.1 Mach number	+/- 0.001
	9.1.2a Steady incidence turntable	+/- 0.002 + 0.0004 * alpha° [°]
	9.1.2b Steady incidence shaft	+/- 0.005°

	9.1.3 Pitch amplitude	+/- 0.005°
	9.1.4 Pitch amplitude	+/- 0.0005
	9.1.5 Steady pressure derivatives	+/- 0.3 per cent
	9.1.6 Unsteady pressure coefficients	+/- 0.5 per cent
9.2	Sensitivity to small changes of parameter	-
9.3	Non-linearity's	-
9.4	Influence of tunnel total pressure	Unsteady measurements had short acquisition times and the total pressure can be assumed constant over each measurement.
9.5	Wall interference corrections	Not applied
9.6	Other relevant tests on same model	Refs. 16, 19 (UTDP VISU test)
9.7	Relevant tests on other models of nominally the same shapes	Ref. 6 (UTDP LCO test), Ref. 16 (UTDP VISU test), Ref. 17 (NLR Subsonic Straked Delta Wing Test)
9.8	Any remarks relevant to comparison between experiment and theory	LCO prediction method mentioned in Ref. 6
9.9	Additional remarks	Structure of file set-up included in README file in database; example of data output indicated in table 3.
9.10	References on discussion of data	Refs. 6, 7, 10, 11, 12, 13, 18

10 Personal contact for further information

Evert G.M. Geurts
Department of Aerodynamic Engineering and Aeroelasticity
Phone: +31 20 5113455
Fax: +31 20 5113210
Email: geurts@nlr.nl

National Aerospace Laboratory NLR
Anthony Fokkerweg 2 — P.O. Box 90502
NL 1059 CM Amsterdam — NL 1006 BM Amsterdam
The Netherlands — The Netherlands
Phone: +31 20 5113113
Fax: +31 20 5113210
Website: http://www.nlr.nl

11 List of references

1 Geurts, E.G.M., den Boer, R.G., (in Dutch) "Eerste uitwerking van voorstel instationaire transsone deltavleugel proeven in HST", NLR Memorandum AE-87-001 U, 1987.

2 Sijtsma, H.A., "Computational assessment of a lower wing surface modification of an F-16A aeroelastic windtunnel model", NLR TR 88143 L, 1988.

3 den Boer, R.G., "Report of the design of two semi-span wind tunnel models with corresponding support system, to be used for unsteady tests in the High Speed Tunnel (HST) of the National Aerospace Laboratory (NLR) in the Netherlands", NLR TR 89057 L, 1989.

4 Geurts, E.G.M., "Experiments with a trial strain gage balance", NLR Memorandum AE-88-005 U, 1988.

5 Geurts, E.G.M., "Continued dynamic experiments with a trial strain gage balance", NLR TR 89052 L, 1988.

6 Cunningham, Jr., A.M., den Boer, R.G., Dogger, C.S.G., Geurts, E.G.M., Retel, A.P., Zwaan, R.J., "Unsteady transonic wind tunnel tests on a 1:9 scaled semi-span model of an F-16 with outboard wing oscillating in pitch and a semi-span straked delta wing model, oscillating in pitch", NLR CR 93386 U (Parts I to IV), 1993.

Part I: Objectives, model, test setup, data acquisition and processing techniques, test program, presentation format

Part II: Selected results of the test on the 1:9 scaled F16 model oscillating in pitch

Part III: Selected results of the test on the semi-span straked delta wing model oscillating in pitch

Part IV: Selected results of the test on the semi-span straked delta wing model simulating pitch manoeuvres

7 Cunningham, Jr., A.M., den Boer, R.G., Dogger, C.S.G., Geurts, E.G.M., Retel, A.P., Zwaan, R.J., "Unsteady transonic wind tunnel test on a semi-span straked delta wing model, oscillating in pitch", NLR CR 93570 L (Parts I to III), 1993

Part I : Description of Model, Test Setup, Data Acquisition and Data Processing, also published as WL-TR-94-3094

Part II: Selected Data Points for Harmonic Oscillation also published as WL-TR-94-3095

Part III:Selected Data Points for Simulated Manoeuvres, also published as WL-TR-94-3096.

8 NN., "Users guide to the High Speed Tunnel (HST): edition 1977".

9 Poestkoke, R., "Hydraulic test rig for oscillating wind-tunnel models", NLR MP 76020 U, 1976.

10 Boer, R.G. den, Cunningham Jr., A.M., "Unsteady Transonic Wind Tunnel Testing of Fighter Type Wings", 31st AIAA / ASME / ASCE / AHS / ASC Structures, Structural Dynamics and Materials Conference, Long Beach, California, 2-4 April 1990.

11 Cunningham Jr., A.M., Boer, R.G. den, "Transonic Wind Tunnel Investigation of Limit Cycle Oscillations on Fighter Type Wings", AGARD SMP Conference Proceedings 507: Transonic Unsteady Aerodynamics and Aeroelasticity, San Diego, California, 7-11 October 1991.

12 Cunningham Jr., A.M., Boer, R.G. den, "Transonic Wind Tunnel Investigation of Limit Cycle Oscillations on Fighter Type Wings - UPDATE", 33rd AIAA / ASME / ASCE / AHS / ASC Structures, Structural Dynamics and Materials Conference, Dallas, Texas, April 13-17, 1992.

13 Geurts, E.G.M., den Boer, R.G., Cunningham, Jr., A.M., "Unsteady Transonic Wind Tunnel Test of a Pitching Straked Wing at High Incidences", 33rd AIAA / ASME / ASCE / AHS / ASC Structures, Structural Dynamics and Materials Conference, Dallas, Texas, April 13-17, 1992 (also NLR MP 92155 L, 1992).

14 den Boer, R.G., "Application of the New NLR Measurement System PHARAO in Unsteady Wind Tunnel Tests on Straked Delta Wings", 18th ICAS Congress, Beijing, China, September 21-25, 1992 (also NLR TP 92441 U, 1992).

15 Geurts, E.G.M., "Presentation and Analysis of Results of an Unsteady Transonic Wind Tunnel Test on a Semi-Span Delta Wing Model, Oscillating in Pitch", International Forum on Aeroelasticity and Structural Dynamics, Manchester, United Kingdom, 26-28 June 1995 (also NLR TP 95523 U, 1995).

16 Geurts, E.G.M., "Flow Visualization and Particle Image Velocimetry on a Semi-Span Straked Delta Wing, Stationary and Oscillating in Pitch", European Forum on Wind Tunnels and Wind Tunnel Test Techniques – Proceedings P.48.1-P.48.11, Cambridge, United Kingdom, 14-16 April 1997.

17 Cunningham, Jr., A.M., den Boer, R.G., et.al., "Unsteady low speed wind tunnel test of a straked delta wing, oscillating in pitch", NLR TR 87146 L Parts I to VI, (also "published" in April 1988 as AFWAL-TR-8-3098, Parts I-VI).

Part I: General description and discussion of results

Part II: Plots of steady and zeroth and first order harmonic unsteady pressure distributions

Part III: Plots of zeroth and first order harmonic unsteady pressure distributions (concluded) and plots of steady and zeroth and first order harmonic overall loads

Part IV:Plots of time histories of pressures and overall loads

Part V: Plots of the overall loads spectra and the response of overall loads to single step (1-cos) inputs

Part VI: Presentation of the visualization program.

18 Cunningham, Jr, A.M., den Boer, R.G. , "Overview of Unsteady Transonic Wind Tunnel Test on a Semi-span Straked Delta Wing Oscillating in Pitch", WL-TR-94-3017, 1994.

19 Cunningham, Jr., Geurts, E.G.M., Dogger, C.S.G., Persoon, A.J., "Transonic Wind Tunnel Test on the Flow-Visualization of a Semi-Span Simple Straked Delta Wing Model', NLR CR 97577 L (Parts I to II), 1997.

Part 1: General Description

Part II: Presentation of (Selected) Test Results

20 Cunningham, Jr., Atlee M., Geurts, Evert G.M., "Analysis of Limit Cycle Oscillation/Transonic High Alpha Flow Visualization, Part 1: Discussion", AFRL-VA-WP-TR-1998-3003, 1998.

21 Cunningham, Jr., Atlee M., Geurts, Evert G.M., "Analysis of Limit Cycle Oscillation/Transonic High Alpha Flow Visualization, Part 2: Stationary Model Data", AFRL-VA-WP-TR-1998-3004, 1998.

22 Cunningham, Jr., Atlee M., Geurts, Evert G.M., "Analysis of Limit Cycle Oscillation/Transonic High Alpha Flow Visualization, Part 3: Oscillating Model Data", AFRL-VA-WP-TR-1998-3005, 1998.

Mach	0.225									
Reynolds	~ 3.8 *10^6		~ 8.0*10^6							
Frequency	5.7		5.7			7.6			11.4	15.2
Amplitude	0.5	0.5	0.5	4.0	8.0	2.0	4.0	8.0	2.0	2.0
Alpha		#								
4.0										
5.0										
6.0	7	36	107	135	147	158	172	185	199	213
7.0										
8.0	8	37	108							
9.0										
10.0	9	38	109	136	148	159	173	186	200	214
10.5										
11.0										
11.5										
12.0	10	39	110							
12.5										
13.0										
14.0	11	40	111	137	149	160	174	187	201	215
15.0										
16.0	12	41	112							
17.0	13	42	113							
18.0	14	43	114	138	150	161	175	188	202	216
19.0	15	44	116							
20.0	16	45	117							
21.0	17	46	118							
22.0	6 18	35 47	106 119	139	151	162	176	189	203	217
23.0	19	48	120							
24.0	20	49	121							
25.0										
26.0	21	50	122	134 140	145 152	157 163	171 177	184 190	198 204	212
27.0										
28.0	22	51	123							
29.0										
30.0	23	52	124	141	146 153	164		191	205	218
32.0	24 25	53	125				178			
34.0	26	54	126	142	154	165		192		219
36.0	27	55	127				179			
38.0	28	56	128	143	155	166		193	207	220
40.0	29	57	129							
42.0	30	58	130	144	156	167	180	194	208	221
44.0		59	131			168	181	195	209	
46.0		60	132			169	182	196	210	
48.0			133			170	183	197		

Table 1a: Simple Strake test programme, harmonic oscillations at Mach = 0.225

without fillerplate

Remark: The y=0 plane was located on a distance of 7 mm from the tunnel sidewall which corresponded to the local displacement thickness of the tunnel sidewall boundary layer. To impose the start of the vortex on the apex, a little flat plate, the filler plate was attached to the model.

Mach	0.600							
Reynolds	~ $8.0*10^6$							
Frequency	5.7	7.6	11.4	15.2				
Amplitude	0.5	4.0	8.0	2.0	4.0	8.0	2.0	2.0
Alpha								
4.0	325							
5.0								
6.0	326	357	371	382	394	406	420	438
7.0								
8.0	327							
9.0								
10.0	328	358	372	383	395	407	421	439
10.5								
11.0	329							
11.5								
12.0	330							
12.5								
13.0	331							
14.0	332	359	373	384	396	408	422	440
15.0	333							
16.0	334							
17.0	335							
18.0	336	360	374	385	397	409	423	441
19.0	337							
20.0	338							
21.0	339							
22.0	340	361	375	386	398	410	424	442
23.0	341							
24.0	342	363	370	381	393	405	419	437
25.0	343							
26.0	324 344	356 364	376	387	399	411	425	443
27.0								
28.0	345							
29.0								
30.0	346	365	377	388	400	414	426	444
32.0	347					412		
34.0	348	366	378	389	401	415	427	445
36.0	349					413		
38.0	350	367	379	390	402	416	428	446
40.0	351							
42.0	352	368	380	391	403	417	429	447
44.0	353							
46.0	354	369		392	404	418	430	448
48.0	355							

Table 1b: Simple Strake test programme, harmonic oscillations at Mach = 0.6

Mach	0.900								
Reynolds	~ $8.0*10^6$								~$14.0*10^6$
Frequency	5.7			7.6			11.4	15.2	5.7
Amplitude	0.5	4.0	8.0	2.0	4.0	8.0	2.0	2.0	0.5
Alpha									
4.0	499								527
5.0	500								528
6.0	501	566	574	584	592	601	609	617	529
7.0	502								530
8.0	503								531
9.0	504								533
10.0	505	567	575	585	593	602	610	618	534
10.5									535
11.0	506								536
11.5									537
12.0	507								538
12.5									539
13.0	508								540
14.0	509	568	576	586	594 595	603	611	619	541
15.0	510								542
16.0	511								543
17.0	512								544
18.0	513	569	579	587	596	604	612	620	545
19.0	514								548
20.0	515								547
21.0	516								549
22.0	517	570	580	588	597	605	613	621	526 550
23.0	518								551
24.0	519	565	573	583	591	600	608	616	
25.0	520								553
26.0	521	571	581	589	598	606	614	622	554
27.0	522								555
28.0	523								556
29.0	524								557
30.0	525	572	582	590	599	607	615	623	558
32.0	559								
34.0	560								
36.0	561								
38.0	562								
40.0	563								
42.0	564								
44.0									
46.0									
48.0									

Table 1c: Simple Strake test programme, harmonic oscillations

Mach	0.225			0.600		0.900	
Reynolds	~ 3.8*10^6	~ 8.0*10^6		~ 8.0*10^6		~ 8.0*10^6	
Amplitude	8.0	8.0	16.0	8.0	16.0	8.0	16.0
Alpha							
6.0		235 236 237 238 239		454 455 456 457 458		625 639 640 641 642 643	
10.0		240 241 242 243 244					
14.0		245 246 247 248 249	296 297 298 299 300	459 460 461 462 463 464	485 486 487 488 489 490 491	644 645 646 647	662 663 664 665 666 667
18.0	62 63 64 65 66 67 68 69 70 71 72 73 74 75 76 77	250 251 252 253 254	301 302 303 304 305				
22.0		255 256 257 258 259	306 307 308 309 310	449 450 451 452 453	480 481 482 483 484	624 626 627 628 629 630 631 632 633 634 635 636 637 638	656 657 658 659 660 661
26.0	78 79 80 81 82 83 84 85 86 87 88	229 230 231 232 233 234 260 261 262 263 264 265	291 292 293 294 295				
30.0		266 267 268 269	311 312 313 314 315	465 466 467 468 469 470 471 472 473 474	492 493 494 495 496	648 649 650 651 652 653 654	
34.0	89 90 91 92 91 92 93 94 95	276 277 278 279 280	316 317 318 319 320				
38.0		281 282 283 284 285		475 476 477 478 479			
42.0		286 287 288 289 290					

Table 2: Simple Strake test programme, manoeuvres, 1/T = 3.8 Hz, Δt = [1 / (3.8 * 128)]

Unsteady Transonic Delta Program

DPN = 151

test conditions

Simple Strake configuration

alpha	=	22.109 deg	Q	=	6.690 kPa
Mach	=	.225	Ptot	=	195.256 kPa
Re*10^-6	=	7.982	Ttot	=	291.828 K
dalpha	=	8.342 deg			
freq	=	5.700 Hz			
k	=	.192			
harm	=	1			

BALANCE LOADS		aerodynamic coefficients			aero / inertia	angular deflections [deg]		
position	comp.	Zero	Re 1	Im 1	[%]	Zero	Re 1	Im 1
main	CN	1.09156	3.45587	1.20868	3883.88			
	Cm	.08135	.24823	-.06273	174.38	-.056	-.035	.003
	Cl	-.37659	-.78329	-.38618	957.42	-.063	-.008	-.009

ACCELERATIONS					vibration mode			
nr	x [mm]	y [mm]	Amplitude [m/s^2]	Phase angle rel. to LVDT [deg]	section	y/b [%]	heave at p.a [mm]	pitch [deg]
11	-425.6	-12.0	75.286	2.197				
12	-215.6	-12.0	35.066	3.471	1	2.878	1.790	7.946
13	167.4	-12.0	28.761	-178.363				
21	-138.6	-116.9	24.535	16.071				
22	-46.6	-116.9			2	28.034	1.208	8.353
23	121.4	-116.9	24.104	-167.130				
31	-74.6	-189.9	8.681	18.730				
32	-10.6	-189.9			3	45.540	2.749	7.223
33	141.4	-189.9	26.302	-168.691				
41	29.4	-304.9	3.384	-172.471				
42	89.4	-304.9	17.520	-178.576	4	73.118	.588	8.675
43	152.4	-304.9	27.168	-178.495				
51	85.0	-374.9	15.733	-166.775				
52	121.4	-374.9	22.863	-163.986	5	89.904	1.179	8.758
53	157.4	-374.9	29.896	-164.250				

Table 3: Example of data output format of harmonic measurements, page 1

Unsteady Transonic Delta Program

DPN = 151

PRESSURES section 1 c = 300.65 mm y =-209.06 mm

nr. up	nr. low	x/c [%]	Cp 0	ReCp 1	ImCp 1
101		2.00	-1.572	.899	-.972
102		5.00	-1.621	1.512	-.885
103		10.00	-1.557	2.213	-1.058
104		15.00	-1.987	4.878	-1.166
105					
106		30.00	-1.117	-2.346	-1.420
107		40.00	-.878	-2.855	-1.111
108		50.00	-.775	-2.952	-.989
109		60.00	-.756	-3.090	-.913
110		70.00	-.723	-2.848	-.752
111		79.00	-.663	-2.535	-.393
112		82.50	-.615	-2.426	-.177
113		85.00	-.574	-2.331	-.009
114		90.00	-.521	-2.240	.280
115		95.00	-.463	-2.179	.472
	151	10.00	.619	.889	.180
	152	20.00	.509	1.010	.241
	153	40.00	.336	.883	.292
	154	60.00	.247	.592	.295
	155	80.00	.164	.158	.267

PRESSURES section 2 c = 246.21 mm y =-273.97 mm

nr. up	nr. low	x/c [%]	Cp 0	ReCp 1	ImCp 1
201		2.00	-.913	1.992	-.914
202		5.00	-.918	2.009	-1.005
203		10.00	-.929	2.178	-1.034
204		15.00	-.894	2.310	-.948
205		18.00	-.879	1.119	-1.667
206		30.00	-.843	2.697	-.942
207		40.00	-.799	2.012	-.827
208		50.00	-.773	.686	-.814
209		60.00	-.720	-.331	-.827
210		70.00	-.668	-.058	-.047
211		79.00	-.596	-1.451	-.699
212		82.50	-.606	-1.636	-.696
213		85.00	-.569	-1.674	-.637
214		90.00	-.556	-1.878	-.540
215		95.00	-.532	-2.116	-.389
	251	10.00	.601	.765	.217
	252	20.00	.495	.879	.259
	253	40.00	.330	.741	.280
	254	60.00	.224	.452	.273
	255	80.00	.101	-.012	.227

PRESSURES section 3 c = 194.13 mm y =-336.06 mm

nr. up	x/c [%]	Cp 0	ReCp 1	ImCp 1
301	2.00	-.523	1.506	-.653
302	5.00	-.528	1.477	-.653
303	10.00	-.522	1.463	-.702
304	15.00	-.513	1.353	-.698
305	18.00	-.506	.453	-1.029
306	30.00	-.513	.903	-.636
307	40.00	-.528	.339	-.536
308	50.00	-.560	-.051	-.440
309	60.00	-.537	-.248	-.390
310	70.00	-.538	-.468	-.466
311	79.00	-.554	-.692	-.594
312	90.00	-.549	-.931	-.676

PRESSURES section 4 c = 144.42 mm y =-395.32 mm

nr. up	x/c [%]	Cp 0	ReCp 1	ImCp 1
401	2.00	-.300	.666	-.550
402	5.00	-.308	.628	-.552
403	10.00	-.305	.525	-.516
404	15.00	-.315	.469	-.522
405	18.00	-.315	.416	-.523
406	30.00	-.324	.128	-.491
407	40.00	-.349	-.201	-.433
408	50.00	-.378	-.586	-.326
409	60.00	-.389	-.880	-.235
410	70.00	-.399	-1.025	-.221
411	79.00	-.396	-1.078	-.248
412	90.00	-.405	-1.155	-.280

Table 3 (continued): Example of data output format of harmonic measurements, page 2

Unsteady Transonic Delta Program DPN = 151

PRESSURES section 5			b = 82.70 mm x =-269.60 mm	
nr. up	y/b [%]	Cp 0	ReCp 1	ImCp 1
501	6.62	-.440	-1.518	-.267
502	20.43	-.574	-2.557	-.119
503	34.05	-.835	-4.215	.156
504	47.67	-1.298	-5.928	.427
505	54.49	-1.541	-6.029	.374
506	61.29	-1.686	-5.240	.138
507	68.10	-1.645	-4.189	-.141
508	74.91	-1.419	-3.535	-.326
509	81.72	-1.124	-3.077	-.290
510	88.53	-1.123	-2.990	-.316

PRESSURES section 6			b = 233.73 mm x = -60.62 mm	
nr. up	y/b [%]	Cp 0	ReCp 1	ImCp 1
601	38.90	-1.568	-3.997	-.031
602	42.93	-1.771	-4.141	-.364
603	46.93	-1.731	-4.658	-.575
604	50.99	-1.556	-5.500	-.593
605	59.03	-1.258	-5.123	-.664
606	67.07	-1.233	-6.098	-.728
607	71.11	-1.404	-6.762	-.944
608	75.56	-1.965	-4.665	-1.308
609	80.00	-2.647	4.103	-1.041
610	84.44	-1.874	3.100	-.957
102	89.45	-1.621	1.512	-.885

PRESSURES section 7			b = 417.90 mm x = 100.71 mm	
nr. up	y/b [%]	Cp 0	ReCp 1	ImCp 1
701	22.71	-.036	.673	-.516
702	28.21	-.312	.592	-.066
703	33.72	-.778	-.192	.370
704	39.26	-.891	-2.468	.079
705	44.69	-.870	-3.140	-.631
109	50.03	-.756	-3.090	-.913
706	55.28	-.700	-2.560	-.945
707	60.46	-.752	-.957	-.960
208	65.56	-.773	.686	-.814
708	70.59	-.689	.802	-.668
709	75.54	-.613	.672	-.627
307	80.42	-.528	.339	-.536
710	85.22	-.443	.305	-.517
711	90.19	-.374	.340	-.513
405	94.60	-.315	.416	-.523

SECTION COEFFICIENTS				
section	comp.	Zero	Re 1	Im 1
1	CN_u	.976	1.357	.770
	CN_l	.319	.627	.261
	CN_t	1.295	1.984	1.031
	Cm_u	-.120	-.803	-.061
	Cm_l	-.026	-.065	-.072
	Cm_t	-.146	-.868	-.133
2	CN_u	.733	-.508	.787
	CN_l	.295	.482	.250
	CN_t	1.029	-.026	1.037
	Cm_u	-.140	-.305	-.121
	Cm_l	-.017	-.024	-.062
	Cm_t	-.157	-.329	-.183
3	CN_u	.507	-.118	.604
	Cm_u	-.118	-.199	-.136
4	CN_u	.341	.412	.370
	Cm_u	-.087	-.290	-.060
5	CN_u	.992	3.683	.051
	Cl_u	-.553	-1.968	-.040
6	CN_u	1.531	3.071	.489
	Cl_u	-.745	-1.060	-.355
7	CN_u	.464	.271	.512
	Cl_u	-.266	-.140	-.282

Table 3 (continued): Example of data output format of harmonic measurements, page 3

```
*alpha/306_1*
  6.791   6.868   7.028   7.161   7.300   7.507   7.704   7.892
  8.164   8.474   8.782   9.160   9.575   9.953  10.364  10.836
 11.294  11.771  12.318  12.863  13.412  14.042  14.694  15.319
 15.996  16.714  17.401  18.110  18.866  19.595  20.323  21.109
 21.891  22.647  23.432  24.203  24.925  25.665  26.421  27.135
 27.847  28.577  29.264  29.920  30.578  31.178  31.721  32.274
 32.804  33.274  33.747  34.217  34.620  34.989  35.351  35.662
 35.942  36.237  36.500  36.715  36.931  37.115  37.224  37.299
 37.345  37.329  37.284  37.225  37.112  36.966  36.810  36.597
 36.321  36.018  35.667  35.254  34.828  34.381  33.890  33.397
 32.906  32.368  31.806  31.246  30.636  29.979  29.324  28.648
 27.931  27.217  26.495  25.739  24.985  24.234  23.443  22.645
 21.864  21.068  20.279  19.534  18.778  17.993  17.246  16.526
 15.784  15.071  14.407  13.743  13.098  12.506  11.926  11.359
 10.851  10.366   9.874   9.428   9.029   8.645   8.305   8.022
  7.751   7.502   7.300   7.114   6.948   6.831   6.737   6.655
  6.615   6.585   6.535   6.514   6.522   6.505   6.482   6.485
  6.469   6.447   6.468   6.500   6.502   6.506   6.507   6.477
  6.455   6.462   6.460   6.462   6.489   6.502   6.496   6.507
  6.511   6.485   6.470   6.469   6.462   6.473   6.501   6.512
  6.516   6.522   6.506   6.486   6.490   6.487   6.475   6.497
  6.530   6.538   6.557   6.587   6.581   6.564   6.576   6.584
  6.588   6.619   6.648   6.649   6.659   6.674   6.662   6.647
  6.651   6.659   6.673   6.701   6.718   6.723   6.730   6.724
  6.710   6.711   6.710   6.702   6.722   6.751   6.752   6.757
  6.772   6.755   6.730   6.736   6.739   6.728   6.745   6.773
  6.775   6.778   6.786   6.768   6.745   6.744   6.737   6.733
  6.756   6.776   6.778   6.783   6.779   6.754   6.741   6.743
  6.736   6.740   6.764   6.773   6.772   6.781   6.772   6.746
  6.740   6.742   6.733   6.743   6.767   6.773   6.774   6.777
  6.760   6.738   6.736   6.732   6.728   6.748   6.764   6.762
  6.768   6.772   6.746   6.725   6.723   6.714   6.719   6.750
*Cp101/306_1*
 -0.858  -0.888  -0.828  -0.866  -1.186  -1.506  -1.485  -1.293
 -1.247  -1.316  -1.350  -1.364  -1.392  -1.408  -1.433  -1.494
 -1.564  -1.617  -1.654  -1.690  -1.746  -1.792  -1.775  -1.742
 -1.767  -1.778  -1.699  -1.624  -1.637  -1.659  -1.639  -1.642
 -1.690  -1.745  -1.800  -1.854  -1.889  -1.926  -1.948  -1.891
 -1.799  -1.773  -1.762  -1.681  -1.597  -1.546  -1.442  -1.308
 -1.243  -1.181  -1.045  -0.948  -0.950  -0.950  -0.974  -1.145
 -1.343  -1.365  -1.262  -1.203  -1.214  -1.208  -1.104  -0.953
 -0.943  -1.092  -1.150  -1.072  -1.071  -1.085  -0.910  -0.770
 -0.911  -1.035  -0.906  -0.806  -0.869  -0.889  -0.929  -1.128
 -1.219  -1.043  -0.923  -0.983  -0.974  -0.903  -0.963  -1.069
 -1.121  -1.207  -1.247  -1.099  -0.952  -1.001  -1.098  -1.135
 -1.217  -1.339  -1.390  -1.402  -1.430  -1.449  -1.479  -1.540
 -1.574  -1.576  -1.594  -1.593  -1.544  -1.514  -1.519  -1.495
 -1.434  -1.367  -1.305  -1.262  -1.227  -1.175  -1.149  -1.155
 -1.109  -1.061  -1.157  -1.260  -1.124  -0.878  -0.815  -0.876
 -0.869  -0.840  -0.863  -0.869  -0.848  -0.857  -0.868  -0.853
 -0.854  -0.866  -0.857  -0.852  -0.863  -0.860  -0.852  -0.860
 -0.862  -0.854  -0.858  -0.863  -0.856  -0.856  -0.862  -0.858
 -0.855  -0.861  -0.860  -0.855  -0.860  -0.861  -0.856  -0.858
 -0.862  -0.857  -0.857  -0.862  -0.859  -0.856  -0.861  -0.860
 -0.856  -0.860  -0.861  -0.857  -0.859  -0.861  -0.858  -0.857
 -0.861  -0.859  -0.857  -0.860  -0.860  -0.857  -0.859  -0.860
 -0.857  -0.859  -0.861  -0.858  -0.858  -0.861  -0.859  -0.857
 -0.860  -0.859  -0.857  -0.859  -0.860  -0.857  -0.859  -0.860
 -0.858  -0.858  -0.860  -0.859  -0.858  -0.860  -0.859  -0.857
 -0.859  -0.860  -0.858  -0.859  -0.860  -0.858  -0.858  -0.860
 -0.859  -0.858  -0.860  -0.859  -0.858  -0.860  -0.860  -0.858
 -0.859  -0.860  -0.858  -0.858  -0.860  -0.859  -0.858  -0.860
 -0.859  -0.858  -0.860  -0.860  -0.858  -0.859  -0.860  -0.858
 -0.859  -0.860  -0.859  -0.858  -0.860  -0.859  -0.858  -0.860
 -0.860  -0.858  -0.859  -0.860  -0.859  -0.859  -0.860  -0.859
```

Table 4: Example of data output format of manoeuvre measurements; $\Delta t = [\ 1 / (3.8 * 128)\ ]$

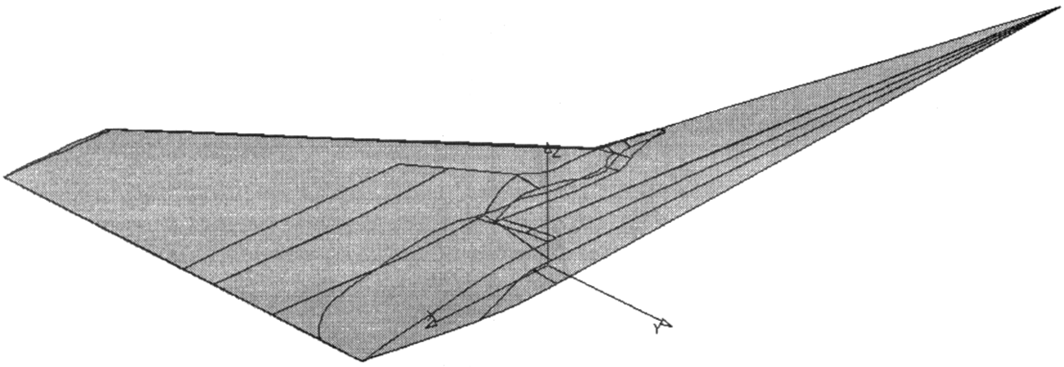

Figure 1: CATIA example of NLR Transonic Simple Straked Delta Wing

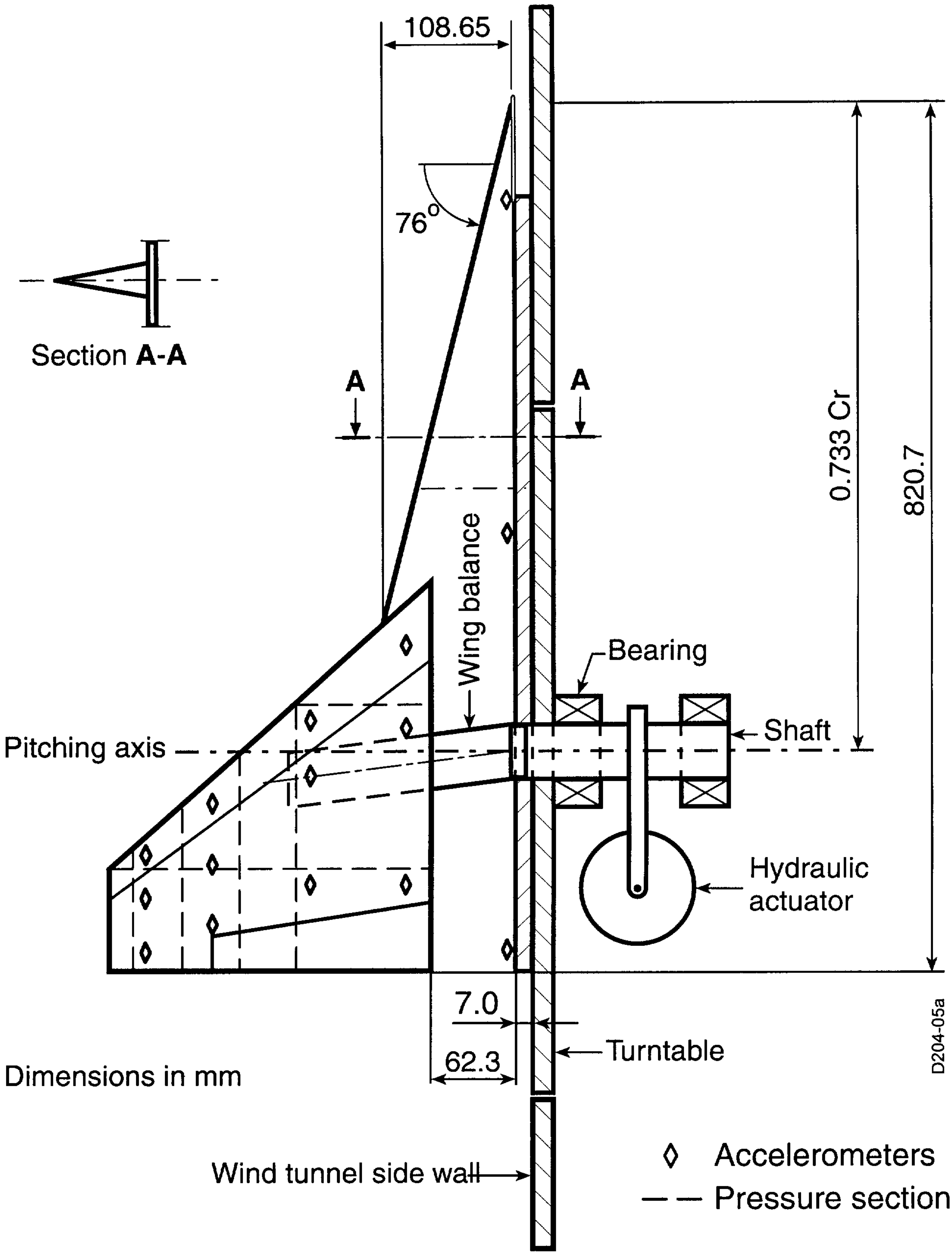

Figure 2: NLR Transonic Simple Straked Delta Wing configuration (dimensions in mm)

20. M219 CAVITY CASE

M J de C Henshaw
British Aerospace (Operations) Ltd.,
Military Aircraft and Aerostructures
Skillings Lane, Brough,
East Riding of Yorkshire,
HU 15 1 EQ
U.K.

INTRODUCTION

The data contained in this set consists of pressure time histories measured on the ceiling of an empty rectangular cavity, and were measured as part of a joint BAe./DERA programme at the ARA wind tunnel at Bedford during November 1991. The overall programme consisted of several configurations, with bodies positioned at various proximities to the cavity, but the data presented here only considers the empty cavity, configured for both shallow and deep cases. Data were measured using Kulite transducers along the centreline of the rig, (which did not coincide with the centreline of the cavity itself), and, in an alternative configuration, on the centreline of the cavity. Measurements taken off the cavity centreline, but not included here, indicated that 3D effects were not significant.

DEFINITIONS

d	Depth of Cavity
L	Length of Cavity (20 in.)
M	Mach Number
P	Pressure (KPa)
X, Y, Z	Co-ordinate directions: X is in direction of the flow, Y is span-wise and Z the vertical directions.

Note that all lengths are given in feet or inches except for boundary layer and transition lengths which are given in mm.

FORMULARY

1 GENERAL DESCRIPTION OF MODEL

1.1 Designation	Model M219 (referred to as 'generic cavity rig')
1.2 Type	Empty Cavity (shallow and deep configurations).
1.3 Derivation	DERA model manufactured at ARA
1.4 Additional remarks	The data are for 3D cavity. However, further data is available which suggests that there is no variation across the inner 50% of cavity width.
1.5 References	1,2

2 MODEL GEOMETRY

2.1 Plan-form	Rectangular cavity 20 in. X 4 in. (length X width). Two depths: 2 in. and 4 in.
2.2 Rig geometry	Flat surface model with inset cavity (see fig 1)
2.3 Cavity position in rig	Cavity offset by 1 in. from flat surface centreline (see fig 1). Cavity leading edge 31 in. aft of flat plate leading edge.
2.4 Additional remarks	Full geometry in attached figures.
2.5 References	1,2

3 WIND TUNNEL

3.1 Designation	ARA TWT (Transonic Wind Tunnel)
3.2 Type of tunnel	Continuous flow
3.3 Test section dimensions	9 X 8 (ft.)

3.4 Type of roof and floor	Ventilated
3.5 Type of side walls	Ventilated
3.6 Ventilation geometry	Perforated steel plate, 22% open area
3.7 Thickness of side wall boundary layer	Typically 13 mm at model centre-of-rotation station, (empty tunnel with centreline probe).
3.8 Thickness of boundary layers at roof and floor	Typically 13 mm at model centre-of-rotation station, (empty tunnel with centreline probe).
3.9 Method of measuring Mach number	Settling chamber and working section static pressures with calibrated corrections.
3.10 Flow angularity	<0.2°
3.11 Uniformity of Mach number over test section	<±0.0005, (low subsonic, fan only), to <±0.01, (high supersonic, nozzle setting plus plenum suction).
3.12 Sources and levels of noise in empty tunnel	Noise: Broadband rms. C_P < 0.5% across Mach range. Turbulence, (subsonic): u′/U<0.1%, v′/U<0.2%
3.13 Tunnel resonance's	Fan blade passing frequency and harmonics.
3.14 Additional remarks	None
3.15 References on tunnel	3, 4

4 MODEL MOTION

4.1 General description	No motion. On-line monitoring of accelerometers indicated no significant model motion. Output from datum pressure transducers, positioned on the flat plate (K1 and K2, see table 1), is available, although not included in this report. This indicated that there were no significant model or tunnel contributions to the unsteady cavity data.
4.2 Angle of attack	zero

5 TEST CONDITIONS

5.1 Model plan-form area/tunnel area	11.81%
5.2 Model span/tunnel width	15.74%, (17in/9ft)
5.3 Blockage	1.16% (119.91 in^2)
5.4 Position of model in tunnel	Rig support sting centreline 6in above tunnel centreline at zero incidence.
5.5 Range of Mach numbers	0.6, 0.85, 1.35
5.6 Range of tunnel total pressure	1.0032 to1.0121 bar
5.7 Range of tunnel total temperature	302.32 to 311.35 deg. K
5.8 Range of model steady, or mean incidence	Zero incidence only.
5.9 Definition of model incidence	N/A
5.10 Position and type of transition trip	40 mm aft of leading edge of flat plate. Stream-wise width of strip 4 mm. Sparsely distributed ballotini 0.13 to 0.15 mm diameter.
5.11 Flow instabilities during tests	None
5.12 Changes to mean shape of model due to steady aerodynamic load	Not measured, very stiff model
5.13 Additional remarks	None
5.14 References	1,2

6 MEASUREMENTS AND OBSERVATIONS

6.1 Steady pressures for the mean conditions	No
6.2 Steady pressures for small changes from the mean conditions	No
6.3 Quasi-steady pressures	Yes (for all conditions, but data not included in this report).
6.4 Unsteady pressures	Yes
6.5 Steady section forces for the mean conditions by integration of pressures	No
6.6 Steady section forces for small changes from the mean conditions by integration	No
6.7 Quasi-steady section forces by integration	No
6.8 Unsteady section forces by integration	No
6.9 Measurement of actual motion at points on model	No
6.10 Observation of measurement of boundary-layer properties	No
6.11 Visualisation of surface flow	No
6.12 Visualisation of shock wave movements	No
6.13 Additional remarks	None

7 INSTRUMENTATION

7.1 Steady/Quasi steady pressures	
7.1.1 Position of orifices span-wise and chord-wise	Front plate, rear plate, cavity ceiling, cavity sidewalls, cavity front wall. For distribution see attached figures and table 2.
7.1.2 Type of measuring system	Pressure orifices in model surfaces. Pressure measurement by PSI electronic scanning modules.
7.2 Unsteady pressures	
7.2.1 Position of orifices span-wise and chord-wise	2 on flat plate ahead of cavity, 2 on front wall of cavity, 10 positioned along ceiling of cavity either on its centreline, (shallow cavity), or 1 inch offset, (deep cavity; note this <u>is</u> the centreline of the rig), and 1 on flat plate aft of cavity. (See figure 1 and table 2)
7.2.2 Diameter of orifices	0.09in diameter transducers behind 0.063in diameter orifices.
7.2.3 Type of measuring system	High speed digital data acquisition system. Data sampled at 6000 Hz
7.2.4 Type of transducers	Kulite miniature high response XCQ 25PSI differential.
7.2.5 Principle and accuracy of calibration	Calibrated in situ by application of range of steady pressures
7.3 Model motion	
7.3.1 Method of measuring motion reference co-ordinate	N/A
7.3.2 Method of determining spatial mode of motion	N/A
7.3.3 Accuracy of measured motions	N/A

7.4 Processing of unsteady measurements	
7.4.1 Method of acquiring and processing measurements	High speed digital data acquisition system. Data sampled at 6000 Hz
7.4.2 Type of analysis	Spectral analysis using FFT to obtain power spectral density, rms. amplitude versus frequency and rms. total sound pressure level. Block size 2048 and summation of moving averages.
7.4.3 Unsteady pressure quantities obtained and accuracies achieved	Time history data. Spectral data
7.4.4 Method of integration to obtain forces	N/A
7.5 Additional remarks	None
7.6 References on techniques	Standard "Text Book" techniques have been used.

8 DATA PRESENTATION

8.1 Test cases for which data could be made available	M=0.4, 0.80, 0.98, 1.10 and 1.19.
8.2 Test cases for which data are included in this document	Two configurations (shallow and deep) each at M=0.6, 0.85, 1.35
8.3 Steady pressures	N/A
8.4 Quasi-steady or steady perturbation pressures	No
8.5 Unsteady pressures	Pressure time history for each pressure tap on cavity ceiling. RMS pressure for each pressure tap on cavity ceiling.
8.6 Steady forces or moments	N/A
8.7 Quasi-steady or steady perturbation forces	N/A
8.8 Unsteady forces and moments	N/A
8.9 Other forms in which data could be made available	Spectral data in rms. amplitude versus frequency form or power spectral density. It is recommended that the reader carry out signal analysis of the experimental data with the same tools that will be used to analyse the CFD data.
8.10 References giving other presentation of data	The data for empty cavity geometries has not been discussed in the open literature. Other reports on related work with non-empty cavities may be made available through application to DERA.

9 COMMENTS ON DATA

9.1 Accuracy	
9.1.1 Mach number	±0.001
9.1.2 Steady incidence	±0.01deg
9.1.3 Steady pressure coefficients	Basic accuracy of system in measuring a steady pressure coefficient at total pressures around atmospheric has been shown to be ±0.5%. However, for the current data steady or quasi-steady pressure coefficients are essentially a time average of a varying pressure and will be less accurate. Quasi-steady pressure coefficients measured at different times have been shown to be repeatable to within ±3%.
9.1.4 Steady pressure derivatives	N/A
9.1.5 Unsteady pressure coefficients	Combined non-linearity and hysteresis of Kulite transducers 0.1% of full-scale output; refer to DERA calibration of entire measurement chain.
9.2 Sensitivity to small changes of parameter	The only parameter varied was Mach number; changes other than those listed were not investigated.

9.3 Non-linearities — N/A

9.4 Influence of tunnel total pressure — Tunnel total pressure remained nominally constant at 1 bar.

9.5 Effects on data of uncertainty, or variation, in mode of model motion — N/A

9.6 Wall interference corrections — Corrections have been made to Mach number for tunnel blockage due to presence of the model and support system.

9.7 Other relevant tests on same model — Other tests have been made on the same model with stores mounted within the cavity.

9.8 Relevant tests on other models of nominally the same shape — N/A

9.9 Any remarks relevant to comparison between experiment and theory — Methods, under development, for the computation of cavity flow fields gave reasonable agreement between experiment and theory for time averaged or quasi-steady pressures. Early computations of rms. unsteady pressure levels using 2-D methods significantly over-predicted levels in comparison with the measured values.

9.10 Additional remarks — None.

9.11 References on discussion of data — The data for empty cavity geometries has not been discussed in open literature. Other reports on related work with non-empty cavities may be made available through application to DERA.

10 PERSONAL CONTACT FOR FURTHER INFORMATION

J A Ross, HWA, Bld 37, DERA Bedford, MK41 6AE

11 LIST OF REFERENCES

1. Aircraft Research Association Ltd., Model Test Note M219/6 "Details of tests in the ARA 2.74m x 2.44m transonic wind tunnel measuring the release disturbance of weapons carried in cavities. " Feb 1993.
2. Aircraft Research Association Ltd. Model Test Note M157/5 "Feasibility study for the measurement of release disturbance of weapons carried in cavities. April 1989.
3. Green J. E., McHugh C.A., Baxendale A.J. and Stanniland D. R., 'The use of a deep honeycomb to achieve high flow quality in the ARA 9' x 8' Transonic Wind Tunnel', presented at 18th Congress of ICAS, Beijing, September 1992.
4. Stanniland D. R., McHugh C.A. and Green J.E., 'Improvement of the flow quality in the ARA Transonic Tunnel by means of a long cell honeycomb', paper 54, RAeS conference on "Wind Tunnels and Wind Tunnel Test Techniques", Southampton, 1992.

EXPERIMENTAL ARRANGEMENT

The test rig dimensions are given in figure 1, the spoiler was not in place for the tests reported herein and is noted for information only. The location of the kulite transducers for which data is recorded in this database are shown in table 1 and illustrated in Figure 2. for the deep cavity. The cavity centreline is displaced by 1" relative to the rig centreline (see figure 1). For the deep (4") cavity the kulites are positioned on the rig centreline (Y=0), which is 1" to port of cavity centreline[1]. For the shallow (2") cavity the kulites are positioned at Y=1.0 (equivalent to the cavity centreline).

There were also 28 static pressure measurement transducers ahead of the cavity (on the rig centreline) and 14 aft of the cavity. Static measurement locations inside the cavity are noted in table 2.

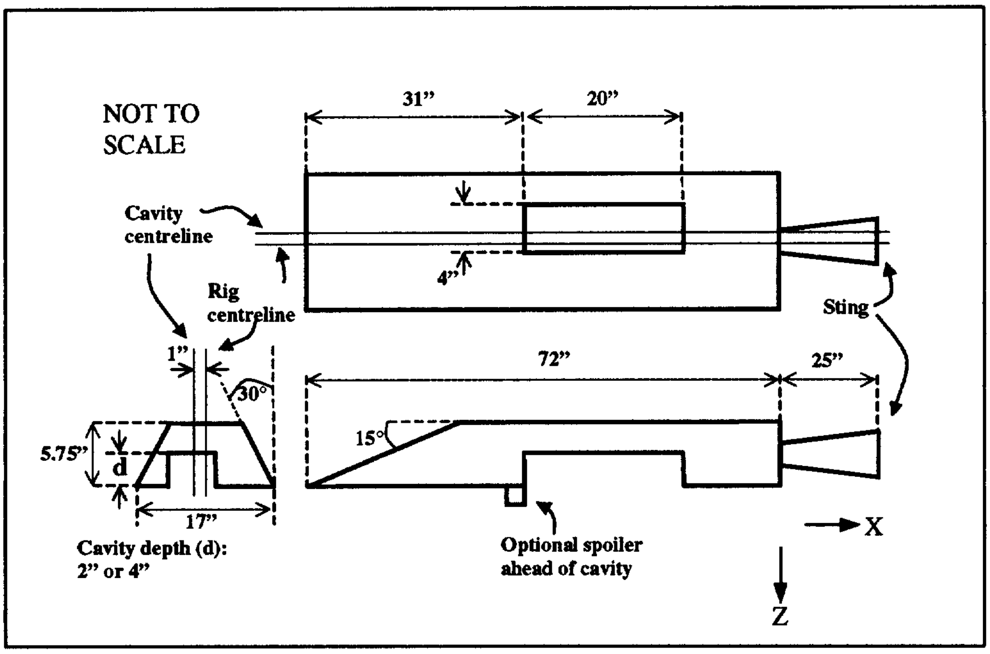

Figure 1: Test Rig and Dimensions

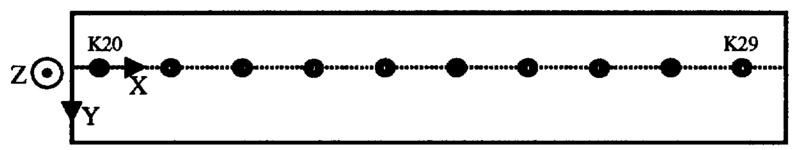

Figure 2: Position of Kulite Transducers on Cavity Ceiling (deep cavity)

[1] Cavity is on the rig underside.

DATA LAYOUT

The data is stored in six files (one for each flow condition), and consists of ten columns corresponding to the ten ceiling transducers in the order K20 to K29 (figure 2). Each column contains the pressure time history in KPa, with each row written in the FORTRAN format 10F14.6.

The time step for the data is implicit in the sampling rate per channel, i.e. a time step of $1/6000$ seconds.

Data files are located in the tree shown in figure 3.

Plots and values of the rms. pressure are included in table 3 (see figures 4 and 5) for the purpose of checking data quality. The values are derived including power up to 3000Hz, using the following parameters:

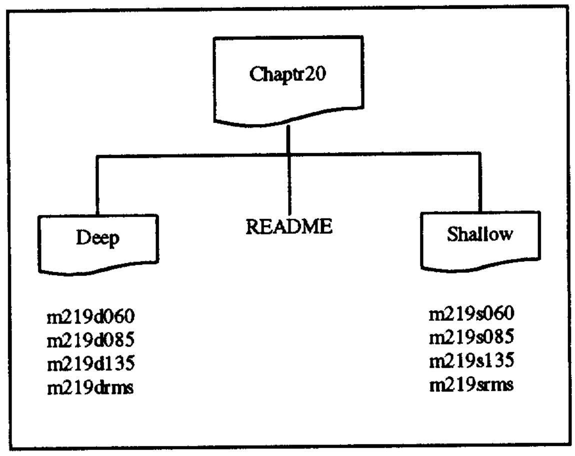

Figure 3: Layout of electronic data

Sampling frequency (samples/second)	6000	Block size	1024
Block period (seconds)	0.17067	Number of averages	20

No windowing was used in this analysis.

Kulite	X(in)	X/L	Location	Y(in)	
K1	-7.0		Front plate	0.0	
K2	-4.0			0.0	
K4	39.9		Rear plate	-3.0	
K7	0.0		Front wall (Z=-1.0) 2" cavity	2.5	
K8	0.0			-0.5	
K9	0.0		Front wall (Z=-1.0) 4" cavity	2.5	
K10	0.0			-0.5	
				Deep	Shallow
K20	1.0	0.05	Cavity ceiling	0.0	1.0
K21	3.0	0.15		0.0	1.0
K22	5.0	0.25		0.0	1.0
K23	7.0	0.35		0.0	1.0
K24	9.0	0.45		0.0	1.0
K25	11.0	0.55		0.0	1.0
K26	13.0	0.65		0.0	1.0
K27	15.0	0.75		0.0	1.0
K28	17.0	0.85		0.0	1.0
K29	19.0	0.95		0.0	1.0
K37	Port wall working section		Tunnel wall		

Table 1 Locations of Kulite transducers, only measurements from those on the cavity ceiling are included in this database.

	2" Depth Cavity	4"Depth Cavity
Ceiling	16 at Y=0", 16 at Y=2"	16 at Y=2"
Front Wall	8 at Y=2"	8 at Y=0", 8 at Y=2"
Port Side Wall	20 at Y=-1", Z=-0.25"	20 at Y=-1", Z=-0.25"
Starboard Side Wall	20 at Y=3", Z=-0.25"	20 at Y=3", Z=-0.25"

Table 2 Static Pressure Measurements Inside Cavity

X/L	Deep Cavity			Shallow Cavity		
	M=0.6	M=0.85	M=1.35	M=0.6	M=0.85	M=1.35
0.050	0.469	1.053	2.699	0.229	0.325	0.565
0.150	0.462	0.923	1.835	0.286	0.381	0.523
0.250	0.486	1.083	1.590	0.488	0.555	0.707
0.350	0.654	1.366	2.947	0.814	0.858	0.873
0.450	0.897	1.716	4.498	0.908	1.221	1.101
0.550	1.046	2.079	4.742	0.721	1.285	1.372
0.650	1.157	2.318	4.280	0.595	1.209	1.720
0.750	1.489	2.572	3.864	0.586	1.241	1.917
0.850	1.929	3.490	5.724	0.799	1.604	2.263
0.950	2.068	4.117	8.505	1.606	3.030	3.358

Table 3 RMS Pressure on cavity ceiling.

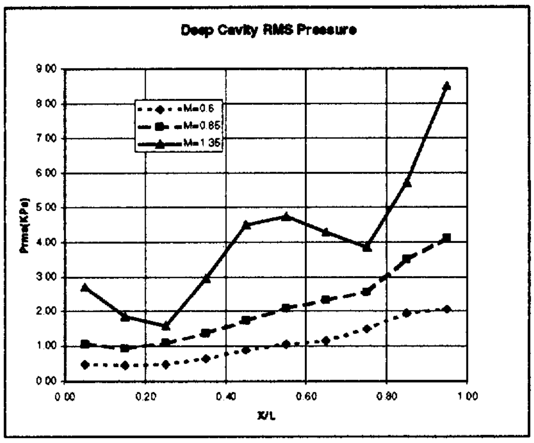

Figure 4: RMS Pressure distribution along the ceiling of the 'deep' empty cavity.

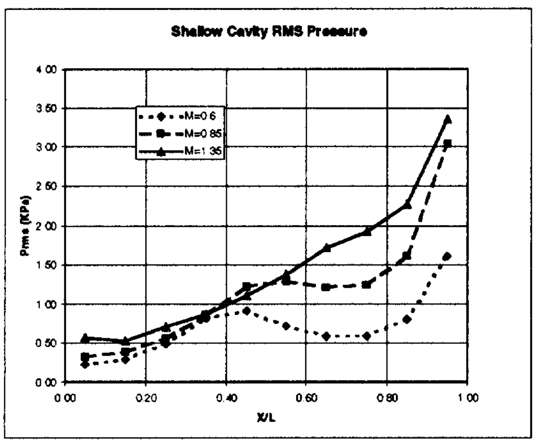

Figure 5: RMS Pressure distribution along the ceiling of the 'shallow' empty cavity.

ACKNOWLEDGEMENTS

Dr. J A Ross of DERA, Bedford, U.K., Mr. Andrea C Hill of ARA Aero. Dept., U.K., and Dr. P E Flood of BAe., Warton, U.K.

21E. DLR CAVITY PRESSURE OSCILLATIONS, EXPERIMENTAL

Jan Delfs
Institute of Design Aerodynamics
DLR German Aerospace Center
Braunschweig
Germany

INTRODUCTION

Windtunnel tests were carried out with the aim of establishing a measured unsteady surface pressure data set in and around a box-shaped shallow cavity, subject to tangential flow in the transonic Mach number range. Apart from the baseline case, for which systematic Mach number and Reynolds number variations were completed, the main purpose of the tests was to investigate the effect of certain upstream mounted passive flow control devices on the cavity oscillations for selected Mach numbers. This chapter contains the description of two baseline case data sets of unsteady surface pressures for freestream Mach number M_∞ =0.8 and M_∞ =1.33 respectively, made available to RTO.

The main purpose of the experiment was to test techniques for the passive control of pressure oscillations occurring in and near cavities exposed to tangential transonic flows. Moreover, the phase relation among the different cavity modes were investigated since the design of devices (passive and especially active) for control, critically depends on the knowledge and an understanding of the underlying physical mechanisms responsible for the resonances driving the phenomenon. Despite its long term investigation and the corresponding vast literature on cavity oscillations, reliable prediction schemes exist only for the frequencies of the oscillation modes. An insight into the phase relations among the modes however is necessary e.g. in order to lay out the characteristics of a controller for a closed loop active control of the oscillations. Therefore the present tests were also performed to reveal the spatio-temporal phase relation among the modes in the cavity.

The tests were done in the DLR wind tunnel TWG (Transonic Windtunnel Göttingen) in November 1997. The closed system tunnel has a test section area of 1m x 1m and is operated continuously. The cavity oscillation model is mounted on a cropped sting and consists basically of a flat plate, containing the cutout for the box-shaped cavity of length L = 0.202 m, width W = 0.03 m and depth D = 0.05 m, which in turn is hosted in the fuselage carrying the model (for details of the geometry see section 2 and Figures 1-5). Unsteady surface pressures were measured using flush mounted Kulite pressure transducers as specified in Table 1 and Figures 1 and 5. The static pressures at three positions on the plate surface upstream of the cavity (details see section 7) were measured in order to determine the actual Mach number of the flow above the cavity. A geometrical angle of attack of $\alpha = 1^{\circ}$ was set in order to assure non-separating flow at the sharp leading edge of the plate.

The cavity's bottom surface was made of an aluminium plate, which could be translated along the *x*-direction (streamwise) with the help of a remote-controlled electric motor. Six equally (in *x*) spaced Kulite sensors were flush mounted into the moveable plate. It was possible to take measurements at arbitrary *x*-positions of the cavity's bottom surface by moving the plate (and thus the six sensors) to the desired setting. For each flow parameter this was done for 12 positions of the plate. From one position to the next, the plate was advanced upstream in steps of 3 mm. For each of these settings the time histories of all Kulite sensors (including all non-moveable sensors) were recorded simultaneously along with the static flow data. Thus for each of the 12 positions the phase relation between all sensors can be evaluated.

LIST OF SYMBOLS AND DEFINITIONS

D	depth of cavity (50.0 mm)
L	length of cavity (202.0 mm)
W	width of cavity (30.0 mm)
M_∞	freestream Mach number
α	angle of attack, degrees
β	angle of sideslip, degrees
T_0	stagnation temperature, K

FORMULARY

1 General description of model

1.1 Designation	COM TWG 1
1.2 Type	empty cavity
1.3 Derivation	model manufactured at DLR Braunschweig central workshop
1.4 Additional remarks	none
1.5 References	none

2 Model geometry

2.1 Planform	rectangular shallow cavity in flat rectangular plate with triangular 50° side ears, plate width 300 mm
2.2 Cavity dimensions	length: 202 mm, width: 30 mm, depth: 50 mm

2.3 Leading edge sweep	cavity: 0°, plate: 0° inner l.e., 50° outer l.e.
2.4 Trailing edge sweep	cavity: 0°, plate: 50°
2.5 Taper ratio	n/a
2.6 Twist	0°
2.7 Root chord	plate root chord: 620 mm
2.8 Span of model	plate span : 700 mm
2.9 Area of planform	n/a
2.10 Definition of profiles	symmetrical flat plate with sharp 5°-leading and 20°-trailing edges, plate thickness 10 mm, cavity's leading edge 250 mm downstream of leading edge of plate
2.11 Additional remarks	dihedral = 0°; full geometry in attached figures.
2.12 References	none

3 Wind tunnel

3.1 Designation	DLR Transonic Wind Tunnel Göttingen, Germany
3.2 Type of tunnel	continuous flow
3.3 Test section dimensions	closed section: height: 1.00 m, width: 1.00 m
3.4 Type of roof and floor	smooth ($1.3 \leq M_\infty \leq 2.2$), perforated ($0.5 \leq M_\infty \leq 1.2$)
3.5 Type of side walls	like roof and floor
3.6 Ventilation geometry	perforated test section: 60° inclined 10 mm holes, 5.8% opening ratio
3.7 Thickness of side wall boundary layer	at test position: 70mm ($M_\infty = 0.5$), 59mm ($M_\infty = 0.9$), 39mm ($M_\infty = 1.2$), 38mm ($M_\infty > 1.3$)
3.8 Thickness of boundary layers at roof and floor	like side walls
3.9 Method of measuring velocity	perforated test section: calibrated function of plenum to total pressure, laval test section: calibrated laval nozzle
3.10 Flow angularity	perforated test section: $\Delta\alpha$, $\Delta\beta < 0.03°$, laval test section: $\Delta\alpha < 0.1°$, $\Delta\beta < 0.05°$
3.11 Uniformity of Mach number over test section	$\Delta v/v < 0.1$ %
3.12 Sources and levels of noise in empty tunnel	no specs
3.13 Tunnel resonances	no evidence of resonance in tests
3.14 Additional remarks	accuracy of Mach number $\Delta M_\infty < 0.001$ ($M_\infty \leq 0.9$), $\Delta M_\infty < 0.005$ ($M_\infty > 0.9$)
3.15 References on tunnel	1

4 Model motion

4.1 General description	no motion
4.2 Natural frequencies and normal modes of model and support system	response to momentarily released load in vertical direction *(z)* revealed only one dominant eigenfrequency of $f = 12.5$ Hz of a bending mode (no interferences with cavity oscillations)

5 Test conditions

5.1 Model plan-form area/tunnel area	0.305 (based upon cross section of test section)
5.2 Model span/tunnel width	0.7
5.3 Blockage	2.36% (frontal blockage, including sting interface)
5.4 Position of model in tunnel	plane of plate 50 mm above center of test section, cavity leading edge in streamwise center of test section
5.5 Range of Mach numbers	0.7, 1.46 (freestream)
5.6 Range of tunnel total pressure	$0.79\ 10^5$ Pa (M_∞=1.33), $0.82\ 10^5$ Pa (M_∞=0.8)
5.7 Range of tunnel total temperature	$300\ K < T_0 < 320\ K$
5.8 Range of model steady, or mean incidence	$-1.0° < \alpha < 0°$, $\beta = 0$
5.9 Definition of model incidence	model incidence defined relative to the plate's plane
5.10 Position of transition, if free	not measured
5.11 Position and type of trip, if transition fixed	no tripping

5.12 Flow instabilities during tests	cavity oscillations
5.13 Changes to mean shape of model due to steady aerodynamic load	not measured, negligible
5.14 Additional remarks	boundary layer thickness at leading edge $x = l_{LE} = 250$ mm of cavity not measured; estimated to be about 4.4 mm for both considered cases (estimation based upon transition from laminar to turbulent boundary layer at $Re_{Tr} = 3.5*10^5$)
5.15 References describing tests	none

6 Measurements and observations

6.1 Steady pressures for the mean conditions	yes, freestream values (wind tunnel) and 3 pressure taps in plate upstream of cavity
6.2 Steady pressures for small changes from the mean conditions	no
6.3 Quasi-steady pressures	no
6.4 Unsteady pressures	yes, KULITE pressure sensors in front, behind and in the cavity
6.5 Steady section forces for the mean conditions by integration of pressures	no
6.6 Steady section forces for small changes from the mean conditions by integration	no
6.7 Quasi-steady section forces by integration	no
6.8 Unsteady section forces by integration	no
6.9 Measurement of actual motion at points on model	no
6.10 Observation of measurement of boundary-layer properties	no
6.11 Visualisation of surface flow	no
6.12 Visualisation of shock wave movements	high speed schlieren movie to visualize sound radiation from cavity
6.13 Additional remarks	accuracy of floor plate sliding mechanism: ±0.15 mm

7 Instrumentation

7.1 Steady pressures	
7.1.1 Position of orifices span-wise and chord-wise	P1 (x = 50 mm, y = 0 mm, z = 0 mm), P2 (x = 100 mm, y = 0 mm, z = 0 mm), P3 (x = 120 mm, y = 0 mm, z = 0 mm), see also Fig.1
7.1.2 Type of measuring system	pressure orifices in model surfaces. connected to PSI pressure measurement system
7.2 Unsteady pressures	
7.2.1 Position of orifices span-wise and chord-wise	see Fig. 5 and Tab. 1
7.2.2 Diameter of orifices	transducers flush mounted
7.2.3 Type of measuring system	PSI modules, KULITE pressure transducers
7.2.4 Type of transducers	KULITE pressure transducers LQ3A-064-25A having 3.14 mm diameter
7.2.5 Principle and accuracy of calibration	PSI: 3 calibration pressures (magnitudes adapted to the expected values of the experiment) applied to each module. Kulite: static calibration at beginning of tunnel entry
7.3 Model motion	
7.3.1 Method of measuring motion reference co-ordinate	N/A
7.3.2 Method of determining spatial mode of motion	N/A
7.3.3 Accuracy of measured motions	N/A
7.4 Processing of unsteady measurements	
7.4.1 Method of acquiring and processing measurements	amplified Kulite signals input to DLR DEAS data acquisition system. Data sampling rate 30 kHz for 0.25 s simultaneously for all Kulites, repeated for 12 positions of the set of 6 Kulites, fixed to the translateable floor plate of cavity, translations in steps of 3 mm

7.4.2 Type of analysis	none
7.4.3 Unsteady pressure quantities obtained and accuracies achieved	time history data
7.4.4 Method of integration to obtain forces	N/A
7.5 Additional remarks	no mean pressure information from Kulite-signals
7.6 References on techniques	none

8 Data presentation

8.1 Test cases for which data could be made available	$0.7 \leq M_\infty \leq 1.2$ in steps of $\Delta M_\infty = 0.05$ (except $M_\infty = 1.0$) for Re(0.1 m) = 1.7 10^6 M_∞ = 0.8, 1.2, 1.33, 1.41, 1.46 for Re(0.1 m) = 1.1 10^6 M_∞ = 0.8, 1.33 for Re(0.1 m) = 0.55 10^6
8.2 Test cases for which data are included in this document	M_∞ = 0.8, 1.33 for Re(0.1 m) = 1.1 10^6
8.3 Steady pressures	freestream conditions and data from 3 pressure taps
8.4 Quasi-steady or steady perturbation pressures	N/A
8.5 Unsteady pressures	see above
8.6 Steady forces or moments	N/A
8.7 Quasi-steady or steady perturbation forces	N/A
8.8 Unsteady forces and moments	N/A
8.9 Other forms in which data could be made available	none
8.10 References giving other presentation of data	none

9 Comments on data

9.1 Accuracy	
9.1.1 Mach number	see 3.14
9.1.2 Steady incidence	-1°
9.1.3 Reduced frequenciy	N/A
9.1.4 Steady pressure coefficients	N/A
9.1.5 Steady pressure derivatives	N/A
9.1.6 Unsteady pressure coefficients	N/A
9.2 Sensitivity to small changes of parameter	no evidence
9.3 Non-linearities	N/A
9.4 Influence of tunnel total pressure	indirect effect through Reynolds number
9.5 Effects on data of uncertainty, or variation, in mode of model motion	N/A
9.6 Wall interference corrections	none
9.7 Other relevant tests on same model	none
9.8 Relevant tests on other models of nominally the same shapes	none
9.9 Any remarks relevant to comparison between experiment and theory	the tests were not performed as dedicated validation experiments for CFD/CAA (Computational Aeroacoustics), but were used to show that some new concepts of reducing cavity pressure oscillations were indeed able to destroy the resonances. Special flow devices were installed upstream the cavity to modify favourably the aerodynamic properties of the cavity shear layer. The devices were able to act in a way as to not increase the broadband level of the pressure oscillations
9.10 Additional remarks	none
9.11 References on discussion of data	none

Personal contact for further information

Dr. Jan Delfs
DLR, Institut für Entwurfsaerodynamik
Lilienthalplatz 7
38108 Braunschweig, Germany
jan.delfs@dlr.de

List of references

1 Binder, B; Riethmüller, L; Tusche, S.; Wulf, R.; Modernisierung des Transsonischen Windkanals in Göttingen.DGLR Jahrbuch 1992 Band1, pp 37-249

FORMAT OF DATA SET

There exists one ASCII data file for each position of the bottom plate of the cavity, in correspondance with the recording of the experimental data. The position is given and identified by a designation, which is a number $i = 0,...,11$ with the following meaning: The position of the plate is called i, when the x-position of plate-mounted sensor 8 is at $x_8 = (285.0 - i \cdot 3)$ mm. The mean position of sensor 8 is indicated in Table 1 and Figure 5. The position i is also indicated in the header of each of the files as well as in the name of the respective file. The data files of the two mentioned test cases ($M_\infty = 0.8$ and $M_\infty = 1.33$) are given as 080_0i.dat or 133_0i.dat for $i < 9$ and 080_i.dat or 133_i.dat for $i > 9$. All mean flow data defining the case considered are given in the header of each file. All data are given in SI-units. The sampling rate of the unsteady pressure data was 30 kHz for all cases. The corresponding time history of all 18 Kulite sensors is listed in the form of 18 respective columns in each of the mentioned data files. The files are compressed using the Unix command `compress` , i.e. they appear with an additional extention ".Z".

Is is emphasized that the Mach number and the dynamic pressure of the flow above the cavity are slightly different from the specified freestream values. The true values are to be computed from the standard oblique shock relations, taking into account the measured static pressures at the pressure taps.

It is noted, that in the case $M_\infty = 0.8$ the positions $i = 0,1,2$ are missing, because of a defect of the sliding mechanism of the cavity's bottom plate. Moreover, for the same Mach number the Kulite sensor No. 6 gave incorrect data. In the case $M_\infty = 1.33$ the signal from Kulite sensor No. 3 is incorrect (the signals of No. 6 being correct). All further details of the experiments are given in sections 1-12. The first lines of a sample data file are printed below. The columns corresponding to Kulites 4 to 17 are omitted in the sample.

```
#    cavity oscillation experiment, DLR COMTWG1
#
#    0.800000 E+00         freestream Mach number
#    1.043000 E+06         Reynolds number Re (0.1m)
#    1.000000 E+00         angle of attack (in degree)
#    0.817914 E+05         total pressure  in [Pa]
#    3.113927 E+02         stagnation temerature in [K]
#    5.370493 E+04         static pressure tap1 in [Pa]
#    5.378215 E+04         static pressure tap2 in [Pa]
#    5.428271 E+04         static pressure tap3 in [Pa]
#    3.000000 E+04         temporal sampling rate in [s^-1]
#    3                     number of position of translatable plate
#   p1             p2             p3             ...      p18              p19
  .64695008E+03  -.77032927E+03  -.79613503E+03  ...  -.10798857E+04  -.11891270E+04
  .42323837E+03  -.10607813E+04  -.97915458E+03  ...  -.11894393E+04  -.10731146E+04
  .22371171E+03  -.13680711E+04  -.13695963E+04  ...  -.15838324E+04  -.15168620E+04
 -.47765473E+03  -.12572223E+04  -.12628349E+04  ...  -.14492379E+04  -.20911233E+04
 -.32045191E+03  -.86854976E+03  -.81443698E+03  ...  -.17027763E+04  -.21389784E+04
```

TABLES

Kulite no.	*x [mm]*	*y [mm]*	*z [mm]*
1	246.5	0.0	0.0
2	250.0	0.0	-5.5
3	250.0	0.0	-11.5
4	250.0	0.0	-17.5
5	250.0	0.0	-23.5
6	250.0	0.0	-29.5
7 not exist.	-	-	-
8	268.5±16.5	0.0	-50.0
9	301.5±16.5	0.0	-50.0
10	334.5±16.5	0.0	-50.0
11	367.5±16.5	0.0	-50.0
12	400.5±16.5	0.0	-50.0
13	433.5±16.5	0.0	-50.0
14	455.5	0.0	0.0
15	452.0	0.0	-5.5
16	452.0	0.0	-11.5
17	452.0	0.0	-17.5
18	351.0	15.0	-17.5
19	351.0	-15.0	-17.5

Table 1: Positions of Kulite sensors. Kulites 8-13 are mounted on a motor-driven translatable plate, such that any position along the cavity floor can be measured. In the given set of data, the plate was moved in steps of $\Delta x = 3$ mm.

FIGURES

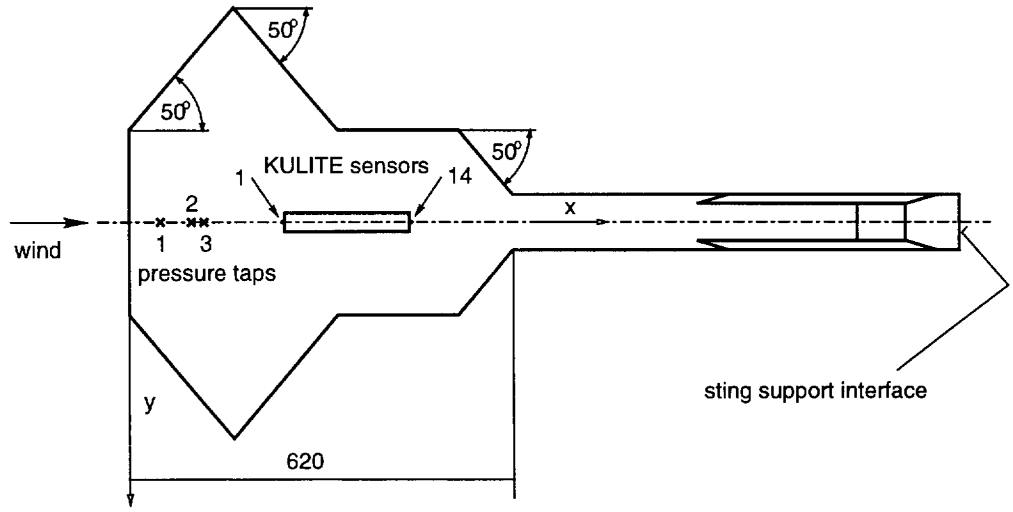

Figure 1: Lower side of model, housing the cavity; position and number of pressure taps and KULITE sensors

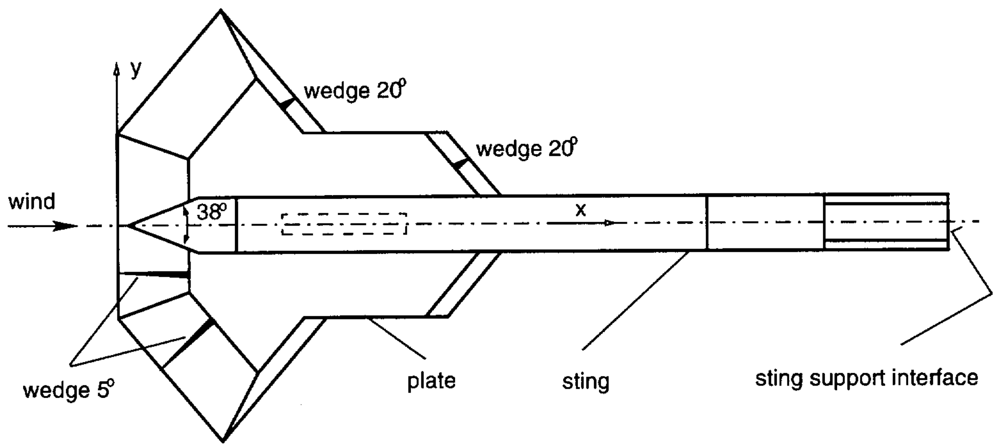

Figure 2: Upper side of the model

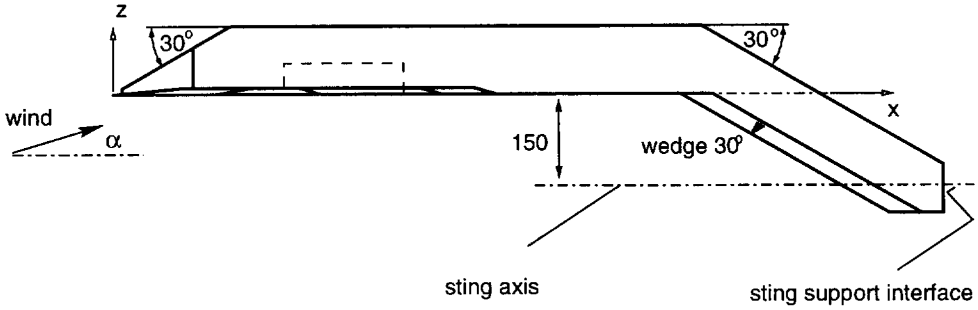

Figure 3: Side view of the model

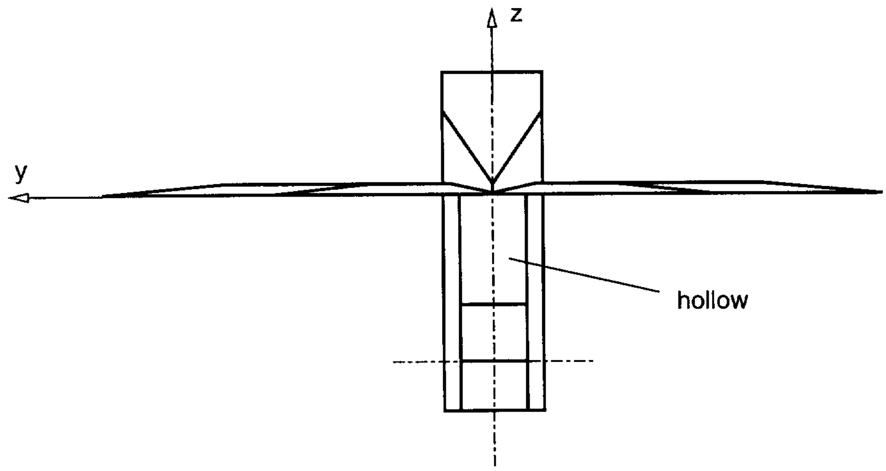

Figure 4: Front view of the model

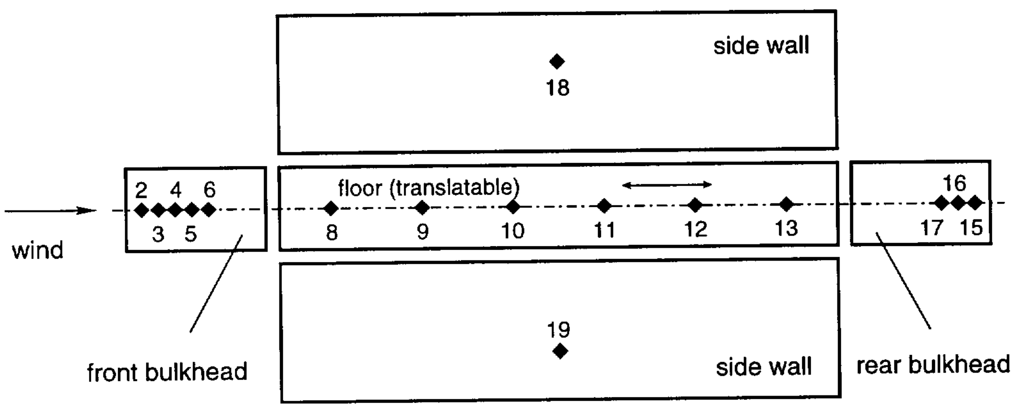

Figure 5: Arrangement and numbering of KULITE sensors on cavity walls

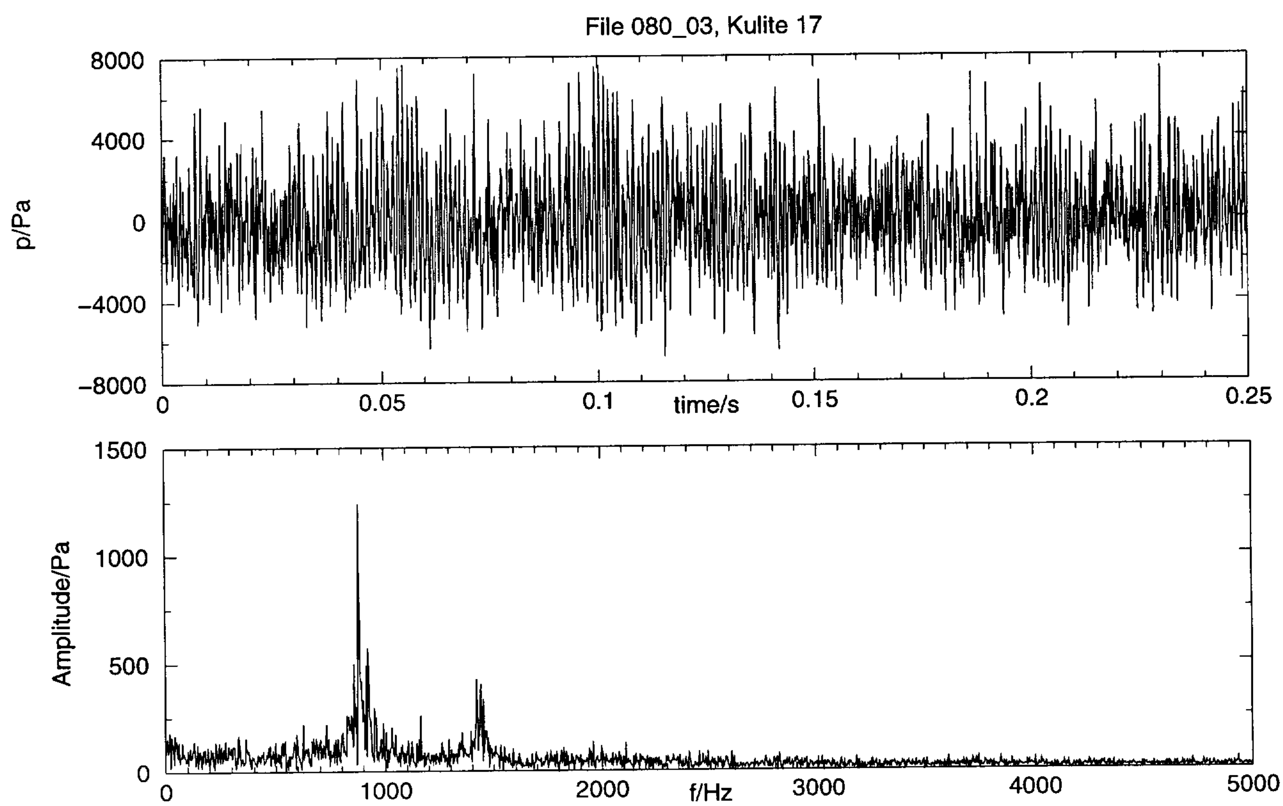

Figure 6: Typical time series and corresponding amplitude spectrum of non-averaged narrow-band Fourier coefficients of Kulite signal

22-E. DYNAMIC STALL DATA FOR 2-D AND 3-D TEST CASES

Professor R A McD Galbraith
Dr F N Coton
Dr R B Green
Dr M Vezza

University of Glasgow

INTRODUCTION

Background

Although substantial work has been carried out and much understanding gained of the phenomena associated with dynamic stall, our description and understanding of it is incomplete. Even if we consider the nominally two-dimensional flow associated with most experiments, some significant anomalies have yet to be explained. Fully three-dimensional experiments are few and, as might have been expected, raise more questions than have been answered.

The purpose of the selected cases herein is to provide the computational fluid dynamic specialists with a variety of test data to assess the output of their codes. The experimentalists may then obtain additional information from the CFD specialists so that together the knowledge and understanding of dynamic stall and the associated anomalies may be enhanced.

As described by Young (ref 1), the nominally two-dimensional case is considered to be characterised by a dynamic overshoot of the aerodynamic coefficients followed by stall onset and the roll-up of the shed vorticity into a coherent vortex that convects over the upper surface of the aerofoil and then off into the mainstream. It is the convection speed of the main vortex (dynamic stall vortex) in which a distinctive anomaly has been identified by Green et al (ref 2). It was observed that certain data indicated an independence of the convection speed from the motion of the model, whilst others did not. (see Fig 1). Of all the influencing factors that could have contributed to that clear difference of result, such as aerofoil shape, aspect ratio, surface finish, data reduction software and Mach number, all but the Mach number had no effect on the observed trends. Green and Galbraith concluded (ref 3) that the most likely contender causing the two very different results would be the difference in the Mach number between the experimental set-ups. Albeit the data sets contained in section 1 are for low Mach numbers (M = 0.12) they do cover a wide range of reduced pitch rate. If CFD results reproduce the constancy of "stall vortex" convection speed observed, then it would be helpful to recalculate for a few higher Mach numbers; say, 0.2, 0.4 and 0.7.

Although the Glasgow data (covering 14 different models) indicated an independence of convection speed with regard to the reduced pitch rate and the reduced frequency, there was a variation between different models. It was observed, however, (ref 2 and 3) that the speed did appear to be dependent on the shape of the aerofoil and the method of transition. It appeared that, if a transition strip was placed at the leading edge (consisting of filtered grit) then the convection speed was reduced and, similarly, the scatter (ref 4). Suitably "tripped" data are contained in section 2.

Section 2 presents data from two NACA 0015 aerofoils of different aspect ratio. It is hoped that the spread of test cases can be used to assess the quality of prediction of low-speed dynamic stall. The data are for motions of "ramp-up", "ramp-down" and oscillatory pitch. Both the ramp-up and ramp-down are important because they isolate the stalling mechanisms from the re-attachment process. As such, the mix, where the aerofoil is simultaneously attempting to stall and "re-attach", during some oscillatory modes, is absent.

In addition, the ramp-downs will provide a most interesting case because the data clearly show that, at the high pitch rates, one can achieve negative lift at high incidence. Figure 2 shows the effect of pitch rate upon the normal force during ramp-down tests of the Sikorsky SSC-A09 aerofoil. Although this was not the most severe case, it does indicate (see Fig 2) that it has negative lift at incidence as high as 8 degrees; other, uncambered aerofoils produced negative lift at incidences as high as 10 degrees.

Both the NACA 0015 aerofoils are for a nominally two-dimensional test set-up, although, at least for the steady case, the flows are likely to be highly three-dimensional in the stall condition. Nonetheless, the data are very comparable and show very similar trends, especially in the ramp-down motion. The only significant difference between the high aspect and the low aspect ratio models is, of course, the Reynolds number. This manifests itself in the ramp-down mode only in the latter stages of re-attachment. This is a consequence of the Reynolds number effects on the boundary layer.

The section 3 data from a finite wing with a NACA 0015 section is presented and provides a very severe test case for any current CFD code.

Summary of Test Cases

All of the models referred to herein were tested for the following motion types: static, linear ramp-up, linear ramp-down and sinusoidal. Actual test cases presented in the following sections are summarised in table 1.

NOMENCLATURE

c	chord (m)
Cm	pitching moment coefficient (ref point 1/4c)
Cn	normal force coefficient
Cp	pressure coefficient
Ct	thrust coefficient (+ve towards leading edge)
DP	dynamic pressure (N/m^2)
g	acceleration due to gravity (m/s^2)
k	reduced frequency $\left(\omega c / 2U\right)$
M	Mach number
r	reduced pitch rate $\left(\frac{\partial \alpha}{\partial t} c / 2U\right)$
Re	Reynolds No $\left(\frac{Uc}{\nu}\right)$
s	span (m)
x	chordwise direction (m)
y	direction normal to chord (m)
z	spanwise direction (m)
U	velocity (m/s)

angle of attack (degrees)

ν	kinematic viscosity (m/s)
ω	rotational frequency (rads/s)

22E(1) SIKORSKY SSC-A09 DATA (NOMINALLY TWO DIMENSIONAL)

INTRODUCTION

The tests described were carried out in the University of Glasgow's 'Handley Page' wind tunnel, which is a closed-return, low-speed type with a 2.13m x 1.61m octagonal working section (Fig 3). The model span and chord were 1.61m and 0.55m respectively, and its construction was of a fibreglass skin filled with an epoxy foam bonded to an aluminium spar. The model was pitched about the quarter chord by a linear hydraulic actuator and crank mechanism. The actuator was a Unidyne 907/1 type with a dynamic thrust of 6.1kN controlled by a MOOG 76 series 450 servo valve. Thirty five Kulite 093-5 PSI G ultra-miniature pressure transducers were installed below the skin in a removable pod at the centre-span of the model. The transducers were of the vented gauge type with one side open, via tubes, to ambient pressure outside the tunnel. Each transducer was fitted with a temperature compensation module to minimize changes in the zero-offset and sensitivity. Model incidence was determined using an angular potentiometer geared to the model's main spar. This provided feedback to the hydraulic actuator control system and the angle of incidence signal for the data recording system. The model incidence waveform was provided by a PC fitted with an ANALOGUE DEVICES RT 1815 input/ output board. The dynamic pressure in the working section was determined by measuring the difference between the static pressure in the working section, just upstream of the model leading edge, and the static pressure in the settling chamber. These pressure tappings were connected to a Furness FC012 micromanometer which provided an analogue signal for the data acquisition module.

The model was tested with a view to an investigation of the dynamic stall vortex convection speed anomaly (ref 2, 4 and 10). The model was instrumented with 35 pressure transducers placed asymmetrically over the upper and lower surfaces at the mid-span of the model. A particularly high resolution around the leading edge was chosen. Two motion types were considered, namely ramp-up and ramp-down. The model was rotated about the quarter chord point. For the ramp-tests the model was pitched over a preset arc at a constant pitch rate. At low pitch rates excellent ramp-profiles were obtained, but at higher pitch rates acceleration and deceleration of the model produced non-linearities. For ramp tests each test case was performed 5 times, and the data were phase averaged to produce the results presented here.

FORMULARY

1 General Description of model

1.1	Designation	Model 15
1.2	Type	Nominally two-dimensional
1.3	Derivation	Not applicable
1.4	Additional remarks	None
1.5	References	6

2 Model Geometry

2.1	Planform	Nominally two-dimensional
2.2	Aspect ratio	2.93
2.3	Leading edge sweep	None
2.4	Trailing edge sweep	None
2.5	Taper ratio	No Taper
2.6	Twist	No Twist
2.7	Wing centreline chord	0.55m
2.8	Semi-span of model	0.805m
2.9	Area of planform	$0.8855m^2$ gross wing area
2.10	Location of reference sections and definition of profiles	Sikorsky SSC-A09 profile: 9%c thick, lightly cambered with 0.7%c leading edge radius (see table 2).
2.11	Lofting procedure between reference sections	Constant section
2.12	Form of wing-body junction	None
2.13	Form of wing tip	Not applicable
2.14	Control surface details	None
2.15	Additional remarks	None
2.16	References	6, 7

3 Wind Tunnel

3.1	Designation	University of Glasgow 'Handley-Page'
3.2	Type of tunnel	Closed section, closed return, atmospheric
3.3	Test section dimensions	2.13m (width) x 1.61m (height) x 2.8m (length)
3.4	Type of roof and floor	Closed – vented at downstream end of working section
3.5	Type of side walls	Closed - vented at downstream end of working section
3.6	Ventilation geometry	60 rectangular slots (0.028m x0.055m) on floor, roof and walls downstream of working section. 13 rectangular slots (0.028m x 0.105m) at same section on angled surfaces.
3.7	Thickness of side wall boundary layer	Unknown
3.8	Thickness of boundary layers at roof and floor	Unknown
3.9	Method of measuring velocity	Working section and settling chamber static pressure tappings related to wind tunnel speed calibration
3.10	Flow angularity	Not available
3.11	Uniformity of velocity over test section	Dynamic pressure constant to within 1% over a $1.5m^2$ reference plane normal to the flow axis in the working section
3.12	Sources and levels of noise or turbulence in empty tunnel	Not available
3.13	Tunnel resonances	Not available
3.14	Additional remarks	None
3.15	References on tunnel	8

4 Model Motion Actuation

4.1	General description	Four motion types: Static, Linear Ramp Up, Linear Ramp Down and Sinusoidal. All incidence variations about quarter chord. Actuation is via Unidyne 907/1 type with a dynamic thrust of 6.1kN controlled by a MOOG 76 series 450 servo valve.
4.2	Natural frequencies and normal modes of model and support system	Not available

5 Test Conditions

5.1	Model planform area/tunnel area	0.258
5.2	Model span/tunnel height	0.756
5.3	Blockage	Function of angle of attack 2.3% - 16.6%
5.4	Position of model in tunnel	Vertical on tunnel centre-line. Mounted through floor. (see Fig. 3)
5.5	Range of velocities	45 m/s to 55 m/s
5.6	Range of tunnel total pressure	Approximately 102.5kPa to 103kPa
5.7	Range of tunnel total temperature	Approximately 293K to 306K
5.8	Range of model steady or mean incidence	-5° to 42°
5.9	Definition of model incidence	Deviation of chord line from tunnel centreline
5.10	Position of transition, if free	Not available
5.11	Position and type of trip, if transition fixed	None
5.12	Flow instabilities during tests	Not available
5.13	Changes to mean shape of model due to steady aerodynamic load	Not available
5.14	Additional remarks	None
5.15	References describing tests	6

6 Measurements and Observations

6.1	Steady pressures for the mean conditions	No

6.2	Steady pressures for small changes from the mean conditions	No
6.3	Quasi-steady pressures	No
6.4	Unsteady pressures	Yes
6.5	Steady section forces for the mean conditions by integration of pressures	Yes
6.6	Steady section forces for small changes from the mean conditions by integration	No
6.7	Quasi-steady section forces by integration	No
6.8	Unsteady section forces by integration	Yes
6.9	Measurement of actual motion at points of model	No
6.10	Observation or measurement of boundary layer properties	No
6.11	Visualisation of surface flow	No
6.12	Visualisation of shock wave movements	No
6.13	Additional remarks	None

7 Instrumentation

7.1	Steady pressure	
7.1.1	Position of orifices spanwise and chordwise	Chordwise only. See Table 3.
7.1.2	Type of measuring system	Thirty five Kulite 093-5 PSI G ultra-miniature pressure transducers mounted close to wing surface connected to 200 parallel channel data acquisition system.
7.2	Unsteady pressure	
7.2.1	Position of orifices spanwise and chordwise	Chordwise only. See Table 3.
7.2.2	Diameter of orifices	1.0mm
7.2.3	Type of measuring system	Thirty five Kulite 093-5 PSI G ultra-miniature pressure transducers mounted close to wing surface connected to 200 parallel channel data acquisition system.
7.2.4	Type of transducers	Kulite CJQH-187 differential
7.2.5	Principle and accuracy of calibration	Steady state sensitivity from applied reference and calibration procedures. Accuracy as stated by manufacturer.
7.3	Model motion	
7.3.1	Method of measuring motion reference coordinate	Quarter chord location specified by manufacture
7.3.2	Method of determining spatial mode of motion	Feedback from potentiometer geared to shaft.
7.3.3	Accuracy of measured motion	0.1°
7.4	Processing of unsteady measurements	
7.4.1	Method of acquiring and processing measurements	35 individual Kulite sensors mounted close to wing surface connected to 200 parallel channel Bakker Electronics BE256 sample and hold modules. Signal conditioning modules on each individual channel. Gain and offset removal automatic. Acquired data downloaded to PC.
7.4.2	Type of analysis	Phase averaging of cycles. Five cycles for ramp function tests.
7.4.3	Unsteady pressure quantities obtained and accuracies achieved	Basic unsteady pressure signal. Cycle repeatability variable depending on amplitude and reduced pitch rate.
7.4.4	Method of integration to obtain forces	Trapezoidal rule
7.5	Additional remarks	None
7.6	References on techniques	None

8 Data presentation

8.1	Test cases for which data could be made available	Two motion types: Linear Ramp Up and Linear Ramp Down. Tests cover a range of reduced pitch rate. In total 54 test cases. All incidence variations about quarter chord.
8.2	Test cases for which data are included in this document	One motion type: Linear Ramp Up. Three test cases as detailed in Table 4. A series of plots are also presented which are illustrative of the data supplied in electronic form. Figure 4 shows a sample upper surface pressure distribution, C_n, C_m and incidence history.
8.3	Steady pressures	None
8.4	Quasi-steady or steady perturbation pressures	No
8.5	Unsteady pressures	For all dynamic cases
8.6	Steady forces or moments	None
8.7	Quasi-steady or unsteady perturbation forces	No
8.8	Unsteady forces and moments	For all dynamic cases
8.9	Other forms in which data could be made available	None
8.10	Reference giving other representations of data	N/A

9 Comments on data

9.1	Accuracy	
9.1.1	Mach number	±0.5%
9.1.2	Steady incidence	±0.1°
9.1.3	Reduced frequency	±0.5%
9.1.4	Steady pressure coefficients	±0.5%
9.1.5	Steady pressure derivatives	Not estimated
9.1.6	Unsteady pressure coefficients	±0.5%
9.2	Sensitivity to small changes of parameter	N/A
9.3	Non-linearities	N/A
9.4	Influence of tunnel total pressure	Not examined
9.5	Effects on data of uncertainty, or variation, in mode of model motion	N/A
9.6	Wall interference corrections	None
9.7	Other relevant tests on same model	None
9.8	Relevant tests on other models of nominally the same shapes	None
9.9	Any remarks relevant to comparison between experiment and theory	None
9.10	Additional remarks	The electronic data supplied with this report comprises three file types. The first type of file contains the aerofoil co-ordinates. There is only one file of this type, and it is identified by the name ssca09_coords.dat. The second type contains the transducer coordinates. There is only one file of this type and it is identified by the name ssca09_xducers.dat. The last file type contains pressure data, and three examples are provided (described in table 4) The first 128 parameters are the run information data (described in table 5), and the remaining parameters are 1024 blocks each comprising the dynamic pressure, pressure coefficients (35 values) and angle of incidence. A MATLAB program to read in the data is listed in appendix A. The pressure transducer locations correspond to the order contained in the file ssca09_xducers.dat, which is the same as in table 3.
9.11	References on discussion of data	3, 6

10 Personal contact for further information

Dr. R.B. Green
Department of Aerospace Engineering
University of Glasgow
Glasgow
G12 8QQ
U.K.
Tel. +44 141 330 4312
Email: richardg@aero.gla.ac.uk

22E(2) NACA 0015 DATA (NOMINALLY TWO-DIMENSIONAL)

INTRODUCTION

The tests described were carried out in the University of Glasgow's 'Handley Page' wind tunnel, which is a closed-return, low-speed type with a 2.13m x 1.61m octagonal working section. The model span was 1.61m, and its construction was of a fibre glass skin filled with an epoxy foam bonded to an aluminium spar. The model was pitched about the quarter chord by a linear hydraulic actuator and crank mechanism. The actuator was a Unidyne 907/1 type with a dynamic thrust of 6.1kN controlled by a MOOG 76 series 450 servo valve. Thirty Kulite 093-5 PSI G ultra-miniature pressure transducers were installed below the skin in a removable pod at the centre-span of the model. The transducers were of the vented gauge type with one side open, via tubes, to ambient pressure outside the tunnel. Each transducer was fitted with a temperature compensation module to minimize changes in the zero-offset and sensitivity. Model incidence was determined using an angular potentiometer geared to the model's main spar. This provided feedback to the hydraulic actuator control system and the angle of incidence signal for the data recording system. The model incidence waveform was provided by a PC fitted with an ANALOGUE DEVICES RT 1815 input/ output board. The dynamic pressure in the working section was determined by measuring the difference between the static pressure in the working section, just upstream of the model leading edge, and the static pressure in the settling chamber. These pressure tappings were connected to a Furness FC012 micromanometer which provided an analogue signal for the data acquisition module.

Two NACA 0015 models were tested, namely a "full" chord, low aspect ratio model, and a "short" chord, high aspect ratio model. The former, of 0.55m chord was tested as part of the research programme at the time to investigate the dynamic stall over a family of aerofoil profile shapes. The latter model, of 0.275m chord was tested with a view to an investigation of the dynamic stall vortex convection speed anomaly (reference 2, 4 and 10). Each model was instrumented with 30 pressure transducers placed symmetrically over the upper and lower surfaces at the mid-span of the model. Four motion types were considered, namely static, ramp-up, ramp-down and oscillatory (sinusoidal). The models were both rotated about the quarter chord point. In static tests each model was positioned at an incidence of -1^{o} and pitched to 30^{o} and back down to -1^{o} in 1^{o} increments allowing a settling time for each new incidence. For the ramp-tests the models were pitched over a preset arc at a constant pitch rate. At low pitch rates excellent ramp-profiles were obtained, but at higher pitch rates acceleration and deceleration of the model produced non-linearities. For ramp tests each test case was performed 5 times, and the data were phase averaged to produce the results presented here. For the sinusoidal tests 10 cycles of motion were recorded, and again the data were phase averaged

FORMULARY

1 General Description of model

1.1	Designation	Full Chord	Model 5
		Short Chord	Model 12
1.2	Type	Nominally two-dimensional	
1.3	Derivation	Not applicable	
1.4	Additional remarks	None	
1.5	References	9	

2 Model Geometry

2.1	Planform	Nominally two-dimensional	
2.2	Aspect ratio	Full Chord	2.93
		Short Chord	5.86
2.3	Leading edge sweep	None	
2.4	Trailing edge sweep	None	
2.5	Taper ratio	No Taper	
2.6	Twist	No Twist	
2.7	Wing centreline chord	Full Chord	0.55m
		Short Chord	0.275m
2.8	Semi-span of model	0.805m	
2.9	Area of planform	Full Chord	$0.8855m^2$ gross wing area
		Short Chord	$0.443m^2$ gross wing area

2.10	Location of reference sections and definition of profiles	NACA 0015 profile nominal ± 0.05mm accuracy
2.11	Lofting procedure between reference sections	Constant section
2.12	Form of wing-body junction	None
2.13	Form of wing tip	Not applicable
2.14	Control surface details	None
2.15	Additional remarks	None
2.16	References	9

3 Wind Tunnel

3.1	Designation	University of Glasgow 'Handley-Page'
3.2	Type of tunnel	Closed section, closed return, atmospheric
3.3	Test section dimensions	2.13m (width) x 1.61m (height) x (length)
3.4	Type of roof and floor	Closed – vented at downstream end of working section
3.5	Type of side walls	Closed - vented at downstream end of working section
3.6	Ventilation geometry	60 rectangular slots (0.028m x0.055m) on floor, roof and walls downstream of working section. 13 rectangular slots (0.028m x 0.105m) at same section on angled surfaces.
3.7	Thickness of side wall boundary layer	Unknown
3.8	Thickness of boundary layers at roof and floor	Unknown
3.9	Method of measuring velocity	Working section and settling chamber static pressure tappings related to wind tunnel speed calibration
3.10	Flow angularity	Not available
3.11	Uniformity of velocity over test section	Dynamic pressure constant to within 1% over a $1.5m^2$ reference plane normal to the flow axis in the working section
3.12	Sources and levels of noise or turbulence in empty tunnel	Not available
3.13	Tunnel resonances	Not available
3.14	Additional remarks	None
3.15	References on tunnel	8

4 Model motion

4.1	General description	Four motion types: Static, Linear Ramp Up, Linear Ramp Down and Sinusoidal. All incidence variations about quarter chord.
4.2	Natural frequencies and normal modes of model and support system	Not available

5 Test Conditions

5.1	Model planform area/tunnel area	Full Chord	0.258
		Short Chord	0.129
5.2	Model span/tunnel height	0.756	
5.3	Blockage	Full Chord	Function of angle of attack 3.9% - 16.6%
		Short Chord	Function of angle of attack 1.9% - 8.4%
5.4	Position of model in tunnel	Vertical on tunnel centre-line. Mounted through floor. (see Fig. 3)	
5.5	Range of velocities	45 m/s to 55 m/s	
5.6	Range of tunnel total pressure	Approximately 102.5kPa to 103kPa	
5.7	Range of tunnel total temperature	Approximately 293K to 306K	
5.8	Range of model steady or mean incidence	-5° to 42°	
5.9	Definition of model incidence	Deviation of chord line from tunnel centreline	
5.10	Position of transition, if free	Not available	

5.11	Position and type of trip, if transition fixed	Full Chord	None
		Short Chord	When applied, grit layer from leading edge to 2% chord on upper and lower surfaces.
5.12	Flow instabilities during tests	Not available	
5.13	Changes to mean shape of model due to steady aerodynamic load	Not available	
5.14	Additional remarks	None	
5.15	References describing tests	9	

6 Measurements and Observations

6.1	Steady pressures for the mean conditions	Yes
6.2	Steady pressures for small changes from the mean conditions	No
6.3	Quasi-steady pressures	No
6.4	Unsteady pressures	Yes
6.5	Steady section forces for the mean conditions by integration of pressures	Yes
6.6	Steady section forces for small changes from the mean conditions by integration	No
6.7	Quasi-steady section forces by integration	No
6.8	Unsteady section forces by integration	Yes
6.9	Measurement of actual motion at points of model	No
6.10	Observation or measurement of boundary layer properties	No
6.11	Visualisation of surface flow	No
6.12	Visualisation of shock wave movements	No
6.13	Additional remarks	None

7 Instrumentation

7.1 Steady pressure

7.1.1	Position of orifices spanwise and chordwise	Chordwise only. See Table 6.	
7.1.2	Type of measuring system	Full Chord	30 Individual Kulite sensors mounted close to wing surface connected to DEC MINC parallel channel data acquisition system.
		Short Chord	30 Individual Kulite sensors mounted close to wing surface connected to Bakker Electronics BE256 parallel channel data acquisition system.

7.2 Unsteady pressure

7.2.1	Position of orifices spanwise and chordwise	Chordwise only. See Table 6.	
7.2.2	Diameter of orifices	1.0mm	
7.2.3	Type of measuring system	Full Chord	30 individual Kulite sensors mounted close to wing surface connected to DEC MINC parallel channel data acquisition system.
		Short Chord	Individual Kulite sensors mounted close to wing surface connected to Bakker Electronics BE256 parallel channel data acquisition system.
7.2.4	Type of transducers	Kulite CJQH-187 differential	
7.2.5	Principle and accuracy of calibration	Steady state sensitivity from applied reference and calibration procedures. Accuracy as stated by manufacturer.	

7.3 Model motion

7.3.1	Method of measuring motion reference co-ordinate	Quarter chord location specified by manufacture

7.3.2	Method of determining spatial mode of motion	Feedback from potentiometer geared to shaft.	
7.3.3	Accuracy of measured motion	0.1°	
7.4	Processing of unsteady measurements		
7.4.1	Method of acquiring and processing measurements	Full Chord	30 individual Kulite sensors mounted close to wing surface connected to parallel channel DEC MINC sample and hold modules. Signal conditioning modules on each individual channel. Gain and offset removal manual. Acquired data downloaded to PC.
		Short Chord	30 individual Kulite sensors mounted close to wing surface connected to parallel channel Bakker Electonics BE256 sample and hold modules. Signal conditioning modules on each individual channel. Gain and offset removal manual. Acquired data downloaded to PC.
7.4.2	Type of analysis	Phase averaging of cycles. Five cycles for ramp function tests, ten cycles for oscillatory function tests.	
7.4.3	Unsteady pressure quantities obtained and accuracies achieved	Basic unsteady pressure signal. Cycle repeatability variable depending on amplitude and reduced pitch rate.	
7.4.4	Method of integration to obtain forces	Trapezoidal rule	
7.5	Additional remarks	None	
7.6	References on techniques	None	

8 Data presentation

8.1	Test cases for which data could be made available	Full Chord	Four motion types: Static, Linear Ramp Up and Linear Ramp Down and Sinusoidal. Tests cover a range of reduced pitch rate, mean incidence and amplitude and reduced frequency. In total 479 test cases. All incidence variations about quarter chord.
		Short Chord	Four motion types: Static, Linear Ramp Up and Linear Ramp Down and Sinusoidal. Tests cover a range of reduced pitch rate, mean incidence and amplitude and reduced frequency. In addition ramp and oscillatory tests with leading edge sand strip. In total 240 test cases. All incidence variations about quarter chord.
8.2	Test cases for which data are included in this document	Full Chord	Four motion types: Static, Linear Ramp Up and Linear Ramp Down and Sinusoidal. 10 test cases as detailed in Table 7. A series of plots are also presented which are illustrative of the data supplied in electronic form. Figure 5 shows a sample upper surface pressure distributions, C_n, C_m and incidence histories for a ramp-up case.
		Short Chord	Four motion types: Static, Linear Ramp Up and Linear Ramp Down and Sinusoidal. 16 test cases as detailed in Table 8. A series of plots are also presented which are illustrative of the data supplied in electronic form. Figure 6 shows a sample upper surface pressure distributions, C_n, C_m and incidence history for a ramp-up case.
8.3	Steady pressures	For static case	
8.4	Quasi-steady or steady perturbation pressures	No	
8.5	Unsteady pressures	For all dynamic cases	
8.6	Steady forces or moments	For static case	
8.7	Quasi-steady or unsteady perturbation forces	No	

8.8	Unsteady forces and moments	For all dynamic cases
8.9	Other forms in which data could be made available	None
8.10	Reference giving other representations of data	N/A

9 Comments on data

9.1	Accuracy	
9.1.1	Mach number	±0.5%
9.1.2	Steady incidence	±0.1°
9.1.3	Reduced frequency	±0.5%
9.1.4	Steady pressure coefficients	±0.5%
9.1.5	Steady pressure derivatives	Not estimated
9.1.6	Unsteady pressure coefficients	±0.5%
9.2	Sensitivity to small changes of parameter	N/A
9.3	Non-linearities	N/A
9.4	Influence of tunnel total pressure	Not examined
9.5	Effects on data of uncertainty, or variation, in mode of model motion	N/A
9.6	Wall interference corrections	None
9.7	Other relevant tests on same model	None
9.8	Relevant tests on other models of nominally the same shapes	None
9.9	Any remarks relevant to comparison between experiment and theory	None
9.10	Additional remarks	The electronic data supplied with this report comprises two file types. The first type of file contains the transducer co-ordinates. There is only one file of this type, and it is identified by the name naca0015_xducers.dat. The second type contains the test data. The first 128 parameters are the run information data (described in table 5), and the remaining parameters are blocks each comprising the dynamic pressure, pressure coefficients (30 values) and angle of incidence. The number of blocks depends upon the motion type. A MATLAB program to read in the data is listed in appendix B. The pressure transducer locations correspond to the order contained in the file naca0015_xducers.dat, which is the same as in table 6.
9.11	References on discussion of data	2, 5, 4, 10

10 Personal contact for further information

Dr. R.B. Green
Department of Aerospace Engineering
University of Glasgow
Glasgow
G12 8QQ
U.K.
Tel. +44 141 330 4312
Email: richardg@aero.gla.ac.uk

22E(3) NACA 0015 DATA (THREE-DIMENSIONAL)

INTRODUCTION

The tests described herein were carried out in the University of Glasgow's 2.13m × 1.61m 'Handley Page' wind tunnel which is a low-speed closed-return type. The test model was a straight wing with a NACA 0015 cross-section and had simple solids of revolution at its tips. Because the lift behaviour at low aspect-ratios (AR) is quite different from that at high aspect ratios, particularly when AR is less than 2.0, the AR of this model was chosen as 3.0 to avoid strong three-dimensional effects at the mid-span in steady flow. When testing in a closed working section, it is very important to reduce the wall effects. In order to diminish the effect of upwash on the angle attack near the wing tips of the model and to reduce the blockage effect to minimum, the model size was carefully determined. The final overall dimensions were 126cm × 42cm which resulted in a variation of model blockage from a minimum of 2.6% to a maximum of 11.35% (not including the fairing of struts) and a model span to tunnel width ratio of 0.592. According to previous studies of the blockage effect for 2-D dynamic stall testing, these dimensions were considered acceptable. The model was supported on three struts, as shown in Fig. 7. These were, in turn, connected to the main support structure and actuation mechanism which was situated below the tunnel. Movement of the model was produced by displacement of the two rear struts and the model was pivoted about the quarter chord position on a tool steel shaft connected to the front support via two self-aligning bearings. The model was constructed with an aluminium framework of ribs and stringers and an outer epoxy glass fibre skin. Figure 8 illustrates this construction.

Altogether, 192 pressure transducers were placed within the model predominantly to the starboard side. There were six chordal distributions at various spanwise locations, each of which had 30 transducers. In the region of the tip, additional transducers were placed between the above mentioned sections to provide a better assessment of the tip vortex movement and structure. In order to check on the overall symmetry of the flow, two transducers were placed on the left side of the wing in corresponding positions to their counterparts on the starboard side. Additionally three accelerometers were embedded in the wing, two of which were at the rear tip locations and a final one mounted centrally. Details of the transducer distribution is given Table 12.

Four particular types of tests were considered in the study. These were static tests, ramp up tests, ramp down tests and sinusoidal tests. In all cases, the model was rotated about its quarter-chord axis to achieve the desired motion type. In the static tests, the straight wing was positioned at the incidence at which the first set of data was to be recorded. Usually, this was approximately -5^{o}. The model's angle of attack was then increased in steps of 1^{o} up to 42^{o} allowing an appropriate settling time at each angle. During a ramp test, the straight wing was rotated over a preset arc at a constant pitch-rate. For the lower pitch rates, excellent ramp functions were obtained but, at the higher values, the starting and stopping sequences induced non-linearities. The ramp motion was repeated several times at each pitch rate and data from 4 cycles of motion were recorded. These were then averaged to produce the results presented here. In the sinusoidal tests, the model was pitched about a mean angle in such a manner that its angle of attack varied sinusoidally with time. An AMSTRAD function generator controlled the mean angle, amplitude and frequency and 8 cycles of motion were recorded. Once again, these were averaged to provide the results presented in this report.

FORMULARY

1 General Description of model

1.1	Designation	Model 16
1.2	Type	Full Wing
1.3	Derivation	Rectangular Wing
1.4	Additional remarks	None
1.5	References	11

2 Model Geometry

2.1	Planform	Rectangular Wing (see Fig. 8)
2.2	Aspect ratio	3.0
2.3	Leading edge sweep	None
2.4	Trailing edge sweep	None
2.5	Taper ratio	No Taper
2.6	Twist	No Twist
2.7	Wing centreline chord	0.42m
2.8	Semi-span of model	0.63m
2.9	Area of planform	$0.516m^2$ gross wing area
2.10	Location of reference sections and definition of profiles	Mid-span, NACA 0015 profile

2.11	Lofting procedure between reference sections	Constant section
2.12	Form of wing-body junction	None
2.13	Form of wing tip	Solid of revolution
2.14	Control surface details	None
2.15	Additional remarks	None
2.16	References	11

3 Wind Tunnel

3.1	Designation	University of Glasgow 'Handley-Page'
3.2	Type of tunnel	Closed section, closed return, atmospheric
3.3	Test section dimensions	2.13m (width) x 1.61m (height) x (length)
3.4	Type of roof and floor	Closed – vented at downstream end of working section
3.5	Type of side walls	Closed - vented at downstream end of working section
3.6	Ventilation geometry	60 rectangular slots (0.028m x0.055m) on floor, roof and walls downstream of working section. 13 rectangular slots (0.028m x 0.105m) at same section on angled surfaces.
3.7	Thickness of side wall boundary layer	Unknown
3.8	Thickness of boundary layers at roof and floor	Unknown
3.9	Method of measuring velocity	Working section and settling chamber static pressure tappings related to wind tunnel speed calibration
3.10	Flow angularity	Not available
3.11	Uniformity of velocity over test section	Dynamic pressure constant to within 1% over a $1.5m^2$ reference plane normal to the flow axis in the working section
3.12	Sources and levels of noise or turbulence in empty tunnel	Not available
3.13	Tunnel resonances	Not available
3.14	Additional remarks	None
3.15	References on tunnel	8

4 Model motion

4.1	General description	Four motion types: Static, Linear Ramp Up, Linear Ramp Down and Sinusoidal. All incidence variations about quarter chord.
4.2	Natural frequencies and normal modes of model and support system	Not available. Accelerometers located as shown in Fig 8 and outputs contained in logged data (See table 14)

5 Test Conditions

5.1	Model planform area/tunnel area	0.173
5.2	Model span/tunnel height	0.782
5.3	Blockage	Function of angle of attack 2.6% - 11.35%
5.4	Position of model in tunnel	Horizontal on tunnel centre-line. Mounted through floor. (see Fig. 7)
5.5	Range of velocities	45 m/s to 55 m/s
5.6	Range of tunnel total pressure	Approximately 102.5kPa to 103kPa
5.7	Range of tunnel total temperature	Approximately 293K to 306K
5.8	Range of model steady or mean incidence	-5° to 42°
5.9	Definition of model incidence	Deviation of chord line from tunnel centreline
5.10	Position of transition, if free	Not available
5.11	Position and type of trip, if transition fixed	None
5.12	Flow instabilities during tests	Not available
5.13	Changes to mean shape of model due to steady aerodynamic load	Not available

5.14	Additional remarks	None
5.15	References describing tests	11

6 Measurements and Observations

6.1	Steady pressures for the mean conditions	Yes
6.2	Steady pressures for small changes from the mean conditions	No
6.3	Quasi-steady pressures	No
6.4	Unsteady pressures	Yes
6.5	Steady section forces for the mean conditions by integration of pressures	Yes
6.6	Steady section forces for small changes from the mean conditions by integration	No
6.7	Quasi-steady section forces by integration	No
6.8	Unsteady section forces by integration	Yes
6.9	Measurement of actual motion at points of model	No
6.10	Observation or measurement of boundary layer properties	No
6.11	Visualisation of surface flow	No
6.12	Visualisation of shock wave movements	No
6.13	Additional remarks	None

7 Instrumentation

7.1 Steady pressure

7.1.1	Position of orifices spanwise and chordwise	See Table 12
7.1.2	Type of measuring system	192 individual Kulite sensors mounted close to wing surface connected to 200 parallel channel data acquisition system.

7.2 Unsteady pressure

7.2.1	Position of orifices spanwise and chordwise	See Table 12.
7.2.2	Diameter of orifices	1.0mm
7.2.3	Type of measuring system	192 Individual Kulite sensors mounted close to wing surface connected to 200 parallel channel data acquisition system.
7.2.4	Type of transducers	Kulite CJQH-187 differential
7.2.5	Principle and accuracy of calibration	Steady state sensitivity from applied reference and calibration procedures. Accuracy as stated by manufacturer.

7.3 Model motion

7.3.1	Method of measuring motion reference coordinate	Quarter chord location specified by manufacture
7.3.2	Method of determining spatial mode of motion	Feedback from optical shaft encoder.
7.3.3	Accuracy of measured motion	0.02°

7.4 Processing of unsteady measurements

7.4.1	Method of acquiring and processing measurements	192 Individual Kulite sensors mounted close to wing surface connected to 200 parallel channel Bakker Electronics BE256 sample and hold modules. Signal conditioning modules on each individual channel. Gain and offset removal automatic. Acquired data downloaded to PC.
7.4.2	Type of analysis	Phase averaging of cycles. Four cycles for ramp function tests, eight for sinusoidal tests.
7.4.3	Unsteady pressure quantities obtained and accuracies achieved	Basic unsteady pressure signal. Cycle repeatability variable depending on amplitude and reduced frequency.
7.4.4	Method of integration to obtain forces	Trapezoidal rule

7.5	Additional remarks	None
7.6	References on techniques	None

8 Data presentation

8.1	Test cases for which data could be made available	Four motion types: Static, Linear Ramp Up, Linear Ramp Down and Sinusoidal. Tests cover a range of incidence and reduced frequency/pitch rate. In total 100 test cases. All incidence variations about quarter chord.
8.2	Test cases for which data are included in this document	Four motion types: Static, Linear Ramp Up, Linear Ramp Down and Sinusoidal. 10 test cases as detailed in Tables 9, 10 and 11. A series of plots are also presented which are illustrative of the data supplied in electronic form. Figure 9 illustrates the integrated normal force coefficients at six span locations on the wing for test case 11441 (file: ntm11441.dat). In the figure, these are contrasted with the static test case 00011(file: ntm 00011.dat). Figure 10 presents the integrated pitching moment coefficients at the same span positions for the ramp-up case 20962 (file: ntm20962.dat). Again, a comparison is made with the static case. Figure 11 presents chordwise pressure distributions at three span locations and at four angles of incidence for the ramp-down case 30681 (file: ntm30681.dat). Finally, in Figs12, 13 and 14, the variation of upper surface chordal pressure distribution with changing incidence is presented at the 57.14%, 80% and 97.2% span positions for the ramp-up test case 21042 (file: cp21042.dat).
8.3	Steady pressures	For static case
8.4	Quasi-steady or steady perturbation pressures	No
8.5	Unsteady pressures	For all dynamic cases
8.6	Steady forces or moments	For static case
8.7	Quasi-steady or unsteady perturbation forces	No
8.8	Unsteady forces and moments	For all dynamic cases
8.9	Other forms in which data could be made available	None
8.10	Reference giving other representations of data	N/A

9 Comments on data

9.1	Accuracy	
	9.1.1 Mach number	±0.5%
	9.1.2 Steady incidence	±0.02°
	9.1.3 Reduced frequency	±0.5%
	9.1.4 Steady pressure coefficients	±0.5%
	9.1.5 Steady pressure derivatives	Not estimated
	9.1.6 Unsteady pressure coefficients	±0.5%
9.2	Sensitivity to small changes of parameter	N/A
9.3	Non-linearities	N/A
9.4	Influence of tunnel total pressure	Not examined
9.5	Effects on data of uncertainty, or variation, in mode of model motion	N/A
9.6	Wall interference corrections	None
9.7	Other relevant tests on same model	None
9.8	Relevant tests on other models of nominally the same shapes	None
9.9	Any remarks relevant to comparison between experiment and theory	None
9.10	Additional remarks	The electronic data supplied with this report comprise three file types. The first type of file contains the wing co-ordinates, in the

form of pressure transducer locations, as specified in Table 12. There is only one file of this type and it is identified by the name 3dmcrd16.dat. The file contains four numbers in the first line followed by the three columns of 192 co-ordinates presented in Table 12. The numbers in the first line represent, in order, number of transducers in one chordal array, number of upper surface transducers in one chordal array, number of chordal arrays, total number of transducers. It should be noted that there are six chordal arrays of thirty transducers giving a total of 180 transducers. The remaining transducers are distributed in the region of the tip vortex, to provide definition of the pressure response there, and on the other side of the wing to indicate flow symmetry.

The second type of file is designated cp'case number'.dat (e.g. cp00011.dat) and there is one of these files for each test case. This type of file consists mainly of the measured pressure coefficient data but also contains all other information relating to the test case. The first twenty-two values in each file are known as the Run Information Block (RIB) and correspond to the RIB locations 0-21 detailed in Table 13. It should be noted that RIB location 19 is set to zero because the dynamic pressure information is contained elsewhere in the file. Following the RIB, the next value in the file is the number, N, of data samples. For all cases, other than the static case, N is set to 201. For the static case, 00011, the value is 48. After this value, the file contains N rows of 200 data values. The content of each row is illustrated in Table 14.

The FORTRAN write statement used to produce the cp*****.dat files is illustrated below.

```
Note:   DIMENSION RINFO(22), CPMS1(200,201)
        WRITE(9,*)RINFO
        WRITE(9,*)NUMBER
        DO 222 I=1,NUMBER
        WRITE(9,*)(CPMS1(J,I),J=1,200)
222     CONTINUE
```

The final file type, designated ntm'case number'.dat (e.g. ntm00011.dat), contains integrated values of Cn, Ct and Cm (quarter chord) for each of the chordal arrays and for the entire wing. There is one of these files for each test case. The first value in the file corresponds to N in the corresponding cp file and this indicates the number of rows to follow. The contents of each subsequent row are described in Table 15 and the FORTRAN write statement used to produce the file is given below.

```
      WRITE(8,*)NUMBER
      DO 15 KK =1,NUMBER
      WRITE(8,*)ANG(KK),(CN(I),I=1,NSECT),(CT(I),I=1,
     * NSECT), (CM(I),I=1,NSECT),CN3D,CT3D,CM3D
15    CONTINUE
```

9.11 References on discussion of data — 12, 13

10 Personal contact for further information

Dr. F. Coton
Department of Aerospace Engineering
University of Glasgow
Glasgow
G12 8QQ
U.K.
Tel. +44 141 330 4305
Email: f.coton@aero.gla.ac.uk

ACKNOWLEDGEMENTS

All the work carried out herein was funded by the EPSRC, DERA, GKN Westland Helicopters Ltd, ETSU and Glasgow University. The authors are most grateful for their significant and continued support.

22E(4) REFERENCES

1. Young, W.H. Jnr (1981) "Fluid Mechanics mechanism in the stall process for helicopters" NASA TM 81956
2. Green, R.B, Galbraith, R.A.McD., & Niven, A.J. (1992) "Measurements of the dynamic stall vortex convection speed" Aero. Journal, vol. 96, pp 319-325.
3. Green, R.B. & Galbraith, R.A.McD. (1996) "Dynamic stall vortex convection: thoughts on compressibility effects" Aer. Journal, vol. 100, pp 367-372
4. Green, R.B. & Galbraith, R.A.McD. (1994) "An investigation of dynamic stall through the application of leading edge roughness" Aero. Journal, vol. 98, pp 17-19
5. Green, R.B. & Galbraith, R.A.McD. (1995) "Dynamic recovery to fully attached aerofoil flow from deep stall" American Institute of Aeronautics and Astronautics Journal, vol. 33, No. 8, pp1433 - 1440
6. Green, R.B., Galbraith, R.A.McD., Gilmour, R. & Leitch, E. "Ramp test data from the Sikorsky SSC-A09 aerofoil model" University of Glasgow, Department of Aerospace Engineering, G.U. Aero. Report 9613, (1996)
7. Lorber, P.F. & Carta, F.O. "Unsteady stall penetration experiments at high Reynolds number" United Technologies Research Center, East Hartford, CT 06108, U.S.A. UTRC Report R87-956939-3, AFOSR TR-87-1202 (1987)
8. Hounsfield, F.R.C., "The Handley Page Wind Tunnel", Aircraft Engineering, July 1940, pp 202-205
9. Galbraith, R.A.McD., Gracey, M.W. & Leitch, E. "Summary of pressure data for thirteen aerofoils on the University of Glasgow's aerofoil database" University of Glasgow, Department of Aerospace Engineering, G.U. Aero. Report 9221, (1992)
10. Green, R.B., Galbraith, R.A.McD "A demonstration of the effect of the testing environment on unsteady aerodynamics experiments" Aeronautical Journal, vol. 98, pp 83-90, (1994)
11. Jiang, D., Coton, F.N., Galbraith, R.A.McD., Gilmour, R., 'Collected data for tests on a NACA 0015 section rectangular wing (aspect ratio 3). Vols 1 -8 , Glasgow University Aero. Repts. 9515 - 9522
12. Coton, F.N., Galbraith, R.A.McD., Jiang, D., Gilmour, R., 'An experimental study of the effect of pitch rate on the dynamic stall of a finite wing', Conference on Unsteady Aerodynamics, The Royal Aeronautical Society, London, April 1996
13. Galbraith, R.A.McD., Coton, F.N., Jiang, D., Gilmour, R., Preliminary results from a three-dimensional dynamic stall experiment of a finite wing. 21st European Rotorcraft Forum, Russia, September 1995

APPENDIX A

Parameter 14, which describes the number of samples, is important. This is essentially the number of time points at which data were sampled.

The data from the test case are then given. The test data for each sample are contained in a block consisting of the instantaneous dynamic pressure reading in Nm^{-2} followed by the pressure coefficient at each transducer location (from location 1 to location 35 in sequence) and finally the instantaneous incidence in degrees.

A program to read in the test data should therefore read in the run information block first. The rest of the information may then be read in according to the number of samples indicated by parameter number 14.

A sample MATLAB code fragment to read in the data is given below:

```
fid=fopen(fname);                //open data file
rib=fread(fid,'%g',128); //read in run information block (rib)...
//data is in '%g' general format, and there are 128 samples
nsamps=rib(14);          //extract number of data samples from rib
model_number=rib(30); //extract model number from rib
//model 15 (sikorsky) has 35 transducers, other models have 30...
if (model_number == 15) then
        nxducers=35;
else
        nxducers=30;
end
//model 12 (high AR NACA 0015 has chord length of 0.275m, others have //chord=0.55m
if (model_number==12) then
        chord=0.275;
else
        chord=0.55;
end
//read in data
for i = 1, nsamps;               //loop for number of samples...
        //construct non-dimensional time array....
        //ndt=tU/c, c=model chord
        ndt(i)=(i-1)*rib(23)/(chord*rib(18));
        q(i)=fread(fid,'%g',1);           //read in dynamic pressure
        cp((1,nxducers),i)=fread(fid,'%g',nxducers);        //read in pressure data
        alpha(i)=fread(fid,'%g',1);       //read in incidence
end
```

APPENDIX B

Parameter 14, which describes the number of samples, is important. This is essentially the number of time points at which data were sampled.

The data from the test case are then given. The test data for each sample are contained in a block consisting of the instantaneous dynamic pressure reading in Nm^{-2} followed by the pressure coefficient at each transducer location (from location 1 to location 30 in sequence) and finally the instantaneous incidence in degrees.

A program to read in the test data should therefore read in the run information block first. The rest of the information may then be read in according to the number of samples indicated by parameter number 14.

A sample MATLAB code fragment to read in the data is given below:

```
fid=fopen(fname);                  //open data file

rib=fread(fid,'%g',128); //read in run information block (rib)...

//data is in '%g' general format, and there are 128 samples
nsamps=rib(14);            //extract number of data samples from rib
model_number=rib(30); //extract model number from rib
//model 15 (sikorsky) has 35 transducers, other models have 30...
if (model_number == 15) then
        nxducers=35;
else
        nxducers=30;
end
//model 12 (high AR NACA 0015 has chord length of 0.275m, others have //chord=0.55m
if (model_number==12) then
        chord=0.275;
else
        chord=0.55;
end
//read in data
for i = 1, nsamps;                 //loop for number of samples...
        //construct non-dimensional time array....
        //ndt=tU/c, c=model chord
        ndt(i)=(i-1)*rib(23)/(chord*rib(18));
        q(i)=fread(fid,'%g',1);              //read in dynamic pressure
        cp((1,nxducers),i)=fread(fid,'%g',nxducers);        //read in pressure data
        alpha(i)=fread(fid,'%g',1);          //read in incidence
end
```

Table 1 Presented Test Cases

Section No	Model	No of Test Cases	Motion Type
1	Sikorsky SSC-AO9 (2D)	3	RU
2	NACA 0015, low aspect ratio (2D)	10	ST, RU, RD, S
	NACA 0015 high aspect ratio (2D)	16	ST, RU, RD, S
3	NACA 0015 (3D)	10	ST, RU, RD, S

Table 2 SSC-A09 Profiles Co-ordinates

x (% chord)	y upper (% chord)	y lower (% chord)
0.0	0	0
0.0199	0.2	-0.1454
0.0798	0.3946	-0.2869
0.1994	0.6482	-0.4573
0.2991	0.8029	-0.5446
0.4487	0.9868	-0.6445
0.6979	1.2392	-0.7703
0.9970	1.4921	-0.8877
1.5952	1.9076	-1.0704
2.1934	2.2500	-1.2175
2.7916	2.5445	-1.3447
3.3898	2.8039	-1.4588
3.9881	3.0369	-1.5631
4.5863	3.2494	-1.6594
5.1845	3.4449	-1.7487
5.7827	3.6249	-1.8314
6.7797	3.8903	-1.9568
7.7767	4.1143	-2.0691
8.7737	4.3016	-2.1706
9.7707	4.4583	-2.2638
11.2663	4.6504	-2.3910
12.7618	4.8054	-2.5064
14.2573	4.9345	-2.6124
15.7529	5.0444	-2.7104
17.2485	5.1385	-2.8013
18.7440	5.2184	-2.8853
20.2395	5.2860	-2.9628
21.7350	5.3427	-3.0339
23.2305	5.3911	-3.0988
24.7261	5.4322	-3.1579
27.7171	5.4958	-3.2594
30.7082	5.5369	-3.3402
33.6992	5.5564	-3.4007
37.6873	5.5494	-3.4506
41.6754	5.5039	-3.4637
43.6694	5.4663	-3.4558
45.6635	5.4182	-3.4376
47.6575	5.3595	-3.4087
49.6515	5.2899	-3.3683
51.6456	5.2093	-3.3165
53.6935	5.1176	-3.2532
55.6336	5.0149	-3.1790
57.6277	4.9009	-3.0949
59.6217	4.7755	-3.0018
61.6157	4.6381	-2.9002
63.6097	4.4875	-2.7904
65.6039	4.3220	-2.6720
67.5979	4.1391	-2.5448
69.5919	3.9368	-2.4088
71.5860	3.7140	-2.2642
73.5800	3.4719	-2.1121
75.5740	3.2138	-1.9540
77.5680	2.9445	-1.7918
79.5621	2.6681	-1.6272
81.5561	2.3871	-1.4617
83.5501	2.1012	-1.2957
85.5442	1.8089	-1.1289
87.5382	1.5093	-0.9598
89.5323	1.2051	-0.7863
91.5264	0.9046	-0.6081
93.5204	0.6229	-0.4290
95.5144	0.3849	-0.2610
97.5084	0.2288	-0.1325
98.5055	0.1987	-0.0992
99.5025	0.2135	-0.0863
100.0000	0.2408	-0.0803

Table 3 Pressure Transducer Location

There were 35 pressure transducers installed in the model, with 19 on the upper surface. Particular attention was given to a concentration around the leading edge. The transducer coordinates are as follows:

Transducer Number	x (% chord)	y (% chord)
1	98.4	0.19983
2	94.4	0.51594
3	87.5	1.51509
4	78.4	2.82985
5	67.8	4.11950
6	56.7	4.95535
7	46.13	5.40543
8	36.98	5.55342
9	30.10	5.53031
10	26.00	5.46219
11	19.10	5.23536
12	14.82	4.97868
13	10.20	4.51809
14	5.94	3.66964
15	2.50	2.40601
16	1.00	1.49445
17	0.50	1.04388
18	0.25	0.73581
19	0.12	0.46899
20	0.50	-0.67456
21	2.50	-1.28479
22	5.94	-1.85216
23	10.2	-2.30172
24	14.82	-2.65090
25	19.10	-2.90438
26	26.00	-3.20377
27	30.10	-3.32542
28	36.98	-3.44437
29	46.13	-3.43183
30	56.70	-3.13519
31	67.80	-2.53142
32	78.40	-1.72332
33	87.50	-0.96308
34	94.40	-0.35254
35	98.40	-0.10222

Table 4 Test Cases

Run Number	Reduced Pitch Rate	Incidence Range
15020021	0.04091	-1^o to 40^o
15020121	0.02035	-1^o to 40^o
15020201	0.00214	-1^o to 40^o

The nominal Mach and Reynolds numbers are 0.12 and 1.5×10^6.

Table 5 Run Information Data

Parameter	Description		
1	run number		
2	test day		
3	test month		
4	test year		
5	temperature (^{o}C)		
6	pressure (mm Hg)		
7	test type:	0=static, 1=oscillatory, 2=ramp-up, 3=ramp-down	
8	ramp test:	requested pitch rate ($^{o}s^{-1}$)	(This is the desired pitch rate. However, actual pitch rate can be obtained from the logged data.)
	oscillatory test:	mean incidence (deg)	
9	ramp test:	ramp arc (deg)	
	oscillatory test:	amplitude (deg)	
10	ramp test:	linear pitch rate ($^{o}s^{-1}$)	
	oscillatory test:	oscillation frequency (Hz)	
11	sweeps per cycle	(This is the number of times all transducers are logged per cycle)	
12	values per cycle		
13	number of cycles		
14	total no. of samples		
15	no. of blocks on disc		
16	clock (irate)		
17	clock (iprset)		
18	sampling rate (Hz)		
19	dynamic pressure (Nm^{-2})		
20	Reynolds number		
21	Mach number		
22	ramp test:linear reduced pitch rate		
	oscillatory test:	reduced frequency	
23	free stream velocity (ms^{-1})		
24	blocks per cycle		
25	no. data points in unfilled silo		
26	data type: 1=averaged data, 2=unaveraged data		
27	no. processed blocks		
28	data type: 1=volts, 2=pressure coefficients		
29	dynamic pressure (Nm^{-2})		
30	model number		
31	coordinate file number		
32	ramp start angle (deg)		
33 to 64:	transducer calibration values		
65 to 96:	channel gain values		
97 to 128:	channel offset values		

Table 6 Pressure Transducer Location

The pressure transducers were positioned symmetrically on the upper and lower surfaces of the model. The transducer number and the chordwise position are listed below:

Transducer Number		Chordwise Station (%chord)
Upper Surface	Lower Surface	
1	30	98.0
2	29	95.0
3	28	83.0
4	27	70.0
5	26	59.0
6	25	50.0
7	24	37.0
8	23	26.0
9	22	17.0
10	21	10.0
11	20	5.0
12	19	2.5
13	18	1.0
14	17	0.25
15	16	0.025

Table 7 Test Cases for Low Aspect Ratio Model

Static test:

Run Number	Incidence Range
05000051	-1° to 30° to -1°

Ramp tests:

Run Number	Reduced Pitch Rate	Incidence Range
05025451	0.0116	-1° to 40°
05025491	0.0187	-1° to 40°
05025551	0.0274	-1° to 40°
05036461	-0.0119	40° to -1°
05036511	-0.0193	40° to -1°
05036581	-0.0277	40° to -1°

Oscillatory tests:

Run Number	Reduced Frequency	Mean Incidence	Amplitude
05014181	0.153	6°	10°
05014201	0.153	15°	10°
05014211	0.153	20°	10°

Table 8 Test Cases for High Aspect Ratio Model

Static test:

Run number	Incidence range
12001251	-1° to 30° to -1°

Ramp tests (clean leading edge):

Run Number	Reduced Pitch Rate	Incidence Range
12021761	0.0110	-1° to 40°
12021411	0.0188	-1° to 40°
12021441	0.0242	-1° to 40°
12031861	-0.0126	40° to -10°
12031901	-0.0192	40° to -10°
12031951	-0.0281	40° to -10°

Ramp tests (with leading edge sand strip):

Run Number	Reduced Pitch Rate	Incidence Range
12822001	0.0108	-1° to 40°
12822321	0.0190	-1° to 40°
12822101	0.0271	-1° to 40°
12832361	-0.0128	40° to -10°
12832141	-0.0197	40° to -10°
12832191	-0.0284	40° to -10°

Oscillatory tests:

Run Number	Reduced Frequency	Mean Incidence	Amplitude
12010712	0.167	6°	10°
12010732	0.167	15°	10°
12010772	0.167	20°	10°

Table 9 Static Test Case

Run No.	Incidence Range (°)	Reynolds No. x 10^{-6}	Sampling Frequency (Hz)
00011	-5~42	1.52	2000

Table 10 Ramp Test Cases

Run No.	Ramp Arc (°)	Pitch Rate (° s^{-1})	Reduced Pitch Rate	Reynolds No. × 10^{-6}	Sampling Frequency (Hz)
20912	- 5 ~ 39	160.24	0.0110	1.48	13790
20962	- 5 ~ 39	280.96	0.0190	1.48	22220
21042	- 5 ~ 39	404.44	0.0270	1.50	33330
30621	39 ~ -5	-161.12	- 0.012	1.37	15380
30681	39 ~ -5	-263.56	- 0.019	1.39	24390
30751	39 ~ -5	-380.37	- 0.028	1.38	33330

Table 11 Sinusoidal Test Cases

Run No.	Mean Angle (°)	Amplitude (°)	Reduced Frequency	Reynolds No. × 10^{-6}	Sampling Frequency (Hz)
11261	5	10	0.17	1.50	20830
11381	15	10	0.16	1.49	20830
11441	20	10	0.17	1.47	20830

Table 12 Pressure Transducer Location

No.	x/c	y/c	z/s
1	0.98	0.00504	0.57143
2	0.95	0.01008	0.57143
3	0.83	0.02856	0.57143
4	0.7	0.0458	0.57143
5	0.59	0.05806	0.57143
6	0.5	0.06618	0.57143
7	0.37	0.07376	0.57143
8	0.26	0.07454	0.57143
9	0.17	0.06911	0.57143
10	0.1	0.05854	0.57143
11	0.05	0.04443	0.57143
12	0.025	0.03268	0.57143
13	0.01	0.02129	0.57143
14	0.0025	0.01089	0.57143
15	0.00025	0.0035	0.57143
16	0.00025	-0.0035	0.57143
17	0.0025	-0.01089	0.57143
18	0.01	-0.02129	0.57143
19	0.025	-0.03268	0.57143
20	0.05	-0.04443	0.57143
21	0.1	-0.05854	0.57143
22	0.185	-0.07053	0.57143
23	0.26	-0.07454	0.57143
24	0.355	-0.07422	0.57143
25	0.49	-0.06695	0.57143
26	0.59	-0.05806	0.57143
27	0.7	-0.0458	0.57143
28	0.835	-0.02784	0.57143
29	0.95	-0.01008	0.57143
30	0.98	-0.00504	0.57143
31	0.98	0.00504	0.68175
32	0.95	0.01008	0.68175
33	0.83	0.02856	0.68175
34	0.7	0.0458	0.68175
35	0.59	0.05806	0.68175
36	0.5	0.06618	0.68175
37	0.37	0.07376	0.68175
38	0.26	0.07454	0.68175
39	0.17	0.06911	0.68175
40	0.1	0.05854	0.68175
41	0.05	0.04443	0.68175
42	0.025	0.03268	0.68175
43	0.01	0.02129	0.68175
44	0.0025	0.01089	0.68175
45	0.00025	0.0035	0.68175
46	0.00025	-0.0035	0.68175
47	0.0025	-0.01089	0.68175
48	0.01	-0.02129	0.68175
49	0.025	-0.03268	0.68175
50	0.05	-0.04443	0.68175
51	0.1	-0.05854	0.68175
52	0.185	-0.07053	0.68175
53	0.26	-0.07454	0.68175
54	0.355	-0.07422	0.68175
55	0.49	-0.06695	0.68175
56	0.59	-0.05806	0.68175
57	0.7	-0.0458	0.68175
58	0.835	-0.02784	0.68175

No.	x/c	y/c	z/s
59	0.95	-0.01008	0.68175
60	0.98	-0.00504	0.68175
61	0.98	0.00504	0.8
62	0.95	0.01008	0.8
63	0.83	0.02856	0.8
64	0.7	0.0458	0.8
65	0.59	0.05806	0.8
66	0.5	0.06618	0.8
67	0.37	0.07376	0.8
68	0.26	0.07454	0.8
69	0.17	0.06911	0.8
70	0.1	0.05854	0.8
71	0.05	0.04443	0.8
72	0.025	0.03268	0.8
73	0.01	0.02129	0.8
74	0.0025	0.01089	0.8
75	0.00025	0.0035	0.8
76	0.00025	-0.0035	0.8
77	0.0025	-0.01089	0.8
78	0.01	-0.02129	0.8
79	0.025	-0.03268	0.8
80	0.05	-0.04443	0.8
81	0.1	-0.05854	0.8
82	0.185	-0.07053	0.8
83	0.26	-0.07454	0.8
84	0.355	-0.07422	0.8
85	0.49	-0.06695	0.8
86	0.59	-0.05806	0.8
87	0.7	-0.0458	0.8
88	0.835	-0.02784	0.8
89	0.95	-0.01008	0.8
90	0.98	-0.00504	0.8
91	0.98	0.00504	0.9
92	0.95	0.01008	0.9
93	0.83	0.02856	0.9
94	0.7	0.0458	0.9
95	0.59	0.05806	0.9
96	0.5	0.06618	0.9
97	0.37	0.07376	0.9
98	0.26	0.07454	0.9
99	0.17	0.06911	0.9
100	0.1	0.05854	0.9
101	0.05	0.04443	0.9
102	0.025	0.03268	0.9
103	0.01	0.02129	0.9
104	0.0025	0.01089	0.9
105	0.00025	0.0035	0.9
106	0.00025	-0.0035	0.9
107	0.0025	-0.01089	0.9
108	0.01	-0.02129	0.9
109	0.025	-0.03268	0.9
110	0.05	-0.04443	0.9
111	0.1	-0.05854	0.9
112	0.185	-0.07053	0.9
113	0.26	-0.07454	0.9
114	0.355	-0.07422	0.9
115	0.49	-0.06695	0.9
116	0.59	-0.05806	0.9

Table 12 Pressure Transducer Location

No.	x/c	y/c	z/s
117	0.7	-0.0458	0.9
118	0.835	-0.02784	0.9
119	0.95	-0.01008	0.9
120	0.98	-0.00504	0.9
121	0.98	0.00504	0.94603
122	0.95	0.01008	0.94603
123	0.83	0.02856	0.94603
124	0.7	0.0458	0.94603
125	0.59	0.05806	0.94603
126	0.5	0.06618	0.94603
127	0.37	0.07376	0.94603
128	0.26	0.07454	0.94603
129	0.17	0.06911	0.94603
130	0.1	0.05854	0.94603
131	0.05	0.04443	0.94603
132	0.025	0.03268	0.94603
133	0.01	0.02129	0.94603
134	0.0025	0.01089	0.94603
135	0.00025	0.0035	0.94603
136	0.00025	-0.0035	0.94603
137	0.0025	-0.01089	0.94603
138	0.01	-0.02129	0.94603
139	0.025	-0.03268	0.94603
140	0.05	-0.04443	0.94603
141	0.1	-0.05854	0.94603
142	0.185	-0.07053	0.94603
143	0.26	-0.07454	0.94603
144	0.355	-0.07422	0.94603
145	0.49	-0.06695	0.94603
146	0.59	-0.05806	0.94603
147	0.7	-0.0458	0.94603
148	0.835	-0.02784	0.94603
149	0.95	-0.01008	0.94603
150	0.98	-0.00504	0.94603
151	0.98	0.00504	0.9719
152	0.95	0.01008	0.9719
153	0.83	0.02856	0.9719
154	0.7	0.0458	0.9719
155	0.59	0.05806	0.9719
156	0.5	0.06618	0.9719
157	0.37	0.07376	0.9719
158	0.26	0.07454	0.9719
159	0.17	0.06911	0.9719
160	0.1	0.05854	0.9719
161	0.05	0.04443	0.9719
162	0.025	0.03268	0.9719
163	0.01	0.02129	0.9719
164	0.0025	0.01089	0.9719
165	0.00025	0.0035	0.9719
166	0.00025	-0.0035	0.9719
167	0.0025	-0.01089	0.9719
168	0.01	-0.02129	0.9719
169	0.025	-0.03268	0.9719
170	0.05	-0.04443	0.9719
171	0.1	-0.05854	0.9719
172	0.185	-0.07053	0.9719
173	0.26	-0.07454	0.9719
174	0.355	-0.07422	0.9719

No.	x/c	y/c	z/s
175	0.49	-0.06695	0.9719
176	0.59	-0.05806	0.9719
177	0.7	-0.0458	0.9719
178	0.835	-0.02784	0.9719
179	0.95	-0.01008	0.9719
180	0.98	-0.00504	0.9719
181	0.17	0.06911	0.92302
182	0.37	0.07376	0.92302
183	0.59	0.05806	0.92302
184	0.83	0.02856	0.92302
185	0.37	0.07376	0.86667
186	0.59	0.05806	0.86667
187	0.83	0.02856	0.86667
188	0.59	0.05806	0.83333
189	0.83	0.02856	0.83333
190	0.83	0.02856	0.77619
191	0.5	0.06618	0.35
192	0.1	0.05854	0.1

Table 13 Layout of Run Information Block

RIB LOCATION	STATIC/ UNSTEADY STATIC	SINUSOIDAL	RAMP UP/ RAMP DOWN
0	Run Number		
1	Date of Test: Day		
2	Date of Test: Month		
3	Date of Test: Year		
4	Temperature (^{o} Celsius)		
5	Barometric Pressure (mm Hg)		
6	Motion Type (0)	Motion Type (1)	Motion Type (2/3)
7	Starting Incidence(^{o})	Mean Incidence (^{o})	Starting Incidence(^{o})
8	Arc (^{o})	Amplitude (^{o})	Ramp Arc (^{o})
9	Empty	Oscillation Frequency (Hz)	Linear Pitch-Rate (^{o} s^{-1})
10	Number of Samples in One Block		
11	Number of Total Samples		
12	Number of Data Blocks (Cycles)		
13	Sampling Frequency (Hz)		
14	Dynamic Pressure (Psi)		
15	Reynolds Number		
16	Mach Number		
17	Empty	Reduced Frequency	Reduced Pitch-Rate
18	Incoming Velocity (ms^{-1})		
19	Dynamic Pressure (Nm^{-2})		
20	Model Number		
21	File ID		

Table 14 Data presented in each row of file cp***.dat**

Channels 1-192	Pressure coefficients corresponding to the transducer locations in Table 5.4
Channel 193	Temperature Channel (Uncalibrated since RIB contains temperature)
Channels 194-196	Accelerometer channels (units of g) (Channel 195 Faulty)
Channels 197-198	Empty
Channel 199	Incidence (deg)
Channel 200	Dynamic Pressure (psi)

Table 15 Data presented in each row of file ntm***.dat**

Position in row	Description of Parameter
1	Angle of Incidence (deg)
2 – 7	Integrated Cn for span stations 57.14%, 68.1%, 80%,90%,94.6%,97.2%
8 - 13	Integrated Ct for span stations 57.14%, 68.1%, 80%,90%,94.6%,97.2%
14–19	Integrated Cm for span stations 57.14%, 68.1%, 80%,90%,94.6%,97.2%
20	Integrated Cn for full wing
21	Integrated Ct for full wing
22	Integrated Cm for full wing

ST – Static RU – Linear Ramp-up RD – Linear Ramp-Down S – Sinusoidal

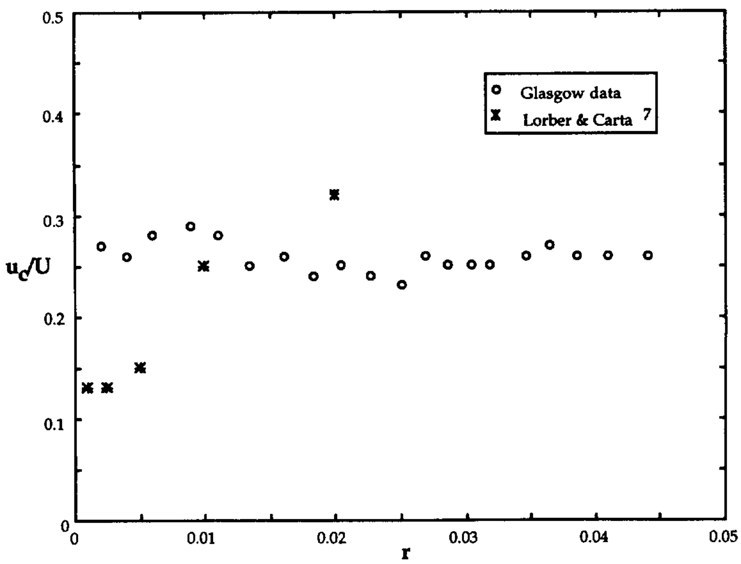

Fig 1 Variation of dynamic stall vortex convection with reduced pitch rate for the SSC-A09 tested at Glasgow. Lorber & Carta [7] results are also shown.

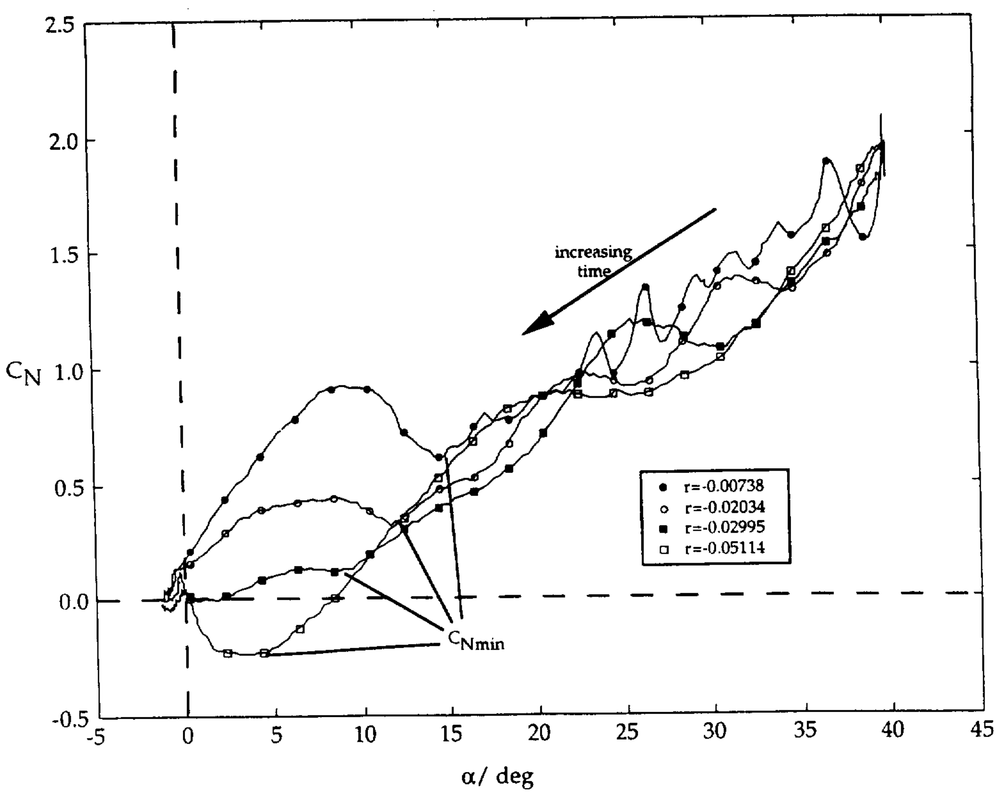

Fig 2 Normal force coefficient as a function of incidence during ramp-down tests of the Sikorsky SSC-A09 aerofoil. Normal Mach and Reynolds numbers are 0.12 and 1.5 million. The effect of reduced pitch rate is shown. Note the indicence at which C_{Nmin} occurs for each test case.

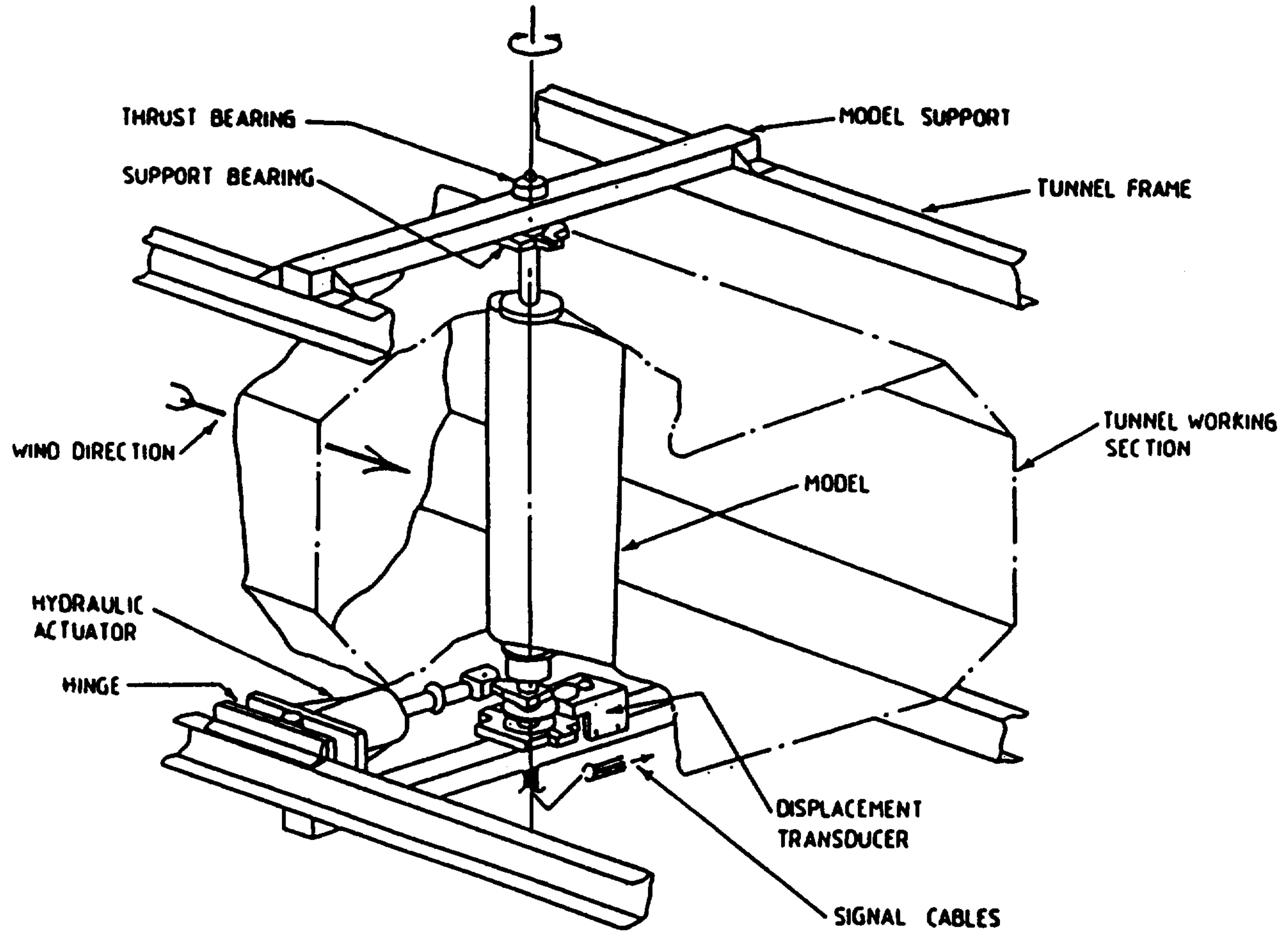

Fig 3 Installation of the Sikorsky SSC-A09 model in the Handley-Page wind tunnel

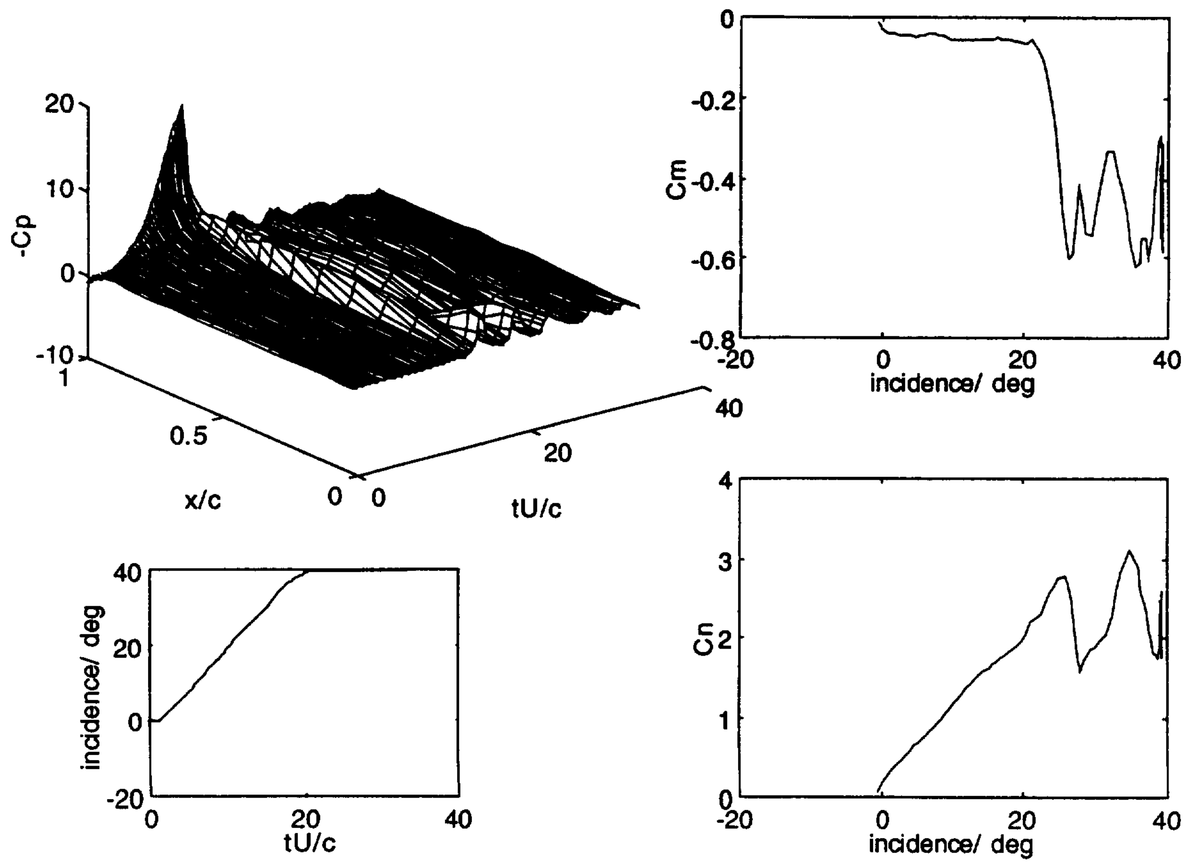

Fig 4 Pressure, normal force and pitching moment behaviour during ramp-up motion for the Sikorsky SSC-A09. r=0.02

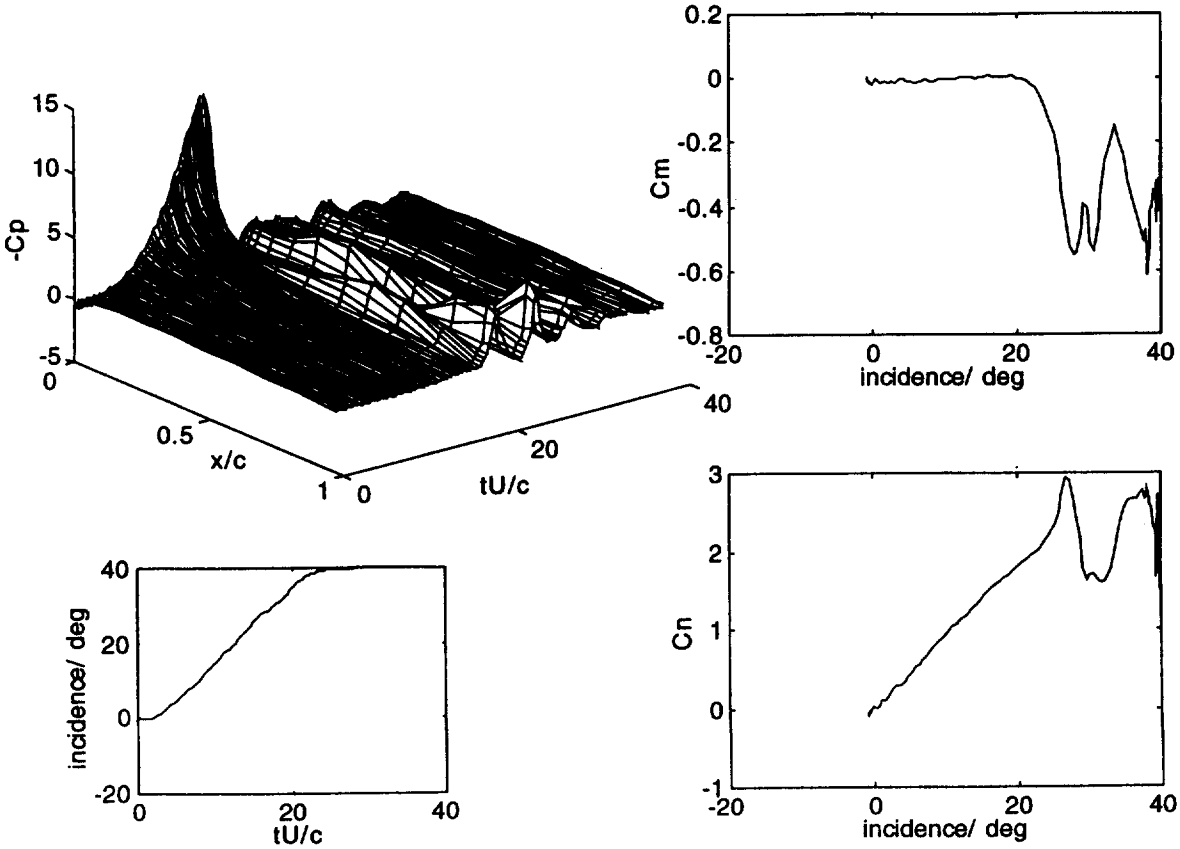

Fig 5 Pressure, normal force and pitching moment behaviour during ramp-up motion for the full chord NACA 0015. r=0.0187

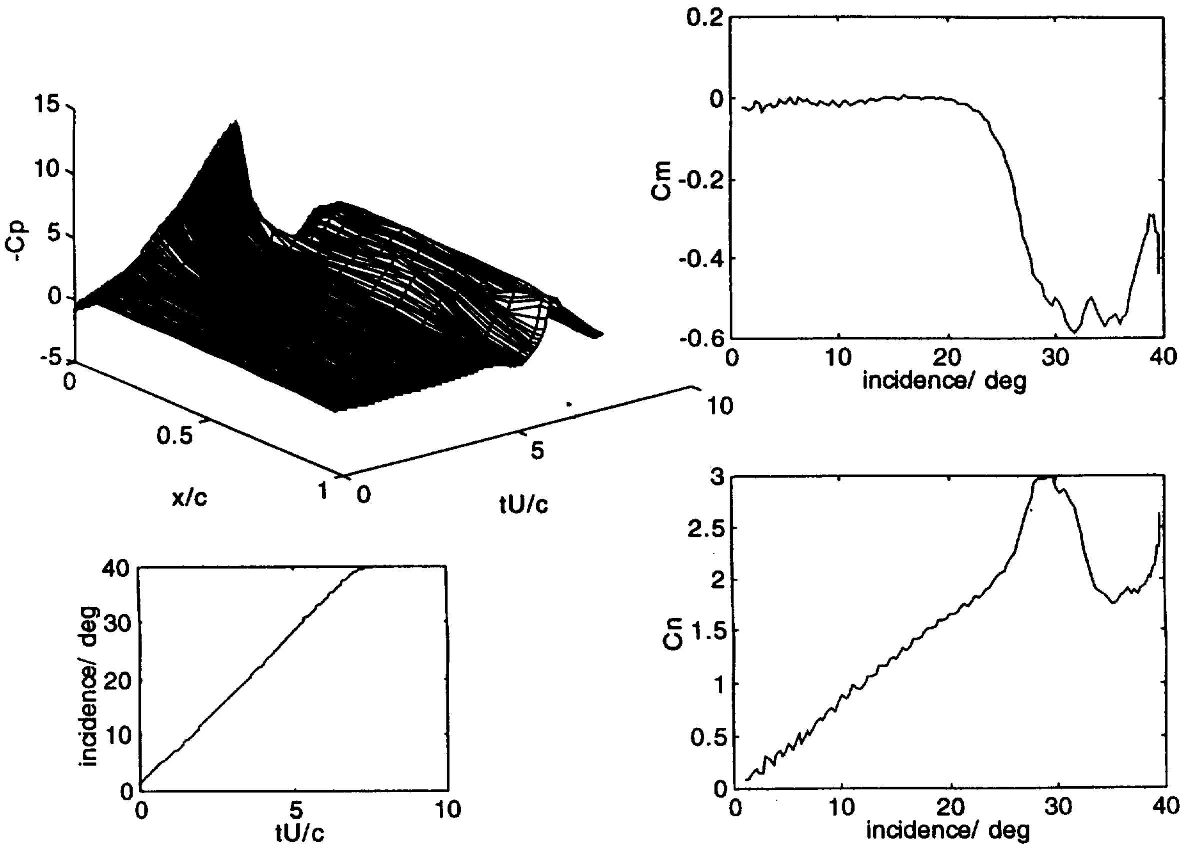

Fig 6 **Pressure, normal force and pitching moment behaviour during ramp-up motion for the high aspect ratio NACA 0015. r = 0.0188.**

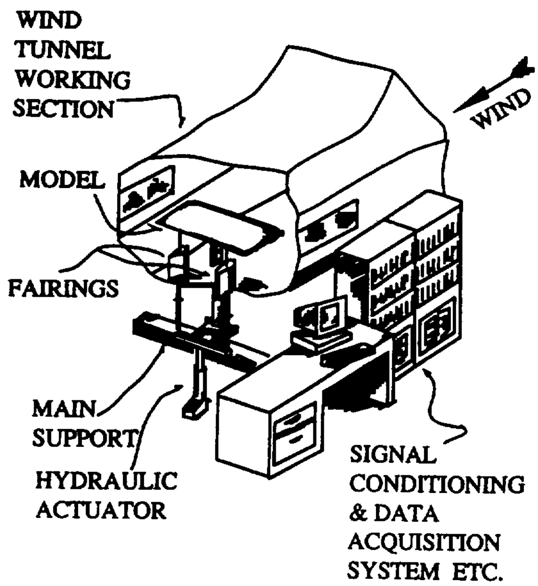

Fig 7 Test set-up for 3-D dynamic stall tests

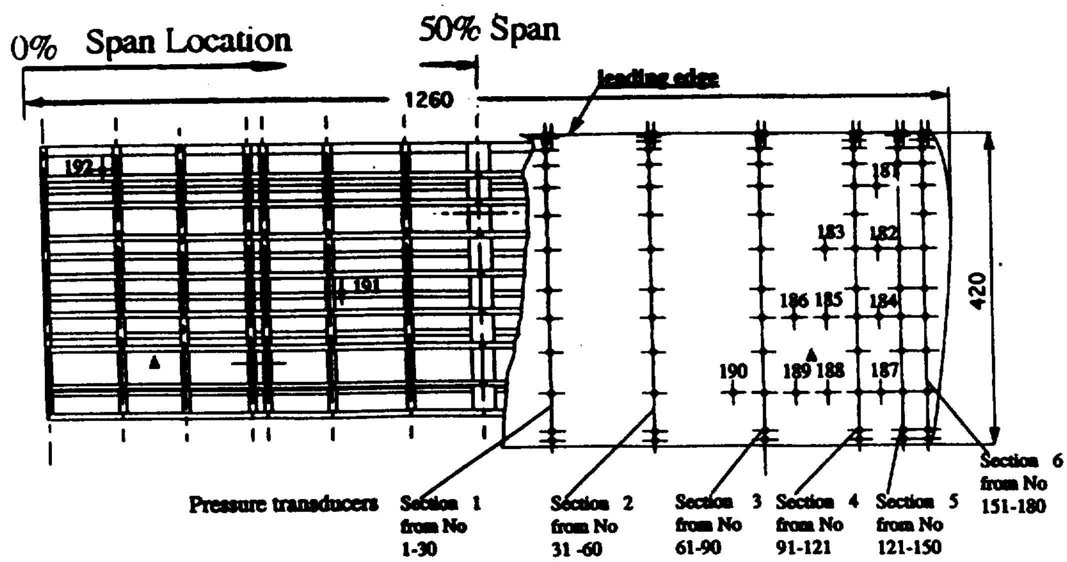

Fig 8 Rectangular wing model showing transducer placement
(▲ accelerometers)

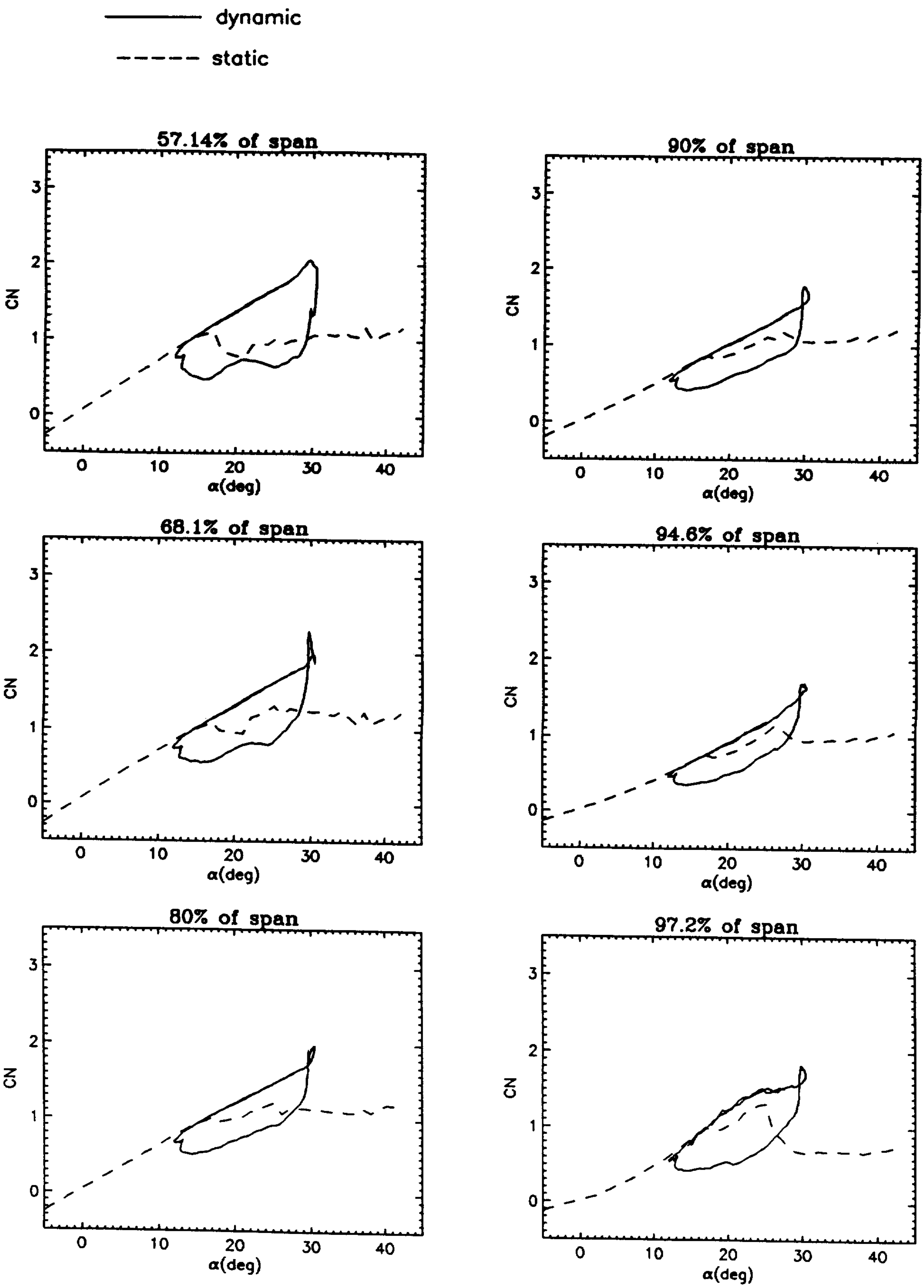

Fig 9 C_n against incidence at six span locations (case 11441)

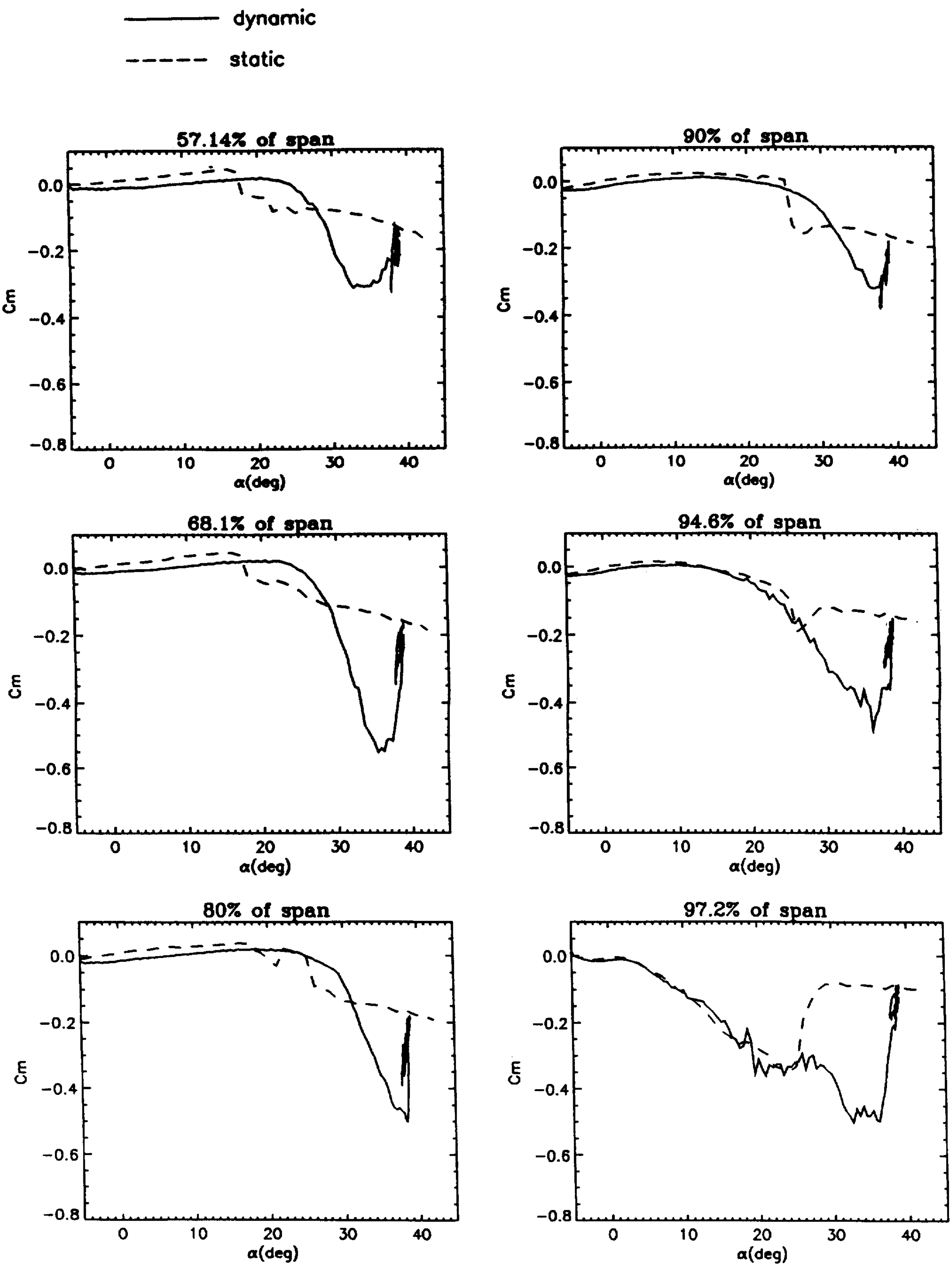

Fig 10 C_m against incidence at six span locations (case 20962)

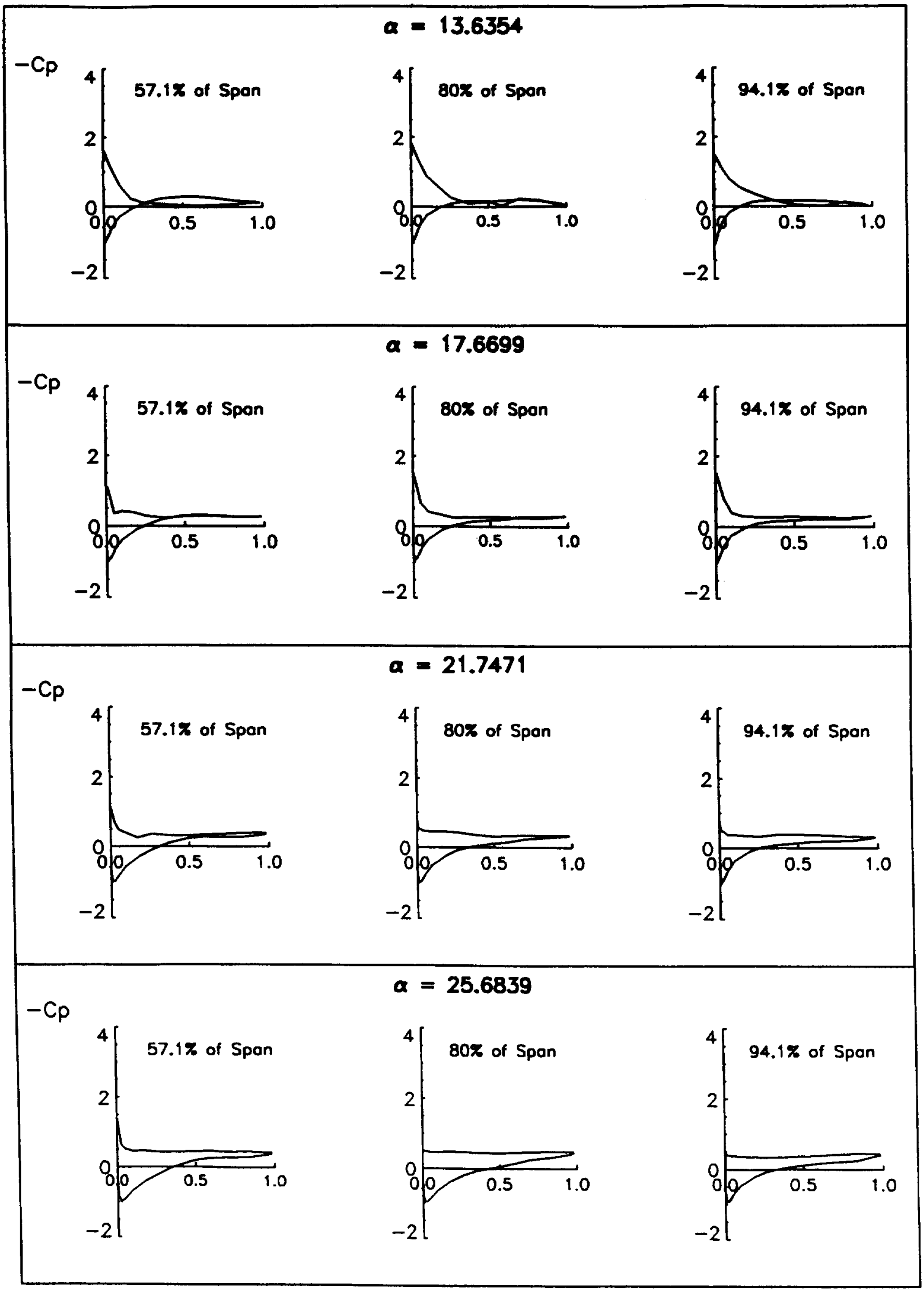

Fig 11 Chordwise pressure distributions (case 30681)

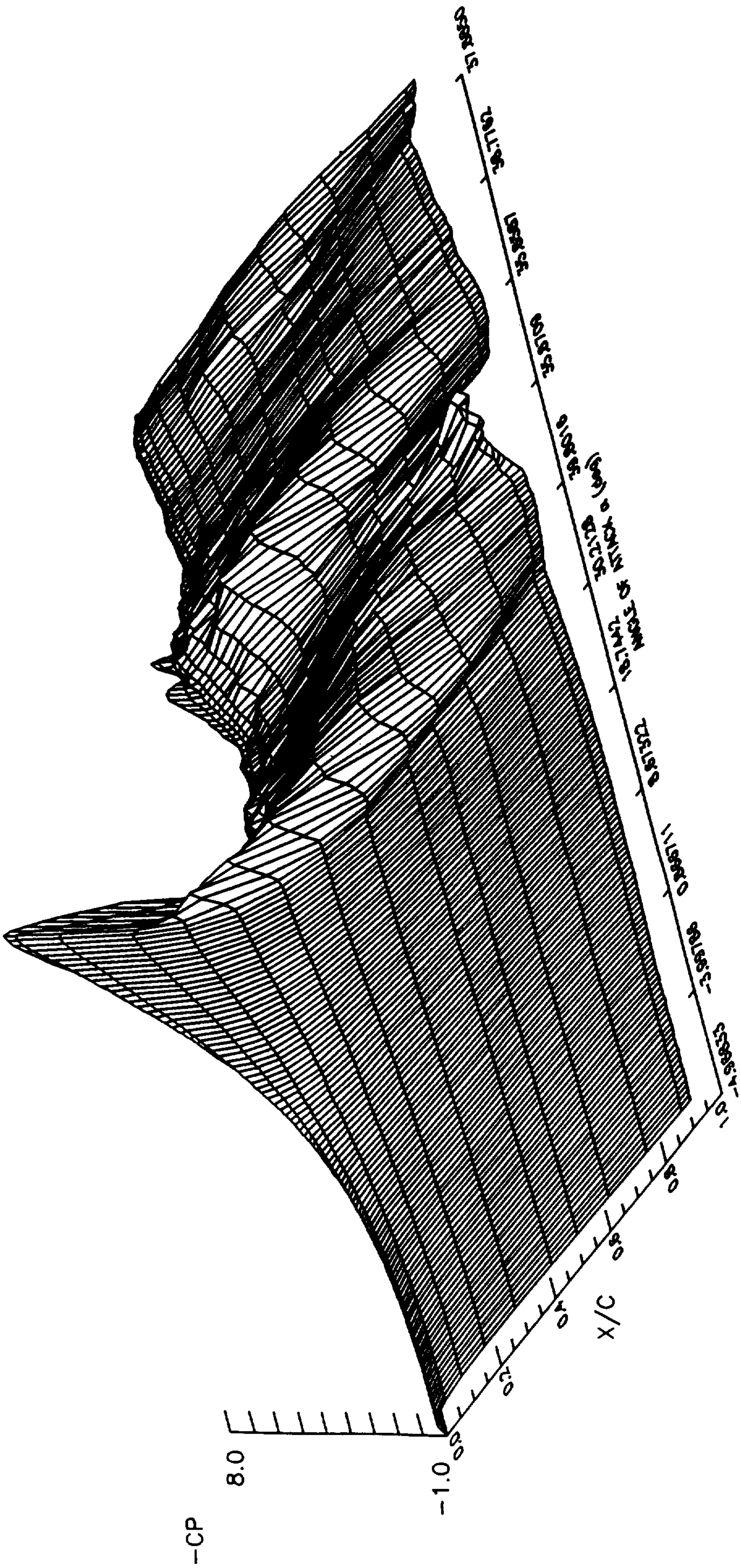

Fig 12 Upper surface variation of chordwise pressure at 57.14% span (case 21042)

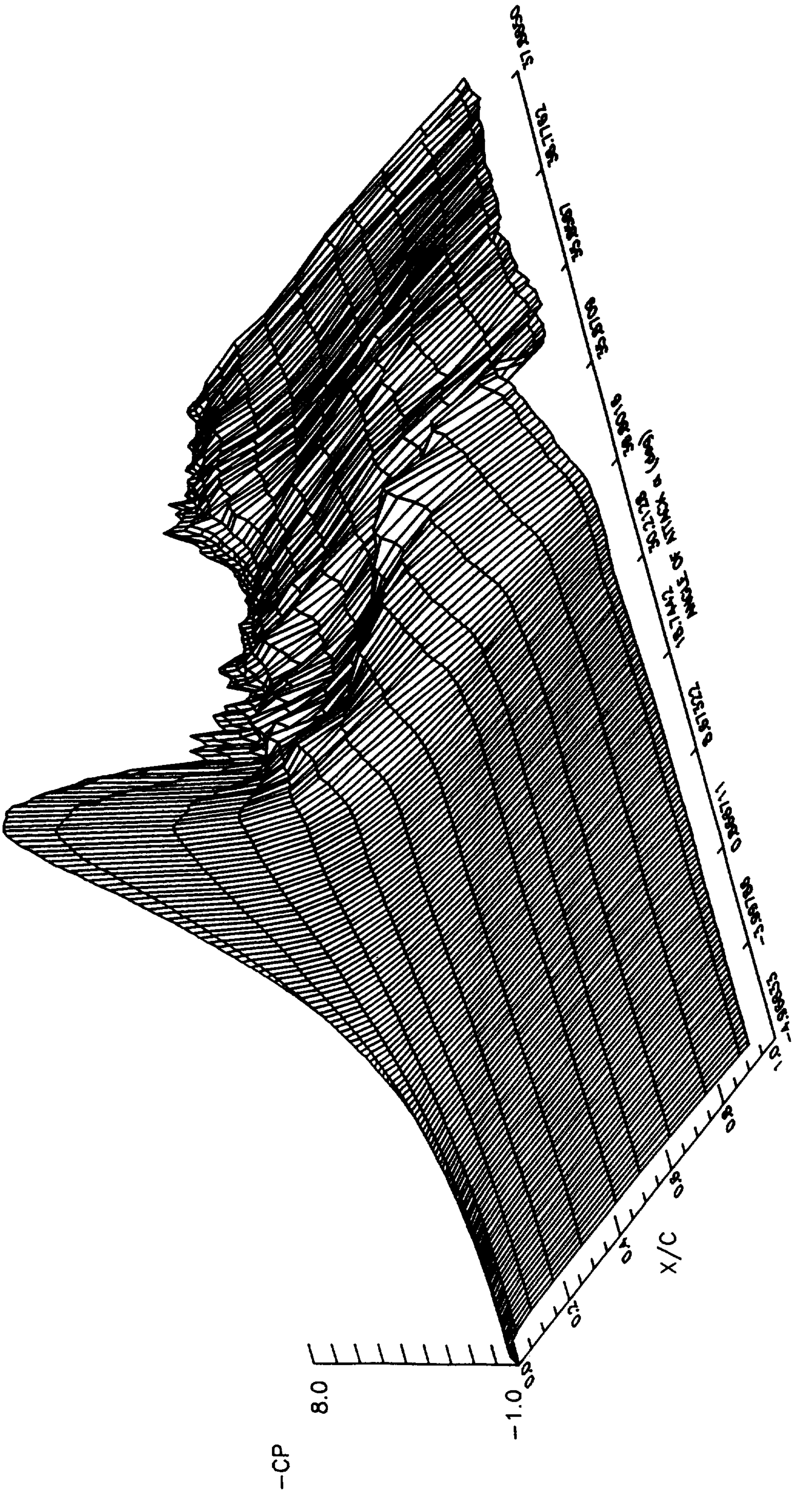

Fig 13 Upper surface variation of chordwise pressure at 80% span (case 21042)

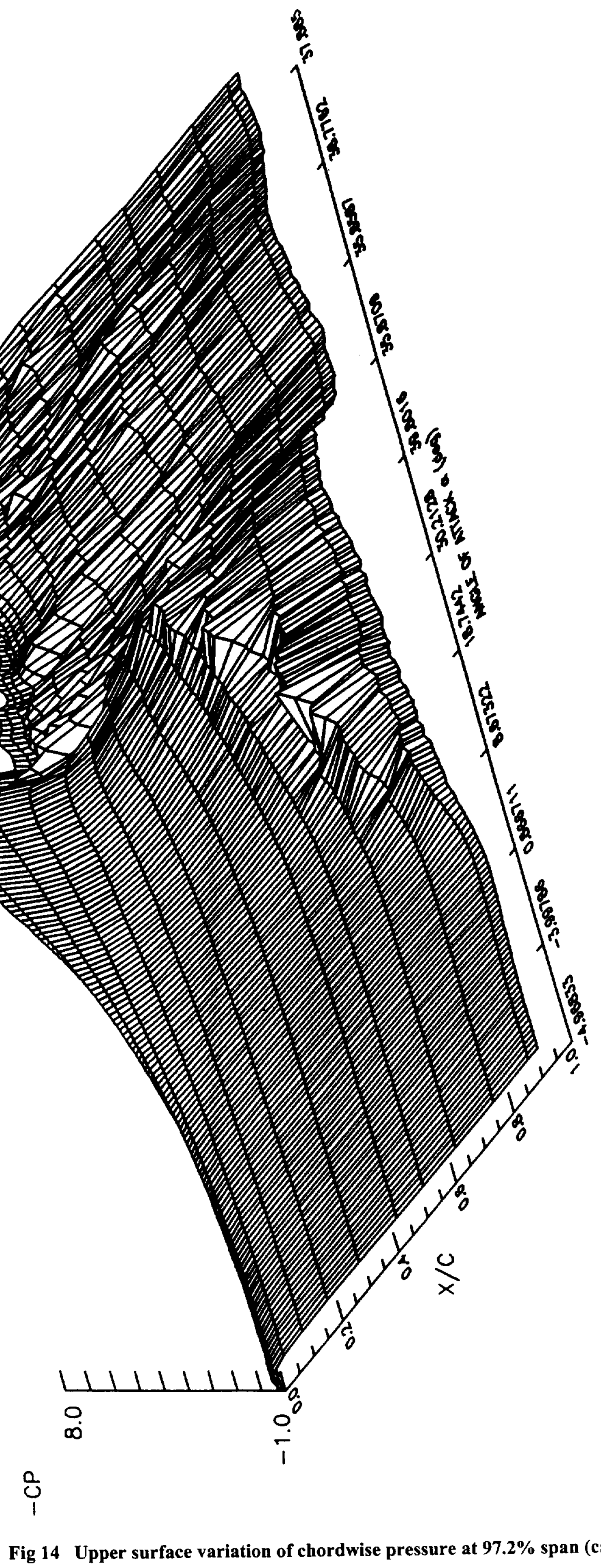

Fig 14 Upper surface variation of chordwise pressure at 97.2% span (case 21042)

23. GENERIC WING, PYLON, AND MOVING FINNED STORE

John H. Fox, PhD
Sverdrup Technology, Inc./AEDC Group
Arnold Engineering Development Center (AEDC)
Arnold AFB, TN 37389-6001, USA

INTRODUCTION

Background

A Computational Fluid Dynamics (CFD) Program of the U. S. Air Force Research Laboratory (AFRL), formerly (AFATL), funded and supported this wind tunnel test. The data support the ongoing validation efforts for CFD codes. A review at AEDC, completed June 12, 1996, determined the data were unrestricted.

The test met the objectives of providing pressure data from geometrically simple wing and store shapes under mutual interference conditions with the store both at its carriage position and at selected points along a realistic store separation trajectory. AFRL chose AEDC's 4-Foot Transonic Aerodynamic Wind Tunnel (4T) for the test. AEDC's Captive Trajectory Support (CTS) system, a moving store-support mechanism, simulated the motion of the store. Dr. L. Liejewski, AFRL, Eglin AFB, FL 32542, designed and executed the test. E. Rolland Heim, Sverdrup Technology, MS 6001, Arnold AFB TN, 37388, an AEDC project engineer, conducted the experiment.

A generic finned-store shape and a clipped delta wing with a 45-degree leading edge sweep were the primary test articles. Store pressure data were acquired with a pressure model with orifices at radial locations in 36, 10-degree intervals around the store and at 8 span-wise locations from 10 to 80 percent span on both surfaces of each fin. Wing upper and lower surface orifices at locations inboard, outboard, and in the plane of the pylon also provided pressure data. The pylon had orifices as well. These data requirements in combination with store size constraints required testing at locations on both the left and right sides of the wing model. However, the resultant data are from a virtual, single store released from the pilot's right wing. Thus, the virtual configuration is asymmetric. A force model of the store provided force and moment data at carriage for comparison with the pressure model. The rig was positioned such that the store model at carriage nearly touched the left or right pylons, as required to initiate a trajectory, Fig 1, Appendix. The store fins were positioned at carriage in a rotated cruciform style and were numbered such that Fin 1 is positioned 45 degrees ccw of the pylon looking upstream. Fin 2 is 90 degrees ccw of Fin 1, and so on.

Summary of Data

The data set contains wind tunnel data for a generic wing/pylon/finned store configuration. Although the store and wing represent no full-scale system, AEDC uses full-scale and subscale terminology and references. In this case, the subscale test article is 5% of an imaginary full-scale wing/pylon/store. All files contain ASCII numeric data that were written out with the FORTRAN FORMAT statement (6(1PE12.5)). The dimensions in the data are full-scale feet. They are left unconverted, for it is a simple matter to perform the conversion to International Units while reading the files. The set contains the following files:

M12BODY.DAT	Store body surface pressures, Mach=1.2, Alpha=0.0
M12FIN.DAT	Store fin surface pressures, Mach=1.2, Alpha=0.0
M12WING.DAT	Wing/pylon surface pressures, Mach=1.2, Alpha=0.0
M12TRAJ.DAT	Entire trajectory data set (store position, forces, moments, velocities, and accelerations), Mach=1.2, Alpha=0.0
M12CAPLOAD.DAT	Store captive loads data, Mach=1.2, Alpha=0.0
M12FREESTR.DAT	Store free-stream data, Mach=1.2, Alpha=0.0
M95BODY.DAT	Store body surface pressures, Mach=0.95, Alpha=0.0
M95FIN.DAT	Store fin surface pressures, Mach=0.95, Alpha=0.0
M95WING.DAT	Wing/pylon surface pressures, Mach=0.95, Alpha=0.0
M95TRAJ.DAT	Entire trajectory data set (store position, forces, moments, velocities, and accelerations), Mach=0.95, Alpha=0.0
M95CAPLOAD.DAT	Store captive loads data, Mach=0.95, Alpha=0.0
M95FREESTR.DAT	Store free-stream data, Mach=0.95, Alpha=0.0

Surface pressure files (General)

The surface pressure files (M12BODY.DAT, M12FIN.DAT, M12WING.DAT, M95BODY.DAT, M95FIN.DAT, and M95WING.DAT) each contain five sets of pressure data corresponding to the store in its carriage position and at four selected points along a trajectory. An ID number indexes the information within the file. The correlation of ID number with store position is as follows:

ID	Mach	Store Position
1	.95	Carriage
7	.95	First point selected from the trajectory
8	.95	Second point selected from the trajectory
9	.95	Third point selected from the trajectory
10	.95	Fourth point selected from the trajectory
4	1.20	Carriage
11	1.20	First point selected from the trajectory
12	1.20	Second point selected from the trajectory
13	1.20	Third point selected from the trajectory
14	1.20	Fourth point selected from the trajectory

For each ID number, a Point Number, as described below, sequences the pressure data.

Wing/Pylon Pressure Data (M12WING.DAT and M95WING.DAT)

Obtaining store body pressure data in 10-degree increments around the body, and store fin pressure data on both sides of each fin, required a total of eight wind tunnel runs for a given ID number. Four runs were required with the store mounted on the left side of the wing and four more were needed with the store mounted on the right side of the wing. To position the body and fin taps at the appropriate locations, the store had to be rotated 90 degrees after each run. Data for the wing/pylon are ordered from Point Number 1 through Point Number 4 for each ID number, corresponding to the four runs made with the store mounted on the instrumented, or right, side of the wing.

Store Body Pressure Data (M12BODY.DAT and M95BODY.DAT)

For the store body, pressure data were collected in 10-degree increments around the store, beginning at an angular location of 5 degrees and ending at 355 degrees. The pylon is the roll reference or zero degree line. Therefore, for each ID number the data are ordered from Point Number 1 (corresponding to measurements at 5 degrees) through Point Number 36 (corresponding to measurements at 355 degrees). The angular position of any store body pressure measurement is denoted by the parameter PHIR.

Store Fin Pressure Data (M12FIN.DAT and M95FIN.DAT)

Similarly, the fin surface pressures are ordered from Point Number 1 through Point Number 32 corresponding to the eight pressure measurements taken at the four fin orientations for a given ID number. Point Numbers 1 through 8, 9 through 16, 17 through 24, and 25 through 32 correspond to fin orientations of 45, 135, 225, and 315 degrees, respectively. Fin orientation is specified in the parameter PHIF.

Trajectory data (M12TRAJ.DAT and M95TRAJ.DAT)

The files M12TRAJ.DAT and M95TRAJ.DAT contain the trajectory data for wind tunnel runs at Mach=1.2 and Mach=0.95, respectively. There is only one set of trajectory data at each Mach number so there is no ID number indexing, as was the case with the pressure data. These files contain the store position and its forces, moments, velocities, and accelerations as a function of time throughout the trajectory. Data were recorded every .01 seconds. In these files, the Point Number corresponds to a specific time during the trajectory. The store pressure information in files M12BODY.DAT and M95BODY.DAT corresponds directly to five selected times during the trajectory. For the trajectory at Mach 0.95, the store pressures in M95WING.DAT, M95FIN.DAT, and M95BODY.DAT correspond to trajectory points denoted by Point Numbers 4, 16, 23, 31, and 38 in the M95TRAJ.DAT file. Similarly, for the trajectory at Mach 1.2, the store pressures in M12WING.DAT, M12FIN.DAT, and M12BODY.DAT correspond to trajectory points denoted by Point Numbers 4, 16, 22, 33, and 43 in the M12TRAJ.DAT file.

At-carriage store force and moment data (M12CAPLOAD.DAT and M95CAPLOAD.DAT)

The files M12CAPLOAD.DAT and M95CAPLOAD.DAT contain the force and moment data from the force-model store in the carriage position at Mach numbers of 1.2 and 0.95, respectively. These data are included to provide a point of comparison with the forces and moments measured on the pressure-instrumented store in the carriage position during the trajectory run.

Free-stream store force and moment data (M12FREESTR.DAT and M95FREESTR.DAT)

The files M12FREESTR.DAT and M95FREESTR.DAT contain the force and moment data for the force-model store in the free stream. These data were collected to obtain the lateral and longitudinal characteristics of the store.

LIST OF SYMBOLS AND DEFINITIONS

ALPHA	Angle of attack of the wing model, deg
ALPHAS, ALPSRB	Angles of attack of the force and pressure models of the store, respectively, deg
BETA	Wing model angle of sideslip, deg
BETAS, BETSRB	Angles of sideslip of the force and pressure models of the store, respectively, deg
BL	Model Butt Line (spanwise location of an orifice row relative to the wing model centerline), cm.
C	Local chord length, cm.
CAT	Axial-force coefficient of the force model of the store, (axial force)/(Q)(S)
CBAR	Mean aerodynamic chord length, 21.59 cm.
CLL	Rolling-moment coefficient of the force model of the store (rolling moment)/(Q)(S)(d)
CLM	Pitching-moment coefficient of the force model of the store calculated about the store center of gravity located 7.09 cm aft of the store nose (pitching moment)/(Q)(S)(d)
CLMRB	Pitching-moment coefficient of the pressure model of the store calculated about a point 45.03 cms aft of the model nose
CLM1	Pitching-moment coefficient of the wing calculated about a point 18.75 cms aft of the leading edge of the wing centerline, (pitching moment)/(Q)(S1)(CBAR)
CLN	Yawing moment coefficient of the force model of the store calculated about the store center of gravity located 7.09 cms aft of the model nose, (yawing moment)/(Q)(S)(d)
CLNRB	Yawing moment coefficient of the pressure model of the store calculated about a point 47.22 cms aft of the model nose
CN	Normal-force coefficient of the force model of the store, (normal force)/(Q)(S)
CN1	Normal-force coefficient of the wing model, (normal force)/(Q)(S1)
CP	Pressure coefficient column heading on tabulated data
CPWXXX	Pressure coefficients (PWXXX – P)/Q
CY	Side-force coefficient of the force model of the store, (side force)/(Q)(S)
d	Diameter of the store centerbody, 2.54 cm.
DPHI, DPSI, DTHA	Identical to PSI, PHI, and THETA for present purposes.
ID	Sequential indexing number for referencing data
L	Store model length, 15.09 cm; chord length.
LP	Pylon model length, 11.43 cm.
M	Free-stream Mach number
P	Free-stream static pressure, psf; lower case addenda signify character: inf = free stream, etc.
P, Q, R	Angular velocities of store: roll, pitch, and yaw, radians/sec; see PHI, THETA, and. PSI
PHI	Roll angle of the store relative to the non-rolling body axes, deg. Zero at pylon position, deg.
PSI	Yaw angle of the store: Angle between the projection of the store longitudinal axis in the flight axis horizontal plane and the X-axis, deg.
PHIF	Radial location of a row of fin pressures, positive clockwise looking upstream, deg
PHIR	Radial location of a row of (store) pressures, positive clockwise looking upstream, deg
PWXXX	Model (wall) pressure at orifice xxx, psfa
PT	Free-stream total pressure, psfa
Q	Free-stream dynamic pressure, psf

Re	Free-stream unit Reynolds Number, $(10)^{-6}$/ft
RUN	Sequential indexing number for referencing on-line data
S	Store model cross-sectional area, 5.07 cm^2
S1	Wing model planform area, 1425.5 cm^2
T	Free-stream static temperature, deg R; Time, sec
TT	Total temperature, deg F
THETA	Pitch angle of the store: Angle between the store longitudinal axis and its projection in the flight axis horizontal plane, deg.
VX, VY, VZ	Velocity components of store cg in flight-axis system, as determined from the local wind velocity, ft/sec
X, Y, Z	Flight-axis system. Origin fixed in space. X is positive in direction of flight path, Y is positive to pilot's right, Z is positive downward. Not used in data presentation.
X	Model pressure orifice location measured from the store nose or the leading edge of the wing, pylon, or fin at the local chord, cm.
X/LW, X/LB, X/LF	X position non-dimensionalized by local chord length of Wing, Store Body, Store Fin, respectively.
XXX	Orifice Identification Number.
XP, YP, ZP	Pylon-axis system, full-scale ft. Origin is coincident with cg of store in carriage position. Used for description of store cg motion.
XP	Distance of the store cg from the pylon-axis system origin in the direction of the flight path.
YP	Distance of the store cg from the pylon-axis system origin parallel to X-Y plane, positive to pilot's right.
ZP	Distance of the store cg from the pylon-axis system origin perpendicular to X-Y plane, positive downward.

FORMULARY

1 General Description of model

1.1 Designation	Clipped generic delta wing with pylon and generic finned store positioned initially in its carriage position at pylon.
1.2 Type	Full 3-D model of wing, pylon, and finned store.
1.3 Derivation	Generic. For time-accurate CFD code validation purposes.
1.4 Relative motion control	Store is attached to sting that is moved with computer-controlled motors. An online 6-DOF computer program solves equations of motion which gives next position of store using sting-balance readings of forces and moments as initial conditions for each step. Steps are usually 0.0002 seconds in pseudo time (falling-store real time).
1.5 References	2, Section 4 in Appendix

2 Model Geometry

2.1 Wing planform	45-degree-leading-edge, clipped delta wing
2.2 Wing aspect ratio	1.73 (38.1 cm mid-wing chord; 66.04 cm full span)
2.3 Leading-edge sweep	45 degrees
2.4 Trailing-edge sweep	0.0 degrees
2.5 Taper ratio	0.133
2.6 Twist	None
2.7 Root chord	38.1 cm
2.8 Span of model	66.4 cm
2.9 Area of planform	1425.8 cm^2
2.10 Location of reference of profiles and definition of profiles	NACA 64A010 airfoil section over entire span
2.11 Lofting procedure between reference sections	Straight line
2.12 Form of wing-body, or wing-root junction	NACA 64A010 airfoil section; note references below
2.13 Form of wing tip	NACA 64A010 airfoil section
2.14 Wing centerbody	Ogive-cylinder: Tangent at trailing edge of wing. Nose 16.51 cm from wing leading edge. Maximum diameter of centerbody is 4.23 cm
2.15 Pylon elevation view	Rectangular blade: 11.43 cm long by 3.05 cm vertical distance from wing reference plane (plane through LE and TE of wing).
2.16 Pylon profile shape	Leading and trailing edge shapes are identical. Ogive tangent 1.47 cm back from leading and trailing edges. Blade is 0.75 cm thick.
2.17 Pylon locations	Centerline is 16.51 cm from wing centerline, both left and right. Pylon LE positioned 1.95 cm back from wing LE.
2.18 Store diameter	2.54 cm
2.19 Store fin leading-edge sweep	60 degrees
2.20 Store fin length	0.89 cm measured from maximum diameter of store
2.21 Store fin root chord	4.23 cm centerline projection
2.22 Form of store fins at body junctions	NACA 0008 airfoil section
2.23 Control surface details	None
2.24 Store model shape	Store shape is tangent-ogive forebody and afterbody. Tangent at point 4.23 cm back from radii intersections on centerline. Store model is 2.54 cm in diameter. Afterbody is truncated 2.39 cm aft of aft tangent point.
2.25 Full-scale store and ejector characteristics	
2.25.1 Weight	8896.4 N
2.25.2 Center of Gravity	XCG = 1.416 m aft of store nose
2.25.3 Roll Inertia	IXX = 27.12 kg-m^2
2.25.4 Pitch Inertia	IYY = 488.1 kg-m^2
2.25.5 Yaw Inertia	IZZ = 488.1 kg-m^2
2.25.6 Roll damping Coefficient	CLP = -4.0/rad
2.25.7 Pitch damping Coefficient	CMQ = -40.0/rad
2.25.8 Yaw Damping Coefficient	CNR = -40.0/rad
2.25.9 Forward Ejector Location	1.24 m aft of store nose
2.25.10 Forward Ejector Force	10675.7 N, constant (No forward-aft time differential)
2.25.11 Aft Ejector Location	1.75 m aft of store nose

2.25.12 Aft Ejector force	42702.9 N, constant (No forward-aft time differential)
2.25.13 Ejector Stroke Length	0.10 m
2.26 Model references	1, 3

3 Wind Tunnel

3.1 Designation	AEDC Aerodynamic 4T
3.2 Type of tunnel	Continuous, variable pressure
3.3 Test section dimensions	1.22 x 1.22 x 3.8 m
3.4 Type of roof and floor	Porous, adjustable
3.5 Type of side walls	Porous, adjustable
3.6 Ventilation geometry	Variable, 0.5 to 10.0 % open
3.7 Thickness of side wall boundary layer	Not recorded
3.8 Thickness of boundary layers at roof and floor	Not recorded
3.9 Method of measuring velocity	Total pressure, static pressure, and temperature in test section: Mach no. x sound speed
3.10 Flow angularity	Less than 0.1 degree in test section
3.11 Uniformity of velocity over test section	See Flow angularity
3.12 Sources and levels of noise or turbulence in empty tunnel	Compressor blade tips and edge tones from porous walls; level is typical; considered of secondary-tertiary importance
3.13 Tunnel resonances	None recorded; high frequency and of no concern
3.14 Additional remarks	Honeycomb addition has nearly eliminated free-stream turbulence
3.15 References on tunnel	AEDC www home page

4 Model motion

4.1 General description	CTS generated trajectories of store from pylon
4.2 Reference coordinate and definition of motion	Bottom of pylon is reference point. Move-pause motion. Quasi-steady.
4.3 Range of amplitude	Not applicable
4.4 Range of frequency	Not applicable
4.5 Method of applying motion	CTS rig
4.6 Time-wise purity of motion	Not time accurate; yaw, pitch, roll then pause
4.7 Natural frequencies and normal modes of model and support system	Not applicable
4.8 Actual mode of applied motion including any elastic deformation	Not applicable
4.9 Additional remarks	Trajectory is calculated on-line from equations of motion using measured forces and moments as input. Induced velocity is accounted for in algorithm (to account for changed wind vector from effect of dynamic store motion: considered as a secondary effect)
4.10 References on model motion	2

5 Test Conditions

5.1 Model planform area/tunnel area	0.098
5.2 Model span/tunnel width	0.54
5.3 Blockage	Not given
5.4 Position of model in tunnel	Inverted; store on tunnel centerline
5.5 Range of Mach number	0.95 and 1.2

5.6 Range of tunnel total pressure	5.75 N/m^2
5.7 Range of tunnel total temperature	300 K to 333 K
5.8 Range of model steady, or mean, incidence	0.0
5.9 Definition of model incidence	None
5.10 Position of transition, if free	Unknown
5.11 Position and type of trip, if transition fixed	No trips anywhere on test articles. Free transition.
5.12 Flow instabilities during tests	None
5.13 Changes to mean shape of model due to steady aerodynamic load	Not measured; very stiff model; store/CTS rig position corrected for deflection by aerodynamic forces.
5.14 Additional remarks	Concerns have been raised in subsequent tests in 4T regarding transition. There is evidence that transition has occurred far aft on some store models.
5.15 References describing tests	3-5

6 Measurements and Observations

6.1 Steady pressures for the mean conditions	Yes
6.2 Steady pressures for small changes from the mean conditions	No
6.3 Quasi-steady pressures	Yes
6.4 Unsteady pressures	Not applicable
6.5 Steady section forces for the mean conditions by integration of pressures	Balances only
6.6 Steady section forces for small changes from the mean conditions by integration	Balances only
6.7 Quasi-steady section forces by integration	Balances only
6.8 Unsteady section forces by integration	Not applicable
6.9 Measurement of actual motion at points of model	Yes, using CTS rig
6.10 Observation or measurement of boundary layer properties	None
6.11 Visualisation of surface flow	None
6.12 Visualisation of shock wave movements	None
6.13 Additional remarks	Store loads from strain-gauge balances only

7 Instrumentation

7.1 Steady pressure	
7.1.1 Position of orifices	On wing, there are 7 spanwise locations with 6-11 chordwise orifices each, with orifices both on top and bottom of wing. See Fig. 3 in Section 4 in Appendix. Store has 28 orifices arranged longitudinally at five azimuthal positions chosen so that swapping store across CL and rotating store 90 degrees 3 times at both locations gives 36 equally spaced orifice rows. See Section 2 of Appendix. There are two rows of fin orifices on <u>one</u> side of each fin; each is positioned at a different span location. Opposite side is taken when store is moved across CL. Using the swapping across CL and rotations of store, 8 effective rows of taps are on each side of each fin. There are two rows of four orifices each on each side of the pylon (inboard and outboard).
7.1.2 Type of measuring system	Electronically Scanned Pressure (ESP) module
7.2 Unsteady pressures	None
7.3 Model motion	CTS rig
7.3.1 Method of measuring motion	Touch point on pylon

reference coordinate	
7.3.2 Method of determining next position of store	Error signal to motors. (Spatial mode of motion.)
7.3.3 Accuracy of measured motions	Uncertainty of trajectory position is recorded as ± 0.15 cm for model-scale position and ± 0.15 degs for attitude.
7.4 Processing of unsteady measurements	
7.4.1 Method of acquiring and processing measurements	Orifices, tubes, and transducers. Strain gauges. On-line computer. Off-line data reduction through Engineering Unit conversion FORTRAN codes
7.4.2 Type of analysis	Discretized equations of motion
7.4.3 Unsteady pressure quantities obtained and accuracy achieved	None
7.4.4 Method of integration to obtain forces	None
7.5 Additional remarks	None
7.6 References on techniques	3-5

8 Data presentation

8.1 Test cases for which data could be made available	Mach =0.95 and 1.2 at Re = 7.87 x10^6/m simulated store drops to equivalent real time of approximately 0.35 secs
8.2 Test cases for which data are included in this document	Same
8.3 Steady pressures	See files on CD-ROM
8.4 Quasi-steady or steady perturbation pressures	No
8.5 Unsteady pressures	No
8.6 Steady forces or moments	See files on CD-ROM
8.7 Quasi-steady or unsteady perturbation forces	No
8.8 Unsteady forces and moments	No
8.9 Other forms in which data could be made available	None
8.10 Reference giving other representations of data	3-5.

9 Comments on data

9.1 Accuracy	
9.1.1 Mach number	± 0.01 with 0.003 uncertainty
9.1.2 Steady incidence	0.15 degs uncertainty
9.1.3 Reduced frequency	Not given
9.1.4 Steady pressure coefficients	0.0069 uncertainty
9.1.5 Steady pressure derivatives	None
9.1.6 Unsteady pressure coefficients	None
9.2 Sensitivity to small changes of parameter	Not recorded
9.3 Non-linearities	Not recorded
9.4 Influence of tunnel total pressure	Not recorded
9.5 Effects on data of uncertainty, or variation, in mode of model motion	Not recorded
9.6 Wall interference corrections	CTS rig has no effect; subsequent CFD solutions confirm
9.7 Other relevant tests on same model	None
9.8 Relevant tests on other models of nominally the same shapes	None

9.9 Any remarks relevant to comparison between experiment and theory	References 3-5 present comparisons with CFD solutions. All the CFD solutions use the Euler equations. All CFD solutions show excellent agreement with the store's cg displacement. Good agreement was shown comparing pitch, yaw, and roll angles. Pitch angles compared least well. See Section 5 of Appendix.
9.10 Additional remarks	None
9.11 References on discussion of data	3-5

10 Personal contact for further information

Dr. L. Liejewski, AFRL, Eglin AFB, FL 32542

11 List of references

1. Abbott, Ira H., and von Doenhoff, Albert E., "Theory of Wing Sections." Dover Publications, New York, New York, 1959.
2. Carman, J. B., Hill, D., Christopher, J. P., "Store Separation Testing Techniques at the AEDC. Vols. I-II," AEDC TR-79-1, Arnold Engineering Development Center, Arnold AFB, TN 37389, 1980.
3. Liejewski, L. and Suhs, N. E. "Chimera-Eagle Store Separation." AIAA-92-4569, August 1992.
4. Jordan, J. K., Suhs, N. E., Thoms, R. E., Tramel, R. W., Fox, J. H., and Erickson, J. C. Jr., "Computational Time Accurate Body Movement: Methodology, Validation, and Application." AEDC-TR-94-15, October 1995.
5. Nichols, R. H., "Applications of a Highly Efficient Numerical Method for Overset-Mesh Moving Body Problems." AIAA-97-2255.

APPENDIX

1 Test Points

Mach Number	Equivalent Real Time of Trajectory	Data Recorded
0.95	0.01 second increments through complete trajectory	Position, Forces, Moments, Velocities, and Accelerations
1.20	0.01 second increments through complete trajectory	Position, Forces, Moments, Velocities, and Accelerations
Mach Number	**Position Points in Trajectory**	**Additional Data Recorded**
0.95	4	Wing, Store, and Pylon Pressures
	16	Wing, Store, and Pylon Pressures
	23	Wing, Store, and Pylon Pressures
	31	Wing, Store, and Pylon Pressures
	38	Wing, Store, and Pylon Pressures
1.20	4	Wing, Store, and Pylon Pressures
	16	Wing, Store, and Pylon Pressures
	22	Wing, Store, and Pylon Pressures
	33	Wing, Store, and Pylon Pressures
	43	Wing, Store, and Pylon Pressures

Table 1 Test Points

2 Identification of Orifices

Span Position	21.1 cm		19.5 cm		18.0 cm		16.5 cm		15.0 cm
Chord LW	17.0 cm		18.5 cm		20.1 cm		21.6 cm		23.1 cm
Orifice Number Bottom-Top	X/LW	Orifice Number Bottom-Top	X/LW	Orifice Number Bottom-Top	X/LW	Orifice Number Bottom-Top	X/LW	Orifice Number Bottom-Top	X/LW
102-302	0.1194	108-308	0.1096	115-315	0.1013	123-323	0.0941*	202-332	0.0879
103-303	0.2388	109-309	0.2192	116-316	0.2025	xxx-324	[0.1882]	203-333	0.1758
104-304	0.3582	110-310	0.3288	117-317	0.3038	xxx-325	[0.2824]	204-334	0.2637
105-305	0.4776	111-311	0.4384	118-318	0.4051	xxx-326	[0.3765]	205-335	0.3517
106-306	0.5970	112-312	0.5480	119-319	0.5063	xxx-327	[0.4706]	206-336	0.4396
107-307	0.7164	113-313	0.6575	120-320	0.6076	140-328	0.5647*	207-337	0.5275
		114-314	0.7671	121-321	0.7089	141-329	0.6588	208-338	0.6154
				122-322	0.8101	142-330	0.7529	209-339	0.7033
						143-331	0.8471	210-340	0.7912

Table 2 Wing Orifice Positions

Span Position	13.5 cm		11.9 cm		3.8 cm		-3.8 cm
Chord LW	24.6 cm		26.2 cm		34.3 cm		34.3 cm
Orifice Number Bottom-Top	**X/LW**	**Orifice Number Bottom-Top**	**X/LW**	**Orifice Number Bottom-Top**	**X/LW**	**Orifice Number Bottom-Top**	**X/LW**
211-402	0.0825	221-412	0.0777	232	(0.2259)	239	(0.2259)
221-403	0.1650	222-413	0.1553	233	(0.3000)	240	(0.3000)
213-404	0.2474	223-414	0.2330	234	(0.3741)	241	(0.3741)
214-405	0.3299	224-415	0.3107	235	(0.4482)	242	(0.4482)
215-406	0.4124	225-416	0.3884	236	(0.5222)	243	(0.5222)
216-407	0.4949	226-417	0.4660	237	(0.5963)	244	(0.5963)
217-408	0.5773	227-418	0.5437	238	(0.6704)	245	(0.6704)
218-409	0.6598	228-419	0.6214				
219-410	0.7423	229-420	0.6990				
220-411	0.8247	230-421	0.7767				
		231-422	0.8544				

* Orifices partially covered by pylon on bottom surface
[ ] Orifices unavailable on bottom surface
( ) Orifices with no counterpart on top surface
xxx Orifices 124 to 139 unavailable on bottom surface

Table 2 (continued) Wing Orifice Positions

Pylon Orifice Numbers and Positions

The Pylon pressure data is the last 16 CPWs in the Wing data set. There are two rows of four orifices each on each side of the pylon (inboard and outboard). The orifice numbers run from 124 through 139. Orifice numbers 126, 130, 134, 138 make the outboard row of taps closest to the store. Orifices 125, 129, 133, 137 make the outboard row closest to the Wing. Similarly, orifices 127, 131, 135, 139 make the inboard row closest to the store, and 124, 128, 132, 136 make the inboard row closest to the wing. Orifices 126 and 127, which correspond to outboard and inboard respectively, are on straight rows (call them Row 1OB and Row 1IB) positioned 0.25 cm inward from the edge attached to the store and parallel to it, and they are 2.1 cm aft of the leading edge of the pylon. Each orifice is equally spaced along the row by 2.03 cm. The rows closest to the wing (call them Row 2OB and Row 2IB) are positioned 1.52 cm in from the edge attached to the store and parallel to Rows 1OB and IB with their orifices exactly aligned vertically with those in Rows 1OB and IB.

Store Body Orifice Rows

Row 1 is 45 degs ccw from pylon looking upstream. Row 1 is also coincident with Fin 1 footprint chord.

Row 2 is 30 degs ccw from Fin 1.

Row 3 is 20 degs cw from Fin 3, which is diametrically opposite Fin 1.

Row 4 is 80 degs ccw from Fin 3. Fin 4 is 10 degs ccw from Row 4, 90 degs ccw from Fin 3.

Row 5 is 40 degs cw from Fin 1.

Store Fin Orifice Rows

There are two rows of orifices on each fin. They are positioned differently on each fin.

Rows 1 and 5 are on Fin 4. Fin 4: Row 5 is 0.44 cm in from Fin tip and Row 1 is 0.80 cm in from Fin tip.

Rows 2 and 6 are on Fin 3. Fin 3: Row 6 is 0.35 cm in from Fin tip and Row 2 is 0.71 cm in from Fin tip.

Rows 3 and 7 are on Fin 2. Fin 2: Row 7 is 0.27 cm in from Fin tip and Row 3 is 0.62 cm in from Fin tip.

Rows 4 and 8 are on Fin 1. Fin 1: Row 8 is 0.18 cm in from Fin tip and Row 4 is 0.53 cm in from Fin tip.

	BODY ORIFICE ROWS					FIN ORIFICE ROWS							
	1	2	3	4	5	1	2	3	4	5	6	7	8
	ORIFICE IDENTIFICATION NUMBER												
Numbers increment aftward													
1	502	522	604	632	714	932	906	828	806	920	841	818	742
2	503	523	605	633	715	933	907	829	807	921	842	819	743
3	504	524	606	634	716	934	908	830	808	922	843	820	744
4	505	525	607	635	717	935	909	831	809	923	844	821	745
5	506	526	608	636	718	936	910	832	810	924	845	822	746
6	507	527	609	637	719	937	911	833	811	925	846	823	747
7	508	528	610	638	720	938	912	834	812	926	847	824	802
8	509	529	611	639	721	939	913	835	813	927	902	825	803
9	510	530	612	640	722	940	914	836	814	928	903	826	804
10	511	531	613	641	723	941	915	837	815	929	904	827	805
11	512	532	614	642	724	942	916	838	816	930	905		
12	513	533	615	643	725	943	917	839	817	931			
13	514	534	616	644	726	944	918	840					
14	515	535	617	645	727	945	919						
15	516	536	618	646	728								
16	517	537	619	647	729								
17	518	538	620	702	730								
18	519	539	621	703	731								
19	520	540	622	704	732								
20	521	541	623	705	733								
21	---	542	624	706	734								
22	---	543	625	707	735								
23	---	544	626	708	736								
24	---	545	627	709	737								
25	---	546	628	710	738								
26	---	547	629	711	739								
27	---	602	630	712	740								
28	---	603	631	713	741								

Table 3 Store Orifice Numbers

	BODY ORIFICE ROWS		FIN ORIFICE ROWS							
	1	2 – 5	1	2	3	4	5	6	7	8
	X/LB		X /LF							
1	0.0337	0.0337	0.0623	0.0647	0.0673	0.0702	0.0733	0.0767	0.0805	0.0846
2	0.0673	0.0673	0.1245	0.1294	0.1347	0.1404	0.1466	0.1535	0.1610	0.1692
3	0.1010	0.1010	0.1868	0.1942	0.2020	0.2107	0.2199	0.2302	0.2415	0.2538
4	0.1347	0.1347	0.2491	0.2589	0.2694	0.2809	0.2933	0.3070	0.3221	0.3384
5	0.1683	0.1683	0.3113	0.3236	0.3367	0.3511	0.3666	0.3837	0.4026	0.4280
6	0.2020	0.2020	0.3736	0.3883	0.4040	0.4213	0.4399	0.4605	0.4831	0.5076
7	0.2357	0.2357	0.4359	0.4531	0.4714	0.4916	0.5132	0.5372	0.5636	0.5922
8	0.2693	0.2693	0.4981	0.5178	0.5387	0.5618	0.5865	0.6140	0.6441	0.6768
9	0.3030	0.3030	0.5604	0.5825	0.6061	0.6320	0.6598	0.6907	0.7246	0.7614
10	0.3366	0.3366	0.6227	0.6472	0.6734	0.7022	0.7331	0.7675	0.8052	0.8460
11	0.3703	0.3703	0.6849	0.7120	0.7407	0.7725	0.8065	0.8442		
12	0.4040	0.4040	0.7472	0.7767	0.8081	0.8427	0.8798			
13	0.4376	0.4376	0.8095	0.8414	0.8754					
14	0.4713	0.4713	0.8717	0.9061						
15	0.5050	0.5050								
16	0.5386	0.5386	LF (cm)							
17	0.5723	0.5723	4.08	3.93	3.77	3.62	3.46	3.31	3.15	3.00
18	0.6060	0.6060								
19	0.6396	0.6396								
20	0.6733	0.6733								
21	-----	0.7071								
22	-----	0.7406								
23	-----	0.7743								
24	-----	0.8079								
25	-----	0.8416								
26	-----	0.8753								
27	-----	0.9089								
28	-----	0.9426								

LB = 15.1 cm

Table 4 Store Pressure Orifice Locations

3 Format of Data on CD-ROM

For files M12BODY.DAT and M95BODY.DAT, there are 55 items in each list. For example, below is the first list in file:

M12BODY.DAT FORMAT(6(1PE12.5))

9.12200E+03	4.00000E+00	1.00000E+00	1.00000E+00	1.15188E+03	9.40000E+01
2.04393E+03	1.20030E+00	4.78861E+02	4.74823E+02	2.43897E+00	4.29820E+02
-1.10000E-01	0.00000E+00	8.58740E-02	8.48428E-03	7.05405E+00	-6.80302E+00
2.10713E-02	1.42177E-02	1.41720E-02	2.41153E-02	8.37489E-03	7.29932E-02
5.00000E+00	5.07298E+00	6.92000E+02	8.63788E-01	6.74838E-01	5.24998E-01
4.01009E-01	3.07119E-01	2.80552E-01	3.82871E-01	5.73961E-01	3.01025E-01
7.88166E-02	-1.67391E-01	-3.31710E-01	-3.93508E-01	-3.58220E-01	-3.55254E-01
-3.15861E-0-	-2.76891E-01	-2.55959E-01	-2.53289E-00	-2.27156E-01	-1.52431E-01
-1.68920E-01	-2.24603E-01	-2.52846E-01	-3.29054E-01	-5.11267E-01	-6.51763E-01
-6.48532E-01					

Table 5 Data List, Store Body

Nomenclature Map of Above and M95BODY.DAT List:

Test number	ID number	Point	Configuration	PT	TT
Patm	M	Q	P	Re	T
ALPHA	BETA	ALPSRB	BETSRB	CLMRB	CLNRB
XP	YP	ZP	THETA	PSI	PHI
ROW	PHIR	RUN	CPW01	CPW02	CPW03
CPW04	CPW05	CPW06	CPW07	CPW08	CPW09
CPW10	CPW11	CPW12	CPW13	CPW14	CPW15
CPW16	CPW17	CPW18	CPW19	CPW20	CPW21
CPW22	CPW23	CPW24	CPW25	CPW26	CPW27
CPW28					

Table 6 Nomenclature Map, Store Body

The FORTRAN STATEMENTS to recover the data could be as follows for this dataset.

```
C     READ DATA

      REAL F(55)
      OPEN (UNIT = 5, FILE = 'c:\FTN\M95BODY.DAT')
      OPEN (UNIT = 8, FILE = 'c:\FTN\M95BODY.OUT')

      REWIND 8
      DO 105, K=1,99999
      READ (5,100,END=105)F
100   FORMAT(6(1PE12.5))

      Write (*,100)(F(I), I= 1,55)
C     Convert to MKS (International) units from Anglo-American
C     Psf to Pascals
      F(5) = F(5) * 47.8802
      F(7) = F(7) * 47.8802
      F(10)= F(10)* 47.8802
C     Farenheit to Kelvin
      F(6) = (F(6)+459.69) / 1.8
C     Rankine to Kelvin
      F(12)= F(12)/ 1.8
```

Table 7 FORTRAN Statements to Read Data, Store Body

```
C     Feet to Centimeters. Note these are full-scale. Multiply by
C     0.05 to recover subscale (tunnel scale) lengths.
         F(19) = F(19)*30.48
         F(20) = F(20)*30.48
         F(21) = F(21)*30.48
C     10**6 per foot to 10**6 per Meter
         F(11) = F(11)/.3048
         Write (8,101)(F(I), I= 1,18)
         Write (8,102)(F(I), I=19,39)
         Write (8,103)(F(I), I=40,55)
101 FORMAT(///,'  Test   =',F9.1,'  ID     =',F9.1,'  Point ='
   x ,F9.1,/,
   x '  Config =',F9.1,'  PT     =',F9.2,'  TT     ='
   x ,F9.4,/,
   x '  Patm   =',F9.2,'  M      =',F9.4,'  Q      ='
   x ,F9.4,/,
   x '  P      =',F9.2,'  Re     =',F9.4,'  T      ='
   x ,F9.4,/,
   x '  ALPHA  =',F9.4,'  BETA   =',F9.4,'  ALPSRB ='
   x ,F9.4,/,
   x '  BETSRB =',F9.4,'  CLMRB  =',F9.4,'  CLNRB  ='
   x ,F9.4,/)
102 FORMAT('  XP     =',F9.4,'  YP     =',F9.4,'  ZP     ='
   x ,F9.4,/,
   x '  THETA  =',F9.4,'  PSI    =',F9.4,'  PHI    ='
   x ,F9.4,/,
   x '  ROW    =',F9.4,'  PHIR   =',F9.4,'  RUN    ='
   x ,F9.2,//,
   x '  CPW01  =',F9.4,'  CPW02  =',F9.4,'  CPW03  ='
   x ,F9.4,/,
   x '  CPW04  =',F9.4,'  CPW05  =',F9.4,'  CPW06  ='
   x ,F9.4,/,
   x '  CPW07  =',F9.4,'  CPW08  =',F9.4,'  CPW09  ='
   x ,F9.4,/,
   x '  CPW10  =',F9.4,'  CPW11  =',F9.4,'  CPW12  ='
   x ,F9.4)
103 FORMAT('  CPW13  =',F9.4,'  CPW14  =',F9.4,'  CPW15  ='
   x ,F9.4,/,
   x '  CPW16  =',F9.4,'  CPW17  =',F9.4,'  CPW18  ='
   x ,F9.4,/,
   x '  CPW19  =',F9.4,'  CPW20  =',F9.4,'  CPW21  ='
   x ,F9.4,/,
   x '  CPW22  =',F9.4,'  CPW23  =',F9.4,'  CPW24  ='
   x ,F9.4,/,
   x '  CPW25  =',F9.4,'  CPW26  =',F9.4,'  CPW27  ='
   x ,F9.4,/,
   x '  CPW28  =',F9.4)
104 CONTINUE
105 CONTINUE
    END
```

Table 7 (continued) FORTRAN Statements to Read Data, Store Body

For a typical fin data list, there are 58 items, but the map is somewhat different.

NOMENCLATURE MAP OF M12FIN.DAT OR M95FIN.DAT

Test number	ID number	Point	Configuration	PT	TT
Patm	M	Q	P	Re	T
ALPHA	BETA	ALPSRB	BETSRB	CLMRB	CLNRB
XP	YP	ZP	THETA	PSI	PHI
ROW	PHIF	RUN	CPF01L	CPF02L	CPF03L
CPF04L	CPF05L	CPF06L	CPF07L	CPF08L	CPF09L
CPF10L	CPF11L	CPF12L	CPF13L	CPF14L	RUN
CPF01R	CPF02R	CPF03R	CPF04R	CPF05R	CPF06R
CPF07R	CPF08R	CPF09R	CPF10R	CPF11R	CPF12R
CPF13R	CPF14R				

Note that the suffix L and R indicate right and left looking upstream, with store virtually positioned on pilot's right wing.

Table 8. Nomenclature Map, Fin

For a typical wing data list, there are 171 items.

NOMENCLATURE MAP OF M12WING.DAT OR M95WING.DAT

Test number	ID number	Point	Configuration	PT	TT
Patm	M	Q	P	Re	T
ALPHA	BETA	ALPSRB	BETSRB	CN	CLM
XP	YP	ZP	THETA	PSI	PHI
RUN	CPW102	CPW103	ETCETERA	ETC.	CPW106
CPW107	ETC.	ETC.	ETC.	ETC.	CPW112
CPW113	ETC.	ETC.	ETC.	ETC.	CPW118
CPW119	ETC.	ETC.	ETC.	CPW123	CPW140
CPW141	CPW142	CPW143	CPW202	CPW203	CPW204
CPW205	ETC.	ETC.	ETC.	ETC.	CPW210
CPW211	ETC.	ETC.	ETC.	ETC.	CPW216
CPW217	ETC.	ETC.	ETC.	ETC.	CPW222
CPW223	ETC.	ETC.	ETC.	ETC.	CPW228
CPW229	ETC.	ETC.	ETC.	ETC.	CPW234
CPW235	ETC.	ETC.	ETC.	ETC.	CPW240
CPW241	CPW242	CPW243	CPW244	CPW245	CPW302
CPW303	ETC.	ETC.	ETC.	ETC.	CPW308
CPW309	ETC.	ETC.	ETC.	ETC.	CPW314
CPW315	ETC.	ETC.	ETC.	CPW319	CPW320
CPW321	CPW322	CPW323	CPW324	CPW325	CPW326
CPW327	ETC.	ETC.	ETC.	ETC.	CPW332
CPW333	ETC.	ETC.	ETC.	ETC.	CPW338
CPW339	CPW340	CPW402	CPW403	CPW404	CPW405
CPW406	ETC.	ETC.	ETC.	ETC.	CPW411
CPW412	ETC.	ETC.	ETC.	ETC.	CPW417
CPW418	ETC.	ETC.	ETC.	CPW422	CPW126
CPW130	CPW134	CPW138	CPW127	CPW131	CPW135
CPW139	CPW125	CPW129	CPW133	CPW137	CPW124
CPW128	CPW132	CPW136			

Table 9. Nomenclature Map, Wing

For a typical free-stream data list, there are 27 items.

NOMENCLATURE MAP OF M12FREESTR.DAT OR M95FREESTR.DAT

Test number	Run Point	Point	PT	TT	Patm
M	Q	P	Re	T	ALPHA
BETA	ALPHAS	BETAS	CAT	CY	CN
CLL	CLM	CLN	XP	YP	ZP
THETA	PSI	PHI			

Table 10. Nomenclature Map, Free Stream

For a typical carriage loads data list, there are 27 items. Nomenclature map is identical to that of free-stream data.

NOMENCLATURE MAP OF M12CAPLOAD.DAT OR M95CAPLOAD.DAT

Test number	Run Point	Point	PT	TT	Patm
M	Q	P	Re	T	ALPHA
BETA	ALPHAS	BETAS	CAT	CY	CN
CLL	CLM	CLN	XP	YP	ZP
THETA	PSI	PHI			

Table 11. Nomenclature Map, Carriage Loads

For a typical trajectory data list, there are 38 items.

NOMENCLATURE MAP OF M12TRAJ.DAT OR M95TRAJ.DAT

Test number	Run Point	Point	PT	TT	Patm
M	Q	P	Re	T	ALPHA
BETA	ALPHAS	BETAS	CAT	CY	CN
CLL	CLM	CLN	XP	YP	ZP
THETA	PSI	PHI	DPSI	DTHA	DPHI
VX	VY	VZ	P	Q	R
ETIME	T (Time)				

Table 12. Nomenclature Map, Trajectory

4 Drawings of Test Articles

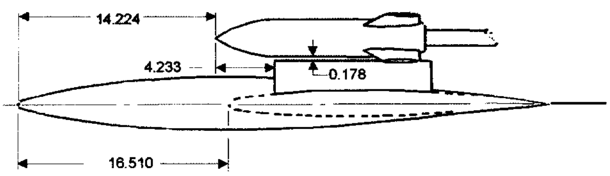

Dimensions in Centimeters

Fig. 1 Store at Carriage

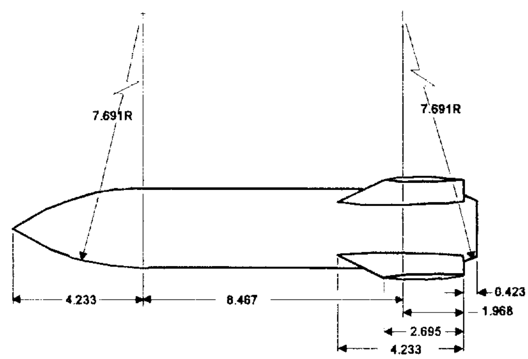

Fig. 2 Store Model

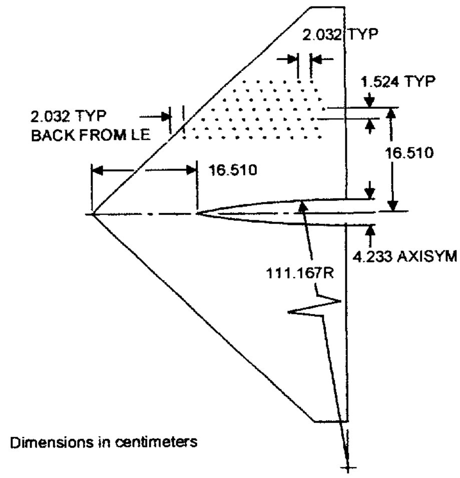

Fig. 3 Wing Upper Surface

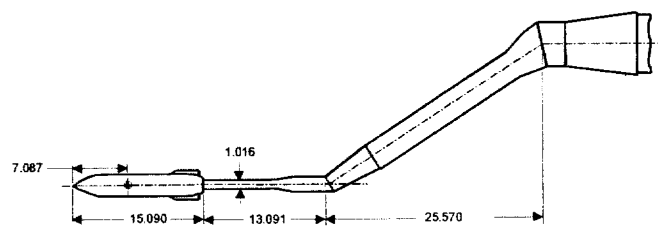

Fig. 4 Captive Trajectory Support Rig

5 Inviscid CFD Comparisons, Reference 5

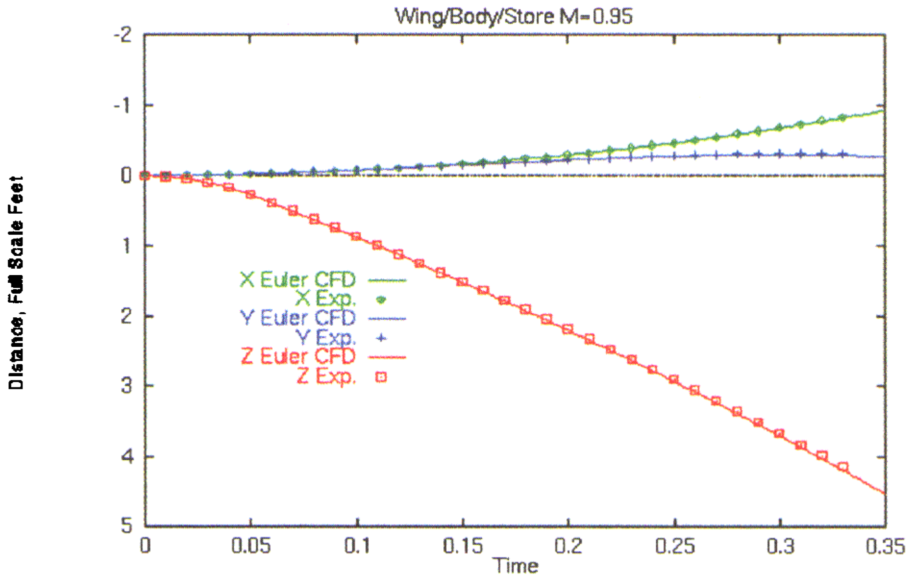

Fig. 5 Position vs Time

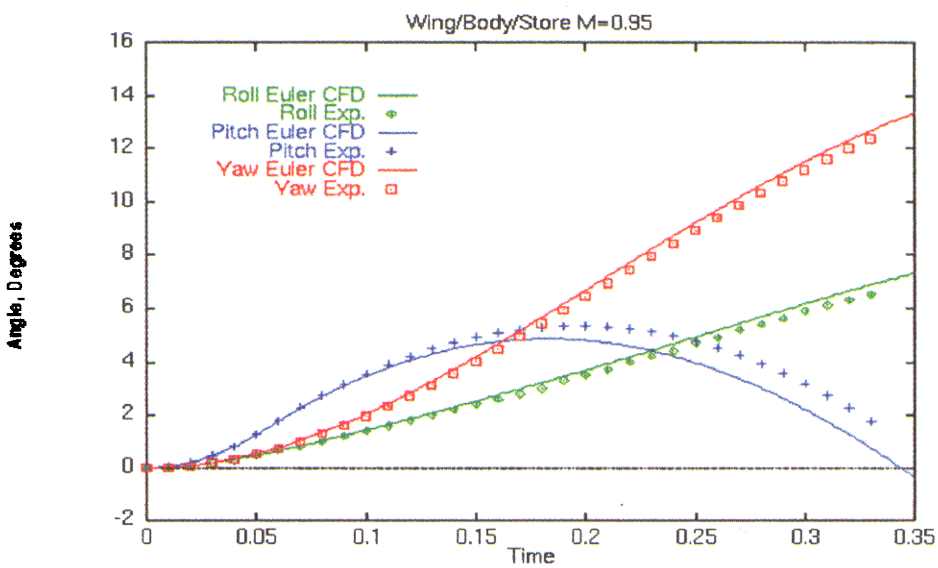

Fig. 6 Attitude vs Time

REPORT DOCUMENTATION PAGE

1. Recipient's Reference	2. Originator's References	3. Further Reference	4. Security Classification of Document
	RTO-TR-26 AC/323(AVT)TP/19	ISBN 92-837-1048-7	UNCLASSIFIED/ UNLIMITED

5. Originator Research and Technology Organization
North Atlantic Treaty Organization
BP 25, 7 rue Ancelle, F-92201 Neuilly-sur-Seine Cedex, France

6. Title
Verification and Validation Data for Computational Unsteady Aerodynamics

7. Presented at/sponsored by
the RTO Applied Vehicle Technology Panel (AVT).

8. Author(s)/Editor(s)	9. Date
Multiple	October 2000

10. Author's/Editor's Address	11. Pages
Multiple	568

12. Distribution Statement There are no restrictions on the distribution of this document. Information about the availability of this and other RTO unclassified publications is given on the back cover.

13. Keywords/Descriptors

Unsteady flow	Aerodynamic characteristics
Aerodynamics	Flight control
Computerized simulation	Stalling
Proving	Cavities
Experimental data	Fluid flow
Verifying	External stores
Computation	Separation
Flutter	Wings
Buffeting	Computational fluid dynamics (CFD)
Aerodynamic stability	Computer codes

14. Abstract

Computational Unsteady Aerodynamics computer codes are being increasingly used. In order to validate their results they must be tested against valid experimental data. The present report aims at collecting reliable experimental data on unsteady aerodynamics and presenting them in a form which permits use for verification of codes. For ease of handling, the data are also presented in machine readable form (CD-ROM). Data on increasingly complex generic forms were selected and the following categories are covered: flutter, buffet, stability and control, dynamic stall, cavity flows, store separation. Computational solutions are included in order to permit evaluation of codes and analysis of solutions which differ from experimental data.

NORTH ATLANTIC TREATY ORGANIZATION

RESEARCH AND TECHNOLOGY ORGANIZATION
BP 25 • 7 RUE ANCELLE
F-92201 NEUILLY-SUR-SEINE CEDEX • FRANCE
Télécopie 0(1)55.61.22.99 • E-mail mailbox@rta.nato.int

DIFFUSION DES PUBLICATIONS
RTO NON CLASSIFIEES

L'Organisation pour la recherche et la technologie de l'OTAN (RTO), détient un stock limité de certaines de ses publications récentes, ainsi que de celles de l'ancien AGARD (Groupe consultatif pour la recherche et les réalisations aérospatiales de l'OTAN). Celles-ci pourront éventuellement être obtenues sous forme de copie papier. Pour de plus amples renseignements concernant l'achat de ces ouvrages, adressez-vous par lettre ou par télécopie à l'adresse indiquée ci-dessus. Veuillez ne pas téléphoner.

Des exemplaires supplémentaires peuvent parfois être obtenus auprès des centres nationaux de distribution indiqués ci-dessous. Si vous souhaitez recevoir toutes les publications de la RTO, ou simplement celles qui concernent certains Panels, vous pouvez demander d'être inclus sur la liste d'envoi de l'un de ces centres.

Les publications de la RTO et de l'AGARD sont en vente auprès des agences de vente indiquées ci-dessous, sous forme de photocopie ou de microfiche. Certains originaux peuvent également être obtenus auprès de CASI.

CENTRES DE DIFFUSION NATIONAUX

ALLEMAGNE
Streitkräfteamt / Abteilung III
Fachinformationszentrum der Bundeswehr, (FIZBw)
Friedrich-Ebert-Allee 34
D-53113 Bonn

BELGIQUE
Coordinateur RTO - VSL/RTO
Etat-Major de la Force Aérienne
Quartier Reine Elisabeth
Rue d'Evère, B-1140 Bruxelles

CANADA
Directeur - Recherche et développement - Communications et gestion de l'information - DRDCGI 3
Ministère de la Défense nationale
Ottawa, Ontario K1A 0K2

DANEMARK
Danish Defence Research Establishment
Ryvangs Allé 1, P.O. Box 2715
DK-2100 Copenhagen Ø

ESPAGNE
INTA (RTO/AGARD Publications)
Carretera de Torrejón a Ajalvir, Pk.4
28850 Torrejón de Ardoz - Madrid

ETATS-UNIS
NASA Center for AeroSpace Information (CASI)
Parkway Center
7121 Standard Drive
Hanover, MD 21076-1320

FRANCE
O.N.E.R.A. (ISP)
29, Avenue de la Division Leclerc
BP 72, 92322 Châtillon Cedex

GRECE (Correspondant)
Hellenic Ministry of National Defence
Defence Industry Research & Technology General Directorate
Technological R&D Directorate
D.Soutsou 40, GR-11521, Athens

HONGRIE
Department for Scientific Analysis
Institute of Military Technology
Ministry of Defence
H-1525 Budapest P O Box 26

ISLANDE
Director of Aviation
c/o Flugrad
Reykjavik

ITALIE
Centro di Documentazione Tecnico-Scientifica della Difesa
Via XX Settembre 123a
00187 Roma

LUXEMBOURG
Voir Belgique

NORVEGE
Norwegian Defence Research Establishment
Attn: Biblioteket
P.O. Box 25, NO-2007 Kjeller

PAYS-BAS
NDRCC
DGM/DWOO
P.O. Box 20701
2500 ES Den Haag

POLOGNE
Chief of International Cooperation Division
Research & Development Department
218 Niepodleglosci Av.
00-911 Warsaw

PORTUGAL
Estado Maior da Força Aérea
SDFA - Centro de Documentação
Alfragide
P-2720 Amadora

REPUBLIQUE TCHEQUE
Distribuční a informační středisko R&T
VTÚL a PVO Praha
Mladoboleslavská ul.
197 06 Praha 9-Kbely AFB

ROYAUME-UNI
Defence Research Information Centre
Kentigern House
65 Brown Street
Glasgow G2 8EX

TURQUIE
Millî Savunma Başkanliği (MSB)
ARGE Dairesi Başkanliği (MSB)
06650 Bakanliklar - Ankara

AGENCES DE VENTE

NASA Center for AeroSpace Information (CASI)
Parkway Center
7121 Standard Drive
Hanover, MD 21076-1320
Etats-Unis

The British Library Document Supply Centre
Boston Spa, Wetherby
West Yorkshire LS23 7BQ
Royaume-Uni

Canada Institute for Scientific and Technical Information (CISTI)
National Research Council
Document Delivery
Montreal Road, Building M-55
Ottawa K1A 0S2, Canada

Les demandes de documents RTO ou AGARD doivent comporter la dénomination "RTO" ou "AGARD" selon le cas, suivie du numéro de série (par exemple AGARD-AG-315). Des informations analogues, telles que le titre et la date de publication sont souhaitables. Des références bibliographiques complètes ainsi que des résumés des publications RTO et AGARD figurent dans les journaux suivants:

Scientific and Technical Aerospace Reports (STAR)
STAR peut être consulté en ligne au localisateur de ressources uniformes (URL) suivant:
http://www.sti.nasa.gov/Pubs/star/Star.html
STAR est édité par CASI dans le cadre du programme NASA d'information scientifique et technique (STI)
STI Program Office, MS 157A
NASA Langley Research Center
Hampton, Virginia 23681-0001
Etats-Unis

Government Reports Announcements & Index (GRA&I)
publié par le National Technical Information Service
Springfield
Virginia 2216
Etats-Unis
(accessible également en mode interactif dans la base de données bibliographiques en ligne du NTIS, et sur CD-ROM)

Imprimé par St-Joseph Ottawa/Hull
(Membre de la Corporation St-Joseph)
45, boul. Sacré-Cœur, Hull (Québec), Canada J8X 1C6

NORTH ATLANTIC TREATY ORGANIZATION

RESEARCH AND TECHNOLOGY ORGANIZATION
BP 25 • 7 RUE ANCELLE
F-92201 NEUILLY-SUR-SEINE CEDEX • FRANCE
Telefax 0(1)55.61.22.99 • E-mail mailbox@rta.nato.int

DISTRIBUTION OF UNCLASSIFIED RTO PUBLICATIONS

NATO's Research and Technology Organization (RTO) holds limited quantities of some of its recent publications and those of the former AGARD (Advisory Group for Aerospace Research & Development of NATO), and these may be available for purchase in hard copy form. For more information, write or send a telefax to the address given above. **Please do not telephone**.

Further copies are sometimes available from the National Distribution Centres listed below. If you wish to receive all RTO publications, or just those relating to one or more specific RTO Panels, they may be willing to include you (or your organisation) in their distribution.

RTO and AGARD publications may be purchased from the Sales Agencies listed below, in photocopy or microfiche form. Original copies of some publications may be available from CASI.

NATIONAL DISTRIBUTION CENTRES

BELGIUM
Coordinateur RTO - VSL/RTO
Etat-Major de la Force Aérienne
Quartier Reine Elisabeth
Rue d'Evère, B-1140 Bruxelles

CANADA
Director Research & Development Communications & Information Management - DRDCIM 3
Dept of National Defence
Ottawa, Ontario K1A 0K2

CZECH REPUBLIC
Distribuční a informační středisko R&T
VTÚL a PVO Praha
Mladoboleslavská ul.
197 06 Praha 9-Kbely AFB

DENMARK
Danish Defence Research Establishment
Ryvangs Allé 1, P.O. Box 2715
DK-2100 Copenhagen Ø

FRANCE
O.N.E.R.A. (ISP)
29 Avenue de la Division Leclerc
BP 72, 92322 Châtillon Cedex

GERMANY
Streitkräfteamt / Abteilung III
Fachinformationszentrum der Bundeswehr, (FIZBw)
Friedrich-Ebert-Allee 34
D-53113 Bonn

GREECE (Point of Contact)
Hellenic Ministry of National Defence
Defence Industry Research & Technology General Directorate
Technological R&D Directorate
D.Soutsou 40, GR-11521, Athens

HUNGARY
Department for Scientific Analysis
Institute of Military Technology
Ministry of Defence
H-1525 Budapest P O Box 26

ICELAND
Director of Aviation
c/o Flugrad
Reykjavik

ITALY
Centro di Documentazione Tecnico-Scientifica della Difesa
Via XX Settembre 123a
00187 Roma

LUXEMBOURG
See Belgium

NETHERLANDS
NDRCC
DGM/DWOO
P.O. Box 20701
2500 ES Den Haag

NORWAY
Norwegian Defence Research Establishment
Attn: Biblioteket
P.O. Box 25, NO-2007 Kjeller

POLAND
Chief of International Cooperation Division
Research & Development Department
218 Niepodleglosci Av.
00-911 Warsaw

PORTUGAL
Estado Maior da Força Aérea
SDFA - Centro de Documentação
Alfragide
P-2720 Amadora

SPAIN
INTA (RTO/AGARD Publications)
Carretera de Torrejón a Ajalvir, Pk.4
28850 Torrejón de Ardoz - Madrid

TURKEY
Millî Savunma Başkanliği (MSB)
ARGE Dairesi Başkanliği (MSB)
06650 Bakanliklar - Ankara

UNITED KINGDOM
Defence Research Information Centre
Kentigern House
65 Brown Street
Glasgow G2 8EX

UNITED STATES
NASA Center for AeroSpace Information (CASI)
Parkway Center
7121 Standard Drive
Hanover, MD 21076-1320

SALES AGENCIES

NASA Center for AeroSpace Information (CASI)
Parkway Center
7121 Standard Drive
Hanover, MD 21076-1320
United States

The British Library Document Supply Centre
Boston Spa, Wetherby
West Yorkshire LS23 7BQ
United Kingdom

Canada Institute for Scientific and Technical Information (CISTI)
National Research Council
Document Delivery
Montreal Road, Building M-55
Ottawa K1A 0S2, Canada

Requests for RTO or AGARD documents should include the word 'RTO' or 'AGARD', as appropriate, followed by the serial number (for example AGARD-AG-315). Collateral information such as title and publication date is desirable. Full bibliographical references and abstracts of RTO and AGARD publications are given in the following journals:

Scientific and Technical Aerospace Reports (STAR)
STAR is available on-line at the following uniform resource locator:
http://www.sti.nasa.gov/Pubs/star/Star.html
STAR is published by CASI for the NASA Scientific and Technical Information (STI) Program
STI Program Office, MS 157A
NASA Langley Research Center
Hampton, Virginia 23681-0001
United States

Government Reports Announcements & Index (GRA&I)
published by the National Technical Information Service
Springfield
Virginia 22161
United States
(also available online in the NTIS Bibliographic Database or on CD-ROM)

Printed by St. Joseph Ottawa/Hull
(A St. Joseph Corporation Company)
45 Sacré-Cœur Blvd., Hull (Québec), Canada J8X 1C6

ISBN 92-837-1048-7